DX 7947 7

TITLE THE XENOLITHIC SUITE OF THE STRONTIAN GRANITE

AUTHOR Barbara M. Kruszewska

UNIVERSITY London Polytechnic, C.N.A.A. 1990

THE XENOLITHIC SUITE OF THE STRONTIAN GRANITE

by

Barbara M. Kruszewska

Submitted to the Council for National Academic Awards

in partial fulfillment of the requirement for the degree of

Doctor of Philosophy

City of London Polytechnic, April 1990

THE XENOLITHIC SUITE OF THE STRONTIAN GRANITE

by

Barbara M. Kruszewska

The Strontian Granite in Argyllshire, is a composite pluton of late Caledonian age, emplaced into Moinian psammitic and pelitic rocks. It is composed of an outer tonalitic granodiorite (dated at 435 Ma.) passing into a porphyritic granodiorite, both xenolithic, and intruded by a younger alkali granite (ca. 400 Ma.). The wide variety of dioritic xenoliths show compositional variations from biotite and hornblende-rich ultramafic varieties through diorites to rarer acid types, with some being particularly sphene - rich. Others have quartz xenocrysts. All the xenoliths occur as dark finer grained, flat ellipsoidal inclusions, lying parallel to the main foliation. Crudely mineralogically layered mafic diorites occur throughout the complex as heterogenous bodies ranging from appinites through biotite-rich diorites to plagioclase-rich types. They appear to form small independent intrusive bodies. They are texturally and mineralogically different from the xenoliths. Conclusions offered in the literature have led to a number of interpretations including: 1) they represent restites from partial melting; 2) the xenoliths are the result of magma mixing - specifically acid and intermediate; 3) they are related by fractional crystallization and assimilation to the host granite. Present work favours the view that the host rocks are the result of fractionation and mixing processes; from field and geochemical observations the xenoliths are the result of hybridization with some being fragments of earlier diorite chills and that from texture and geochemistry displayed the diorites are independent bodies formed by accumulation.

ACKNOWLEDGEMENTS

I would like to take this opportunity to thank both my supervisors, Dr Alistair Baxter and Dr Ian Platten, who have given me their time, effort and help in writing this thesis, and for their patience and friendship; and to Prof RR Skelhorn for his encouragement.

I am grateful also to the Department of Geology, City of London Polytechnic (now Thames Polytechnic) which provided analytical facilities, financial assistance and a base for this study.

Additional facilities were given by Kings College London and Nick Walsh (ICP-AES) and by Edinburgh University, where I thank Dr Peter Hill for allowing me as a guinea-pig on the Camebax Electron Microprobe.

I thank all on the Ardtornish Estate, Morvern Peninsula Argyllshire for giving me free access to their estate, whether by foot or by boat and for being able to stay in such beautiful surroundings as Ardtornish house.

Lastly I thank my husband Jaś, my mother and brother Andrzej for continual support and never having lost faith in me.

I dedicate this work to all those people who can
now easily distinguish and appreciate
GRANITE.

CONTENTS

Appendix C Electron Microprobe Analyses

Appendix D Analytical Techniques

LIST OF FIGURES IN THE TEXT

Chapter 1

Fig.1 Map of the Scottish Highlands showing outcrops of the principal Geological Groups and some of the late Caledonian Intrusive Complexes.

Fig.1.1 Sketch map of the Strontian Granite Complex showing the main geological features.

Fig.1.2 Map of locations visited and mentioned in the text.

Fig.1.3 A map to show the location of all samples collected and analyzed.

Fig.1.4 Location of region and distribution of the Morar, Glenfinnan and Loch Eil divisions of the Moinian, after Johnstone et al (1969).

Chapter 2

Fig.2.1A A sketch map to show the whole area displaying the developed layering.

Fig.2.1B A sketch diagram to show closer detail of the layering from Fig.2.1A.

Fig.2.1C A sketch diagram to show the layering in the quarry (Location B), with analyzed samples marked also.

Fig.2.2 A sketch diagram to show details of the microdioritic, granitic sheet and porphyritic granodiorite host relationships, at A Fig.1.2.

Fig.2.3 A sketch map to show the details of the granitic sheet found in the Moine country rock.

Chapter 3

Fig.3.1 A sketch diagram to show details of zoning and twinning in the host rock feldspars.

Fig.3.2 A sketch diagram to show details of amphibole and K-feldspars of the host rocks.

Fig.3.3 A sketch diagram to show details of zoning and twinning in the host rock feldspars.

Fig.3.4A Host rock feldspar compositions plotted into the system Or-Ab-An.

Fig.3.4B Xenolith feldspar compositions plotted into the system Or-Ab-An.

Fig.3.4C Caledonian dyke feldspar compositions plotted into the system Or-Ab-An.

Fig.3.4D Diorite feldspar compositions plotted into the system Or-Ab-An.

Chapter 4

Fig.4.24 Bivariate plot of Ba/Sr ratio : SiO_2.

Fig.4.25 Bivariate plot of Ba/Rb ratio : SiO_2.

Fig.4.26 Bivariate plot of Sr : Rb.

Fig.4.27 Bivariate plot of Cr : SiO_2.

Fig.4.28 Bivariate plot of Ni : SiO_2.

Fig.4.29 Bivariate plot of V : SiO_2.

Fig.4.30 Bivariate plot of Sc : SiO_2.

Fig.4.31 Bivariate plot of Sc : FeO* (all rocks).

Fig.4.32 Bivariate plot of V : FeO* (all rocks).

Fig.4.33 Bivariate plot of V : TiO_2 (all rocks).

Fig.4.34 Bivariate plot of Cu : SiO_2.

Fig.4.35 Bivariate plot of Zn : SiO_2.

Fig.4.36 Bivariate plot of Li : SiO_2.

Fig.4.37 Chondrite normalised REE patterns for the host rocks of Strontian.

Fig.4.38 Bivariate plot of Al_2O_3 & minerals.

Fig.4.39 Bivariate plot of CaO & minerals.

Fig.4.40 Bivariate plot of TiO_2 & minerals.

Fig.4.41 Bivariate plot of FeO* & minerals.

Fig.4.42 Bivariate plot of K_2O & minerals .

Fig.4.43 Bivariate plot of MgO & minerals.

Fig.4.44 Bivariate plot of Na_2O & minerals.

Fig.4.45 Bivariate plot of P_2O_5 & minerals.

Fig.4.45A Plot of Ba vs SiO2 with extract paths calculated from Figs.4.38 to 4.44.

Fig.4.45B Plot of Sr & Rb against SiO2 with calculated extract path.

Fig.4.46 Logarithmic bivariate plot of Ba : Rb (host rocks only).

Fig.4.47 Logarithmic bivariate plot of Ba : Sr (host rocks only).

Fig.4.48 Logarithmic bivariate plot of K : Rb (host rocks only).

Fig.4.49 Logarithmic bivariate plot of Ce : Yb (host rocks only).

Fig.7.16 Bivariate plot of CaO : Sr.

Fig.7.17 Bivariate plot of Sr/Ca ratio : SiO_2.

Fig.7.18 Bivariate plot of Ba : Sr.

Fig.7.19 Bivariate plot of Ba/Sr ratio : SiO_2.

Fig.7.19A Bivariate plot of K_2O : Sr.

Fig.7.20 Bivariate plot of Rb : MgO.

Fig.7.21 Bivariate plot of Sr : Rb.

Fig.7.22 Bivariate plot of Rb : K_2O.

Fig.7.23 Bivariate plot of K/Rb ratio : SiO_2.

Fig.7.24 Bivariate plot of Cr : MgO.

Fig.7.25 Bivariate plot of Ni : MgO.

Fig.7.26 Bivariate plot of V : MgO.

Fig.7.27 Bivariate plot of Sc : MgO.

Fig.7.28 Bivariate plot of Cu : MgO.

Fig.7.29 Bivariate plot of Zn : MgO.

Fig.7.30 Bivariate plot of Li : MgO.

Fig.7.31 Chondrite normalised REE patterns for the xenoliths.

Fig.7.31A Ce plotted against MgO & SiO2 for the xenoliths.

Fig.7.31B Eu & Ce plotted against major elements MgO & P2O5.

Fig.7.32 Bivariate plot of Al_2O_3 & minerals.

Fig.7.33 Bivariate plot of CaO & minerals.

Fig.7.34 Bivariate plot of FeO* & minerals.

Fig.7.35 Bivariate plot of K_2O & minerals.

Fig.7.36 Bivariate plot of MgO & minerals.

Fig.7.37 Bivariate plot of Na_2O & minerals.

Fig.7.38 Bivariate plot of P_2O_5 & minerals.

Fig.7.39 Bivariate plot of TiO_2 & minerals.

Fig.7.40 Logarithmic bivariate plot of Rb : Ba (xens & diorites).

Fig.7.41 Logarithmic bivariate plot of K : Rb (xens & diorites).

Fig.7.42 Logarithmic bivariate plot of Ba : Sr (xens & diorites).

Fig.7.43 Logarithmic bivariate plot of Ce : Yb (xens only).

Chapter 8

Fig.8.1 Chondrite normalised REE patterns for the microdiorite dykes.

Chapter 9

Fig.9.1A Sketch map to show the internal detail of the Ranachan diorite.

Fig.9.1B Sketch map to show the internal detail of the Rubha-na-Sroine diorite.

Fig.9.1C Sketch map to show the internal detail of the Liddesdale diorite.

Fig.9.1D Sketch map to show details of the traverses across the Sheet diorite.

Fig.9.1E Sketch map to show the internal detail of the elongate Uileann diorite - southern body (no.5 Fig.1.2).

Fig.9.1F Sketch map to show the internal detail of the round Uileann diorite - northern body (no.5 Fig.1.2).

Chapter 10

Fig.10.1 Total Aliv content of all the rock types plotted against SiO2 content.

Fig.10.2 A plot of titanium against Aliv in amphiboles for all rocks of Strontian.

Fig.10.3 A plot of Alvi against Aliv in amphiboles for all rock types of Strontian.

Fig.10.4 A plot of (Na+K) against Aliv in amphiboles for all rock types of Strontian.

Fig.10.4A A plot of (Ca+Na+K) against Aliv in amphiboles for all rock types of Strontian.

Fig.10.5 Hornblende and biotite plotted on the Ca-Mg-Fe triangle (atomic %).

Fig.10.6 A plot of Fe/Mg against Aliv in amphiboles for all rocks types of Strontian.

Fig.10.7 Pyroxenes plotted on the Wo-En-Fs triangle.

Chapter 11

Fig.11.1 Bivariate plot of SiO_2 : MgO.

Fig.11.2 Bivariate plot of Al_2O_3 : MgO.

Fig.11.2A Bivariate plot of Al_2O_3 : SiO_2.

Fig.11.3 Bivariate plot of TiO_2 : MgO.

Fig.11.3A Bivariate plot of TiO_2 : SiO_2.

Fig.11.4 Bivariate plot of FeO* : MgO.

Fig.11.5 Bivariate plot of MnO : MgO.

Fig.11.5A Bivariate plot of TiO_2 : FeO* (all rocks).

Fig.11.5B Bivariate plot of MnO : FeO* (all rocks).

Fig.11.6 Bivariate plot of CaO : MgO.

Fig.11.6A Bivariate plot of CaO : SiO_2.

Fig.11.7 Bivariate plot of Na_2O : MgO.

Fig.11.8 Bivariate plot of K_2O : MgO.

Fig.11.9 Bivariate plot of P_2O_5 : MgO.

Fig.11.10 Bivariate plot of Ba : MgO.

Fig.11.11 Bivariate plot of Ba/Rb ratio : SiO_2 (all rocks).

Fig.11.11A Bivariate plot of Ba/Rb ratio : SiO_2.

Fig.11.12 Bivariate plot of Ba/Sr ratio : SiO_2 (all rocks).

Fig.11.12A Bivariate plot of Ba/Sr ratio : SiO_2.

Fig.11.13 Bivariate plot of K_2O : Ba.

Fig.11.14 Bivariate plot of Rb : Ba.

Fig.11.15 Bivariate plot of Sr : MgO.

Fig.11.16 Bivariate plot of Sr/Ca ratio : SiO_2 (all rocks).

Fig.11.17 Bivariate plot of Sr/Ca ratio : SiO_2.

Fig.11.18 Bivariate plot of CaO : Sr.

Fig.11.19 Bivariate plot of Sr : K_2O.

Fig.11.20 Bivariate plot of Ba : Sr.

Fig.11.21 Bivariate plot of Rb : Sr.

Fig.11.22 Bivariate plot of Rb : MgO.

Fig.11.23 Bivariate plot of K/Rb : SiO_2 (all rocks).

Fig.11.24 Bivariate plot of K/Rb ratio : SiO_2.

Fig.11.25 Bivariate plot of Rb : K_2O.

Fig.11.26 Bivariate plot of Cr : MgO.

Chapter 12

Fig.12.3B AFM diagram comparing the Strontian diorites to the Lorne and Sidlaw lavas.Bivariate plot of FeO* : SiO_2 (all rocks).

Fig.12.4 Bivariate plot of Al2O3: SiO_2 (all rocks).

Fig.12.5 Bivariate plot of CaO : SiO_2 (all rocks).

Fig.12.6 Bivariate plot of FeO* : SiO_2 (all rocks).

Fig.12.7 Bivariate plot of MgO : TiO_2 (all rocks).

Fig.12.8 Bivariate plot of TiO2 : SiO_2.

Fig.12.9 Bivariate plot of Sr : TiO2.

Fig.12.10 Bivariate plot of Ba : SiO_2 (all rocks).

Fig.12.11 Bivariate plot of Cr : SiO_2 (all rocks).

Fig.12.12 Bivariate plot of Li : SiO_2 (all rocks).

Fig.12.13 Bivariate plot of Rb : SiO_2 (all rocks).

Fig.12.14 Bivariate plot of Sc : SiO_2 (all rocks).

Fig.12.15 Bivariate plot of Sr : SiO_2 (all rocks).

Fig.12.16 Bivariate plot of V : SiO_2 (all rocks).

Fig.12.17 Bivariate plot of Y : SiO_2 (all rocks).

Fig.12.18 Total REE patterns for all Strontian rocks.

Fig.12.19 Bivariate plot of La : P_2O_5.

Fig.12.20 Bivariate plot of La : TiO_2.

Fig.12.21 Bivariate plot of Light REE : MgO.

Fig.12.22 Bivariate plot of Heavy REE : MgO.

Fig.12.23 ENd vs 87Sr/86Sr initial ratios for Strontian host rocks and enclaves.

Fig.12.24 Rb/Sr isochron for all reported Strontian data.

LIST OF PLATES IN THE TEXT

Chapter 1

Plate 1.1 View of the structures within the Moine schist towards Loch Tearnait (G.Ref. 7100-4730)

Chapter 2

Plate 2.1 The western margin of the complex following the A884 towards Lochaline, at Beinn Chlaonleud - Fig.1.2 - the change in the colour of the vegetation on the distant hillside denotes the contact (G.Ref. 7462-5343).

Plate 2.1A The northern shore of Loch Sunart showing rounded outcrops of the porphyritic granodiorite close to Location A - Fig.1.2 (G.Ref. 8010-6094).

Plate 2.1B View on the contact of the complex and the Moine - denoted by the break in slope, NNE of Achagavel (G.Ref. 7675-5695).

Plate 2.2 shows the contact between the tonalitic granodiorite and Moine found west of Liddesdale, shows coarse tonalitic granodiorite - albeit finer grained than the bulk (G.Ref. 7746-5998).

Plate 2.2A View of the schlieren in the tonalitic granodiorite (G.Ref. 7458-5080). Hammer shaft 550mm.

Plate 2.3 The curved layering close to Locality A on the N. shore of Loch Sunart, in the porphyritic granodiorite (G.Ref. 8008-6100). Hammer shaft 550mm.

Plate 2.4 Closer detail of the layering showing the concentration of mafics in the layers (G.Ref. 8008-6100).

Plate 2.5 Closer detail of the hornblende - rich lenses found in the layering (G.Ref. 8008-6100). Lens cap 50mm.

Plate 2.6A View eastwards onto Loch Linnhe and Lismore (middle ground) from Glen Sanda (G.Ref. 8118-4800).

Plate 2.6B A view more south-eastwards than 2.6A onto Glensanda, Loch Linnhe and Lismore. Outcrops are very limited (G.Ref. 7800-4911).

Plate 2.7 View SW from the same place as 2.6B onto Loch Tearnait (in the back ground). The Isle of Mull is in the far distance.

Plate 2.8 Looking from Meall a' Chaorainn towards Kingairloch (G.Ref. 7990-5310).

Plate 2.9A The contact between the porphyritic granodiorite and the later granitic sheet (ctG). Lens cap 50mm. (G.Ref. 7716:5702).

Plate 2.9B Closer detail of a later granitic sheet showing large feldspar phenocrysts on the N. shore of Loch Sunart, note rounded inclusion - rich core in central megacryst. Hammer head 170mm. (G.Ref. 8195-6088).

Plate 2.10 A later granitic sheet cutting across a xenolith in the porphyritic granodiorite. (G.Ref.8199-6086).

Plate 2.11A The relationship of the microdiorite, granitic sheet and porphyritic granodiorite found at Locality A Fig.1.2. (G.Ref. 8006-6107).

Plate 2.11B Detail of the microdiorite veinlets that pass into the porphyritic granodiorite, as seen on Fig.2.2.

Plate 2.12 A later granitic sheet present outside the complex in the Moine. Refer to Fig.2.3. (G.Ref. 7405-5036).

Chapter 5

Plate 5.1 Xenoliths present in the granodiorite porphyry sheet (ctG) located at D, Fig.1.2. (G.Ref.7620-5465).

Plate 5.2A View of the lamprophyre dyke found at Locality E, Fig.1.2 (G.Ref. 8394-6097). Hammer shaft 550mm.

Plate 5.2B View of the lamprophyre dyke showing the texture and mineralogy which is still contains primary pyroxenes. Sample XG92.

Plate 5.3A Plane view of a cluster of xenoliths close to the A884 (G.Ref. 7725-5740).

Plate 5.3B Wider view of the same cluster. Hammer shaft 550mm.

Plate 5.4A Narrow cluster of xenoliths found on the northern shore of Loch Sunart (G.Ref. 8010-6095).

Plate 5.4B Closer detail of cluster showing the xenoliths moulding over each other(G.Ref. 8010-6095).

Plate 5.5 Close - up detail of another cluster showing more rounded xenoliths, with Types 1A, 1B, 2 and 4, on the S. shore of Loch Sunart (G.Ref. 8123-6017).

Plate 5.6A Two xenoliths of different appearance - Types 1B (left) and 2 (right).

Plate 5.6B A cluster of elongate sub-angular xenoliths on the washed southern shore of Loch Sunart (G.Ref.8140-6170). Hammer shaft 550mm.

Plate 5.6C A smaller group of sub-angular to rounded xenoliths, just west of Rubha-na-Sroine. (G.Ref. 7880-5973).

Plate 5.6D Samples XG64A, XG64B, XG65 and host SGVIII from the ctG sheet at Locality D (Fig.1.2). (G.Ref. 7620-6465).

Plate 5.7 More outstanding xenoliths on the S. shore of Loch Sunart. (G.Ref. 7805-5980).

Plate 5.8 Xenolith showing a very diffuse contact with the surrounding granodiorite. (G.Ref. 8092-6017).

Plate 5.9 Two xenoliths with an irregular crenulate margins, found close to the Rubha-na-Sroine diorite. Samples XD1/1A are collected from the right xenolith (G.Ref. 7933-6011).

Plate 5.10 An example of a xenolith within a xenolith, a round Type 1A centre surrounded by a tear-drop shaped Type 4 (G.Ref. 7932-6009).

Chapter 6

Plate 6.1 View of Type 1A in PPL showing the general equigranular texture - Sample XG32. Field of view 3mm.

Plate 6.2 View of Type 1B in PPL with a hornblende phenocryst in an equigranular groundmass - Sample XG45. Field of view 3mm.

Plate 6.3A View of Type 1B xenolith in PPL showing a pyroxene core to the amphibole - Sample XG7. Field of view 3mm.

Plate 6.3B As in 6.3A but in XPL showing the clinopyroxene core with higher birefringence than the surroundings - Sample XG7.

Plate 6.4 View of Type 2 xenolith in PPL displaying a coarser grained rock with a mafic aggregate on the left and a poikilitic sphene on the right - Sample XG28. Field of view 3mm.

Plate 6.5A View of Type 2 xenolith in PPL showing the abundant hornblendes as individual crystals or as aggregates (bottom right corner) - Sample XG61A. Field of view 3mm.

Plate 6.5B View of Type 2 xenolith in PPL showing a large euhedral hornblende - Sample XG48. Field of view 3mm.

Plate 6.6 View of Type 2 xenolith in PPL showing the magnetite-rich zone within the hornblende crystal - Sample XG33. Field of view 3mm.

Plate 6.7 View of Type 2 xenolith in XPL showing a subhedral poikilitic sphene in extinction - Sample XG36. Field of view 3mm.

Plate 6.8 View of Type 3 xenolith in PPL showing the hornblende and sphene-rich nature of the xenoliths - Sample XG18. Field of view 3mm.

Plate 6.9 View of Type 4 xenolith in PPL showing a large hornblende and intergrowth of hornblende and biotite in the right hand side - Sample XG88. Field of view 3mm.

Plate 6.10 View of Type 4 xenolith in PPL showing a feldspar phenocryst with numerous inclusions of hornblende and biotite surrounded by an altered zone within the crystal - Sample XG27. Field of view 3mm.

Plate 6.11A View of Type 5 xenolith in PPL showing the highly biotite-rich nature with 2 feldspar phenocrysts in opposite corners showing inclusions in the core and alteration in specific zones - Sample XG30. Field of view 3mm.

Plate 6.11B View of Type 5 xenolith in PPL showing a biotite phenocryst in a biotite-rich matrix - Sample XG5. Field of view 3mm.

Chapter 9

Plate 9.1 View of the heterogenous granitic sheet within the Rubha-na-Sroine diorite, showing the coarse interior and finer grained mafic margin - Samples GS3 and GS3A (G.Ref. 7935-6017).

Plate 9.2 View of the D29 diorite found east of Beach, showing the diffuse margins with the granodiorite (G.Ref. 7792-5311). Hammer head 170mm.

Plate 9.3 View onto the Uileann diorite (Fig.9.1E), looking northwards. The mafic diorite at A (G.Ref. 7865-5030)

Chapter 10

Plate 10.1A View of biotite in PPL (Ranachan) pseudomorphing a euhedral hornblende - Sample D35. Field of view 3mm.

Plate 10.1B View of 10.1A in XPL (Ranachan) - Sample D35.

Plate 10.1C View of biotite in PPL (Ranachan) in 2 orientations pseudomorphing hornblende - Sample D41, Fig.9.1A. Field of view 3mm.

Plate 10.2 View of a large hornblende in PPL (Ranachan) pseudomorphing an earlier cpx (bottom left corner) - sample D33, Fig.9.1A. Field of view 3mm.

Plate 10.3 View of an anhedral sphene in PPL (Ranachan) found within hornblende - Sample D33, Fig.9.1A. Field of view 3mm.

Plate 10.4A View of the general texture of the Rubha-na-Sroine diorite with large poikilitic biotites in PPL - Sample D2, Fig.9.1B. Field of view 3mm.

Plate 10.4B View of the general texture of the Rubha diorite with large biotite crystals with associated sphene exsolution along the cleavage in PPL - Sample D5A, Fig.9.1B. Field of view 3mm.

Plate 10.4C View of a large biotite in PPL showing its poikilitic nature - Sample D1, Fig.9.1B. Field of view 3mm.

Plate 10.5A View of a once brown hornblende jacketed by a pale green hornblende in PPL (Liddesdale) with biotite and opaques in the core - Sample D50, Fig.9.1C. Field of view 3mm.

Plate 10.5B The same view in XPL - Sample D50.

Plate 10.6 View of green prismatic hornblende in PPl (Liddesdale) with numerous apatites in the surrounding matrix - Sample D58, Fig.9.1C. Field of view 3mm.

Plate 10.7A View of euhedral to subhedral opx and green/brown hornblende in PPL (Liddesdale) - Sample D11. Field of view 3mm.

Plate 10.7B The same view as 10.7A, but in XPL showing clearly the interstitial plagioclase - Sample D11.

Plate 10.8A View of larger biotite crystal with cross cutting smaller biotite lathes in PPL (Liddesdale) - Sample D12. Field of view 3mm.

Plate 10.8B View of biotite aggregate pseudomorphing a hornblende crystal in PPL (Liddesdale) - Sample D11. Field of view 3mm.

Plate 10.8C View of a large hornblende crystal being pseudomorphed by biotite in 2 orientations in PPL (Liddesdale) - Sample D11. Field of view 3mm.

Plate 10.9A View of a plagioclase crystal showing inclusions of hornblende and apatite in PPL, also with alteration in the core - Sample D58, Fig.9.1C. Field of view 3mm.

Plate 10.9B The same view as 10.9A, but in XPL showing the twinning and zoning of the plagioclase - Sample D58.

Plate 10.10A View of a hornblende-rich aggregate (top half) and a single hornblende phenocryst in PPL (Sheet) - Sample D45, Fig.9.1D. Field of view 3mm.

Plate 10.10.B The same view as 10.10A but in XPL with the hornblende phenocryst in extinction (except inclusions) - Sample D45. Field of view 3mm.

Plate 10.11 View of a hornblende aggregate surrounded by biotite lathes in PPL (Sheet) - Sample D25. Field of view 3mm.

Plate 10.12 View of a single subhedral hornblende crystal in PPL (Sheet) showing inclusion-rich zone within and biotite around the margins - Sample D25. field of view 3mm.

Plate 10.13 View of the general hornblende texture in PPL (Sheet) - Sample D27. Field of view 3mm.

Plate 10.14A View of a plagioclase phenocryst with a spongy/skeletal texture in PPL (Sheet), full of rounded inclusions of hornblende and biotite - Sample D28. Field of view 3mm.

Plate 10.14B The same view as 10.14A, but in XPL, showing the plagioclase twinning and the optical continuity of the included hornblende - Sample D28.

Plate 10.14C View of a plagioclase phenocryst with a core full of inclusions and a highly altered zone in PPL (Sheet) - Sample D25. Field of view D25.

Plate 10.15A View of the general texture of the Loch Tearnait diorite, showing the alignment of the biotite around a large hornblende in PPL - Sample D80. Field of view 3mm.

Plate 10.15B View of the general texture of Loch Tearnait diorite - Sample D80. Field of view 3mm.

Plate 10.16 View of the fine grained pale green hornblende aggregate surrounded by biotite in PPL (Uileann) - Sample D73, Fig.9.1F. Field of view 3mm.

Plate 10.17 View of a large poikilitic biotite in PPL from the core of Uileann - Sample D57, Fig.9.1E. Field of view 3mm.

Plate 10.18 View of a quartz xenocryst (top left corner) surrounded by biotite and hornblende in PPL - Sample D63, Fig.9.1E. Field of view 3mm.

LIST OF TABLES IN THE TEXT

Chapter 1

Chapter 3

Chapter 4

Chapter 5

Chapter 6

Chapter 7

Table 7.1 Samples and minerals used in IGPET.

Table 7.2 Mixing xenoliths using IGPET.

Table 7.3 Fractional crystallization of xenoliths by IGPET.

Table 7.4 Partition coefficients used in trace element modelling for the xenoliths and diorites.

Chapter 8

Table 8.1 Pressures for the dyke amphiboles.

Table 8.2 Major and trace element geochemistry data with norm data.

Chapter 10

Table 10.1 Modes of the mafic diorites.

Table 10.2 Representative plagioclase analyses for the mafic diorites.

Table 10.3 Representative amphibole analyses for the mafic diorites.

Table 10.4 Pressures for the diorite amphiboles.

Chapter 11

Table 11.1 Samples and minerals used in IGPET.

Table 11.2 Mixing the diorites using IGPET.

Table 11.3 Fractional crystallization of diorites by IGPET.

Chapter 12

Table 12.1 Nd and Sr isotope data for Strontian from various authors.

Chapter 1 INTRODUCTION

1.1 GENERAL GEOLOGY OF THE STRONTIAN GRANITE

The Strontian Granite is a large (12 x 25km.) composite, late Caledonian pluton found on the Morvern peninsula in Argyllshire. It lies on the NW side of the Great Glen Fault, which apparently cuts off its south - eastern margin (Fig. 1). This complex has been mapped and described in detail by Scott (1928), MacGregor and Kennedy (1932), Sabine (1963) and Munro (1965). There is also more recent structural work done by Hutton (1988).

Scott described the Granite as being of two kinds - a pink and a grey. MacGregor and Kennedy (1932) describe it as "a complex mass made up of three major intrusions of different granitic types with, almost everywhere, sharp mutual junctions". The later work however shows that the complex is composed of only two clearly separate plutons. An early , outer body, varying in composition from a tonalitic to a porphyritic granodiorite, is cut by a later pluton of relatively uniform alkali granite (Sabine 1963) BGS sheet 52E (Fig.1.1 Map of complex).

The Strontian granite was also considered as being Lower O.R.S. by the H.M.Geological Survey because:

- It is subsequent to the regional movements and metamorphism of the adjoining Highland schists.
- It has close petrological affinities with the Ben Nevis, Etive and Southern Upland granites (Scott 1928).

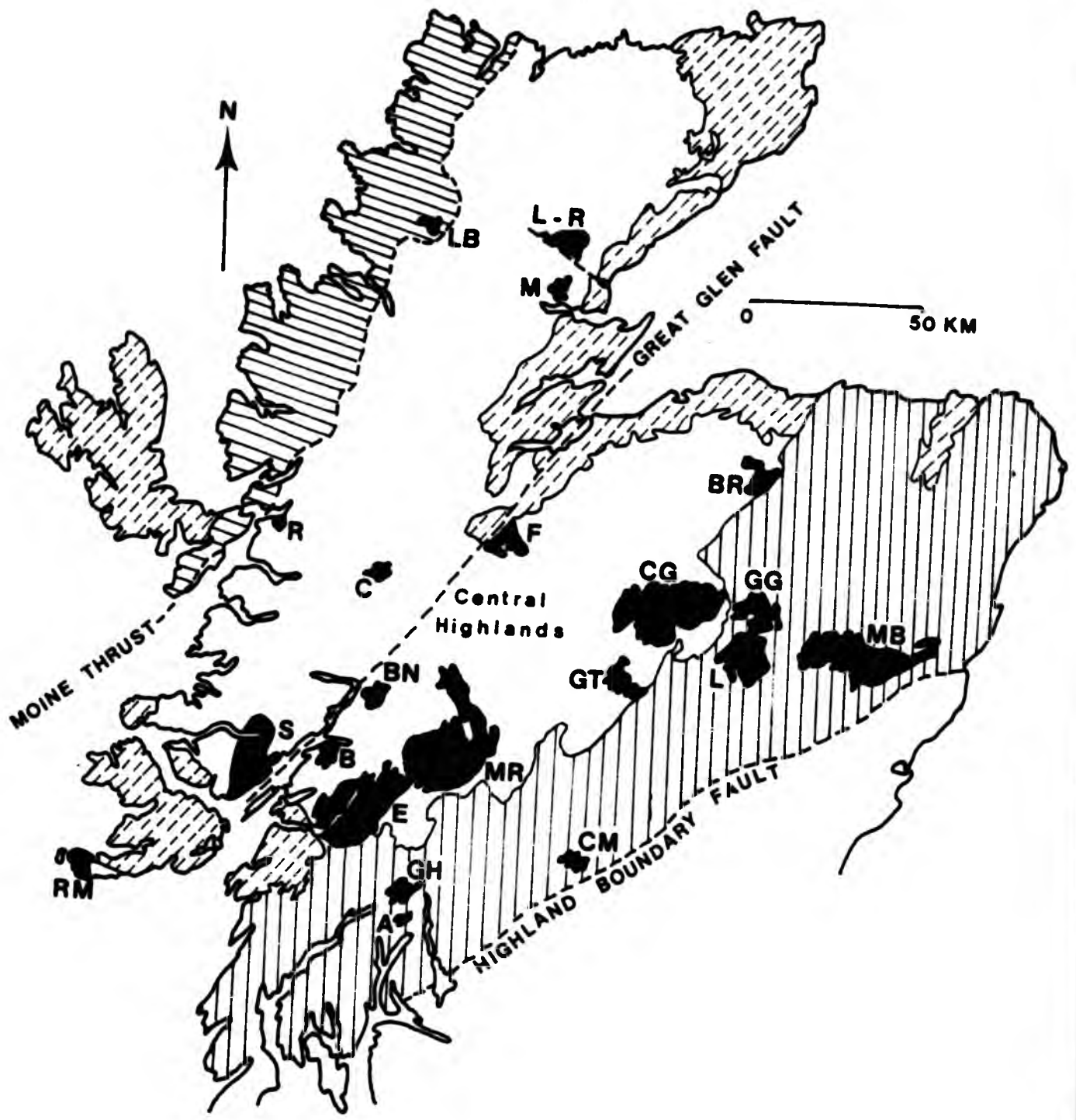

Fig.1. Map of the Scottish Highlands showing outcrops of the principal Geological Groups and some of the late Caledonian intrusive Complexes.

Late Caledonian intrusive Complexes

Old Red Sandstone & younger rocks

Moinian

Dalradian

Lewisian & Torridonian

A – Arrochar B – Ballachulish BN – Ben Nevis BR – Ben Rinnes C – Cluanie
CG – Cairngorm CM – Comrie E – Etive F – Foyers GG – GlenGairn
GH – Garabal Hill GT – Glen Tilt L – Lochnagar LB – Loch Borralan
L-R – Lairg-Rogart M – Migdale MB – Mount Battock MR – Moor of Rannoch
R – Glenelg-Ratagain RM – Ross of Mull S – Strontian

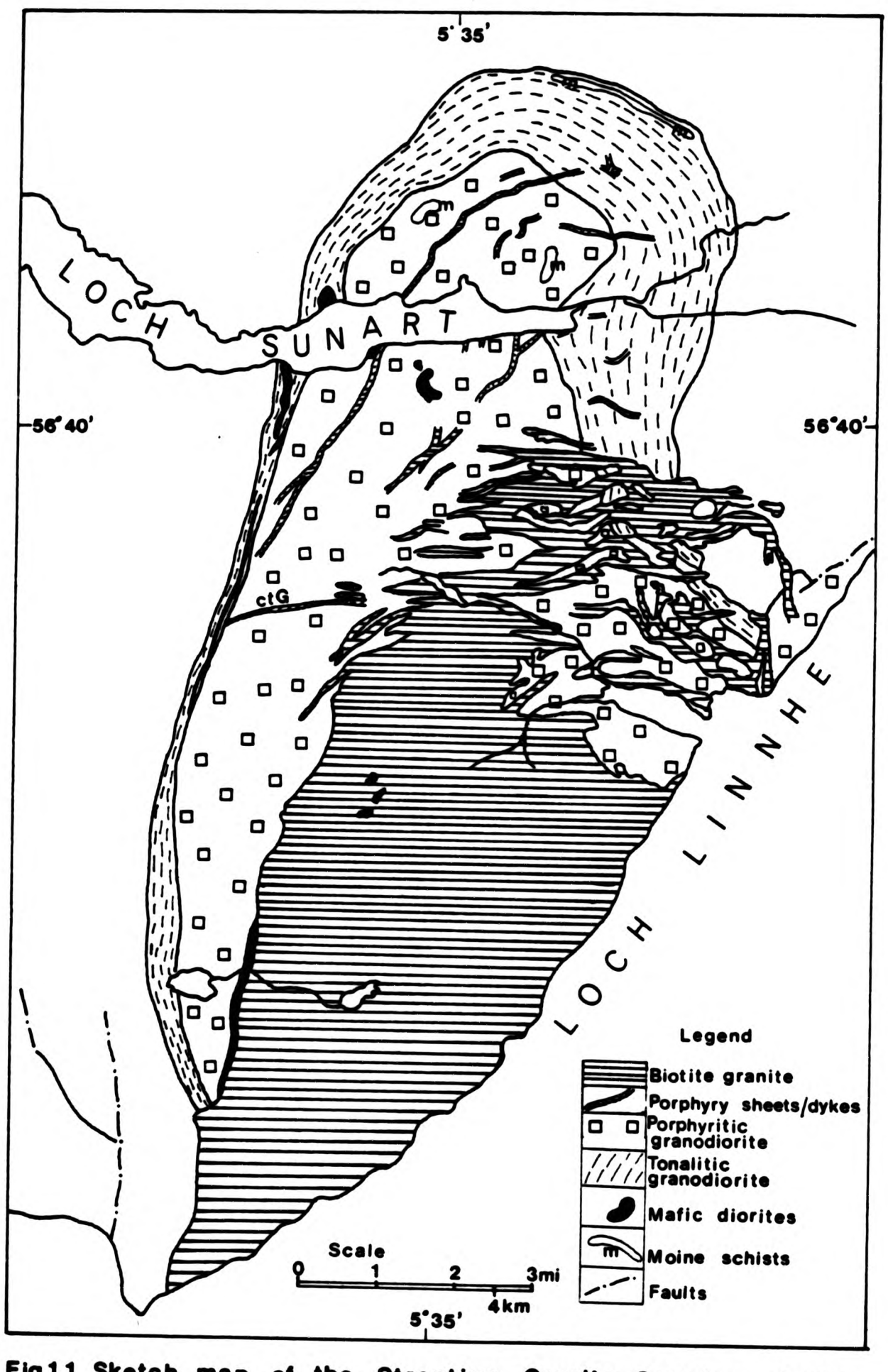

Fig.1.1 Sketch map of the Strontian Granite Complex showing the main geological features. Place and local names are given on Fig.1.2
Taken from P A Sabine 1963

The tonalite of the Strontian complex has been dated by Miller & Brown (1965; K/Ar in biotites), Pidgeon & Aftalion (1978; U/Pb), Brown & Locke (1979; K/Ar), Pankhurst (1979; U/Pb) and by Halliday et al (1979) and Hamilton et al (1980) both using lead isotopes in inherited zircons. An assumed age of emplacement was given by Halliday et al(1979), Brown & Locke (1979) and Hamilton et al (1980) of 435 Ma. More recently Rogers & Dunning (1989 and in press) give dates of 425+/-3 Ma (U/Pb in zircons) and 423+/-3 Ma ($^{206}Pb/^{238}U$ in titanites) for the tonalite. Miller & Brown (1965) give a K/Ar age of 381+/-17 Ma for the biotite granite, which represent a final cooling age not the emplacement age. The biotite granite was emplaced under brittle fracturing conditions and the earlier tonalite and granodiorite were capable of being plastically deformed (Munro 1965). Although clearly the biotite granite is structurally younger, it is not thought that the complex has such a long emplacement history. A gap of 1-2 Ma is sufficient and more believable. It is a part of the Siluro-Devonian suite, described by Brown & Locke (1979), of large volume, mobile magmas intruded under tensional conditions like The Etive and Rannoch Moor.

Nockolds & Mitchell (1946), Joplin (1959), Read (1961), Mercy (1965) and Munro (1965, 1973) all describe Caledonian igneous activity and geochemistry in detail. The Strontian complex is very similar in many aspects to other Caledonian intrusions (Fig.1). It is calc-alkaline in composition and has the tri-partite structure of tonalitic and porphyritic granodiorite and biotite granite/adamellite portions. Fluxion structures are confined to earlier tonalitic and dioritic members. Also the deflection of strike of the country rocks into conformity with the tonalitic granodiorite margin is very common. This shows that the tonalitic granodiorite intrusion belongs

to Read's (1961) group of forcefully emplaced Newer Granites. The later alkali granite does not deform its host rocks and is believed to have been emplaced by stoping. It belongs to Read's (1961) permissively emplaced group of Newer Granites. Hutton (1988) also describes the emplacement of the pluton. Both foliation dip of the complex and strain determinations of the xenoliths present in the granodiorites, suggest a more complicated emplacement history than a diapir/balloon (Hall 1987). It is thought that the pluton was intruded as a synformal shape into an already pre-existing country rock fold (as it is seen to truncate some large stratigraphic units in the area) (Hutton 1988).

Dioritic xenoliths are known to be particularly common in the early tonalitic granodiorite pluton (Scott 1928, MacGregor & Kennedy 1932; Sabine 1963), while Moine country rock xenoliths are rare. Diorite xenoliths have also been found in the later alkali granite, but there they are rare. Some seven large (greater than 100 metres) mafic diorite bodies occur within the granodioritic pluton and three occur within the late alkali granite pluton (BGS sheet 52E). The xenolith distribution has been determined and the large bodies have been mapped in detail in this study (chapter 9).

Diorite plugs, of sufficient diameter to produce xenoliths of the size of the observed mafic bodies, are not seen in the surrounding country rocks (BGS sheet 52). Thin microdiorite sheets do occur in the country rocks, but they form much less than 1% of the surrounding area. Derivation of both the large and small diorite masses as xenoliths from the country rocks without the formation and/or preservation of vast numbers of Moine xenoliths in the granite would appear to require very special conditions. The close spatial

relationships between any source for the large bodies and the present limits of the complex, suggest that a genetic rather than accidental relationship exists between the diorites and granite host. This relationship between granitic and dioritic rock types is reinforced by the occurrence of a few large diorite bodies within the later alkali granite pluton at sites where the nearest contact is with relatively sparsely xenolithic early granodiorite (Fig.1.2) not Moine metasediment.

1.2 MODERN HYPOTHESES ON XENOLITHS

Diorite xenoliths or enclaves are common in worldwide calc-alkaline plutons (Didier 1973). Four hypotheses have been put forward in the literature to explain the associated assemblages of acid and intermediate rocks in calc-alkaline provinces: the melt/restite, the magma mixing, the earlier, more mafic material (accidental xenoliths) and fractional crystallization hypotheses.

1. The concept of the restite model is that "..the products of partial melting (both melt and restite) can move upwards to form granitoid plutons or volcanic rocks.." (White & Chappell 1977), with the restite, the unmelted solid residue, being represented by the diorite xenoliths. Vernon (1983) in general argues that such xenoliths cannot be of restite origin, as microstructural evidence such as mafic aggregates (present in Strontian) and corroded plagioclase cores, is meagre or even absent, so processes such as magma mixing need to be considered.

2. Magma mixing and the textures resulting from the co-existence of two different magmas, was first recognized in basaltic provinces and

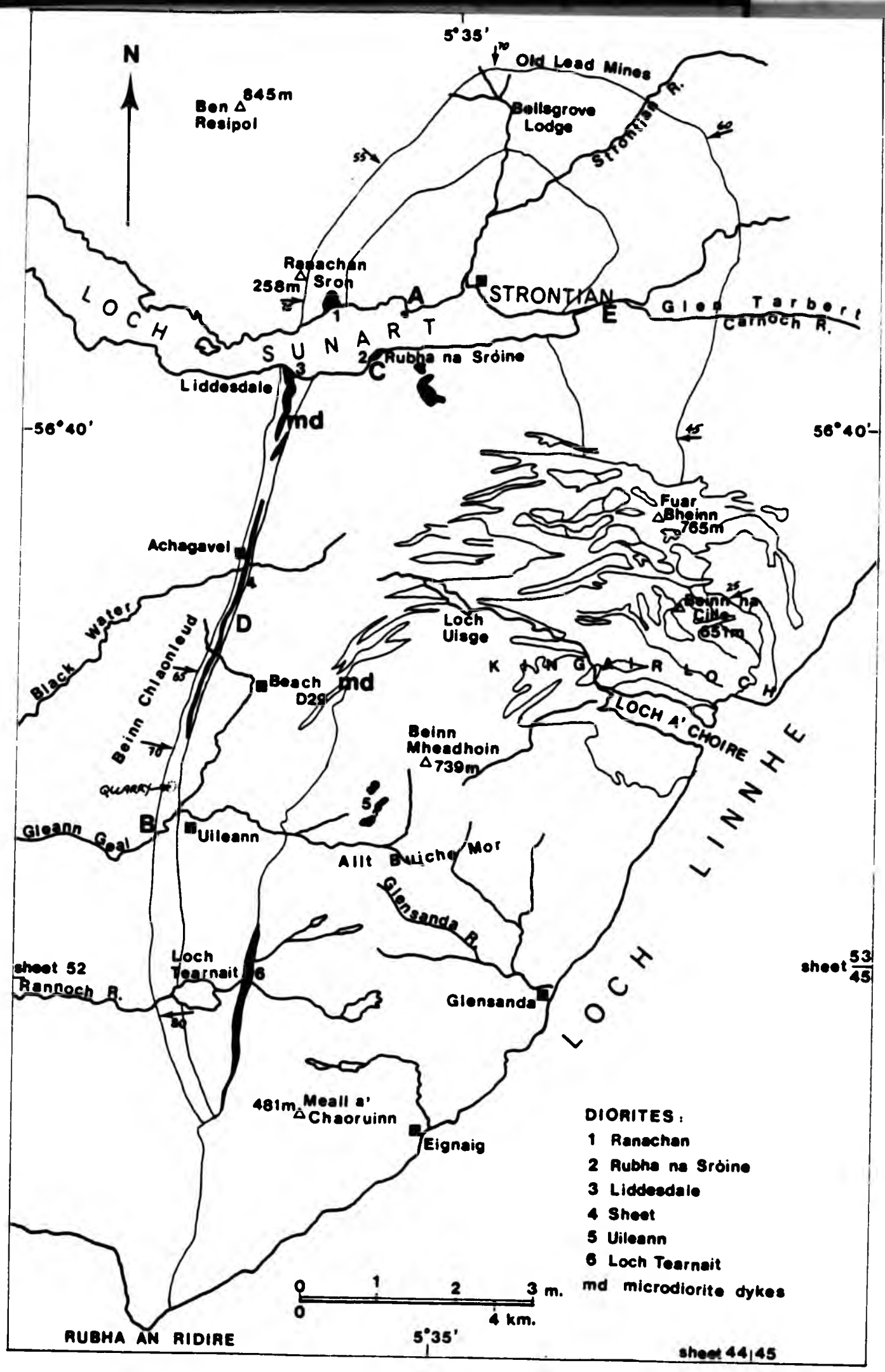

Fig. 1·2 Map of locations visited and mentioned in the text.
Observed dips of outer margin of complex are shown.
A - Microdiorite sheet relationships (section 2·3)
B - Moine sheet (section 2·3)
C - Samples GS3 / GS3A (section 9·2·1)
D - Xenolithic ctG sheet (section 5·4)
E - Lamprophyre dyke (section 5·1)

a detailed account is given of examples from the North Atlantic Tertiary Volcanic Region by Walker & Skelhorn (1966). Evidence of mixing of co-existing acid and intermediate magmas in calc-alkaline volcanic suites is becoming increasingly recognized eg. California & Alaska, Anderson (1970); California, Eichelberger (1974;1975); Labrador, Canada, Wiebe (1980). Glassy volcanic rocks show complex xenocryst assemblages in a uniform glass which require the efficient blending of magmas prior to eruption (Eichelberger 1974). The mixing of porphyritic basaltic and rhyolitic magmas can result in the hybrid rocks possessing two plagioclase phenocrysts (calcic and sodic), quartz xenocrysts and Mg-olivines. This phenomenon will be discussed more fully later in more relevant chapters. Heterogenous glass or fine grained rocks with inclusions of basic and intermediate material floating in more acidic matrices, show signs of incomplete mixing between magmas subsequently quenched and preserved by eruption onto the surface. These processes are all considered to have occurred within the magma chamber before eruption at the surface. Sparks et al (1977) propose that "..the injection of basic magma into acid magma causes superheating of the acid magma and vigorous convection which may eventually trigger an explosive eruption..". If the products of mixing are not erupted at the surface, but crystallize at depth, some record of the process ought to be preserved. Eichelberger (1978,1980) and Sparks et al (1977) suggest that the common dioritic inclusions in calc-alkaline plutons are the holocrystalline equivalents of the glassy porphyrytic andesite inclusions in heterogenous lavas and tuffs. Eichelberger (1980) states that observations indicate that the inclusions represent mafic magma injected into and chilled within cooler, more silicic magma reservoirs.

3. Accidental xenoliths are fragments of foreign rock which have no common origin with the igneous rock that contains it eg. the Moinian xenoliths found in Strontian.

4. Xenoliths derived from earlier rocks and related by fractional crystallization to the present host are called cognate xenoliths. The crystallization process would progress with particular minerals coalescing. Very few xenoliths appear to be the result of any form of mineral accumulation.

The Strontian Complex with its abundant intermediate xenoliths, provides an opportunity to study the relationship between acid and intermediate magmas in a plutonic environment and assess the mixing, accidental xenoliths and restite hypotheses.

1.3 XENOLITH TERMINOLOGY

Though the term "xenolith" was not then used "spheroidal arrangements or pseudofragmentary concretions" have been observed and described by authors such as Dr. John Macculloch (1821), Johann Jokely (1855) and J.A.Phillips (1879).

Dark objects in granitic rocks have long been termed "xenoliths", a term meaning "pieces of foreign material enclosed in igneous rocks" (Sollas 1894 quoted by Didier 1973). The term xenolith is currently defined by the Penguin Dictionary of Geology (Whitten & Brooks 1972) as an inclusion surrounded by an igneous rock, following clearly Sollas' original definition.

Other terms are often used in the literature to describe dark inclusions in granite, similar in composition but more mafic than the enclosing rock, for example: "enclave", "autolith", "cognate xenolith", "microgranitoid enclaves", which suggest great difficulty in naming them consistently (Didier 1973). Also terms as homeogenic, consanguineous or mafic inclusions are used (Lacroix 1893, Grout 1937, Loewinson-Lessing 1940 & Goodspeed 1948; from Fershtater & Borodina 1977). The French term "enclave", derived from Lacroix's system (Didier 1973), means a piece of foreign material contained within an eruptive rock, affectively a translation of the English xenolith, but the other terms have more complex genetic implications.

The qualified "enclave homoeogene" (Lacroix 1893) being a piece of igneous rock contained in another igneous rock and linked to it in composition and origin, also called "cognate inclusion" in the Dictionary of Geological Terms (American Geological Institute 1962). This latter term after careful study may be more acceptable than "xenolith", which is used at present. "Inclusions" (Grout 1937) is best reserved for inclusions of mineral grains in other mineral grains. "Autolith" (Pabst 1928) recognizes the close relationship to the enclosing granitoid. It implies material generated entirely from the granitoid itself and from within the granitoid magma, which is not necessarily always the case (Vernon 1983). Vernon & Flood (1982) used the term "microgranitoid xenolith" to emphasize more the granitoid microstructure and the close compositional relationship, which was recognized by Phillips (1880).

The simple term xenolith will be used for the small dioritic objects throughout the descriptive sections, but this use will be reviewed in the conclusions.

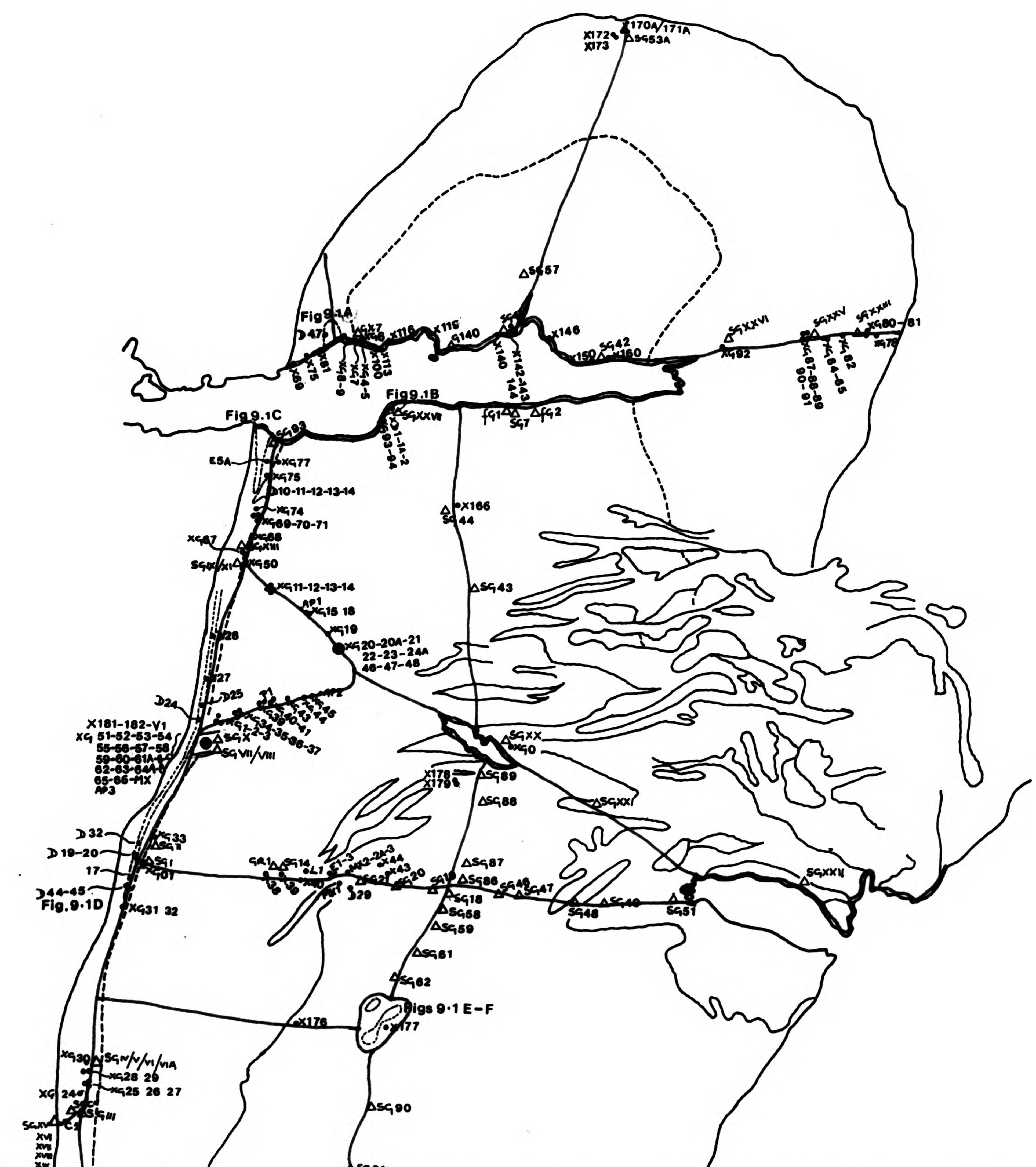
X170A/171A
X172
X173
ΔSG53A
ΔSG57
Fig 9.1A
D 47
X116
X115
X140
X146
SG42
X160
X150
SGXXVI
SGXXV
XG92
XG80–81
XG82
XG84–85
XG87–88–89
90–91
X113
X100
XG4–5
XG7
XG8–9
X81
X75
X69
X142–143
144
Fig 9.1B
SGXXVII
Fig 9.1C
SG93
D 1–1A–2
XG93–94
ΔSG2
SG7
E5A
XG77
XG75
D10–11–12–13–14
XG74
XG69–70–71
XG68
SGXIII
XG67
XG50
XG11–12–13–14
AP1
XG15 18
XG19
XG20–20A–21
22–23–24A
46–47–48
X166
SG44
ΔSG43
D28
D27
D24
D25
X181–182–V1
XG 51–52–53–54
55–56–57–58
59–60–61A
62–63–64A
65–66–MX
AP3
SG VII/VIII
SGXX
XG90
X178
X179
ΔSG89
ΔSG88
SGXXI
SGXXII
D 32
D 19–20
17
D44–45
Fig. 9·1D
XG31 32
XG33
XG101
SG29
ΔSG87
ΔSG86
ΔSG47
SG18
ΔSG58
ΔSG59
SG48
ΔSG40
SG51
ΔSG61
ΔSG62
Figs 9·1 E–F
X177
X176
ΔSG90
ΔSG91
XG30
SGIV/V/VI/VIA
XG28 29
XG25 26 27
XG 24
SGIII

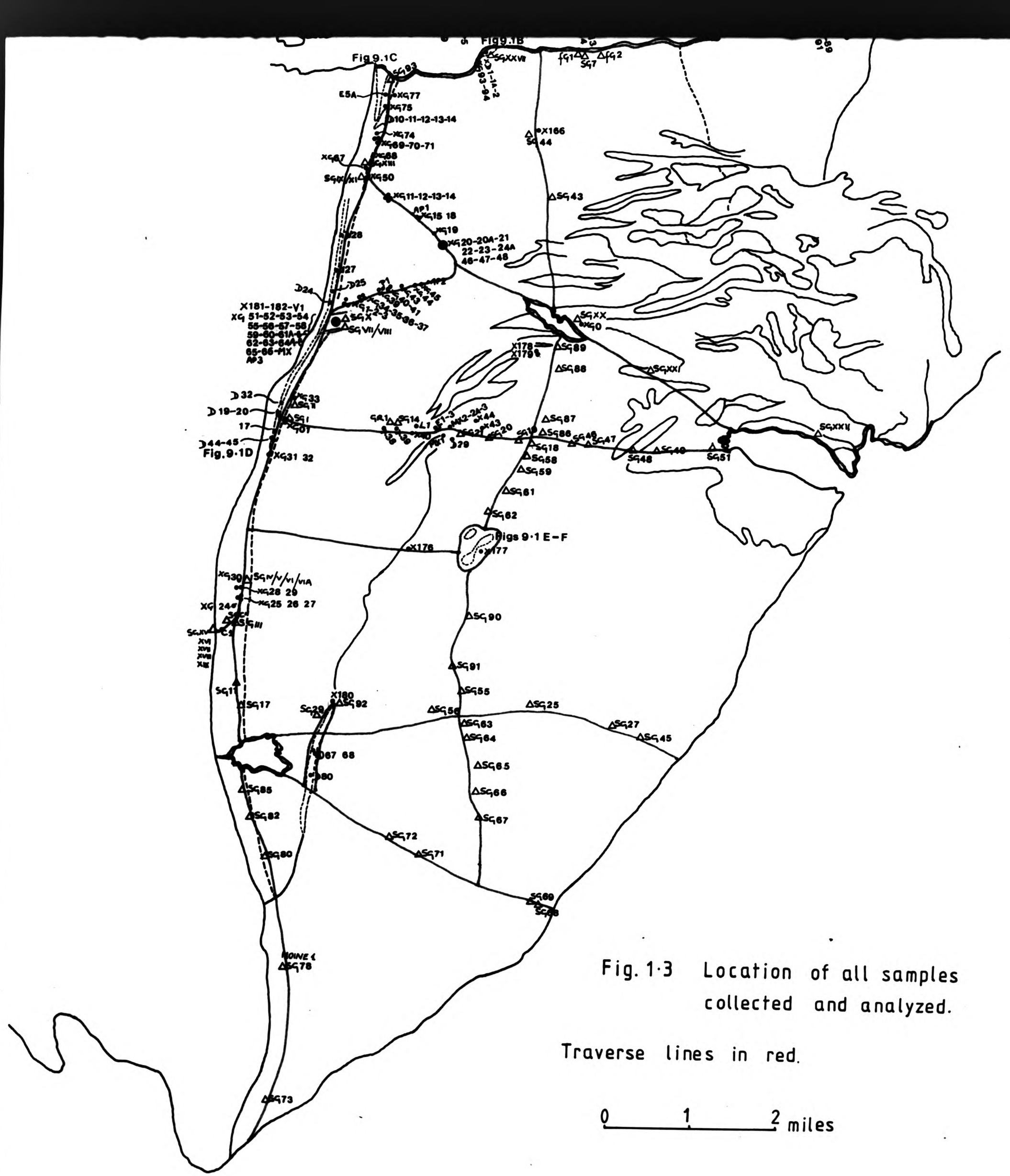

Fig. 1·3 Location of all samples collected and analyzed.

Traverse lines in red.

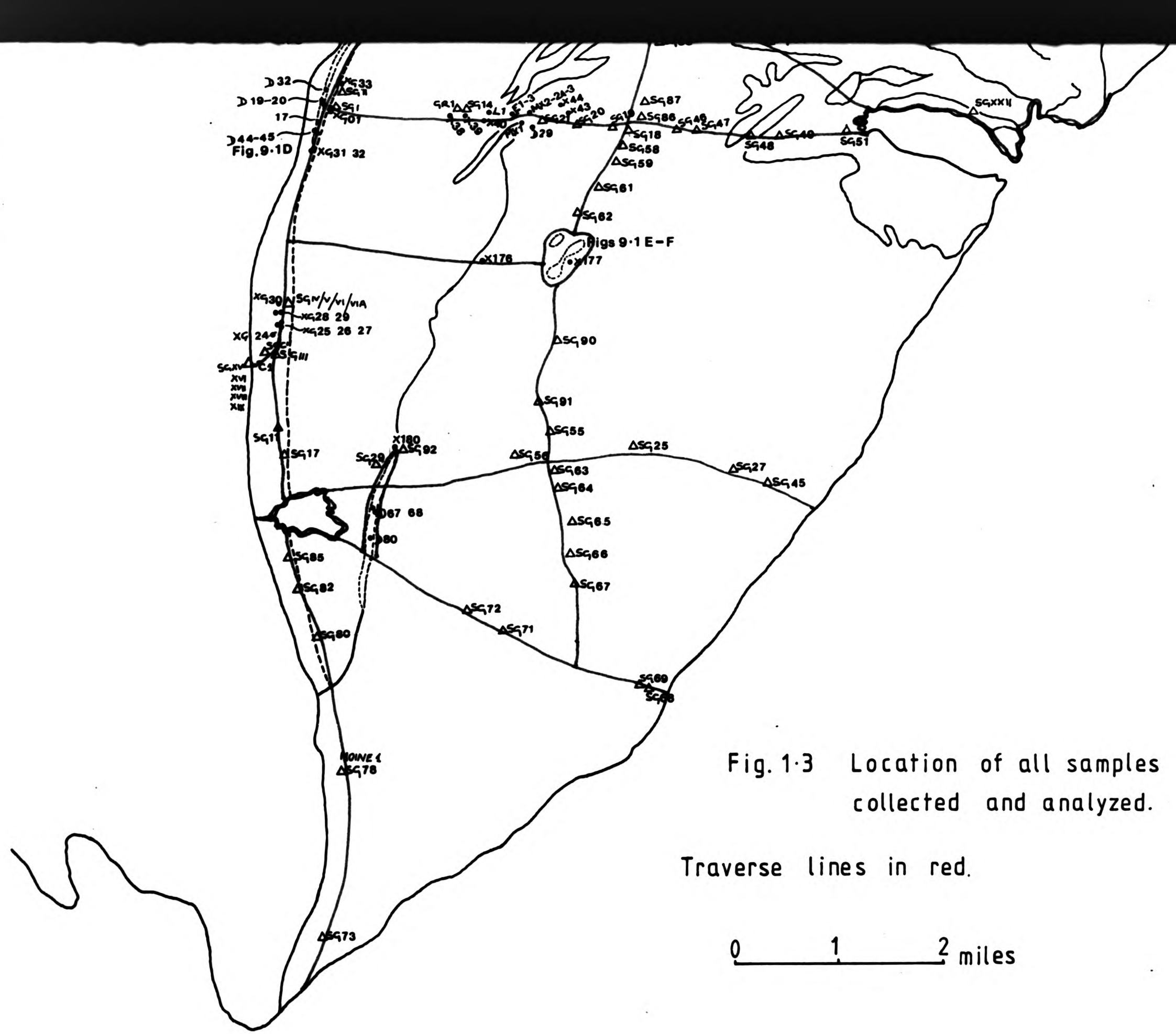

Fig. 1·3 Location of all samples collected and analyzed.

Traverse lines in red.

1.4 METHOD OF SAMPLING - FIELD TECHNIQUES

Good maps of the complex already exist along with general structural and petrographical descriptions (BGS sheets 52E and 44, Sabine 1963, Munro 1965 and Hutton 1988). These authors have described the general features of the xenoliths. To build on this base, detailed chemical and mineralogical work is needed, coupled with rigorous local field control. The sampling needed to be systematic and to cover the whole of the pluton. The plan was to sample the complex using a grid of traverses through the best exposed areas, but also covering the spectrum of rock types (Fig.1.1). There are 2 north-south lines and 5 east-west lines along which the host pluton, as well as the xenoliths, were mapped and sampled (Fig.1.3).

Outcrop mapping and sampling were carried out for 50m. either side of the traverse lines and will be quantified in chapter 5 and Fig.5.1A. Geochemical sampling was not uniform along the traverses, as more detailed work was done where the xenoliths were present; the closest spacing of sampling was every 0.5-1.0 metres in some xenolithic areas, while homogeneous areas of granite were only sampled every 50m. The general features of the host granite found along the traverses are consistent with the work done by Munro (1965) and Sabine (1963) and MacGregor & Kennedy (1932), which essentially substantiates the original decision to accept their mapping. It has been accepted that the late biotite granite has an intrusive and structurally later relationship with the rest of the complex and will be discussed in later chapters.

1.5 LABORATORY TECHNIQUES AND GEOCHEMISTRY

The major, trace and rare earth element (REE) geochemistry of the Strontian Complex has been determined. The major elements SiO_2, Al_2O_3, TiO_2, *FeO, MgO, MnO, CaO, Na_2O, K_2O were analyzed in a lithium metaborate fusion solution using a Pye Unicam SP1900 Atomic Absorption Spectrophotometer. P_2O_5 was analyzed in the same solution using a colorimetric technique. The trace elements Ba, Cr, Cu, Li, Ni, Rb, Sc, Sr, V and Zn were analyzed after an open acid digestion using a Philips PV8210 Inductively Coupled Plasma Atomic Emission Spectrometer (ICPAES). Rb was determined by AA using the lithium metaborate solution. Zr was not analyzed. The REE were analyzed by ICPAES following pre-concentration by a cation exchange procedure (Walsh et al 1981).

Details of analytical procedures are given in Appendix D. The geochemistry has been plotted on a range of variation diagrams in order to display and help in the interpretation. They have been plotted initially using SiO_2 as abscissa since the rock types discussed exhibit a wide range of SiO_2 values. However where necessary the abscissa has been changed to MgO.

294 samples were analyzed and the distribution of sample composition/lithology is as follows:

Granodiorite and biotite granite.....84

Xenoliths (All Types).....133

Mafic diorites (all classes).....64

Dykes and veins.....13

and their distribution is shown on Map 1.3.

The method of sampling is as described in section 1.3. Specimens chosen for analysis were selected on the basis of their petrography and geographical position to cover the chemical variation of each series from: basic types at 48% SiO_2 to acidic at 73%; very high silica types (78% SiO_2) represent pegmatites and aplites.

The geochemical data for all the analyzed samples are given in Appendix B. Each main rock group ie. host, xenolith and diorite, will have their geochemistry very generally described in their respective chapters, but representative analyses are given in Table 1.1.

Table 1.1 REPRESENTATIVE ANALYSES OF THE THREE MAIN GROUPS

	1	2	3	4	5	6	7
SiO_2	49.00	56.00	53.00	59.00	64.00	66.00	72.00
Al_2O_3	10.00	17.70	14.20	15.00	14.00	14.50	15.00
TiO_2	0.90	1.45	1.08	0.95	0.62	0.65	0.20
FeO*	8.70	6.80	7.80	5.20	4.05	3.05	1.00
MnO	0.14	0.09	0.12	0.07	0.05	0.03	0.01
MgO	13.51	4.10	6.75	4.30	3.90	2.15	0.60
CaO	9.65	4.60	6.85	6.55	5.70	3.50	0.85
Na_2O	2.19	5.25	4.34	4.20	4.03	4.54	4.70
K_2O	2.43	2.30	1.70	2.08	2.63	3.30	3.73
P_2O_5	0.53	0.43	0.25	0.32	0.07	0.70	0.06
H_2O+	1.92	1.36	2.82	1.70	1.22	0.84	0.76
CO_2	0.09	0.03	0.11	0.08	0.05	0.14	0.08
Total	99.06	100.10	99.00	99.45	100.15	99.10	99.00

Analyses 1 and 2 are samples of the mafic diorites
Analyses 3, 4 and 5 are samples of xenoliths
Analyses 6 and 7 are samples of the host rocks

1.5.1 Rare Earth Elements

The lanthanides or rare earth elements (REE) consist of a coherent geochemical group from La to Lu, which exhibit closely similar chemical properties. REE are dominantly tri-valent in igneous rocks

and show a progressive decrease in ionic radii from 1.03 A for La to 0.86 A for Lu (Shannon 1976). They can be divided into 2 main subgroups a) light REE (LREE) La-Gd and b) heavy REE (HREE) Dy-Lu.

Overall the REE behave similarly, but the LREE can be fractionated from the HREE particularly by such minor mineral phases as apatite, sphene, zircon, garnet and especially allanite and monazite. In Strontian these latter two minerals are not found. Europium commonly occurs in the 2+ and 3+ state, with ratio depending on oxygen fugacity in the magma at the time of crystallization (Drake 1975). In the divalent form Eu can substitute for Ca^{2+} in plagioclase feldspar. Therefore Eu can be fractionated relative to the other REE during plagioclase crystallization.

Twelve of the fourteen naturally occurring REE (not Tb and Tm) have been analyzed in a selected number of samples using the ICPAES following a preconcentration of solution by a cation exchange procedure (Walsh et al 1981, Appendix D). The REE data is given in Appendix B, Table B.5.

The REE have been normalized to average chondrite (Nakamura 1974) and are plotted against the elements in order of increasing atomic number. Yttrium, though not strictly a member of the Lanthanide group, displays similar behaviour to the HREE (Mason 1966) and so has been included here.

1.6 MICROPROBE ANALYSES

Mineral chemistry provides additional data that can be used in later petrogenetic modelling and can relate petrography with the overall

bulk rock chemistry. The chemistry of the major mineral phases was determined by a wavelength dispersive electron microprobe and all details of analysis are given in Appendix D.

Table 1.2 TO SHOW THE NUMBER OF ANALYSES DETERMINED FOR EACH ROCK SAMPLE

Sample	Rock Type	Am	Fl	Bi	Py	Ap	Sp	Su	Ox
SGiii	Ton.Gdi	13	12	8	-	2	6	-	2
SGvii	Late	7	17	8	-	3	4	-	-
SGviii	Late	15	18	7	-	-	8	-	2
SGix	Ton.Gdi	7	10	3	-	2	2	-	1
SGx	Late	9	22	11	-	-	7	-	-
SGxiii	Ton.Gdi	16	32	15	-	-	10	-	-
SGxxvi	Ton.Gdi	6	10	4	-	1	2	-	-
SG49	Por.Gdi	6	19	10	-	3	8	-	4
SG78	Biot.Gr	-	15	9	-	-	6	-	1
SG93	Ton.Gdi	17	16	12	-	1	-	-	-
G24	Ton.Gdi	9	10	8	-	1	3	-	1
XG4	Xenolith	9	12	8	-	1	3	-	2
XG7	Xenolith	8	10	7	-	1	-	-	3
XG24	Xenolith	15	17	13	-	-	10	-	-
XG25	Xenolith	8	10	5	-	3	-	-	-
XG32	Xenolith	-	19	11	-	-	7	-	-
XG44	Xenolith	15	15	12	-	4	5	-	3
XG61B	Xenolith	7	9	9	-	-	4	-	-
XG61C	Xenolith	15	20	10	-	-	8	-	-
XG64A	Xenolith	9	14	11	-	-	9	-	-
XG65	Xenolith	5	18	10	-	-	6	-	-
XG89	Xenolith	9	10	10	-	2	-	-	2
X181	Xenolith	16	15	9	-	-	9	-	-
D1	Di(Rubh)	4	1	10	-	3	1	-	-
D2	Di(Rubh)	7	9	7	-	3	-	-	-
D8	Di(Rubh)	12	12	14	-	6	-	14	-
D11	Di(Lidd)	7	11	9	13	6	2	24	-
D12	Di(Lidd)	10	12	6	-	-	-	-	-
D19	Di(Shet)	18	15	12	-	3	5	14	-
D41	Di(Rana)	15	16	13	-	5	6	5	-
D63	Di(Uile)	16	17	9	-	6	7	18	-
E1	Dyke	15	17	14	-	1	3	-	-
E3	Dyke	13	16	9	-	5	7	-	-
E5A	Dyke	17	15	11	-	-	6	-	-
L1	Dyke	-	7	5	-	-	-	-	-

NB. - = phases that were absent, not analyzed or too altered for analysis.

The 36 rocks chosen for mineral analysis cover a representative range of SiO_2 concentrations from 48% to 70%, from granites to xenoliths, diorites and dykes. The major silicate phases analyzed from each main rock type consist of: amphibole, feldspar and biotite, smaller numbers of accessory minerals such as sphene, apatite and sulphides, with very occasional pyroxenes and oxides. In total there were over 1500 analyses determined for 36 rock samples. Table 1.2 shows the number of analyses for each sample and all analyses are given in Appendix C. They will be described according to the rock groups.

1.6.1 Amphibole Classification

A wide range of amphibole compositions is seen from the different rock groups within the Strontian complex. 350 analyses were determined and major element (SiO_2, TiO_2, Al_2O_3, FeO, MnO, MgO, CaO, Na_2O, K_2O) compositions, structural formulae and names are given in Appendix C. Water has been excluded from the analyses as it was theoretically calculated by the electron microprobe software. The microprobe does not allow independent determination of Fe^{3+} in the amphibole, so all is reported as Fe^{2+}. Dodge et al (1968) has concluded that about 25% of the Fe is Fe^{3+} in calc-alkaline plutons.

All the amphiboles have been recalculated to 23 oxygens per formula unit according to the widely adopted classification of Leake (1978), as water plus the halogen content is uncertain. The standard amphibole formula is:

$$A_{0-1}\ B_2\ C_5^{vi}\ T_8^{iv}\ O_{22}(OH,F,Cl)_2$$

The allocation of cations to each site as recommended by Leake (1978), is as follows:

Sum T to 8.00 using Si, Al then Cr^{3+}, Fe^{3+} and Ti^{4+}

Sum C to 5.00 using excess Al, Cr, Ti, Fe^{3+}, Mg and Fe^{2+}

Sum B to 2.00 using excess Fe^{2+}, Mn, Mg, Ca and Na

Sum A 0.00 to 1.00 using excess Na and K

After analysis, the amphibole can then be classified into one of four major amphibole groups as proposed by Leake (1978) on the basis of the number of cations of $(Ca + Na)^B$ and Na^B. The amphiboles from Strontian all fall into the calcic amphibole group as they have $(Ca + Na)^B$ greater than 1.34 and Na^B less than 0.67. Further subdivisions can be made by using the appropriate two dimensional diagram (Table 1.3 Leake 1978). This uses the atomic ratio of $Mg/Mg+Fe^{2+}$, the proportion of silica atoms and (Na+K) in the A site.

These amphiboles fall into the main igneous amphibole field, according to Nockolds and Mitchell's classification (1947), which is divided into either the primary hornblende field or secondary hornblende formed at the expense of pyroxenes and primary hornblende. Textural evidence supports this classification by showing either well formed crystals or monomineralic aggregates of tiny crystals with rare pyroxene cores (sections 3.1, 3.3, 6.2.2, 6.2.4, 6.2.6, 10.2.3, 10.2.4 and 10.3). (Table 1.3, classification of calcic amphiboles from Leake (1978)).

In general the amphiboles range from actinolite/actinolitic hornblende $Ca_2(Mg;Fe^{2+})5Si_8O_{22}(OH,F)_2$ to magnesio-hornblende and hornblende $(Na,K)_{0-1}Ca_2\ (Mg,Fe^{2+},Fe^{3+},Al)_5[Si_{6-7}Al_{2-1}O_{22}](OH,FO_2)$ and

CALCIC AMPHIBOLES: $(Ca + Na)_B \geq 1.34$; $Na_B < 0.67$

A. $(Na + K)_A < 0.50$; $Ti < 0.50$

$\frac{Mg}{(Mg+Fe^{2})}$	8.00 – 7.75	7.50 – 7.25	7.00 – 6.75 (Si)	6.50 – 6.25	6.00 – 5.75
1.00 – 0.90	TREMOLITE	TREMOLITIC HORNBLENDE	MAGNESIO-HORNBLENDE	TSCHERMAKITIC HORNBLENDE	TSCHERMAKITE (ALUMINO-TSCHERMAKITE)
0.90 – 0.50	ACTINOLITE	ACTINOLITIC HORNBLENDE			
0.50 – 0.00	FERRO-ACTINOLITE	FERRO-ACTINOLITIC HORNBLENDE	FERRO-HORNBLENDE	FERRO-TSCHERMAKITIC HORNBLENDE	FERRO-TSCHERMAKITE

B. $(Na + K)_A \geq 0.50$; $Ti < 0.50$; $Fe^{3} \leq Al^{VI}$

$\frac{Mg}{(Mg+Fe^{2})}$	8.00 – 7.75	7.50 – 7.25	7.00 – 6.75 (Si)	6.50 – 6.25	6.00 – 5.75
1.00 – 0.70	SILICIC EDENITE	EDENITE	EDENITIC HORNBLENDE	PARGASITIC HORNBLENDE	PARGASITE
0.70 – 0.50				FERROAN PARGASITIC HORNBLENDE	FERROAN PARGASITE
0.50 – 0.30	SILICIC FERRO-EDENITE	FERRO-EDENITE	FERRO-EDENITIC HORNBLENDE	FERRO-PARGASITIC HORNBLENDE	FERRO-PARGASITE
0.30 – 0.00					

C. $(Na + K)_A \geq 0.50$; $Ti < 0.50$; $Fe^{3} > Al^{VI}$

$\frac{Mg}{(Mg+Fe^{2})}$	8.00 – 7.75	7.50 – 7.25	7.00 – 6.75 (Si)	6.50 – 6.25	6.00 – 5.75
1.00 – 0.70	SILICIC EDENITE	EDENITE	EDENITIC HORNBLENDE	MAGNESIO-HASTINGSITIC HORNBLENDE	MAGNESIO-HASTINGSITE
0.70 – 0.50				MAGNESIAN HASTINGSITIC HORNBLENDE	MAGNESIAN HASTINGSITE
0.50 – 0.30	SILICIC FERRO-EDENITE	FERRO-EDENITE	FERRO-EDENITIC HORNBLENDE	HASTINGSITIC HORNBLENDE	HASTINGSITE
0.30 – 0.00					

D. $Ti \geq 0.50$

$\frac{Mg}{(Mg+Fe^{2})}$	6.50 – 6.25	6.00 – 5.75
1.00 – 0.50	KAERSUTITE	
0.50 – 0.00	FERRO-KAERSUTITE	

ORDINATE SCALES $Mg/(Mg+Fe^{2})$

ABSCISSA SCALE Si: 8.00 7.75 7.50 7.25 7.00 6.75 6.50 6.25 6.00 5.75

Table 1·3 Classification of calcic amphiboles after Leake (1978).

edenite $Na,Ca_2,Mg_5Si_7AlO_{22}(OH)_{22}$. Though in nomenclature, the amphiboles of each main group overlap, this is where the similarity ends. As seen on Fig.3.6, 6.2 & 10.5 of Ca-Mg-Fe, the amphiboles of the mafic diorite group plot separately from the amphiboles of the granite and xenoliths. Therefore each group will be discussed separately.

1.6.2 Feldspar Analysis

A difference has been noted between anorthite values determined optically using the Michel-Levy test (which is a statistical method) and the electron microprobe. The Michel-Levy values are always lower. The problem is the sampling of very coarse rocks, as only a few crystals will be present in each thin section and this optical method relies on the maximum value of extinction:

eg.	SGIII:	optically	An10-11
		microprobe	An33-40

1.6.3 Biotite Analysis

Analyzed micas have been classified according to the scheme of Heinrich et al (1953) on the basis of their Mg:Fe atomic ratio. Samples with a ratio greater than 2:1 are classified as phlogopites, while those with less than 2:1 are biotites. Complete solid solution exists between phlogopite and biotite and so the division at 2:1 for Mg:Fe is purely arbitrary. The micas of Strontian have accordingly been classed as biotites.

1.7 REGIONAL SETTING OF THE STRONTIAN GRANITE

The complex is emplaced in regionally metamorphosed rocks of the Pre Cambrian Moine Series on the western side of the Caledonian metamorphic belt. The stratigraphical succession of the country rock has been described by Johnstone et al (1969), who proposed the division of the Moinian Assemblage into three structural / stratigraphical units: the Morar, Glenfinnan and Loch Eil divisions and the relationships of these constituent groups are indicated by sedimentation structures (Powell 1974). These are found to be applicable over a very large of north-west Argyll and western Inverness-shire, from Glenelg in the north to Ardnamurchan in the south (Fig.1.4). Lithologically the divisions range from the dominantly pelitic Glenfinnan Division to the more psammitic rocks of the Morar and Loch Eil Divisions. However the Morar Division does show interbedding with semi-pelites (Powell 1974; Plate 1.1). The Lewisian hornblendic and acid gneisses are present in the cores of primary isoclinal folds of the Moine cover of the Morar-Knoydart area of W. Inverness-shire reaching Loch Eilt (Powell 1974). In the Strontian area, the Lewisian is not seen.

The Moine schists and gneisses have undergone a polyphase deformation history and Dalziel & Johnson (1963); Dalziel & Brown (1965) and Brown et al (1970) recognize 4 phases (F1-F4) of deformation and metamorphism, which is outlined below:

F1 - Isoclinal folds with a strong axial plane foliation (S1); these folds have only been recognized on a mesoscopic scale;

F2 - Tight, sometimes isoclinal, folds usually

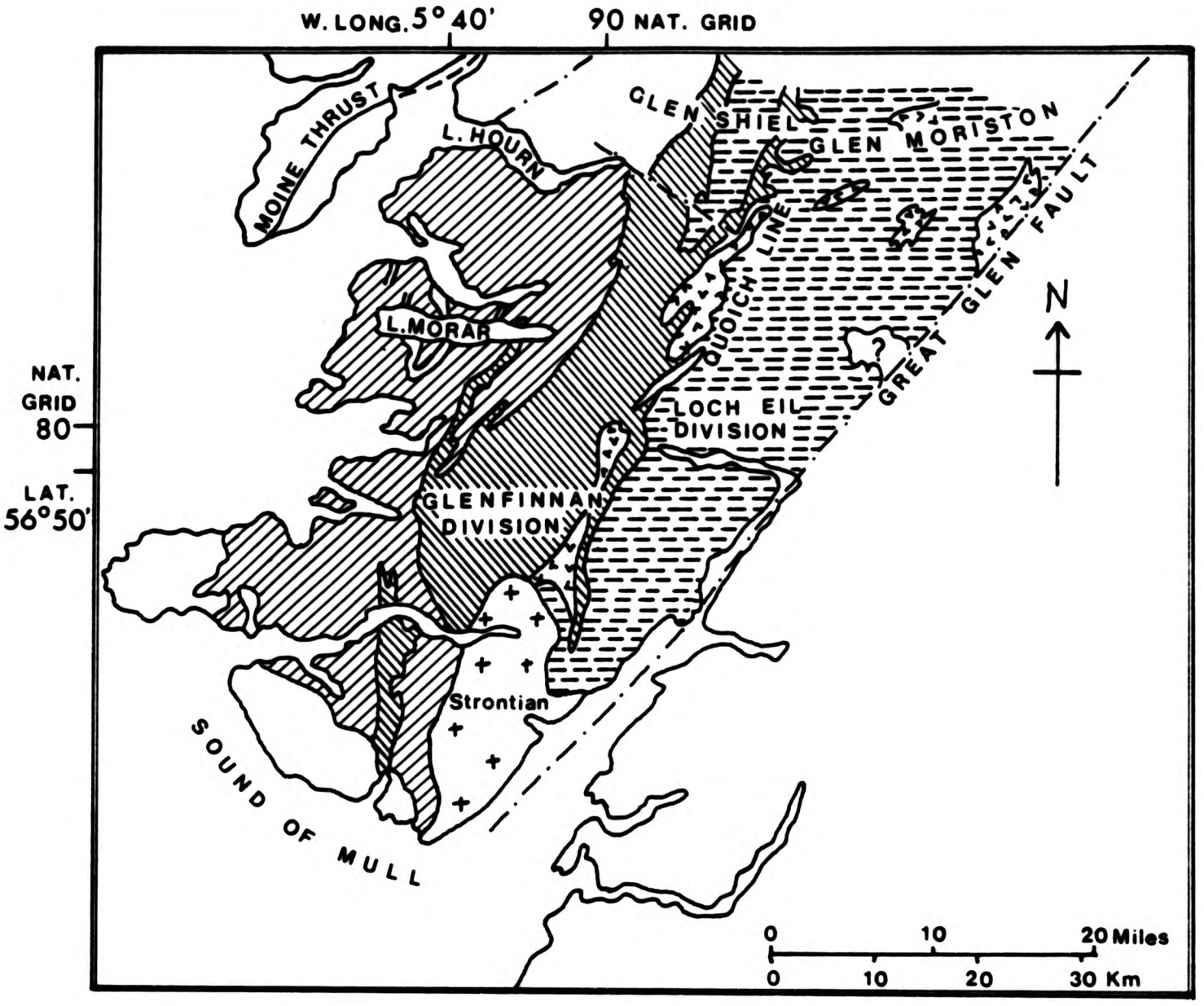

Fig. 1.4 Location of region and distribution of the Morar, Glenfinnan and Loch Eil Divisions of the Moinian, mainly after Johnstone et al. (1969) from Brown, Dalziel & Johnson (1970).

Loch Eil Division
"Flat" belt
Upper psammitic group

Glenfinnan Division

Morar Division

Strontian Complex

Granitic Gneiss

Plate 1.1 View of the structures within the Moine schist towards Loch Tearnait (G.Ref. 7100-4730)

accompanied by a strong axial plane foliation (S2);

F3 - Major and minor folds varying in style from open to moderately tightly compressed; an axial plane foliation (S3) is only developed locally in the cores of the tightest folds. Axial planes of the F3 folds trend in a N-S or NNE-SSW direction;

F4 - Open folds with no axial plane foliation.

Brook et al (1977) considered all available isotopic work and have described the tectono-metamorphic history of the Morar pelite in the Morar area as:

- Grenvillian events (1024+/-96 Ma) comprising first isoclinal folding (D1), low grade metamorphism (M1), then intense penetrative deformation (D2), accompanied by a medium grade metamorphism;
- Caledonian deformation and mild retrogression, occurring between 470-410 Ma, dated by Rb-Sr whole rock data (Brewer et al 1979).

The Strontian area lies 30km south of Morar and is considered to have suffered a similar sequence of events, although the maximum metamorphic temperatures were higher, producing migmatitic rocks (Winchester 1974).

The Moine can be divided into two structurally contrasting parts: a) the "flat"belt; and b) the "highly inclined" belt. The "flat" belt includes the semi-pelitic schists of the Loch Eil Division, while the "highly inclined" belt includes the psammitic Morar and Glenfinnan Divisions. However the structural division does not exactly match the lithological division. The boundary between the two areas is

called the Loch Quoich Line (after Clifford 1957) and it runs parallel to the Great Glen Fault from the Sound of Mull into Ross and Cromarty, trending NNE-SSW (Leedal 1951; Dalziel 1966). It forms the eastern outcrop boundary of the regional migmatite belt and is marked by the outcrop of the granitic gneiss belt (Dalziel 1966). Leedal (1951) writes that the Strontian Granite has been intruded at a significant structural position near the junction of the "flat" and "highly inclined" belts of the Moine rocks. The three Moinian Divisions have been deformed as a result of the emplacement of the Strontian Complex, so that their structures now strike parallel to the intrusion contacts.

Swarms of minor microdiorite and lamprophyre dykes and sheets cut all folds, but are themselves locally foliated and metamorphosed. These record late Caledonian igneous and structural events in the area. They are part of a swarm of minor intrusions north of the Great Glen Fault, in which Smith (1979) has described 3 major suites (younging from a to c):

a) The amphibolite suite - was intruded between D1-D2 deformations.

b) The microdiorite suite (also classed as lamprophyres) - was emplaced during the last phases of Caledonian tectonism.

c) The minette suite - is a post tectonic dyke swarm marking the end of igneous activity in the North Highlands Caledonides.

It is this second group, the microdiorite suite, that is the most significant with regards to this study of the Strontian Complex. These occur as dyke swarms and sills in the surrounding country rocks (Sheet 52E) and a single xenolith has been found in this study. They are reported to form inclusions in the complex (MacGregor & Kennedy 1932) and have been observed in this study deformed into boudins in the aureole of the complex.

Microdiorite dykes located in Moidart as well as along Loch Sunart have been found to possess metamorphic fabrics (Johnson & Dalziel 1966). Although they post date the last deformation (F4 of Brown et al 1970) of the Moine, and belong to the Smith post-tectonic calc-alkaline suite, they underwent a separate greenschist facies metamorphism. It is an important fact that they still occur in this state a long way from the Strontian intrusion itself, so metamorphism is not solely the result of the intrusion of the Strontian complex, (Johnson & Dalziel 1966), but the result of the regional thermal state of the country rocks, load pressure, water vapour pressure and the strain energy due to deformation.

The complex was emplaced after the intrusion of the microdiorites and a rare composite xenolith of Moine schist has been found, which contains a typical foliated lamprophyre dyke (Plate 5.2 A-B). Dyke and foliation are sharply truncated at the margin of the xenolith by the unfoliated host granodiorite. This clearly shows that in some cases the foliation and its regionally associated greenschist metamorphism pre-date emplacement of the Strontian complex.

Isotopic data (Miller & Brown 1965; Halliday et al 1979) support the view that the Strontian Complex post dates the fold phases in the

Moine (MacGregor & Kennedy 1932). Dearnley (1967) and Smith (1979) show that the relationship between the complex and dyke suite may be:

- Intrusions of lamprophyre dyke suite in relatively "brittle" conditions.
- Intrusion of the Strontian granodiorite under more "plastic" conditions prior to or about the time of the metamorphism and foliation of the dykes.
- Intrusion of the Strontian alkali granite and vein complex under cooler, comparatively "brittle" conditions.
- Intrusion of later cross-cutting felsites and different lamprophyres (minette).

Field evidence from this study shows however that the intrusion of the granodiorite took place after the development of the foliation of some of the dykes.

As a result of the high grade of earlier regional metamorphism and the psammitic nature of the country rock, contact metamorphic effects around the pluton are limited to its immediate vicinity. A metamorphic aureole is not obvious (Macgregor & Kennedy 1932; Sabine 1963 and Watson 1964), however Tyler and Ashworth (1982), Ashworth and Tyler (1983) have observed a change in metamorphic state towards the granite contact. These zones are best observed in the pelitic rocks of the Glenfinnan Division. These range from muscovite + quartz to sillimanite + potash feldspar assemblages, with cordierite bearing assemblages occurring adjacent to the contact. The inner cordierite zone is wider on the north east of the complex than along the western. As there is an asymmetry to the aureole around Strontian, Ashworth & Tyler (1983) suggest that the cause may be the

emplacement of the intrusion into rocks with a horizontal regional thermal gradient, with aureole temperatures of 645ºC in the west and north-west and 690ºC in the east. This temperature was increasing eastwards in the plane of present exposure at approximately 5ºC/km (Ashworth & Tyler 1983). These conditions relate to the emplacement of the earlier tonalitic granodiorite pluton. The later alkali granite is mostly emplaced in earlier granitic materials, which are not sensitive to contact metamorphic effects.

It has been suggested that the intrusive styles of the "Newer Granites" were governed by both the depth of cover and temperature of the country rock (discussed above in respect of the Strontian Granite). The earliest granites do not possess obvious thermal aureoles and often have marginal zones of injection and migmatization eg.Strontian. So these granites were intruded at greater depths and into warmer country rock (Brown, Miller & Grasty 1968).

1.8 THESIS FRAMEWORK

The aims of the project are: first to describe the nature of the xenoliths along with their occurrence, chemistry and mineralogy and the nature of the host granite; second to determine whether or not they are in any way genetically related to the granite complex or the mafic dioritic bodies also found in the complex. It will then be possible to assess the relative merits of various hypotheses of the origin of diorite xenoliths and the relationship of the phenomena observed here in the calc-alkaline plutonic environment to those described in the literature for calc-alkaline volcanic rocks.

Each rock type (host rocks, xenoliths, diorites and dykes) will be

described separately in a combination of 3 chapters, which cover field work; petrography and mineralogy and geochemistry. Chapter 12 will bring all conclusions of these chapters together and will also review all common and related points present in the preceding chapters.

Chapter 2 THE HOST ROCKS OF THE XENOLITHS: FIELD RELATIONSHIPS OF THE STRONTIAN GRANITE

2.1 INTRODUCTION

The host rocks of the xenoliths are composed of an early pluton of foliated tonalitic granodiorite and porphyritic granodiorite, which are both cut by a later alkali granite pluton with associated sheets and dykes. The tonalitic and porphyritic granodiorites contain the bulk of the xenolith population. The SE margins are truncated by the Great Glen Fault and the granite is reddened and chloritized along the shores of Loch Linnhe.

2.2 THE EARLY GRANODIORITE PLUTON

The granodiorite pluton is well exposed along the shores of Loch Sunart, as well as on higher ground, forming rounded smooth outcrops (Plate 2.1). The extent of the outcrops of each rock type can be seen on Fig 1.1. There are two facies of granodiorite forming an annular outcrop pattern with a tonalitic granodiorite everywhere separating a porphyritic granodiorite from the surrounding Moine country rock (Fig 1.1). Sabine (1963) reports that the contact of the two granodiorites is a relatively sharp one, taking place within approximately 1-2 metres, where there is a gap between the outcrops, and forming a readily mapped line at 1:10,000 scale. In some places the porphyritic granodiorite becomes finer grained as the contact is approached. He also describes the tonalitic granodiorite as appearing baked at Gleann Geal (location shown on Fig 1.2, grid ref: 740-500) adjacent to the porphyritic granodiorite. Mercy(1963) and Munro(1965) however consider the relationship of the two rock types

Plate 2.1 The western margin of the complex following the A884 towards Lochaline, at Beinn Chlaonleud - Fig.1.2 - the change in the colour of the vegetation on the distant hillside denotes the contact (G.Ref. 7462-5343).

Plate 2.1A The northern shore of Loch Sunart showing rounded outcrops of the porphyritic granodiorite close to Location A - Fig.1.2 (G.Ref. 8010-6094).

Plate 2.1B View on the contact of the complex and the Moine - denoted by the break in slope, NNE of Achagavel (G.Ref. 7675-5695).

Plate 2.2 shows the contact between the tonalitic granodiorite and Moine found west of Liddesdale, shows coarse tonalitic granodiorite - albeit finer grained than the bulk (G.Ref. 7746-5998).

to be gradational and that " the tonalite may merely be a marginal modification of the granodiorite " (Munro 1965).

New detailed work along the shores of Loch Sunart, especially the northern side, where outcrop is continuous, has shown the contact between the two granodioritic types is gradational with an increase in the number of alkali feldspar phenocrysts over a distance of 300 metres here. This suggests there is a continuous process going on between the two facies. Crystal size remains uniform across the transitional zone. No xenoliths of the tonalitic facies are found in the porphyritic granodiorite, nor are veins of porphyritic granodiorite encountered cutting the tonalitic facies. The contact is also parallel to the foliation discussed below. All this suggests that the emplacement of the two granodiorite facies occurred as a continuous process rather than as two separate phases of intrusion.

The external contact generally dips steeply inwards at 70-80º (Sabine 1963), though it is locally more gently dipping, being as little as 25º by Beinn na Cille (grid ref:854-542). South of Loch Tearnait, the junction dips outwards at 80º (Sabine 1963; Munro 1965) (Fig.1.2). Nearing the outer margins, the tonalitic granodiorite becomes slightly finer grained than the main mass and where the contact with the Moine is visible (Plate 2.2 shows a coarse rock albeit finer grained than the bulk) e.g. on the southern shore of Loch Sunart (Fig.1.1), apophyses of the tonalitic granodiorite are also found in the country rock, making the contact less distinct.

Munro (1965) describes the pluton as possessing a foliation and a lineation which is particularly conspicuous in the marginal areas of the complex ie. in the tonalitic granodiorite. In general the

Plate 2.2A View of the schlieren in the tonalitic granodiorite (G.Ref. 7458-5080). Hammer shaft 550mm.

Plate 2.3 The curved layering close to Locality A on the N. shore of Loch Sunart, in the porphyritic granodiorite (G.Ref. 8008-6100). Hammer shaft 550mm.

foliation is parallel to the margin of the pluton (Munro 1965) and present observations have confirmed this pattern. The foliation is best seen by the orientation of the platy plagioclase crystals and also by the biotite crystals in the marginal areas of the tonalite (Munro 1965), while the lineation is the preferred orientation of the longest axes of tabular plagioclase crystals and prismatic hornblendes (Munro 1965). These fabrics imply the former presence of flow within the granodiorites, parallel to the country rock contact. The undeformed, prismatic hornblendes suggest a magmatic event controlling the fabrics rather than late plastic deformation (Munro 1965). Hutton (1988) also describes the foliation in the granodiorite pluton as a pre-full crystallization fabric concordant with the outer contact, dipping inwards and being nearly vertical in the west. The pluton lies in a major southward plunging synform in the country rocks (Hutton 1988).

The planar structure formed by the biotite crystals is most pronounced where they form concentrated layers, called streaks, parallel to the flow structure. These streaks are most evident close to the contacts and, as described by Munro(1965), the tonalitic granodiorite "..may appear gneissose..", this being the result of an abundance of biotite crystal aggregates plus hornblende prisms. These may even be described as schlieren (Didier 1973) which are defined as being "..an irregular mass, generally streaky in form, occurring in a body of igneous rock..". Plate 2.2A shows well developed schlieren only.

Detailed field work in this study has shown that the fabric vanishes in the xenolithic rich areas or clusters. The fabric is also very poorly developed, if at all, in some layers with concentrations of

mafic minerals and will be discussed in the concluding section on xenoliths.

Although the granodiorites are generally massive, layering is seen at two sites near the contact of the complex. These layers lie at right angles to the contact. Well developed, curved layering has been found in the clean, washed outcrops of the porphyritic granodiorite on the northern shore of Loch Sunart (Fig.2.1A & B). It is clearly a local feature trending NE then N to NW at 006°, defined by alternate layers rich or poor in mafic minerals. The zone of layering appears to have a sharply arcuate form, with a radius of curvature of ten's of metres (Plate 2.3 & 2.4). The sharply curved layering is picked out by coarse hornblende prisms concentrated into streaks and layers (Plate 2.5). Bifurcation of the layers is well developed on the more northern side of the outcrop. One set of layering is seen to truncate another. The contacts of the layering with the granodiorite are sharp. The dip of the layers is steep overall reaching 56° N. These mafic layers are also considered to occupy regions of highest relative shearing stress (Wilshire 1969). These hornblende-rich bands also form discrete pockets or lenses (Plate 2.5).

The rock between these layers ranges from a very coarse, almost pegmatitic porphyritic granodiorite of 15 to 30mm grains to a more finer grained rock than the usual porphyritic granodiorite. There is a form of grading of grain size within some of these layers (Fig 2.1B). The layers with a greater concentration of mafic minerals tend to be finer grained and non-porphyritic. These grade into coarser, more leucocratic porphyritic layers. So the grain size increases gradually within the layers and then a sharp contact is crossed into the finer grained part of the next layer. There also

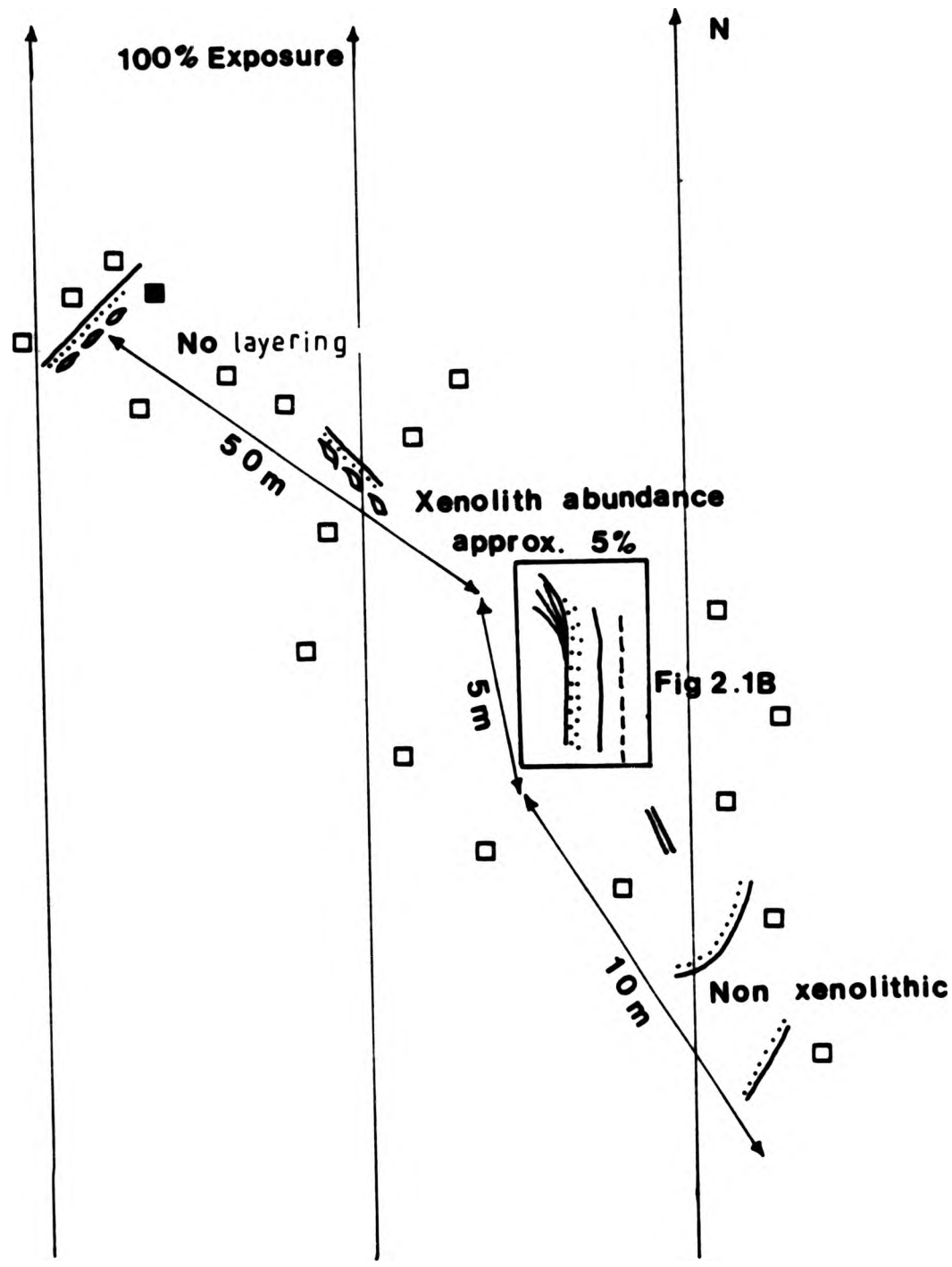

Fig. 2·1A Sketch map of the area showing developed layering.

□ fine to medium grained porphyritic granodiorite

■ coarse grained porphyritic granodiorite

schlieren (dots denote coarser rock)

xenoliths present

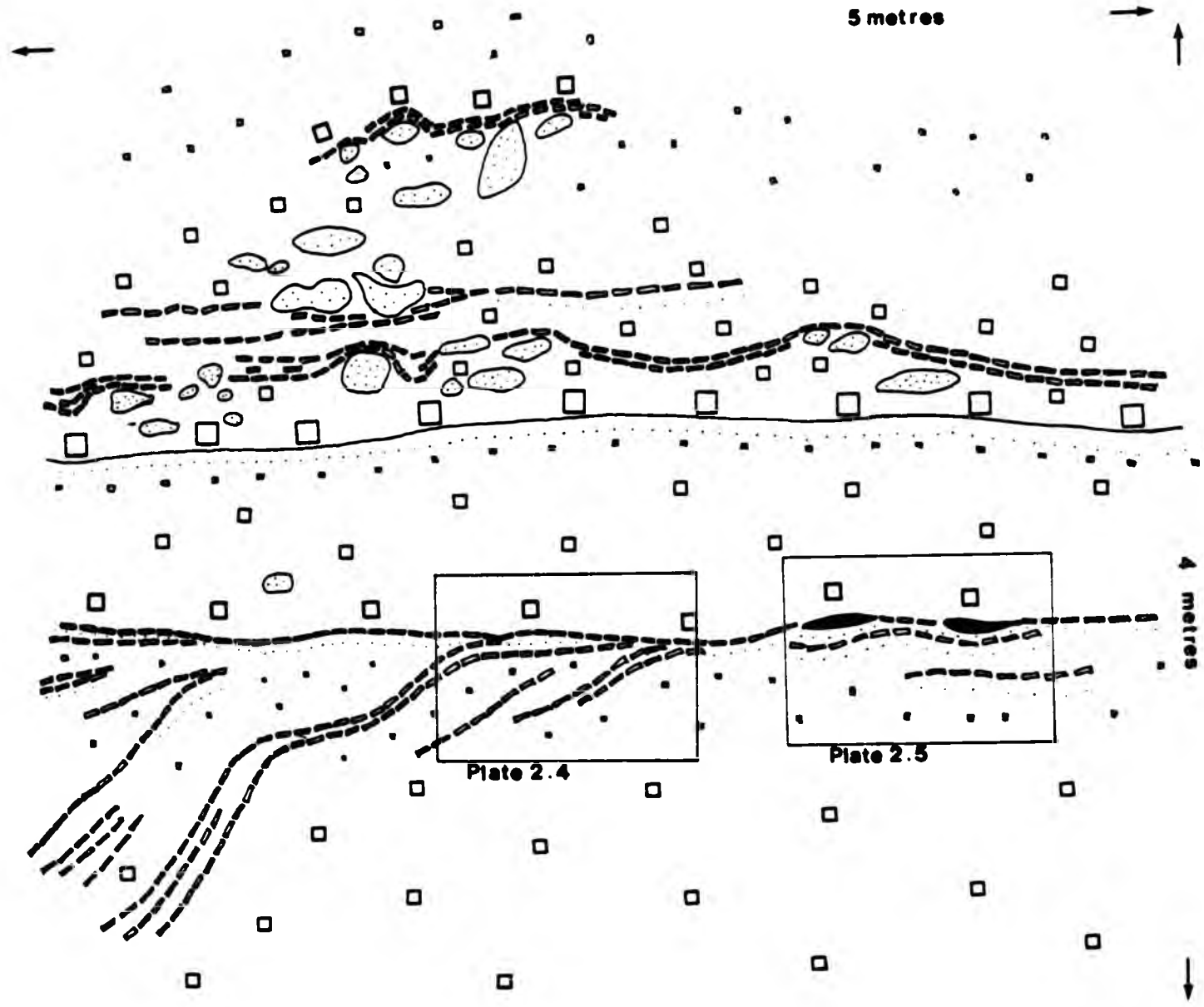

Fig. 2·1B Sketch diagram showing detail of layering from Fig. 2·1A. (Plate 2·3)

- "Pegmatitic" porphyritic granodiorite
- Coarser porphyritic granodiorite facies
- Normal to fine grained porphyritic granodiorite
- Xenoliths
- Prismatic hornblende layers
- Lenses of hornblende

Plate 2.4 Closer detail of the layering showing the concentration of mafics in the layers (G.Ref. 8008-6100).

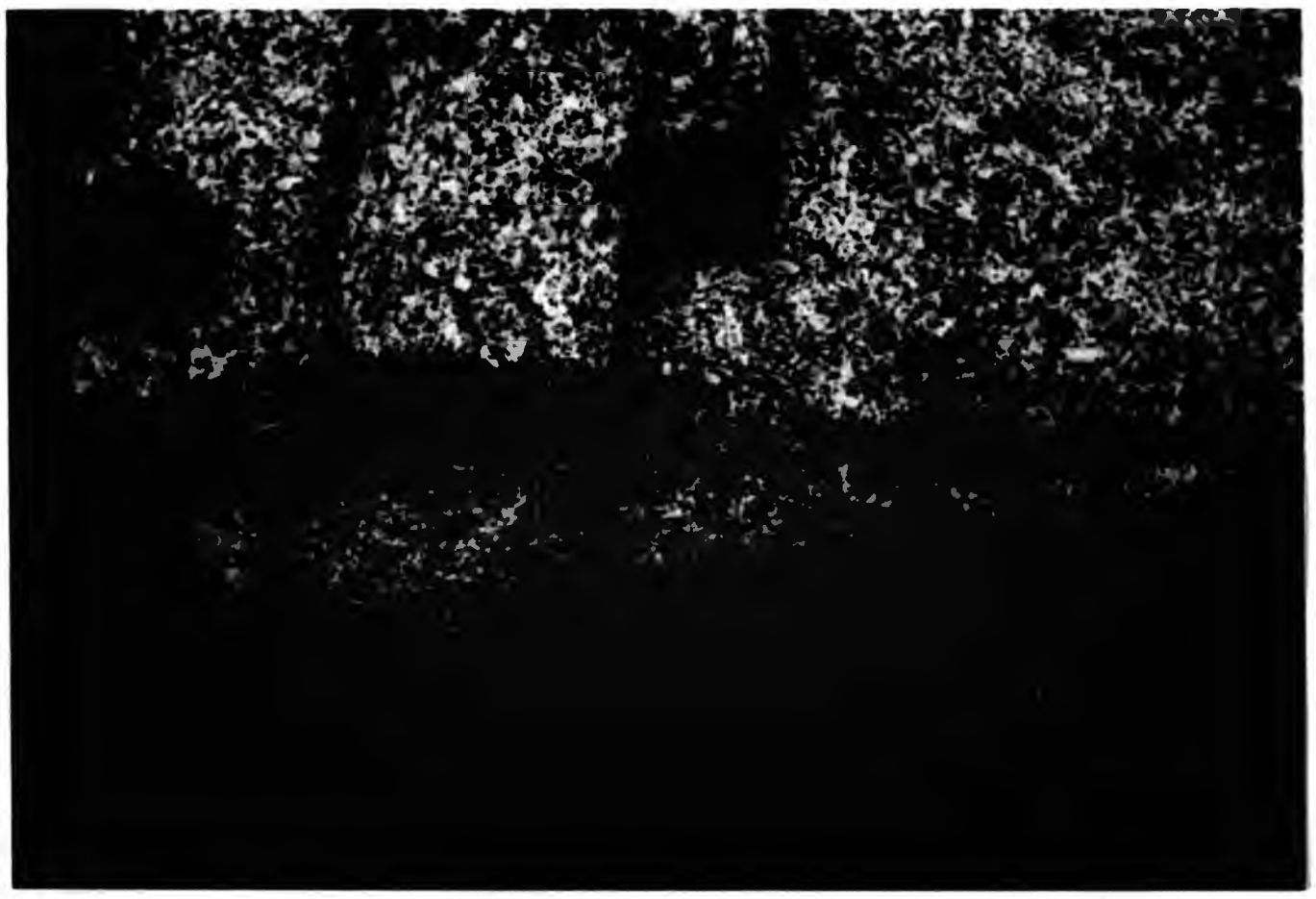

Plate 2.5 Closer detail of the hornblende - rich lenses found in the layering (G.Ref. 8008-6100). Lens cap 50mm.

appears to be a succession of internal contacts within the main layers. Concentration of phenocrysts does not vary along the strike of the layers. Xenoliths are not present in all the bands or layers, but where they are the hornblende layer is draped around the outer margins of the xenoliths. The xenoliths are undeformed so the layering would have to form either in contact with a large body of liquid or by deformation of a liquid/crystal system, which was very fluid by comparison with the xenoliths. The mechanism that produced the lineation and foliation, would also be responsible for any layering effects that have been noted in the field, since the structures are coplanar. This structure indicates at least restricted flow and crystal sorting within the crystallizing Strontian complex, but it should be stressed that these structures are restricted in occurrence. This form of layering has also been noted in the Twin Lakes granodiorite, Colorado (Wilshire 1969). There is no preferred orientation within the layers, even though it might be expected if magma flow was responsible for the structures observed. The absence of this may be due to interference between crystals in the liquid/crystal suspension. The branching of the layers may resemble sedimentary structures and so some kind of sorting theory would be applicable together with variations in shear stress and grain size of crystals in suspension. Wall accretion would give layers with random fabrics.

The second site of layering is found just north of Locality B (Fig. 1.2). By the roadside is a very small quarry in which there are a number of quartz dolerite dykes. Sharp contacts are present at the base of the mafic-rich layers. Then gradation from the finer grained more mafic to the slightly coarser, more leucocratic part takes place. The layers dip at 35 to 40° towards 323°. They appear

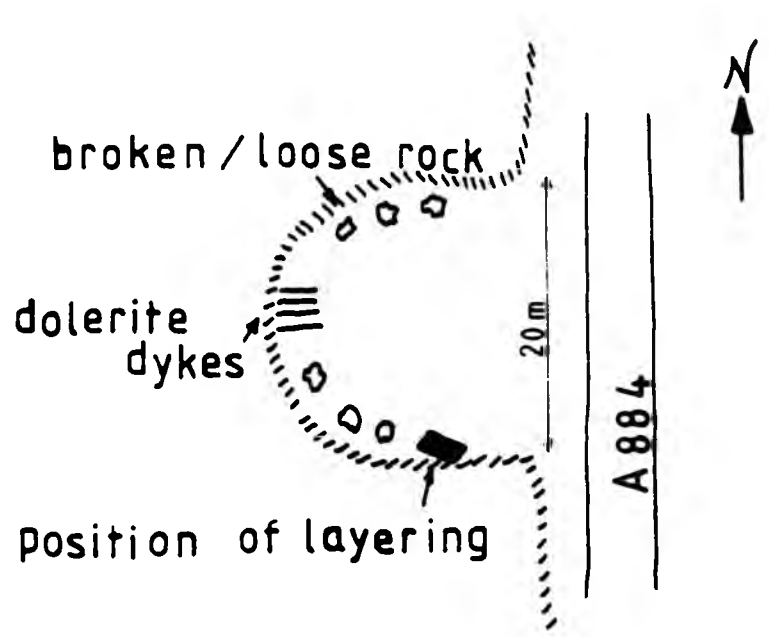

Sketch location of layered block in Quarry B (Figs.1·3 & 4·1B).

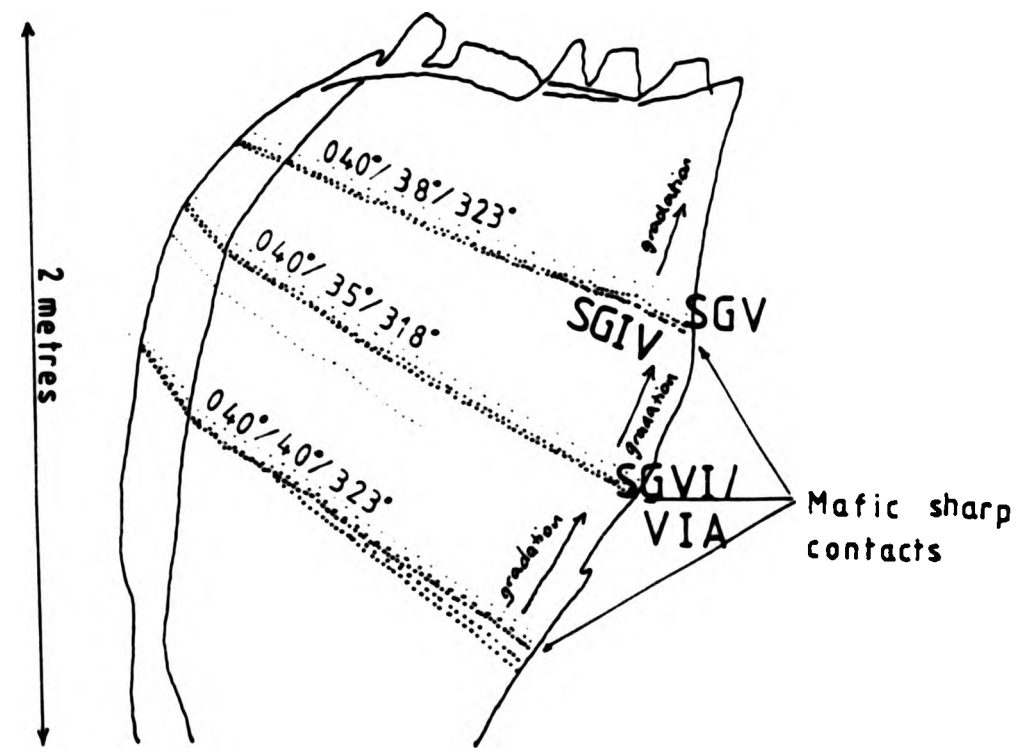

Fig. 2·1C Diagram to show layering and positions of analyzed samples.

not to be as well developed as those along the shore of Loch Sunart (described above). Fig.2.1C shows details of the layering with the analyzed sample sites.

Aplites and pegmatites are present throughout the complex, especially in the granodiorite, but are not particularly abundant. They range from a few millimetres in width to over 300mm, though these latter are rare. The aplites are more common and are seen to cut across not only the porphyritic granodiorite and late granodioritic sheets, but also the very mafic diorite bodies found along Loch Sunart.

2.3 THE BIOTITE GRANITE PLUTON

The biotite granite is the last main intrusion of the Strontian complex. It occupies the whole of the most southerly part of the pluton and is found along the western shores of Loch Linnhe (Plate 2.6 A & B). It is exposed as rounded outcrops especially on higher ground, where there is an extensive cover of grass and peat bog (Plate 2.7 & 2.8). The outcrops are quite highly weathered on the higher ground too. The junction between the biotite granite and the earlier granodiorites is a sharp, steep, nearly vertical contact, nowhere suggesting any transition. There is no evidence of chilling between the granite and the granodiorites, though local fining of grain size has occasionally been observed.

The biotite granite was emplaced broadly following the shape of the earlier intrusion. The NNE trending dexteral shear zone of the granodiorite extended eastwards into the site of the biotite granite before its emplacement (Hutton 1988). Its movement continued after the biotite granite intrusion to produce a weak pre-full

Plate 2.6A View eastwards onto Loch Linnhe and Lismore (middle ground) from Glen Sanda (G.Ref. 8118-4800).

Plate 2.6B A view more south-eastwards than 2.6A onto Glensanda, Loch Linnhe and Lismore. Outcrops are very limited (G.Ref. 7800-4911).

Plate 2.7 View SW from the same place as 2.6B onto Loch Tearnait (in the back ground). The Isle of Mull is in the far distance.

Plate 2.8 Looking from Meall a' Chaorainn towards Kingairloch (G.Ref. 7990-5310).

crystallization fabric in the marginal part of the granite (Hutton 1988). On its western margin, this junction obliquely transgresses the tonalitic and porphyritic granodiorite to come into contact with the Moine schists. The contact of the granite with the Moine is sharp and is observed to either cut across the banding in the Moine or lie parallel to it (Sabine 1963). Numerous inclusions or pods of the Moine and granodiorite are observed here in the granite within 150 to 200m of the contact. The Moine is also cut by granitic and pegmatitic veins coming from the intrusion. The granite shows a strongly developed foliation near the contact.

Just north of the transgression and east of Loch Tearnait (Fig.1.1), the biotite granite is separated from the porphyritic granodiorite by a narrow strip of fine grained dioritic rock, some 2.5 kilometres long and upto 200 metres in width (MacGregor & Kennedy 1932; Sabine 1963). Present work has shown that exposure of this mass is very limited, being restricted to stream sections and occasional outcrops on higher ground, so the relation with the biotite granite is unknown.

North of Loch Uisge (Fig.1.1), the granite becomes a complex of irregular branching, steeply inclined sheets which strike NE-SW, on occasion cutting across the granodiorite pluton to reach the Moines on the eastern margin (marked fG on the B.G.S. map). They show very similar textural and mineralogical features to the main granite pluton and have no foliation or lineation. There appears to be no evidence to suggest that these sheets or the main pluton have disturbed the host rock types in any way. The present study has shown that at the contacts of both the main biotite granite body and the sheets, there may be a slightly finer grained facies, but there

is no conspicuous chilled margin. These sheets and the main biotite granite pluton contain only rare diorite xenoliths that contrast with the greater abundance of microdiorite xenoliths in the granodiorite pluton. There does not appear to be a separate metamorphic aureole detectable around the biotite granite.

Present work also shows that the biotite granite has a systematic internal variation in petrography, which is described in section 3.2.

The biotite granite, according to Munro (1973), appears to have been emplaced by a process of brittle fracture (Hutton 1988), which suggests a somewhat higher level of emplacement in the crust than the granodioritic pluton and that a considerable interval passed between the two events. This is supported by different radiometric ages given for both the granodiorite and the biotite granite by several authors (Miller & Brown 1965; Pankhurst 1979; Halliday et al 1979; Hamilton et al 1980 and Rogers & Dunning 1989 & in press).

2.4 THE GRANODIORITE PORPHYRY DYKES/SHEETS (marked as ctG on BGS sheet 52)

These intrusions were originally mapped by Dr.A.G.MacGregor after the war and are not very common in the complex (BGS sheet no.52). They have also been reported by Sabine (1963). MacGregor and Kennedy (1932) suggest that from similarities with the granodiorite, the sheets are only slightly younger than the main mass, but older than the biotite granite. The bodies occur as vertical and horizontal sheets, have the same petrography and so there is uncertainty as to the correct terminology to use ie.dykes or sheets. However for the

purpose of simplicity, they will be referred to as sheets. The abbreviation ctG has been taken from the B.G.S. map and used to distinguish the later sheets in the granodiorite; while fG (also from the B.G.S. map) refers to the biotite granite related sheets.

Most of the examples mapped by the B.G.S. were encountered by the traverse lines in the study. They are found in the porphyritic granodiorite pluton (one exception in the Moine), where they reach lengths of several kilometres and about 40 metres width and trend east to north-east. They do not cut across the biotite granite, nor has any example of a porphyritic sheet been seen to be cut by the biotite granite. Therefore no relationship can be established between the two as to whether the ctG sheets pre-date the the biotite granite and its sheets or whether they are just earlier intruded variations of the differentiating biotite granite.

The sheets(fG) of the biotite granite reach the granodiorite pluton north of Loch Sunart (Fig 1.1). It has also been noted from the B.G.S. map that some of the very long sheets have been labelled fG at one end and ctG at the other (none have been analyzed in this study). This may provide evidence of a genetic relationship between the rock types. On comparison of Plates 2.9A (fG), 2.9B (fG), 2.10 (fG), 2.11A (ctG), 5.1 (ctG) and 5.6D (ctG) there does appear to be an overall similarity in the petrography and texture of both sheet types.

In the Criffell-Dalbeattie granodiorite complex there are also a great number of porphyry granite dykes, which do not enter the centre of the pluton. It is suggested that they were intruded while the core was still unconsolidated. The occurrence of these dykes

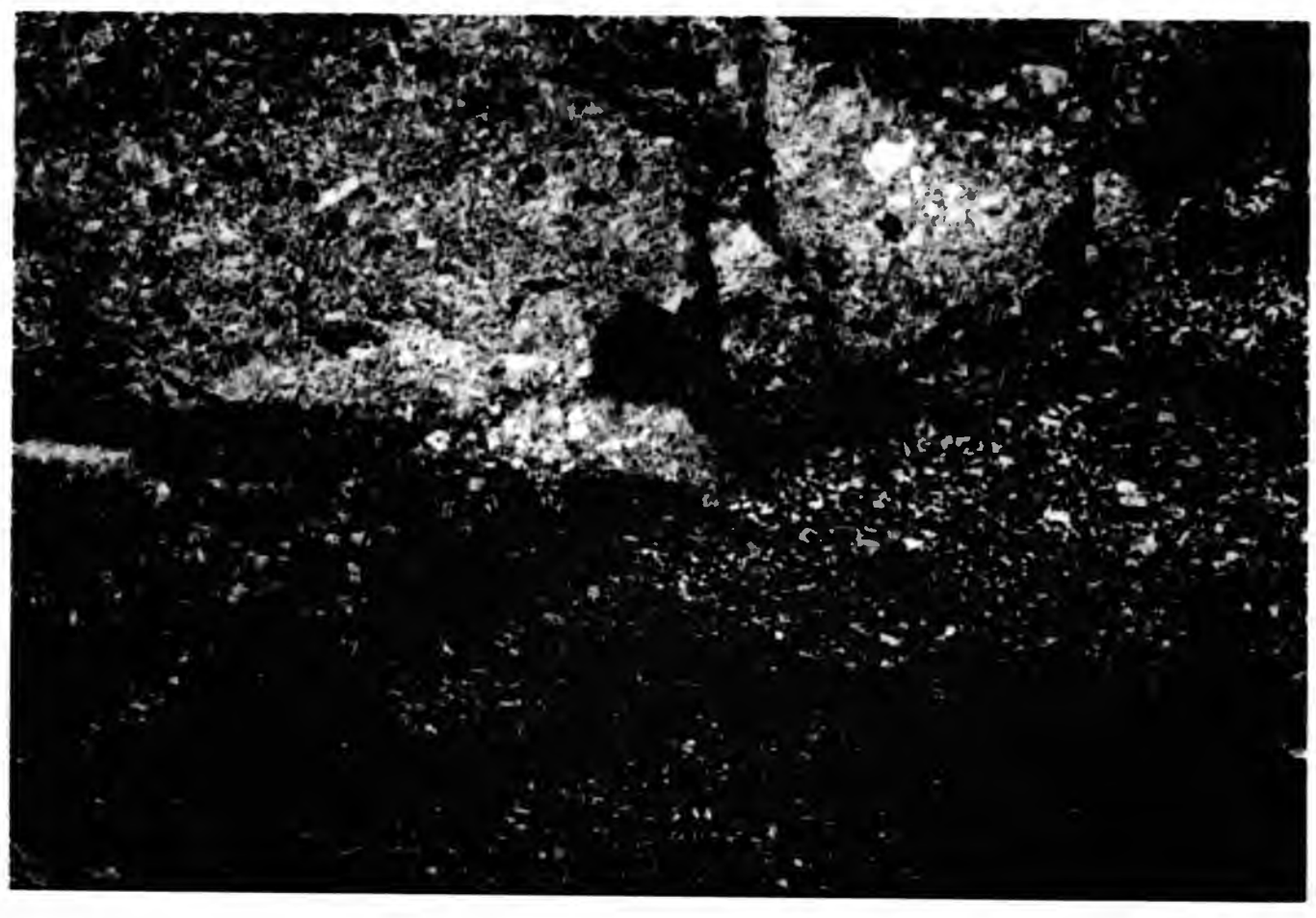

Plate 2.9A The contact between the porphyritic ganodiorite and the later granitic sheet (ctG). Lens cap 50mm. (G.Ref. 7716-5702).

Plate 2.9B Closer detail of a later granitic sheet showing large feldspar phenocrysts on the N. shore of Loch Sunart, note rounded inclusion-rich core in central megacryst. Hammer head 170mm. (G.Ref. 8195-6088).

indicates that porphyritic magma was available for intrusion when later fractures were formed (W.J.Phillips 1956). Therefore in the Strontian granodiorite complex a similar occurrence could be the case.

Though these sheets are very granitic in nature, they are patchy with variations being in the proportions of the modal minerals as well as in the textures. The granodiorite porphyry sheets have sharp, steeply inclined contacts with the surrounding host granodiorite. Plate 2.9A & B suggest some groundmass chilling at the contacts, but this is not very well developed. One of these sheets shows a xenolith of the host granodiorite in it and another cuts across a xenolith present in the host granodiorite (Plate 2.10). These sheets show complex relationships with some of the large dioritic bodies: eg. they form veins in the Loch Sunart diorites and have gradational/mixing relations with the diorite along the Strontian western margin (No.4 Fig.1.1). These relationships are discussed in detail in Chapter 9.

One sheet found along the northern shore of Loch Sunart, close to the island Eilean a' Mhuirich (Grid ref. 8008-6109 Fig.1.2 Location A), shows a complex composite intrusion of a leucocratic porphyritic granodiorite sheet with an associated microdiorite containing patches of coarser mafic dioritic material.

The sheet is asymmetric and is approximately 16m wide (Fig.2.2). There are in fact 4 different contacts within this one unusual exposure:

1 NW - the granitic sheet with the porphyritic granodiorite

Fig. 2·2 Details of microdioritic, granitic sheet porphyritic granodiorite host relationships (at A, Fig. 1·2)

Xenoliths

Granitic sheet
Porphyritic granodiorite
Microdiorite sheet

■ Feldspar phenocrysts

□ Coarser granodiorite facies

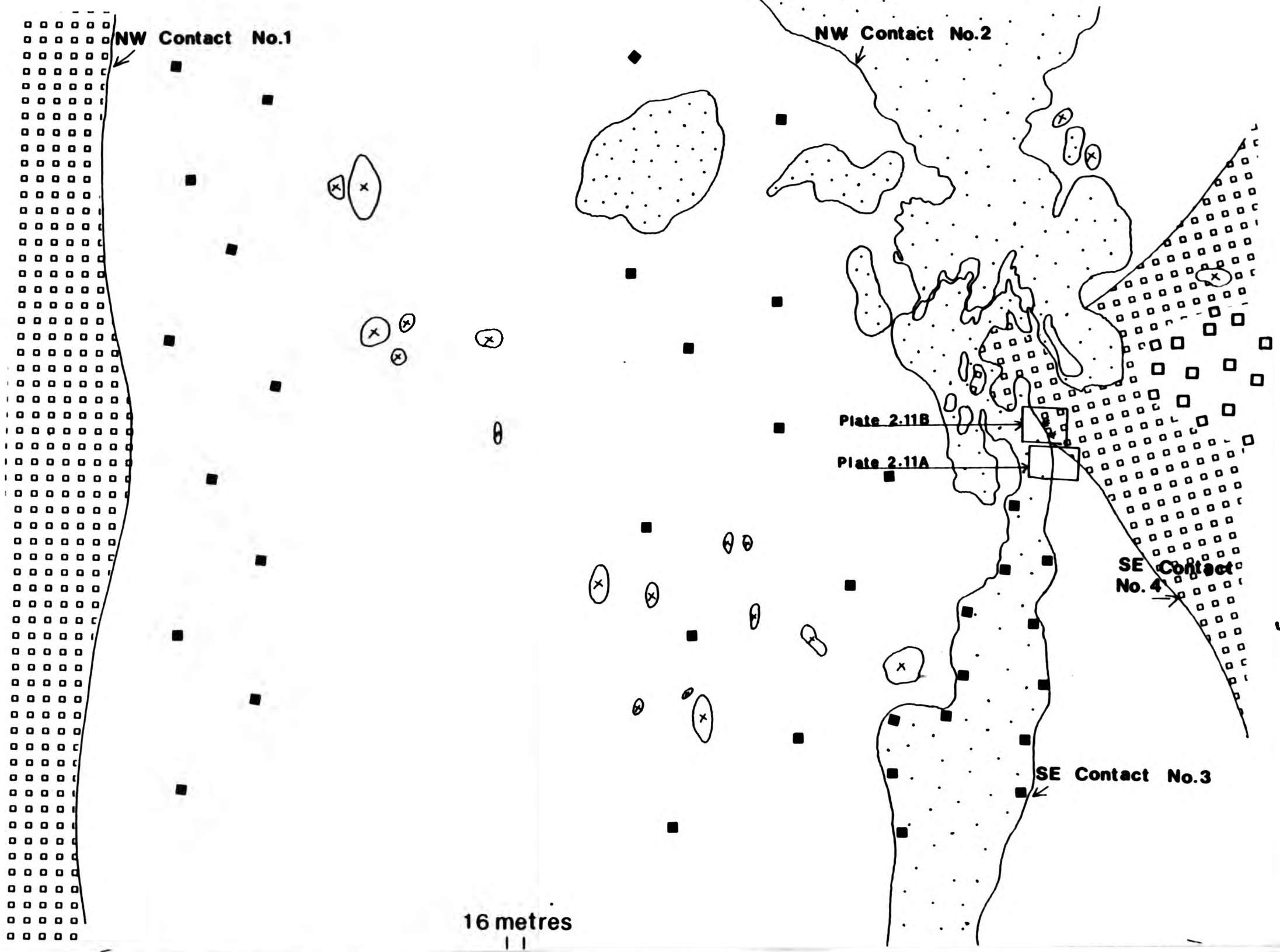
NW Contact No.1
NW Contact No.2
Plate 2.11B
Plate 2.11A
SE Contact No. 4
SE Contact No.3
16 metres

Fig. 2.2

Plate 2.10 A later granitic sheet cutting across a xenolith in the porphyritic granodiorite. (G.Ref.8199-6086).

Plate 2.11A The relationship of the microdiorite, granitic sheet and porphyritic granodiorite found at Locality A Fig.1.2. (G.Ref. 8006-6107).

pluton. It has a sharp outward dipping contact. The porphyritic granitic sheet is quite uniform in grain size at the contact, though moving away it becomes more feldspar-rich and ferromagnesian poor. Also inwards from the contact small microdiorite xenoliths occur, which increase in size further inwards. However this contact has no evidence of the microdiorite sheet (described below in 2 and 3).

2 NW - the microdiorite with the granitic sheet. This contact appears sharp, as the microdiorite is darker and finer grained than the sheet. From the undulating nature of the contact, it is thought to be very shallow dipping too. The sheet here is also xenolithic and there are also large (300-500mm) more mafic patches of the microdiorite material. The granitic sheet has very large alkali feldspar phenocrysts (20mm or more) with plagioclase jackets, in rapakivi-style.

3 SE - the microdiorite with granitic sheet and also locally with the pluton. The microdiorite sheet here again has a sharp contact with the granitic sheet. At the contact, the microdiorite has large feldspar phenocrysts, which have clearly been picked up from the coarser granitic sheet (Plate 2.11A). The microdiorite sheet then transgresses the granitic sheet and comes into contact with the host granodiorite. The contact is sharp with no phenocrysts. Close to this there are also patches/xenoliths of the host granodiorite in the microdiorite sheet. Plate 2.11B shows "flame-like" structures of the microdiorite material in the host

Plate 2.11B Detail of the microdiorite veinlets that pass into the porphyritic granodiorite, as seen on Fig.2.2.

Plate 2.12 A later granitic sheet present outside the complex in the Moine. Refer to Fig.2.3. (G.Ref. 7405-5036).

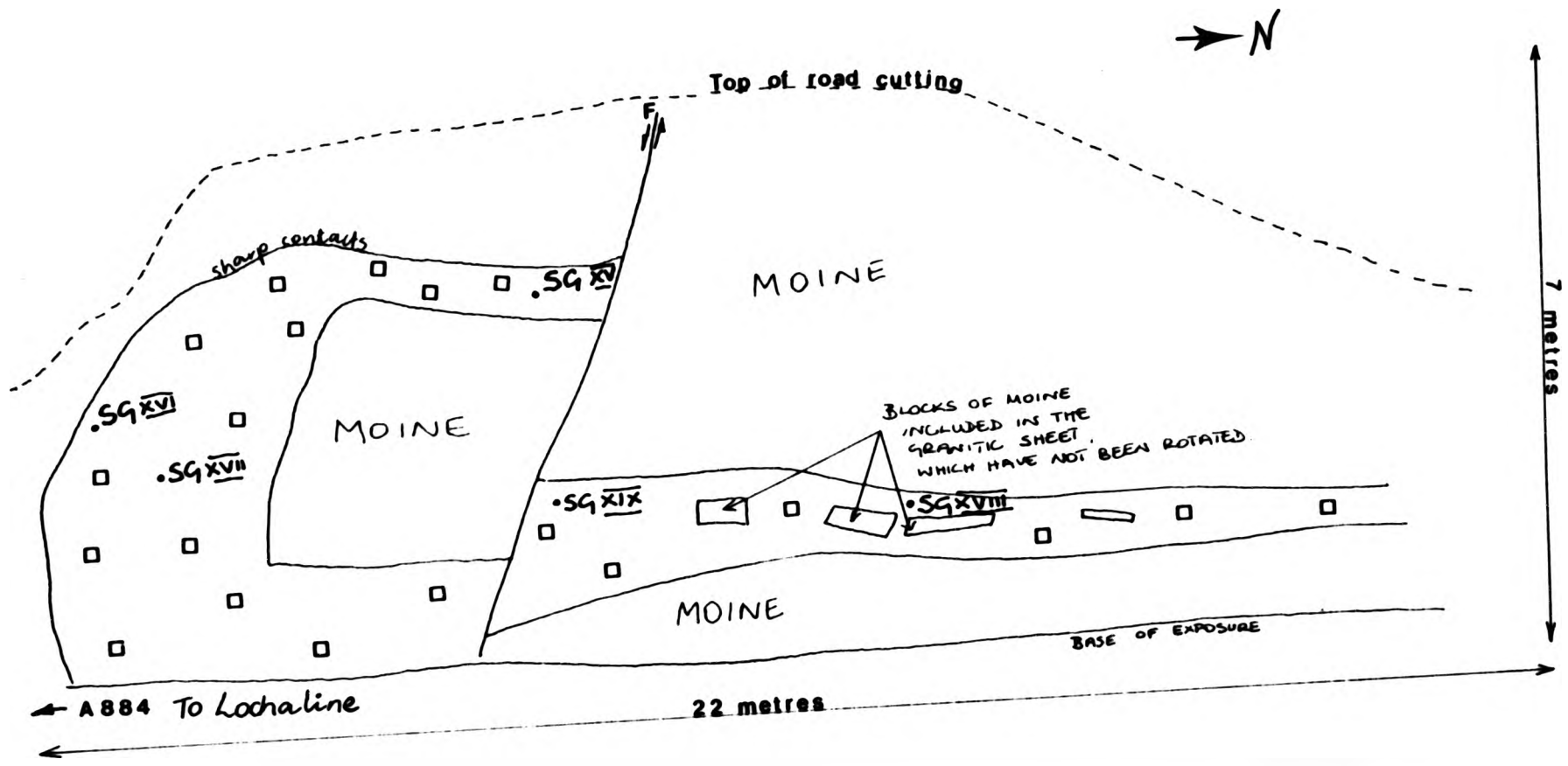

Fig. 2·3 Details of the granitic sheet found in the Moine country rock

Location B, Fig. 1·2 & Plate 2·12

▫Granitic sheet

granodiorite, suggesting it was still fluid of semi-fluid when it came into contact with the granodiorite.

4 SE - the granitic sheet with the granodiorite pluton. This contact is sharp and unchilled with the granitic sheet, being overall finer grained than the pluton, though both are porphyritic.

All four contacts do seem to be different, but it is the contact of the microdiorite with the granodiorite porphyry that is particularly important. It is known that these sheets post-date the granodiorite. From the field evidence it appears that the microdiorite post-dates the granodiorite porphyry (where it transgresses). However it was intruded at a time when both the sheet and the pluton were a crystal mush allowing incorporation of the phenocrysts, formation of the "flame-structures" and the non-chilled contacts.

One example is known to cut the Moines (Grid Ref: 7392-5034; Plate 2.12) and will be named the Moine sheet (Location B, Fig.1.2). It is an isolated outcrop and there is no evidence of it actually cutting across the contact (Fig.2.3). Therefore it could be only a differentiated vein of the main pluton. It has very sharp straight contacts and the banding in the Moine is truncated by the intrusion. There are angular blocks of Moine incorporated into the sheet, which indicates that this intrusion simply pushed apart the surrounding rock as it was being intruded. This is the outcrop that has 5 analyzed samples that often plot separately (described in chapter 4).

A highly xenolithic sheet cuts across the road at Locality D

(Fig.1.2). It has in this case near vertical contacts. The observed microdiorite xenoliths show nearly the full range of types found in the granodiorite pluton.

2.5 DISCUSSION

The field relations observed in this study confirm and extend the previous work. The Strontian igneous complex, as with many Caledonian intrusions, is multiple with two main intrusive events - the tonalitic and porphyritic granodiorites followed by the biotite granite. Field work supports the view that the granodiorite types are two facies from one continuous intrusion. The evidence of rare layering and internal contacts within the granodiorites suggest that at some time both rock and magma existed together in the granodiorite pluton and they had sharp interfaces. The lack of chilling at the porphyritic granodiorite contacts and some microdiorite suggest that the granodiorite was still relatively hot at the time of their emplacement. Porphyritic granodiorite - microdiorite sheet relationships show that both acid and intermediate magmas co-existed at this stage at depth.

In general the Strontian complex was a 2 phase emplacement of a near horizontal removal of a segment of country rock out of the core of the plunging synform, by extensional stresses. Magma exploited the space created and was deformed in the process (Hutton 1988). The siting and space made available for a pluton is likely to be a combination of tectonic structures making the space and the magnitude of tectonic stresses determining pluton emplacement mechanisms (Hutton 1988).

Chapter 3 THE HOST ROCKS OF THE XENOLITHS: PETROGRAPHY AND MINERALOGY

3.1 PETROGRAPHY OF THE GRANODIORITE

As both the tonalitic and porphyritic granodiorites show very similar mineralogical characteristics, it was decided to describe them in one section.

Both granodiorite types are white/grey in colour and are medium to coarse grained (3 to 10mm size range) acid igneous rocks with an inequigranular texture consisting of dominantly hypidiomorphic plagioclase feldspar, hornblende, biotite and quartz with variable amounts of alkali feldspar (Table 3.1). The transition from tonalitic granodiorite to porphyritic granodiorite results from i) an increase in the amount of euhedral, 10-30 mm pink perthitic alkali feldspar phenocrysts, and ii) an increase in the amount of quartz, particularly as large rounded grains. There is an increase in the mafic content (and so colour index) from the tonalitic to porphyritic granodiorite (Table 3.1). The porphyritic granodiorite contains 10-20% K-feldspar with the majority occurring as phenocrysts; while in the tonalitic granodiorite they occur interstitially, rarely as phenocrysts. Representative modes of the two types are given below to show the difference.

The alkali feldspar phenocrysts are large subhedral to euhedral crystals varying in length from 10-30 mm. They are often sparsely perthitic, with little albite showing, and show Carlsbad twinning and concentric zoning. There is occasional microcline twinning. They often have an uneven undulating extinction. Inclusions such as small

euhedral biotite, hornblende, quartz and occasional sphenes and plagioclase occur randomly within the alkali feldspar crystals (Fig. 3.1A). The margins of the phenocrysts can be quite irregular and serrated, suggesting porphyroblastic or simultaneous growth of other minerals. Graphic textures occur locally on the crystal edge, but are not common. Where alkali feldspar is not present as phenocrysts it is found in the groundmass as anhedral interstitial grains, occasionally showing perthitic textures but free of inclusions.

Table 3.1. REPRESENTATIVE MODES OF THE GRANODIORITES

	TONALITIC	PORPHYRITIC
Plagioclase	61.1	40.1
K-Feldspar	7.0	17.7
Quartz	20.9	28.5
Hornblende	5.9	7.3
Biotite	5.0	6.3
Accessory min.	0.7	0.7
Q	22.8	32.3
A	8.0	20.7
P	69.2	46.9
	Tonalite	**Granodiorite**

The second set of columns refer to the QAP coordinates of Streckeisen's classification (1975) from where the names are derived. Q, A and P are Streckeisen's Qz, Alk. Feld and Plag. values.

The modal amount of plagioclase varies inversely with the total amount of alkali feldspar present. Plagioclase feldspar (andesine-oligoclase) forms tabular, euhedral crystals of upto 10mm in length. It is found both in the matrix and as phenocrysts in the tonalitic granodiorite; while in the porphyritic granodiorite plagioclase is found mainly in the matrix and only very occasionally as phenocrysts. The feldspars are generally fresh, with alteration being limited to certain zones. They show multiple lamellar twinning

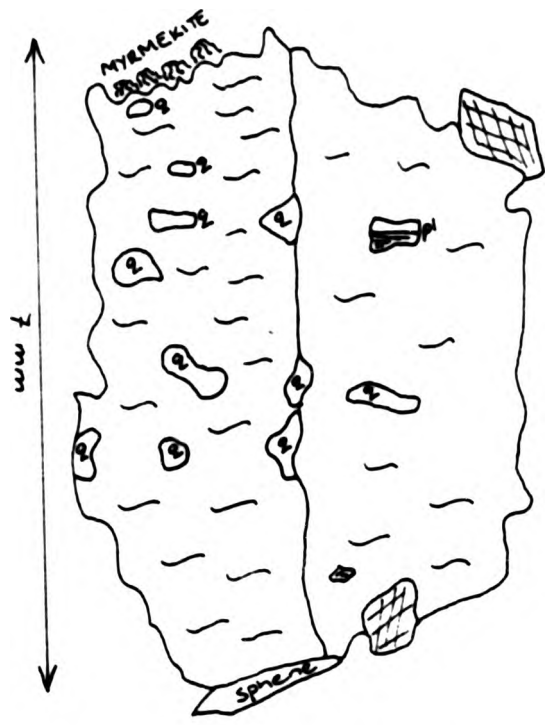

A. SG II K-feldspar

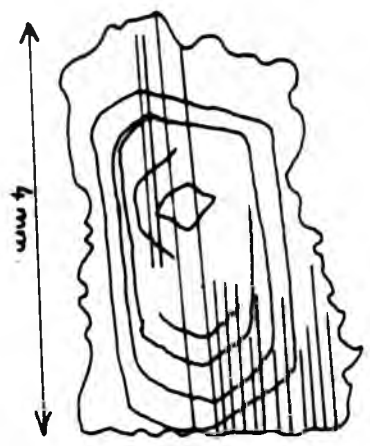

B. SG II Plagioclase

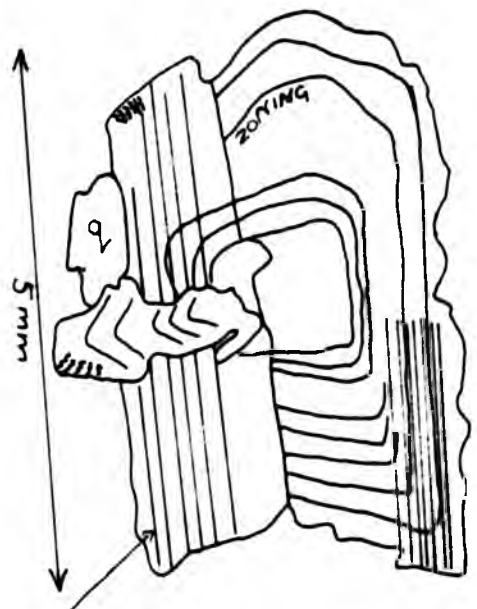

C. SG I Plagioclase

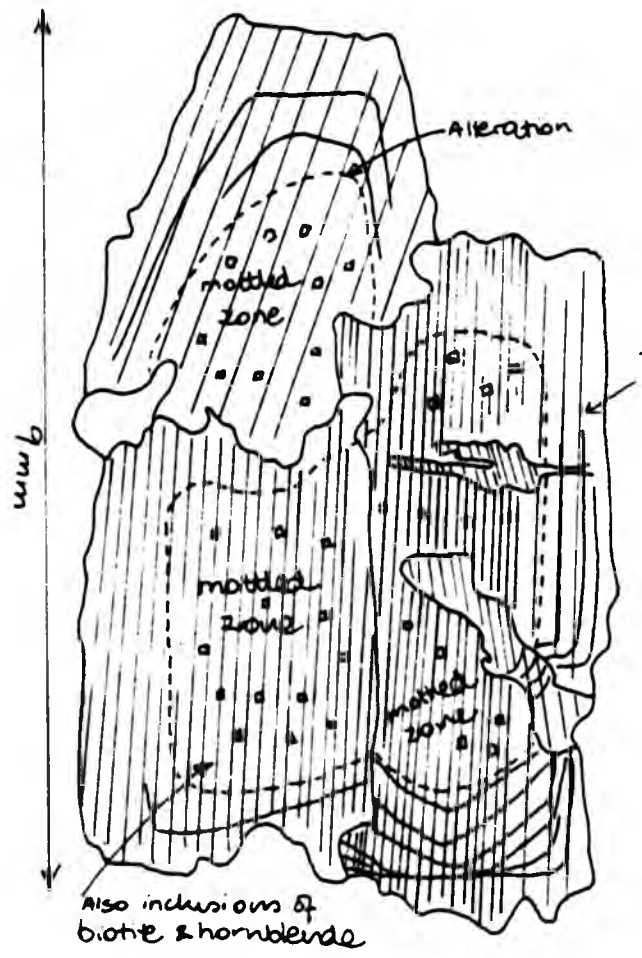

E. SGIX Plagioclase

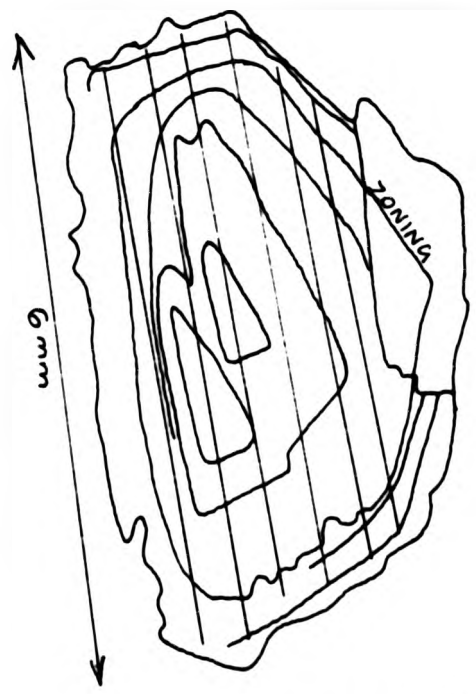

D. SGXXVII Plagioclase

Fig. 3-1 Details of host rock feldspars.

and concentric normal and oscillatory zoning, quite often in the same crystal (Fig.3.1 B-C-D). Oscillatory zoning within the plagioclase has euhedral and rounded outlines and occasional rounded zones possess inclusions of euhedral biotite and hornblende crystals that follow the line of the zone. Microprobe plagioclase compositions, as a whole range, from mid-andesine to mid-oligoclase (An41-22), with the cores An41-36 and the rims An32-22. Myrmekitic texture in plagioclase also occurs on a small scale at the margins of the crystals and antiperthitic exsolution of alkali feldspar is also observed.

Another phenomenon is a mottled extinction in the plagioclase. Similar spongy textures have been noted in volcanic rocks by Anderson (1976) and Eichelberger (1978). In Strontian this spongy texture has had new growth/crystallization superimposed onto the original feldspar during a phase of magma mixing. It occurs within particular zones of a zoned plagioclase, or in the core itself (Fig.3.1E).

The main ferromagnesian minerals are a green edenitic to magnesio-hornblende and a dark brown pleochroic biotite. Their modal amounts vary throughout the whole granodiorite pluton, but not substantially enough to cause any heterogeneity, except in the more mafic schlieren. While in xenolithic areas, the host rock has a slightly higher modal proportion of mafic minerals. Biotite and hornblende may show alignment in the tonalitic granodiorite close to the contact.

Hornblende is the dominant mafic mineral (Table 3.1) and modally ranges from 5 to 10%. Its form ranges from single euhedral elongated prisms, upto 10mm in length, through subhedral-anhedral finer grained

crystals to fine grained, monomineralic aggregates upto 10mm in diameter. There is a slight tendency for the finer grained hornblendes to be found closer to the complex margins. In some large hornblendes and in the aggregates, rounded grains of magnetite occur in variable amounts. They may well be the result of pyroxene altering into hornblende and a single remnant core of clinopyroxene has been found with a hornblende jacket (Fig.3.2A). Spongy hornblendes with quartz and pyroxene cores have been found. The origin of the quartz would result from the alteration of pyroxene to amphibole, as amphiboles have a lower silica content than pyroxene.

Biotite is found as subhedral to euhedral individual flakes (1-5mm across) or as books. Biotite can also occur together with hornblende in fine grained irregularly shaped aggregates, the minerals having crystallized together, and on occasion is seen replacing hornblende. Biotite is altered to chlorite along its cleavage surfaces, where it occurs as 5 to 30% of the books or aggregates. Inclusions of apatite, zircon, and occasional sphenes are noted in the biotites. Where mafic schlieren is well developed close to the margins of the pluton, the aligned biotite crystals all show varying signs of alteration to chlorite.

Colourless quartz varies considerably in abundance and distribution, but is generally found as large anhedral grains (1-3mm), while irregular interstitial patches of fine grained crystals do also occur. The quartz content is seen to increase from the tonalitic to the porphyritic granodiorite. Most have a primary texture, though some show recrystallization into polygonal grains and many show some form of strained extinction.

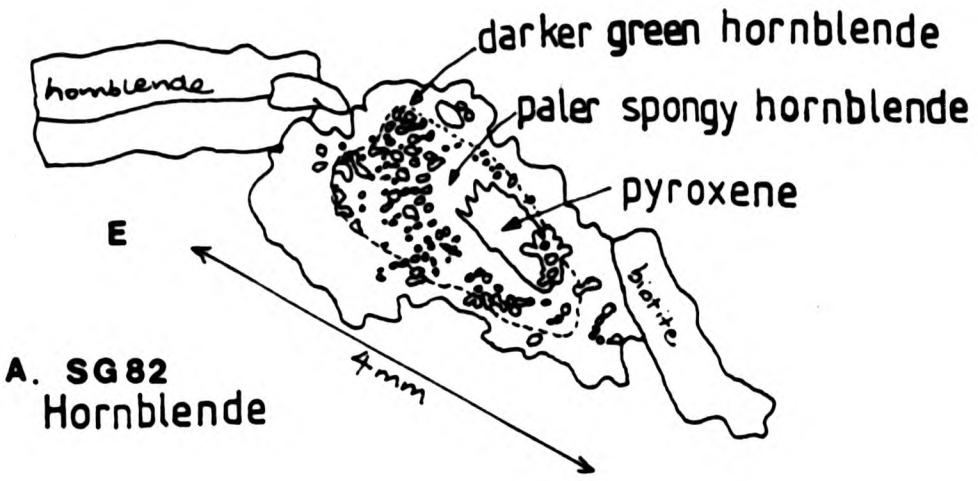

A. SG82
Hornblende

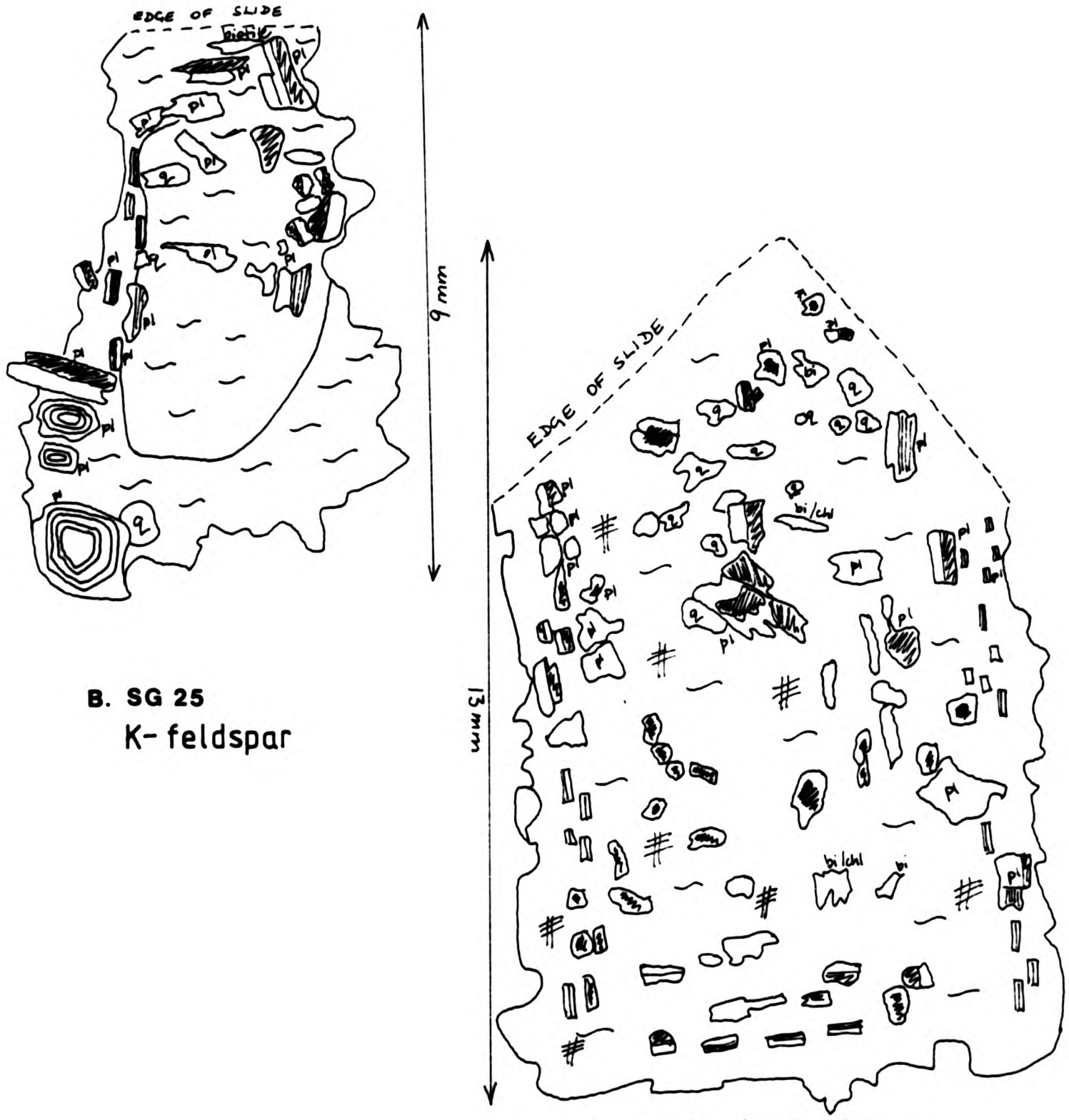

B. SG 25
K- feldspar

C. SG 59 K-feldspar

Fig. 3·2 Details of hornblende & K-feldspar

In general all the accessory minerals have a tendency to be found within or in the close proximity to the mafic minerals.

Sphene is the most prominent and characteristic accessory mineral in the Strontian granodioritic complex. It is a brown mineral with crystals of 2mm in length in some cases. Sphene appears in three different forms: 1. most commonly as large euhedral crystals in the groundmass, which are considered magmatic but also as tiny euhedral crystals included in the margins of the plagioclase, which could represent refractory material from the source - restite (Noyes et al 1983); 2. as subhedral/skeletal crystals with inclusions of quartz and plagioclase; and 3. occasionally as a secondary alteration product of biotite within the hornblende/biotite aggregates. This suggests that sphene crystallization occurred at a number of stages in the cooling history.

Euhedral, stubby, prismatic apatites are most readily found as inclusions in hornblende and biotite, but occur occasionally in plagioclase. They are not distributed uniformly in the matrix.

Rounded magnetite (now altered to haematite) are seen individually in the groundmass or within the confines of the hornblende crystals or hornblende/biotite aggregates. The modal amount of magnetite is no more than 1%. Rare zircons are found in the granodiorite, as inclusions in the aggregates, close to the mafic minerals or within the alkali feldspar phenocrysts.

3.2 PETROGRAPHY OF THE BIOTITE GRANITE

Mineralogically, the biotite granite is very different from the

earlier granodioritic body and the bulk of it is a pale, creamy pink, unfoliated, medium grained (upto 5 mm) acid igneous rock. It consists mainly of hypidiomorphic plagioclase and alkali feldspar and a lot of allotriomorphic quartz. The main ferromagnesian mineral is a green-brown biotite, which is present in only small quantities (Table 3.2). The branching sheets (described in section 2.2) have similar textural and mineralogical features to the biotite granite and so can be regarded as being included in this section.

The regional variation in the biotite granite results from changes in modal mineralogy and texture. This is best seen towards the Loch Linnhe side (Fig.1.1) of the granite, where the proportions of quartz and orthoclase increase dramatically, while plagioclase remain nearly the same. Associated with these changes is a grain size increase, with quartz reaching 10 mm in diameter in the most quartz-rich rocks.

Table 3.2 REPRESENTATIVE MODES OF BIOTITE GRANITE
(refer to Fig.1.1)

	BEACH Western	EIGNAIG Eastern	GLENSANDA Eastern
Plagioclase	30.0	27.4	33.1
K-feldspar	27.4	28.6	24.9
Quartz	29.7	41.3	36.2
Hornblende	0.5	0.4	0.0
Biotite	11.4	1.8	5.2
Accessory min.	0.8	0.5	0.7
Q	34.4	42.4	38.4
A	31.5	29.4	26.4
P	34.1	28.1	35.1
	GRANITE	GRANITE	GRANITE

All samples are granites according to Streckeisen's classification.

In general the granite is non-porphyritic, though random local variations in the pluton and sheets may show some phenocryst-like

alkali feldspars of upto 20mm in length. However most of the alkali feldspar, often with microcline twinning, forms subhedral to anhedral crystals reaching 3 to 10mm in length. It is also likely that all the alkali feldspar is microcline, but that some of the grains have not developed the characteristic twinning. They often have simple twins and occasional concentric zoning parallel to the crystal margins is defined by inclusions. Larger crystals sometimes show zones with anhedral outlines, suggesting periods of resorption during their crystallization history (Fig.3.2B). Perthitic textures are developed in many feldspars. The quantity of exsolved albite varies from 1% to a maximum 10%. The alkali feldspars are fairly fresh, but where alteration occurs it is found along certain zones in the albite rods of the perthitic texture. The crystal margins of the alkali feldspar are very often quite irregular showing signs of recrystallization and graphic intergrowth. Inclusions of plagioclase and quartz crystals in the alkali feldspar are very common often and seem to be randomly distributed. The inclusions of euhedral plagioclase can be regularly oriented parallel to the crystal faces of the host K-feldspar (Fig.3.2C). Quartz is found, always as rounded grains, closer to the crystal margins. Biotite is occasionally present as inclusions (Fig.3.2B-C). The plagioclase inclusions are all altered. Graphic intergrowths are more common than in the granodiorites.

Plagioclase is present in similar amounts to the alkali feldspar, but is seen as small subhedral crystals varying in size from 0.1 to 7mm, though they can be occasionally anhedral and even interstitial. They range compositionally from mid-andesine to oligoclase (An41-23) and are chemically zoned, becoming more sodium-rich towards the margins. Rim compositions range from An31-23, while the core values overlap a

little from An41-29. In the biotite granite sheets, as well as in the pluton as a whole, plagioclase forms occasional phenocrysts, but is always less abundant than alkali feldspar (alkali:plagioclase ratio of 4:1). They all have highly sericitized cores, which on occasion follow the twinning planes or zones. The sericite (muscovite) also forms coarser flakes dispersed randomly within the crystals. Fine lamellar twinning is very common in the plagioclase while concentric zoning is only occasionally seen. Myrmekitic intergrowths and antiperthitic textures are also seen throughout the different granitic types.

Quartz is far more abundant in the biotite granite than in the granodiorite. Its form ranges from large subhedral to euhedral grains upto 3mm across with high quartz bipyramid habit to patches of finer crystals and individual anhedral grains. They occur within zoned plagioclase and alkali feldspar, close to their respective margins as rounded grains. Quartz appears in concentrated zones in plagioclase and alkali feldspar crystals (along old euhedral crystal margins), where it is thought to have nucleated simultaneously as the feldspar grew. Subsequently these were buried by the continual growth of the feldspar.

The most common ferromagnesian mineral present is biotite (max. 15%), occurring as fine grained lathes. Alteration of the biotite to chlorite occurs with the release of needles of rutile. Very occasional muscovites have been found. Hornblende is only present in very minor amounts as grains of 0.5mm in size. Alteration is common throughout the the grains and where it is nearly complete, only the original euhedral shape is evidence of hornblende being once present.

Rare accessory minerals include skeletal sphenes, apatites and rounded zircons.

3.3 PETROGRAPHY of the Sheets (ctG on Sheet 52)

Texturally these sheets seem to be distinct from the biotite granite sheets (mentioned above). They are medium to fine grained porphyritic acid igneous intrusions, consisting of both alkali feldspar and plagioclase feldspar, quartz, hornblende and biotite. The modes fall on the granite - adamellite border of Streckeisen's classification, although they are called granodiorite on the BGS sheet. Modally the sheets vary internally with variable amounts of feldspar phenocrysts. The sheets have a high mafic colour index, which is more than the granodiorite body, as the minerals are finely disseminated throughout the groundmass as well as being present as large individual crystals. The combination of high quartz and a high colour index is an indication of a hybrid origin.

Table 3.3 MODES REPRESENTATIVE OF THE RANGE OF THE SHEETS

Plagioclase	17.5	40.0
Alkali feldspar	33.1	27.2
Quartz	31.2	19.4
Mafics + Accessory	18.0	13.4
Q	38.1	22.4
A	40.5	31.4
P	21.4	46.2

Conspicuous phenocrysts of both feldspars are present (Fig 3.3A-B-C).

However the modal phenocryst abundance does vary from sheet to sheet from 40% to less than 5%. Euhedral pink alkali feldspars (max. length 35mm) are seen (Plate 2.9B) with fine grained inclusions of

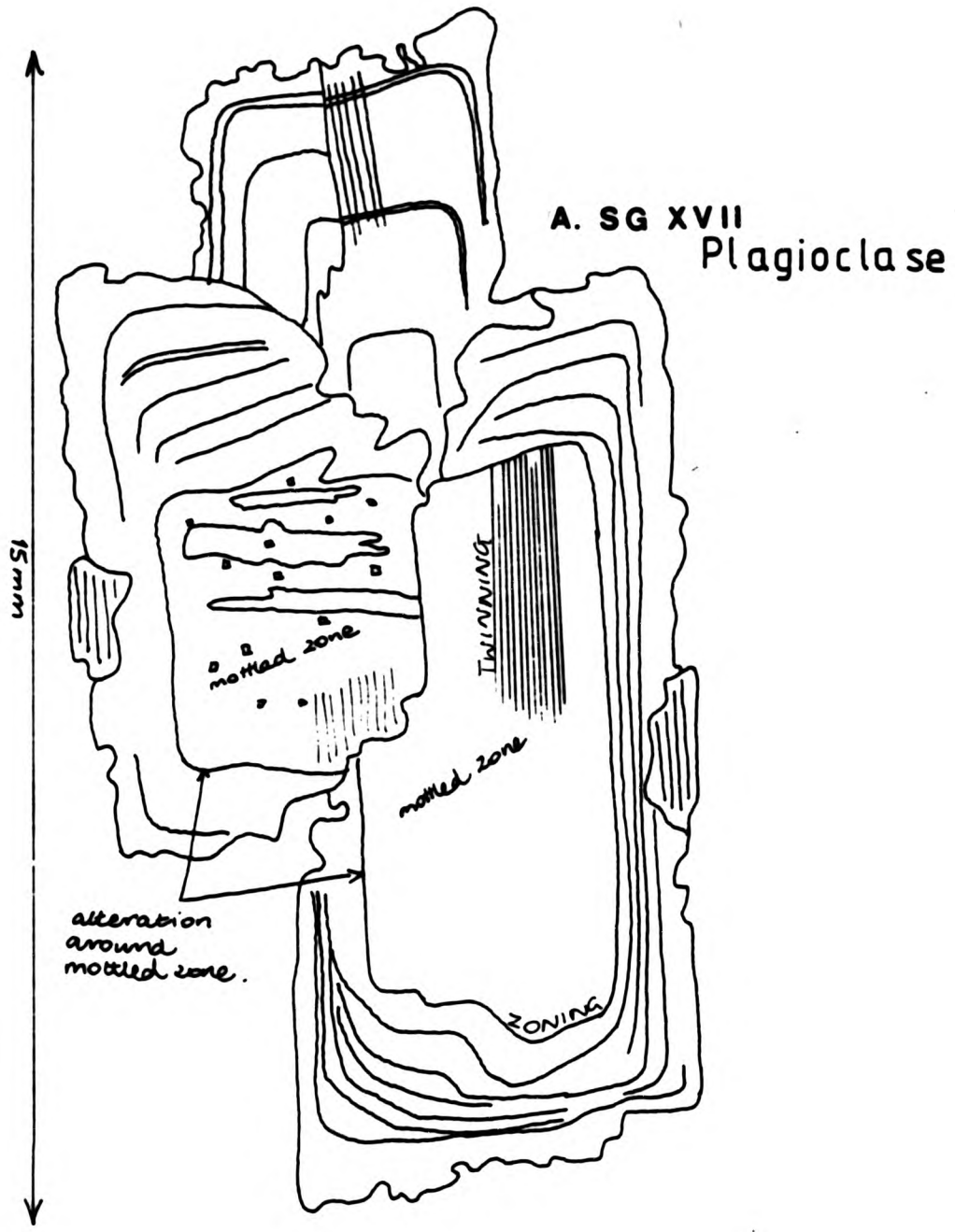

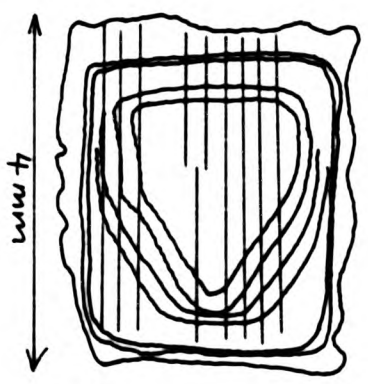

B. SG X
Plagioclase

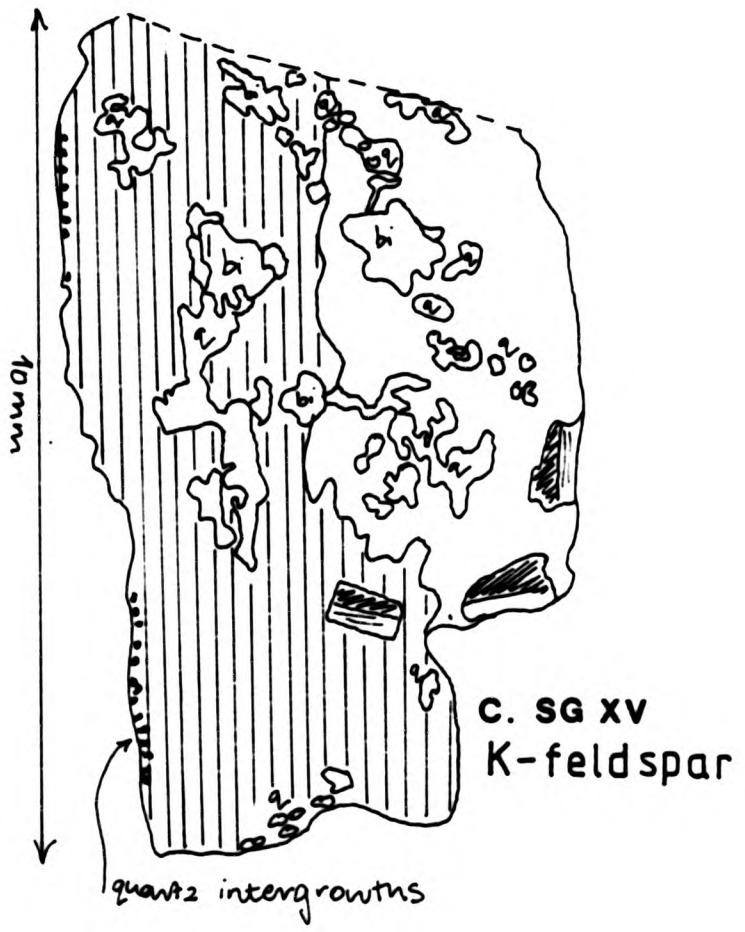

Fig. 3·3 Details of host rock feldspars

ferromagnesian minerals such as biotite and hornblende. The central megacryst in Plate 2.9B shows a rounded inclusion-rich core. In some cases the alkali feldspar shows a jacket of plagioclase around it as seen in the sheet at location D (Fig.1.2). Plagioclase does not form such large phenocrysts (max. 15mm, Fig.3.3). Compositionally they are oligoclase to andesine An22-38. It appears in two forms:

- Euhedral white crystals, which have inclusions of ferromagnesians.
- Subhedral clear crystals showing good twinning. These crystals range in size from 5 to 10mm. Their form appears to be only rounding of the original crystal which suggests that they could be xenocrysts.

Both alkali and plagioclase feldspars are found in the fine grained matrix, where they form subhedral to euhedral crystals, showing good normal concentric zoning in the plagioclase.

Quartz occurs as rounded bi-pyramid phenocrysts, reaching 4 mm across and many are surrounded by ferromagnesian minerals as a jacket. It is also present interstitially in the matrix as tiny subhedral to anhedral crystals showing signs of a recrystallized granoblastic texture, which is not very abundant.

The ferromagnesian minerals are biotite and hornblende. They are both found in a number of different forms:

- As fine (less than 1mm) crystals disseminated throughout the matrix.
- As coarse, greater than 2 mm crystals, locally as phenocrysts,

in which hornblende occurs in primatic form and biotite as books.

- As rounded aggregates of both minerals reaching 7 mm across.

3.4 MINERAL CHEMISTRY

The main phases of the host rocks were analyzed by the electron microprobe and will be discussed together. The total number of grains analyzed is 470.

3.4.1 Plagioclase

The host rocks of Strontian have a low bulk rock MgO value, on average 2.5% (discussed in chapter 4), and their plagioclase falls into an overall range of An22-42 mid-oligoclase to mid andesine. The granodiorites range from An22-43, the biotite granite An23-41 and the porphyry sheets from An 22-38. There is in fact a very small range of maximum An values between the 3 groups and this could suggest very similar crystallizing conditions for the pluton. There is an extreme core value of An63 in the granite, which suggests it could be a xenocryst from mixing. The range of compositions determined has been plotted onto the K-Na-Ca (atomic percent) triangle to display the gross variation in plagioclase chemistry (Fig.3.4A). The diagram clearly shows the wide range of compositions for all the rock types.

In a single sample similar crystals may have compositions that vary greatly from core to rim eg. An38-22 and will display limited normal zoning with cores typically of An41-36; intermediate An36-32 and rims of An32-22. In larger phenocrysts oscillatory zoning of core

An35-An39-rim An30 can occur but it is not very common. Reverse zoned crystals An36-An37-An42 are also rare, but can occur in samples with normal zoning. The later ctG sheets show reverse and oscillatory zoning more often than the granodiorites; while the biotite granite shows normal zoning only. The K20 levels are very low in the plagioclase range from 0.16 to 0.4% throughout the host rock types and could be the result of antiperthitic textures.

Table 3.4 REPRESENTATIVE FELDSPAR ANALYSES FROM THE STRONTIAN HOST ROCKS

	SGIX TGD 8Rim	SGIX TGD 9Mid	SGX TGD 16	SG49 PGD 15	SGXIII TGD 1 Rim
SiO2	65.86	63.05	61.49	62.16	64.62
TiO2	-	-	-	-	-
Al2O3	22.09	22.91	23.69	23.36	18.71
FeO*	0.17	0.15	0.14	0.15	0.08
MgO	0.01	0.01	-	-	0.01
CaO	3.45	4.46	4.86	4.61	0.03
Na2O	9.62	8.79	8.78	8.90	1.59
K2O	0.34	0.41	0.30	0.39	14.43
BaO	0.06	0.07	0.05	0.02	1.02
Total	101.60	99.86	99.33	99.60	100.51
Ab	71.8	64.4	63.0	63.9	9.9
Or	2.4	3.0	2.2	2.8	89.9
An	25.8	32.6	34.8	33.3	0.2
	Olig.	Ande.	Ande.	Ande.	Orth.

When anorthite content is plotted against bulk rock MgO (Fig.3.5) it does not show a trend. The An content of the host rocks and xenoliths are very similar with comparable MgO content, with the granites having a more limited range which is more sodic. There is no positive or negative correlation between the two parameters as in the Skaergaard intrusion (Wager & Brown 1968), which shows a positive correlation throughout the range of rock types. The Ba content is greater in the alkali feldspars than the plagioclase and reflects the preference of substitution of Ba in the former. The plagioclase Ba

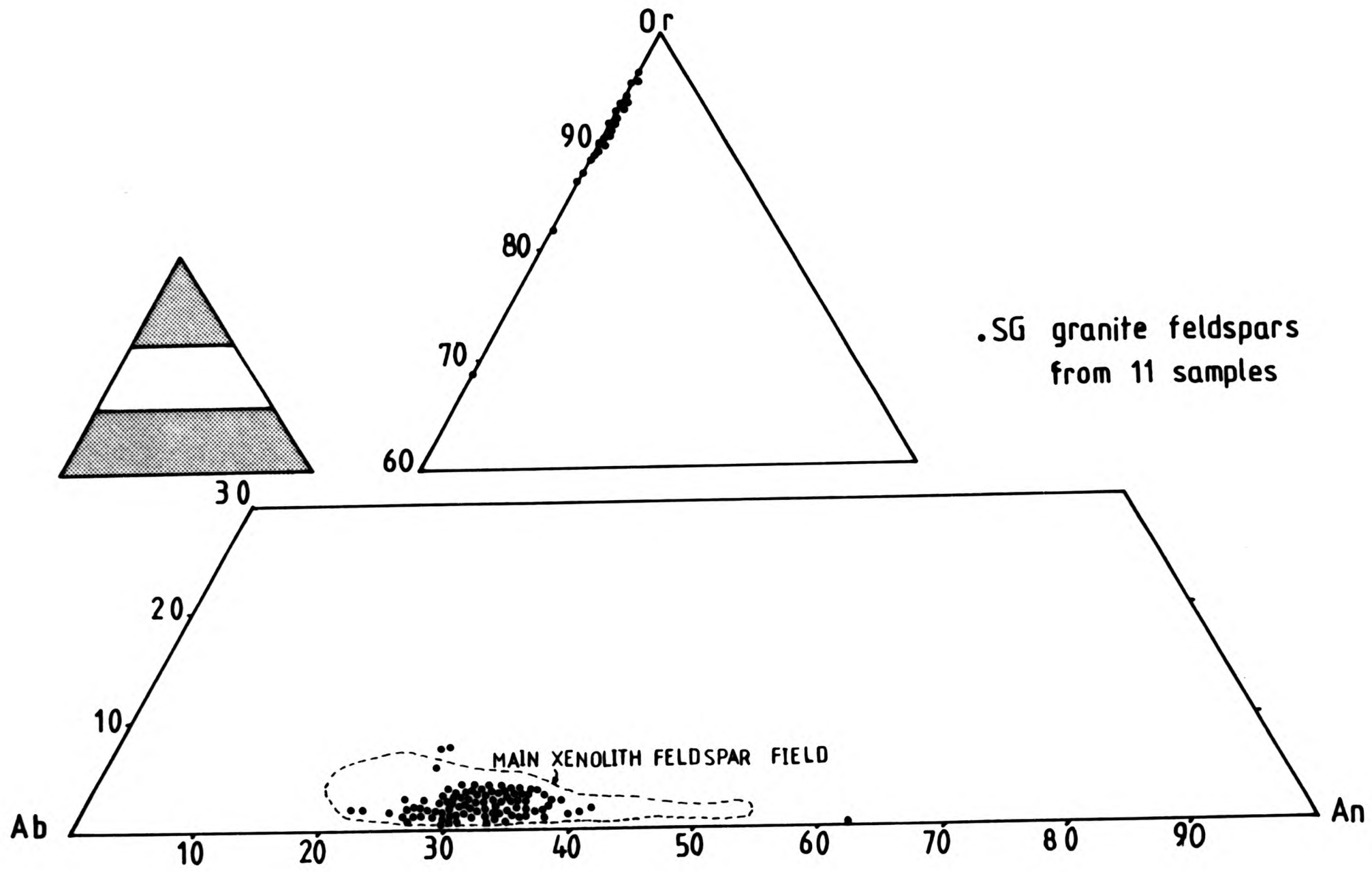

Fig. 3·4A Host rock feldspar compositions plotted onto the system Or - Ab - An.

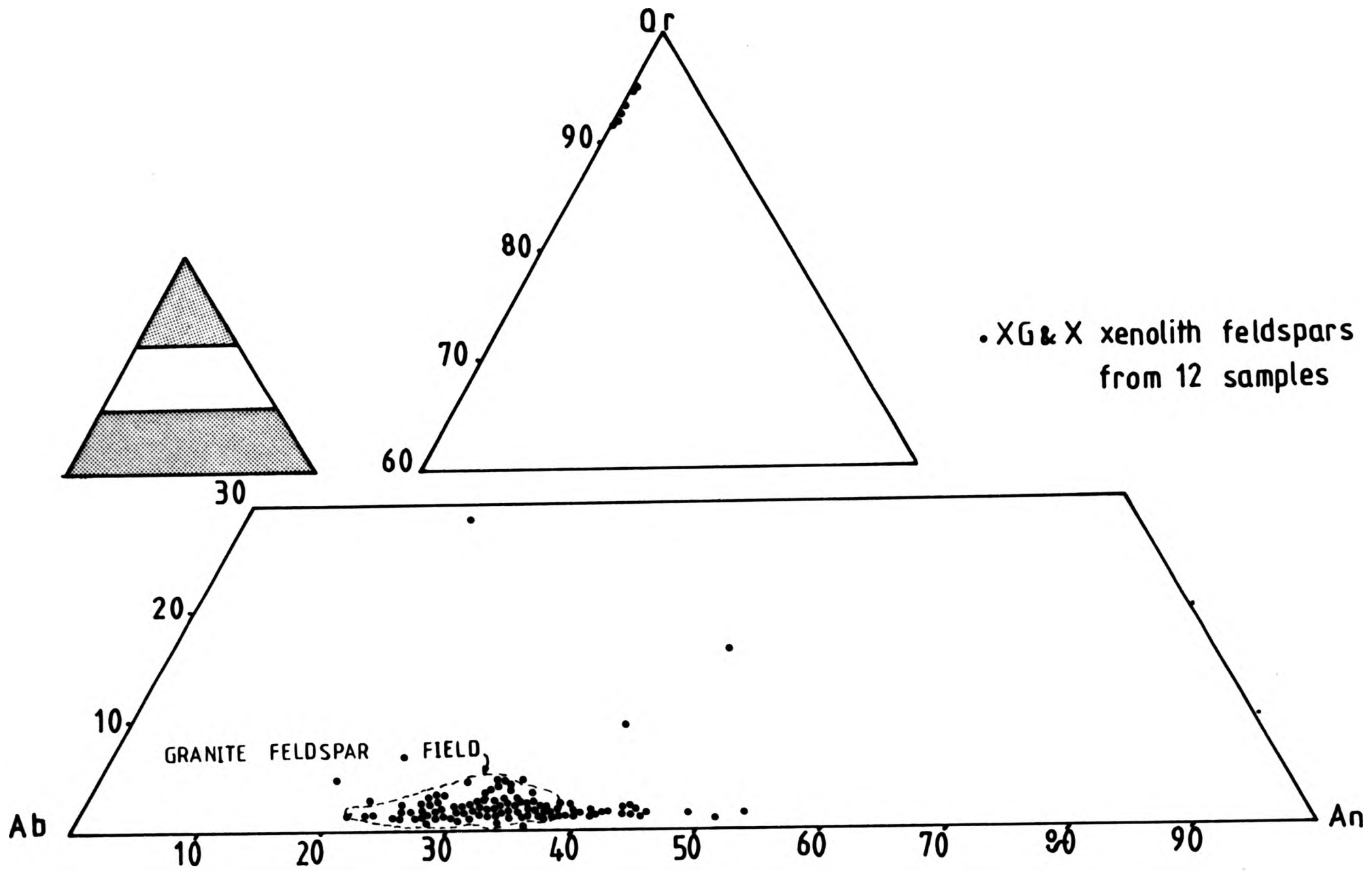

Fig. 3·4B Xenolith feldspar compositions plotted onto the system Or - Ab - An.

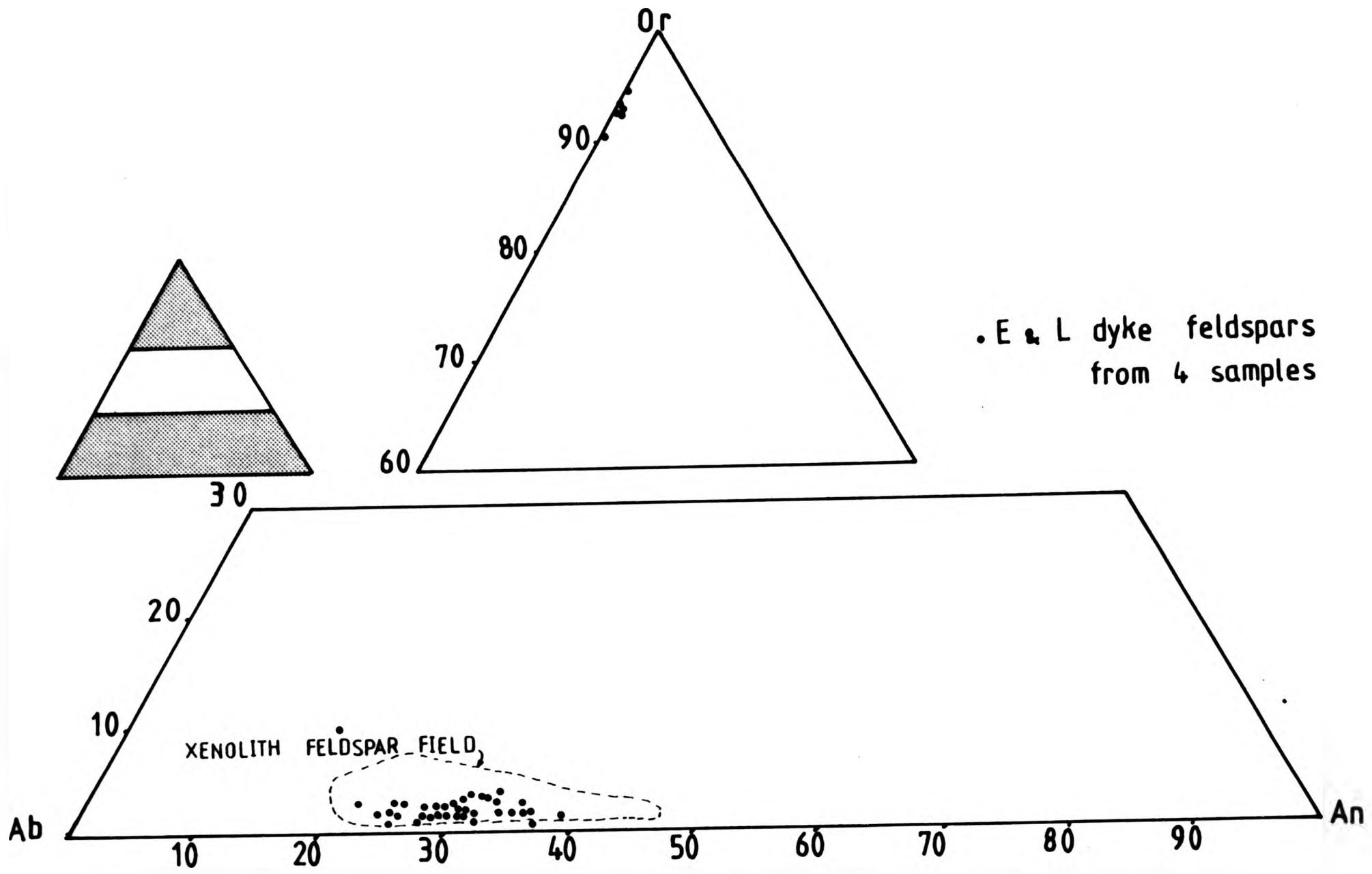

Fig. 3·4C Dyke feldspar compositions plotted onto the system Or - Ab - An.

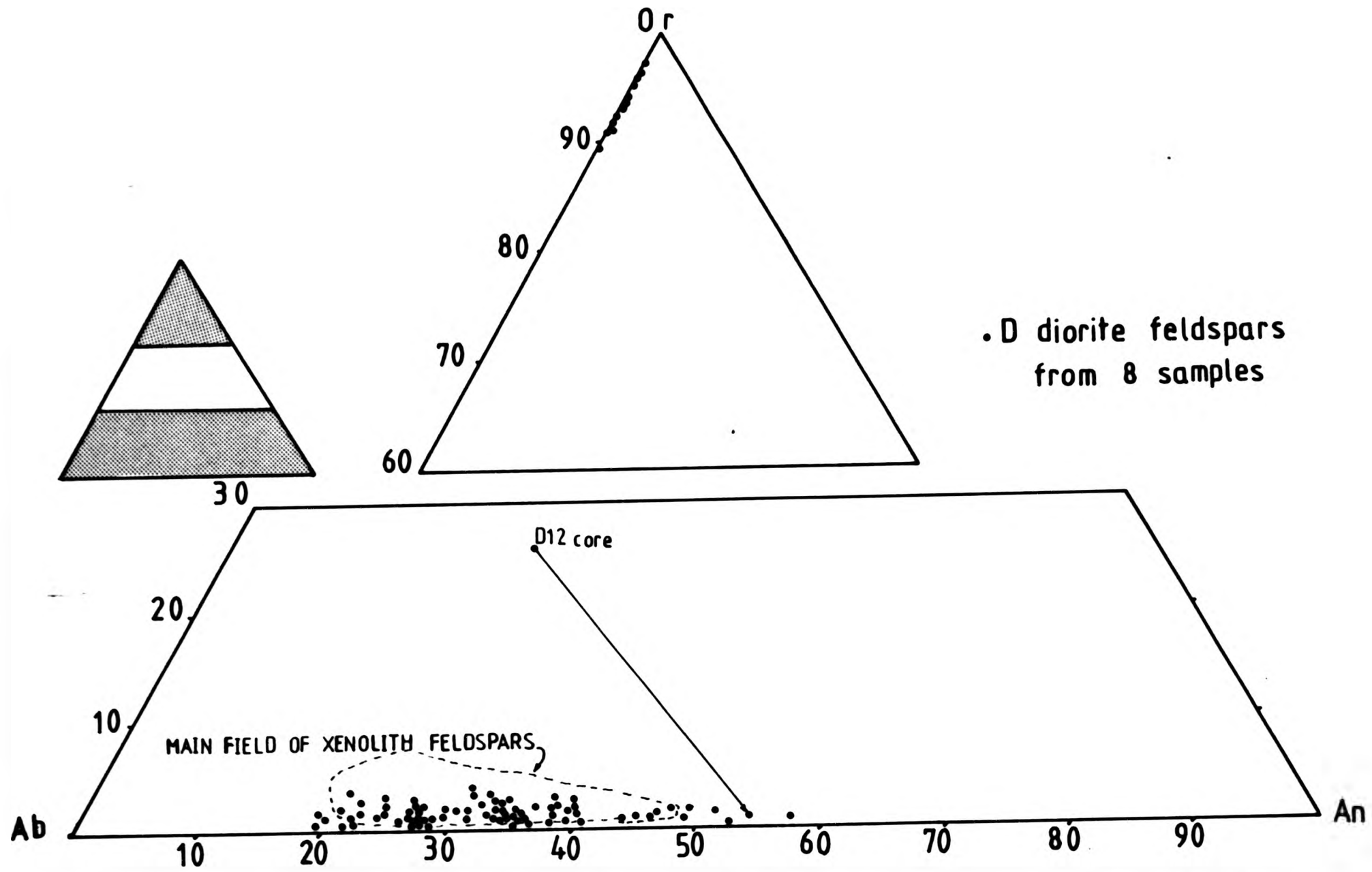

Fig. 3·4 D Diorite feldspar compositions plotted onto the system Or - Ab - An.

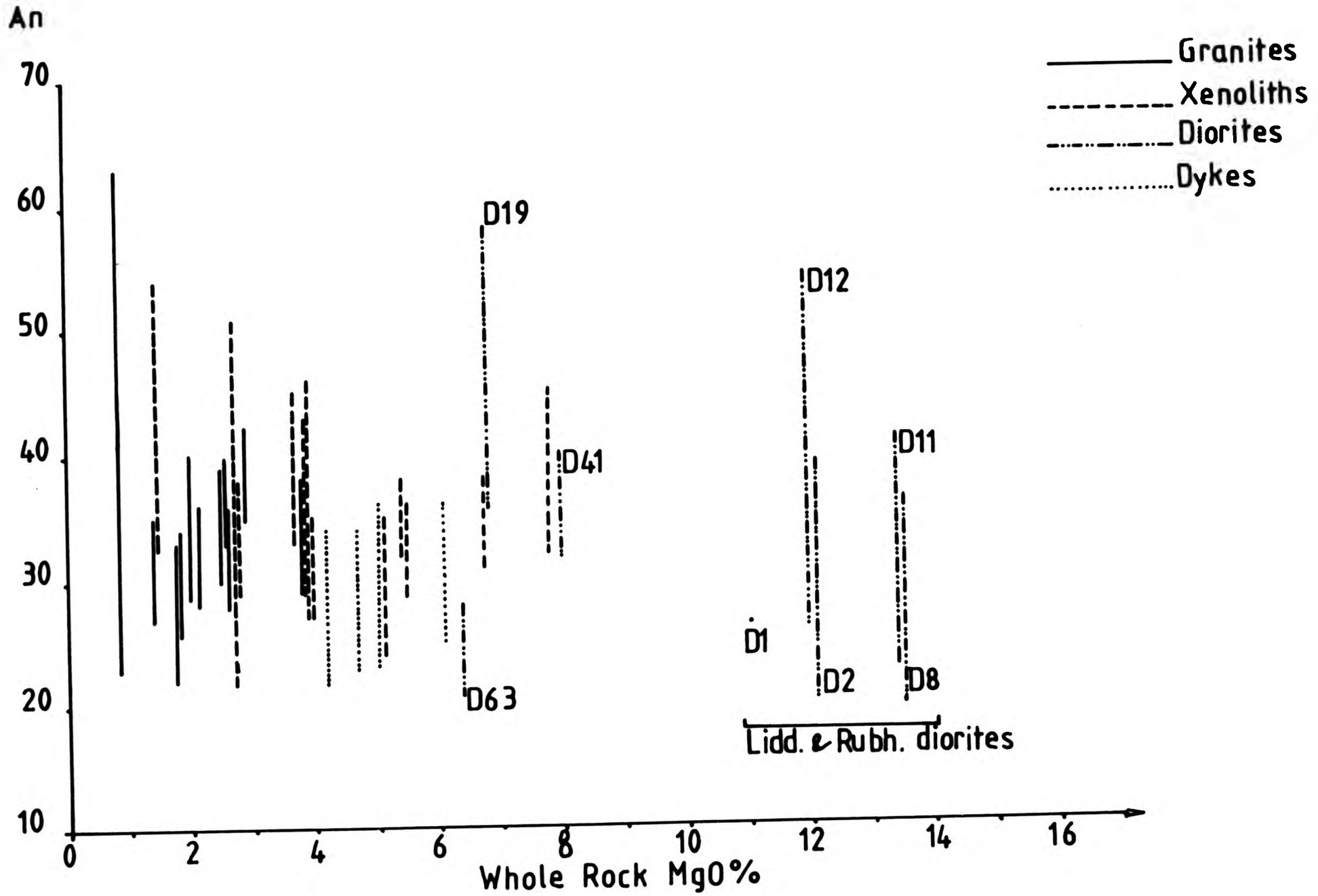

Fig. 3·5 Anorthite content of plagioclase plotted against whole rock MgO for the Strontian Complex.

content of Strontian is similar to that of composite dykes on Iona (Rock & Hunter 1987), while alkali feldspars are similar to those quoted by Deer et al (1982).

Alkali feldspar in the granite and granodiorite hosts have compositions of Ab5-13 Or95-87 An0, are very pure and classed as orthoclase. There are some signs of unmixing ie limited perthite. This K-rich and Ca-depleted nature of the alkali feldspars may suggest a subsolidus equilibration (Barnes 1983). Upto 10% exsolution lamellae have been observed in both the alkali and plagioclase feldspars. This allows little shift in the feldspar composition to the "original" composition. This could suggest low temperature crystallization controlled by a wide solvus. Also there is a small amount of exsolution in the respective feldspars and so the original K-feldspar was Na-poor and plagioclase had slightly higher Or values though still low overall.

3.4.2 Amphibole

When classifying the amphiboles of the host rocks according to Leake (Table 1.3), magnesio-hornblende and edenite are by far the most common found, with occasional actinolitic hornblende and one actinolite. Many were on the border of the two divisions and only the Na+K total could separate them.

They are dark green in colour in the granodiorites and biotite granite and show relatively uniform compositions throughout . Each rock sample may contain more than one habit of amphibole. The site of the analysis may vary from individual crystals to clusters of small crystals but the result may give the same amphibole type.

Table 3.5 REPRESENTATIVE ANALYSES OF AMPHIBOLES

	SGXIII TGD 5Rim	G24 TGD 2Core	G24 TGD 4Core	SG93 TGD 1Mid	SGVIII Late 3Mid
SiO2	46.82	45.80	46.83	52.90	50.59
TiO2	1.09	1.00	0.83	0.29	0.48
Al2O3	6.99	7.79	6.74	3.06	4.20
FeO*	14.28	15.19	14.52	9.87	13.01
MgO	13.37	12.22	12.95	17.29	14.65
MnO	0.36	0.41	0.41	0.26	0.35
CaO	11.71	11.46	11.86	12.57	12.13
Na2O	1.47	1.37	1.08	0.43	0.82
K2O	0.69	0.83	0.67	0.19	0.34
Total	96.83	96.11	95.93	96.89	96.61
Si	6.971	6.916	7.048	7.605	7.445
Aliv	1.029	1.084	0.952	0.395	0.555
Alvi	0.201	0.304	0.245	0.125	0.175
Ti	0.125	0.114	0.095	0.035	0.055
Fe2+	1.781	1.920	1.829	1.184	1.600
Mn	0.044	0.054	0.052	0.034	0.044
Mg	2.971	2.751	2.906	3.707	3.208
Ca	1.879	1.856	1.913	1.936	1.090
Na	0.429	0.403	0.317	0.121	0.229
K	0.125	0.162	0.130	0.034	0.070
	Eden.	Eden.	Mag-H.	Actin.	Act-H.

There is a corresponding increase in the amount of silica present from the edenite to actinolite amphiboles 6.8 to 7.6 atoms per formula unit, which is accompanied by a decrease in Aliv substitution in the T site (1.23 to 0.65).

The Mg/Mg+Fe ratio varies from 0.54 to 0.63 in the edenites and 0.57 to 0.67 in the magnesio hornblendes to over 0.70 in the actinolitic hornblendes and actinolites. Mg is also known to be substituted by Ti and Fe. This is noted in a slight zoning from core to rim in the amphiboles. It is common for MgO to increase towards the rim and is seen in edenites and magnesio-hornblendes, though the reverse has also been noted. Fig.3.6 shows the range of Strontian hornblendes plotted on the Ca-Mg-Fe triangle with tie lines for their co-exiting biotites. However the MgO content from core to rim has only limited

changes in the Strontian amphiboles:

eg. SGIX core 13.04% G24 core 13.05%
rim 13.5% rim 12.47%

Fig.6.3 shows quite a wide range of Mg/Mg+Fe ratios for the amphiboles for a smaller range of bulk rock ratio of 0.364 to 0.45.

The extensive substitution of cations in the amphibole lattice is considered to be controlled by a number of physical and chemical parameters. Both Binns (1965) and Henderson (1966) have demonstrated that the colour of calcic amphiboles is a function of the TiO2 content. The analyzed samples from Strontian all have low TiO2 and show a correlation with the colour as all have variable shades of green. This is a feature also observed in primary amphiboles from the Glenelg-Ratagain Complex (Nicholls 1950).

The TiO2 is relatively low in the actinolites. A plot of Ti amph. vs Aliv amph. shows a positive correlation of the granitic amphiboles (Fig.10.2). The rims of the amphiboles tending to have lower Ti and Aliv contents, so reflecting lower temperatures.

Total Al data can be used to estimate the pressure of solidification of calc-alkaline plutons to +/- 1kbar in the pressure range of 2-8 kbars (Hollister et al 1987), in rocks which have a common magmatic mineral assemblage (plagioclase, hornblende, biotite, alkali feldspar, quartz, sphene, magnetite or ilmenite +/- epidote) and probably crystallized at similar temperatures (Hammarstrom & Zen 1986; Hollister et al 1987). The Strontian complex possesses the same assemblage and the amphiboles have been calculated on the basis

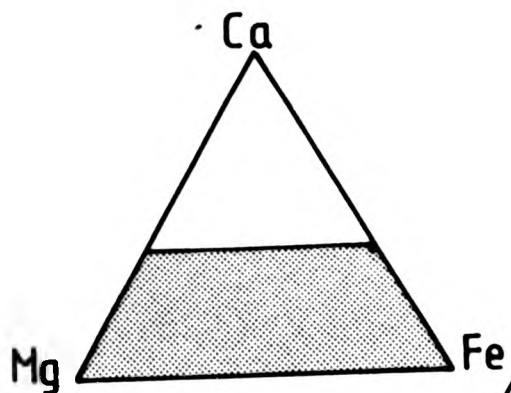

• Hornblende & Biotite analyses from the host rocks of Strontian.
Tie lines link co-existing phases.

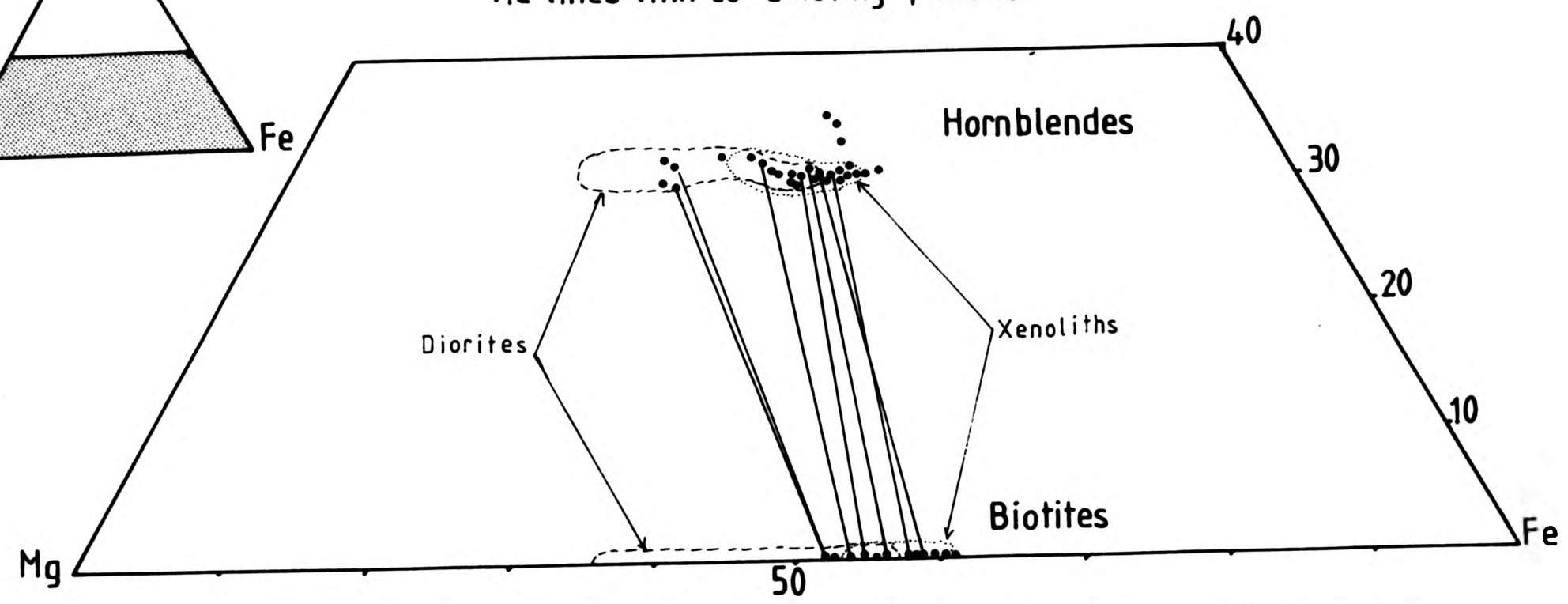

Fig. 3·6 Hornblende and biotite plotted on the Ca-Mg-Fe triangle (atomic %).

of 23 oxygen atoms.

Table 3.6 PRESSURES IN AMPHIBOLES

Total Al in amphibole	Pressure in literature*	P. from regression equation 1	2
SGIII TGD 1.1897-1.4623	2 - 3	2.05-3.43	1.8-2.73
SGIX TGD 1.107 -1.735	1.7 - 5	1.65-4.81	1.56-3.84
SGXIII TGD 0.9667-1.2942	1 - 2	0.94-2.56	1.18-2.13
SGVII Late 0.9543-1.6404	1 - 4.2	0.88-4.33	1.16-4.43
SGVIII Late 0.7039-1.4996	<1 - 3.5	0.38-3.62	0.63-2.87
SGX Late 0.8930-1.3020	<1 - 2	0.57-2.63	1.01-2.16
SGXXVI TGD 0.905-1.167	<1 - 2	0.63-1.95	1.04-1.73
SG49 PGD 0.9815-1.0911	1 - 1.5	1.02-1.57	1.22-1.51
SG93 TGD 0.3237-1.3462	<1 - 3	-2.29-2.85	0.13-2.31
G24 TGD 1.196-1.915	2 - 5.5	2.09-5.71	1.82-4.69

* Pressures estimated from Fig.1 from Hollister et al 1987.

Table 3.6 shows the ranges of total Al for all the analyzed samples and the predicted pressure (from the plot of Hollister et al 1987). Using the regression equations relating pressure and total Al in the hornblendes (Hammarstrom & Zen 1986), columns 1 and 2 of Table 3.6 have been calculated:

- Equation 1 $Y = A + BX$
- Equation 2 $Y = AX^B$

where:

A = -3.92 (eq. 1) and 1.27 (eq. 2)

B = 5.03 (eq. 1) and 2.01 (eq. 2)

X = total Al in hornblende

Y = pressure in kilobars

The tonalitic and porphyritic granodiorite amphiboles give an overall range of 5kb to less than 1 kb, and this is equivalent to a depth of between 15 to 3km. While the later granitic sheets also give crystallization depths of between 12 to 3km. These results will be discussed together with the amphibole data for the other rock types in chapter 12. However the maximum end of the range falls around the calculated cordierite pressure estimates of Tyler & Ashworth (1982).

In general edenite has slightly higher K2O core values 0.84 -1.23% than magnesio-hornblende 0.64 - 0.78%. K2O levels in edenites can either increase towards the rims or decrease eg: core 0.73% rim 0.66% K2O and core 0.62% to rim 0.72% K2O. These values fall within the total range of K2O of 0.12 - 1.23%.

Sodium can also show this variation of slight increase or decrease from core to rim, within the total range of 0.82 -1.61%, for example:

- Core 1.36% to rim 1.5% Na2O
- Core 1.43% to rim 1.28% Na2O.

These features are not peculiar to one type of amphibole. Fig.10.4 plots the (Na+K) vs total Aliv and shows the drop in alkalis from core to rim in the green hornblendes. This again indicates the

control of temperature and magma composition over the primary magmatic hornblendes. The composition of cpx essentially reflects an "anhydrous" actinolitic amphibole of which there are occasional analyses in the tonalitic granodiorite.

3.4.3 Biotite

Biotite is the only mica present in the Strontian host rocks, with a Mg:Fe ratio is less than 2:1. It appears as dark brown crystals and is zoned chemically with respect to Ti and Fe. Biotite totals shown in Table 3.7 are low as volatiles are not included. Fluorine data ia available for some biotites (Appendix C.3). They can have cores of upto 3.2% TiO2 and 17.0% FeO*, while the rims have 1.7% TiO2 and 19.4% FeO*. There seems to be little variation in MgO from core to rim of 12.6 to 13.3%. These levels are quite similar to those from the Sierra Nevada Batholith, where MgO in biotites from rocks containing hornblende range from 10.7 to 13.1%. (Dodge et al 1969).

Table 3.7 REPRESENTATIVE ANALYSES OF BIOTITES

	G24 TGD 1Core	SGIX TGD 2Core	SGXIII TGD 3Core	SGXXVI TGD 1Rim
SiO2	37.00	37.13	37.57	36.84
TiO2	3.18	3.45	2.64	2.81
Al2O3	14.42	13.37	14.08	13.85
FeO*	17.07	17.47	17.52	18.89
MgO	12.66	13.11	12.97	12.72
MnO	0.25	0.24	0.25	0.35
Na2O	0.09	0.10	0.09	0.13
K2O	9.94	9.86	9.79	9.23
Total	94.61	94.73	94.91	94.82
Si	5.906	5.938	5.978	5.906
Aliv	2.094	2.062	2.022	2.094
Alvi	0.621	0.460	0.620	0.524
Ti	0.383	0.415	0.317	0.340
Fe2+	2.279	2.336	2.332	2.533
Mn	0.035	0.033	0.034	0.049
Mg	3.012	3.124	3.076	3.038
Na	0.031	0.033	0.029	0.042
K	2·025	2·012	1·988	1·889

The biotite TiO2 content is considerably higher than that of its associated amphibole and its host rock, being in some cases twice the amount. Albuquerque (1973) gives biotite TiO2 levels of 2.61 - 3.48%, while Dodge et al (1969) has TiO2 ranging from 1.7 - 3.1%, reaching 4.2% in rocks with hornblende and pyroxene. However in those samples that possess sphene, and in some cases also titaniferous magnetite, the TiO2 in the biotites is not substantially lower. It has been reported in the literature by Albuquerque (1973) that TiO2 is lower in biotites coexisting with sphene. This is not the case in Strontian. There is no variation in TiO2 of the biotite and sphene between the granodiorite and biotite granite. However the amount of biotite increases from the granodiorite to the biotite granite. Znamenskii et al (1962) report that as the amount of biotite in the rock increases, the amount of TiO2 in the biotite increases with a decrease in the sphene content. This has also been noted in the Strontian complex.

The MgO/MgO+FeO* ratios range from 0.434 to 0.480 for the granodiorites and 0.398 to 0.439 for the biotite granite and later sheets. This ratio is less than that for the diorites and so plot separately on the Ca-Mg-Fe diagram (Fig 3.6). So there is a general decrease in the Mg content and increase in Fe content with increasing acidity.

Fluorine can subsitute for OH- in the biotite lattice (Deer et al 1982). Between 70 to 90% of the F in fluorite-free granitoid rocks, is contained in biotite (Grabezhev et al 1979). In Strontian biotites F varies from 0.17 to 0.57% F for the granodiorites and

later sheets and 0.25 to 1.17% F for the biotite granite.

3.4.4 Sphene

Sphene is the most common accessory mineral present in the Strontian complex. It can reach several millimetres in size and stands out clearly in hand specimen as brown euhedral crystals. It is commonly unzoned and is typically 36.0% TiO2, 29.0% SiO2 and 28.0% CaO. Total iron varies from 1.0 to 1.8% suggesting some substitution of Fe for Ti.

Sphenes are well known to contain rare earth elements (REE). During probing several sphenes were scanned to show the wavelength peaks for the different elements and were found to contain 1-2% REE. Light REE enrichment of La and Ce especially was found to be the case. Only 2 sphenes were analyzed for REE and both showed REE-rich patterns. The REE contents of sphene and amphibole are considered in chapter 4 (4.4.1).

3.4.5 Apatite

Apatite crystals across the whole complex are unzoned fluor-apatites as classified by Deer et al (1982). The fluorine levels are consistent, high and range from 3.5% to 4.6% F.

3.4.6 Oxide Minerals

Analyzed samples from the granodiorite and biotite granite include magnetite, titaniferous-magnetite and occasionally haematite pseudomorphs of magnetite.

Magnetite and titaniferous magnetite occur in the granitic samples either as euhedral grains, interstitially or in the amphibole aggregates. The titaniferous magnetite is more common than the Ti-free magnetite. The former is often found together with sphene. The TiO2 content of Ti-magnetite varies from 10-21% and there appears to be no correlation with the bulk rock titanium content. Magnetites have low levels of chromium 0.1-0.2%.

3.5 DISCUSSION

From the field evidence and now petrography, it is seen that the Strontian complex is a series of rocks ranging from the tonalitic granodiorite to the quartz-rich biotite granite of Eignaig. Between the two, there is a large time gap as seen by the isotope data.

The granodiorite and biotite granite suites are modally distinct. Field and modal data suggest a trend from early mainly plagioclase and mafics crystallization with alkali feldspar towards late quartz and alkali feldspar; while normative data (Fig 3.7) define a trend from plagioclase towards quartz and alkali feldspar. The modal and norm trends may indicate both restite separation and fractional crystallization, which may reflect the scatter in the tonalitic granodiorite and the mismatch with the porphyritic granodiorite. The core of the biotite granite is indeed enriched in alkali feldspar and quartz and the Moine sheet is too. Modal variation is much greater than compositional variation of the minerals.

In general the gross igneous texture has been preserved in the form of broadly euhedral plagioclase, K-feldspar in the porphyritic

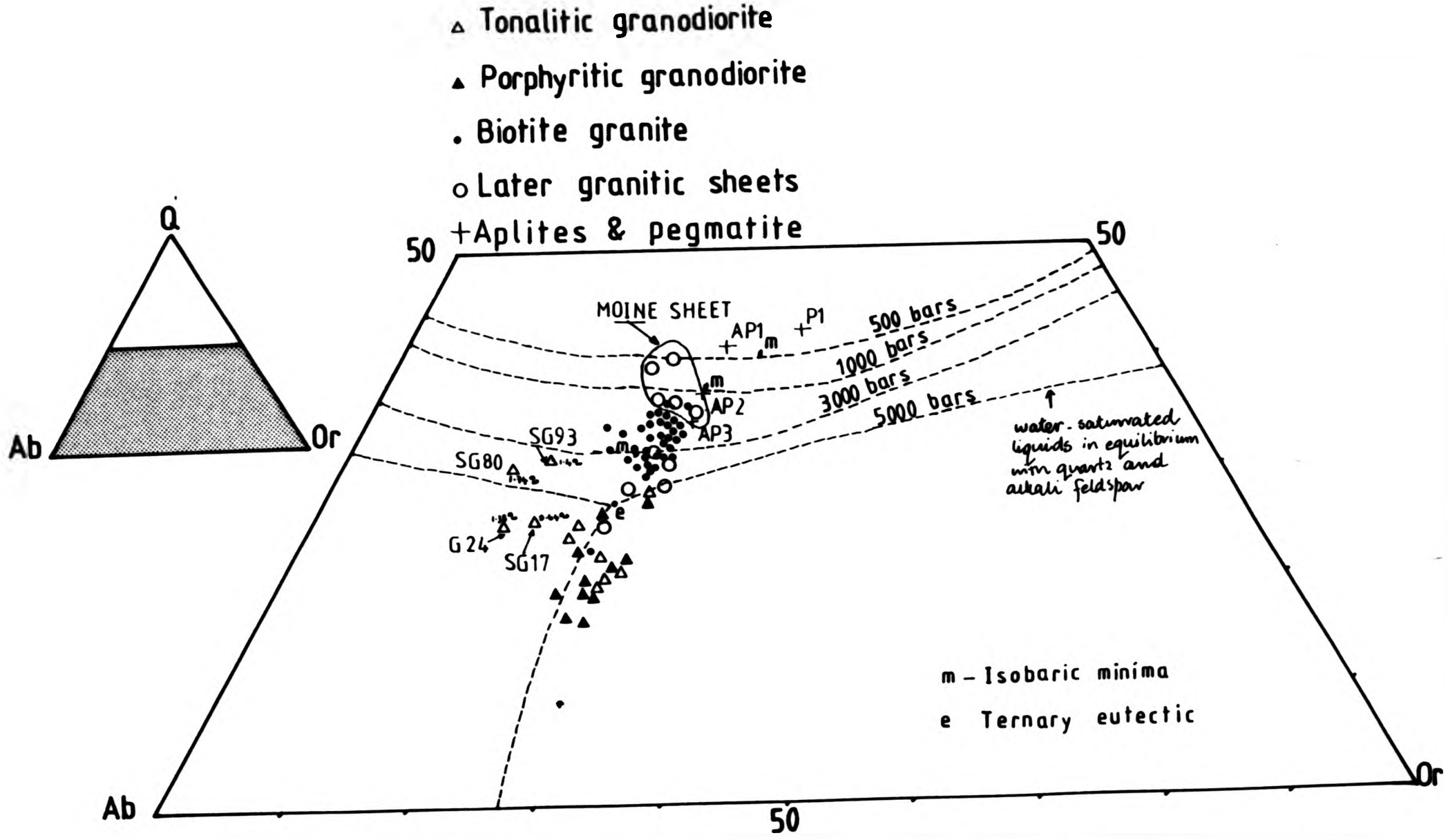

Fig. 3·7 Q - Ab - Or projection of normative data for Strontian.

granodiorite and amphibole prisms. However there is evidence of recrystallization and re-equilibration. This is seen in the leucocratic portion as strained quartz and polygonal grains, perthite/antiperthite, inversion of alkali feldspar to microcline and myrmekite. While in the mafic portion it is the complex aggregates of amphibole and biotite and the rare partially replaced pyroxenes.

The preservation of primary mineral compositions is also varied. Plagioclase has the largest compositional range. The granodiorites have a higher modal plagioclase content than the biotite granite. The zonal patterns of albite-anorthite are still preserved, but present Or contents are lower as a result of the antiperthitic exsolution. The plagioclase ranges of the granodiorites and biotite granite overlap considerably, but are not likely to be the result of simple fractionation. The range of core compositions is very similar for all the groups: An33-37 tonalitic granodiorite; An29-32 porphyritic granodiorite; An27-41 (63) biotite granite and An29-38 sheets. The extreme core value found in the biotite granite suggests that it could be a xenocryst eg. restite material from deeper levels or relics of hybridization with a dioritic magma. The few mottled cores which occur in the granodiorites and sheets, could be interpreted as overgrown spongy resorption residues suggesting magma mixing.

The large solvus produced by plagioclase-alkali feldspar compositions indicates a relatively low temperature equilibration. Restoration of perthite/antiperthite increases the Or in plagioclase and An in alkali feldspar. In Strontian this is not by very much, as relative volumes of exsolution products are small making the calculation of the percentage impossible. Therefore much of this large solvus is a

primary feature.

The preservation of primary mineral compositions in the mafics is poor, with most hornblendes being secondary. Their classification splits the amphiboles artificially for this complex. The Mg- and edenitic - hornblendes form a coherent group regardless of their occurrence ie. single prisms have the same composition as the aggregates and the amphibole-biotite intergrowths. This reflects late magmatic or subsolidus processes, which in turn cannot be separated on the data available. Hornblende textural and compositional variations appear to reflect not only heterogeneity at source, but local differences in conditions during crystallization or subsolidus crystallization.

In general the hornblendes occur in most of the complex. However the amounts do decrease with increasing silica content in the host. This is apparent from the increase in visible quartz in hand specimens. Hornblende is even absent from the biotite granite when SiO2 is over 70%. The presence or absence of hornblendes may be closely related to rock compositions, but their composition is not merely a function of rock composition but differentiation also (Noyes et al 1983). While Deer (1938) noted that the silica content of the hornblendes tends to increase as the rocks become richer in silica. This can also be said to be the case of Strontian.

Tyler & Ashworth (1981) and Ashworth & Tyler (1983) show that the confining pressure of the pluton is around 4.1kb and that the partial water pressure was also high in the aureole. Hydrous mafic mineralogy indicates that the magma was wet, but there is no evidence of it being over saturated. Therefore feldspar crystallization

conditions were somewhere between 3-5kb in a water saturated system. Similar pressures have been calculated by the total Al content of the amphiboles and will be discussed in chapter 12.

The mottled feldspars seen in the granodiorite and later granitic sheets, are not a common feature of andesitic/dacitic volcanism. However what is common is the spongy partly resorbed plagioclase which may form the basis of the mottled plagioclase or subsequent crystallization. Both Anderson (1976) and Eichelberger (1978) report the resorption of sodic plagioclases in quenched conditions; while in Strontian they have had a long slow crystallization history. It is suggested that they grew in more silicic conditions, but underwent mixing. Renewed crystallization would then occur, allowing the growth of new phases appropriate to the new intermediate bulk compositions and temperatures. Overgrowths protect the disequilibrium phases from further reaction (Eichelberger 1978). In Strontian there is also evidence of reverse zoning and together with the mottled feldspars, suggests the possibility of some hybridization within the main granodiorite host.

The ctG sheets are also a source of evidence as to mixing. They display reversed zoning and K-feldspars with plagioclase jackets. There are the mafic jackets surrounding the quartz phenocrysts, which reflect the reaction of the quartz grain with the groundmass. The presence too of quartz and alkali feldspar phenocrysts in the sheets despite the mafic groundmass. All these factors suggest that the sheets are derived from acid magma mixing with a small amount of basic or intermediate magma.

Chapter 4 THE HOST ROCKS OF THE XENOLITHS: GEOCHEMISTRY

4.1 INTRODUCTION

All major element plots for the host rocks are plotted against SiO_2, as it is most suited to display the chemical variation with magmatic evolution and is influenced by all the crystallizing silicate phases. SiO2 was chosen as no totally incompatible elements occur which could have been used and which would not be affected by amphibole and sphene separating. Zr could not be analyzed successfully on the available equipment.

Sabine (1963) reports tonalite, granodiorite and biotite adamellite major element analyses in his 1963 paper with very limited trace element data. Present work expands and supports this data. Only published Strontian isotope data has been used in this study. Pankhurst (1979) reveals that the Strontian isochron plots away from the 415Ma reference isochron and even along its length there is a separation of the granodiorite and biotite granite. This suggests that the magmas of both the granodiorite and biotite granite are quite separate and that they are not simply the result of fractional crystallization.

The tonalitic and porphyritic granodiorite have SiO_2 values from 55% to 69%, while the main biotite granite pluton and associated porphyry sheets all lie at the high silica end of the plots with SiO_2 values of 69 to 75%. The late granodiorite sheets lie on the continuous line of the main granodiorite-granite trend and fall between 66 to 70% SiO_2. Those analyzed are marked on Fig.4.1A & B. Though the petrography of the tonalitic and porphyritic granodiorites are

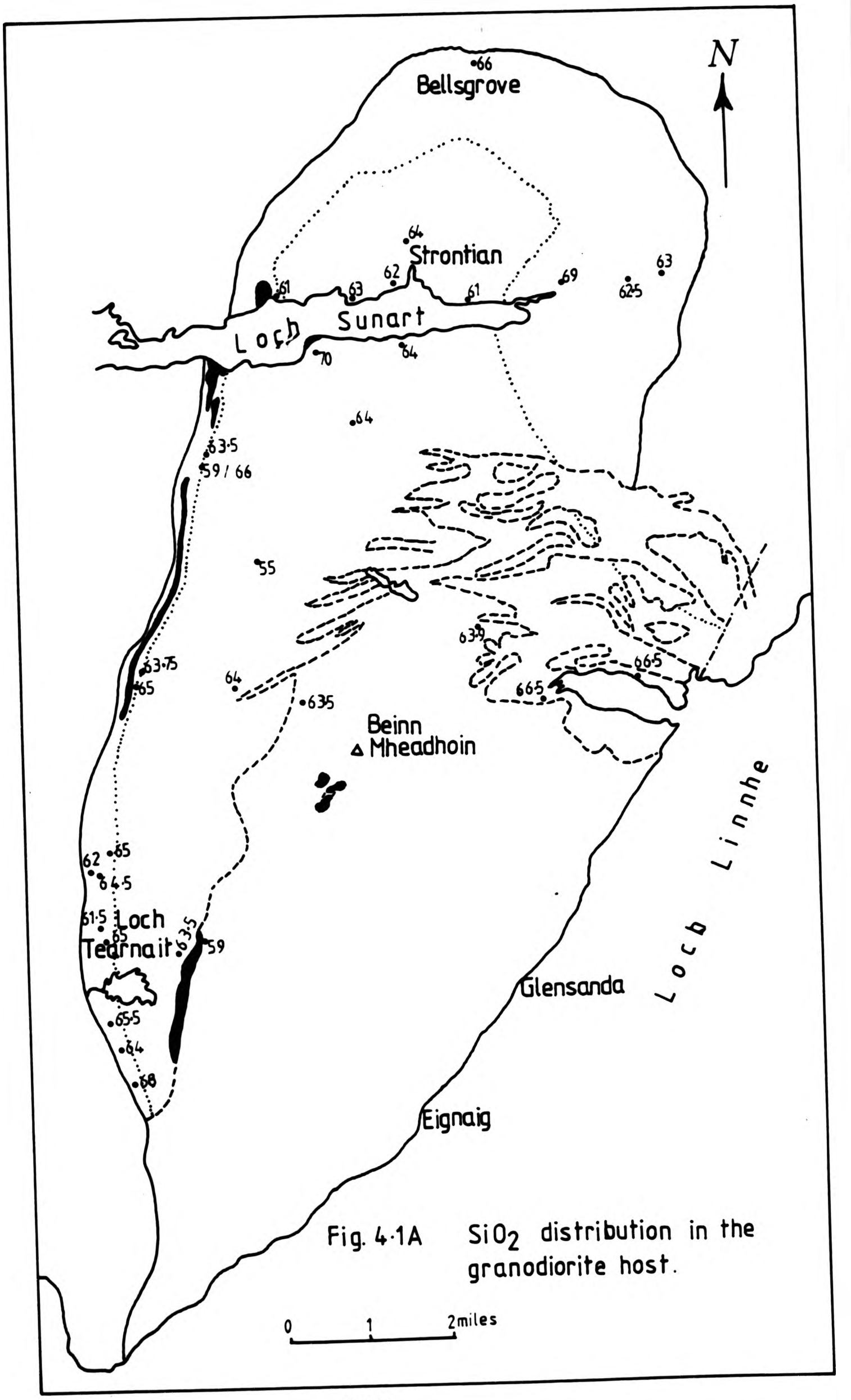

Fig. 4·1A SiO_2 distribution in the granodiorite host.

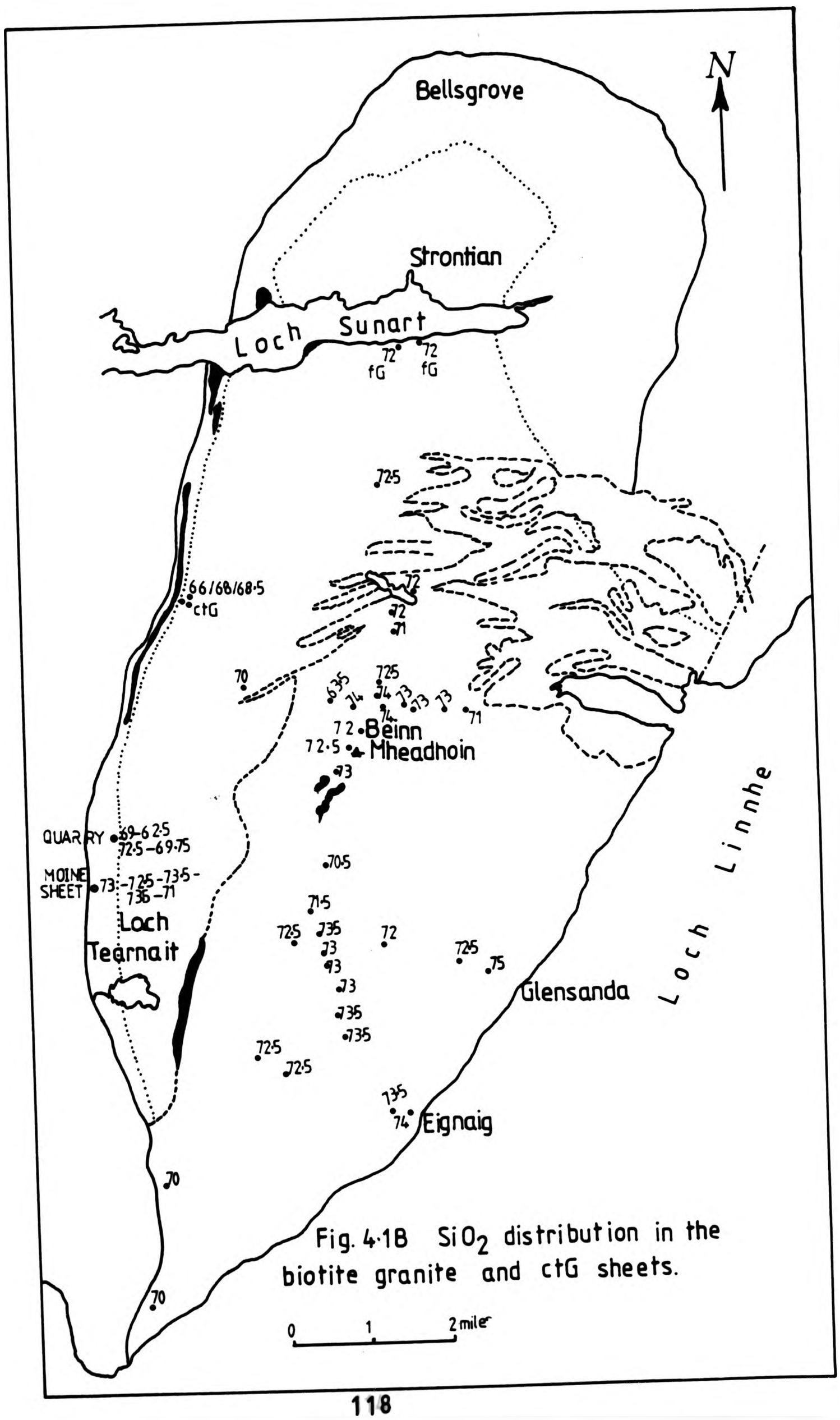

Fig. 4·1B SiO_2 distribution in the biotite granite and ctG sheets.

described together in the previous chapter, here it will be possible to separate the two bodies.

4.2 MAJOR ELEMENTS

The SiO_2 values for all the analyzed samples have been plotted on a map (Fig 4.1A & B) to show their distribution. No systematic geographical pattern of SiO_2 values is detectable in the granodiorite, and the values in tonalitic and porphyritic granodiorites do overlap. Granodiorite and biotite granite SiO_2 values however do not overlap.

Closely spaced granodiorite samples show most commonly variations of only 0.5 to 1.0% SiO_2 with a maximum of 10.0% at the site with a well developed layering in the quarry. Comparison of xenolithic and non-xenolithic areas shows a slight difference in silica (Table 4.1): in the xenolithic areas have a SiO_2 range of 55 to 70%, while the non-xenolithic areas have 63.5 to 68% SiO_2. There are three exceptions:

- A lower value of 55% which is a granodiorite (GX42) next to a xenolith sample.
- A higher value of 70% which is a granodiorite analysis close to the Rubha-na-Sroine diorite (No.2 Fig.1.2).
- A leucocratic layer in the marginal layered granodiorite (quarry Fig.1.2 & 1.3).

The biotite granite has an intrusive contact against the porphyritic granodiorite and is marked by abrupt changes in SiO_2. It ranges from

70% at the contact to 74-75% at Eignaig and Glensanda where hand specimens show coarse quartz grains in the rock. The bulk of the pluton is uniform. Biotite granite sheets in the north span the lower part of the range 70 to 72.5 SiO_2. A single extreme low value (59% SiO_2) is found adjacent to the Loch Tearnait dioritic sheet.

Table 4.1 TO SHOW THE RANGE OF SiO_2 IN XENOLITHIC AND NON-XENOLITHIC AREAS OF GRANODIORITE

Xenolithic areas		Non-xenolithic areas	
Sample		Sample	
SGI	65.00	SGIII	64.50
SGII	63.75	SGXXII	66.50
SGV	62.50	SG7	64.00
SGIX	66.50	SG11	61.50
SGXI	59.00	SG17	65.00
SGXII	63.50	SG29	63.50
SGXXIII	63.00	SG49	66.50
SGXXV	62.50	SG51	66.50
SGXXVI	69.00	SG57	64.00
SGXXVII	70.00	SG80	68.00
SG14	64.00	SG82	64.00
SG21	63.50	SG85	65.50
SG41	62.00	SG93	64.00
SG42	61.00	SGC1	62.00
SG44	64.00		
SG53A	66.00		
SG92	59.00		
GX7	61.00		
G24	65.00		
GX42	55.00		
G140	63.00		

Location of samples refer to Fig.1.3.

Overall the host rocks of the Strontian Complex plot on a well defined trend on the Harker diagrams (Figs 4.2 to 4.12). However more detailed plotting of the individual bodies helped to show internal trends that were present. Figures 4.2 to 4.36 have different symbols to distinguish between the tonalitic and porphyritic granodiorites and the biotite granite and the late granodiorite sheets. These are especially evident between the

tonalitic and porphyritic granodiorites, which show the same range in the major elements in spite of being "separate" bodies. At the lower SiO_2 end, below 65%, the tonalitic and porphyritic granodiorites trends separate, indicating that they are chemically distinct.

4.2.1 Aluminium

Aluminium (Fig 4.2) varies from 16.5 to 13.7% for both the granodiorites, while the biotite granite 16.5 to 13.0% and 15.3 to 13.0% for the late sheets. The host rocks display a horizontal trend with a wide scatter of points. The modal amount of plagioclase feldspar varies considerably in the granodiorite, granite and sheets. Microprobe analyses of the plagioclase from the different rock types show a variation from 20 to 24% Al_2O_3. It is thought that the bulk rock aluminium values reflect the variable abundance of modal plagioclase in the rocks, with the highest reflecting plagioclase accumulation in the tonalitic granodiorite.

The late porphyry sheets (ctG) plot across the whole field of the host rocks in an almost straight line. They stretch from the mafic-rich sample GS3 (58.5% SiO_2, a very porphyritic granitic sheet found at locality C Fig.1.2) to the five more feldspar-rich and mafic-poor samples from locality B (Fig. 1.2). All lie along the Al-poor segment of the plot, while the granodiorites are more Al-rich, which may reflect plagioclase accumulation.

4.2.2 Titanium, Magnesium, Iron and Manganese

These four elements all show tight linear trends of decreasing oxide abundance with increasing SiO_2 for all the host rocks (Figs. 4.3,

FIGURE 4.2 Al2O3 vs SiO2

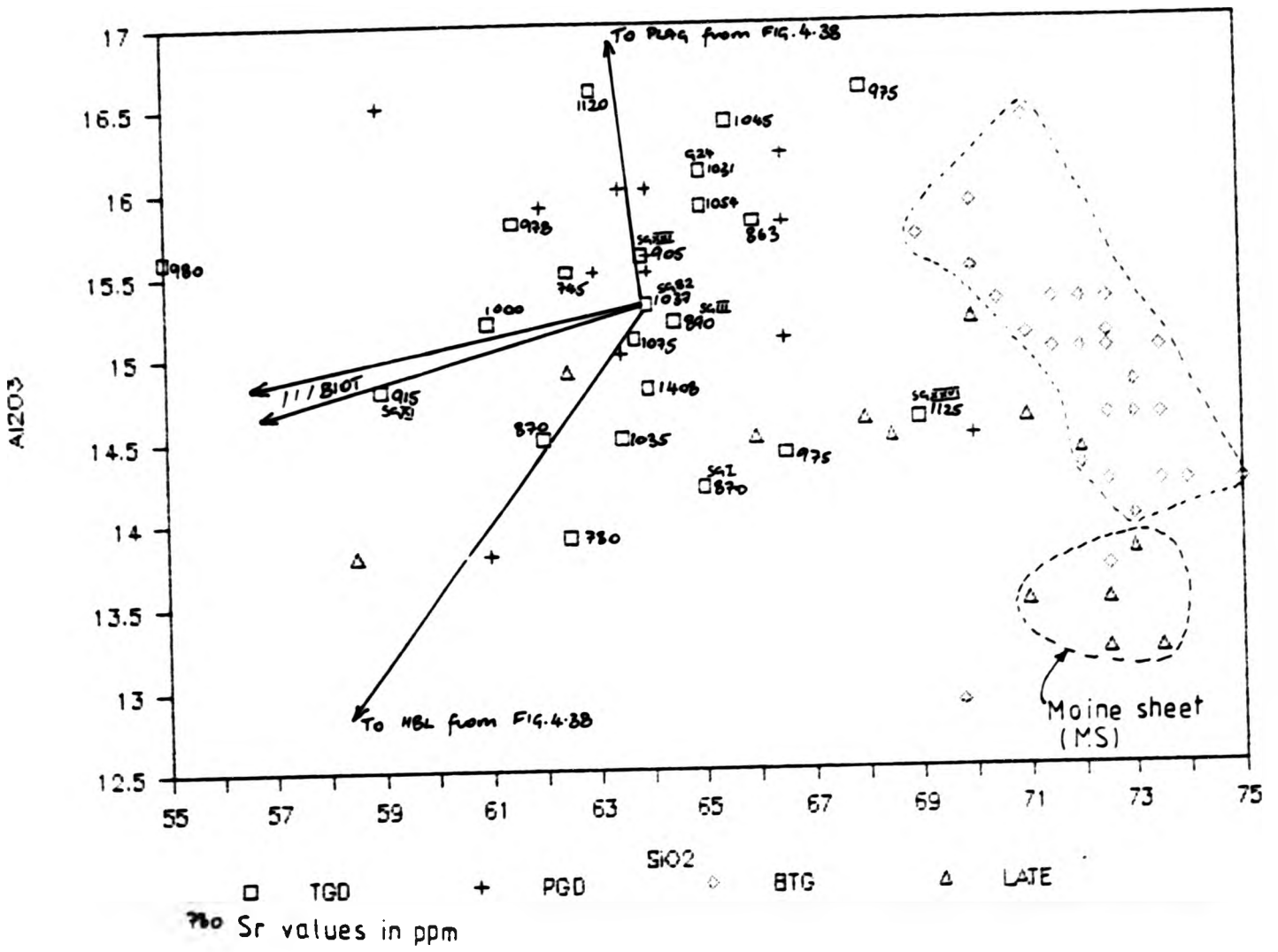

FIGURE 4.3 TiO2 vs SiO2

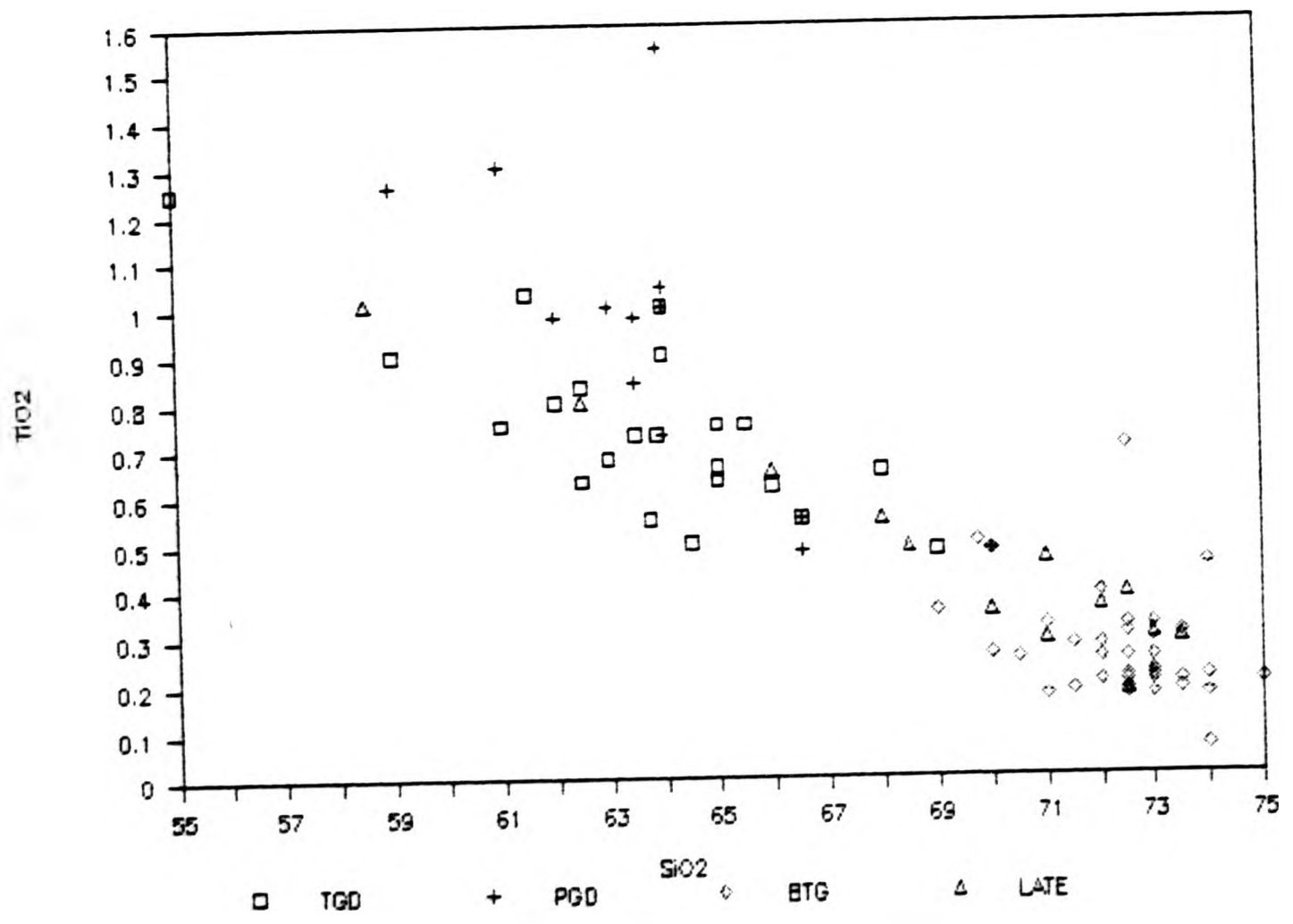

4.4, 4.5 & 4.6), with the least variation with the porphyritic sheets.

The granodiorites display a wider range of TiO_2, FeO*, MnO and MgO values over a wide range of SiO_2 values than the biotite granite: 1.2 to 0.4% TiO_2, 7.6 to 2.0% FeO* 0.12 to 0.02% MnO and 5.5 to 1.4% MgO; while the biotite granite: 0.84 to 0.06% TiO_2, 3.01 to 0.75% FeO*, 0.03 to 0.01% MnO and 2.2 to 0.4% MgO and the porphyry sheets: 1.01 to 0.18% TiO_2, 6.5 to 1.1% FeO*, 0.09 to 0.01% MnO and 5.4 to 0.45% MgO.

The tonalitic and porphyritic granodiorites plot very closely throughout the diagrams, but below 65% SiO_2 they separate. This is most clearly seen on the TiO_2 graph (Fig.4.3), where the porphyritic granodiorite has a higher TiO_2 content and where the porphyritic granodiorite shows evidence of sphene fractionation. The later sheets trend straight through the tonalitic granodiorite field with very similar TiO_2 values as the granodiorite. While MgO, FeO* and MnO show a smaller separation , if one at all, as seen on the FeO* plot (Fig.4.5).

The MgO and FeO* plots, especially for the tonalitic and porphyritic granodiorites, show a very large variation, which is probably a result of the variation in the modal amounts of mafic minerals present throughout these bodies. The low levels of FeO*, MnO and TiO_2 probably also reflects the general absence of modal magnetite and ilmenite, but covariance in Fe vs Ti or Mn is also a reflection of ferromagnesian silicates. Figures 4.7 and 4.8 both display positive correlations between MnO : FeO* and TiO_2 : FeO*, may reflect the substitution of titanium and manganese for iron in the

FIGURE 4.4 MgO vs SiO2

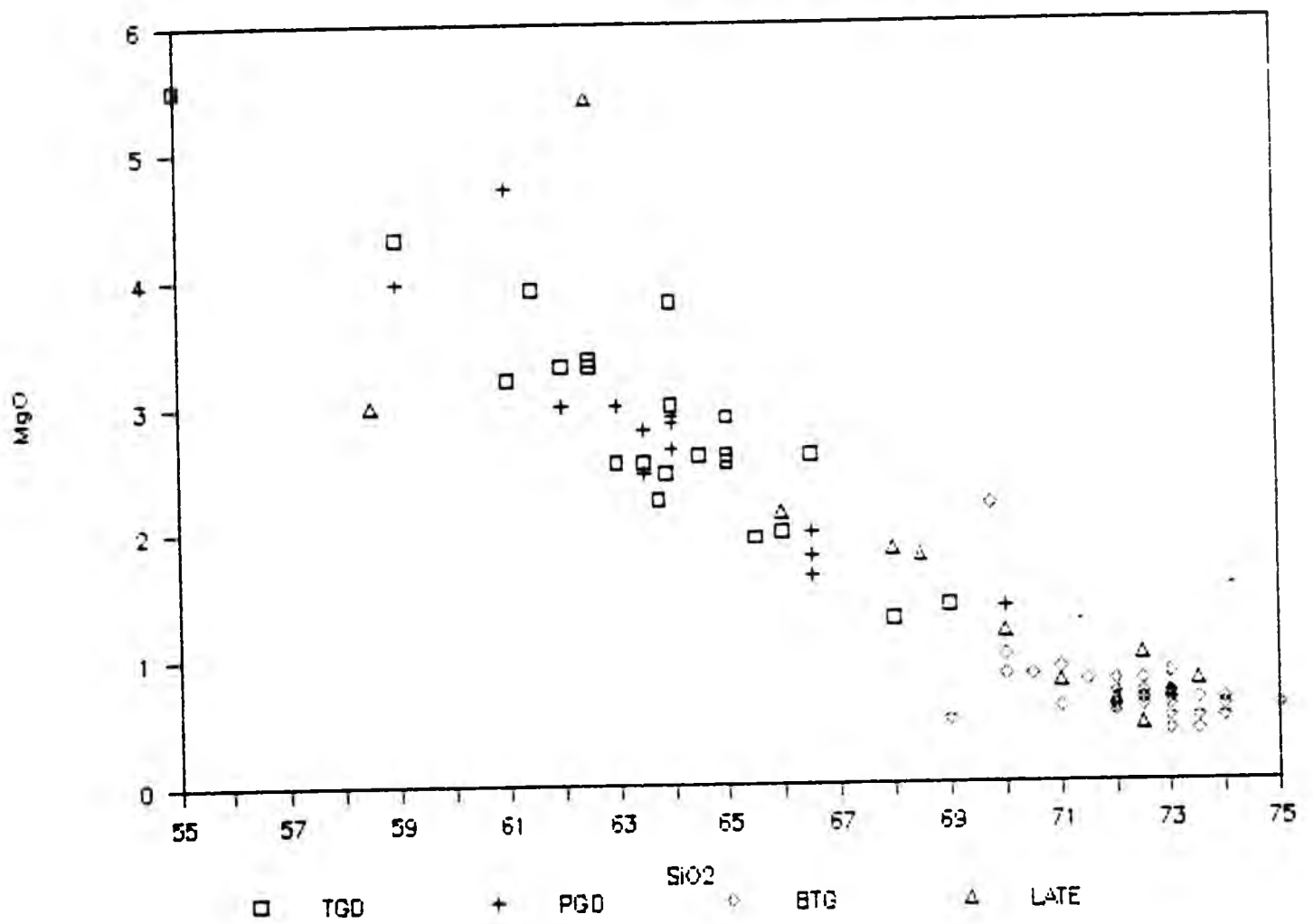

FIGURE 4.5 FeO* vs SiO2

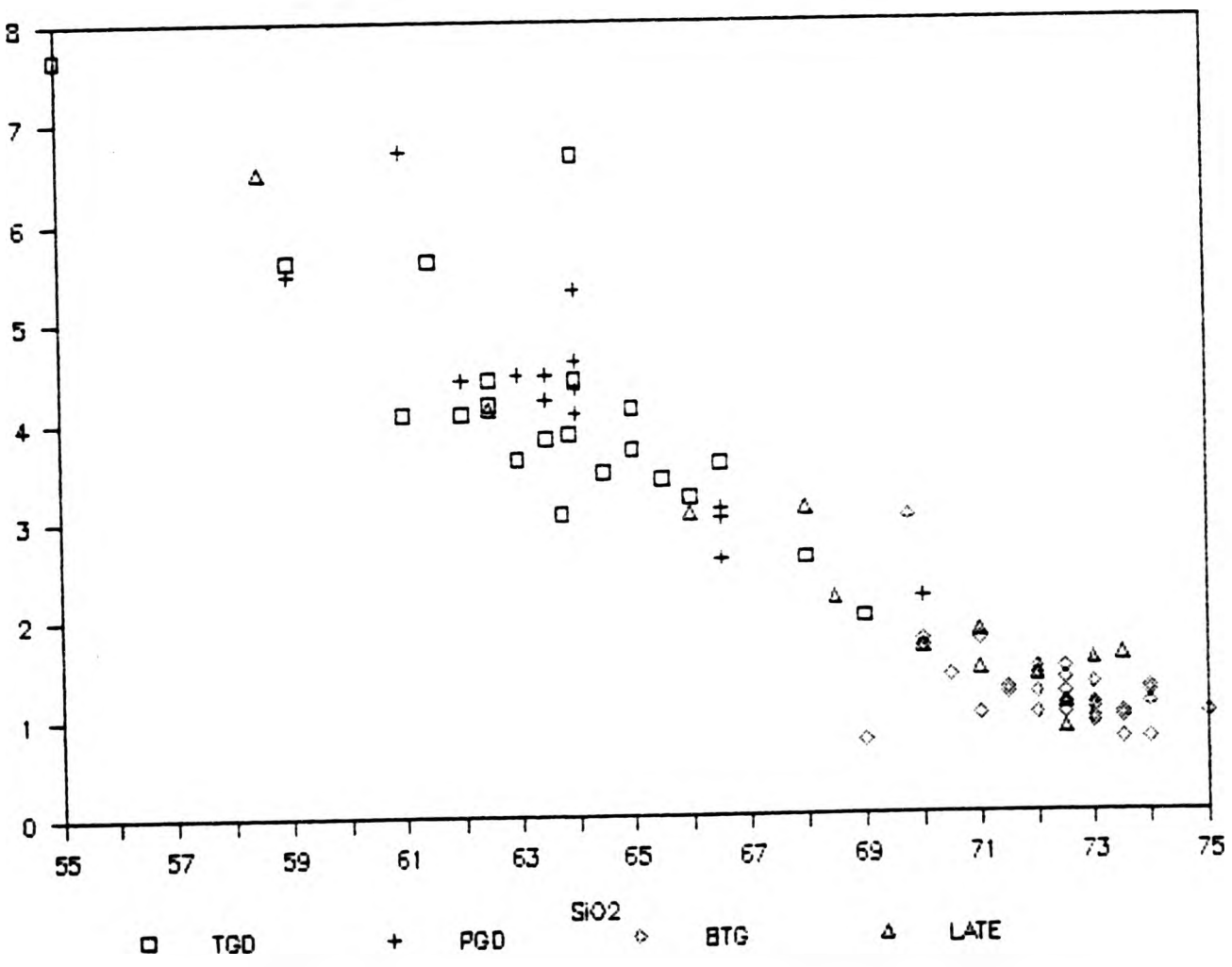

FIGURE 4.6 MnO vs SiO2

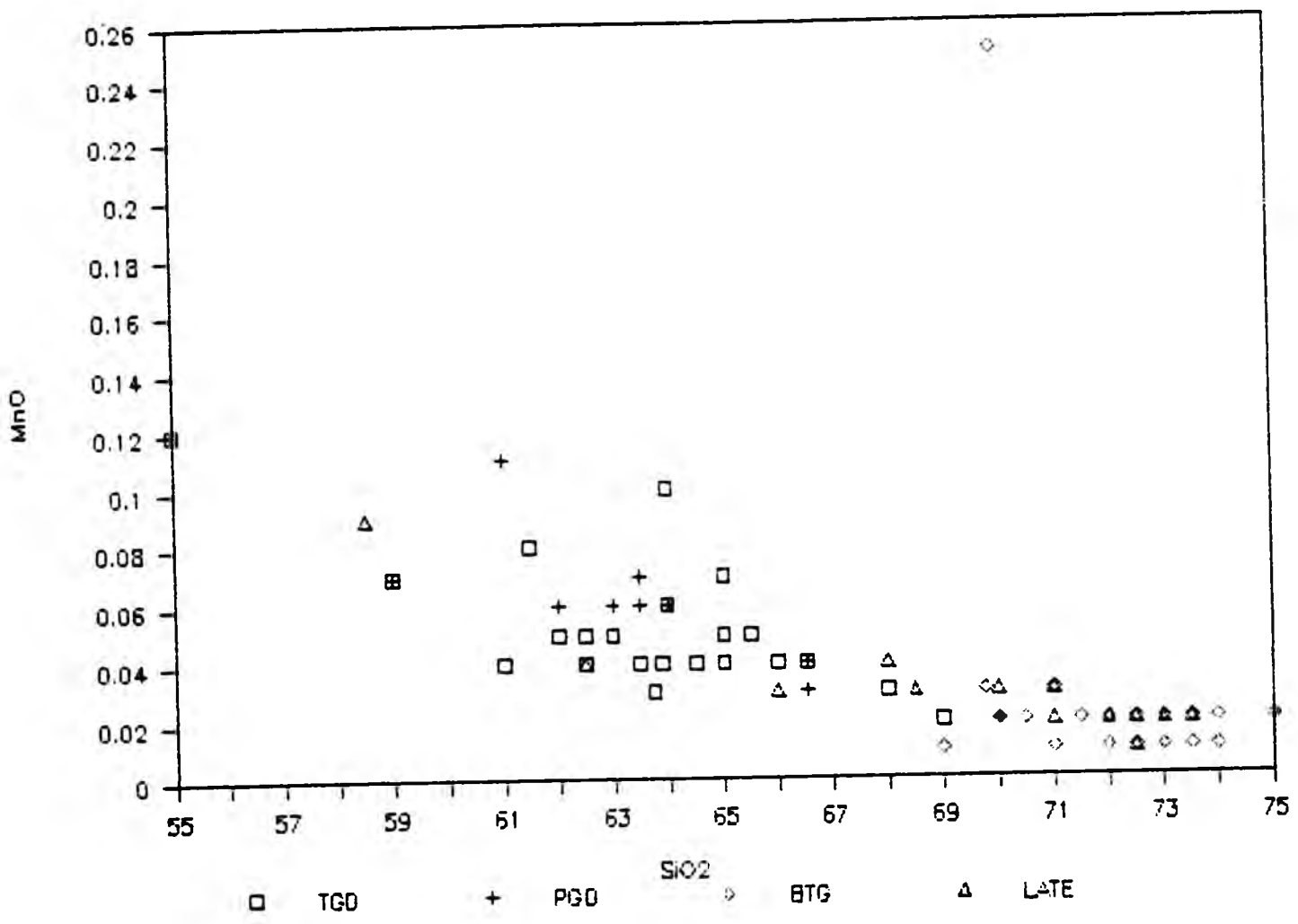

FIGURE 4.7 MnO vs FeO*

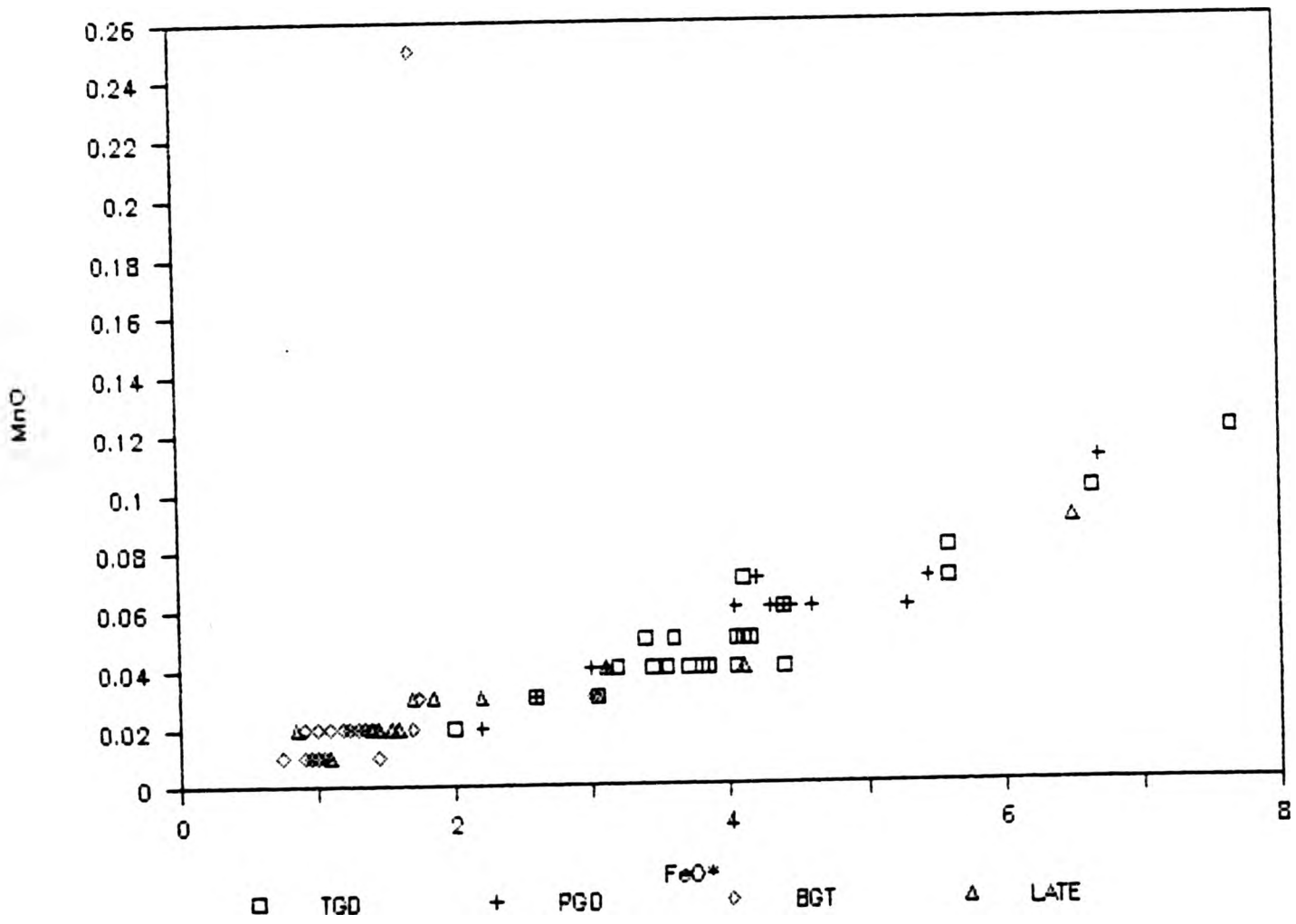

oxide minerals. A break of slope occurs in the FeO* vs MnO plot at 5% FeO*. However the low levels of these elements in the acidic rocks of the Strontian complex suggest that these minerals are uncommon or in fact absent. The positive trends of Fig.4.7 and 4.8 show that the granodiorites have higher levels than the biotite granite and so it is possible that the titanium substitutes in hornblende and biotite. These mafic minerals are more abundant in the granodiorites than the granite.

4.2.3 Calcium

The tonalitic and porphyritic granodiorite (5.5 to 2.0% CaO) plot completely separately from the biotite granite (2.3 to 0.5% CaO) (Fig.4.9). As with the other major elements CaO shows an overall decrease with increasing SiO_2. The higher CaO values are found in the tonalitic granodiorite, where fresh plagioclase feldspar is the dominant leucocratic mineral, even cumulate. This occurs below 65% SiO_2 where the tonalitic and porphyritic granodiorites separate as on the TiO_2 plot. Higher Al_2O_3 values for the granodiorites correspond with lower CaO values. The highest CaO values may therefore relate to more mafic rocks such as the granodiorites as Al is low in amphibole. The modes (Table 3.1 & 3.2) show the drop in the level of mafic minerals from the granodiorites to the biotite granite. Part of the later sheets plot along the "axis" of the tonalitic granodiorite trend; while the others plot close by the biotite granite. The biotite granite has a very tight grouping with hardly any change in the CaO content. This is reflected in the lower levels of plagioclase and mafic minerals present.

FIGURE 4.8 TiO2 vs FeO*

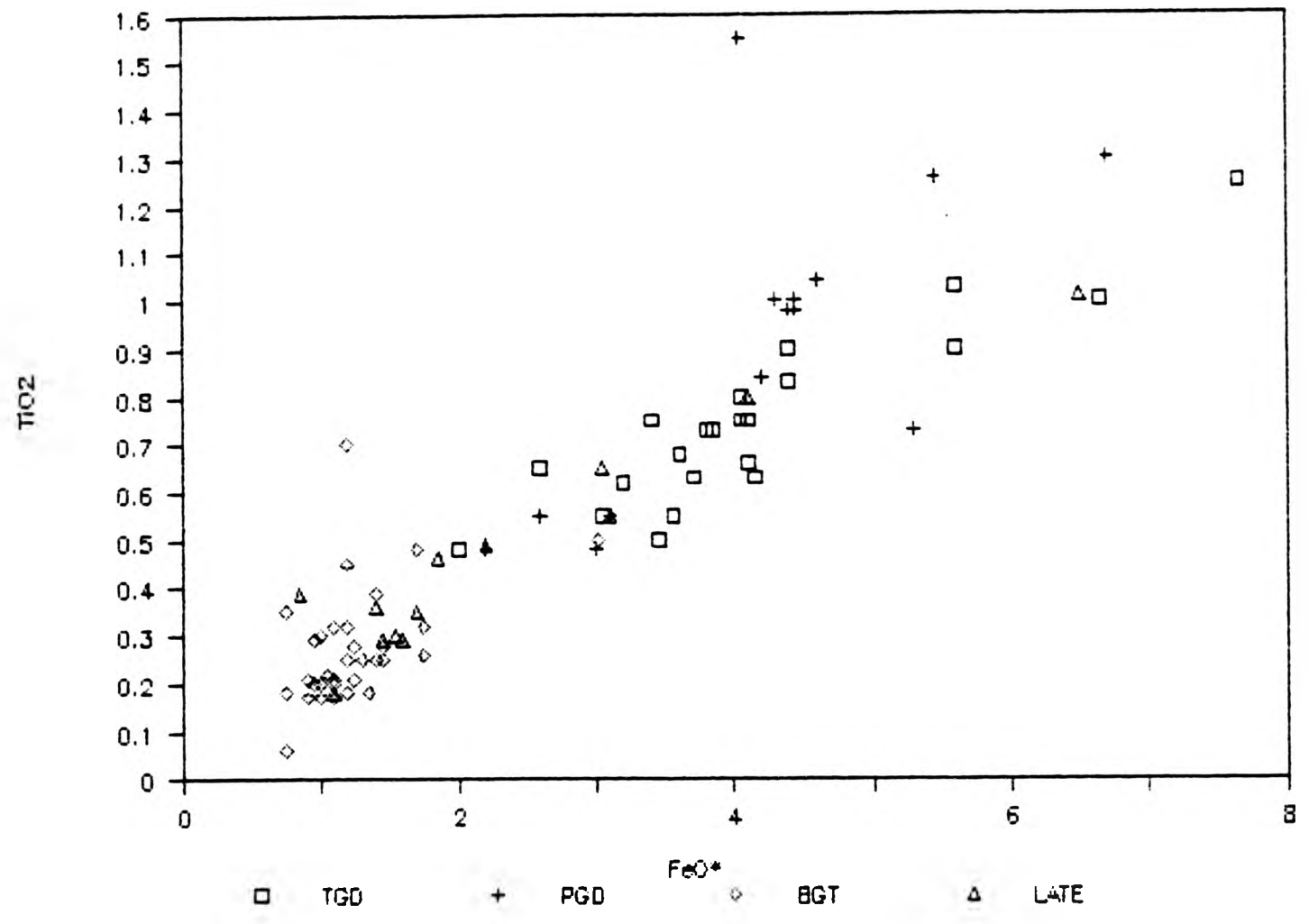

FIGURE 4.9 CaO vs SiO2

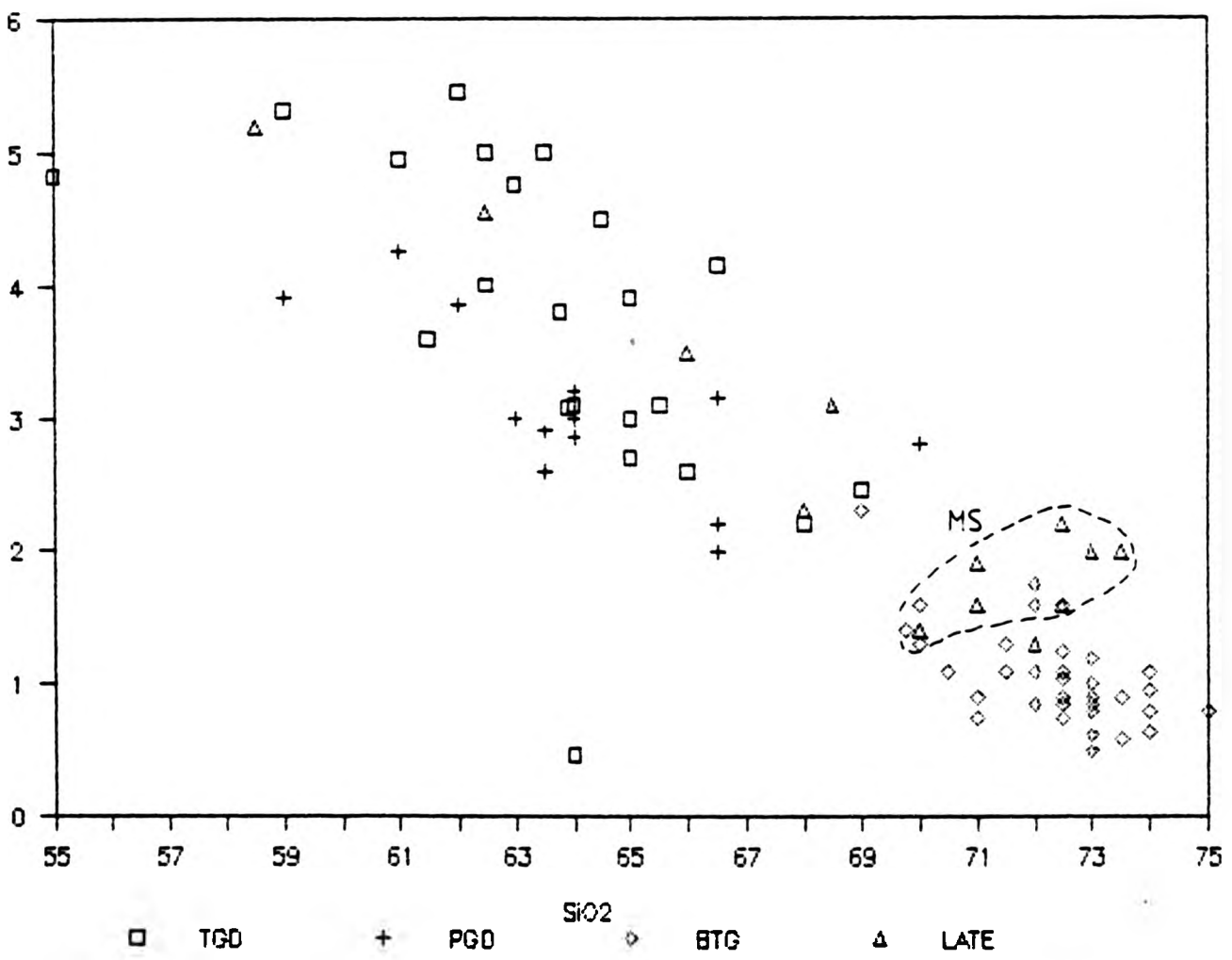

4.2.4 Sodium and Potassium

The alkali metals, sodium and potassium, display broadly more scattered plots in comparison with the previous elements, with Na_2O showing a gentle decrease and K_2O a gentle but definite increase with increasing silica.

The tonalitic and porphyritic granodiorite contain 5.45 to 4.2% Na_2O and are far more widely scattered than the biotite granite 4.99 to 4.05% (with an extreme sample at 5.45% Na_2O).

The later sheets have a considerable spread of values across the whole sodium plot (Fig.4.10). Most of the sheet samples are found within the porphyritic granodiorite in the field, except the extreme group at the high SiO_2 and low Na_2O end, which are located at B (Fig 1.2) just outside the complex in the Moine. The Na_2O values do not appear in any pattern on the sheet ie. they do not increase/decrease systematically inwards from the margins or along its length.

The potassium trends are a little more tightly grouped, but still with some scatter (Fig 4.11). The tonalitic and porphyritic granodiorite range from 2.47 to 3.6% K_2O, however there is a small group of tonalitic samples that plot between 1.8 and 2.1% K_2O and are completely separate from the main trend. All these samples occur close to the contact and are scattered along its length from Liddesdale to Loch Tearnait and do not form such a separate group together on any plot. In fact half of this group is in the higher CaO, Al_2O_3 and Na_2O field, which may indicate that they are cumulates. They have higher modal plagioclase than the other half which has average CaO, Al_2O_3 and Na_2O values and lower but variable

FIGURE 4.10 Na2O vs SiO2

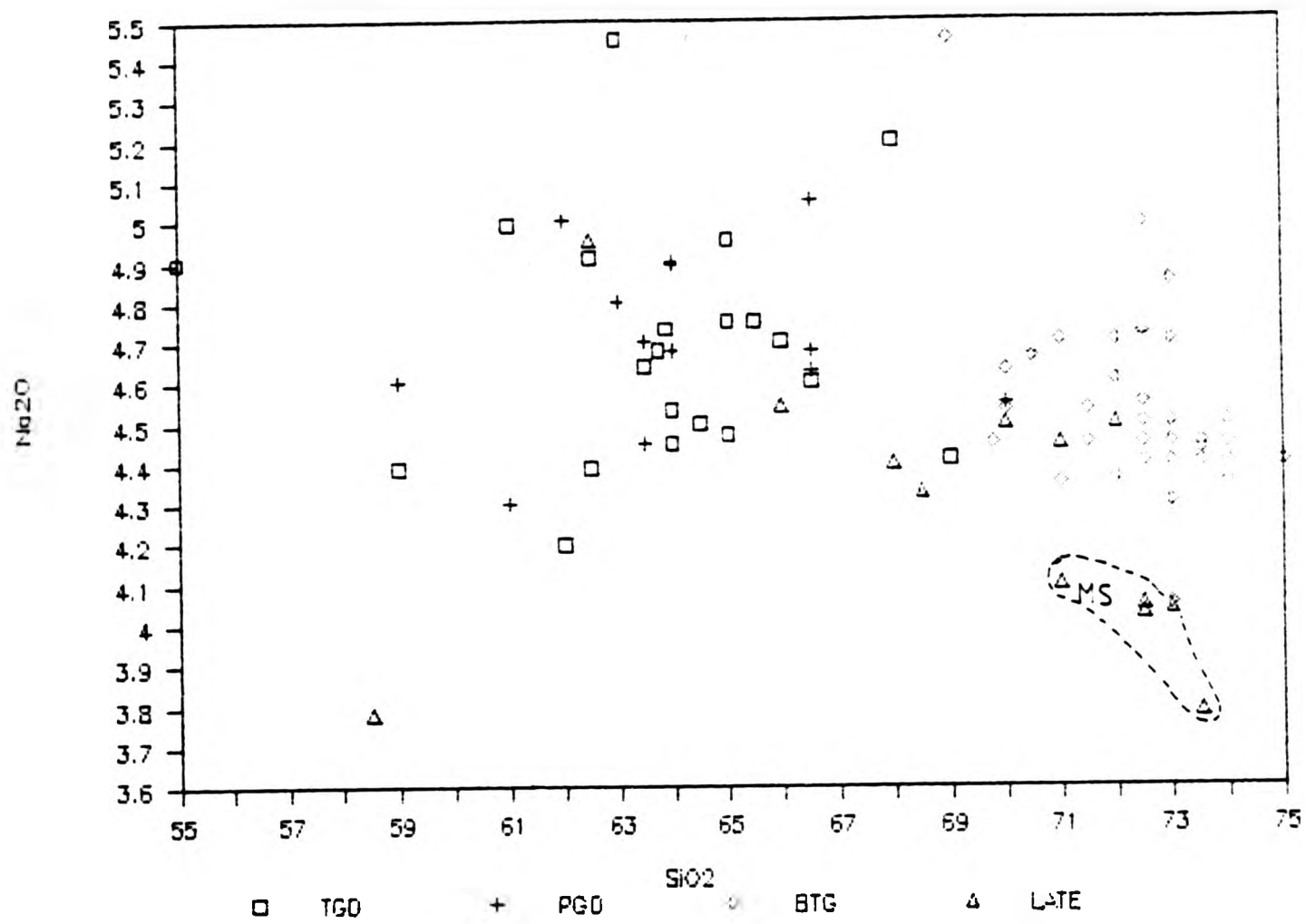

FIGURE 4.11 K2O vs SiO2

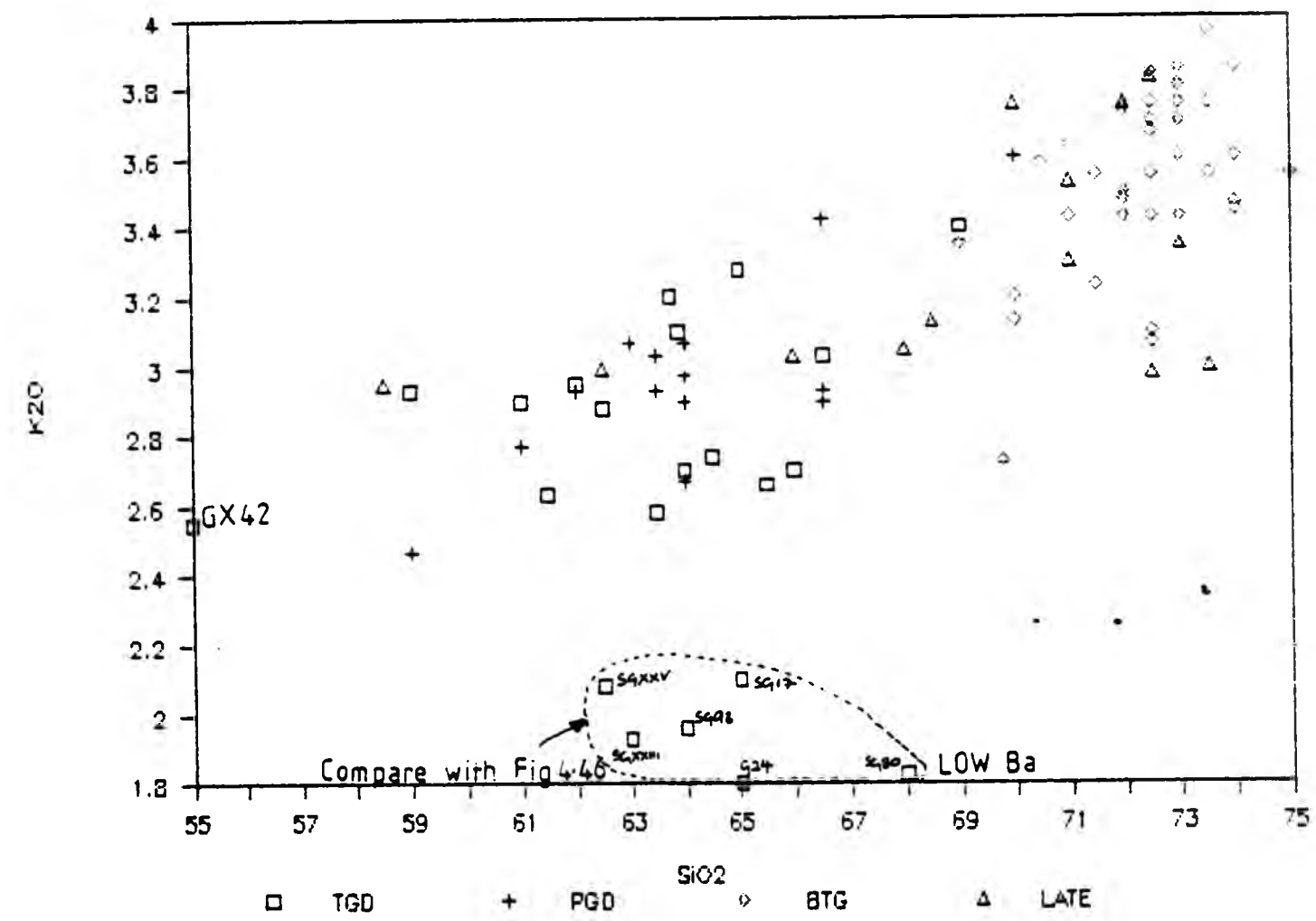

modal plagioclase. Biotite is an abundant mafic mineral in the granodiorites and has a high K_2O content, which may reflect the K_2O levels on Fig.4.11.

The biotite granite contains 2.73 to 3.96% K_2O and the alkali feldspar content increases from the western margin to Eignaig and Glensanda. The late sheets trend obliquely at a lower gradient through the granodiorite field and range from 2.95 to 3.83% K_2O.

Both alkali felspars and biotites contain significant amounts of potassium: 9.8 to 15.2% for K-feldspar and 8.1 to 9.94% for biotites. It is these two minerals which vary quite considerably in modal amounts from the granodiorites to the biotite granite.

4.2.5 Phosphorus

The distribution of phosphorus is shown in Fig.4.12 and shows an overall linear tight trend of decreasing P_2O_5 with increasing silica. The biotite granite has a small range of P_2O_5 values: 0.01 to 0.14%. Between 59 to 64% SiO_2 the porphyritic granodiorite (0.46 to 0.14% P_2O_5) has greater P_2O_5 content than the tonalitic (0.35 to 0.22% P_2O_5). However the tonalitic granodiorite has a number of extreme samples which have values of 0.02% and reach 1.09%. One of the more phosphorus-rich samples is present in the low K_2O field and in the extremely low CaO sample (Fig.4.9); while none of the extreme values occur in the layered rocks. The most common phosphorus bearing mineral in calc-alkaline rocks is apatite. It is found in all the rocks of the Strontian Complex, where the modal amounts vary considerably.

FIGURE 4.12 P205 vs SiO2

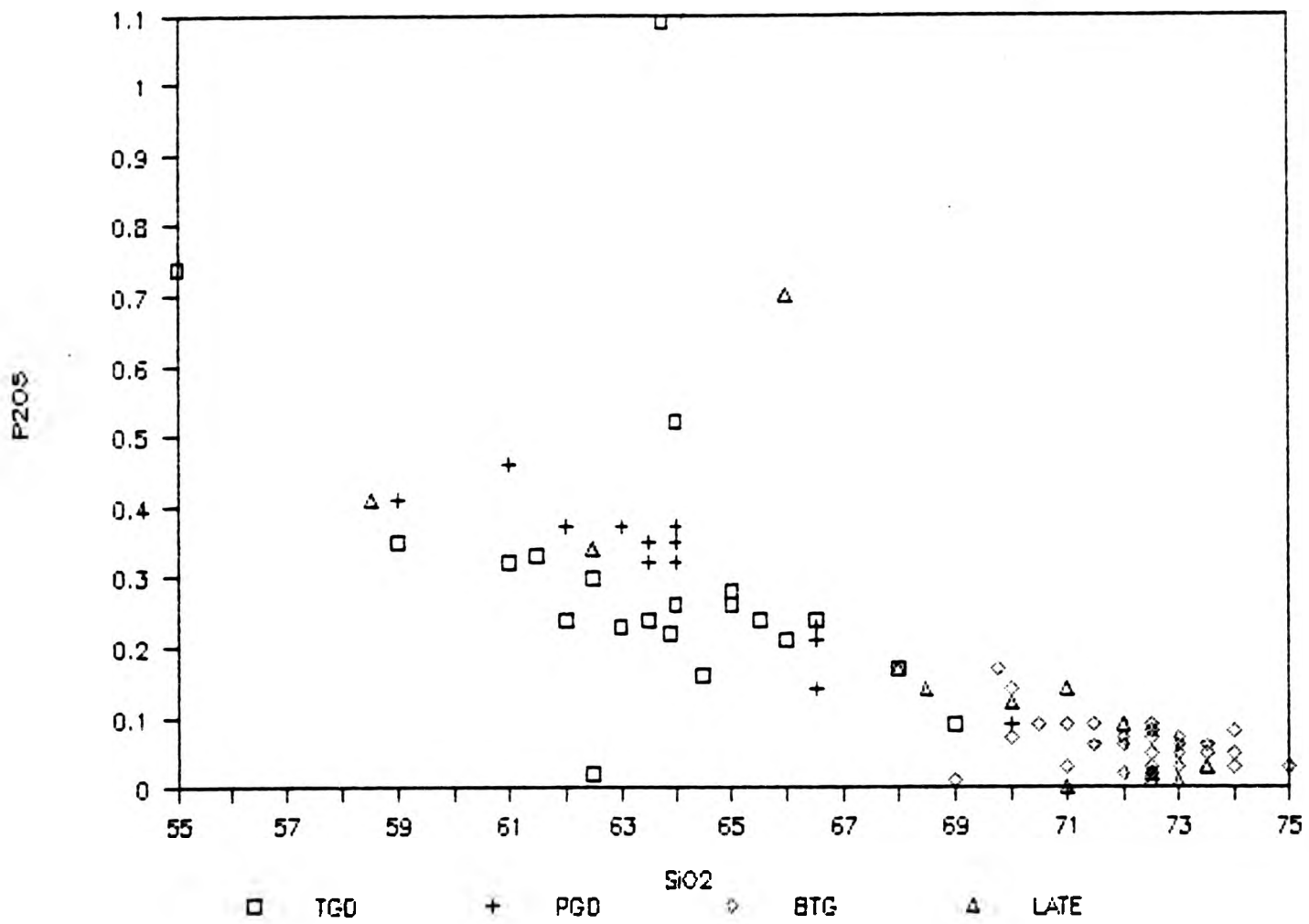

FIGURE 4.13 Ba vs SiO2

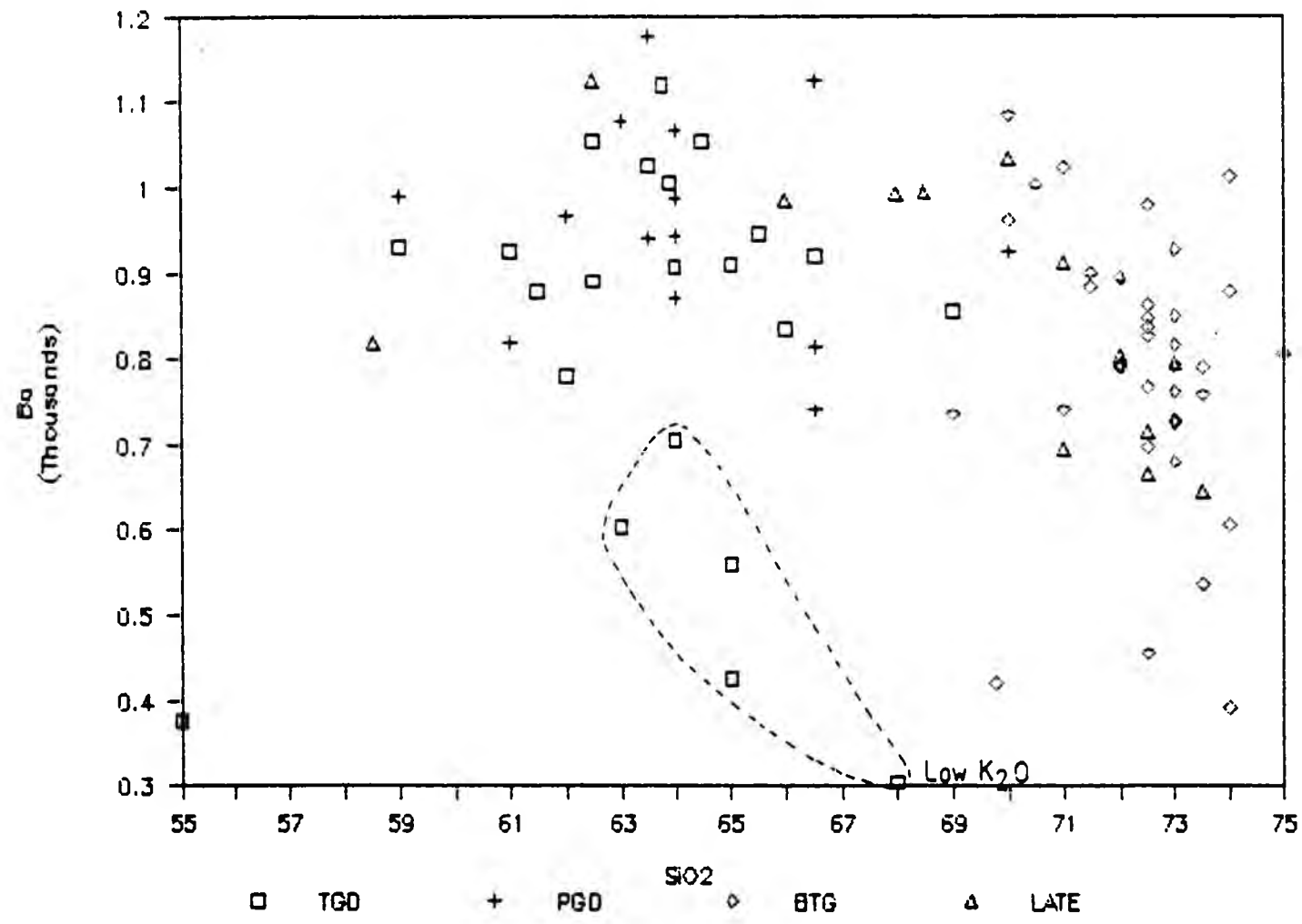

4.3 TRACE ELEMENTS

The variation diagrams for the trace elements are figures 4.13 to 4.36 and in general show similar trends with the major elements of decreasing values with increasing SiO_2. The relationship of the individual trace element to the major element is discussed and details of their ionic radius, charge or electronegativity will be given where appropriate.

4.3.1 Barium, Strontium and Rubidium

Ba, Sr and Rb are widely distributed in acidic rocks and are closely interelated in their behaviour.

Barium (Fig.4.13) shows a wide distribution of data with a uniform trend with increasing SiO_2. The tonalitic and porphyritic granodiorites contain between 305 to 1175ppm Ba and are scattered between 61 to 65% SiO_2. Ba continues at the same levels in the biotite granite, which also shows a wide scatter of 1020 to 390ppm between 70 to 74% SiO_2. These values are high in comparison with the Loch Doon complex, where a range of 548 to 724ppm for the granites (Brown et al 1979) and 612 to 907ppm for the tonalite and granodiorite (Tindle and Pearce 1981).

Ba^{+2} (ionic radius 1.43 A) can replace K+ in either biotite or K-feldspars. The wide scatter and no substantial change with increasing silica suggests that the earlier granodiorites have significant amounts of Ba entering biotite and progressively becoming enriched in the K-feldspar of the biotite granite. The tonalitic granodiorite samples which have low K_2O values (Fig.4.11), also have

lower Ba content (Fig.4.13). These are the early formed host rocks and all are found within 500m of the complex margins. Fig.4.14 shows Ba vs K_2O where the granodiorites have lower K_2O and Ba than the biotite granite.

Strontium shows a definite decrease with increasing SiO_2 (Fig.4.15). The granodiorites vary from 1408 to 745ppm Sr. The porphyritic granodiorite lies on the main trend, but the tonalitic granodiorite shows a weak transverse positive trend, which reflects the variable amphibole and plagioclase content. The biotite granite varies from 760 to 350ppm Sr. The Loch Doon have 554 to 306ppm Sr for the granodiorites (Tindle & Pearce 1981) and 200 to 502 ppm Sr for the granites (Brown et al 1979).

Sr^{+2} (1.12A) can substitute for Ca^{+2} (0.99A) in crystal lattices. The Sr plot is very similar to the CaO plot of decreasing values with increasing silica (Fig.4.9). Those samples with lower CaO tend to have slightly higher Sr content. When plotted against each other Ca and Sr show a definite positive correlation of decreasing Ca and Sr with the more evolved biotite granites (Fig.4.16). This may also reflect the Sr being substituted in amphibole which is a major ferromagnesian mineral of the granodiorites. In acid rocks Sr^{+2} can substitute for K+ in alkali feldspars and this may result in an increase in the bulk rock Sr/Ca ratio. This is seen in Fig.4.17 where the ratio increases with increasing silica, which suggests that Sr substitutes in the K-feldspars. K_2O vs Sr also shows a significant decrease in Sr with decreasing K_2O (Fig.4.18). Fig.4.19 plots Ba vs Sr which shows a significant increase on a curved trend from the biotite granite to the granodiorites of increasing Ba with increasing Sr. The curved path precludes the use of simple mixing

FIGURE 4.14 K2O vs Ba

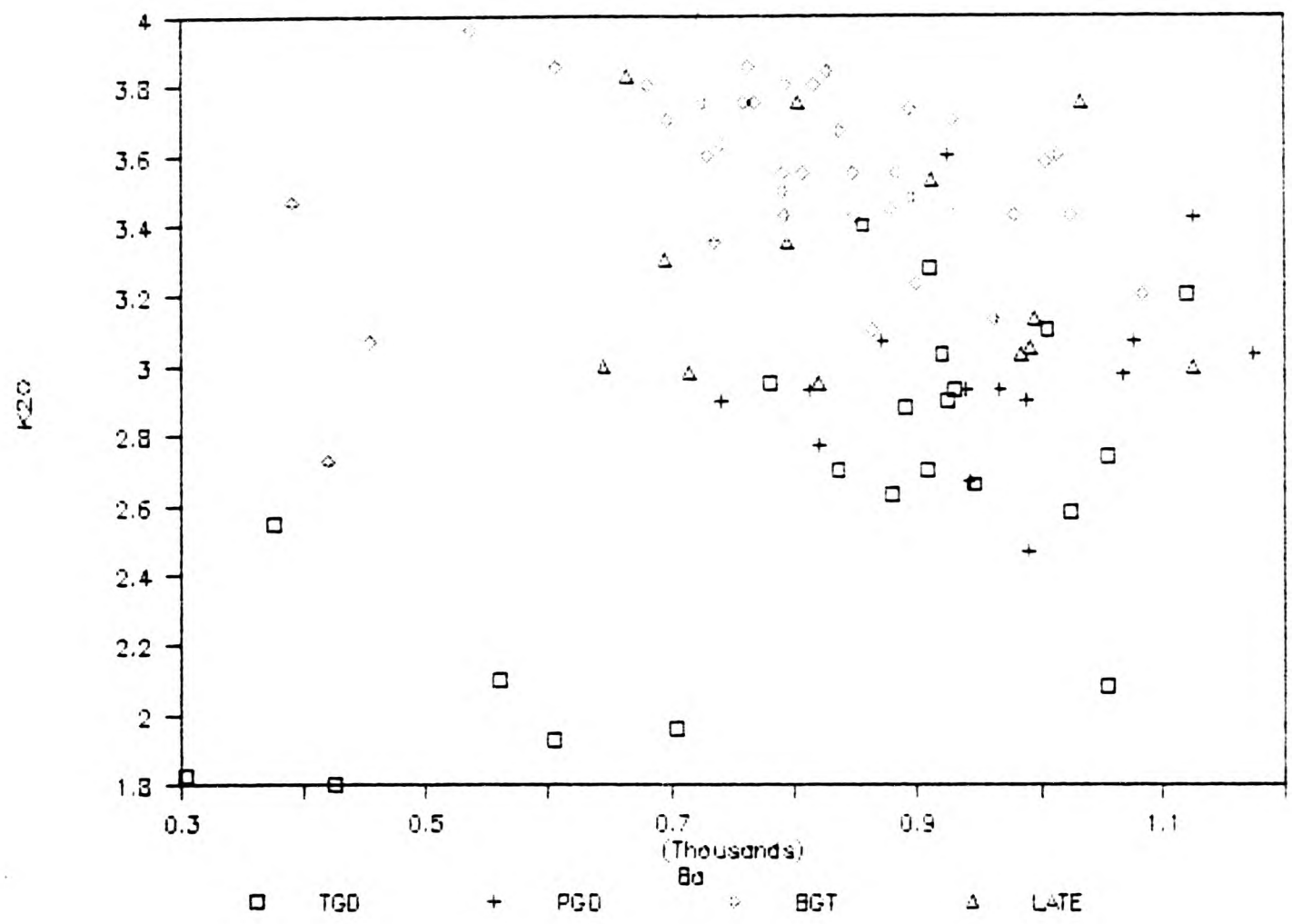

FIGURE 4.15 Sr vs SiO2

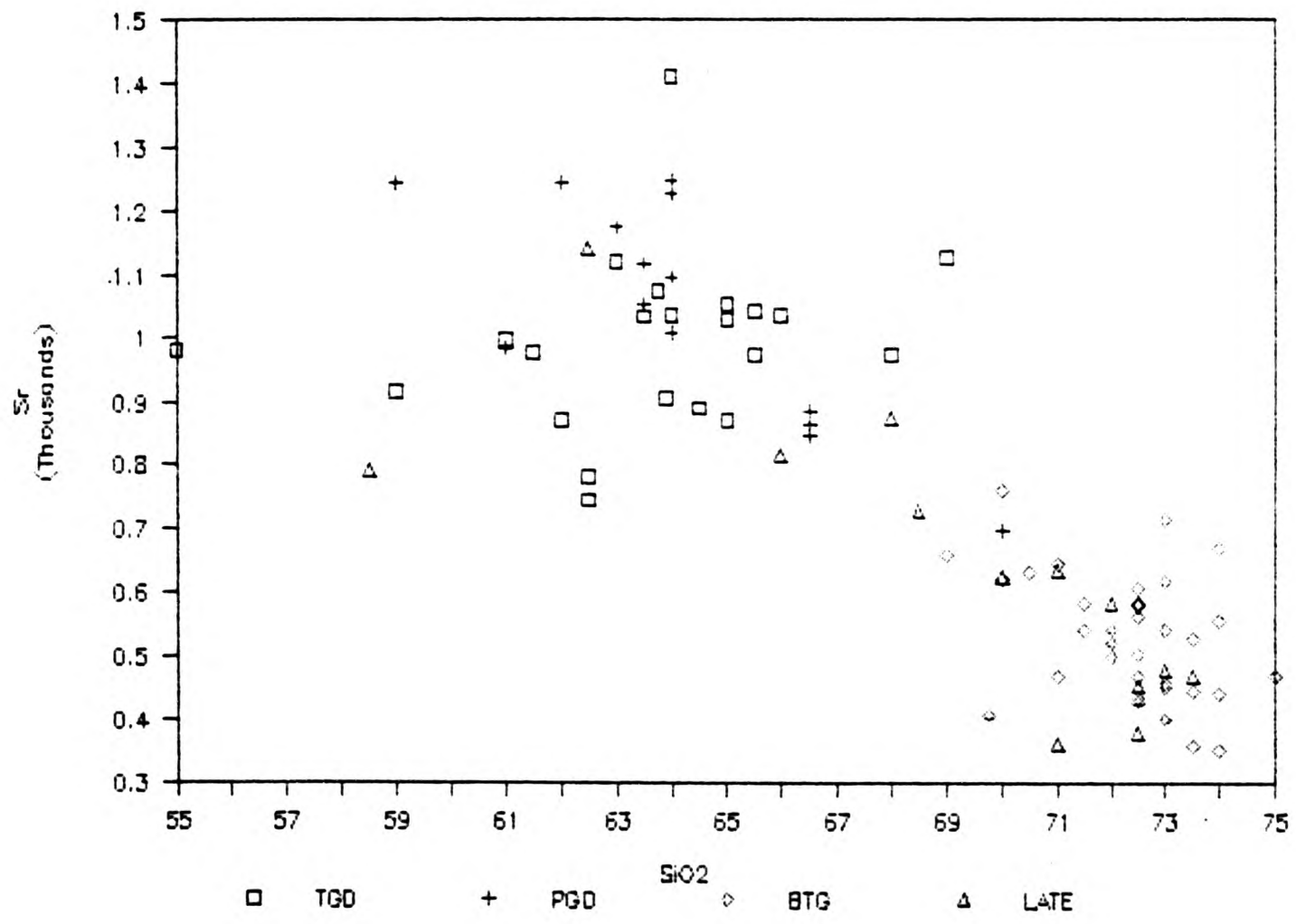

FIGURE 4.16 Ca vs Sr

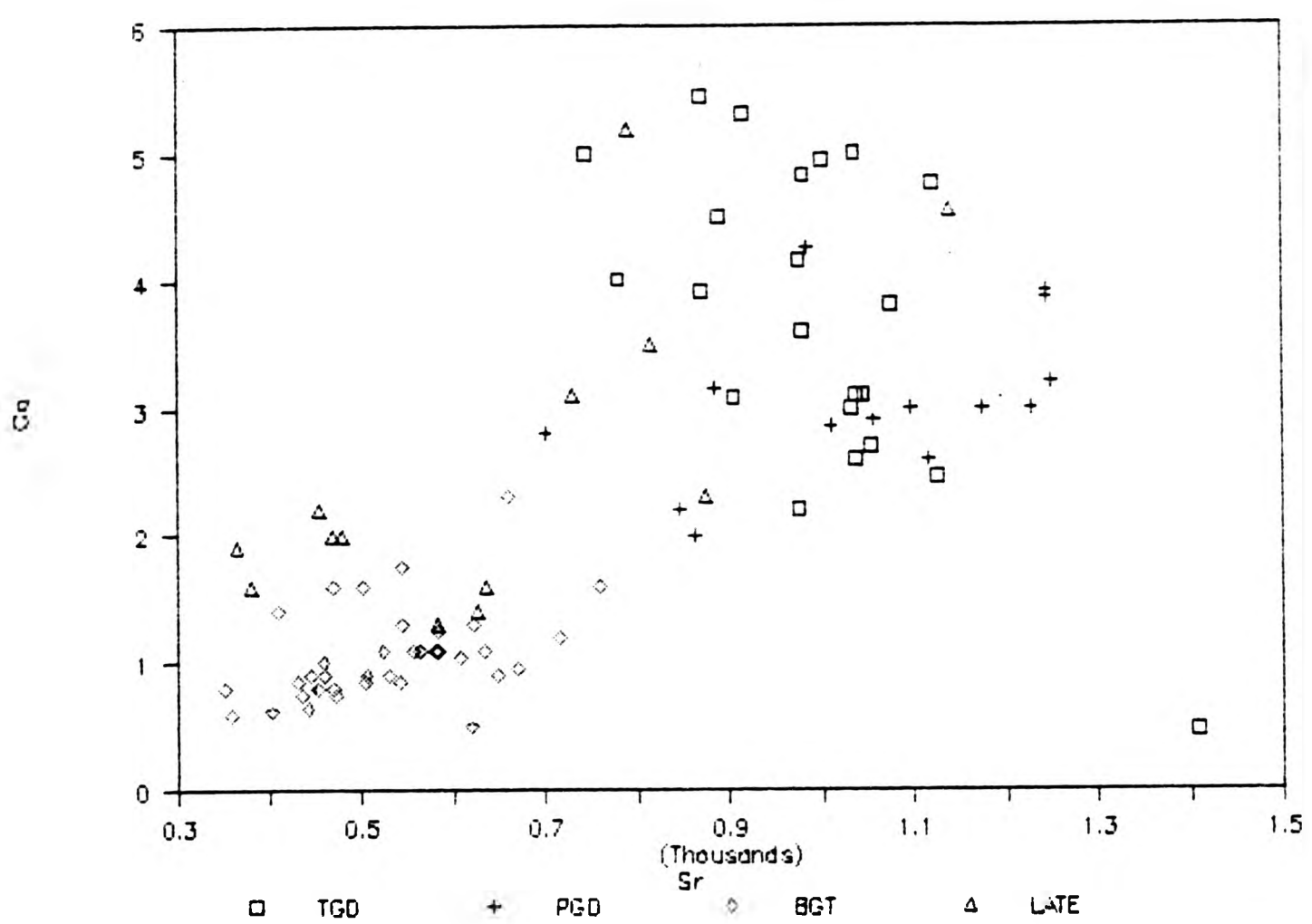

FIGURE 4.17 Sr/Ca vs SiO2

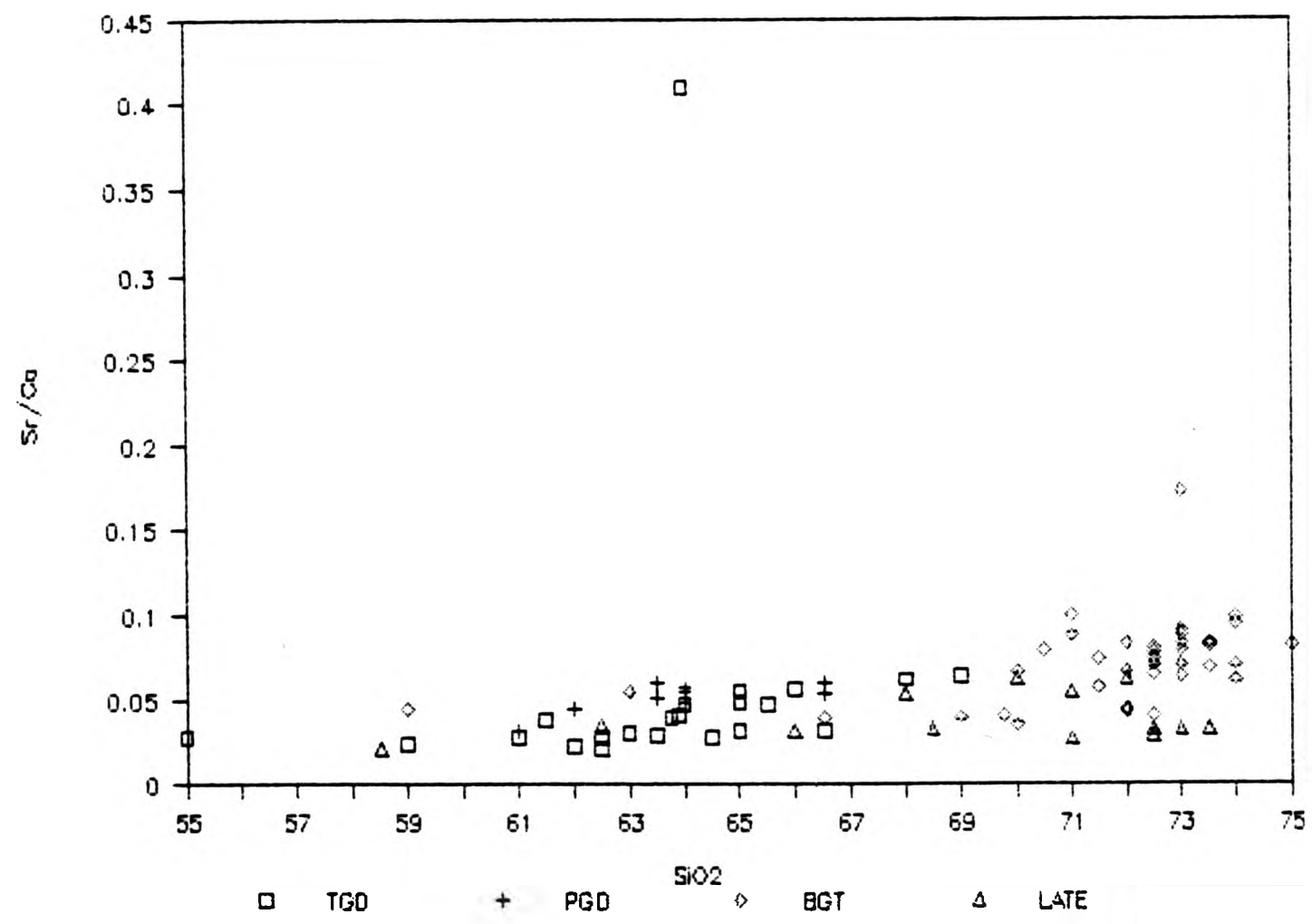

FIGURE 4.18 K20 vs Sr

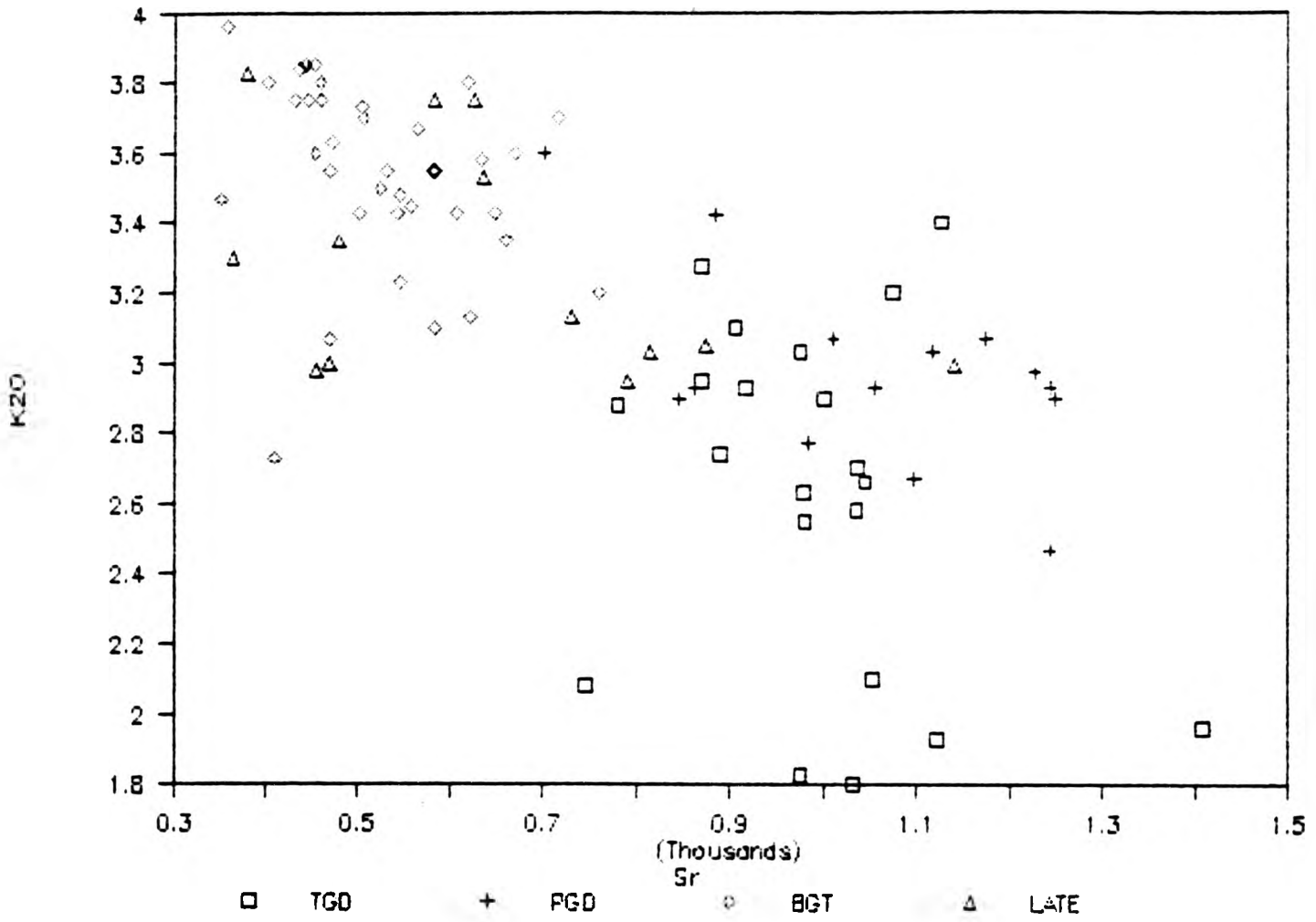

FIGURE 4.19 Ba vs Sr

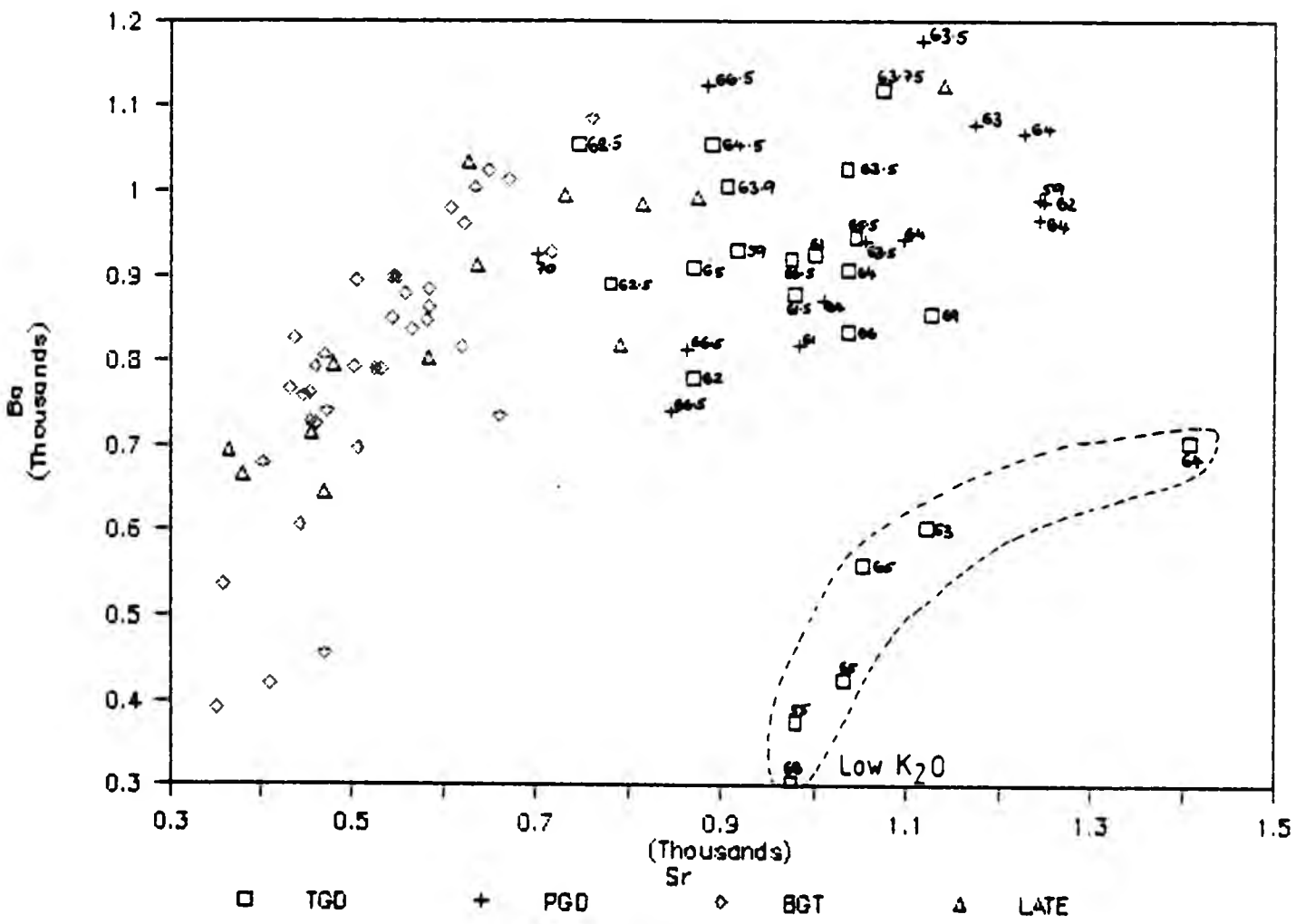

models for the whole suite involving only two end member compositions. Acid rocks with Sr >500ppm and Ba >800ppm can give linear trends on this diagram, but Sr-poor and Ba-poor end members would not account for the trend. Limited mixing from multiple acid end members remains possible. The crystallization of biotite, K-feldspar and plagioclase in all rocks means that the accelerated depletion of Ba and Sr is not attributed to a new phase crystallized, but would have to result from a change in the proportion of plagioclase to K-feldspar. The tonalitic granodiorites that plot completely separately with lower Ba but high Sr content, are the same samples which have the lower K_2O contents. This would reflect their lower modal alkali feldspar contents.

Rubidium clearly shows an increase of levels with increasing silica. Typically both granodiorites vary from 40 to 90ppm Rb; the biotite granite 70 to 162 ppm Rb and the later sheets 75 to 105ppm Rb. In comparison the Loch Doon has substantially higher levels: 144 to 104ppm Rb for the granodiorites (Tindle & Pearce 1981) and the granites 130 to 238ppm Rb (Brown et al 1979). BGT samples with lower Rb levels than the main BGT field include samples close to the BGT margin with the Moine (south of Loch Tearnait) as well as from the quarry. The data (Fig.4.20) almost separates the granodiorite field, which has a small vertical change with increasing SiO_2, from the biotite granite, which has a wide scatter for a small range of silica. The tonalitic granodiorite plots transversely across the field and does not really fit the porphyritic granodiorite and biotite granite pattern, reflecting its variable mineralogy.

Rb^{+1} (1.47A) commonly replaces potassium (1.33A) in biotite and alkali feldspar. The K/Rb ratio (Fig 4.21) typically decreases with

FIGURE 4.20 Rb vs SiO2

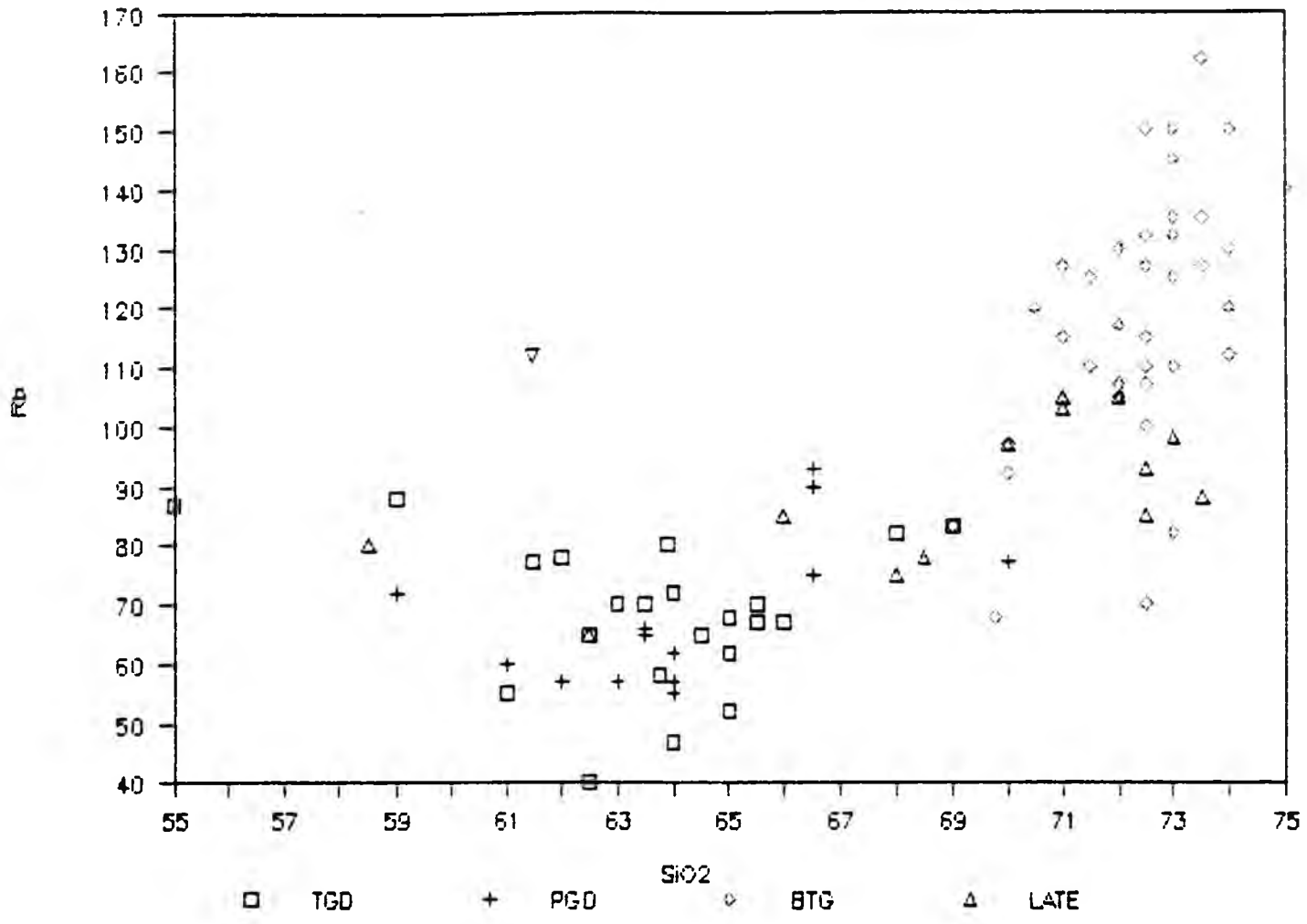

FIGURE 4.21 K/Rb vs SiO2

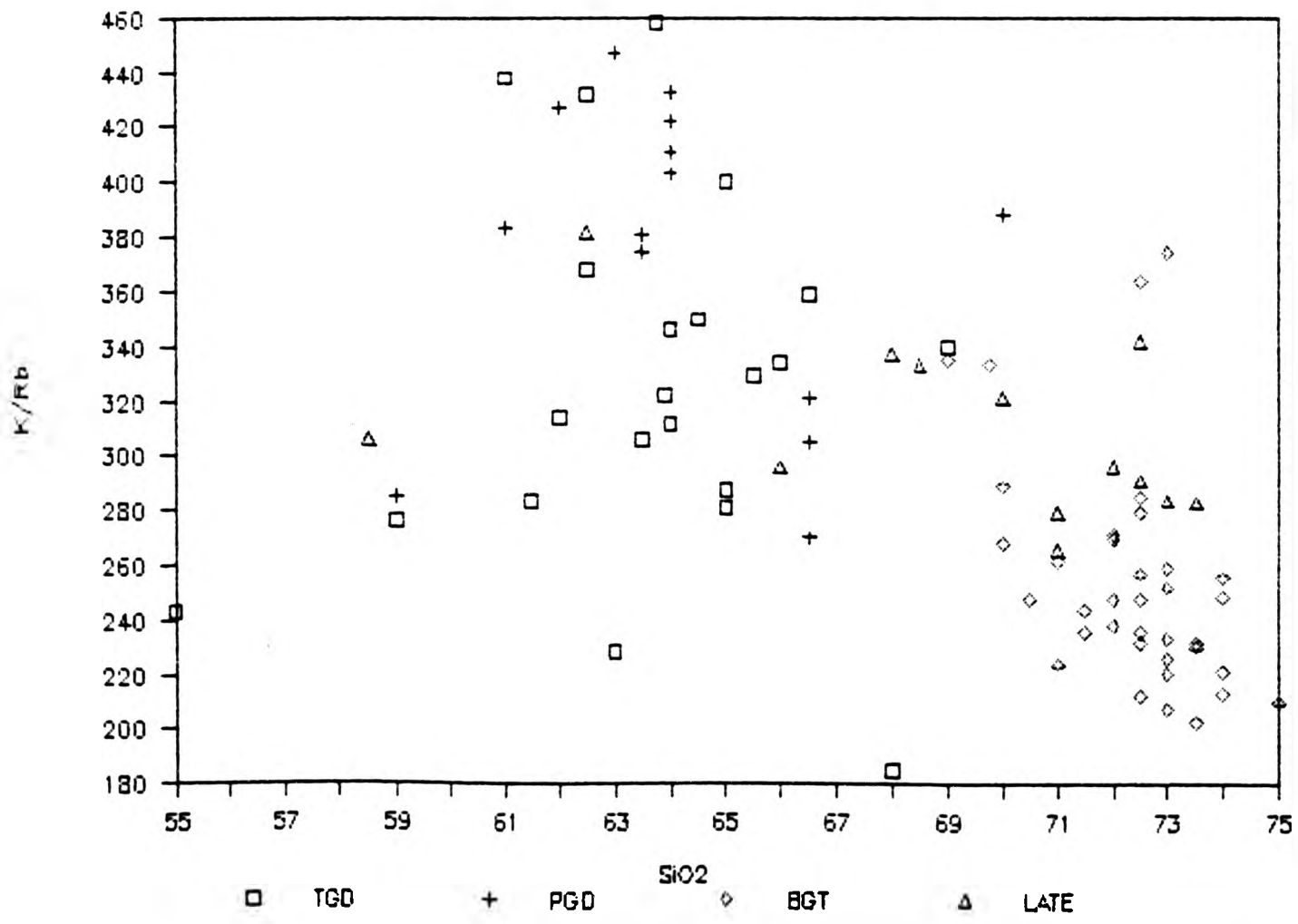

increasing SiO_2, which various authors suggest can be attributed to fractional crystallization of a magma or the crystallization of amphibole which preferentially concentrates K+ (eg. Taylor 1969). When plotted against each other there is a positive correlation with increasing levels towards the biotite granite (Fig 4.22). The higher Rb content in the tonalitic granodiorites correspond to hornblende/biotite rich rocks.

These three elements are best discussed together rather than in binary relationships (El Bouseily & El Sokkary 1975). On the ternary diagram (Fig.4.23) they plot mainly in the high-Ca field of Turekian & Wedepohl(1961) from El Bouseily & El Sokkary (1975), while a small group of tonalitic granodiorites plot completely separately on the border with the diorite field. This group has also been noted as being separate on Fig.4.11, 4.13 and 4.19, where they have substantially lower K_2O and Ba levels. Ba depletion leads to either Rb or Sr enrichment (El Bouseily & El Sokkary 1975) and this is seen on the ternary diagram Fig 4.23. In the differentiation sequence of diorites - quartz diorites - granodiorites - normal granites (described in El Bouseilly & El Sokkary 1975) the Ba/Sr is a governing factor and is found to increase with differentiation from the granodiorites to the biotite granite of Strontian (Fig.4.24). Also in the sequence of normal granite - strongly differentiated granite the Ba/Rb ratio is very sensitive in following differentiation and this is also seen in Strontian as a rapid decrease with increasing silica in Fig.4.25. While Fig.4.26 Sr vs Rb shows a decrease of Sr with decreasing Rb from the granodiorites to the biotite granite. There appears to be a small break in the trend between the two groups. This is supported by the fact that they are separate intrusions.

FIGURE 4.22 Rb vs K20

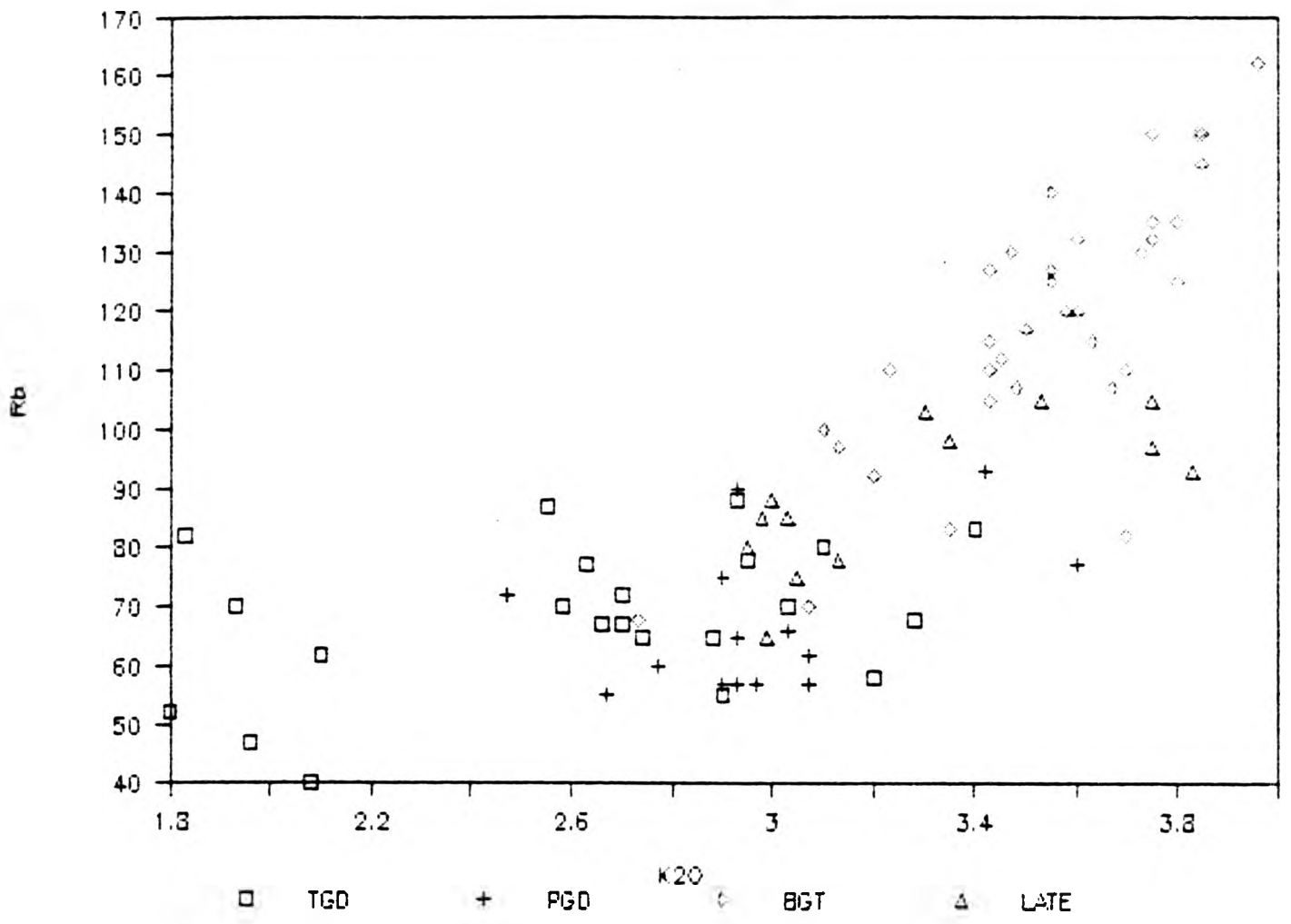

FIGURE 4.24 Ba/Sr vs SiO2

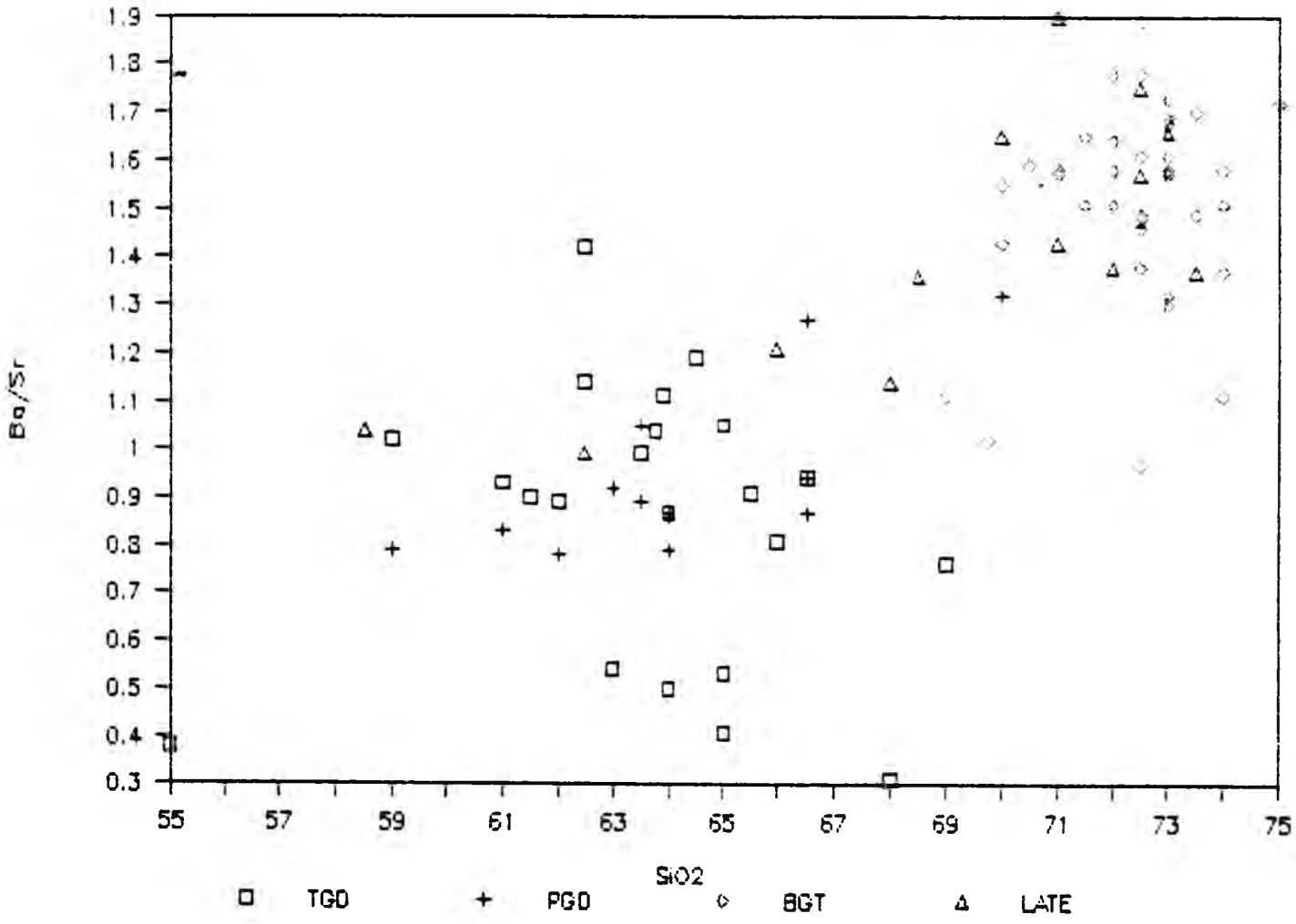

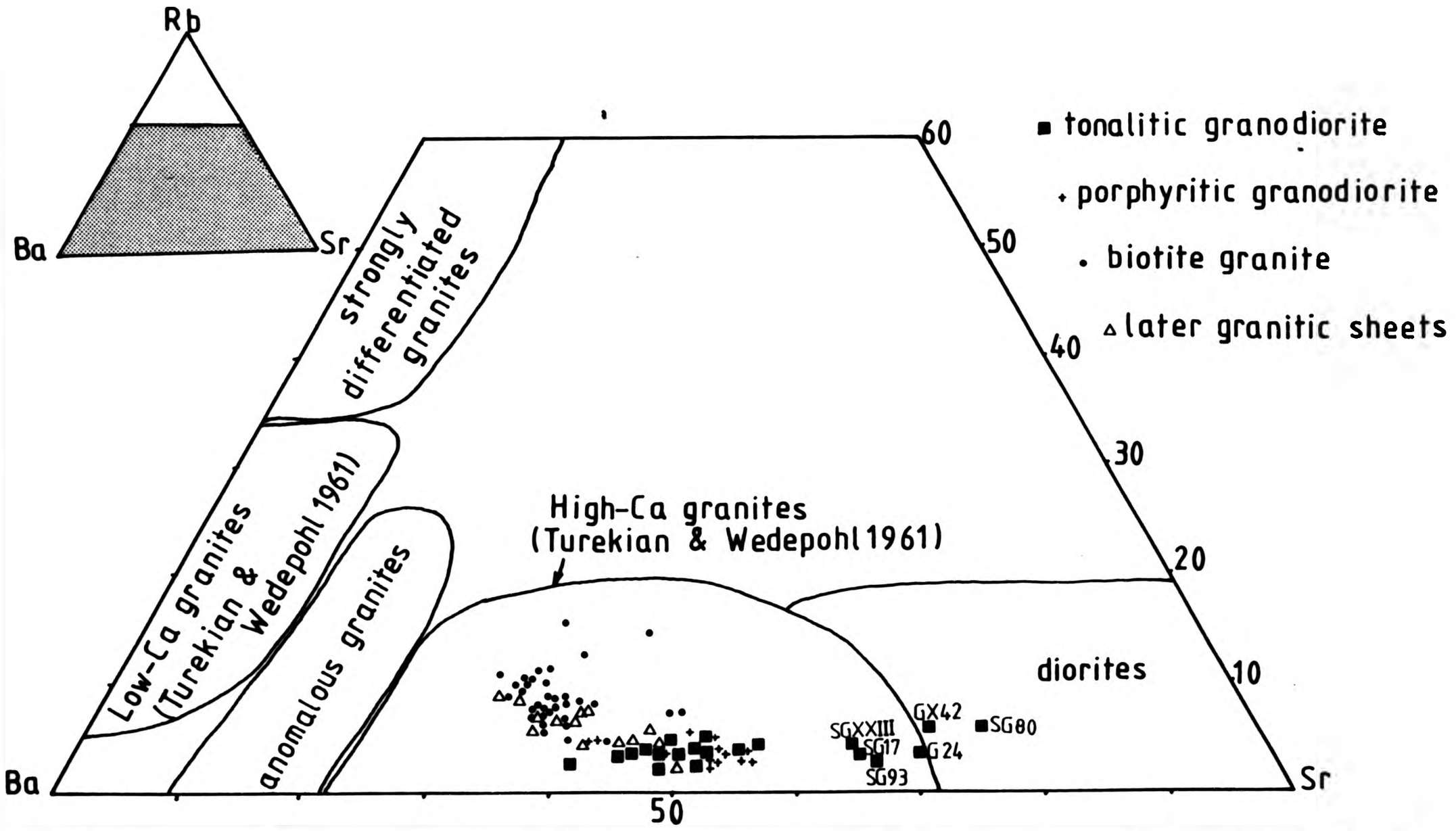

Fig. 4·23 The relationship between Rb, Ba and Sr in the various host rocks of Strontian (from El Bouseily & El Sokkary 1975).

FIGURE 4.25 Ba/Rb vs SiO2

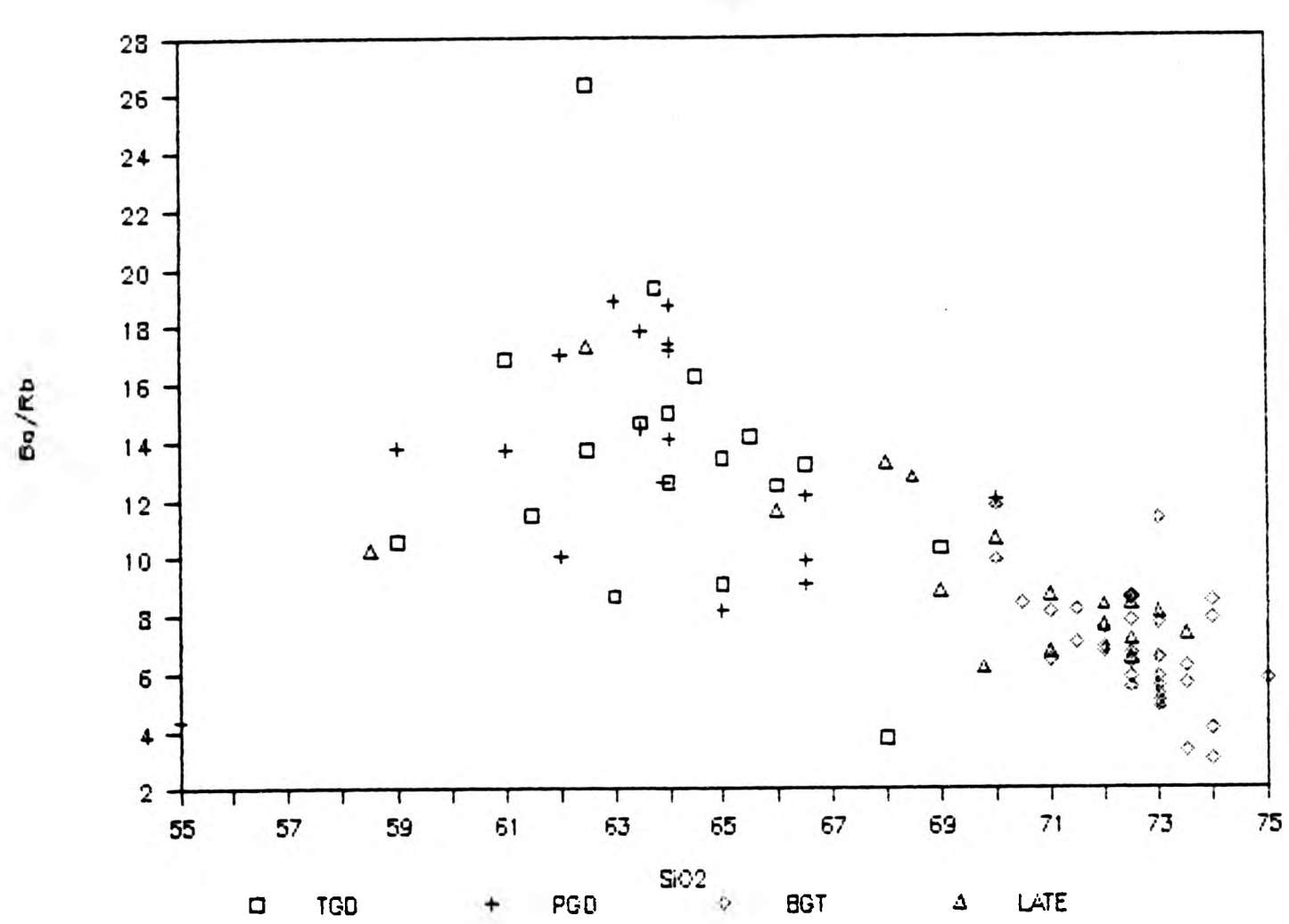

FIGURE 4.26 Sr vs Rb

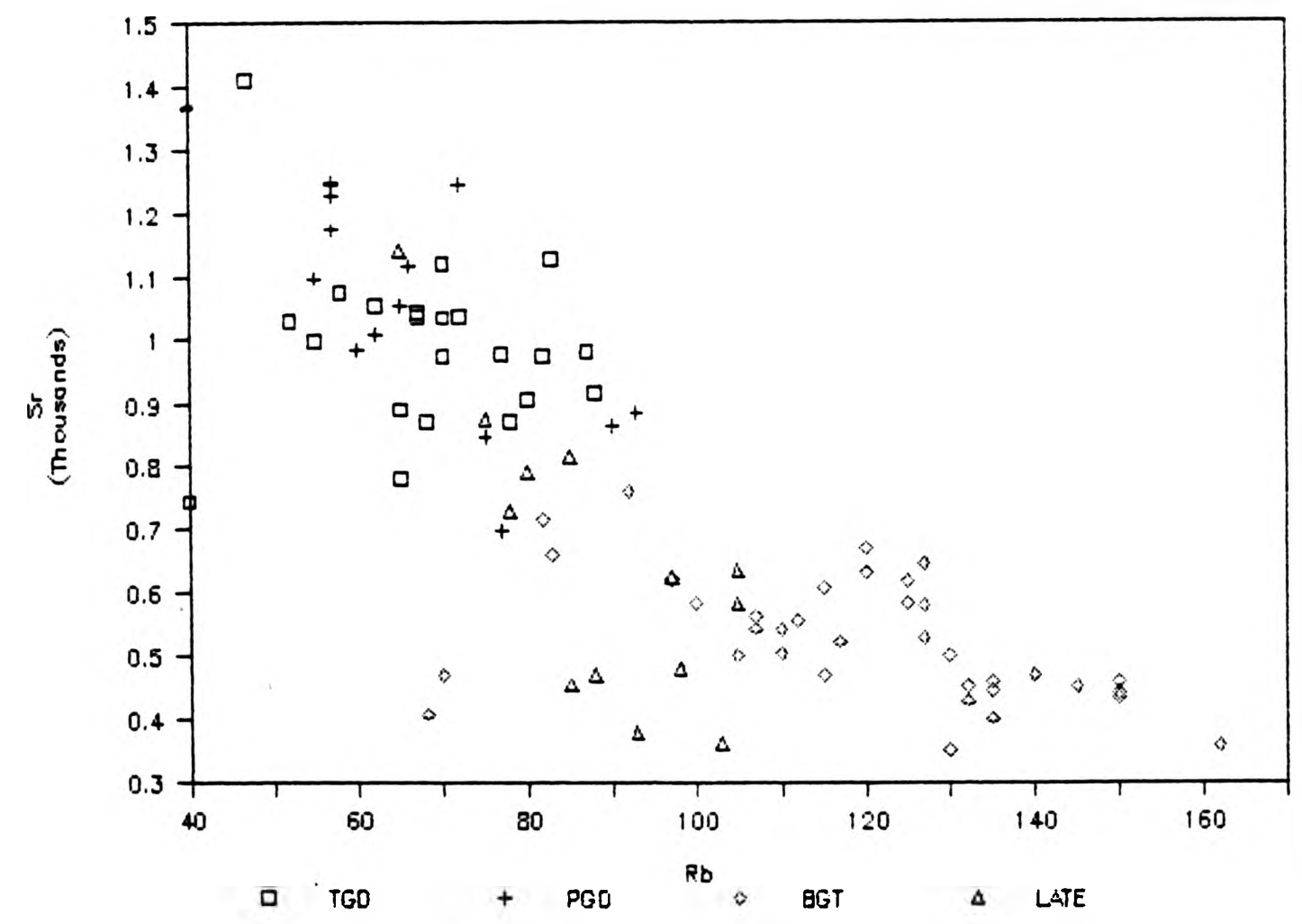

4.3.2 Nickel and Chromium

The distribution of Cr and Ni are shown on Figs 4.27 & 4.28. A similar pattern is seen on both diagrams of decreasing values with increasing silica, with levels falling from 220 to 10ppm Cr and 160 to less than 10ppm Ni.

Chromium in the tonalitic granodiorite shows the greatest scatter with values from 220 to 30ppm and the porphyritic granodiorite within these limits at 145 to 37ppm Cr. The biotite granite forms a very tight group 30 to 8ppm, with an average 12 to 10ppm Cr. The later sheets either follow the overall trend or are found as a separate group with overall higher levels of Cr than in the biotite granite (Fig 4.27). This separation has not been noted in on many other elements.

Cr^{+3} (0.63A) commonly substitutes for Fe^{+3} (0.69A) and so the lower Cr levels will reflect lower FeO* in the host rocks. There are no minerals which readily concentrate Cr such as chrome bearing spinels or clinopyroxene. However a small number of titaniferous magnetites (Chapter 3, sec.3.4.6) were analyzed and Cr_2O_3 contents of 0.039 to 0.169% were recorded. Chromium was also found in oxide analyses of haematite, giving values of 0.15 to 0.40%. Cr plotted against MgO also shows a positive correlation.

Nickel shows two parallel linear trends (Fig.4.28), but these reflect two different analysis batches and must be considered suspect, probably an error on standards. If the trends were moved together they would show a coherent linear trend of decreasing Ni with increasing silica. The tonalitic granodiorite: 160 to 12ppm Ni and

FIGURE 4.27 Cr vs SiO2

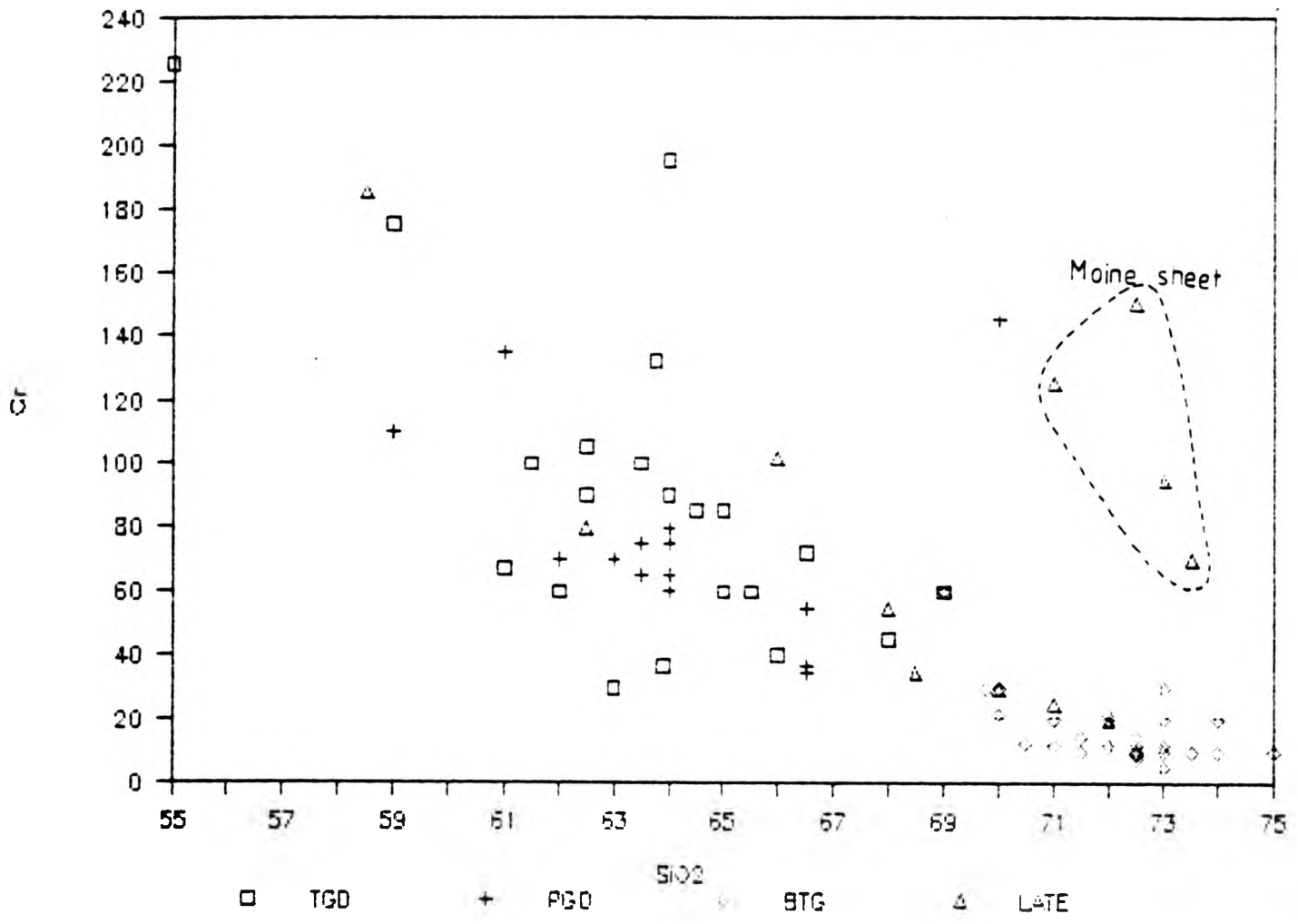

FIGURE 4.28 Ni vs SiO2

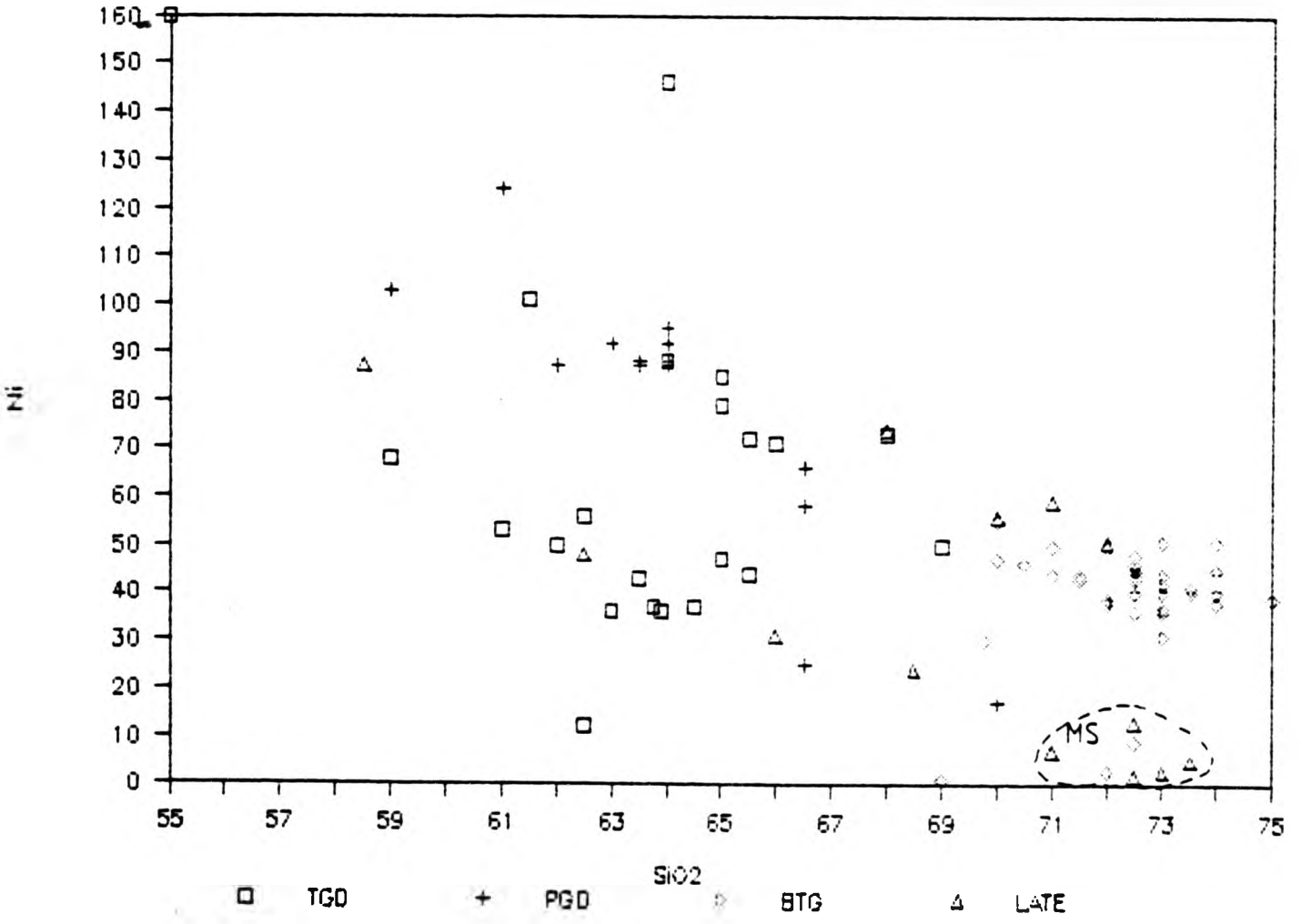

the porphyritic granodiorites 124 to 60ppm Ni. The biotite granites have a more restricted range of 55 to 31ppm Ni and the later sheets 74 to 51ppm Ni. The other sheets (ctG on the map) have 87 to 2ppm Ni.

Ni^{+2} (0.69A) has the same ionic radius as Mg^{+2} (0.68A), and substitution can also occur with Fe^{+2}. Levels are low and early formed crystals in the magma are no longer present eg. pyroxene, which would contain substantial amounts. Minor amounts of Ni can substitute for Mg in amphiboles or pyroxenes, but the nickel content of these minerals has not been measured. When Ni is plotted against Cr it shows a positive correlation, indicating a close relationship between the two elements.

4.3.3 Vanadium and Scandium

Vanadium (Fig 4.29) and scandium (Fig 4.30) both display similar linear trends. V has a steep plot with values ranging from 150 to 40ppm V for the granodiorites, while the biotite granite forms a tight group at the high silica end with 60 to 20ppm V. The later sheets fall on the main trend.

The Sc plot shows a little more scatter with abundances for the granodiorites at 16 to 2ppm Sc and the biotite granite 5 to 2ppm Sc.

These distribution patterns follow closely those of FeO* and TiO_2. Both V and Sc can substitute for iron in ferromagnesian and oxide minerals. V^{+3} (0.74A) whose ionic radius is greater than Fe^{+3} (0.64A) has a lower electronegativity, so substitutes for Fe^{+2} in magnetite. While Sc^{+3} (0.732A) has almost the same ionic radius as

FIGURE 4.29 V vs SiO2

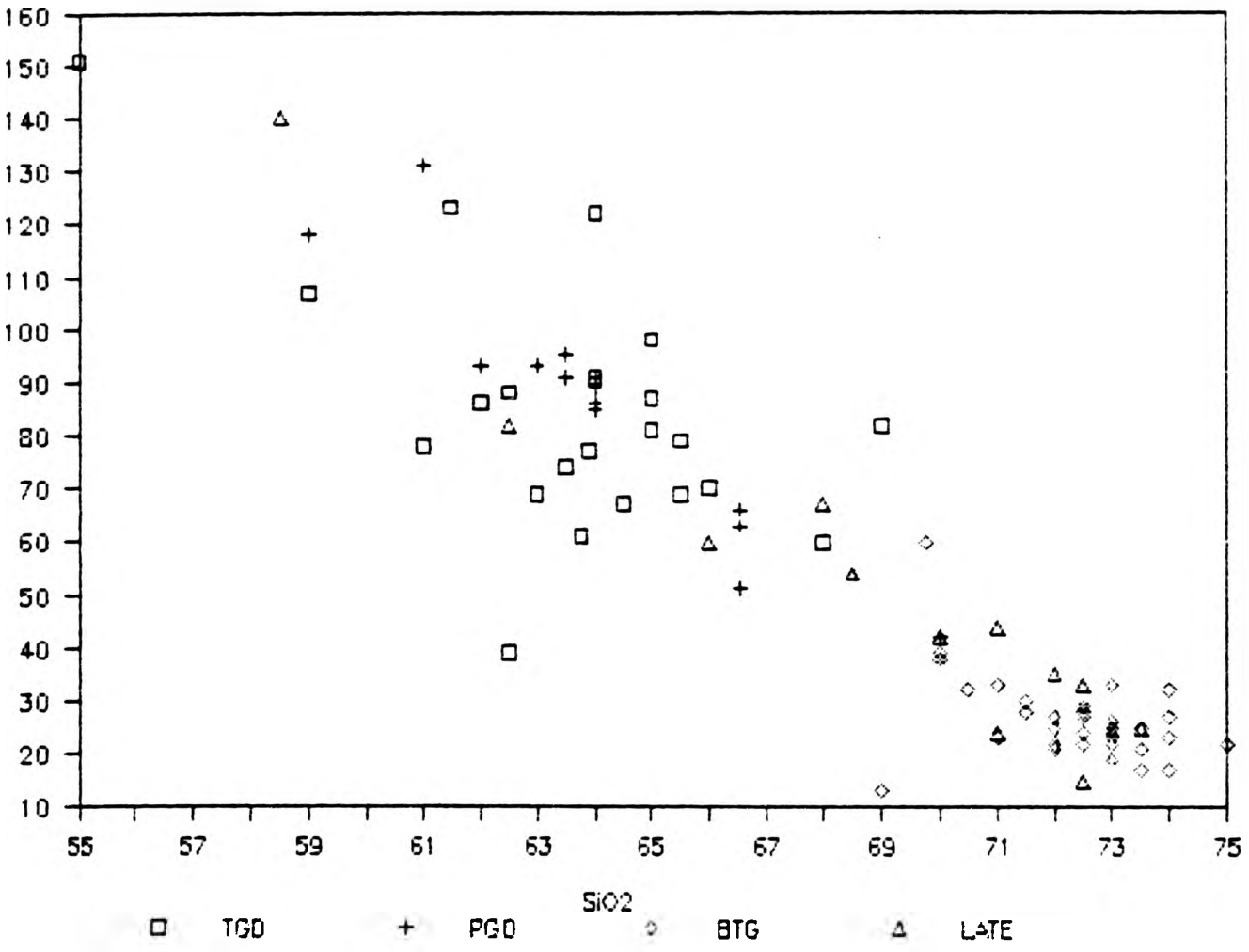

FIGURE 4.30 Sc vs SiO2

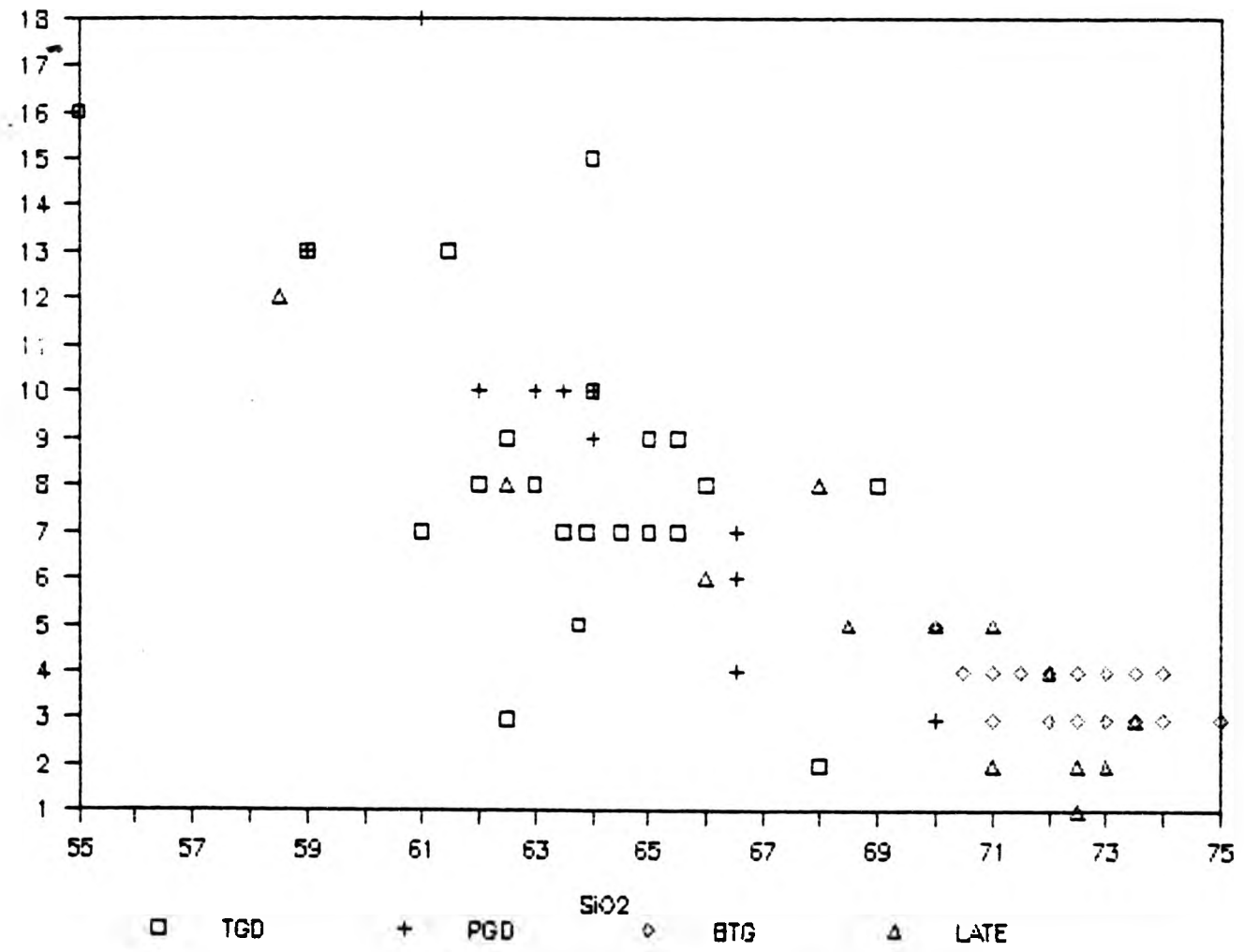

Fe^{+2} (0.74A) and so can substitute in pyroxene, amphibole and biotite. Plots of FeO* vs Sc, FeO* vs V and TiO_2 vs V (Figs 4.31, 4.32 & 4.33) all show positive linear correlations and they are all consistent with the data of substitution for iron and titanium.

4.3.4 Copper, Zinc, Lithium and Yttrium

Figures 4.34, 4.35 & 4.36 display the distribution patterns for these elements. Cu and Zn show gentle linear trends of decreasing values, while Li has a definite but scattered increase with increasing SiO_2.

The abundance of Cu varies from 57 to less than 10ppm Cu for the granodiorites and 20 to 5ppm Cu for the biotite granite and later sheets. Zn levels are 120 to 45ppm for the granodiorites and 70 to 20ppm for the biotite granites and later sheets.

Zn^{+2} (0.74A) has the same ionic radius as Fe^{+2} (0.74A), allowing substitution in ferromagnesian minerals like pyroxene, amphibole and biotite and also in iron oxide where the iron is in the ferrous form (Mason 1966). Copper commonly occurs in the Cu^{+2} state in igneous rocks and so substitutes for Fe^{+2} even though the electronegativity is greater than iron or zinc.

Lithium shows a scattered but positive correlation increasing from 10 to 45ppm for the granodiorites (exception at 70ppm) over the range of 61 to 65% SiO2 and 2 to nearly 60ppm for the biotite granite. Li^{+1} has the same small ionic radius as Mg^{+2} (0.68A) and only limited substitution takes place in pyroxene, amphibole and biotite. It is thought that it frequently remains in the magma until late stage differentiation (Mason 1966). The scatter of the Li data may be

FIGURE 4.31 Sc vs FeO

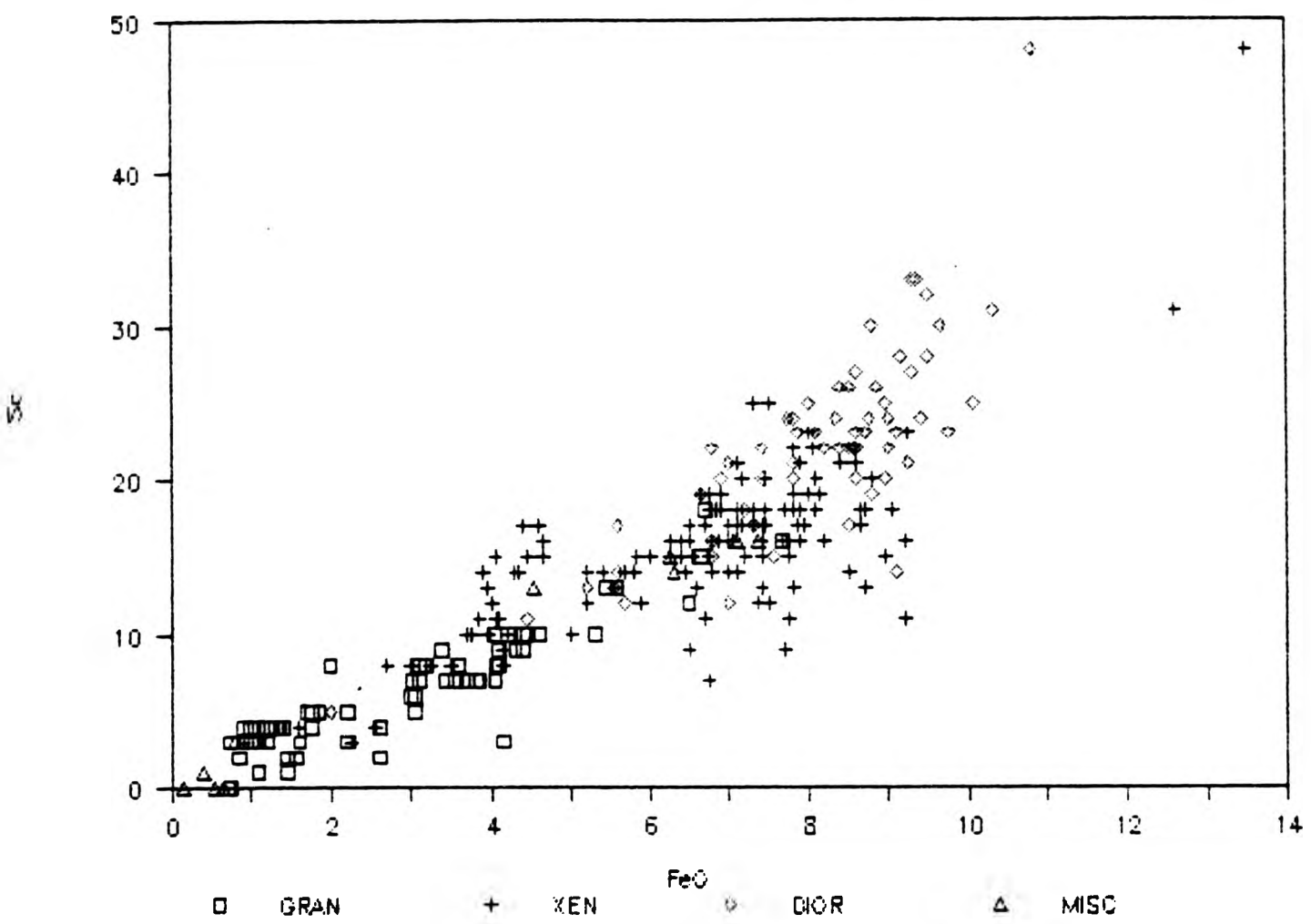

FIGURE 4.32 V vs FeO

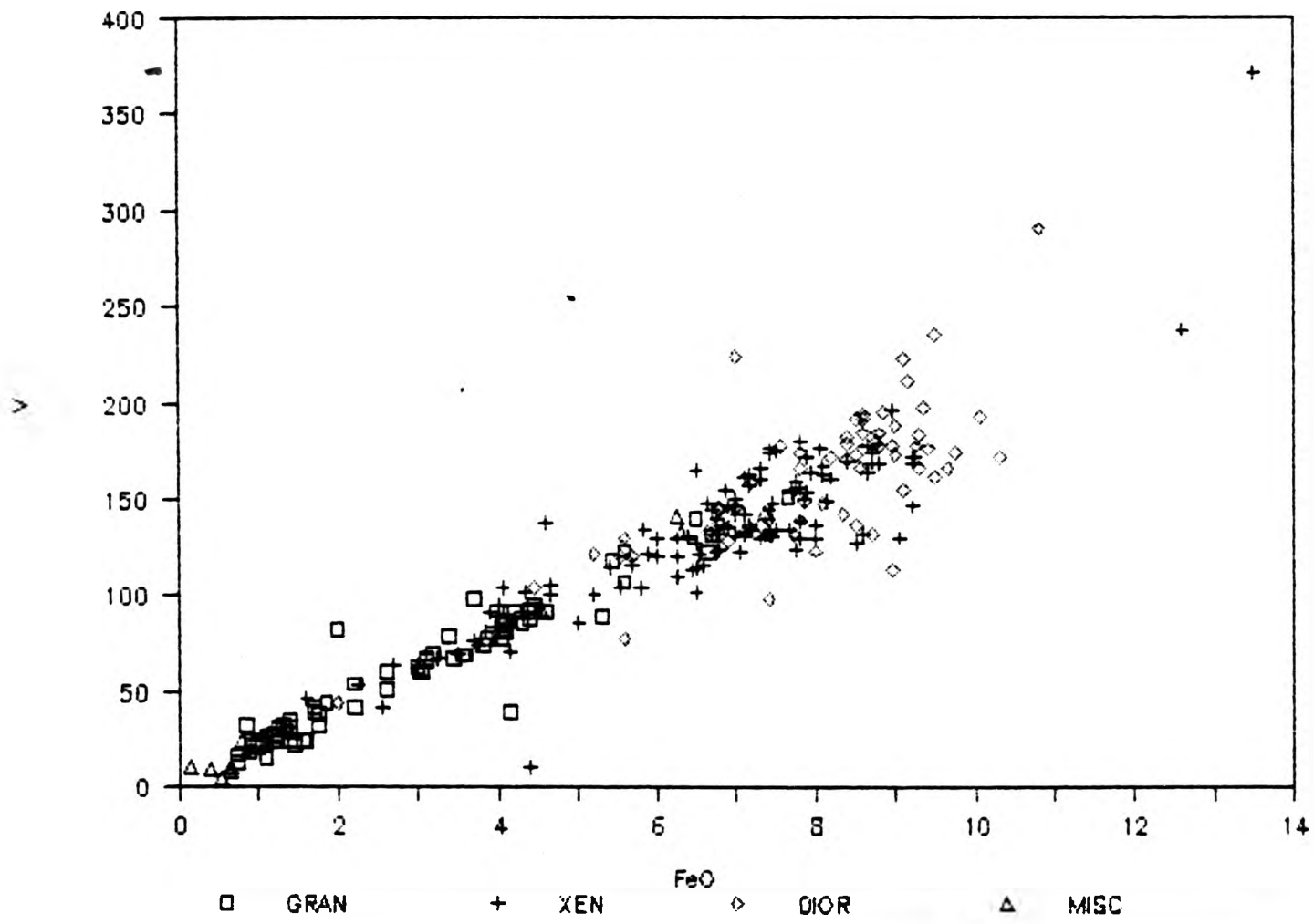

FIGURE 4.33 V vs TiO2

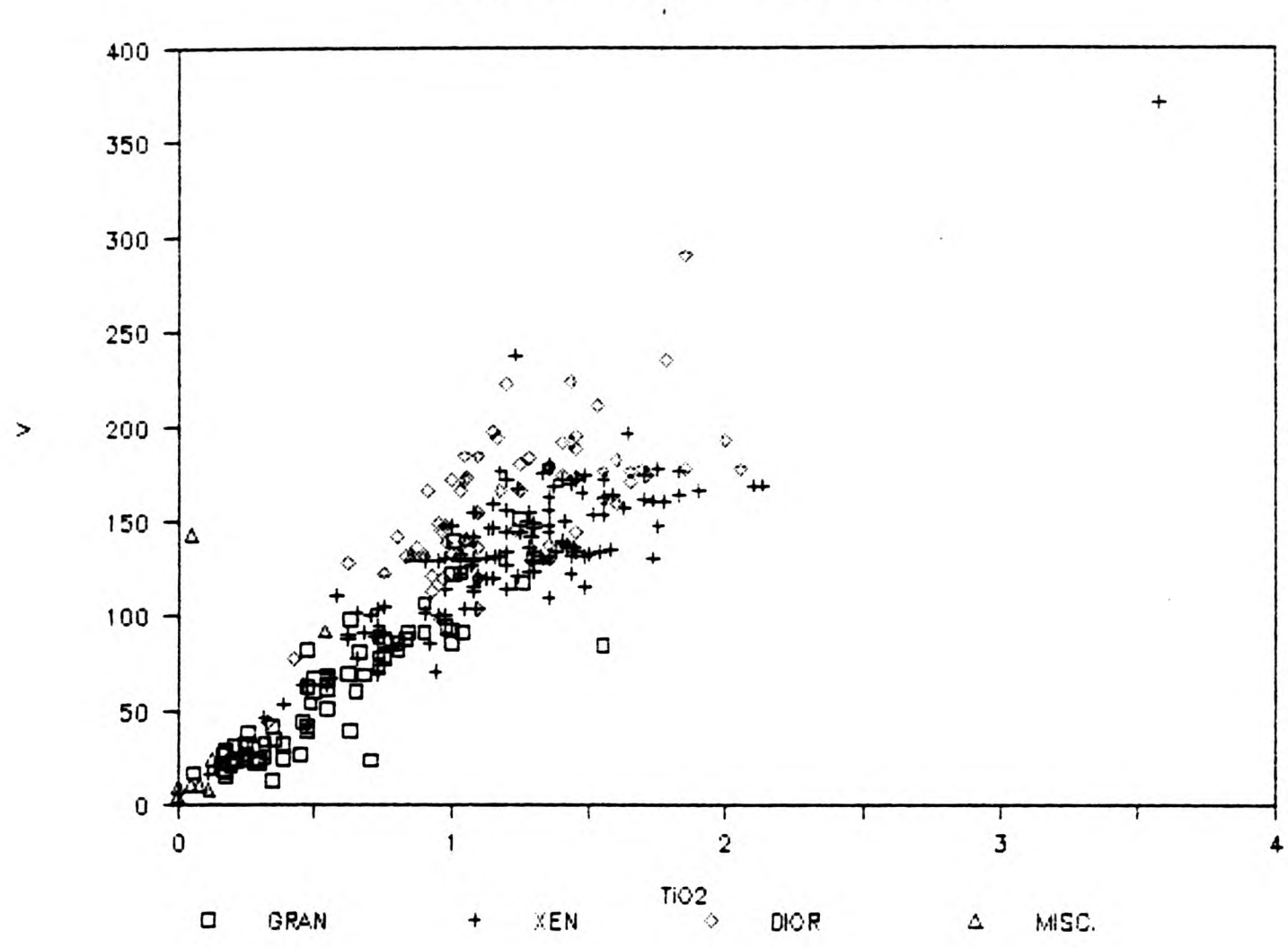

FIGURE 4.34 Cu vs SiO2

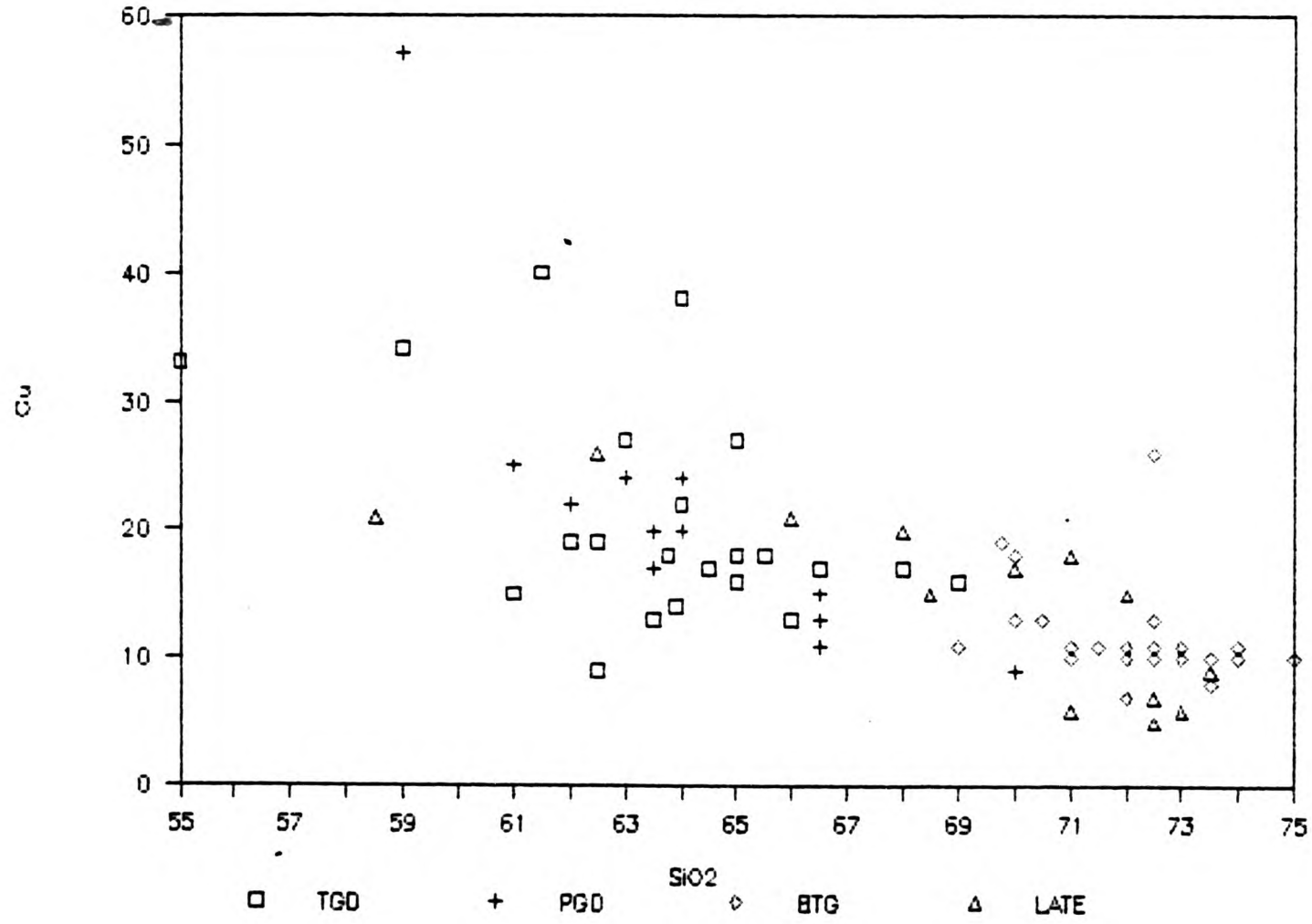

FIGURE 4.35 Zn vs SiO2

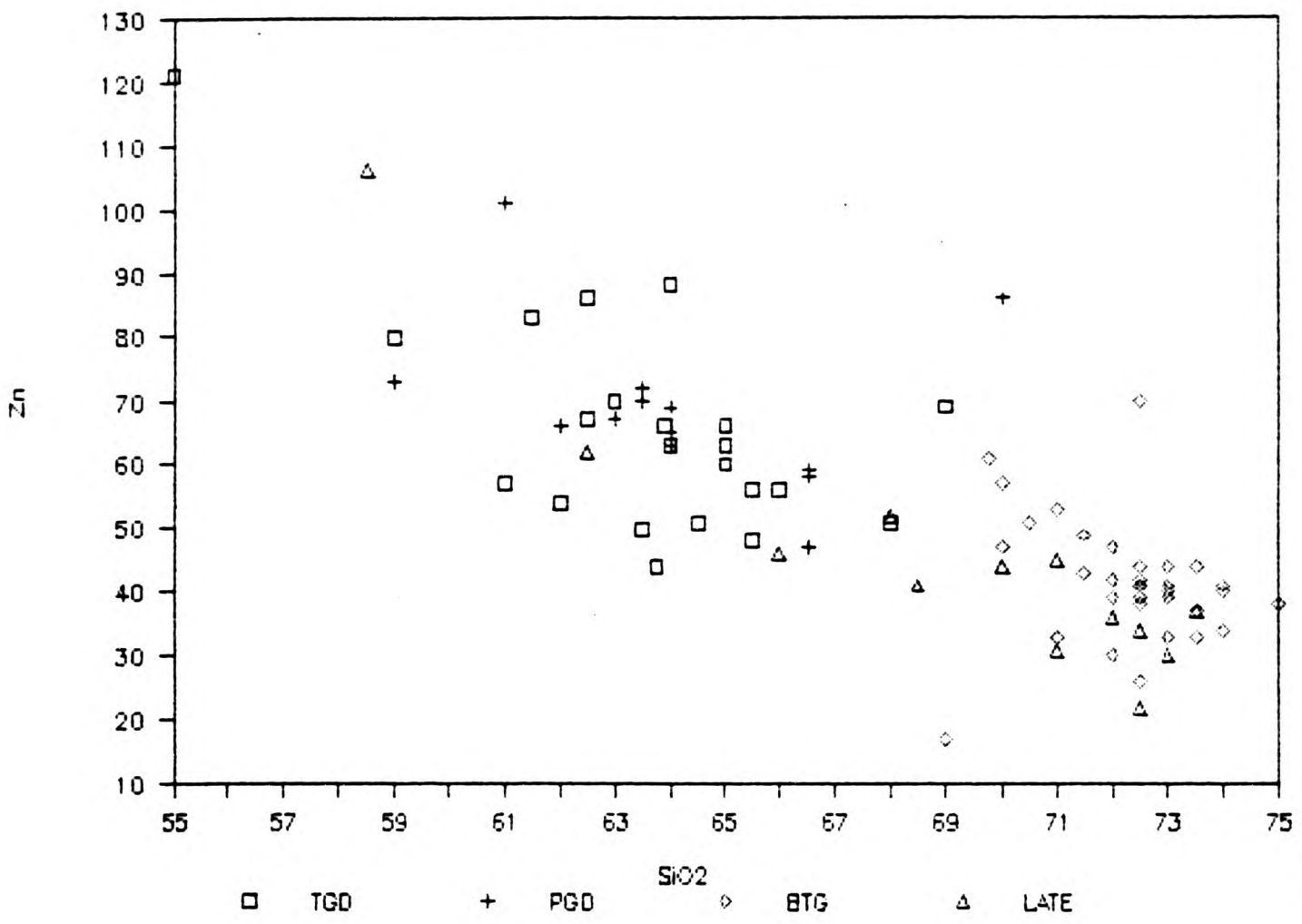

FIGURE 4.36 Li vs SiO2

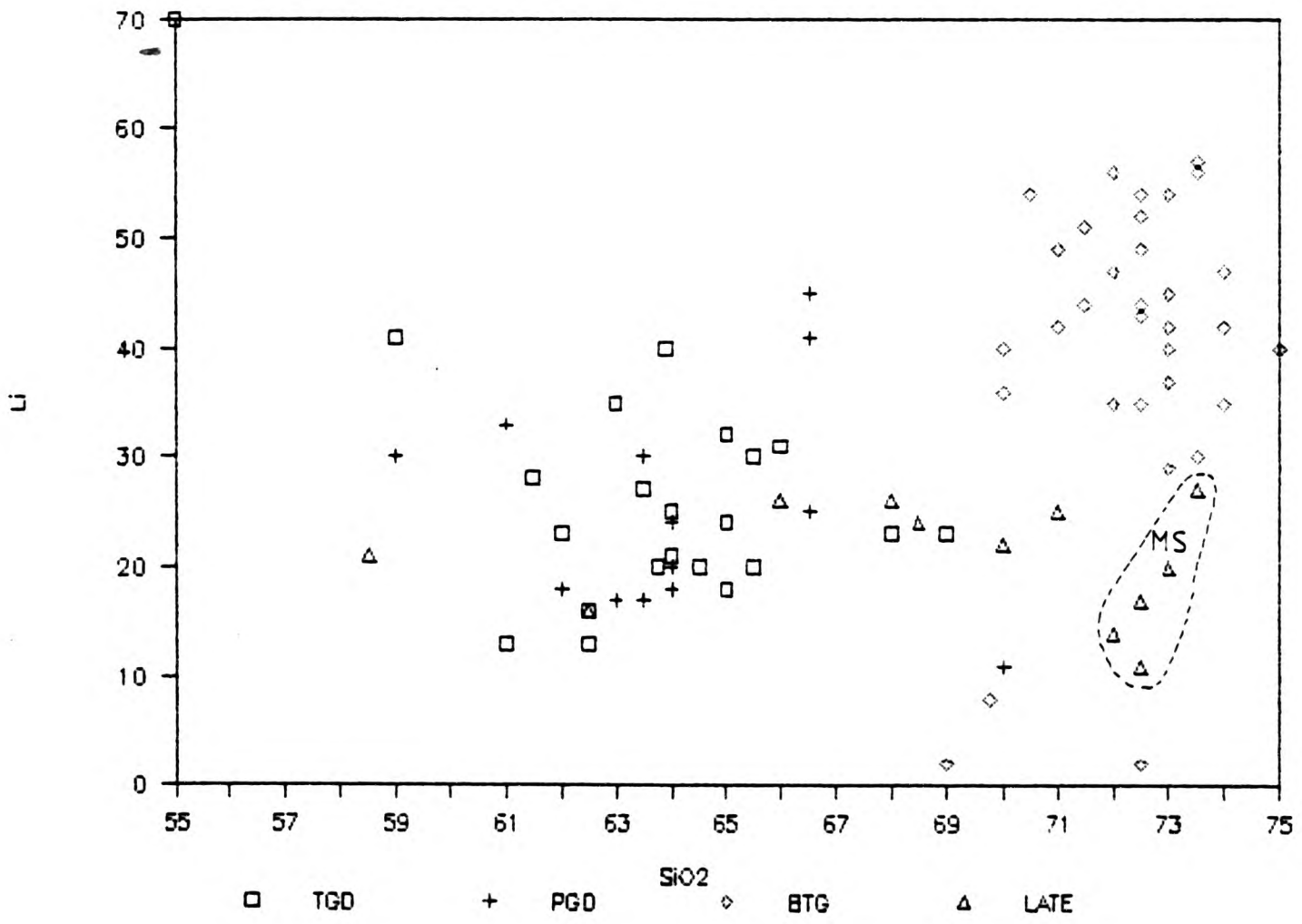

controlled by the modal abundance of ferromagnesian minerals, which does decrease in the host rocks with increasing silica. The Moine sheet samples again plot separately from the biotite granite and the main trend indicating it may be from a different source and /or has undergone a separate stage of differentiation.

Yttrium shows a scattered but linear decrease in levels with increasing differentiation. The granodiorites have 31 to 8ppm Y, while the biotite granite have a smaller range of 18 to 4ppm.

4.4.1 Host Rock REE Patterns

The host rocks are variable in the degree of La enrichment. The chondrite normalized patterns for these rocks are relatively steep with La/Yb ratios from 21.8 to 38.0 with an average of 29.9. LaN varies from 73 to 197x chondrite and LuN from 3 to 9x chondrite. The profiles are essentially parallel and smooth. Slight positive and negative Eu anomalies have been noted on the host rock diagrams (Fig. 4.37). There are in fact several granodiorite samples which show a positive Eu anomaly. They are SGC1, SGIX and GX7 and all are located within 500m of the complex margin. They have a higher plagioclase content than the other granodiorite samples. Negative Eu anomalies in the REE patterns of granitic rocks are usually interpreted as evidence of earlier separation of a mineral phase such as plagioclase (Fowler & Doig 1983). Miller & Mittlefehldt (1982) believe that fractionation of a very felsic magma results in the depletion of LREE in liquids, because of the early and continuing crystallization of small quantities of highly enriched accessories.

McCarthy & Kable (1978), Exley (1980), Henderson (1980) and Gromet &

Fig. 4·37 Chondrite normalised REE patterns for the host rocks of Strontian.

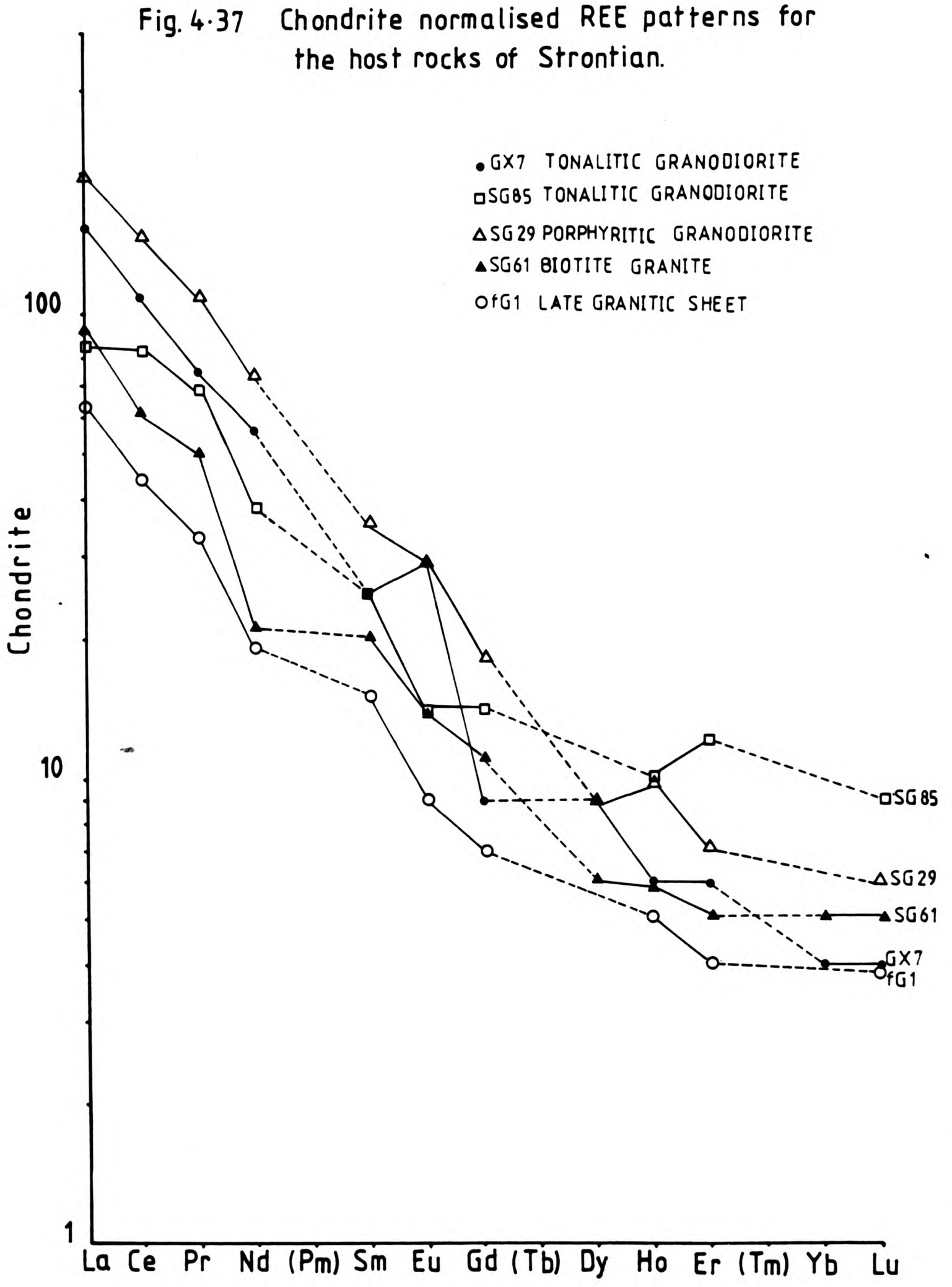

Silver (1983) all show that amphibole and minor minerals such as sphene, apatite and allanite are enriched in REE and that they have an important role in the behaviour of REE in granitic magmas. Therefore the early fractionation of amphibole, apatite and sphene will capture the REE and cause a fall in the REE (except Eu) content of the magma; while crystallization of plagioclase will cause a rise in the REE (except Eu). The Eu anomalies are well documented in Sawka (1988) where hornblende, apatite and sphene all show negative anomalies, but with relatively flat chondrite normalized plots. So if all 4 phases were crystallizing, particularly amphibole and plagioclase, the net effect would be of the Eu anomalies cancelling themselves out. This could be the case in Strontian with such poorly developed Eu anomalies. However the samples showing positive Eu anomalies are noted as being more plagioclase-rich than ferromagnesian-rich.

The absolute abundance of the REE tends to decrease with increasing whole rock silica content. The La/Yb ratio falls with increasing silica ie. from 38 (at 61% SiO_2) to 22 (at 72.5% SiO_2). This trend is the reverse of normal igneous trends (Pankhurst 1979), but is similar to the pattern in the Galway Granite (Coats & Wilson 1971). The aplitic veins analyzed show very low values and extreme patterns which may well be the result of poor analysis.

REE profiles for the Loch Doon Complex (Tindle & Pearce 1981 & 1983) for diorite and granodiorite compositions are typically shallow, broadly parallel with La/Yb ratios of 10.3 and display negative europium anomalies. The sequence of rocks in Loch Doon is thought to be the result of in-situ fractional crystallization and so the distribution of the REE controlled by the crystallization of minor

phases such as apatite, zircon, sphene and allanite.

The primitive andesite lavas of the Lorne Plateau and the Sidlaw Hills (Thirlwall 1982) have a SiO_2 range of 48.9 to 60.3, which spans the lower half of the Strontian granodiorite range. They display relatively steep, smooth patterns (La/Yb - 29). The Sidlaw lavas show an increase in the LREE/HREE ratio with increasing silica, a feature typical of a magma undergoing fractional crystallization and where the REE are behaving essentially as incompatible elements. This is the opposite to the Strontian complex where Pankhurst (1979) regards the REE as behaving as compatible elements.

4.5 PETROGENESIS

This section integrates the data and observations from mineral chemistry (Chapter 3) and bulk rock chemistry, therefore allowing the development of possible models for the evolution of the Strontian granite. As demonstrated in the earlier sections the Strontian granite comprises of a suite of lithologies ranging from a tonalitic granodiorite to a very quartz rich biotite granite. They show in general continuous trends from the low silica end to the high. The silica-poor members of the TGD and PGD show differences although compositional fields still overlap partially. TGD is relatively poor in TiO_2 and P_2O_5 and richer in CaO than the PGD. For Sr, Sc, V and Cu vs SiO_2, PGD produces a well defined linear trend whilst the TGD shows substantial scatter and/or oblique trends. On the normative Qz-Or-Ab plot (Fig.3.7) the TGD data is also more scattered than PGD. These differences indicate that the two units identified in the field do have different histories of evolution. Some minor chemical characteristics however separate the two granodiorites from each

other and from the biotite granite.

The biotite granites are shown by Pankhurst (1979) to have different isotopic characteristics from the granodiorites; BGT initial $^{87}Sr/^{86}Sr$ ratios are .707167 to .7071861, whilst the PGD/TGD initial ratios are .703148 to .706003. Unfortunately he does not relate these inferred initial ratios to full analyses of specific rocks. Ba and Rb vs SiO_2 show very wide ranges of values gently increasing with SiO_2 that do not match well with the granodiorite pattern. The silica-rich end of the granodiorites in TiO_2 vs SiO_2 plots flatten and only passes through the highest TiO_2 BGT. Ba vs Sr shows good correlation in BGT forming a linear trend that passes along the Sr-poor side of the granodiorite data.

Some changes in gradient and pattern are exhibited by the linear trends particularly at 64% and 70% SiO_2. As SiO_2 increases above 64% the gradients decrease in FeO*, MnO, TiO_2 and CaO; the scatter of data points decreases abruptly for FeO*, MgO, MnO, TiO_2, Cr and Cu; Ba registers a well defined maximum values and Zn minimum values. These changes occur in the middle of the TGD-PGD compositional range and indicate the possibility of a change in process eg. new phases crystallize or a change from cumulates to liquids. The changes in trend with increasing SiO_2 at 70% SiO_2 are decreases in gradient to nearly zero for TiO_2, FeO* and MgO, decrease for K_2O and very abrupt changes from zero to a positive gradient for Rb. These are in addition to the discriminations in patterns described above.

All major and many minor elements produce broadly linear trends when plotted against silica. Such linear trends result from mixing magmas, variable extraction of residuum by filter pressing or

fractional crystallization of several phases from the magma. In the latter case the observed rocks may represent a sequence of magma compositions or a sequence of cumulates. Mixing may occur as a result of assimilation of crustal rocks by a rising magma or may involve two magmas in the process of hybridization. Therefore it must be regarded as an open system, where new material may always come in. Hybrid rocks are sometimes easy to recognize, whether streaks and patches of varying compositions or by the presence of 2 suites of phenocrysts not normally expected to be in equilibrium with each other. Parent compositions for magma mixing would be found as extreme end members of the trend or outside the analyzed trend of the granodiorite. Filter pressing involves the extraction of the interstitial liquid from a semi-solid magma. Parent compositions chosen for this method of crystallization would be found within the observed trend. Fractional crystallization will be reviewed in section 4.5.2 with regard to trace elements.

4.5.1 Major Element Modelling

Major element modelling for fractional crystallization uses the observed mineral assemblages and plots them on the bulk rock data (Figs.4.38 to 4.45). The smaller scale used for these diagrams tends to eliminate the more subtle gradient changes at 64% SiO_2 though the changes at 67 to 70% which remain visible. The mineral compositions here were all analyzed by microprobe and are given in Appendix C. The overall positions of the mineral triangles are the result of taking the middle of the compositional ranges for all the minerals except amphibole. Mg-rich amphibole compositions are chosen however as these may be less affected by subsolidus alteration. For the purpose of this initial modelling the parent liquid composition is

taken initially as the most primitive rock composition and assumes that analyzed rocks represent liquid compositions. X-X represents the tonalitic and porphyritic granodiorite crystal extract compositions while Xa-Xa represents the biotite granite extract needed to produce the observed rock variations. In Fig.4.39 (Cao vs SiO_2) the assumed parent lies within the extract triangle. The latter shows that some of the observed rocks can represent pure cumulates. For other oxides the parents lie outside the extract triangle.

Considering first only the tonalitic granodiorite Figs.4.38 (Al_2O_3), 4.39 (CaO), 4.41 (FeO*), 4.42 (K_2O), 4.43 (MgO) and 4.44 (Na_2O) all favour a crystal extract composition at about 45 to 50% SiO_2. Fractionation of a mixture of mainly hornblende, higher Ca-plagioclase with any small amount of biotite would allow the generation of the main granodiorite trend. Because the extract trend passes through the biotite composition in Al_2O_3 vs SiO_2 plot and through the plagioclase compositions of the extract triangle on CaO vs SiO_2, it is possible to estimate Amphibole : Plagioclase (1 : 0.895) and Amphibole : Biotite (1 : 0.4) ratios of extract. This would give a bulk extract of 44% amphibole, 39% plagioclase and 17% biotite with bulk SiO_2 approximately 50% in the Al_2O_3 vs SiO_2 plot. This composition is marked A on Figs. 4.38 to 4.44 and will work reasonably for all except Na_2O (Fig.4.44). Using this extract composition on the Al_2O_3 : SiO_2 plot (Fig.4.38) it is found that an initial liquid at 59% SiO_2, 36% crystallization must be removed to reduce SiO_2 to 64% and 50% must be removed to reduce SiO_2 to 68%. Conversely if all the rocks are cumulates from magmas with SiO_2 at 68%, the most silica-poor rocks represent 50% cumulate crystals with 50% interstitial liquid. Rocks at 64% SiO_2 would have 13% cumulate

FIGURE 4.38 Al2O3 vs SiO2

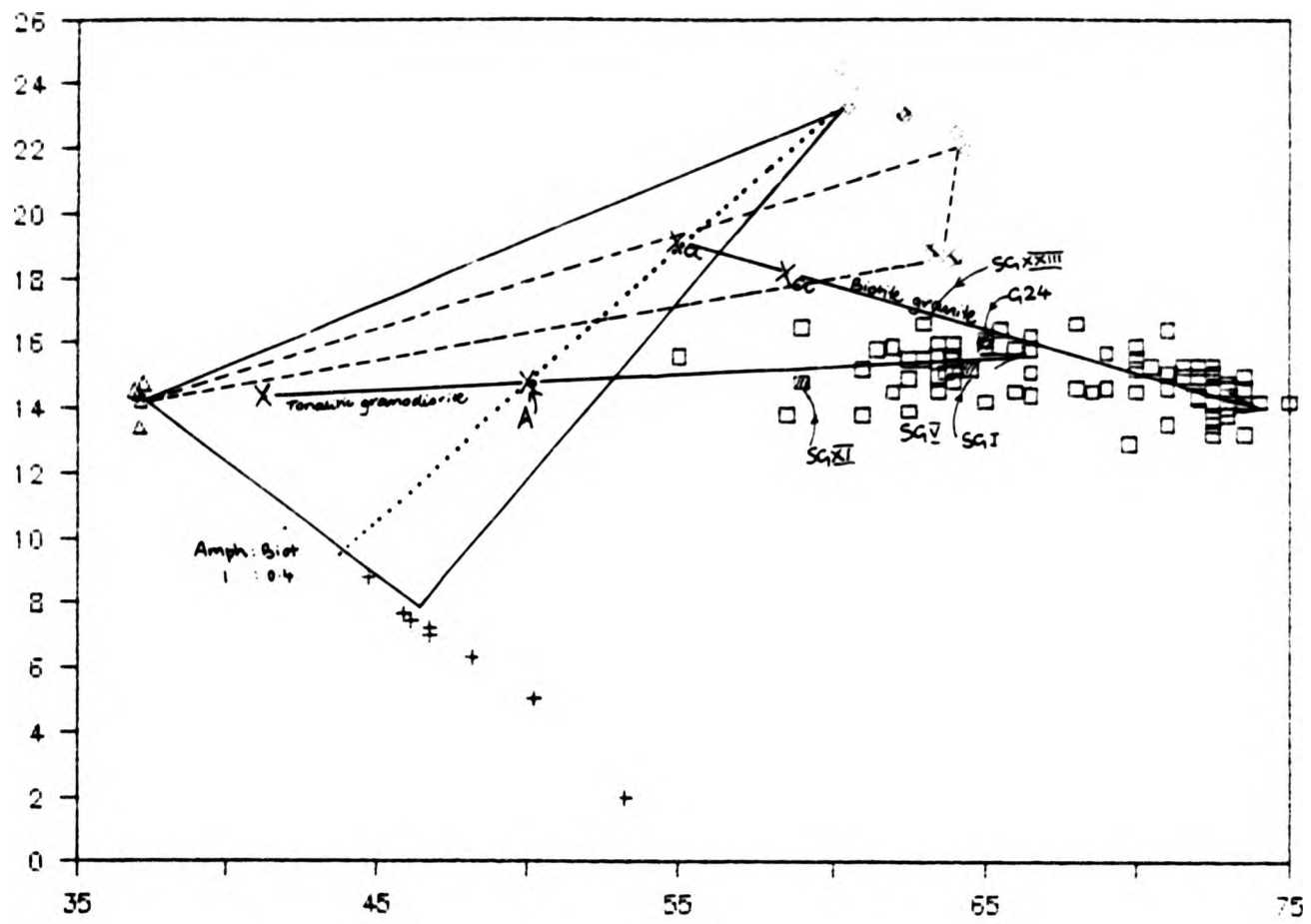

FIGURE 4.39 CaO vs SiO2

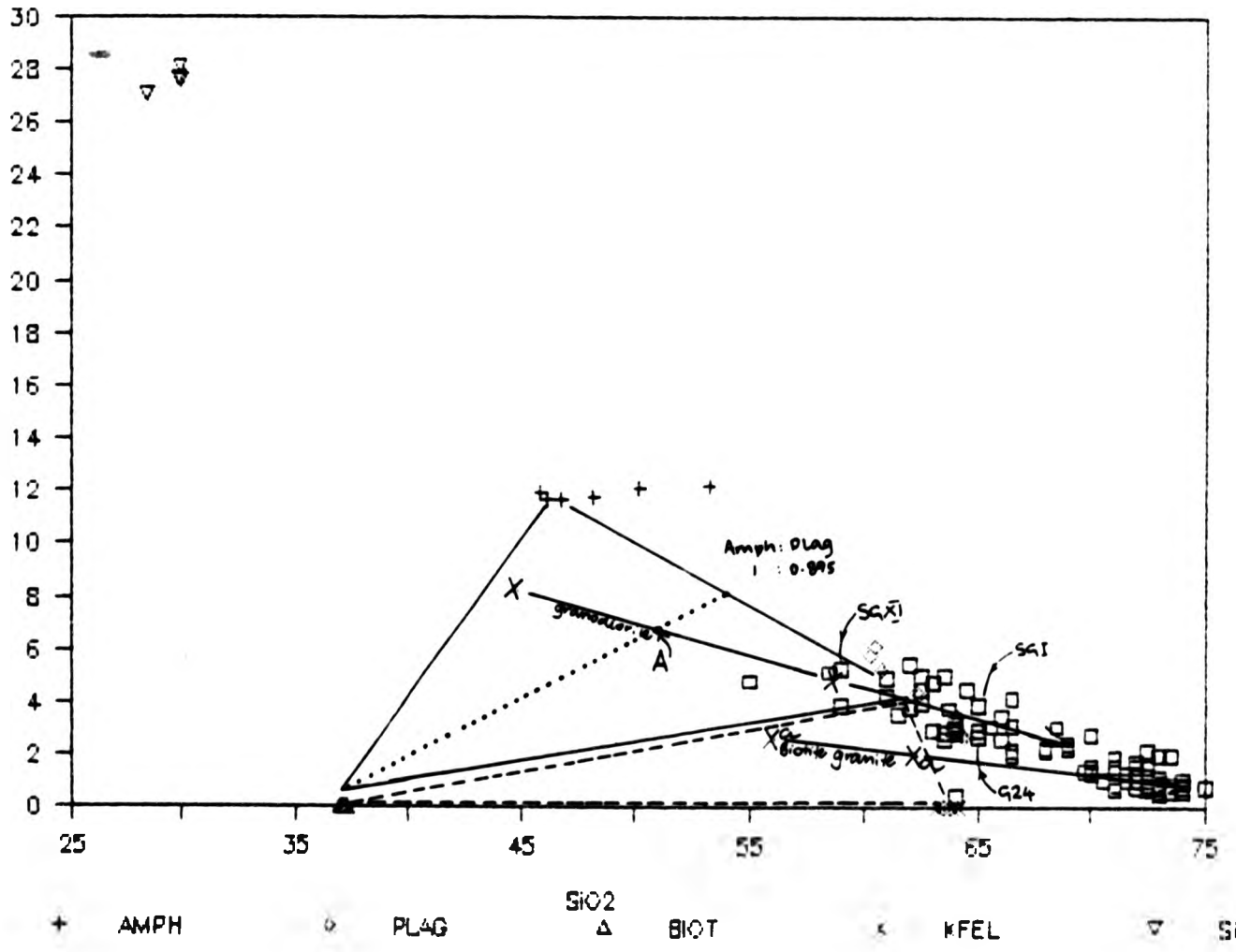

FIGURE 4.40 TiO2 vs SiO2

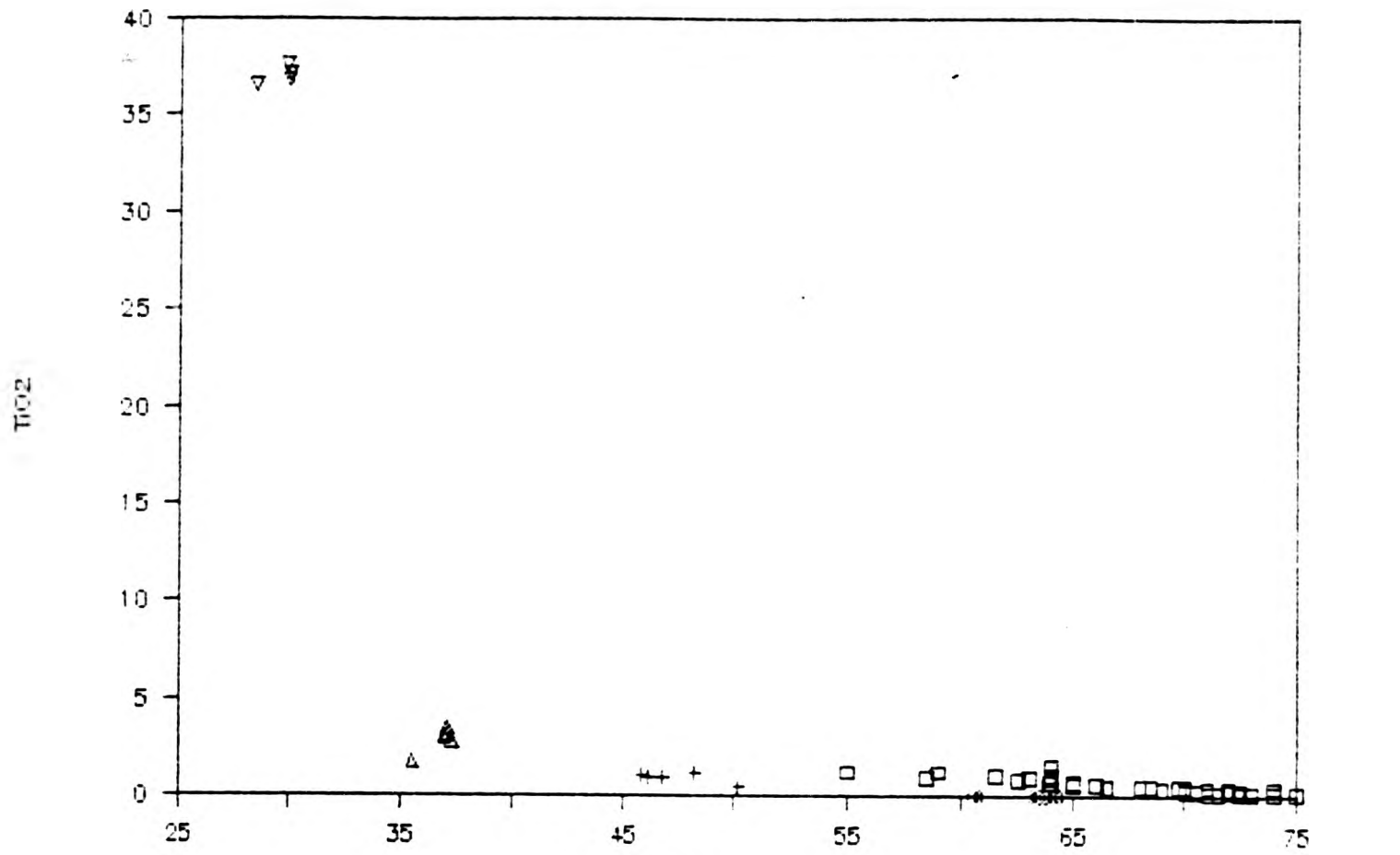

FIGURE 4.41 FeO* vs SiO2

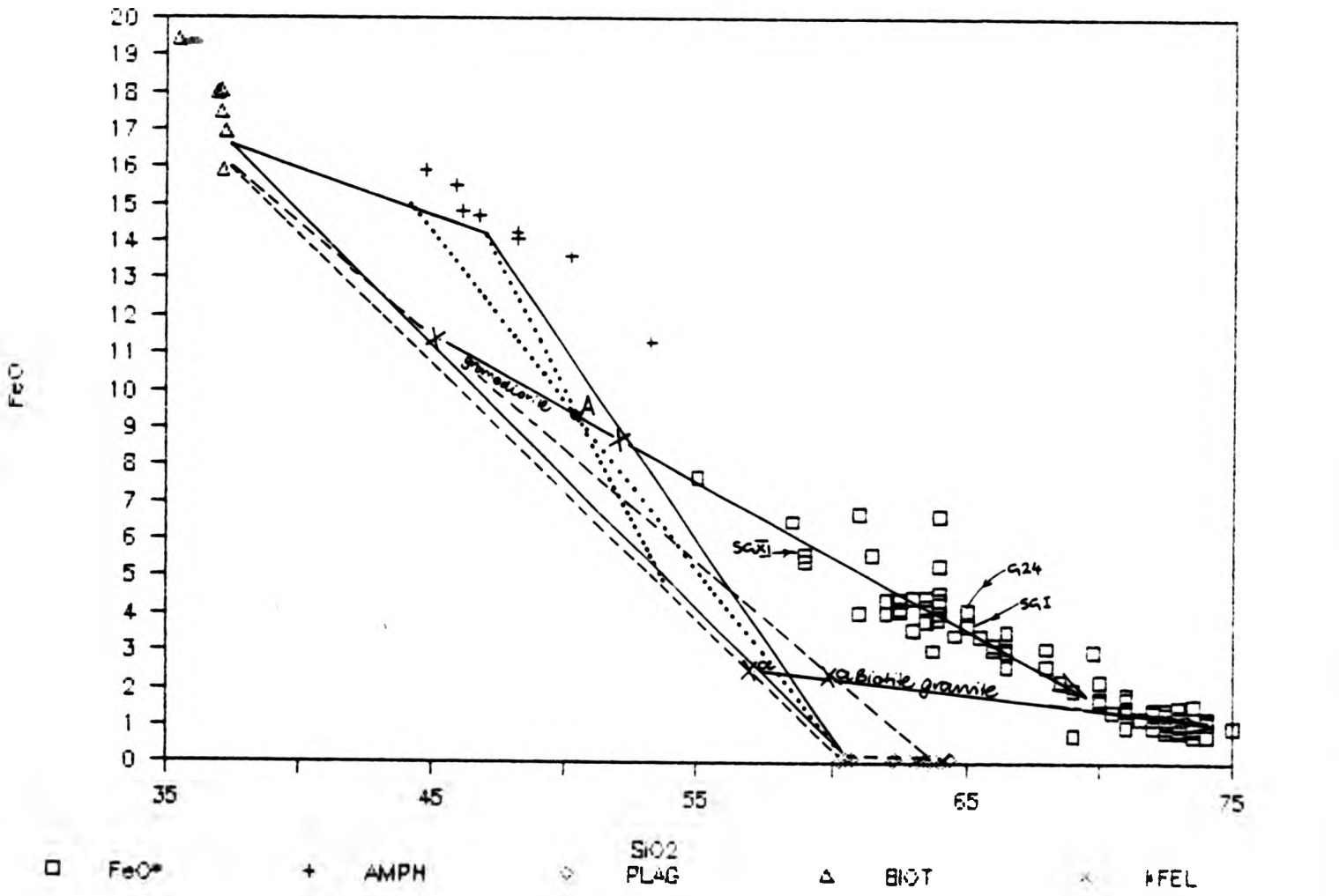

FIGURE 4.42 K2O vs SiO2

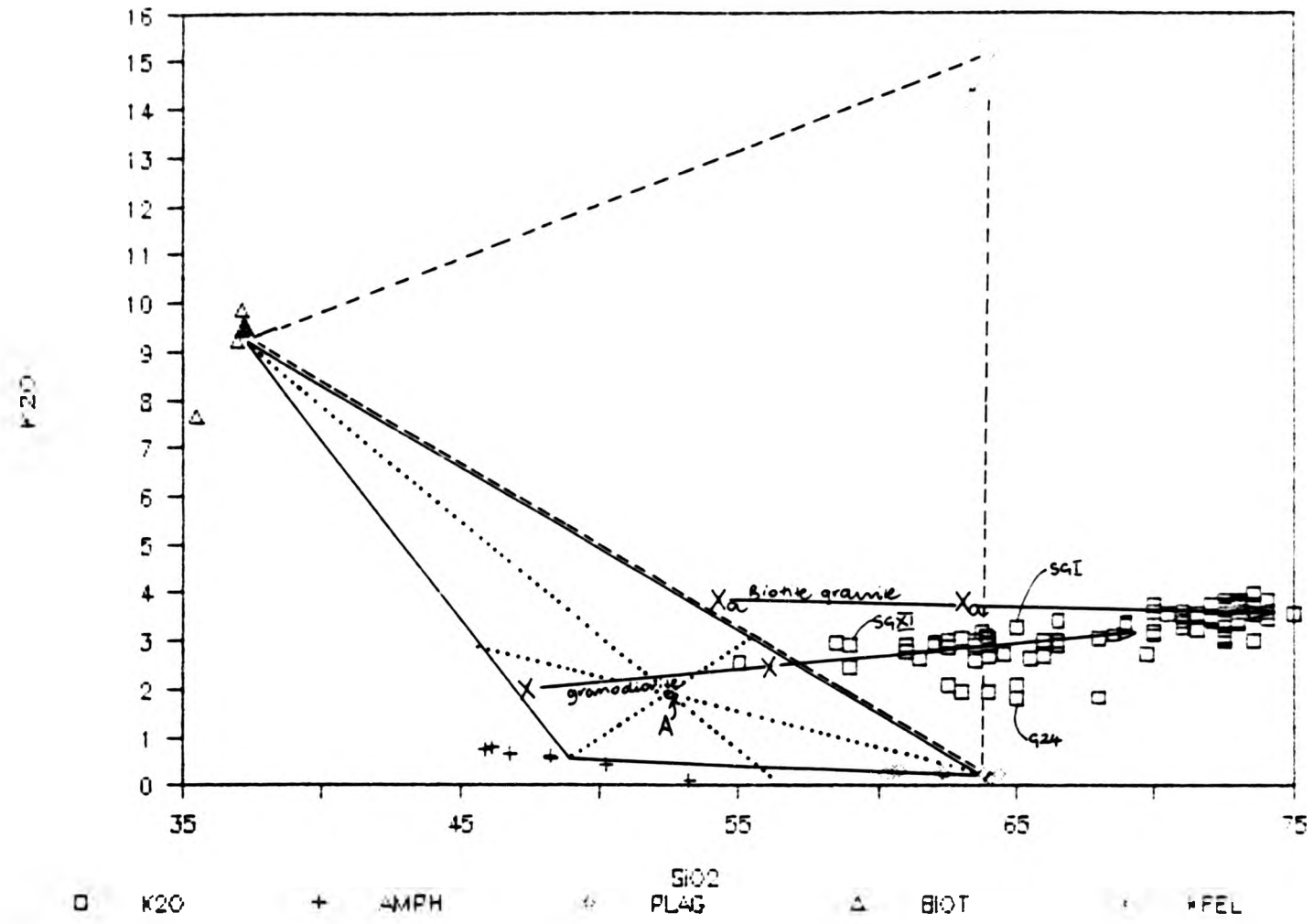

FIGURE 4.43 MgO vs SiO2

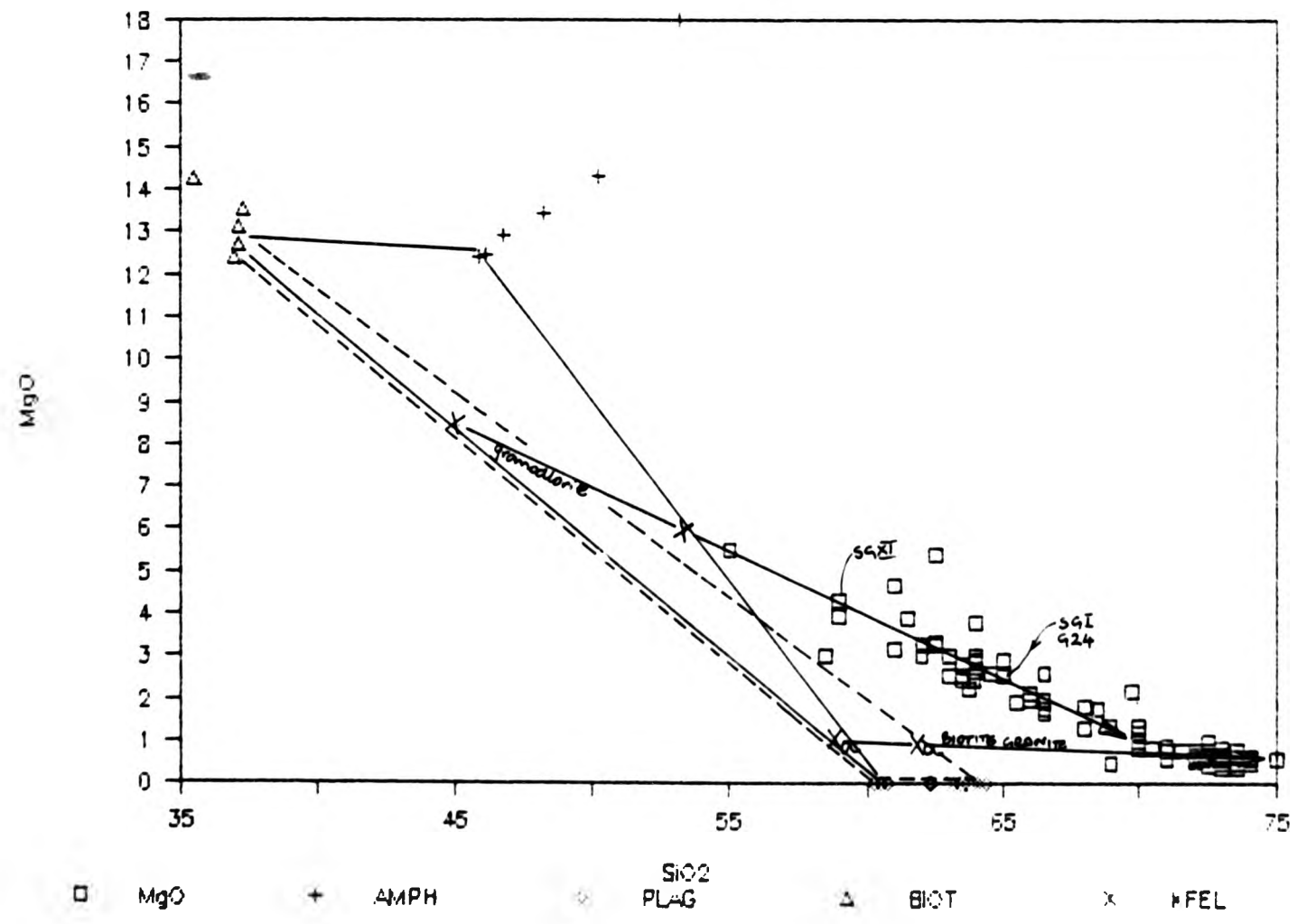

FIGURE 4.44 Na2O vs SiO2

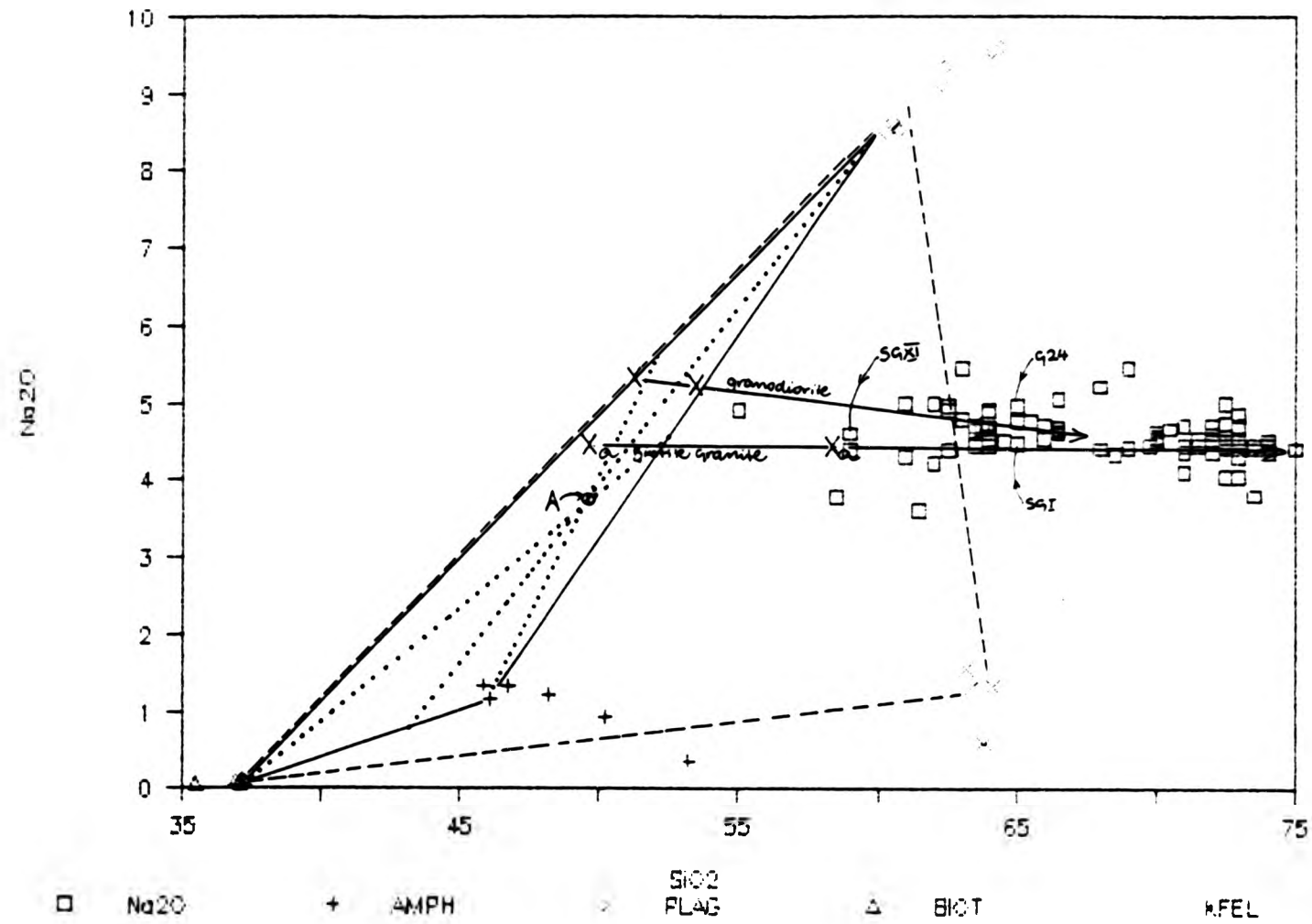

FIGURE 4.45 P2O5 vs SiO2

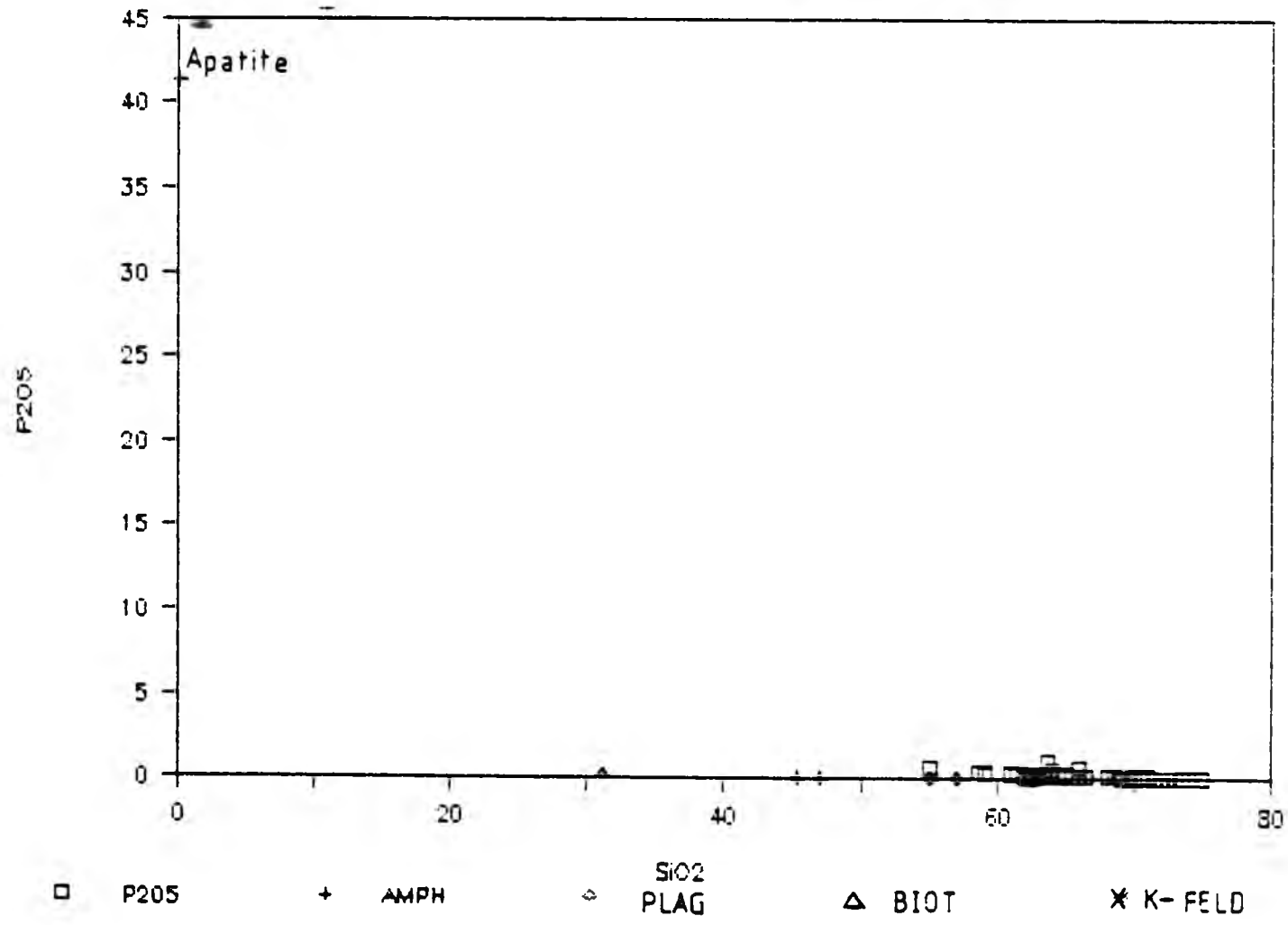

crystals and 78% intercumulus and are almost certainly outside the limit for crystal framework of plagioclase to form. If the composition range results from a parent liquid at 64% SiO_2, then SiO_2-poor rocks (59% SiO_2) could be cumulates with 36% framework and acid liquid at 68% SiO_2 would require extraction of 13%.

The bends/gradients noted in the major element plots reflect the change in crystallizing minerals in relation to each other: for example the reduced FeO* gradient results from the decrease in ferromagnesians relative to plagioclase; while the CaO gradient results from the increase in biotite relative to amphibole and also a new CaO-poor phase such as K-feldspar.

The scatter at low SiO_2 from mean lines on Figs.4.38 to 4.44, indicates a variation in mineral proportions in extract or cumulate component for individual samples for Al_2O_3 (Figs.4.2 and 4.38), eg. going from a mid-trend rock at 64% SiO_2 (SG82) to an Al_2O_3-rich rock (SGXXIII) requires 14 to 16% of a cumulate component composed of almost pure plagioclase. In contrast moving from SG82 to Al_2O_3-poor SGCI, this lies directly on a hornblende control line and would imply addition of 11% of pure hornblende to SG82. These are significant variations.

The PGD has basically a similar trend, therefore similar extracts/cumulates are possible. However large, near euhedral K-feldspars enclosing plagioclase suggests that K-feldspar is a relatively early crystallizing phase and might be a fourth component of the extract assemblage. This would certainly produce more of a K_2O-rich extract in Fig.4.42, which would fit the flat trend of K_2O in PGD better.

On the present plot of TiO_2 (Fig.4.40) the trend passes through the biotite corner of the extract field, but does not enter the triangle. Since 100% biotite extract cannot remotely fit the data for other elements, removal/accumulation of small amounts (<2%) of sphene is indicated. The sample amph + plag + biot extract is also P_2O_5-free, so the extract must indicate apatite (<2%) to account for the negative linear trend of P_2O_5 (Fig.4.43). As both are Ca-bearing phases they will reduce the proportions of amphibole to other phases. The PGD is slightly richer in P_2O_5 and TiO_2 at the silica-poor end. These would indicate slightly enriched magmas if all the rocks represent liquids or more efficient separation of sphene and apatite if a cumulate mode of origin.

Major element modelling has also been undertaken with the IGPET Least squares mixing computer program, using mineralogy seen in hand specimen, mineral compositions obtained by probing and major element data. This is a similar program to that developed by Wright & Doherty (1970) for the Hawaiian lavas and uses techniques summarized by Banks (1979). This tests, but in no way proves, that the processes causing the observed chemical variations could be a combination of partial melting, fractional crystallization, assimilation and mixing, of which mixing and fractional crystallization were used. The program then can calculate the proportions of each mineral which may be added to the "daughter" composition to produce the "parent" composition. Variations in compositions can be continually changed until the smallest difference is achieved.

TABLE 4.2 SAMPLES AND MINERALS USED FOR IGPET

Samples	SiO_2	Rock		Minerals
SGXI	59%	TGD	1	Mg-hbl(6C)...rock G24
SGI	65%	TGD	2	Plag (6C)...rock G24 An35
G24	65%	TGD	3	Biot (8M)...rock G24
SGIV	69%	BGT	4	Mag ...rock G24
SGXXVI	69%	TGD	5	Sph ...rock SGIII
SGVIA	69.75%	BGT	6	K-fel ...rock SGIII
SG48	71%	BGT	7	Apat ...rock G24
SG59	71.5%	TGD	8	Eden (7) ...rock SGX
SGVI	72.5%	BGT	9	Plag (4R) ...rock SG78
SG19	73%	BGT	10	Biot ...rock SG78
SG20	74%	BGT	11	Sph ...rock SG78
SG68	74%	BGT	12	K-fel ...rock SG78

The parent composition used was one of the most silica-poor granodiorites SGXI (59%), while daughter samples used included SGI (65%), SGXXVI (69%) and G24 (65%). The program itself takes no account of the geological validity of its conclusions nor the errors on the initial data, but merely provides one of many possible combinations of minerals that will fit the given data best. Individual components are varied separately rather than together, so any error estimates based on independent variation will underestimate the real uncertainty of the results. Banks (1979) stresses the importance of considering observed mineralogy and other modelling techniques in conjunction with this technique, as this linear program by no means gives an absolute answer. Banks also concludes that additional data such as trace element analyses need to be incorporated into the constraints to reduce the errors and therefore strengthen the conclusions.

TABLE 4.3 FRACTIONAL CRYSTALLIZATION OF GRANODIORITES BY IGPET

(refer to Table 4.2 for mineral & rock data)

	1	2	3	4	5	6
Parent	SGXI	SGXI	SGXI	SGXI	SGXI	SGXI
Daughter	SGI	SGI	SGI	SGI	G24	G24
Plag(2)	46.2	45.4	44.5	44.2	42.1	30.8
Amph(1)	38.3	33.0	33.9	34.5	43.6	42.8
Biot(3)	15.5	19.2	17.0	14.8	14.4	-1.3
K-fel(6)	-	-	2.5	4.2	-	24.5
Sph(5)	-	1.0	1.0	0.8	-	0.9
Mag(4)	-	-	-	0.4	-	1.3
Apat(7)	-	1.4	1.2	1.1	-	1.0
Daughter %	57.9	58.9	57.0	55.9	60.9	47.1
Residuals	0.188	0.011	0.006	0.002	2.300	0.116

	7	8	9	10	11	12
Parent	SGXI	SGXI	SGXI	SGXI	SGXI	SGXI
Daughter	SGXXVI	SGXXVI	SGXXVI	SGXXVI	SGIV	SGIV
Plag(2)	44.5	45.0	43.3	41.2	35.8	33.8
Amph(1)	38.4	40.7	34.9	41.1	48.3	44.1
Biot(3)	15.4	14.2	18.8	3.2	15.9	13.0
K-fel(6)	-	-	-	12.9	-	5.9
Sph(5)	1.7	-	1.0	-	-	0.4
Mag(4)	-	-	-	1.5	-	1.3
Apat(7)	-	-	1.9	-	-	1.5
Daughter %	44.8	44.5	46.6	35.7	47.4	46.2
Residuals	0.387	0.549	0.101	0.164	0.504	0.011

The results achieved with the fractional crystallization modelling program (Table 4.3) were broadly compatible with the visual estimates of the Harker rock and mineral plots Figs.4.38 to 4.45. The program was run with 3, 4, 5, 6 and 7 phase extracts. Gross proportions of amphibole, plagioclase and biotite and extract residue proportions are relatively insensitive to the addition of other possible extract phases. Alternatively the SiO_2-poor SGXI can be viewed as a cumulate from SGI parent liquid having a 42% crystal framework with 58% intercumulus liquid SGI trapped. SGXI modelled to SGI lie close to the average trend of some of the plots, while just off the trend on others eg. Na_2O and K_2O. The extracts are crudely similar to the graphical estimates, but rely more on plagioclase and biotite.

Table 4.4 RESULTS OF MIXING OF GRANODIORITES BY IGPET

	Parent 1 P1		Parent 2 P2	Hybrid Magma	P1	P2	Residuals
1	SGXI	+	SGIV	SGI	55.5	44.5	0.771
	SiO_2 59		69	65			
2	SGXI	+	SG20	SGI	61.2	38.8	0.269
	SiO_2 59		74	65			
3	SGXI	+	SG20	SGIV	16.4	83.6	3.820
	SiO_2 59		74	69			
4	SGXI	+	SG20	G24	62.2	37.8	3.149
	SiO_2 59		74	65			
5	SGXI	+	SG20	SGVI	13.4	86.6	0.572
	SiO_2 59		74	72.5			
6	SGI	+	SG20	SGIV	27.8	72.2	3.660
	SiO_2 65		74	69			
7	SGI	+	SGXI	G24	91.5	8.5	4.416
	SiO_2 65		59	65			
8	SGXI	+	SGXXVI	SGI	44.6	55.4	0.159
	SiO_2 59		69	65			

The gross proportions change by small amounts when additional phases are added. Apatite and sphene increase the biotite proportions and decrease amphibole. The sum of the squares of the residuals decreases from 0.188 to 0.002 with the biggest jump being achieved by going from 3 phases to 5 phases (apatite + sphene). The addition of K-feldspar and magnetite does improve the residuals, however as the extract now encompasses all the minerals except quartz, this is of little value (Table 4.4). Additional K-feldspar seems to decrease the biotite proportions and has a marked effect on the extract in some rocks: 5 & 6 in Table 4.3.

Results for modelling the TGD suite as a series of hybrids are given in Table 4.4. The best fitting results occurred with both end members being granodioritic - SGXI(TGD) to SGXXVI(TGD), producing a hybrid lava SGI with a small residual value of 0.159.

The biotite granite in a number of cases has a "dog-leg" change in trend from granodiorite at 67% SiO_2. This requires a change in the extract assemblage from that in TGD and /or a separate magma.

TABLE 4.5 FRACTIONAL CRYSTALLIZATION OF BIOTITE GRANITE BY IGPET

Parent	G24	SGXXVI	SGXXVI	SGXXVI	SGXXVI	SG48
Daughter	SG48	SG48	SG19	SG19	SG68	SG68
Plag(9)	56.2	74.3	65.5	63.8	56.3	75.5
Amph(1)	37.0	-	31.1	25.2	37.3	-
Biot(10)	6.8	25.5	3.4	6.7	0.7	24.5
K-fel(12)	-	0.2	-	-	-	-
Sph(11)	-	-	-	4.4	5.7	-
Daughter %	59.0	87.6	80.5	80.8	79.4	85.5
Residuals	0.838	2.098	0.221	0.098	0.182	0.105

Table 4.6 RESULTS OF MIXING OF BIOTITE GRANITE BY IGPET
(refer to Table 4.2 for rock & mineral data)

	Parent 1 Pl		Parent 2 P2	Hybrid Magma	Pl	P2	Residuals
1	SGVIA 69.75	+	SG68 74	SG48 71	29.2	70.7	0.846
2	SGIV 69	+	SG19 73	SG48 71	26.4	73.6	1.053
3	SGVIA 69.75	+	SG19 73	SG48 71	20.9	79.1	1.177
4	SGIV 69	+	SG20 74	SG48 71	30.4	69.6	1.526
5	G24 65	+	SG68 74	SGVIA 69.75	48.1	51.9	1.943
6	G24 65	+	SG48 71	SGXXVI 69	27.4	72.6	1.600

Overall the mineral combinations for the generation of the biotite granite trend would be a lower Ca-plagioclase, with the introduction of alkali feldspar and exclusion of hornblende. The crystal extract composition would fall between 55 to 60% SiO_2 and would drive a parent liquid at 67% SiO_2 to the quartz-rich differentiates at 75%

SiO_2 (Figs. 4.38 to 4.43). This assemblage does not however lie within the field of granodiorite rock compositions. The xenolith host rocks appear to reflect a separate, but gradual change in mineralogy for the granodiorite and the biotite granite respectively, but a single liquid line of descent cannot be drawn for the two intrusions.

Fractionation has been modelled with the IGPET program Table 4.5 for BGT. The BGT however displays a considerable difference between the modelling program and the Harker plot results. IGPET fractional crystallization utilising only plag + amph or plag + biot is successful; while plag + biot + K-fel assemblage gives a large residual and includes virtually no K-feldspar. Whilst the Harker mineral plots suggest that the main phases are plag + biot + K-feld:

eg. Fig.4.39 at 59% SiO_2 gives extracts of
plag 51.1% biot 11.4% K-feld 37.5%

Fig.4.42 at 59% SiO_2 gives extracts of
plag 66% biot 19% K-feld 15%

A possible extract was determined using the Harker mineral plots (Figs.4.38 to 4.44). This was modelled onto the Ba vs SiO_2 (Fig.4.45A), Sr vs SiO_2 (Fig.4.45B) and Rb vs SiO_2 (Fig.4.45B). By extracting from this liquid, the path of crystallization of SGXI (Fig.4.45A) plots away from the main TGD trend, with the SGXXI trend being nearly parallel. This SGXXI extract accomodates the downward "dog-leg" part of the TGD trend. By adding amphibole to SGXXI the trend moves towards the silica-poor TGD end. A path from SGIII would probably give a remarkable model straight into the BGT field. Similar extract paths are also noted on the Sr and Rb plots, which model the TGD trends quite well.

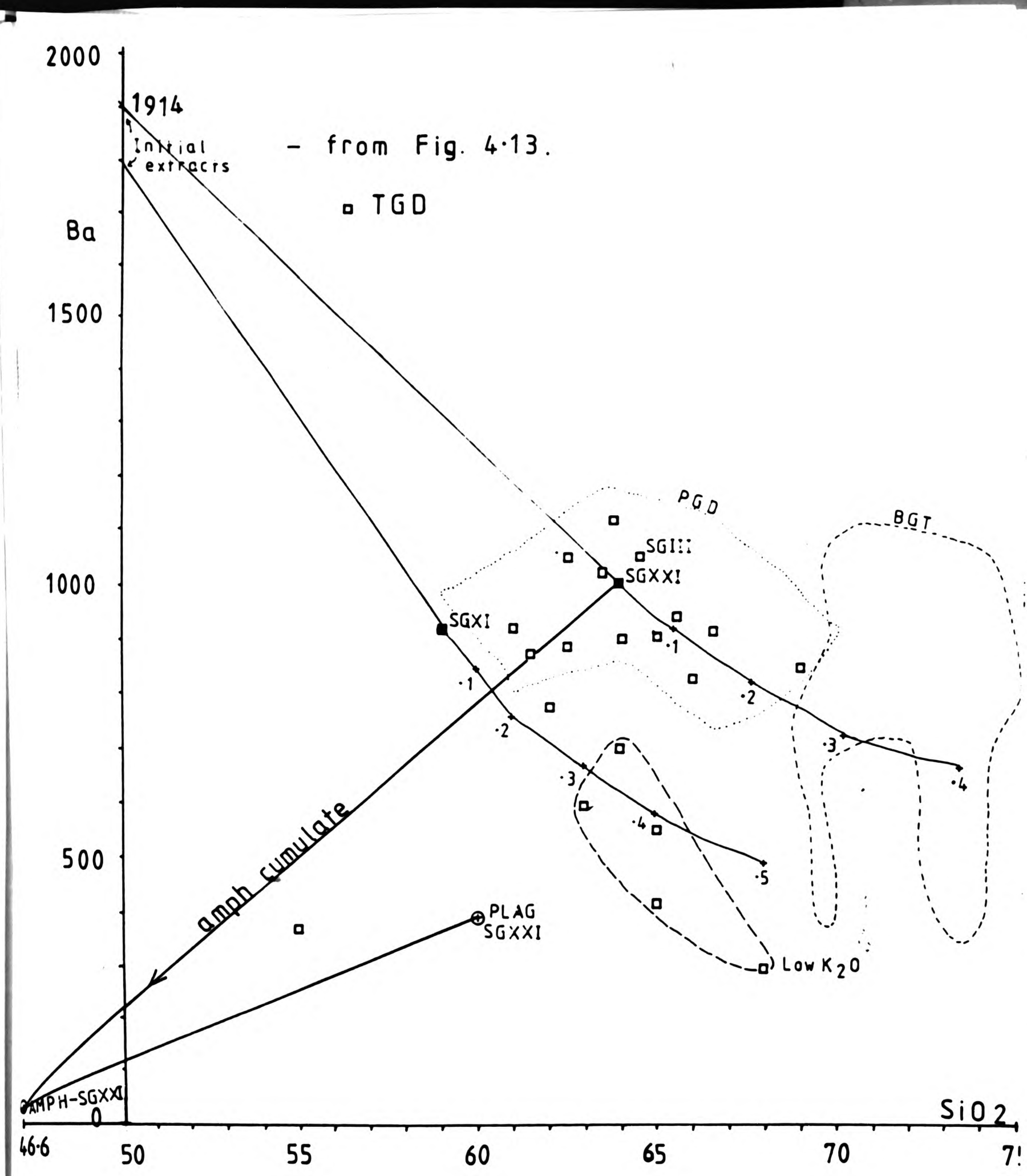

Fig. 4·45A Plot of Ba vs SiO_2 with extract paths calculated from Figs. 4·38 to 4·44

values = % extracted

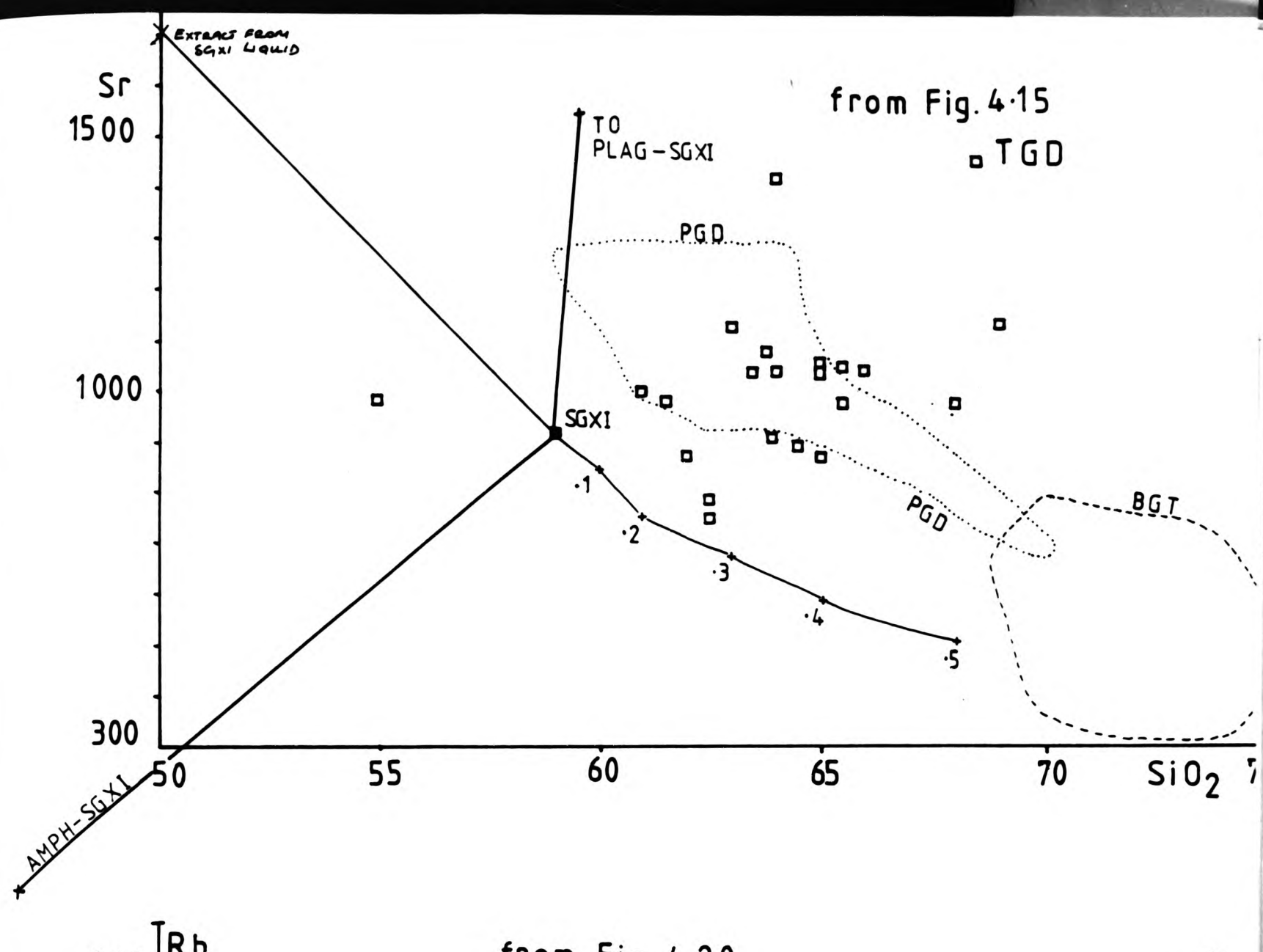

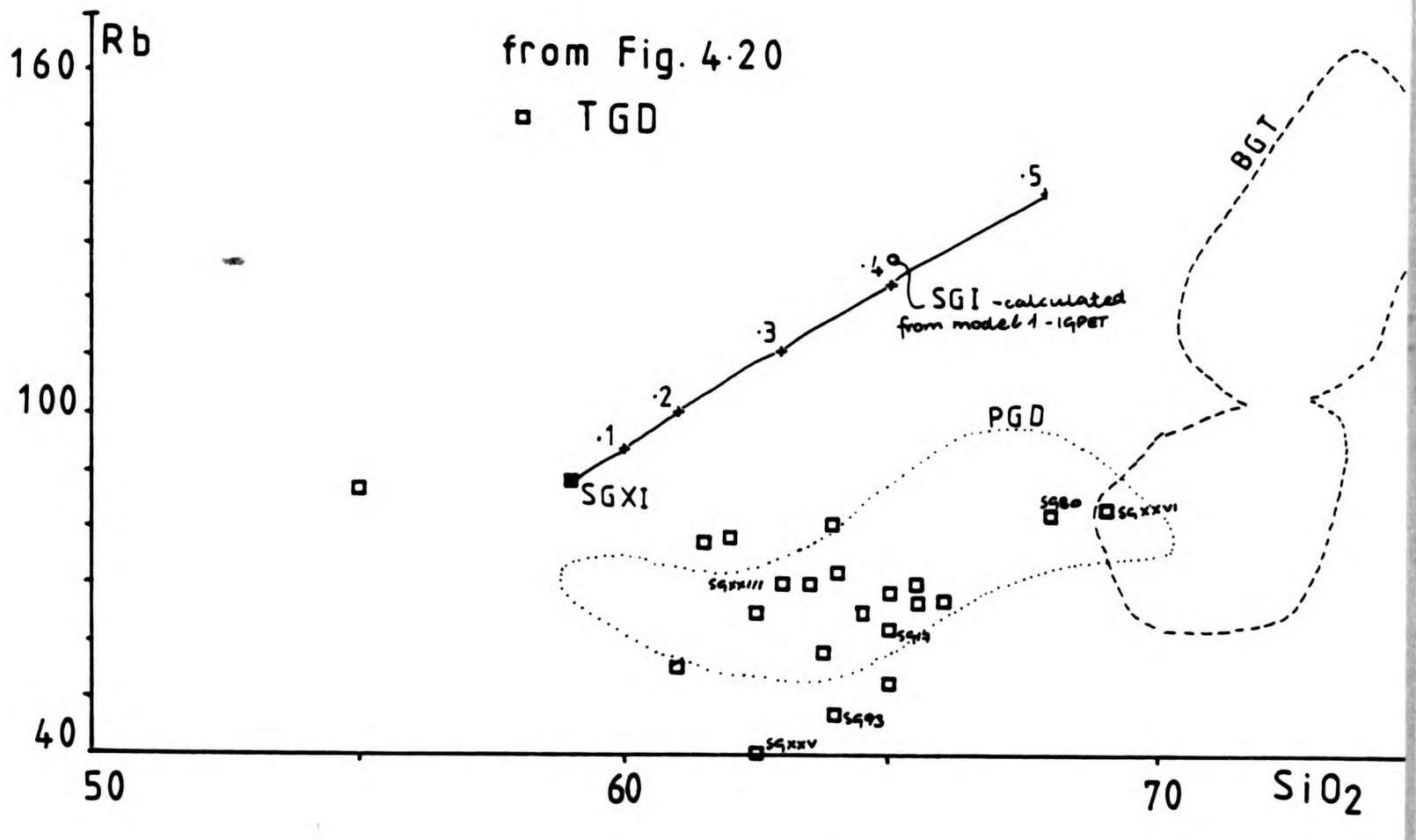

Fig. 4·45B Plot of Sr & Rb against SiO_2 with calculated extract paths

values = % extracted

4.5.2 Trace Element Modelling

Trace element data has been extensively used in an attempt to model petrogenetic evolution of many volcanic and plutonic complexes by Higuchi & Nagasawa (1969); Bouseily & Sokkary (1975); McCarthy & Hasty (1976); Hanson (1978); Hanson & Langmuir (1978); Pearce & Norry (1979); Tindle & Pearce (1981); and Togashi (1984).

Crystallization in plutonic complexes probably lies between two extreme types: perfect equilibrium crystallization, where the entire solid phase is in equilibrium at all times with the host melt; and perfect or Rayleigh fractionation, where only the surface of the crystal is in equilibrium with the melt. Between these extremes lies a continuum of conditions of crystallization involving partial equilibrium between solid and melt. A large body of magma cooling slowly may provide enough time for equilibrium crystallization to occur. However, processes such as convection within the body can prevent a state of equilibrium being reached as well as periodical refilling of the magma chamber by batches of the original parental magma. Trace element distribution during crystallization is also strongly influenced by the extent to which crystals and melt separate as crystallization proceeds.

Shaw (1977,1978) showed that Rayleigh and equilibrium crystallization produce similar trends for small amounts of crystallization and that it is only for relatively large amounts that the trends produced become significantly different. Many authors eg. Tindle & Pearce (1981) have suggested that equilibrium between the crystal surface and the melt is the most likely situation, particularly in cumulate rocks, as the intercumulus melt may frequently change. Therefore

trace element modelling is based on the Rayleigh fractionation equation.

Mineral analyses were carried out using an electron microprobe. Trace element data is not available for the phases analyzed, so partition coefficients for the range of elements needed has been compiled from available literature (Table 4.7). This includes data from Nash & Crecraft (1975) for the natural granitic rocks; Cox et al (1979) for acid to basic rocks and Baxter et al (1985) for the basic rocks.

Table 4.7 PARTITION COEFFICIENTS USED IN TRACE ELEMENT MODELLING FOR THE STRONTIAN HOST ROCKS

	Ba	Sr	Rb	Ce	Yb	K
Plagioclase	0.30	4.40	0.04	0.30	0.05	0.19*
Amphibole	0.04	0.02	0.01	1.50	8.40	0.08
Clinopyroxene	0.13	0.50	0.03	0.50	1.60	0.04
Biotite	10.00	0.29#	2.00	0.32	0.33	2.60*
K-feldspar	6.00	4.00	0.40	0.04	0.01	1.40*
Apatite	-	-	-	35.00	25.00	-
Sphene	-	-	-	80.0@	60.00@	-
Garnet	-	-	-	0.40	40.00	

From: 1. Cox, Bell & Pankhurst (1981)
2. Henderson (1984)*
3. Baxter et al (1985)@
4. Nash & Crecraft (1985)#

The main trace element models are as follows:

- CL / CO = F(D-1) Rayleigh fractionation
- CL / CO = 1/F+D(1-F) Equilibrium crystallization

where:

CO = concentration of the element in the original liquid

CL = concentration of the element in the residual liquid

F = weight fraction of liquid remaining

D = bulk distribution coefficient

These models are the extreme cases proposed for the evolution of magma, but there are many more possible models. It must be noted that magma evolution may not necessarily follow any one model exactly and also in cases where the major element composition of the magmas changes considerably, distribution coefficients may not remain constant .

Trace elements chosen to identify evolutionary mechanisms, should be those which are not essential structural constituents of minor phases in the rocks eg. Cu in sulphides, Zr in zircon, because of the problem of obtaining a representative sample of the rock. While trace elements such as Ba, Rb and Sr are particularly useful in modelling in granitic systems, because they are either incompatible of highly compatible in restricted phases. K has also been recalculated to ppm to see what effects it has on the plots. They also occur only in the major silicate minerals and not in the accessory minerals.

A range of trace element pairs have been used to determine the effects of major and minor phase crystallization within each rock group (in this section the granitic host) and then compare with the observed trend. They have been plotted on log-log paper (Figs. 4.46-4.49) and include pairs such as Ba/Rb, Ba/Sr, K/Rb and Ce/Yb. On each figure mineral vectors calculated using Rayleigh's CL - CO $_{F^{(D-1)}}$, are plotted and give liquid compositions after specific amounts of fractional crystallization or contamination. The values of .8, .6 and .4 in Figs.4.46, 4.47, 4.48 all refer to the percentages of liquid left after crystallization. Since the mineral trends are vectors, any change in the starting composition simply translates their initial position, while the direction and length of

the vectors remains constant. Vectors are also given for the extract of the mineral assemblages indicated by the major element modelling (section 4.5.1). The parent for this type of modelling has been chosen within the trend itself and is assumed to be the liquid composition.

The Rb vs Ba (Fig.4.46) observed trend displays an overall slight decrease of Ba and increase of Rb with differentiation from the granodiorites to the biotite granite. Individual plutons have weak or non-existent trends. The tonalitic granodiorite shows a wide scatter of Ba at right angles to the gross trend.

Crystallization of plagioclase and amphibole appear to be the main phases controlling variation. The granodiorites however do not plot systematically with respect to SiO_2 on this diagram, high and low SiO_2 occurring together. The reason can be appreciated from Figs.4.13 and 4.20, where Ba shows a maximum at 64% SiO_2 and Rb is scattered with a weak minimum at 63% SiO_2. It is therefore difficult to pick a meaningful parent liquid to use to model the variation. Taking an arbitrary point at the top left end of the scatter of points (liquid of Rb 50ppm and Ba 1200ppm), the weak elongation of the TGD main cluster can be modelled as liquids by the extraction of 65% plagioclase; 30% amphibole and 5% biotite (CL1 Fig.4.46). Individual rocks paired to the parent would involve very varied proportions of plagioclase + amphibole to biotite on the extract (CL2 - 38.3% amph, 46.2% plag & 15.5% biot; no.1 in Table 4.3). It is however difficult to see the significance of these models when rocks are not ordered with respect to silica.

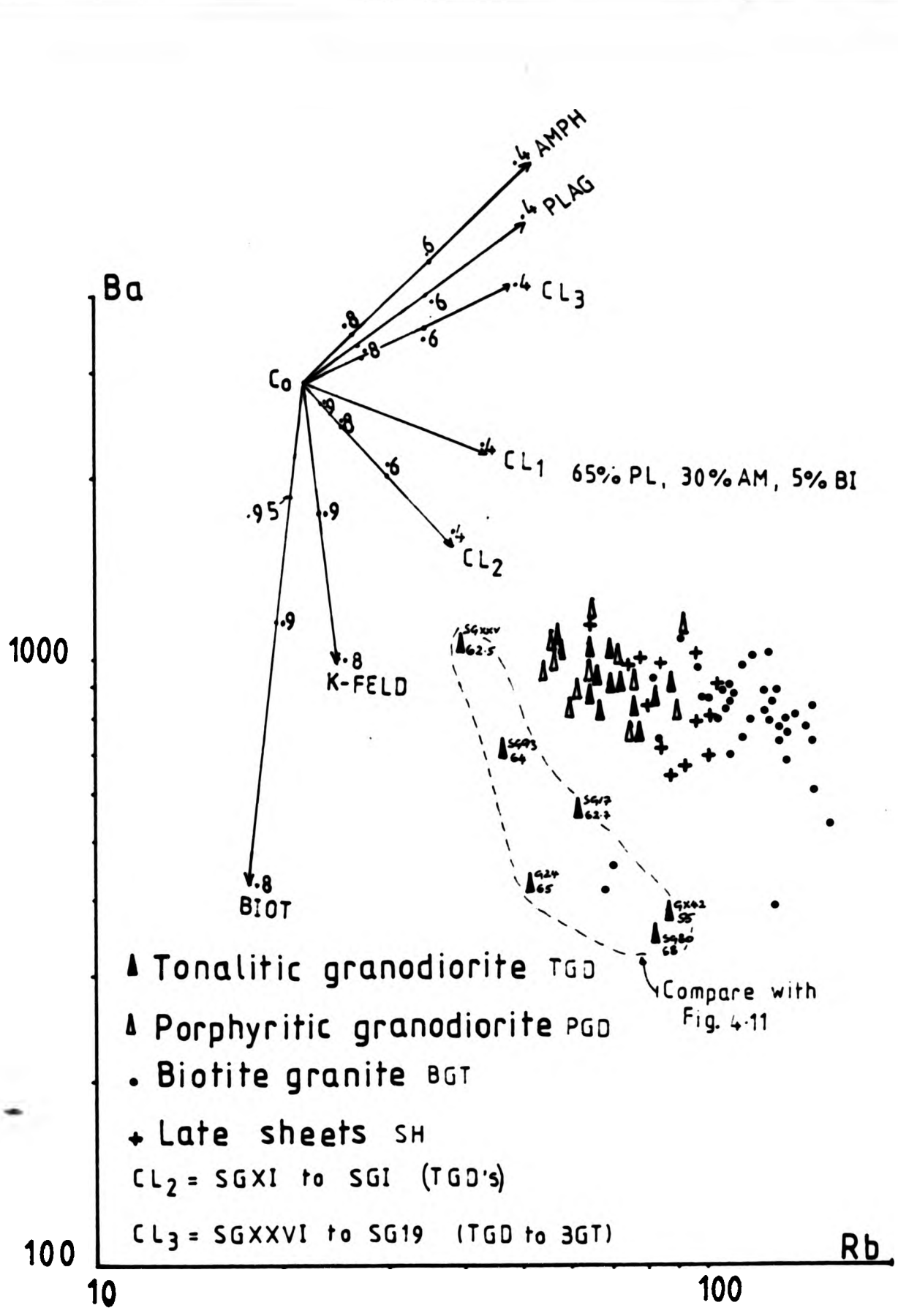

Fig. 4·46 Logarithmic plot of Ba against Rb for the host rocks.

Nos. on vectors = residual liquid fraction

The scatter of very low Rb, very low Ba for the TGD, forms a discrete field, which also has a random SiO_2 pattern. This requires either a different parent with a relatively biotite-rich extract or a hornblende + plagioclase accumulation. The BGT is possibly a little more organised than the granodiorites. However a different starting point could be chosen within the trend itself, while the parent compositions could be found in the middle of the plot with some of the rocks being cumulates and some being the liquid formed from the cumulates. The scatter of Ba could reflect K-feldspar "removal" by eg. filter pressing a granitic, K-rich liquid.

In view of the failure of Fig.4.46 to order the rocks with respect to silica modelled values for selected extracts and compositions have been plotted on Figs.4.13 (Ba) and 4.20 (Rb) Harker diagrams. The diagrams show assumed parents + calculated extract, evolved liquids and possible liquid + crystal cumulate compositions. Trace element in minerals and extracts are calculated using K_D in Table 4.2.

Fig.4.13 (Ba vs SiO_2) shows that extracts from silica-poor SGXI do not produce liquids or normal trends, but taking a parent liquid at 64% SiO_2 (SGXXI) the SiO_2-rich part of the trend is modelled. The silica-poor leg can be then be modelled as cumulate + liquid, but the cumulus must be nearly biotite-free, mainly amph + plag. The model liquids derived from SGXI do however cover the separate low Ba field. Neither of the liquid paths enter in the main part of the BGT field. Extracts would require much reduced biotite contents to produce the high (1000ppm) Ba BGT from SGXXI (1005ppm Ba).

Fig.4.20 (Rb vs SiO_2) models fairly successfully at SiO_2>63%, but fails at the low SiO_2. The low silica trend requires very much

higher biotite contents in the extract. This contrasts with the Ba plot for the region where a biotite-poor extract is required.

Similar gross trends are seen on the Ba vs Sr plot (Fig.4.47). The SiO_2 pattern on Fig.4.47 shows a similar random pattern as with the previous log-log plot. Granodiorites fall in rather equant clusters with again a subset of TGD forming a discrete field with high Sr and low Ba values. The transverse trend of the granodiorites suggests the possibility of plagioclase and amphibole cumulates. The biotite granite shows linear trends with some curvature at low values, which can be explained by a plag + K-feld + biot extract.

On Fig.4.15 (Sr vs SiO_2) a SiO_2-poor parent liquid composition was chosen for modelling, but was a failure. When a 63% SiO_2 starting liquid (SGXXIII) was taken, it appeared to model PGD to BGT with more success, but remained useless for the main field of TGD. The TGD field requires a more mafic dominated assemblage to avoid a negative trend.

The plag + amph controls of Sr were also tested on Fig.4.2 (Al_2O_3 vs SiO_2) and Sr values have been plotted on the TGD rocks. There is no systematic variation with Al_2O_3, though there are slightly lower Sr values in the lower Al_2O_3 region. A model was calculated using SG82 and SGIII as parent liquids. 14% cumulus plagioclase was added to imitate SGXXIII and this produced model Sr values of 1574 and 1314ppm Sr, which are very much higher than the observed 1120ppm Sr. The highest Sr rock is also high in P_2O_5, which lies above the main trend (Fig.4.12, sample SG93 & SGIII). This is a strong indication of the rocks being cumulates. Therefore it was either plagioclase accumulation as well as apatite, or the apatite is very rich in Sr.

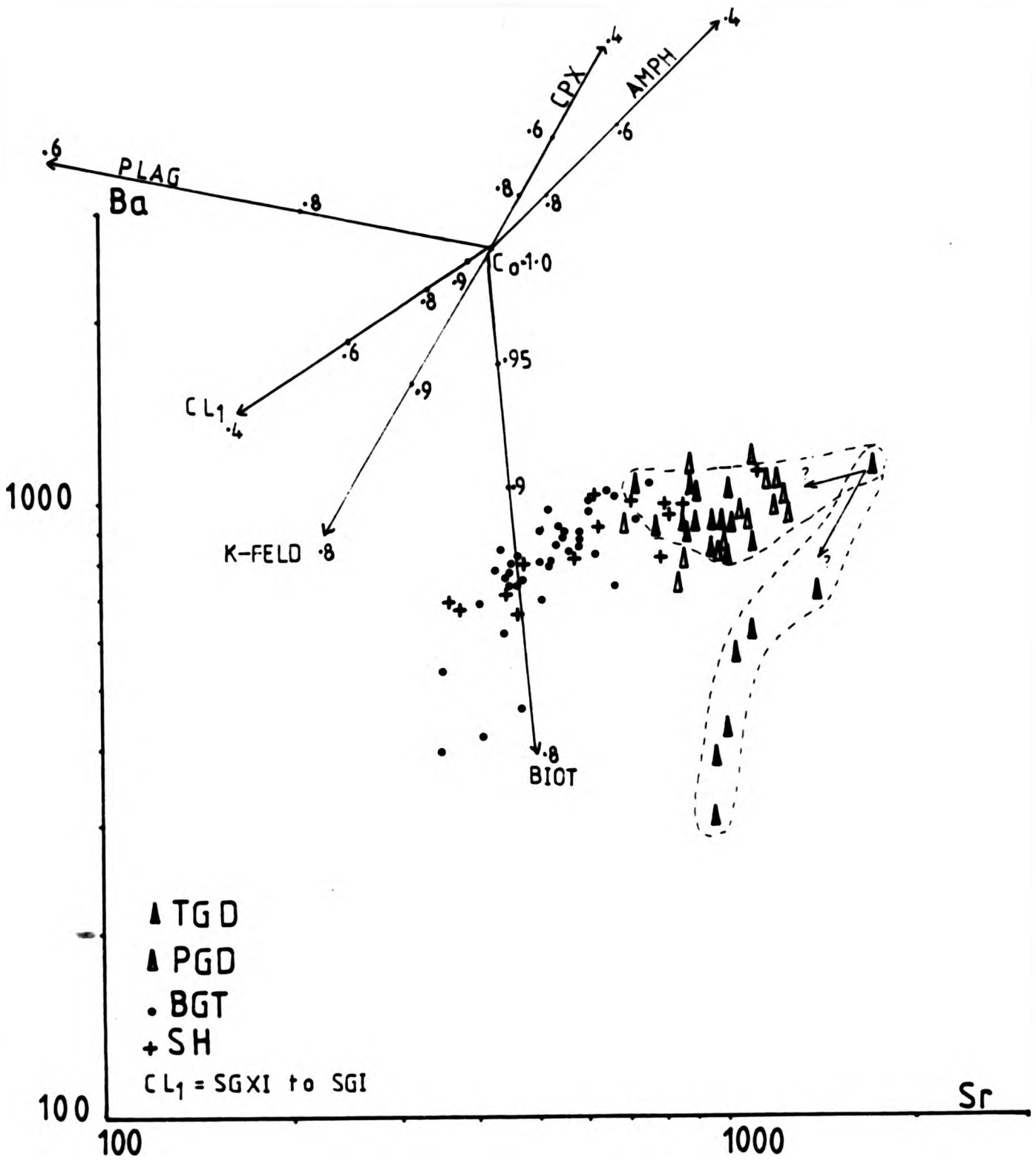

Fig. 4·47 Logarithmic plot of Ba against Sr for the host rocks.

Nos. on vectors = residual liquid fraction

This indicates that there is a difference in the origin of the 2 magmas. The vectors for Ba vs Sr indicate that a combination of plagioclase, amphibole, biotite and clinopyroxene fractionation could produce the observed trend. In fact 50% plagioclase, 35% amphibole and 15% biotite would accomodate the trend.

The K-Rb plot (Fig.4.48) displays a tighter cluster of vectors following the trend defined by the actual data points. PGD, sheets and BGT each define overlapping linear trends with similar directions. TGD falls in 2 fields, an equant cluster in the main trend and as a separate low K field. PGD, sheets and BGT show broad positive correlations of SiO_2 with Rb, so here progressive evolution moves the magma to the right. The TGD SiO_2 pattern is random. The main trend is influenced by plagioclase and chain silicate crystallization. The scatter here can only reflect the proportions of K-feldspar. The substantial overlap of the PGD and BGT fields means that there is not an ordered increase in Rb between the 2 groups as evolution proceeds, although this does occur in previous log-log plots. CL1 models SGXI to G24 using 42.1% plag, 43.6% amph and 14.4% biot (no.5 Table 4.3).

The REE are particularly useful in distinguishing between the effects of major and minor phase crystallization. The minor phases in the Strontian Complex are apatite and sphene in particular and they are known to contain significant amounts of REE. However hornblende is also known to contain REE and in Strontian this mineral is volumetrically more important than apatite and sphene. Fig.4.49 displays Ce vs Yb for the granites. There is substantial overlap of the different rock types. The 5 TGD samples produce a well defined, gently sloping linear trend, showing a rapid change in Ce:Yb ratios

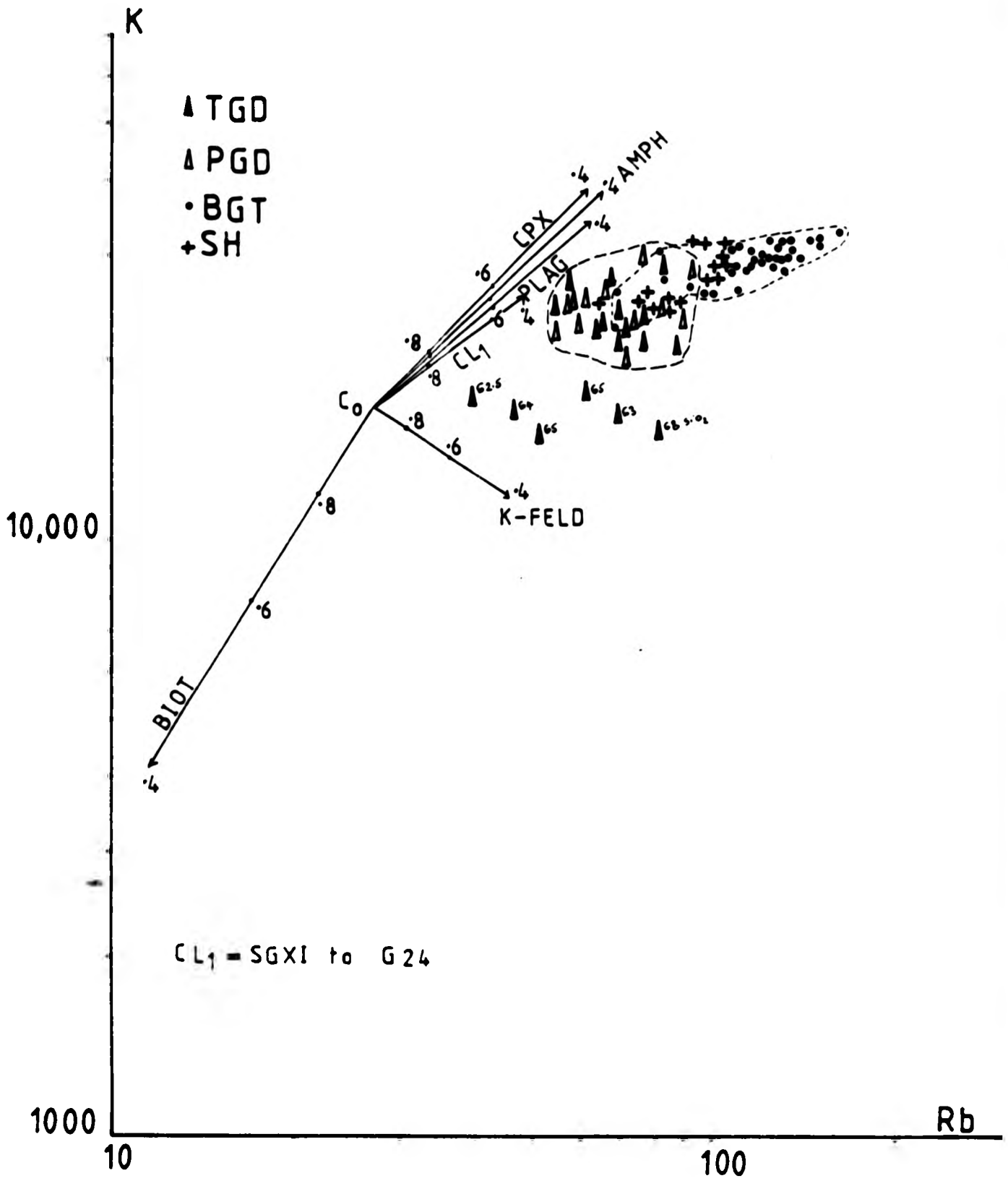

Fig. 4·48 Logarithmic plot of K against Rb for the host rocks.

Nos. on vectors = residual liquid fraction

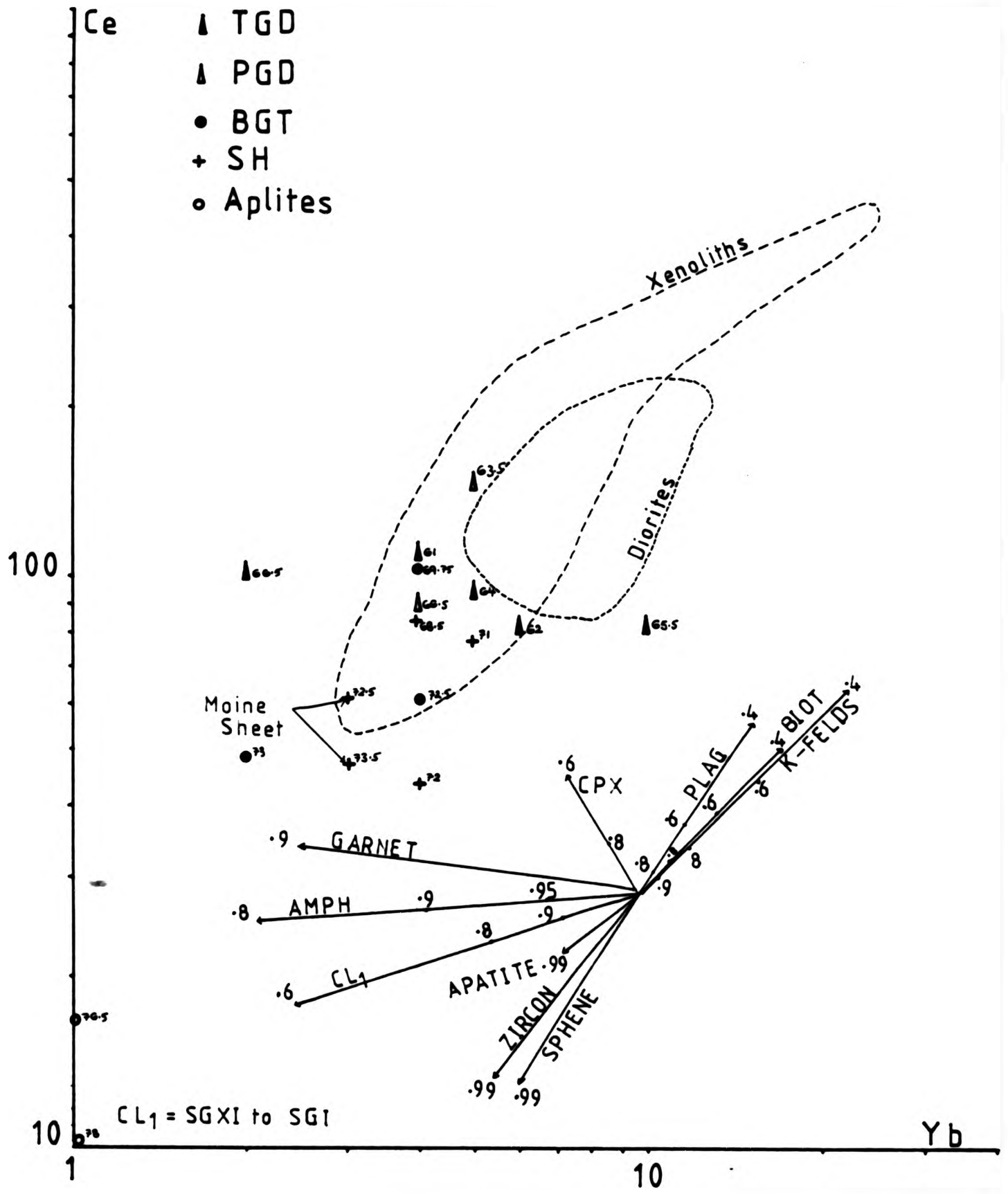

Fig. 4·49 Logarithmic plot of Ce against Yb for the host rocks.

Nos. on vectors = residual liquid fraction

(LREE:HREE). The PGD only has 2 points which seem to be in continuation of the BGT trend. While the BGT has 3 points ordered in a decreasing REE with increasing SiO_2, which is elongated parallel to the accessories and plagioclase vectors. As with the other incompatible element plots, there is no ordered progression of SiO_2 values along the trend. The orientation of the TGD trend is unrelated to the pattern of BGT although it touches the fields of BGT and sheets. The trend indicates the possible influence of amphibole crystallization and is remarkably parallel to the vector for garnet. Since the plagioclase vector is approximately 180deg from the apatite + sphene vectors, it is possible that large amounts of plagioclase are reversing the effects of small values of accessory minerals, this balance leaves amphibole to dominate the effects. The garnet content can only be a reality if the TGD pluton is an imperfect mixture (and so heterogenous) of magmas fractionating at sufficient depth for garnet to be stable. CL1 uses model no.3 from Table 4.3.

4.5.3 Summary

The interesting feature of the host rocks is the significant overlap of the tonalitic and porphyritic granodiorites, supporting the view of the common origin of the two rock types. However at low SiO_2 levels there is a separation of the two granodioritic types. This may be the result of a number of different factors such as a sequence of cumulates comprising of magma + accumulated crystals or cumulates at low SiO_2 and magma at high SiO_2. Trace element modelling has been carried out here for the Strontian host rocks only, assuming fractional crystallization in a closed system. The amount of fractionation required to get from granodiorite to biotite granite for some of the major phases is quite large, between 40-60%. Most of

the log-log plots are rather equant masses rather than the linear trends which would have been formed by fractional crystallization. Therefore the processes involved within the Strontian rocks are more than simple fractionation and so are accompanied by another process such as magma mixing.

The major element modelling was quite good though the scatter of points meant that the extracts or accumulation was very varied. trace elements failed for the SiO_2-poor compositions of TGD, though there was some success with higher values. While the log-log "incompatibles" had variable success. So magma mixing remains a possibility, but Ba eg. Ba vs SiO_2 (Fig.4.13) and Ba vs Sr (Fig.4.19), for example limits greatly the range of compositions involved in mixing.

On Fig.3.7 four TGD samples fall around the albite-quartz cotectic. All are found close to the western margin (Fig.1.3). Interestingly these samples are all non-porphyritic and possess only plagioclase and quartz with ferromagnesians and K-feldspar is only interstitial. This suggests the formation of quartz phenocrysts is possible, but they are not seen in TGD hand specimens. However with the TGD magma at depth, there is the possibility of it being a source of xenocrystic quartz as seen in some xenoliths and diorites. Their water content ranges from 0.64 to 1.74% H_2O+. The main PGD field lies along the 5kb cotectic and at the 5kb eutectic. This is also noted in hand specimen where the PGD possess subsolidus K-feldspar phenocrysts. While the BGT field lies around the low 3kb cotectic supporting the view of a separate magma at a different time and position, with substantial quartz content.

In another approach to evaluating the evolution of the granite phase boundaries for the Qz - Or - Ab - H_2O system has been drawn onto Fig.3.7 showing normative Qz- Or - Ab. Aplites and BGT contain more than 75 % normative Qz-Or-Ab and approximates closely to the experimental system of BGT (77.5% to 91.6% Qz-Or-Ab) and TGD (70.7% to 85.9% Qz-Or-Ab) are projected in and so may deviate more from the experimental system. Observed water contents of rocks are low 0.28 to 2.52% BGT; 0.48 to 1.56% PGD and 0.8 to 2.32% TGD and would lead to saturation at <<1kb. No higher water contents are likely to be preserved or recorded with the present mineralogy as virtually all ferromagnesian minerals are hydrous (amphibole and biotite). No drusy cavities or vugs are observed in any of the rocks. Most samples in Fig.3.7 plot on the line of the thermal minima and its high water pressure content as the plag-K-felds cotectic. Four TGD samples however plot on a quite separate trend, lying on the the line of the 5kb Qz-Ab cotectic.

Of the rocks that are very close to the Qz-Or-Ab composition the BGT samples cluster near the 3kb water saturated nepheline minima on the Qz-feld cotectic, which is comparable with the K-feldspar and quartz textures observed but not its present water content. The pegmatites and aplites plot on the line of minima, but curiously, at lower pressures than for BGT. No evidence has been encountered to suggest that BGT rocks do not represent liquids.

The projected PGD lie very close and parallel to the Na-feldspar-K-feldspar water saturated cotectic at 5kb in an An-free system, which appears to be compatible with the evidence of contemporary crystallization of plag and K-feld (refer to Fig.3.1A & 3.2B/C). These rocks however contain considerable normative An (7.73

(SG51) to 15.82 (SG92)) and the presence of An displaces the plag-k-feld cotectic towards more K-feld-rich compositions (Ehlers, Fig.190, 1972). Then if they represented liquids they would lie in the plag only field of the projection and the evolutionary trend would have a different trend, moving directly away from the "Ab" corner of the triangle. An alternative view maybe that the quartz-poor members do not represent liquids but are cumulates from liquids with lower normative An. As the plag - K-feld projection of the cotectic is approximately a straight line, the extracts will on fractionation have approximately constant plag:K-feld ratios and extract-residual melt mixtures will lie approximately along the plag-K-feld cotectic. On this basis the quartz-rich portion of the field could represent the liquid composition and would lie on the cotectic, but not necessarily at the Qz-Plag-K-feld minima, which is displaced (Fig.190, Ehlers 1972) into the quartz-rich side of the An free minimum. The silica-poor rocks then represent mixtures of plag + K-feld extract and their original liquid and so lie on a line joining the two. A cumulate chemistry for some PGD has been considered a possibility for the pattern on the Harker diagrams, but could not be discriminated from other models. This presentation of the data does suggest that it is a better explanation of some PGD variation than the other models. The heterogeneity observed in the plot might then result from differential separation of residual liquid from the crystal framework.

TGD distribution partly overlaps (in more silica-rich) PGD, but 4 rocks plot completely separately, scattered along the line of the 5kb water saturated plag-qz cotectic (Fig.3.7). Since these rocks contain normative An, the above association is fortuitous. Increasing An contents in the liquid shifts the qz-feldspar cotectic

to higher quartz contents (Fig.190, Ehlers 1972). Thus the observed trend would have to relate to >>5kb water saturated crystallization in An + Ab + Or + Qz + H_2O system. The work of Johannes (1984) also shows anhydrous 5kb cotectics more SiO_2-rich than saturated cotectics, so similarity implies fractionation at >5kb. Whatever the water pressure or total pressure, this indicates that TGD series magmas reached the plag + qz cotectic surface when they evolved from a one phenocryst to a 2 phenocryst assemblage. Subsequent fractionation brought them to the plag + K-feld + qz phenocryst point and there was more of the fractionation on the plag + K-feld cotectic surface that is shown by PGD. The observed spread along the qz - plag cotectic could arise either from a series of fractionated liquids or from a series of cumulates + melt mixes from a parental low temperature melt at the now Or-rich end of the trend, as the cotectic is really a straight line. It is not possible to discriminate evolved liquid sequences from cumulate + parent liquid mixes in this situation. The rocks plotting on the Qz -Feld surface would all appear to be members of the group of low K TGD separated on several of the Harker and log-log plots.

It is evident that SiO_2 was not always a satisfactory measure of fractionation in some Harker plots and the patterns shown by TGD on Fig.3.7 is further evidence. Consideration of the effects of varying An content in Qz + Or + Ab + An + H_2O at elavated water pressure (Fig.190 Ehlers, 1972, for 2kb H_2O; Fig.18.6 Winkler 1979) show that a fractionating system that is crystallizing Qz + Plag + K-feld with initial An would show decreasing SiO_2 as plagioclase fractionation reduced the An content (Fig.4.50). For a 5kb water saturated system, quartz decreases from 34 to 27% as An dips from 9 to 5%. At the same time the projection of the qz - feld cotectic moves to lower SiO_2

From – Ehlers, Fig.190 (1972)

Winkler, Fig.18-6 (1976)

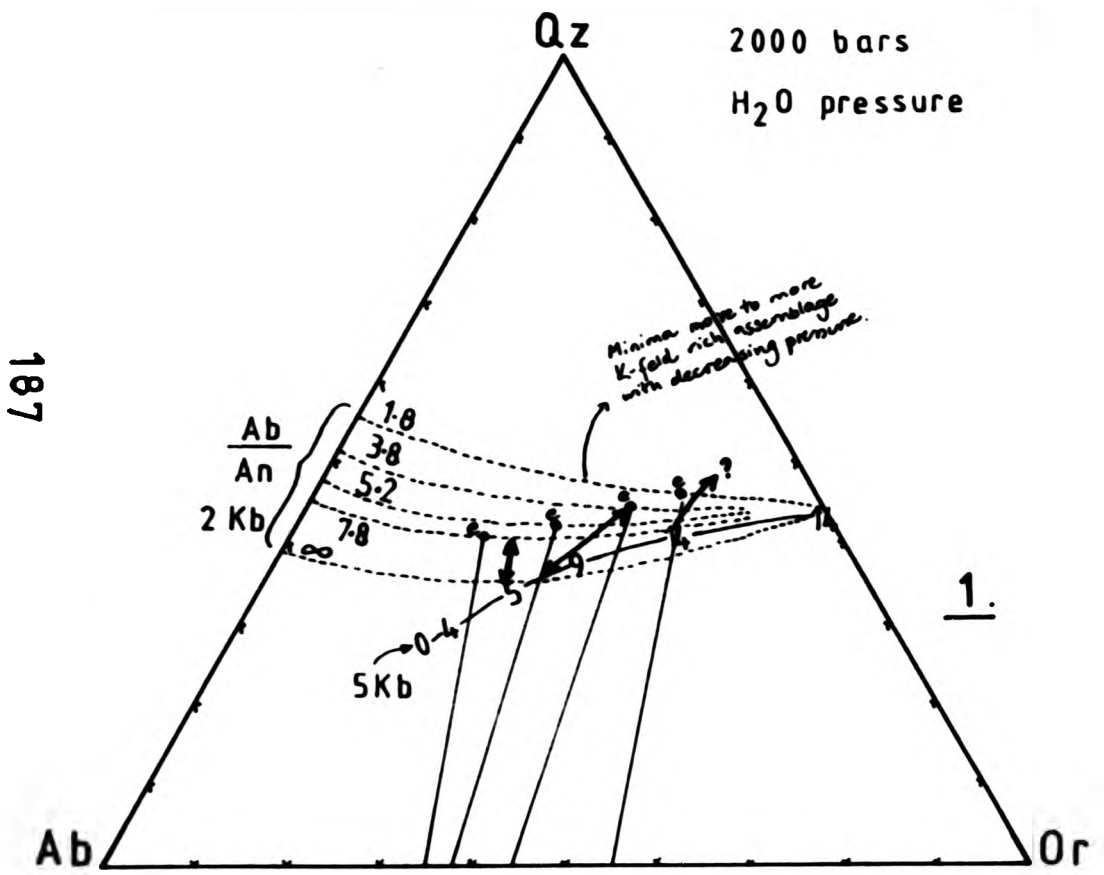

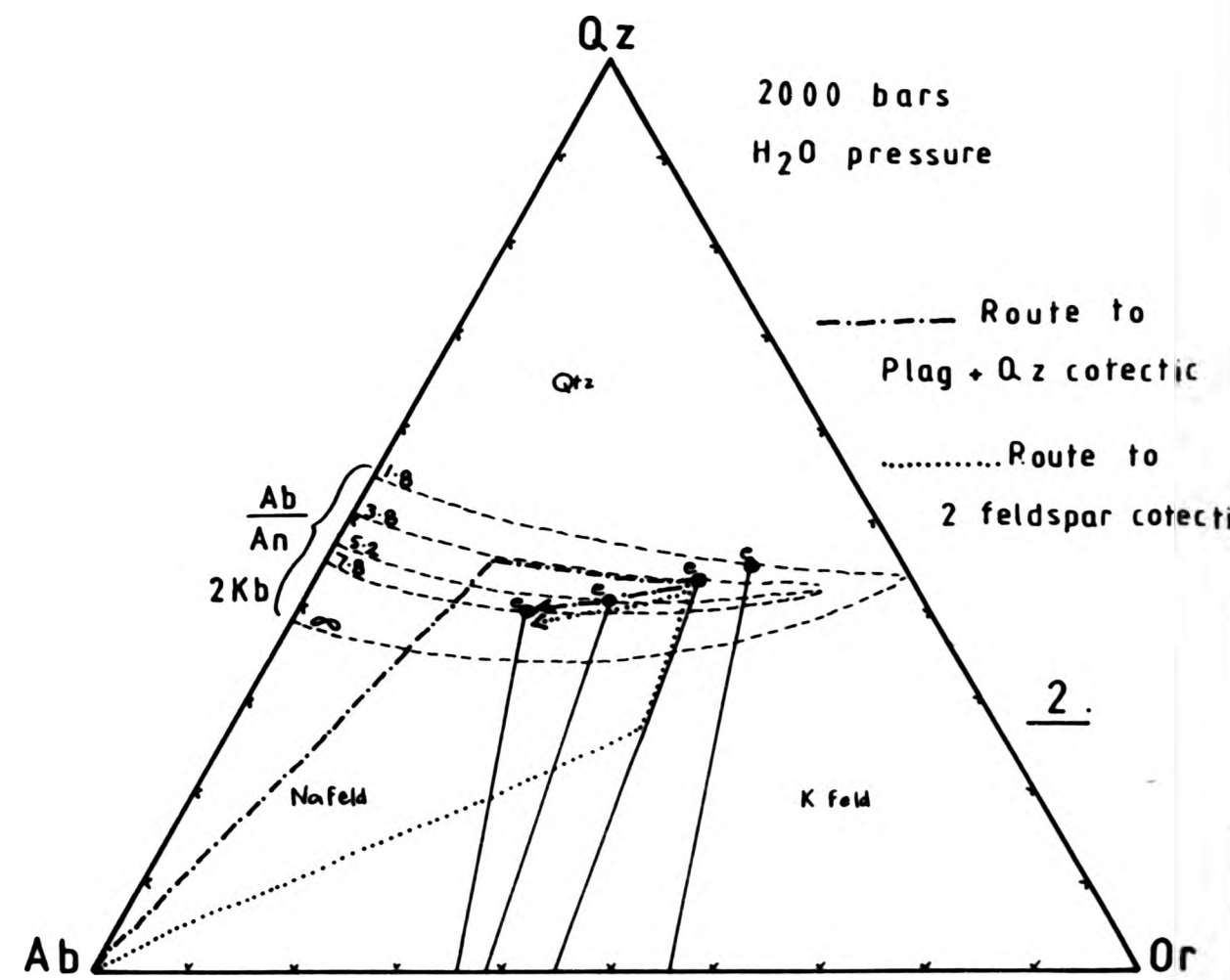

Fig. 4·50 The system Qz-Ab-Or at 2Kb/H_2O with various proportions of anorthite added (weight% is Qz + Ab + An + Or = 100; in 1.). e = eutectic

Both after Von Platen, 1965.

values. Thus fractionating liquids driven onto the quartz - feld cotectic by increasing silica will cross to the Or-rich side of the triangle with a small decrease in silica. They will then show further steady decreases in SiO_2 as they follow the minima for successively lower An values with decreasing Or and SiO_2. Such a pattern, if it is maintained in the presence of ferromagnesian minerals, will render SiO_2 based Harker diagrams very difficult to interpret. It will lead to considerable scatter on the Harker plots for minor and major elements undergoing contemporary rapid changes in concentration as a result of fractionation: eg. Ba, K, but will have less effect on the 4 oxides already reduced to small values.

Consideration must be given to the likelyhood that 1. PH_2O <, possibly << than P Total; 2.F was present in addition to H_2O; and 3. Cl was present in addition to H_2O. The low present water contents, very limited muscovite and lack of druses all suggest that, if the confining pressure was 4.1kb (Ashworth & Tyler, 1983) the water pressure was << P Total. The work of Steiner et al (1975) and Huang & Wyllie (1975) shows that 4 and 5kb quartz cotectics in Ab + Or + Qz + H_2O lies at a crudely similar position in the Ab + Or +Qz space, the most marked deviation being on the Ab side of the triangle, where the anhydrous cotectic is more quartz-rich. Thus the pressures estimated for BGT and SiO_2-rich PGD would effect the total pressure rather than P H_2O.

The analyzed apatites and biotites contain upto 4.65 and 1% F respectively. Amphiboles were not analyzed for F, but their potential F sites are similar to those in biotite, so similar values are to be expected. These indicate bulk rock values of 0.07% F and 4.0% (assuming modal biotite + amphibole of 13.5% and 0.5% apatite

and mineral F contents of 0.5%) compared with present water contents of 1-2%. Manning & Picharavant (1983) show that the addition of F to the Qz - Or - Ab - H_2O system not only lowers the liquidus further, but shifts the quartz - feldspar cotectic to even more silica-poor values, 1% F causing a reduction of approximately 10% in SiO_2 content of cotectic minima at 1kb confining pressure. The presence of F in the biotite and apatite must indicate that the "pressures" read on Fig.3.7 must be maxima, but the effect is small in relation to the scatter of points on the diagram.

There is no data for Cl, as it is usually considered a fugitive component (Carmichael, Turner & Verhoogen 1974). However Winkler (1979) notes that work by Von Platen (1965) shows that the HCl also sharply moves the cotectic to more quartz-poor compositions.

Chapter 5 THE XENOLITHS: FIELD RELATIONSHIPS

5.1 INTRODUCTION

The xenoliths occur as grey, relatively fine-grained inclusions found most commonly in the tonalitic and porphyritic granodiorites, and more rarely in the biotite granite (MacGregor & Kennedy 1932; Sabine 1963; Munro 1965 & Hutton 1988). The xenoliths are extremely variable in size, abundance, distribution and composition (Fig. 5.1). They are composed of similar minerals to the enclosing rock and have an igneous texture, but are finer grained and have a higher mafic colour index. An attempt to classify the xenoliths has been made (Table 5.1) in order to facilitate their description in later chapters. 133 analyses are reported in Appendix B, Table B.2.

The xenoliths are most abundant in the tonalitic and porphyritic granodiorite, with also a large number being present in the late sheets (ctG) eg. location D on Fig. 1.2, Plate 5.1. The sheets also possess a wide variety of xenoliths ie. shape and petrography.

A number of major inclusions of schist occur in the granodiorite mass (Fig. 1.1). Their foliation lies generally parallel to the pluton outer margins and to the foliation in the country rock. Their size varies from 15 metres in width to dimensions of 230m x 140m. Small xenoliths of pelite or psammite are rare and have a minimum size of 100 to 200mm. Compositionally they are siliceous and semipelitic schists which on occasion show baking against and invasion by the surrounding host granodiorite (Sabine 1963).

A solitary example of an accidental igneous xenolith incorporated

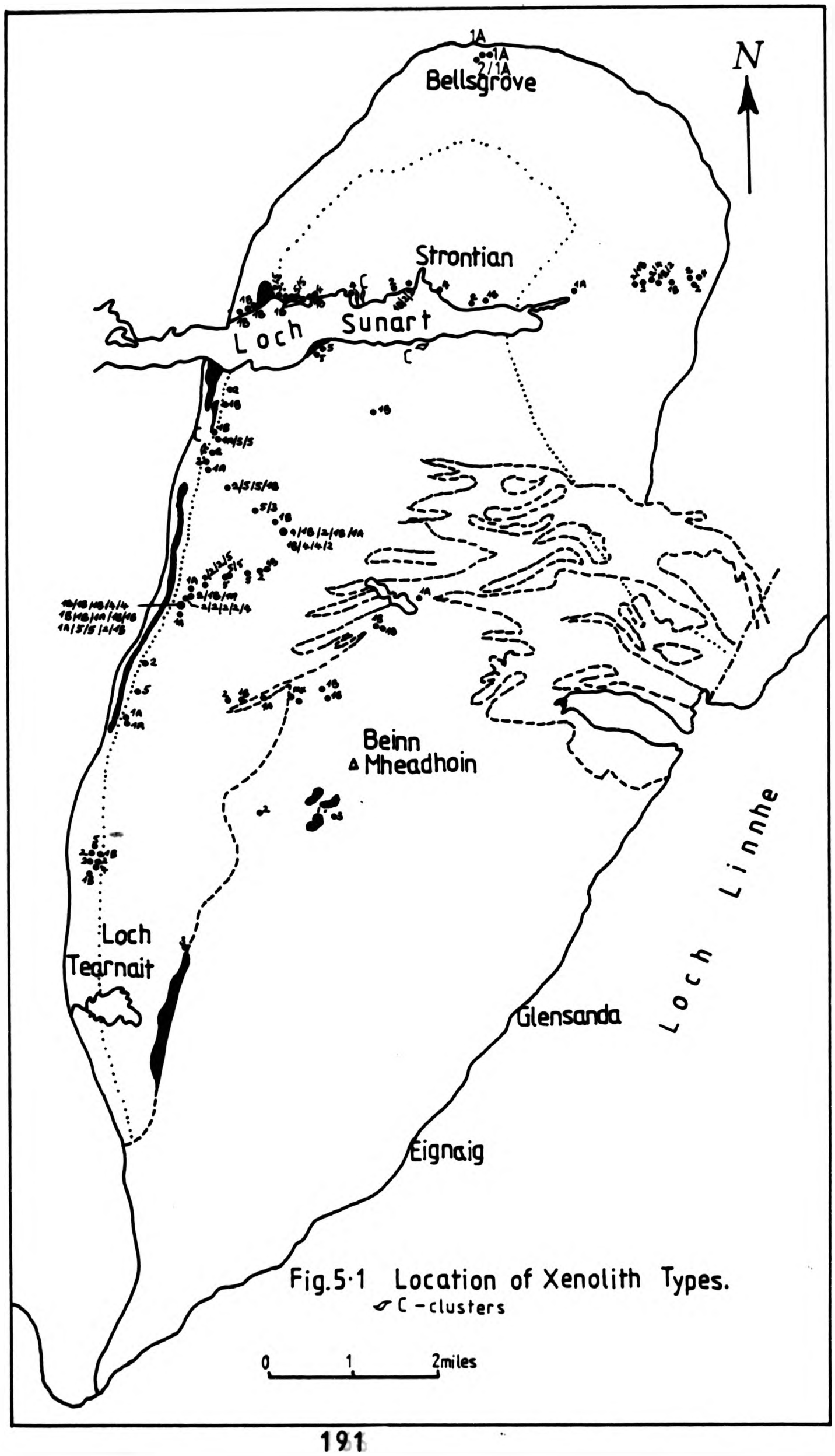

Fig.5·1 Location of Xenolith Types.
C - clusters

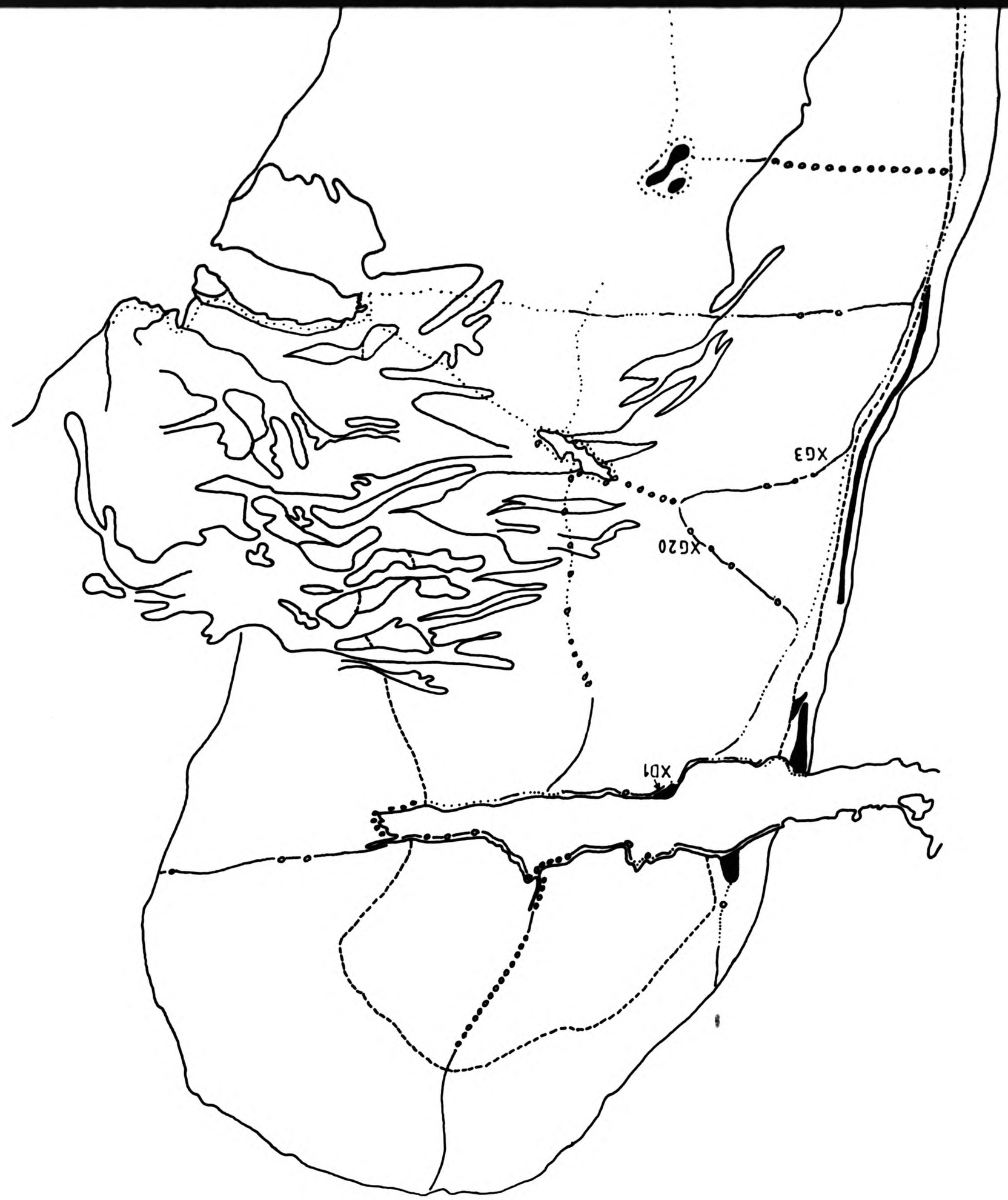
XG3
XG20
XD1

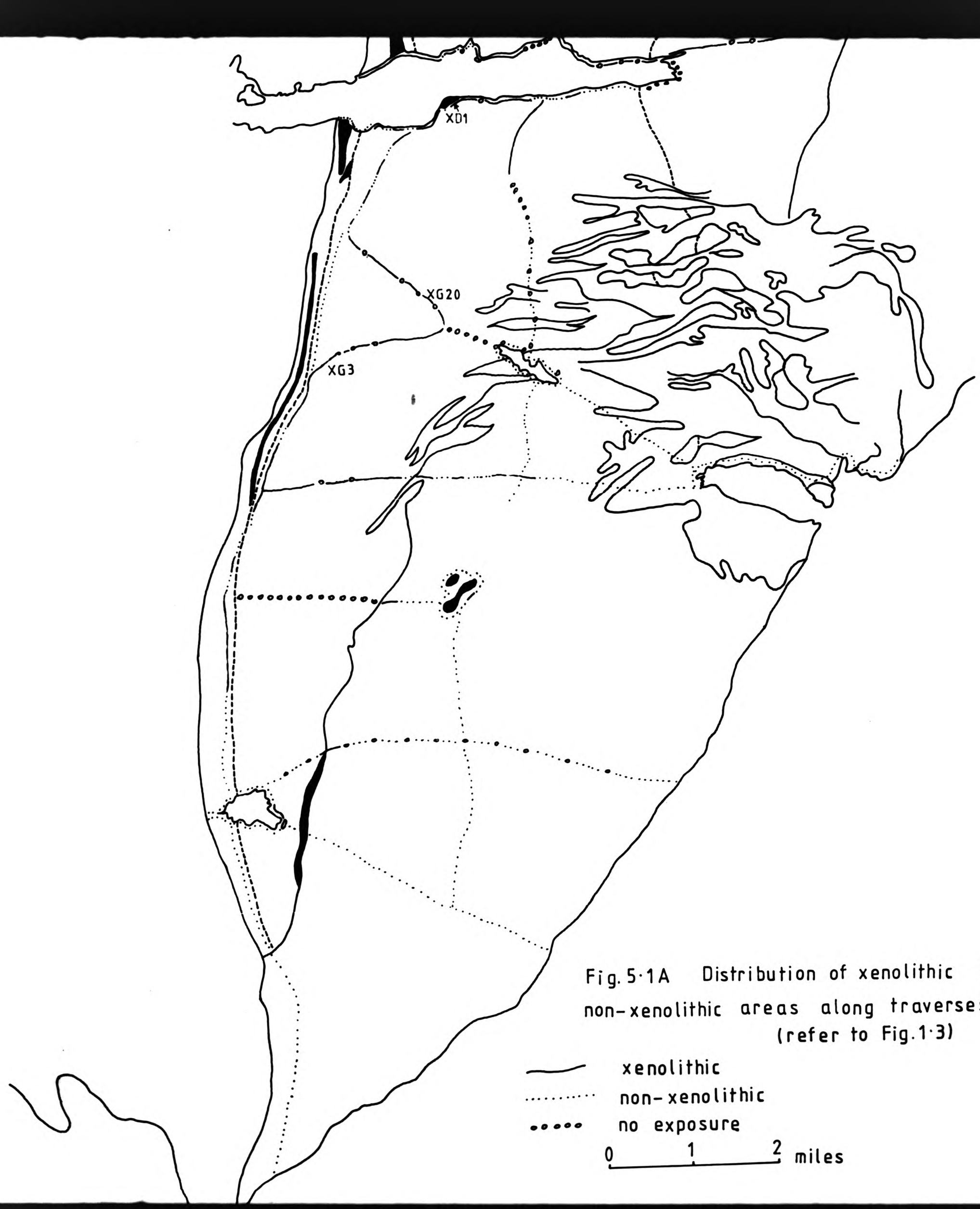

Fig. 5·1A Distribution of xenolithic & non-xenolithic areas along traverses. (refer to Fig. 1·3)

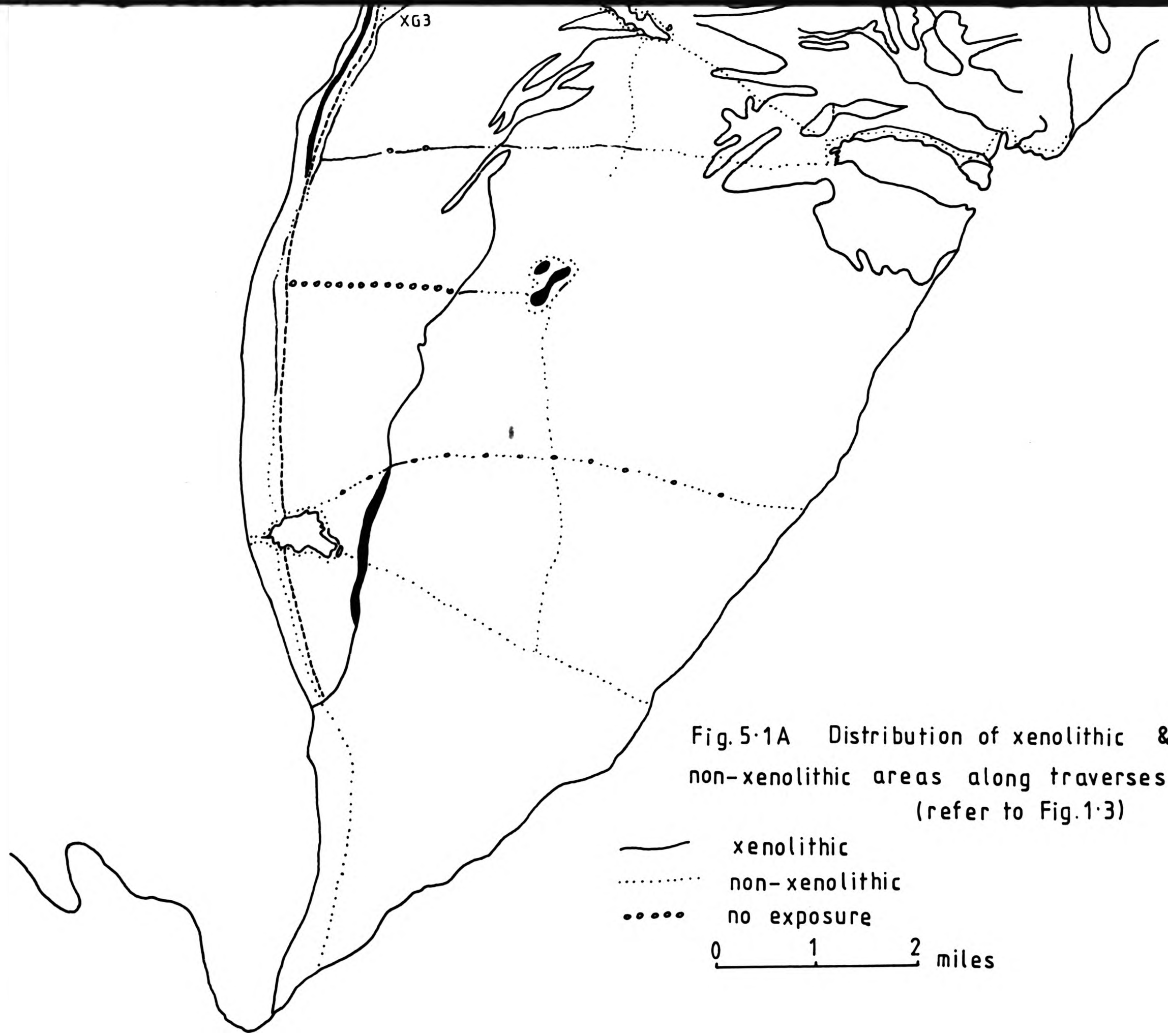

Fig. 5·1A Distribution of xenolithic & non-xenolithic areas along traverses. (refer to Fig. 1·3)

xenolithic

non-xenolithic

no exposure

0 1 2 miles

Plate 5.1 Xenoliths present in the granodiorite porphyry sheet (ctG) located at D, Fig.1.2. (G.Ref.7620-5465)

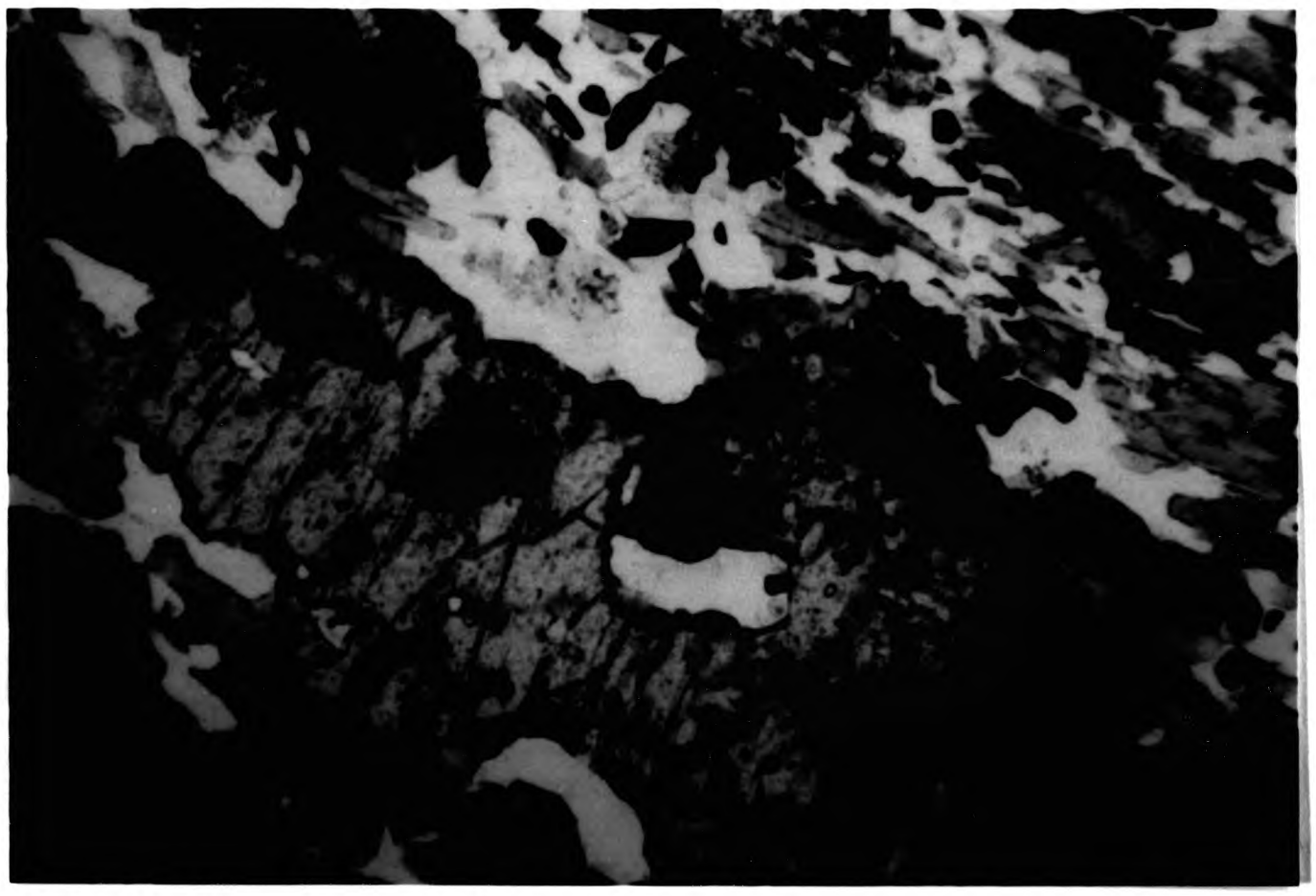

Plate 5.2A View of the lamprophyre dyke found at Locality E, Fig.1.2 (G.Ref. 8394-6097). Hammer shaft 550mm.

into the host Strontian granodiorite, is a fragment of a foliated lamprophyre dyke from the Moine (Plate 5.2 A & B Location E Fig. 1.2). Moine fragments are still present on its margins which are angular steps in the Moine-lamprophyre contact. In the dyke granitic material and the Moine have been recrystallized into coarse quartz-rich patches. It is an important point that the foliation in the dyke is preserved, which counters any suggestion that the bulk of the xenoliths are recrystallized older lamprophyres and microdiorites. A sample of the dyke was collected and analyzed as XG92 (Appendix B, Table B.2).

5.2.1 Occurrence and Distribution in The Granodiorite

The xenoliths are variable in size throughout the complex, ranging from 0.03 to 1.78 metres in length. The bulk lying in a well defined size range of 100 - 300 mm as measured along their long axis. Xenoliths of more than 0.5m are distinctly rare. The width of the xenoliths ranges from 0.02 to 0.46m, while more rounded xenoliths have diameters reaching 0.35m.

In general the distribution of the xenoliths is most irregular (Fig. 5.1 and Table 5.1). Along the traverses, it was noted that there is no distinct increase in xenolith numbers when approaching the mafic diorites. There is also a mix of shapes at single sites (Plate 5.6B & C). In the granodiorite body, the non - xenolithic areas are by far the most common, occupying 65% of the traverses and individual areas of up to 500 square metres (Fig.5.1A shows the percentage distribution of xenolithic and non-xenolithic areas). The main xenolithic areas are sparsely populated, with less than 5% xenoliths

present. These xenoliths show the full range of sizes (0.03 to 1.78mm). Moving into areas where xenoliths form 10 to 20% of the bulk rock, the size range is a little more restricted (100 to 400mm). The greatest concentration is reached in the rare densely populated areas, termed clusters (or swarms by Pabst 1928), where 55% or more of the bulk rock is xenolithic material and host rock is reduced to the role of a binding material. Here size range is restricted to 100 to 300mm. Where this occurs it may well indicate a form of size sorting. These clusters form less than 1% of the total traverse lengths visited.

The clusters seen in the field (Fig 1.2; Plate 5.3 to 5.5) have a flattened ellipsoidal outline, which in a number of examples is very elongate, while a number are quite rounded. They range in dimensions from the largest found 4 metres long by 2 metres wide (Plate 5.3A & B) to 6-7 metres long by 500mm wide, (Plate 5.4A, B & C) with occasional rounded clusters of about 1 square metre or less (Plate 5.5). The clusters are all sharply bounded, with no apparent change in grain size in the surrounding host rock. The long axes of the clusters in plan view have approximately the same trend as the fabric in the granodiorite. In a vertical plane the clusters have steep walls so are probably parallel to the granodiorite planar fabric, though the fabric itself is lost in between the xenoliths. The long axis of individual xenoliths always lies parallel to the long axis of the clusters. There are at least 9 clusters located in the field and they commonly occur in the porphyritic granodiorite or near the contact between the tonalitic and porphyritic granodiorites (Fig. 5.1).

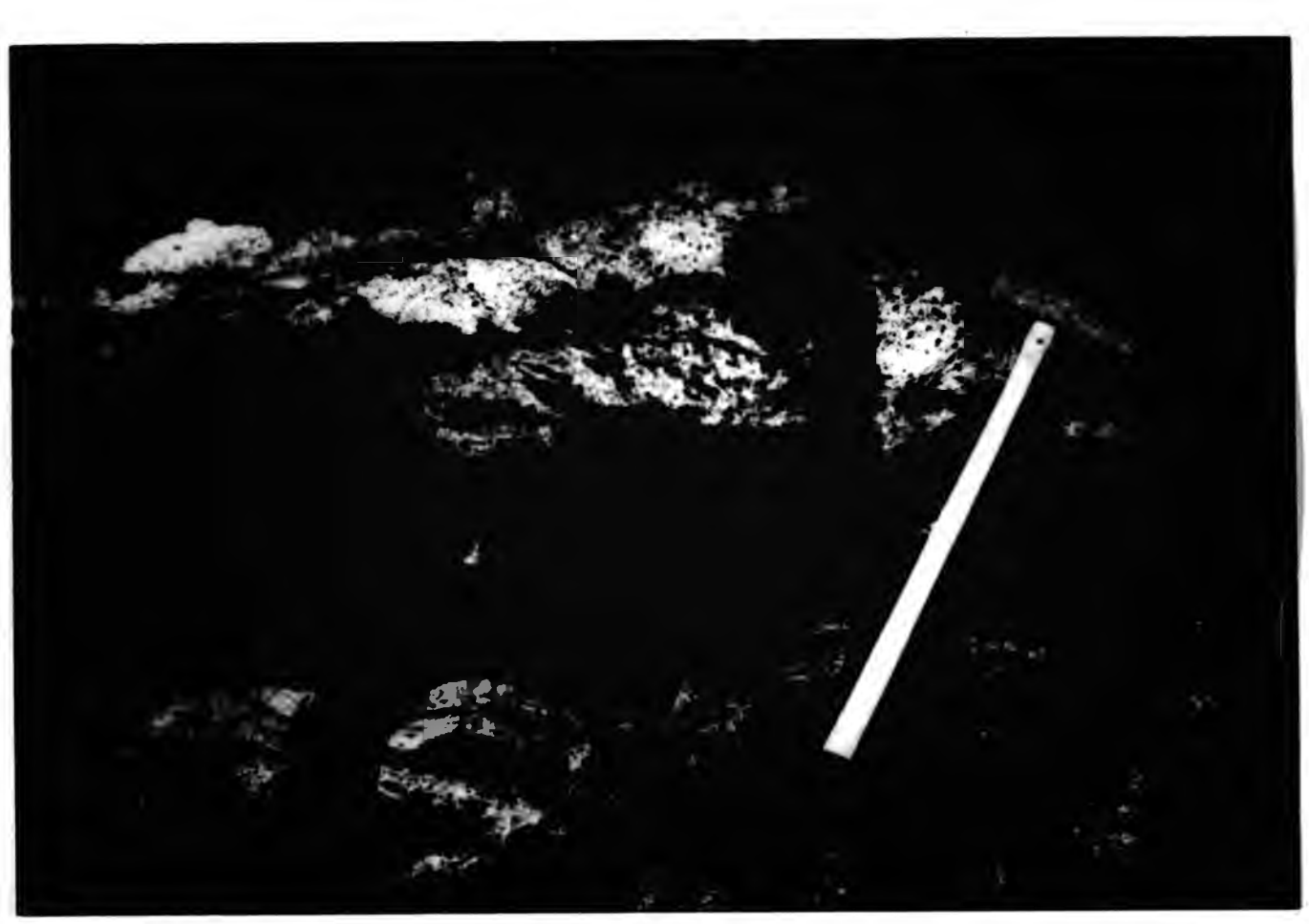

Plate 5.2B View of the lamprophyre dyke showing the texture and mineralogy which is still contains primary pyroxenes. Sample XG92.

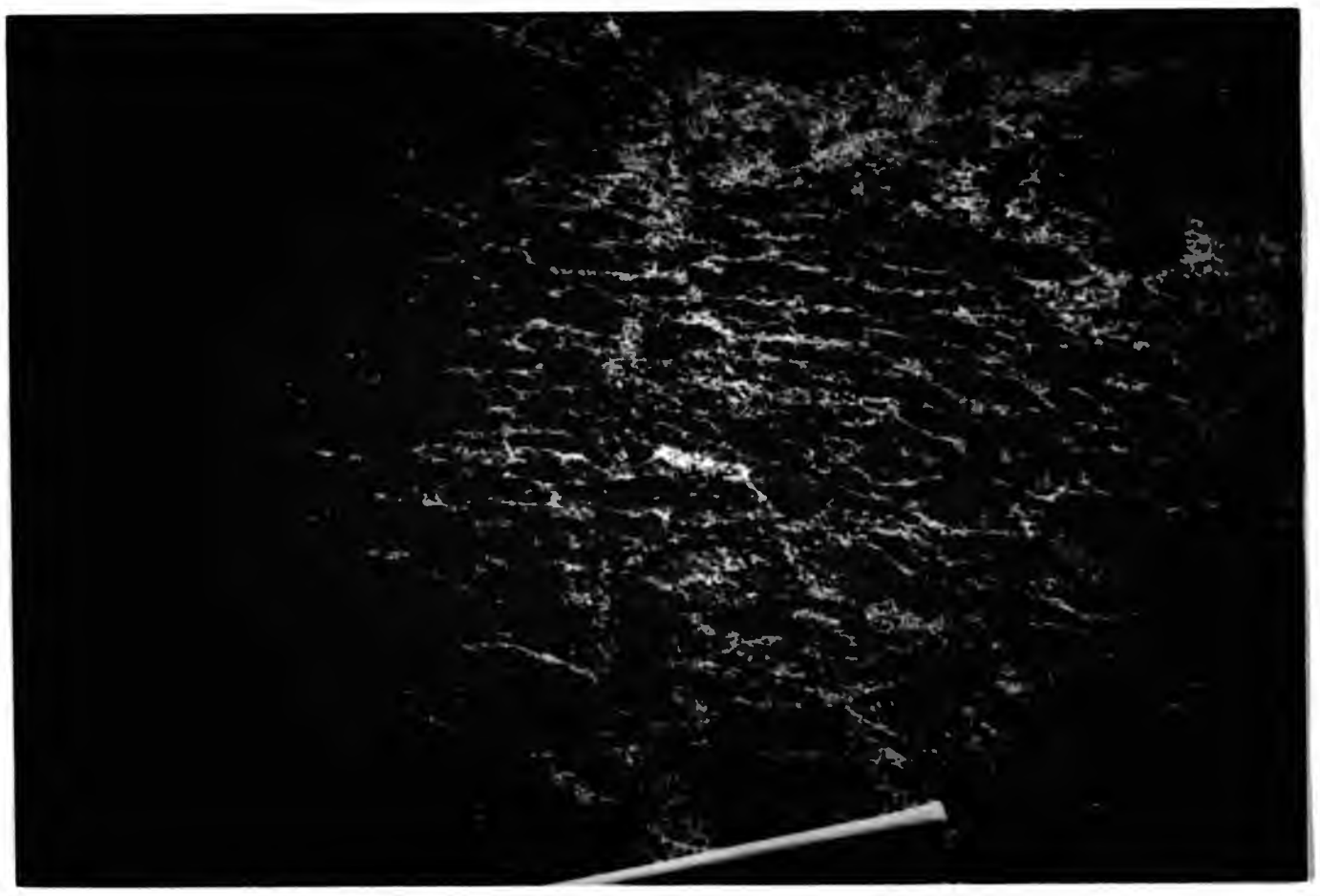

Plate 5.3A Plane view of a cluster of xenoliths close to the A884 (G.Ref. 7725-5740).

Plate 5.3B Wider view of the same cluster. Hammer shaft 550mm.

Plate 5.4A Narrow cluster of xenoliths found on the northern shore of Loch Sunart (G.Ref. 8010-6095).

Plate 5.4B Closer detail of cluster showing the xenoliths moulding over each other(G.Ref. 8010-6095).

Plate 5.5 Close - up detail of another cluster showing more rounded xenoliths, with Types 1A, 1B, 2 and 4, on the S. shore of Loch Sunart (G.Ref. 8123-6017).

Plate 5.6A Two xenoliths of different appearance - Types 1B (left) and 2 (right).

Plate 5.6B A cluster of elongate sub-angular xenoliths on the washed southern shore of Loch Sunart. Hammer shaft 550mm.

Plate 5.6C A smaller group of sub-angular to rounded xenoliths, just west of Rubha-na-Sroine. (G.Ref. 7880-5973).

Plate 5.6D Samples XG64A, 64B, XG65 and host SGVIII from the ctG sheet at Locality D (Fig.1.2). (G.Ref. 7620-6465).

Table 5.1. **XENOLITH CLASSIFICATION FOR THE WHOLE OF THE STRONTIAN COMPLEX**

The percentages given at the end of each class refers to the proportion of each group from the total collected.

Type 1: Microdiorite (fine grained)

A Non-porphyritic. These contain plagioclase + hornblende + biotite + quartz +/- <0.5 to 1.5mm sphene +/- magnetite. Occasional aggregates of hornblende / biotite.
14.4%

B Porphyritic. These contain phenocrysts of plagioclase +/- hornblende +/- biotite in a matrix of plagioclase + hornblende + biotite + quartz +/- sphene. Occasional quartz xenocrysts.
27.5%

Type 2: Diorites (medium to coarse grained): with hornblende aggregates.

Aggregates of hornblende (+ magnetite + biotite) upto 2.5mm across + plagioclase phenocrysts set in a groundmass of plagioclase + hornblende + biotite + quartz +/- sphene + magnetite. Primary assemblage anhydrous.
18.6%

Type 3: Diorites (coarse grained appinitic texture).

Appinitic - type texture of elongate euhedral prisms of hornblende and plagioclase phenocrysts with quartz, biotite and upto 3mm long sphenes.
1.9%

Type 4: Diorites (medium grained): with phenocrysts but no hornblende aggregates.

These are similar to Type 2, but have no hornblende aggregates; containing plagioclase and hornblende phenocrysts in a matrix of quartz + plagioclase, with hornblende being the dominant mafic mineral + biotite +/- sphene +/- magnetite. Primary assemblage hydrous.
21.5%

Type 5: Diorites (medium grained): biotite-rich.

These are more mafic looking, as their matrix is biotite dominated; containing plagioclase phenocrysts +/- biotite phenocrysts +/- hornblende - biotite aggregates, in a matrix of biotite + plagioclase + quartz + hornblende +/- sphene +/- magnetite.
14.4%

Petrographically the clusters are a heterogenously mixed group of xenolith types (described below in Table 5.1). This is not only a feature of these clusters, but of smaller groups of xenoliths and even pairs (Plate 5.6 A, B, C & D).

5.2.2 Shape and Orientation of the Xenoliths

The orientation and shape of the xenoliths present in the granodiorite host, reflect the intensity of the lineation and foliation. The xenoliths can be divided into two main groups:

a) Spherical and slightly ellipsoidal xenoliths;

b) Strongly flattened.

a) These xenoliths are by far the most common in the pluton with a rounded to subangular shape. Angular xenoliths are rare and most are only found at the western margin (Plate 5.6C). Most xenoliths are spherical to flattened ellipsoids (max:min axial ratio 2:1) in three dimensions (Plate 5.7). Markedly inequant xenoliths are rare. The ellipsoids are generally concordant with the flow fabric and when prolate, their longest axes lie parallel to the lineation. However these ellipsoidal xenoliths are not only found near the margin where the fabric is well developed, but also away from it. Though where the fabric becomes less pronounced away from the pluton contacts, the xenoliths become more spherical and are therefore unable to exhibit any preferred orientation. Spherical and ellipsoidal xenoliths occur together, as seen in some of the smaller clusters (Plate 5.5 & 5.6B),

Plate 5.7 More outstanding xenoliths on the S. shore of Loch Sunart. (G.Ref. 7805-5980).

Plate 5.8 Xenolith showing a very diffuse contact with the surrounding granodiorite. (G.Ref. 8092-6017).

so the ellipsoidal shape is not the result of a penetrative deformation. The igneous fabric is retained within the ellipsoids, confirming the lack of penetrative deformation. This also suggests that the xenoliths could either have crystallized after the deformation or have been plastic at the time the fabric was being formed.

b) The strongly flattened xenoliths, max:min ratios are greater than 3:1, are only found at the margins (Fig 5.1), where they are parallel to the steep planar fabric. They can also show an igneous fabric even though they are flattened. They are not abundant, but where they do occur they appear to be associated with the biotite - rich streaks or schlieren. Some xenoliths that have been subjected to penetrative deformation, become elongated, show an internal foliation of parallel feldspars lying parallel to the external one of the host but these are rare. Hutton (1988) discusses the stresses that occurred in both the granodiorite and biotite granite pluton of Strontian, using strain determinations from numerous deformed xenoliths. They indicate that deformation was highest around the contact. However these stresses vary throughout the pluton as not all the xenoliths found near the contacts have been deformed.

The distribution of xenoliths as isolated individuals and small groups comprising of more than one type, indicates dispersal and mixing of xenoliths within the magma. Orientation shows that they were related by the flow of magma. The dense clusters may either represent accumulation of xenoliths or areas that have not been dispersed by the flow.

The xenoliths have sharp, smooth contacts with the surrounding host rocks. The contact of the xenoliths is less smooth in thin section

than it appears to the unaided eye, since there is an interlocking of grains and a larger crystal may be seen to lie partly in the host and partly in the xenolith (Plate 5.6A). Rarely, xenoliths show diffuse margins indicating assimilation into the host (Plate 5.8). Rare examples of xenoliths show irregular crenulate margins with lobes 10 to 20mm across separated by inward pointing cusps of granite (Plate 5.9). This relationship has been found in the study of the intimate associations of acid and basic magmas (Blake et al 1965; Walker & Skelhorn 1966). These examples were interpreted as the result of the simultaneous liquidity of acid and basic magma.

Most xenoliths are internally uniform, but uneven distribution of minerals or phenocrysts may give the impression of a xenolith within a xenolith. This internal zoning is generally clear in hand specimen, but may look more diffused at microscope level. Very occasional examples of xenoliths containing smaller xenoliths occur with the mutual internal contact being sharp. These types of xenoliths indicate that they have undergone at least 2 different phases in their earlier history than all the other xenoliths. Not only are these xenoliths rare, but they were difficult to collect and so many were left in the field. Only 3 xenoliths were successfully collected: XG3/3A, XG20/20A and XD1/1A. It is seen clearly on XD1/1A, where the centre is hornblende aggregate-rich with a narrow fine grained outer margin. This margin is not a chill as the fine grained nature is the same as the matrix interior between the aggregates. All grid references are given in Appendix A, separate geochemical analyses in Appendix B and their locations are marked on Fig.5.1A.

In general the xenoliths show an internal fine grained Type 1(A)

Plate 5.9 Two xenoliths with an irregular crenulate margins, found close to the Rubha-na-Sroine diorite. Samples XD1/1A are collected from the right xenolith (G.Ref. 7933-6011).

Plate 5.10 An example of a xenolith within a xenolith, a round Type 1A centre surrounded by a tear-drop shaped Type 4 (G.Ref. 7932-6009).

surrounded by Type 4 xenolithic material. Plate 5.10 clearly shows this occurrence and is located at grid ref.: 7932 - 6009. This is along the southern shore of Loch Sunart, close to the SW contact of the Rubha-na-Sroine diorite (Fig.1.2, Locality 2 and described in chapter 9). This xenolith appears very clear as it is present on the washed shoreline and weathering has exaggerated the difference between the 2 Types.

The centres of the xenoliths are also occasionally biotite-rich (Type 5). There are no examples in these xenoliths of the porphyritic part being surrounded by non-porphyritic material, but one xenolith XG20/20A has a non-porphyritic medium grained rim which passes into a finer grained biotite-rich centre. The centre is sharply bounded only by the hand specimen difference in petrography.

Field collection and geochemical analysis was not restricted to xenoliths within xenoliths. When larger xenoliths were encountered, serial samples within a single homogenous xenolith were taken. These xenoliths are not zoned or jacketed by a different xenolith type, but were collected to study any internal geochemical variation (refer to chapter 7, section 7.1). This is the case for xenoliths XG61A/B/C and XG64A/B, both from the ctG sheet found at Locality D on Fig.1.2, which is very xenolith-rich. They are large xenoliths and so sampling from core to rim was possible. However there is no great difference between the core and rim in terms of grain size or the presence of phenocrysts.

5.3 OCCURRENCE AND DISTRIBUTION IN THE BIOTITE GRANITE

The alkali granite is a poorly xenolithic rock. The later granitic

sheets associated with the biotite granite (fG on the BGS map) are also poorly xenolithic and have been noted to truncate xenoliths (Plate 2.10). The occasional xenoliths that were found, were scattered throughout the host granite (Fig. 5.1). Their total size range is smaller than that in the granodiorite, 250mm to less than 100mm. Xenolith types present include Type 1A, 1B and occasional Type 2 and 3. Those found closer to the mafic diorites, are more mafic themselves, eg. close to the Uileann and Loch Tearnait bodies. While those xenoliths away from the diorite bodies are more leucocratic in appearance, with occasional quartz xenocrysts.

The xenoliths also have the rounded to flattened ellipsoidal shape, which is interesting as there is no developed fabric in much of the biotite granite. They are sharply bounded like the xenoliths in the granodiorite.

5.4 OCCURRENCE AND DISTRIBUTION IN THE GRANODIORITE PORPHYRY SHEETS

The granodiorite porphyry sheets (ctG) of Strontian are xenolithic (Plate 5.1 & 5.6D) eg Location A & D Fig 1.2.

The large sheet at location D, which crosses the A884, was found to possess a very high proportion of xenoliths. Their total size range is similar to the granodiorite, 0.15 to 1.0m. The xenolith classes found are Type 1B to 4. There is no fabric developed within the sheets and xenolith shape ranges greatly from large flattened ellipsoids (Plate 5.1) to rounded/sub-angular (Plate 5.6D). They all have sharp contacts with the granodiorite porphyry.

5.5 SUMMARY AND DISCUSSION

The intermediate dioritic xenoliths of Strontian commonly occur as dark finer grained ellipsoids in the host tonalitic and porphyritic granodiorite (rare examples in the biotite granite), from which they are different. A very limited percentage of Moine xenoliths were found in the complex and show little local country rock contribution to the xenolith assemblage. There is only a little overlap of the size range of the Moine and psammitic xenoliths.

When accounting for the origin certain facts must be considered: 1. The flattening and orientation of the xenoliths in certain localities gives evidence that they were able to undergo plastic deformation at the time of emplacement of the surrounding rock, and that they were not fully crystallized; 2. Their position within the host is not restricted by the surrounding host; 3. Their distribution is apparently related to magmatic movement; and 4. the xenoliths are composed of similar minerals to the host rock (but are always finer grained) and chemically and texturally the xenoliths have igneous rock characteristics (to be discussed in chapters 6 & 7). The origin of the xenoliths is the basis of this study and at this stage a plausible suggestion is that the xenoliths are fragments of an earlier crystallized phase of each intrusive mass. However a basic border facies of the Strontian complex has not been observed and the mafic diorites have not been described. Preliminary evidence in the Strontian host rock chapters points to early conclusions of magma mixing/hybridization, which can now be extended to the xenoliths. They show quartz xenocrysts and xenolith within xenolith relationships, which suggest a more complicated history possibly at depth.

The possibilty of xenoliths being formed by magma mixing is suggested by Hyndman & Foster (1988) who describe the formation of the Idaho Batholith. They regard the granitic magma as having been formed by the injection of high-temperature mantle magmas causing partial melting of the continental crust. These mafic magmas are now represented at the surface by numerous synplutonic mafic dykes and tonalite/quartz diorite plutons around the margins of the batholith. Also variable amounts of mixing of the mafic magma and the granites would produce all the rock types presently seen in the batholith.

The efficiency of this mechanical magma mixing and associated textural features would depend on the rates of convective velocity, crystal content and viscosity of the granite at the time of mafic magma intrusion (Furman & Spera 1985). For example rapid convection rates (1km/year) at low crystal content of the host (0-30%), would produce textures such as clots, isolated xenocrysts, disequilibrium mineral assemblages and small rounded inclusions; while slow convection rates (0 to a few cm/year) at high crystal content (50-70%) could result in deformed synplutonic dykes and large inclusion swarms (Furman & Spera 1985, from Hyndman & Foster 1988).

Chapter 6 THE XENOLITHS: PETROGRAPHY AND MINERALOGY

6.1 INTRODUCTION

Xenoliths were classified in the field by gross textural and mineralogical features (refer to Table 5.1). This chapter is concerned with their petrography and mineral chemistry. To prevent repetition in the case of xenolith classification, some points will be described once and where necessary reference will be made to the appropriate point.

6.2 XENOLITH PETROGRAPHY FOR THE GRANODIORITE, BIOTITE GRANITE AND GRANITIC SHEETS

The xenoliths found always contrast sharply with the light grey and pink colour of the tonalitic and porphyritic granodiorite and biotite granite. They are finer grained than the surrounding host and most large mafic dioritic bodies. They have a typically hypidiomorphic texture with a grain size range from 0.1 to 3mm. At first all the xenoliths appear uniform, though on closer inspection small differences in composition, texture, grain size and abundance of phenocrysts become apparent. The different xenolith types, as described in Table 5.1, have been plotted on Fig.5.1 and there is no pattern to their distribution. The more leucocratic or mafic xenoliths mentioned in chapter 5 are incorporated into the descriptions of each type, but are elaborated on where necessary. The petrography of the xenoliths found in the ctG sheets is also included in these descriptions and all appear uniform with those found outside the sheets. However where any differences were observed, these are pointed out.

Phenocrysts which range from 4 to 20mm in length are conspicuous in many xenoliths. The commonest phenocryst phase is plagioclase, hornblende and biotite are common and quartz rare. Their concentration varies not only from xenolith to xenolith, but may well show the entire range in a single xenolith. Nearly half of all the xenoliths collected have feldspar phenocrysts, though in 40% of those the phenocrysts are not abundant. Hornblende phenocrysts are most commonly found with the feldspars. While a third of the hornblende-phyric xenoliths have only hornblende as their main phenocrysts phase. The remaining 20% of the xenoliths, that have neither plagioclase or hornblende phenocrysts, have a variable petrography of biotite-rich (occasional phenocysts) with or without sphene; "spotty" xenoliths with or without sphene and aphyric xenoliths with no sphene. Xenocryst quartz is widespread but not abundant and does not define a separate xenolith Type. The xenocrysts reach a maximum of 5% in any type.

The sampling traverses have established that a variety of xenoliths are present and they range from mafic and quartz diorites to microdiorites. The dioritic xenoliths have a variable colour index ranging from mafic to leucocratic dominated. Mineralogically the xenoliths are very similar to the surrounding host rocks, with an increase in the proportion of biotite and hornblende and a corresponding decrease in quartz and K-feldspar. The main constituents are: plagioclase, hornblende, biotite, quartz and some alkali feldspar, with accessory minerals such as sphene, apatite, magnetite and occasional zircons and allanite. Very rare remnants of pyroxene have been seen. Occasional secondary minerals include epidote, chlorite and sericite. However these will not be considered

further.

The xenoliths often retain an original igneous texture varying from a porphyritic texture with an interlocking matrix to an appinitic texture. Porphyritic textures are better preserved than the groundmass textures in Types 2 and 3 (Plates 6.4 & 6.8). Granoblastic textures (Plates 6.1 & 6.2) have been noted in varying amounts in the different xenolith classes, especially in the groundmass where interlocking, equigranular crystals suggest recrystallization. The recrystallization of mafics is also seen in the form of aggregates noted in Types 2 and 5 (Plates 6.4 & 6.5A).

6.2.1 TYPE 1A : Plate 6.1A.

This xenolith type is a very fine grained crystals, upto 1mm in length, and non-porphyritic, seen in hand specimen in Plate 5.6C and 5.10 (centre).

Plagioclase is present as euhedral to anhedral crystals of upto 1mm in length. Their compositions range from labradorite to oligoclase An54-28. Pronounced continuous zoning is present in many of the feldspars but not oscillatory zoning. Some plagioclase grains shows a uniform basic core succeeded by a more sodic rim with a sharp boundary between the two zones. Rare reverse zoning was found during analysis on the electron microprobe. Good Carlsbad twins are noted and albite twinning can be seen poorly to well developed.

Alkali feldspar is also present, but not as abundantly as plagioclase, as subhedral to anhedral grains. Occasional examples of microcline twinning are observed.

Both myrmekitic and graphic textures occur occasionally. Alteration of the plagioclase is unevenly distributed throughout this class, within the xenolith and between the xenoliths. Plagioclase is either fresh or has alteration in the cores or along certain compositional zones.

Biotite and hornblende are the main ferromagnesian minerals present in Type 1A, with biotite being slightly more abundant.
Biotite occurs as euhedral to subhedral crystals of 0.1 to 1mm in length. It is found as either fine individual grains in the groundmass or in aggregates. Some aggregates are small and are solely biotite, while larger ones of upto 2.5mm are associated with hornblende.

Hornblende is found as small euhedral to subhedral, stubby to elongate prisms of 1mm to 3mm in length. Compositions will be discussed later on in this chapter in section 6.3.2, but range from magnesio-hornblende to edenite.

Hornblende either forms fine grained aggregates, possibly replacing an earlier mafic mineral suggested by the shape of the aggregate or is one larger crystal. In the more highly altered xenoliths, where nearly all the plagioclase has been weathered, the hornblendes are present as tiny subhedral to euhedral grains; while biotite has been altered to chlorite and shows exsolution along its cleavage.

Magnetite is also found in the aggregates. It is unevenly distributed throughout Type 1A xenoliths. Some have magnetite present as rounded grains in the matrix, while in others magnetite is

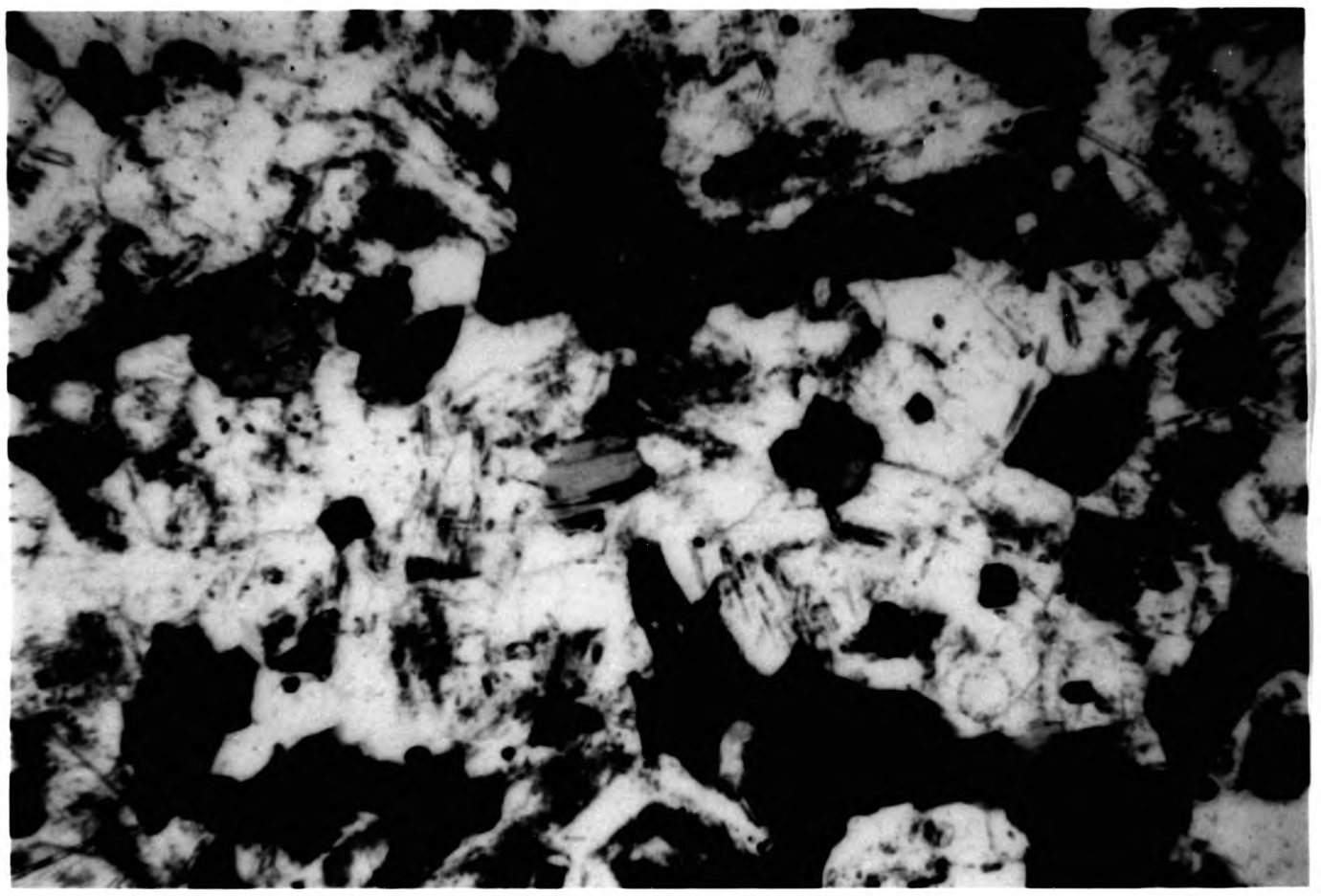

Plate 6.1 View of Type 1A in PPL showing the general equigranular texture - Sample XG32. Field of view 3mm.

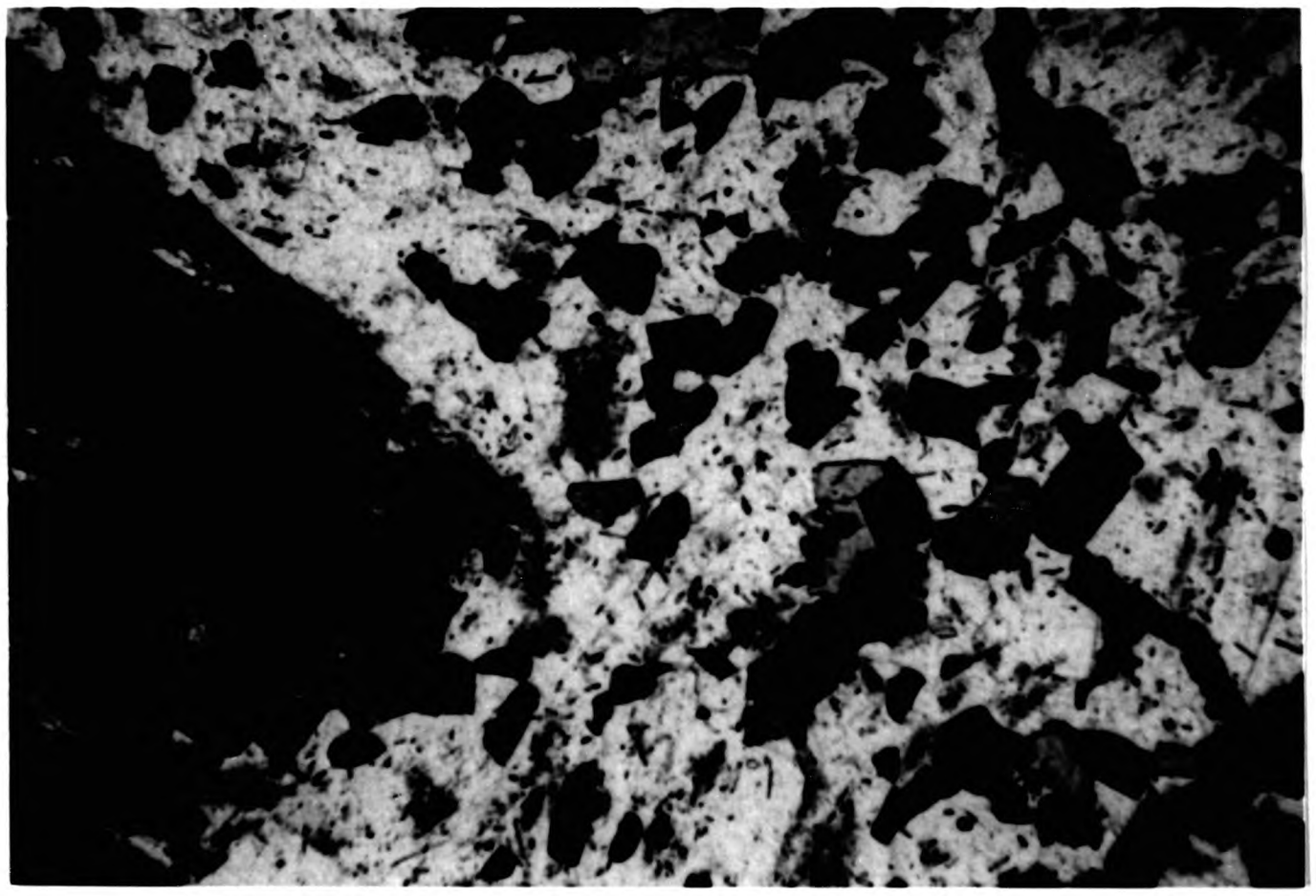

Plate 6.2 View of Type 1B in PPL with a hornblende phenocryst in an equigranular groundmass - Sample XG45. Field of view 3mm.

restricted to the biotite and hornblende aggregates with nothing in the groundmass.

Sphene and apatite are present. Sphene occurs in two forms, as small 0.1mm euhedral crystals and as 1mm skeletal grains. In the xenoliths with weathered feldspars, sphene forms tiny euhedral grains with very high relief and occasional rounded inclusions of green hornblende. Apatite forms very fine acicular needles present as inclusions in feldspar and quartz.

Quartz occurs as anhedral, interstitial grains upto 1mm in diameter.

6.2.2 TYPE 1B : Plate 6.2.

These xenoliths are also fine grained, but distinguished from Type 1A by being porphyritic, seen in Plate 5.6A (left hand xenolith).

The phenocrysts of plagioclase are exactly the same as the plagioclase in the groundmass, but reach 10mm in length. They are subhedral in shape often showing signs of irregular marginal intergrowth with, and partial enclosure of , the surrounding matrix. This margin in the phenocrysts appears narrower in the phenocrysts than in the groundmass plagioclase. However poor the crystal faces, they seem more prominent by the presence of the albite twinning commonly combined with Carlsbad twinning.

Compositionally phenocryst and groundmass plagioclase is the same, ranging from andesine to oligoclase An45-29. There are only occasionally mottled plagioclases, where the twinning is disrupted, but is not as well developed as in the host rocks. Oscillatory and continuous zoning are found with examples such as phenocryst

compositions from An35-37 in alternating zones or simply from core to rim An 40-32. Occasional abrupt compositional boundaries between zones in the earlier stages of growth seen by probe data, suggest discontinuous zoning of a more basic core mantled by a more sodic rim. There are too few examples of this to see if it is important.

Within the phenocrysts individual annular subhedral zones are also marked by small subhedral to euhedral mineral inclusions, especially of biotite and hornblende with the occasional apatite and / or sphene. Plagioclase with cores containing abundant inclusions are also found. There seems to be no regularity in the occurrence of these inclusions throughout the xenoliths. There are some examples of antiperthitic texture. Myrmekite does occur where there is opportunity, but it never grows to such fine examples as seen in the granitic hosts.

Alteration in the plagioclase phenocrysts and in the groundmass is commonly observed in the core of the crystals, in zones immediately around it and in those rich in inclusions.

Alkali feldspar is not so abundant, but occurs as phenocrysts reaching 10mm in length. They are often found in the xenoliths of the porphyritic granodiorite sheets and only occasionally in the xenoliths of the tonalitic and porphyritic granodiorites. They are subhedral to anhedral in shape and are slightly perthitic. They display various stages of development of cross-hatch or microcline twinning. One such K-feldspar shows signs of resorption in the core and then being jacketed by plagioclase feldspar (Fig.6.1D). K-feldspar in the groundmass occurs as interstitial anhedral grains of 1mm or less in size with microcline. A very large, 20mm, rare

poikilitic grain of alkali feldspar has a very coarse granophyric texture and is perthitic. The grain has also 4mm crystals of plagioclase within its margins. This is a rare occurrence and was found in a Type 1B xenolith.

As in Type 1A, hornblende and biotite are the main ferromagnesian minerals.

Hornblende is found in the groundmass forming subhedral to anhedral individual grains or in aggregates of 5mm in diameter. The individual acicular grains can reach 1mm in length. Occasional phenocrysts of hornblende are euhedral to subhedral elongate prisms between 5 to 10mm in length containing very rare examples of remnant pyroxene cores (Plate 6.3 A & B).

Most aggregates are of hornblende, but some have magnetite in the core or in annular zones. They also on occasion possess rare clinopyroxene cores, so suggesting that the aggregates have replaced and pseudomorphed earlier formed pyroxene phenocrysts. Some aggregates are associated with biotite, which is seen to form a jacket around the aggregate.

Biotite occurs mainly in the groundmass as individual subhedral to anhedral grains of 0.5mm grading to larger euhedral to subhedral phenocrysts of 5mm in diameter. It is distributed throughout the groundmass, but can form concentrations of larger crystals or simply aggregates. These aggregates are often associated with hornblende where the biotite is either chemically replacing the hornblende or has grown simultaneously.

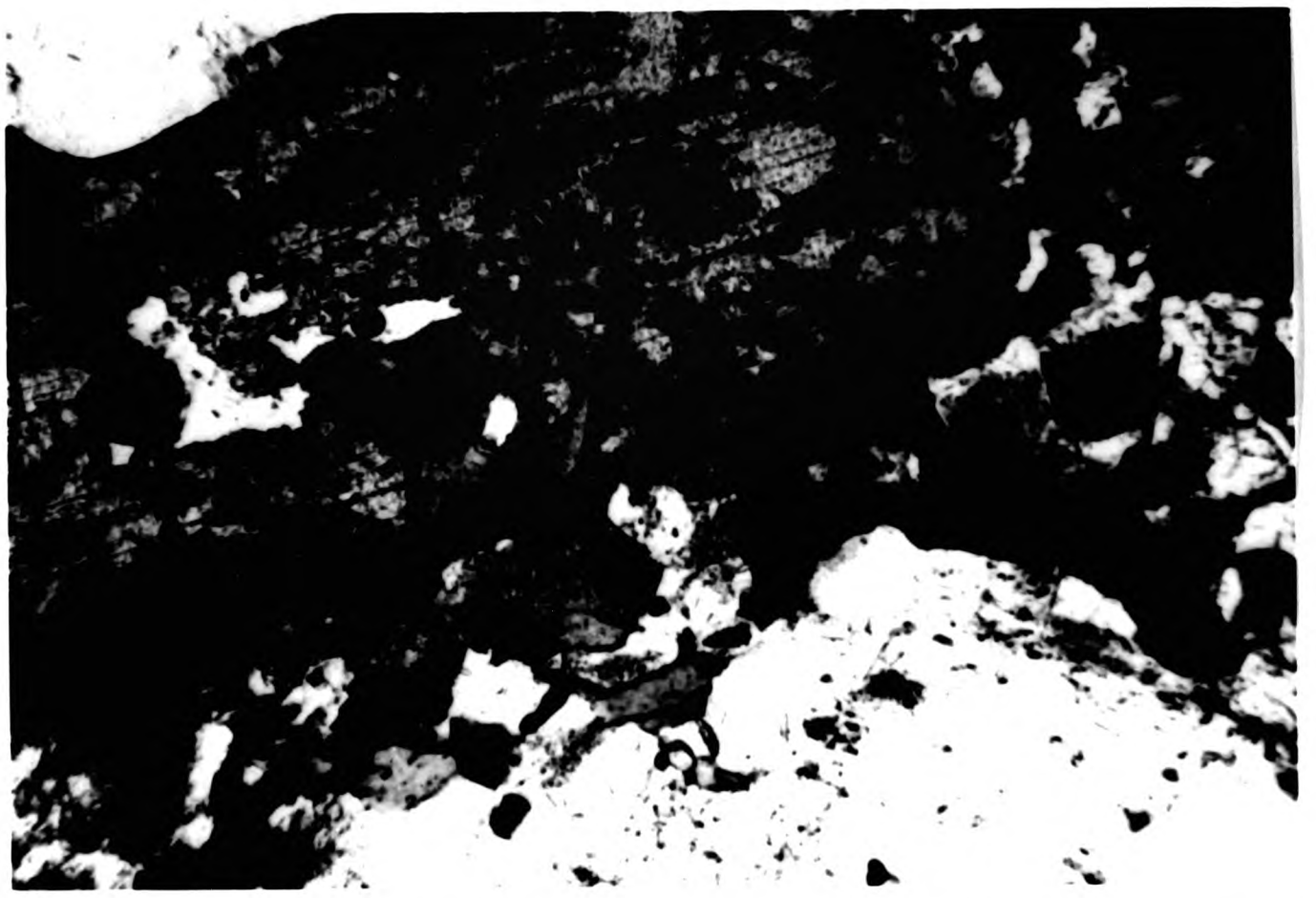

Plate 6.3A View of Type 1B xenolith in PP1 showing a pyroxene core to the amphibole - Sample XG7. Field of view 3mm.

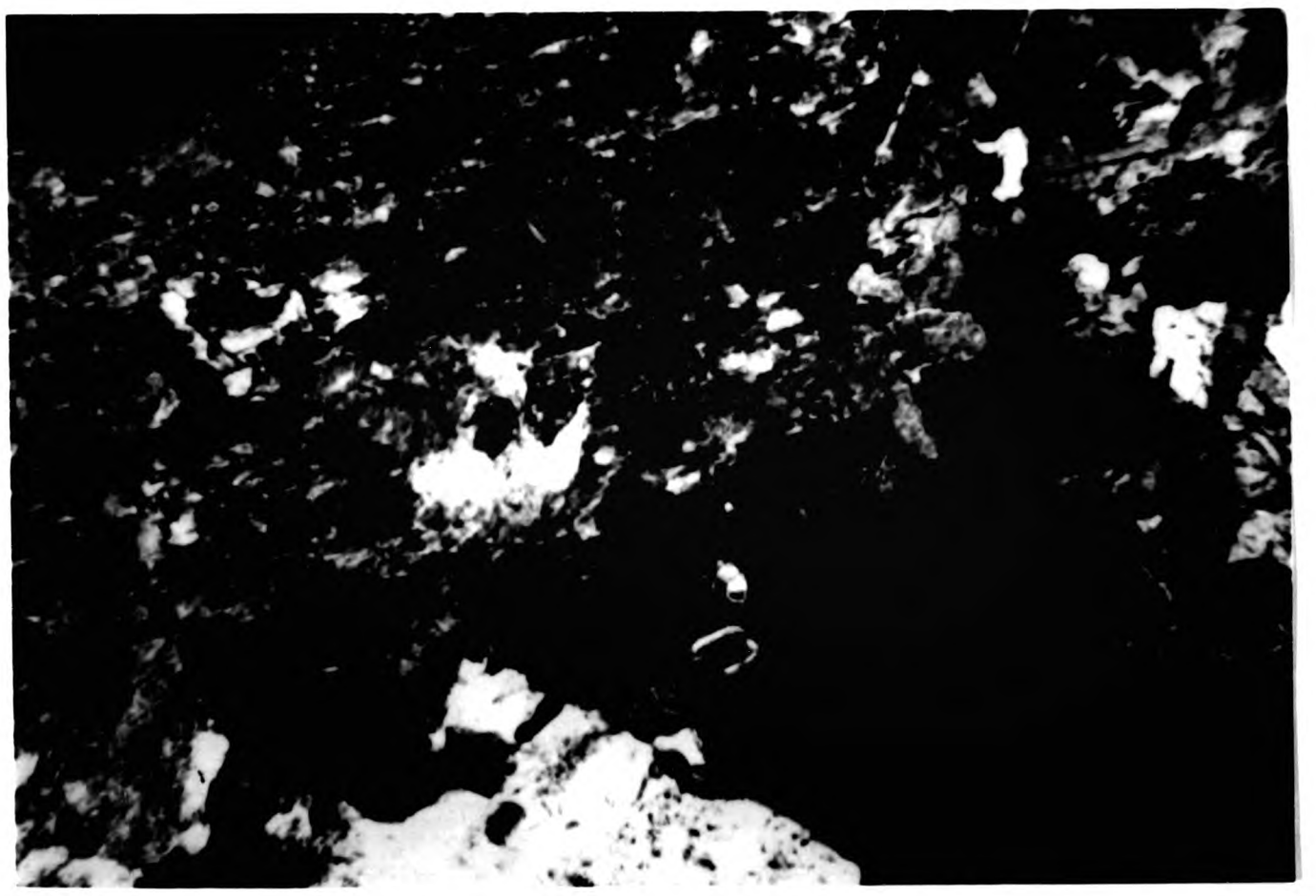

Plate 6.3B As in 6.3A but in XPL showing the clinopyroxene core with higher birefringence than the surroundings - Sample XG7.

Quartz is found in varying amounts and forms. Most commonly it is interstitial amongst the feldspar, where it shows myrmekitic and graphic intergrowths. Coarser grains of quartz often show euhedral apatite needles within the crystal. They are also poikilitic in texture, enclosing the groundmass plagioclase, biotite and hornblende.

The occurrence of quartz xenocrysts has been observed. They reach 3-4mm in diameter and consist of either a single crystal or two quartz grains together. They are always surrounded by mafic jackets which consist of mainly fine euhedral to subhedral crystals of hornblende and occasionally biotite and sphene. Xenocryst abundance usually ranges from only a few grains to a few percent and occasionally to 10-15%. Even when sparse they are conspicuous on the weathered surfaces of the xenoliths. These xenocrysts are always found in the thin section of the xenolith seen to have xenocrysts in the field. 8% of the xenoliths collected and analyzed have quartz xenocrysts and are found close to the margin of or within the biotite granite, or along the shores of Loch Sunart.

Quartz in some Type 1B xenoliths show a good metamorphic granoblastic texture of variable intensity, suggesting a certain amount of strain and recrystallization of the groundmass.

Magnetite, sphene and apatite are the most common accessory minerals. Magnetite is not only found associated with the hornblende aggregates, but is found individually as euhedral to subhedral grains reaching 0.5mm in diameter.

Sphene is found throughout Type 1B in varying amounts. Its form is

either euhedral crystals of 1-2mm showing good cleavage traces or anhedral skeletal grains of less than 1mm. These latter sphenes are also found either in the groundmass or associated with biotite or hornblende crystals. While the euhedral sphenes often have tiny euhedral inclusions of plagioclase feldspar.

Apatite varies from very fine acicular needles of 1.0mm in length to stubbier needles of 0.1mm in length. They are found throughout the groundmass, often within the quartz.

6.2.3 TYPE 2 : Plate 6.4.

Type 2 xenoliths are coarser grained than Type 1A and 1B and are all characterized by aggregates of hornblende, a higher proportion of mafic minerals and very occasional K-feldspar phenocrysts (or xenocrysts) and seen in Plates 5.6B and 5.6C.

Plagioclase as phenocrysts forms grains of 8 to 12mm in length. They show good Carlsbad and albite twinning with faint concentric zoning. Feldspar compositions range from labradorite to oligoclase, an extreme An51 core to An24 rim with an average core composition of An35-30, with some cores greater than An35. Only one example in the phenocryst shows reverse zoning from core to rim of An37-An34-An45. Rounded inclusions of hornblende and biotite together with apatite needles, occasional magnetite and sphene, have been noted concentrated in the rounded cores of some plagioclase phenocrysts (Fig.6.1B - XG44). These cores are seen in at least 40% of the phenocrysts. Mottling seems to be present with the most inclusion-rich cores. These xenoliths are all found within the granodiorite with occasional ones in the ctG granitic sheet.

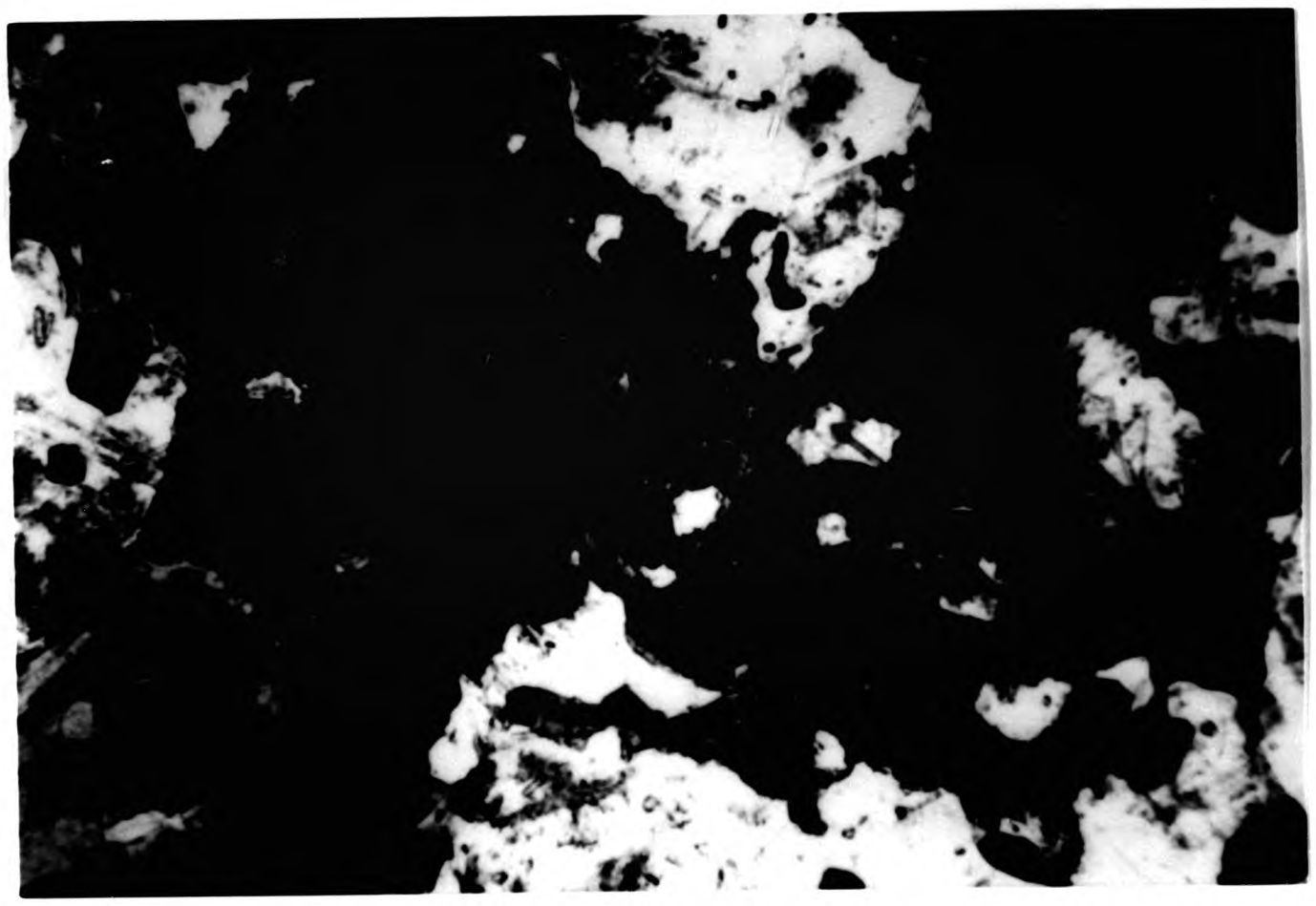

Plate 6.4 View of Type 2 xenolith in PPL displaying a coarser grained rock with a mafic aggregate on the left and a poikilitic sphene on the right - Sample XG28. Field of view 3mm.

Plate 6.5A View of Type 2 xenolith in PPl showing the abundant hornblendes as individual crystals or as aggregates (bottom right corner) - Sample XG61A. Field of view 3mm.

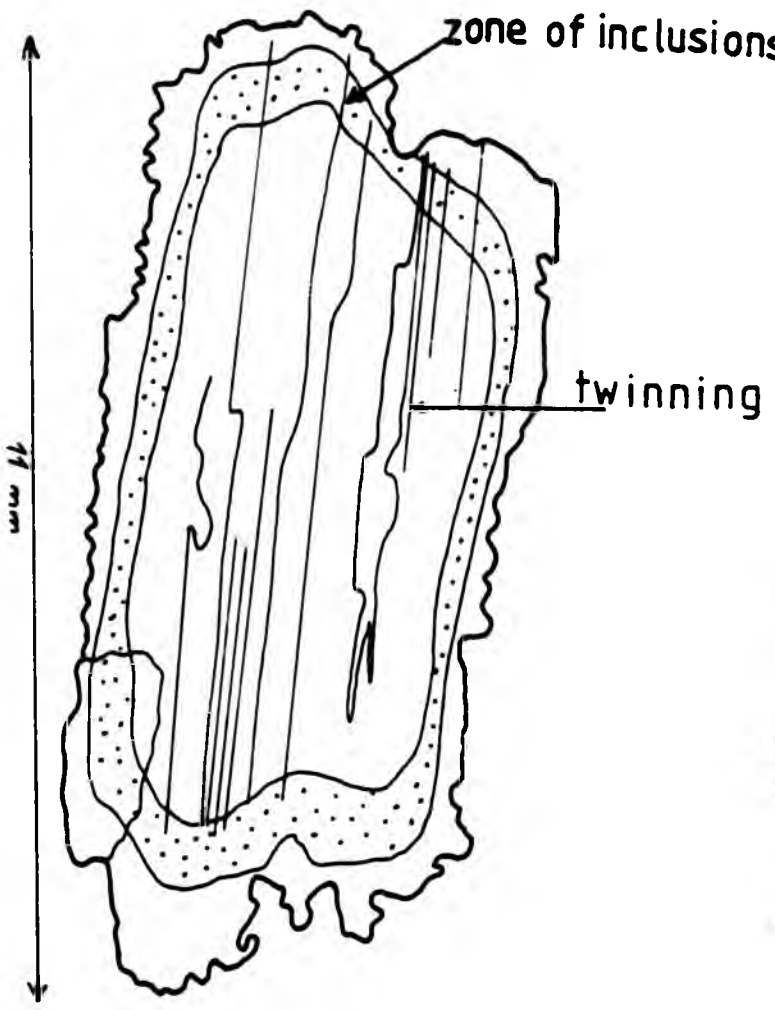

A. XG4
Plagioclase

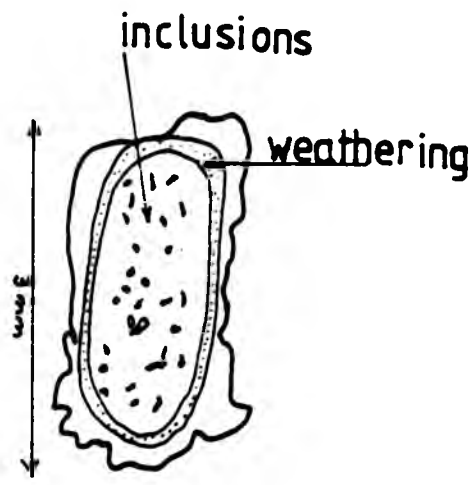

B. XG 44
Plagioclase

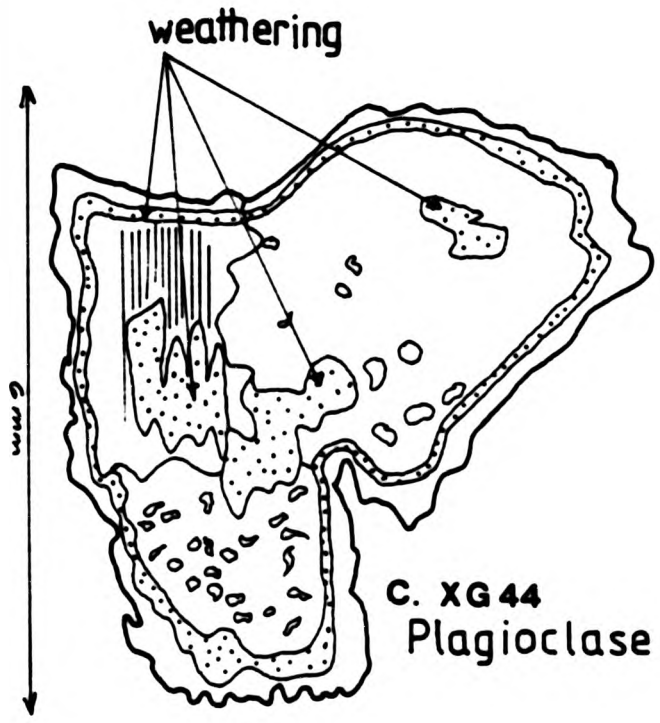

C. XG 44
Plagioclase

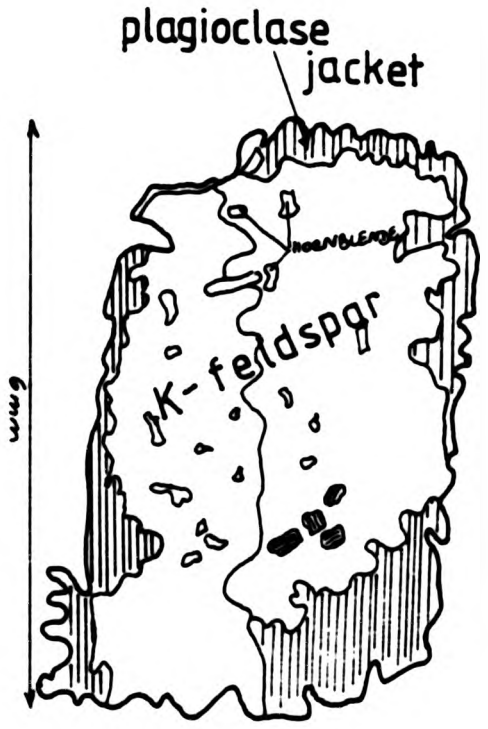

D. XG 64B

Fig.6-1 Details of xenolith feldspars

Alteration occurs along the albite twins and specific zones or in the cores.

Alkali feldspar is also found as occasional phenocrysts, showing the first signs of exsolution. They occur as subhedral grains of 8 to 10mm in size, that are jacketed by plagioclase feldspar, a texture which has not been seen in the host rocks and forms less than 3% of the rock. Alkali feldspar is also present interstitially as subhedral to anhedral grains of 1mm or less.

Plagioclase in the groundmass exhibits similar features to the phenocrysts such as good albite twins with some pericline twinning, normal zoning and alteration in the cores. Their form is interlocking subhedral elongate grains of 1-2mm in length. They also contain fine acicular apatites in varying amounts.

Hornblende is the more abundant mafic mineral forming large aggregates as well as individual grains within the groundmass. In the groundmass it forms euhedral to anhedral grains of 1-4mm in length (Plate 6.5 A & B).

The aggregates vary in size from 2 to 8mm and consist mainly of green hornblende. Biotite, sphene and magnetite are seen to be associated in a variety of habits. Biotite in some cases seems to be jacketed by or have been crystallized with the hornblende rather than being the alteration product of the hornblende in the aggregates. Sphene is quite often found close to or within the aggregate.

Magnetite can form specific zones within the aggregate eg. in the core, close to the margins or both, and here the magnetite grains are

Plate 6.5B View of Type 2 xenolith inPPL showing a large euhedral hornblende - Sample XG48. Field of view 3mm.

Plate 6.6 View of Type 2 xenolith in PPl showing the magnetite-rich zone within the hornblende crystal - Sample XG33. Field of view 3mm.

usually rounded and of the same size (Plate 6.6). While in examples where the magnetite is scattered uniformly throughout the aggregate, the grains are of variable size.

Magnetite is more abundant in Type 2 xenoliths than in the others and is very often seen intergrown with individual larger hornblendes and biotites in the groundmass. It is also present as euhedral to subhedral grains of nearly 1mm.

Biotite ranges from medium grained individual plates of 1mm in diameter, through finer grained subhedral to anhedral forms of less than 0.5mm to small aggregates. These aggregates are often solely biotite, but do occur close to or together with hornblendes with a high magnetite content. Sphene and magnetite are also seen associated with the biotite aggregates. Alteration of biotite into chlorite is noted along the cleavage traces.

Throughout Type 2 xenoliths quartz is found as anhedral interstitial grains of upto 1mm in diameter. Occasional examples of myrmekitic and graphic textures are noted.

Sphene is not only found in and around the mafic aggregates, but in its larger form, is found as single sub- to poikilitic crystals and as euhedral rhombs or prisms (Plate 6.7). They are often associated with small subhedral to euhedral plagioclase feldspar grains. This latter sphene is observed clearly in hand specimen as pinkish brown patches surrounded by a white rim. This was one of the original hand specimen characteristics used in discriminating Type 2. Small anhedral grains of sphene are also not uncommon throughout this xenolith class.

Medium to fine acicular apatites in the groundmass are seen mainly as inclusions in quartz and plagioclase, but also occur in biotite and hornblende. They have euhedral to rounded basal sections.

6.2.4 TYPE 3 : Plate 6.8.

These xenoliths are coarse grained, non-porphyritic, rich in ferromagnesian minerals especially hornblende and biotite, with rare pyroxenes. They appear very similar to appinites in mineralogy and texture. They are also very uncommon and only 4 were collected of which 3 were found within 50m of the contact with a mafic diorite. Their abundance in the field is less than 5% of the total xenoliths observed.

Hornblende forms very conspicuous, coarse, green euhedral elongate prisms of 2.5 to 6mm in length. They often show inclusions of small biotite lathes, quartz and apatite needles within the crystal. Magnetite occurs randomly within the hornblende as subhedral to anhedral grains. There are rare inclusions of sphene and rounded zircon. There are no finer grained aggregates of hornblende but a rare example of a remnant clinopyroxene was found with magnetite surrounding the core, all within the hornblende crystal. A paler green variety of hornblende, is found as cores within the larger green prisms or around their margins. This pale hornblende is intergrown with biotite.

Biotite forms large single euhedral to subhedral crystals of 1 to 4mm as well as finer grains of less than 1mm in length. Inclusions of apatite are the most common with occasional zircons, magnetites and

Plate 6.7 View of Type 2 xenolith in XPL showing a subhedral poikilitic sphene in extinction - Sample XG36. Field of view 3mm.

Plate 6.8 View of Type 3 xenolith in PPL showing the hornblende and sphene-rich nature of the xenoliths - Sample XG18. Field of view 3mm.

sphenes. Alteration of biotite occurs along its cleavage traces and includes chlorite as well as exsolution of rutile and sphene.

Plagioclase forms large, upto 4mm in length subhedral crystals showing good multiple twinning and very pronounced zoning (refer to Type 1B xenoliths). All the plagioclase cores are highly weathered. Alkali feldspars are present as anhedral interstitial grains and appear to be slightly more abundant than in Type 1 and 2 xenoliths. There are also good examples of perthitic and graphic textures and the beginning of microcline.

Quartz also forms larger interstitial grains than in Type 1 and 2, but overall is present in similar amounts. Both quartz and feldspar have inclusions of rounded hornblende and biotite, as well as apatite needles.

Sphenes are a very prominent and abundant accessory mineral in this xenolith type, forming euhedral crystals of maximum length 3mm (average 1mm). They occur close to the hornblende and biotite crystals. They also have inclusions of apatite and occasional magnetite. There are occasional examples of skeletal sphene.

Magnetite occurs not only as inclusions in hornblende, biotite and sphene, but also in the rest of the xenolith. It forms subhedral to anhedral grains of 0.1 to 1mm in diameter, with a tendency to occur in and around the mafic fraction.

Apatites occur as small stubby needles of less than 0.5mm in length and are most often seen as inclusions.

6.2.5 TYPE 4 : Plate 6.9.

Type 4 xenoliths are similar to Type 2 xenoliths, but do not have the characteristic hornblende aggregates, seen in Plate 5.10 (external part of xenolith).

Plagioclase feldspar is present as phenocrysts and in the groundmass. The phenocrysts reach 10mm in length and are subhedral in form showing signs of irregular intergrowth with and partial enclosure of the surrounding matrix. They possess the same characteristics as Type 2 feldspar phenocrysts, with inclusions, alteration and composition (Plate 6.10).

In the groundmass, the form of plagioclase varies from subhedral lathes to anhedral interstitial grains of 1mm in length. A high proportion of the zoned groundmass plagioclase have weathered cores. There is also more abundant myrmekitic intergrowth, than in any other xenolith class, which is related to the larger amount of quartz present.

Alkali feldspar also occurs in the groundmass as anhedral interstitial grains showing varying degrees of development of a perthitic and microcline textures. A graphic texture is not as common as myrmekitic. Rare alkali feldspar phenocrysts are noted from the porphyritic granodiorite host. They are anhedral in shape with a minor amount of inclusions close to the margins and are likely to be xenocrysts.

Type 4 xenoliths have proportionately more quartz than any other xenolith type. This is seen as more interstitial quartz grains,

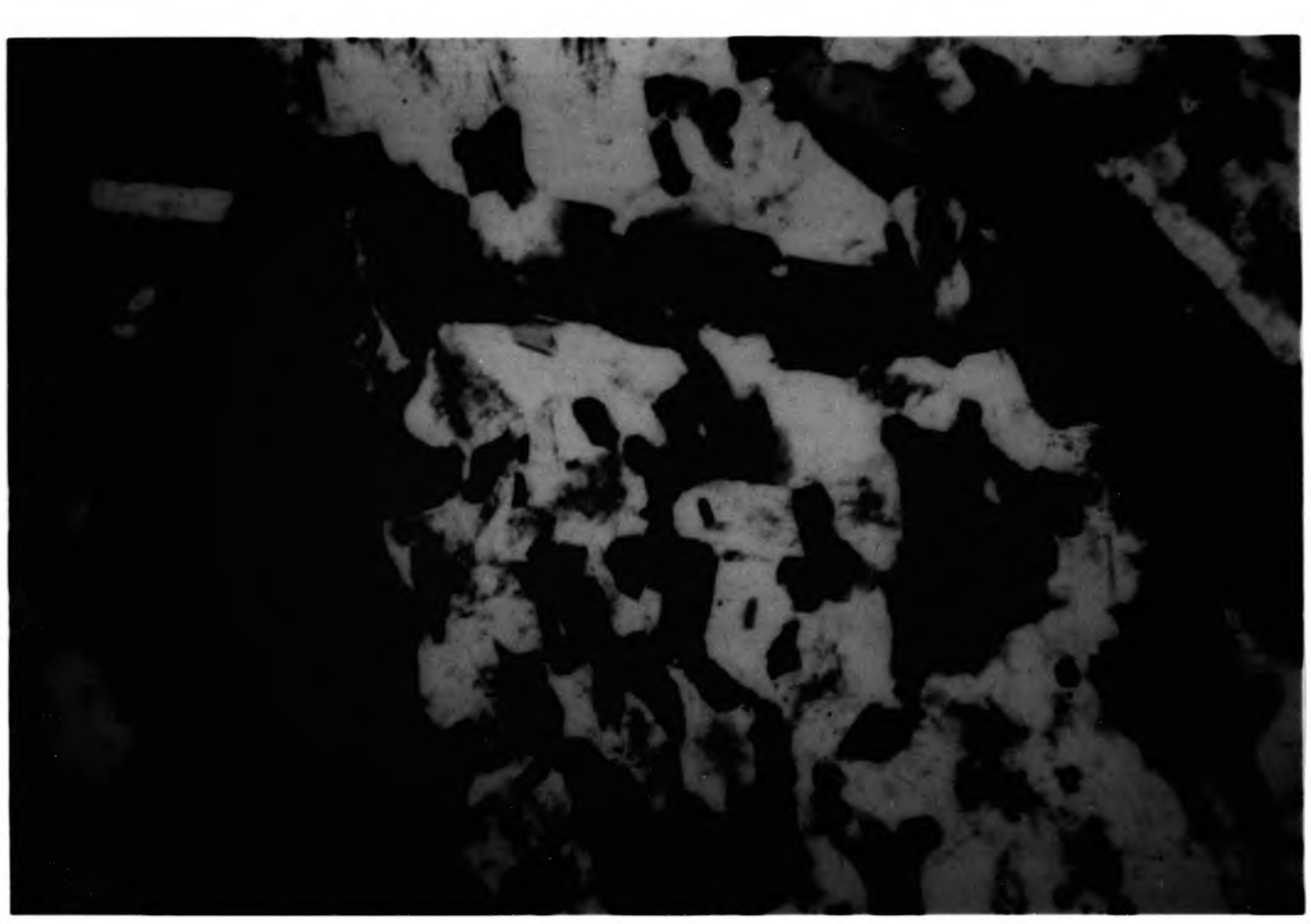

Plate 6.9 View of Type 4 xenolith in PPL showing a large hornblende and intergrowth of hornblende and biotite in the right hand side - Sample XG88. Field of view 3mm.

Plate 6.10 View of Type 4 xenolith in PPL showing a feldspar phenocryst with numerous inclusions of hornblende and biotite surrounded by an altered zone within the crystal - Sample XG27. Field of view 3mm.

which have in a number of examples been recrystallized into a low intensity granoblastic texture, or show strongly intergrown boundaries. These do not appear to have any quartz xenocrysts.

Overall, hornblende is the more abundant mafic mineral present in the groundmass. There are occasional larger hornblende crystals, but none reach phenocryst size. Most commonly they are small euhedral to subhedral in form ranging from stubby to elongate prisms. Hornblende is present either as individual grains or associated with another mineral. In this case it is most commonly with biotite, which appears to have been intergrown rather than be an alteration product. Plate 6.9 shows this intergrowth of hornblende and biotite in the right hand side, with even a discordant biotite growing across the length of the crystal.

Biotite is mainly found in the groundmass as fine grained subhedral to anhedral lathes, with some reaching 1.0mm in size. Alteration is not very common, but where it occurs along the cleavage, it is mainly chlorite with a little exsolution of rutile.

Sphene is the main accessory mineral present as in Type 2, as poikilitic crystals enclosing rounded grains of quartz and plagioclase, surrounded by plagioclase feldspar. They reach 2-3mm in length. Smaller euhedral to subhedral sphenes do also occur.

Magnetite is present as fine rounded anhedral grains are in the groundmass. Occasional large nearly 1mm size grains are found. However it is not as abundant in the hornblende-biotite aggregates as seen in Type 3 xenoliths.

Stubby needles of apatite of 0.2mm in length are seen and not as abundantly as in the other xenolith types. Very fine acicular apatite of less than 0.01mm in size are observed. They are most often noted as inclusions in quartz and feldspar and occasionally in biotite.

6.2.6 TYPE 5 : Plate 6.11A & B.

These xenoliths are medium to coarse grained diorites with a predominance of biotite as the mafic mineral. They are porphyritic with hornblende-biotite aggregates. Textures and overall petrography is similar to Type 2, with examples in Plates 5.5 and 5.6A (right hand xenolith).

Plagioclase forms phenocrysts and is abundant in the groundmass. Compositionally these plagioclase are very similar to the other xenoliths with ranges of An35-18. Phenocrysts reach 11mm in length (Fig.6.1A). There is also a pattern of inclusions within the phenocrysts which is slightly different. A subhedral zone of rounded grains of hornblende and biotite with very fine acicular apatites occurs parallel to the outline of the plagioclase phenocryst and lying close to the crystal margin. This zone is often altered, while the outer part is always clear of inclusions and alteration. Scattered inclusions also occur throughout the core of some crystals. Alkali feldspar phenocrysts occur showing variable degrees of mottling. Fig.6.1 D shows an alkali feldspar xenocryst surrounded by plagioclase. 38% of the xenoliths collected and analyzed have these phenocrysts and all are located in the porphyritic granodiorite and one in the ctG sheet.

Plate 6.11A View of Type 5 xenolith in PPL showing the highly biotite-rich nature with 2 feldspar phenocrysts in opposite corners showing inclusions in the core and alteration in specific zones - Sample XG30. Field of view 3mm.

Plate 6.11B View of Type 5 xenolith in PPL showing a biotite phenocryst in a biotite-rich matrix - Sample XG5. Field of view 3mm.

In the groundmass plagioclase forms subhedral to anhedral grains that are full of apatite needles. The plagioclase shows good albite and Carlsbad twinning with continuous zoning. There is rare myrmekitic growth. Alkali feldspar is also found in the matrix as anhedral grains.

Quartz is only present interstitially throughout Type 5 and in smaller amounts than in the other xenolith types, often as sub- to poikilitic grains around plagioclase, hornblende and biotite.

Biotite is the dominant ferromagnesian mineral. It forms large euhedral crystals of upto 5mm in diameter to small stubby euhedral to subhedral crystals of 0.5mm or less. The larger biotites often have inclusions of apatite, magnetite and tiny subhedral hornblende.

In the groundmass biotite can occur as 1. individual grains; 2. in aggregates of biotite; 3. in aggregates together with hornblende, where biotite is either chemically replacing the hornblende or has grown simultaneously.

The individual grains range from the less than 0.5mm to 2mm in length. In some cases there is a slight alignment. They also show rounded forms with partial enclosure by plagioclase and quartz mainly. The biotite aggregates can reach 3-4mm across and are often found associated with sphene and a little magnetite. While the aggregates with hornblende, often show hornblende as small subhedral to anhedral grains with zones of magnetite within the limits of the aggregate.

Larger single prisms of hornblende upto 4mm in length show the

intergrowth with biotite. These hornblendes also have a few rounded grains of magnetite. Very rare remnants of pyroxene have been found within the larger hornblende crystals. Smaller euhedral to subhedral hornblendes occur as grains of 1mm or less in size.

Sphene ranges from large 2mm poikilitic crystals to tiny less than 1mm subhedral to anhedral grains. These anhedral sphenes are often found close to or within the biotite aggregates, as rounded and elongate grains.

Magnetite is most commonly found in the hornblende aggregates, but it does occur separately in the groundmass as subhedral grains reaching 0.5mm in diameter.

Apatite occurs as fine acicular inclusions in feldspar, quartz and biotite. Coarser, stubbier grains reach 0.5mm in length.

Zircons are more abundant in Type 5 xenoliths than in any other, reaching 1% of the whole rock.

6.3 MINERAL CHEMISTRY

The petrography of the xenoliths has been described in the separate classes, however for the mineralogy it is simpler to describe the minerals chemistry for the xenoliths as a whole group, as there is little difference between the classes. 12 xenolith samples were analyzed by the probe of which 3 are from the tonalitic granodiorite, 4 from the porphyritic granodiorite, 5 from the ctG sheet, but none from the biotite granite.

6.3.1 Plagioclase

Plagioclase feldspars of the xenoliths have a wider range An22-54, oligoclase to high labradorite than the host rocks. They are summarized on the Or-Ab-An diagram Fig.3.4B. In Fig 3.5 where An content is plotted against bulk rock MgO, the xenoliths show a wider range of MgO than the host rocks.

In a single sample compositions may vary from An22-51. For the whole xenolithic suite analyzed core-middle-rim values overlap (the rim includes the actual edge plus a narrow margin; the core includes the centre plus a small area aroud it and the middle is the area left between the rim and the core), for example:

Small to medium crystals:

rim An24-37, middle An22-45 & core An26-54

Calcic cores with compositions greater than An46 are not very abundant.

Phenocrysts also show an overlapping pattern, with some strongly reversed zoning:

eg: rim An28-45, middle An29-36 & core An32-37.

The phenocrysts have a wider range of rim values in a single rock than the small to medium crystals, while the core values are more restricted.

Both normal and oscillatory zoning are common and can occur in the same rock sample. This is observed in both the smaller crystals and in the phenocrysts. Reverse zoning is rare, but does occur in the

phenocrysts of the xenoliths in the porphyritic granodiorite and ctG sheet with mottled cores. No one type of zoning is peculiar to any one type of xenolith, for example:

- XG61C groundmass oscillatory - rim An24, inner rim An30, middle An29
- XG65 groundmass reverse - rim An34, core An31
- XG61B phenocryst oscillatory - rim An28, inner rim An37, core An32
- X181 phenocryst oscillatory - rim An30, inner rim An27, middle An29, core An33
- X181 phenocryst normal - rim An28, core An41
- XG89 phenocryst reverse - rim An45, middle An34, core An37

Table 6.1 REPRESENTATIVE PLAGIOCLASE ANALYSES FROM THE XENOLITHS

	XG4 PGD 7Rim	XG25 TGD 1Rim	XG65 ctG 10	XG24 TGD 16Mid	X181 ctG 16Core
SiO2	62.85	63.02	60.47	59.14	57.68
TiO2	0.01	-	-	-	-
Al2O3	22.22	22.97	24.23	24.99	26.34
FeO*	0.11	0.08	-	0.01	-
MgO	0.01	-	-	-	-
CaO	3.38	4.20	5.61	6.44	7.87
Na2O	9.47	8.89	8.58	7.92	7.29
K2O	0.25	0.23	0.15	0.30	0.14
BaO	-	-	-	0.02	-
Total	98.30	99.39	99.04	98.82	99.32
Ab	72.3	66.7	59.9	54.0	47.6
Or	1.9	1.7	1.0	2.0	1.0
An	25.8	31.5	39.1	44.0	51.4
	Olig.	Ande.	Ande.	Ande.	Labr.

Occasional alkali feldspars have also been analyzed in the xenoliths. Together their overall compositions are Ab9-5 Or91-95 An 0, which are very similar to the host rocks.

6.3.2 Amphiboles

The dominant amphibole of the xenoliths is a dark green hornblende which falls into groups of 1. magnesio-hornblende (defined by Leake 1968) and edenite and 2. actinolitic hornblende, with a rare actinolite. One sample may contain more than one type of amphibole with magnesio- and actinolitic hornblende being the most common combination.

They vary from euhedral prisms to large aggregates. The xenolith amphiboles match those in the immediate host rocks, so suggesting that they may either be derived from the host granite itself or they may have equilibrated with the host. Amphiboles occurring as clusters show the same range of compositions as individual crystals in their surrounding matrix and are often magnesio-hornblende with occasional actinolitic-hornblende.

Fig 6.3 displays the MgO/MgO+FeO*(rock) ratio against the MgO/MgO+FeO*(amph) ratio using weight percent of the oxides. The xenolith amphiboles lie on a broad linear trend of decreasing MgO/MgO+FeO* (amph) with decreasing MgO/MgO+FeO* (rock). All xenolith host samples are from the granodiorites as no probe data for biotite granite amphiboles was possible. The minimum MgO/MgO+FeO* values for amphiboles in general lie very close to a straight line with 45 deg gradient. This ratio in ferromagnesian minerals therefore reflects the ratio in the bulk rock. This is an indication of the development of secondary subsolidus amphiboles. The xenoliths have a wider range of whole rock ratios than the hosts, while the hosts have a wider amphibole ratio range. On Fig.6.3 co-existing

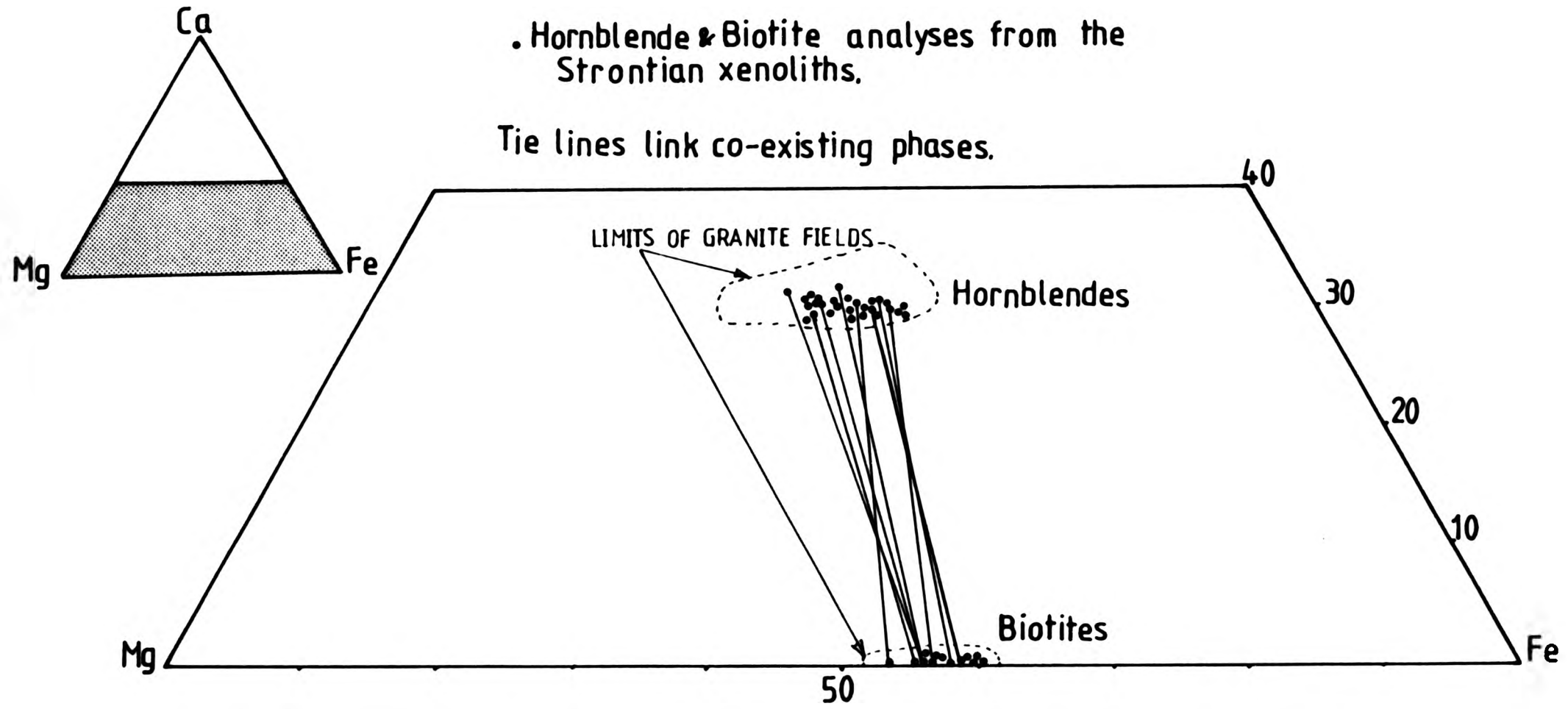

Fig. 6·2 Hornblende and biotite plotted on the Ca-Mg-Fe triangle (atomic%).

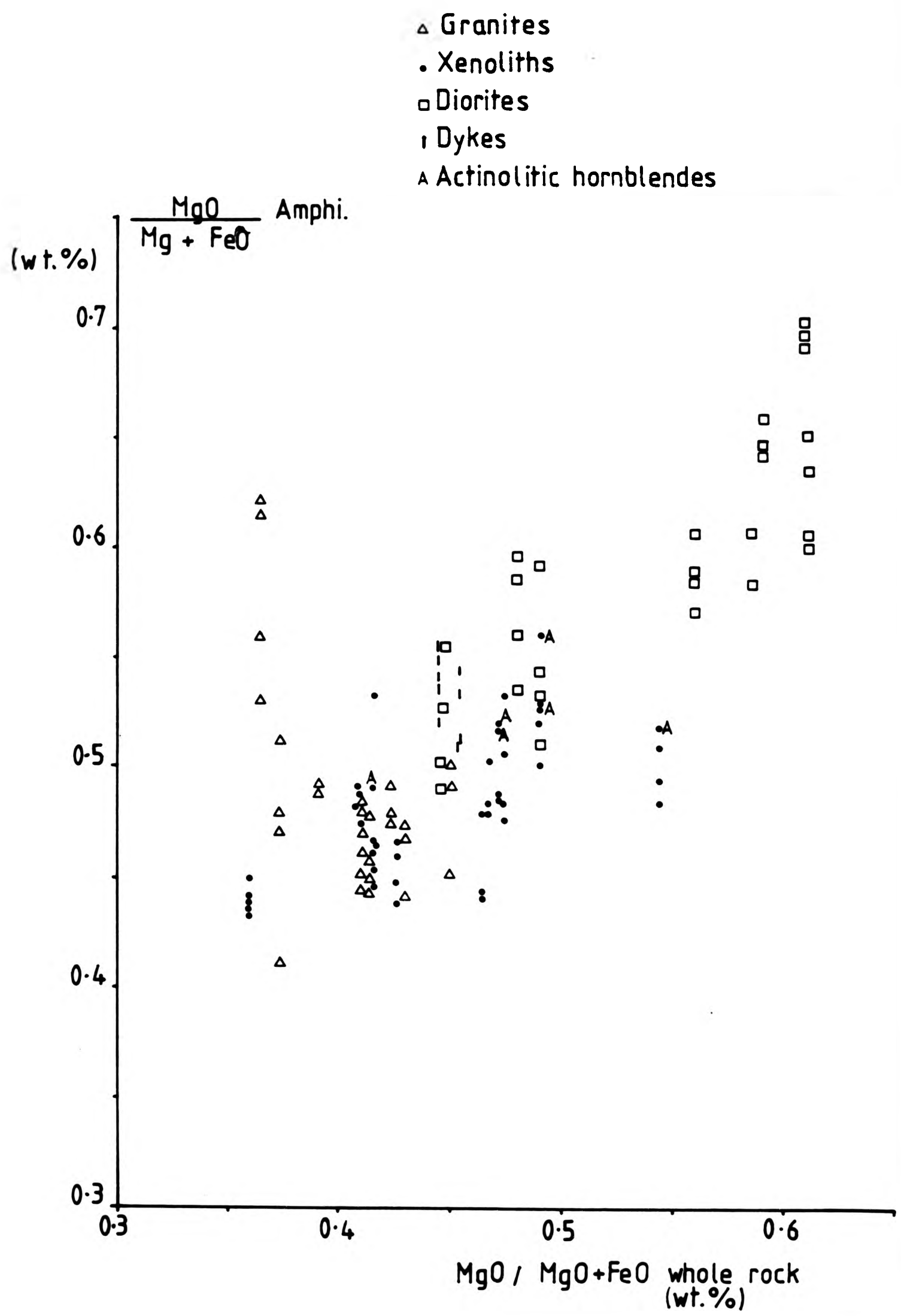

Fig.6·3 Amphibole and whole rock magnesium-iron ratios plotted for the Strontian Complex.

actinolitic - and magnesio-hornblendes are distinguished only for the xenoliths. The range of the Mg/Mg+Fe ratio for each xenolith has the actinolitic hornblendes systematically at the top of its range. This is because actinolitic hornblendes from clinopyroxenes preserve magmatic Mg/Mg+Fe ratios more faithfully than other amphiboles, reflecting simple hydration without reaction with biotite and plagioclase.

The MgO/MgO+FeO* ratios of the individual amphiboles in a single thin section varies considerably ie. mag-hornblende 0.541 to 0.459, edenite 0.494 to 0.419 and actinolitic-hornblende 0.560 to 0.518. Fig. 6.2 shows the range of compositions on the Ca-Mg-Fe plot.

The amphiboles of the xenoliths contain moderate amounts of Al2O3 (4.6 to 10.7%), with amounts increasing from the actinolitic to the edenites and respectively lower amounts of silica. This will result in a progressive substitution of Aliv for Si in the T site. The Si levels of the actinolitic-hornblendes and occasional actinolites are high compared (7.25-7.6 Si) with the other amphiboles (6.7-7.23 Si) and so their Aliv is overall lower (0.39-0.76 Aliv; others 0.86-1.3). Though values are close, they do not overlap.

The pressures of formation for the total Al of the xenolith amphiboles are given in Table 6.2, where the regression equations have been calculated according to Hammarstrom & Zen (1986). Overall the pressures are low, with most being less than 1kbar. This is equivalent to less than 3km indepth (a temperature of less than 1070 °C). This follows that much of the amphibole assemblage is low temperature and secondary in many cases.

Nockolds & Mitchell (1948) suggest a correlation between amphibole composition and rock type and that amphiboles with high Si and hence low Aliv are commonly secondary. Also the highest Mg/Mg+Fe values for the actinolitic hornblendes may reflect hydration of early crystallized Ca-pyroxene.

Table 6.2 PRESSURES IN XENOLITH AMPHIBOLES

Total Al in amphibole	Pressure in literature	P. from regression eq. 1	2
XG4			
0.901-1.740	<1 - 5	0.61-4.8	1.0-3.8
XG7			
1.058-1.191	1 - 2	1.4-2.1	1.4-1.8
XG24			
1.3656-1.4419	3 - 3.5	2.9-3.3	2.4-2.6
XG25			
1.138-1.355	1.5 - 3	1.8-2.9	1.6-2.3
XG44			
0.8535-1.2088	<1 - 2	0.4-2.2	0.9-1.8
XG61B			
0.840-1.177	<1 - 1.7	0.3-2	0.9-1.8
XG61C			
0.4850-1.720	<1 - 1.7	1.5-1.9	1.0-1.7
XG64A			
1.0479-1.1633	1 - 2	1.4-1.9	1.4-1.7
XG65			
1.0786-1.2703	1 - 2.7	1.5-2.5	1.5-2
XG89			
0.982-1.199	<1 - 2	1.0-2.1	1.2-1.8
X181			
0.7607-1.4826	<1 - 3.5	-0.1-3.5	0.7-2.8

TiO_2 and Na_2O levels are also higher in edenite than in the other amphiboles (1.4% Na_2O and 0.9% TiO_2 for edenite; 1.1% Na_2O and 0.7% TiO_2 for magnesio and 0.8% Na_2O and 0.3% TiO_2 for actinolites) and

this represents substitution of Ti for MgC and Na for CaB. This low titanium level may reflect low titanium of the parent.

Table 6.3 REPRESENTATIVE ANALYSES OF AMPHIBOLES

	XG61B ctG 1Rim	XG4 PGD 1Mid	XG25 TGD 5Mid	XG61C ctG 4	XG44 PGD 10
SiO2	48.62	48.65	46.69	49.45	47.68
TiO2	0.71	0.73	0.98	0.71	1.06
Al2O3	5.69	5.89	7.47	5.39	6.62
FeO*	13.79	14.08	15.25	12.87	14.06
MgO	13.70	13.87	12.17	14.69	13.52
MnO	0.33	0.37	0.36	0.30	0.34
CaO	11.83	11.71	11.68	12.12	11.87
Na2O	0.97	1.27	1.32	0.95	1.32
K2O	0.51	0.58	0.80	0.43	0.69
Total	96.15	97.15	96.72	96.91	97.16
Si	7.236	7.185	6.993	7.265	7.297
Aliv	0.764	0.815	1.007	0.735	0.700
Alvi	0.235	0.213	0.312	0.195	0.190
Ti	0.079	0.081	0.111	0.080	0.079
Fe2+	1.717	1.740	1.910	1.579	1.592
Mn	0.042	0.047	0.046	0.035	0.044
Mg	3.039	3.053	2.718	3.212	3.194
Ca	1.888	1.854	1.875	1.906	1.884
Na	0.279	0.364	0.385	0.264	0.318
K	0.098	0.110	0.154	0.088	0.088
	Mg-hbl.	Mg-hbl.	Eden.	A-hbl.	A-hbl.

The sodium levels decrease from core to rim for the actinolitic-hornblendes, but remain the same for edenite and magnesio-hornblende. TiO2 and FeO* levels appear quite uniform across the amphibole types and from core to rim with little zoning.

When plotted on the Ca-Mg-Fe diagram (Fig.6.2), the amphiboles of the xenoliths fall directly over the field of the host rocks.

6.3.3 Biotites

The micas of the xenoliths classify as biotites, as they have less

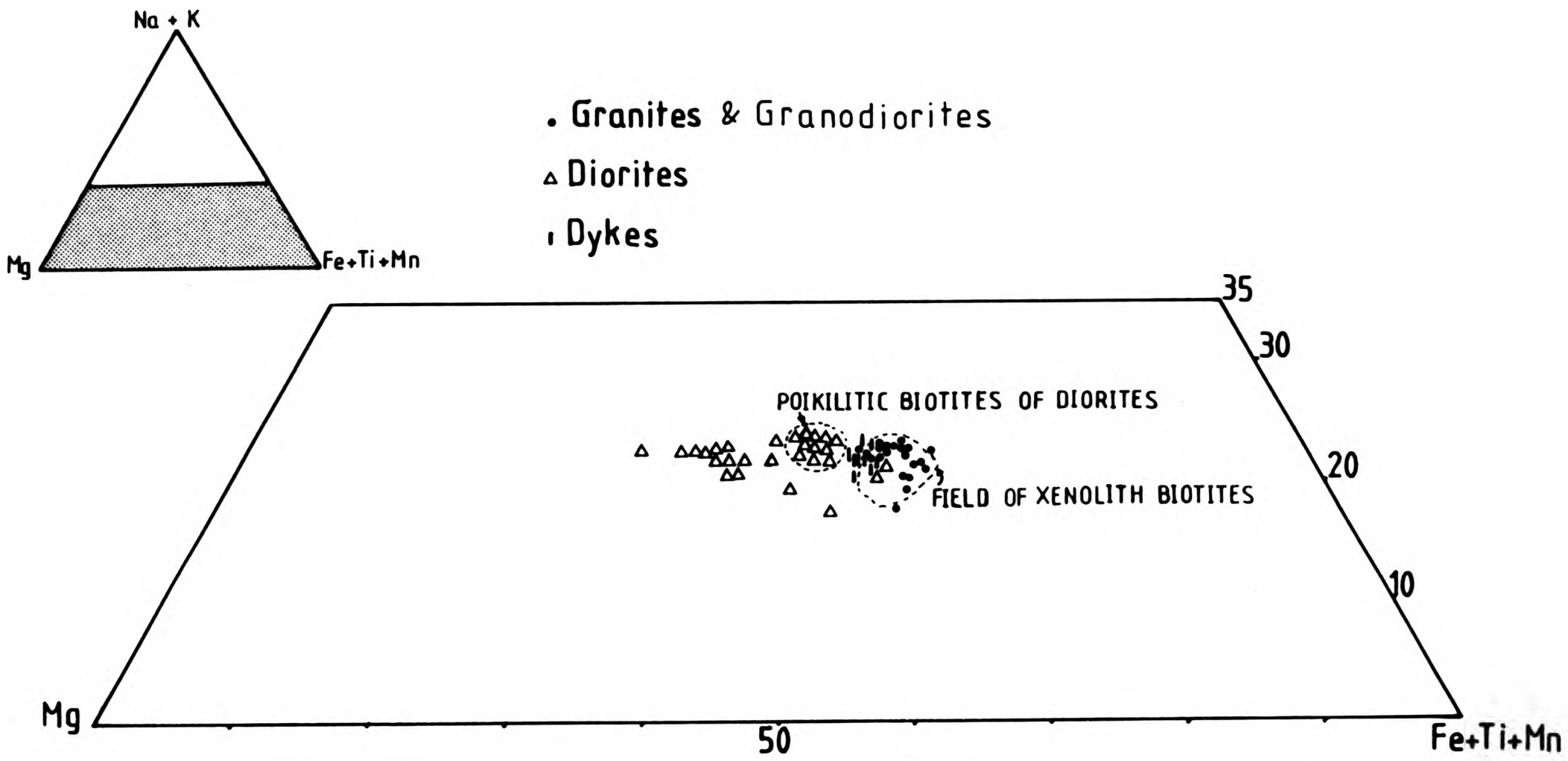

Fig.6·4 Biotite compositions plotted onto the Mg-(Na+K)-(Fe+Ti+Mn) triangle (atomic %)

than 2:1 Mg:Fe. On the Ca-Mg-Fe diagram (Fig.6.2) the biotites of the xenoliths fall in the field of the host rocks biotites. They also have a considerably lower MgO/MgO+FeO* ratio (0.404 to 0.46) than the amphiboles (0.434 to 0.56). These biotites are all dark brown and do not show any systematic zoning.

The range of biotite composition has been plotted on a (Na+K)-Mg-(Fe+Ti+Mn) diagram (Fig.6.4). The elements that commonly substitute (Mason 1966) are included together eg. Na+K. The xenoliths and host rocks overlap each others ranges, while the mafic diorites (discussed later on) plot separately. No distinction can be made between the biotites and the different xenolith types.

There appears to be no great change in the FeO* (16.9 to 17.4%) and TiO2 (2.8 to 3.3%) levels from core to rim, though these levels are more than twice the amount in the bulk rock xenoliths.

K2O does show a change of 10.0 to 9.5% in the cores to rims of 9.9 to 7.9%. Though these values do depend on the size of the crystal, as small lathes may give values of 10% K2O.

Fluorine levels range from 0.16% to 0.48% and show almost as wide a range as the host granodiorites.

6.3.4 Sphene

Sphene is the most common accessory mineral of the xenoliths and was used as one of the criteria for classification of the xenoliths. The sphenes are uniform in composition and typically 38% TiO2, 28% CaO and 29% SiO2 with little variation throughout the xenolith classes.

There may be slight zoning with an increase in TiO2 towards the rim.

6.3.5 Apatite

Apatites are the second most common accessory mineral whose habit varies greatly. The apatites are all classified as fluor-apatites (Deer et al 1982) with fluorine levels for the xenoliths of 3.6 to 4.8% F, which is only 0.2% greater than the apatites in the xenoliths host rocks. The major element chemistry of the apatites is consistent throughout the xenoliths with 54-55% CaO.

6.3.6 Oxide Minerals

Titaniferous-magnetite and ilmenite are the only two oxides present in the xenoliths. Ti-magnetite occurs in a variety of of forms, while the occasional ilmenite analyses are of only rounded grains. TiO2 levels vary from 10.6 to 20.1% TiO2 in the Ti-magnetite and 42.1 to 49.0% TiO2 in the ilmenite. Ti substitutes for Fe2+ in the ilmenite lattice (Deer et al 1967). MnO varies from 0.87 to 2.7% and against TiO2 and FeO* it has a positive correlation. The ilmenites also have approximately 0.04% Cr2O3.

6.4 DISCUSSION

The xenoliths show a diverse range of types within which variation is also great. Though in hand specimen they do appear different from their surrounding host, their mineral chemistry does overlap considerably in some cases. Two important features must be stressed here: 1. the evidence for magma mixing for the xenoliths; and 2. the uniformity of hornblende and biotite compositions within the

xenoliths and between the xenoliths and their host and not the diorites.

1. In the porphyritic rocks the evidence includes A. quartz xenocrysts with mafic reaction rims (which are most likely to be relict bipyramids); B. the alkali feldspar crystals showing resorption textures and rarely jacketed by plagioclase; and C. the complex reverse and normal zoning of the plagioclases within the same rock sample, also with some evidence of mottling.

A and B indicate hybridization with very acidic magmas as quartz is present as a phenocryst phase. It is not likely to be the local magma of the tonalitic or porphyritic granodiorite as quartz is essentially interstitial in both. While C has mixed feldspar compositions, including limited reverse zoning and marked Ca-rich zones, which are an indication of hybridization though the source is more difficult to tie in. It could possibly be associated with a K-feldspar and quartz phenocryst assemblage if the the source was a very phenocryst-rich magma eg. a granodiorite that has crystallized 50-60% solid. However the xenoliths in the later, quartz-rich, biotite granite could easily hybridize with their immediate host rock.

The sharp boundaries of the xenoliths are also incompatible with in situ mixing therefore mixing occurred at depth.

The origin of the mafic clusters whether solely hornblende or biotite, or a combination of the two, suggest a phase of mineralogical disequilibrium. The rare examples of pyroxene cores within the hornblende aggregates, are evidence that some of the

aggregates at least are the result of alteration of pyroxene to amphibole.

2. The interesting feature is the uniformity of the compositions of single crystals, monomineralic aggregates and multimineralic aggregates from the biotite and hornblende between the xenoliths and both granodiorite and granite hosts. This also supports the evidence for the host rocks having a subsolidus reaction and re-equilibration of its mafics, as with the xenoliths.

Chapter 7 THE XENOLITHS: GEOCHEMISTRY

7.1 INTRODUCTION

The xenoliths lie on the same general trend and are chemically coherent with the granodiorites and biotite granite host rocks (Fig. 7.1 to 7.11). They are initially inferred to be cognate. The norm (Appendix B) was calculated with an assumed Fe_2O_3 value of 0.25. The xenolith norms surprisingly contrast sharply with the granodiorites and diorites. 30% of the xenoliths are nepheline normative rocks (Table B.2), which indicates critical silica-undersaturation. All these xenoliths occur within the tonalitic and porphyritic granodiorites (none in the biotite granite or later granitic sheets). The host rocks have quartz and hypersthene in the norm (and so are silica-oversaturated) and the diorites have olivine and hypersthene, with only 4 diorites (D7, D8, D12 & D13) having nepheline in the norm (and so are silica-undersaturated).

In general there appears to be a continuum of compositions with little chemical separation of the 5 classes recognized in hand specimen. Some classes do appear characterized by distribution of extreme values eg. SiO_2, TiO_2 and K_2O, while some plots eg. Al_2O_3, Ba and Na_2O give a partial separation into 2 fields that is not based on xenolith types. The xenoliths have been plotted against SiO_2 and MgO to see if any scatter is reduced or resolved into discrete fields. The choice of major elements is the same as for the host rocks, that there is no wholly incompatible element that could have been used. Both abscissi give similar plots, but MgO was chosen as some of the xenoliths are quite mafic. MgO will be used for most of this discussion, SiO_2 plots only reviewed when relevant. The 'e' symbol

in Figs.7.1 to 7.30 refer to the Caledonian dyke samples. They are plotted here as there are too few to be plotted on separate diagrams.

Features such as multiple analyses from one xenolith ie. zoning of a xenolith or analyses of xenoliths from clusters will all be considered together with the majority of the xenoliths, but will be described separately when they are distinctive. Fig.7.0 plots the core to rim analyses of the 3 xenoliths within xenoliths (XG3/3A, XG20/20A and XD1/1A) and also the serial sampling of XG61A/B/C and XG64A/B. MgO and SiO_2 were plotted as the probably "immobile" elements, while K_2O and Rb were the late crystallizing "mobile" elements.

The serial sampling of single xenoliths shows no change in MgO or SiO_2 and only small changes in K_2O and Rb. Thus supporting the view that the xenoliths have not undergone wholesale metasomatism. Single analyses of xenoliths may thus be taken as representative of the bulk xenolith. K_2O for xenoliths within xenoliths is the only element that shows a slight decrease from rim to core for any size of xenolith and indicates some limited exchange which may be related to biotite growths. While Rb decreases inwards only for the xenoliths within xenoliths. These xenoliths between them span a wider SiO_2 range of 50.25 to 65.5% than xenoliths found in the clusters. The difference of the elements from margin inwards (50.25 to 64% SiO_2; 2.03 to 2.75% K_2O; 4.1 to 8.85% MgO and 53 to 105ppm Rb) is still lower than the gross values for the whole xenolith assemblage, SiO_2 48 to 71%; Rb 5 to 22ppm; MgO 1 to 12% and K_2O 1.6 to 4.4%, apart from Rb which is greater.

Fig.7 Multiple analyses from single xeno

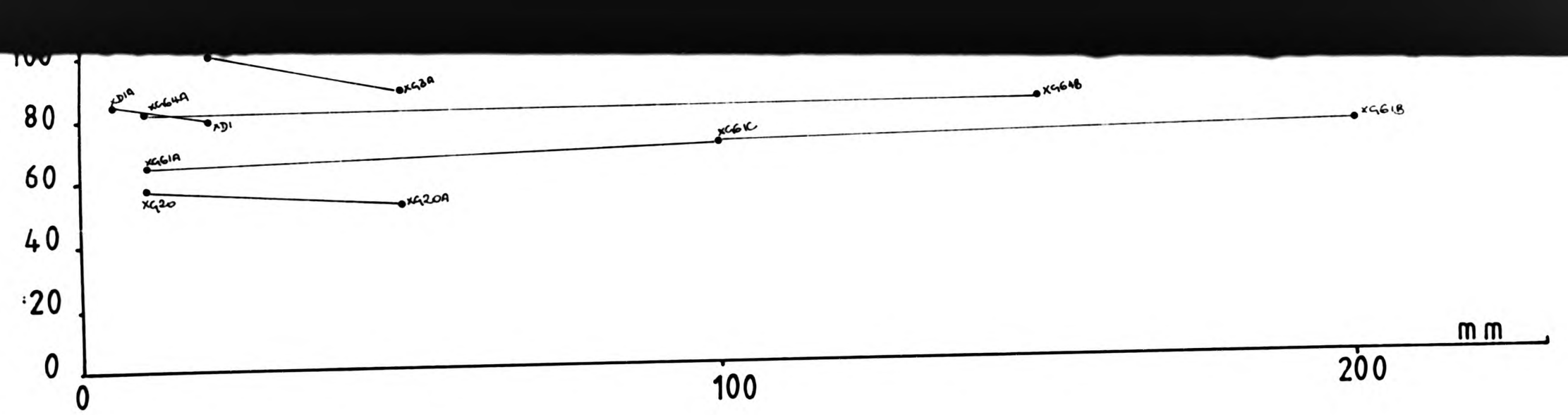

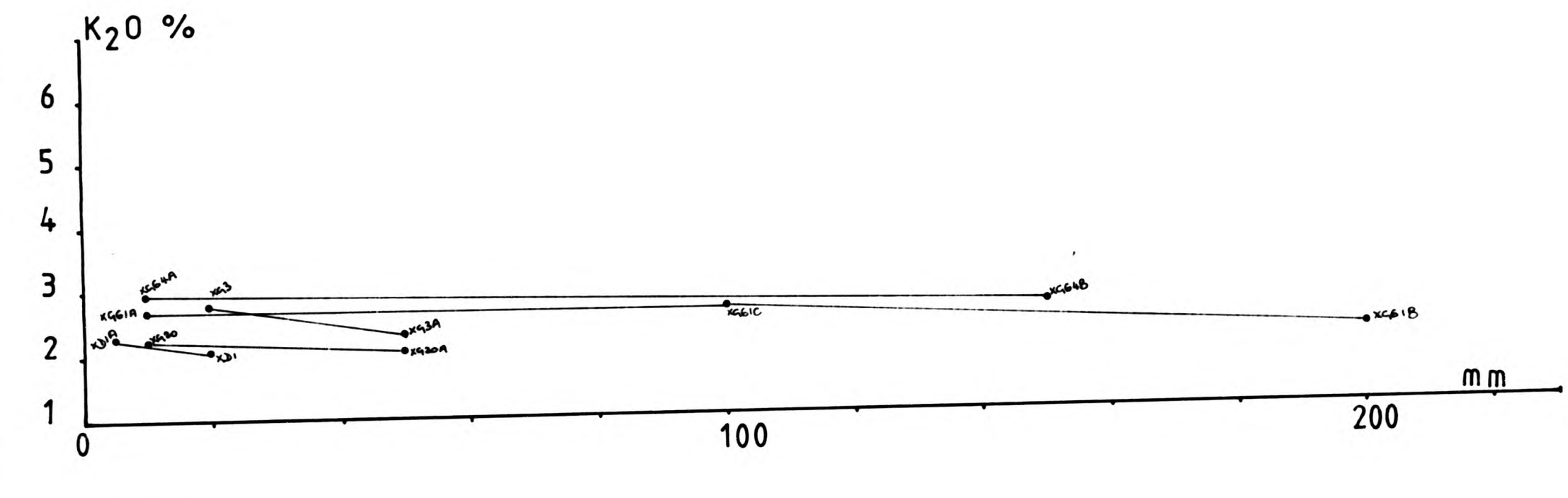

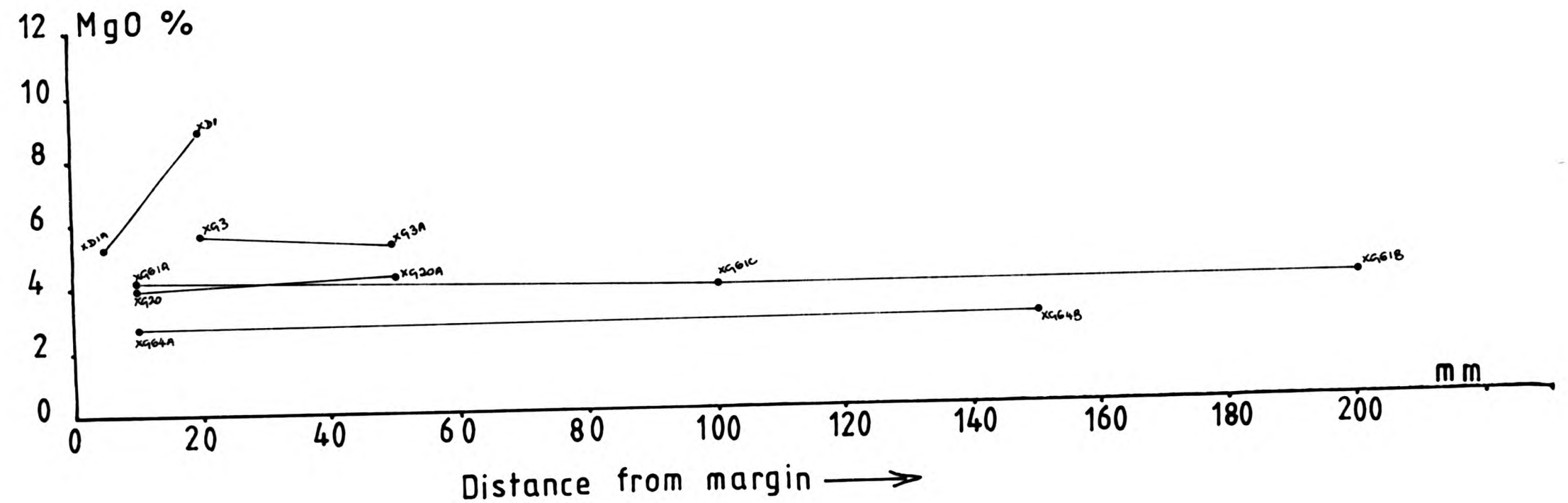

(ii)

Fig. 7 Multiple analyses from single xenoliths.

Xenoliths collected from the single clusters, all located in the granodiorite host, are [X113, X116], [X142, X143, X144] and [XG20/20A, XG22/22A/22B, XG23, XG46, XG47, XG48]. This population shows a more limited SiO_2 range from 52% to 59.5% than the zoned xenoliths and include all the xenolith types (except Type 3 which are very rare overall). Overall they do not appear to plot in any distinctive way and fall onto the main xenolith trend.

7.2 MAJOR ELEMENTS

7.2.1 Silica

Fig.7.1 displays a coherent decreasing linear trend with increasing MgO, upto 8% MgO. There is little variation in more magnesian xenoliths, this trend however changes abruptly at 8% MgO and 50 to 54% SiO_2. The SiO_2 variation is the greatest for any of the group of rocks, ranging from 48% for the more mafic to 71% for the more acidic. The xenoliths show a similar range to that of the basalts and andesites of the Sidlaw (50 to 64% SiO_2) and Lorne lavas (49 to 62% SiO2), while the granodiorites 55-70% and biotite granite 66-75% SiO_2 overlap the SiO_2-rich xenolith compositions.

The extremes of the plot ie. the very low and very high MgO are characterized by distinct xenolith classes. The high SiO_2/low MgO have Type 1A xenoliths which are very leucocratic; while low SiO_2/high MgO have Type 3 & 5 xenoliths rich in ferromagnesian minerals. In between is the full range of xenolith types. Above 60% SiO_2 all the xenoliths (regardless of class) lie within the biotite granite or the ctG sheet or are located close to the complex contacts.

FIGURE 7.1 SiO2 vs MgO

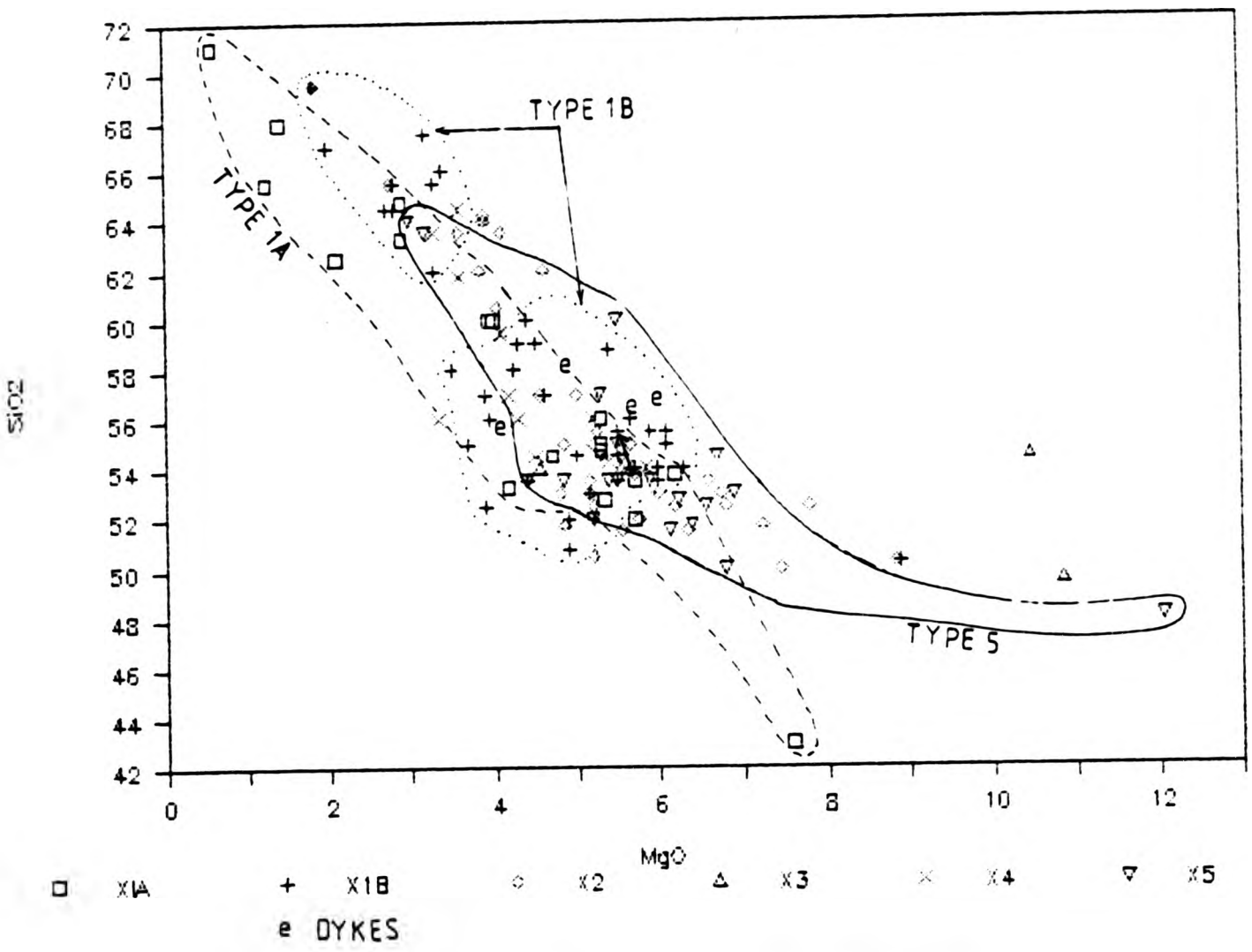

FIGURE 7.2 Al2O3 vs MgO

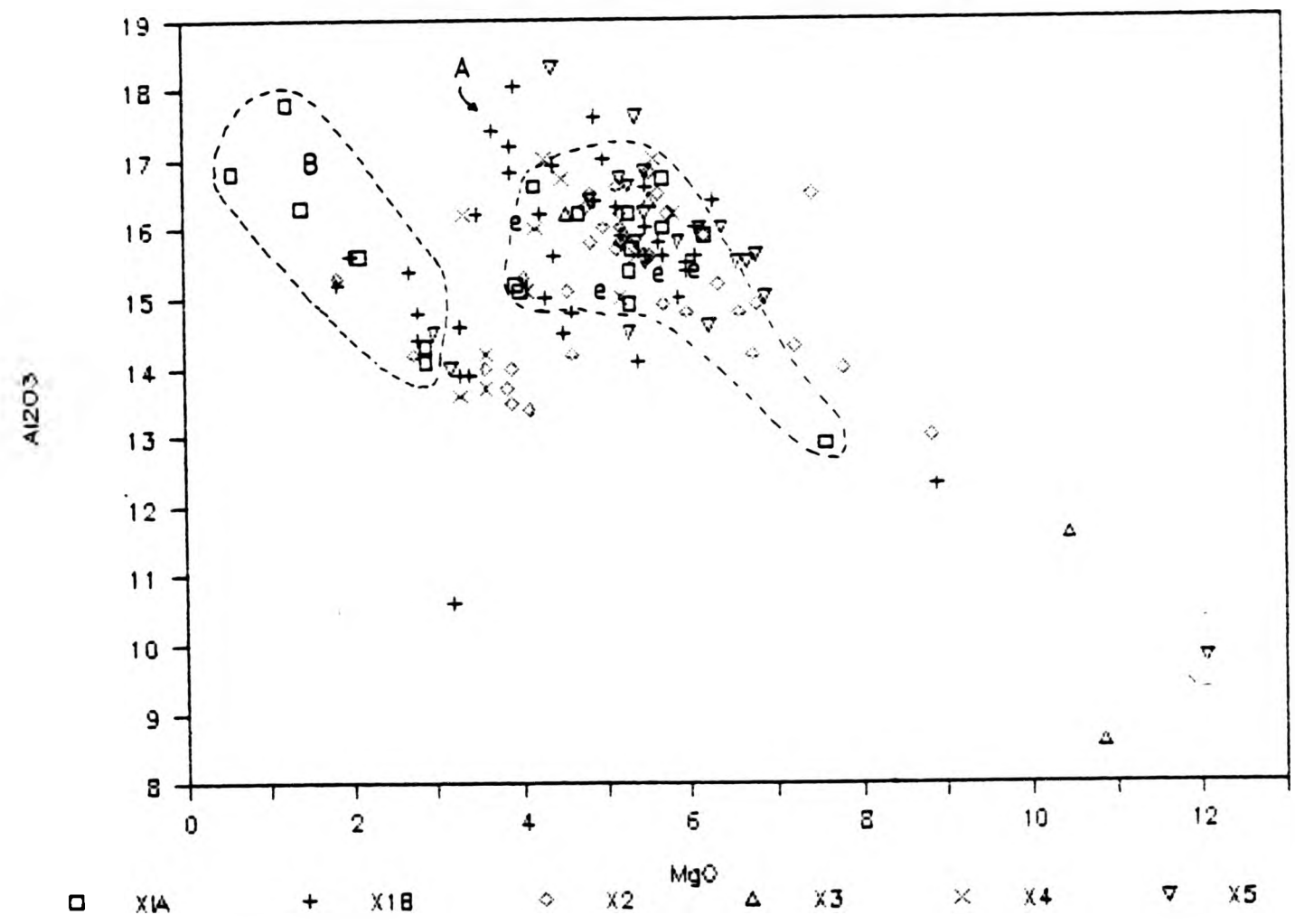

More than half the xenoliths have 55% or less SiO_2 (this includes the whole spectrum of xenolith types) and no xenoliths are more SiO_2 rich than their immediate host. When plotted on a map of the complex they are located in a variety of places (Fig.5.1):

- Close to the complex margins.
- Majority are in the tonalitic/porphyritic granodiorite.
- If in the biotite granite, they are close to the mafic diorites.
- If in the clusters, there is a mixture of those xenoliths with less than 55% SiO_2 with those with more than 55.5% SiO_2.

The rare xenoliths found in the biotite granite have smaller range 54.0 to 69.5% SiO_2, which falls well within the limits of the main xenolith group. The majority of them are microdioritic Type 1A/B and xenolith types 4 and 5 are not found.

7.2.2 Aluminium

Aluminium (Fig.7.2) varies from 0.6 to 12.05%, displaying a uniform trend of decreasing Al_2O_3 with increasing MgO. Below 5% MgO the plot is far more scattered with the formation of two separate fields, labelled A and B on Fig.7.2. This separate group (B) of xenoliths are all located close to the margin of the complex, within the biotite granite or within the late porphyry granodiorite sheet (Location D Fig.1.2).

This great variation in the Al_2O_3 results from the highly variable modal amount and composition of the feldspar in the xenoliths, as phenocrysts or in the matrix. The Al_2O_3 of the feldspar from microprobe analyses varies from 21.9 to 24.4% Al_2O_3. This split into

two fields also correlates with the two fields shown by Na_2O (section 7.2.5).

7.2.3 Titanium, Iron and Manganese

Figures 7.3, 7.4 and 7.5 display the positive linear trends of increasing TiO_2, FeO* and MnO with increasing MgO. FeO* has the tightest plot followed by MnO and TiO_2.

Values range from 0.14 to 3.58% TiO_2; 0.9 to 13.5% FeO* and 0.02 to 0.3% MnO. In all 3 diagrams the trend is linear starting from zero to approximately 7.0% MgO at which point the trend is either scattered (Figs.7.4 & 7.5) or as in the case of TiO_2 (Fig.7.3) follows a more uniform trend of constant TiO_2 with increasing MgO. This inflexion corresponds to a similar one at 6% MgO in Fig.7.1. TiO_2 shows peak TiO_2 at different MgO values for different xenolith groups. Type 1A and 4 peak at about 4.5% MgO. This is not seen on the SiO_2 vs TiO_2 plot.

The higher amounts of MnO and FeO* in the samples above 7.0% MgO is reflected in higher modal amounts of mafic minerals as well as sphene and oxide minerals.

7.2.4 Calcium

The xenoliths on the calcium plot (Fig.7.6) show an overall increase of CaO with increasing MgO, even though the plot is not as tight as FeO*. CaO ranges from 1.7 to 11.0%.

The high MgO xenoliths are scattered around the high CaO and this in

FIGURE 7.3 TiO2 vs MgO

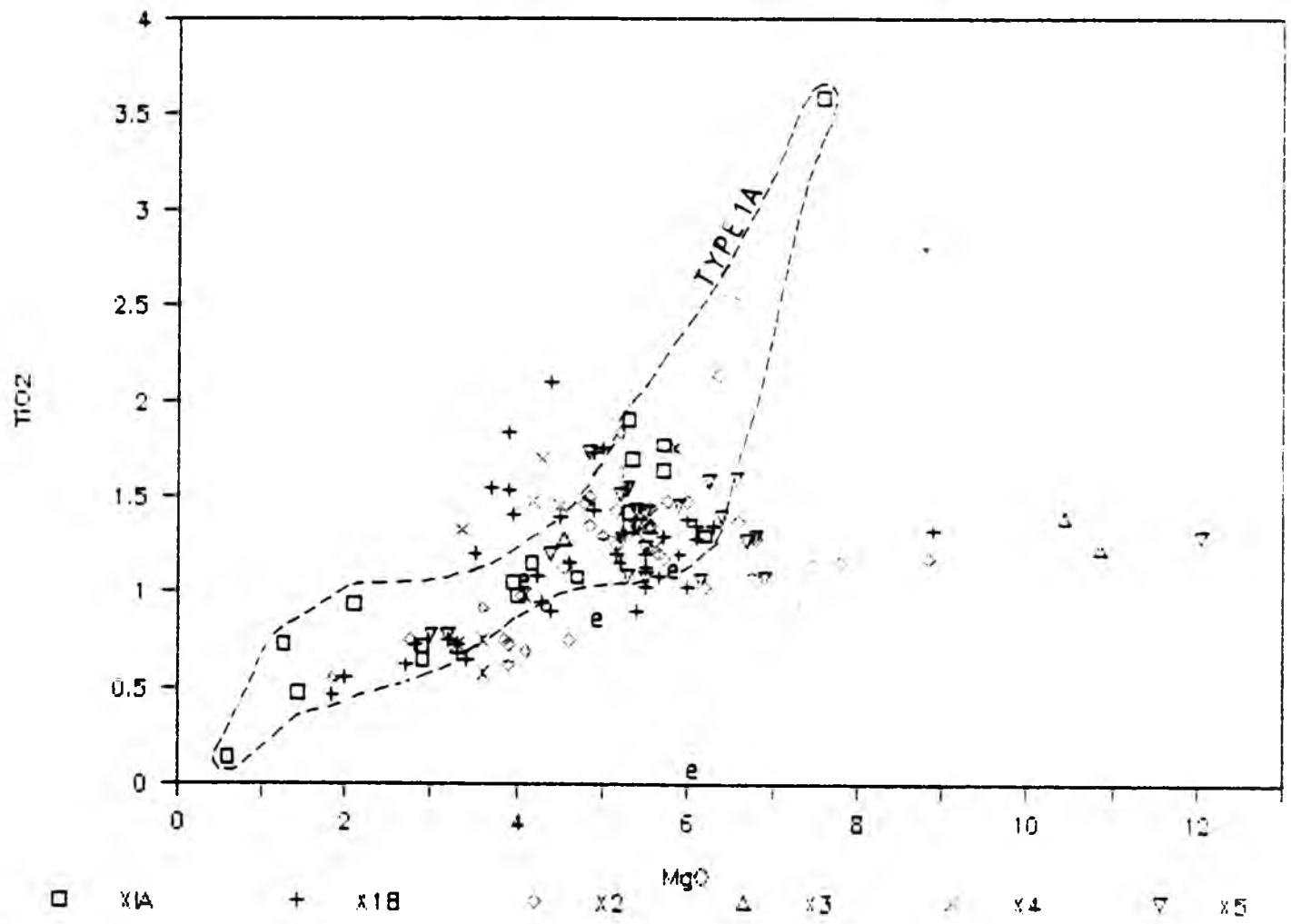

FIGURE 7.4 FeO* vs MgO

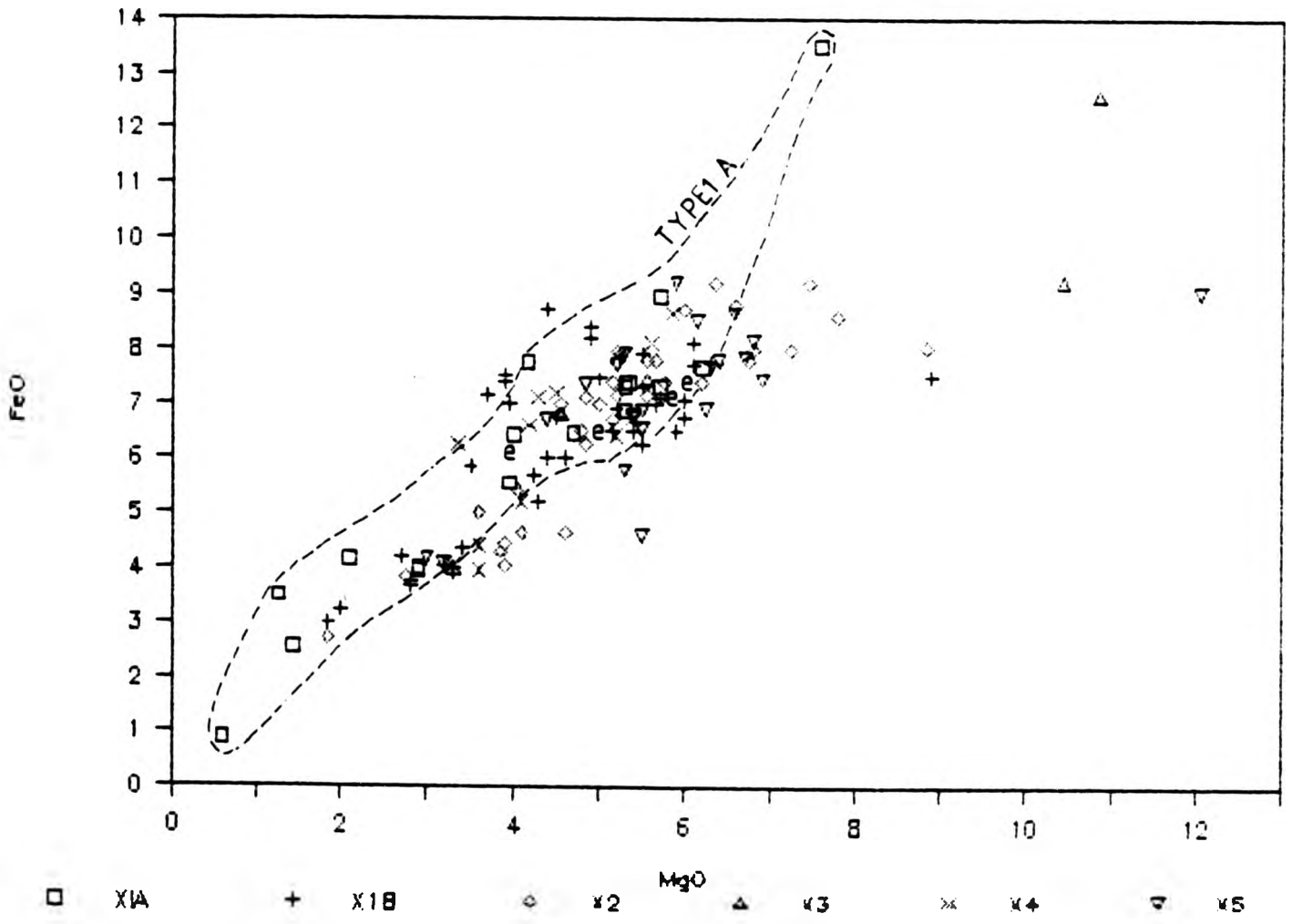

FIGURE 7.5 MnO vs MgO

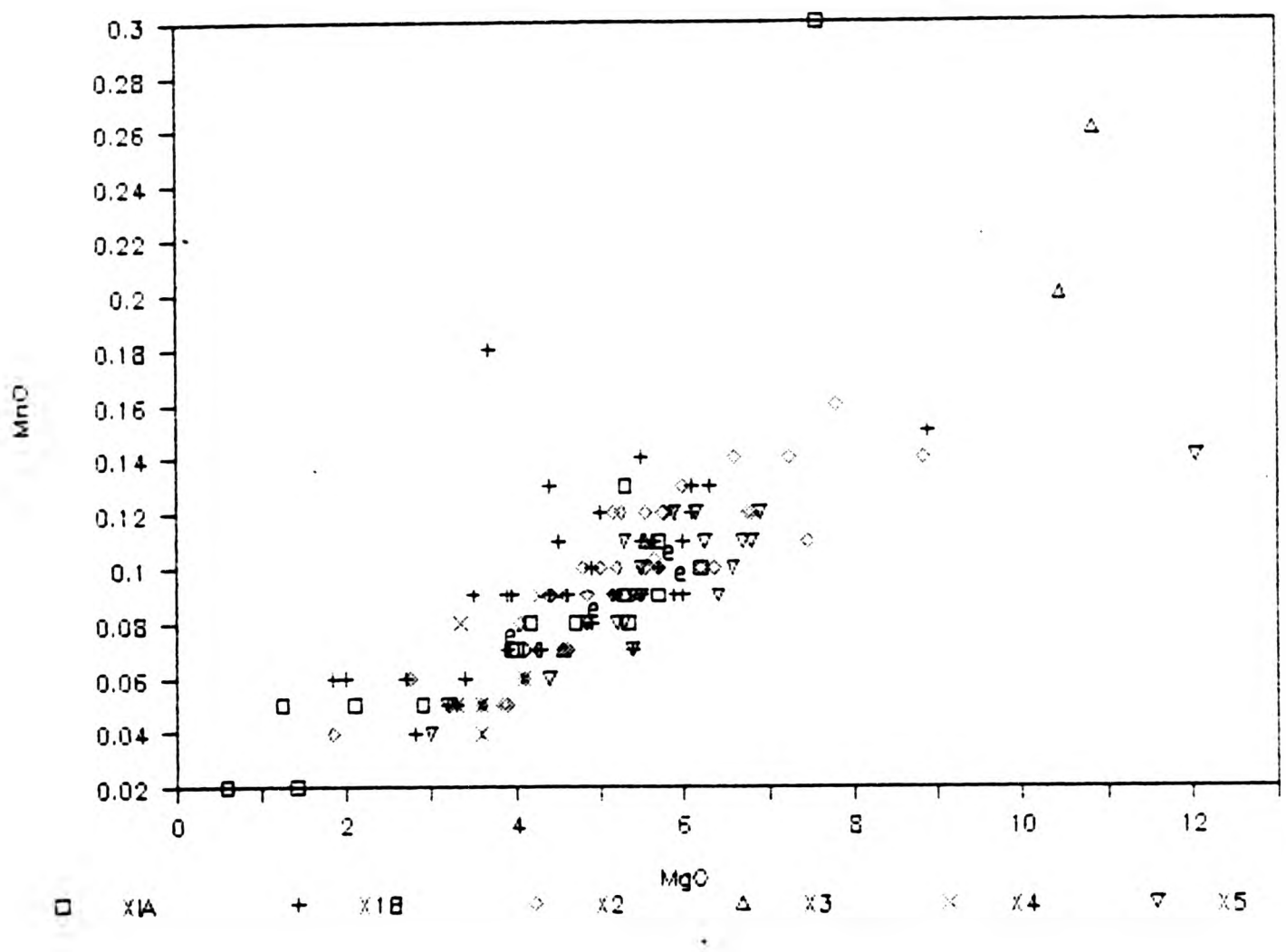

FIGURE 7.6 CaO vs MgO

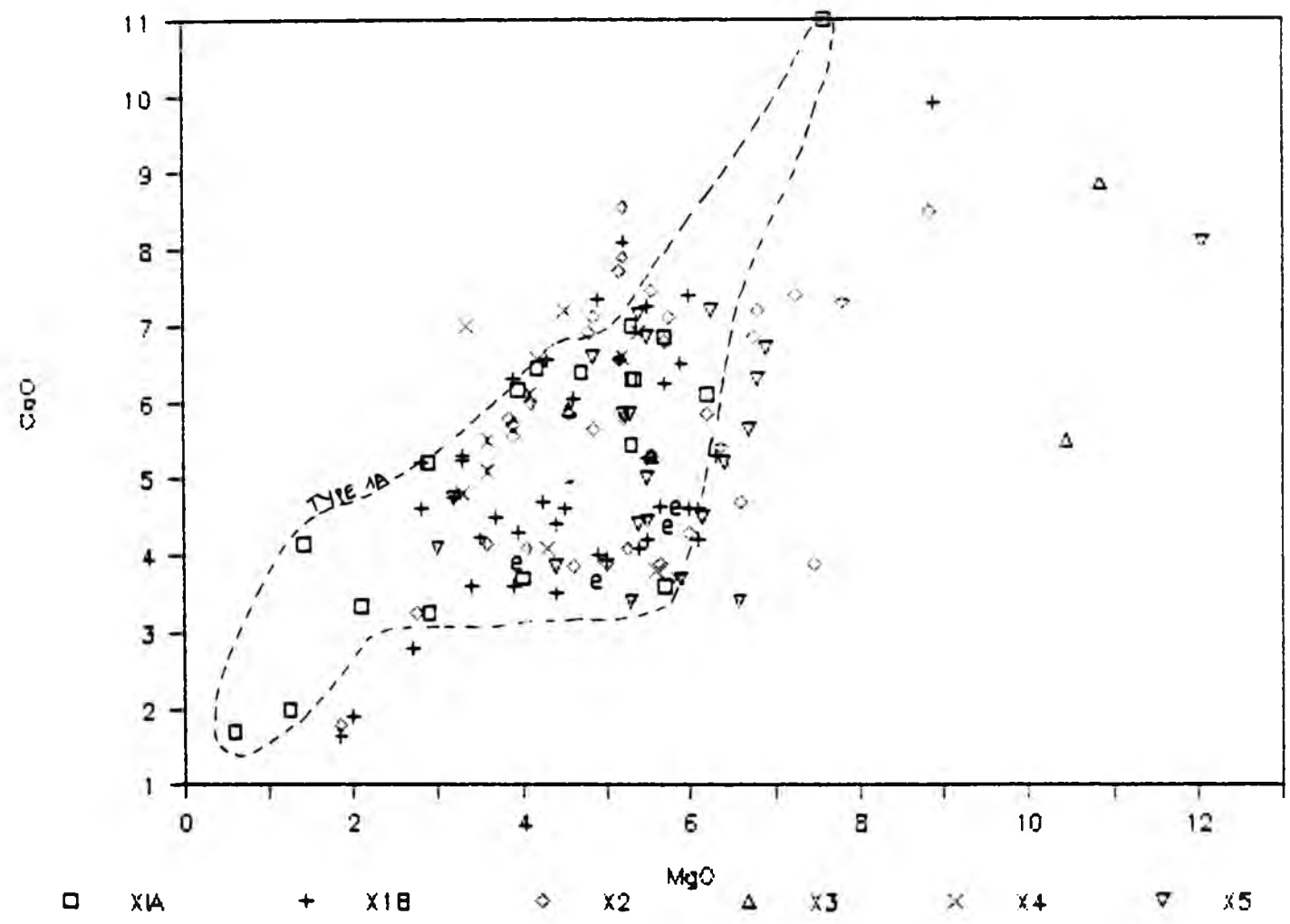

turn is reflected by low Al_2O_3 levels (Fig.7.2). In between 3.0 and 7.0% MgO the xenoliths show a scattered but rounded plot with no obvious trend, which may be the result of the variable amounts of mafic minerals and feldspar.

On the CaO vs MgO for all the rocks (Fig.7.7) the xenoliths lie in the middle of the overall trend of increasing CaO with increasing MgO. The region of wide scatter lies outside the main granodiorite field.

7.2.5 Sodium and Potassium

Sodium and potassium display quite different plots from each other (Figs.7.8 & 7.9A-B). Both elements show a greater range for the xenoliths than in the host rocks ie. 1.1 to 6.5% Na_2O (host 4.2 to 5.45% Na_2O) and 1.6 to 4.4% K_2O (host 4.05 to 4.99% K_2O). The core to rim of the zoned xenoliths show an increase on both Na_2O and K_2O of maximum 1.5% Na_2O and 0.45% K_2O (Fig.7).

Na_2O (Fig.7.8) shows a very similar pattern to that of Al_2O_3 (Fig. 7.2). It has a main field (A) with a trend of decreasing Na_2O with increasing MgO with the Type 3 & 5 xenoliths with the lowest Na_2O values. This is supported by the smaller amounts of plagioclase feldspar of these more mafic xenoliths. A low Na_2O field (B) is seen in MgO poor rocks and it corresponds with the Al_2O_3 field (B) rocks.

K_2O (Fig.7.9A) has a more scattered horizontal plot, with only the very low and very high MgO xenoliths showing any signs of separation. The high MgO xenoliths have higher levels of K_2O, also higher CaO levels, but lower Na_2O and these are Type 5 xenoliths with abundant

FIGURE 7.7 CaO vs MgO

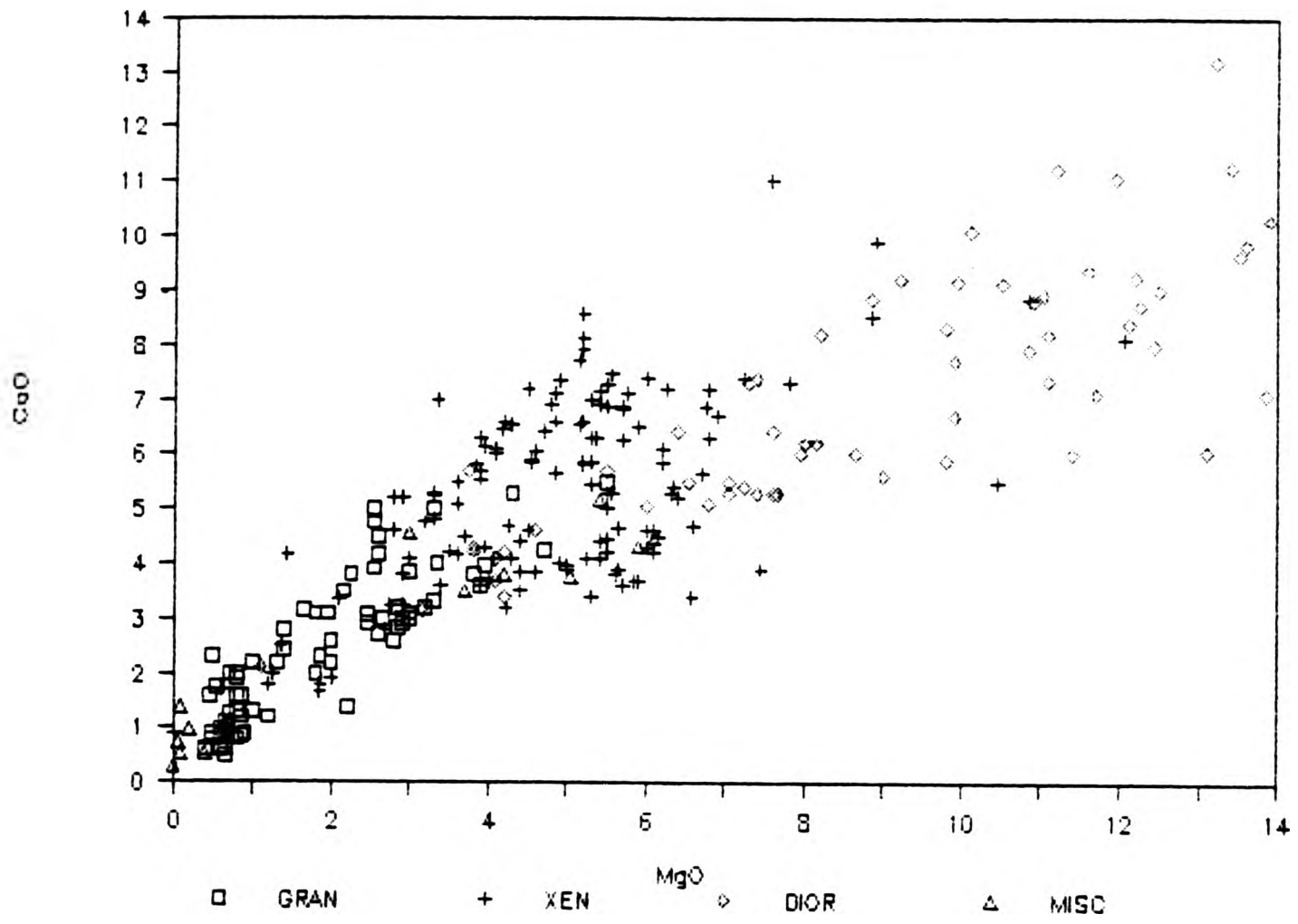

FIGURE 7.8 Na2O vs MgO

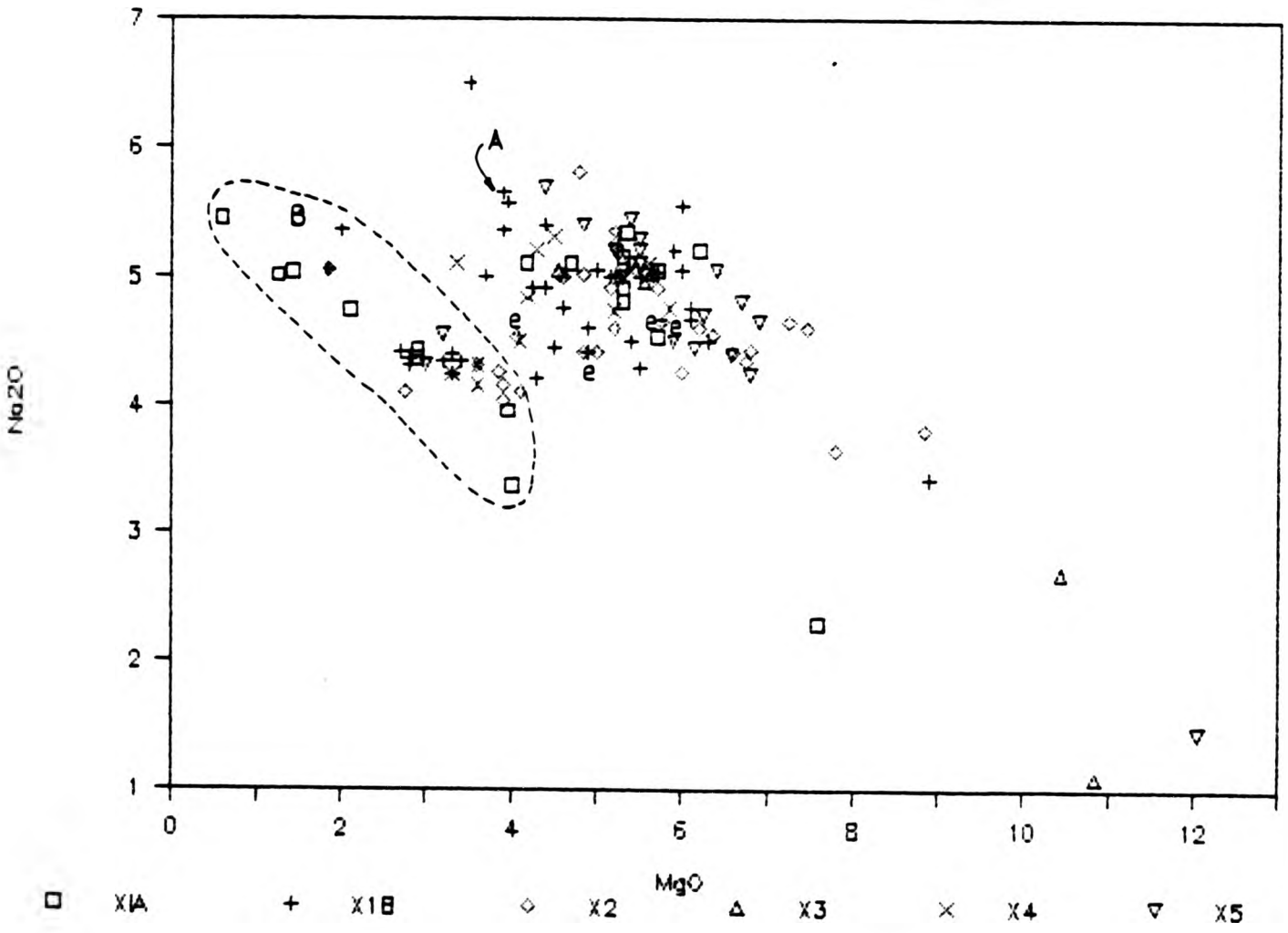

FIGURE 7.9A K20 vs MgO

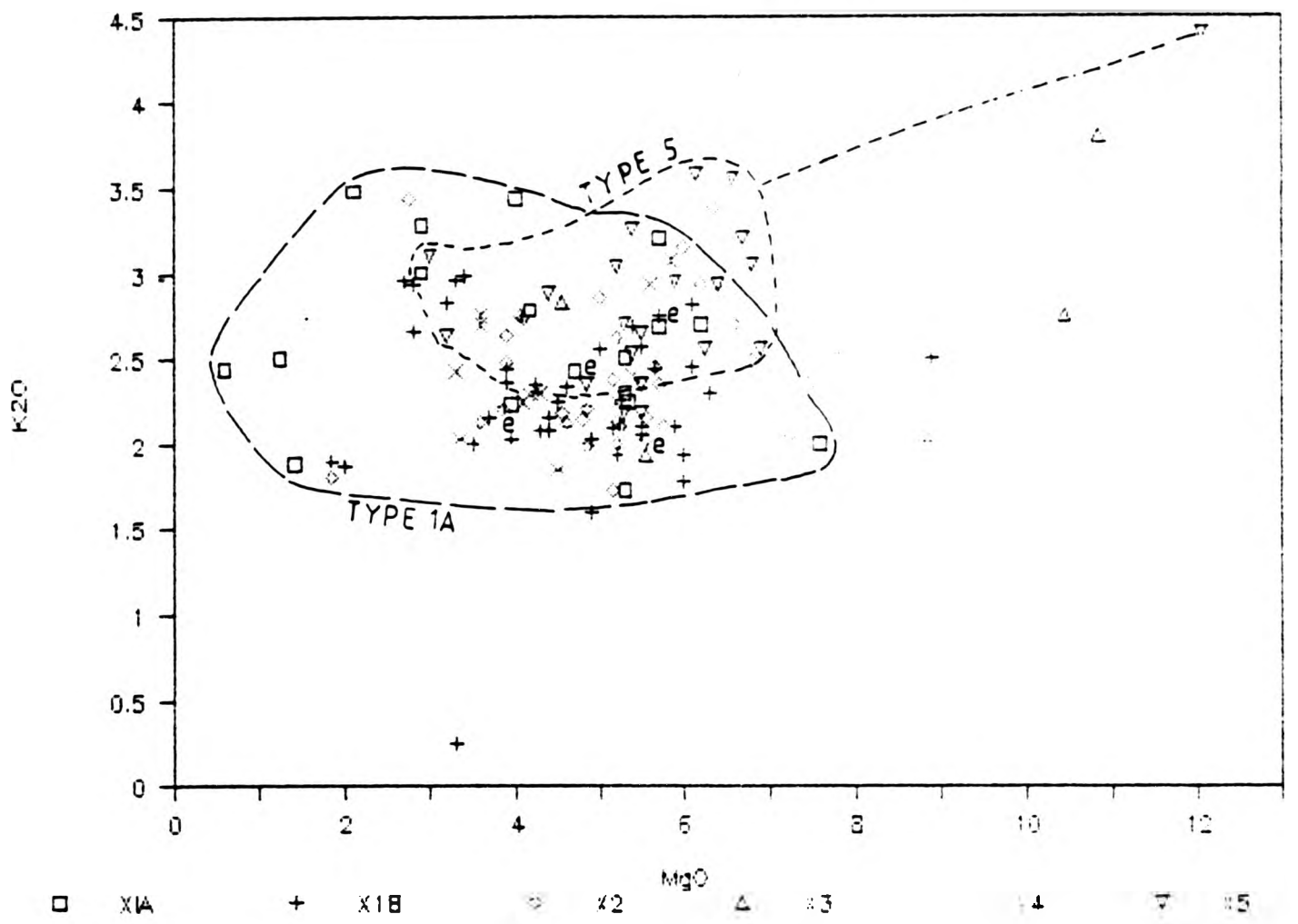

FIGURE 7.9E K20 vs SiO2

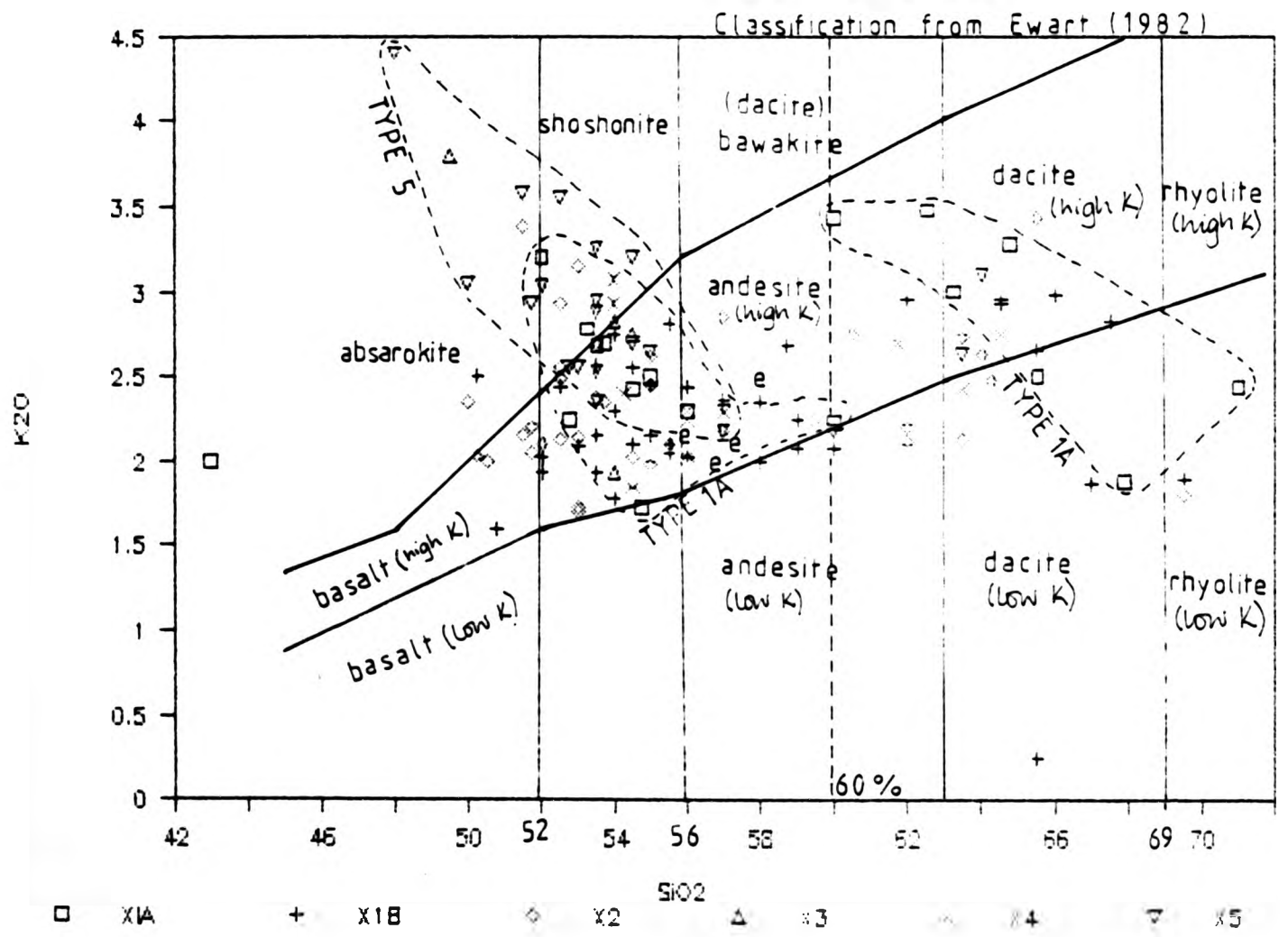

biotite; while the low MgO xenoliths have low K_2O and low CaO with higher Na_2O. On the SiO_2 vs K_2O (Fig.7.9B) the fields are also well defined with the dividing line being at 60% SiO_2. Above 60% all the xenoliths (regardless of class) lie within the biotite granite or the ctG sheet or are located close to the complex contacts. Both the Sidlaw (Gandy 1972) and Lorne lavas (Groome & Hall 1974) have smaller overall ranges than the xenoliths K_2O range : 0.63 to 2.88% K_2O Sidlaw and 3.31 to 4.28% K_2O Lorne, with the groundmass of the Lorne porphyritic appinites having similar values 2.31 to 5.15% K_2O for similar MgO values as the xenoliths.

Figure 7.10 with total alkalis Na_2O+K_2O shows again the scattered majority of xenoliths between 3.0 -7.0%, while the high MgO xenoliths have an overall lower total alkali content. The generally variable Na_2O/K_2O ratio in the xenoliths is another indication of the variable metasomatism that affects all the xenoliths.

K_2O in the xenolith biotites varies from 8.4 to 10.1% which is almost exactly the same as the range for the host rocks. Biotite certainly varies in its modal amounts in the xenoliths and is then likely to influence the K_2O in the whole rock eg. the biotite rich xenoliths.

7.2.6 Phosphorus

Phosphorus (Fig.7.11) has a highly scattered, but positive trend. The range is 0.06 to 1.52% P_2O_5. The high values occur at high MgO values which is not a usual feature of P_2O_5. The high P_2O_5 samples correspond with the high CaO samples. The overall plot reflects the very variable modal amounts of apatite present throughout the different Types. The widest scatter of maximum values is at 4-6.5%

FIGURE 7.10 Na & K2 vs MgO

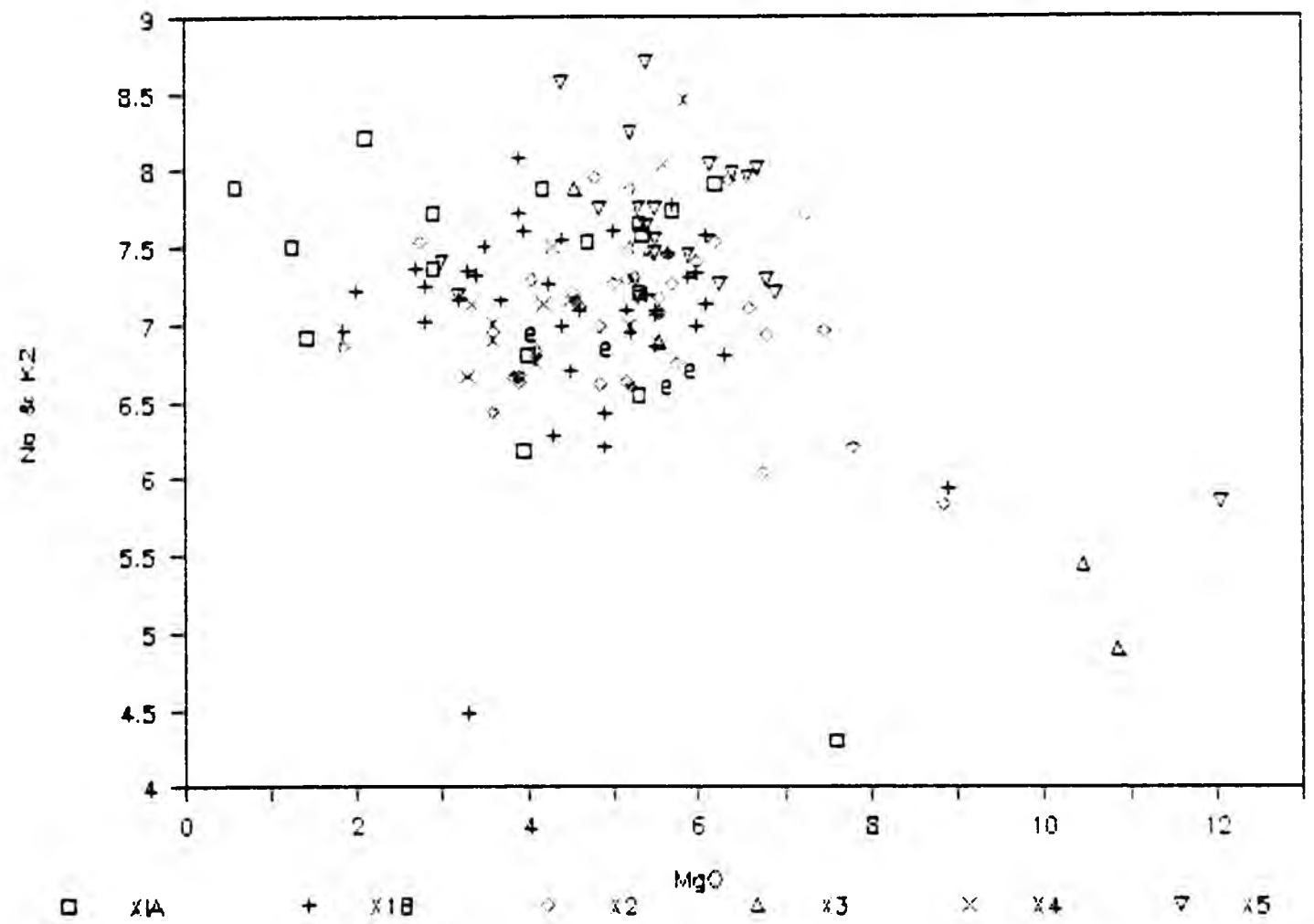

FIGURE 7.11 P2O5 vs MgO

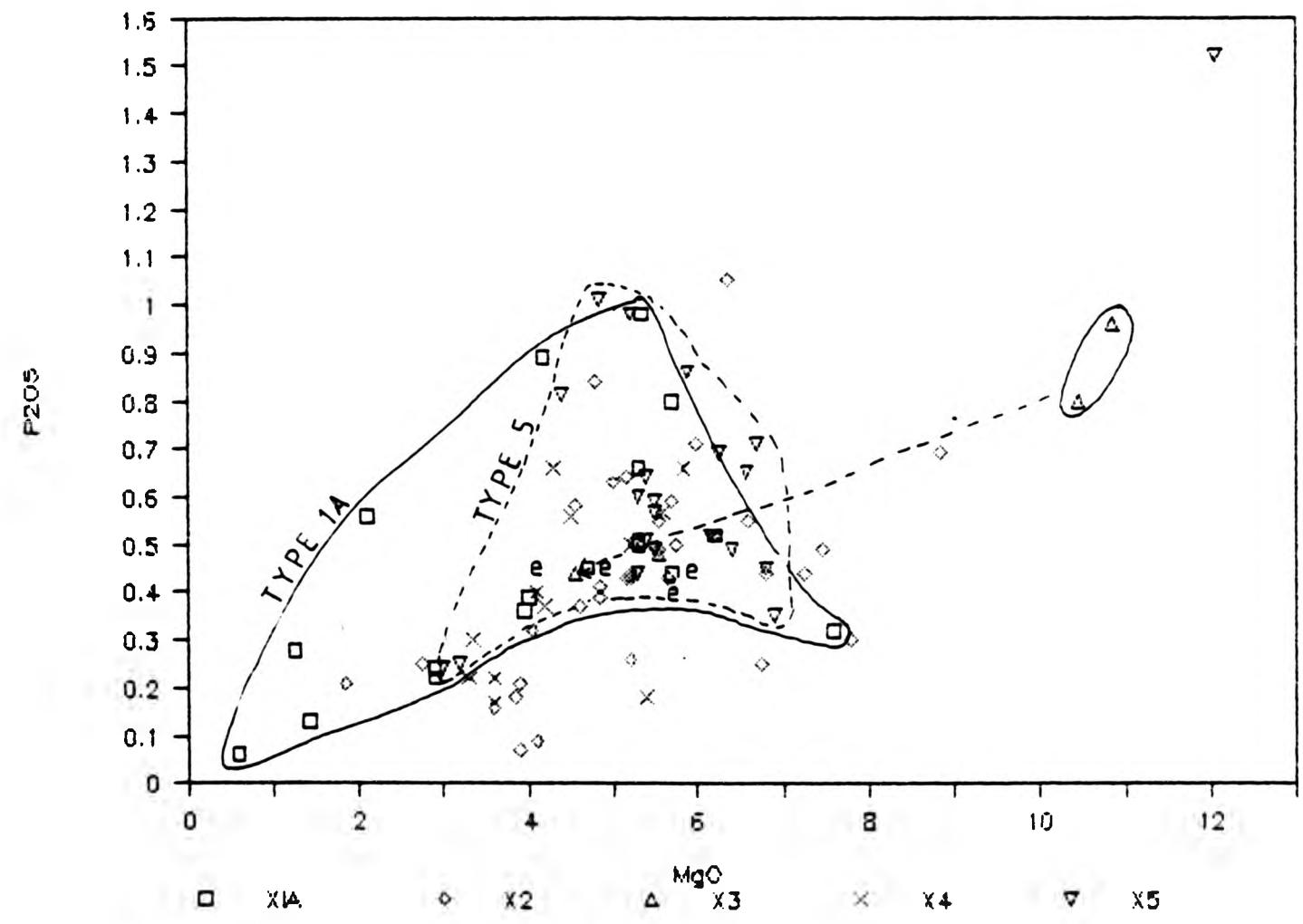

MgO, which is within the same peak ranges of TiO_2. Type 1A and Type 5 show the most clearly defined maximum P_2O_5 at 4-6% MgO. The range of P_2O_5 for Lorne and Sidlaw lavas is far more restricted - 0.12 to 0.24% P_2O_5 Lorne (0.4 to 0.61% for the porphyritic appinites) and 0.24 to 0.61% P_2O_5 Sidlaw.

7.3 TRACE ELEMENTS

The variation diagrams for the xenoliths trace elements are from Figure 7.12 to 7.31. Many of the trace elements show very similar trends to the major element plots. Details of ionic radii, charge and electronegativity have been discussed in Chapter 4, sections 4.3 to 4.3.4.

7.3.1 Barium, Strontium and Rubidium

These three elements show a wide variation throughout the xenoliths (Figs.7.12, 7.15 & 7.19).

Barium (Fig 7.12) varies from 200 to 1525ppm. In the MgO range 3.0 to 7.0%, there is a very wide scatter of data points, ranging from 200 to 1300ppm. This scatter is somewhat greater than that for K_2O (Fig.7.9A), which indicates a variable amount of substitution. Type 1A occupies a diffuse curved field with a broad maximum at 2-5 SiO_2.

When Ba is plotted against K_2O (Fig.7.13), the diagram shows very little coherent trend, suggesting a very great deal of unrelated substitution throughout the xenolith Types. The Ba/Rb ratio vs SiO_2 (Fig.7.14) shows a very constant ratio with increasing SiO_2 unlike the granites (Fig.4.23). Again there appears to be some separation

FIGURE 7.12 Ba vs MgO

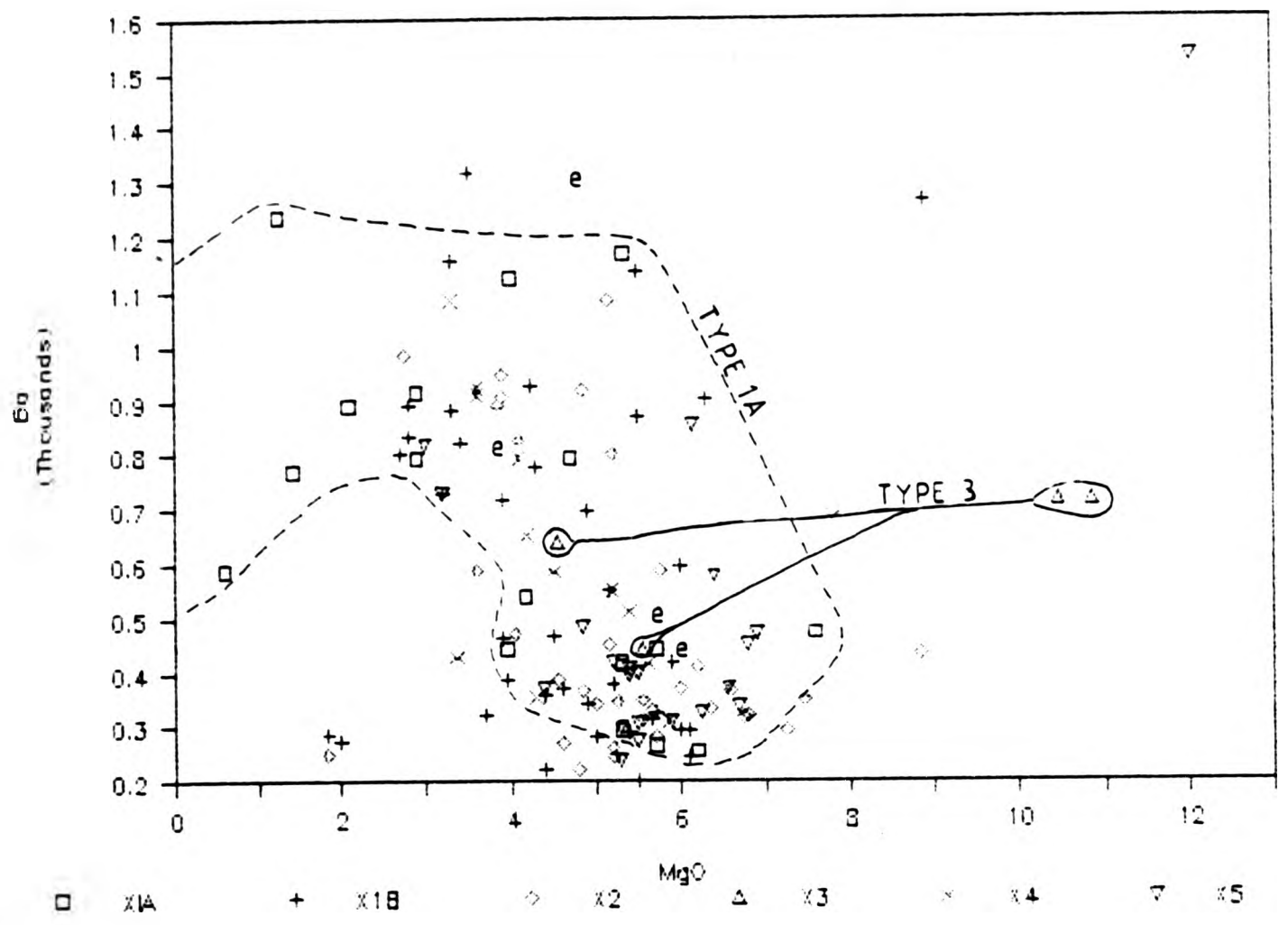

FIGURE 7.13 K2O vs Ba

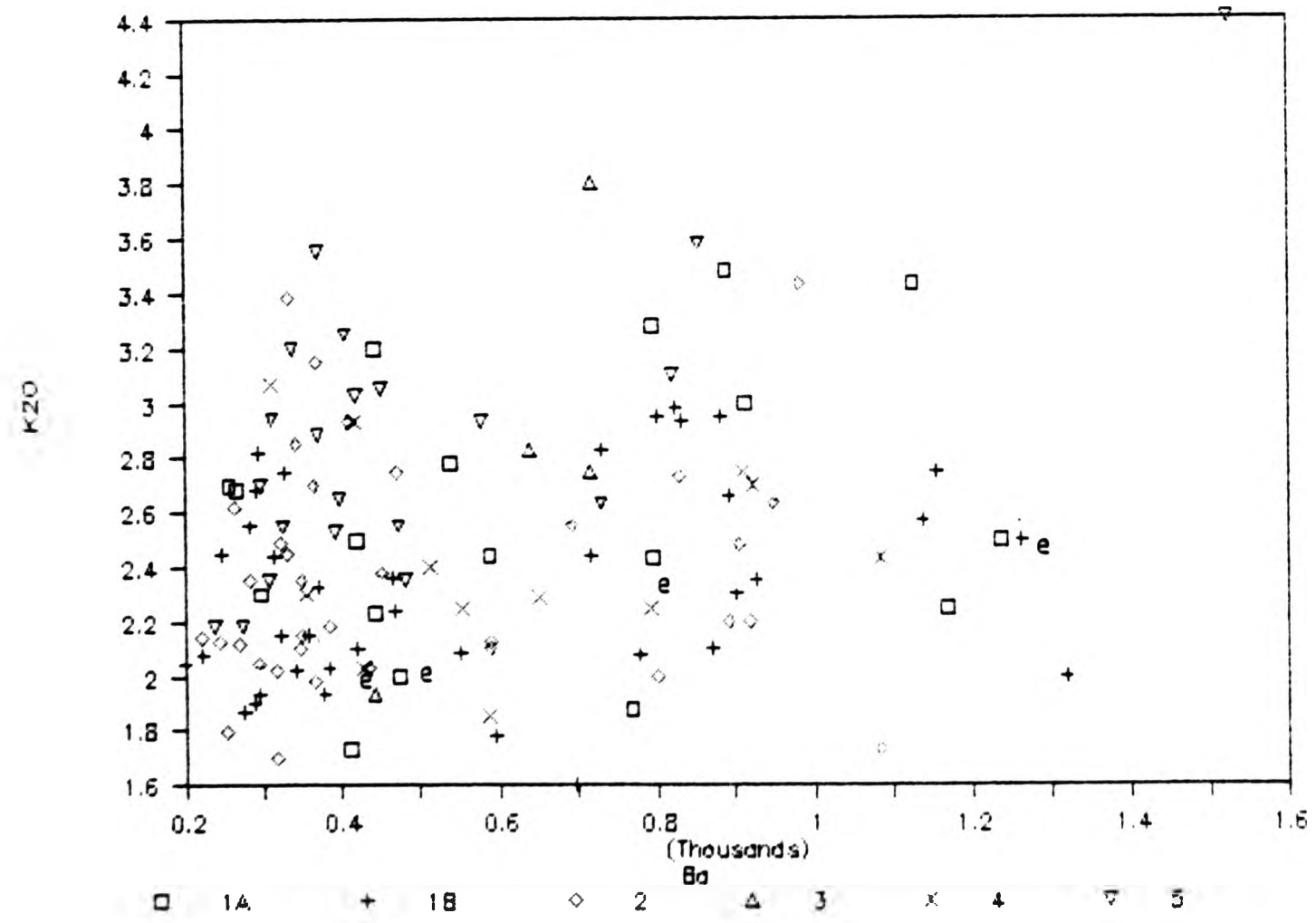

FIGURE 7.14 Ba/Rb vs SiO2

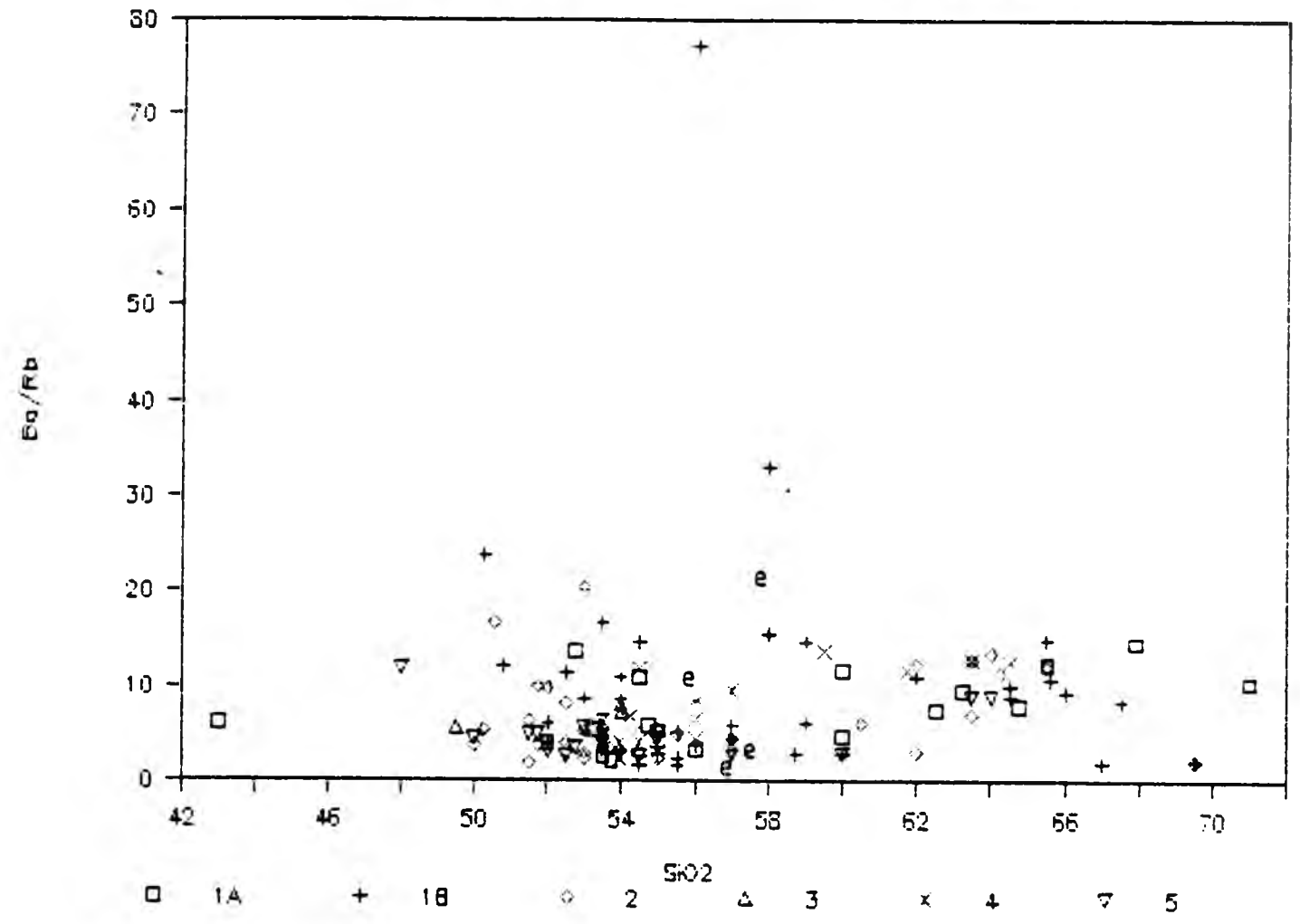

FIGURE 7.15 Sr vs MgO

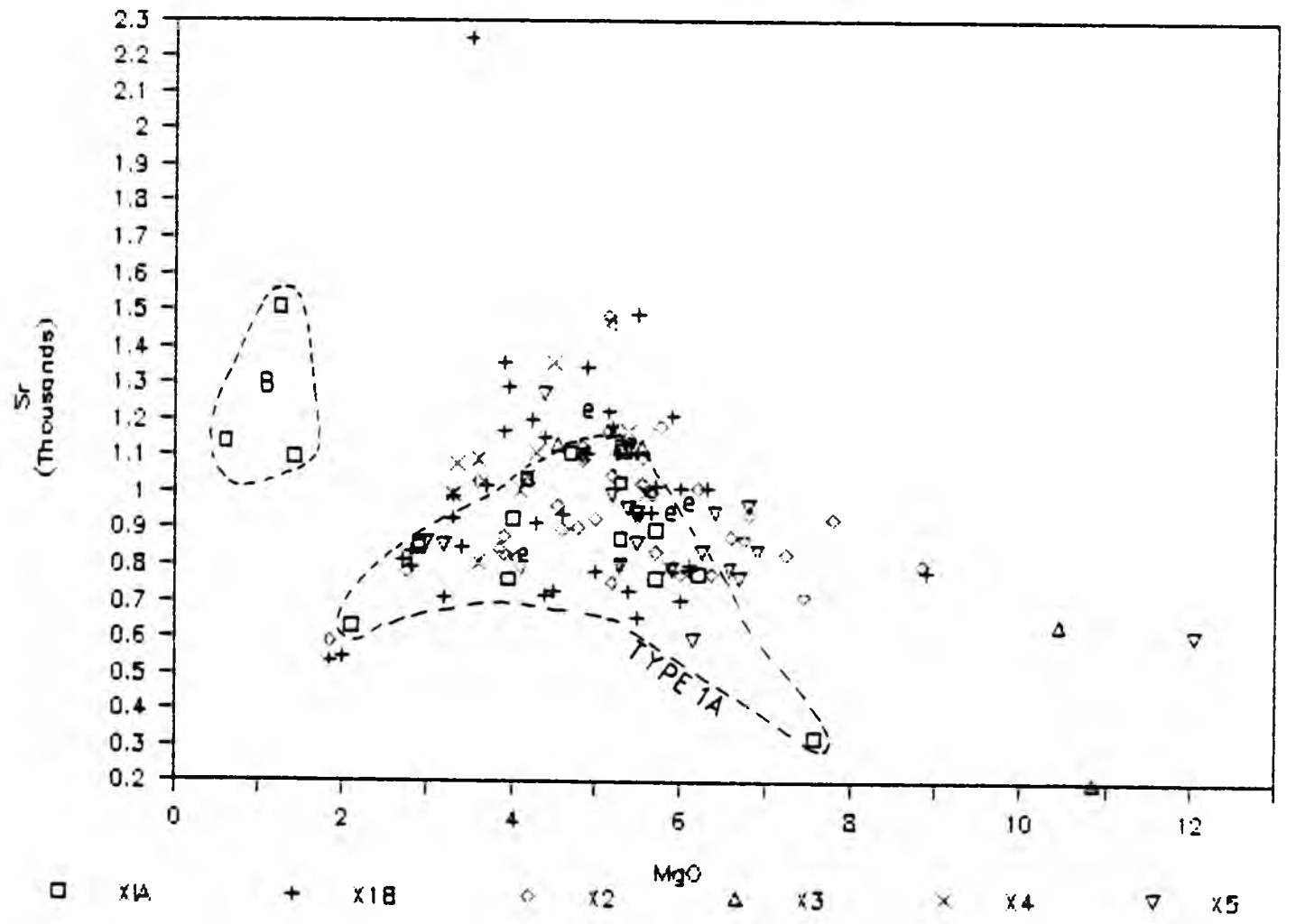

at 60%, which corresponds to the group mentioned in section 7.2.5.

Strontium vs MgO (Fig.7.15) is a tighter plot with the same extreme low and high MgO xenoliths plotting slightly separately from the main trend. This should be compared with Na_2O and Al_2O_3 results. The Sr range is from 201 to 2248ppm. The sample with 2248ppm Sr also has the highest Na_2O - 6.5%. There is no linear trend though a distant peak occurs at 5% MgO with minimum values of about 700ppm below 2 and above 8% MgO.

Those samples that have low Sr, have high CaO, Ba and K_2O. When Sr and CaO are plotted against each other (Fig.7.16), it shows a slight positive correlation with only a few extremely low ratios. While the Sr/Ca ratio vs SiO_2 (Fig.7.17) shows little change with increasing SiO_2. A number of very high values are 3 samples which have very low CaO levels (Fig.7.6).

When Sr is plotted against Ba (Fig.7.18) and K_2O (Fig.7.19A), there is wide scatter with no trend. The Ba/Sr ratio (Fig.7.19) shows little change with increasing SiO_2 though a weak maximum at 63% SiO_2 occurs. The most extreme values are found in rocks with <52% SiO_2.

Rubidium (Fig.7.20) has a very similar trend to K_2O (Fig.7.9), with even the extreme xenoliths at both ends showing medium to high levels of Rb. Rb ranges from 5 to 220ppm. There are Rb values greater than 100ppm at high MgO eg. Type 5 xenoliths (X5) which will correspond to their biotite-rich petrography. Rb ranges for Sidlaw (6 to 89ppm) and Lorne (75 to 116ppm) are again far more restricted.

When plotted against Sr and K_2O, Rb displays quite linear trends.

FIGURE 7.16 CaO vs Sr

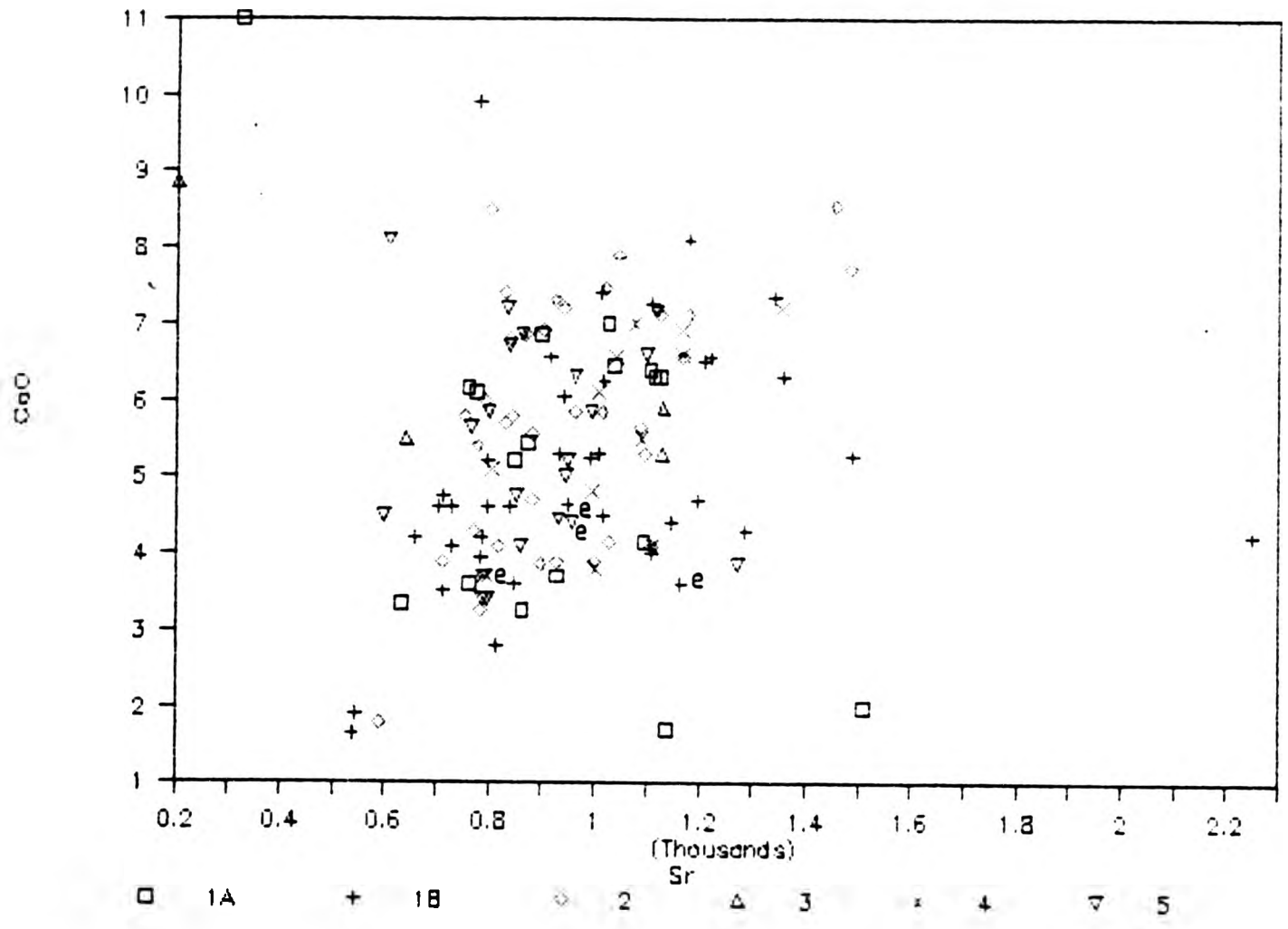

FIGURE 7.17 Sr/Ca vs SiO2

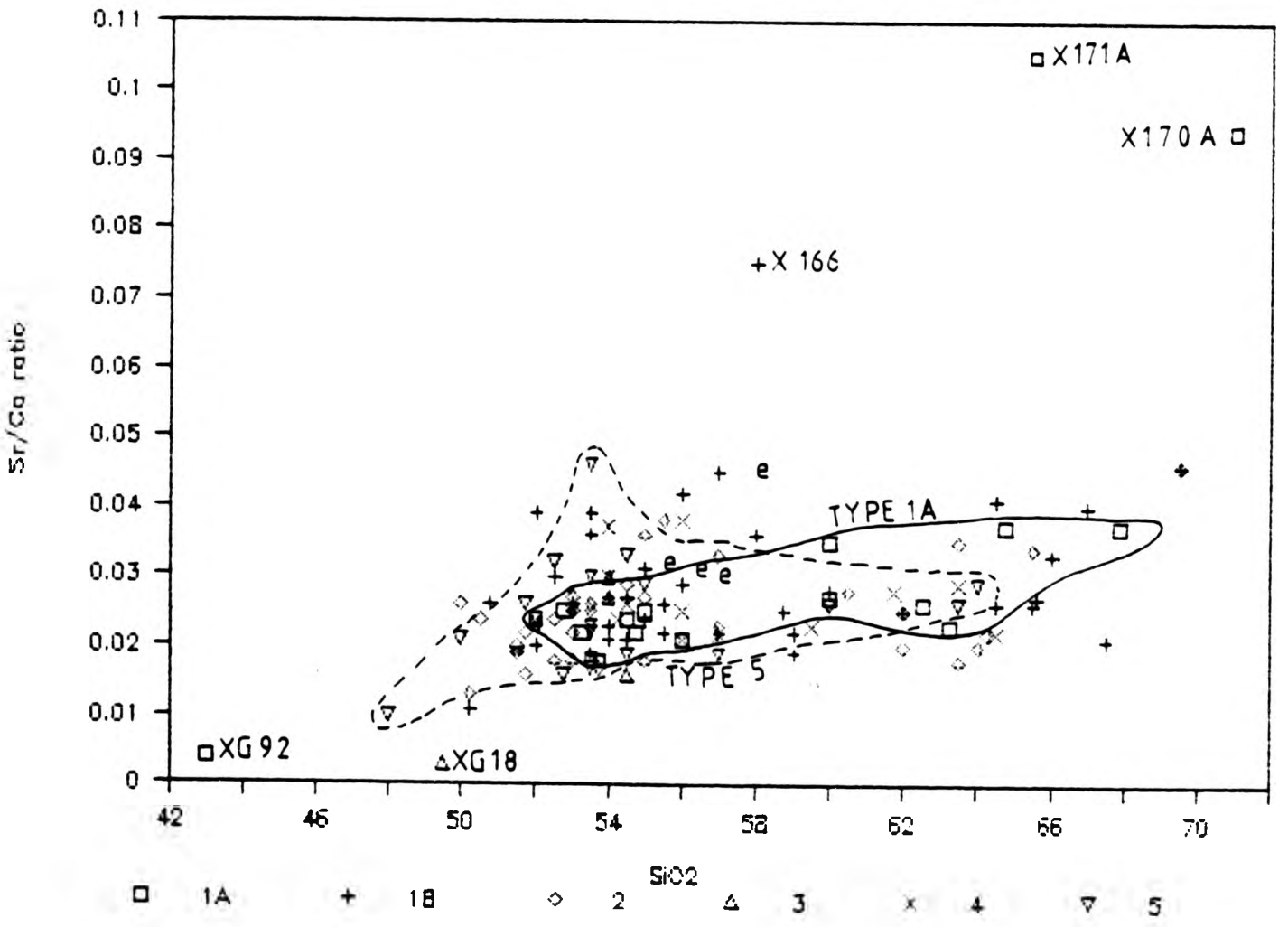

FIGURE 7.18 Ba vs Sr

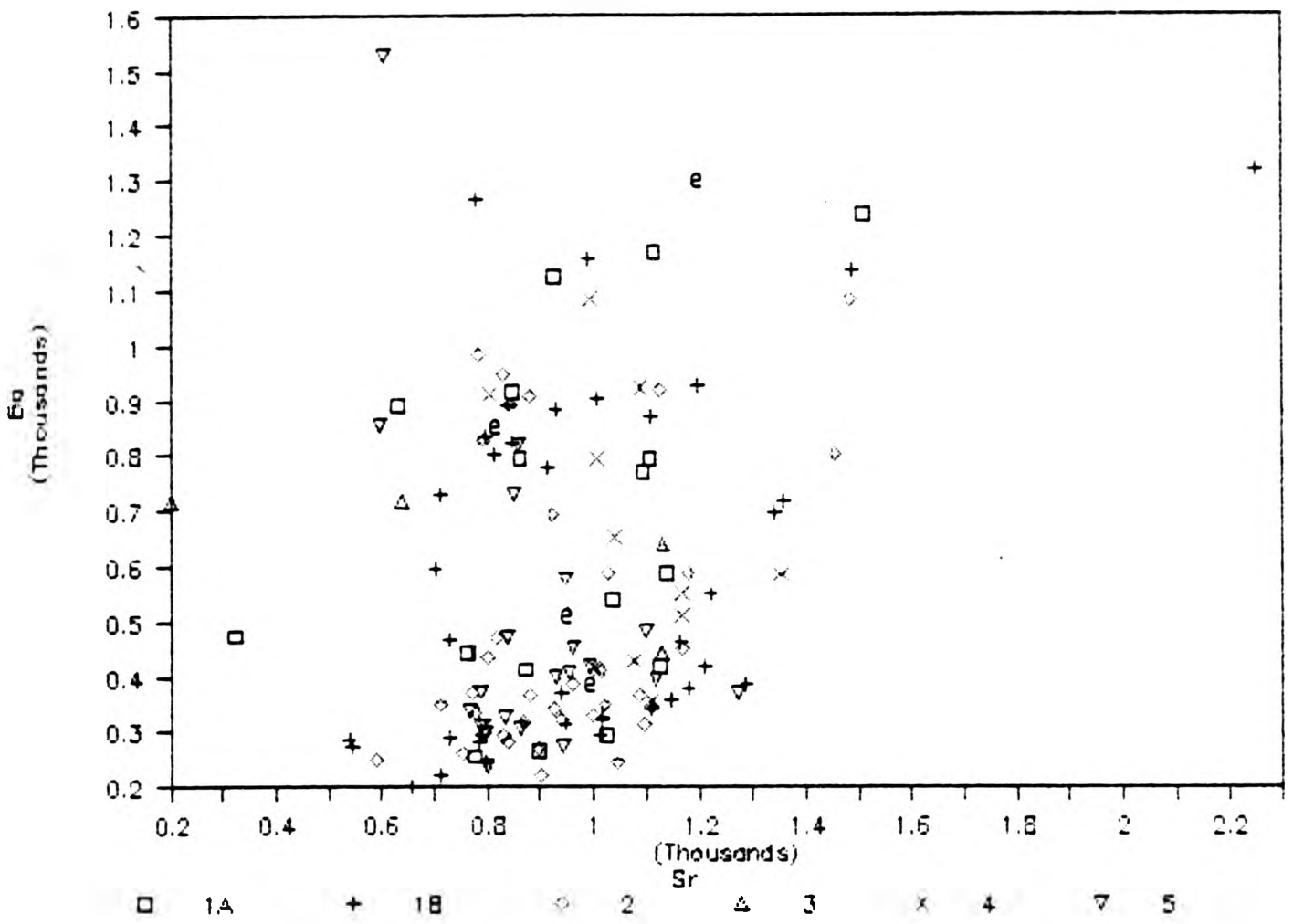

FIGURE 7.19 Ba/Sr vs SiO2

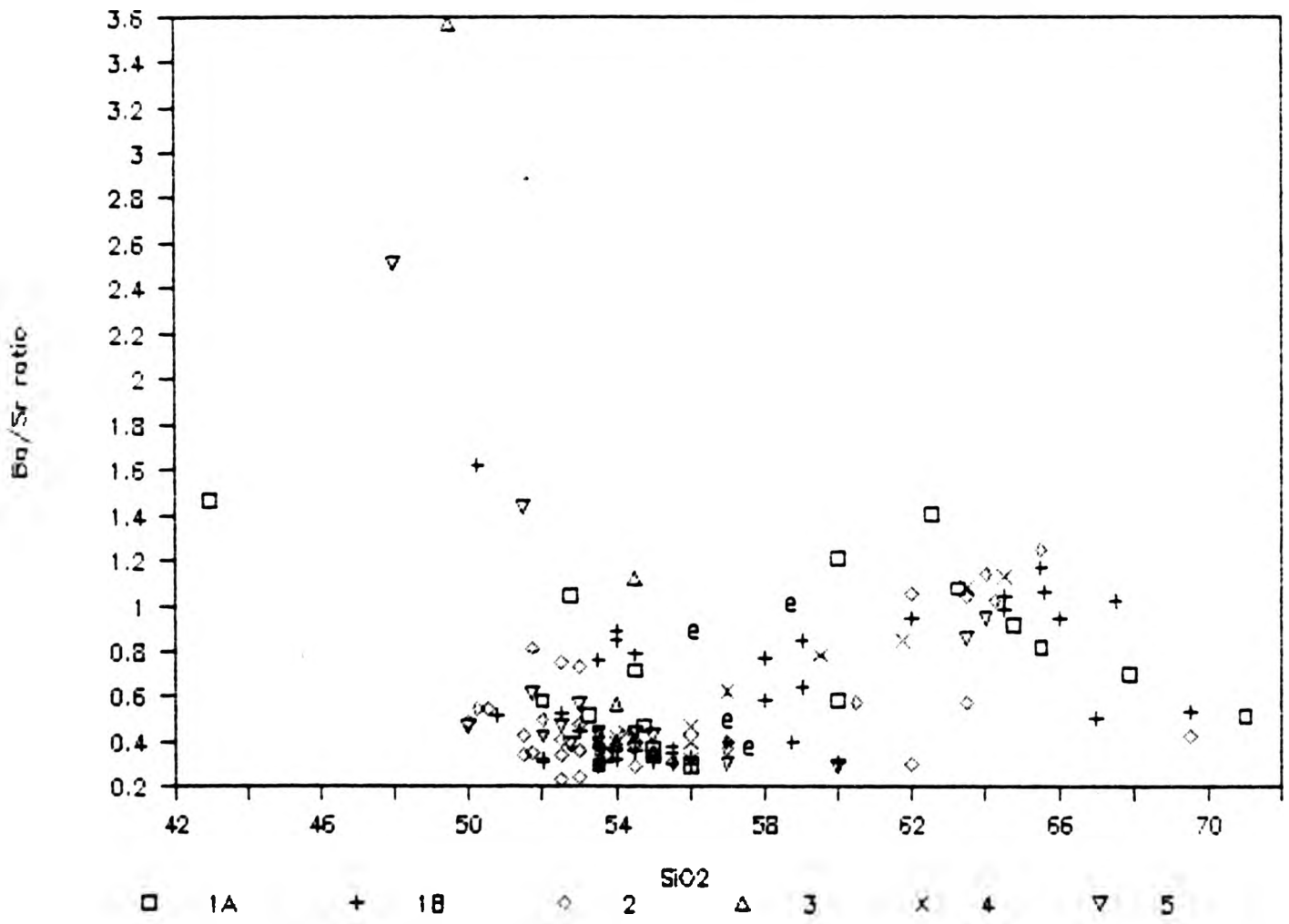

FIGURE 7.19A K20 vs Sr

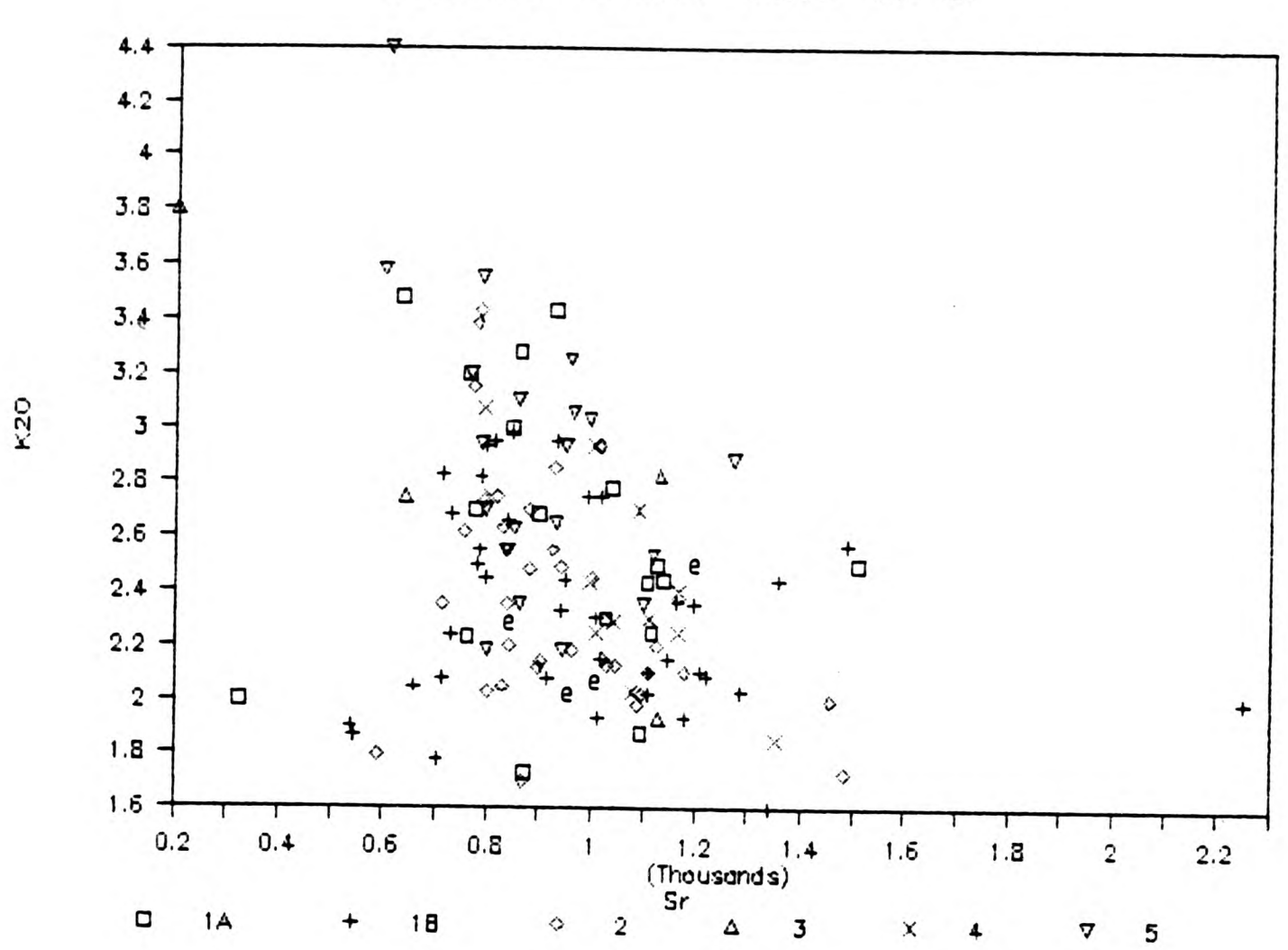

FIGURE 7.20 Rb vs MgO

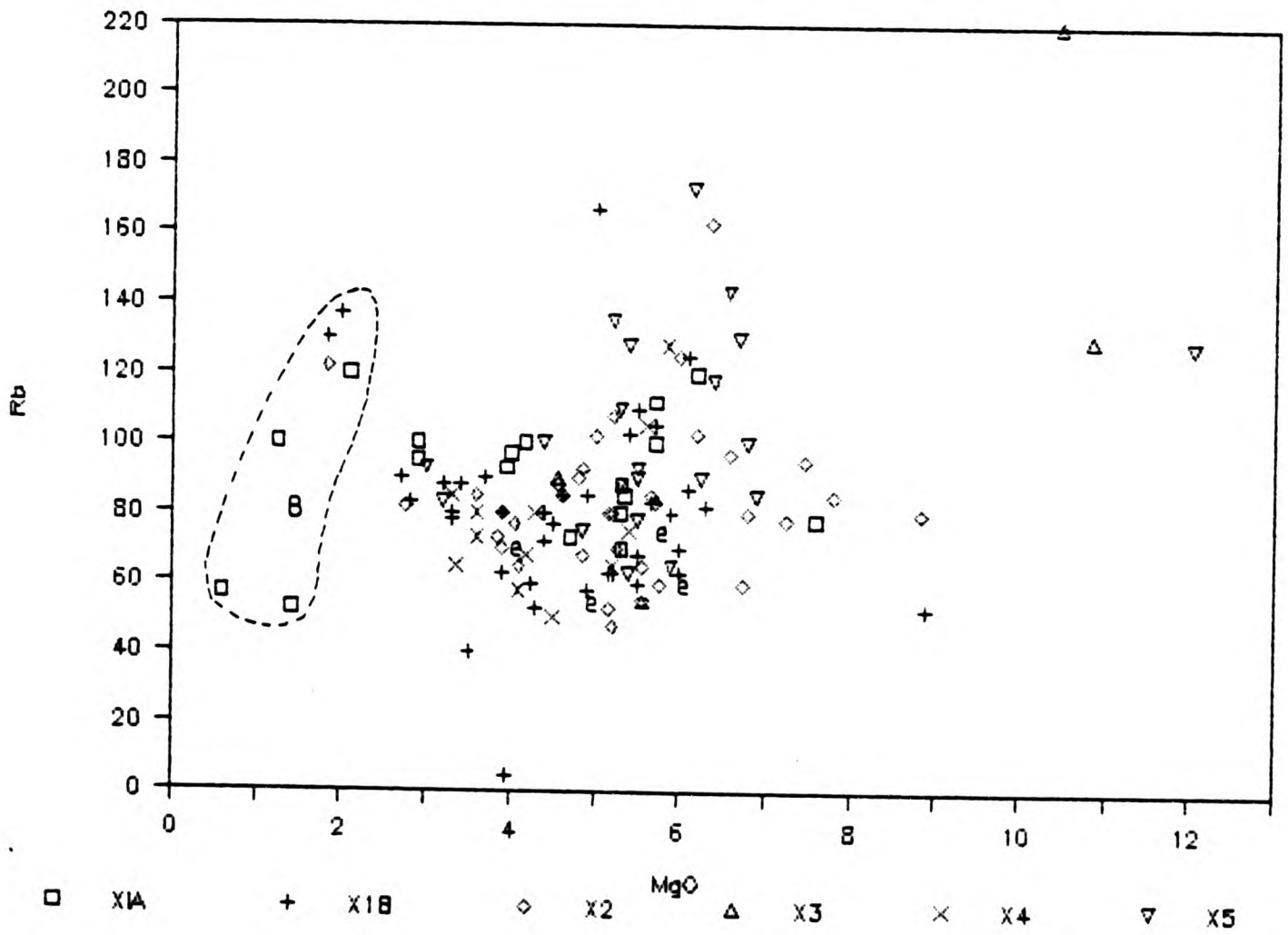

Rb vs Sr (Fig.7.21) has a negative decreasing Sr with increasing Rb and Rb vs K_2O (Fig.7.22) shows a positive correlation of increasing K_2O with increasing Rb, which indicates a certain amount of substitution. The normal chemical coherence of these 2 elements (Rb and K_2O) is preserved inspite of the random variation in other elements, but the trend does not quite go through the origin and there is a very wide scatter of Type 1B data. K/Rb ratio vs SiO_2 (Fig.7.23) does not show any real trend, but instead a wide scatter of values throughout the xenoliths. The best correlation is with the K-Rb plot which is controlled by the crystallization of biotite and K-feldspar. The Ba and Rb content increases in the outer xenolith of the xenolith within xenolith, but decreases in the serial sectioning of uniform xenoliths (Fig.7), with an average Ba increase of 56ppm (max. 733ppm) and Rb of 5ppm.

7.3.2 Chromium and Nickel

Figures 7.24 and 7.25 show the distribution of Cr and Ni respectively against MgO.

Both display positive correlations with increasing levels with increasing MgO, with 20 to 530ppm Cr and 24 to 403ppm Ni. They can substitute for iron and magnesium so the higher the levels of MgO and FeO*, the higher the Cr and Ni levels. Cr levels are noted to be lower in the biotite-rich xenoliths.

7.3.3 Vanadium and Scandium

Vanadium (Fig.7.26) and scandium (Fig.7.27) both display very similar trends with each other. They have good linear trends of increasing

FIGURE 7.21 Sr vs Pb

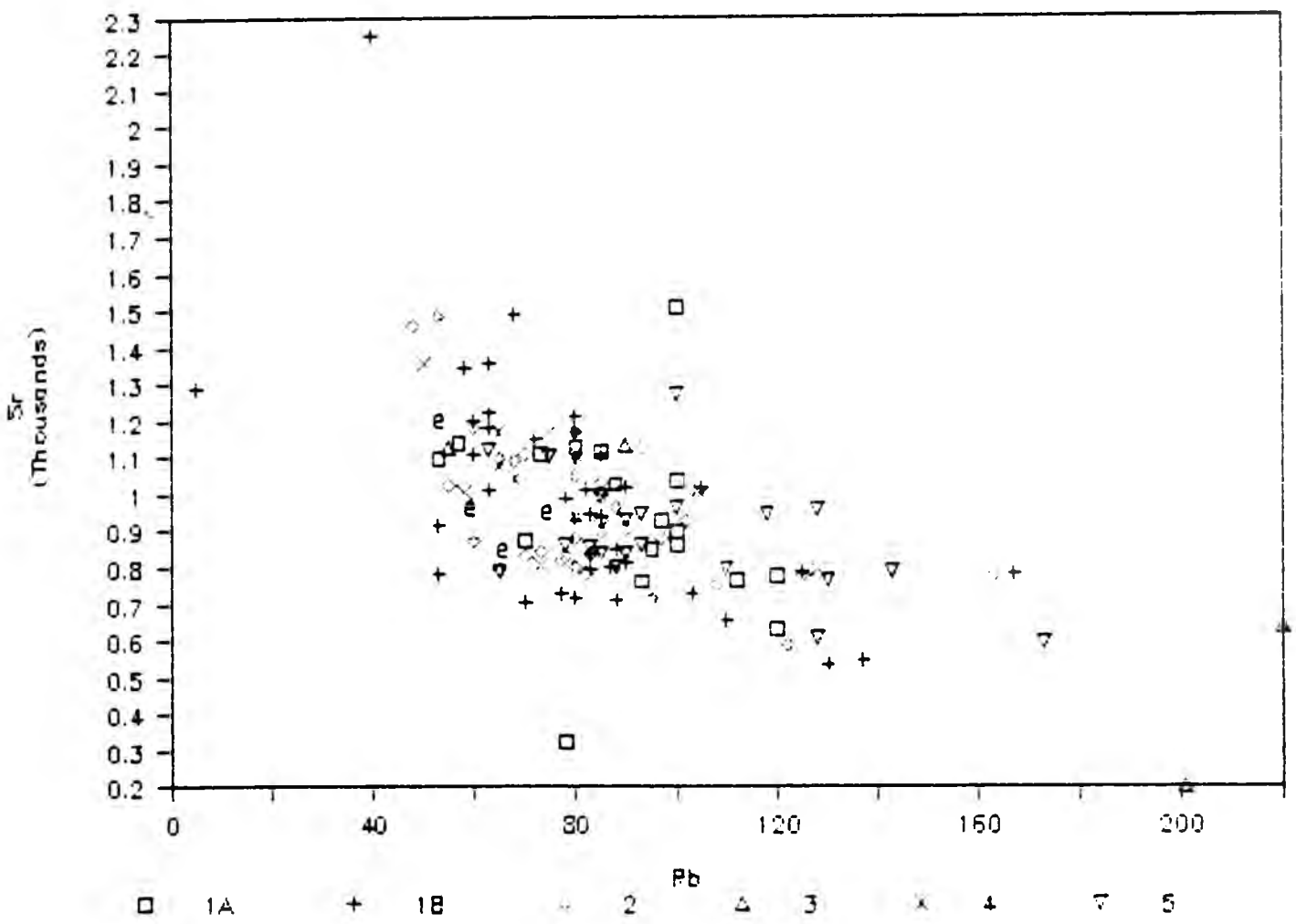

FIGURE 7.22 Rb vs K20

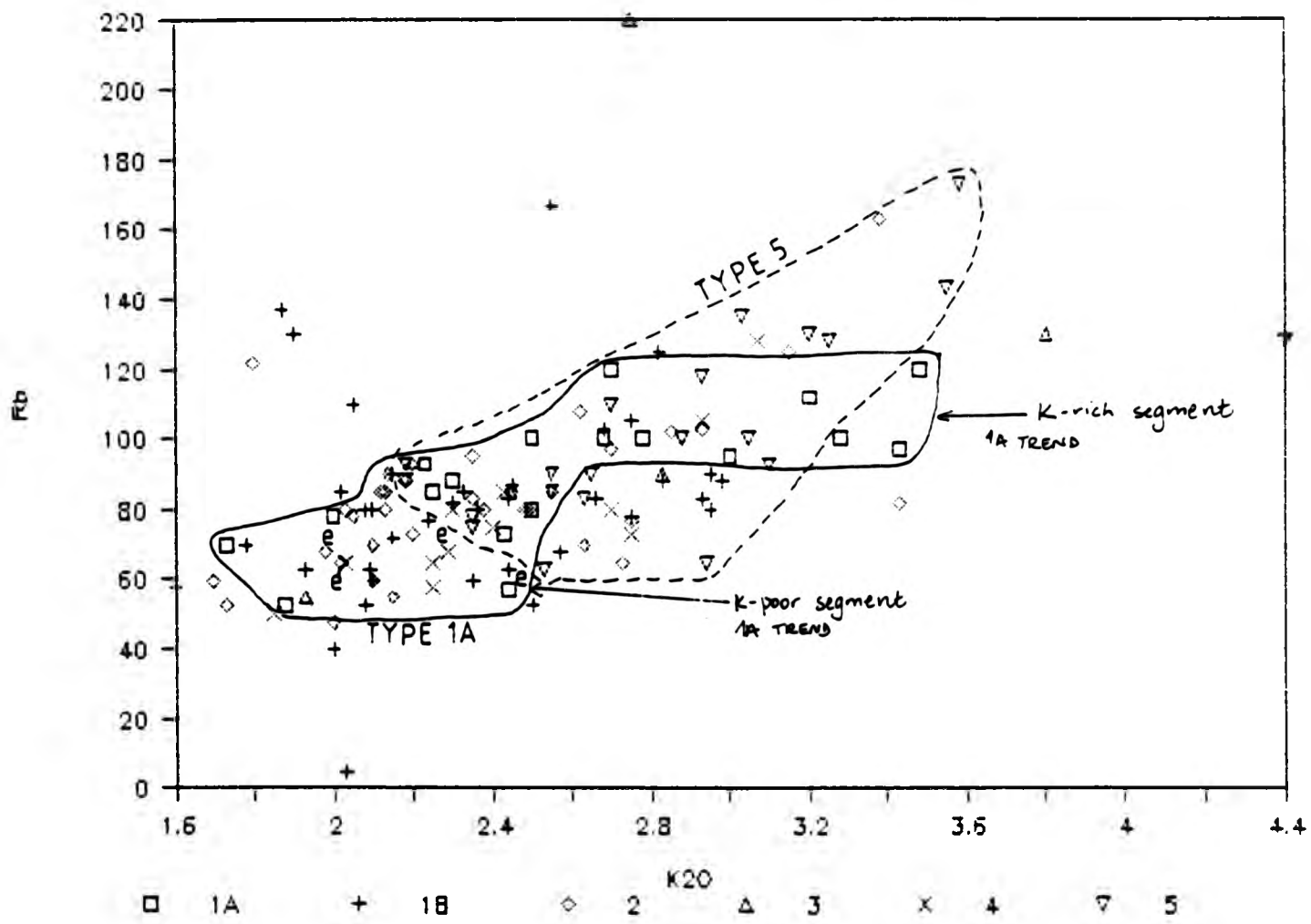

FIGURE 7.23 K/Rb VS SiO2

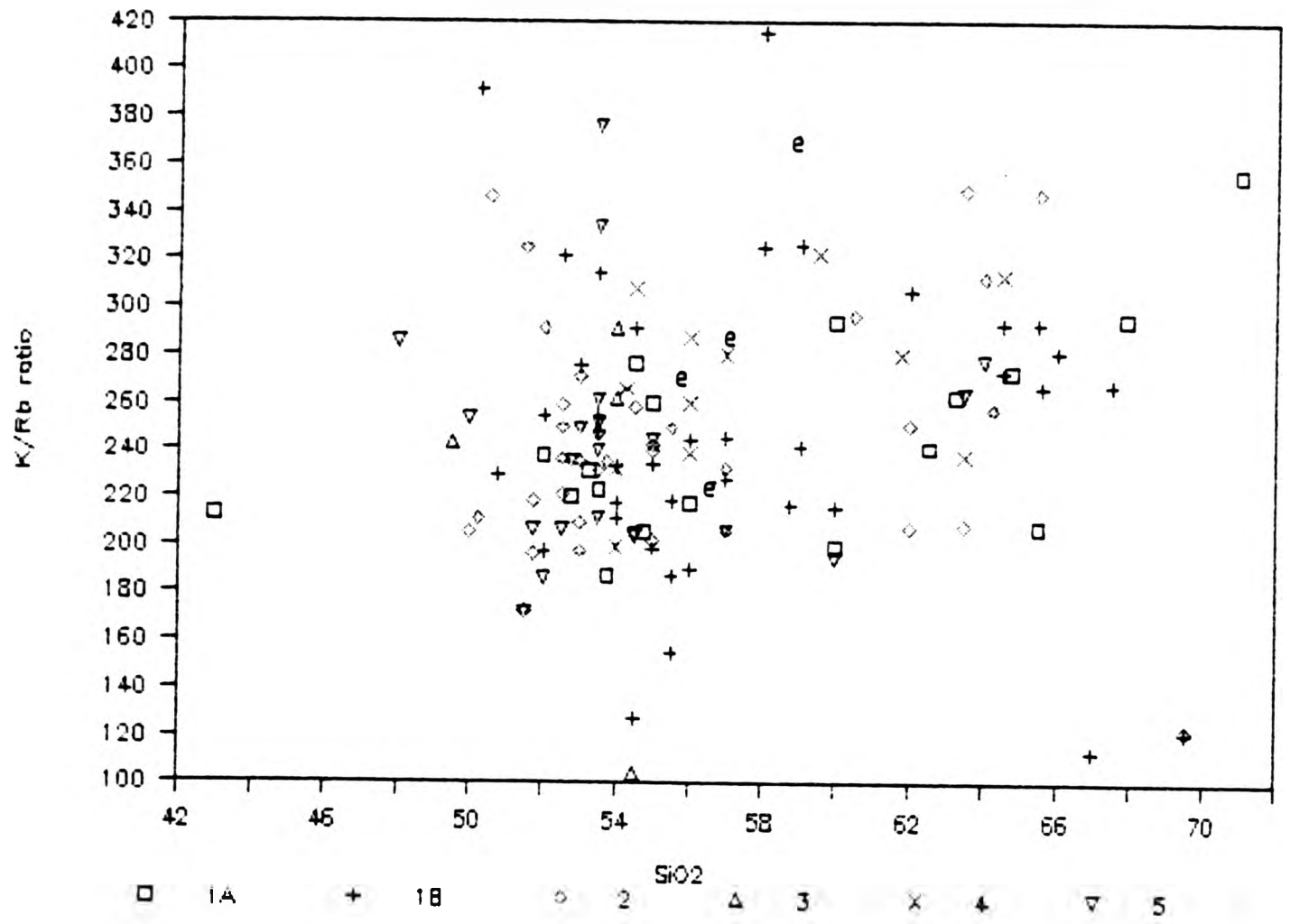

FIGURE 7.24 Cr vs MgO

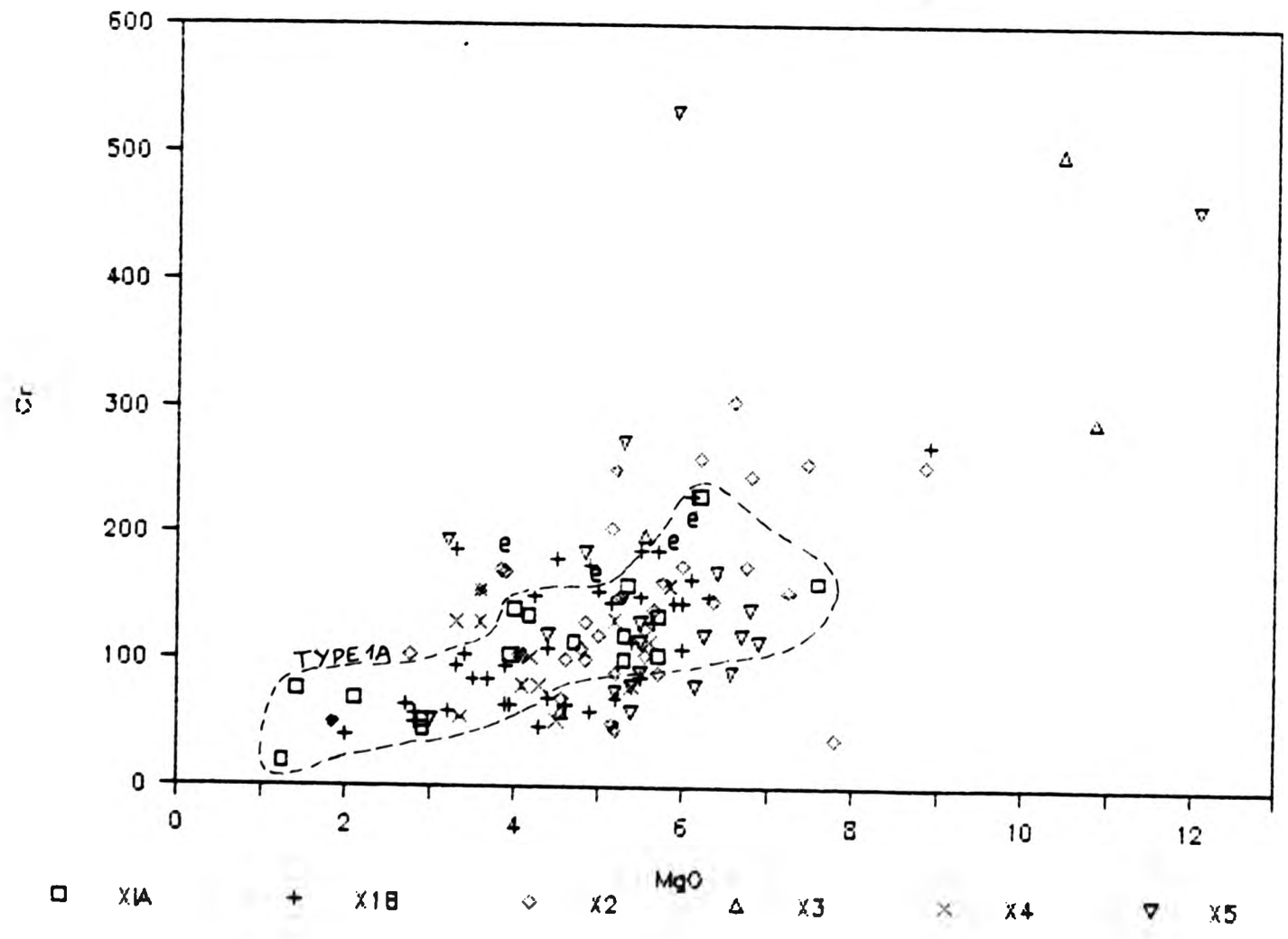

FIGURE 7.25 Ni vs MgO

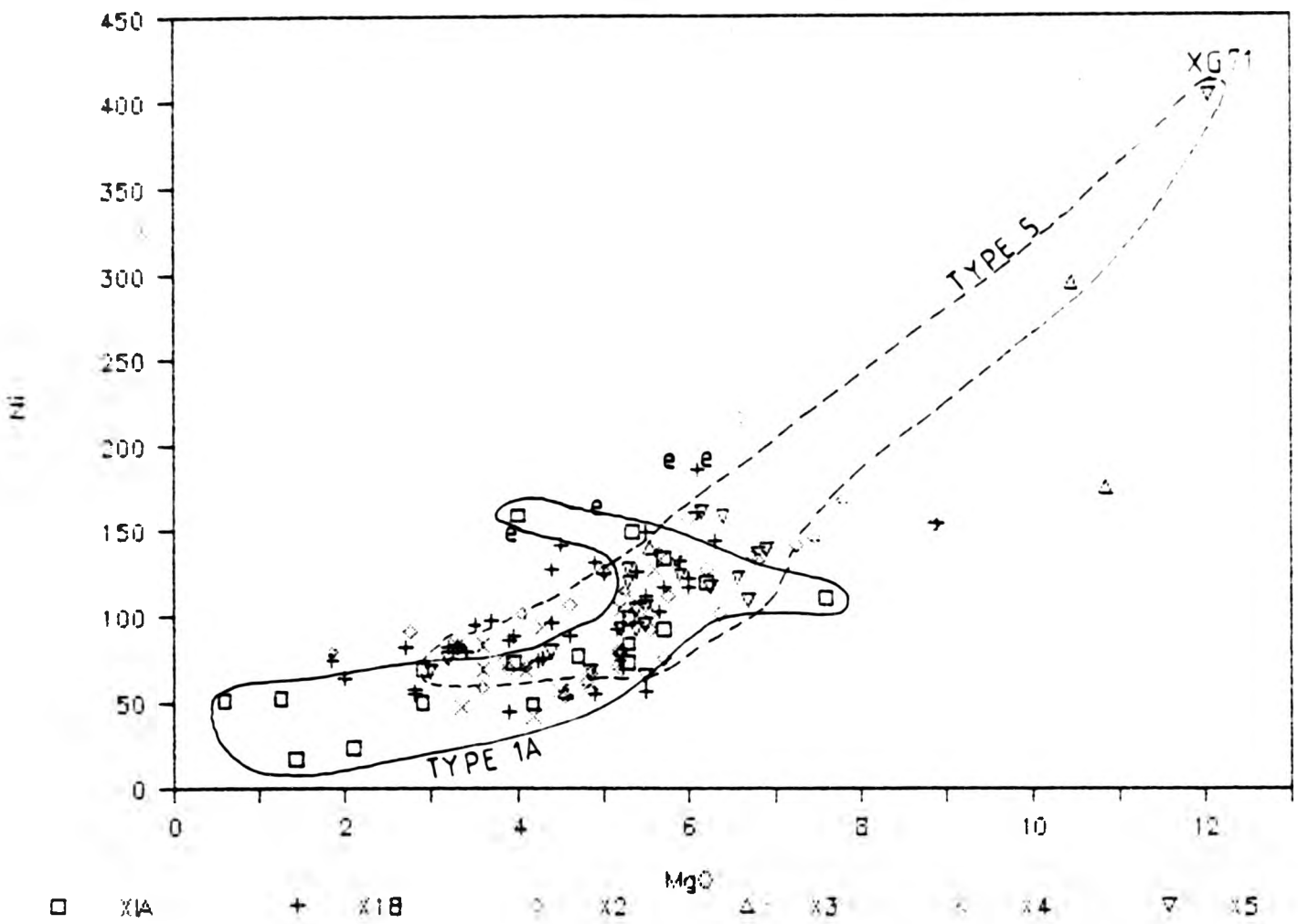

FIGURE 7.26 V vs MgO

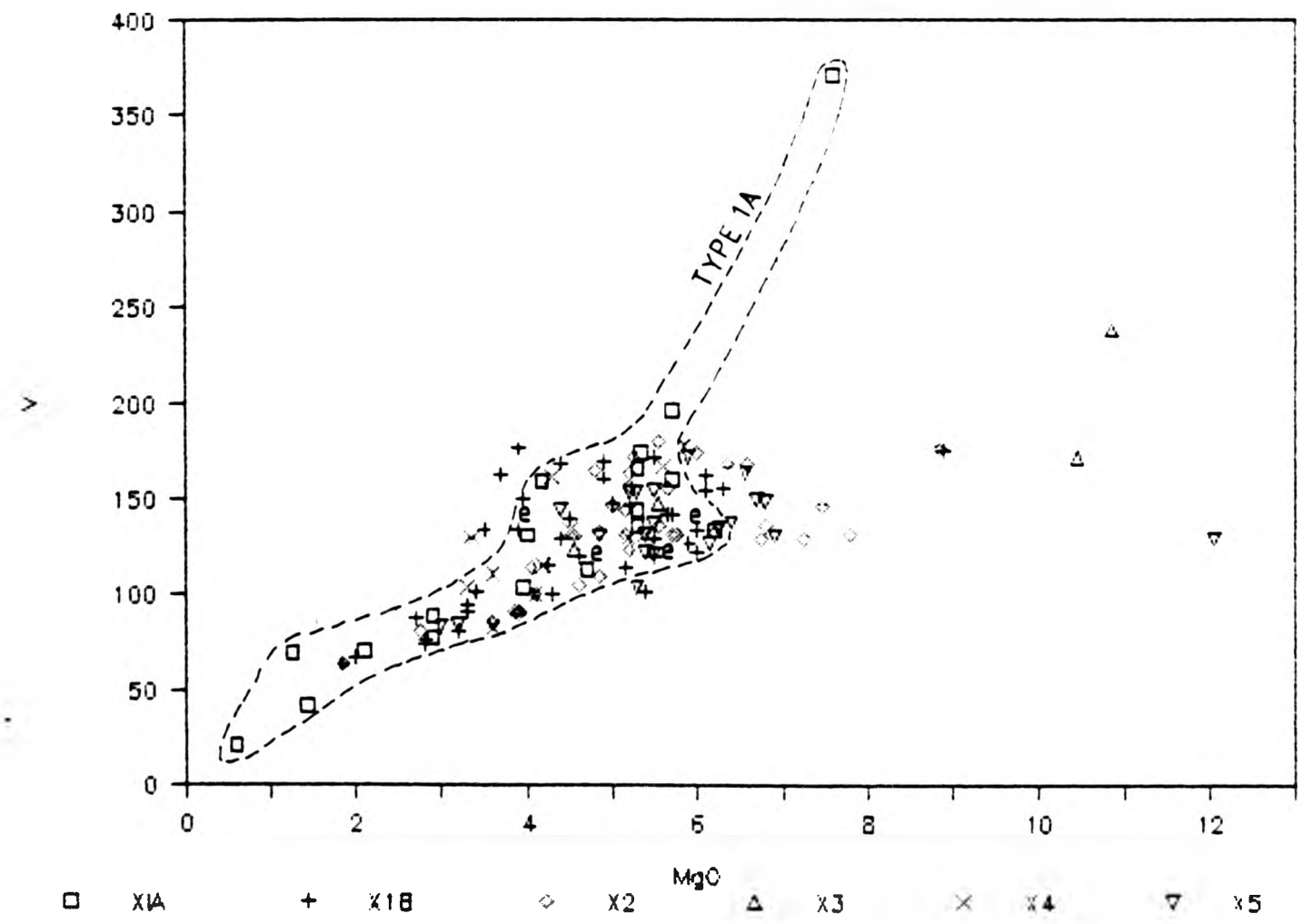

FIGURE 7.27 Sc vs MgO

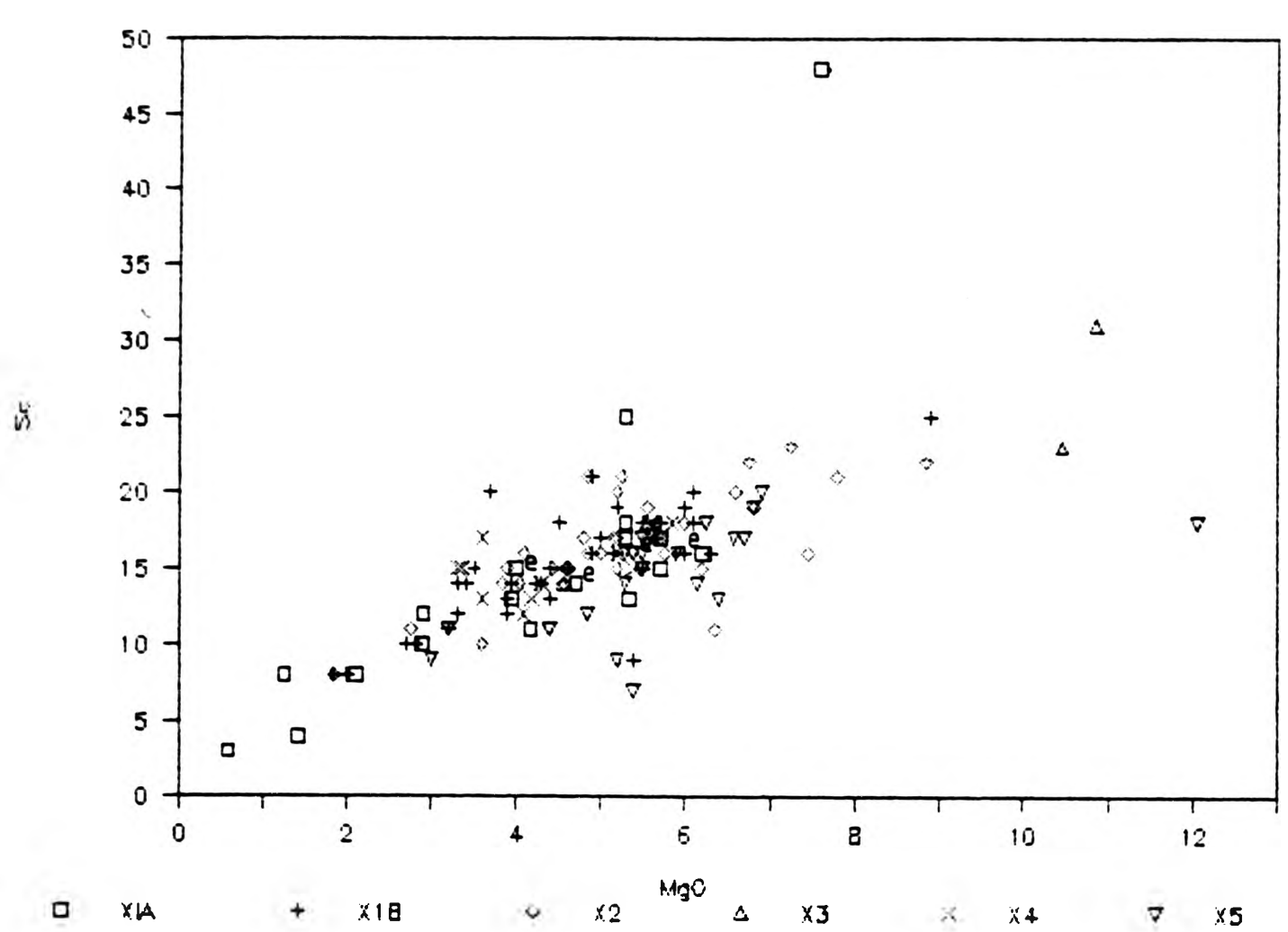

FIGURE 7.28 Cu vs MgO

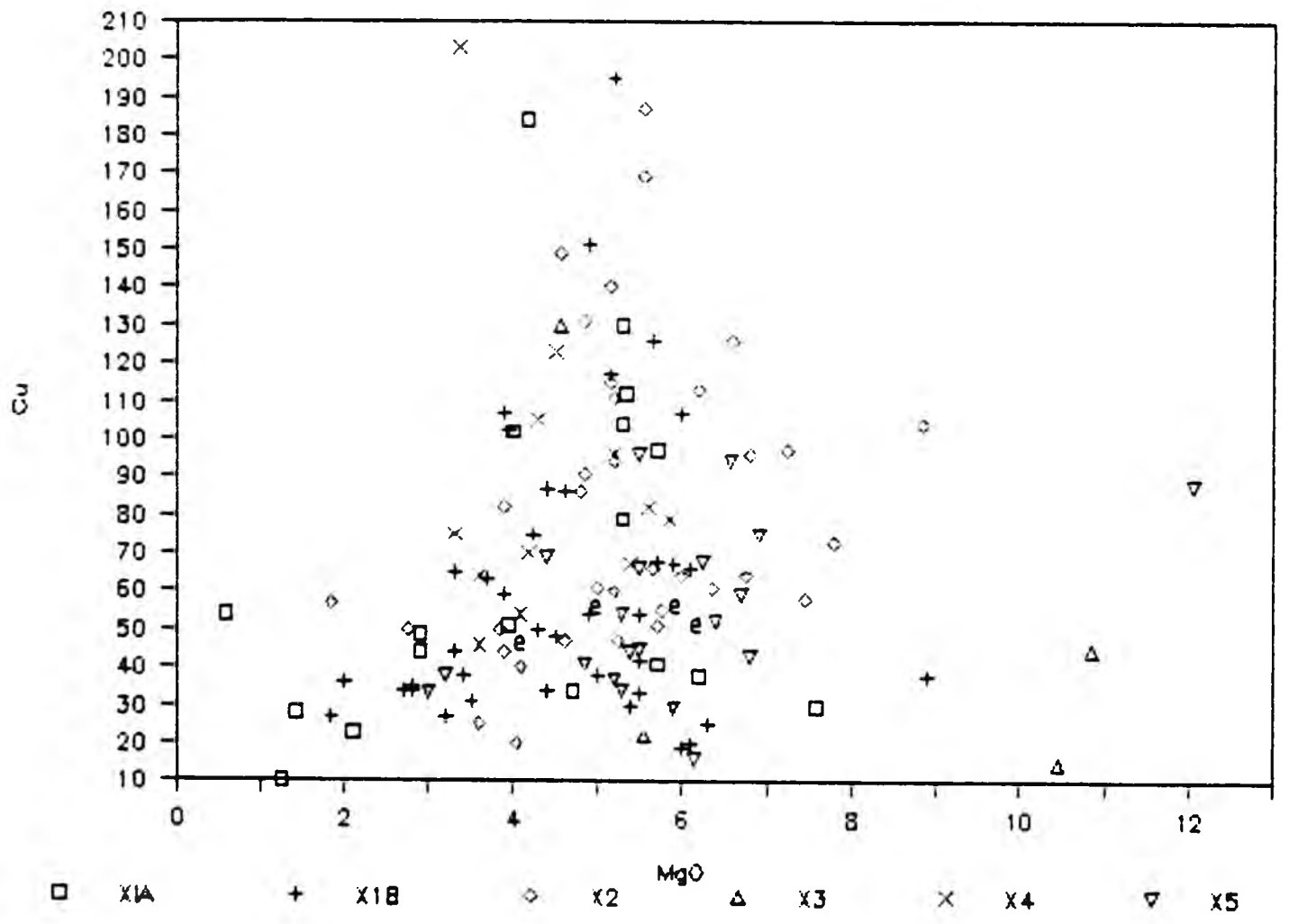

levels with increasing MgO. V ranges from 21 to 371ppm and Sc 4 to 48ppm. These high V and Sc levels correspond to high FeO* (Fig.7.4) and when plotted against FeO* (Figs.4.32 & 4.31) they show very tight linear trends. Also TiO_2 vs V (Fig.4.33) has a very positive correlation. Therefore the Cr & Ni and V & Sc plots are related to the percentage of mafics present.

7.3.4 Copper, Zinc and Lithium

Figures 7.28, 7.29 and 7.30 display copper, zinc and lithium against MgO.

The abundance of Cu varies from 10 to 203ppm and show a very wide scatter of values between 4.0-6.0% MgO. The level of sulphides in thin section is low, but nevertheless would influence the Cu content.

Zn (32 to 208ppm) has a very similar tight trend to FeO* with the same samples being scattered at the high MgO end. While at the low MgO end there is a separate but parallel field, which is the same group as mentioned before with SiO_2 greater than 60% (Fig.7.8 Na_2O and Fig.7.9A K_2O). They are found either within 100m of the complex margin or are those in the biotite granite.

Li displays a scattered plot with abundances ranging from 15-131ppm. A wide range is found at 0-2% MgO in spite of the limited range at 2-4% MgO. At 4-6% MgO again the scatter is wide and this is similar to the copper plot. These high Li values correspond to xenoliths with more abundant biotite. Li (Fig.7.30) and Rb (Fig.7.20) correlate with a wide scatter at 6% MgO (the result of Type 5 xenoliths) and give a linear plot through the origin. The separation of the group

FIGURE 7.29 Zn vs MgO

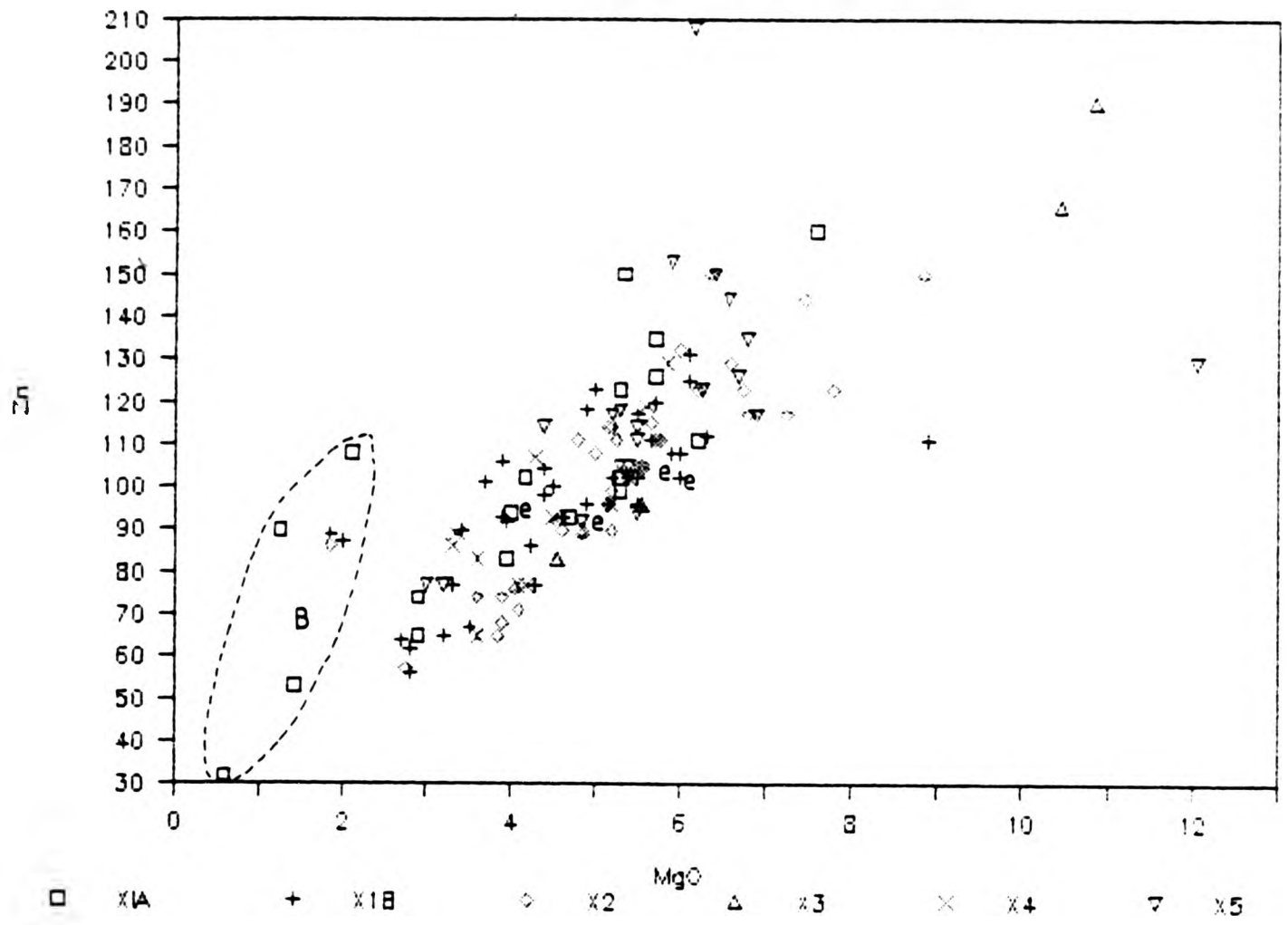

FIGURE 7.30 Li vs MgO

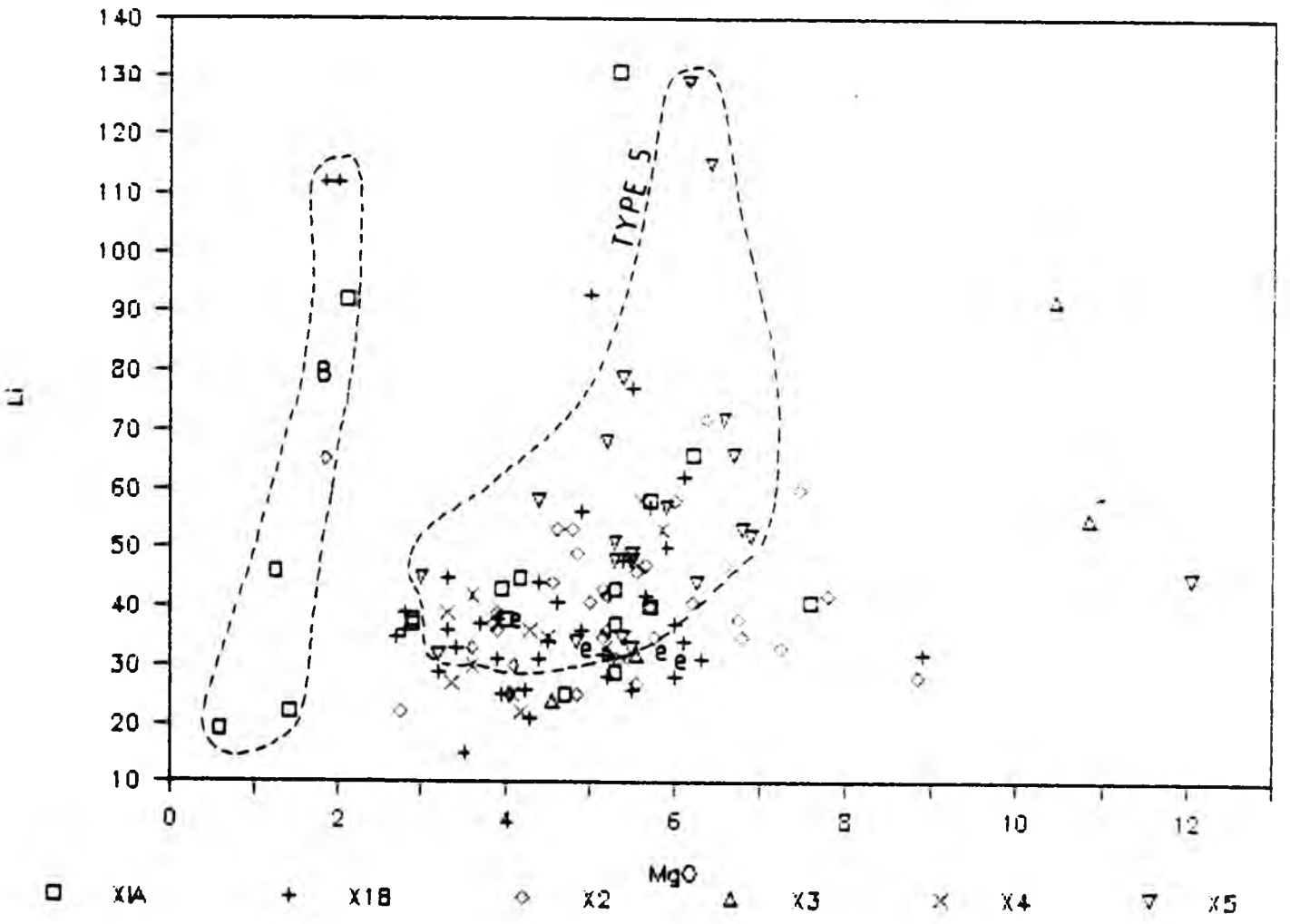

at low MgO has the xenoliths with biotite rather than hornblende as the mafic phase.

7.4 XENOLITH REE PATTERNS

Although not strictly a member of the Lanthanide group, yttrium displays similar behaviour to the HREE (Mason 1966). Y has been plotted against MgO and shows a uniform trend with a slight decrease at the low MgO end. Above 35ppm Y there is a separation of a line of samples and also above 70ppm. None of the samples appear to have any outstanding petrographic feature which would explain such great separation ie from the preferential concentration of REE.

The xenoliths display a wider range of REE compositions than the host granites and in consequence have a higher absolute abundance (Fig.7.31). Their La/Yb ratios range from 20.2 to 61.2; LaN varies from 79 to 464x and LuN 3 to 21x chondrite. There is no pattern to the ratios with increasing silica. Changes are minor and too few xenoliths are analyzed to see if the changes are consistent within each class.

The profiles are slightly steeper than the host granites with higher LREE contents and exhibit both minor negative and positive Eu anomalies (Fig.7.31). Those xenoliths with negative Eu anomalies are XG18, XG22B, XG44 and X69 and all are characterized by having hornblende phenocrysts; while the positive Eu anomalies in XG6, XG20, XG52, XG53, X116 and X177 are feldspar-phyric. The phenocryst phases would influence the REE contents (Sawka 1988) as already discussed in section 4.4.1.

Fig.7-31 Chondrite normalised REE patterns for the Strontian xenoliths.

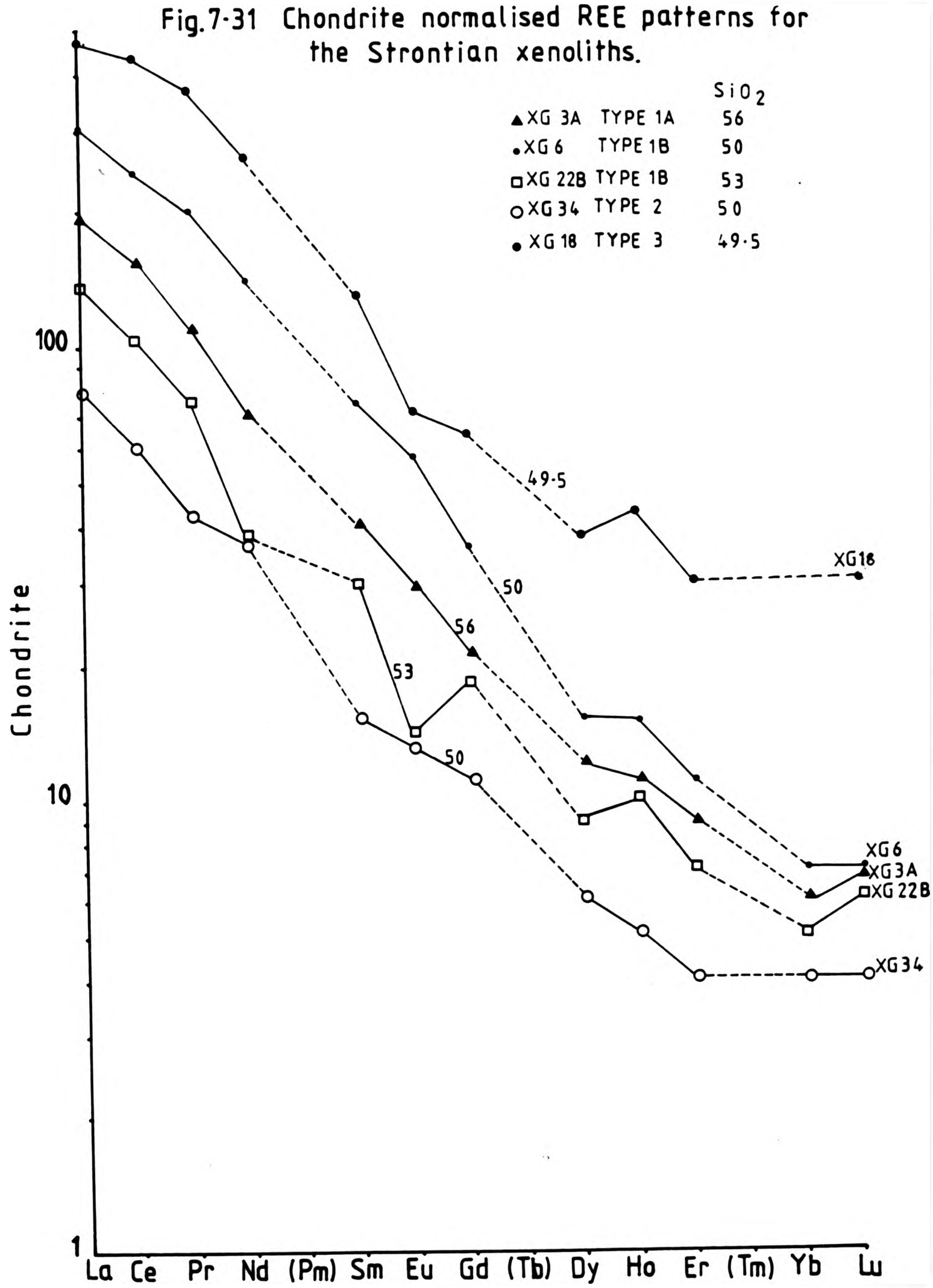

On Fig.7.31 rocks at 50% SiO_2 show both very high and very low REE contents, which is not normal, as REE-bearing accessories are not usually phenocryst phases in such mafic magmas: eg. very high REE content in XG71 and "low" REE in XG66 (Appendix B.5). Both are Type 5 xenoliths, but there is no visible phenocryst mineral present. Therefore there is no obvious crystal fractionation mechanism available to explain the range of values here.

When plotting REE (Ce) vs P_2O_5 (Fig.7.31B) a clear negative correlation is noted, with the most mafic xenoliths having the highest Ce contents. While Ce against MgO and SiO_2 (Fig.7.31A) shows a negative and positive trend respectively. On Fig.7.31B Eu has been plotted against MgO. This is to see whether there is an inflection at 5% MgO similar to the Sr vs MgO plot (Fig.7.15). The plot shows a very uniform Eu content upto 5-6% MgO, after which the more basic xenoliths show a dramatic increase. If the inflection had been similar it might further have been evidence of cpx only fractionation.

7.5 SUMMARY

The xenoliths as a whole group display a wide range of compositions and lithologies. On the whole the xenoliths and their host are chemically coherent on the variation diagrams, so suggesting they are chemically linked in their origin. These microdiorite xenoliths, common in the granodiorite complex of Strontian, are fine grained, variably porphyritic and containing rare quartz xenocrysts. The quartz xenocryst bearing xenoliths are also feldsparphyric. The xenolith found in the biotite granite close to the granodiorite/biotite granite contact (X44 Fig.1.3) is far more MgO

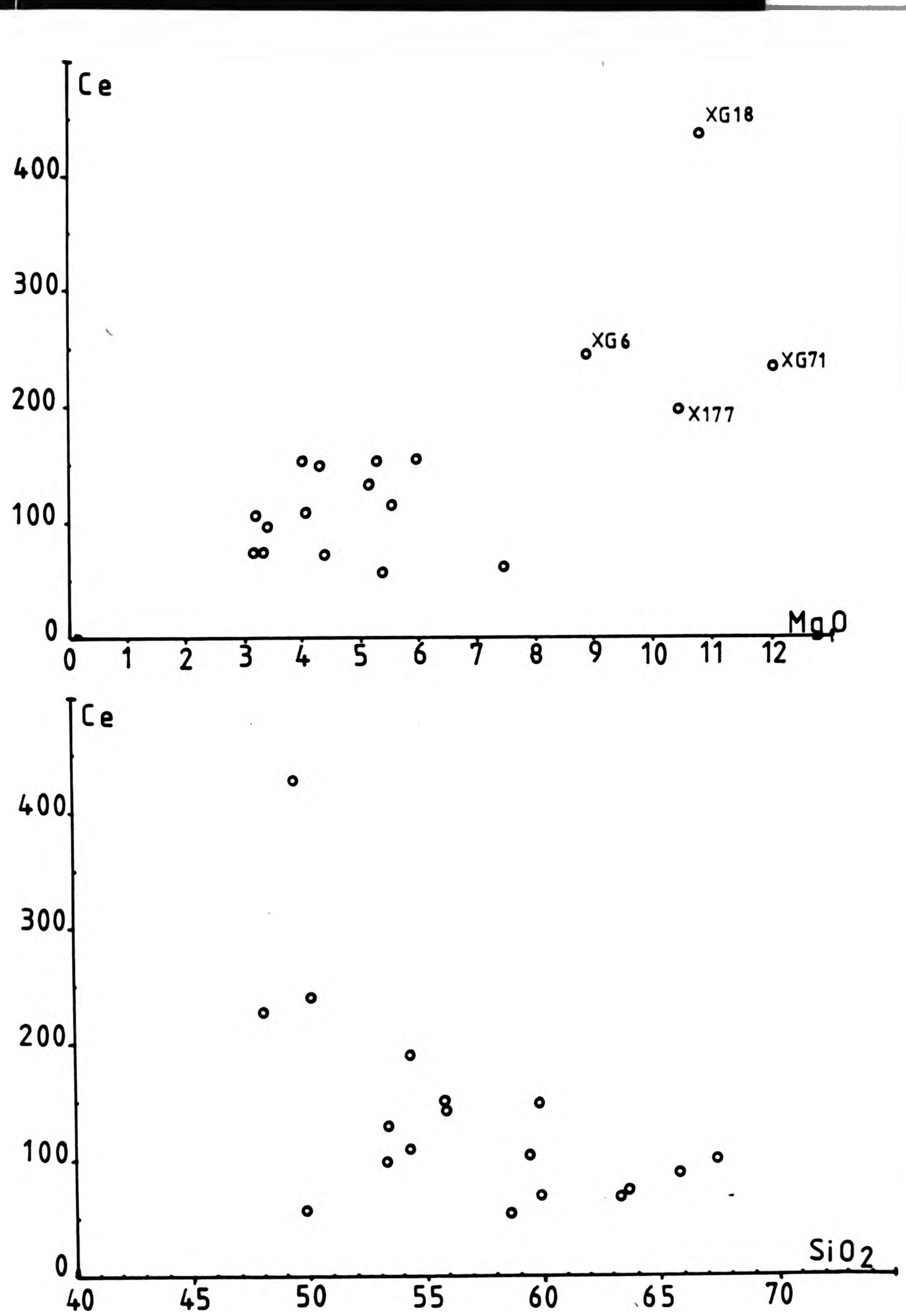

Fig. 7·31A Ce plotted against MgO and SiO_2 for the xenoliths.

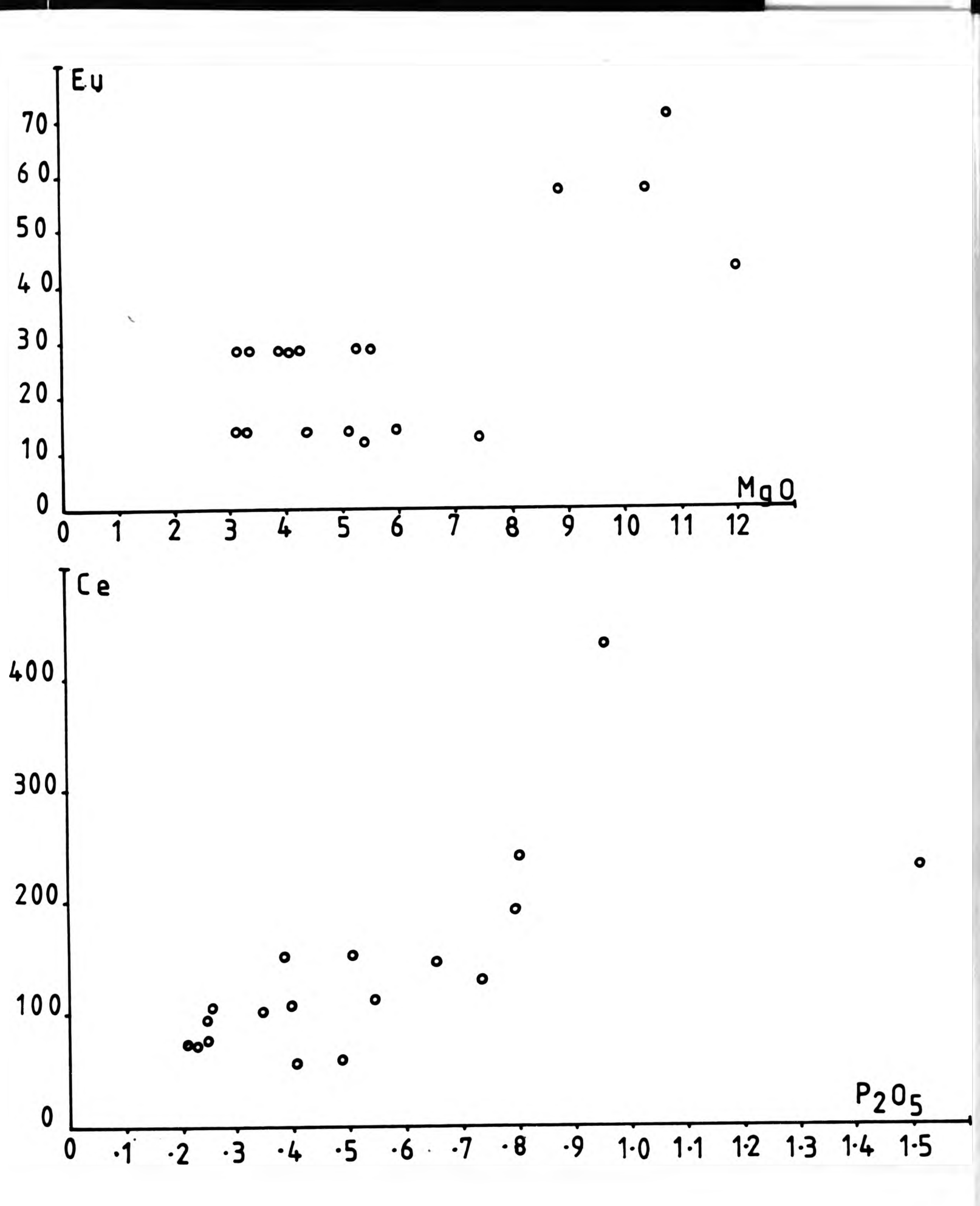

Fig. 7·318 Eu and Ce plotted against major elements MgO and P_2O_5.

and FeO* rich than the others.

The xenoliths though mineralogically so similar to their surrounding host, do have some major differences. Very rare cores of pyroxene indicate that both orthopyroxene (opx) and clinopyroxene (cpx) were once present and that many hornblendes are secondary. Therefore when modelling the trace elements amphiboles are not always included as crystallizing components.

7.5.1 Major elements

These figures have been plotted against silica and not MgO so an easy straight comparison can be made with the granite hosts. The xenolith composition variation could be the result of metasomatism, hybridization and fractional crystallization.

Metasomatism has been investigated in Fig.7 where distance from xenolith margin was plotted against element concentration for uniform looking xenoliths. Potassium showed significant change, decreasing inwards, but overall there was no consistency in the results as Rb increased slightly inwards. The recrystallization of mafics and the exchange of components of granitic interstitial residual melts could have some influence on xenolith composition, but is clearly too small.

The mixing process with a "granitic" magma is indicated by the presence of quartz xenocrysts. The straight line trends can be explained by mixing using an evolved Strontian granite sample as a model end member. It appears, for example, that 50% biotite granite added to a Type 1 xenolith could produce the mean leucocratic

xenolith composition. However it should be noted that the rocks falling off the main trend eg. high CaO and K_2O at <54% SiO_2, cannot be explained this way and applicability is also limited by the changes in pattern and maximums shown on the oxide-MgO plots.

The main variations of the xenoliths all lie on a straight line and the extracts for a fractional crystallization model will lie on the projection of these lines to lower SiO_2 values. The mineral compositions used try to incorporate the full range analyzed eg. the amphiboles include actinolitic-hornblendes to Mg-hornblendes and the plagioclase ranges from oligoclase to labradorite (An29-54). Figures 7.32 to 7.39 display the analyzed mineral data together with the bulk rock xenolith data. If the rock analyses are considered to represent liquids then the parent composition can be seen to range between 47 to 50% SiO_2 and lies inside the triangle field of extract compositions for most elements.

At around 60% SiO_2 there is a break and a change in the trend. This separation is visible on all the plots, but it does not always change direction. It indicates a change in the fractionation process for SiO_2-rich xenoliths. These plots are very similar to those for the host rocks. Similar mineralogy for the xenoliths and host supports the view of a coexisting origin.

Figs.7.32, 7.34, 7.35, 7.36 shows Al_2O_3, FeO*, K_2O and MgO are plotted against SiO_2, with amphibole, plagioclase, biotite and K-feldspar. The potential crystal extract composition (marked X-X on all Figures) ranges from about 40% to 50% SiO_2, which varies from figure to figure. Al_2O_3 has the widest choice for extracts. While CaO, FeO*, K_2O and MgO have a slightly more limited range of extract

FIGURE 7.32 Al2O3 vs SiO2

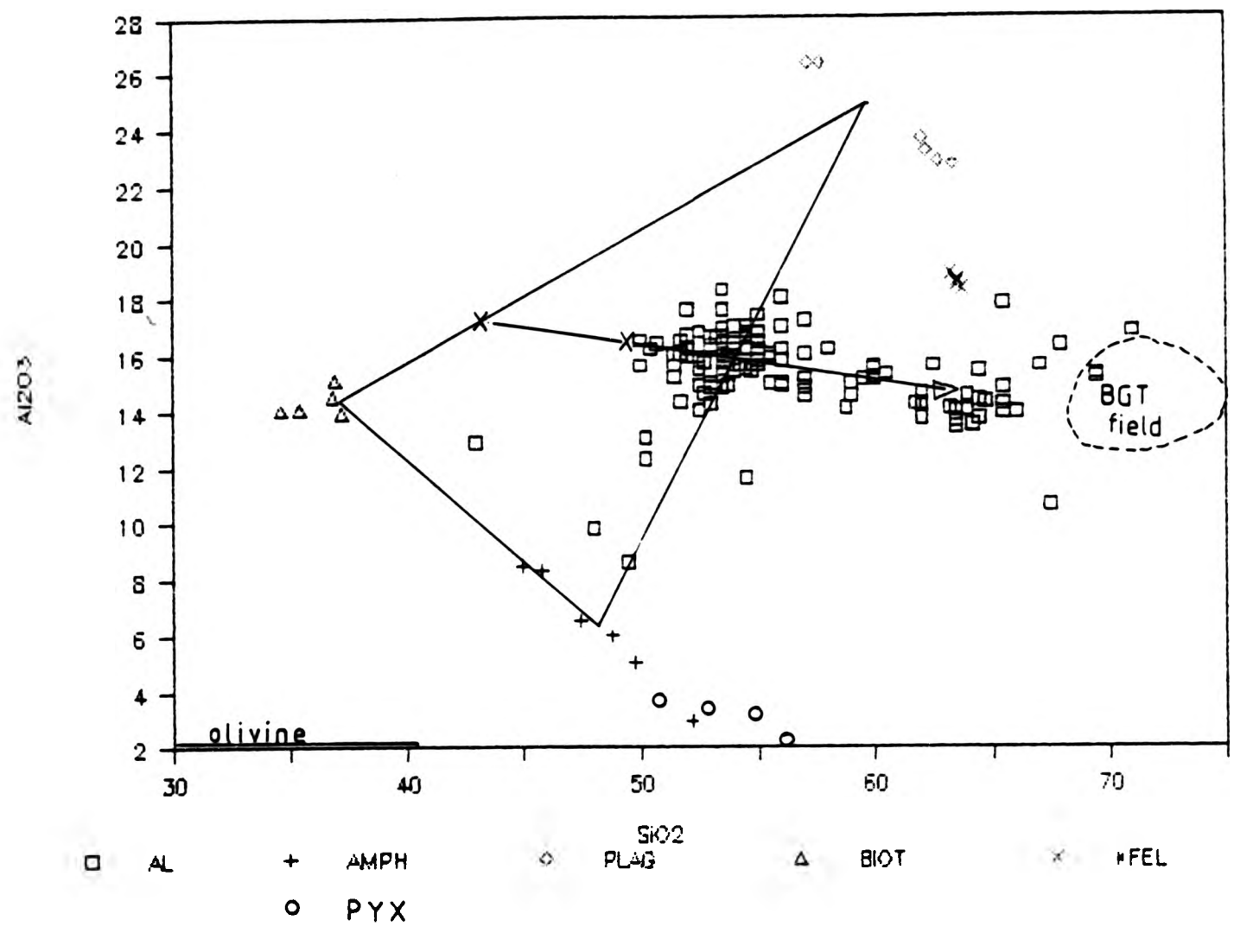

FIGURE 7.33 CaO vs SiO2

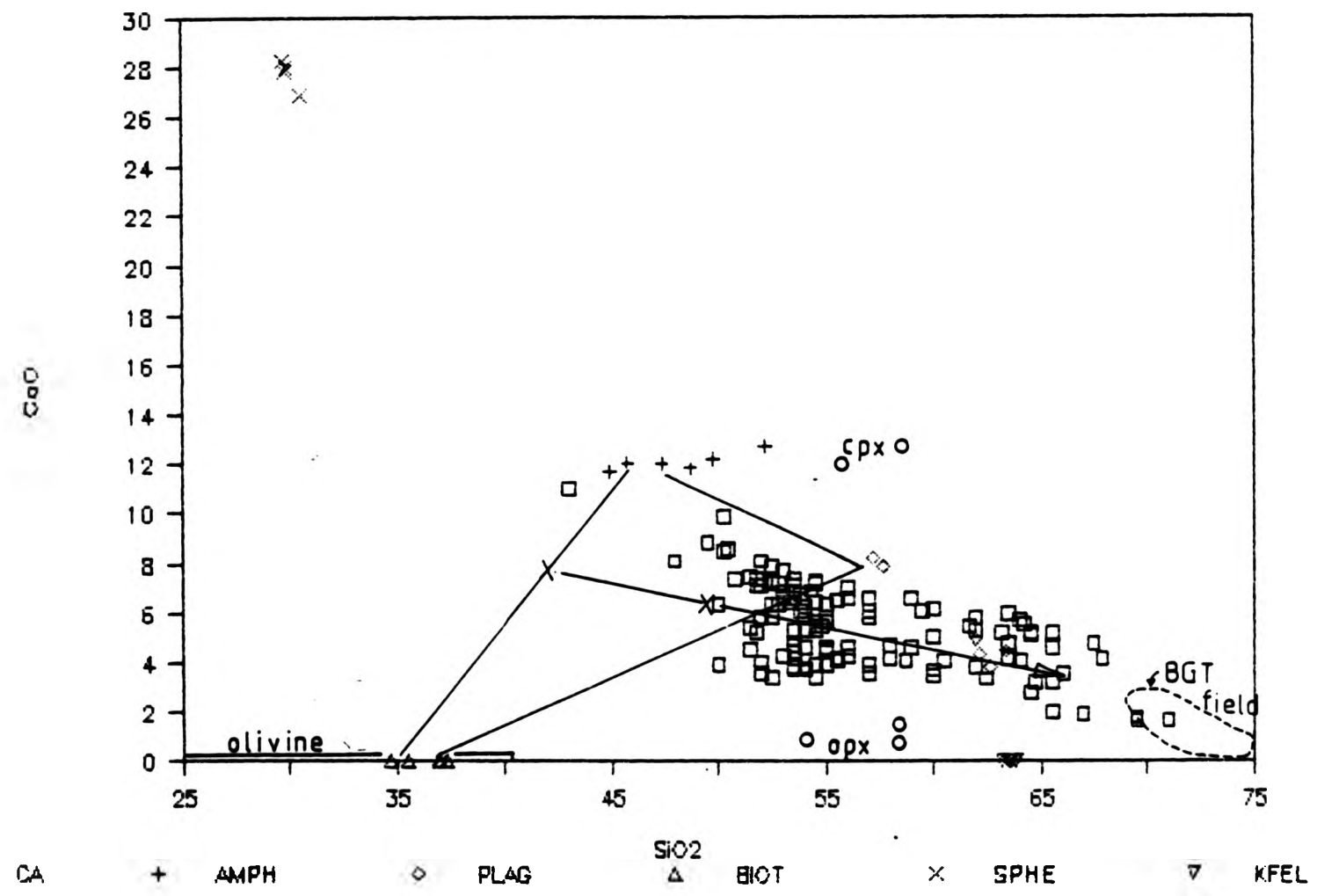

FIGURE 7.34 FeO* vs SiO2

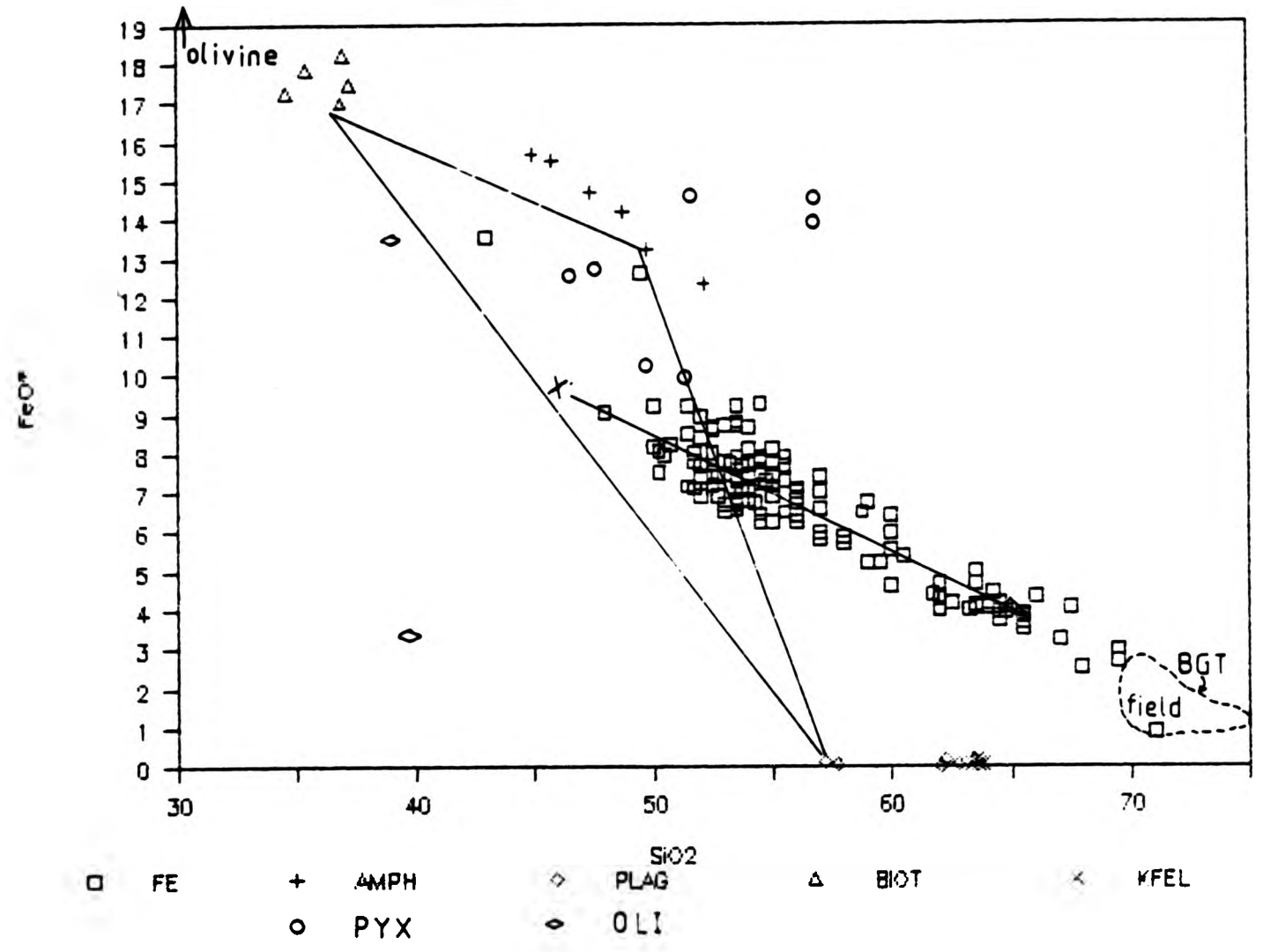

FIGURE 7.35 K20 vS SiO2

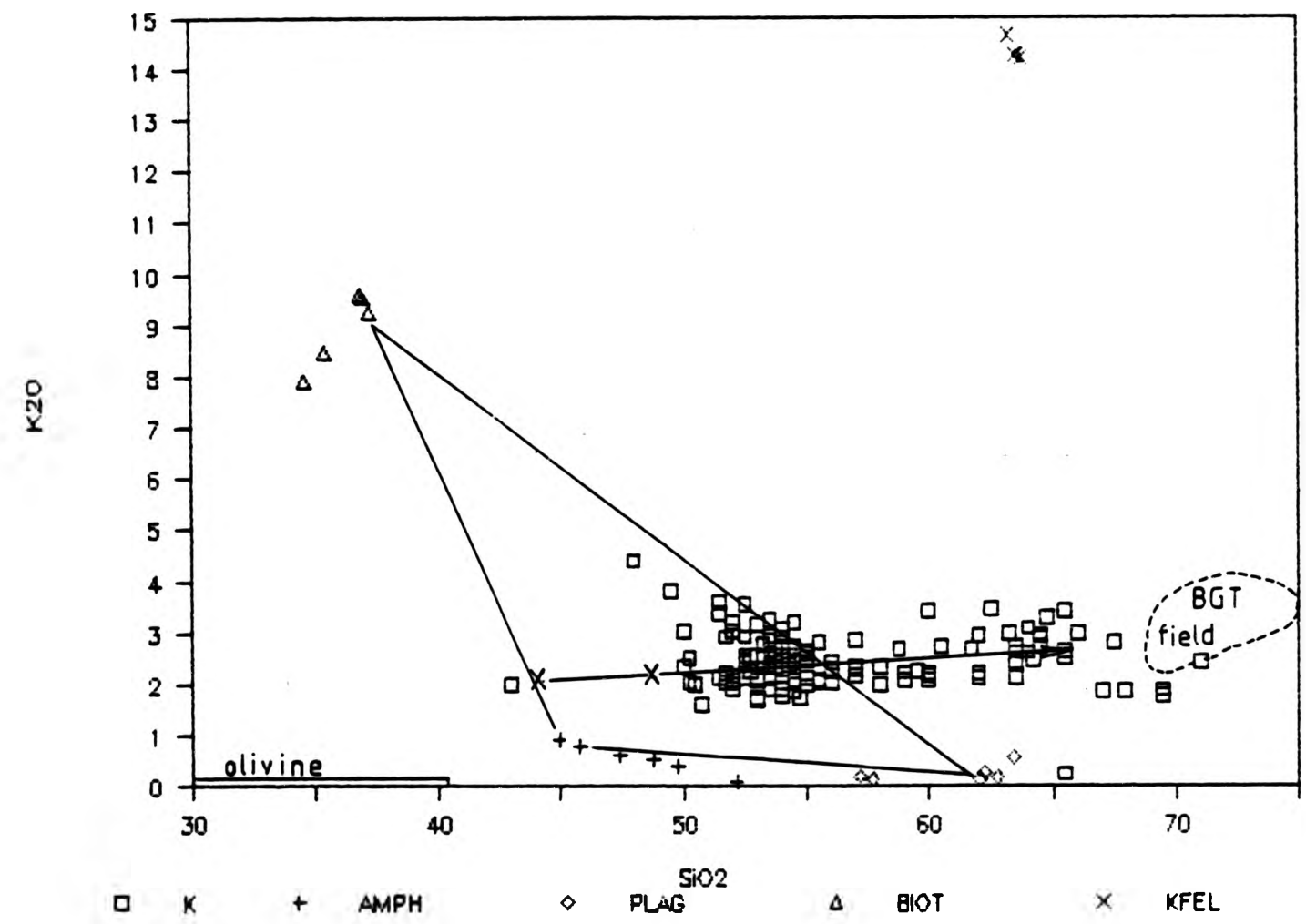

FIGURE 7.36 MgO vs SiO2

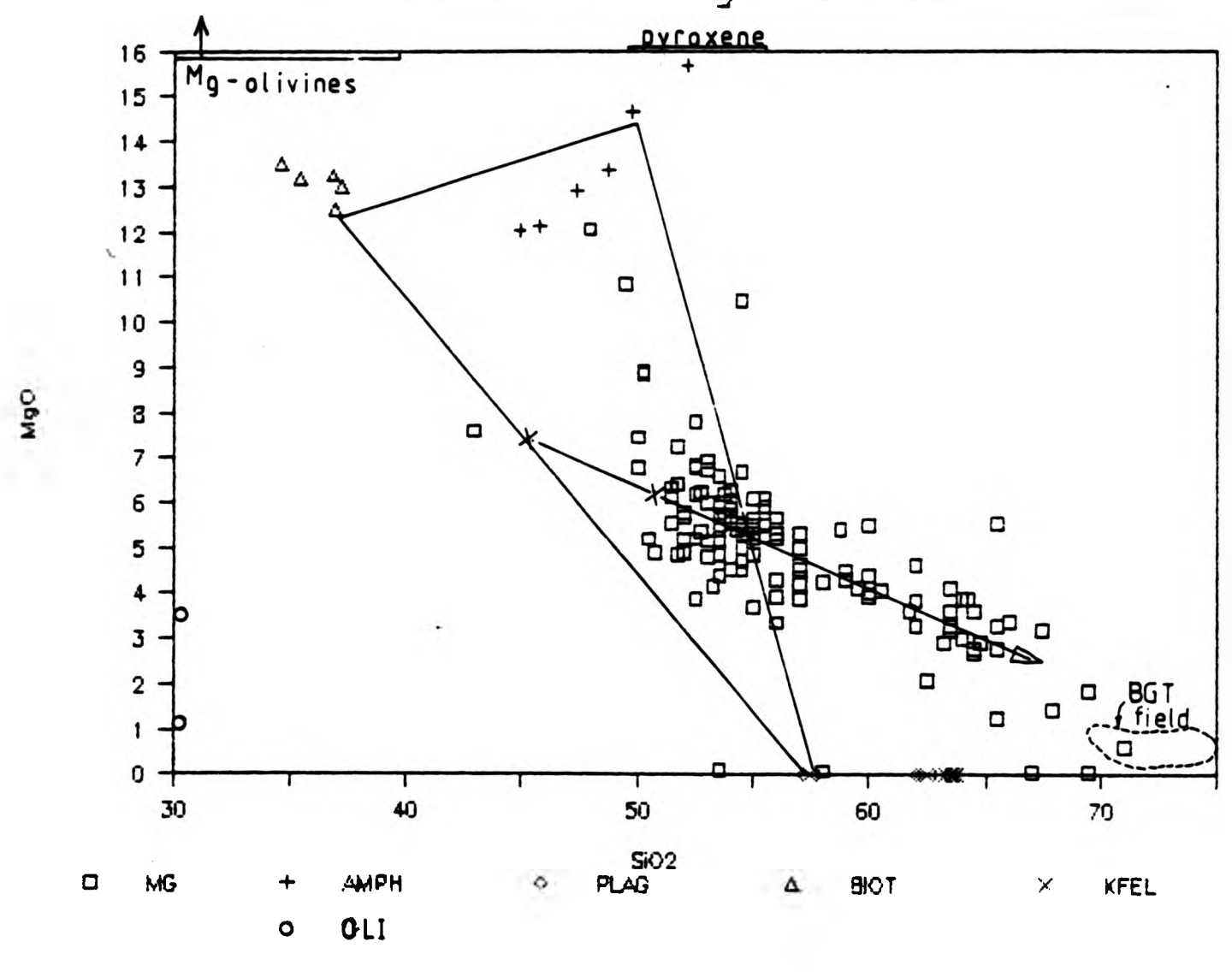

FIGURE 7.37 Na2O vs SiO2

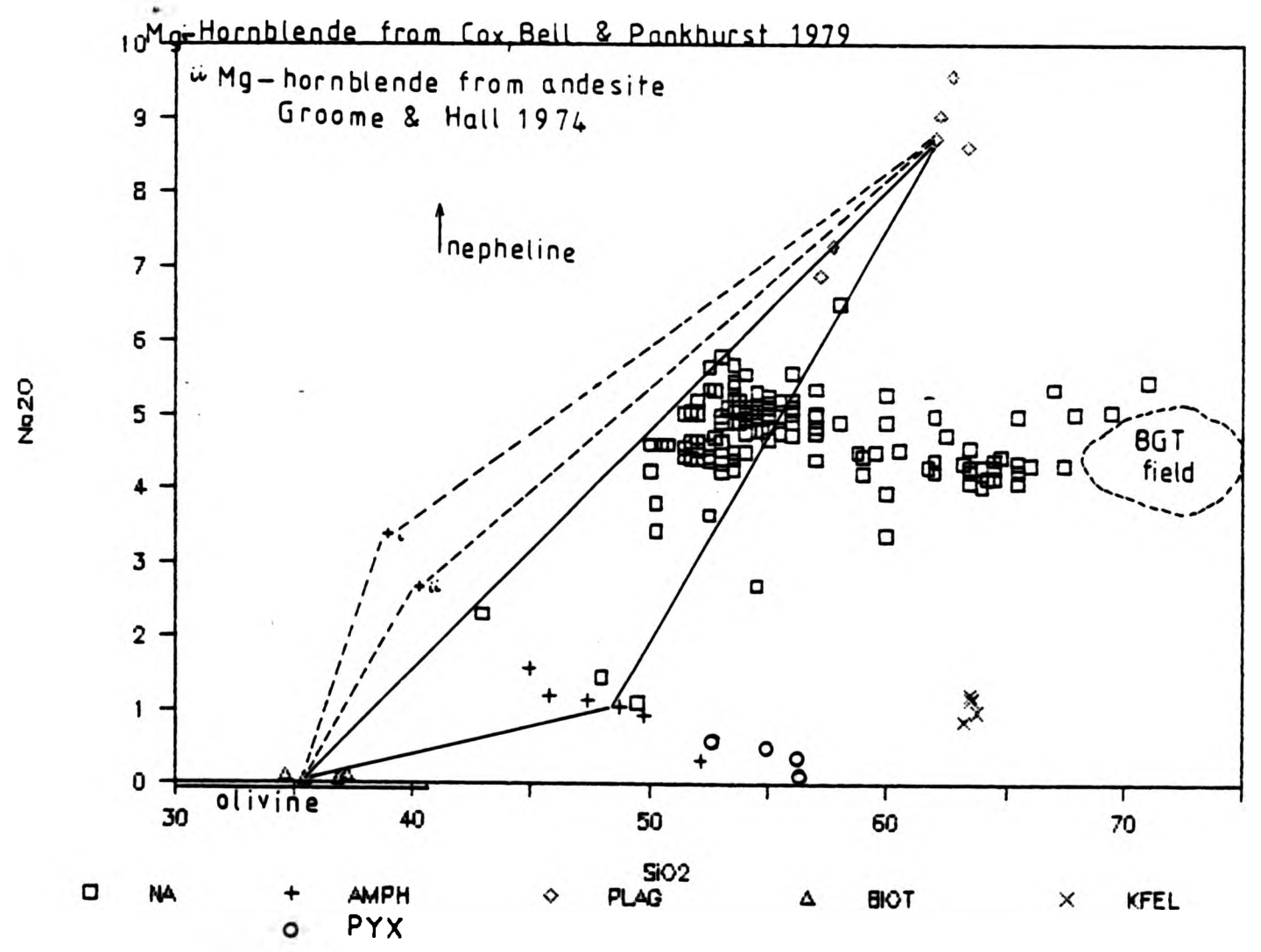

FIGURE 7.38 P205. vs SiO2

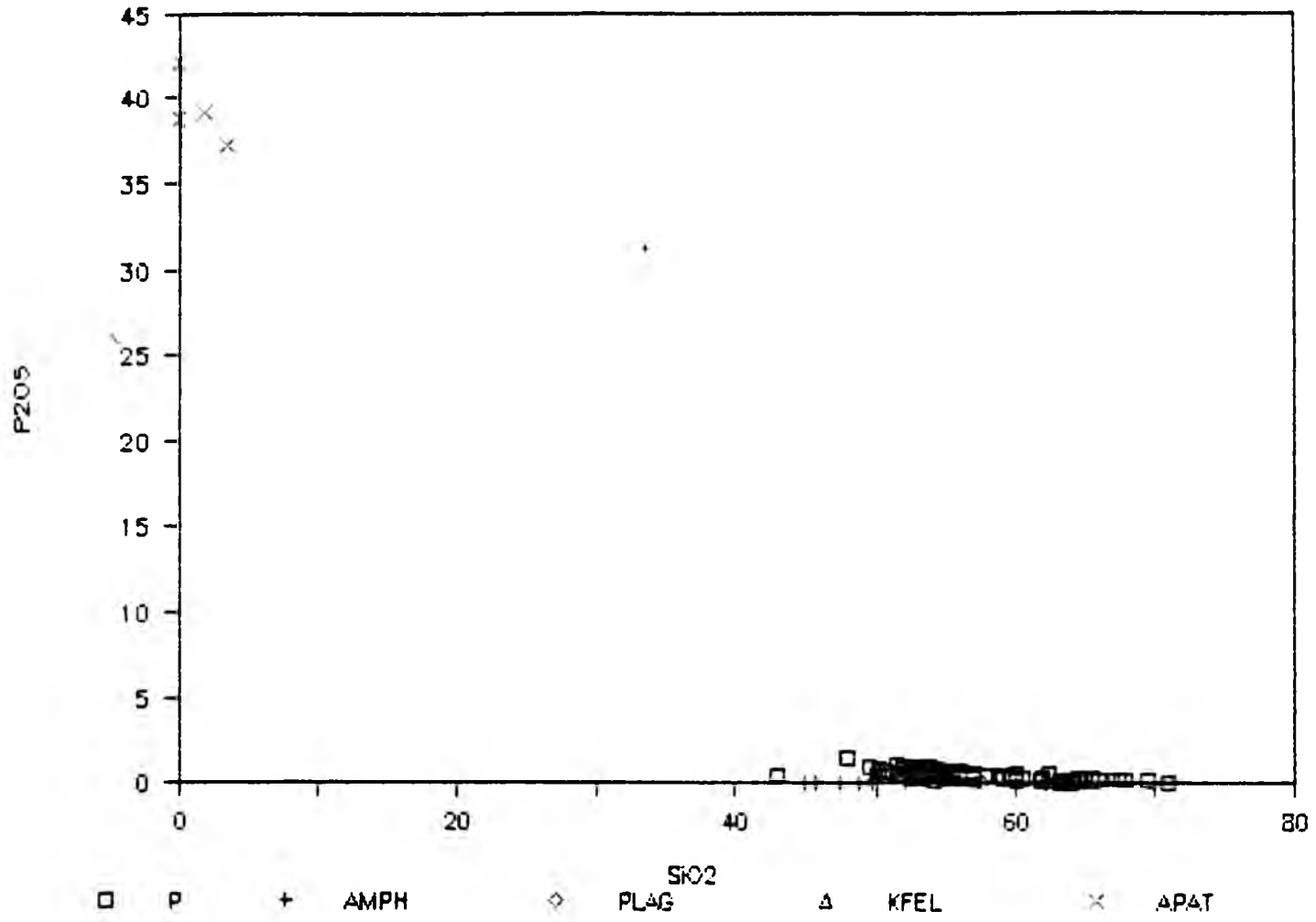

FIGURE 7.39 TiO2 vs SiO2

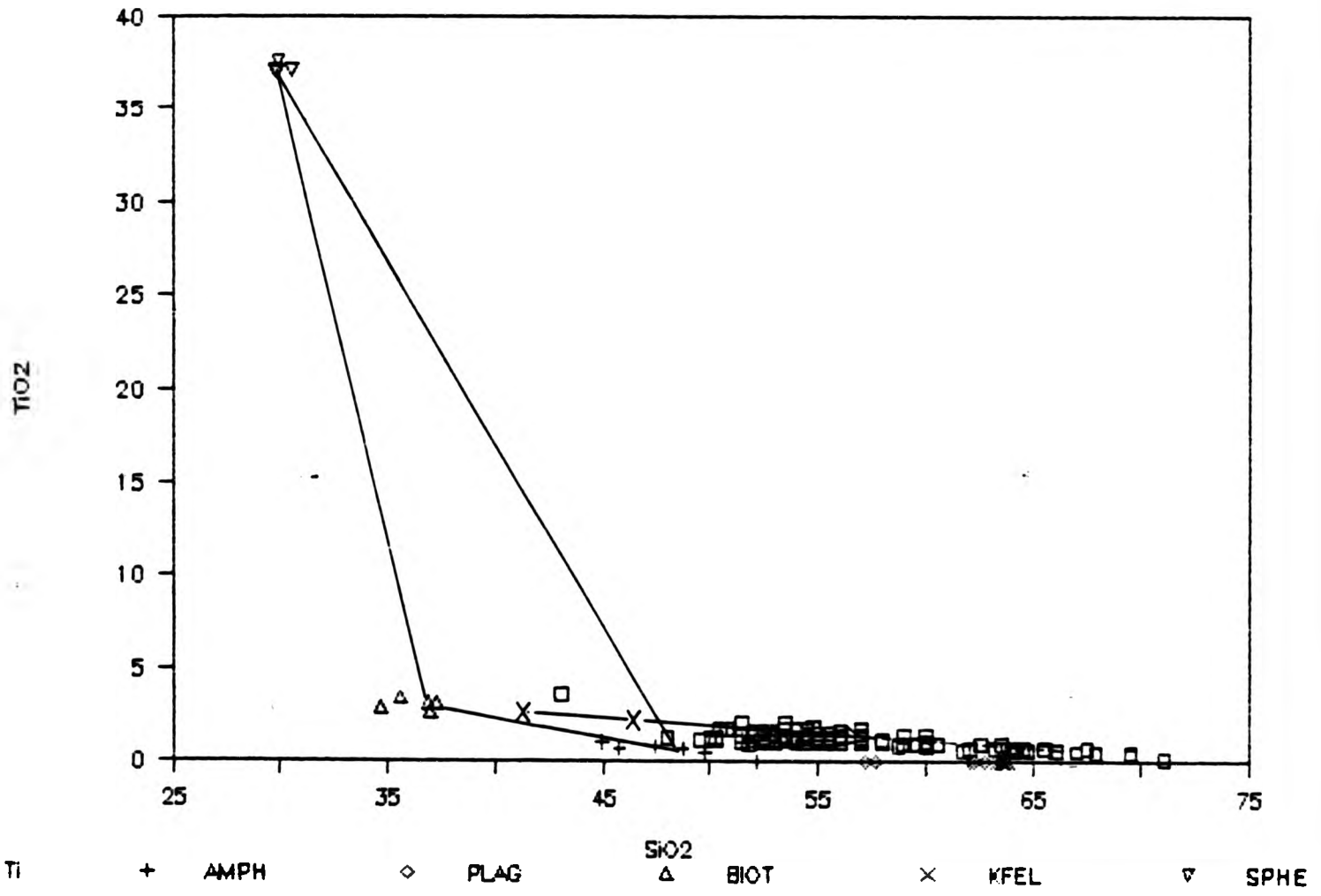

compositions. However Na_2O (Fig.7.37) has the assumed parent liquid lying on the SiO_2-poor side of the triangle and so no extracts within the triangle could achieve fractionation.

The minerals used are from the Type 1A and 5 xenoliths. However there are traces of former anhydrous minerals in the shape of equant hornblende aggregates. This suggests that a different mineral extract eg. opx, cpx or olivine could move the extract to the more SiO_2-poor values. As seen on Fig.7.37, if olivine compositions are added to the Na_2O vs SiO_2 plot then the extract triangle would be moved further to the SiO_2-poor side. This would accomodate the xenolith field more and give a more convincing possibility as to the extracts influencing the trend. Groome for example gives an Appin andesite phenocryst hornblende as 41% SiO_2 and 2.38% Na_2O, which if substituted for the amphiboles plotted reduces the SiO2 in the possible extract. It also reduces the problem with Na_2O vs SiO_2 to a minimum as possible extract compositions would then lie on the end of the observed trend of rock compositions and not overlap completely as in Fig.7.37 at present. This would also support the view that the xenolith amphiboles are not the original magmatic amphiboles, but secondary compositions.

Figs.7.38 of P_2O_5 vs SiO_2 displays a very limited liquid composition range. Apatite being the main phosphorus-bearing phase would only need to crystallize a few percent to drive the trend. A similar pattern is seen on the TiO_2 vs SiO_2 (Fig.7.39), where sphene is the main minor phase crystallizing.

So modelling the xenolith trend under the assumption of X-X being a crystallizing extract from a SiO_2-poor liquid, the observed xenolith

trends could be produced by crystal fractionation of amphibole, biotite and plagioclase, with minor phases such as apatite and sphene for most elements. Approximate extract compositions would have such a range:

40 - 50%	SiO_2
2 - 2.5%	TiO_2
16 - 17%	Al_2O_3
9 - 10%	FeO*
6.5 - 7.5%	MgO
6 - 7.5%	CaO
5%	Na_2O
2 - 2.3%	K_2O

However, the extract percentage would have to be very large in view of the similarity of the assumed parent liquid and possible extracts. In the case of Na_2O, there is no extract for the most SiO_2-poor xenoliths that can change Na_2O in the residual liquid with a concomitant decrease in SiO_2. As phenocryst contents are generally small, the opportunity for generating the linear array by crystal accumulation from SiO_2-rich parents is also limited.

The BGT has been plotted on Figs.7.32 to 7.37 to see the possibility of its playing a role in the contamination of the xenoliths. It does give fairly good explanations for the mean trends. However the weakest plot is MgO with some CaO values not being possible from contamination. Overall there is greater scatter of the xenolith data on these diagrams then the granodiorites. Individual rocks lie well off the main trend eg. Al_2O_3, CaO and MgO, which might indicate the preferential accumulation of hornblende or cpx.

Type 1A and 5 xenoliths were chosen for the IGPET modelling as in a number of Harker plots they appear to fall onto good linear trends. However the overall range is poor for modelling purposes and it is likely that a multiple of processes has occurred. The results are

also poor because an important phase may well have been missed.

TABLE 7.1 SAMPLES AND MINERALS USED IN IGPET

SAMPLES			MINERALS		
Type 1A	XG92	43% SiO_2	Type 1A	Mg-hbl	1...XG65
	XG1	53.5% SiO_2		Eden	3...XG65
	XG65	60% SiO_2		Labr	6C..XG32
	X170A	71% SiO_2		Olig	5C..XG65
				Biot	10..XG32
				Aug	1...D11
				Opx	3...D11
				Orth	14..XG32
Type 5	XG71	48% SiO_2	Type 5	Eden	7C..XG4
	XG70	53% SiO_2		Olig	9R..XG4
	XG60	64% SiO_2		Sph	1R..XG4
				Apat	1...XG4

The graphical extract triangles overlap the primitive xenolith compositions suggesting phases such as olivine are extractable (discussed above). The best fits for the IGPET modelling (Table 7.3) occur at the acid end, where amphibole dominates with plagioclase as the main controlling extract. Type 5 xenolith modelling was not as successful as Type 1A. This may be due to modelling attempted at too great a step.

TABLE 7.2 MIXING XENOLITHS USING IGPET

Parent 1 P1		Parent 2 P2	Hybrid Magma	P1	P2	Residuals
XG1 53.5	+	X170A 71	XG65 60 SiO2	49.8	50.2	8.903
XG92 43	+	X170A 71	XG65 60 SiO2	40.5	59.5	1.283
XG92 43	+	X170A 71	XG1 53.5 SiO2	74.0	26.0	16.689
XG92 43	+	XG65 60	XG1 53.5 SiO2	58.6	41.4	19.436
XG92 43	+	X170A 71	XG60 64 SiO2	18.9	81.1	6.097

In the Harker plots type 1A and 5 xenoliths appeared to show the best trends or ones which were suitable for attempts at IGPET modelling. Table 7.2 shows the mixing of the xenoliths, but with lesser success than expected. This is most probably a result of the ranges being too extreme for the IGPET program as well as too many factors influencing the xenoliths' composition.

TABLE 7.3 FRACTIONAL CRYSTALLIZATION OF XENOLITHS BY IGPET

	1*	2*	3	4*	5	6
Parent	XG65	XG65	XG65	XG65	XG65	XG1
Daughter	X170A	X170A	X170A	X170A	X170A	X170A
Plag	34.3	32.4	38.2	36.4	55.2	17.6
Amph	51.0	49.9	53.0	61.6	-	17.6
Biot	10.6	14.5	8.8	2.0	19.8	70.7
K-fel	-	-	-	-	-	-
Sph	4.1	-	-	-	6.5	11.7
Apat	-	3.2	-	-	-	-
Pyx	-	-	-	-	18.5	-
Daughter%	49.9	52.4	47.9	45.9	37.0	15.2
Residuals	0.631	0.799	1.390	2.984	7.039	36.833

	7	8	9	10	11	12
Parent	XG1	XG1	XG60	XG71	XG70	XG71
Daughter	X170A	X170A	X170A	XG60	XG1	XG60
Plag	33.5	33.2	37.6	7.3	67.0	8.0
Amph	33.6	33.4	52.2	58.5	-	92.0
Biot	32.5	32.5	10.1	30.5	30.7	-
K-fel	-	-	-	-	-	-
Sph	-	0.6	-	-	-	-
Apat	0.4	0.2	-	3.6	1.7	-
Pyx	-	-	-	-	-	-
Daughter%	9.900	10.0	78.7	19.9	44.0	18.2
Residuals	19.600	19.548	9.289	21.109	13.842	31.494

* models used in trace element modelling

7.5.2 Trace Element

The log-log plots for trace element modelling include Rb:Ba, K:Rb and Ba:Sr (Figs.7.40 to 7.42) and REE Ce:Yb (Fig.7.43). The mineral vectors have been calculated using the partition coefficients in Table 7.4.

Table 7.4 PARTITION COEFFICIENTS FOR TRACE ELEMENT MODELLING FOR THE XENOLITHS AND DIORITES

	K	Rb	Ba	Sr	Ce	Yb
Plagioclase	0.200	0.070	0.200	2.20	0.100	0.03
Cl-pyroxene	0.002	0.001	0.001	0.07	0.100	0.28
Or-pyroxene	0.001	0.001	0.001	0.01	0.003	0.05
Amphibole	1.000	0.300	0.400	0.50	0.200	0.49
Biotite	2.700	3.100	1.100	0.08	0.030	0.04
K-feldspar	-	0.040	6.000	-	-	-
Sphene	-	-	-	-	80.00	60.00
Apatite	-	-	-	-	25.00	25.00
Garnet	-	-	-	-	0.02	4.00

Source: Cox, Bell & Pankhurst (1981).

The trends are linear for K-Rb (Fig.7.41) and Ce-Yb (Fig.7.43); while in Ba-Sr (Fig.7.42) and for Ba-Rb (Fig.7.40) (also Ba-Y) they are non-linear. This variation supports the view of a number of processes going on. Wholly fractional crystallization cannot be accepted for the modelling of the xenoliths, as from field observations there is some evidence of mixing. The xenoliths also have overlapping trends with their host rocks, so suggesting that the processes controlling the development are mutual. Vectors are drawn from an arbitrary point in each diagram. The vectors represent liquid compositions for the simplest model. The modelled data here limits the crystallizing phases, allows an assessment of the data and the processes involved. The calculations made here were on the assumption of a closed fractionating system. However the scattered points of the xenoliths suggests this was not the case.

Figure 7.40 Ba vs Rb shows the majority of the xenoliths fall in a highly scattered pattern completely enclosing the granite fields. The Ba variation is not controlled by K-feldspar fractionation. It should be noted that there is no coherent variation of Ba vs MgO (Fig.7.12), which also supports this question. Separation or accumulation of the other phases would generate the spread in Rb values. The scatter of the xenolith data points to a combination of processes such as fractionation and mixing. The crystallization of biotite would deplete the liquid of Rb and possibly the variable amounts of modal biotite present could account for this scatter in data points of Rb and Ba. Type 1A xenoliths give a more restricted linear trend with a wide variation in Ba for a little change in Rb. This linear feature does not produce a unidirectional order of SiO_2 values, as seen on Fig.7.40A. Low SiO_2 rocks occur at the extremities, while high SiO_2 rocks are found in the middle and near the BGT field.

The scatter of xenoliths on the Ba-Rb plot is too difficult to accomodate by simply using the percentages from the IGPET fractional crystallization model. The 2 vectors, CL1 and CL2, would produce the trend seen within the diorite field and also the diorites.

The IGPET models used are modelling XG65 to X170A (Table 7.3):

CL1 (no. 2) Amph 51.5%, Plag 33.5%, Biot 15.0% (no apatite)

Cl2 (no. 4) Amph 61.6%, Plag 36.4%, Biot 2.0%

Figure 7.41 K vs Rb displays a linear trend of increasing K with increasing Rb, overlapping the field of the host rocks. Mineral vectors for opx, cpx, plagioclase and biotite would clearly influence the linear trend of the xenolith data points with only 0.6 of the

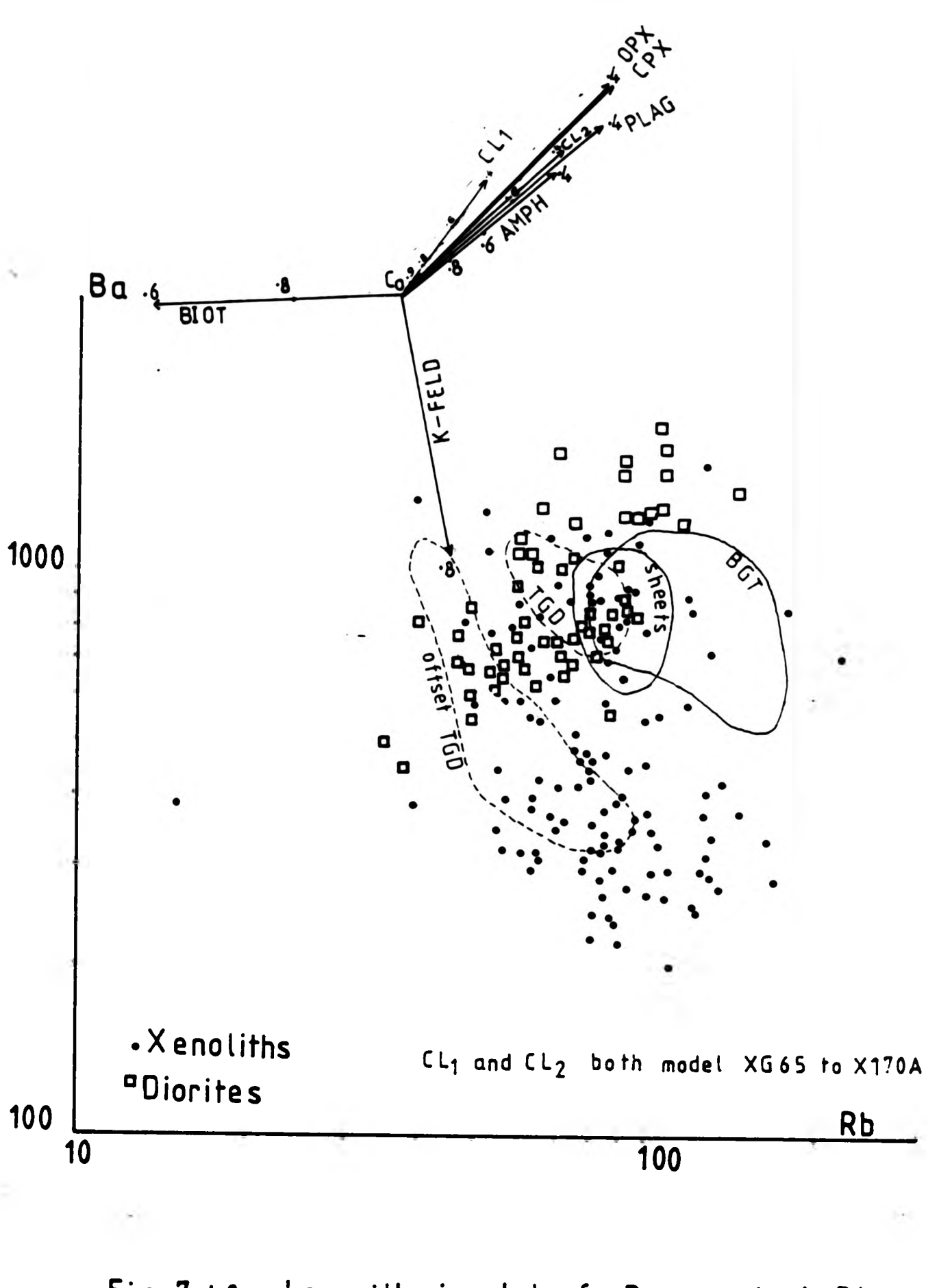

Fig. 7·40 Logarithmic plot of Ba against Rb for the xenoliths & diorites.

Nos. on vectors = residual liquid fraction

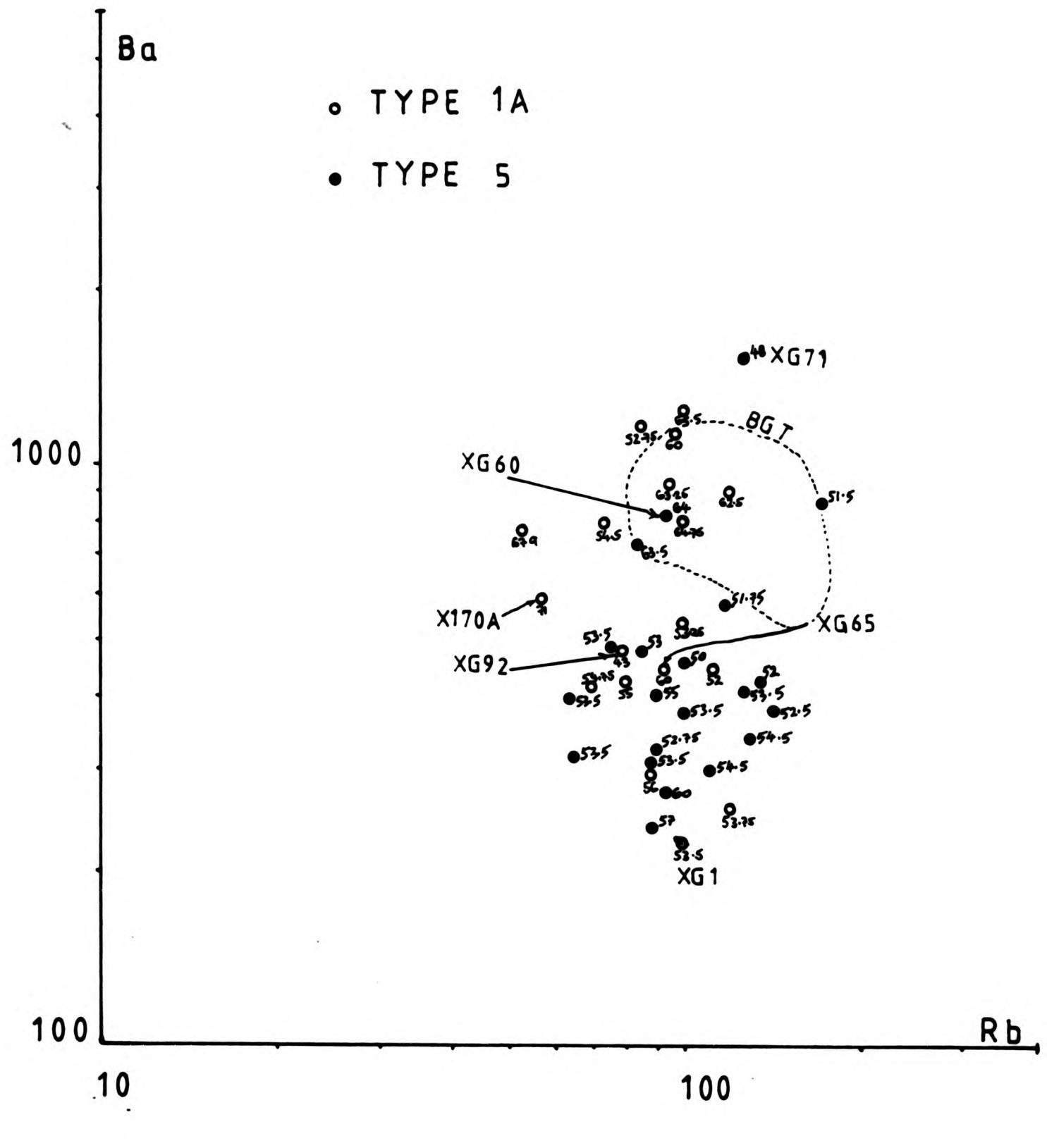

Fig. 7·40A Type 1A and 5 xenoliths showing distribution of SiO_2

Samples named used in IGPET.

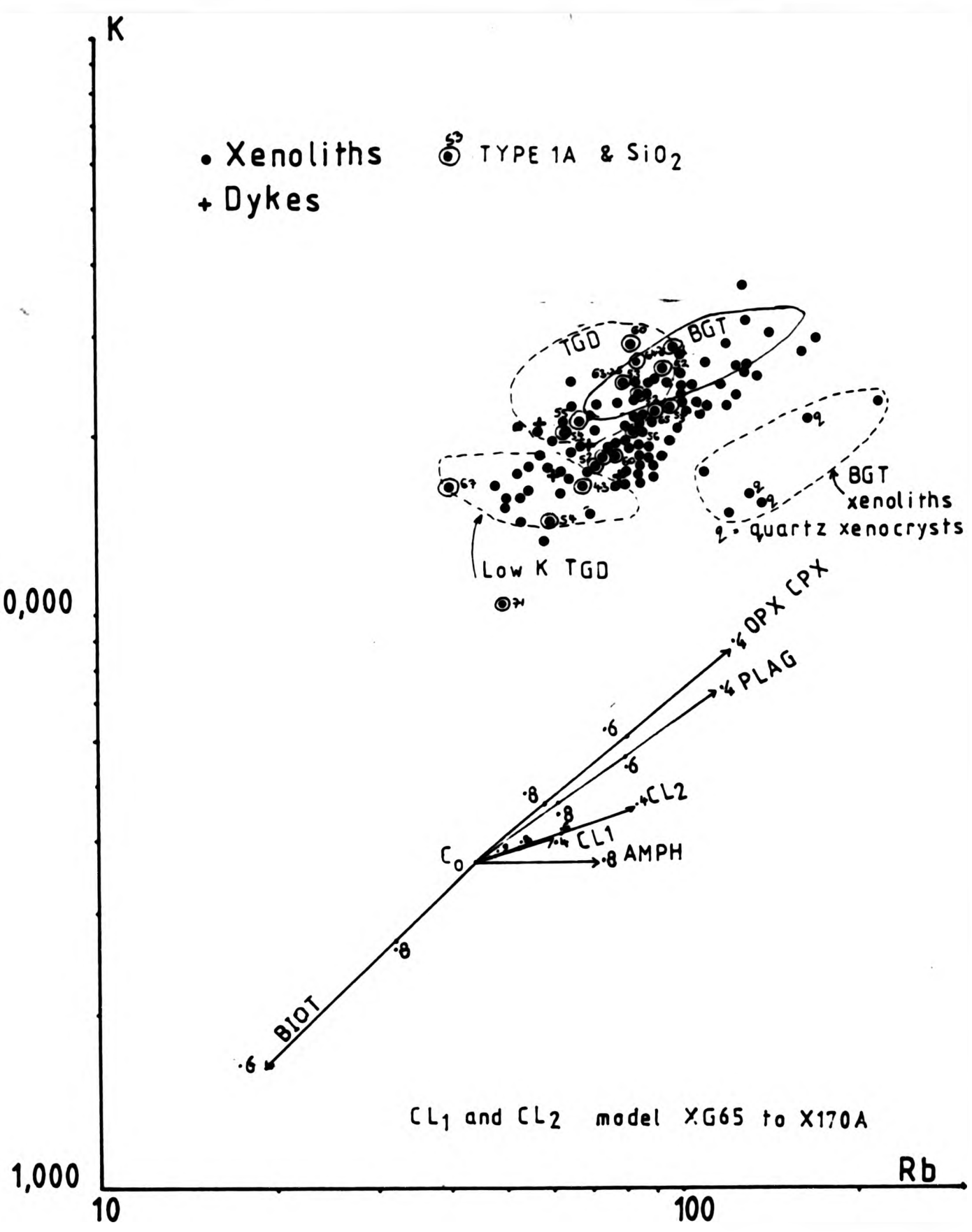

Fig. 7·41 Logarithmic plot of K against Rb for the xenoliths & dykes.

Nos. on vectors = residual liquid fraction

liquid fraction left, with plagioclase and pyroxene being more important. The BGT xenolith group requires an amphibole dominated extract to bring this off the main trend. The quartz xenocryst xenolith field are obviously contaminated xenoliths, but it is odd that they lie off the main trend and away from the bulk BGT field.

The Type 1A xenoliths are scattered throughout the main trend, together with the SiO_2 values, which have a random pattern. The variation shown in Fig.7.41 is very large and needs a large amount of plagioclase and amphibole extraction. Any biotite removal makes it impossible to achieve the range by fractional crystallization. Both CL1 and CL2 vectors plot very closely together as the biotite vector opposes the plag & pyx and so will reduce the overall effect.

Ba vs Sr (Fig.7.42) is very similar to Ba vs Rb (Fig.7.40) as a result of the wide variation of in Ba. The large xenolith field displays a rapid decrease of Ba with decreasing Sr (Fig.7.42), with a small overlap with the main granite field. Type 1A xenoliths (Fig.7.42A) show a scattered pattern of SiO_2 values from the most Ba-poor to Ba-rich. Type 5 xenoliths also form a scattered plot. The range of Ba is outside the realms of possibility of fractional crystallization. The spread of Ba values would seem to require a very large extract yet SiO_2 or MgO variation is small. Fractional crsytallization is possibly not a good model for the Ba field range. This central part of the trend is associated with high SiO_2 and may reflect contamination with BGT-type material. The disordered SiO_2 also limits hybridization as this will order them and though they will not lie on a straight vector. The low Ba and low K of the TGD falls in the low Ba region of the xenoliths, but the SiO_2 of the xenoliths and TGD is very different, so the association may be

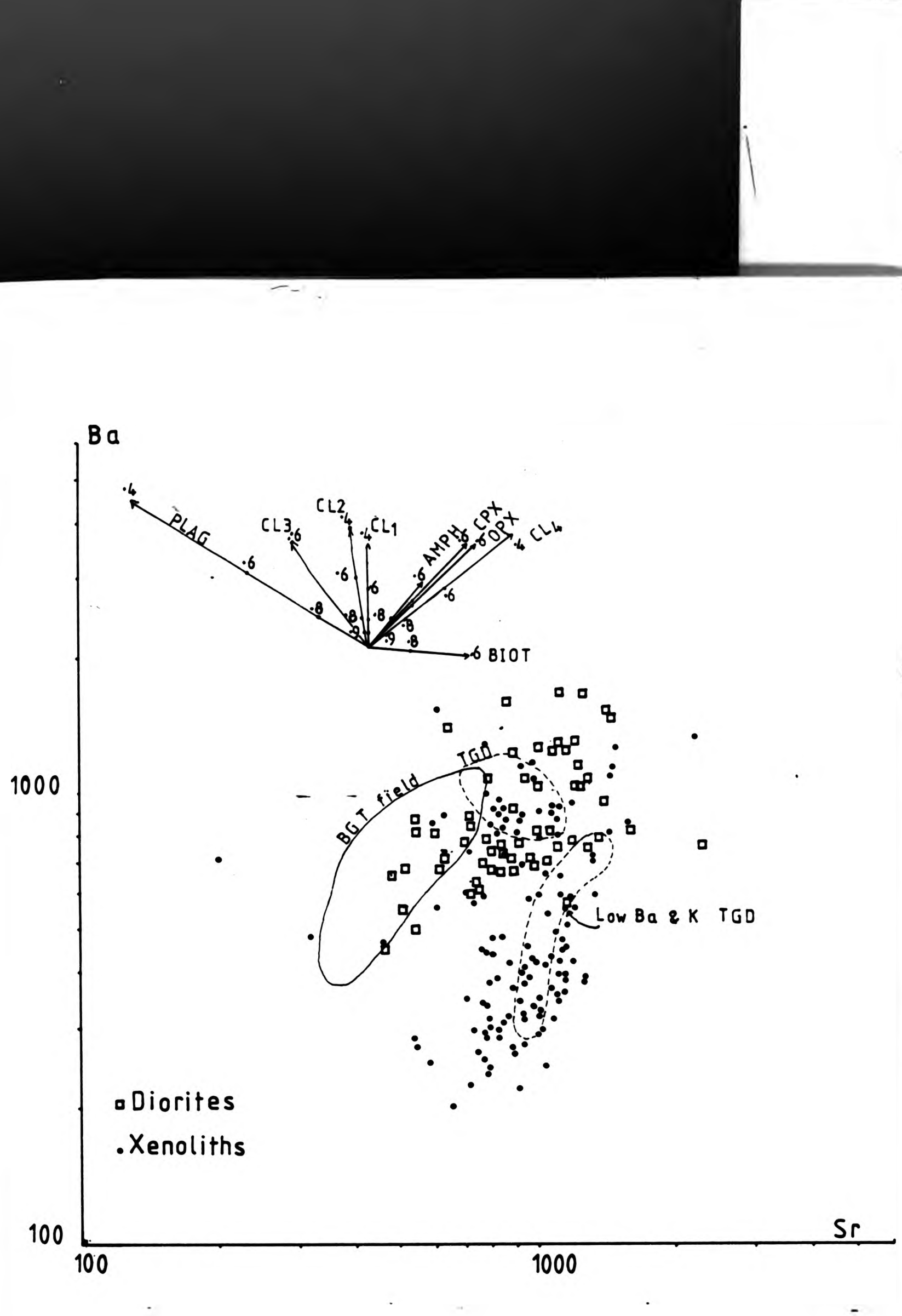

Fig. 7·42 Logarithmic plot of Ba against Sr for the xenoliths & diorites.

Nos. on vectors = residual liquid fraction

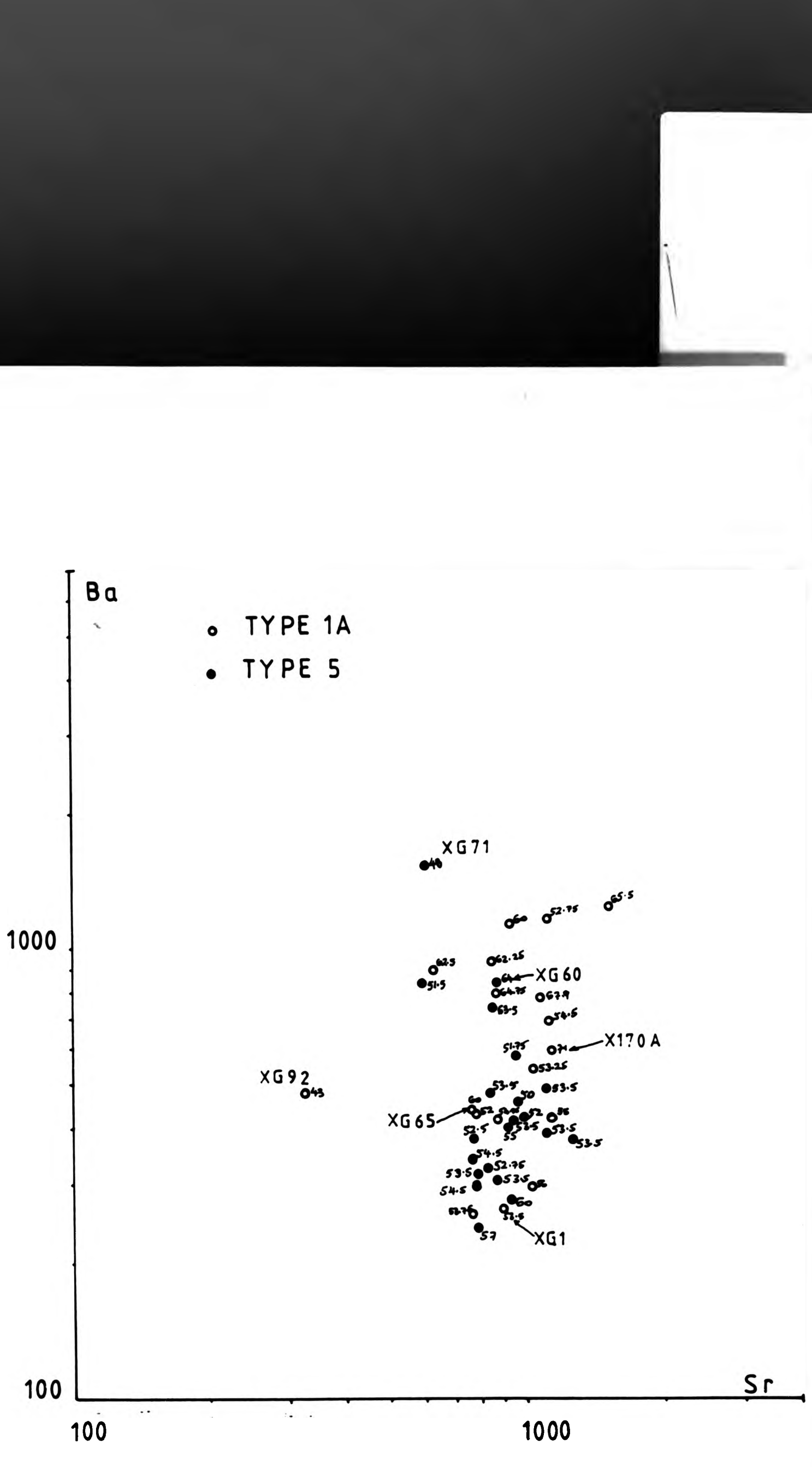

Fig. 7·42A Type 1A and 5 xenoliths showing the distribution of SiO_2

Samples named used in IGPET.

chance. Using the IGPET models, CL1 & CL2 produce vectors which would cover the upward trend of the Ba trend. While CL3 & CL4 are not generated from IGPET, but from the mineral vectors themselves. CL3 is generated from 75% plag and 25% opx; while CL4 is a combination of of 45% opx + 10% cpx + 10% plag + 35% biot.

Fig.7.43 displays the REE Ce vs Yb of the xenoliths. They fall in a linear trend with increasing Ce with increasing Yb and mainly within both the granite and diorite trends. Again there is no order to the SiO_2 values. Only the Type 3 xenoliths plot on the Ce-Yb richer end, because of their greater amphibole content then the other xenolith types (REE in amphibole discussed in chap.4, section 4.4.1). This trend is different from the other plots as it either requires extensive major silicate fractionation or several percent crystallization of accessories. However there is no real evidence of any accessories in a phenocryst assemblage. Vector CL1 uses the same mineral proportions as in the other figures and would successfully drive the liquid up, while CLA (no.1 Table 7.3) contains 4.1% sphene which reverses and strongly influences the vector.

7.6 SUMMARY

The origin of xenoliths could conceivably be: 1. partly crystallized, quenched margins of the granites; 2. repeated mingling of a variety of more mafic or hybrid magmas with the granite; 3. a more mafic layer within the pluton which is mixed with the granitic material and 4. the result of partial melting of an igneous parent (possibly quartz diorite, Tindle & Pearce 1983). Figs.7.32 to 7.42 investigate the possibilities that fractional crystallization could develop the observed trend. The xenoliths show too great a range of petrography and scatter in the geochemistry to be able to put down their origin

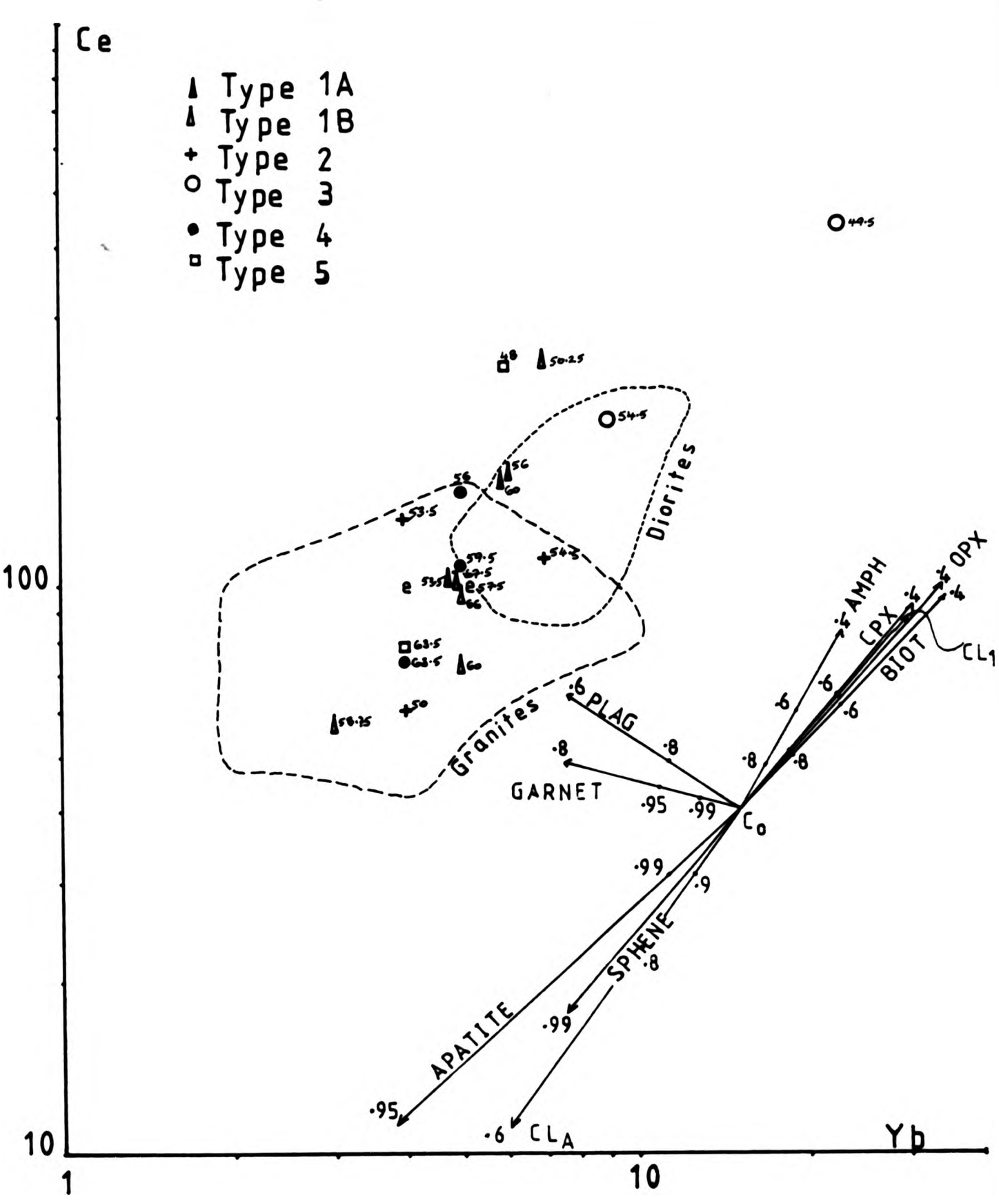

Fig. 7·43 Logarithmic plot of Ce against Yb for the xenoliths.

Nos. on vectors = residual liquid fraction

60 = SiO_2 values

merely to fractional crystallization. However the effects of mixing should not be disregarded. The presence of plagioclase with resorbed cores, K-feldspar megacrysts with oligoclase rims and rounded quartz xenocrysts with mafic rims is mineralogical evidence of hybridization. The mineralogy is similar to the phenocryst assemblage in granites that have reached the Qz -feld cotectic, and would be the only record when the granite magma is completely mixed with xenoliths. Therefore the xenoliths may be products of magma mixing either at depth in the same pluton, or at a site located away from the present level of exposure. The coexistence of xenoliths with variable compositions and microstructural evidence of hybridization, suggest that the xenoliths could be produced away from the present site of exposure. Vernon (1983) states that the mixing of a variety of magmas of a granitic suite would help explain the compositional range of xenoliths. Also magma mixing would explain the rarity of more acidic/felsic xenoliths in the host rocks, as acidic melt in mafic melt would disappear more quickly than mafic melt in acidic melt (Kouchi & Sunagawa 1982; 1983).

There is moderate success with the major element fractionation model, which is similar to the level of success with BGT-type contamination for majors. The xenoliths Harker plots display a variety of patterns eg. Type 1A in Figs. 7.12, 7.22 & 7.26, especially in the trace elements. This would limit the mixing models for the MgO-poor compositions. While the wide range of Ba, K_2O, REE at 50+/-1 SiO_2 exceeds the limits of normal fractional crystallization and therefore points to diverse immediate parents to the xenolith magmas.

Chapter 8 THE MICRODIORITE DYKES

8.1 INTRODUCTION

Four microdiorite dykes have been found cutting the granodiorite pluton (Fig.1.2, Locations named - md), in addition to the microdiorite - granodiorite composite intrusion described in chapter 2. They were not reported by either MacGregor & Kennedy (1932) or Sabine (1963) and are not on the B.G.S. map. Exposure is poor and extremely limited, being restricted to stream sections. The dykes have not been observed cross-cutting the biotite granite sheets or vice versa, so their time relationship cannot be accurately assessed. However an occasional aplitic vein has been seen crossing the dyke into the surrounding granodiorite, so post dating both.

8.2 OCCURRENCE IN THE STRONTIAN GRANODIORITE

They are very fine grained , medium grey dykes were found varying in width from 0.75 to 3 metres. The dykes trend from 030º to 062ºN dipping 80ºSE, where dip measurement is possible.

They have sharp undulating contacts showing signs of slight chilling with the surrounding host. There is also, in all the dykes seen, a lineation and foliation, that is picked out by the alignment of biotite, which is best developed at the contact and dies away inwards. The foliation is oblique to the contact and is cut off at the contact. It is picked out by small biotite crystals of < 3mm in length, which have all become aligned in the process. The adjacent granodiorite is also very biotite rich.

Dilational features such as veinlets, are noted along the contact infilled with later stage feldspar and quartz, cutting the dyke. This material is part of the host granodiorite and not the dyke. The sharp contact displays a slightly metamorphosed chilled surface with the foliation/lineation in the dyke. Tiny apophyses of the dyke material pass into the granodiorite. These apophyses are present at or very close to the granodiorite contact and are located along the length of the whole outcrop. They are small in size, reaching a maximum length of 20mm and are elongated in shape. Small globules of microgranite are also present.

8.3 PETROGRAPHY AND MINERALOGY

These dykes are medium grey and fine grained. They are very mafic-rich and porphyritic with upto 5% feldspar phenocrysts, often alkali feldspar. They do not possess their original igneous texture, but show variable stages of development of a granoblastic texture and foliation.

Plagioclase and alkali feldspar are both found in the groundmass as well as phenocrysts. Both phenocrysts show definite subhedral crystals. The alkali feldspar in the dykes is mainly present as phenocrysts and is clustered around Ab6-7 Or94-93 An 0. They reach 10mm in length.

Plagioclase compositions range from An39-22 in the groundmass (within the xenolith range) and show compositional normal and reverse zoning (Fig.3.4C). A large plagioclase phenocryst found in a single example

has a very gentle compositional change from core to rim of An34-An31-An33-An29-An23 displaying some oscillatory zoning. They have a smaller range of overlapping plagioclase compositions than the xenoliths, with rims of An22-31, middle An25-34 and cores An30-36.

Occasional fresh plagioclase feldspars are found in equilibrium with the dyke. They often have a highly altered zone close to the crystal margin, which has many inclusions of rounded biotites and acicular apatites. Occasional myrmekitic intergrowths have been noted too. While others are turbid throughout with only remnants of unaltered plagioclase, though all inclusions are altered too.

Biotite and hornblende are the main mafic minerals present in the groundmass, as individual euhedral to subhedral grains or in small aggregates together. Occasional larger crystals of hornblende are found, showing alteration. The aggregates also suggest they are altered earlier formed mafic minerals.

The dominant amphibole in the dykes are actinolitic hornblendes, with some magnesio-hornblendes and very occasional edenitic hornblendes. They all appear dark green in colour. The dykes plot on the MgO/MgO+FeO* (amph) ratio against the MgO/MgO+FeO* (rock) ratio (Fig 6.3) in the middle of the xenolith field of decreasing amphibole ratio with decreasing rock ratio. The MgO/MgO+FeO* ratios of the individual amphiboles varies throughout all the thin sections from: 0.527 to 0.581 for actinolitic and 0.419 to 0.555 for the magnesio-hornblendes (again actinolitic hornblendes with more MgO). The dykes have a similar pattern to the xenoliths of increasing amounts of Al substitution from the actinolitic hornblendes to the magnesio-hornblendes and rare edenitic. Due to the fine grained

nature of the dykes any zoning in the amphiboles was too difficult to assess during probing. On Figs. 6.2 and 6.3 the dykes amphibole plot very closely to the host rock and xenolith fields.

The hornblendes of the dykes show a pressure range of <1 to 5kbar (Hammarstrom & Zen 1986; Hollister et al 19870. After using the regression equations in chapter 3 similar values were calculated in Table 8.1. The actinolitic hornblendes give the lowest pressures of less than 1kbar, supporting the view that they are secondary. This is the case for the xenoliths too.

Table 8.1 PRESSURES FOR THE DYKES

Total Al in amphibole	Pressure in literature	P from regression eq. 1	2
E1			
0.8715-1.725	<1 - 5	0.46-4.81	0.96-3.84
E3			
0.8512-1.2985	<1 - 3	0.36-2.61	0.92-2.15
E5A			
0.6352-1.0009	<1 - 1	0.72-1.11	0.51-1.27

The biotites of the dykes are dark brown and overlap the ranges of the host rocks and xenoliths (Fig 6.4). Overall the biotites do not appear to be zoned with quite uniform compositions: TiO2 3.3 - 2.1%; FeO* 16.7 - 15.9% and K2O 9.6- 9.0%. Fluorine has as wide a range as the xenoliths of 0.15 to 0.47% F.

Quartz is present mainly in the groundmass as interstitial grains. Rare examples of xenocrysts have been found as spherical grains surrounded by a narrow jacket of fine grained hornblendes and biotites in one of the dykes only.

Sphenes and apatites are present in small amounts. Sphene is seen as

fine euhedral to anhedral grains throughout the matrix. It is almost identical to those of the xenoliths and host rocks.

Apatite forms very fine acicular crystals and are found as inclusions in feldspar and quartz. They are also fluor-apatites with F levels of 3.7-4.7%.

8.4 GEOCHEMISTRY

Only 4 dyke samples have been analyzed and so their contribution to the general geochemical history of the Strontian complex will be extremely limited. The microdiorite dykes have a similar range to the xenoliths of 56 to 58.5% SiO2. They fall into the main granodiorite -granite-xenolith trend, though more towards the mafic end and lie in the overlap area between the xenoliths and mafic diorites (Figs.7.1 to 7.30).

The dykes range from 16.2 to 15.3% Al2O3, which has a reasonably constant value with little scatter.

They range from 0.05 to 1.06% TiO2; 6.25 to 7.35% FeO* and 0.08 to 0.11% MnO and all fall on the main xenolith trend.

The dykes fall within the xenolith range of CaO with 3.8 to 4.5% CaO. They have a much narrower range of sodium and potassium than the xenoliths, of 4.35 to 4.6% Na2O and 2.05 to 2.33% K2O. Phosphorus levels fall in the middle at 0.42 to 0.45%. Fig.8.1 displays the REE patterns for the dykes.

Table 8.2 MAJOR AND TRACE ELEMENT GEOCHEMICAL DATA WITH NORM DATA

	L1 C.Dyke	E1 C.Dyke	E2 C.Dyke	E3 C.Dyke
Major Elements				
SiO_2	56.00	58.50	57.00	57.50
TiO_2	1.06	0.85	1.03	0.05
Al_2O_3	16.20	15.30	15.50	15.50
FeO	6.25	6.30	7.10	7.35
MnO	0.08	0.09	0.11	0.10
MgO	4.20	5.05	5.90	6.10
CaO	3.80	3.75	4.30	4.50
Na_2O	4.60	4.35	4.53	4.53
K_2O	2.33	2.50	2.05	2.07
P_2O_5	0.45	0.44	0.42	0.45
H_2O	2.52	1.58	1.82	1.24
CO_2	2.40	0.30	0.13	0.34
Total	99.89	99.01	99.88	99.73
Trace Elements				
Ba	825	1305	528	432
Cr	190	175	195	220
Cu	50	56	56	54
Li	37	34	34	32
Ni	157	158	172	172
Rb	70	57	77	60
Sc	15	14	16	16
Sr	856	1227	984	1006
V	141	133	134	143
Y	19	19	20	19
Zn	93	88	102	99
Norm				
Q	11.08	7.27	3.56	2.95
C	5.84	0.37	-	-
Or	13.77	14.77	12.11	12.23
Ab	38.91	36.79	28.31	38.31
An	0.74	13.83	15.91	15.85
Lc	-	-	-	-
Ne	-	-	-	-
Di	-	-	1.50	1.12
Wo	-	-	-	-
Hy	16.36	18.90	20.99	23.57
Ol	-	-	-	-
Mt	2.32	2.34	2.64	2.73
Il	2.01	1.61	1.96	0.09
Ap	1.07	1.04	1.00	1.07
Cc	5.46	0.68	0.30	0.77

8.5 DISCUSSION

The dykes found in the Strontian complex show geochemical, mineralogical and hybrid similarities with the xenoliths. The dykes cannot be considered as the source of the xenoliths, as they are seen cutting the granodiorite which contains xenoliths. However the dyke magma-type may have been available earlier and therefore been the parent to the xenoliths and dykes.

The dykes contain xenocrysts of quartz. The alkali feldspar present is unlikely to be a phenocryst phase in such a magma and so would also be a xenocryst. Therefore the dyke magma is likely to have been hybridized with a porphyritic granitic magma. Since the dyke contacts are sharp it is probable that hybridization took place at depth.

The dykes show similar petrographical features to the composite microdiorite-granodiorite body described in chapter 2 (section 2.3). Both bodies are very mafic, display the presence of feldspars from the surrounding host and have apophyses of microdioritic material passing into the host granodiorite. So it is likely that both intrusions are the result of mixing at depth. The composite body also brings the relatively uncontaminated acid end member to the present surface.

Fig. 8·1 Chondrite normalised REE patterns for the Microdiorite Dykes.

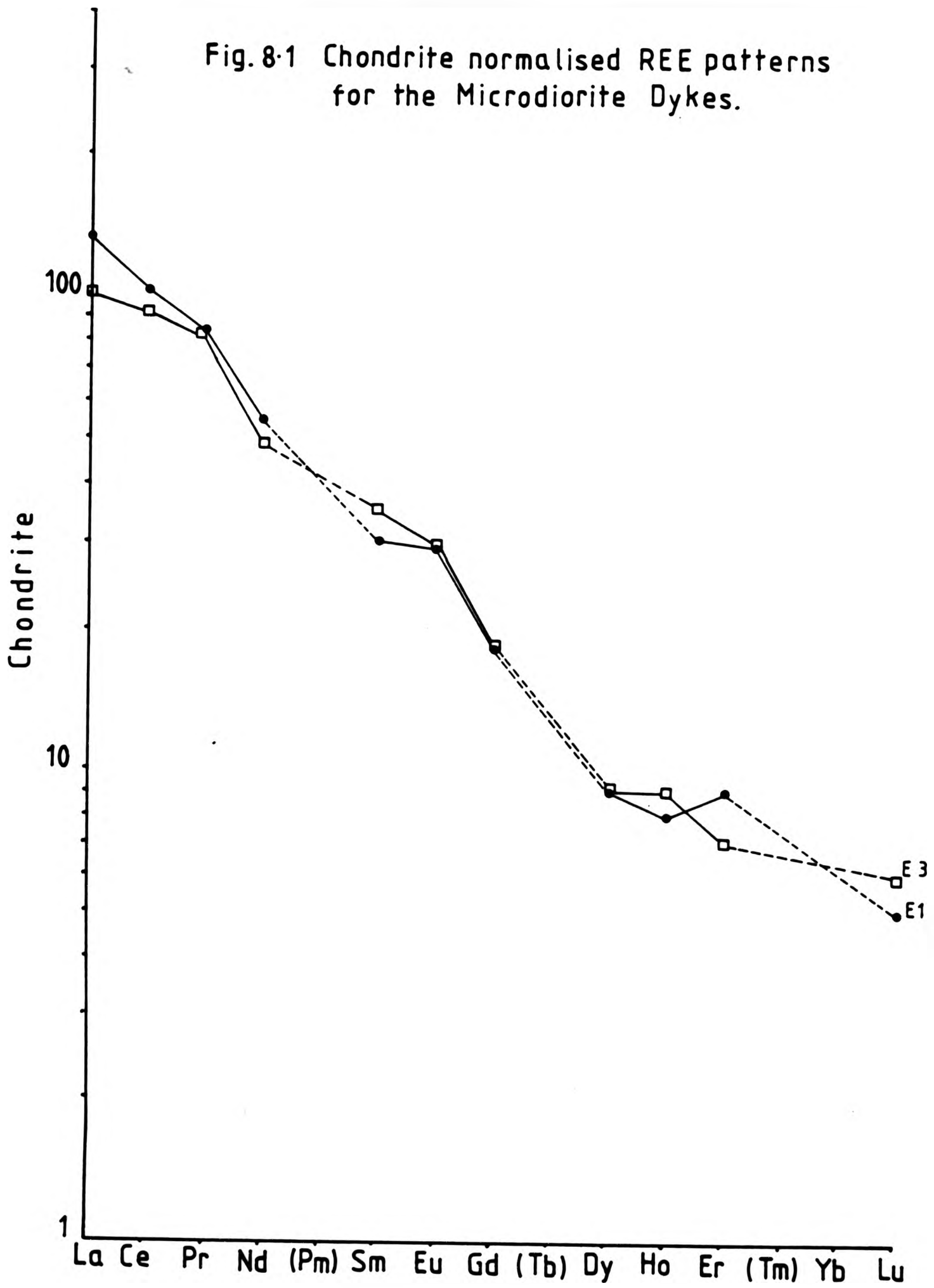

Chapter 9 THE DIORITES: FIELD RELATIONSHIPS

9.1 INTRODUCTION

The twelve diorites (called appinites on the BGS sheet no.52E) in the Strontian complex, are found as large bodies varying in shape from the "long narrow sheet-like" structure on the western margin of the pluton to large bodies with sub-rounded outlines found throughout the two plutons (Fig 1.1). They have all been reported to a greater or lesser extent by Scott (1928), MacGregor & Kennedy (1932) and Sabine (1963). The majority of the bodies are within 3.5km of the margins of the complex (Fig 1.1) in the tonalitic and porphyritic granodiorite pluton; while a small group is found nearly in the centre of the complex in the biotite granite, but lying near the margin of that unit.

The mapped outlines of the equidimensional bodies have in general proved similar to those on the maps of MacGregor & Kennedy(1932) and Sabine(1963). The sheet-like body of diorite (no.4 on Fig 1.1) was mapped as a single body by Sabine (1963), reaching 5km in length, but is shown as number of discrete lens-shaped bodies all lying in the same orientation on the earlier map of MacGregor & Kennedy (1932). My own field work has shown that the earlier interpretation is correct. However there are some bodies shown on the map that are no longer significantly exposed eg. just south of Loch Sunart (Fig. 1.1).

The better exposed bodies have been mapped at a 1:10,000 scale and local detailed plans at 1:2000 and 1:500 scales prepared from well exposed coastal sections Fig 9.1 A, B, C, D, E & F). Eight of these

bodies could be studied to show the internal features and relationships with the surrounding host rocks, no such details of the diorites are given in the literature. The rest were unexposed or so poorly exposed that little useful information could be obtained by mapping. In the field, variation in the colour index, from rare hornblendite through meladiorite to diorite, and the textural features of the mafic minerals were used to map subdivisions within the bodies. Each of the mapped bodies shows its own unique assemblage of diorites, though they do have similarities (Fig 9.1A, B, C, D, E & F). The diorite bodies will be discussed in 2 groups:

- Those found in the granodioritic host.
- Those found in the biotite granite host.

9.2 THE DIORITES IN THE GRANODIORITE

The main 5 bodies that were mapped in the granodioritic pluton are marked on Fig 1.1 as:

1. Ranachan
2. Rubha-na-Sroine
3. Liddesdale
4. Sheet
5. Loch Tearnait

Ranachan, Rubha-na-Sroine and Liddesdale are well exposed only along the shores of Loch Sunart (Fig 1.1). This is by no means the entire body, but further mapping inland was not possible due to the lack of outcrops. These coastal outcrops reach 250-350 metres in length and 2-40 metres in width (above the high water mark). Below high water

mark the rocks are heavily covered with seaweed. Each diorite has been mapped (Fig 9.1A, B, C) and each has been seen to be very different, therefore their field relationship will be reviewed separately.

9.2.1 Ranachan (Fig 1.2, Location 1 & Fig 9.1A)

This body is found on the northern shore of Loch Sunart, close to the western contact of the complex (Gr.Ref: 7855-6114 to 7880-6120). Both contacts of the diorite body are sharp and nearly vertical. There are small rounded clots of acidic material similar to the host granodiorite, reaching 0.5m in diameter. They have been incorporated into the diorite and this gives the impression of irregularity to the contact. The grain size in the dioritic material becomes finer towards both contacts from an average 8mm in the core to 2-3mm at the contacts, but there is no evidence of any very fine grained chill.

Large patches of granodiorite host were encountered within the limits of the diorite. The contacts are sharp, but irregular with apophyses of the granodiorite penetrating into the diorite. There is no change in grain size of the granodiorite patches towards the contacts. The patches are all tonalitic granodiorite and have microdiorite xenoliths, which are the same as in the main pluton. These patches are not considered to be proved inclusions or veins as all the sides of the contacts were not exposed. The apophyses suggest that they are most likely veins.

The Ranachan diorite is not a uniform diorite body and could be described as: 1.a fine to medium grained mafic diorite with biotite crystals, bladed hornblende and mafic aggregates, with an uneven

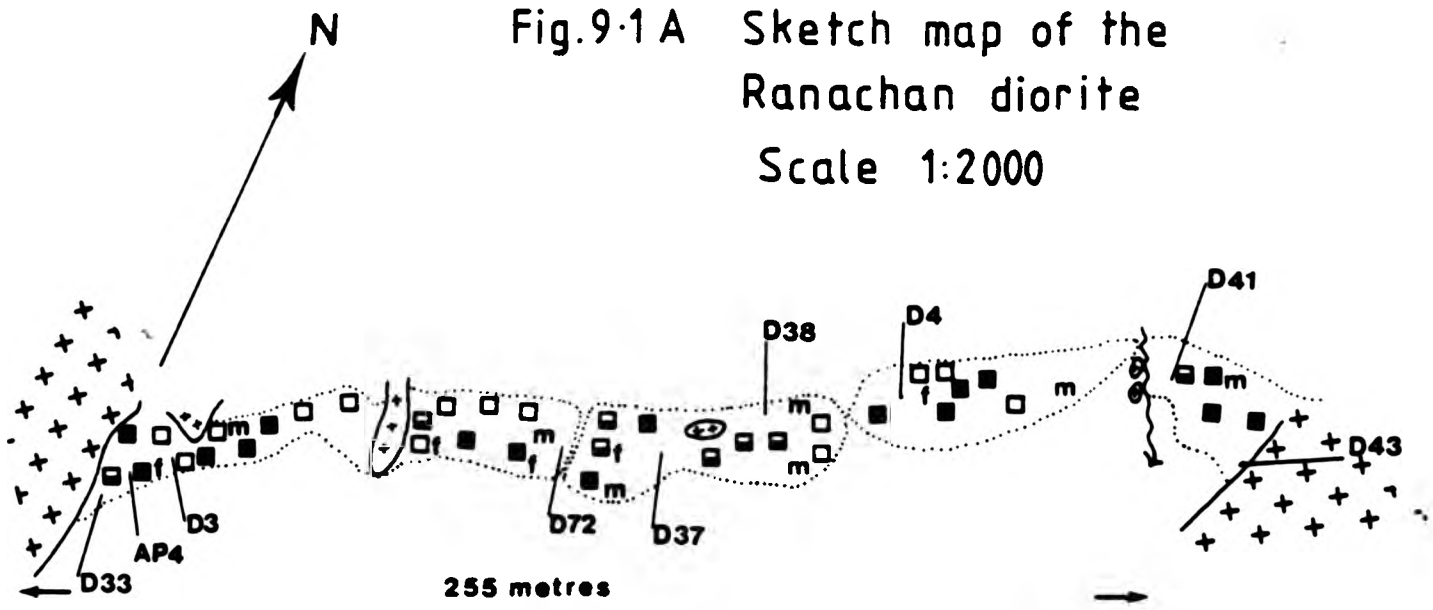

Fig.9·1A Sketch map of the Ranachan diorite
Scale 1:2000

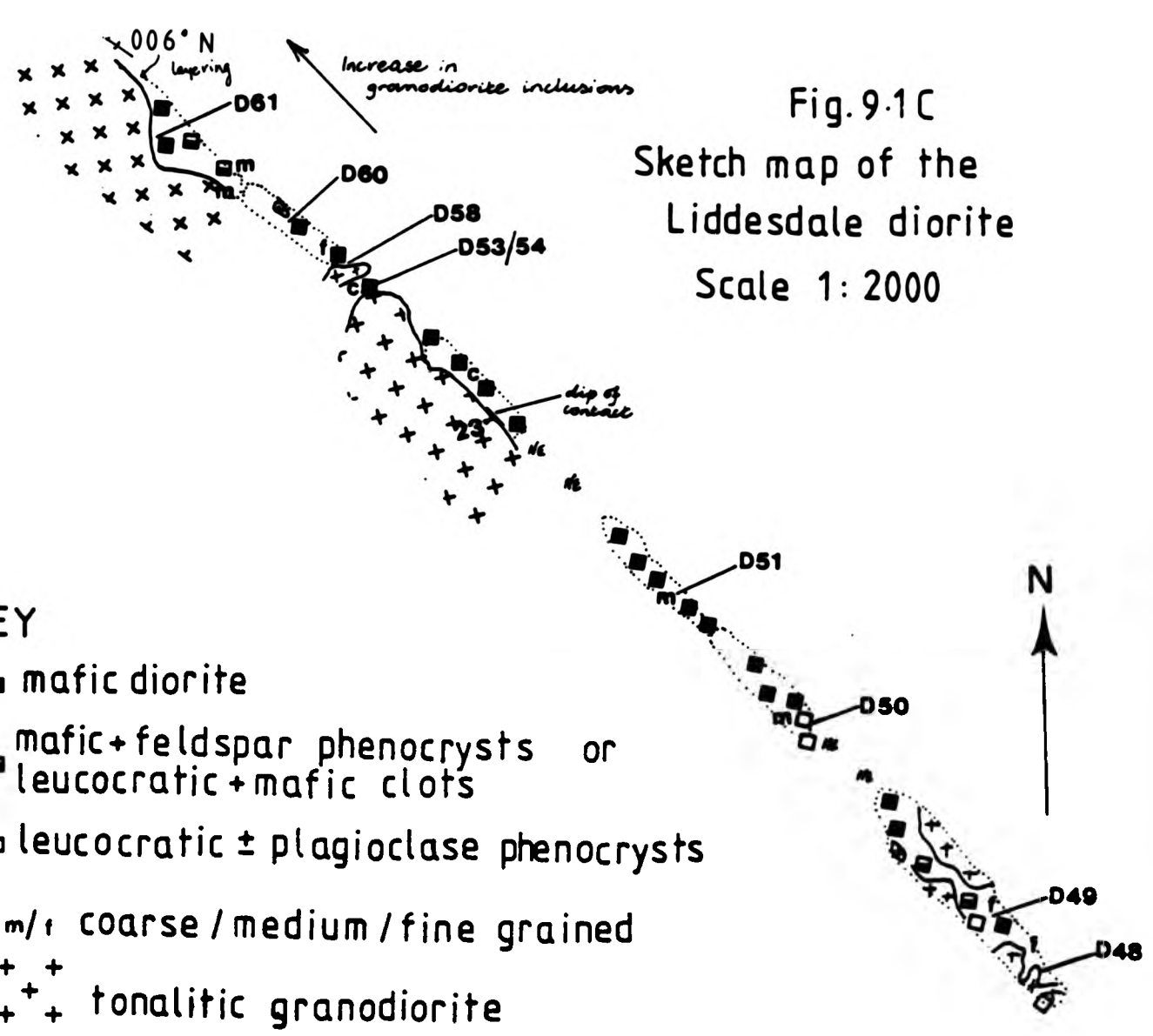

Fig.9·1C Sketch map of the Liddesdale diorite
Scale 1:2000

interstitial leucocratic faction; and 2. a fine grained (2-3mm) mafic diorite with biotite and hornblende in the matrix as well as individual crystals together with plagioclase phenocrysts upto 5mm long. The two dioritic types grade into each other across the whole body over a distance of between 10 to 40m (marked on map 9.1A). The finer grained nature of the margins is local to the contact and so is separate from the variation in the main body. Both types have sphenes and sulphides present in variable amounts. There are also rare aplitic veins and dykes that cut across the body.

9.2.2 Rubha-na-Sroine (Fig 1.2, Location 2 & Fig 9.1B)

This diorite is located on the south shore of Loch Sunart (Gr.Ref:6010-7930 to 6012-7972). It is a completely different body to the Ranachan diorite. Not only in its petrography, but in its internal features. The contact of the main diorite with the granite is only very locally noted as being sharp. This diorite is far more mafic than Ranachan with no feldspar phenocrysts. Rubha displays a crude layering seen by the distribution of large (25mm) and small (3mm) poikilitic biotite crystals. This layering dips at 51º. The boundaries between the layering observed in sample D3/D3A are gradational and not sharp and planar (Fig.9.1B). D3 has coarser 8mm biotite and within 20mm D3A exhibits 3mm biotites.

One unusual feature in this diorite is the intrusion of a coarse heterogenous granitic sheet (GS3 & GS3A) that reaches 2 metres in width (Plate 9.1). Its outer margin is grey, fine grained and non-porphyritic and varies in width from 20 to 40mm. The interior zone is granitic, but looks more like a mixture of very large granite feldspar phenocrysts and the coarse biotite-rich facies of the

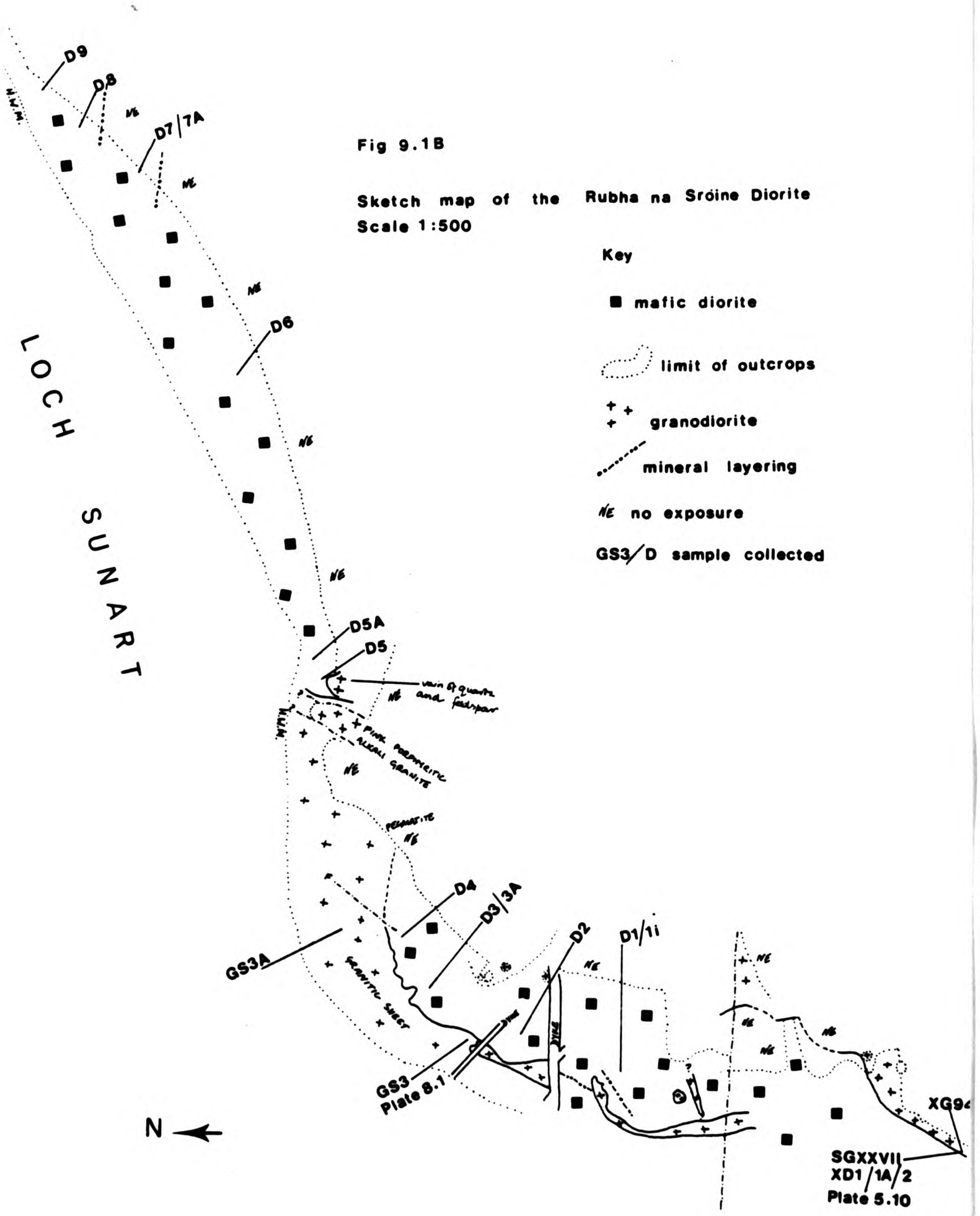

Fig 9.1B

Sketch map of the Rubha na Sróine Diorite
Scale 1:500

Plate 9.1 View of the heterogenous granitic sheet within the Rubha-na-Sroine diorite, showing the coarse interior and finer grained mafic margin - Samples GS3 and GS3A (G.Ref. 7935-6017).

Plate 9.2 View of the D29 diorite found east of Beach, showing the diffuse margins with the granodiorite (G.Ref. 7792-5311). Hammer head 170mm.

diorite. Further along its length it comes into contact with a dioritic sheet that cuts the main diorite. The plane of contact is a crenulated or cusp-like, but this feature may be due to the level of exposure that gives this crenulated contact. The grain size of the diorite sheet is finer grained at the granite margin and coarsens away from it. This whole sheet complex is regarded as being a local feature within the diorite rather than a regional one, as this has not been seen outside the diorite.

Along the entire length of the coastal exposure of the Rubha-na-Sroine diorite, it is in contact with a porphyritic granodiorite sheet. There are microdiorite xenoliths found within the sheet, which are not as mafic as the diorite itself. The abundance of the xenoliths is slightly less than the sparsely populated areas in the host granodiorite (<5%). Aplite and coarse pegmatite veins are more common in this diorite body than any other, but do not occur in the host rock.

9.2.3 Liddesdale (Fig 1.2, Location 3 & Fig 9.1C)

This body is found further west from Rubha-na-Sroine, but still along the south shore of the loch (Gr.Ref: 5995-7740 to 5982-7762), close to the pluton margin in the tonalitic granodiorite. There are very rare inland outcrops of the Liddesdale diorite, which are unfortunately deeply weathered.

It differs from the Ranachan and the Rubha-na-Sroine diorites, by having more abundant hornblende as equant crystals and as aggregates. This body is a coarse to fine grained mafic diorite of dominantly hornblende, with biotite and the leucocratic minerals varying in

abundance. The amount of sphene also varies throughout.

The western contact with the host granodiorite is sharp, planar and near vertical (as far as exposure allows). The diorite at the contact has a grain size of 2mm increasing inwards to 6-8mm. At 20m into the diorite a near vertical layering trending at 006ºN, parallel to the contact, is encountered. It can also be recognized upto 40m away from the contact. It is not seen in the core or on the eastern contact of this body. The layers are of alternating mafic and leucocratic diorite of a width of 10mm or less. The leucocratic layers are mostly feldspar (3mm grain size) with the appearance of occasional feldspar phenocrysts; whilst the mafic layers are composed of hornblende and biotite occurring as single crystals (3-4mm) or as aggregates. The aggregates are elongate masses (of 3-10mm), probably pseudomorphed large hornblendes, which appear to show a regularly oriented fabric close to this contact, similar to the layering of 006'N. Otherwise they are more rounded in shape and are randomly oriented.

The Liddesdale diorite, like the Rubha diorite, shows some form of internal zoning. The dioritic types vary from a very mafic diorite with interstitial plagioclase to a more leucocratic version, with the same texture. It differs from the Rubha diorite as it is not picked out by large poikilitic biotites. The mafic diorite is richer in hornblende as equant prisms to acicular crystals, in monomineralic aggregates or together with biotite. The abundance of biotite also varies and it occasionally has poikilitic tendencies (as in Rubha). The overall grain size of the core is around 5-8mm. The leucocratic parts of this body are feldspar and quartz-rich and where occasional feldspar phenocrysts are encountered.

As the eastern contact is approached the diorite becomes more leucocratic, though mafic aggregates are still present. There is only a slight reduction of grain size to between 4-6mm. The actual contact with the tonalitic granodiorite is not visible, as there is an irregular grouping of tonalitic patches around this point. As in the Ranachan body, the whole patch is not seen therefore they are assumed not to be inclusions within the diorite.

An area of tonalitic granodiorite was mapped on the landward side of the centre of the diorite strip. A dip for this contact was measured (Fig.9.1C) at 23º to the south.

Actual granodiorite patches occur locally at or close to the western contact. They appear at about the same distance as the banding. They are quite large, over 2m in some cases, at the first encounter. Moving towards the contact they become smaller and more elongate. They have sharp, non-chilled contacts. The tonalitic granodiorite patches, whether at the eastern or western contact, is xenolithic with abundance more or less the same as the sparsely populated areas of the external granodiorite. The xenoliths are microdiorite and different from the Lidd diorite.

South of the Liddesdale diorite, along the A884, there is a separate 300m exposure of diorite (Fig 1.2) in a road side drainage ditch. This body has very similar poikilitic biotite (4-10mm) textures as seen in the Rubha diorite, but from the B.G.S. map is too far away to be part of that body. Therefore this body will be discussed here with the nearby main Liddesdale body for convenience. It is a mafic diorite with biotite as well as hornblende phenocrysts (upto 15mm in size) as the main phases, while feldspar and a small amount of quartz

are interstitial. The outcrop trends at 030ºN. The contacts trending N-S with the granodiorite host are sharp, planar and show no signs of chilling. The diorite has no developed fabric. It is a very mafic body with only small local signs of segregation. There are no granitic or aplitic veins cutting across this narrow exposure.

9.2.4 Sheet (Fig 1.2, Location 4 & Fig 9.1D):

This is by far the longest diorite in the Strontian complex, stretching for nearly 5km along the western contact of the intrusion. MacGregor & Kennedy (1932) and Sabine (1963) both recorded this diorite on their maps as a number of discrete shorter bodies or as a long single body respectively. Though exposure is poor along most of this section, several stream sections provided much information. A number of traverses were completed in the present study in the north and south. Sample collection was along the length of the body where outcrop allowed. The continuation of the diorite across the valley at Achagavel (Fig.1.2) is only assumed as there is heavy cover of peat and heather. The northern end of this sheet is separated into discrete lens shaped bodies. The contacts are steep as observed from mapping up the hillsides and along stream sections.

The dioritic sheet is a medium to fine grained dark rock (not as mafic as the other diorites) with mafic aggregates(10mm in diameter) giving a "spotty" appearance as well as single crystals of biotite and hornblende, subhedral to euhedral plagioclase and K-feldspar phenocryst (upto 11mm in length) and a variable amount of quartz xenocrysts. This sheet has a different texture to the other diorites. Many of the plagioclase feldspars have jackets of a different plagioclase composition. No examples of plagioclase

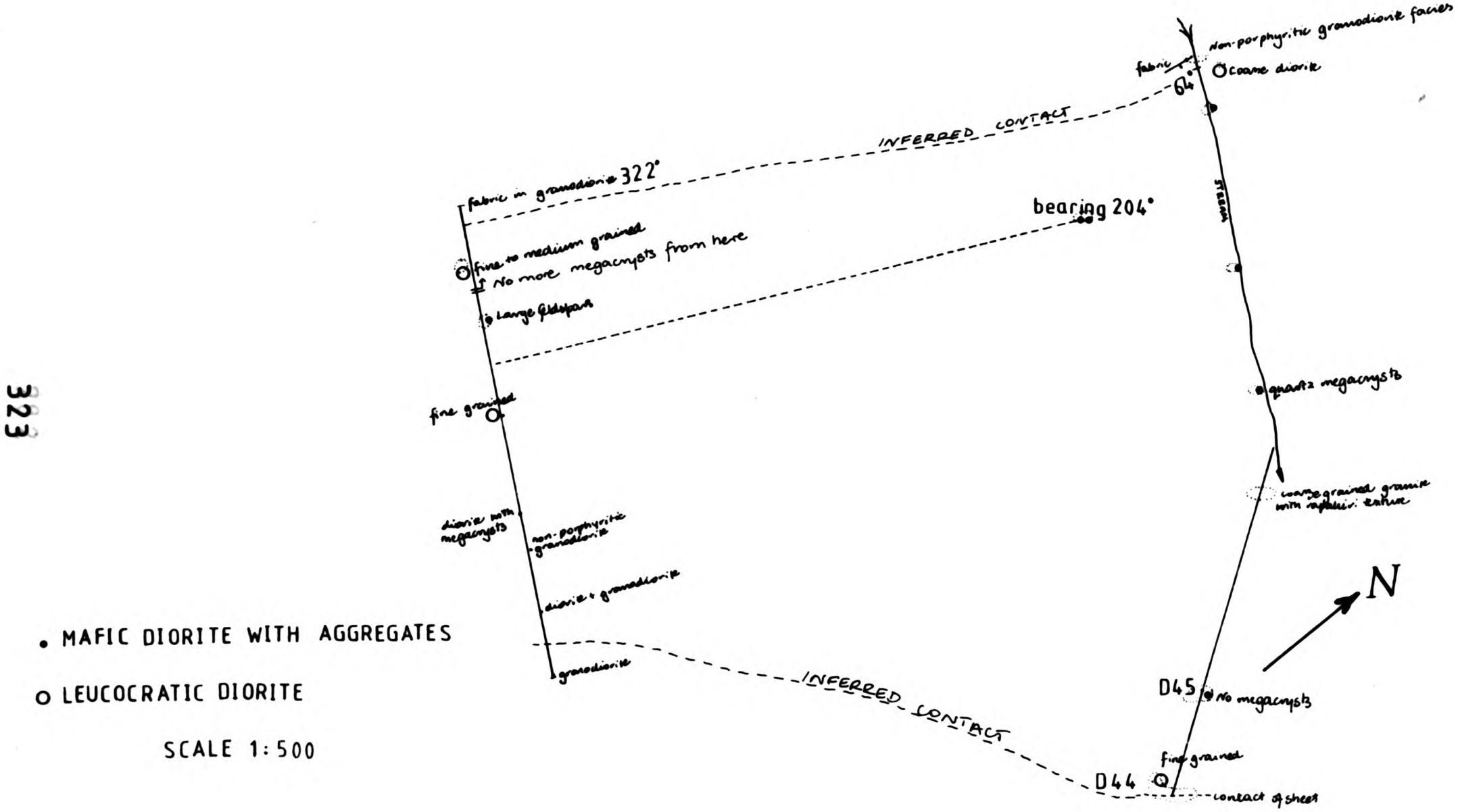

Fig. 9·1 D Sketch map of the traverses across the Sheet diorite.

jacketing alkali feldspar or vice versa have been seen.

The two traverses (Fig.9.1D) at Clounlaid (Fig.1.2) show that the body is locally composite with a zone of porphyritic granite similar to the ctG sheets occurring at its eastern margin with the porphyritic granodiorite. The granodiorite has an igneous foliation on the east side of the body, while on the west it is locally coarser at the contact than the usual granodiorite with the foliation heading at 009º (dipping at 64º) skew to the contact. The description of the traverse will be from the west to east, starting with the familiar sheet diorite.

The western contact with the porphyritic granodiorite is sharp, with granodiorite veining the diorite. The diorite is fine grained (3mm) with the usual mafic aggregates, feldspar phenocryst and quartz xenocrysts. The groundmass coarsens inwards over 1m and for 105m eastwards the diorite is uniform with abundant mafic aggregates and quartz with mafic reaction rims. Patches of coarse granite with K-feldspar megacryst showing rapakivi-style white plagioclase jackets occur within the diorite. They are subhedral in shape and reach 15mm in length. The feldspars are aligned parallel to their diorite contacts.

As the granitic sheet is approached, the plagioclase phenocrysts and "spots" become less frequent and at about 15m from the contact with the sheet, the diorite is non-porphyritic. The diorite also becomes more leucocratic, finer grained with finely disseminated biotite and has occasional quartz xenocrysts. The contact with the sheet is gradational as seen in the increase in abundance of feldspar phenocrysts within 2m.

The contact of the porphyritic sheet with the porphyritic granodiorite is sharp, but irregular and follows the planar structure of the granodiorite. It is generally near vertical and lies on an approximate bearing of 026°, which is parallel to the diorite.

The sheet is clearly a hybrid with one parent being a porphyritic granite and pre-dates the solidification of the porphyritic granodiorite. The fine grained margin also suggests that the body is still largely intact.

9.2.5 Loch Tearnait (Fig 1.2, Locality 5)

There is a diorite body located between the porphyritic granodiorite and the biotite granite in the south by Loch Tearnait. This diorite has been described by Sabine (1963), who notes that compositionally it is a microdiorite being invaded from the west by the porphyritic granodiorite and from the east by the biotite granite.

It is poorly exposed throughout its length and extensively covered by peat and grass. Rare outcrops were found in the stream sections, but these were often quite weathered. Its contacts on both sides are not sharp or clear-cut. The granodiorite contact facies has a well developed fabric with a medium to fine grained mica-rich groundmass with plagioclase phenocrysts. Xenoliths in the granodiorite show no similarities to the diorite. The biotite granite contact displays more of an interdigitating contact giving the impression of the diorite being streaky xenoliths in the biotite granite.

The diorite is very mafic, medium grained in general and highly foliated (Plate 10.15 A & B). This fabric is picked out by biotite

and trends at 006ºN. It has plagioclase phenocrysts in a fine grained matrix of quartz, feldspar, prismatic hornblende and +/- sphene. While the host rocks are commonly slightly coarser than described in earlier sections. The porphyritic granodiorite has alkali feldspars reaching 50mm in length.

9.2.6. D29 (Fig.1.2)

D29 is a single exposure of a diorite rock found close to Beach (Fig 1.2). The exposure is no more than 1 sq m and shows a medium grey, fine grained rock with mafic aggregates and occasional feldspar phenocrysts in a matrix of plagioclase, quartz and biotite. Plate 9.2 shows the contacts of the diorite with the porphyritic granodiorite. The contact at the base of the print is N-S. It is irregular and diffuse, with the granodiorite present in the diorite as little blebs. While the upper contact is sharp, trending 010º.

9.3 DIORITES IN THE BIOTITE GRANITE

(Fig.1.2, Location 6 & Figs.9.1E & F)

Three diorite bodies were found just south of Beinn Mheadhoin (Fig 1.1 & 1.2) in the biotite granite near the contact with the porphyritic granodiorite. These have been termed the "Uileann Diorites" and have also been reported by Sabine (1963).

These outcrops are located on the north side of Allt Buidhe Mor valley and from the south side are clearly seen as slight depressions of darker material with somewhat greener vegetation (Plate 9.3). They occur as sub-rounded bodies reaching several hundred metres wide and have been mapped on a scale of 1:2,000 (Fig.9.1E & F). From

Plate 9.3 View onto the Uileann diorite (Fig.9.1E), looking northards. The mafic diorite at A (G.Ref. 7865-5030)

this mapping it was apparent that two of the bodies were connected by a narrow "arm" of dioritic material. All three are broadly the same ie. mafic diorites locally grading to ultramafic rocks. The diorites are exceedingly rich in poikilitic biotite and also have amphibole, with little feldspar and sulphides.

Unlike the diorites of Loch Sunart, the contacts of the Uileann diorites are difficult to locate, because of the extensive cover of grass, peat bog and drift and because of the deep weathering of the diorite outcrops. However, some contacts were located during the mapping of the bodies, using the outcrop method and stream sections. The contacts of these diorites were all found to be gradational. Sabine (1963) suggests either mixing or growth of hornblende in the biotite granite, as there is no sign of chilling in either rock.

An outstanding and unique feature of these diorites is the occurrence of the intensive net-veining and granite intrusion at the margins of these bodies(Fig.9.1E & F). Two zones are recognizable within the bodies:

a) The cores of the diorites; and
b) The marginal zone of the diorites.

a) The cores of the diorites represent dioritic material untouched by the invading granite and are very black in colour, they are very similar to the Rubha-na-Sroine diorite. They remain very mafic with a predominance of coarse poikilitic biotite crystals with rarer examples of amphibole-rich types. There are no quartz xenocrysts in the cores.

Fig. 9·1E Sketch map of the elongate Uileann diorite southern body — Fig.1·2, no. 5.
Scale 1: 2000

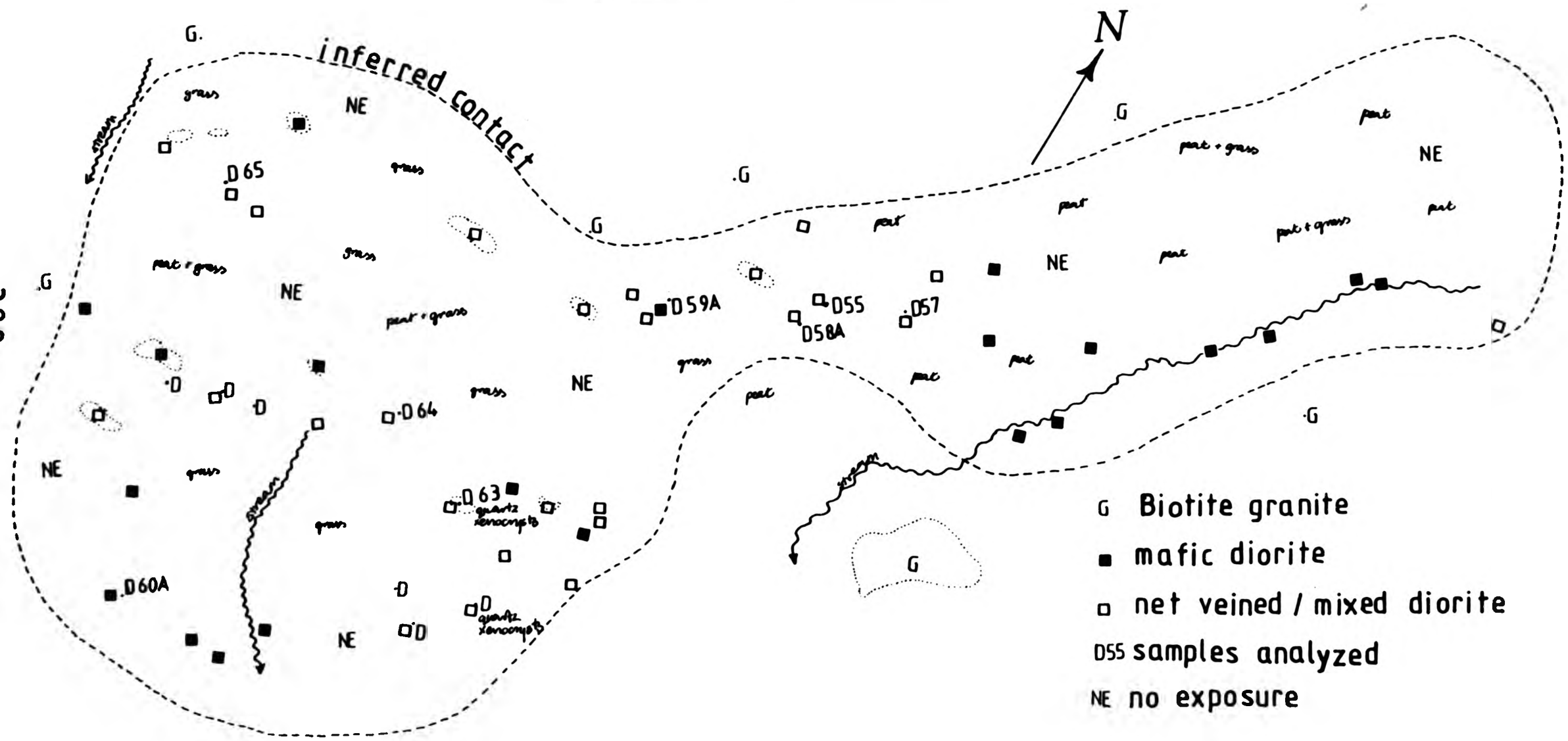

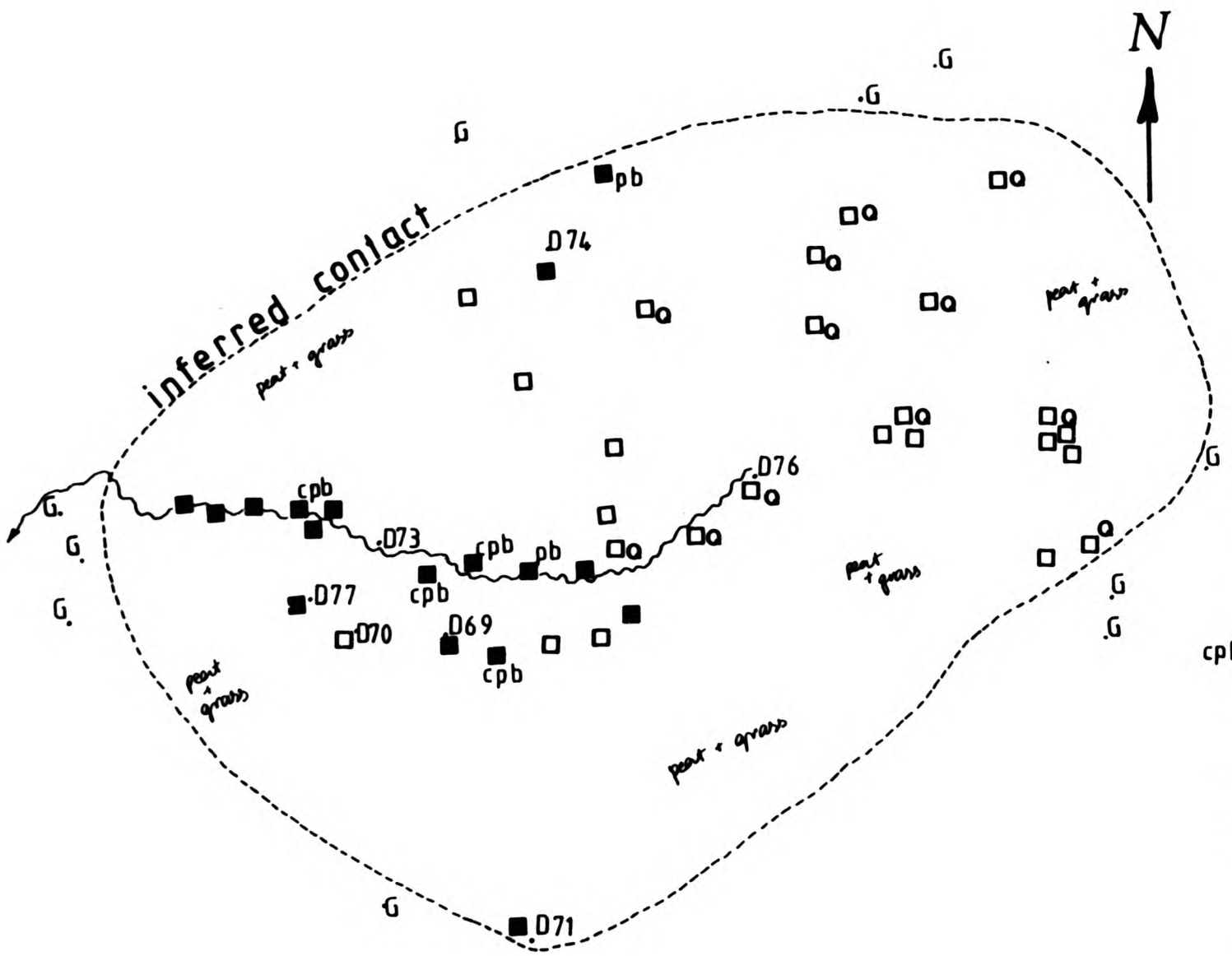

Fig. 9·1F Sketch map of the rounded Uileann diorite northern body — Fig. 1·2, no. 5.

G biotite granite

cpb/pb (coarse) poikilitic biotites

o quartz xenocrysts

■ mafic diorite

□ net veined/mixed diorite

Scale 1: 2000

The area of the core compared with the overall dimensions of the diorite body, is small. In fact the cores or non-net veined diorite can range from just a single exposure to an area 10 metres across as the net-veining and the marginal zones are very extensive. There are some 20 of them and they indicate the nature of the original material. They are coarse grained (6 to 8mm), biotite-rich, and locally hornblende-rich meladiorites. All are more biotite-rich than the other described diorites. Biotites occur as poikilitic crystals (upto 8mm) enclosing finer grained mafic material. Feldspar phenocrysts and quartz xenocrysts are absent.

b) The marginal zone varies in thickness from a few metres to several tens of metres. No contacts showing diorite intruding granite (ie. veining or including granite blocks or xenoliths) have been found, which suggests they are not intrusions post-dating the solidification of the host granite. The granite net-veining however implies that the biotite granite may post-date the diorites and that they are the remnants of some larger body that was slowly being incorporated into the host granite.

Traced towards the main contacts the diorites become finer grained, locally 1-2mm. Quartz xenocrysts appear and reach locally 10% of the rock. They are relatively large, most are 2mm, but some reach 4-5mm and have well developed mafic reaction rims. Feldspar phenocrysts or xenocrysts appear in the rounder Uileann body (Fig.9.1E). They are not very common and occur in only several outcrops. They are subhedral to anhedral plagioclases, with occasional jackets of K-feldspar. This is an unusual feature and supports the view of some sort of mixing occurring.

The marginal zone displays a variety of rock types. There is the mafic diorite, which is the same as in the diorite cores. The net veining is sharply defined by the leuco-granite against this. There is also a more leucocratic mottled diorite, which is distinguished from the core material by mafic aggregates (Plate 10.16) and by being much finer grained than the adjacent mafic diorite. It also bears quartz xenocrysts. In the marginal zones the mottled diorite is cut by the leucocratic net veining. The presence of a more leucocratic xenocrystic member in the diorite cut by net-veining indicates early mixing with alkali granite. As there are contacts visible the relationship of mafic and mottled can only be inferred.

A heterogenous look to the rock appears where the mottled and net-veining becomes extensive, with the diorite material being very fine grained (which could have originally been chilled against the granite during the invasion). This mottled phenomenon gives rise to a pock-marked surface, where the dark mafic-rich clots are weathered out. The granitic material in between is medium to fine grained.

Rare xenoliths have been found in the vicinity of the diorites. They appear to be more leucocratic than the diorite, are finer grained, non porphyritic with plenty of quartz and feldspar, and could be classed as Type1(A).

The Uileann diorites are clearly hybrids in their outer parts against the biotite granite. The quartz xenocrysts in the diorites are larger than quartz in the adjacent host rock, therefore hybridization with the immediate host is unlikely. The fine grained diorite and margins suggest the bodies are close to their original dimensions in spite of the invasion by the biotite granite. These diorites are

similar to the Sheet in that both are hybrids. They differ however as the Uileann diorites are dominated by biotite and amphibole, have coarser interiors and have very limited plagioclase phenocrysts/xenocrysts.

9.4 DISCUSSION

All the diorite bodies located and studied have extended the work presented by MacGregor & Kennedy (1932) and Sabine(1963). In Strontian these mafic diorites all occur within the limits of the whole complex. This contrasts with the small early intrusions around Ballachulish Granite (Bailey 1950, Bowes et al 1964) and larger peripheral intrusions Garabal Hill (Nockolds 1941), Glen Tilt (BGS sheet 63), though similar to the Ross of Mull (BGS sheet 43) and Foyers (Marston 1971).

The present work has far extended the available data on the mafic diorites present in the Strontian complex. There is an ambiguity as to the time relationship of the diorites to the host rocks. As there is no isotope data for these bodies it is inferred from field observations such as local finer grained diorite margins and granitic veining that they do not post-date their surroundings, but are contemporaneous with the granites. Field evidence shows that each of the mafic bodies is heterogenous and very different from each other, not only petrographically but also in their relationship with the surrounding host eg. the sheet or Uileann. Some diorites, sheet or Uileann, are shown to be hybrids involving granitic magmas, while others lack evidence of hybridization.

All appear to be intruded by the immediate host rock, but decreases

in grain size towards the margins suggest that much of the original body is preserved. If the diorites represent large, pre-granite accidental xenoliths then the xenoliths of the former psammite host rock would be expected at the contacts with a chilled facies. Such xenoliths are never seen.

If the the mafic diorite can be regarded as being contemporaneous with granodiorite then the origin of the granodiorite patches or "inclusions" found in the Ranachan and Liddesdale diorites can be questioned. The diorite and host granodiorite may have been semi-solid allowing mixing on a more massive heterogenous scale rather than complete homogenization.

Xenoliths found adjacent to the diorites, apart from the those in the Sheet diorite, do not have the same hand specimen petrography as the diorites, but are the same as those found in the host granite. Xenolith abundance near the bodies is no greater or lesser than the normally sparsely populated host granodiorite (<5%). Xenoliths within the diorite bodies do not occur unless they are present in a patch of granodioritic material.

Chapter 10 THE DIORITES: PETROGRAPHY AND MINERAL CHEMISTRY

10.1 INTRODUCTION

Each diorite body, whether in the granodiorite or biotite granite host, varies mineralogically and texturally from the others, showing great internal heterogeneity. Therefore the eight diorites studied will be described separately. However they do have in common a high colour index.

In chapter 9 a number of the diorite bodies were described with the help of hand specimen petrography. Some of these descriptions were divided into 2 main dioritic types eg Ranachan. This was only an aid for mapping and now a fuller description will be given.

The dominant minerals in these essentially meladiorites are: hornblende and biotite, but where biotite becomes smaller and less abundant, feldspar becomes more dominant and probably shows the greatest variety of composition and crystal form in all the dioritic types. All mineral chemistry will be discussed later in this chapter. The rock types range from rare hornblendites through meladiorites to diorites and occasional appinitic diorites. Modal analyses are given in Table 10.1 with names according to Streckeisen's classification (1975). The tendency for the monzonite - monzo-diorite character appears as a result of the granitic component coming into the mafic diorite. The bodies especially influenced are Uileann and the Sheet, where the granitic invasion (or mixing) is seen to have occurred.

10.2.1 Ranachan (Fig 1.2, loc.1)

This body is a fine to medium grained mafic-rich diorite (mafic colour index 30-45). Hornblende is the dominant ferromagnesian mineral with biotite being less abundant, but more constant in percentage. There is no regularly orientated fabric in this diorite body.

Some brown hornblendes have been observed as remnants within green hornblende. Green hornblende occurs in two forms, but not as phenocrysts:

- Individual euhedral prisms that have grown with a spongy/skeletal appearance together with biotite (both showing good crystal form) and within occasional plagioclase. Coarser biotite is seen to be pseudomorphing the euhedral hornblendes (Plate 10.1A, B & C).
- Aggregates (of upto 5mm across) free of biotite but with accompanying magnetite. Remnants of clinopyroxene are seen in some aggregates. These could all be replacements of earlier formed clinopyroxene (Plate 10.2).

Hornblende is seen to alter to chlorite, epidote and sphene, often along its cleavage planes.

Biotite is only seen in association with hornblende and also often pseudomorphs a mineral with an elongate prismatic habit (upto 5mm long). Biotite 'hornblende' intergrowths have two occurrences of biotite (Plate 10.1A, B & C): a) a zone of biotite with a basal pinacoid parallel to the hornblende front pinacoid (which gives

Plate 10.1A View of biotite in PPL (Ranachan) pseudomorphing a euhedral hornblende - Sample D35. Field of view 3mm.

Plate 10.1B View of 10.1A in XPL (Ranachan) - Sample D35.

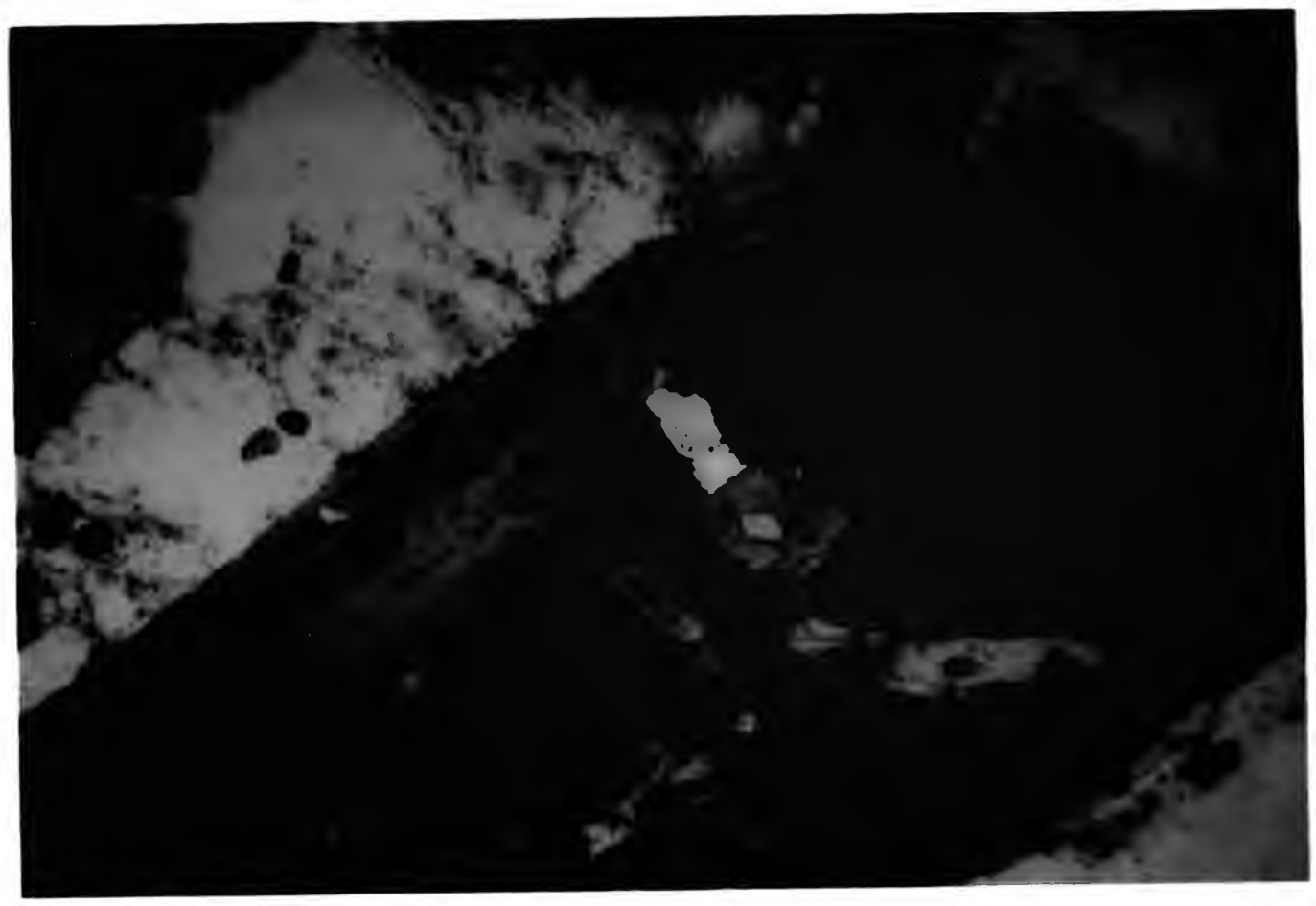

Plate 10.1C View of biotite in PPL (Ranachan) in 2 orientations pseudomorphing hornblende - Sample D41, Fig.9.1A. Field of view 3mm.

Plate 10.2 View of a large hornblende in PPL (Ranachan) pseudomorphing an earlier cpx (bottom left corner) - sample D33, Fig.9.1A. Field of view 3mm.

straight extinction parallel to the length of the aggregate), which is also seen in some Appin diorites (Platten, pers.comm.); and b) discordant irregularly orientated biotite lathes in the a) type biotite and in the hornblende.

Table 10.1 MODES FOR THE MAFIC DIORITES

	1	2	3	4
Plagioclase	58.6	30.0	36.0	19.0
K-feldspar	-	10.7	10.7	32.0
Quartz	9.0	15.4	4.0	29.7
Mafics+ Accessory	32.4	41.3	49.3	19.3
Q	13.3	22.7	7.9	36.9
A	-	26.1	21.1	39.8
P	86.7	51.2	71.0	23.2

	5	6	7
Plagioclase	39.3	39.3	33.3
K-Feldspar	12.0	11.4	-
Quartz	11.0	4.0	20.0
Mafics + Accessory	37.7	45.3	46.7
Q	17.8	7.3	37.5
A	19.5	20.7	-
P	62.7	71.9	62.5

1 Loch Tearnait (D80) : Diorite
2 Ranachan (D33) : Diorite
3 Uileann (57) Core : Monzodiorite
4 Uileann (D76) Marginal : Granite
5 Sheet (D45) : Quartz monzodiorite
6 Rubha (D1) : Monzodiorite
7 Liddesdale (D11) : Quartz diorite

The QAP values are for Streckeisen's classification.

Anhedral sphene is also associated with some of these aggregates. It is thought that this is a late magmatic or even a subsolidus reaction between an original Ti-bearing hornblende and K-bearing fluids leading to a new amphibole (possibly not hornblende) + biotite with the release of Ti.

There are two forms of plagioclase feldspar:

- As phenocrysts upto 15mm in length (10-20%).
- As interstitial or sub-poikilitic crystals.

Both phenocrysts and interstitial plagioclase is strongly zoned with cores of An32-34 and mid to high andesine margins (showing reversed zoning). Multiple twinning is variably developed and any alteration occurs along the twin planes.

Quartz is present only interstitially and in a small amount. It often has inclusions of apatite and sphene.

Apatite occurs as large euhedral stubby crystals upto 2mm in length and 0.5mm in diameter with occasional subhedral grains. They are often poikilitically surrounded by plagioclase.

Sphene is found as dark brown crystals of variable habit. They can be euhedral to subhedral in the groundmass or anhedral in quartz crystals. Anhedral sphene is also found in hornblende and could possibly be secondary from primary titanium-hornblendes (Plate 10.3). Exsolution of granular sphene is thought to be the result of low temperature alteration.

Magnetite is found only in the hornblende aggregates and has been found to be pseudmorphed by haematite.

Some sulphides are present interstitially, such as pyrite and chalcopyrite, in very low amounts, and are obvious against such a mafic background. Rare zircons are present.

Plate 10.3 View of an anhedral sphene in PPL (Ranachan) found within hornblende - Sample D33, Fig.9.1A. Field of view 3mm.

Plate 10.4A View of the general texture of the Rubha-na-Sroine diorite with large poikilitic biotites in PP1 - Sample D2, Fig.9.1B. Field of view 3mm.

10.2.2 Rubha-na-Sroine (Fig 1.2, loc 2)

The Rubha-na-Sroine diorite is a very mafic looking medium to coarse grained diorite with appinitic affinities and is a monzodiorite according to Streckeisen (Table 10.1). It consists mainly of biotite and hornblende with subordinate feldspar, never as phenocrysts, and quartz. This body shows crude layering, that is picked out by the poikilitic biotite crystals. This layering has been measured as dipping at 51º and striking at the diorite margin (Fig 9.1B). The difference between the layers is firstly in the size of the poikilitic biotites, 25mm in coarse layers and 3mm in fine layers, and secondly the leucocratic portion of the groundmass becomes finer grained and more disseminated in the finer grained layers.

Dark brown poikilitic biotite crystals commonly range in size from 3 to 10mm in diameter with some reaching 25mm. They are subhedral in form with ragged edges. They also form smaller crystals of less than 1mm, intimately associated with hornblende in aggregates. Biotite is seen to be commonly altered to chlorite, but sphene, clinozoisite (also yellow epidote) and occasionally rutile and prehnite (which is not uncommon in the Appinite suite) also occur as alteration products. All this occurs along the cleavage planes. Inclusions of apatite are relatively common (Plate 10.4A, B & C). The biotites enclose aggregates of pale hornblende that could be pseudomorphs of clinopyroxene prisms (Plate 10.4).

The modal amount of poikilitic biotite does vary greatly in this body from 25-30% to less than 5%. Where biotite is present as fine grained crystals, there is a higher proportion of hornblende, feldspar and quartz, but this is not apparent in hand specimen,

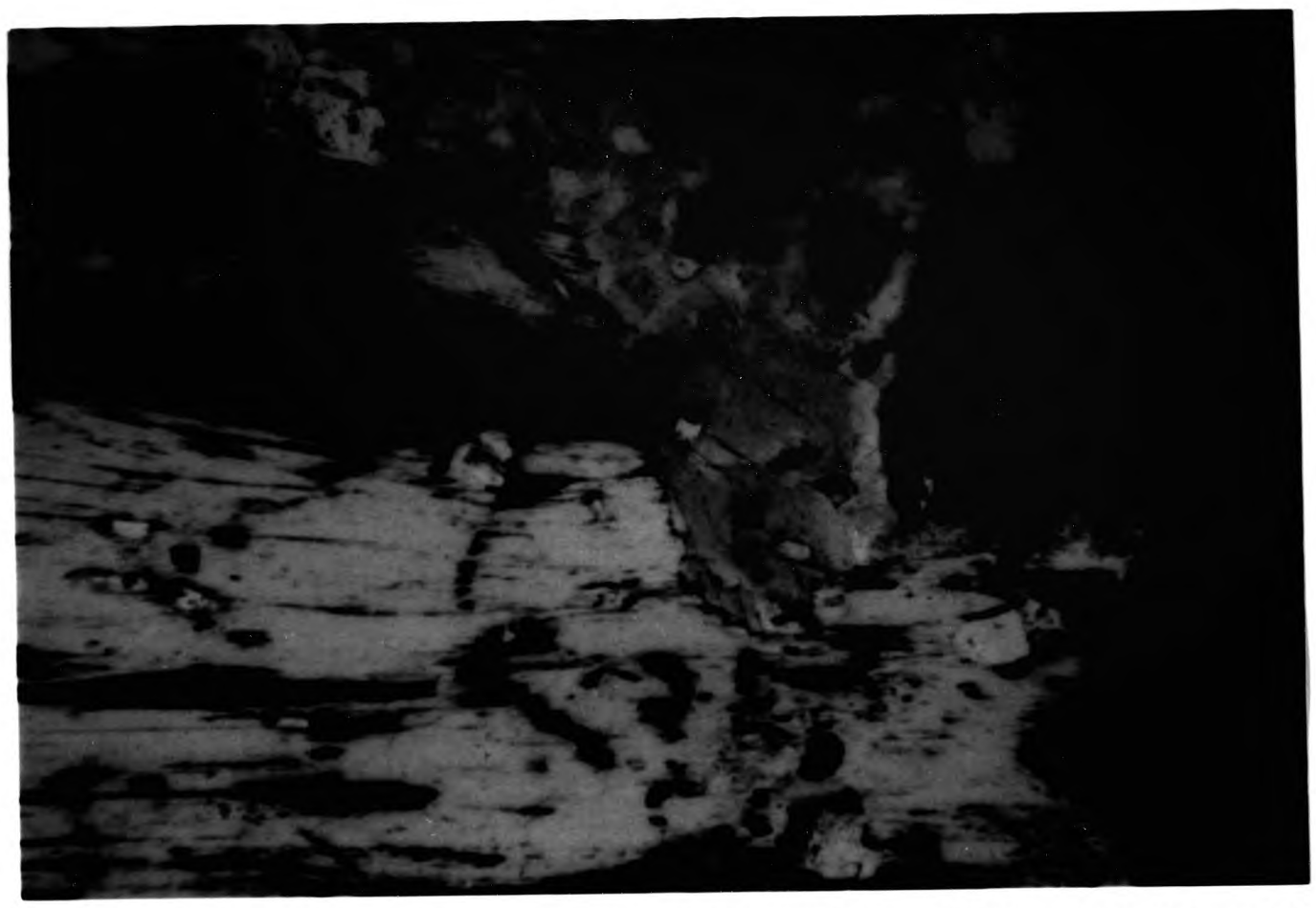

Plate 10.4B View of the general texture of the Rubha diorite with large biotite crystals with assocaiteed sphene exsolution along the cleavage in PPL - Sample D5A, Fig.9.1B. Field of view 3mm.

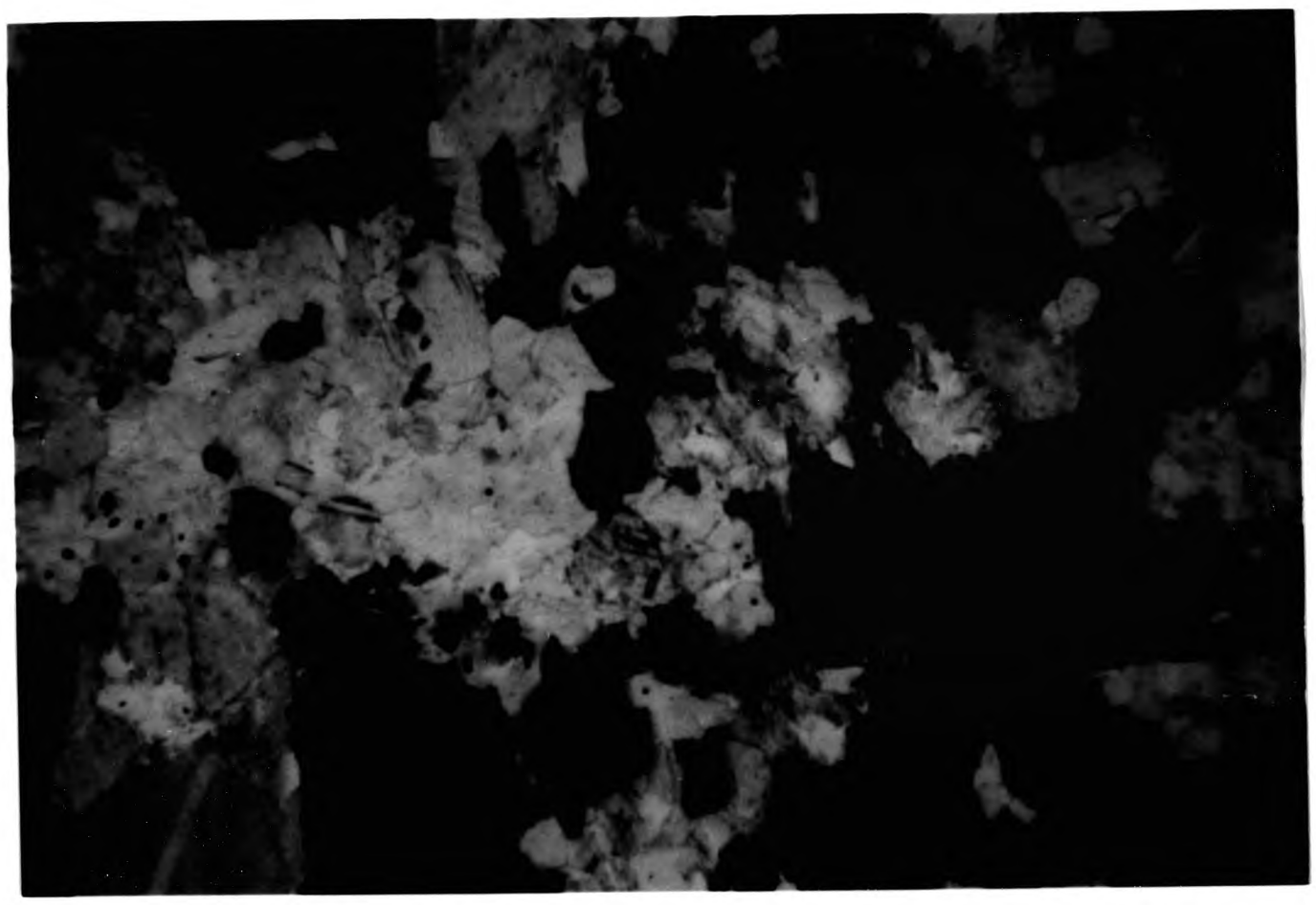

Plate 10.4C View of a large biotite in PPl showing its poikilitic nature - Sample D1, Fig.9.1B. Field of view 3mm.

only under the microscope. Poikilitic biotite encloses other smaller biotite crystals and often part of the leucocratic groundmass.

Hornblende occurs as equigranular subhedral to anhedral stubby prisms of 1-4mm in the matrix or in aggregates of upto 5mm in diameter. It is not found as phenocrysts in any part of this body. In any form hornblende usually is medium green in colour. Rare examples of brown hornblende are noted. Biotite is present in the hornblendes and is far more common in the green hornblendes.

The grains in the hornblende aggregates are very fine, generally less than 1mm in length. It appears that there is no primary hornblende in the aggregates or as single crystals, but all is the result of alteration. Single crystals of biotite are seen to be surrounded by a larger skeletal hornblende that is in optical continuity.

Feldspar is interstitial as poikilitic grains or as small single interstitial grains throughout the diorite and has variable modal amounts, but is still essentially subordinate. Both plagioclase and alkali feldspar have been found, though alkali feldspar is not so common.

Alkali feldspar very often shows a granophyric texture and only minor perthitic exsolution. It is also seen to jacket the plagioclase grains on occasion.

Plagioclase shows a compositional range from mid-andesine to oligoclase(An36-20) with individual anhedral poikilitic crystals reaching 5mm in size. They enclose acicular apatites and tiny

biotite and hornblende crystals. Multiple twinning is well developed in plagioclase and normal zoning is often seen surrounding the twinned cores. Alteration to sericite is very common and varies from complete alteration to limited alteration along the twin planes. Plagioclase is also seen in small amounts in the perthitic texture of the uncommon alkali feldspar.

Myrmekitic and graphic intergrowths are also found.

Quartz is present in only minor amounts and always found interstitially together as small grains with feldspar. Its modal percentage is less than 5%.

Sphene occurs as small subhedral to anhedral crystals upto 1mm. It is often found together with biotite and hornblende and in some cases gives the appearance of being the result of biotite alteration.

Apatite forms medium to coarse euhedral needles of upto 0.2mm in diameter, occasionally possessing tiny inclusions of biotite.

Opaque minerals such as sulphides and magnetite do occur, but in relatively minor amounts. The sulphides found commonly include pyrite with occasional chalcopyrite and millerite. Subhedral to euhedral magnetite is scattered throughout the diorite, but is most often associated with biotite and the hornblende aggregates.

10.2.3 Liddesdale (Fig 1.2, loc 3)

This is a mafic medium to coarse grained diorite, with occasional porphyritic types. The types of diorite that occur in this body

range from very mafic rich types to leucocratic diorites with euhedral hornblende prisms ie appinitic types.

Hornblende appears to be the most abundant of the mafic minerals. Both brown and green forms are present. The habit of brown hornblende before alteration was probably stubby subhedral to euhedral crystals, but more commonly it is found as remnants within green hornblende and surrounding amphibolized pyroxene. There is also linear exsolution of sphene and opaques in these hornblendes. Brown hornblende generally is jacketed by a later paler green amphibole with included opaques (Plate 10.5A & B). This jacket is in optical and therefore physical continuity with the brown hornblende.

The green hornblende is seen in a variety of habits from euhedral acicular and stubby prisms (upto 7mm long; Plate 10.6) to occasional very fine grained crystals in aggregates. The hornblendes in the aggregates are usually randomly oriented. They are also seen to be intergrown with biotite (described below). In the finer groundmass green hornblende is also present as euhedral crystals, showing few signs of any form of alteration.

Subhedral crystals of quite fresh orthopyroxene and occasional cpx are also quite commonly present (Plate 10.7A & B). They are often highly altered to hornblende, which pseudomorphs its original form.

There is a reasonably high proportion (15-25%) of biotite and it is often an alteration product of prismatic mafics. In the Liddesdale body biotite is found as single subhedral to euhedral crystals reaching 5mm, but on average 1 to 3mm in length. Biotite is also seen in aggregates where it appears in two distinct forms. It is

Plate 10.5A View of a once brown hornblende jacketed by a pale green hornblende in PPL (Liddesdale) with biotite and opaques in the core - Sample D50, Fig.9.1C. Field of view 3mm.

Plate 10.5B The same view in XPL - Sample D50.

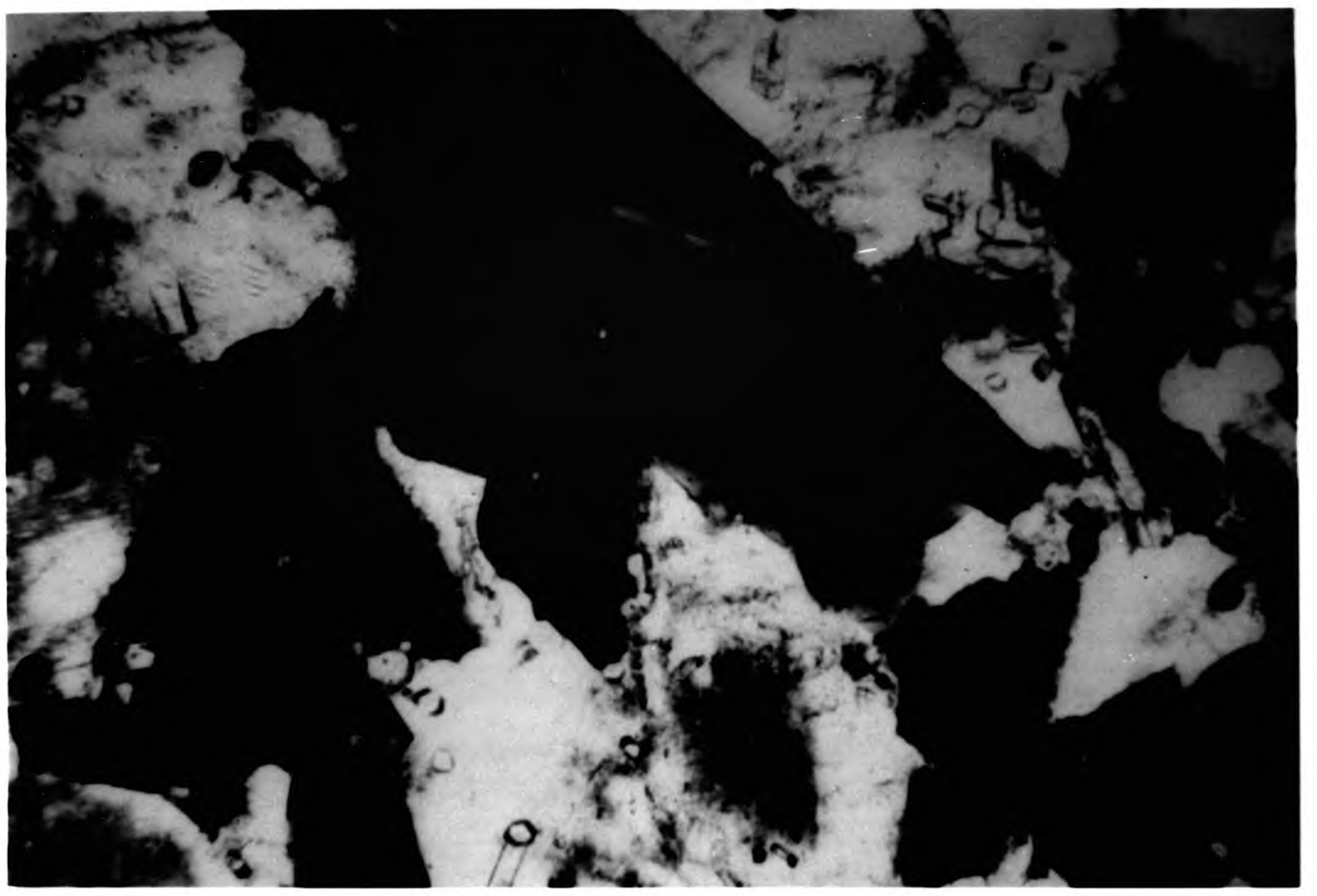

Plate 10.6 View of green prismatic hornblende in PPl (Liddesdale) with numerous apatites in the surrounding matrix - Sample D58, Fig.9.1C. Field of view 3mm.

Plate 10.7A View of euhedral to subhedral opx and green/brown hornblende in PPL (Liddesdale) - Sample D11. Field of view 3mm.

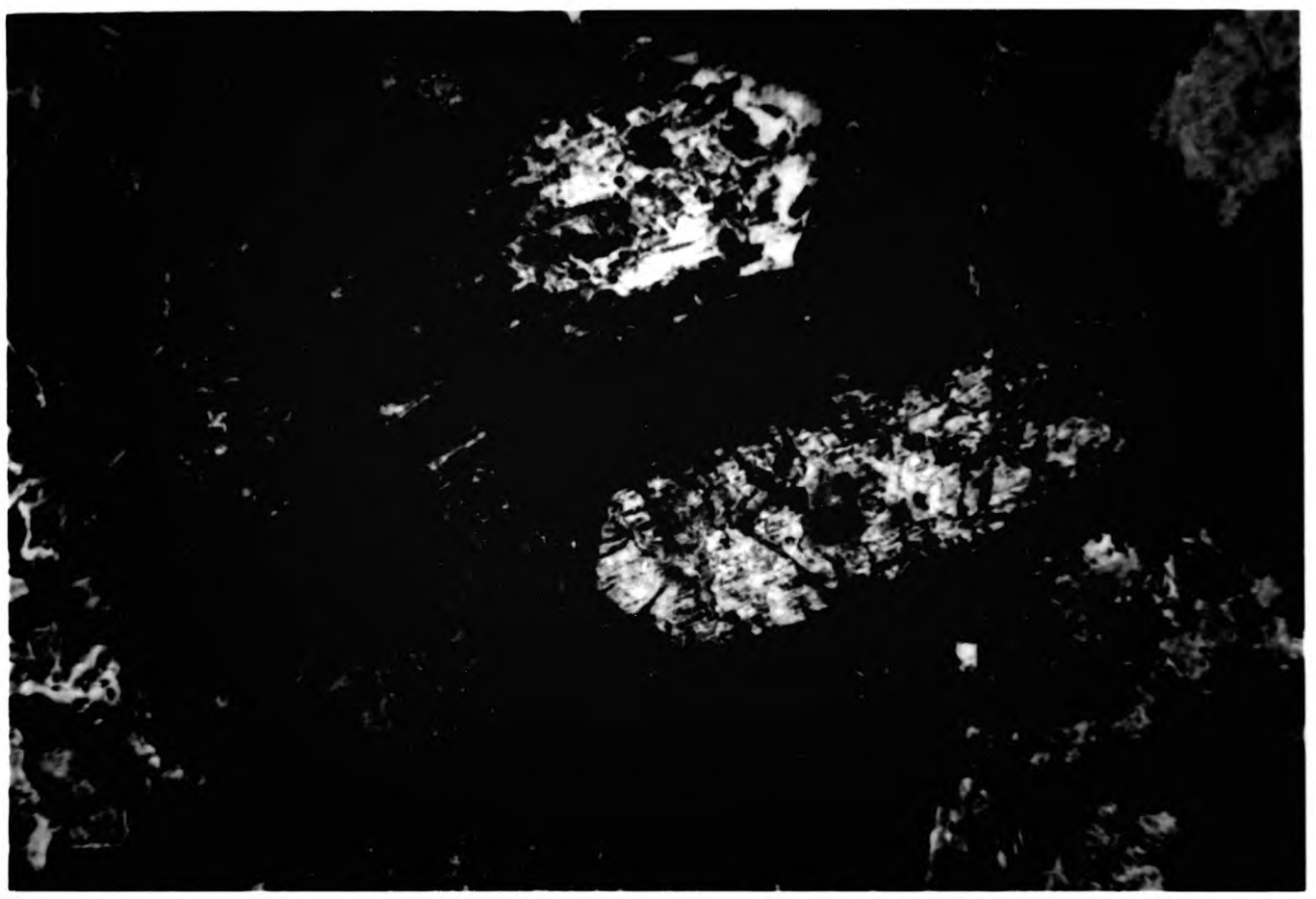

Plate 10.7B The same view as 10.7A, but in XPL showing clearly the interstitial plagioclase - Sample D11.

Plate 10.8A View of larger biotite crystal with cross cutting smaller biotite lathes in PPL (Liddesdale) - Sample D12. Field of view 3mm.

seen as large anhedral crystals, often skeletal, associated with hornblende and present within the hornblende crystal. This is often where it suggests that they are the result of alteration of an earlier brown hornblende or even pyroxene. These larger biotite crystals often have smaller acicular biotite lathes cutting across (Plate 10.8A). Biotite is present in small fine grained aggregates pseudomorphing what was once a hornblende (Plate 10.8B). Here the crystals are well developed and randomly orientated in the original crystal limits. These two forms have even been noted on one crystal (Plate 10.8C). Biotite is reasonably fresh in the Liddesdale body, only occasional chlorite and epidote replacement are seen.

Plagioclase is generally interstitial as anhedral crystals occasionally showing poikilitic habits. Such individual grains can reach 7mm in size and surround the remnant pyroxene, green hornblende and apatite.

All the feldspars show good multiple twinning and variably developed normal zoning, usually a uniform core with zoned margin. Alteration most commonly follows the twin planes or is found in the cores of the grains (Plate 10.9A & B).

Quartz is only present in small amounts as single interstitial grains or as finer anhedral grains with plagioclase. There are rare examples of myrmekitic texture.

Apatite is present in a number of habits and in variable amounts. Most commonly they are found as numerous 1mm long acicular needles surrounded by biotite or plagioclase. Coarser grained apatites are found in areas without apatite needles.

Plate 10.8B View of biotite aggregate pseudomorphing a hornblende crystal in PPL (Liddesdale) - Sample D11. Field of view 3mm.

Plate 10.8C View of a large hornblende crystal being pseudomorphed by biotite in 2 orientations in PPL (Liddesdale) - Sample 11. Field of view 3mm.

Plate 10.9A View of a plagioclase crystal showing inclusions of hornblende and apatite in PPL, also with alteration in the core - Sample D58, Fig.9.1C. Field of view 3mm.

Plate 10.9B The same view as 10.9A, but in XPL showing the twinning and zoning of the plagioclase - Sample D58.

PAGE
MISSING

Sphene is not so abundant as in the other diorites, but is most commonly observed associated with biotite and hornblende or as individual anhedral grains. Larger and more euhedral sphenes are present in the more leucocratic diorite.

Magnetite is found within the hornblende aggregates or pseudomorphed hornblende crystals. It forms anhedral to subhedral grains with size ranging from 0.1 to 1mm across.

10.2.4 Sheet (Fig 1.2, Location 4 & Fig.9.1D)

This shows a very different assemblage to the Loch Sunart diorites. The diorite varies from a fine to medium grained fairly mafic diorite with a 'spotty' appearance to a medium grained mafic diorite with hornblende and biotite not only in aggregates, but as individual crystals in the matrix. When this 'spotty' type occurs the general groundmass is much finer grained, slightly paler grey in colour and relatively more biotite-rich. It contains large plagioclase phenocrysts and quartz xenocrysts, with mafic aggregates of hornblende and biotite similar to those of Liddesdale and Ranachan. This diorite has no preferred orientation or fabric. There is little original primary texture left in the mafic component, with brown hornblende surrounding pyroxene, then altered by green hornblende. Though plagioclase appears to be primary.

Green hornblende is observed in a number of habits, though many of them are not primary. There are a few rare remnants of brown hornblende amid a jacket of green hornblende together with biotite. The brown amphibole is also zoned with the interior being full of opaque exsolution products and the margins free of inclusions.

Most commonly hornblende is secondary as fine grained subhedral to anhedral crystals either individually or in aggregates (Plate 10.10A & B). These (Plate 10.11) aggregates range in size from 1 to nearly 10mm and are surrounded by an equigranular corona of biotite lathes. The aggregates have a hornfels texture. Sphene and magnetite occur in these aggregates, though their amounts are variable.

Hornblende is also present as medium grained, single subhedral to anhedral crystals. Some may have a mottled aggregate core, full of inclusions, with a jacket of magmatic origin (Plate 10.12 & 10.13). The single hornblendes are often jacketed by a paler green hornblende, which produces a more subhedral to euhedral form. They also have sphene alteration along their cleavage planes.

The core may be due to a subsolidus change of pyroxene or even brown hornblende. The inclusions within the single hornblende (Plate 10.12) occur either in the core or in a particular zone within the crystal margins. These inclusions are commonly very fine apatites together with euhedral magnetites.

Rare clinopyroxenes have been found. They occur within the single crystal hornblendes, never in the aggregates, suggesting that the aggregates may represent some other early anhydrous mafic eg. opx/pigeonite or even olivine. Those pyroxenes which are not being altered have been observed to be surrounded by the interstitial feldspar. So the pyroxene is either being replaced by or co-exists with the amphibole.

Biotite is not as common as hornblende in this diorite body and is generally seen as an alteration product or as individual crystals in

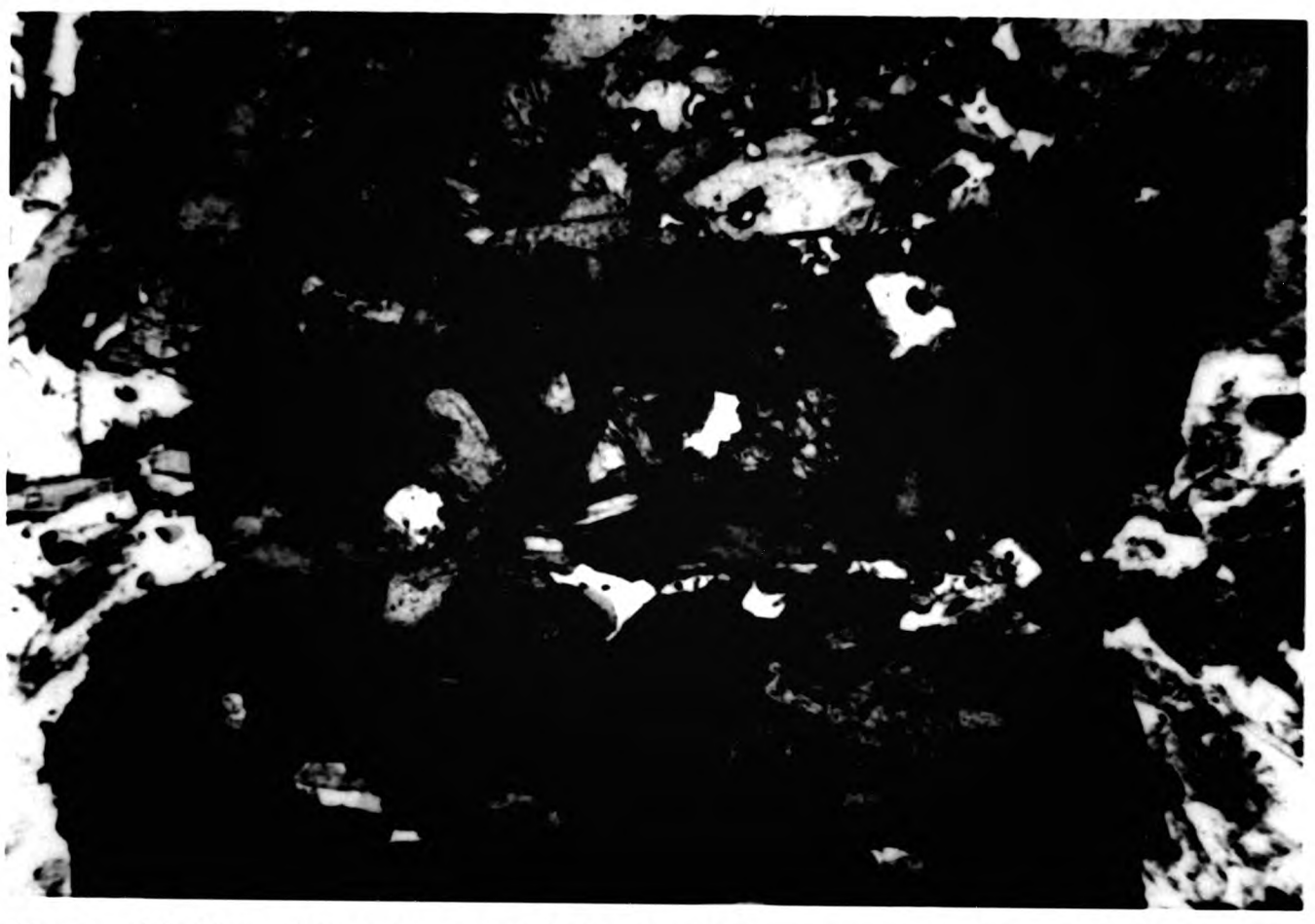

Plate 10.10A View of a hornblende-rich aggregate (top half) and a single hornblende phenocryst in PPL (Sheet) - Sample D45, Fig.9.1D. Field of view 3mm.

Plate 10.10.B The same view as 10.10B but in XPL with the hornblende phenocryst in extinction (except inclusions) - Sample D45. Field of view 3mm.

Plate 10.11 View of a hornblende aggregate surrounded by biotite lathes in PPL (Sheet) - Sample D25. Field of view 3mm.

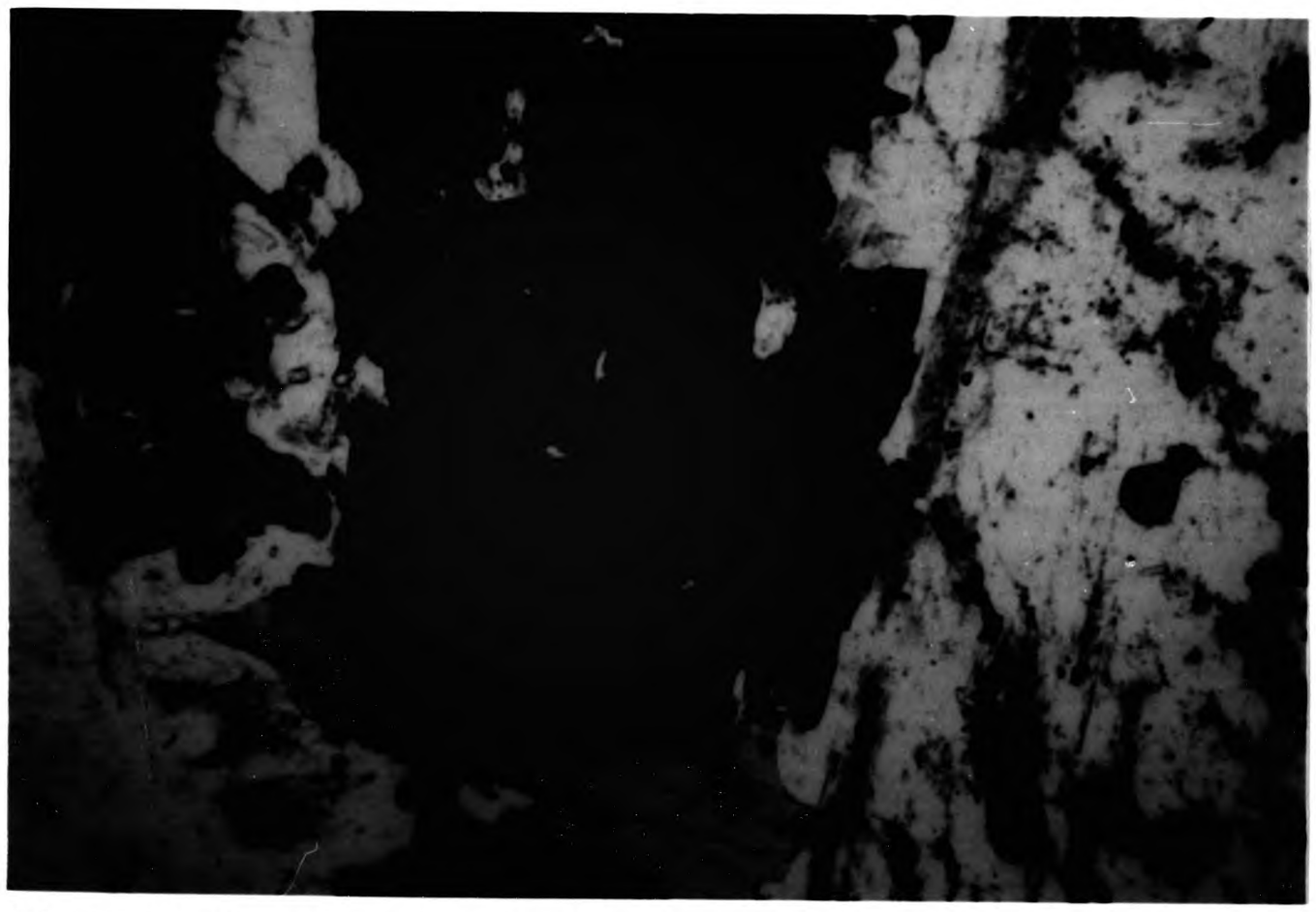

Plate 10.12 View of a single subhedral hornblende crystal in PPL (Sheet) showing inclusion-rich zone within and biotite around the margins - Sample D25. field of view 3mm.

the groundmass. When replacing hornblende, biotite either appears as fine grained crystals within the hornblende crystal or as larger grains cutting across the limits of the hornblende. Its size ranges from 0.1 to 2mm in length and form from anhedral to subhedral. Alteration products of biotite include chlorite and epidote.

Both plagioclase and alkali feldspar are present, though plagioclase is dominant. Both are seen as phenocrysts. The plagioclase shows a range of forms from subhedral lathes of 0.5 to 4mm in length in the groundmass to phenocrysts of 10mm. The groundmass plagioclase show very fine lamellar twinning and compositionally are often in the labradorite to andesine range (An58-36) from core to rim (Plate 10.14B). Zoning is more common in the slightly larger lathes and includes simple continuous zoning and occasional examples of reverse zoning. Many of the plagioclase crystals show signs of alteration and this is more common in the cores, though certain twin planes are susceptible too.

The plagioclase phenocrysts appear blotchy and spongy. The spongy plagioclase core is full of hornblende and the outer margin is completely free of it (Plate 10.14A, B & C). Just outside the core there is always a highly sericitized zone. This spongy/skeletal texture could result from skeletal growth or partial absorption of plagioclase as seen in hybrid andesites. The latter seems more plausible as the outlines of the zones (as seen in Plates 10.14A, B & C) are anhedral. Plate 10.14C shows a plagioclase with inclusions in its core and a highly altered compositional zone.

Alkali feldspar is mainly found in these diorites as subhedral phenocrysts, reaching 10mm in length. They commonly have euhedral to

Plate 10.13 View of the general hornblende texture in PPL (Sheet) - Sample D27. Field of view 3mm.

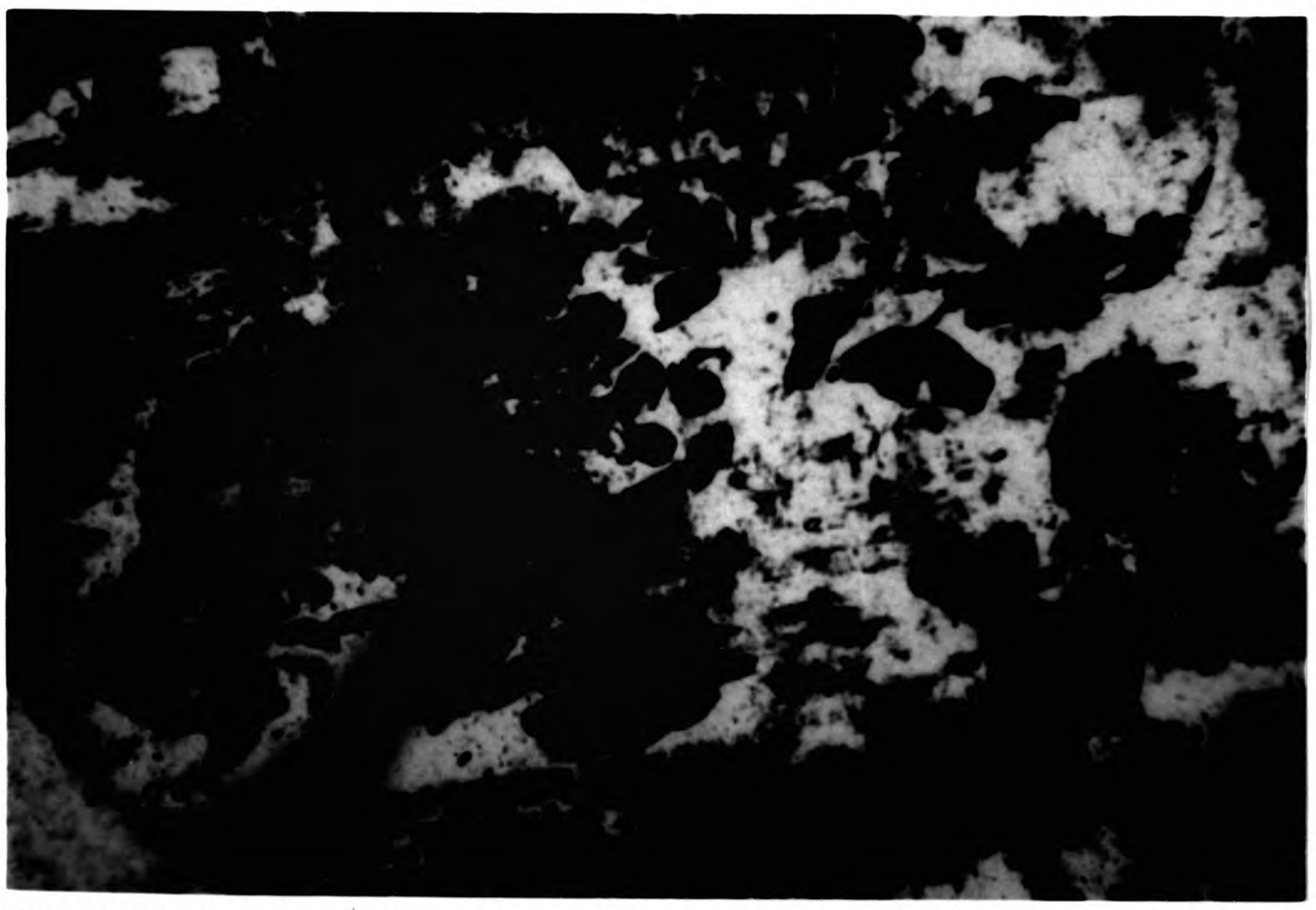

Plate 10.14A View of a plagioclase phenocryst with a spongy/skeletal texture in PPL (Sheet), full of rounded inclusions of hornblende and biotite - Sample D28. Field of view 3mm.

Plate 10.14B The same view as 10.14A but in XPL, showing the plagioclase twinning and the optical continuity of the included hornblende - Sample D28.

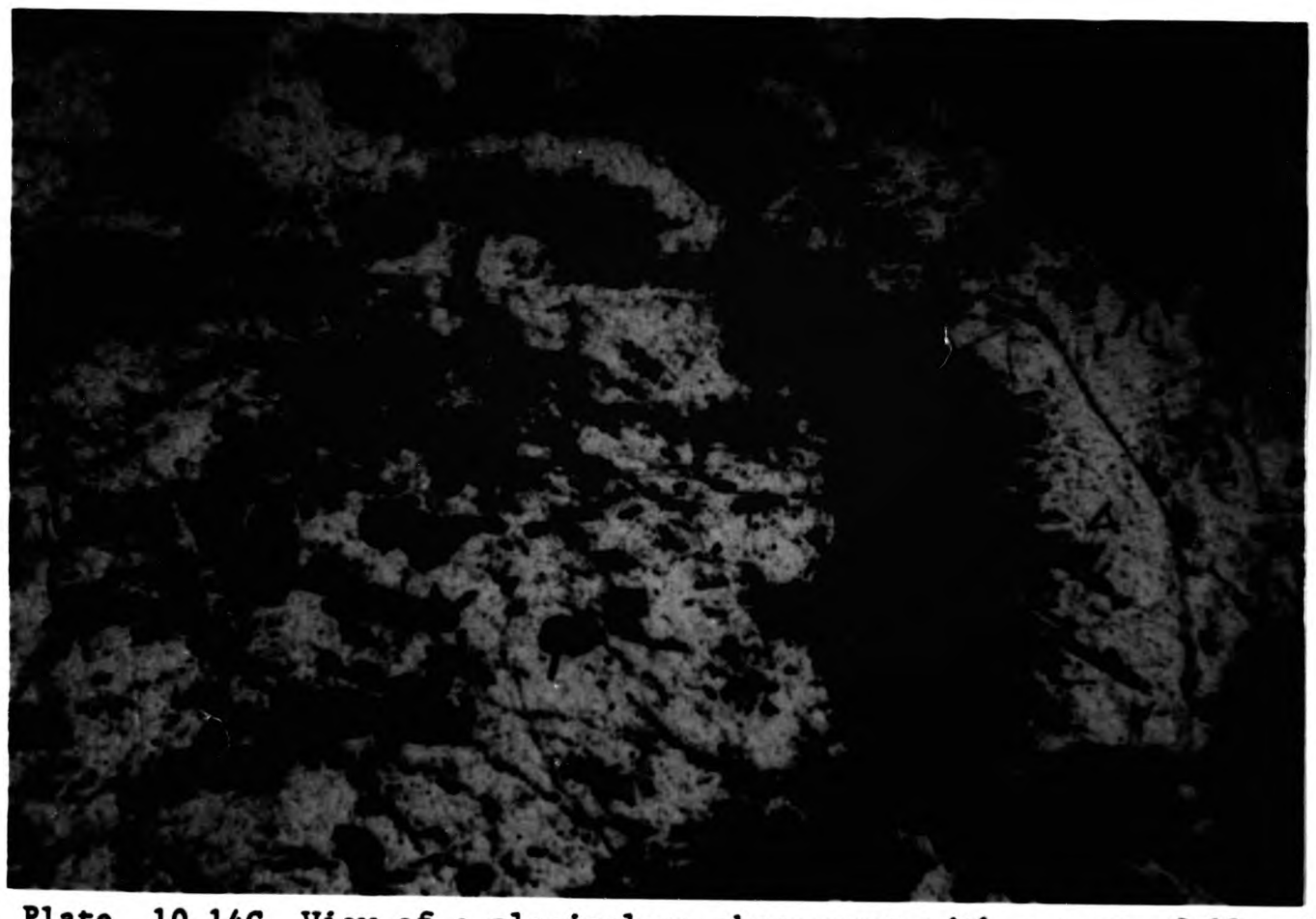

Plate 10.14C View of a plagioclase phenocryst with a core full of inclusions and a highly altered zone in PPL (Sheet) - Sample D25. Field of view D25.

subhedral inclusions of green hornblende and occasionally biotite and apatite. The hornblende inclusions are sometimes found concentrated in the core.

Quartz is present in extremely variable amounts and is more abundant in the leucocratic patches together with the feldspar. Some anhedral grains reach 1mm, while most (15% or less) quartz is mainly small and interstitial.

Quartz xenocrysts have been observed in this dioritic body and occur right across to the most western side of the diorite away from the granitic sheet, but not along its entire length. These xenocrysts (or even megacrysts) reach 3mm in diameter and are roughly rounded in shape with a trace of a bi-pyramid habit. They are often outlined by fine crystals of biotite and occasionally hornblende. Since the quartz in the host granodiorite is interstitial these cannot result from in situ mixing, but mixing may have occurred with a porphyritic alkali granite magma at depth.

Accessory minerals occur in varying amounts and include sphene, apatite, magnetite and primary sulphides.

Sphene is very common throughout this body as anhedral to subhedral brown crystals of upto 1mm in length. It is also seen as skeletal/spongy crystals together with hornblende.

Apatites are not as abundant as in the other diorite bodies, but small stubby crystals are seen throughout as inclusions especially in the leucocratic parts.

Magnetite only is found associated with hornblende. It is subhedral to euhedral in form and located either in the core or as discrete zones in the aggregates. The most common sulphides are pyrite and chalcopyrite.

10.2.5 Loch Tearnait (Fig.1.2, Location 6)

Loch Tearnait is a medium to fine grained porphyritic mafic diorite with a well developed fabric, which is picked out by the alignment of mainly biotite and amphibole. Plate 10.15A & B show this texture clearly.

Green hornblende forms large single euhedral crystals of upto 4mm. A slightly darker green hornblende forms smaller subhedral crystals of upto 1mm in the groundmass. They occur as single crystals or in small aggregates together with biotite. No pyroxene or brown hornblende have been found.

Biotite is also present as subhedral to euhedral lathes or with hornblende, but never pseudomorphing hornblende.

Plagioclase and quartz have a semi-granoblastic texture, which is also aligned. Zoning in the plagioclase is very common throughout all the grains regardless of size. Occasional plagioclase phenocrysts show good multiple twinning and zoning. Alteration occurs along certain compositional zones and inclusions in cores are not uncommon.

Euhedral sphenes and abundant fine acicular apatites (in the plagioclase) are present.

Plate 10.15A View of the general texture of the Loch Tearnait diorite, showing the alignment of the biotite around a large hornblende in PPL - Sample D80. Field of view 3mm.

Plate 10.15B View of the general texture of Loch Tearnait diorite - Sample D80. Field of view 3mm.

10.3 PETROGRAPHY OF THE UILEANN DIORITES

(Fig.1.2, Location 5 & Figs.9.1E & F)

The rocks of these diorites range from pink leucocratic types to the ultramafic rich in hornblendes. They are medium to fine grained and consist of green hornblende, biotite, plagioclase and alkali feldspar and quartz.

Green hornblende in both the core and marginal zone of the body, is the dominant mafic mineral with rare examples of brown hornblende. The habit of green hornblende varies from small equigranular crystals in the groundmass and fine to medium grained aggregates of upto 5mm in diameter to larger skeletal single crystals. The aggregates possess a very variable amount of anhedral to subhedral magnetites of grain sizes from minute 0.01mm grains to 0.5mm across. There is often a paler green amphibole jacketing the aggregates (Plate 10.16). Single earlier hornblendes are present. Rare examples are seen of earlier formed pyroxene or brown hornblende within green hornblende. Compositionally hornblende is an actinolitic hornblende with occasional edenitic and magnesio-hornblendes.

Biotite occurs in a variety of forms. They quite commonly form large poikilitic types (as in Rubha-na-Sroine Plate 10.17) and smaller subhedral grains in the ground mass to small lathes, associated with the hornblende aggregates. There is evidence to suggest two forms of biotite in the aggregates ie one where the biotite shows a syntaxial texture with hornblende and the other where lathes of biotite randomly cut across the aggregates and the equigranular hornblende. Biotite is also seen to form a very fine grained jacket around the green hornblende aggregates (Plate 10.16) which are pseudomorphing

Plate 10.16 View of the fine grained pale green hornblende aggregate surrounded by biotite in PPL (Uileann) - Sample D73, Fig.9.1F. Field of view 3mm.

Plate 10.17 View of a large poikilitic biotite in PPL from the core of Uileann - Sample D57, Fig.9.1E. Field of view 3mm.

earlier euhedral minerals. It has also been observed around remnant brown hornblendes where it has grown in optical continuity.

Biotite shows little chlorite alteration, but very often has anhedral skeletal sphene either at its margins or throughout the grain itself. In the zone of extensive net-veined diorite, the amount of biotite is much reduced and that present is patchy and unevenly distributed (Table 10.1). This is the case for the granite too.

Both plagioclase and alkali feldspar are present and both are equally highly altered. Plagioclase gives compositions of oligoclase - An 28-21. The feldspars range in form from medium grained anhedral lathes, and interstitial grains to occasional phenocrysts. In the marginal zone of the mafic diorite small plagioclase lathes (now highly weathered) are seen to be completely enclosed by a large interstitial alkali feldspar.

In the net-veined dioritic parts of this complex, the proportion of interstitial alkali feldspar increases. It shows some granophyric texture, simple twinning and often has inclusions of biotite and apatite, though not much evidence of any perthitic texture.

There is some interstitial quartz throughout the dioritic types but in the marginal zone, it also forms xenocrysts. The xenocrysts reach 4mm in diameter and have a rim of mafic minerals, mainly hornblende, which completely surrounds them (Plate 10.18). These xenocrysts are more rounded and generally larger than the quartz found in the surrounding host biotite granite. They also have a layer of feldspar around them inside the mafic reaction rim.

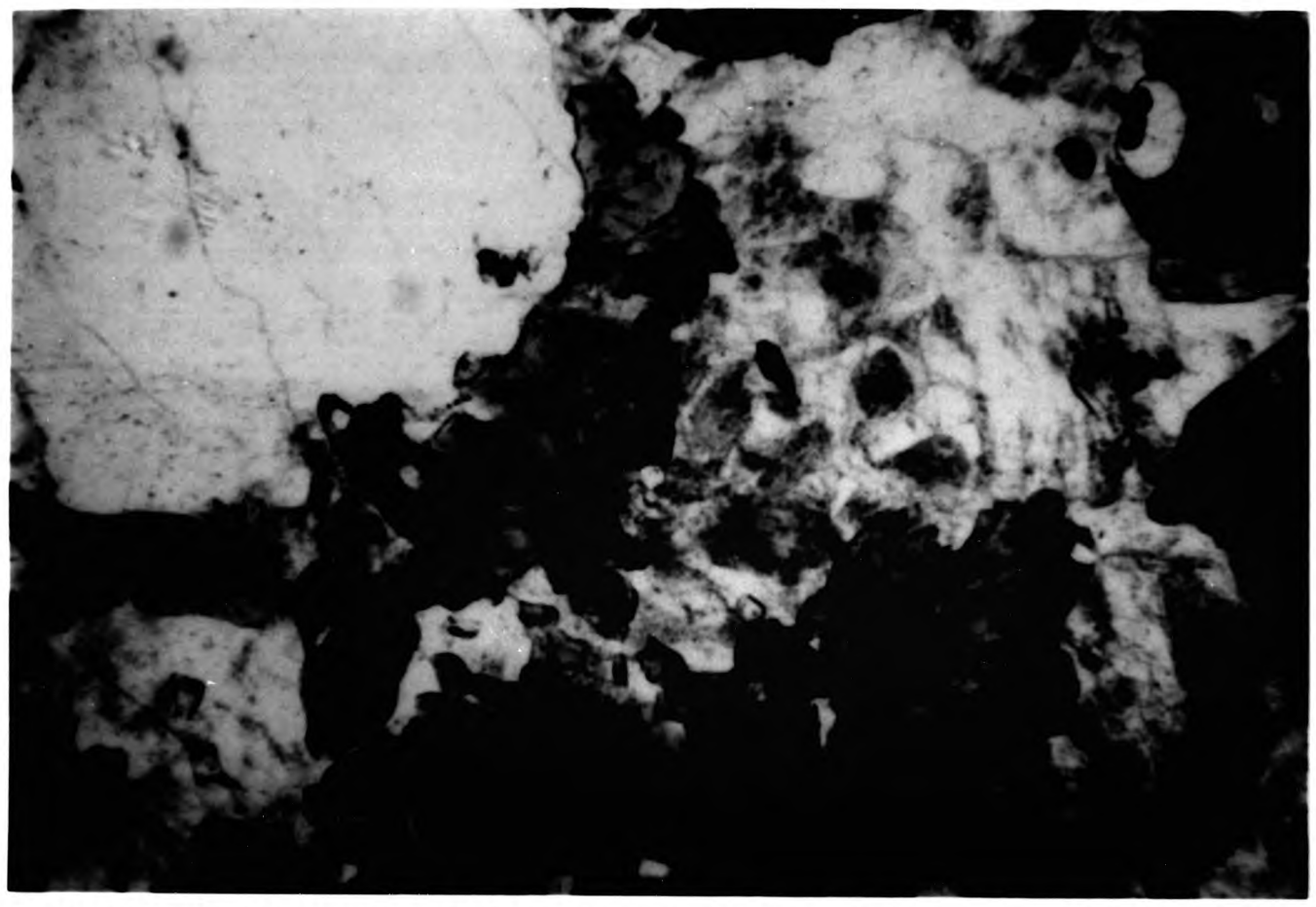

Plate 10.18 View of a quartz xenocryst (top left corner) surrounded by biotite and hornblende in PPL - Sample D63, Fig.9.1E. Field of view 3mm.

Accessory minerals in these Uileann diorites are mainly apatite, sphene and magnetite. Apatite is generally present in the core as large stubby prisms of 2mm in length and 1mm in diameter, whilst in the marginal and mottled zone it forms numerous fine acicular needles reaching 2mm in length. Sphene is only present as small anhedral or skeletal/spongy grains generally associated with biotite and hornblende. Magnetite is found in the hornblende rich aggregates as subhedral grains.

10.4 MINERAL CHEMISTRY

Analyses of the different minerals are all given in Appendix C together with those from the host rocks and xenoliths. Mineral chemistry of all the diorite bodies will be discussed together and where any outstanding feature is present it will be described separately.

10.4.1 Plagioclase

The diorite plagioclase displays a wider range of compositions (An 58-20) than the granites (An42-22), but are nearly equal in range with the xenoliths (An54-22).

The K-Na-Ca (atomic percent) diagram (Fig 3.4D) displays clearly the range of plagioclase compositions. Figure 3.5 where compositional range is plotted against bulk rock MgO, again the diorites show the wider range than the granite or xenoliths. The mafic diorites have an overall higher bulk rock MgO content (upto 13.5%) than the granites and xenoliths. The highest MgO values are associated with some of the lowest An values for the diorites. There is some

separation of 2 of the diorite bodies from the main field, between 11-8% MgO. This is the result of the Liddesdale and Rubha diorites having a higher mafic proportion and lower feldspar content than the other diorites analyzed.

In a single diorite sample the larger non-porphyritic plagioclase in the groundmass may show a very wide range of core to rim values eg. D19 An58-36. Core and rim values may display their own ranges too, which overlap with each other considerably: core An58-28; middle An48-25 and rim An54-20. Smaller interstitial crystals are often unzoned and of andesine to oligoclase (An36-20) composition. There is no plagioclase phenocryst data available.

Zoning is very common in the diorite plagioclase, with normal zoning mainly eg. core An58 to rim An36 or core An49 - middle An44 - rim An45. One unusual feldspar (D12 of Liddesdale) was analyzed (Fig 3.4D) with 25% K component in the core and with a jacket of An54. The probe may well have analyzed sericite instead of the core of the crystal as the feldspar is highly altered and so would give a high K content. Reverse zoning has not been noted at all in the mafic diorites. High Ba values show that whole rock Ba is magmatic and not a secondary feature resulting from $BaSO_4$.

Alkali feldspars have only been analyzed from the Uileann bodies giving compositions of Or97-89, Ab3-11, An0.

Table 10.2 REPRESENTATIVE PLAGIOCLASE ANALYSES FROM THE MAFIC DIORITES

	D2 Rubh 9Rim	D41 Rana 6Mid	D12 Lidd 7Mid	D19 Shet 12Mid	D63 Uile 14
SiO_2	64.04	61.09	60.59	59.15	64.02
TiO_2	-	-	0.02	-	-
Al_2O_3	22.52	23.64	24.04	25.62	18.49
FeO*	0.08	0.07	0.09	0.09	0.11
MgO	0.01	-	0.02	-	0.02
CaO	3.54	4.74	5.61	7.13	-
Na2O	9.18	8.95	8.25	7.66	1.14
K2O	0.35	0.26	0.22	0.24	14.41
BaO	-	-	-	0.02	0.46
Total	99.72	98.75	98.84	99.91	98.65
Ab	70.2	64.2	58.5	50.9	7.4
Or	2.7	1.8	2.0	1.6	92.6
An	27.1	34.0	39.5	47.5	-
	Olig.	Ande.	Ande.	Ande.	Orth.

Table 10.3 REPRESENTATIVE AMPHIBOLE ANALYSES

	D12 Lidd 5Rim	D2 Rubh 4Rim	D11 Lidd 5	D41 Rana 1	D63 Uile 2
SiO_2	49.91	53.51	49.37	50.09	48.21
TiO_2	0.79	0.41	1.23	0.66	1.07
Al_2O_3	5.33	3.17	5.63	5.22	5.95
FeO*	11.21	9.15	9.19	10.90	13.12
MgO	15.16	17.30	17.10	16.17	14.46
MnO	0.25	0.22	0.15	0.22	0.24
CaO	12.21	12.29	11.98	12.29	11.89
Na_2O	0.90	0.66	1.12	0.97	1.46
K_2O	0.39	0.23	0.42	0.43	0.61
Total	96.15	96.94	96.19	96.95	97.01
Si	7.319	7.652	7.188	7.285	7.115
Aliv	0.681	0.348	0.812	0.715	0.885
Alvi	0.241	0.188	0.149	0.175	0.145
Ti	0.088	0.045	0.131	0.069	0.115
Fe^{2+}	1.376	1.095	1.119	1.327	1.623
Mn	0.032	0.027	0.017	0.026	0.035
Mg	3.313	3.688	3.707	3.502	3.184
Ca	1.920	1.884	1.871	1.912	1.880
Na	0.258	0.185	0.314	0.279	0.425
K	0.075	0.043	0.087	0.087	0.124
	A-Hbl.	Acti.	Mg-Hbl.	A-Hbl.	Eden.

10.4.2 Amphiboles

The majority of the amphiboles of the mafic diorites classify, according to Leake, as actinolitic hornblendes (with occasional actinolites) followed by magnesio-hornblende and edenites. Both brown and green amphiboles are present though this is not indicative of any one composition (Table 10.3).

Binns (1965) and Henderson (1966) both demonstrated that the colour of calcic amphibole is controlled by their titanium content. High Ti is correlated with a brown colour and low Ti with a green colour. There does not appear to be a textural difference between the Ti-rich and Ti-poor amphiboles ie. whether they are subhedral to euhedral or present as aggregates. The amphiboles analyzed from Strontian do show a close correlation between Ti content and colour ie. low TiO2 and most amphiboles are green. This has also been noted in the primary amphiboles of the Glen Tilt Complex (Deer 1938) and the Glenelg-Ratagain Complex (Nicholls 1950).

The actinolitic hornblendes have a lower Aliv range of 0.55 to 0.74 (or 2.5 to 5.4% Al2O3) than the magnesio-hornblendes and edenites which have a higher amounts of Aliv 0.75 to 1.1 (or 5.6 to 8.27% Al2O3).

The relationship between Aliv in hornblende and the SiO2 content of its surrounding host rock (whether granite, xenolith or diorite) is shown on Fig. 10.1. The amphiboles of Strontian have lower Aliv content than those of the island arc calc-alkaline rocks (Jakes & White 1972), but overlap with the range of continental calc-alkaline rocks. An average 1.3 Aliv for dioritic hornblendes has been

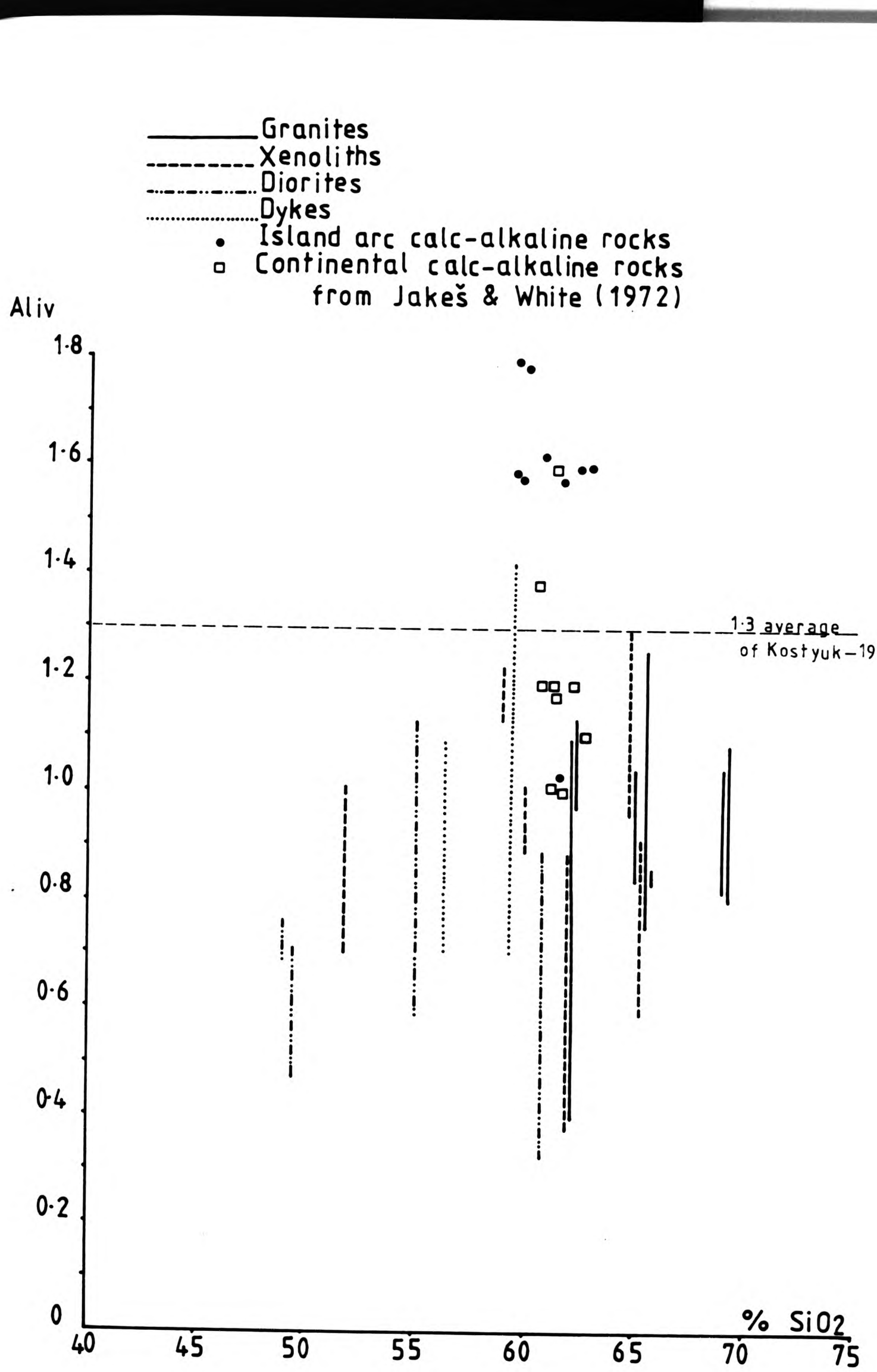

Fig.10·1 Total Aliv content of all the rock types plotted against SiO_2 content.

suggested by Kostyuk & Sobolev (1969). This is also a typical value for Aliv in hornblendes from Andean calc-alkaline rocks, but lies at the top of the range of Strontian data. The dioritic and tonalitic masses (with about 62% SiO2) are barely comparable with Andean andesites and dacites in terms of rock composition (Hamilton 1969 & 1970) and hornblende composition (0.70 to 1.41 Aliv) (Dodge et al 1968).

Table 10.4 PRESSURE FOR THE DIORITE AMPHIBOLES

Total Al in amphibole	Pressure in literature	P. from regression equation	
		1	2
D1 Rubh. 0.792-0.937	<1	0.06-0.8	0.8-1.1
D2 Rubh. 0.536-0.887	<1	-1.2-0.5	0.3-0.9
D8 Rubh. 0.6033-0.9632	<1	-0.9-0.9	0.4-1.2
D11 Lidd. 0.7284-1.1776	<1-1.7	-0.2-2.0	0.7-1.8
D12 Lidd. 0.673-1.423	<1-3	-0.5-3.2	0.6-2.6
D19 Shet. 0.7957-1.1435	<1-1.5	0.08-1.8	0.8-1.7
D41 Rana. 0.7797-1.2349	<1-2	2.3	0.8-1.9
D63 Uil. 0.2402-1.0005	<1-1	-2.7-1.1	0.07-1.3

Crystallization pressure has been calculated from the total Al data for the diorites according to the equations of Hammarstrom & Zen (1986) and Hollister et al (1987) (Table 10.4). The results are obviously nonsense as these diorites are mafic quartz-poor rocks, which are not comparable with those used for the construction of the barometer.

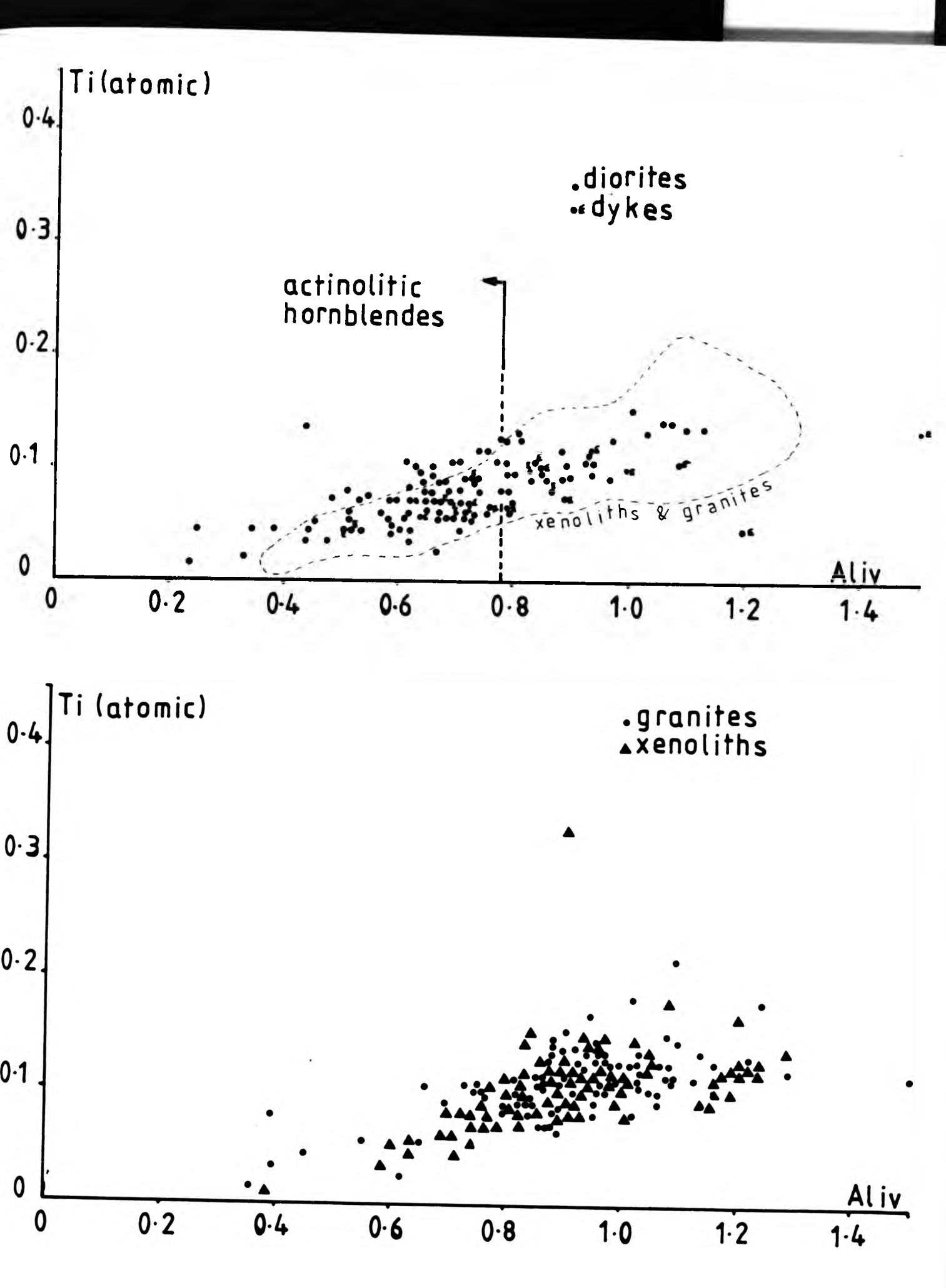

Fig.10·2 Titanium plotted against Aliv in amphiboles for all Strontian rocks.

Temperature is considered to be an important influencing factor on the titanium and aluminium content in amphiboles (Verhoogen 1962; Leake 1965; Green & Ringwood 1968; Holloway & Burnham 1972 and Albuquerque 1974). Higher temperatures favour Ti and Aliv entry into the amphibole structure. Fig 10.2 shows a positive correlation between the Ti amph. and Aliv amph. There is a substantial overlap between the different groups and all lie on the same positive linear trend of increasing Ti with increasing Aliv. The actinolitic amphiboles of the complex lie on the lower Ti and Aliv end. At about 0.8 Aliv there is a dividing line between the actinolitic hornblendes and the edenitic- and magnesio-hornblendes.

It is also suggested by some authors (eg. Leake 1965) that the titanium content of the amphiboles is controlled by the bulk rock titanium. However no such correlation is observed, which may reflect the contemporaneous crystallization of other titanium-bearing minerals such as sphene or ilmenite.

Leake (1971) suggests that high temperatures and low pressure favours high Aliv contents. A plot of Aliv vs Alvi (Fig 10.3) show a general increase of Aliv with Alvi. The amphiboles of the diorites having overall lower aluminium contents than the xenoliths and granites. So the dioritic amphiboles display a wide range of temperatures at which they were formed, supporting the petrographic view that many are secondary.

Figure 10.4 shows a positive correlation between Na+K and Aliv. The amphibole at the higher end are high temperature edenites. Intermediate compositions (Na+K 0.55 to 0.40) are the green magnesio- and edenitic hornblendes of the xenoliths and granite hosts.

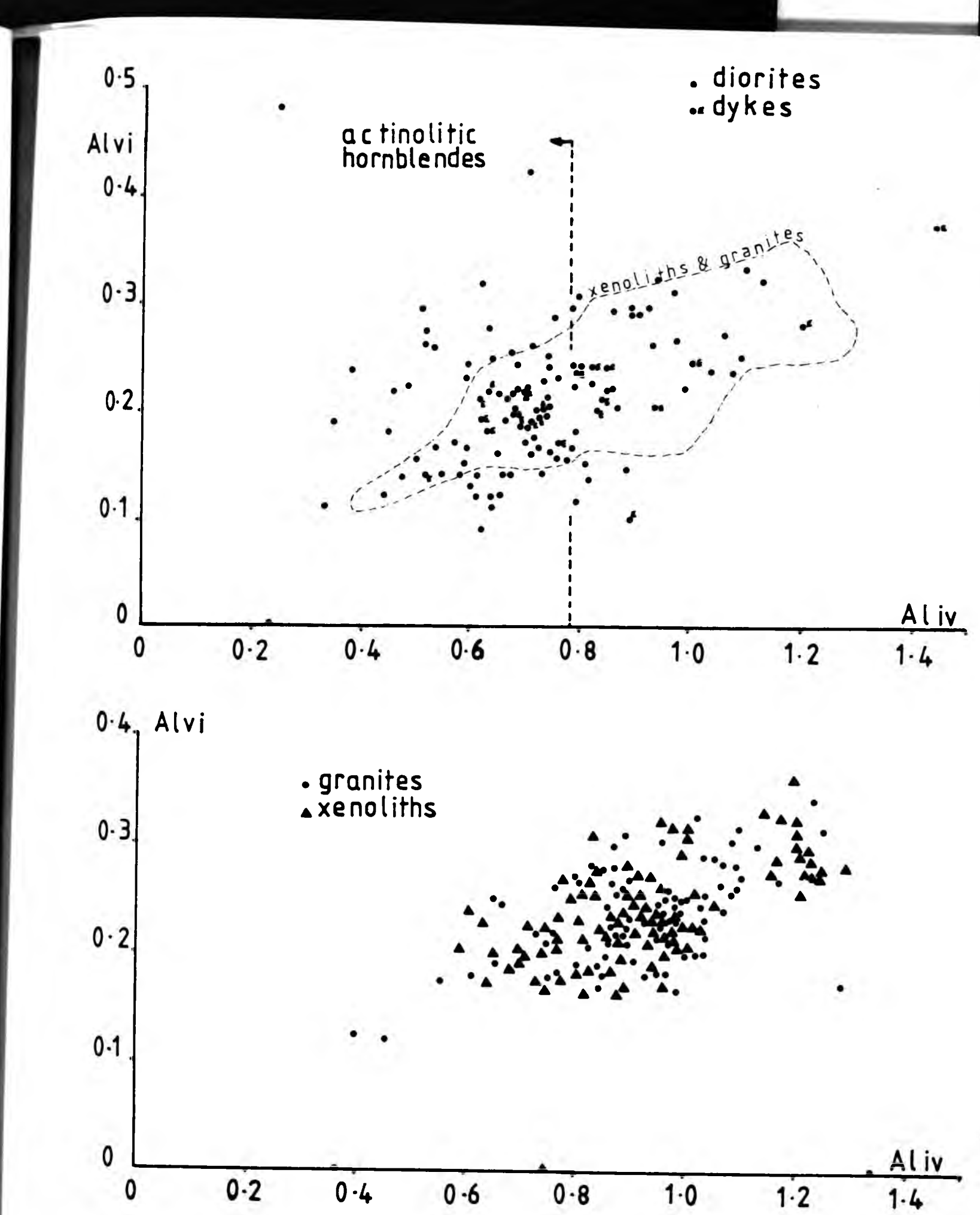

Fig. 10·3 A plot of Alvi against Aliv in amphiboles for all rock types of Strontian.

Dioritic amphiboles also plot in this field. They are the medium green edenitic and magnesio hornblende. At the lower end below 0.40 (Na+K) are the secondary actinolitic hornblendes replacing pyroxene. Zoned crystals in the diorites show an increase in (Na+K) and Aliv towards the rim. Zoned crystals in the xenoliths and granites show decreasing (Na+K) and Aliv towards the rims. Ho wever 11 rims have similar (Na+K) and Aliv. So compositions in these rock assemblages converge on a common value at the slope of growth of the outermost amphiboles. This is further evidence of the amphibole assemblage of the whole complex including a substantial "metamorphic" element.

Ca+Na+K (Fig. 10.4A) increases with increasing substitution of Aliv in the amphiboles from less than 2.1 in the diorites to over 2.5 in the xenoliths. Ranges overlap within the range though few diorite amphiboles exceed 2.45 (Ca+Na+K) and few xenoliths and granites fall below 2.2. The plot trends close to the limit of Ca+Na+K for a given Aliv content normally found in igneous environments (Leake 1971) and supports the view that the amphiboles are of igneous origin and metamorphic (Wones & Gilbert 1982).

During fractional crystallization of a basic magma the MgO/MgO+FeO* ratio decreases with inceasing crystallization. Some authors (eg. Czamanske et al 1981) have plotted MgO/MgO+FeO* of the amphibole against that of the bulk rock. While other authors (Green & Ringwood 1968; Holloway & Burnham 1972) suggest that substitution of cations and overall amphibole compositions are the result of physical crystallization conditions rather than the bulk rock chemistry.

Figure 6.3 shows the amphibole MgO/MgO+FeO* against the bulk rock MgO/MgO+FeO* and it shows a definite linear positive trend. The

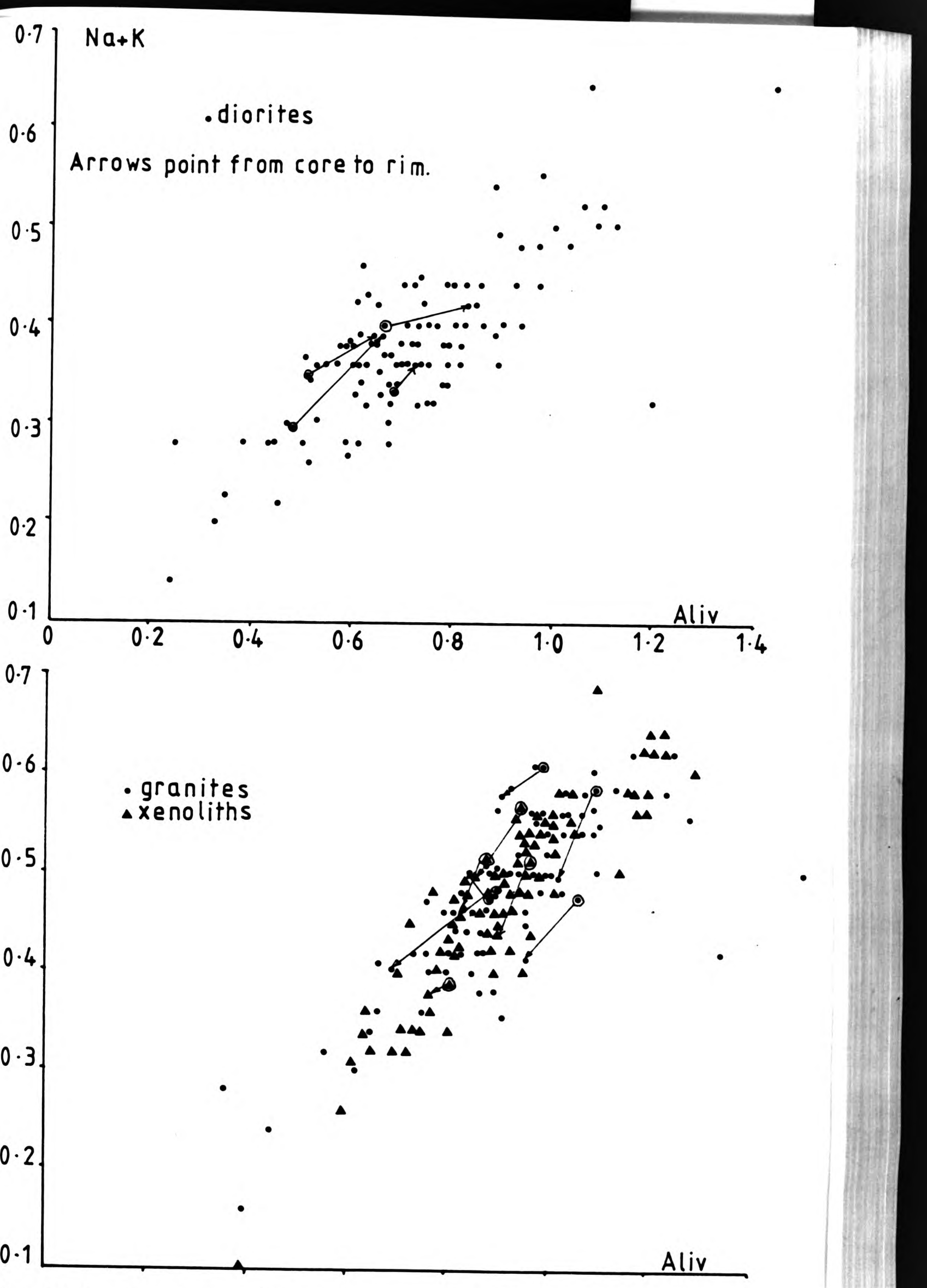

Fig.10·4 A plot of (Na+K) against Aliv in amphiboles for all rock types of Strontian.

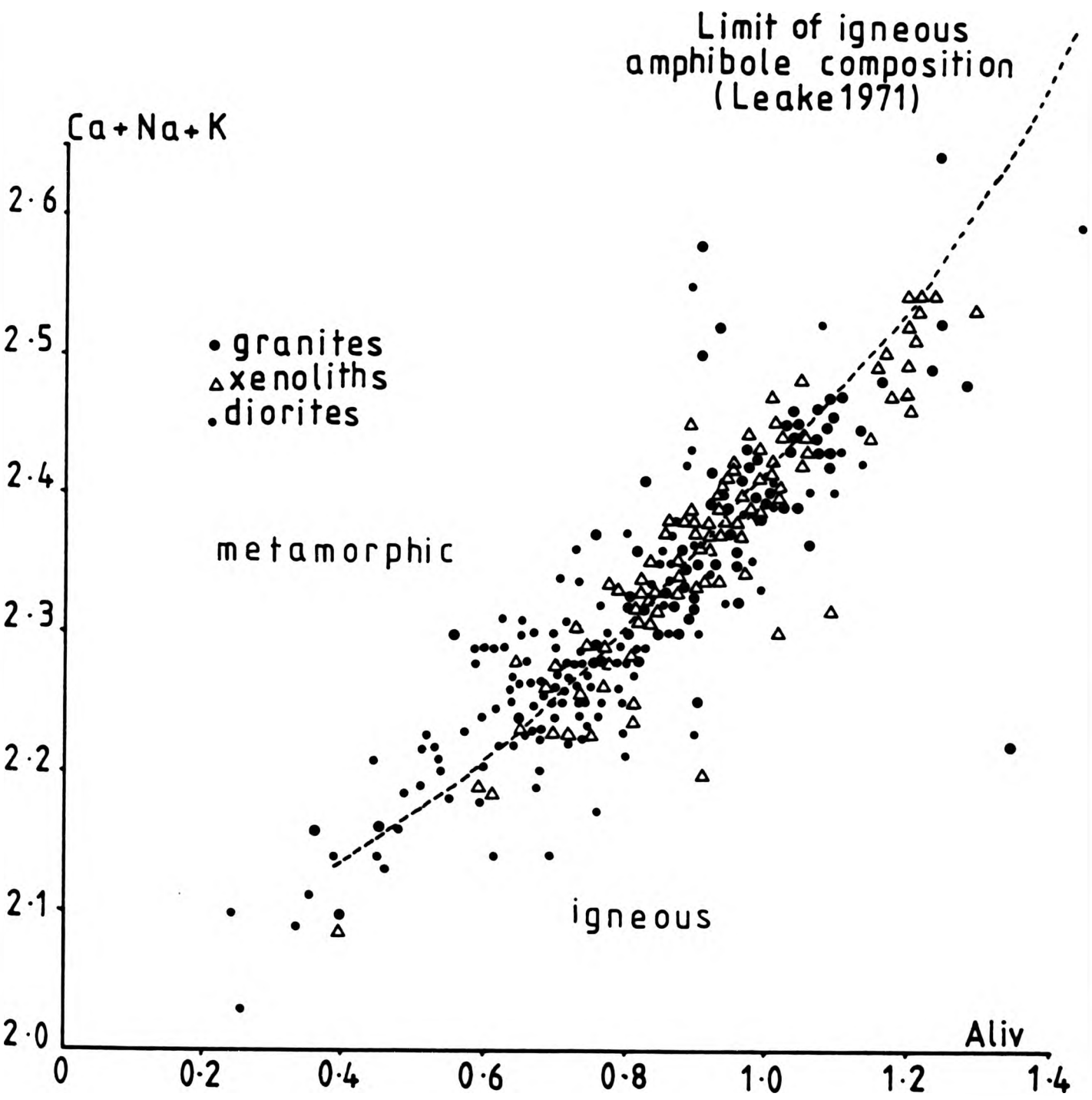

Fig. 10·4A A plot of (Ca+Na+K) against Aliv in amphiboles for all rock types of Strontian.

mafic diorites having the highest ratios, which can be explained by their being regarded as amphibole-biotite cumulates. There is no overlap of the diorite amphiboles with granites or xenoliths, except with the analyses of Uileann diorites.

The MgO/MgO+FeO* ratio for the different amphiboles of the diorites varies overall from 0.570 to 0.695 (14.9 to 17.3% MgO) for the actinolitic hornblendes + actinolite; 0.490 to 0.557 (13.1 to 16.0% MgO) for the magnesio-hornblendes and 0.531 to 0.658 (13.5 to 15.0% MgO) for the edenites. The MgO/MgO+FeO* ratios for the actinolitic hornblendes often show an increase from the core towards the edge of the crystal of about 3.5% MgO eg. core ratios 0.599 to rim ratios 0.634.

The Ben Nevis ferromagnesian minerals have been observed to become enriched in Mg during cooling - if partial pressure of oxygen remains constant at a lower temperature. While the excess iron is accomodated in the formation of a greater quantity of magnetite (Haslam 1968). In Strontian the diorite amphiboles are more Mg-rich (Fig. 10.5 & 10.6) than the granite or xenolith amphiboles. On Fig 10.5 the diorite amphiboles are plotted on a Ca-Mg-Fe diagram and display the range from the mafic-rich Rubha diorite to the Liddesdale and Ranachan bodies, which overlap the xenolith field. Therefore Strontian varies from Ben Nevis.

Both these diagrams reflect the overall higher MgO/MgO+FeO* ratios in the mafic diorites and their respective amphiboles. The ratios(Fig.10.6) change with the bulk rock ratios from the highest in the Rubha body (D1, D2 and D8) to the lowest in the Uileann (D63) and Sheet (D19). The latter 2 also form a separate amphibole field from

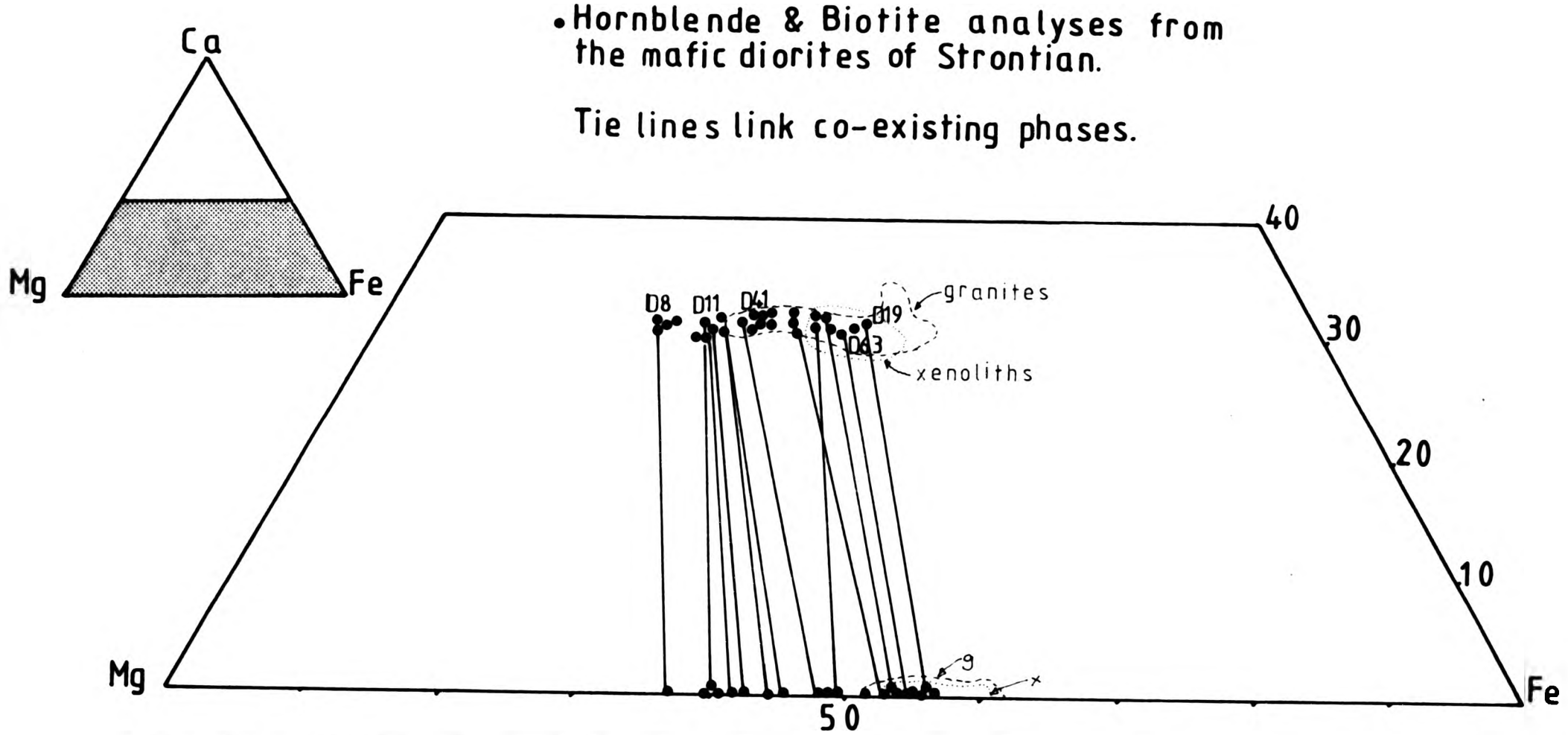

• Hornblende & Biotite analyses from the mafic diorites of Strontian.

Tie lines link co-existing phases.

Fig.10·5 Hornblende and biotite plotted on the Ca-Mg-Fe triangle (atomic %).

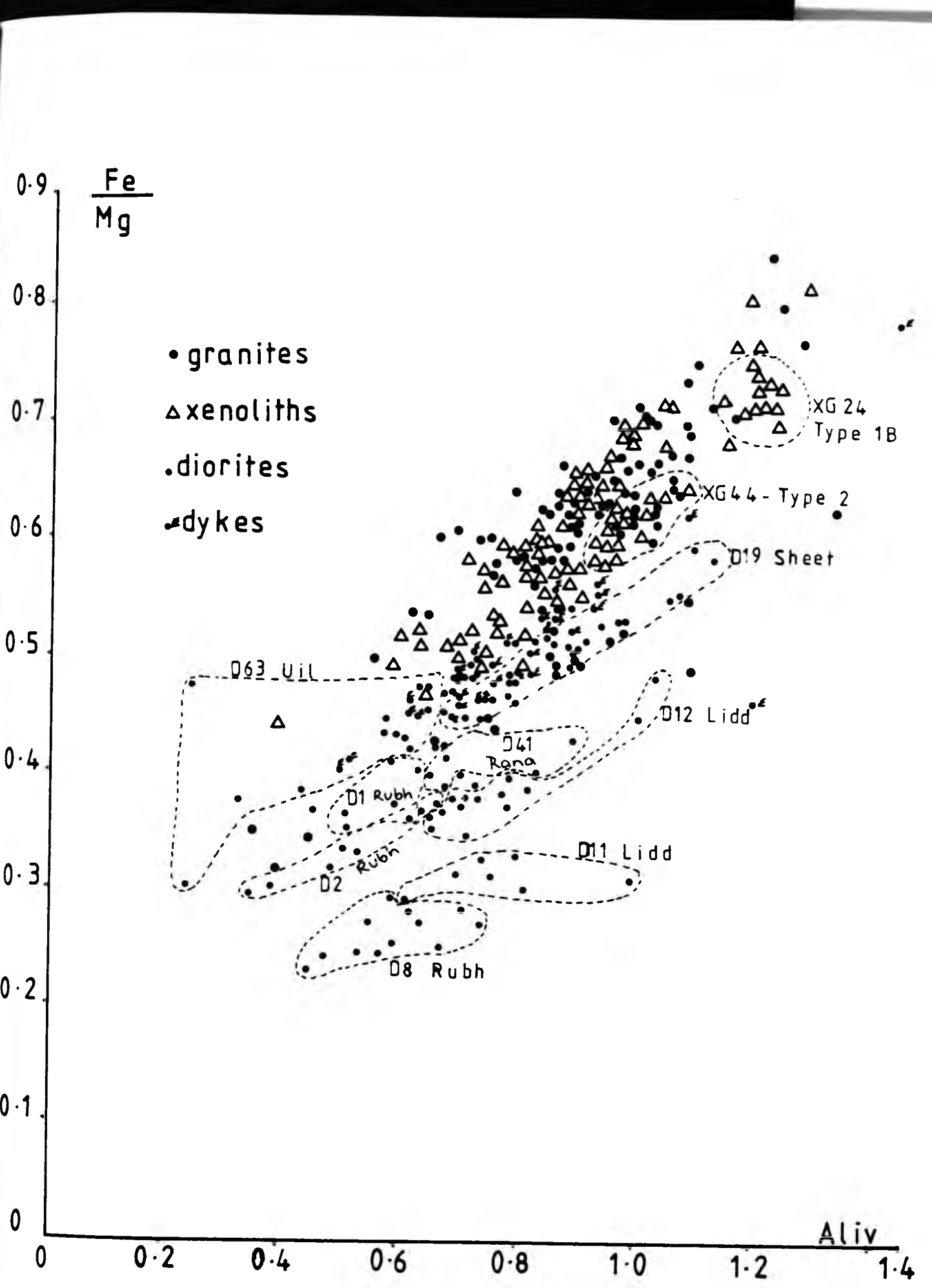

Fig.10·6 A plot of $\frac{Fe}{Mg}$ against Aliv in amphiboles for all rock types of Strontian.

the rest of the diorites on Fig.10.6. This may reflect their more extreme type.

There is some chemical zoning from core to rim in the diorite actinolitic hornblendes and actinolites, but it is not as widespread as in the xenoliths. TiO2 and FeO* decrease from core to rim 0.89 to 0.4% TiO2 and 11.5 to 9.1% FeO*; while MgO increases from 15.2 to 17.0%. The edenite and magnesio-hornblende are not noted to have any substantial zoning at all.

10.4.3 Biotites

The analyzed micas are all classified as biotite according to Heinrich et al (1953). On the Ca-Mg-Fe diagram (Fig.10.5) the diorite biotites plot separately from the host rock and xenolith biotites (Figs. 3.6 & 6.2). The diorite biotites possess higher MgO/MgO+FeO* ratios 0.454 to 0.601 than the granites (0.394 to 0.480) and xenolith biotites (0.400 to 0.460). There is a small amount of overlap of the granite and xenolith ratios with the diorites. However these values are considerably lower compared with the co-existing amphiboles. The biotite analyses here are for a range of forms not simply the very large primary poikilitic biotites. There is a general decrease in the Mg content with increasing acidity. This is noted with the change from the very mafic diorites such as Rubha-na-Sroine to the Uileann diorites:

eg.D8	(Rubha.)	average MgO	17.91%	FeO*	11.82%	Rock SiO2 49%
D63	(Uil.)	average MgO	14.41%	FeO*	16.92%	Rock SiO2 61.5%

The biotites have also been plotted on a (Na+K)-Mg-(Fe+Ti+Mn) diagram

(Fig 6.4) and they show the widest range of compositions of all the rock types. The poikilitic biotites plot in a tight group. This could possibly be a reflection of preserved magmatic compositions. There appears to be a very limited amount of chemical zoning in the biotites with respect to titanium and iron.

Fluorine can substitute in a biotite lattice for OH-. F levels vary from 0.09 to 0.48% with the Sheet diorite showing the lowest levels: 0.091 to 0.265% F. These values are lower than for the host granites, but similar to the xenoliths.

10.4.4 Pyroxenes

The near total absence of preserved pyroxenes in the Strontian Complex diorites makes it difficult to interpret in any fullness those that are present. Rare occurrences of remnant pyroxene were found in the very mafic diorites. However the few analyses possible (overall totals are low) were of pyroxene cores surrounded by hornblende and/or biotite.

They yielded orthopyroxene (an iron-rich bronzite of En72-76) and clinopyroxene (augite of Wo27-En64-Fs9 to Wo28-En58-Fs14) according to the Wo-En-Fs triangle (Fig 10.7).

The Ti content in the pyroxenes varies from 0.029 to 0.56% TiO2; the augites 0.2-0.56% and opx 0.029-0.36%. Due to the lack of analyses no real inference can be made from plotting Ti against Aliv.

Ca-poor pyroxenes have been reported in calc-alkaline magmas in the Garabal Hill Complex (Nockolds 1941); Iceland (Carmichael 1960);

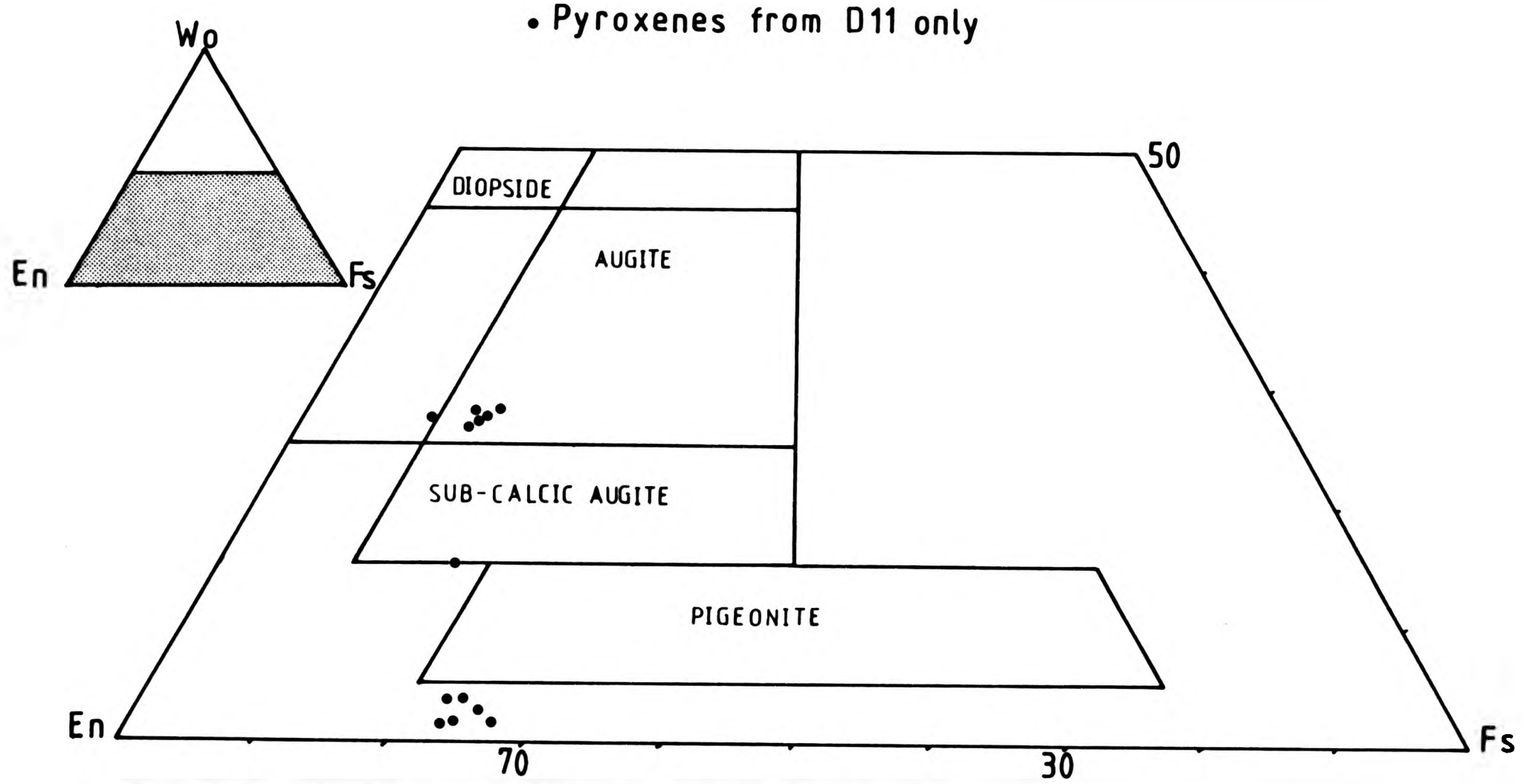

Fig.10·7 Pyroxenes plotted on the Wo-En-Fs triangle.

Guadalupe Complex (Best 1963) and by Cawthorn (1976). In Strontian all the augites have around 6.83 to 12.4% CaO, while the opx have 0.7 to 1.5% CaO.

Cr typically occurs in the 3+ form and commonly substitutes for Mg2+ (Mason 1966). Cr203 levels in both opx and cpx range from 0.01 to 0.13%, suggesting that pyroxene might control Cr fractionation in the diorites.

Overall the Mg/Mg+Fe ratios for the clinopyroxenes are higher (0.698 to 0.785) than for their associated amphiboles (in D11, 0.639 to 0.658); while they are within the same range for the opx 0.599 to 0.647.

Evidence for there having once been pyroxene in the mafic diorites is supported by the amphibole aggregates together with magnetite on the cores and the present amphibole composition. The observed opx are surrounded by amphibole aggregates, while the augites have been observed to be surrounded by a single amphibole crystal or by biotite.

10.4.5 Sphenes

Sphenes are common accessory minerals in the mafic diorites too, with a range of different habits (described in the petrography section). Their major element chemistry is similar to that of the host and xenoliths with 30% SiO2, 35-38% TiO2 and 26-28% CaO.

10.4.6 Apatites

Apatites are also abundant with their habit varying from stubby crystals to very fine acicular crystals. They are all fluor-apatites containing 3.04 to 4.70% F, with particularly high F levels in the Ranachan samples (over 4.0%). The F range is slightly wider than that of the apatites of xenoliths and granites.

10.4.7 Sulphides

Sulphides are only found in the mafic diorite bodies. They are present as tiny individual anhedral, rounded interstitial crystals in the groundmass. The most common are pyrite (FeS2) and chalcopyrite (CuFeS2). The pyrite has constant iron levels of 45-46%, while chalcopyrite has 30% iron and 31-32% copper. Two nickel bearing sulphides also occur, but not in great abundance: pentlandite (Fe,Ni)9S8 with 33% Ni and millerite with 60-62% Ni. In occasional examples the nickel-bearing sulphides are coated by an irregular mass of pyrite. Rare examples of pyrrhotite are found in the diorites. These are not associated with fractionating systems and so are inferred to be primary magmatic sulphides.

10.5 DISCUSSION

The diorite bodies are all modally distinct (Table 10.1), but they could form a complete mineralogical gradation from the more to less mafic varieties eg. from the Rubha-na-Sroine to the sheet. There are no cortlandites found in Strontian, even though the majority of the diorites have a very mafic appearance. In general the gross igneous texture has been preserved, though a substantial amount of the

mineralogy has undergone changes and is no longer primary. The remnant pyroxene cores and brown hornblendes, together with the mafic aggregates, that are so common in all the diorites, suggest a phase of mineralogical disequilibrium within the diorite bodies. These remnants of opx and cpx suggest a higher temperature anhydrous assemblage, which has changed to a lower temperature hydrous amphibole dominated assemblage. However the whole mafic mineralogy for the diorites is quite distinct from the host rocks and xenoliths, as the latter two groups have a common coherence of hornblende and biotite compositions. This suggests that the diorite mineralogy has a different source or are likely to be cumulates.

Indications of hybridization are most evident in the Sheet and Uileann diorites. The occurrence of quartz xenocrysts jacketed by mafics and plagioclase jacketed by a more basic plagioclase composition or by an alkali feldspar are such examples. These relationships with xenocrysts are widely recognized as evidence of hybridization between magmas (Wager & Bailey 1953; Walker et al 1966; Anderson 1979; Eichelberger 1974, 1975, 1978, 1980). At Strontian they show that dioritic magma existed contemporaneously with a porphyritic granitic magma and that efficient mixing could occur. Further magmas with these components co-existed, so relating the early and late stages in the evolution of the complex.

Chapter 11 THE DIORITES: GEOCHEMISTRY

11.1 INTRODUCTION

The mafic diorites of the Strontian Complex appear to fall onto the main xenolith-granodiorite-granite trend, though in fact they have a more scattered pattern with a distinctly separate trend at the lower silica end (Figs. 11.1 to 11.9).

The diorites in the granodiorites and biotite granite will be discussed together to avoid repetition. MgO was chosen as the abscissa due to the diorites being so mafic. However where appropriate SiO_2 will replace it so a direct comparison can be made with the granodiorites and biotite granite. Appendix B - Table B.3 gives the whole rock analyses for the diorites.

Each intrusion has distinctively different compositional characteristics, which in some cases do not overlap with other fields. Names of the diorites have been abbreviated to save repetition: Rubha-na-Sroine = Rubh; Liddesdale = Lidd; Ranachan = Rana; Loch Tearnait = LT; Uileann = Uil; Sheet = Sheet. Sample D29 has been marked on separately on the Figures.

11.2.1 Silica

Fig.11.1 shows a reasonably coherent trend of decreasing SiO_2 with increasing MgO, with the majority of the diorites ranging from 48 to 58% SiO_2. Individual diorites have distinct MgO - SiO_2 fields. The Lidd diorite shows the greatest MgO (3.75-13.85%) range with a small silica range. The variation can be related to the high MgO sample

FIGURE 11.1 SiO2 vs MgO

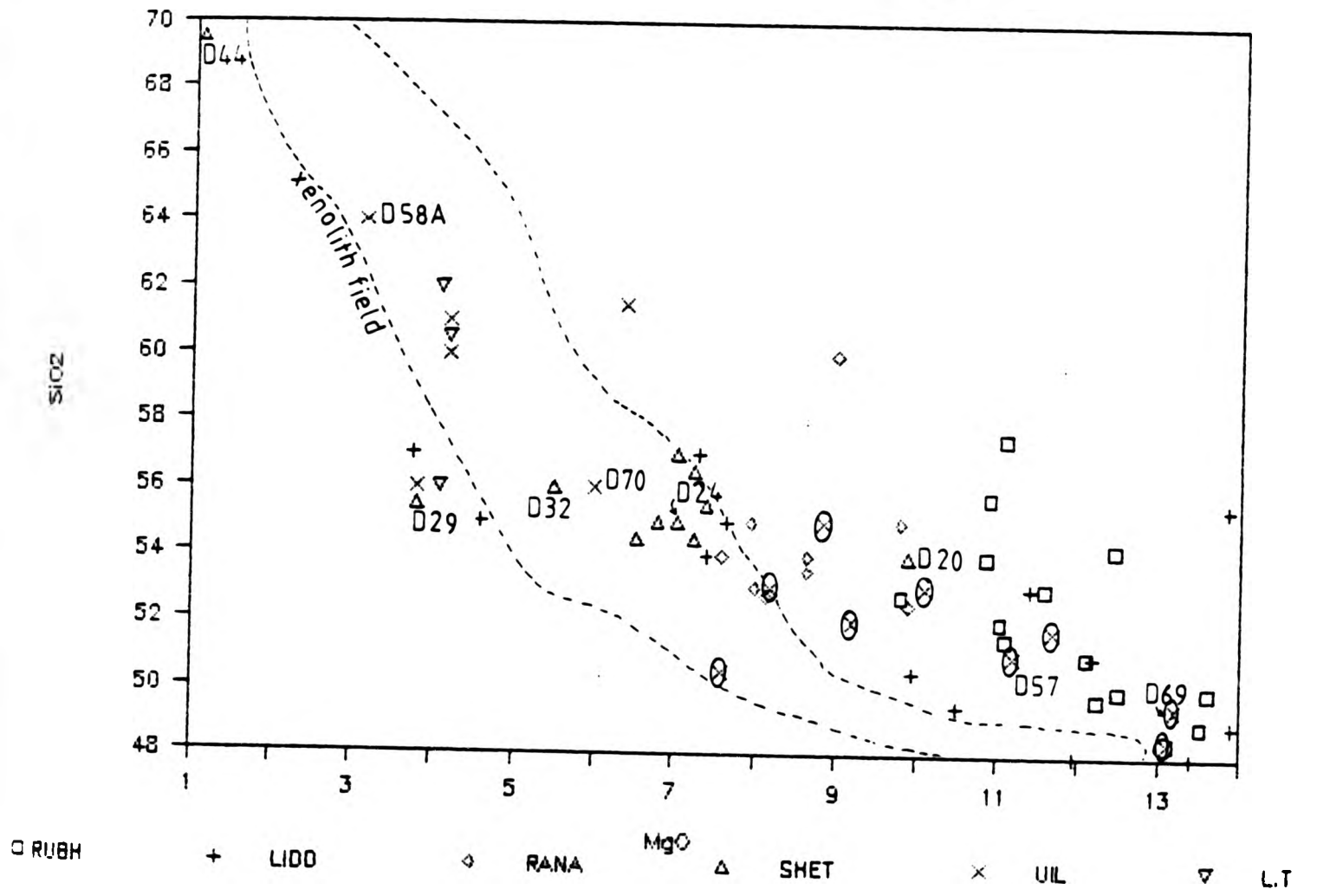

being very biotite-rich while the low MgO sample is not so mafic with plagioclase phenocrysts. Lidd shows a clear linear pattern with a wide variation. The Rubh occupies a completely separate field on many of the plots of which MgO:SiO_2 is one. It has a tighter field, as it is a much more mafic uniform diorite than the others. It also shows a steeper gradient. Uil shows a wide variation of data points with a clear linear pattern. The more mafic core of Uil also falls in the lower SiO_2/higher MgO part of the plot (marked on Fig.11.1); while those quartz-bearing contaminated samples plot at the lower MgO level (D63, D64 D76). The linear fields of Lidd and Uil overlap at high MgO, but diverge at low MgO.

The other diorites show more restricted fields with limited variation of MgO with SiO_2 and less well defined trends. The Sheet shows 5.5-8% MgO with little SiO_2 variation (54-65.5%). There are two extreme Sheet samples - one at the low MgO end (1.1% D44) which is a sample from the granitic component of the composite section of the Sheet and a higher MgO (9.9%) sample rich in mafic aggregates. The LT diorite has a SiO_2 range of 56-62% with no change in MgO. Rana data, as with Rubh, forms a fairly equant cluster with limited MgO and SiO_2. Both these clusters are totally separated on MgO values- Rana 7.5-10% and Rubh 10-14%. Likewise these are separated by MgO from the Sheet and LT fields. Collectively however all the variations yield a broad band of data with a systematic decrease in SiO_2 with increasing MgO.

The diorites above 8% MgO are outside the xenolith composition range and all the Rubh and Rana samples lie in here. The majority of the Rubh and all those above 10% MgO are silica-saturated (ie. have olivine and hypersthene in norm, (according to Cox et al 1979). A

few xenoliths are in this field as they are very mafic-rich themselves. While those below 8% lie within or close to the xenolith field (plotted on Fig.11.1), as the xenoliths have slightly wider field of MgO and SiO_2 contents.

11.2.2 Aluminium

Fig.11.2 displays a linear trend of decreasing Al_2O_3 with increasing MgO, with abundances varying from 18.4 to 7.6% Al_2O_3. There is slight scatter at the very high and very low alumina ends. The Rubh body shows quite a tight plot of 9.2 to 12.4% . Rana falls mainly on the trend with 2 samples (D33-D43, Fig.9.1A map of Ranachan) that have considerably lower levels. These are found very close to the E-W contacts of the body and are slightly finer grained than the main body. The odd Uil (D63) is an analyzed sample of the net-veined facies. The Sheet has variable Al_2O_3 content - 12.0 to 16.8%. There does not appear to be any geographical pattern to the distribution of the samples with respect to Al_2O_3.

The MgO vs Al_2O_3 has a negative trend, which is largely reflected by the variation in the colour index. The Al_2O_3 of the plagioclase and alkali feldspar varies from 18.4 to 26.5% and in the biotites from 13.2 to 15.0% Al_2O_3. On Fig.11.2A Al_2O_3 vs SiO_2 gives a more varied plot with a positive slope. The separation of the fields is possibly due to the fact that some of the diorites have been contaminated.

11.2.3 Titanium, Iron and Manganese

Figures 11.3, 11.4 and 11.5 display the patterns for TiO_2, FeO* and MnO against MgO.

FIGURE 11.2 Al203 vs MgO

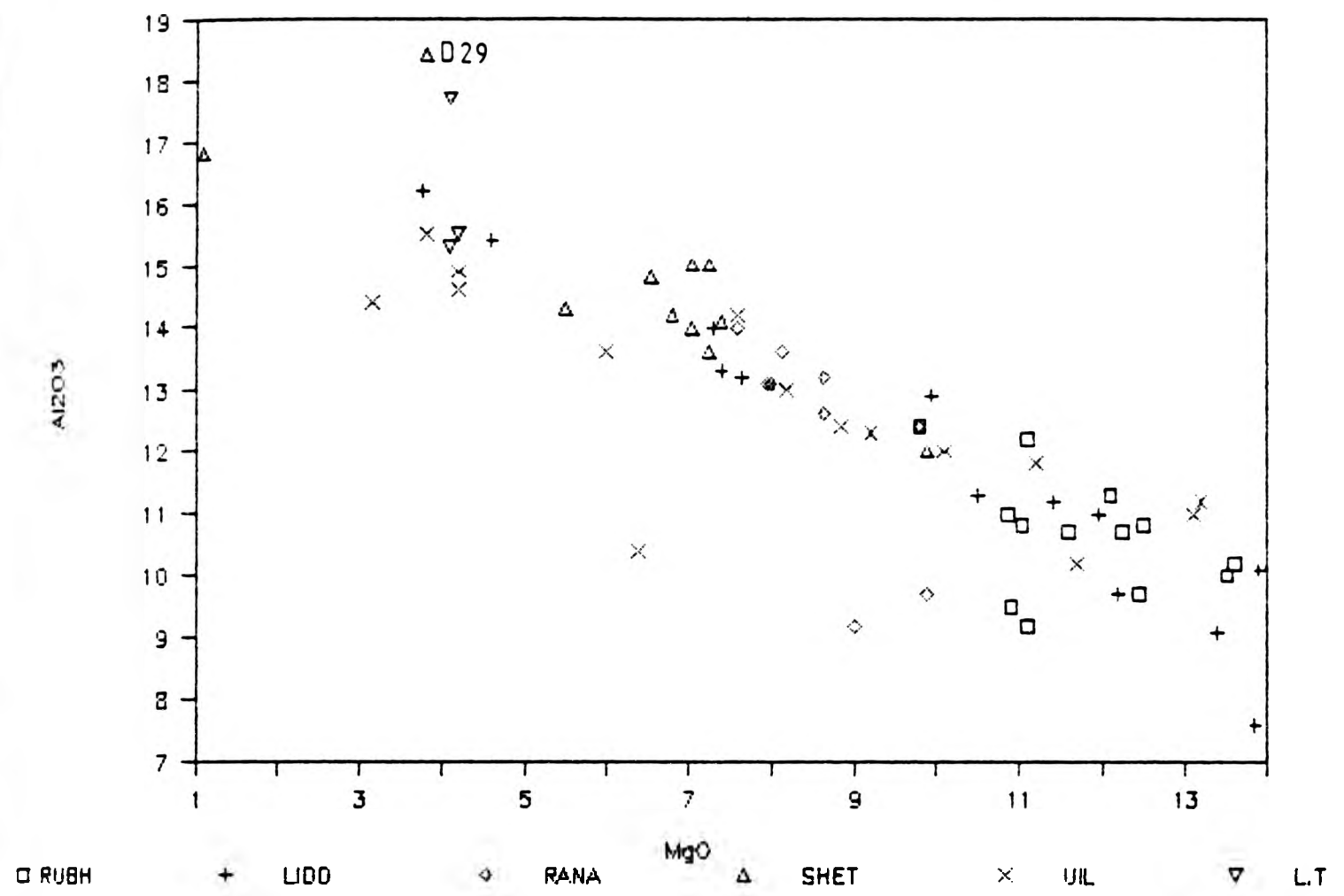

FIGURE 11.2A AL203 vs SiO2

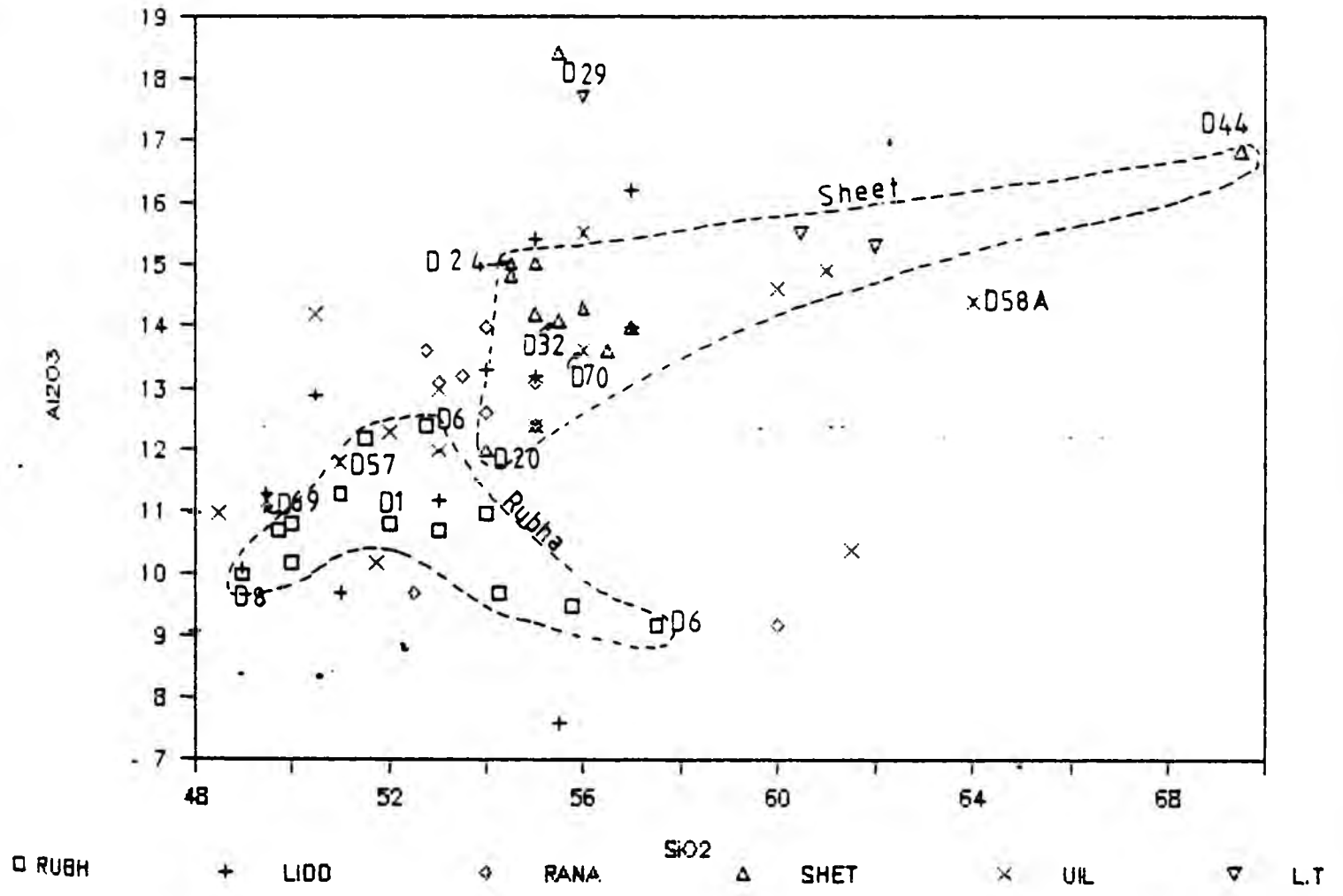

The titanium plot is very highly scattered, but shows an overall horizontal trend with MgO. Fields for LT and Rana show no coherence, but have the highest ranges - LT 0.93-1.45% and Rana 0.75-1.85% TiO_2. Rubh has an equant cluster. The Sheet has a negative linear trend and Lidd and Uil have horizontal trends. There is a discrete separation of the Rubh data from the mafic Lidd and Uil data, which is not seen on the MgO:SiO_2. The Uil diorite shows the greatest scatter of points with TiO_2 ranging from 2.05 to 1.0% across the range of MgO values.

Fig.11.3A shows TiO_2:SiO_2, which unlike TiO_2:MgO, produces a well defined negative linear trend for the Rubh, LT, Uil and Rana. There is virtually no overlap between Rubh, Rana and LT. The intrusions have distinctively different compositional fields, some with no overlap. The SiO_2 ranges of individual bodies are distinctive as well. The extreme Sheet sample at the high SiO_2 and low TiO_2 end is D44 (Fig.9.1D) the marginal granitic sample from the composite section of the detailed traverse. The Sheet however loses its linear trend to form an equant cluster.

Iron (Fig.11.4) has a decrease of FeO* with decreasing MgO. FeO* ranges from 10.8 to 2.0% which is a very large variation (larger than the host rocks but not the xenoliths). Most diorites fall on a gentle linear trend from 13.5 to 5.0 MgO, which then steepens for MgO values <5.0%. Even here there is some separation of the fields, particularly Rubh, which has lower FeO* values but still with a negative correlation with MgO. It is the Sheet that individually has the widest range of iron from 9.0 to 2.0% following a conspicuously curved trend. The Uil FeO* ranges from 10.0 to 4.5% again with a curved rend. Lidd by contrast shows a much more limited

FIGURE 11.3 TiO2 vs MgO

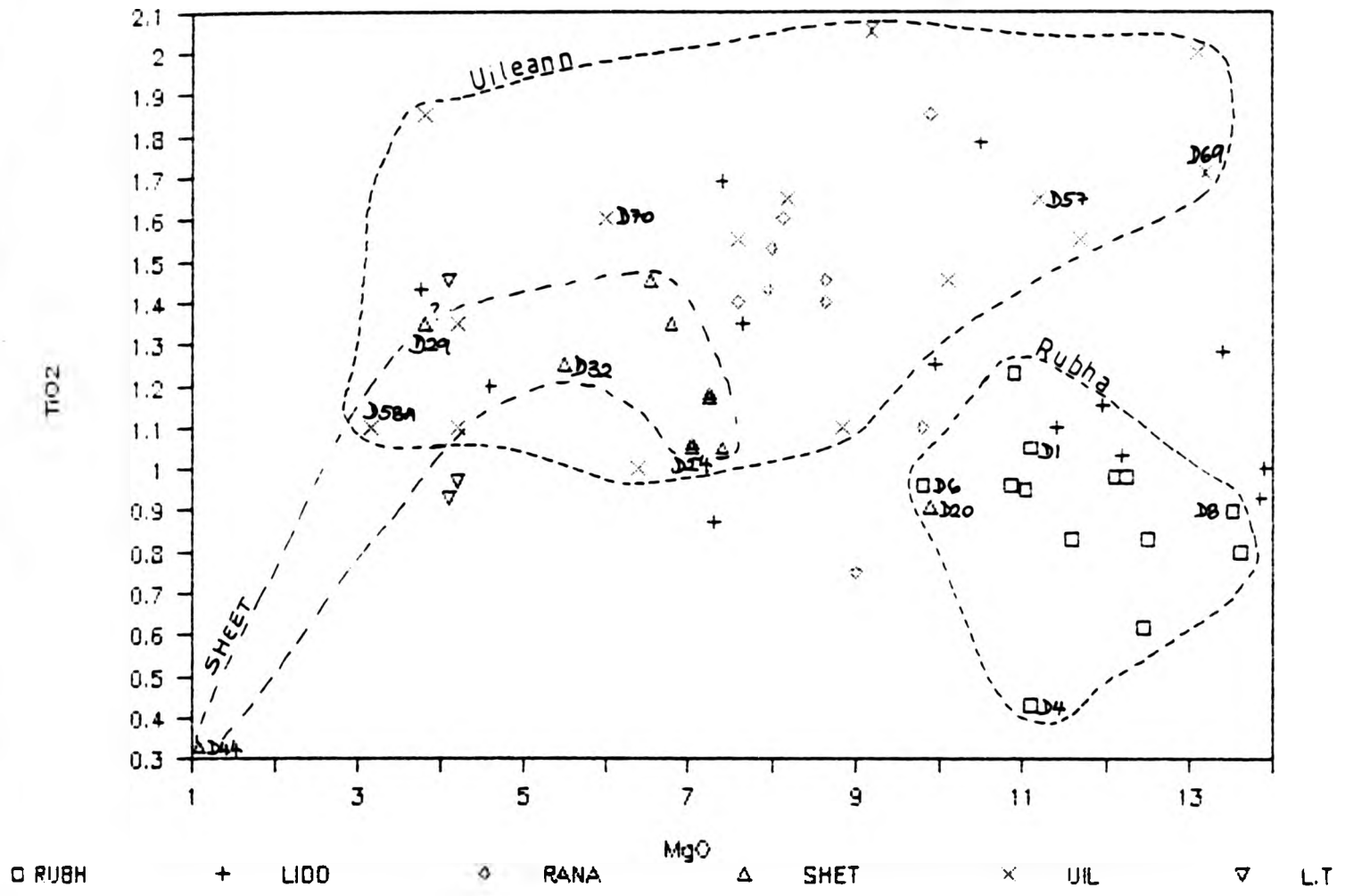

FIGURE 11.3A TiO2 vs SiO2

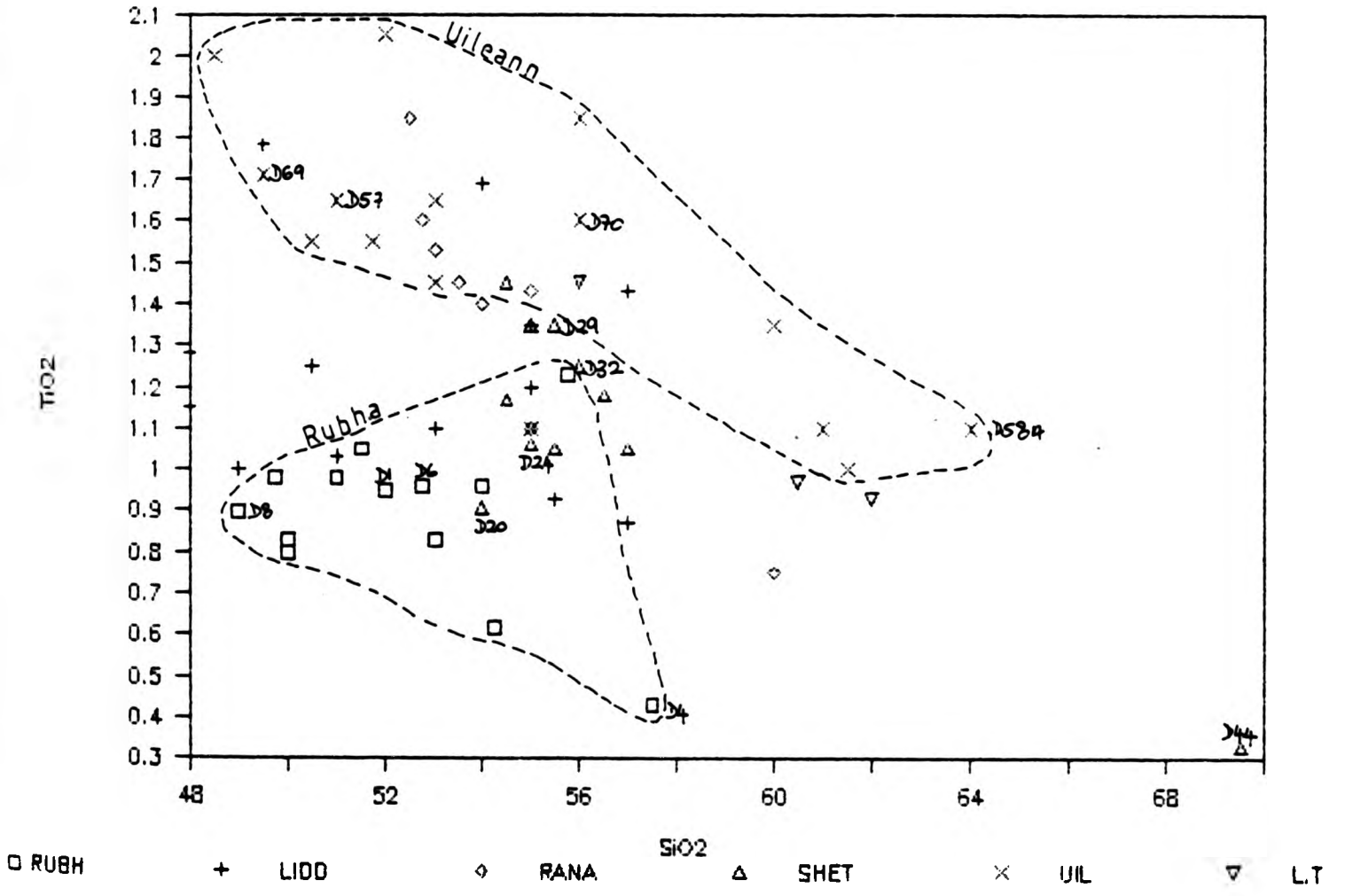

FIGURE 11.4 FeO* vs MgO

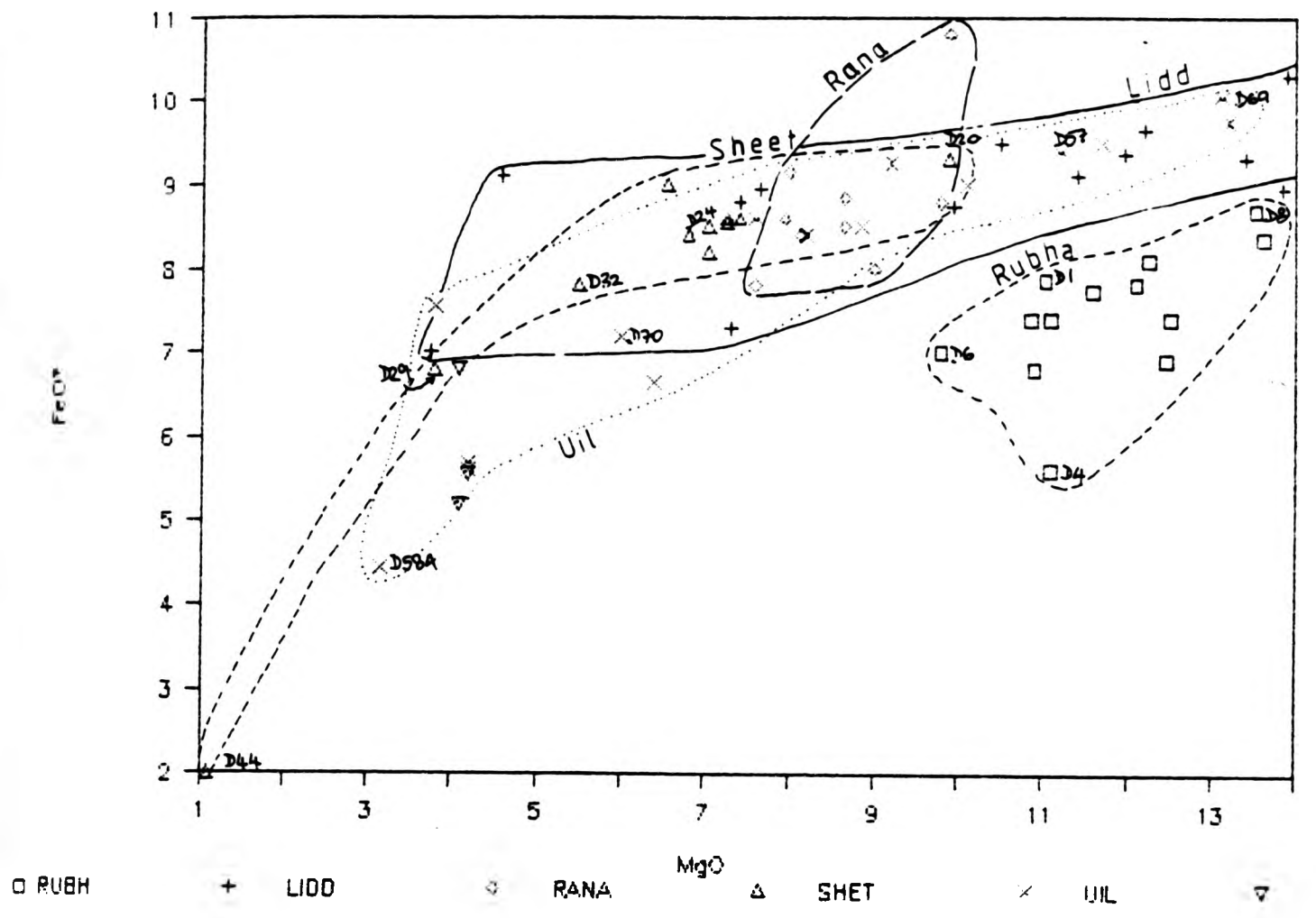

FIGURE 11.5 MnO vs MgO

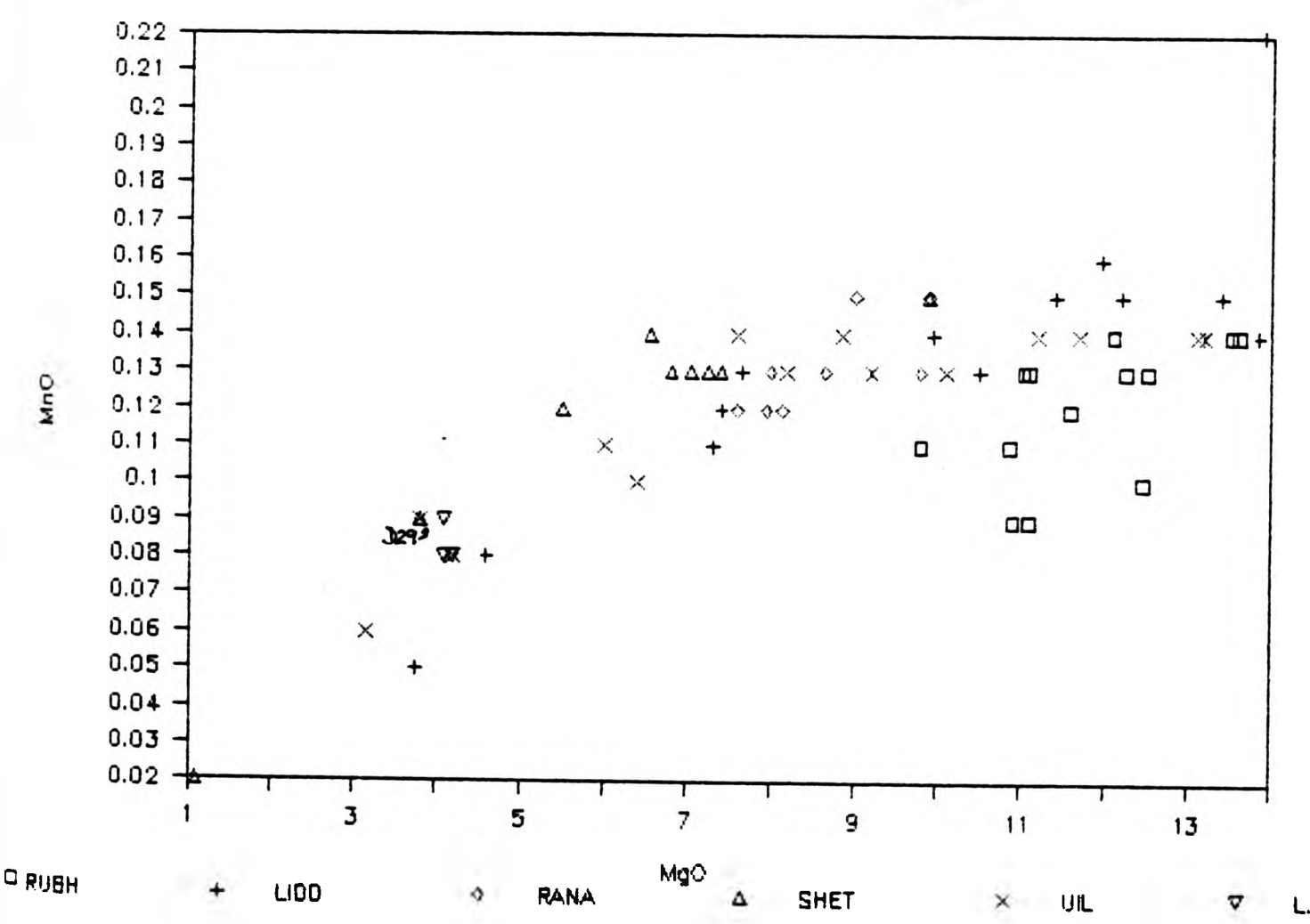

FIGURE 11.5A TiO2 vs FeO* (all rocks)

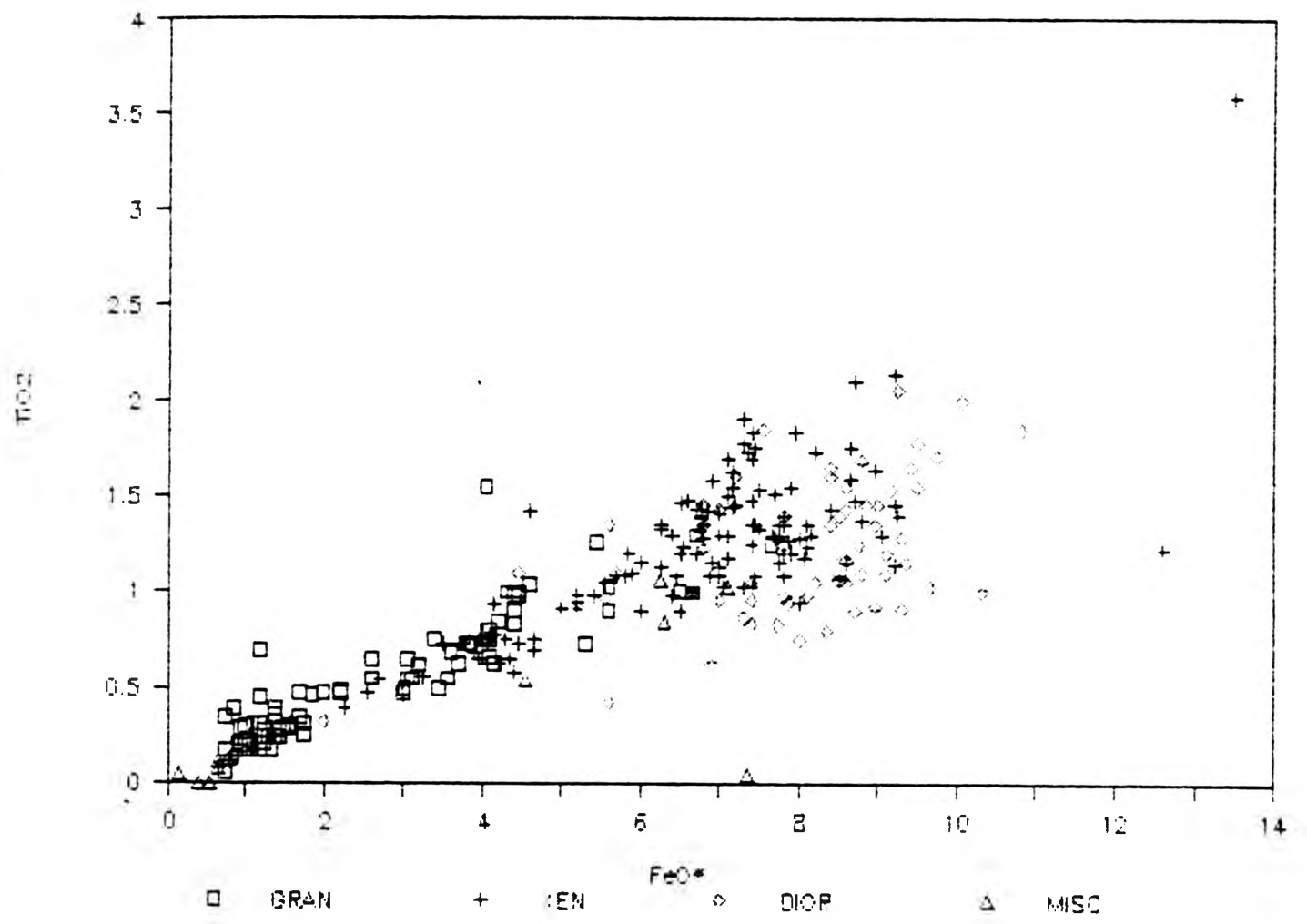

FeO* range with FeO* remaining above 6% for MgO-poor specimens.

This plot displays a large variation which is a result of the variable modal amount of ferromagnesian minerals in the bodies, with Rubh and Uil cores being the most mafic to the sheet and Uil margins being the least mafic.

Manganese (Fig.11.5) shows a very similar pattern to the FeO* plot, with a steepening trend of decreasing values with decreasing MgO. There is a separation of the individual bodies within the main trend. Again the Rubh diorite separates from the main trend with lower MnO content.

The low levels of TiO_2 and MnO reflects the general absence of modal magnetite and ilmenite (not like the host rocks and xenoliths). Opx and cpx do not have Ti, but do have Fe which would give a different pattern. The positive correlations seen between TiO_2 vs FeO* (Fig.11.5A) suggests that crystallization of brown titanium amphibole and biotite may well be important in controlling the distribution of this oxide in the absence of iron oxide minerals. The very tight completely linear plot of MnO vs FeO*, which passes through the origin, is consistent with the well established geochemical similarity of these elements. It functions more as a check of analytical consistency than a local understanding of the evolution of the rocks.

11.2.4 Calcium

Figure 11.6 displays the overall positive linear trend of CaO decreasing from 11.25 to 2.10% with decreasing MgO. There is a

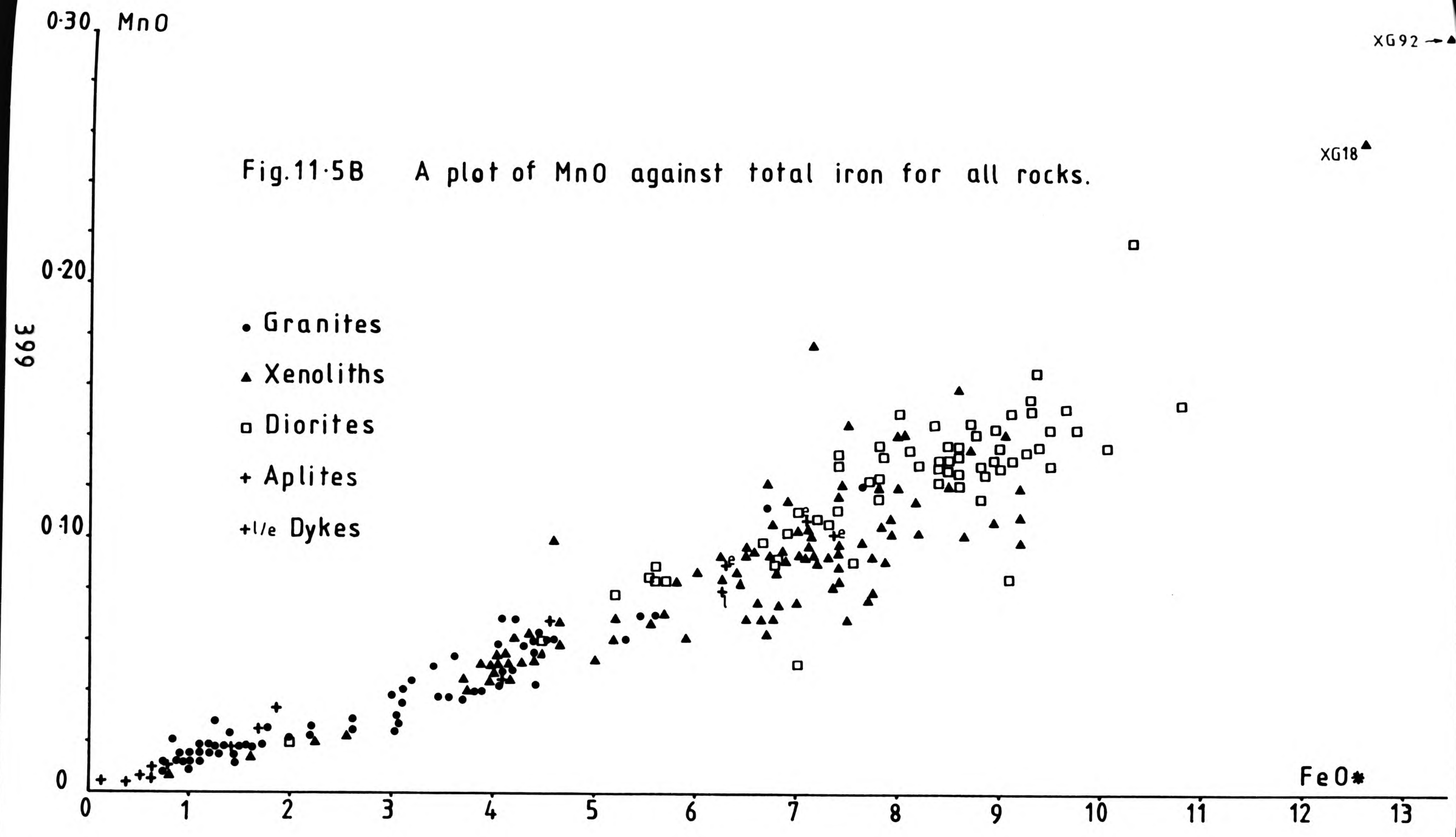

Fig.11·5B A plot of MnO against total iron for all rocks.

FIGURE 11.6 CaO vs MgO

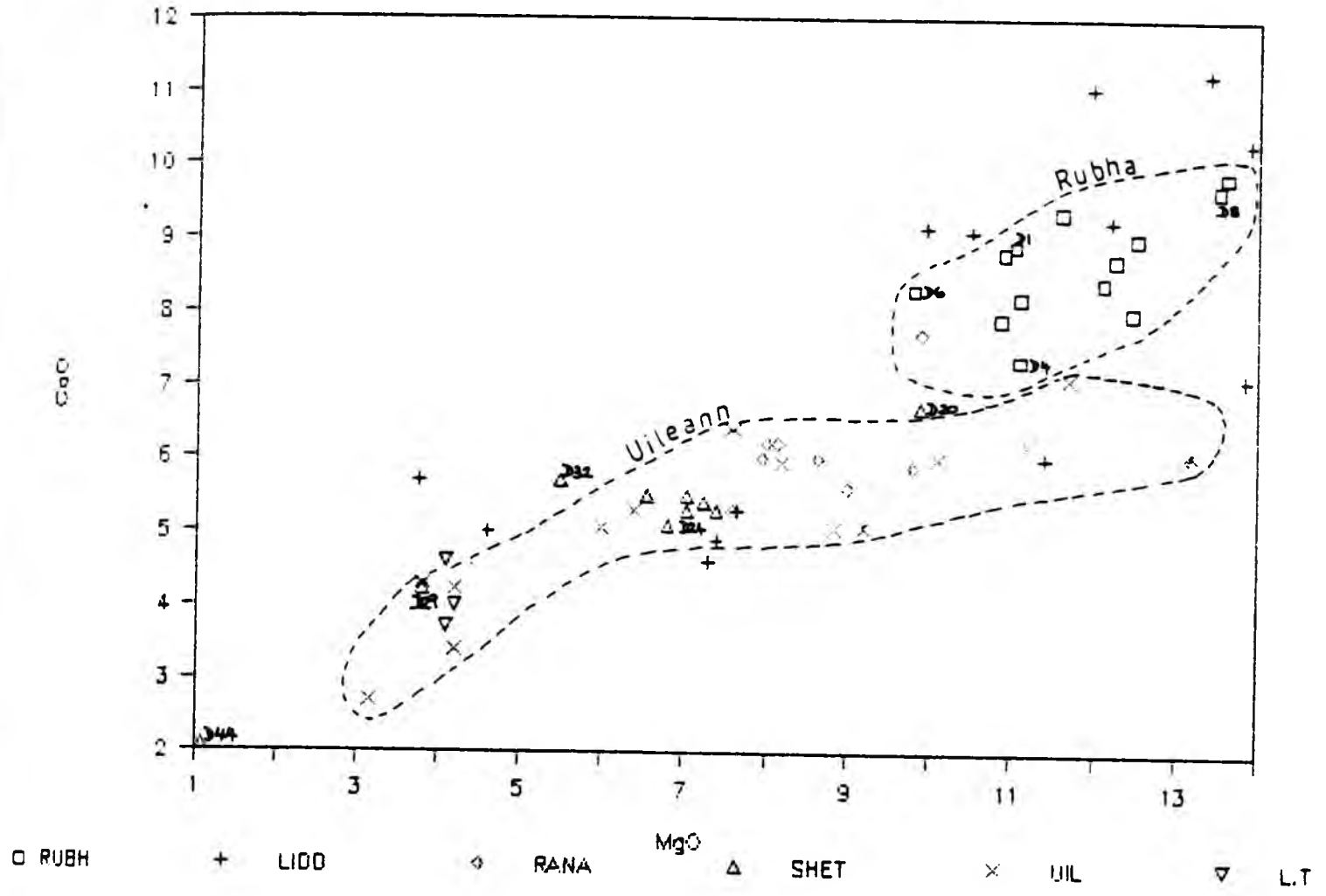

FIGURE 11.6A CaO vs SiO2

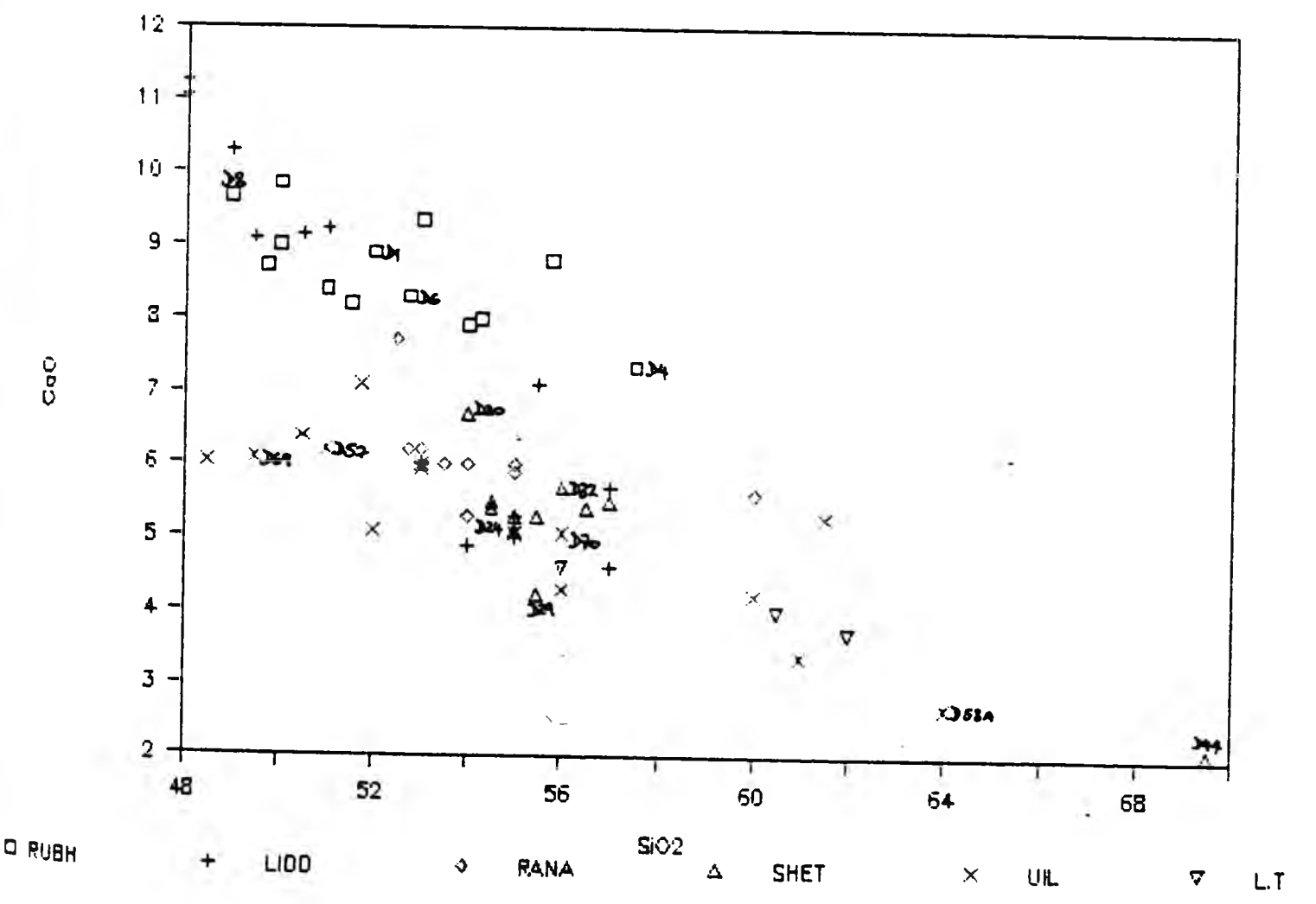

stepped or curved trend on this plot at around 8% MgO, which may indicate a change in the evolutionary pattern eg. a change in the number of cumulate phases or a change from fractionation to hybridization. The Ca values are higher than those displayed by the host rocks (Fig.4.9) and the xenoliths (Fig.7.6) when looking at the total range. The higher (>7.0% CaO) CaO values are found in the Rubh body and in a discrete subset from the Lidd bodies with over 9.0% MgO. These Lidd samples also correspond to the separate field in the TiO_2:SiO_2 plot (Fig.11.3A) but not on TiO_2:MgO (Fig.11.3). The rest of the Lidd data shows a truncated trend on the MgO:CaO plot (Fig.11.6) with the highest CaO and MgO-poor rocks.

Uil (7.0 to 2.55% CaO) follows the trend, but the more mafic cores separate from the Rubh field even though on the Al_2O_3 plot they are together. The Uil data shows a marked change in the trend at 7.0% MgO at 52% SiO_2 with horizontally high MgO and low SiO_2. On Fig.11.6A the Rubh and Uil diorites plot completely separately at the low silica end (not seen on Fig.11.6). This shows that if all the elements are considered, each body is unique. The Rubh data points relate to cpx accumulation as seen on Fig.11.34 to 11.41, while the Uil would relate to hornblende cumulates.

The higher calcium diorites clearly correspond with much lower Al_2O_3 values (Fig 11.2) and probably reflect $CaMgSi_2O_6$ (pyroxene). They not thought to have primary hornblende. This also indicates Rubh and Lidd have more calcic plagioclase and more ferromagnesian minerals and these two factors decrease with decreasing MgO. Sample Dll has the highest CaO value at 11.25% and is the only sample that has had any electron microprobe analysis of pyroxenes (chapter 10).

11.2.5 Sodium and Potassium

Sodium (Fig.11.7) and potassium (Fig.11.8) display different patterns from each other.

Sodium is very similar to the Al_2O_3 (Fig 11.2) and has a very definite increase of Na_2O with decreasing MgO, but has less scatter than Al_2O_3. The diorites contain 1.8 to 5.25% Na_2O. Therefore the diorites with low Al_2O_3 also have low Na_2O. The trend of Na_2O:SiO_2 is very linear too, but with a little more scatter.

Potassium (Fig.11.8) in gross terms has a horizontal trend with scatter. An arbitrary line may be drawn, which divides the Uil and Rubh diorites from the rest. However there are some organised trends lying within K_2O. Uil has a negative correlation with a high K_2O but small range of K_2O values. Lidd shows a negative correlation for MgO >7% and has only limited overlap with Uil. The Sheet also has a negative correlation for MgO >3% and is completely separate from Uil, Rubh and Rana. While Rubh has a wide range of K_2O for limited MgO. Variation is different from the others due to Rubh having the enormous poikilitic biotites.

This wide scatter of K_2O may reflect the variable feldspar content and the higher K_2O could be related to biotite pseudomorphing amphibole. Biotite is an important mineral, which contains 7.9 to 9.8% K_2O typically. Alkali feldspars have also been recorded in the Uil diorites and they typically have 14.0 to 15.7% K_2O. The samples with biotite pseudomorphs were therefore labelled (Fig.11.8). All plot below 2.6% K_2O and tend to have lower K_2O than other rocks in the same intrusion. Late biotite may reflect delayed onset of

FIGURE 11.7 Na2O vs MgO

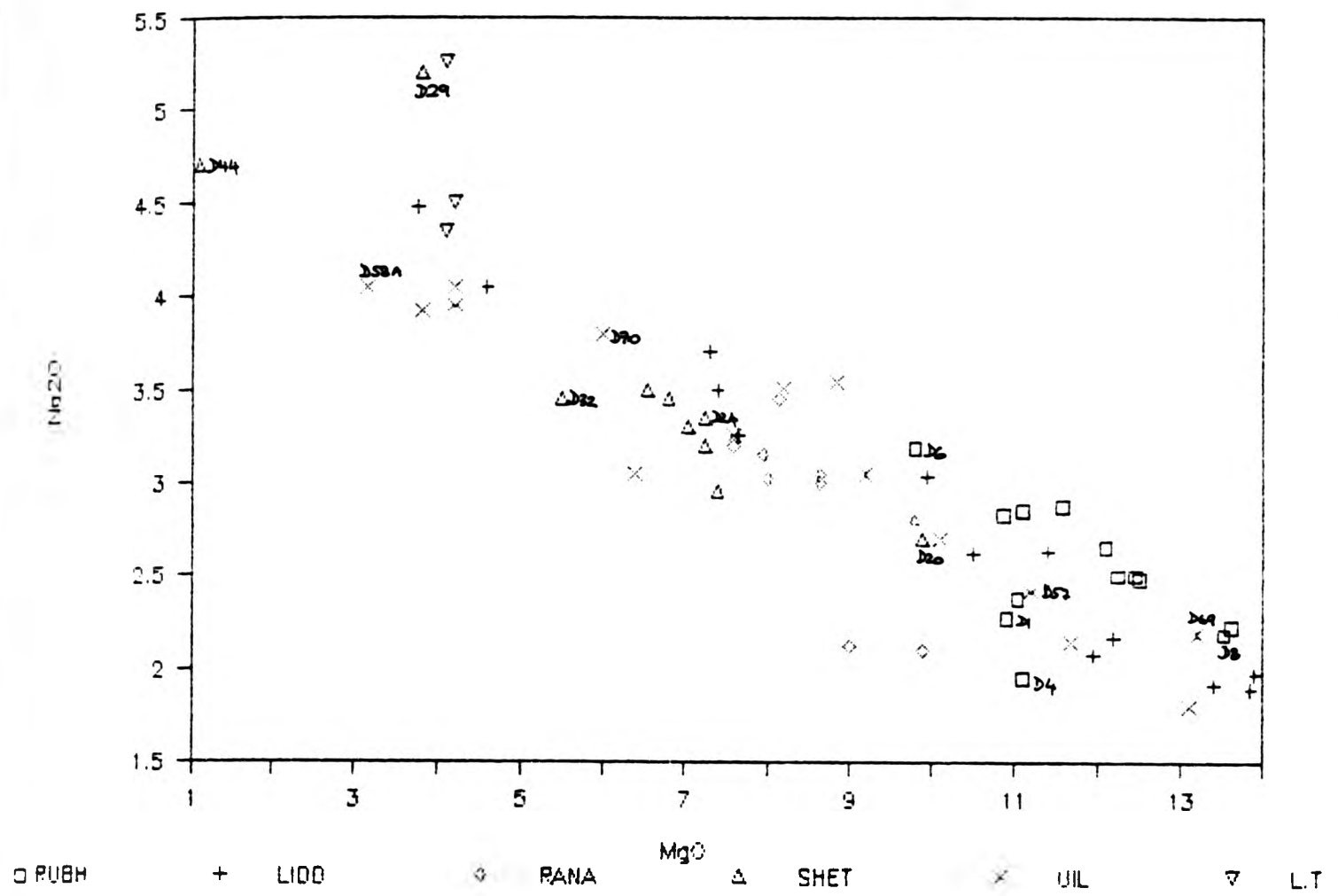

FIGURE 11.8 K2O vs MgO

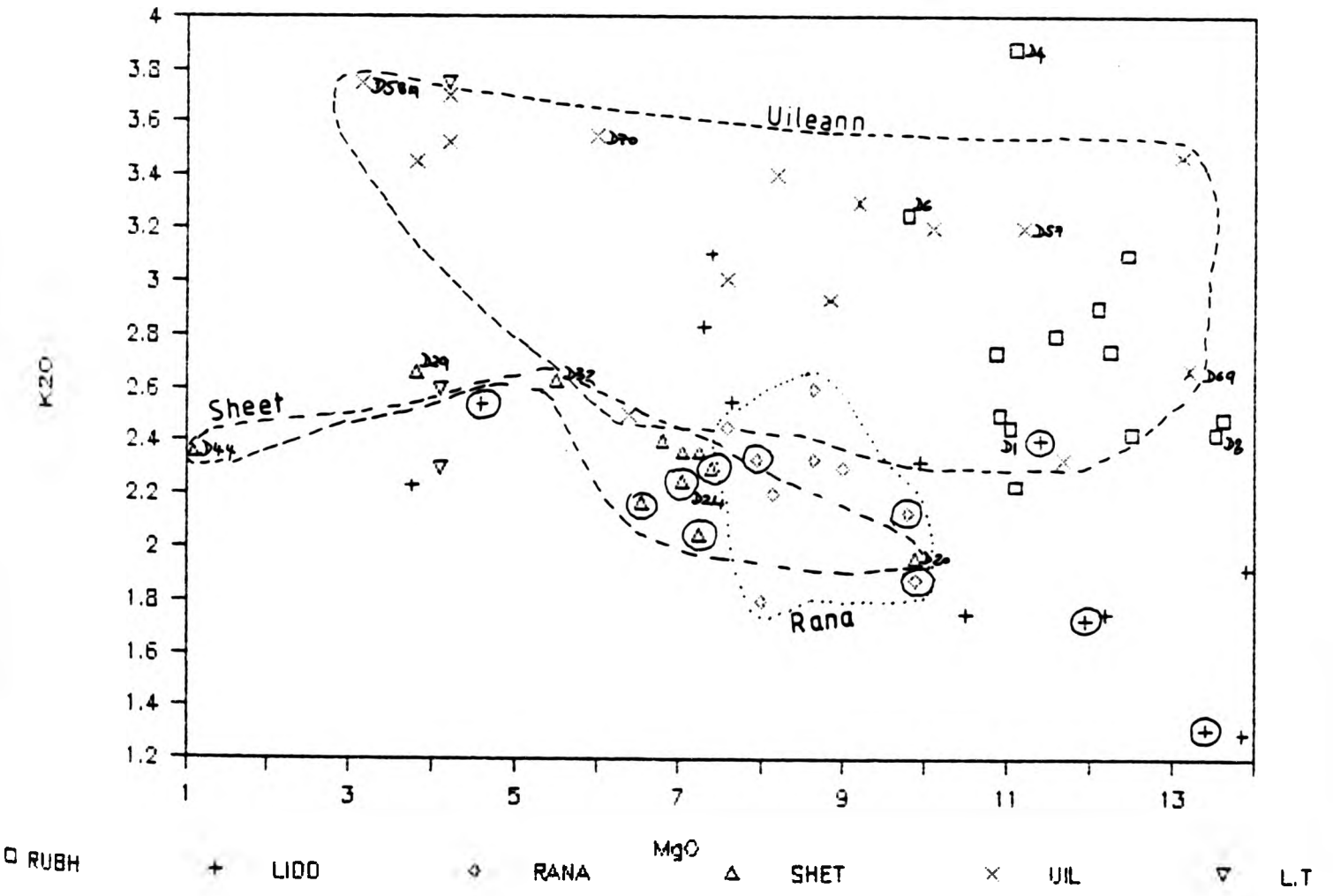

○ Biotite pseudomorphs

biotite stabilizing in the diorites, which although K_2O-poor compared with other Strontian diorites, are still K_2O-rich compared with basaltic rocks of similar MgO content. The possibility of a metasomatic origin for the secondary biotites still remains but the parent material would have carried less K_2O than the observed rocks. Large poikilitic biotites are considered magmatic and the main field of rocks with poikilitic biotites plots above 2.6% K_2O.

11.2.6 Phosphorus

The distribution of P_2O_5 (Fig.11.9) is a wide non-coherent scatter across the full range of MgO. This wide range of P_2O_5 contents at any value of MgO for most of the diorites reflects the occurrence of variable proportions of apatite in the Strontian diorites. The Lidd diorite shows the greatest scatter from 1.2 to 0.1% P_2O_5, though the rocks with >9% MgO fall on a well marked negative linear trend. The Sheet also shows a negative linear trend with a low gradient. There are very low values for Lidd and some Rubh samples at the MgO-rich end, which may reflect a dilution effects of cumulate pyroxene or hornblende. Uil shows a broad horizontal trend for all its samples and is more P_2O_5-rich at high MgO than the others.

11.3 TRACE ELEMENTS

The variations in the trace element chemistry is given in Figures 11.10 to 11.32.

11.3.1 Barium, Strontium and Rubidium

The diorites contain 450 to 1783ppm Ba and show no trend at all in

FIGURE 11.9 P2O5 vs MgO

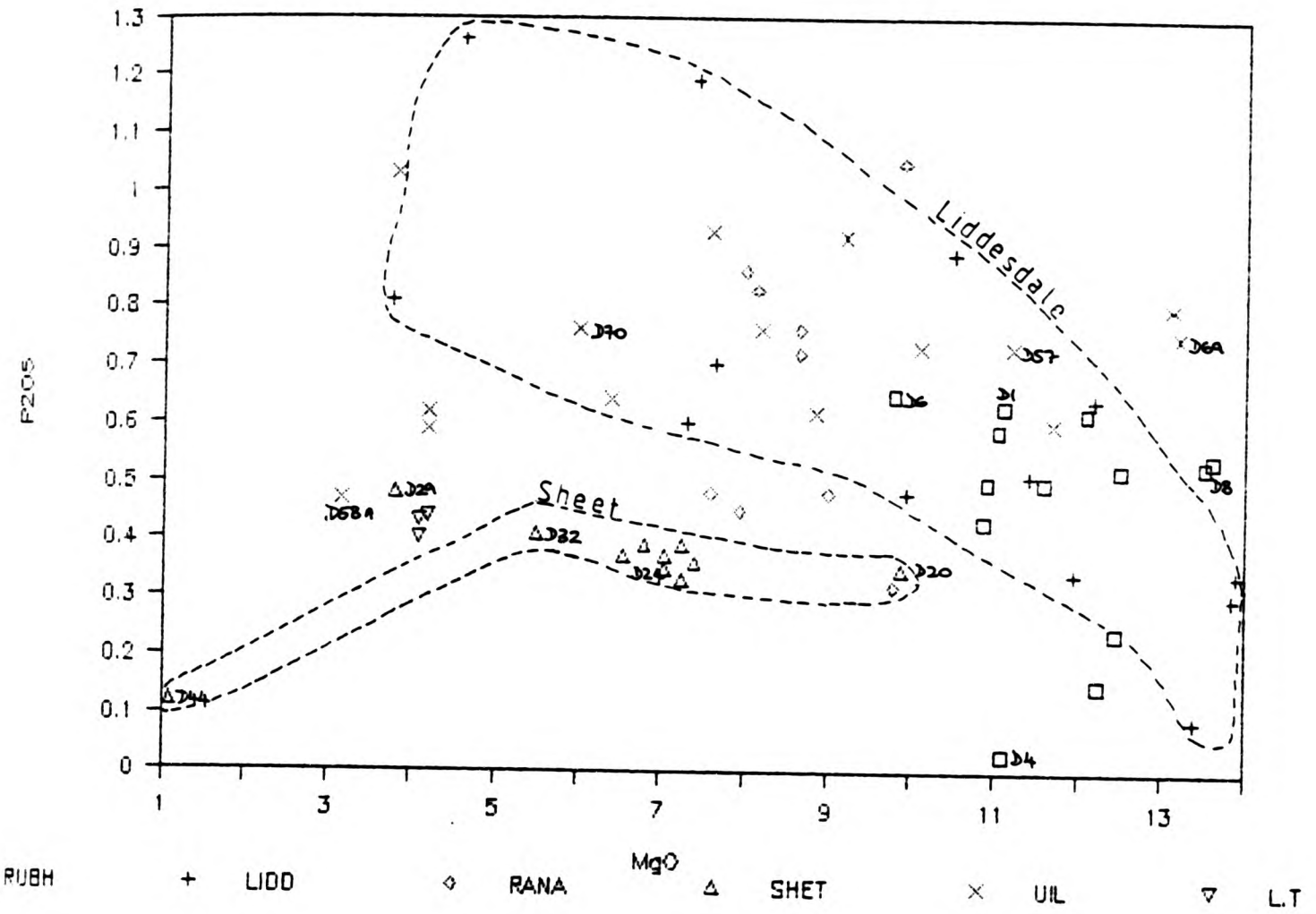

FIGURE 11.10 Ba vs MgO

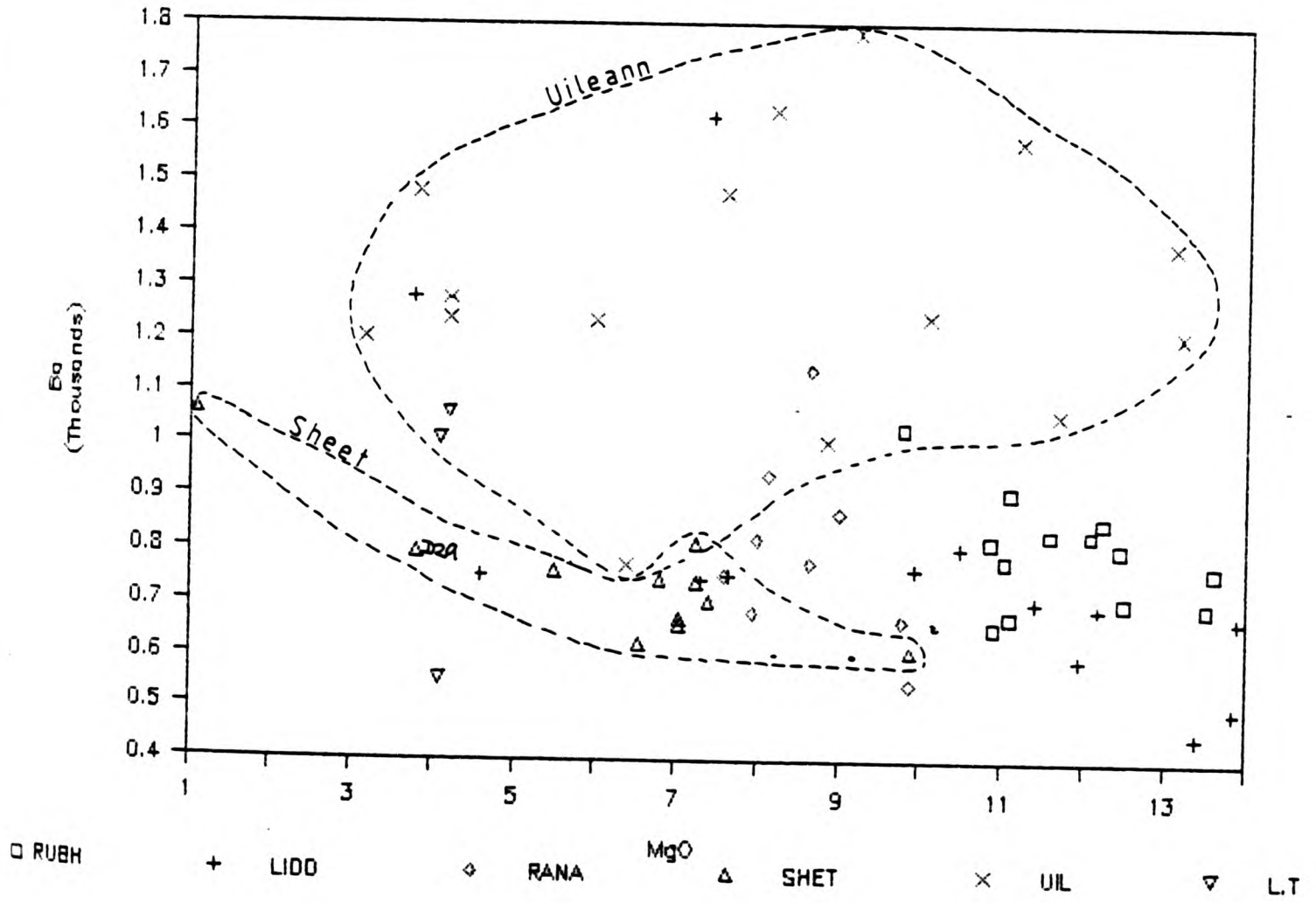

Fig.11.10, but distinct patterns are visible for individual bodies. The Uil diorites show the greatest amounts and scatter of any group, even the more mafic cores have high Ba and forms a completely separate field while the other diorites show only partial separation. The Rubh, Sheet and mafic Lidd all contain between 550 and 1060ppm Ba and show negative trends with MgO. The lowest values are for very mafic rocks which may be pyroxene or hornblende cumulates. The absolute Ba values at Strontian are high 450 to 1783ppm, while Ba content of the Sidlaw lavas, from basalt to dacite, ranges from 272 to 730ppm Ba (Gandy 1975).

On Fig.11.11 Ba/Rb is plotted against SiO_2 for all the rock groups the diorites show a constant ratio with increasing SiO_2 which overlaps the main granite trend, but is separate from the xenoliths; while the Ba/Sr ratio (Fig.11.12) has a more scattered trend and the diorites are separated from the main granite - xenolith trend. The Ba/Rb (Fig.11.11A) and Ba/Sr (Fig.11.11B) ratios for individual diorite bodies show a wide scatter of data with no obvious trend with increasing silica. The Rubh diorite appears to have the tightest grouping of all the diorites in both diagrams and show the lowest Ba/Rb ratios.

Ba vs K_2O (Fig.11.13) and Ba vs Rb (Fig.11.14) both have scattered but linear positive trends pointing to coherent behaviour of these geochemically similar elements. The Uil diorites has the widest scatter and the highest contents, especially in the net-veined and "mixed" samples. Lidd shows a curious banded trend, mostly low K_2O and Rb, but with wide variation at 700-800ppm Ba.

Strontium (Fig.11.15) has a much tighter trend, though there is one

FIGURE 11.11 Ba/Pb vs SiO2 (all rocks)

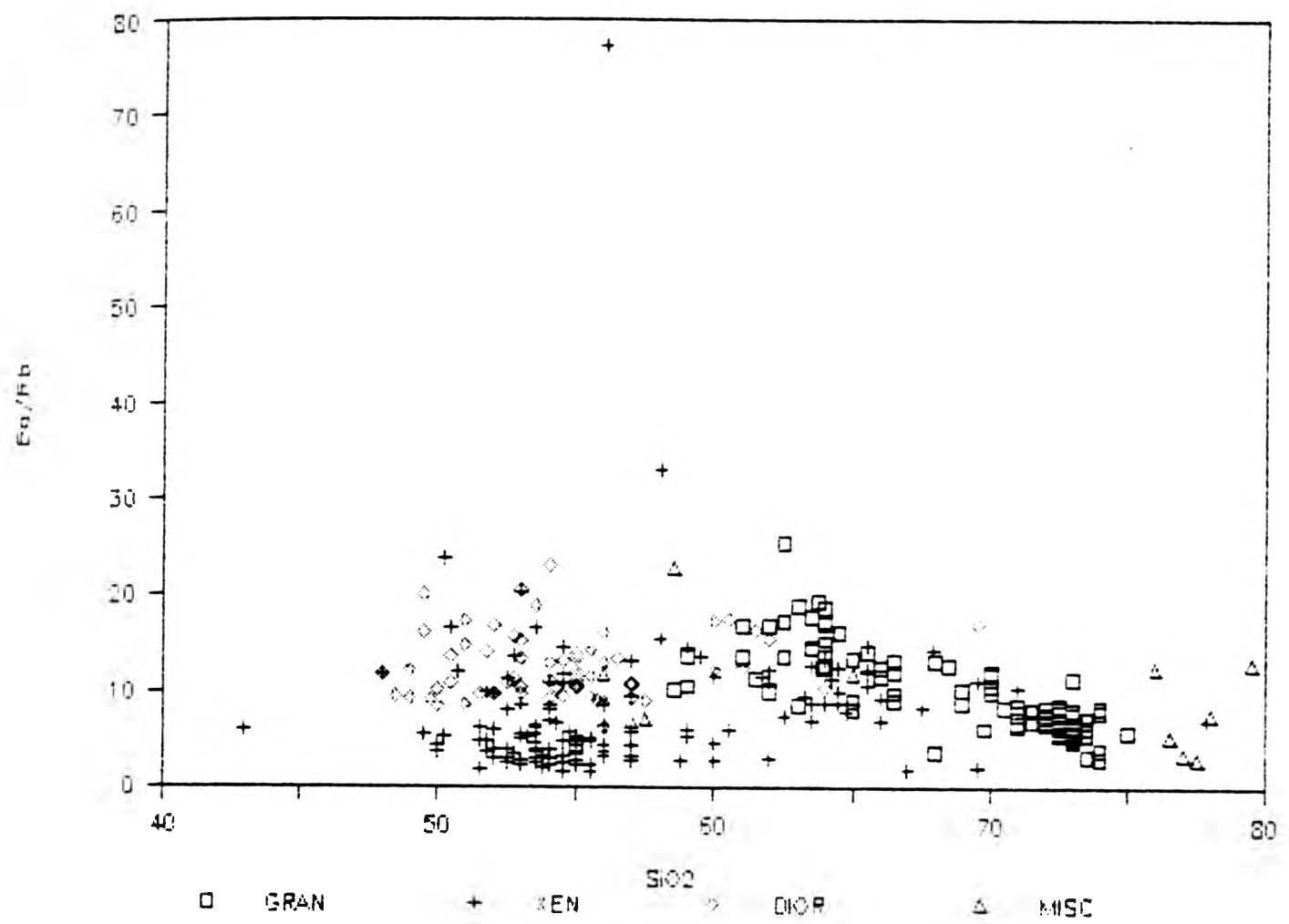

FIGURE 11.11A Ratio Ba/Pb vs SiO2

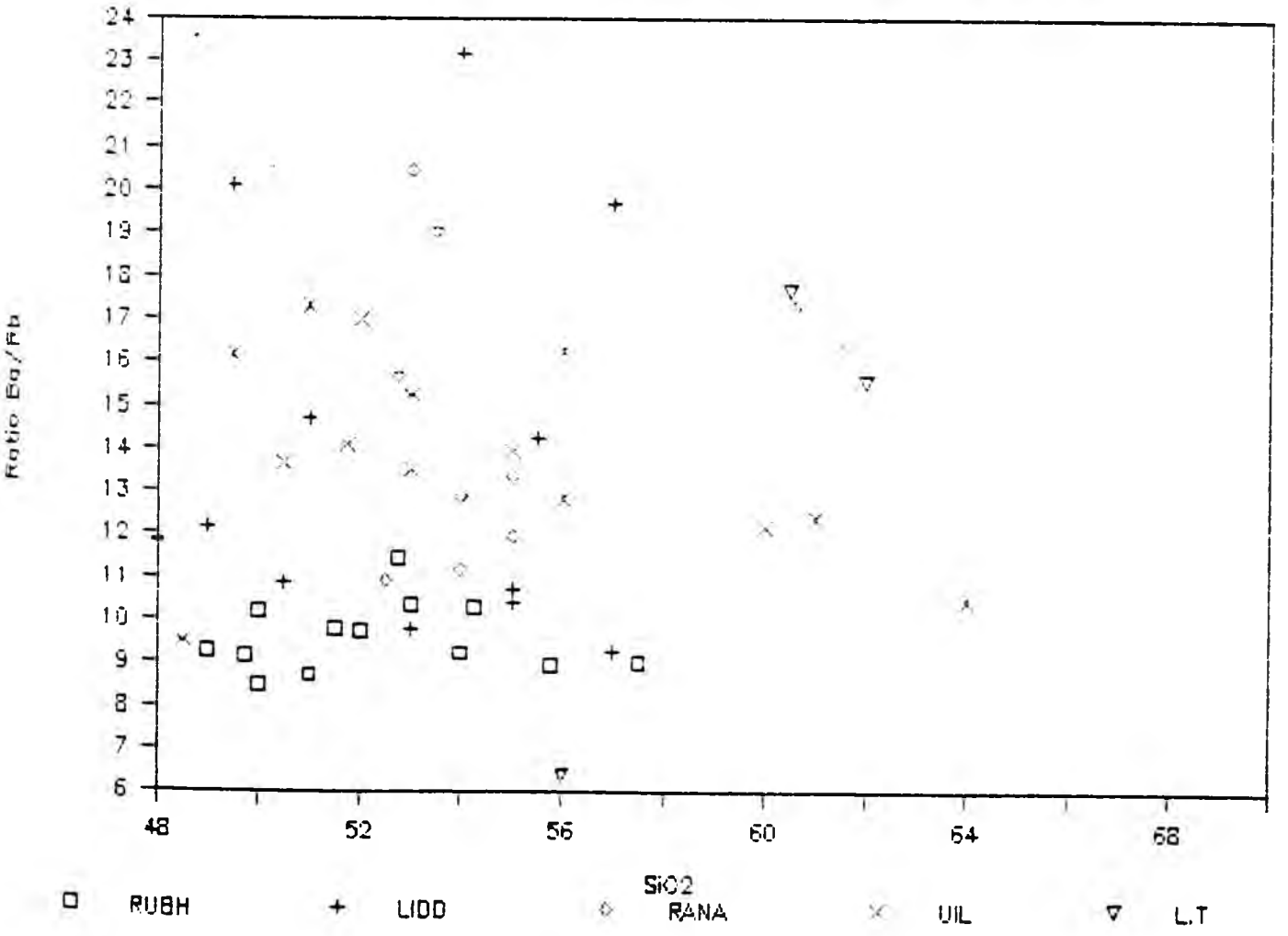

FIGURE 11.12 Ba/Sr vs SiO2 (all rocks)

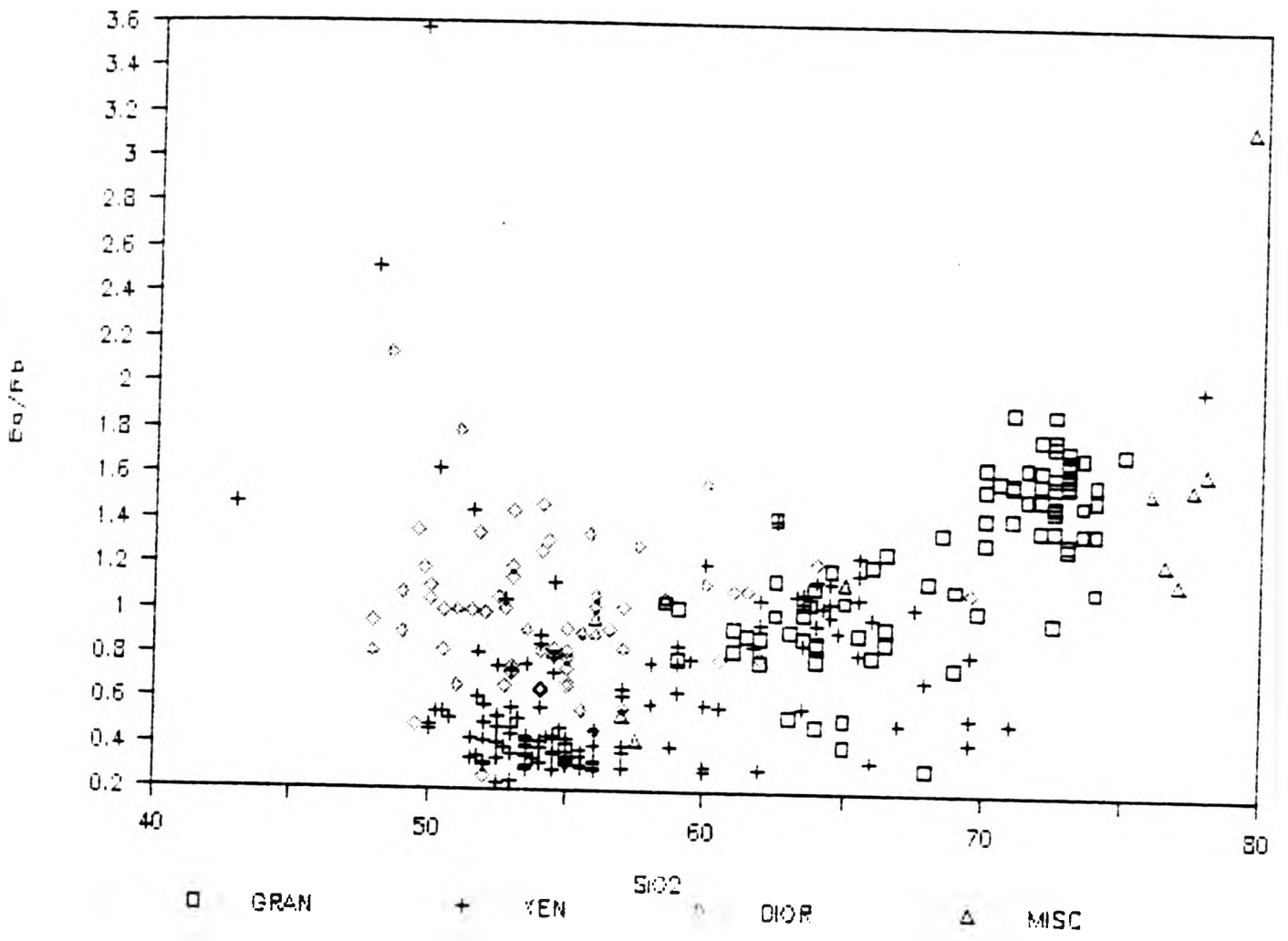

FIGURE 11.12A Ratio Ba/Sr vs SiO2

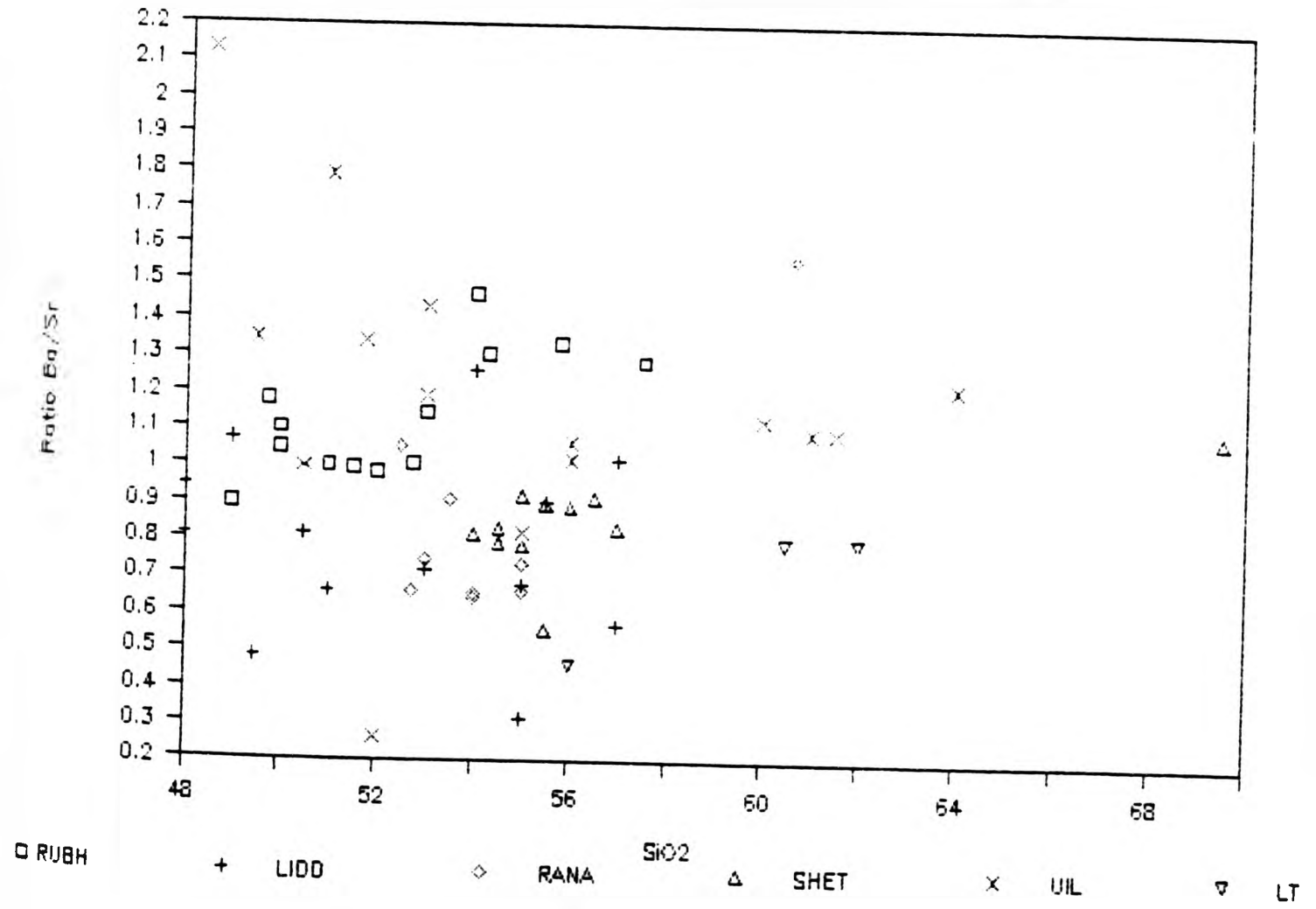

FIGURE 11.13 K20 vs Ba

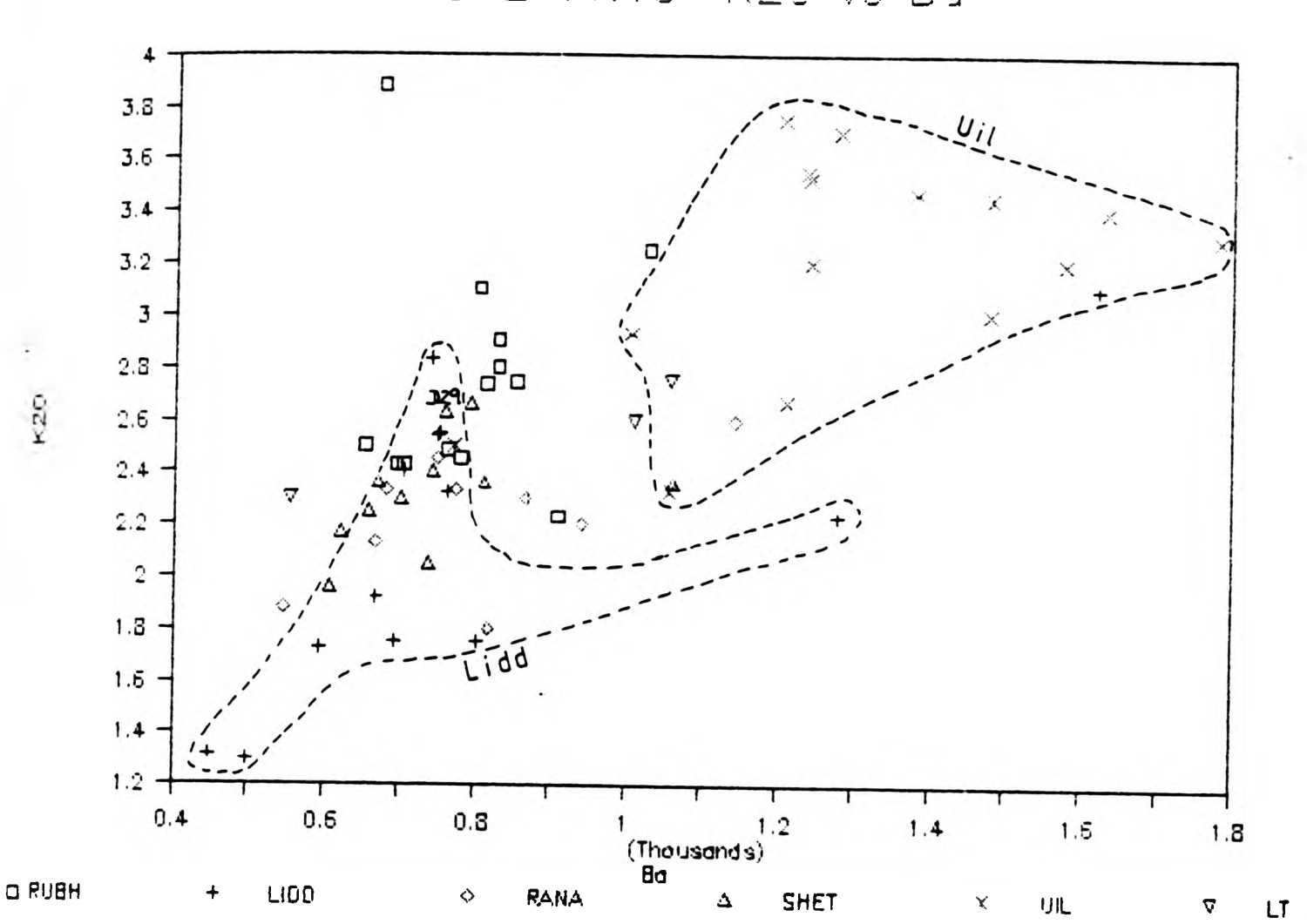

FIGURE 11.14 Rb vs Ba

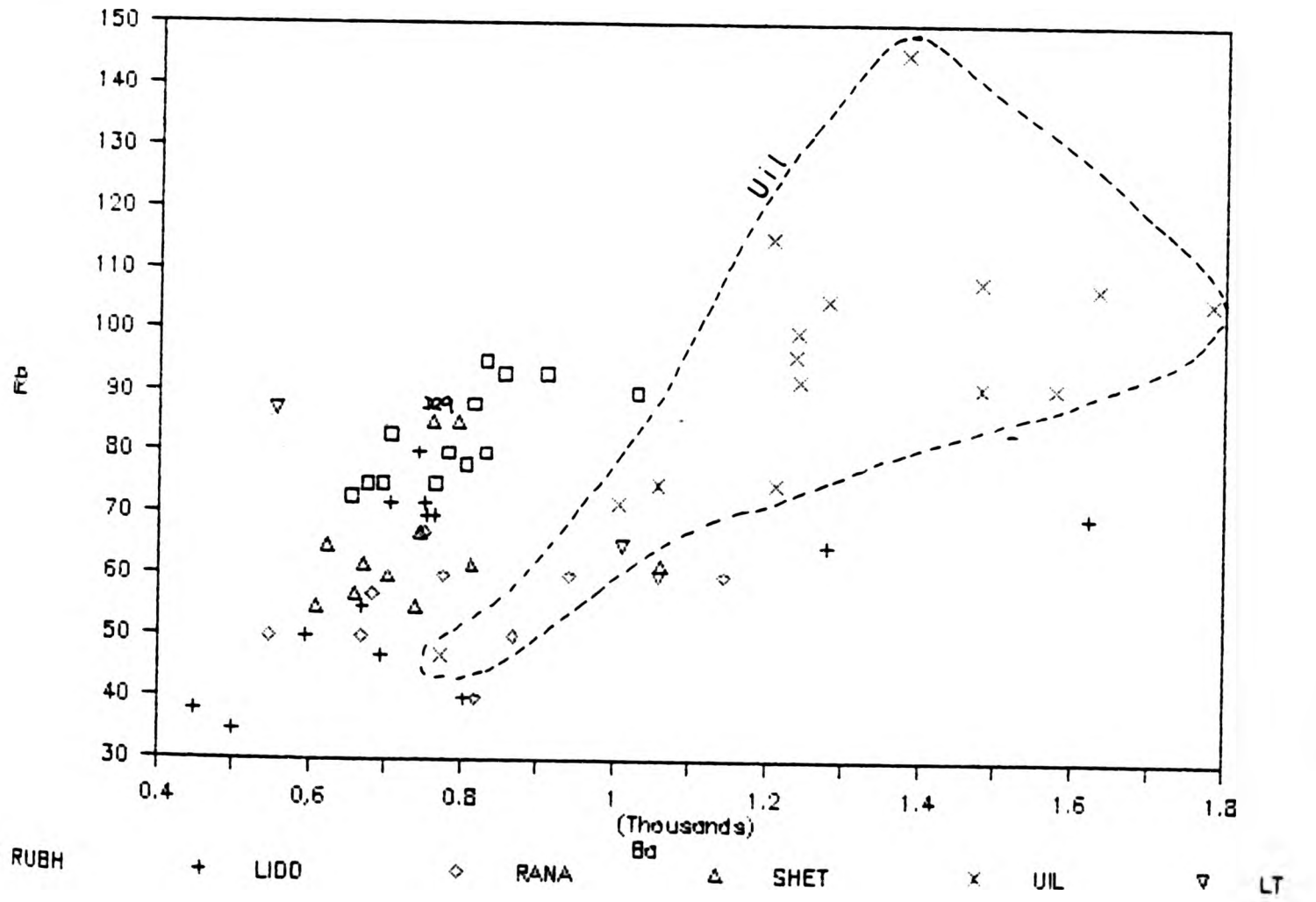

extreme Uil sample (D65) at 6745ppm Sr. The main range is 490 to 2367ppm Sr. The ranges of Sr for each group do overlap somewhat, though the Uil all have Sr contents of over 1000ppm, shows a negative linear trend.

Sr can substitute for Ca and K in crystal lattices. Fig.11.16 displays the increase in the Sr/Ca ratio with increasing SiO_2 for all the groups. The diorites having the lowest ratios and the trend increases towards the host rocks. In the Sr/Ca diagram for the diorites alone (Fig.11.17) the trend is gentle positive linear trend. Rubh shows a consistent ratio. The Sr content is higher in those samples with lower CaO (Fig.11.18) giving a general negative correlation. The Rubh data seems to plot separately from the rest with positive correlation upto 800ppm Sr. Lidd data falls into two fields, high and low CaO with overlapping negative trends. Sr in the Sidlaw and Lorne lavas varies from 412 to 704ppm (Gandy 1975) and 760 to 1410ppm (Groome & Hall 1974) Sr respectively. The Lorne lavas seem to display similar ranges to the diorites.

Sr vs K_2O and Sr vs Ba (Figs.11.19 & 11.20) do not display significant trends. The Uil (in the Sr vs K_2O) have higher contents of both elements than the other diorites, though the Lidd diorite has the greatest range. While Sr:Rb (Fig.11.21) displays a separation of the Rubh and Uil diorites from the remaining trend of increasing Rb with increasing Sr.

Rubidium (Fig.11.22) to a certain extent reflects the distribution of Ba (Fig.11.10) and K_2O, with negative trends again visible for the individual intrusions, but Rb (38 to 145ppm Rb) has a wide scatter. The Uil diorite apart from one extreme point , which is a sample of

FIGURE 11.15 Sr vs MgO

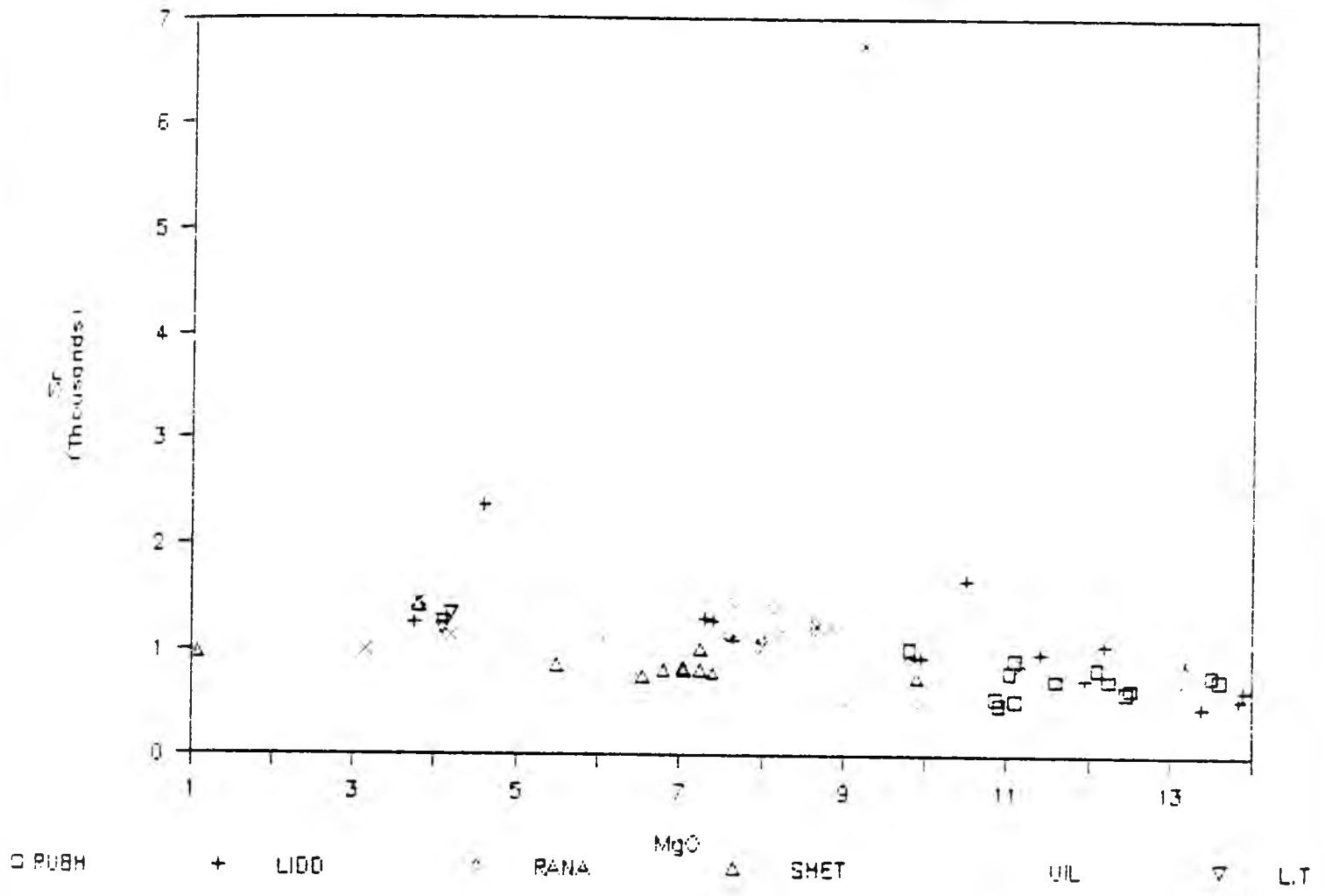

FIGURE 11.16 Sr/Ca vs SiO2 (all rocks)

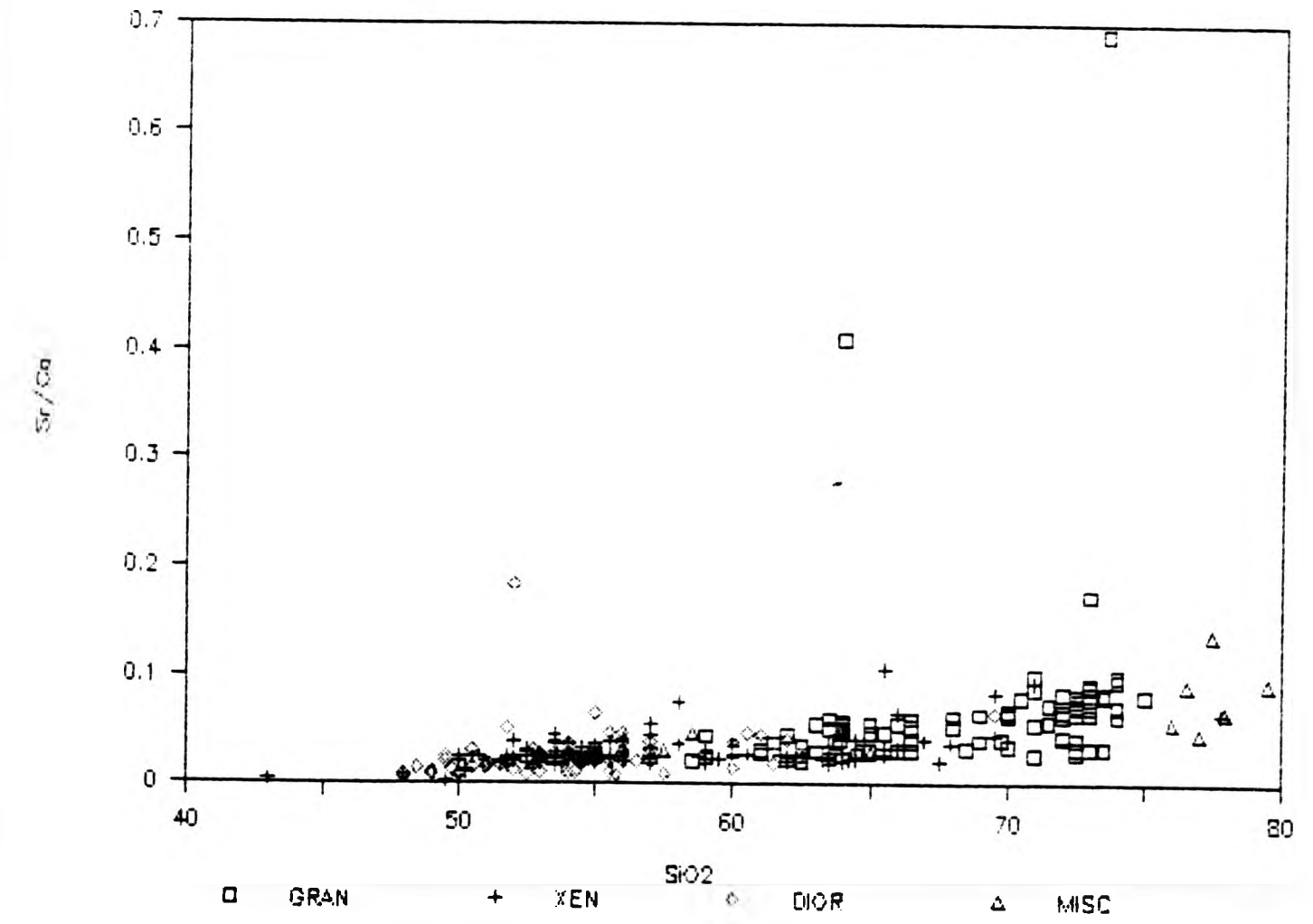

FIGURE 11.17 Sr/Ca vs SiO2

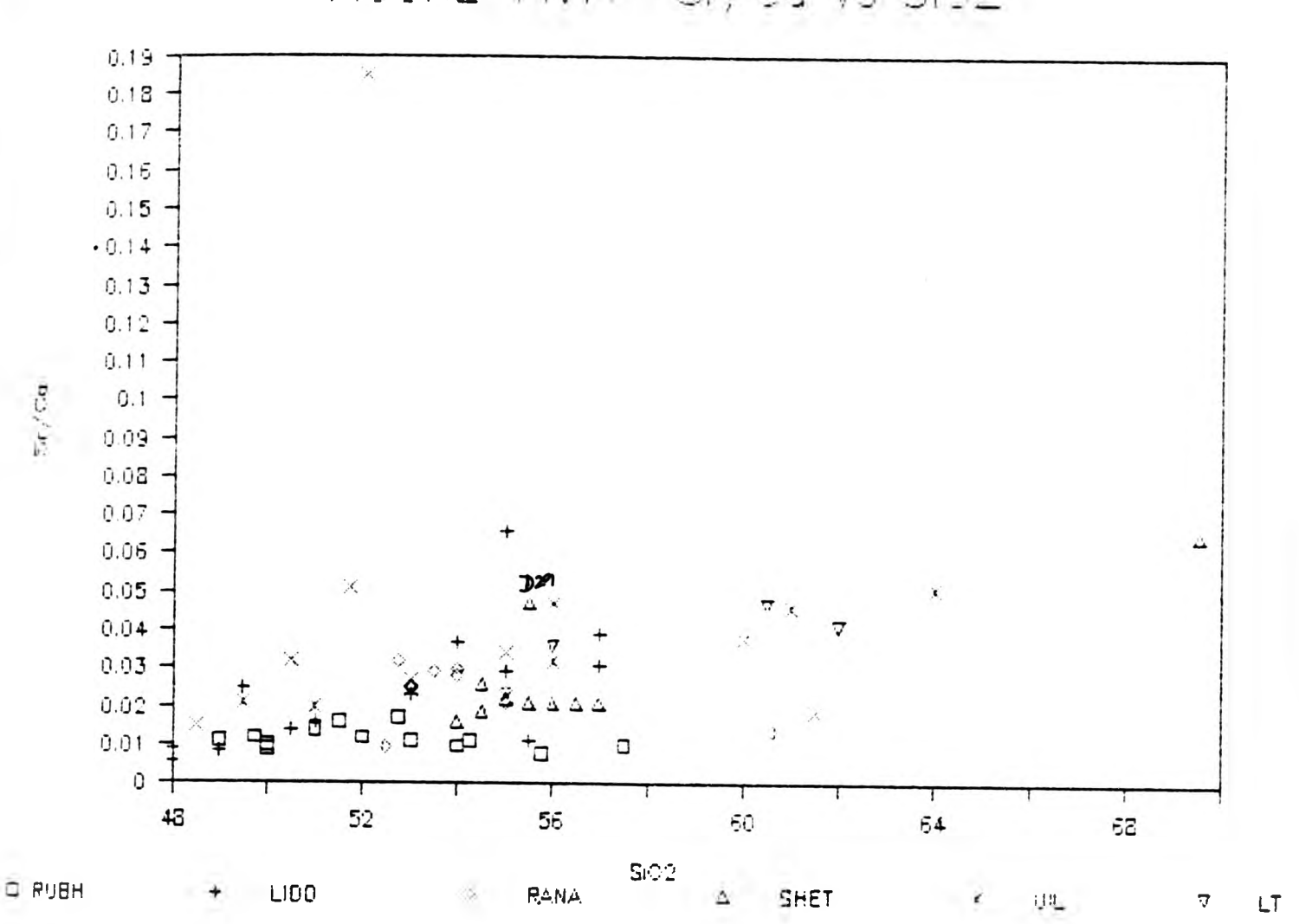

FIGURE 11.18 CaO vs Sr

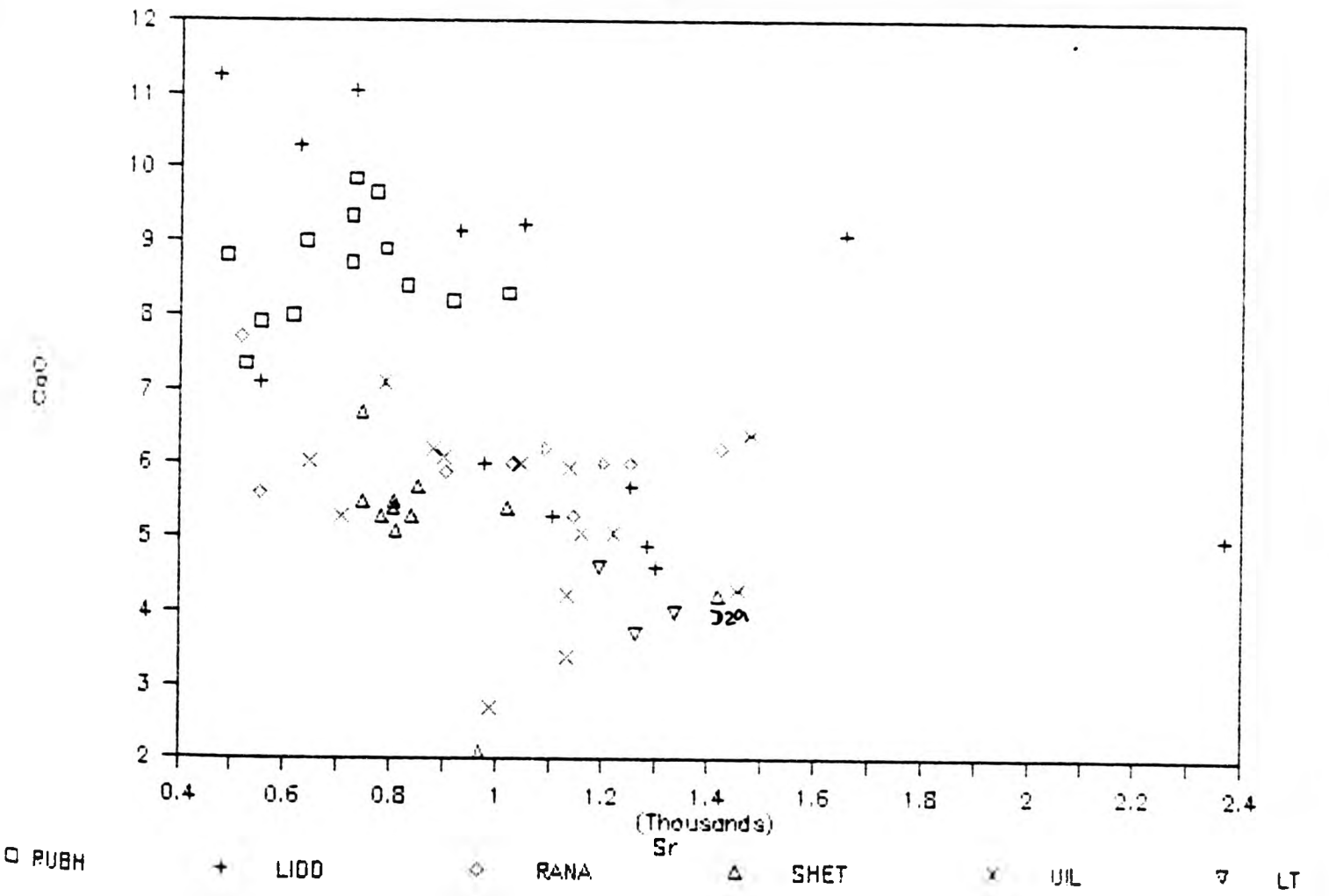

FIGURE 11.19 Sr vs K2O

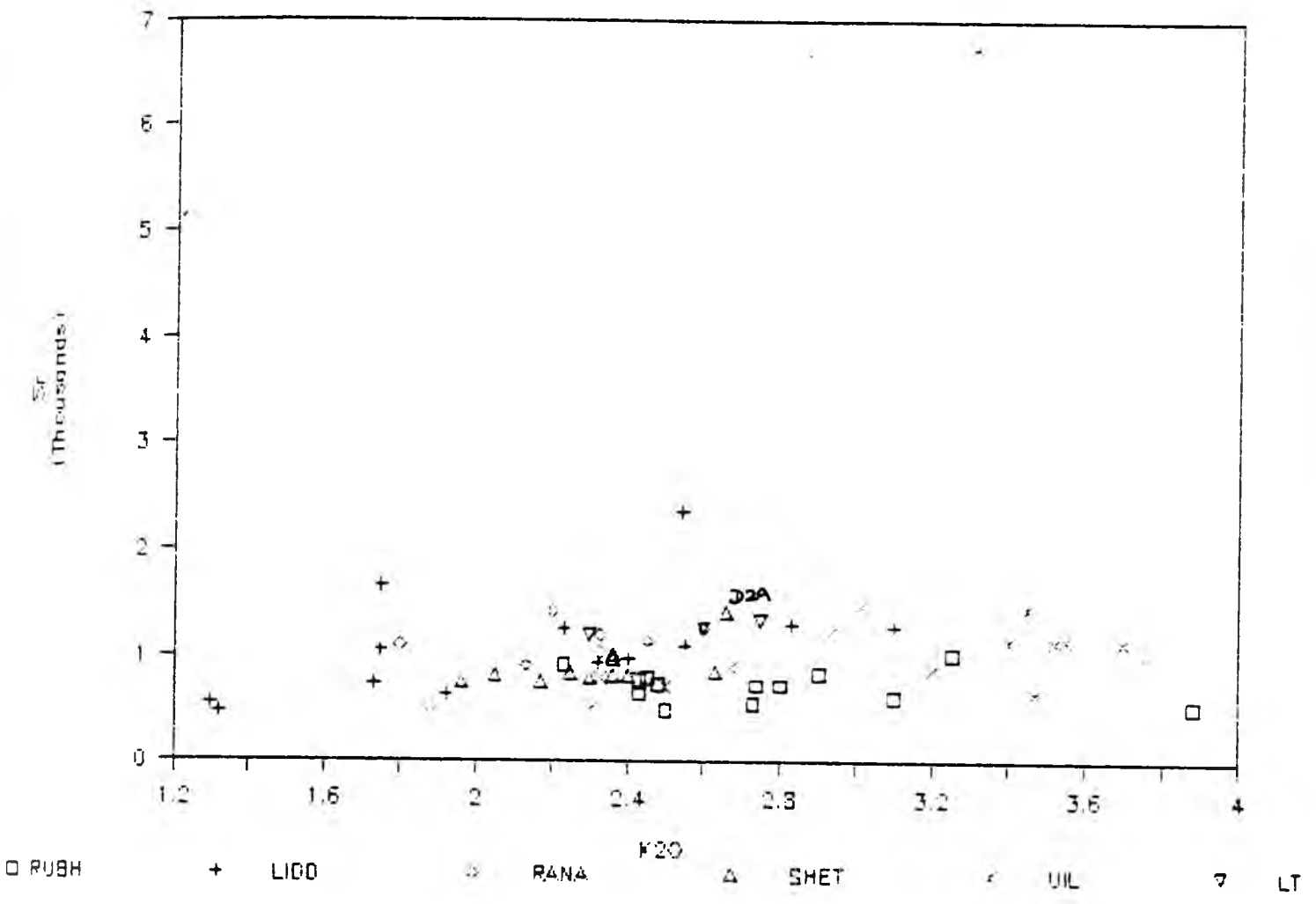

FIGURE 11.20 Ba vs Sr

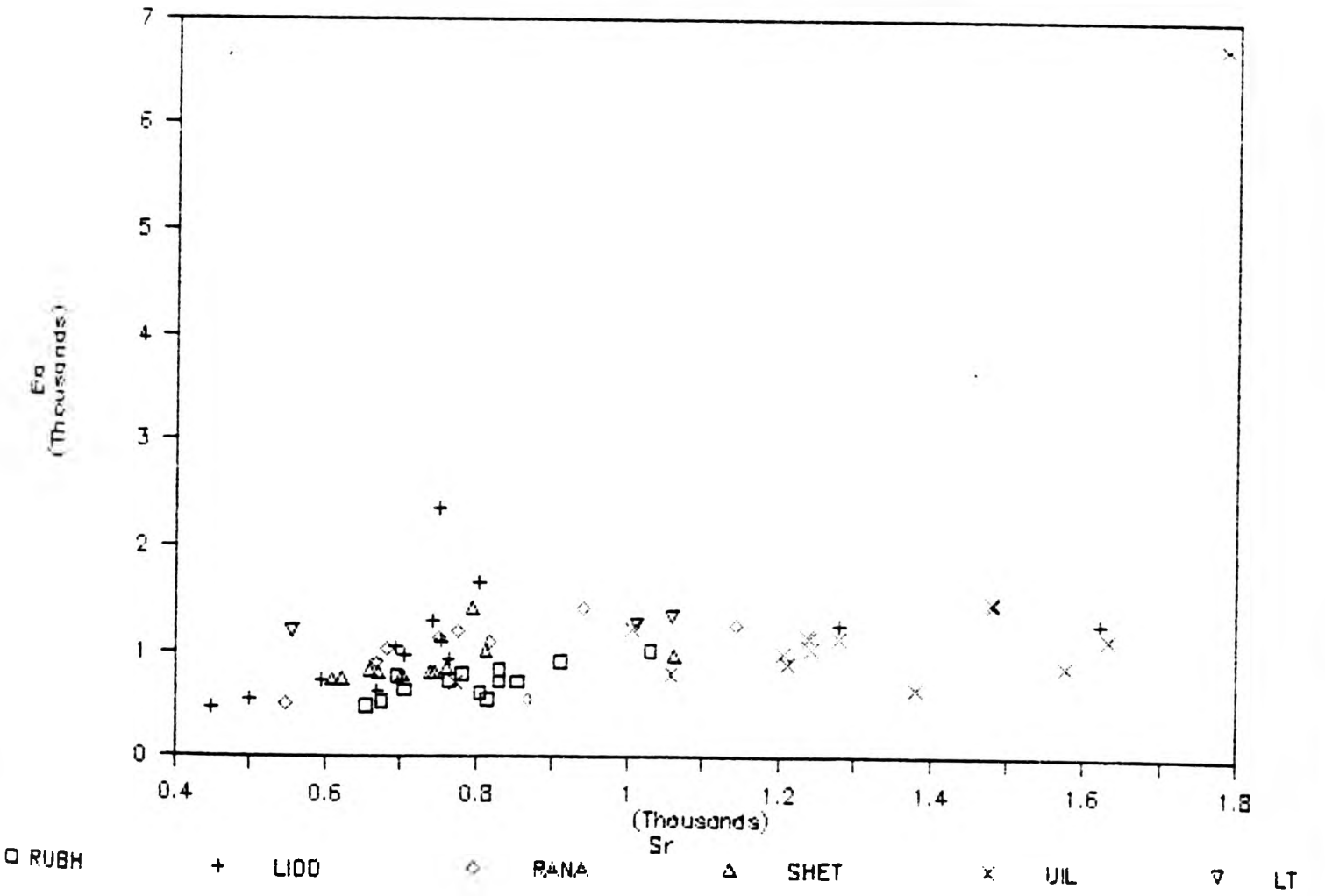

FIGURE 11.21 Rb vs Sr

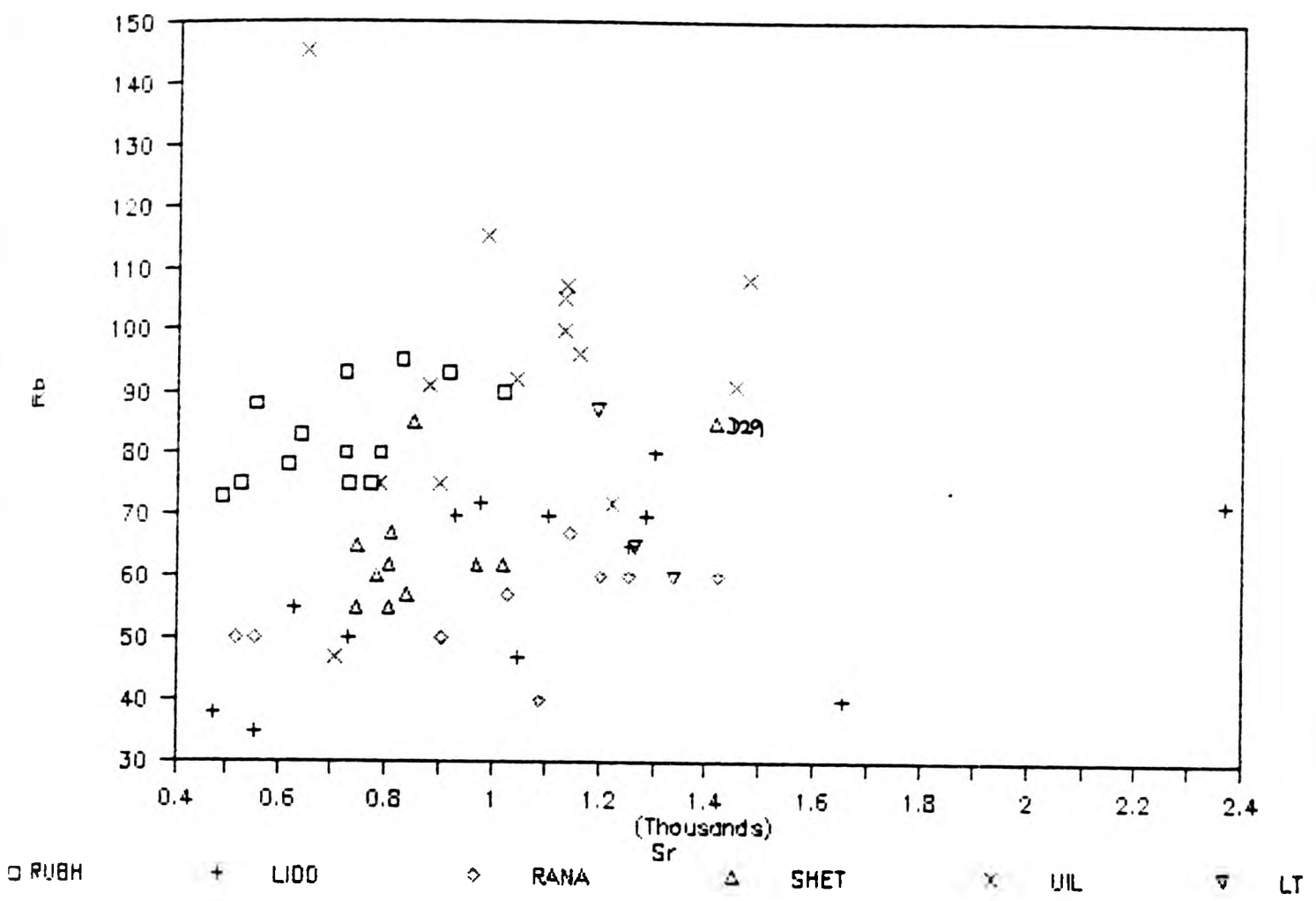

FIGURE 11.22 Rb vs MgO

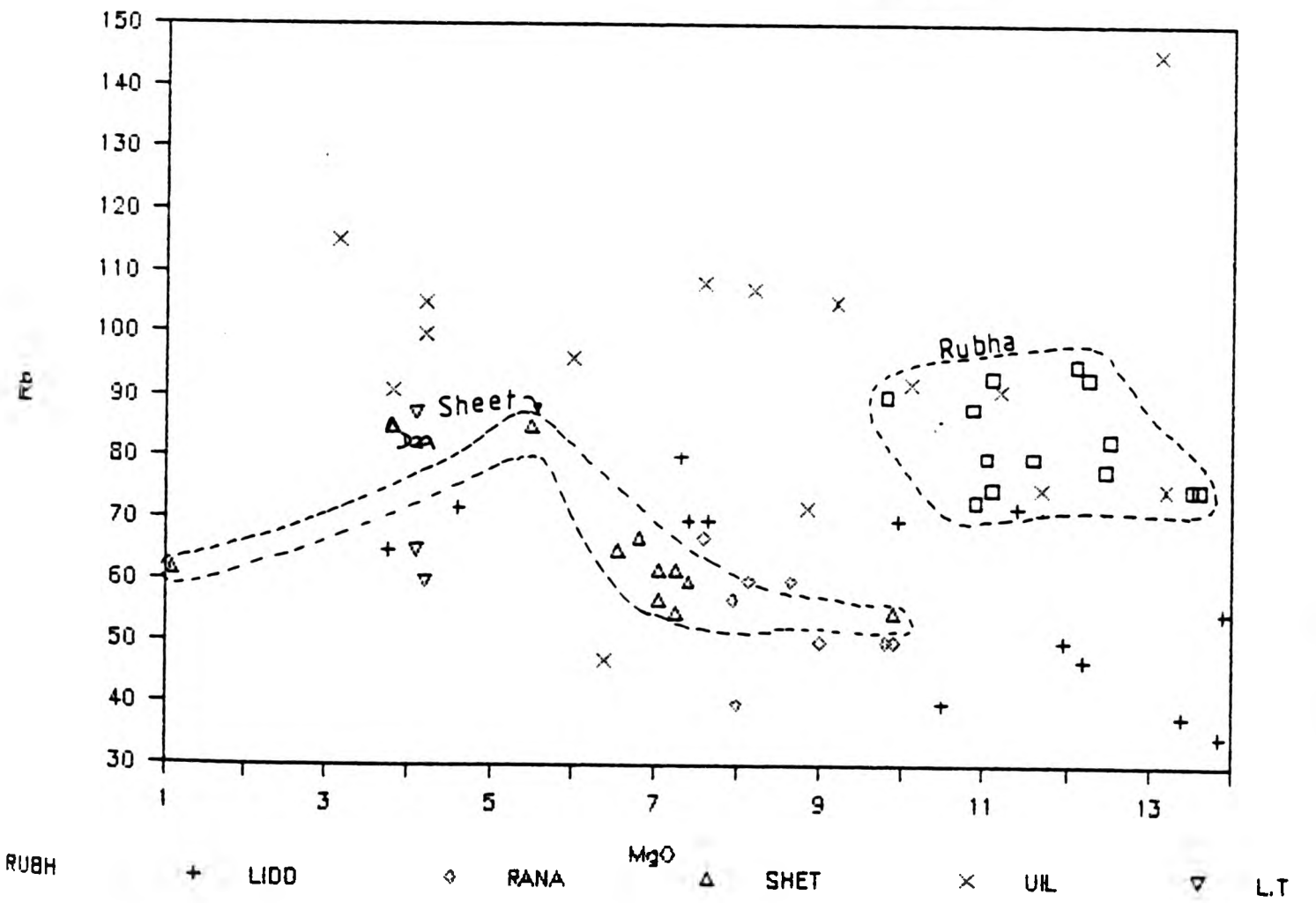

the marginal net-veined facies, is not so separate from the rest of the diorites. Lidd and Sheet both have well defined linear negative trends with narrow ranges. Rubh, the Sheet (a tight trend) and Rana are all separate fields and are relatively coherent as individual bodies. The Strontian diorites have generally high Rb relative to both the Sidlaw (6 to 89ppm) and Lorne (15 to 67ppm) lavas. The higher levels are really only noted in the Uil and Rubh diorites, which respectively have contact with biotite granite and have a higher proportion of biotite.

Rb can replace potassium in biotite and K-feldspar. The K/Rb ratios (Fig.11.23) are variable throughout each main rock group and the ratios plot as a broad band from 100 to 450 (for the host granodiorites). The K/Rb ratio for the diorites (Fig.11.24) shows a completely different trend to that of the host rocks with a positive correlation of increasing ratio with increasing SiO_2. There is a wide scatter which at about 60% SiO_2 meets the negative correlation of the host rocks (Fig.11.23). If the trend for the granodiorites-granites could be attributed to fractional crystallization or amphibole crystallization, then the diorites could be an accumulation of amphibole.

The Rb vs K_2O (Fig.11.25) is a good linear coherent trend passing close to the origin. There is a positive correlation of increasing Rb with increasing K_2O, except Rubh which has uniform Rb and LT, which has a negative trend.

11.3.2 Chromium and Nickel

The distribution of Cr and Ni are given in Figures 11.26 and 11.27.

FIGURE 11.23 K/Rb vs SiO2 (all rocks)

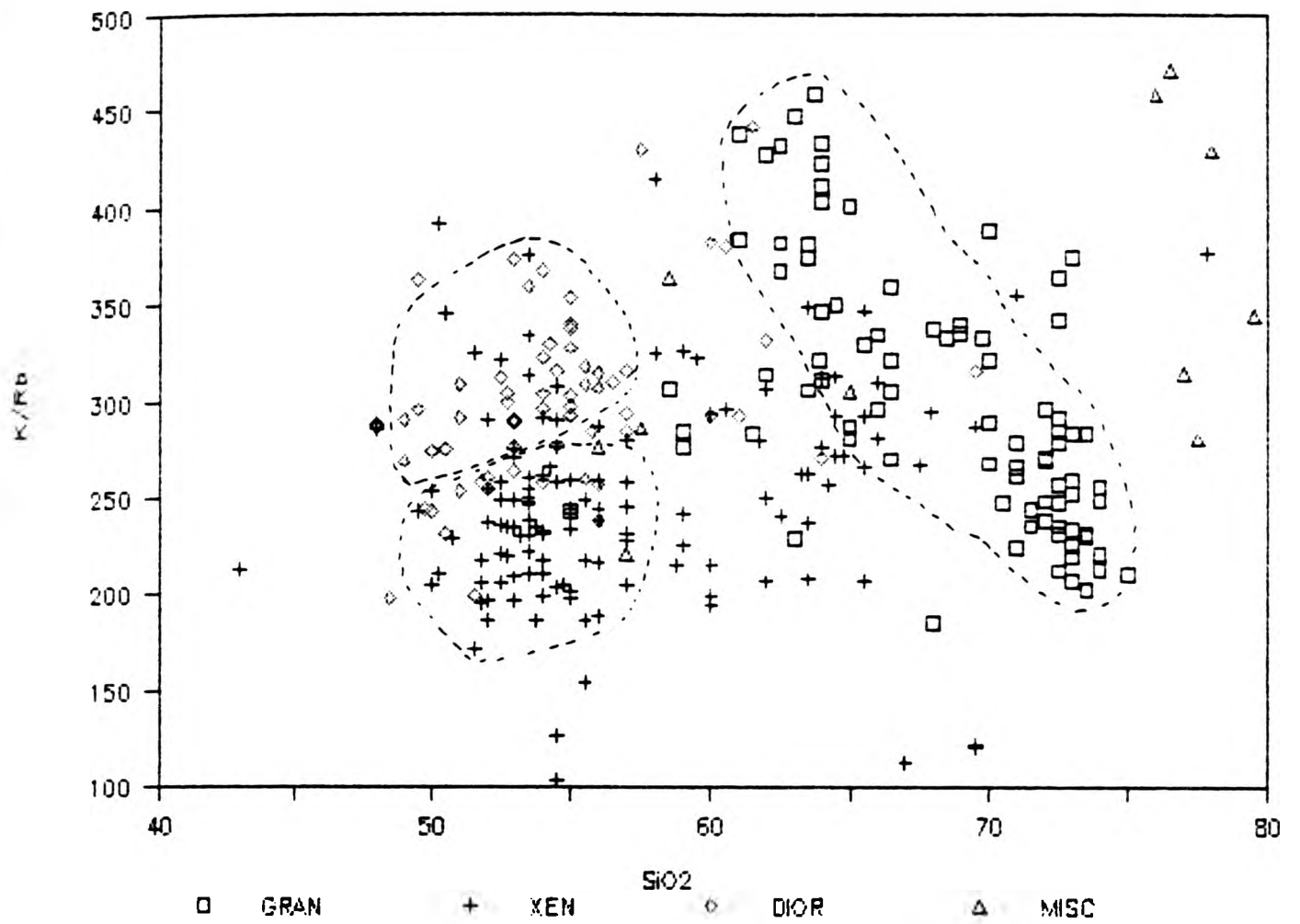

FIGURE 11.24 K/Rb vs SiO2

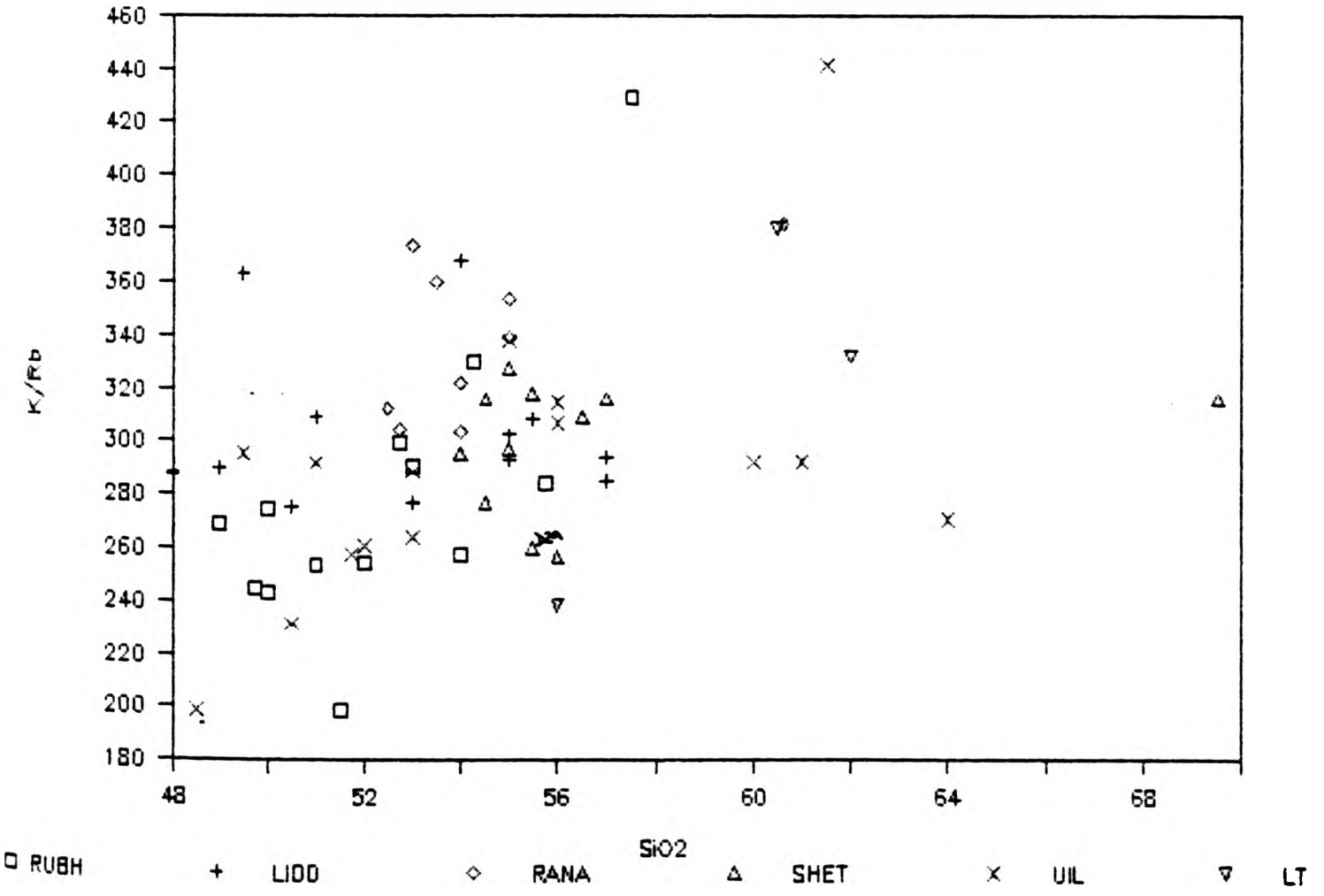

FIGURE 11.25 Rb vs K20

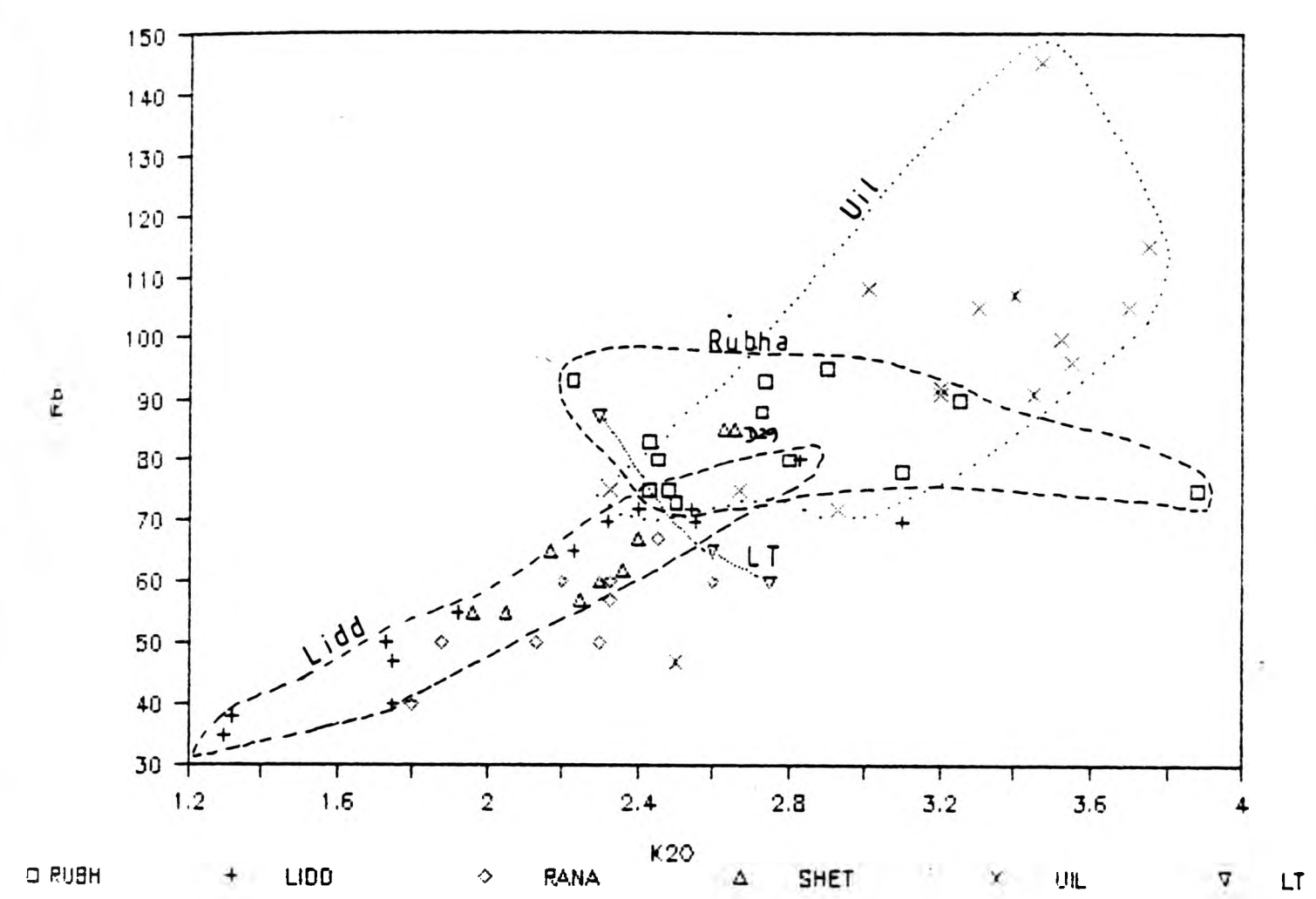

FIGURE 11.26 Cr vs MgO

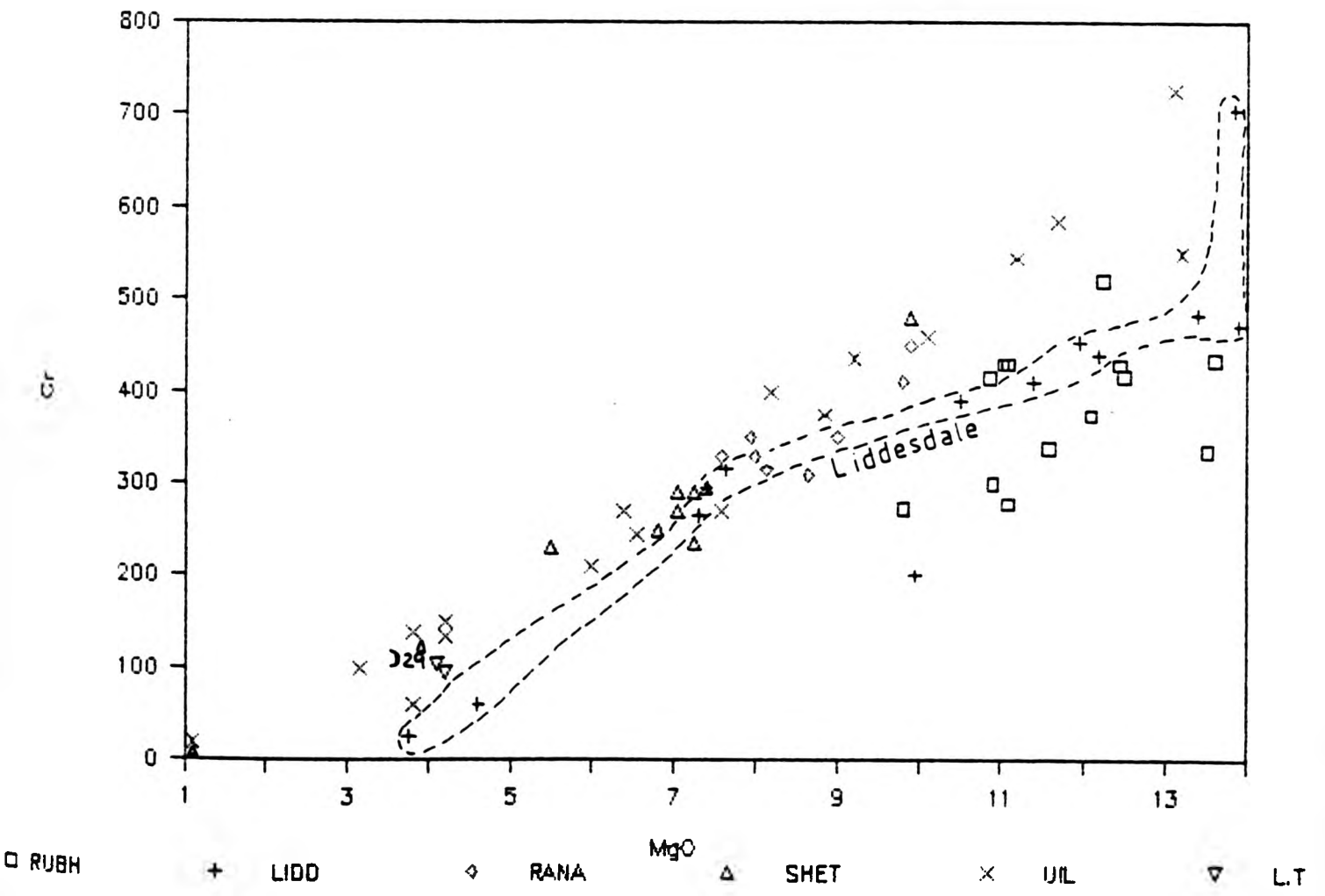

Both show good linear trends of decreasing values with decreasing MgO.

Cr has a slightly tighter trend than for Ni and contents range from 27 (in the sheet) to 725ppm Cr. The Sidlaw lava levels are 14 to 325ppm and the Lorne lavas are 108 to 433ppm Cr for MgO values of 3.05 to 7.34% and 2.45 to 6.37% respectively. The Strontian diorites seem to overlap both sets of data.

The Rubh and the separate Lidd body (on A884) plot parallel to but overall slightly below the main trend, while the remainder form the trend.

Nickel (Fig.11.27) has a more scattered plot with a range from 13 to 351ppm Ni (Sidlaw 7 to 252ppm; Lorne 33 to 190ppm Ni), but still has a good linear trend for all the diorites except for two Rubh samples and a small group from the Lidd. These latter samples are in fact a separate body found along the A884.

The diorites are the only rocks that possess sulphide minerals of any amount. These vary from pyrite and chalcopyrite to millerite. Ni levels vary from 0.15 to 61.3% Ni in the different sulphides. While Cr levels in the rare pyroxene analyses give 0.06 to 0.1% Cr_2O_3, suggesting that pyroxene crystallization may control Cr variation.

11.3.3 Vanadium and Scandium

V and Sc (Figs.11.28 and 11.29) display very similar distribution patterns to FeO* and MnO.

FIGURE 11.27 Ni vs MgO

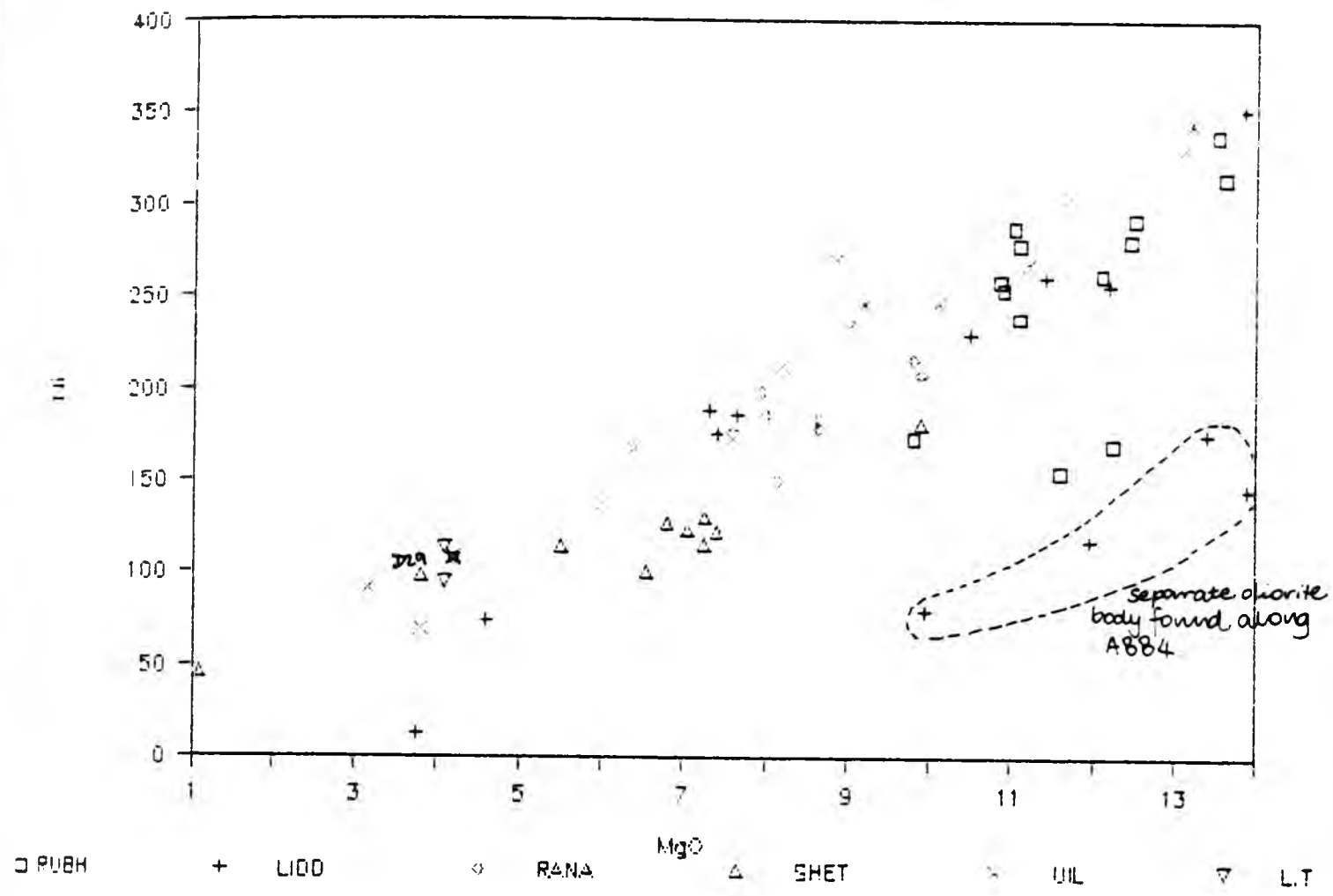

FIGURE 11.28 V vs MgO

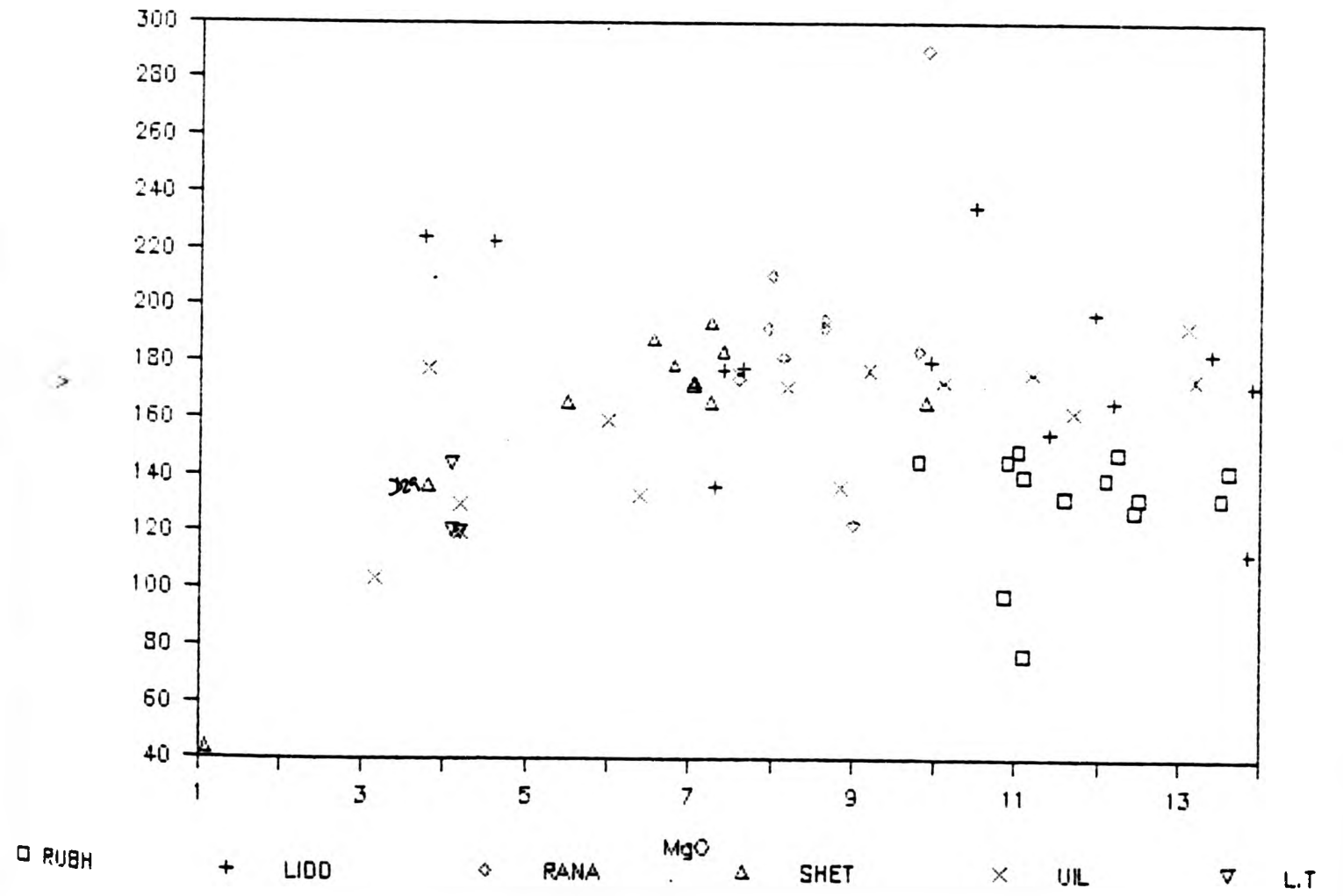

V (Fig.11.28) has a more scattered pattern than any of the major element plots and the trend is very gentle compared with the others. V ranges from 44 to 290ppm. As in the MnO amd FeO*, the Rubh diorite in the V plot lies slightly separately with overall lower V contents.

Sc, 5 to 48ppm, (Fig.11.29) has a more coherent positive linear trend <8% MgO, with only one Rana sample being outstanding at 48ppm. The remainder of the plot is horizontal at >8% MgO.

Both V and Sc can substitute for iron, manganese and titanium. On the plots of FeO* vs Sc (Fig.4.31), FeO* vs V (Fig.4.32) and TiO_2 vs V (Fig.4.33), all three diagrams show good strong positive correlations. This suggests their distribution is most probably controlled by ferromagnesian minerals in the diorites such as pyroxene, amphibole and biotite (as they do not possess any iron oxide minerals).

11.3.4 Copper, Zinc and Lithium

All three elements show plots that are highly scattered (especially Li and Zn) with no obvious trends. The range of each element is reasonably small with the full range of MgO, but there are scattered single samples (Figs.11.30, 11.31, 11.32).

Copper (Fig.11.30) varies from 17 to 228ppm and the average levels for typically calc-alkaline rocks is 10 to 50ppm Cu (Halliday et al 1985). It has a flat trend of quite uniform Cu levels with increasing MgO.

Zinc (Fig.11.31) levels vary from 66 to 122ppm with only one Sheet

FIGURE 11.29 Sc vs MgO

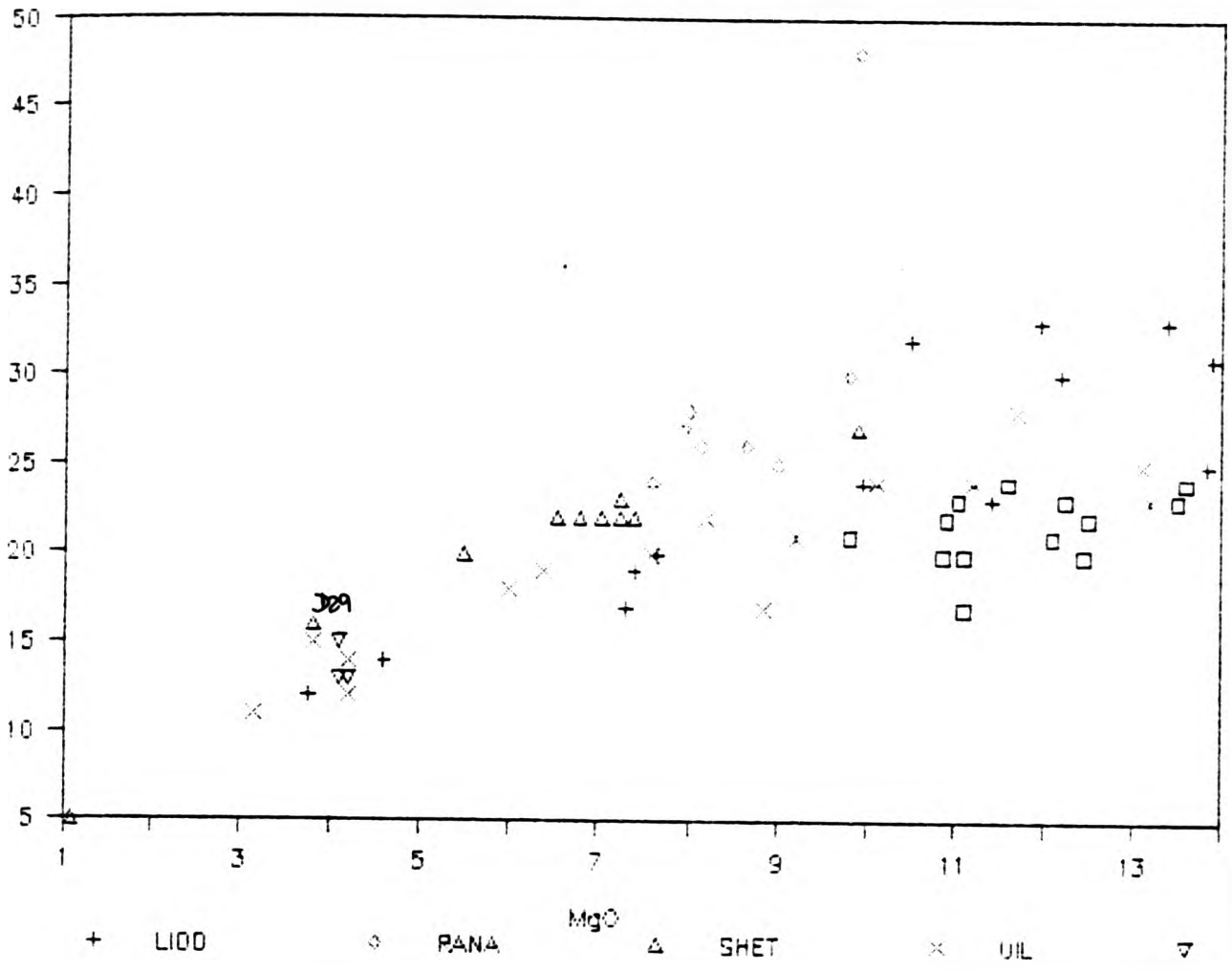

FIGURE 11.30 Cu vs MgO

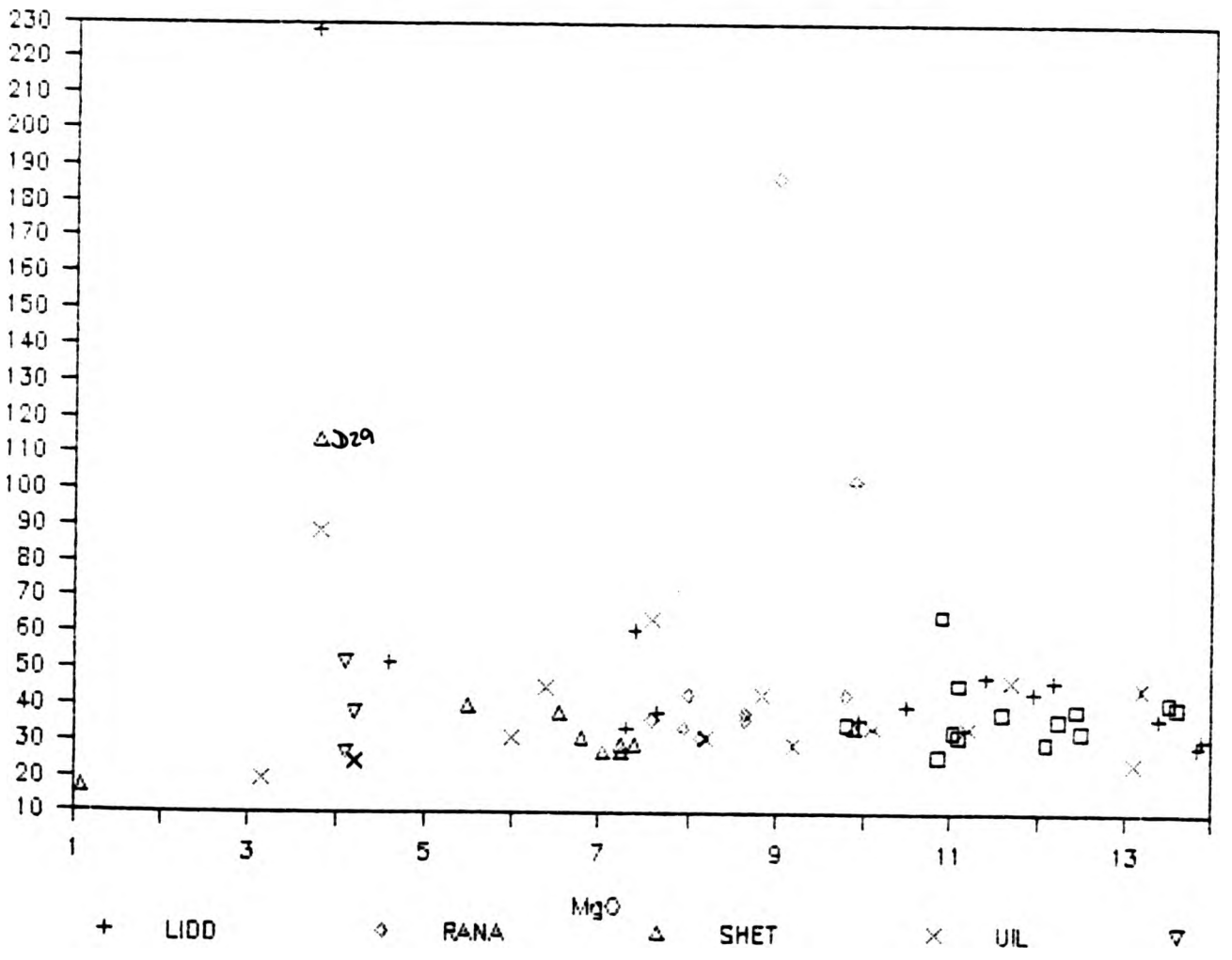

sample falling at 37ppm Zn. These are higher than Halliday et al (1985) who gives typical Zn levels at 40 to 50ppm. Uil and the Sheet display close overlapping linear trends; while Lidd has a step at 8-9% MgO. Rubh data points are low and offset from the overall trend.

Both elements can be incorporated into sulphide minerals and copper is noted as being 30 to 32% in the sulphide analyses. However no Zn data is available for the sulphides.

Lithium plotted against MgO (Fig.11.32) has quite a uniform trend with a small range (13 to 24ppm Li) for all except the Uil diorites. The Uil diorites have a far more scattered distribution with Li levels ranging from 12 (D63 net-veined sample) to 63ppm and they lie almost entirely above all the others with very high levels. The higher Li levels may well correspond to the higher proportion of K-feldspar, which can have upto 0.34% LiO_2 in the matrix (Deer et al 1982). Xenoliths in the biotite granite also have higher Li contents (65 to 112ppm Li) than the other xenoliths.

Little is known of Li substitution, but limited data suggests substitution for magnesium occurs in pyroxenes, amphiboles and biotites. Therefore the observed scatter may be controlled by the variable modal abundances of the mafic minerals of the diorites or it may be inherited from parental materials.

11.4 DIORITE REE PATTERNS

The patterns displayed by the diorites are parallel, but steeper than the xenoliths and have still higher absolute abundances (Fig.11.33).

FIGURE 11.31 Zn vs MgO

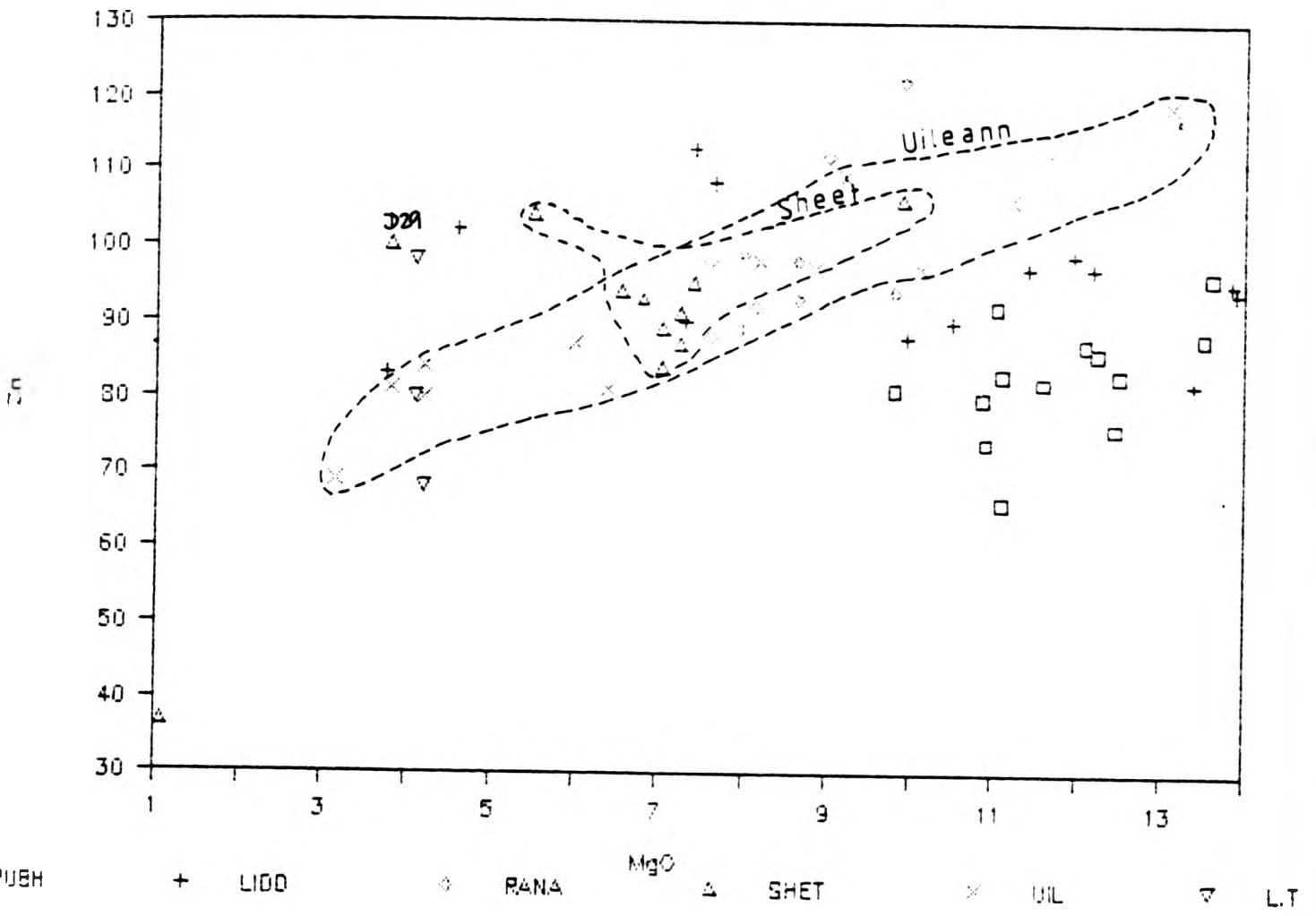

FIGURE 11.32 Li vs MgO

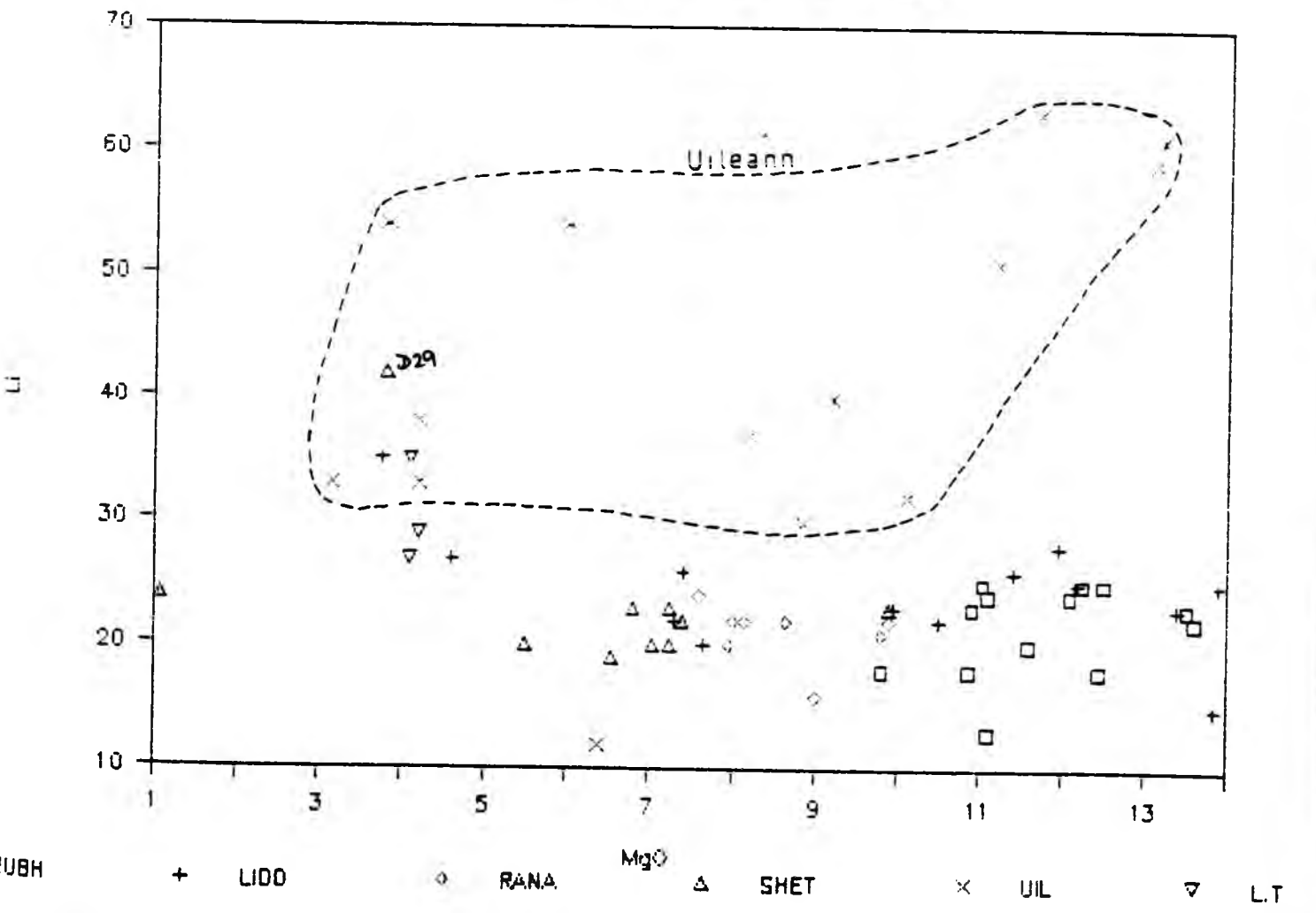

Fig.11·33 Chondrite normalised REE patterns for the mafic diorites.

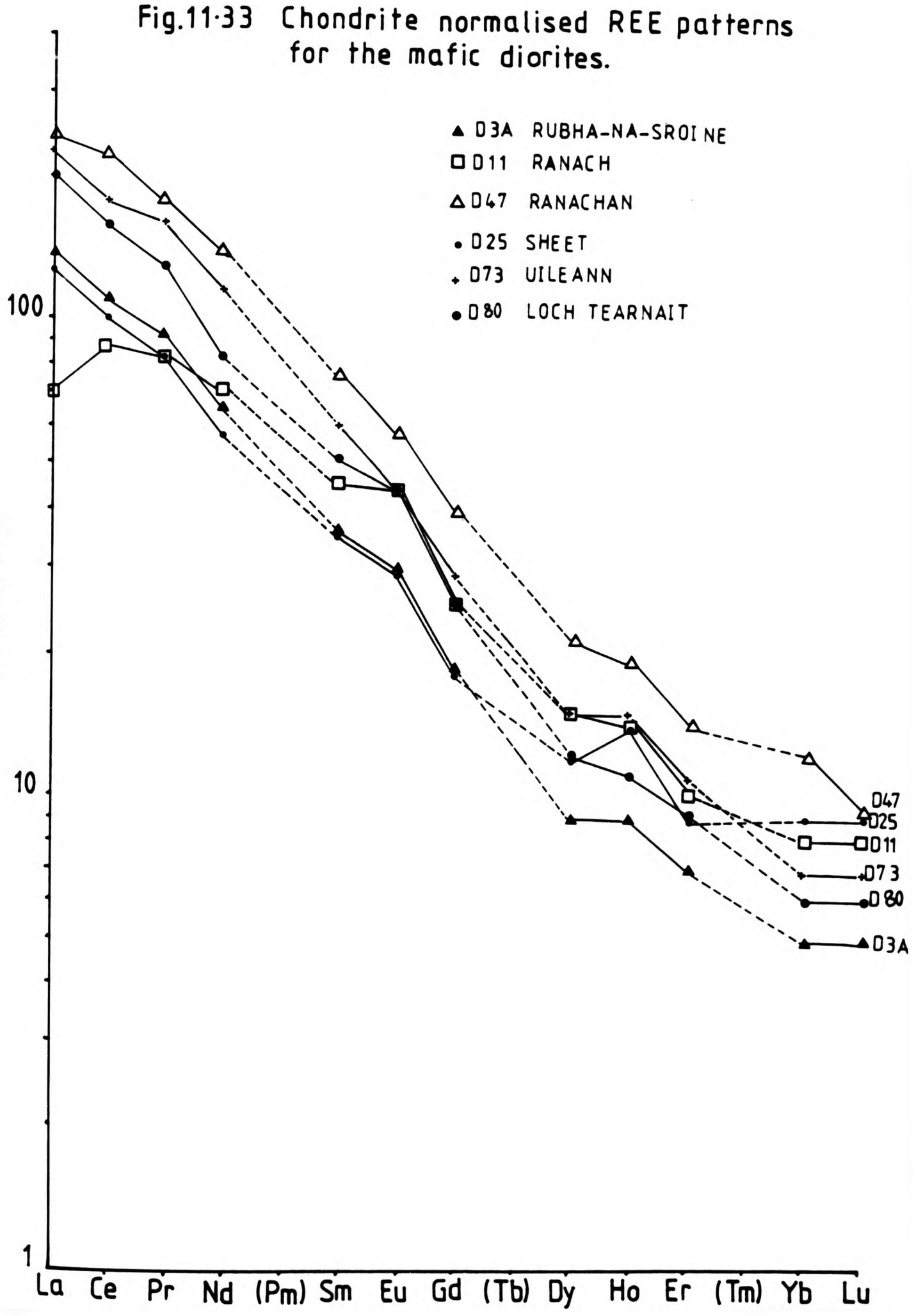

They have consistently higher La enrichment than the host rocks. This would be the result of early and continuing fractionation of highly enriched accessories (Miller & Mittlefehldt 1982). Biotite and amphibole may also be partly responsible. Their La/Yb ratio varies from 8 to 37 with an average of 26; with LaN 70 to 258x and LuN 5 to 13x chondrite. All the patterns for the diorites show either a straight trend or a very slight positive Eu anomaly. Although diorites as a group are richer in REE than the xenoliths and granites, there is not a systematic variation with silica within the diorite group. In fact there are low and high silica samples with high La/Yb ratios, for example:

- D8 48% SiO_2 - 30.7 La/Yb D60 57% SiO_2 - 31 La/Yb
- D73 48.5% SiO_2 - 31.6 La/Yb D58A 64% SiO_2 - 37 La/Yb

There are not enough analyses from each body to see if there are individual REE patterns for each diorite. Though very generally Rubh and Rana show a decrease of the ratio with increasing silica; Lidd and Uil increase the La/Yb ratio with increasing silica and the Sheet is the same.

11.5 SUMMARY

It was initially thought possible that the small microdiorite xenoliths were derived in a crystalline state from these large diorite bodies. This is a possibility that can be tested by using field and hand specimen evidence. In general the textures and mineralogy of the diorites are not represented among the types of xenoliths found. The diorites are generally much coarser and more mafic than the xenoliths. Xenolith Types 1(A) and 4 (section 6.2)

are not represented in the diorite bodies. Though appinitic xenoliths (Type 3) are seen, they have elongate hornblendes, different from the coarse equant hornblendes of the Rubha-na-Sroine and Uileann diorites. While xenolith Types 1(B) and 2 have similar assemblages to the Sheet diorite (no.4 on Fig.1.2), rocks of this type are not found in the diorites around Loch Sunart. The distinct and very coarse (10mm) hornblende diorites, hornblendites and poikilitic biotite meladiorites extensively developed in the diorite bodies along Loch Sunart, are not observed as xenoliths in the granodiorite. The Rubha-na-Sroine diorite (no.2 Fig.1.2) has one finer grained margin, which could be said to be similar to Type 1(A) xenolith. There is therefore only a small overlap between the range of rock types seen in hand specimen in the xenoliths and the large diorite bodies. It is concluded that the crystallizing diorites were not the sources of most of the xenolith material.

11.6 PETROGENESIS

The range of lithologies in the Strontian mafic diorites is wider than for their host rocks or xenoliths, ranging from ultramafic (hornblende and biotite rich) to hornblende and biotite diorites. Their overall geochemistry may display a linear trend, but individually some of the diorites have distinct compositional fields. This indicates that they are not part of a single fractionating body, but must be regarded as having more than one provenance and having more than one mechanism of evolution eg. fractionating or mixing.

The Sheet has strong evidence of magma mixing with quartz xenocrysts and two different feldspar phenocrysts (xenocrysts). It has a straight line variation in most element plots with MgO, but the SiO_2

range of most of the body is limited. The Uil diorites also plot on a straight line and have quartz xenocrysts, but show a wider SiO_2 range. These two dioritic bodies may well be the result of incomplete hybridization with an alkali granite magam. They will be investigated to consider the relative contributions of fractionation and mixing.

The stepped trends can be considered as either being a result of a change in the number of cumulate phases or a change in the mechanism from fractionation to contamination or mixing. The Rubh diorite trends separately from the other diorite plots. This body favours the crystallization and accumulation of mafics first and then mafics and plagioclase (Fig.11.38 MgO vs SiO_2).

The very mafic diorites with MgO >8% eg.Rubh and Uil cores, also have high Cr and Ni contents a feature often associated with cumulates. High Cr, Ni and Mg in lavas in the region has been suggested by Thirlwall (1982) to represent magmas derived from a primitive source region. General geological and geochemical studies by Thirlwall (1979) suggest that the calc-alkaline Lorne lava series are closely related to late Caledonian plutonic complexes. Many of the lavas are basaltic andesites, exhibiting primitive chemistry and possibly representing mantle derived magmas, which have undergone <20% fractional crystallization (Thirlwall 1982, 1986). Therefore these lavas could be considered as parental liquids for the Strontian diorites, with accumulation of mafic minerals taking place to produce the observed rocks.

The diorites are mostly coarse grained and chilling is limited, thoroughly queched rocks are absent, so the recognition of parent

magma compositions is difficult if the rocks requier both crystal accumulation and fractionated liquids. The few finer grained rocks at Rubha and Ranachan were difficult to sample and have not been analyzed.

11.6.1 Major element modelling

Silica was chosen as the abscissa so that straight comparison could be made between the xenoliths and granite host. Major element modelling involves observed mineral assemblages plotted together with bulk rock data (Figs.11.34 to 11.41).

Figs. 11.34 (Al_2O_3), 11.35 (CaO), 11.36 (FeO*), 11.37 (K_2O), 11.38 (MgO) and 11.39 (Na_2O) the crystal extract composition falls within the triangle (marked X-X on the figures) with a maximum SiO_2 range of 40 to 47%. This compositional range takes into account not only a liquid parent but a liquid with cumulate components. Each figure shows that an initial mineral assemblage containing biotite, amphibole and pyroxene would produce the gross diorite trend. For serial oxides MgO, Na_2O, TiO_2, FeO* and CaO an amphibole dominated crystal assemblage would suffice to generate the diorite trend, but it cannot explain Al_2O_3. All other crystal assemblages contain biotite in addition to pyroxene. However biotite is not a common phenocryst phase in basic rocks, though it does occur in lamprophyres. At 55% SiO_2 the trend would require plagioclase to crystallize together with biotite and amphibole/pyroxene. Figs 11.34A to 11.39A discriminate between the individual bodies while the minerals are grouped together, allowing some points to be made body by body.

On Fig.11.34 (Al_2O_3) the high silica Sheet sample could well be used as an end member for contamination purposes of the Sheet trend, as it plots very close to the BGT field. The pyroxene mineral field plots in such a way above the Sheet field that it is possibly a very strong influence on the Sheet evolution.

The Sheet has a porphyritic texture with mafic spots representing a 'phenocryst' phase. Thus rocks are likely to represent quenched liquid compositions. Discounting the acid component of the multiplre intrusion, it shows considerable MgO variation but limited SiO_2 variation. For Al_2O_3 vs SiO_2 and MgO vs SiO_2 the Sheet rocks show a linear trend away from pyroxene compositions suggesting that much of the variation reflects pyroxene extraction. MgO vs FeO* ratios change (Fig.11.4) showing iron enrichment with decreasing MgO, a feature consistent with fractional crystallization. Contamination woth a granite component would spread the data at a high angle to a fractional crystallization trend. The limited extent of this suggests that the component of granite was small and uniform in each sample and it was mixed with already differentiated mafic liquids.

The Uil bodies have no chilled textures therefore it is no guarantee that the rocks are liquids for the MgO-rich compositions.

The Rubha body is coarse and petrographically points to pyroxene accumulation and intercumulus crystallization of feldspar + biotite. There is no evidence of contamination or hybridization. Total MgO >9% is unusual for magmas where cumulates are a possibility. CaO vs MgO (Fig.11.6) shows a positive correlation as expected if cpx or hornblende accumulates. Plots against SiO_2 do not place the analyses in the same order as MgO based plots and so interpretation is more

FIGURE 11.34 Al2O3 vs SiO2

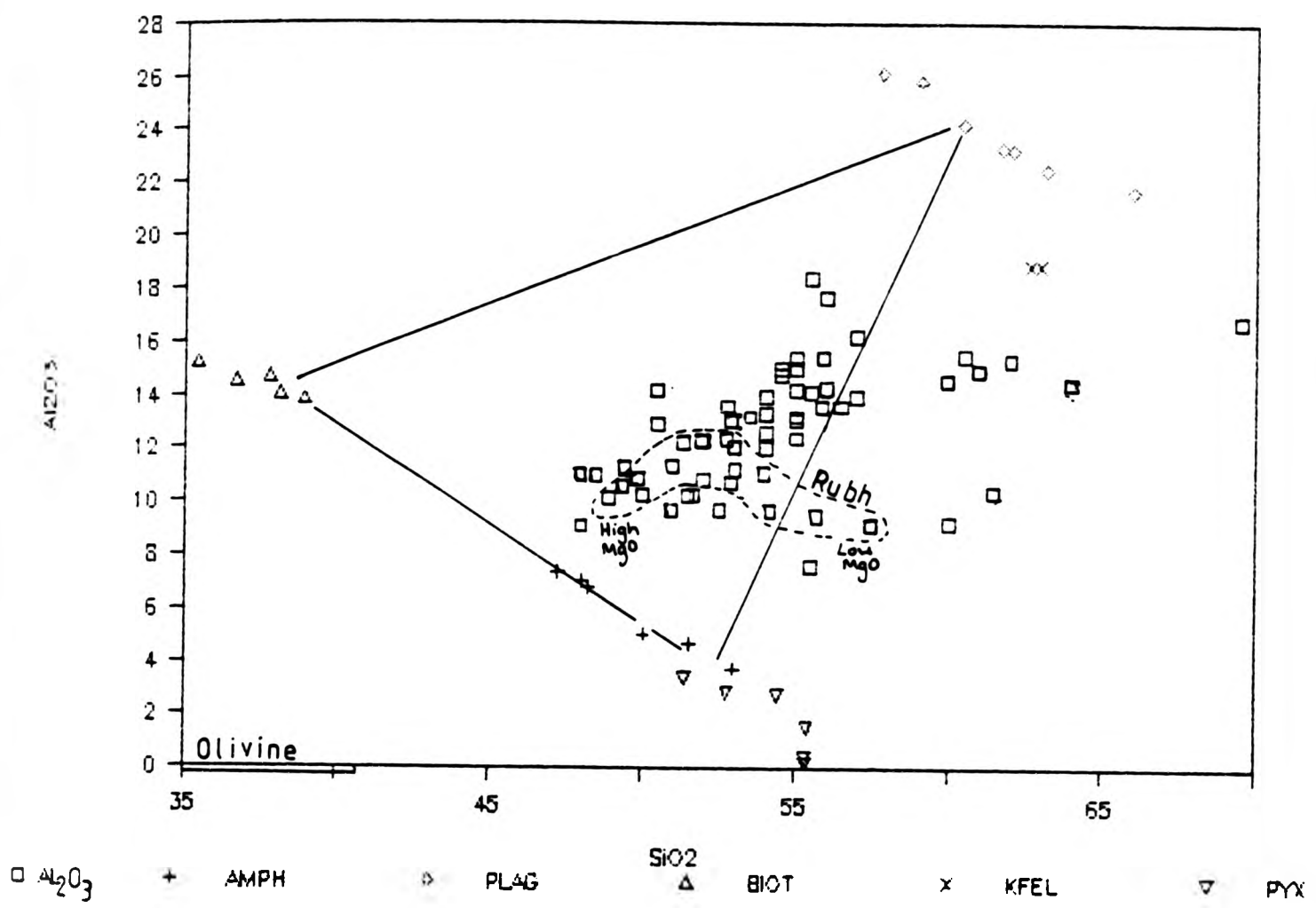

FIGURE 11.35 CaO vs SiO2

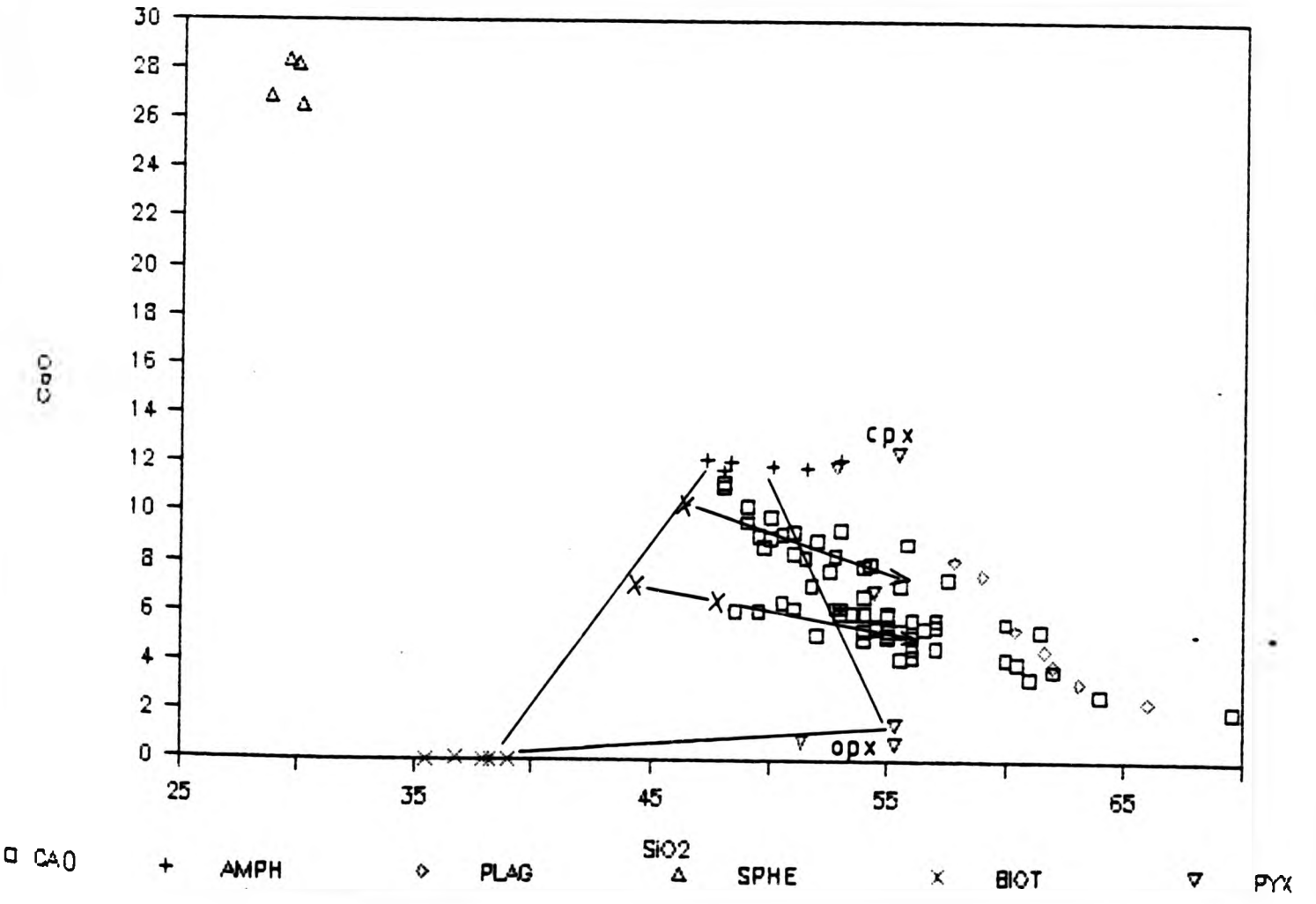

FIGURE 11.34A Al2O3 vs. SiO2

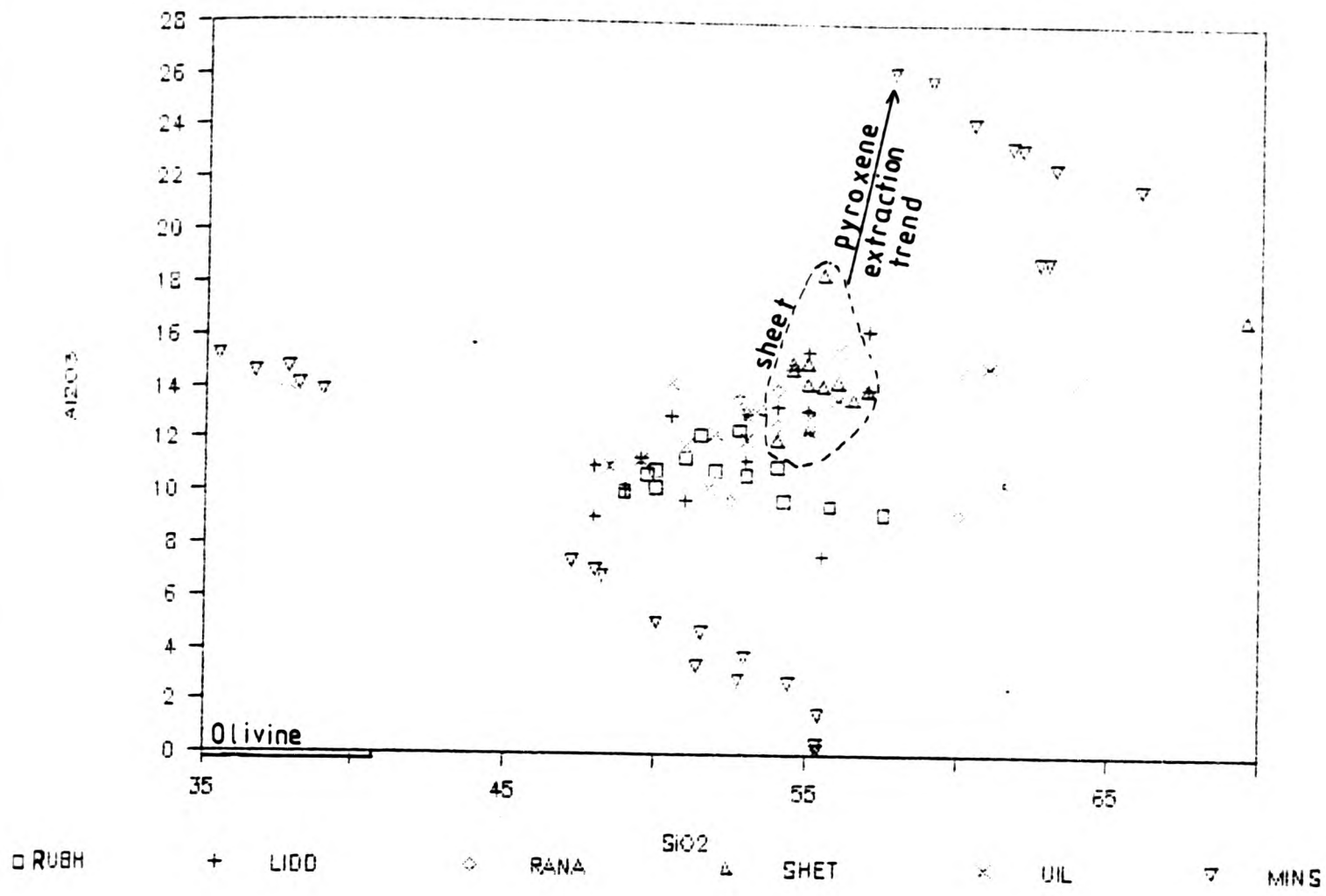

FIGURE 11.35A CaO vs SiO2

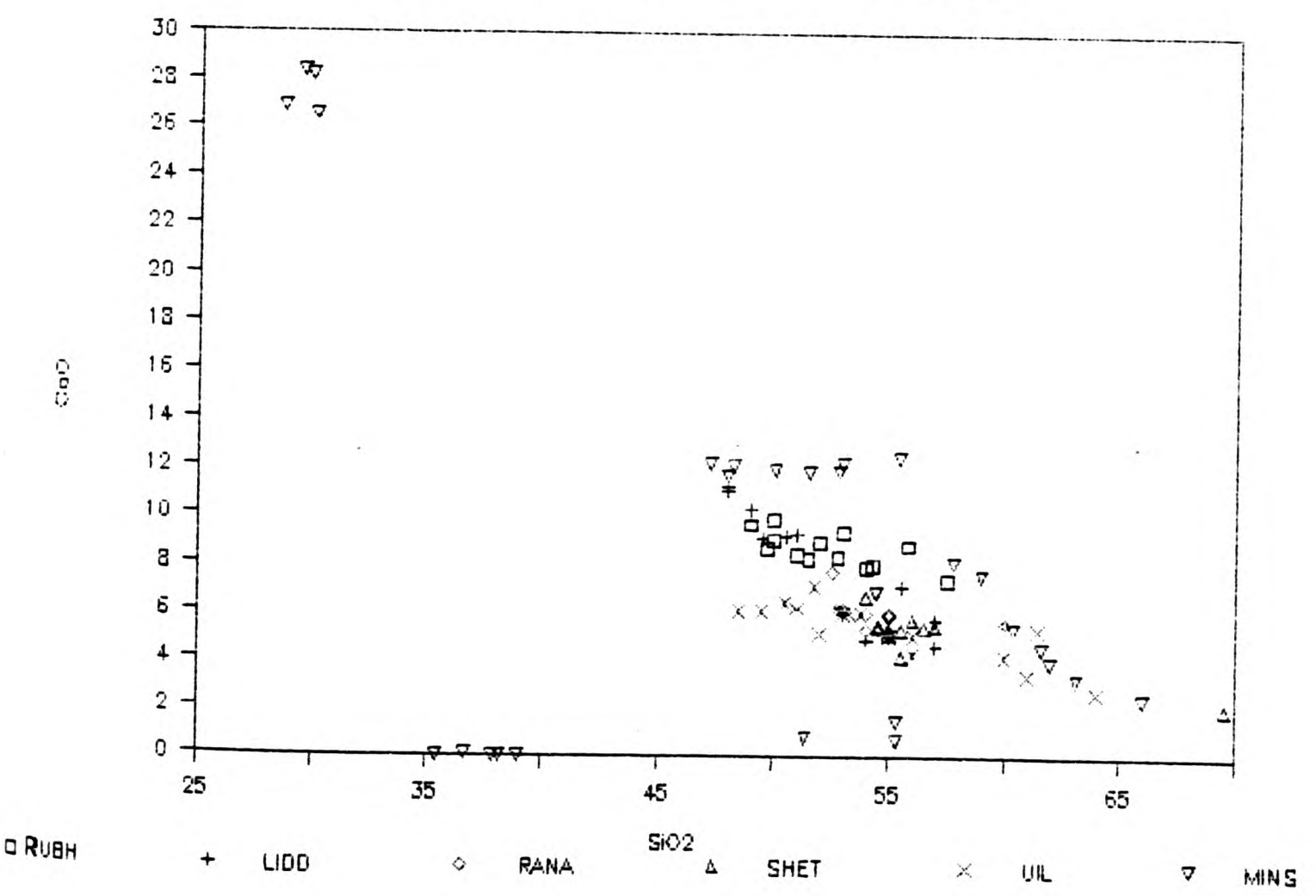

difficult than for Sheet or Uil. CaO vs SiO_2 (Fig.11.35) shows that a significant addition of biotite or hornblende is required to achieve the correct range of SiO_2, if most rocks are cumulates. Pyroxenes all have SiO_2 contents corresponding to the SiO_2-rich end of the Rubh variation trend, so are themselves incapable of generating the trend.

Fig.11.35 displays two well defined trends with the upper one being composed of the Rubh and Lidd diorites and the lower being the remainder (refer to Fig.11.6A). Simple fractional crystallization is not appropriate for some of the Strontian diorites as some are contaminated ie. the lower trend; while the upper line of Rubh and Lidd are those likely to be the result of fractionation and/or accumulation.

Fig.11.40 where P_2O_5 is plotted shows that only a small amount of apatite crystallization would generate the trend, as it is the main phosphorus bearing phase.

As with the xenolith major element modelling Figs. 7.38 to 7.43, adding olivine as an extracting phase provides a better understanding of the diorite body and mineral trends. In Figs. 11.34 (Al_2O_3), 11.36(FeO*), 11.37 (K_2O), 11.38 (MgO) and 11.39 (Na_2O) olivine as an early crystallizing phase can move the extract path through the gross trend with ease. On a number of plots this would otherwise have only been produced by a very substantial amount of biotite.

FIGURE 11.36 FeO vs SiO2

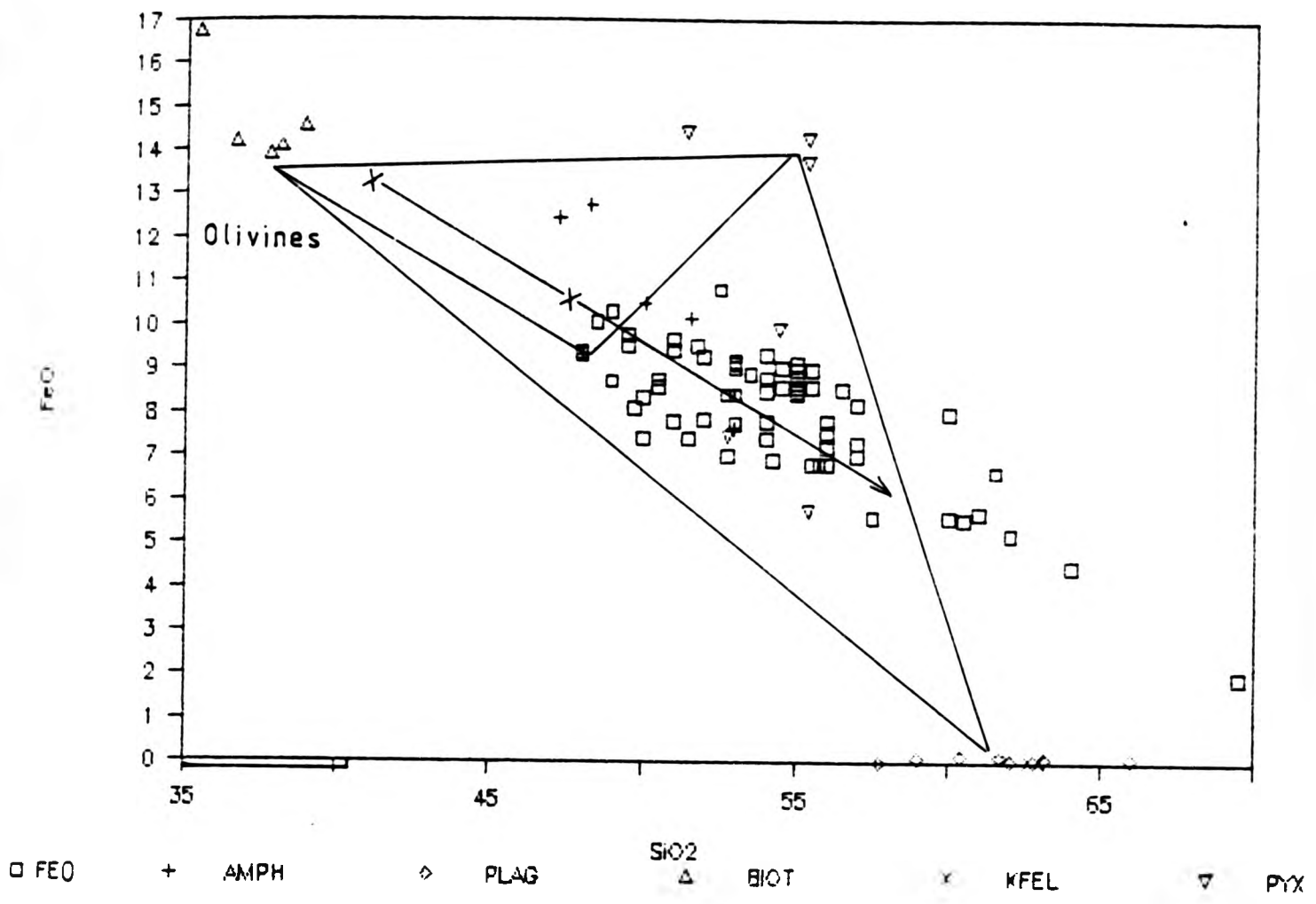

FIGURE 11.37 K2O vs SiO2

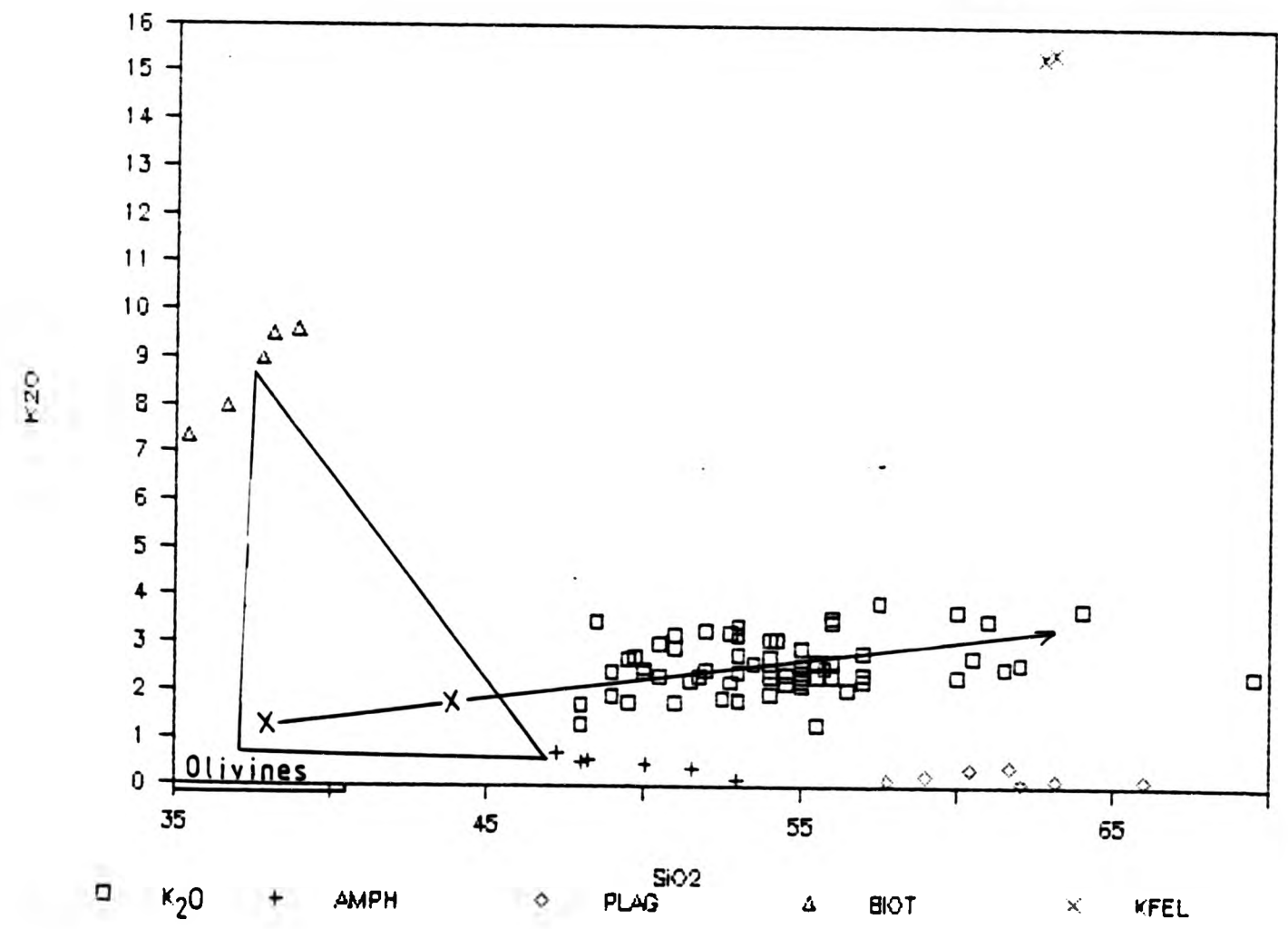

Table 11.36A FeO vs SiO2

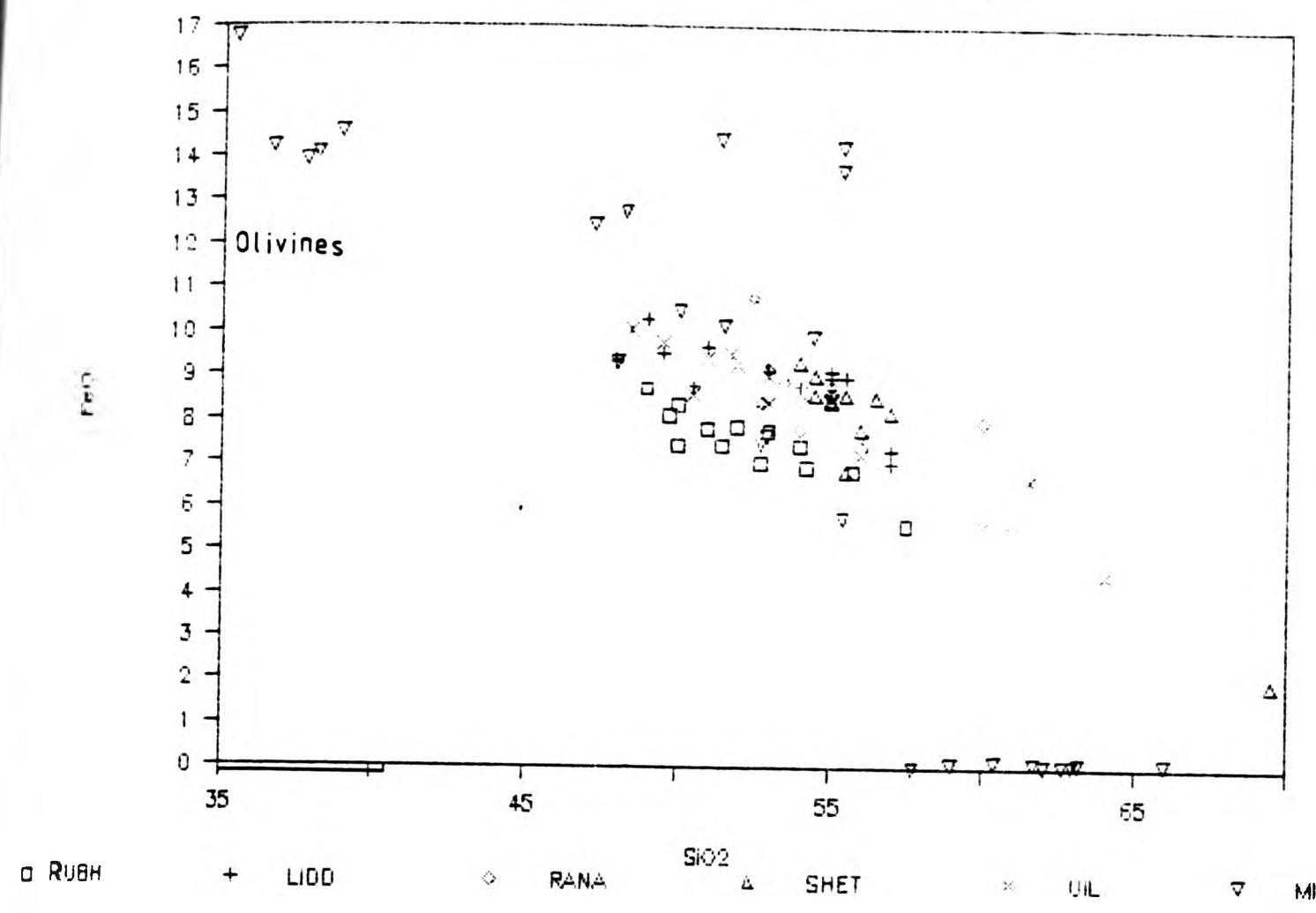

Table 11.37A K2O vs SiO2

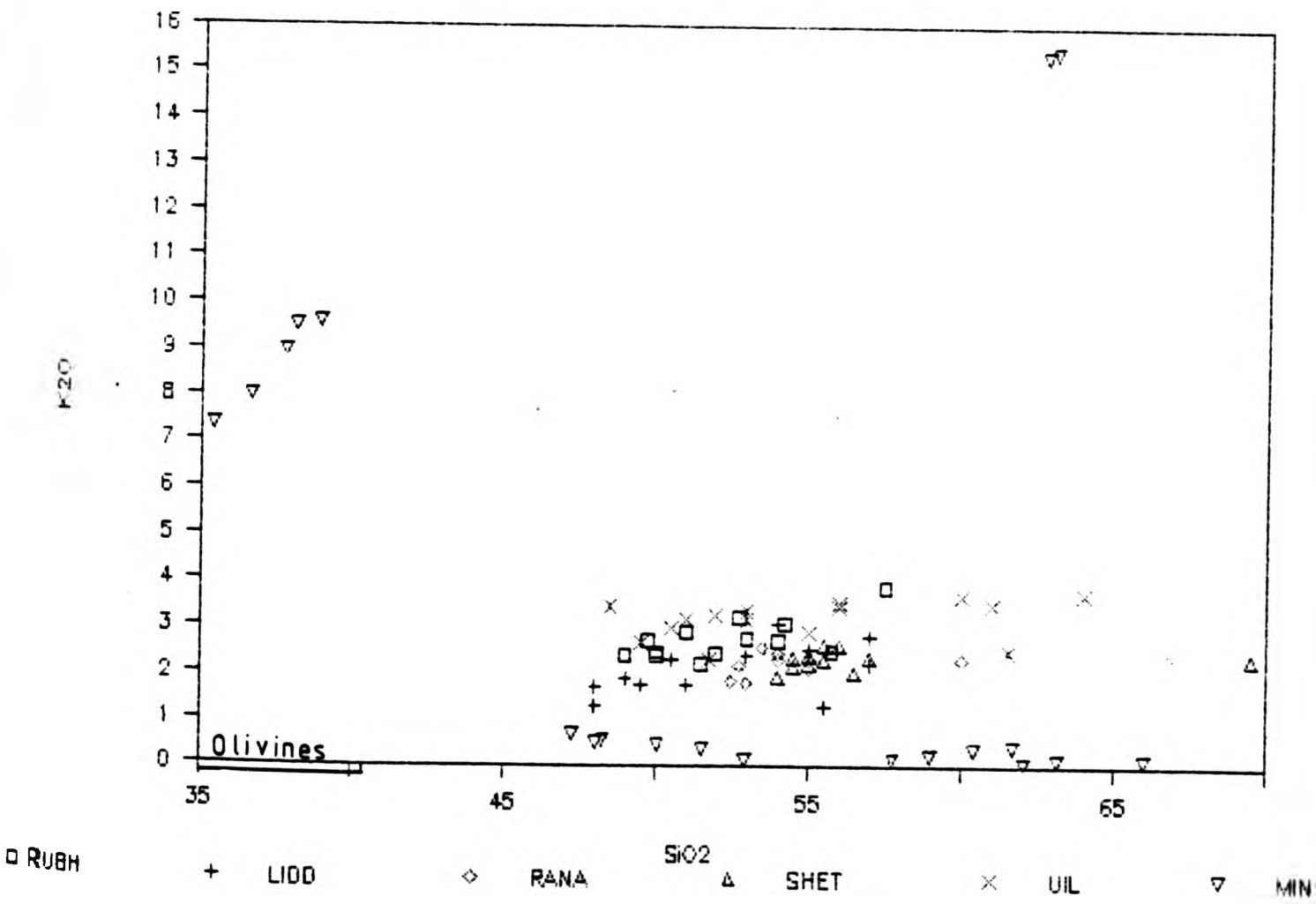

FIGURE 11.38 MgO vs SiO2

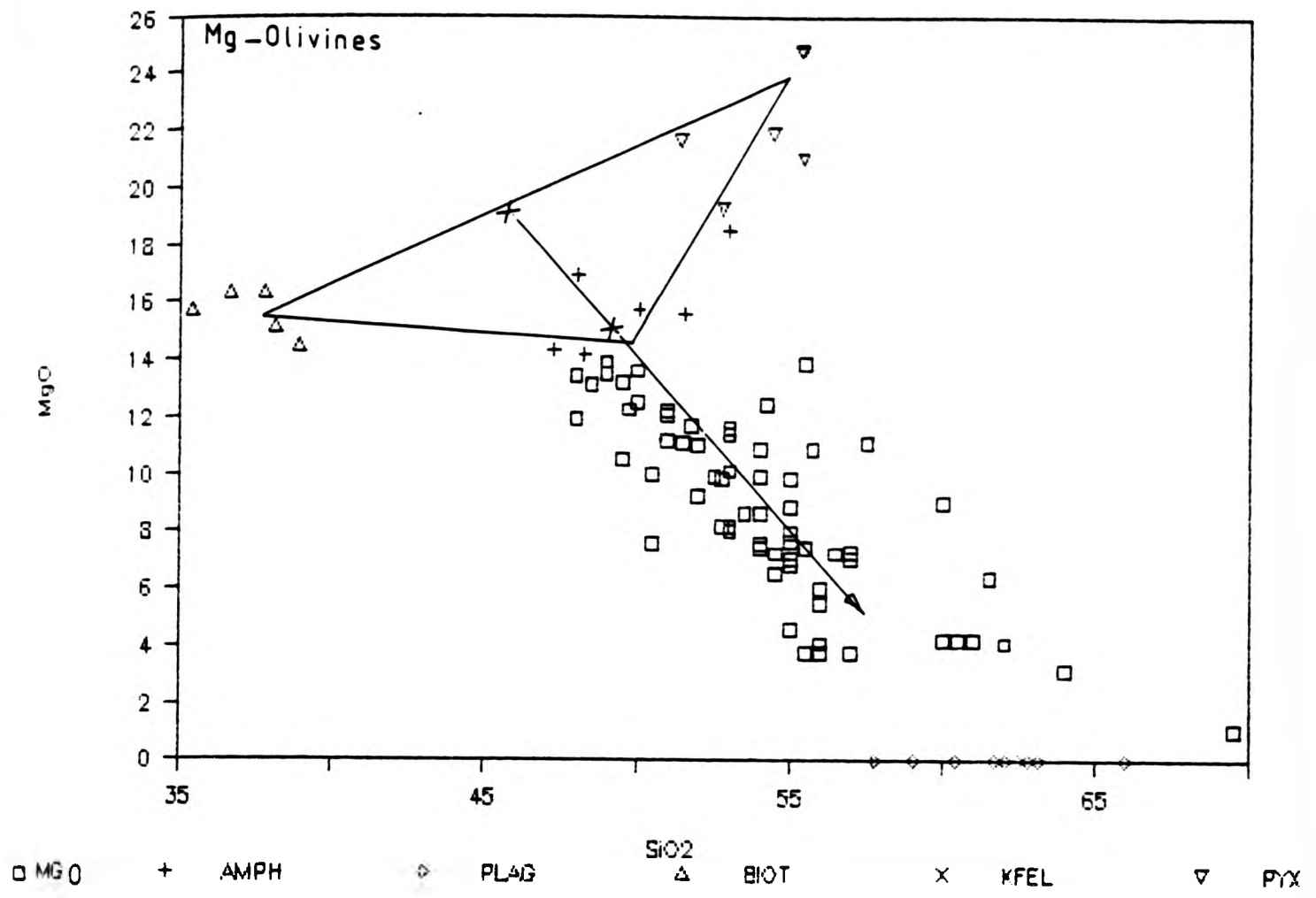

FIGURE 11.39 Na2O vs SiO2

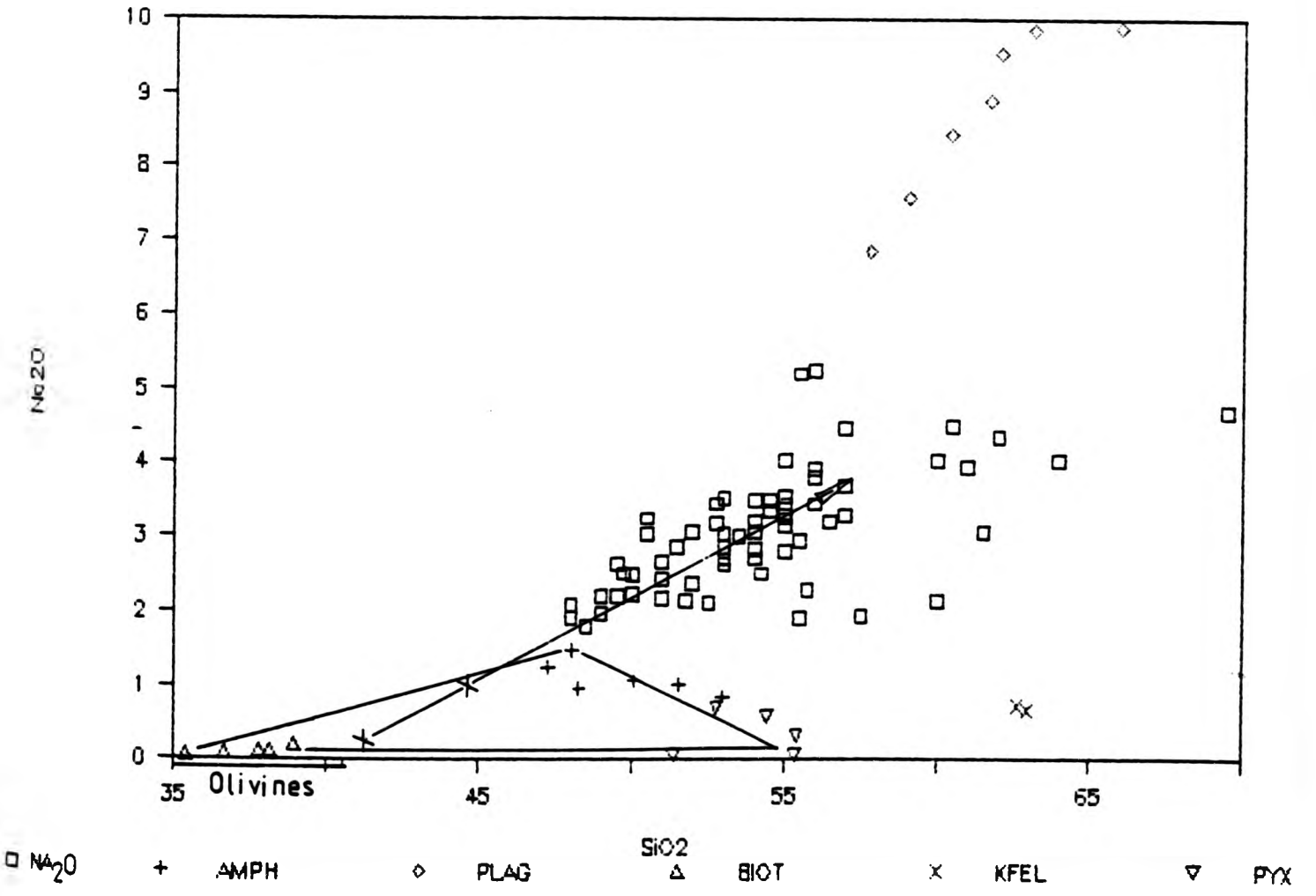

Table 11.38A MgO vs SiO2

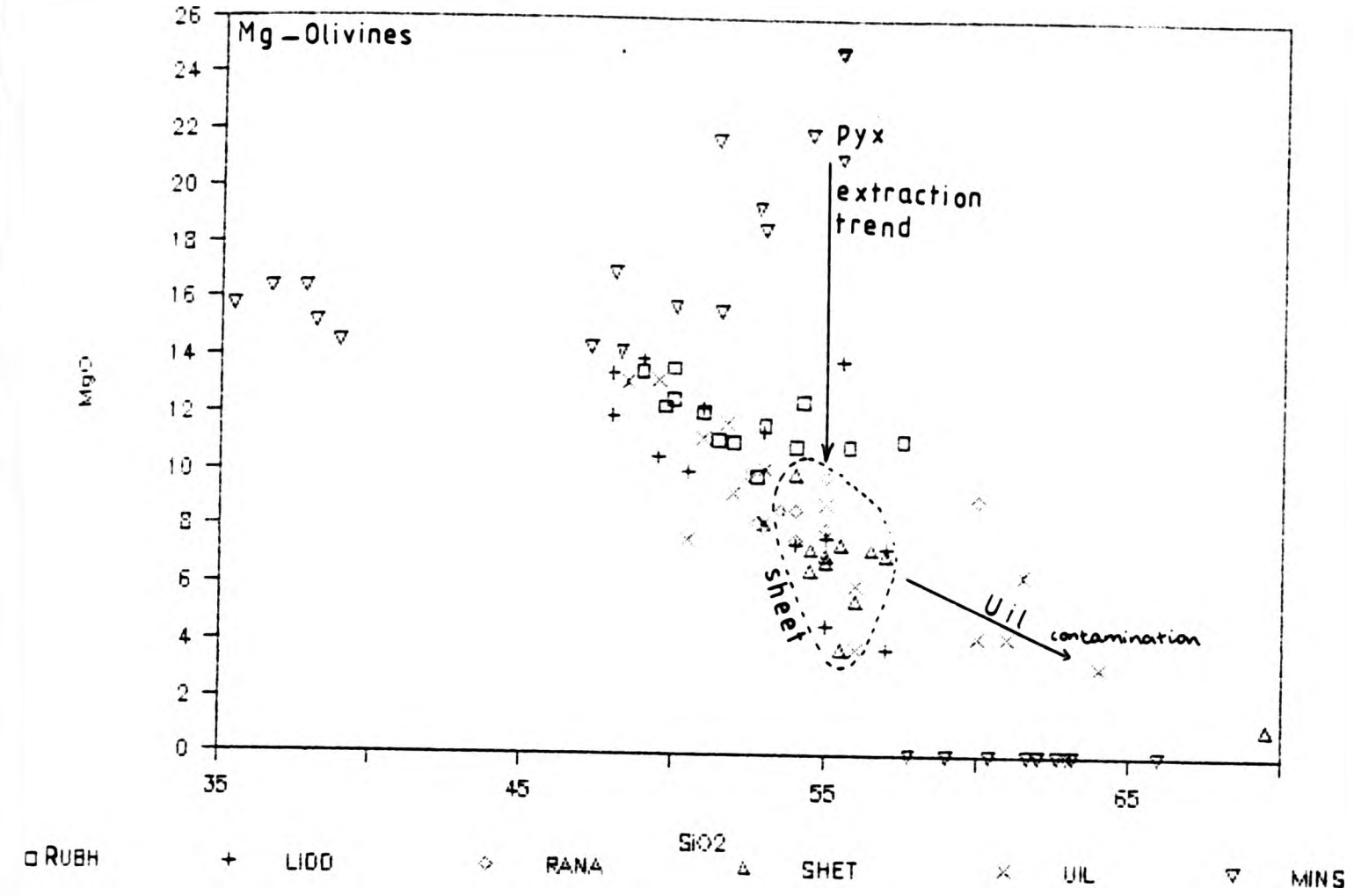

Table 11.39A Na2O vs SiO2

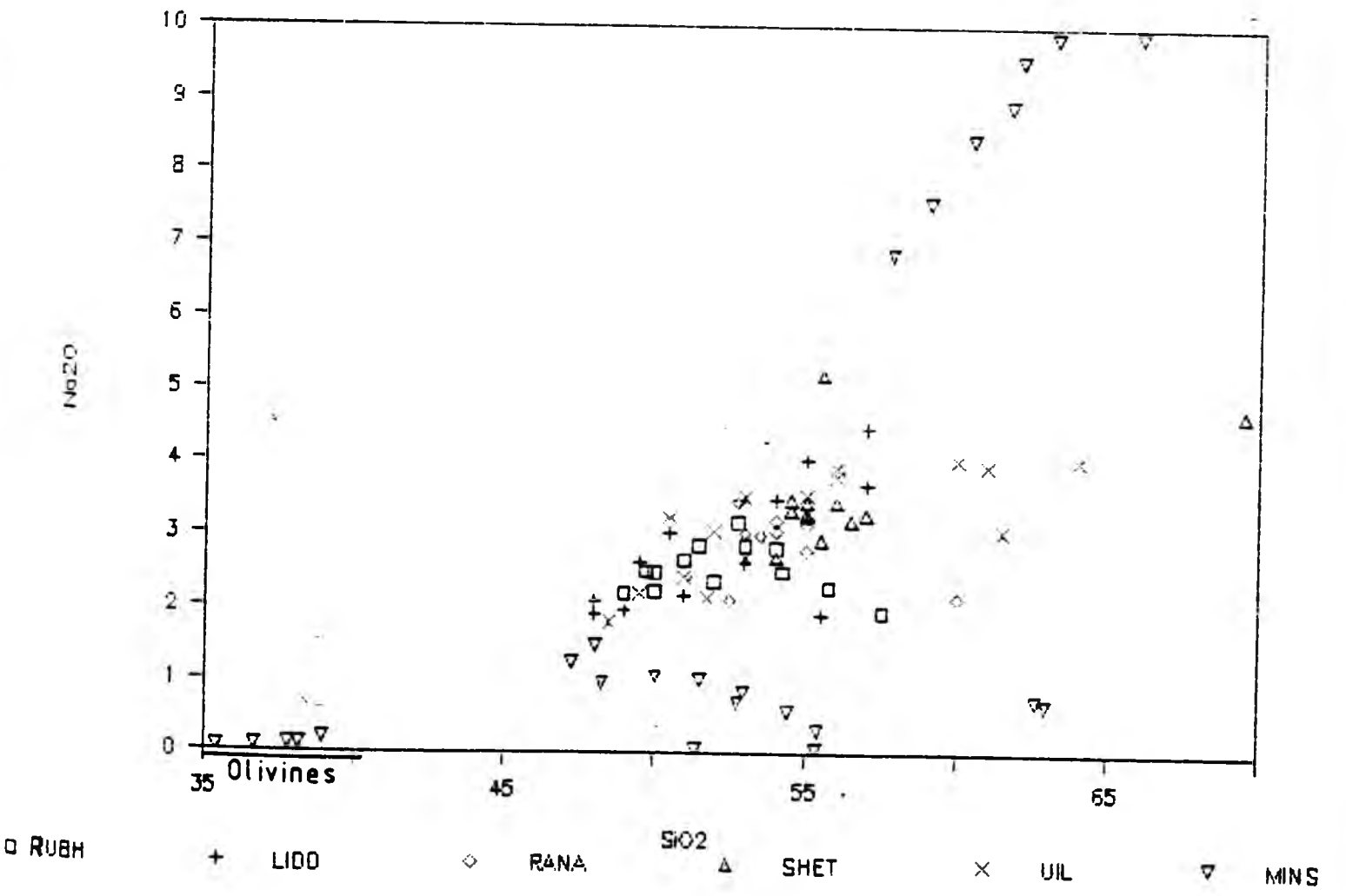

FIGURE 11.40 P205 vs SiO2

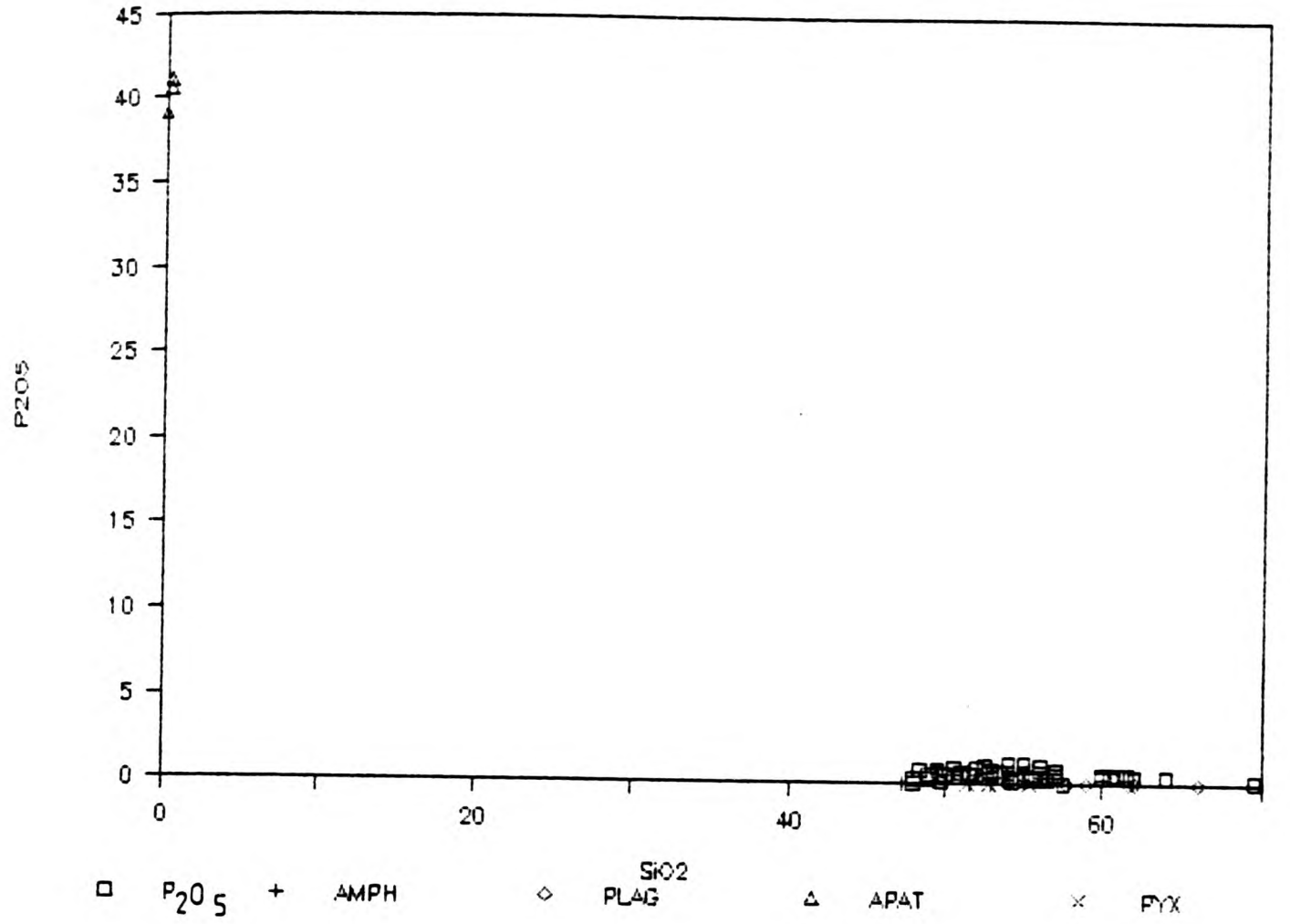

FIGURE 11.41 TiO2 vs SiO2

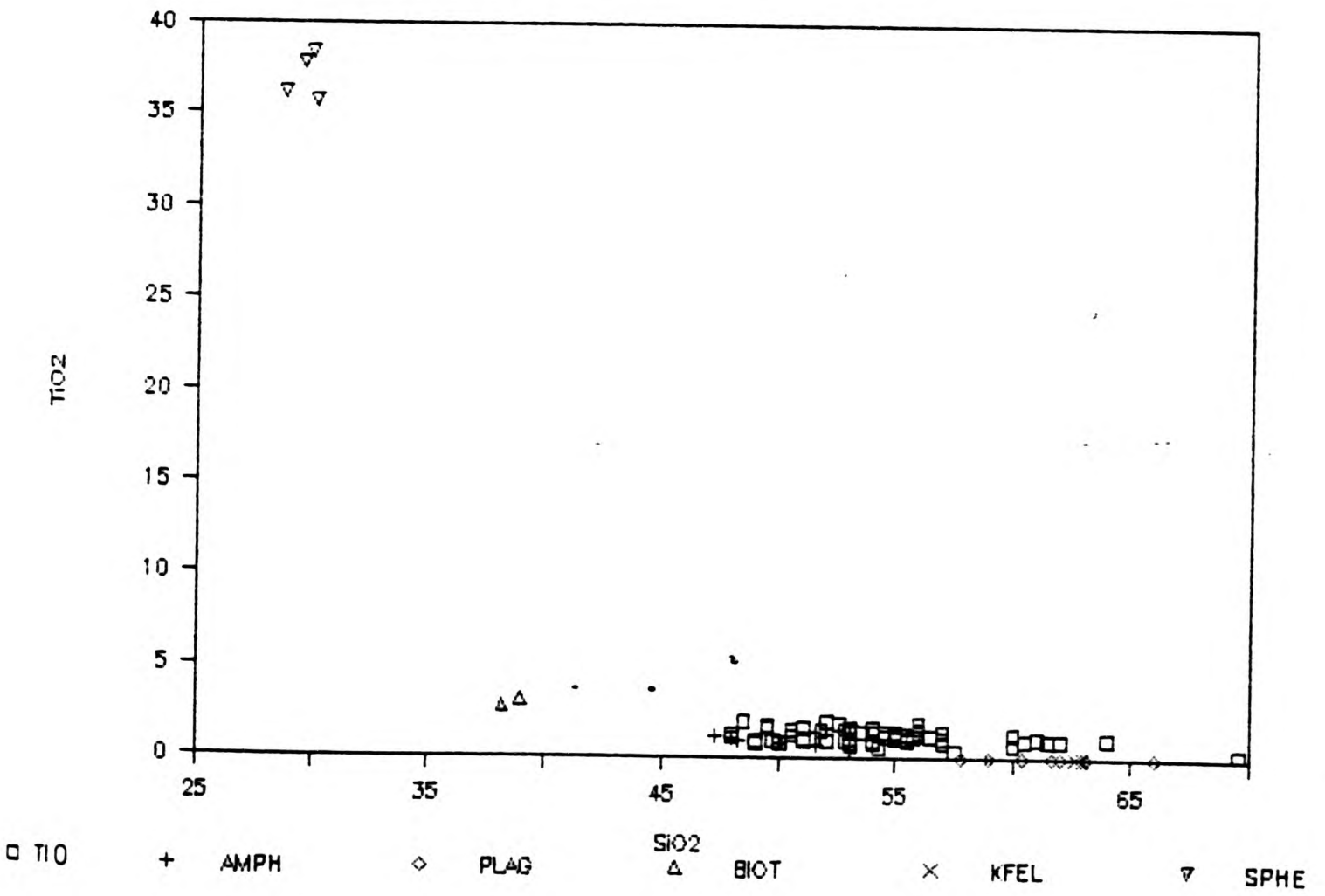

FIGURE 11.40A P2O5 vs SiO2

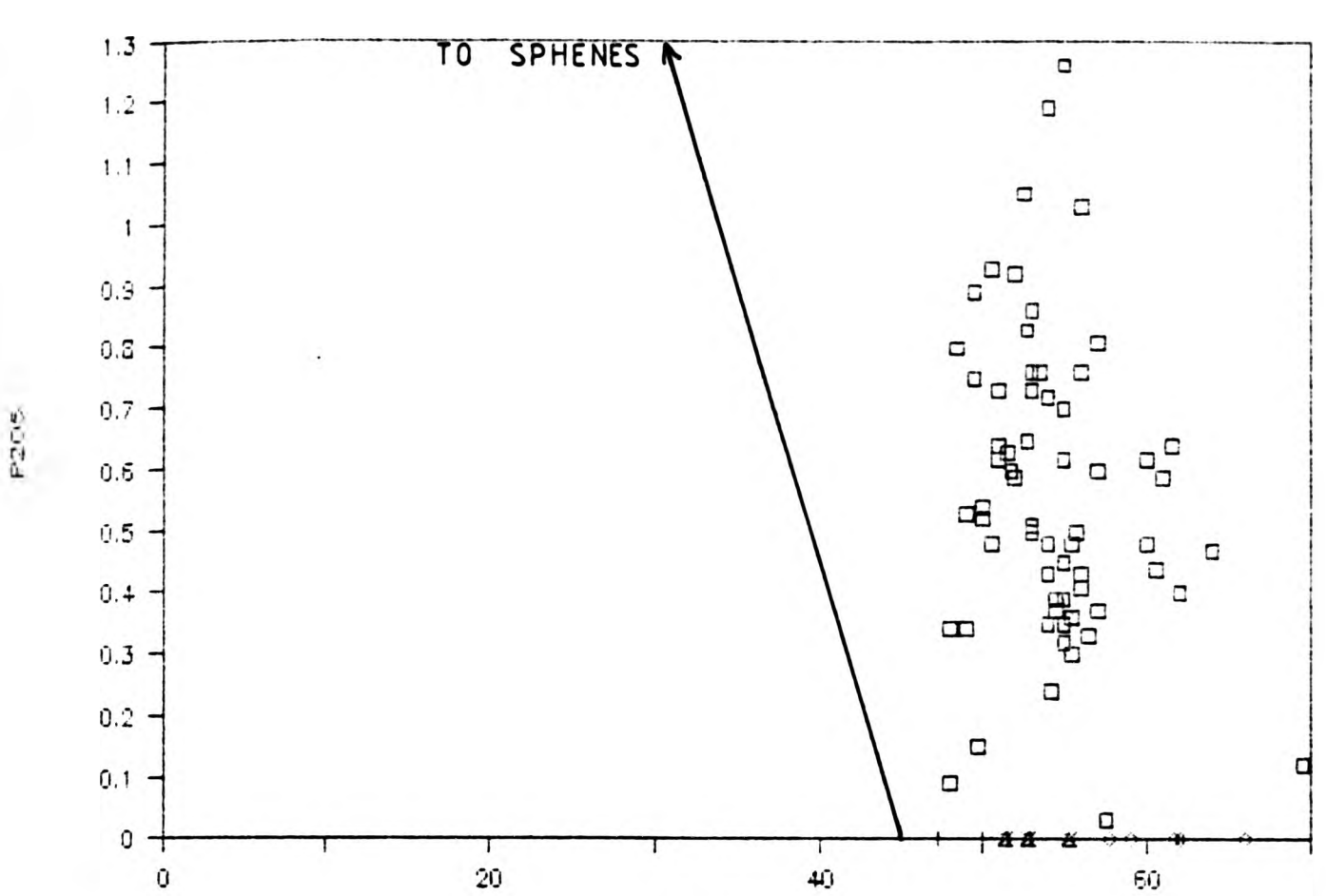

FIGURE 11.41A TiO2 vs SiO2

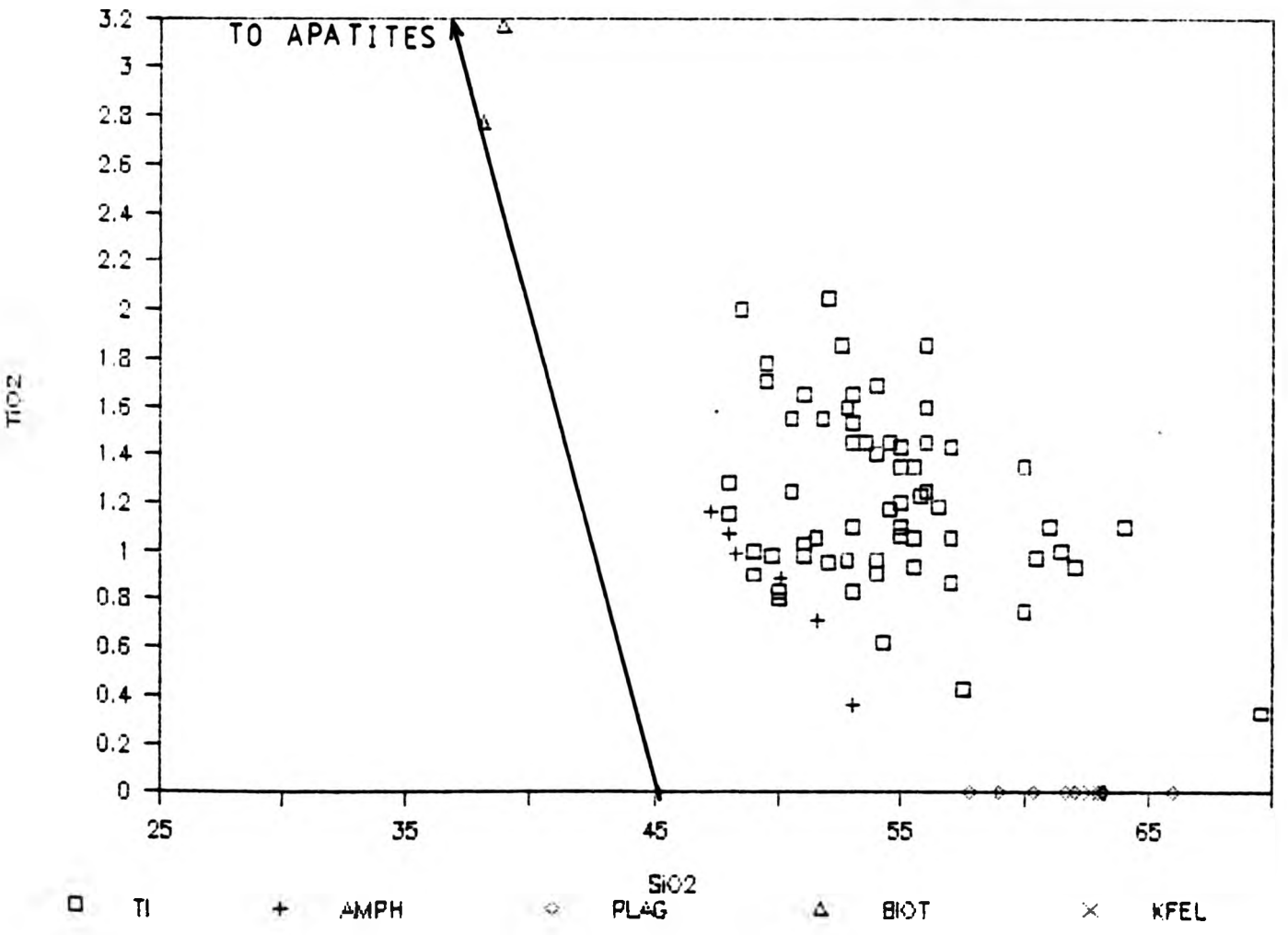

TABLE 11.1 SAMPLES AND MINERALS USED IN IGPET

SAMPLES				MINERALS	
Rubha					
D1	52%	SiO_2		A-hbl	2C...D1
D4	57%	SiO_2		Olig	5R...D2
D6	52.75	SiO_2		Ande	2R...D41
D8	49%	SiO_2		Labr	2C...D19
				Biot	5 ...D11
Sheet				Aug	1 ...D11
D20	54%	SiO_2		Opx	3 ...D11
D24	55%	SiO_2		Sph	5 ...D63
D32	56%	SiO_2		Orth	5 ...D63
D44	69.5%	SiO_2		Apat	1 ...D11
Uileann					
D57	51%	SiO_2	Core		
D69	49.5%	SiO_2	Core		
D58A	64%	SiO_2	Mix		
D70	56%	SiO_2	Mix		

SG48, SG68, G24 & SGXI for contamination

The acidic components used in IGPET allow successful results for hybridizing the Uileann diorites (Tables 11.1 & 11.2), though the residuals are not ideally low. The acidic members used for the mixing range from G24 (65% SiO_2) to SG68 (74% SiO_2). In fact the lower silica samples of G24, SGXI and SGXXVI worked better giving lower residuals than the BGT samples. This suggests that indeed the Uil diorites are mixed with a similarly acidic component at depth. While the Sheet mixing problem is not so easily resolved using the BGT samples (nos. 11 & 12, Table 11.2).

TABLE 11.2 MIXING THE DIORITES USING IGPET

	Parent 1		Parent 2	Hybrid	P1	P2	Residuals
1	SGXI	+	D69	D70	76.1	23.9	1.703
2	G24	+	D69	D70	57.9	42.1	5.456
3	G24	+	D57	D70	49.8	50.2	3.237
4	SG48	+	D57	D70	37.1	62.9	4.263
5	SG68	+	D57	D70	34.6	65.4	5.189
6	SG68	+	D69	D70	41.9	58.1	8.981
7	SGXXVI	+	D57	D70	40.7	59.3	3.625
8	SG48	+	D57	D58A	71.2	28.8	1.352
9	SG68	+	D69	D57	9.6	90.4	1.579
10	SG68	+	D69	D58A	74.8	25.2	2.198
11	SG48	+	D24	D44	90.6	9.4	2.618
12	SG68	+	D20	D44	87.7	12.3	5.365

A number of important points emerged using the fractional crystallization model of IGPET, taking Rubhs as an example (Nos 1 to 12 Table 11.3). It appeared that solutions using amphibole worked better than those with opx/cpx. More often than not the opx/cpx component would produce a negative value for plagioclase, which is equivalent to assimilation of plagioclase. Quite substantial plagioclase assimilation is requiredby some of the models, with occasional pyroxene assimilation also shown in some models. Model numbers 1, 6, 7 & 9 (Table 11.3) require plagioclase assimilation 0f 11 to 77%. This cannot be reversed to give a meaningful answer and so D8 can be regarded as a cumulate. The assimilation of plagioclase in the models may reflect the assimilation of a granodiorite component. TGD is plagioclase-dominated and its hornblende and biotite would be concealed in the calculations in reduced extract values for these phases. The host PGD would also add K-feldspar.The D6 to D4 model(no.11), using an amphibole + biotite + plagioclase assemblage, is one of the "best" results with a low residual and no assimilation. This could therefore be a satisfactory model for the more SiO_2-rich points of Rubha. This assimilation of Na + Ca + Al + Si bearing phases in these models could simply signify the extraction

of a phase completely deficit in these elements eg. olivine. As discussed above for Figs. 11.34 to 11.39, olivine as a crystallizing phase would make a very big difference in the evolutionary path of the diorites.

TABLE 11.3 FRACTIONAL CRYSTALLIZATION OF DIORITES BY IGPET

	1*	2	3*	4*	5*	6*	7*
Parent	D8	D8	D8	D8	D8	D8	D8
Daughter	D1	D1	D1	D1	D1	D1	D6
Plag	-48.8	-	-17.8	100.6	124.4	-28.0	-77.1
Amph	-	83.6	-	-	-	-	-
Biot	36.3	16.4	28.2	2.5	-	21.0	26.1
Pyx	112.4	-	89.6	-3.2	-24.4	107.0	149.9
Sph	-	-	-	-	-	-	1.1
K-fel	-	-	-	-	-	-	-
Apat	-	-	-	-	-	-	-
Daughter	85.1	56.6	77.2	114.6	110.2	72.0	83.3
Residuals	1.478	1.871	1.783	2.906	2.226	2.611	1.89

	8	9*	10	11	12	13	14
Parent	D8	D8	D8	D6	D1	D20	D20
Daughter	D6	D6	D4	D4	D4	D44	D44
Plag	2.3	-11.1	12.0	35.6	23.6	16.5	13.1
Amph	84.5	98.5	74.7	50.5	76.4	62.1	63.3
Biot	13.2	12.6	13.3	14.0	-	21.4	23.6
Pyx	-	-	-	-	-	-	-
Sph	-	-	-	-	-	-	-
K-fel	-	-	-	-	-	-	-
Apat	-	-	-	-	-	-	-
Daughter	39.9	56.2	12.6	28.4	38.4	20.4	25.4
Residuals	1.734	1.660	2.744	2.793	2.362	2.023	1.996

	15	16*	17*	18*	19*	20
Parent	D20	D20	D20	D20	D20	D32
Daughter	D44	D44	D44	D44	D44	D44
Plag	16.2	14.9	21.7	9.0	9.8	28.5
Amph	61.8	61.5	59.2	99.1	101.7	48.6
Biot	21.9	28.0	25.0	21.5	20.6	22.9
Pyx	-	-	-	-29.7	-31.0	-
Sph	-	-	-	-	-1.0	-
K-fel	-	-5.1	-5.8	-	-	-
Apat	-	0.6	-	-	-	-
Daughter	21.6	28.5	21.9	27.3	26.7	37.7
Residuals	1.938	1.781	1.639	0.625	0.532	7.904

* refers to models with either plagioclase or pyroxene assimilation

11.6.2 Trace element modelling

As seen in the host rocks and xenoliths, no one process produced the trends of the mafic diorites. The logarithmic plots Figs.7.40 and 7.42 display quite scattered positive trends, which support the view that fractional crystallization was not the only mechanism. Logarithmic K-Rb plot (Fig.11.42) is more organised. The diorite data in all cases substantially overlaps the granitic data, while the xenolith data is more dispersed and is only partly overlapped by the diorites.

Trace element modelling has been calculated using the partition coefficients in Table 7.4 as for the xenoliths. The mineral vectors are also the same for the Ba vs Rb plot (Fig.7.40) and for the Ba vs Sr plot (Fig.7.42). Crystallization of amphibole, opx, cpx and plagioclase could produce a series of liquids containing increasing amounts of Rb, Ba and Sr. In fact the vectors calculated for the xenoliths show great potential for the diorite trends too. This is seen especially in Fig.7.40 (Ba vs Rb) and Fig.7.42 (Ba vs Sr), where again there is great scatter of the Ba points. In both cases the scatter of the diorite data points is as wide as for the xenoliths. However the xenoliths do plot with substantially lower Ba values than the overall granite-diorite trend. This separation feature has not been seen so clearly in any other plots and suggests that the xenoliths have undergone more than just crystal fractionation. While the diorites are spatially closer to the granite hosts. However in all three rock groups the scatter supports the view that crystal fractionation together with mixing occurred.

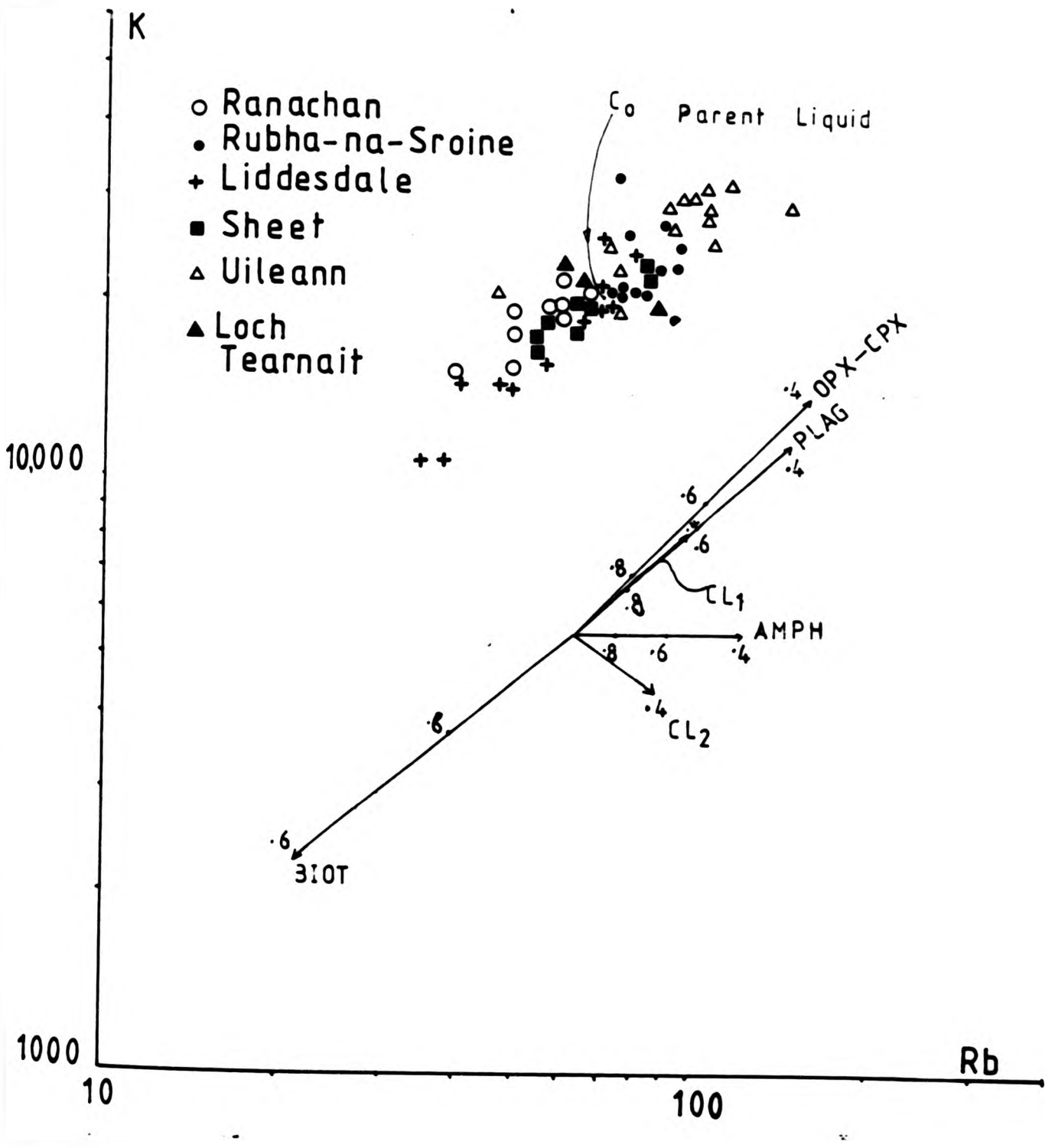

Fig.11·42 Logarithmic plot of K against Rb for the diorites.

Nos. on vectors = residual liquid fraction

The diorites plot (Fig.11.42) in a coherent linear trend of increasing K with increasing Rb, with clear overlapping of the diorite bodies. For single bodies mafic rocks plot at the low K-Rb end of the line, but this relationship does not apply when all the rocks are considered together as mafic Rubh rocks are in the middle of the line. The high K-Rb consists of the net-veined and mixed diorites of Uil. Crystallization of cpx, opx and/or plagioclase from a low K, Rb liquid could produce a series of fractionated liquids along the trend containing increasing amounts of K and Rb. This diagram does not discriminate between the partition coefficient of K-Rb for cpx/or opx as they are the same. The accumulation of crystals of these phases could produce the trend starting from relatively K-Rb rich liquids. The biotite vector is approximately 180 deg. to the pyroxene vectors. Only 20% crystallization of biotite would drive the mafic part of the trend in the opposite direction.

Fig.11.43 plots Ce vs Yb for the diorite bodies. Again there is a trend of decreasing Ce with decreasing Yb, together with a random distribution of SiO_2 levels. The whole trend falls mainly within the granite and xenolith fields. Vectors for the major silicate phases push the trend upwards; while the accessories reverse it. Even garnet could broaden the trend towards Ce. Vector CL1 (using no. 11, from Table 11.3) modelled 35.6% plag, 50.5% amph & 14.0% biot. Unfortunately none of the IGPET fractionation models were successful when using accessories, because of the "assimilation" problem.

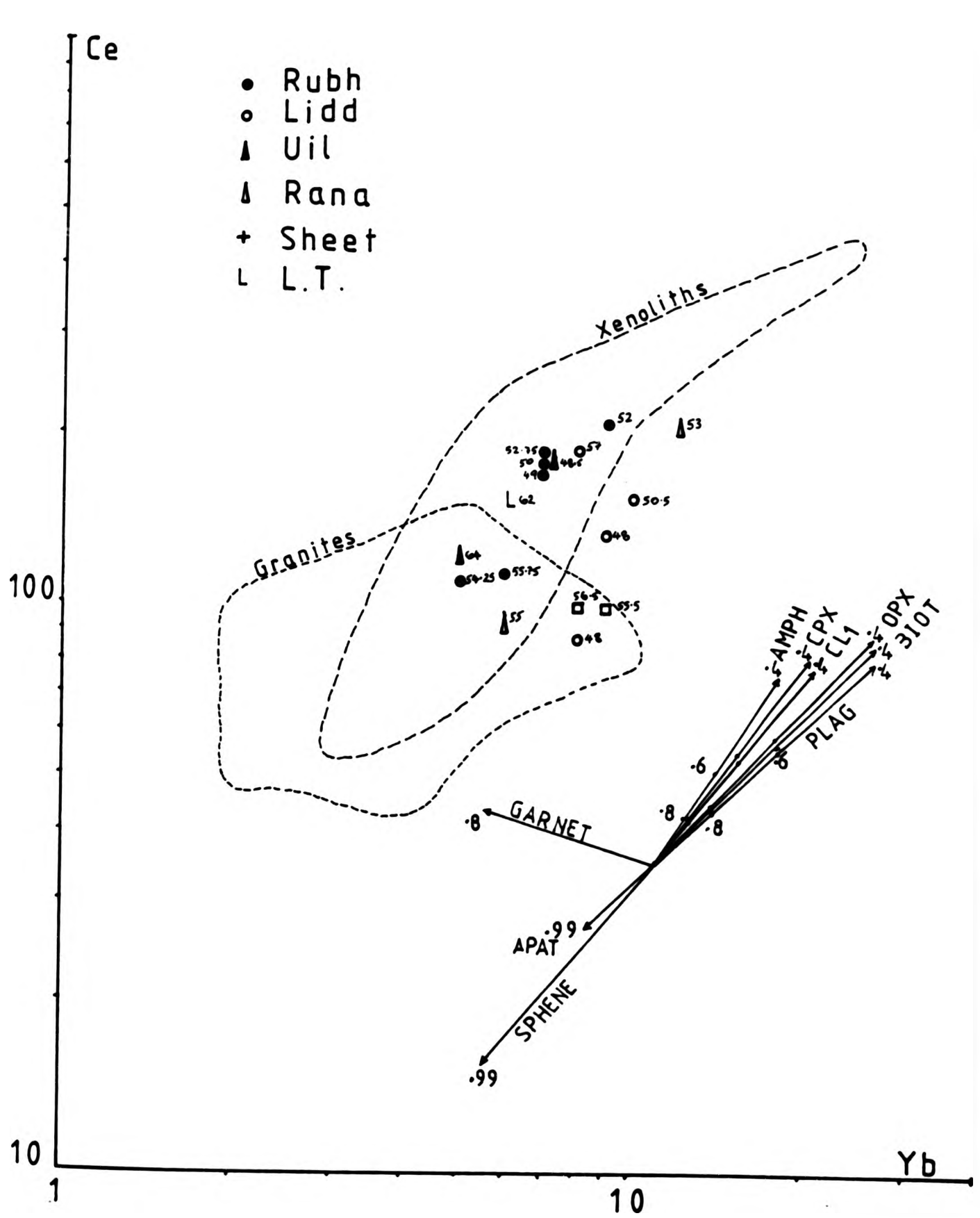

Fig. 11·43 Logarithmic plot of Ce against Yb for the diorites.

Nos. on vectors = residual liquid fraction

48 - SiO_2 values

11.7 DISCUSSION

The diorites display a wide range of petrography and mineralogy, suggesting they are separate individual bodies rather than small parts of a larger body. This is supported by field mapping. Geochemical characters also show the differences between each body, such as the high Li and Rb of the Uil and Rubh diorites. There is no easy way of achieving these compositions, even by very intensive metasomatism and why these diorites in particular. Therefore these diorites must come from more than one basic parent magma source at depth.

The Sheet which has very uniform trends with the greatest MgO variation (refer to Figs. 11.1 to 11.32), also displays evidence of mixing, whose characteristics could not have been gained from the surrounding host. Therefore the mixing took place before emplacement. The effect of mixing is noted in the Uil diorite. Both Uil and the Sheet have quartz xenocrysts. There is evidence of K-feldspars on earlier plagioclases, plagioclase with mottled/spongy cores (supporting the view of unstable conditions and/or recrystallization) and the presence of a variety of feldspars with different compositions whether in the groundmass or as phenocrysts. Mixing at depth and a number of different parent sources would allow for the geochemical variation seen in the diorites.

Chapter 12 REVIEW OF PETROGENESIS AND CONCLUSIONS

12.1 INTRODUCTION

The previous chapters have demonstrated the diverse suite of lithologies present in the Strontian Complex from the mafic diorites through the xenoliths to the host granodiorites and biotite granite. They display characteristics typical of calc-alkaline intrusive complexes found around the world such as: Garabal-Hill (Nockolds 1940); Uusikaupunki-Kalanti, SW Finland (Arth et al 1978); Tuolumne Intrusive series (Bateman & Chappell 1979); Cortlandt complex, USA (Bender et al 1982); Red Lake & Eagle Peak plutons, USA (Noyes et al 1983) and Wooley Creek Batholith, USA (Barnes 1983).

A number of hypotheses have been put forward for the origin and evolution of granitic rocks such as Strontian Complex, including fractional crystallization, mixing (hybridization), unmixing of partial melts from restite and possibly filter pressing and these will be reviewed in a later section.

The rocks of Strontian show an overall lack of hydrothermal alteration, however recrystallization of ferromagnesian minerals indicates some high temperature but subsolidus alteration. Some of the magmatic mineralogy is preserved and this provided an opportunity for a detailed geochemical study of this large, relatively well exposed complex.

12.2 SUMMARY OF ROCK TYPES AND FIELD DATA

12.2.1 The Host Rocks of the Strontian xenoliths

The TGD, PGD and biotite granite are part of a multiple intrusive event. Both granodiorite units show a range of SiO2 and other elements (Ba, Rb, etc) that have no clear geographical pattern. This indicates considerable heterogeneity within the pluton, but analyzed samples are not close enough to identify the size of the domains. The rare local layering in the granodiorite (Fig.2.1A & B) indicates local sharp boundaries existed between effectively solid and effectively liquid materials, that some crystal fractionation can have taken place, but this would not necessarily influence the entire geochemistry of the pluton. The lack of a sharp contact between the tonalitic and porphyritic granodiorites (Chapter 2) suggests that the magma was continuously present in the pluton. Rare examples of baking or fining in grain size between the two granodiorite facies were noted by Sabine (1963). Therefore a completely non-intrusive relationship between the 2 granodiorites should not be disregarded as granitic complexes can possess both. It is inferred that the inner PGD crystallized after the outer TGD.

The biotite granite, in contrast, has sharp, steep, nearly vertical contacts with the earlier granodiorites. There are no signs of chilling between the granite and granodiorites or any interdigitating. Only on the traverse from the most southerly point of the complex, at Rudha-na-Ridire (Fig.1.2), northwards towards Loch Tearnait, are inclusions of Moine seen. Unlike the granodiorite, the BGT does show some geographical pattern to the SiO_2 (Fig.4.1A & B). The silica increases eastwards towards Glensanda and Eignaig,

indicating a fractionating body.

The later features of the Strontian complex include the ctG sheets, aplites and pegmatites. The ctG sheets also have sharp, non-chilled margins (Plate 2.9A, 2.9B & 2.10) with the surrounding granodiorite. The aplites and pegmatites are not particularly abundant in the complex and are only found in the granodiorite pluton.

12.2.2 The Xenoliths

The dioritic xenoliths of Strontian are an example of a phenomenon found in other granitoid complexes around the world eg. Australia - White & Chappell (1977), Chappell (1978), Flood & Vernon (1979) and Bailey (1984); USA - Bateman et al (1963, 1970, 1978, 1979) Dodge et al (1968, 1969), Noyes et al (1983) and in France - Didier (1973).

There are several interpretations for their origins:

- The xenoliths being the result of fragments detached from pre-granite diorites ie. accidental xenoliths from earlier minor intrusions in the psammites. The observed microdiorites and appinites outside the complex are sheets and dykes with a variably developed foliation. A single Moine xenolith was found with a pre-granite foliated microdiorite, this showed that pre-granite microdiorite retains its fabric in the granite. There is also a limited percentage of Moine xenoliths, showing little local country rock contribution to the xenolith assemblage. So this is an unlikely model for Strontian xenoliths.

- The xenoliths are fragments of the observed diorite bodies within the granite. Most of the xenoliths are finer grained, and have different mineralogy and bulk chemistry from most present day exposures of the diorite and so cannot be derived from them. However the marginal diorite chill at Rubha is petrographically similar to Type 1A xenoliths, but there are no analyses of this chill for comparison. The Sheet diorite, which is porphyritic with fine to medium grained matrix, is superficially similar to Type 1B & 2. This diorite is seen to be breaking up into xenoliths at its margin. This single body is hardly enough to account for all the Type 1B & 2 microdiorite xenoliths in the complex as the xenolith distribution is far more widespread (Fig.1.3), occurring in all major granitic bodies. Additional sources are therefore required.

- The restite model infers that dark xenoliths represent the mafic residue after partial melting of intermediate or acid parents. Such residues should show extensive recrystallization with textures resulting from protracted annealling. This is not a characteristic of the Strontian xenoliths, which have a dominantly igneous texture with many euhedral and zoned crystals. The occurrence of xenoliths within xenoliths requires that at least the outer layer of the composite body was able to behave as a fluid. Then the outer layer (Type 4) cannot be restite and it becomes likely that similar materials that are free of inner xenoliths must also have been fluid rather than solid restite.

- Magma mingling is another model for xenolith

formation. This involves the incomplete mixing of contemporary magmas, with the quenching of a more basic component in a matrix of a more acid component. The crenulated and chilled margins of some xenoliths are also consistent with mingling and the co-existence of acid and intermediate magmas.

Coarse grained xenoliths, particularly all the appinitic types, that show no marginal variation in grain size and those xenoliths occurring as angular blocks, are however clearly fragments of pre-existing igneous rocks. Some (Type 1B & 2) could result from the break-up of diorites similar to the Sheet body, some (Type 1A, or possibly 5 in view of bulk chemistry) could be derived from chilled margins of Rubha-na-Sroine type diorites. The other diorites dismembered would not produce the rocks seen as xenoliths. Even The appinitic xenoliths (Type 3) cannot be matched, as the xenoliths have elongated prismatic hornblendes, whilst the dioritic appinities have equant prisms of hornblende. There is no visible external or internal source for most of these xenoliths, so they are considered to be derived from the disruption of contemporary magma and synplutonic dykes (Furman & Spera, 1985). The latter accounting for the coarser grained xenoliths, including the appinitic types and xenoliths with angular outlines. The former producing the rounded microdioritic xenoliths.

Occasional diorite xenoliths carry quartz xenocrysts several millimetres across, which have the equant habit of high quartz and mafic reaction rims showing that they are not in equilibrium with the xenoliths. These quartz grains are similar in size and habit to those found in alkali granite magmas and in particular here are similar to those in the porphyritic granodioritic ctG sheets. They

indicate efficient mixing of dioritic and granitic magmas. The new Qz + Or + Ab (end of Chapter 4) data shows that some toanlitic granodiorite could have reached the plag + qz cotectic. Therefore more varied sources are available in addition to the alkali granite. Reversed zoning in some feldspars supports the view of hybridization. The immediate host TGD and PGD mostly crystallize quartz at a late stage and so cannot be the source of such xenocrysts. The xenocrysts refer to an earlier stage of the magmas evolution at depth before the occurrence of mingling. The xenoliths within xenoliths also show that the xenolith diorite material had an extended history of prior emplacement as the enclosed xenoliths are diorites and not masses of observed country rock.

It is recognized from field, petrographical and probe data that the xenoliths are not merely derived from the host granites, but also attribute their origins to a variable degree of mixing of an acidic and basic components at depth. This then leads to the necessity of reviewing the appropriateness of the term "xenolith". Terms such as "autolith" (Pabst 1928); "inclusions" (Grout 1937); "microgranitoid xenolith" (Vernon & Flood 1982) cannot be used (section 1.3, chapter 1). The one term which does appear applicable is "enclave homoegene" (Lacroix 1893) or "cognate inclusion" (Dictionary of Geological Terms 1962), where an igneous rock (xenolith) is contained in another igneous rock (host granite) and which are linked in composition and origin. Therefore it would now seem correct to refer to the xenoliths as cognate inclusions. This does however seem unfortunate to substitute "xenolith", as it is such an economic and more easily applied word than the others and so will be used until the conclusions part of this chapter.

12.2.3 The Diorites

The detailed mapping of the diorites within the Strontian complex have revealed a range of ultramafic to leucocratic diorites, not fully investigated by earlier authors. The diorite petrography in some areas (Rubha) points to a cumulate model that would explain the gross structures within the rocks ie. wall parallel layering, the chemistry of the silicate phases and the bulk geochemistry. Other diorites show evidence of contamination with alkali granite in the form of xenocrysts. Bulk rock geochemistry suggests that diorites are derived from distinct low K and high K parents. Field relations point to ambiguous time relations with the host rocks. Chills are seen, but only rarely, at diorite margins. Some diorites include bodies of TGD/PGD (Ranachan & Liddesdale), others are veined by granodiorite and aplites and the Sheet locally breaks into xenoliths in the host rock. These contradictory features can be most readily explained if the diorites were emplaced as stocks or pipes in hot and possibly only partly crystallized granites in a manner similar to the emplacement of the synplutonic dykes (Furman & Spera, 1985). The synplutonic intrusions would provide a heat source, so although initially locally quenching to chill against the granite, they subsequently mobilize the hot granite which can invade the diorite. Disintegrating synplutonic dykes have not been seen, but a few dioritic dykes (Chapter 8) are emplaced in the granodiorite and biotite granite. These microdiorites have sharp chilled contacts with the host, but are foliated and partly retrogressed showing that their emplacement occurred when the host was solid but hot. These are considered to represent the latest in a continuous sequence of emplacements of dioritic material.

The granodiorite patches/inclusions noted in some of the mafic diorite bodies suggest a contemporaneous intrusion of the diorite within the granodiorite. There are no signs of chilling or baking on either rock type and they are unlikely to be the result of large scale mixing as neither the granodiorite or diorite are more mafic or leucocratic respectively as a result.

12.2.4 Conclusions

There is widespread evidence within the complex of magma mixing and so pointing to the co-existence of acid and intermediate magmas at depth. Diorite complexes in the granodiorites and biotite granite have been found to contain high quartz xenocrysts, jacketed by mafics. Similar to xenocrysts are seen in some xenoliths. Porphyritic granitic sheets (ctG) carry quartz with mafic reaction rims and K-feldspar. Some porphyritic granitic sheets with small quartz phenocrysts are spatially associated with some of the diorites eg. the Sheet and, at Location A (Fig.1.2, with microdiorite dykes in composite intrusions). A few microdiorite dykes cutting the complex are found to carry quartz xenocrysts and partly resorbed alkali feldspars. This supports the idea that hybridization, the result of efficient mixing, should be considered an important element in the evolution of xenolith, diorites and granites.

Feldspars with mottled extinction are found in the xenoliths and host rocks. If the mottled component of the mottled areas that is in optical continuity with the late crystallizing rim is removed, these feldspars would have a spongy texture. Such textures are common in xenocrystic feldspars in hybrid volcanic rocks (Anderson, 1976 & Eichelberger 1978) and result from partial resorbtion of phenocrysts

of the acid component of the hybrid. In the plutonic environment where the material cools slowly, these spongy textures are overgrown to reconstitute massive crystals in which the new material is slightly different in An content from the spongy substrate. This mottled plagioclase is considered another indication of magma mixing.

The mechanism of emplacement of the xenoliths, dykes and diorites varies for each rock type. For the xenoliths their emplacement will depend greatly on their origin, whether they are eg. basic segregations of early crystallizing phases (Fershtater & Borodina 1976) or fragments of early formed mafic border rocks of the pluton itself (Bateman et al 1963). The xenoliths are regarded as being hybrid in origin, therefore the length of time and convective velocities involved in the mixing process (of a closed system) would influence the physical features of the xenoliths (Furman & Spera 1985). As the host crystallinity increases so does the apparent viscosity, so the evidence of mixing will be sought out in the distribution of xenoliths, swarms and schlieren. The presence of plagioclase phenocrysts or xenocrysts with resorbed cores in the host granodiorite as well as in the xenoliths, favours a magmatic origin for the plagioclase cores and ferromagnesian inclusions rather than a restite (high-grade metamorphic, Mason 1986). This also follows the mixing model.

The diorites would have been intruded into a partly crystallized granodiorite host, as evidence of granodioritic patches and non-chilled contacts shows. While the microdiorite dykes would have been intruded into a completely crystallized but still hot host.

12.3 REVIEW OF GEOCHEMISTRY AND MINERALOGY

12.3.1 Review of geochemical and tectonic associations

The Strontian late Caledonian complex occurs in the western margins of the Caledonides, approximately 50 kilometres from the Moine Thrust and the outcropping of the Lewisian Craton. Of the other scattered late tectonic intrusive complexes only Ross of Mull, Ratagain and the Loch Borolan group occur nearer the craton. All these late Caledonian complexes post-date the end of the severe deformation and prograde metamorphism, though uplift continued together with late Caledonian compression of O.R.S. sediments in the Midland Valley of Scotland.

Various geochemically broad subdivisions of orogenic volcanic rocks that are related to orogenic settings, have been proposed and a particularly useful major element scheme is the use of K_2O vs SiO_2 (Peccarillo & Taylor). Fig.12.1 shows the modified Peccarillo & Taylor scheme used by Ewart (1982) superimposed on the Strontian data. The bulk of the rocks fall in the High K calc-alkaline assemblage, very few rocks fall in the main calc-alkaline field. A significant number of xenoliths and diorites fall in the shoshonite field, but no granitic rocks enter this region.

High K_2O is characteristic of other late Caledonian plutons eg. Garabal Hill and Ratagain (Fig.12.1, Nockolds 1941, Nicholls 1951) though the Strontian acid rocks are not as potassic as the Ratagain suite. Caledonian lavas are also high K calc-alkaline types, but only the Lorne lava field is reported to include shoshonitic types (Fitton et al 1982). The latter reports a tendency for Caledonian

FIGURE 12.1 K2O vs SiO2

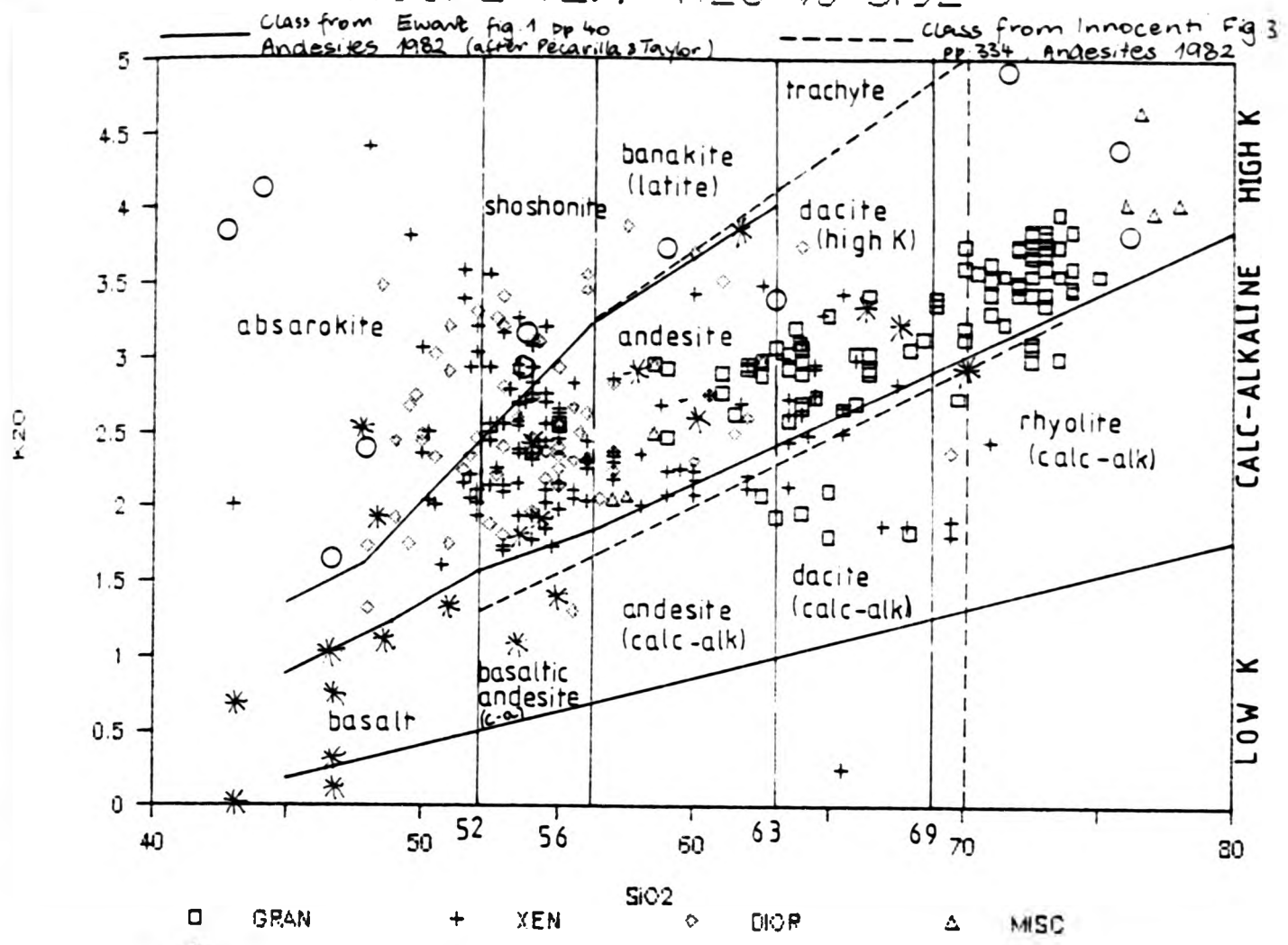

FIGURE 12.2 Na+K vs SiO2

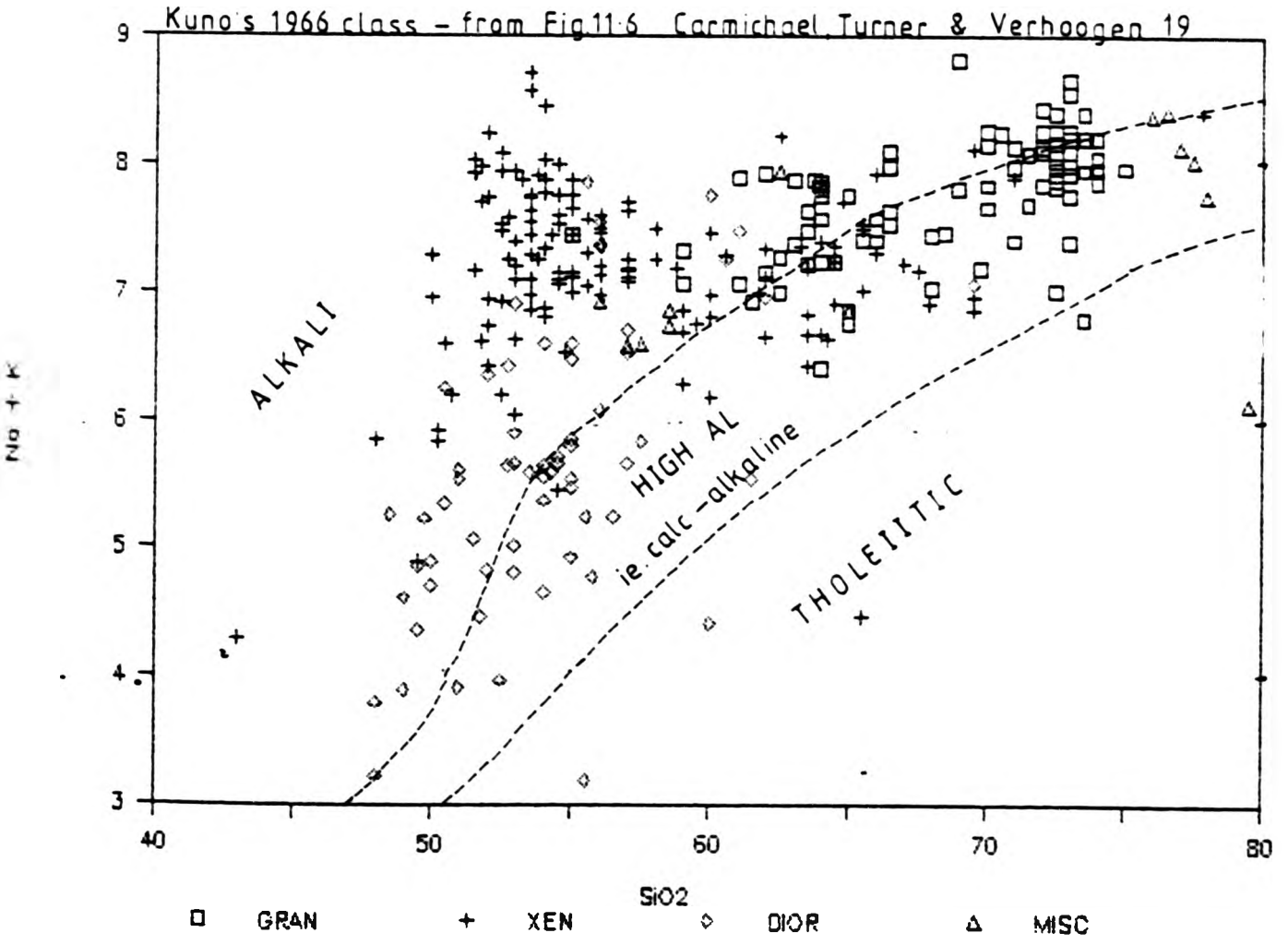

lavas to become more potassic towards the NW and the Strontian intrusions are a continuation of this trend.

Most shoshonitic types at Strontian fall in SiO_2-poor shoshonite and SiO_2-poor absarokite compositions. The xenoliths are likely to approximate to liquids so this shows that absarokite, shoshonite, high K basalt and high K basaltic andesites were all available for incorporation in the granites. It should be noted that high K shoshonitic characters have also been reported at the edge of cratons and continental volcanic arc locations. Strontian shows similar spatial association of diverse basic magmas to those described by Lange & Carmichael (1990). While absarokite composition xenoliths have been reported by Dorais et al (1990). The diorites are affected by cumulate features, but the bulk of the analyses plotting in the shoshonite suite come from two intrusions, Rubh and Uil, which are K-rich throughout and so can be confidently placed in the shoshonite suite. The possibility of pyroxene or hornblende accumulation however means that they cannot necessarily be used to infer absarokite margins for the SiO_2-poor members.

Fig.12.2 plots the total alkalis against silica and the host rocks of Strontian xenoliths fall half in the high alumina (calc-alkaline) series and half in the alkali series. The bulk of the xenoliths lie in the alkali series. There are peaks for the xenoliths, which are as high in total alkalis as the biotite granites. These high alkalic rocks are not adjacent or even nearby samples therefore the high xenolith K_2O+Na_2O values cannot be attributed to reaction with the surrounding hosts. These xenoliths also cannot be mixed with granodiorite or biotite granite to produce the intermediate members of the observed xenolith-granite trend. The xenoliths may be linked

to the diorite trend of increasing (Na+K) with little change in the silica content. The crystallization of amphibole and pyroxene in the diorites results in the increase of Na_2O+K_2O in the liquid (due to the small but significant content of Na_2O and the absence of K_2O in pyroxene; Green & Ringwood 1968).

Iron, magnesium and total alkalis (AFM) plots for the whole Strontian complex have been plotted to display the range of compositions (Fig.12.3A & B). The AFM plot for the Strontian data shows the mafic diorites (Fig.12.3B) lying at the mafic end of the trend with a pronounced MgO enrichment relative to FeO. The host granodiorites and granites, together with the xenoliths, form a continuous nearly straight trend. Aplitic veins, the most alkali-rich members of the complex, are a little offset from this trend. It is a characteristic of magma compositions of calc-alkaline suites, unlike tholeiitic suites, is they fall in an almost straight line extending from the Mg-Fe side to the alkali apex (Green & Ringwood 1968). The granite-xenolith trend is similar to, but with less iron than that defined by the calc-alkaline Cascade lava series (Carmichael 1964). It is markedly displaced from the Aleutian Island and Marianas lavas arc (Green & Ringwood 1968). Nockolds suggested that such a trend may represent a liquid line of descent of a parent magma. However Wilkinson et al (1964) demonstrated that some members of the calc-alkaline series may be produced by hybridization of basic rocks by acid magmas, so illustrating a case where no liquid line of descent occurs.

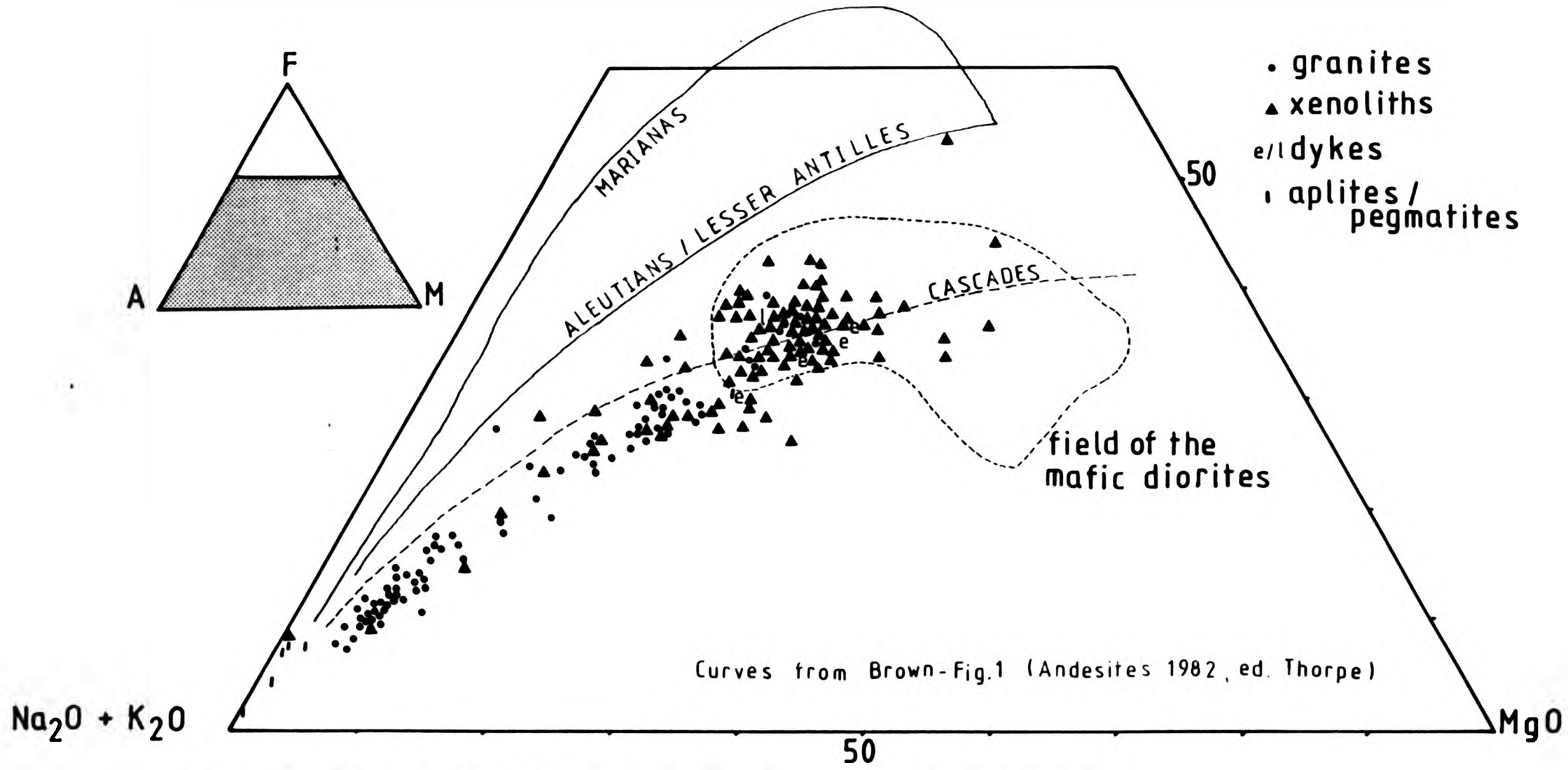

Fig.12-3A AFM diagram for the Strontian Complex.

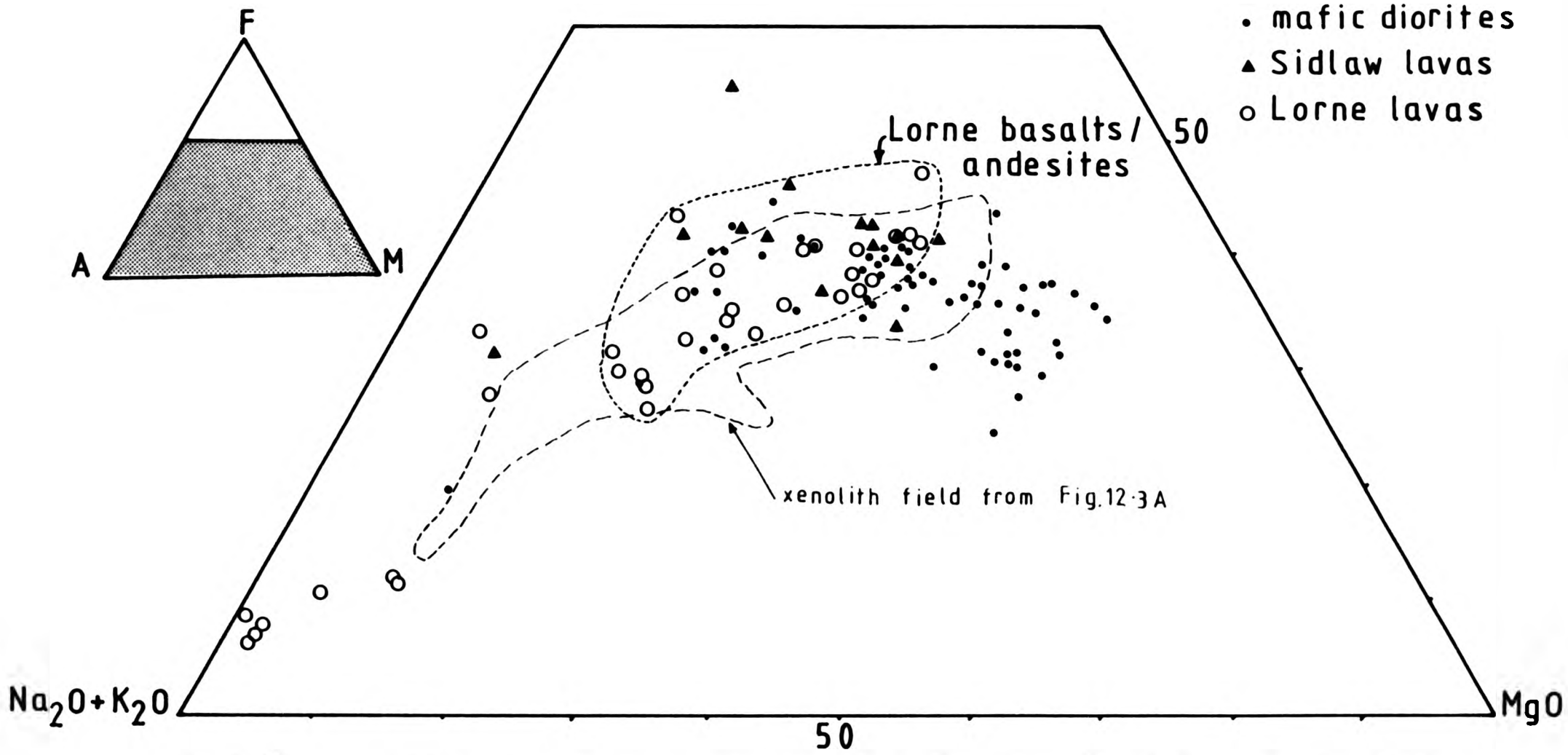

Fig.12·3B A F M diagram comparing the Strontian diorites to the Lorne and Sidlaw lavas.

12.3.2 Geochemical relations of granites, xenoliths, dykes and mafic diorites

In chapter 4, 7, 8 and 11 the geochemistry of granites, xenoliths, dykes and diorites was described and the causes of variation within each group discussed. For the granites various combinations of fractionation involved extraction or accumulation of crystals and magma mixing were shown to be capable of explaining the major element variation and variation in some, but not all, trace elements. Crystal fractionation, particularly accumulation, seems to offer an explanation of most diorite trends albeit modified by contamination with alkali granite in some cases. Xenolith patterns are the most ill defined. This section will consider the geochemical relationships between the granites, xenoliths, dykes and diorites.

The plotting of the elements against SiO_2 was appropriate for the granites, while plotting the diorites and xenoliths against MgO was needed to look at their relationship. To look at all three groups SiO_2 has been used; Figures.12.4 to 12.17. A striking feature of the major element chemistry is the spatial relationship between the data points for the 3 main groups. The main fields of the granite-xenolith-diorite are discrete and exhibit only limited overlap in their SiO_2 plots. FeO*, TiO_2 and V have straight trends with complete overlap of the xenoliths and diorites. It is mostly the xenoliths that link the granite to the diorite fields, which themselves have virtually no overlap. The three fields define a range of patterns from tightly linear (FeO* & V) to irregular and diffuse (K_2O). These patterns place restraints on the likely extent of genetic relationships between the diorites, xenoliths and granites.

FIGURE 12.4 Al203 vs SiO2

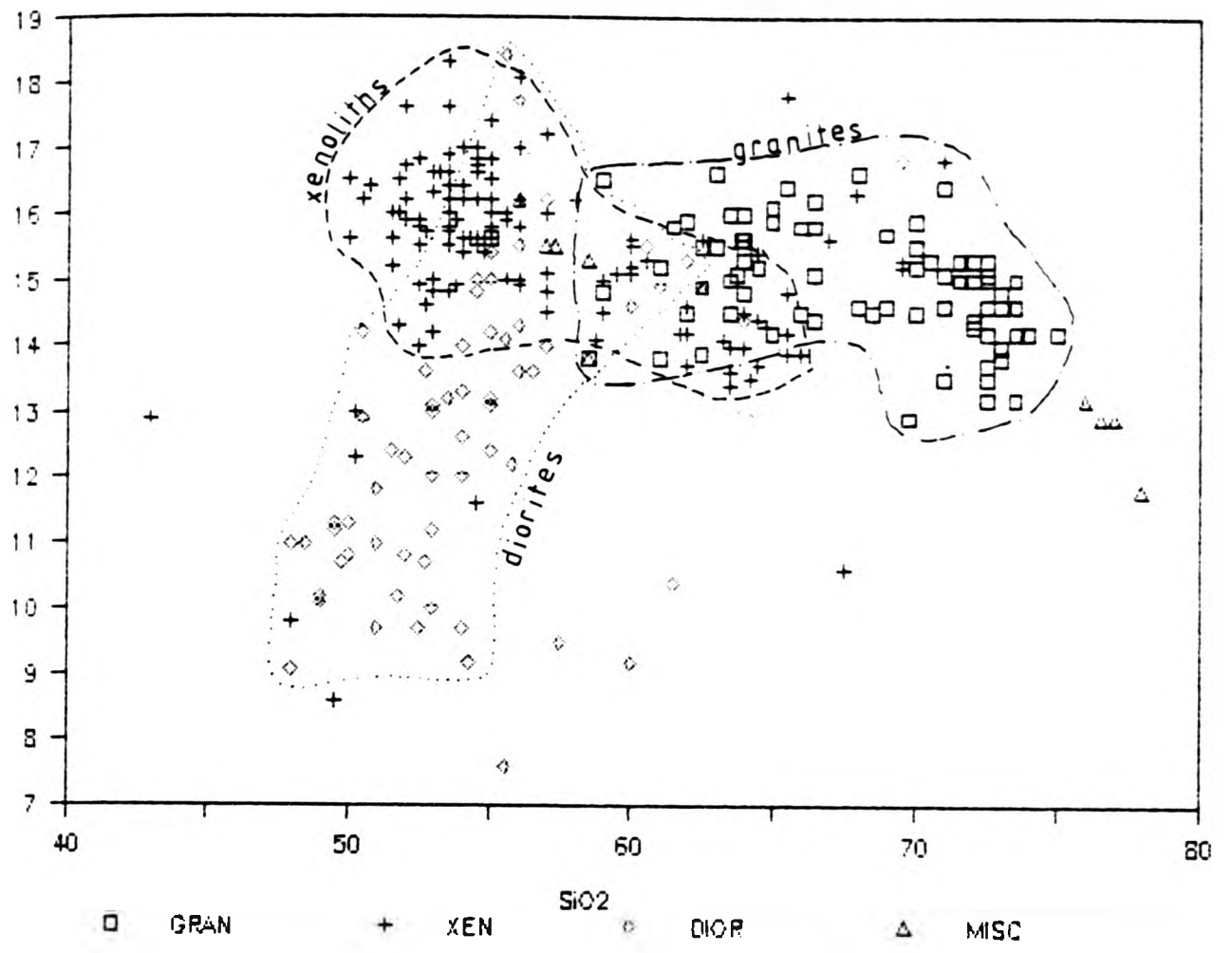

FIGURE 12.5 CaO vs SiO2

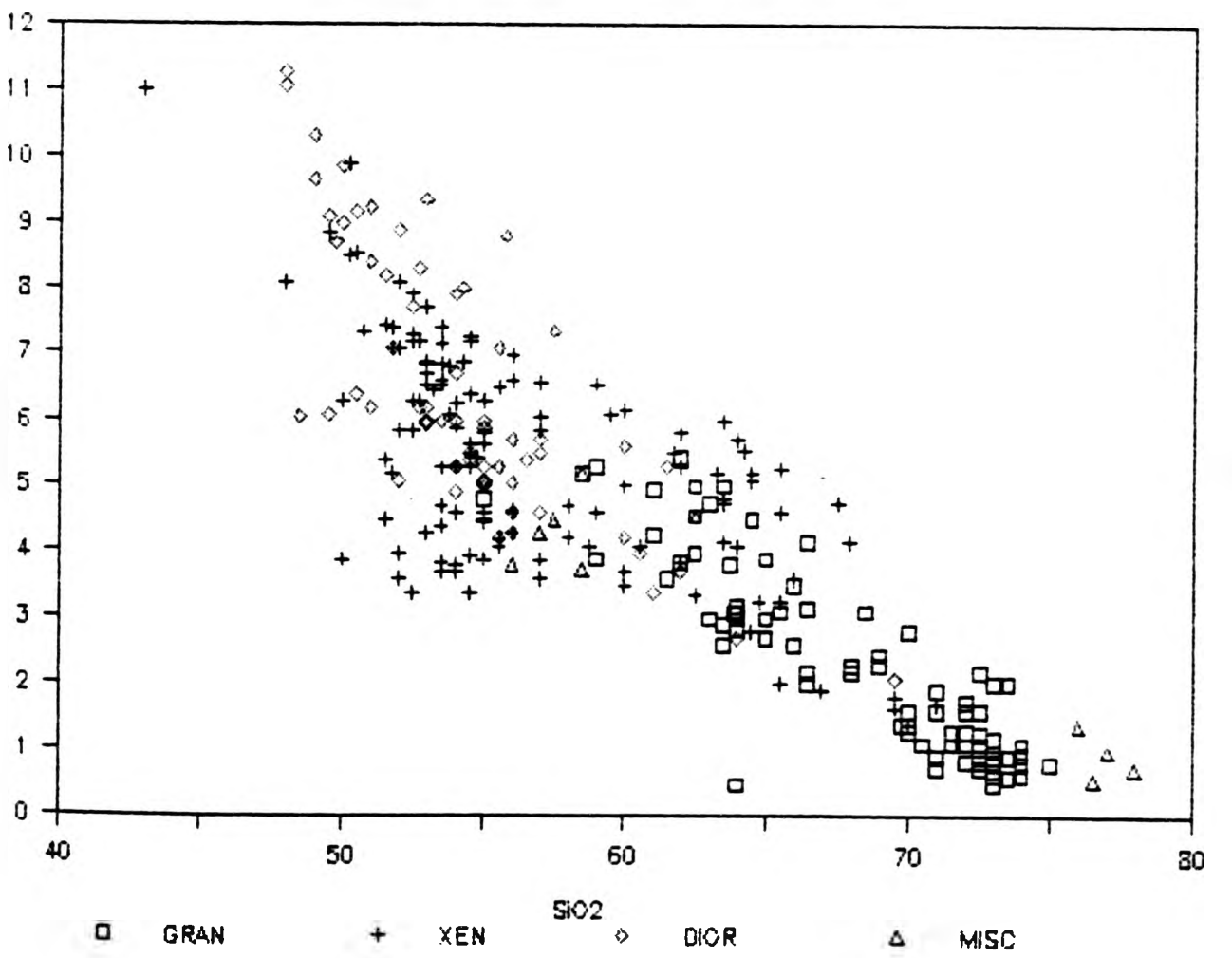

FIGURE 12.6 FeO* vs SiO2

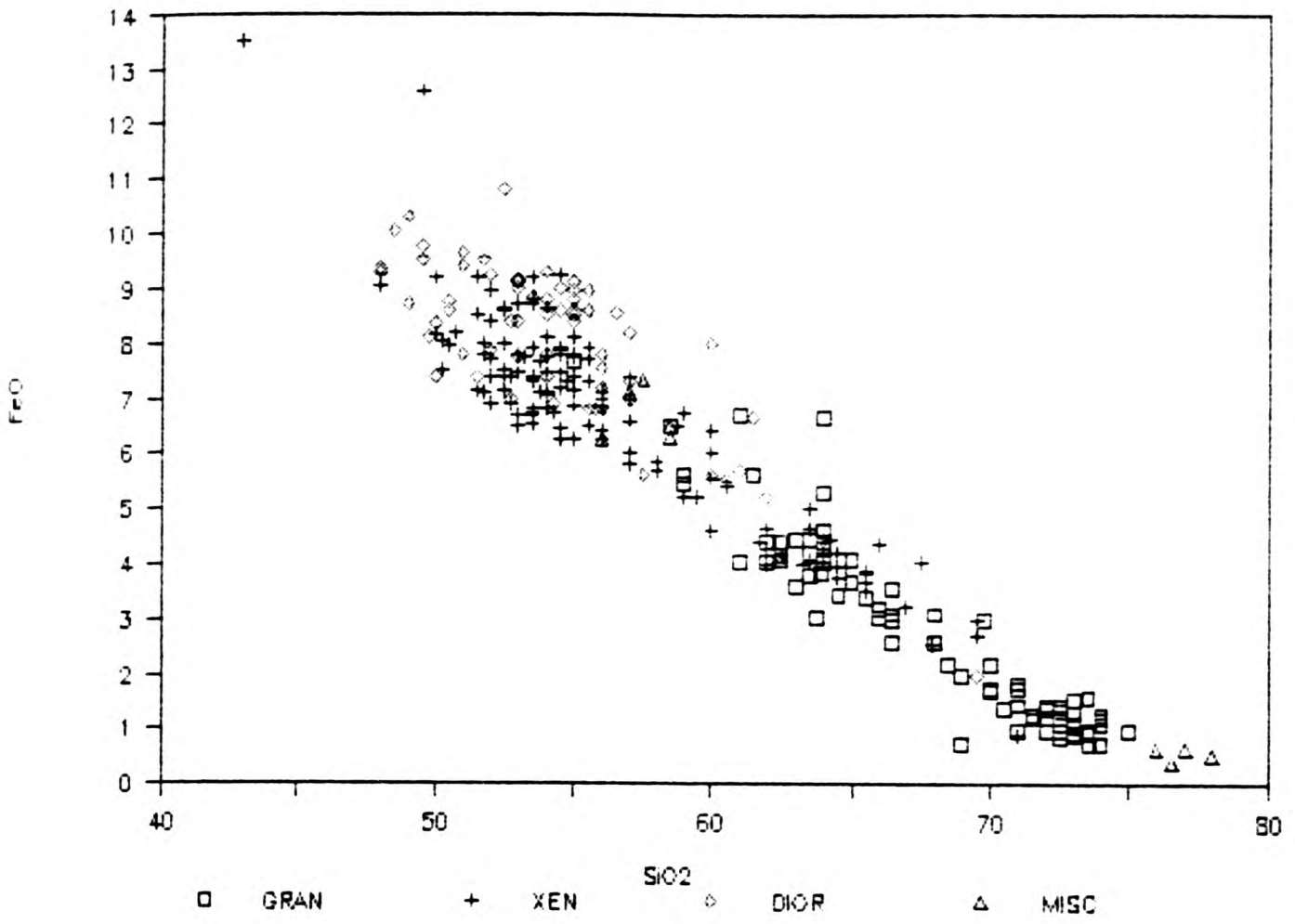

FIGURE 12.7 MgO vs SiO2

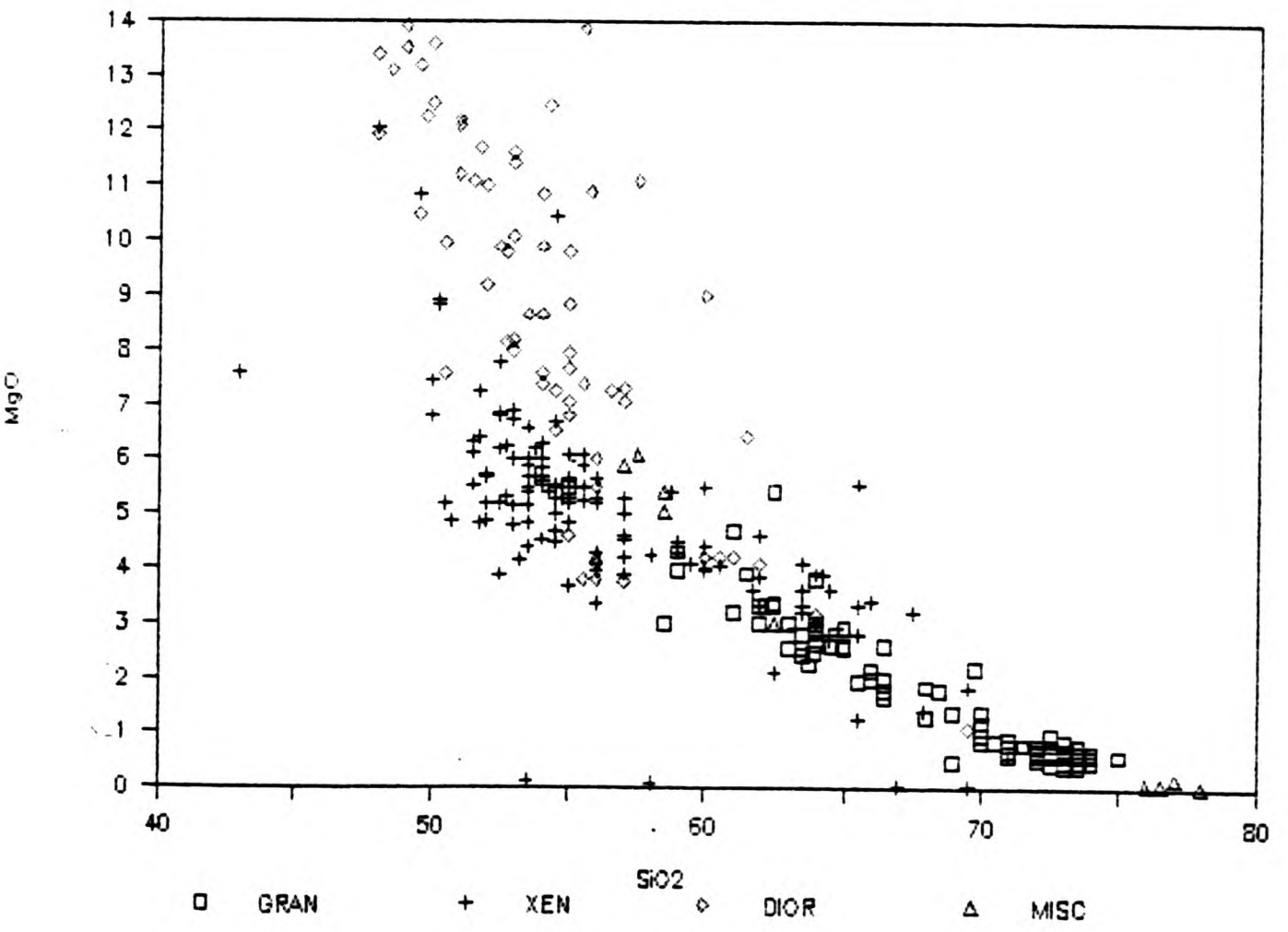

Tight linear negative trends are shown by FeO* vs V (Fig.4.32) and TiO_2 shows a linear trend with slight scatter at low silica values. These show nearly complete overlap of diorite and xenolith fields and tell very little except that total ferromagnesians decrease with increasing silica. The patterns are consistent with both multimineral fractionation and mixing. The coherent behaviour of FeO*, TiO_2 and V in all the rock types (Fig.4.32 FeO* vs V and 4.33 TiO_2 vs V) may indicate that the trend is in part controlled by the fractionation and accumulation of titaniferous magnetite or Ti amphibole. Substitution of V for Fe has been shown to commonly occur in the magnetite phase (Taylor 1969).

Broadly negative linear trends but with a tendency to branch at low SiO_2 are shown by CaO, MgO, Cr, Sc and Y (Figs. 12.5, 12.7, 12.11, 12.14 & 12.17). The overlap of diorites and xenoliths is limited at low SiO_2, but they converge to overlap the granites in medium SiO_2 contents. Two discrete classes are found: i) CaO, Sc and Y show diorites plot on the low SiO_2 continuation of the granites trend; whilst the xenoliths trend deviates , giving a very clear separation of most diorite compositions from the xenolith compositions; ii) MgO and Cr show xenoliths plotting on the granite trend and the diorites deviating. The existence of these two discrete classes means that a simple interpretation with xenoliths as samples of parent liquids from which the diorites are derived by crystal accumulation and granites as fractionated liquids or mixing between extreme end members, cannot work. Only a limited number of more SiO_2-rich xenoliths would satisfy these requirements and the evolution from SiO_2-poor xenoliths to SiO_2-rich xenoliths requires some different mechanism eg. a change in the extract assemblage or more fundamentally changes at the point of magma origin.

FIGURE 12.8 TiO2 vs SiO2

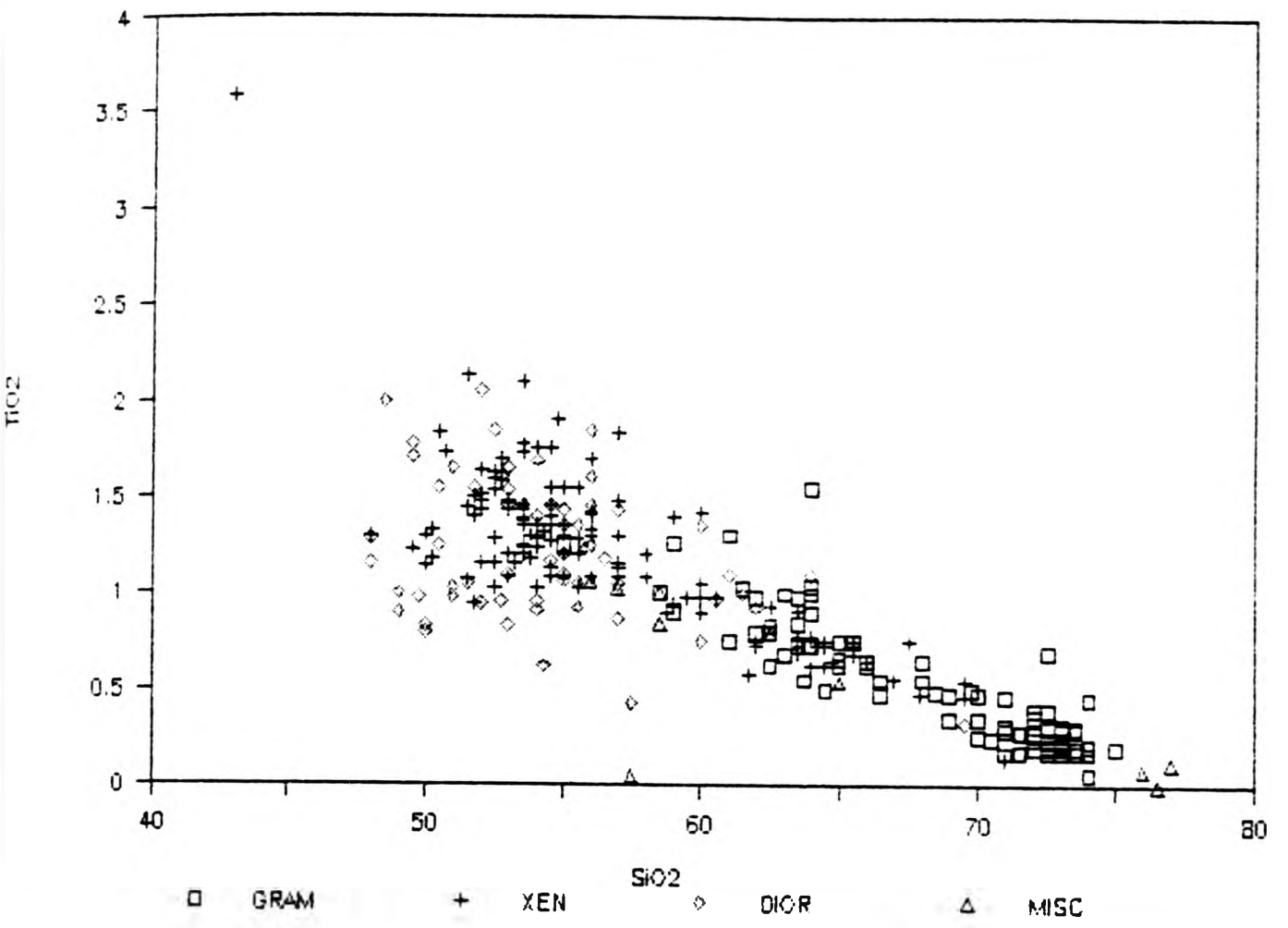

FIGURE 12.9 Sr vs TiO2

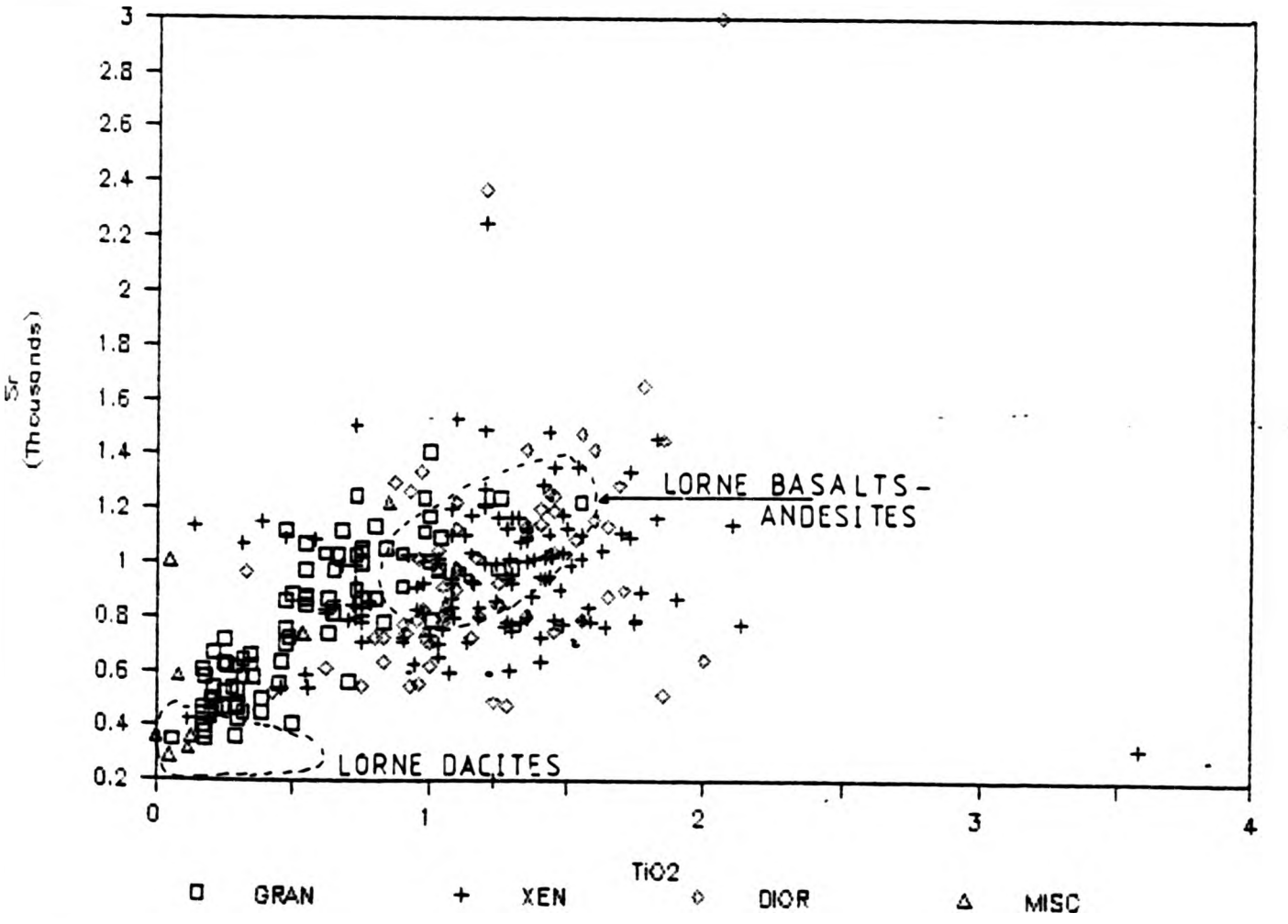

Lorne Lava data from Groome & Hall, 1974.

FIGURE 12.10 Ba vs SiO2

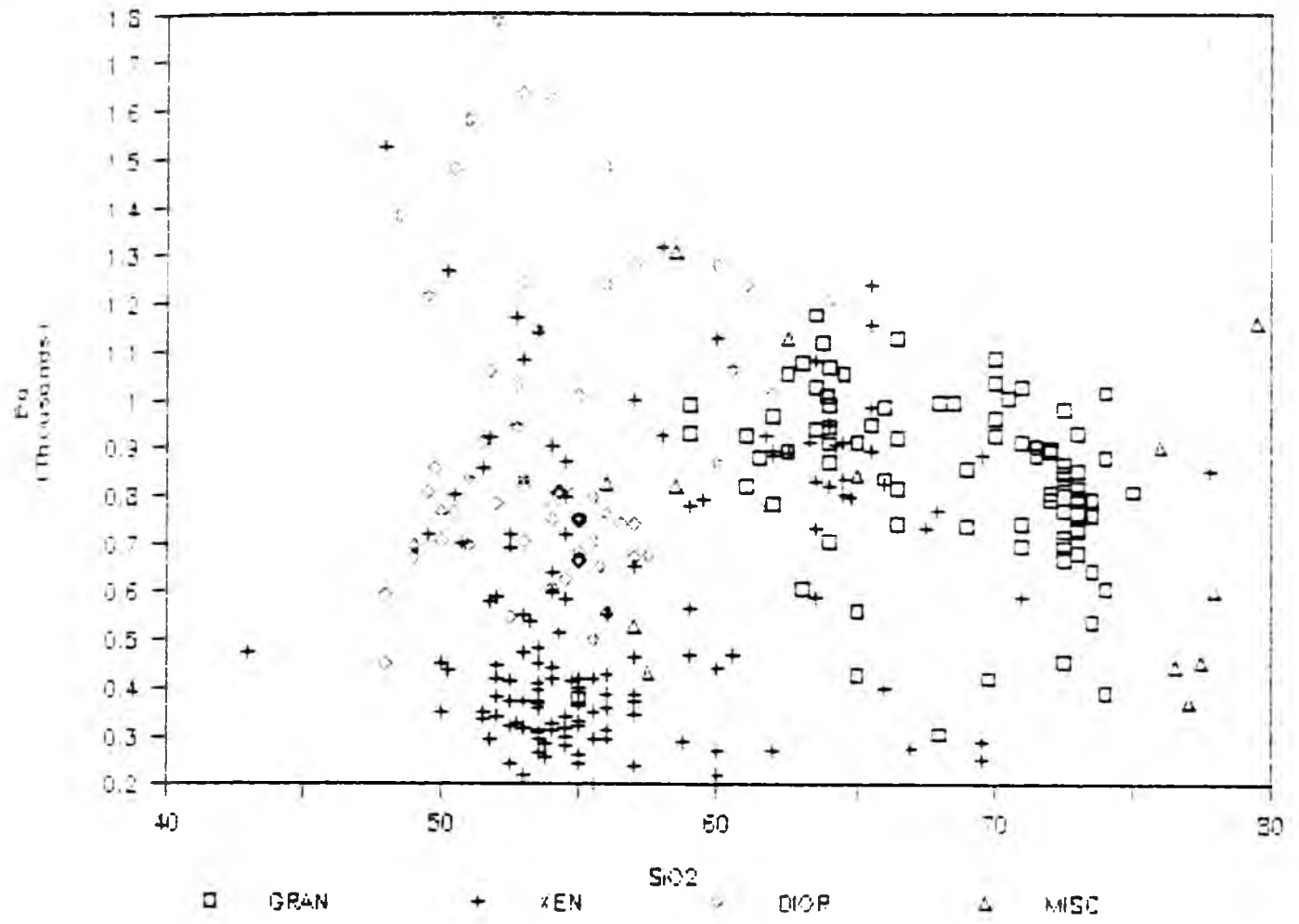

FIGURE 12.11 Cr vs SiO2

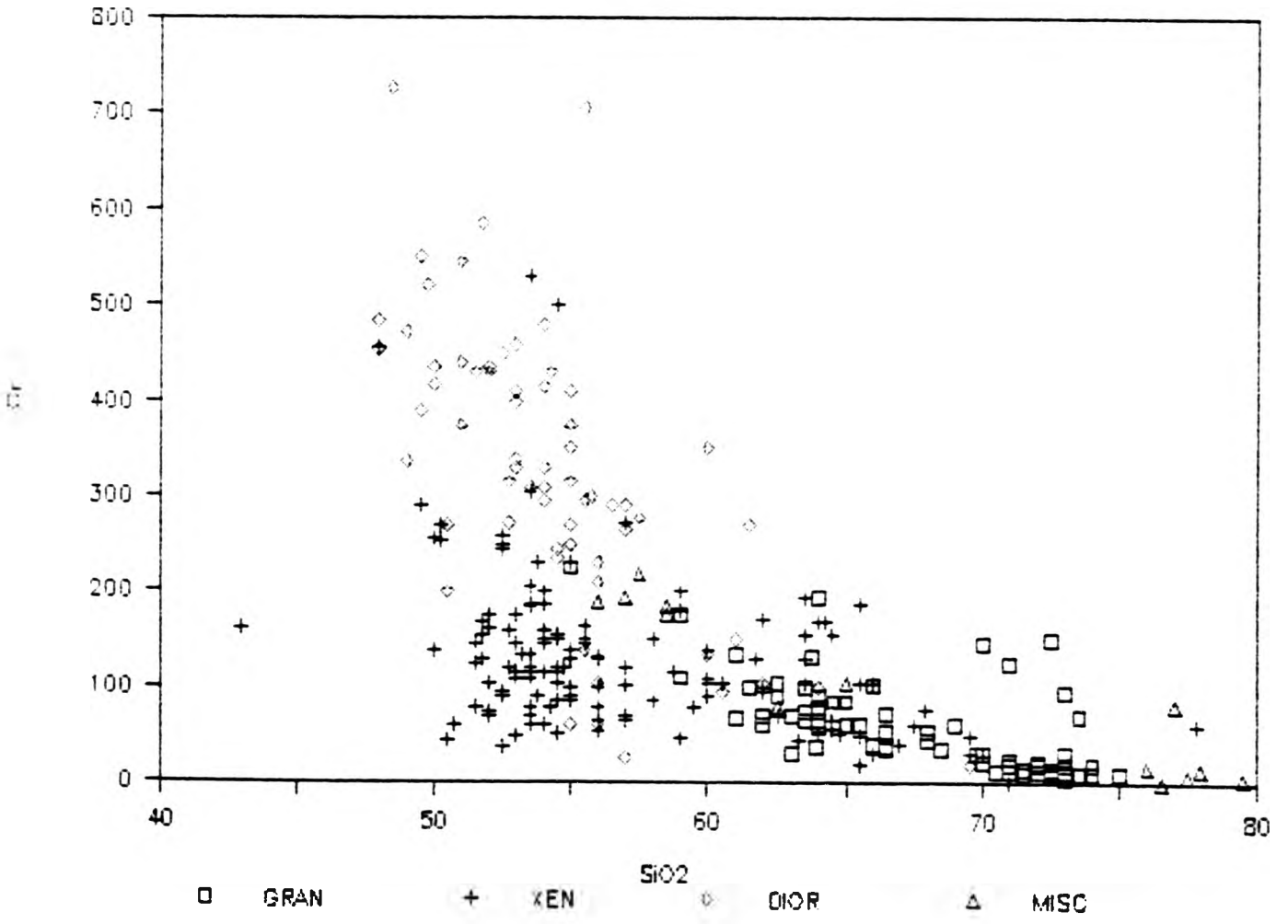

FIGURE 12.12 Li vs SiO2

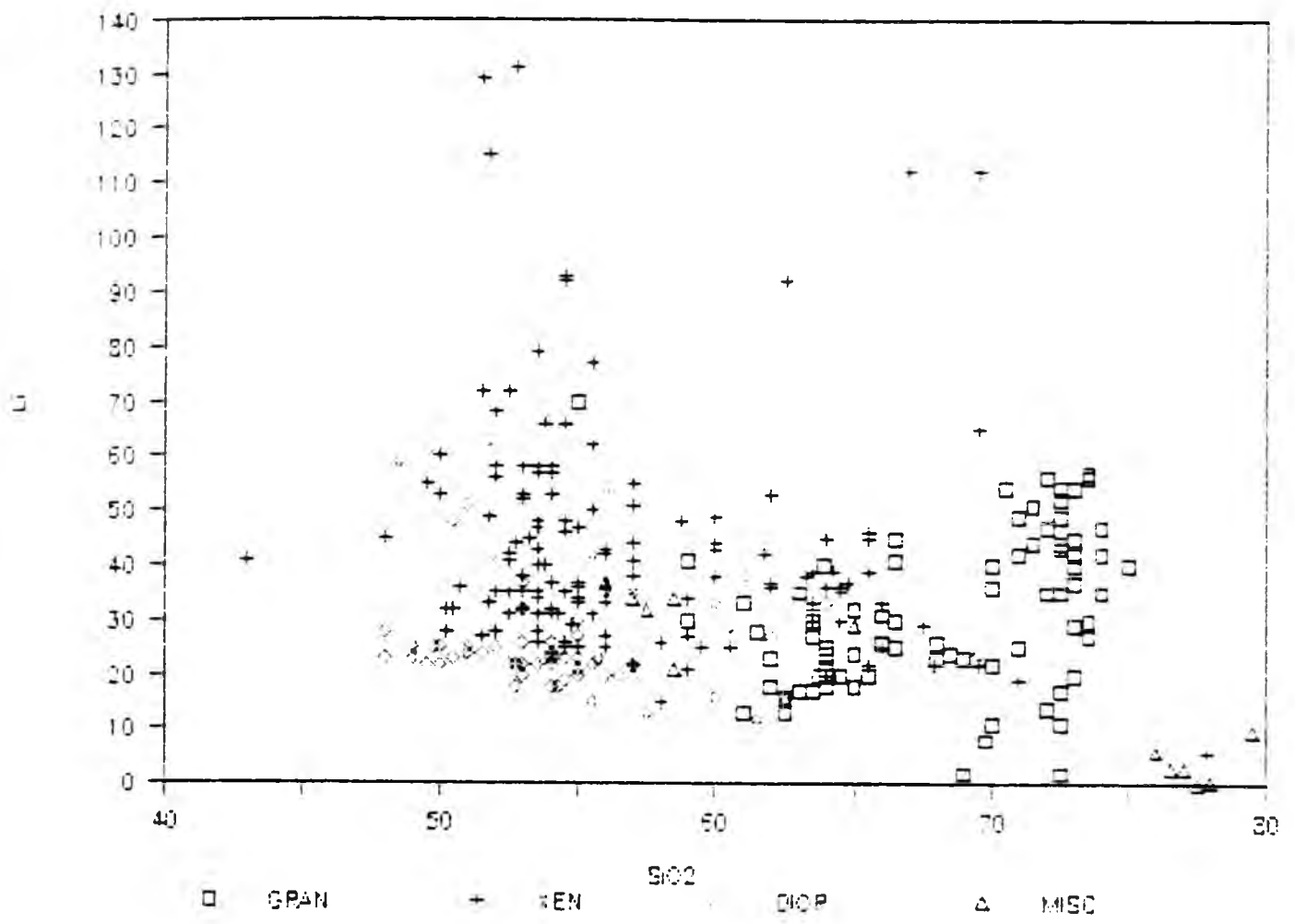

FIGURE 12.13 Pb vs SiO2

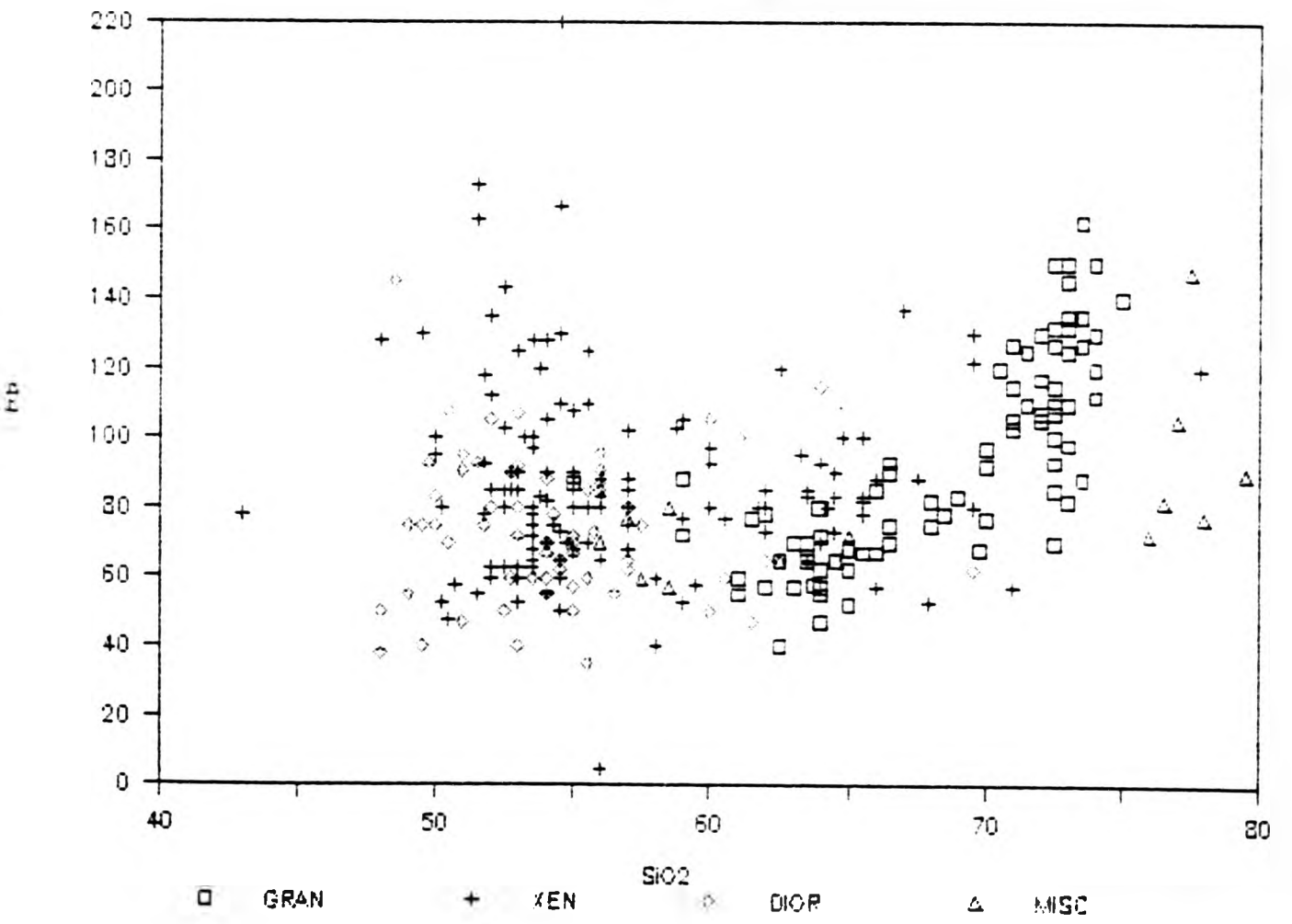

FIGURE 12.14 Sc vs SiO2

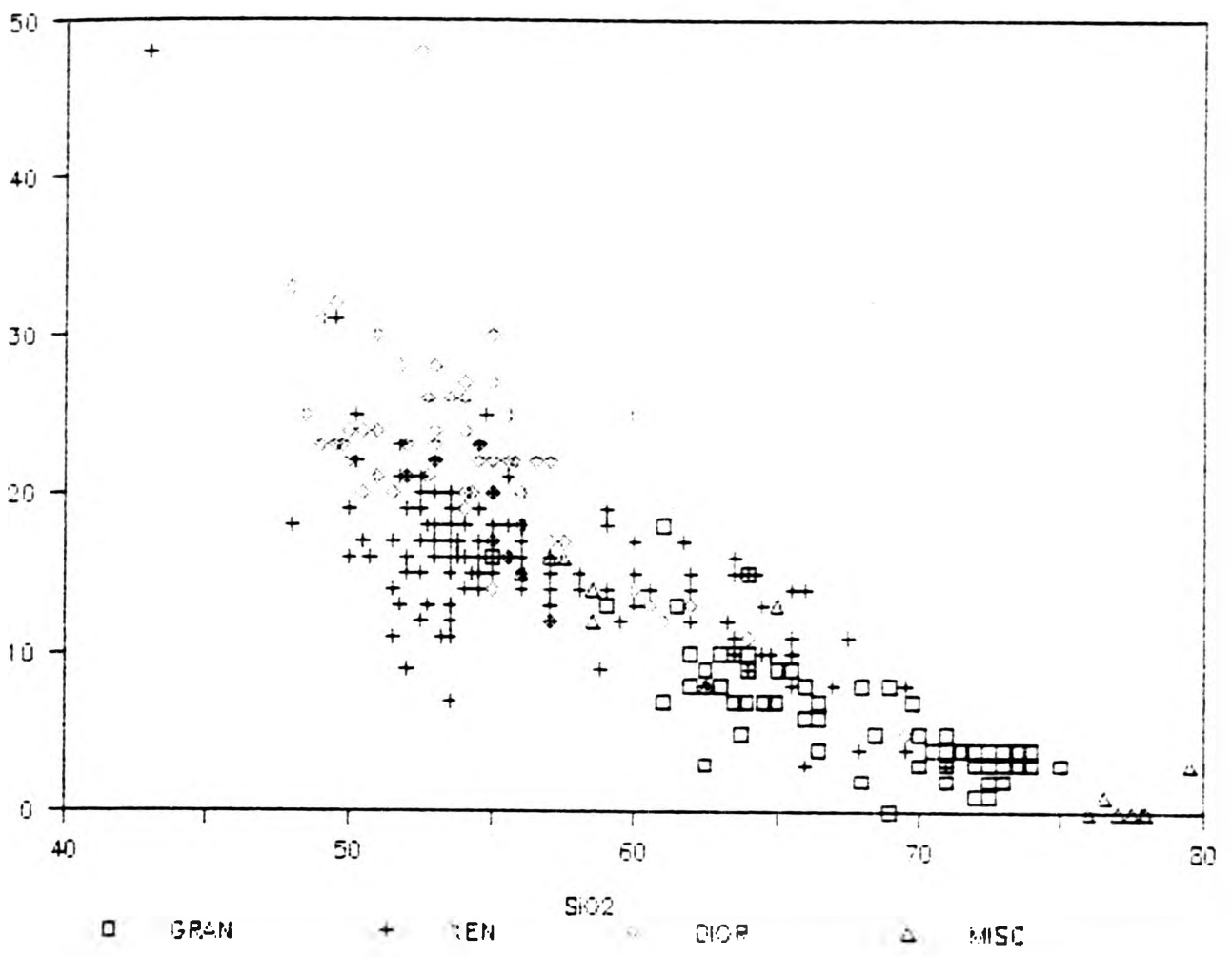

FIGURE 12.15 Sr vs SiO2

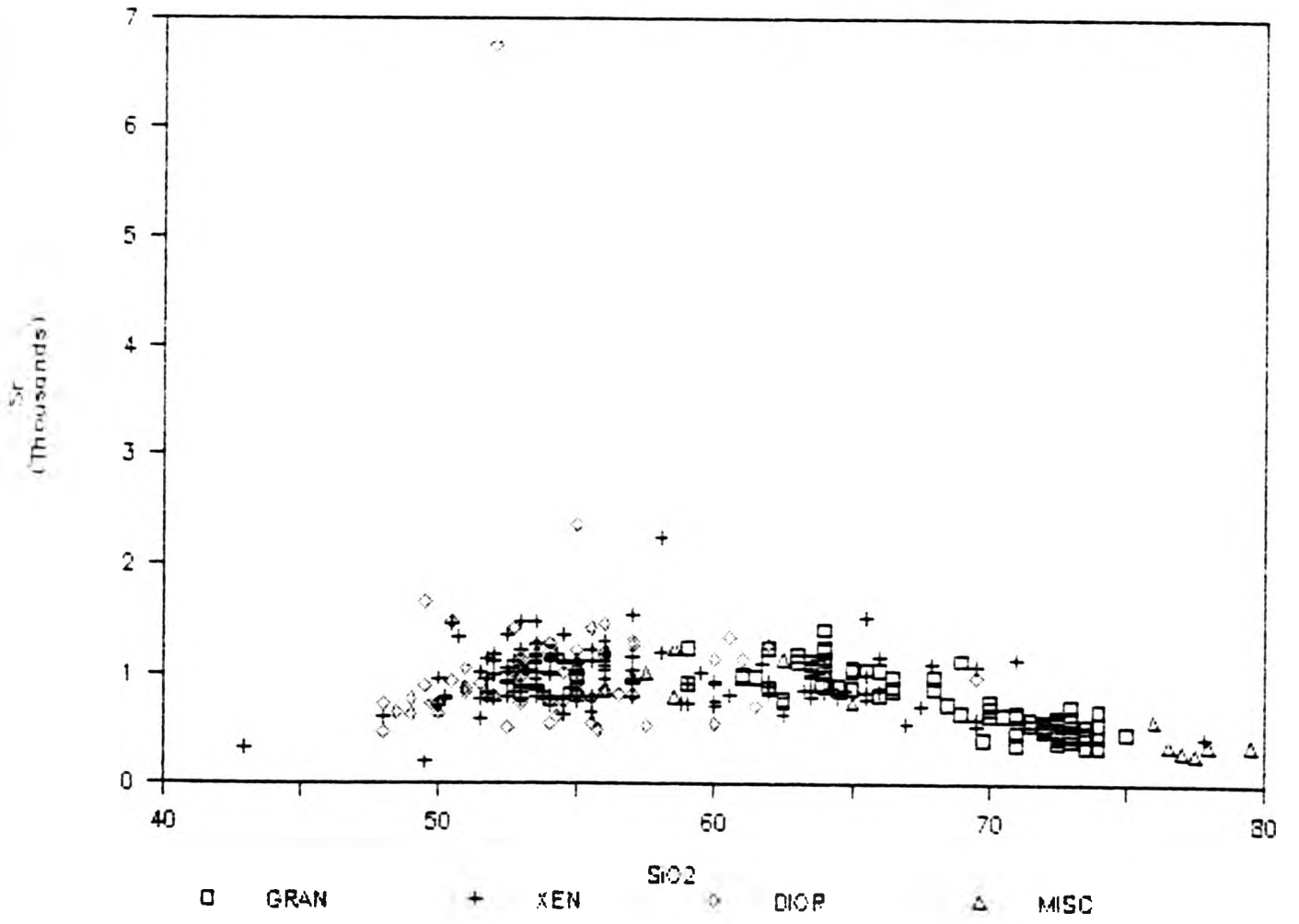

FIGURE 12.16 V vs SiO2

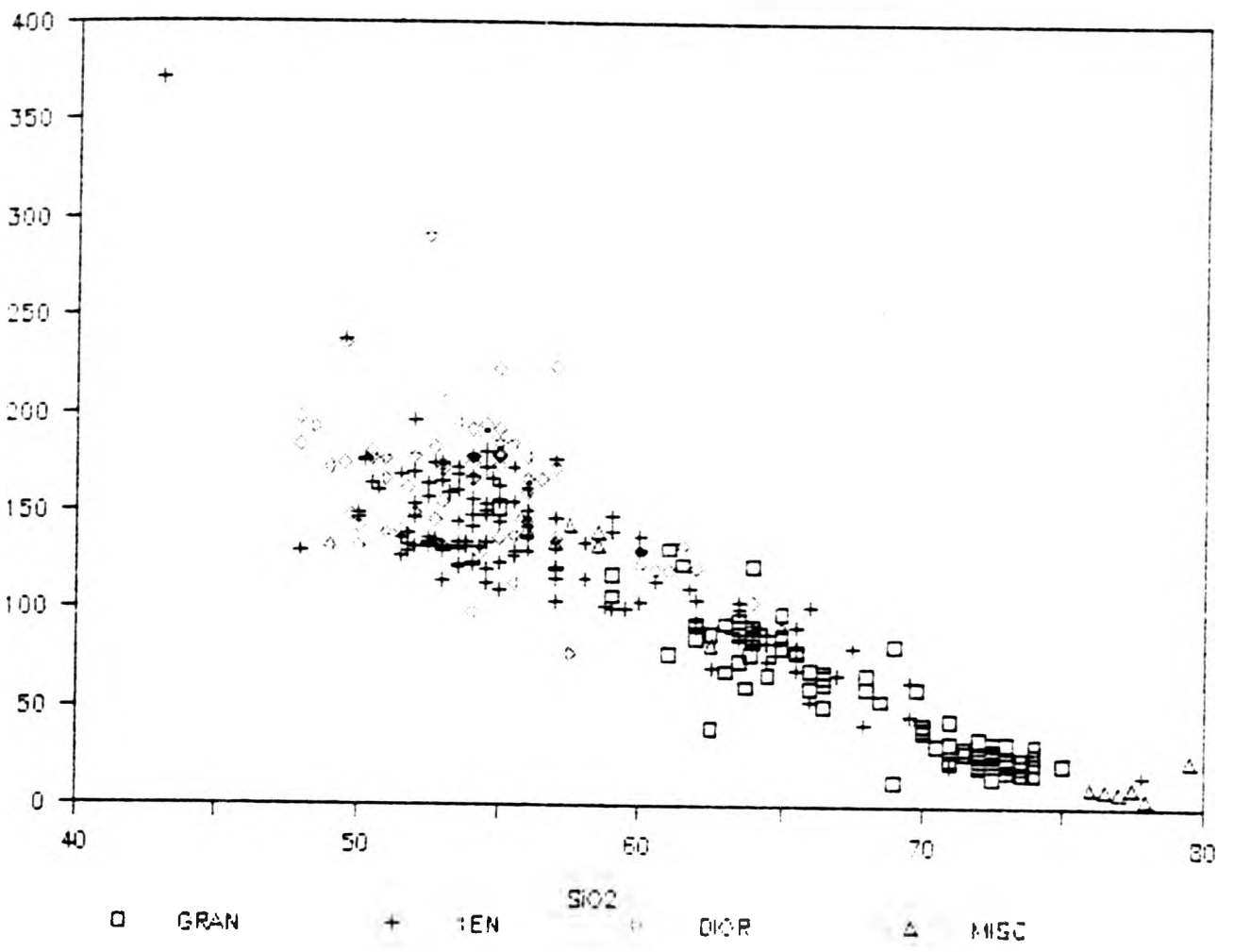

FIGURE 12.17 Ti vs SiO2

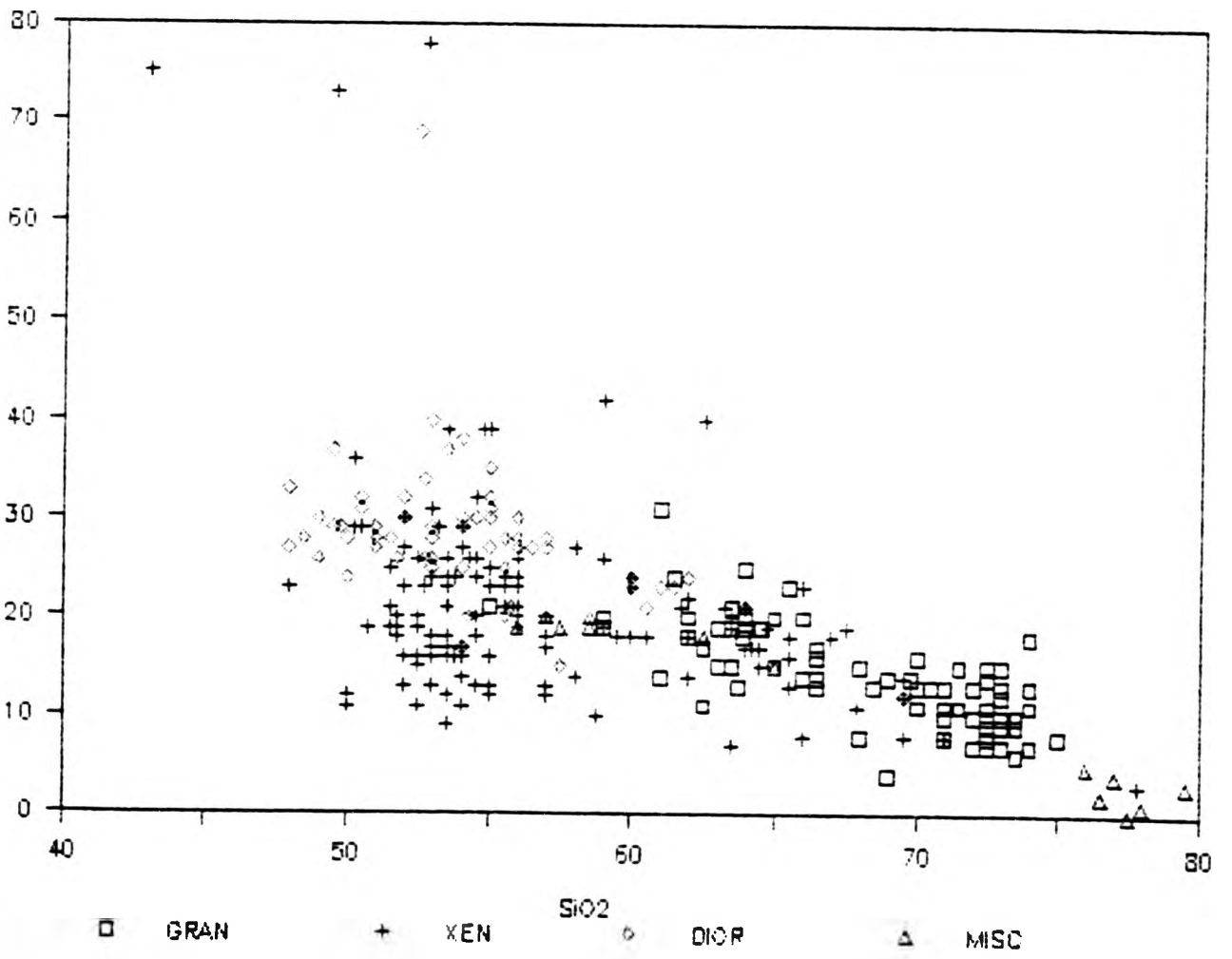

Al_2O_3 and total alkalis vs SiO_2 (Figs. 12.4 & 12.2) show all three groups with different linear trends diverging from a common area. Again only high SiO_2 xenoliths could be possible common parents to the diorites and granites and the evolutionary trends of these are controlled by: i) different mineral assemblages if driven by fractional crystallization or ii) basically different mechanisms. SiO_2-rich xenoliths cannot be the direct parents for the SiO_2-rich diorites. Fractionation for SiO_2-poor xenoliths to SiO_2-rich xenoliths would require some different extract from that identified for the granodiorite evolution.

Ba vs SiO_2 is a very scattered but the densely populated area of the field of xenolith compositions is totally separated from the granodiorite trend. This separation would suggest that only a very small numbers of xenoliths could be directly related to the granodiorite by magmatic evolution. An intermediate stage involving the extraction of Ba-poor phases eg. pyroxene +/-amphibole +/- plagioclase would be required. The very low Ba of the main xenolith population means that any xenolith magma - granitic hybrids will not lie on the granitic trend of slowly decreasing Ba with increasing SiO_2. Hybridization between the two could however account for the scatter of analyses on this plot and the broadening of the field of granite analyses to high and low Ba values. The diorites show a far greater range of Ba than either the other two rock types, but virtually all values with >1000ppm Ba are from the Uileann diorite.

Covariance as seen between CaO and MgO (Fig.7.7) has been suggested to arise from imperfect separation of partial melt from residual source rock xenocrystic material (White & Chappell 1977, from McCarthy & Groves 1979). Many plots show a change in the trend at the

xenolith compositions at 50-55% SiO_2, except with FeO*. This latter continuity may present a possible genetic linkage, but the trend changes discussed above suggest different processes.

The group of elements Rb, Ba and Sr have a decreasing ionic radius from Rb to Sr. During fractional crystallization of a magma the concentration of incompatible elements such as Rb increases. The substitution of Rb for K in alkali feldspars and Sr for Ca in plagioclase can take place, with extreme fractionation. The high (Na+K) is equivalent to high Rb in the xenoliths. When compared with lithium there is no link between high total alkalis and high Li at all. Rb vs SiO_2 (Fig.12.13) shows a definite increase with increasing differentiation, while the xenoliths show the greatest scatter. The high fliers in the Li and Rb plots are all xenoliths found within the biotite granite or in the coarse granitic sheet by the Rubha diorite, suggesting contamination by the granite or a close relationship below the present level of exposure. A plot of K_2O vs Rb for the host rocks and diorites (Figs.4.22 and 11.25) suggest that extensive substitution of Rb for K has taken place in the more evolved rocks ie. the biotite granite and the Uileann diorites.

Although compatible elements like Mn, Ni, V etc show normal expected coherent behaviour with MgO and FeO*, particularly the latter, the "incompatible" elements do not show such well organised mutual correlations. K/Rb ratios (Fig.11.23) vary widely and shows a range of 150 to 450 across the whole plot. The main cluster of diorite, xenolith and granite data are separated, the granites being the most isolated. Taylor (1965) suggests that the K/Rb ratio is a useful clue to fractionation of a suite of rocks. Gast (1965) says a common average for the K/Rb ratio is approximately 300, so the Strontian

rocks have a wider range. There is scatter in the xenolith compositions on the Y plot (Fig.12.17), where the xenoliths lie below the main diorite-granite trend. It therefore limits the interpretation of the xenoliths coming from the same source material as the complex.

Sr vs SiO_2 (Fig.12.15) shows a single convex upward pattern with the maximum values between 55 and 65% SiO_2. Overlaps between diorites and xenoliths is unusually complete and they form a continuous smooth trend with the granites. If controlled by fractional crystallization a considerable variation in extract assemblage and chemistry is implied; initially mafic dominated, then mafic + plagioclase and finally plagioclase dominated to decrease Sr in high SiO_2 rocks. The curvature limits hybridization either to small segments of the trend or, if extremities are involved, to small amounts of intermixed material.

K_2O, Rb and Li (Figs.12.1, 12.13 & 12.12) all show patterns with marked peaks at 50 to 55% SiO_2 and above 70% SiO_2. All these show more regional variation in the lower limits of the range; positive for K_2O and Rb; negative for Li. Diorite and xenolith fields are largely coincident for K_2O and Rb, but Li is systematically lower in the diorites then xenoliths. The conspicuously Li and Rb-rich rocks are xenoliths from the BGT and in a coarse granitic sheet.

K_2O and Rb are normally considered incompatible elements in silica-poor rocks and concentration increases with increasing SiO_2. The xenoliths forming the low SiO_2 - high K_2O, Rb field cannot generate any of the other rocks and although some scatter here may represent contamination or mixing with granite, this must be limited.

Then the high and low K_2O xenoliths must represent liquids from a different source.

Sr, Ba, Rb, Li and K_2O vs SiO_2 together indicate that hybridization between the granites and xenoliths is limited, but may well account for the broadening of trends and scatter of points. The smaller number of more SiO_2-rich xenoliths that overlap the granite trend may however be related either by amph + biot + plag fractionation or mixing, to the granitic trend. Likewise a small number of xenoliths in the 52 to 56% SiO_2 range, potentially could be genetically related to the diorites either as parent liquids for cumulate diorites or as derivative liquids.

Although compatible elements like Mn, Ni, V, etc show the normally expected coherent behaviour with MgO and FeO*, particularly the latter, the "incompatible" elements do not show such well organised mutual correlations. K vs Rb ratios (Fig.11.23) vary widely and the main cluster of diorite, xenolith and granite data are separated, the granites being the most isolated.

The mafic diorites have higher Cr levels (average 327ppm) than other Caledonian plutonic rocks (100 to 250ppm Cr, Nockolds & Mitchell 1946). Both Sr (490 to 2367ppm for Strontian) and Rb (38 to 145ppm for Strontian) fall into the average abundances though into the lower half. One extreme example has over 6000ppm Sr (Fig.12.15). However a plot of Sr vs Ti (Fig 12.9) shows continuity between the acid and basic rocks while in the Lorne lavas there is no continuity (Groome & Hall 1974).

12.3.3 The Rare Earth Elements

The REE have been determined for the range of rock types found in Strontian (Figs.4.37, 7.31, 8.1 and 11.33) and are shown together on Fig.12.18. The xenolith field is by far the broadest, completely enclosing the diorite and dyke fields and overlapping a large part of the granite field. The granite field is displaced to lower abundances relative to the xenolith field. The host rocks also have lower absolute abundances than the diorites with only a small overlap at the LREE end. The dykes lie on the lower margin of the diorite field. The La/Yb ratios are greatest for the host rocks of 72:1 to 8:1; while the xenoliths range from 51:1 to 19:1 and the diorites 34:1 to 8:1.

The minerals which preferentially concentrate REE in granitic rocks are amphibole, zircon, apatite and sphene. Limited electron microprobe analyses of sphenes from Strontian show they contain substantial amounts of REE. A broad positive correlation between La vs P_2O_5 (Fig.12.19) and La vs TiO_2 (Fig.12.20) in the Strontian rocks is seen with the trend passing close, but not through, the origin. Xenolith and diorite fields overlap and are more scattered than the granite data. This correlation suggests that some form of apatite and sphene fractionation may account for some of the variation. Amphiboles must be considered as they are known to contain significant amounts of REE, even though their absolute values are not as high as in sphene or apatite, the volume of amphibole crystals is very large.

Figs.12.21 and 12.22 plot La/Gd (LREE) ratios and Gd/Lu (HREE) ratios vs MgO. They demonstrate the degree of relative enrichment from the

Fig.12·18 Total chondrite normalised REE patterns showing the full range of each rock group in Strontian.

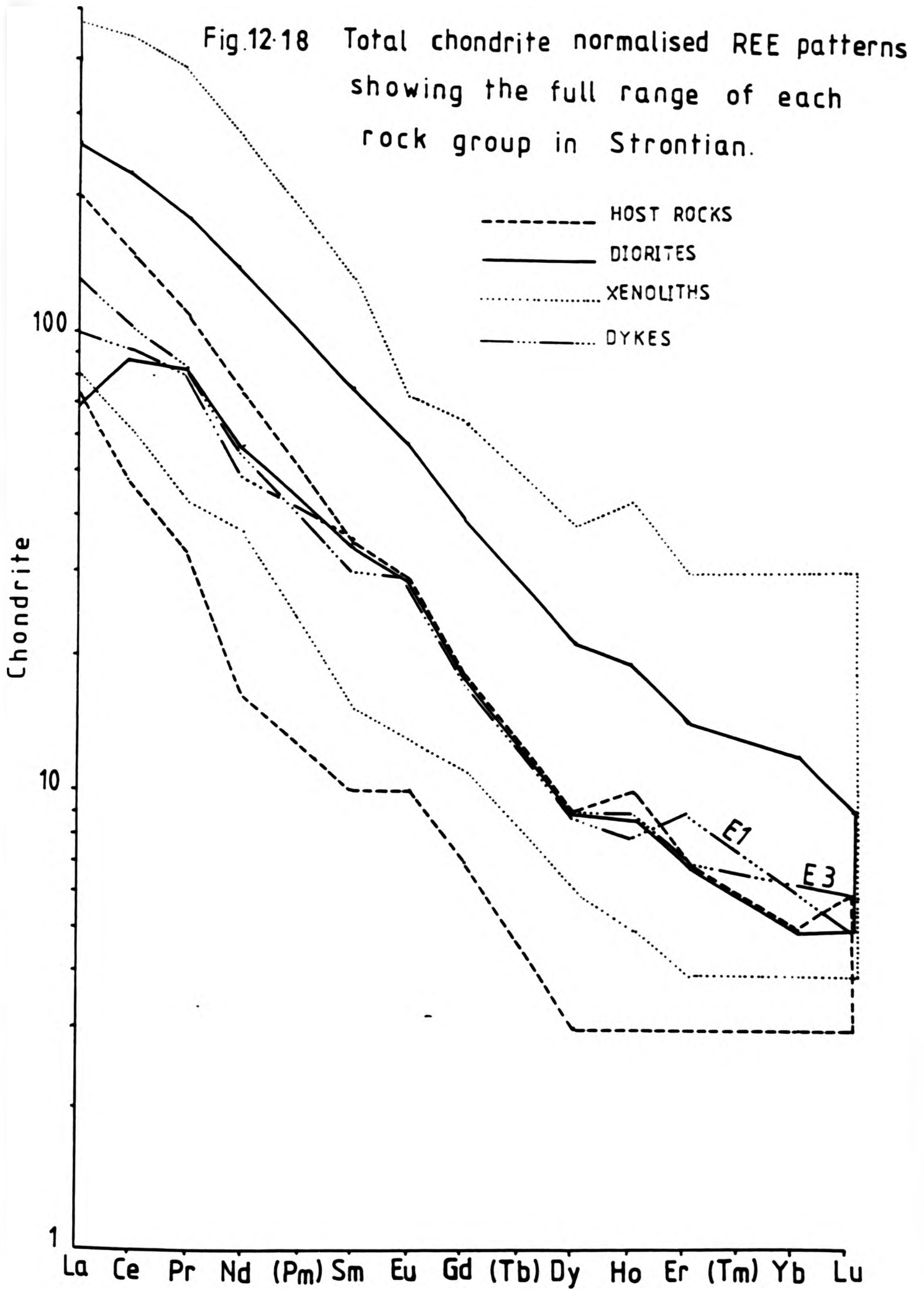

FIGURE 12.19 La vs P2O5

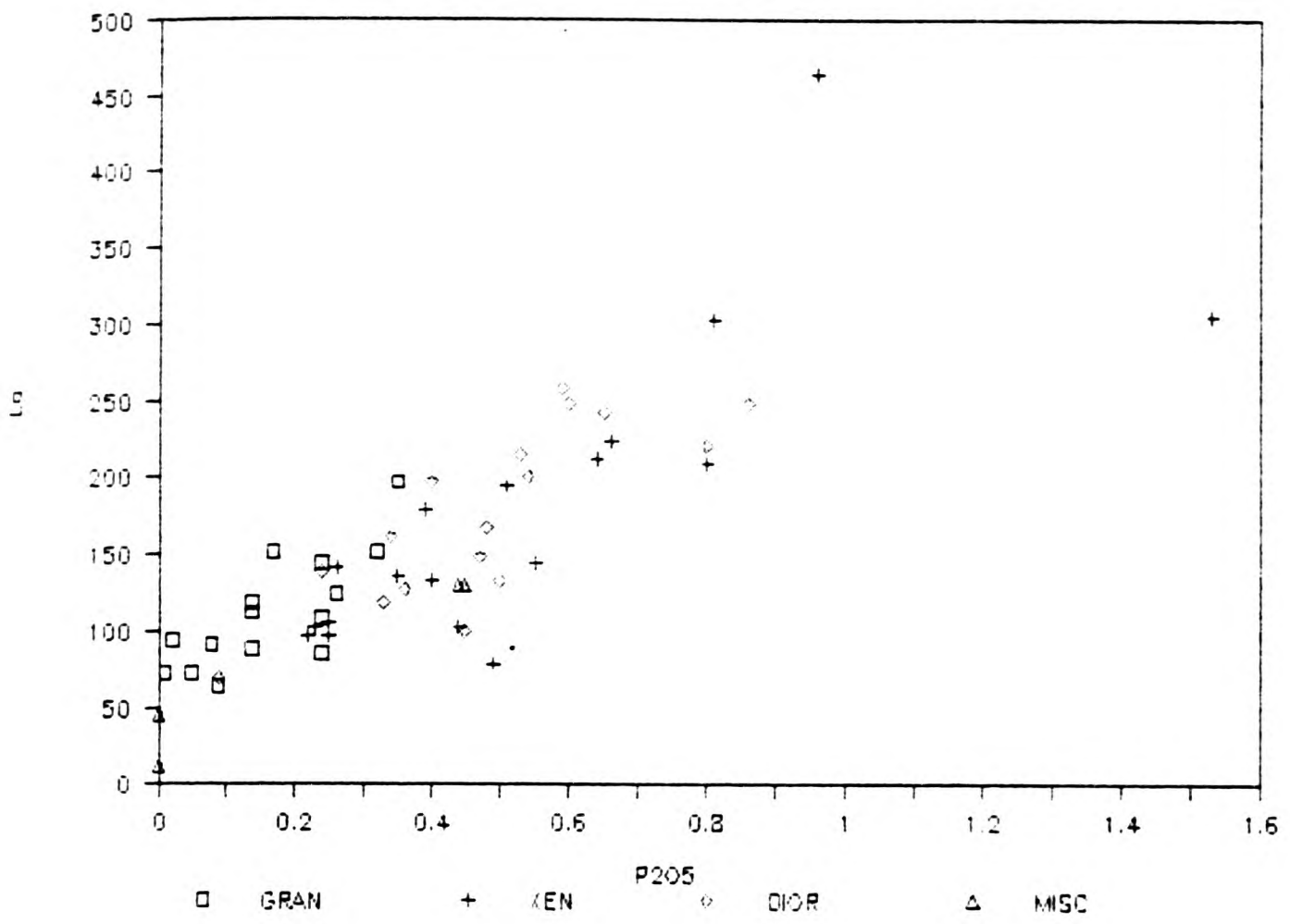

FIGURE 12.20 La vs TiO2

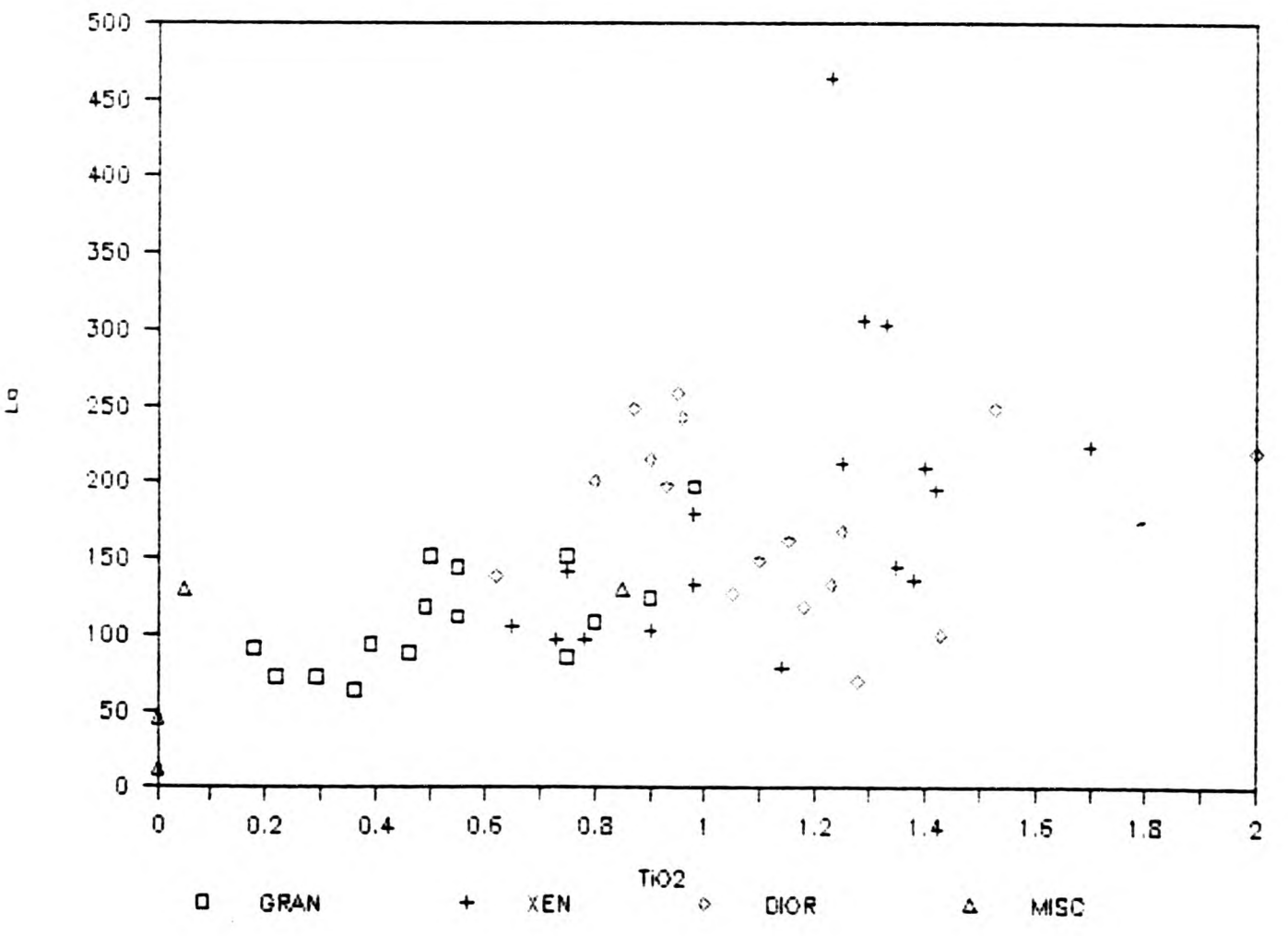

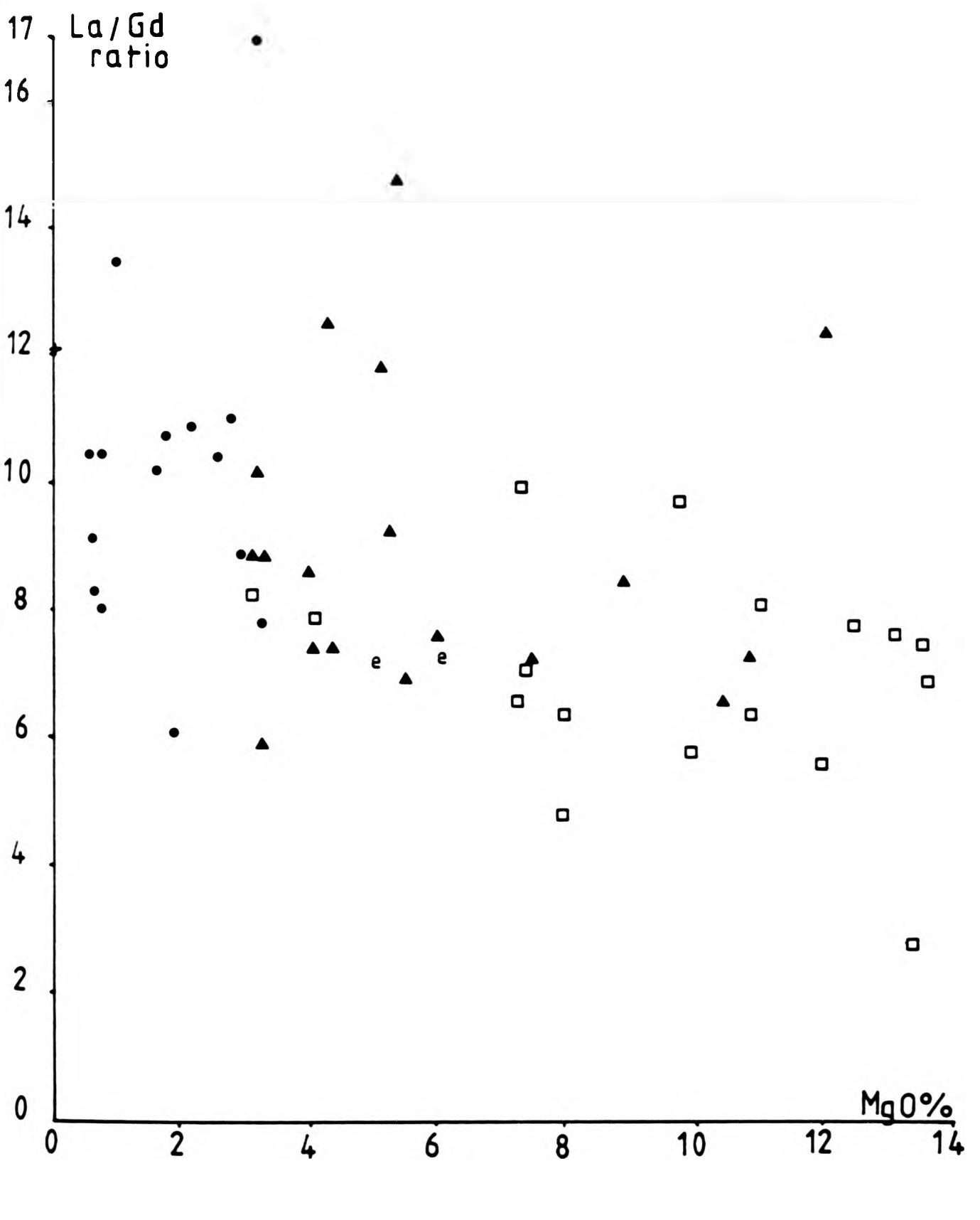

Fig. 12·21 Light REE (La/Gd) plotted against MgO (atomic %).

- Granites
- ▲ Xenoliths
- □ Diorites
- e Dykes
- + Aplite vein

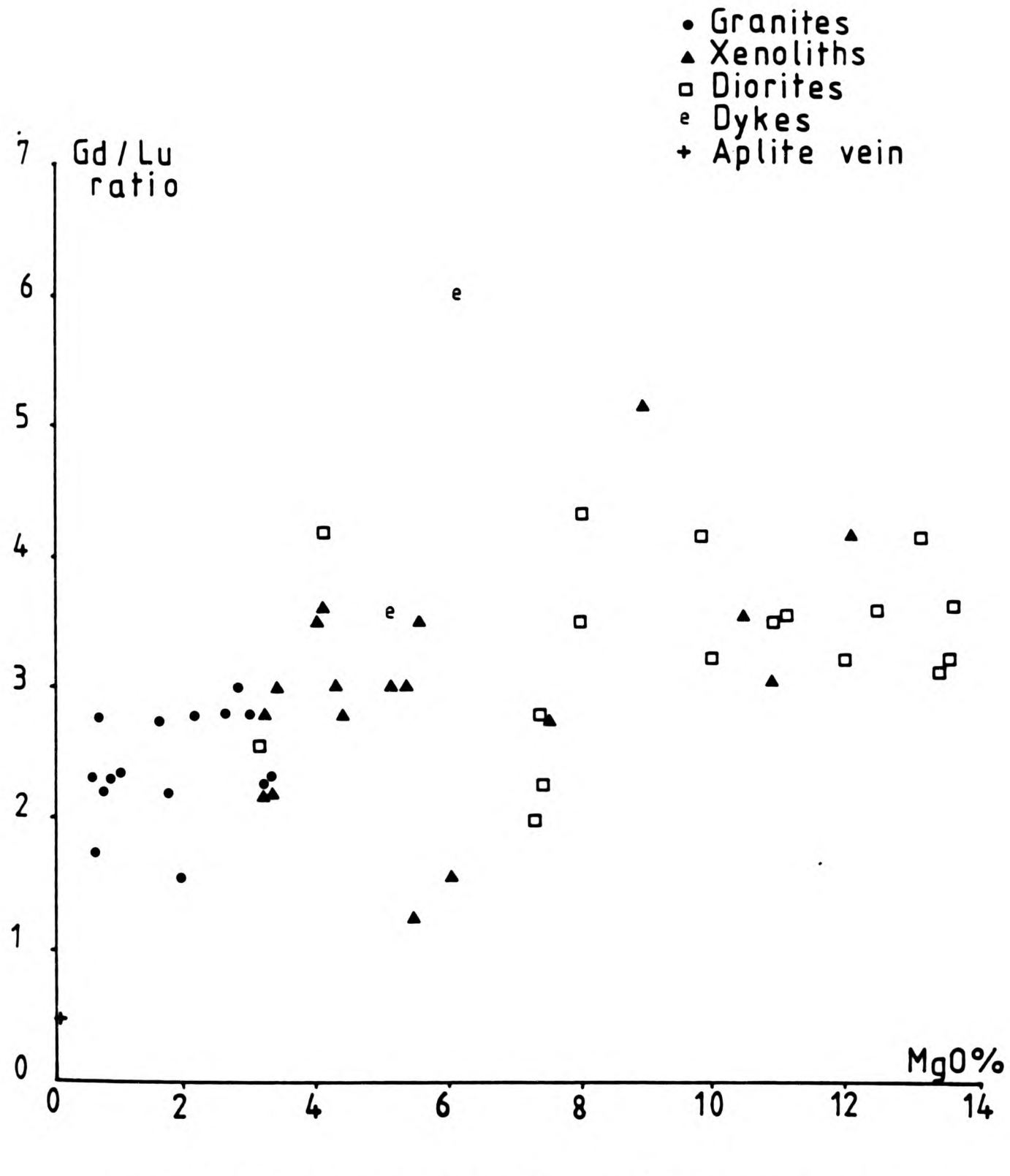

Fig. 12·22 Heavy REE (Gd / Lu) plotted against MgO (atomic %)

diorites to the host granites. If the three groups were linked by fractional crystallization, then these patterns indicate that significant amounts of REE have been removed from the magma prior to crystallization of the granites.

The REE data for other Caledonian complexes has been up till recently very limited. Tindle and Pearce (1981, 1983) have analyzed the diorite and granodiorite rocks from the Loch Doon Complex. They have yielded shallow profiles with La/Yb ratios of 10.3 and have negative Eu anomalies. Loch Doon is thought to be the result of in-situ fractional crystallization and the distribution of REE is controlled mainly by minor,phases such as apatite, zircon, sphene and allanite.

The Lorne and Sidlaw andesite lavas (Thirlwall 1982) display smooth, steeper profiles with La/Yb ratios of 29, which fall within the ranges of the Strontian granites, xenoliths and diorites. The Sidlaw lavas show an increase in the LREE/HREE ratio with increasing silica, which is the opposite to Strontian (Pankhurst 1979). The Sidlaw is a feature typical of a magma undergoing fractional crystallization of ol, cpx, plag, a situation where the REE are behaving essentially as incompatible elements. The Strontian trend indicates compatible behaviour of REE requires crystallization of REE-bearing amphiboles and/or REE bearing accessories. The wide variation in the xenoliths, in which phenocryst cumulates are low, again points to the derivation of xenoliths from different magma sources.

12.3.4 Review of Mineralogy

Although the rock types of Strontian have retained their original igneous texture, the mineralogy is thought to have undergone changes.

This is particularly evident in the ferromagnesian mineralogy where the amphiboles are quite often secondary aggregates pseudomorphing equant or particular patches. Overall there is a similarity and overlap between the xenoliths and host granite mineral assemblage and composition, in spite of the wide range of bulk rock compositions. The mafic diorite minerals show a somewhat different range especially in the mafic minerals, where the MgO/MgO+FeO* ratio is greater than the mafic minerals of the hosts and xenoliths.

The feldspars in the Strontian complex are predominantly sodic , with compositional ranges An20-58 (diorites), An22-54 (xenoliths) and An22-42 (granites), which overall display quite uniform patterns. If the main groups are divided into two using silica content, even then the An content overlaps considerably:

DIORITES	48 to 50% SiO_2	-	An20-54
	52 to 55% SiO_2	-	An20-58
XENOLITHS	52 TO 59% SiO_2	-	An24-45
	60 TO 68% SiO_2	-	An22-54
GRANITES	60 to 64% SiO_2	-	An29-40
	65 to 70% SiO2	-	An22-42

The ferromagnesian minerals, hornblende and biotite, display a wide range of habits and compositions throughout the rock types of Strontian. As a result of this complexity, the hornblendes cannot be all in equilibrium. This has also been noted in the xenoliths, granodiorites and diorites, where particularly biotite is a subsolidus assemblage, eg. in the Ranachan diorite - sample D41 - shows magmatic and subsolidus reaction between an original Ti-bearing hornblende and K-bearing fluids, which lead to the

formation of a new amphibole (possibly not hornblende) and biotite. This seen as 2 sorts of biotite (Plate 10.1C & 10.8C) where a) the zone of biotite with a basal pinacoid parallel to the hornblende front pinacoid (also seen in some Appin diorites) & b) discordant, irregularly oriented biotite plates. They are all pseudomorphs of a mineral with an elongate, prismatic habit.

The hornblende geobarometer of Hammarstrom & Zen (1985) uses Aliv in hornblendes from calc-alkaline assemblages. Although Aliv is temperature dependent, this cannot solely account for the differences in Aliv content between low and high pressure composition, pressure is thought to be a dominant factor (Hammarstrom & Zen 1986). The pressures estimated from hornblende in chapters 3, 6, 8 and 10, range from <1 to 5 kb. The pressure range for the hornblendes is wider than that reported by Ashworth & Tyler (1983) of 4.7 to 4.1 +/- 0.4 kbar for the aureole. The maximum values are similar to Ashworth & Tyler's only for the granites. The others have values that are too low or even negative.

The wide range of amphiboles represented in each slide cannot all be in equilibrium with each other. Similarly they may not all be magmatic or all have been formed in equilibrium with quartz. The replacement amphiboles are metamorphic or subsolidus rather than igneous in many cases. Further screening of amphiboles used is required, because of the wide range of amphiboles present in each sample. First actinolitic hornblendes were removed from the amphibole data. This is because they are derived from cpx and are low temperature. The results are that all the pressures of less than 1kb no longer exist and that the total ranges become more limited (still starting from around 1kb). If only non-actinolitic

rim compositions are used in calculation (these can be immediately adjacent to quartz), granite and xenolith values range from 1.1 to 3.0kb. Rims however are also likely to be post-magmatic since diorite amphiboles are often actinolites or actinolitic hornblendes they cannot be used in any way. It is concluded that the range of pressures calculated initially may include real values, but the extent of recrystallization is such that it is difficult to extract these from the entirely spurious ones.

12.3.5 Isotope data

No new isotope analyses have been undertaken in this study, but the available published data on isotope variation can be integrated with new geochemical data. Halliday et al (1979), Hamilton et al (1984) and Holden et al (1987) provide the bulk of the data on $^{87}Sr/^{86}Sr$ and $^{143}Nd/^{144}Nd$, which is summarized in Table 12.1. This mostly relates to the granites and a few xenoliths, but there is no data on the diorites. The age of the complex is taken as 423 =/-3Ma (Rogers & Dunning 1991). Rogers & Dunning also reported a zircon age of 425+/-3 and the existence of inherited zircons in this granodiorite sample. Inherited zircon was reported in the BGT by Halliday et al (1979), although they did not recognize the inherited component in the PGD. Fig.12.23 (ENd vs $^{87}Sr/^{86}Sr$) shows the tie-lines joining host rock to xenolith and having no consistent slope. This suggests that the host has not equilibrated with the xenoliths from a single homogeneous source. The xenoliths have a higher initial Nd ratio which also rules out a cogenetic origin for these xenoliths, unless the host has been contaminated with low ENd material (Holden et al 1987).

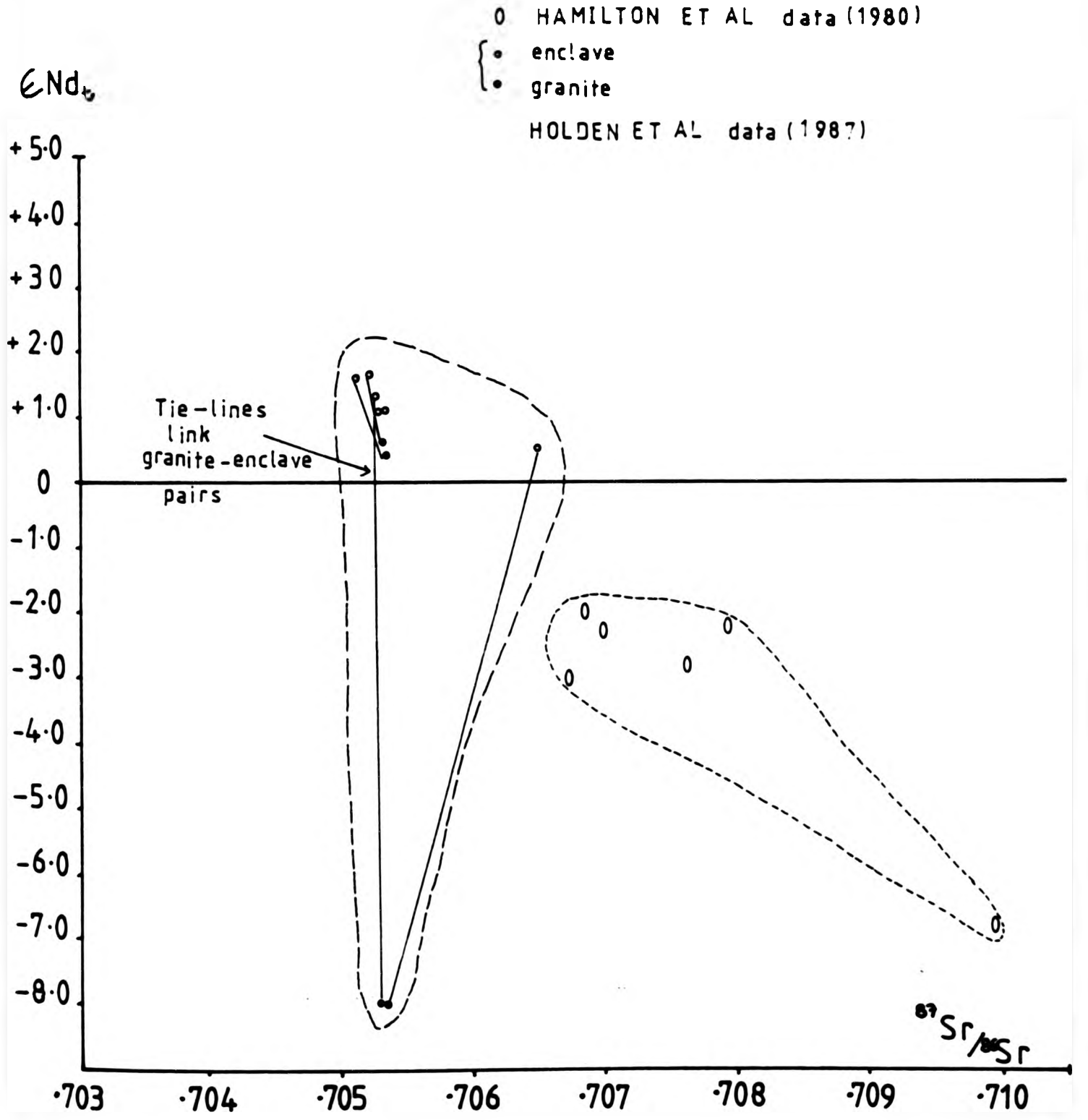

Fig. 12·23 ϵNd vs $^{87}Sr/^{86}Sr$ initial ratios for Strontian host rocks & enclaves. Using the 435 Ma calculated data.

TABLE 12.1 ND AND SR DATA FOR STRONTIAN FROM VARIOUS AUTHORS

Samples	$^{87}Sr/^{86}Sr$		$^{143}Nd/^{144}Nd$	G.Ref.
Age	435 Ma	423 Ma		
1194 PGD	.70612	.705398	-	NM 821608
1840 BGT	.71074	.707184	-	NM 809553
1841 PGD	.70624	.705356	-	NM 780560

from Halliday et al 1979.

Samples	$^{87}Sr/^{86}Sr$		$^{143}Nd/^{144}Nd$
Age	435 Ma	423 Ma	
o202 TGD	.70686	.705515	.512372
o203 TGD	.70700	.706007	.512292
o205 PGD	.70764	.705883	.512240
o207 PGD	.70624	.705368	.512450
o210 PGD	.70795	.705576	.512320
o208 BGT	.70980	.707199	.512050
o212 TGD	.70652	.705716	-
o200 TGD	.70687	.705631	-
o201 PGD	.70621	.705362	-
o204 PGD	.70630	.705292	-
o209 PGD	.70758	.705712	-

from Hamilton et al 1980.

Samples	$^{87}Sr/^{86}Sr$		$^{143}Nd/^{144}Nd$
Age	435 Ma	423 Ma	
SG10X	.70713	.703373	.512446
SG10G TGD	.70606	.704619	.512372
SG38X	.70684	.703805	.512426
SG41X	.70656	.704047	.512417
SG41G PGD	.70613	.704566	.512309
SG45X	.70737	.704764	.512364
SG45G PGD	.70535	.704645	.512381
SG53X	.70706	.703158	.512427
SG53G PGD	.70613	.704574	.512382

from Holden et al 1987.

The Hamilton and Holden data can be recalculated to give $^{87}Sr/^{86}Sr$ from 423 Ma, which shows a slightly greater range and higher values than those using a Strontian age of 435 Ma. Initial Sr isotopic ratios for whole rock samples and host-enclave pairs is .703149 to .704758, which is lower and wider than quoted by Holden et al (.7051 to .7061; 1987). Sr isotopes were calculated using the "isochron equation" in Cox, Bell & Pankhurst (1979) and using the new Strontian age of 423 Ma (from Rogers & Dunning 1991). They fit within the range of granite initial 87Sr/86Sr ratios found in Cox,

Bell & Pankhurst of .700 to .740.

Hamilton et al (Fig.2 1980) shows 2 BGT analyses lying on a line subparallel to the 435 reference isochron, but with an initial ratio of > .707, compared with the .70534 to .705978 (Table 3 1980). This tends to minimize the time difference between the BGT and PGD, but emphasizes the isotopic differences. Fig.12.24 has plotted the Rb/Sr data and shows the difference.

For the Holden data (1987) the xenoliths are different from their host in terms of ENd, therefore simple magmatic relations by fractional crystallization are not possible. The origin must be independent or is related by some contamination mechanism. This is consistent with geochemical evidence provided here, that only a handful of xenoliths are likely to be immediate parents of the granites.

The Holden et al (1987) initial $^{87}Sr/^{86}Sr$ ratios in the TGD and PGD range from .70533 to .70605 using 435 Ma. This has been calculated to .70456 to .70464 using 423 Ma however. The Hamilton et al (1980) initial Sr isotopic data ranges from .70621 to .70795, while recalculations give a range of .70529 to .70600. This is outside the range expected and indicates the heterogeneity at isotopic level that may be similar to the heterogeneity shown by Ba, Rb, Li, K_2O etc interms of chemical variation. It indicates that a) if the TGD and PGD were each wholly fluid magma chambers, then they come from a heterogenous source and have undergone insufficient convection to fully blend the composition; b) the TGD and PGD may have been built up in stages of successive pulses of various magmas or c) an existing body of melt or crystal-melt system must have been locally

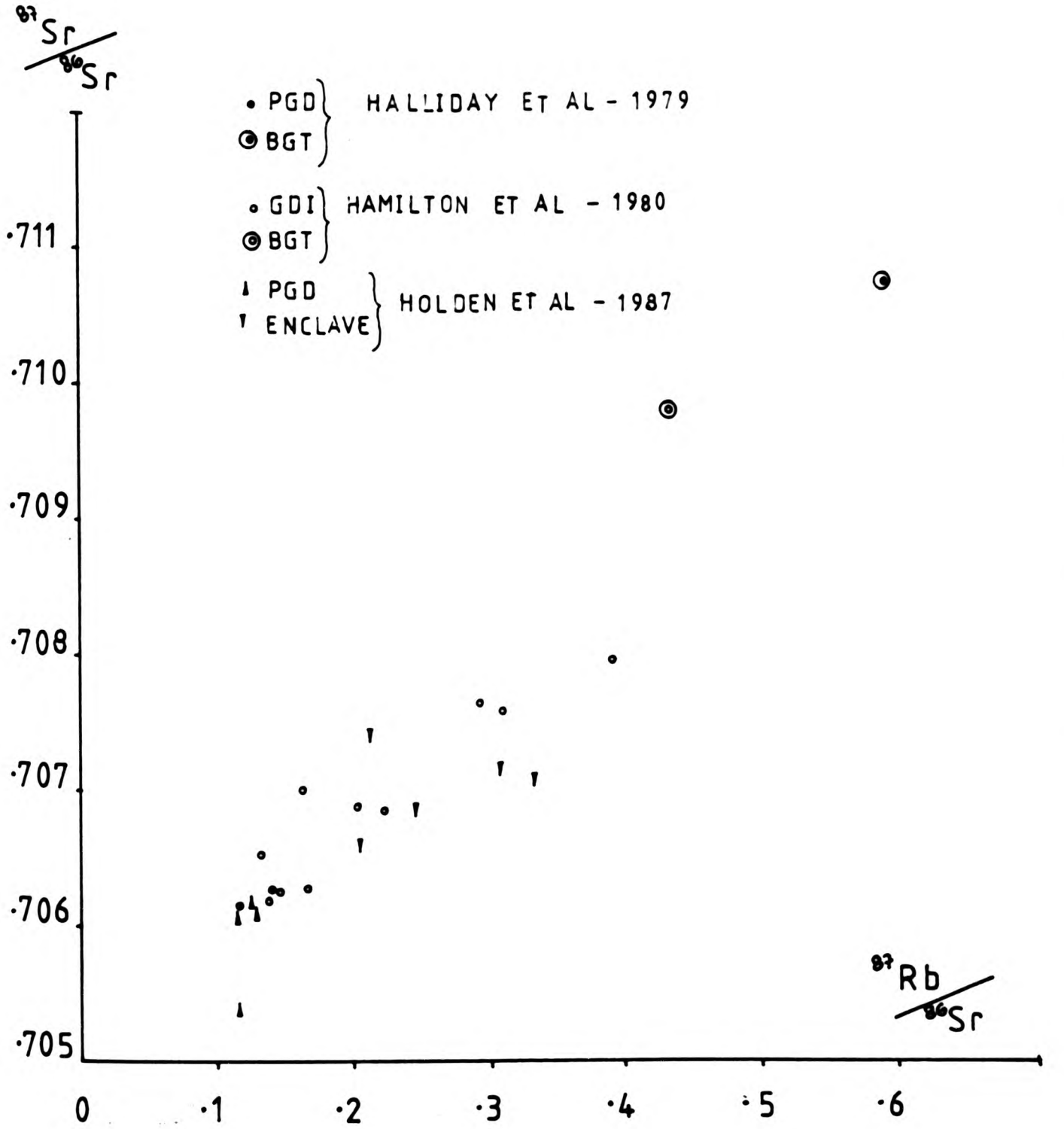

Fig. 12·24 Rb/Sr isochron for all reported Strontian data.

mixed with other materials eg. the dioritic xenoliths. A succession of cycles of injection of synplutonic dykes or plugs which then mobilize the host rock, break and subside, leaving only local xenolith swarms, could generate this kind of heterogeneity.

12.4 CONCLUSIONS

The study of the Strontian Complex reveals that the tonalitic and porphyritic granodiorites are petrographically and geochemically related. On a large scale they appear to have been intruded as a large single intrusion, but detailed geochemistry shows them to be heterogenous. The biotite granite though lying on the same geochemical trend in may cases, is however a separate intrusive event into a still warm granodioritic pluton (due to the lack of any significant chilling). The later biotite granite and ctG sheets are also intrusive events into a warm host.

The geochemical data displays the remarkable linear trends for the xenoliths and granitic host rocks, including the porphyritic alkali granitic sheets. The detailed considerations of geochemistry however shows considerable heterogeneity in the granites and diorites and some elememts show critical "dog-leg" or curved trends that limit the extent of mixing. However modelling magma evolution by fractional crystallization is only partly successful indicating that both processes are likely to have operated.

The integration of xenolith-diorite-granite data in this chapter shows that most xenolith magmas are not suitable parents for diorites or granitic rocks. The isotope data of Holden et al (1987) supports this concusion. Further it is difficult to derive the wide

range of silica-poor xenoliths from each other by fractionation or mixing. It is concluded that different source magmas were available for injection to form the various xenolith compositions.

The normative data shown on Fig.3.7 shows that the TGD points fall onto the quartz-feldspar cotectic. This suggests that both quartz and plagioclase were available as xenocrysts and both have been seen as xenocrysts in the xenoliths. Therefore a TGD liquid could also ahve been available as a contaminant for the xenoliths as well as the alkali granite.

The mafic diorites, though contrasting greatly with the main xenolith-granite trend, display cumulate assemblages. All the diorite bodies appear separate rather than part of a single large body. The Uileann diorites present in the biotite granite have similar mineralogy to the mafic diorites in the granodiorite host.

However their complex net-veining/mixing relationships with the biotite granite suggest they were intruded contemporaneously with and not by the biotite granite. The varied petrography and mineralogy present in the Strontian rocks suggests a variety of processes at work.

The tonalitic and porphyritic granodiorites being part of one and the same intrusion, followed by the formation of the biotite granite by fractional crystallization. The later granitic sheets (ctG and fG), xenoliths and microdiorite dykes are more likely to have been mixed at depth than at the present level of exposure. The mafic diorites, though clearly in many cases formed by accumulation, have also been noted (especially Uileann) as being the result of mixing

and/or contamination. Therefore if mixing took place at depth, there must be a source of more acidic/granitic and basic material available. However this would not simply account for all the rock types exposed. Dioritic material for the xenoliths and microdiorite dykes must have been available already, as was a quartz phenocryst-rich component, which were both ready for mixing, while the magma chamber was fractionating the granodiorites.

Therefore effectively the pluton was functioning as a conduit for a variety of magmas which had mixed to various degrees.

12.5 FUTURE WORK

It is clear from this investigation that there is considerable scope for further work on this interesting pluton. Some suggested avenues for field, minerlogical, isotopic and geochemical studies are outlined below:

1. Field

Field observations and sampling of xenoliths and diorites.

Progress in the history of hybridization could result from the study of xenolith within xenolith and field sections along additional traverses could be made to search them out. Further field investigations for more information on contamination/hybridization investigations of the margins of the diorites. The collection of new samples, especially of xenoliths within xenoliths. Mapping in even greater detail the diorite bodies and the xenoliths.

Further investigations of the microdiorite dykes along new traverses, to see if there are any that show fragmented margins, so contributing to the xenolith assemblage.

2. Mineralogy

Few phenocryst feldpsars were encountered on probed slides and they are important as they may preserve important details of the history of mixing. Further electron microprobe work must have a programme set out to search out and analyze feldspar phenocrysts from the xenoliths, ctG sheets and diorites for comparison with feldspars in the host rocks.

The variation in biotite/ amphibole compositions is likely to record the progress of retrograde cooling and metamorphism. Systematically mapping the chemical variations in single crystals, aggregates and jacketed brown hornblendes may help to analyse the later history. Some of more abundant trace elements must reach substantial concentration in some minerals if partition coefficients and bulk rock analyses are a reliable guide. Some of these concentrations should be in excess of microprobe detection limits eg. Ba & Sr in feldspars; REE in apatite and sphene; Ni & Cr in hornblende and biotite. Determination of these at or near the sites used for major element analysis would provide much better constraints on the trace element modelling.

It has been shown that apatite and biotite contain significant amounts of fluorine. Since fluorine has a significant effect on the stability of hydrous minerals, the determination of F in amphiboles - the dominant ferromagnesian phase, should figure in any future

investigation. Mobilization of F and formation of fluorite, often accompanies mineralization in granites, so the behaviour of F in subsolidus amphibole reactions may be a sigificant feature in explaining the conspicuous lack of Caledonian mineralization at Strontian.

3. Isotope studies

Pankhurst (1979) gives a pseudoisochron for $^{87}Sr/^{86}Sr$ and indicates a range of initial isotope patterns and this has been re-inferred by discussion here. This may point to incomplete pluton-scale homogenization. The variation in SiO_2 in the granodiorites is not directly related to the pluton margins, but shows spatial inhomogeneity. Wide variation in Ba, Li, etc also indicates inhomogeneity. There is a scatter of $^{87}Sr/^{86}Sr$ initial ratios (.704562 to .707186), which also points to inhomogeneity. If this inhomogeneity is real then it has important petrological implications. Detailed geochemical studies of continuously well exposed TGD and PGD sections could be made to study the scale of inhomogeneity and establish whether compositions are continuously variable or the body is a mass of domains that are internally uniform. Existing isotope studies are not tied to fully analyzed samples and so the consideration of isotope systematics is partly decoupled from the geochemistry at present. New isotope work should incorporate the full chemical analyses of the samples to rectify this decoupling.

It is clear that the xenoliths are derived from diverse igneous sources and these need individual investigation. The diorites have not been subject to any isotope study at all. The bulk chemistry

suggests that these also have more than one parent and, although the bulk composition suggests mantle origins, isotope studies would help to characterize the source regions.

Existing isotope work (Pankhurst, 1979 and Rogers, 1991) indicates some crustal component in the granitic rocks. Contamination with crust will partly mimic contamination/mixing with relatively acid igneous rocks in bulk chemistry, but can produce a distinctive isotopic signature. Crustal contamination cannot be addressed effectively in this work but Rb/Sr, Sm/Nd, U/Pb etc can place constraints on its importance. The clearly established subsolidus mineralogy shows that the pluton cooled slowly. With a coarse grained assemblage of amphibole, biotite, sphene, apatite, zircon these rocks provide ideal materials for looking at the cooling and uplift history of the region using isotopic dates. K/Ar dates indicate final cooling circa 400Ma in this part of the orogenic belt, 25 Ma after the granite emplacement, if the Rodgers (1991) date is used.

4. Geochemistry

Further geochemical analyses would provide further material for interpretation and fill in the gaps. This would involve elements such as Zr and Ta together with more REE samples. In spite of the evidence of inherited zircons, Zr may provide a better index of fractionation than SiO_2. Boron is probably wholly incompatible, as there is virtually no tourmaline in these rocks. It too should be investigated as a possible index of fractionation.

REFERENCES

Albuquerque,C.A.R.de, 1971, Petrochemistry of a series of granitic rocks from Northern Portugal: Bull.Geol.Soc.Am., v.82, pp.2783-2798.

Albuquerque,C.A.R.de, 1973, The origin of enclaves in granitic rocks from Northern Portugal: Spec.Publ.G.Soc.S.Af., v.3, pp.479-493.

Albuquerque,C.A.R.de, 1973, Geochemistry of biotites from granitic rocks, Northern Portugal: Geochim. Cosmochim. Acta., v.37, pp.1779-1802.

Albuquerque,C.A.R.de, 1974, Geochemistry of actinolitic hornblendes from tonalitic rocks, Northern Portugal: Geochim. Cosmochim. Acta., v.88, pp.789-803.

Allegre,C.J.,& Minster,J.F., 1978, Quantitative models of trace element behaviour in magmatic processes: Ear.Pl.Sci.Lett., v.38, pp.1-25.

Anderson,A.T., 1970, The hybrid andesite of East Sand Butte, Modoc County, California (abstract): Geol.Soc.Am.Annual Meet., Milwaukee, 1967

Anderson,A.T., 1976, Magma mixing:Petrological process and volcanological tool: J.Volc.& Geotherm.Res., v.3, pp.3-33.

Anderson,J.G.C., 1935, The Arrochar Intrusive Complex: Geol.Mag., v. lxxii, pp.263-283.

Anderson,J.G.C., 1935, The marginal intrusions of Ben Nevis: Trans.Geol.Soc.Glasg., v.19, pp.225-269.

Anderson,J.G.C., 1937, The Etive granite Complex: Q.J.G.S., v.xcii(4), pp.487-533.

Arth,J.G., 1976, Behaviour of trace elements during magmatic processes - A summary of theoretical models and their applications: J.Res.U.S.Geol.Surv., v.4(1), pp.41-47.

Arth,J.G.,& Barker,F., 1976, Rare earth partitioning between hornblende and dacitic liquid and implications for the genesis of trondhjemitic-tonalitic magmas: Geology, v.4, pp.534-536.

Arth,J.G., Barker,F., Peterman,Z.E.,& Friedman,I., 1978, Geochemistry of the Gabbro-Diorite-Tonalite-Trondhjemite suite of SW Finland and its implications for the origin of tonalitic anf trondhjemitic magmas: J.Pet., v.19(2), pp.289-316.

Arth,J.G.,& Hanson,G.N., 1972, Quartz diorites derived by partial melting of eclogite or amphibolite at mantle depths: Contrib.Min.Pet., v.37, pp.161-174.

Ashworth,J.R.,& Tyler,I.M., 1983, The distribution of metamorphic temperatures around the Strontian Granodiorite: Geol.Mag., v.120(3), pp.281-290.

Atherton,M.P.,& Tarney,J., 1979, Origin of granite Batholiths: Geochemical evidence: Shiva Publishing.

Bailey,E.B., 1960, The geology of Ben Nevis and Glen Coe: Mem.Geol.Surv.U.K.

Bailey,J.C., 1984, Geochemistry and origin of hornblende-bearing xenoliths in the I-type Petford granite, north-east Queensland: Aust.J.of Earth Sci., v.31, pp.7-23.

Bailey,S.W., 1984, Micas: Reviews in Mineralogy Min.Soc.Am., v.13.

Banks,R., 1979, The use of linear programming in the analysis of petrological mixing problems: Contrib.Min.Pet., v.70, pp.237-244.

Barker,F.,& Arth,J.G., 1976, Generation of trondhjemitic-tonalitic liquids and Archaen bimodal trondhjemitic-basalt suites: Geol., v.4, pp.596-600.

Barnes, C.G., 1983, Petrology and upward zonation of the Wooley Creek Batholith, Klamath Mts, California: J.Pet., v.24(4), pp.495-537.

Bateman,P.C.,Clark,L.D.,Huber,N.K.,Moore,J.G.,& Rinehart.C.D 1963, The Sierra Nevada Batholith - A synthesis of recent work across the central part: Geol.Surv.Prof.Paper 414-D, U.H.,1979, Microstructural evidence for the origin of xenoliths in an I-type pluton of the New England Batholith: From: Crust and Upper Mantle of Southeast Australia, Summary of Symposium, Canberra Bureau of Mineral Resources, Australia.

Bateman,P.C.,& Dodge,F.C.W., 1970, Variations of major chemical consituents across the Central Sierra Nevada Batholith: Geol.Soc.Am.Bull., v.81, pp.409-420.

Bateman,P.C.,& Nockleberg,W.J., 1978, Solidification of the Mount Givens Granodiorite, Sierra Nevada, California: J.Geol., v.86, pp.563-579.

Bateman,P.C.,& Chappell,B.W., 1979, Crystallization, fractionation and solidification of the Tuolumne Intrusive series, Yosemite National Park, California: Geol.Soc.Am.Bull., v.90(1), pp.465-482.

Baxter,A.N., Upton,B.G.J.,& White,W.M., 1985, Petrology and geochemistry of Rodrigues Island, Indian Ocean: Contrib.Min.Pet., v.80, pp.90-101.

Bender,J.F., Hanson,G.N.,& Bence,A.E., 1982, The Cortlandt complex: evidence of large-scale liquid immiscibility involving granodiorite and diorite magmas: Ear.Pl.Sci.Lett., v.58, pp.330-344.

Berlin,R.,& Henderson,C.M.B., 1968, A re-interpretation of Sr and Ca fractionation trends in plagioclases in basic rocks: Ear.Pl.Sci.Lett., v.4, pp.79-83.

Best,M.G., 1963, Petrology of the Guadalupe Igneous Complex, SW Sierra Nevada foothills, California: J.Pet., v.4, pp.223-259.

Best,M.G.,& Mercy,E.L.P., 1967, Composition and crystallization of mafic minerals in the Guadalupe Igneous Complex, California: Am.Min., v.52, pp.436-474.

Binns,R.A., 1965, Hornblendes from basic hornfelses in the New England region, New South Wales: Min.Mag., v.34, pp.52-65.

Bishop,A.C., 1964, Dark margins at igneous contacts. A critical study with special reference to those in jersey, Channel Islands: Proc.Geol.Assoc., v.74(3), pp.289-300.

Bishop,A.C.,& French,W.J., 1982, Nature and origin of meladiorite layers in northern Guernsey, Channel Islands: Min.Mag., v.46, pp.301-321.

Blake,D.H., Elwell,R.W.D., Gibson,I.L., Skelhorn,R.R.,& Walker,G.P.L., 1965, Some relationships resulting from the intimate association of acid and basic magmas: Q.J.G.S., v.121, pp.31-49.

Blaxland,A.B., Aftalion,M.,& van Breemen,O., 1979, Pb isotopic composition of feldspars from Scottish Caledonian Granites, and the nature of the underlying crust: Scott.J.Geol., v.15(2), pp.139-151.

El Bouseily,A.M.,& El Sokkary,A.A., 1975, The relation between Rb, Ba and Sr in granitic rocks: Chem.Geol., v.16, pp.207-219.

Bottinga,Y., Kudo,A.,& Weill,D., 1966, Some observations on oscillatory zoning and crystallization of magmatic plagioclase: Am.Min., v.51, pp.792-806.

Bowden,P.,& Whitley,J.E., 1974, Rare-earth patterns in peralkaline and associated granites: Lithos, v.7, pp.15-21.

Bowes,D.R., Kinloch,E.D.,& Wright,A.E., 1964: Min.Mag., v.33, pp.963-973.

Bowes,D.R.,& McArthur,A.C., 1976, Nature and genesis of the Appinite suite: Krystalinikum, v.12, pp.31-46.

Brewer,M.S., Brook,M.,& Powell,D., 1979, Dating the tectono-metamorphic history of the southwestern Moine, Scotland: The Caledonides of the British Isles - reviewed.Geol.Soc.Lond., pp.129-137.

Briqueu,L.,& Lancelot,J.R., 1979, Rb-Sr systematics and crustal contamination models for calc-alkaline igneous rocks: Ear.Pl.Sci.Lett., v.43, pp.385-396.

Brooks,C.K., 1968, On the interpretation of trends in element ratios in differentiated igneous rocks, with particular reference to strontium and calcium: Chem.Geol., v.3, pp.15-20.

Brook,M., Powell,D.,& Brewer,M.S., 1977, Grenville events in Moine rocks of the Northern Highlands, Scotland: J.G.S.Lond., v.133, pp.489-496.

Brown,G.C., 1979, Geochemical and geophysical constraints on the origin and evolution of Caledonian granites: The Caledonides of the British Isles - reviewed. Geol.Soc. Lond., pp.645-651.

Brown,G.C., Cassidy,J., Tindle,A.G.,& Hughes,D.J., 1979, The Loch Doon granite: an example of granite petrogenesis in the British Caledonides: J.G.S.Lond., v.136, pp.745-753.

Brown,G.C.,& Locke,C.A., 1979, Space-time variations in British Caledonian granites: Some geophysical correlations: Ear.Pl.Sci.Lett., v.45, pp.69-79.

Brown,G.C., Cassidy,J.,& Locke,C.A., Plant,J.A.,& Simpson P.R., 1981, Caledonian plutonism in Britain:- summary: J.Geophys.Res., v.86, pp.10502-10514.

Brown,M., Topley,C.G.,& Power,G.M., 1980, The origin of the dioritic and associated rocks of Chouet, NW Guernsey, Channel Islands: Min.Mag., v.43, pp.919-930.

Brown,P.E., Miller,J.A.,& Grasty,R.L., 1968, Isotopic ages of late Caledonian Granitic intrusions in the British Isles: Proc.York.Geol.Soc., v.36(3), pp.251-276.

Brown,R.L., Dalziel,I.W.D.,& Johnson,M.R.W., 1970, A review of the structure and stratigraphy of the Moinian of Ardgour, Moidart and Sunart - Argyll and Inverness-shire: Scott.J.Geol., v.6(3), pp.309-335.

Buddington,A.F.,& Leonard,B.F., 1953, Chemical petrology and mineralogy of hornblendes in NW Adirondack granitic rocks: Am.Min., v.38, pp.891-902.

Cantagrel,J-M., Didier,J.& Gourgaud,A., 1984, Magma mixing: origin of intermediate rocks and enclaves from volcanism to plutonism: Phys.Ear.Pl.Inter., v.35, pp.63-76.

Carmichael,I.S.E., 1964, The petrology of Thingmuli, a Tertiary volcano in eastern Iceland: J.Pet., v.5, pp.435-460.

Carmichael,I.S.E., Turner,F.J.& Verhoogen,J., 1974, Igneous Petrology. publ.McGraw-Hill Intern.

Cawthorn,R.G., 1976, Some chemical controls on igneous amphibole compositions: Geochim. Cosmochim. Acta. v.40, pp.1319-1328.

Cawthorn,R.G., 1976, Calcium-poor pyroxene reaction relations in calc-alkaline magmas: Am.Min., v.61, pp.907-912.

Cawthorn,R.G.,& O'Hara,M.J., 1976, Amphibole fractionation in calc-alkaline magma genesis: Am.J.Sci., v.276, pp.309-329.

Chappell,B.W., 1978, Granitoids from the Moonbi District, New England Batholith, E.Australia: J.G.S.Aust., v.25(5), pp.267-283.

Chappell,B.W.,& White,A.J.R., 1974, Two contrasting granite types: Pac.Geol., v.8, pp.173-174.

Chappell,B.W., White,A.J.R.,& Wyborn,D., 1987, The importance of residual source material (restite) in granite petrogenesis: J.Pet., v.28(6), pp.1111-1138.

Clayburn,J.A.P.,Harmon,R.S.,Pankhurst,R.J.,& Brown,J.F., 1983 Sr, O and Pb isotope evidence for origin and evolution of Etive Igneous Complex, Scotland: Nature, v.303, pp.492-497.

Clifford,T.N., 1957, The stratigraphy and structure of part of the Kintail district of southern Ross-shire: its relation to the Northern Highlands: Q.J.G.S.Lond., v.113, pp.57-92.

Coats,J.S.,& Wilson,J.R., 1971, The eastern end of the Galway Granite: Min.Mag., v.38, pp.138-151.

Cox,K.G., Bell,J.D.,& Pankhurst,R.J., 1981, The interpretation of igneous rocks. publ. Allen & Unwin.

Czamanske,G.K., Ishihara,S.,& Atkin,S.A., 1981, Chemistry of rock forming minerals of the Cretaceous-Palaeocene batholith in south-western Japan and implications for magma genesis: J.Geophys.Res., v.86, pp.10431-10469.

Dalziel,I.W.D.,& Johnson,M.R.W., 1963, Evidence for the geological dating of the granitic gneiss of Western Ardgour: Geol.Mag., v.100(3), pp.244-254.

Dalziel,I.W.D.,& Brown,R.L., 1965, The structural dating of the sillimanite-grade metamorphism of the Moines in Ardgour(Argyll) and Moidart (Inverness-shire): Scot.J.Geol., v.1(3), pp.304-311.

Dalziel,I.W.D., 1966, A structural study of the granitic gneiss of western Ardgour, Argyll and Inverness-shire: Scott.J.Geol., v.2(2), pp.125-152.

Dearnley,R., 1967, Metamorphism of minor intrusions associated with the Newer Granites of the Western Highlands of Scotland: Scot.J.Geol., v.3(3), pp.449-457.

Deer,W.A., 1935, The Cairnsmore of Carsphairn Igneous Complex: Q.J.G.S.Lond., v.91, pp.47-76.

Deer,W.A., 1936, The composition and paragenesis of the biotites of the Carsphairn igneous intrusion: Min.Mag., v.XXV, pp.56-74.

Deer,W.A., 1938a, The diorites and associated rocks of the Glen Tilt Complex, Perthshire. I Granites and Intermediate hybrid rocks: Geol.Mag., v.lxxv, pp.174-184.

Deer,W.A., 1938c, The composition and paragenesis of the hornblendes of the Glen Tilt Complex, Perthshire: Min.Mag., v.XXV, pp.56-74.

Deer,W.A., 1950, The diorites and associated rocks of the Glen Tilt Complex, Perthshire. II Diorites and Appinites. Geol.Mag., v.87, pp.181-195.

Deer,W.A., 1953, The diorites and associated rocks of the Glen Tilt Complex, Perthshire, pt.3. Geol.Mag., v. 90, pp.27-35.

Deer,W.A., Howie,R.A.,& Zussman,J.,(1962), An introduction to the rock-forming minerals: publ. Longman (also 1982).

DePaolo,D.J., 1981, Trace element and isotopic effects of combined wallrock assimilation and fractional crystallization: Ear.Pl.Sci.Lett., v.53, pp.189-202.

Didier,J., 1973, Granites and their enclaves: The bearing of enclaves on the origin of granites: publ. Elsevier Scientific Publ Co.

Dodge,F.C.W., 1972, Trace element contents of some plutonic rocks of the Sierra Nevada Batholith: Geol.Surv.Bull., 1314-F, pp.F1-F13.

Dodge,F.C.W., Papike,J.J.,& Mays,R.E., 1968, Hornblendes from granitic rocks of the central Sierra Nevada Batholith, California: J.Pet., v.9(3), pp.378-410.

Dodge,F.C.W., Smith,V.C.,& Mays,R.E., 1969, Biotites from granitic rocks of the central Sierra Nevada Batholith, California: J.Pet., v.10(2), pp.250-271.

Drake,M.J., 1975, The oxidation state of europium as an indicator of oxygen fugacity: Geochim.Cosmochim.Acta., v.39, pp.55-64.

Ehlers,E.G., 1972, Interpretation of geological phase diagrams. publ. Freemans.

Eichelberger,J.C., 1974, Magma contamination within the volcanic pile: Origin of andesite and dacite: Geol., v.2, pp.29-33.

Eichelberger,J.C., 1975, Origin of andesite and dacite: Evidence of mixing at Glass Mountain in California and at other circum-Pacific volcanoes: Geol.Soc.Am.Bull., v.86, pp.1381-1391.

Eichelberger,J.C., 1978, Andesitic volcanism and crustal evolution: Nature, v.275, pp.21-27.

Eichelberger,J.C., 1980, Vesiculation of mafic magma during replenishment of silicic magma reservoirs Nature, v.288, pp.446-450.

Engel,C.E., 1959, Igneous rocks and constituent hornblendes of the Henry Mountains, Utah: Bull.Geol.Soc.Am., v.70, pp.951-980.

Ernst,W.G., 1968, Amphiboles:- Crystal chemistry, phase relations and occurrence: Chapters III & VI.

Exley,R.A., 1980, Microprobe studies of REE-rich accessory minerals: Implications for Skye granite petrogenesis and REE mobility in hydrothermal systems: Ear.Pl.Sci.Lett., v.48, pp.97-110.

Fershtater,G.B.,& Borodina,N.S., 1977, Petrology of autoliths in granitic rocks: Inter.Geol.Rev., v.19(4), pp.458-468.

Fleischer,M., 1978, Relation of the relative concentrations of lanthanides in titanite to type of host rocks: Am.Min., v.63, pp.869-873.

Flood,R.H.,& Vernon,R.H., 1978, The Cooma granodiorite, Australia: An example of in situ crustal anatexis: Geol., v.6, pp.81-84.

Flood,R.H.,& Shaw,S.E., 1979, K-rich cumulate diorite at the base of a tilted granodiorite pluton from the New England Batholith, Australia: J.Geol., v.87, pp.417-425.

Flood,R.H.,& Vernon,R.H., 1979, Microstructural evidence for the origin of xenoliths in an I-type pluton of the New England Batholith: Crust and upper mantle of Southeast Australia (compiled by D.Denham) pp.39-41.

Fourcade,S.,& Allegre,C.J., 1981, Trace element behaviour in granite genesis: A case study: The calc-alkaline plutonic association from the Querigut Complex (Pyrenees, France): Contrib.Min.Pet., v.76, pp.177-195.

Fowler,A.D.,& Doig,R., 1983, The significance of europium anomalies in the REE spectra of granites and pegmatites, Mont Laurier, Quebec: Geochim.Cosmochim.Acta., v.47, pp.1131-37

Frey,F.A., Chappell,B.W.,& Roy,S.D., 1979, Fractionation of rare-earth elements in the Tuolumne Intrusive Series, Sierra Nevada Batholith California: J.Geol., v.87, pp.417-425.

Frost,C.D.,& O'Nions,R.K., 1985, Caledonian magma genesis and crustal recycling: J.Pet., v.26(2), pp.515-544.

Furman,T,& Spera,F.J., 1985, Co-mingling of acid and basic magma with implications for the origin of mafic I-type xenoliths: Field and petro-chemical relations of an unusual dike complex at Eagle Lake, Sequoia National Park, California, U.S.A.: J.Vol.Geoth.Res., v.24, pp.151-178.

Gandy,M.K., 1975, The petrology of the Lower Old Red Sandstone lavas of the Eastern Sidlaw Hills, Perthshire, Scotland: J.Pet., v.16(1), pp.189-211.

Gast,P.W., 1965, Terrestrial ratio of potassium to rubidium and the composition of the Earth's mantle: Science, v.147, pp.858-860.

Gerlach,D.C., & Grove,T.L., 1982, Petrology of Medicine Lake Highland volcanics: Characterization of end-members of magma mixing: Contrib.Min.Pet., v.80, pp.147-159.

Goodspeed,G.E., 1948, Xenoliths and skialiths: Am.J.Sci., v.246, no.8.

Grabezhev et al, 1979, refer to S.W.Bailey, 1984.

Green,N.L., 1982, Co-existing calcic amphiboles in calc-alkaline andesites: possible evidence of a zoned magma chamber: J.Vol.Geoth.Res., v.12, pp.57-76.

Green,T.H.,& Ringwood,A.E., 1968, Genesis of the calc - alkaline igneous rock suite: Contr.Min.Pet., v.18, pp.105-162.

Green,T.H.,& Pearson,N.J., 1986, REE partitioning between sphene and co-existing silicate liquids at high pressure and temperature: Chem.Geol., v.55, pp.105-119.

Griffin,T.J., White,A.J.R.,& Chappell,B.W.,1978, The Moruya Batholith and geochemical constraints between the Moruya and Jindabyne Suites: J.Geol.Soc.of Aust., v.25(4), pp.235-247.

Gromet,L.P.,& Silver,L.T., 1983, Rare earth element distribution among minerals in a granodiorite and their petrogenetic implications: Geochim.Cosmochim.Acta., v.47, pp.925-939

Groome,D.R.,& Hall,A., 1974, The geochemistry of the Devonian lavas of the northern Lorne Plateau, Scotland: Min.Mag., v.39, pp.621-640.

Grout,F.F., 1937, Criteria of origin of inclusions in plutonic rocks: Bull.Geol.Soc.Am., v.48, pp.1521-1572.

Hall,A., 1969, Regional variation in the composition of British Caledonian Granites: J.Geol., v.77(4), pp.466-481.

Halliday,A.N., Aftalion,M., van Breemen,O.,& Jocelyn,J.,1979, Petrogenetic significance of Rb-Sr and U-Pb isotopic systems in the 400 Ma old British Isles granitoids and their hosts: The Caledonides of the British Isles-rd. Geological Society of London pp.653-661.

Halliday,A.N., Stephens,W.E.,& Harmon,R.S., 1980, Rb-Sr and O isotopic relationships in 3 zoned Caledonian graniotic plutons, Southern Uplands, Scotland: evidence for varied sources and hybridization of magmas: J.Geol.Soc.Lond., v.137, pp.329-348.

Halliday,A.N., 1984, Coupled Sm-Nd and U-Pb systematics in late Caledonian granites and the basement under northern Britain: Nature, v.307, pp.229-233.

Hamilton,P.J., O'Nions,R.K.,& Pankhurst,R.J., 1980, Isotopic evidence for the provenance of some Caledonian granites:
Nature. v.287, pp.279-284.

Hamilton,W., 1969, The volcanic central Andes, a modern model for Cretaceous batholiths and tectonics of western North America:
Ore.Dep.Geol.Min.Ind.Bull.. v.65, pp.175-184.

Hamilton,W., 1970, Mesozoic California and the underflow of Pacific mantle:
Bull.Geol.Soc.Am.. v.80, pp.2709-2430.

Hammarstrom,J.M.,& Zen,E-an, 1986, Aluminum in hornblende: An empirical igneous geobarometer:
Am.Min.. v.71, pp.1297-1313.

Hanson,G.N., 1978, The application of trace elements to the petrogenesis of igneous rocks of granitic composition:
Ear.Pl.Sci.Lett.. v.38, pp.26-43.

Hanson,G.N.,& Langmuir,C.H., 1978, Modelling of major elements in mantle-melt systems using trace element approaches:
Geochim.Cosmochim.Acta.. v.42, pp.725-741

Harry,W.T., 1950, Aluminium replacing silicon in some silicate lattices:
Min.Mag.. v.29, pp.142.

Harry,W.T., 1953, The composite granitic gneiss of western Ardgour, Argyll:
Q.J.G.S.. v.109(3), pp.285-308.

Haslam,H.W., 1968, The crystallization of Intermediate and Acid magmas at Ben Nevis, Scotland:
J.Pet.. v.9(1), pp.84-104.

Haslam,H.W.,1970, Appinite xenoliths and associated rocks from the Ben Nevis igneous complex:
Geol.Mag.. v.107, pp.341-356.

Henderson,C.M.B., 1966, Chemistry of hastingsitic amphiboles from the Marangudzi Igneous Complex, Southern Rhodesia:
Proc.5th.Int.Min.Assoc.. pp.291-304.

Henderson,P., 1980, Rare earth element partition between sphene, apatite and other coexisting minerals of the Kangerdlugssuaq Intrusion, E.Greenland:
Contrib.Min.Pet.. v.72, pp.81-85.

Henderson,P., 1984, REE in Geochemistry (Developments in Geochemistry 2):
Chapter 2 and 4.
Publ. Elsevier.

Hibbard,M.J., 1981, The magma mixing origin of mantled feldspars:
Contrib.Min.Pet., v.76, pp.158-170.

Higazy,Riad A., 1954, The trace elements of the plutonic complex of Loch Doon (Southern Scotland) and their petrogenetic significance:
J.Geol., v.62, pp.172-181

Higuchi,H.,& Nagasawa,H., 1969, Partition of trace elements between rock-forming minerals and the host volcanic rocks:
Ear.Pl.Sci.Lett., v.7, pp.281-287.

Hine,R., Williams,I.S., Chappell,B.W.,& White,A.J.R.,1978, Contrasts between I- and S-type granitoids of the Kosciuszko Batholith:
J.Geol.Soc.of Aust., v.25(4), pp.219-234.

Hollister,L.S., Grissom,G.C., Peters,E.K., Stowell,H.H.,& Sisson,V.B., 1987,
Confirmation of the empirical correlation of Al in hornblende with pressure of solidification of calc-alkaline plutons:
Am.Min., v.72, pp.231-239.

Holloway,J.R.,& Burnham,C.W., 1972, Melting relations of basalt with equilibrium water pressure less than total pressure:
J.Pet., v.13, pp.1-29.

Hubbard,F.H.,& Whitley,J.E., 1978, Rapakivi granite, anorthosite and charnokitic plutonism:
Nature, v.271, pp.439-440.

Hutton,D.H., 1988, Granite emplacement mechanisms and tectonic controls: inferences from deformation studies:
Trans.Roy.Soc.Edin: Earth Sciences, v.79(2&3), pp.245-255.

Hyndman,D.W.,& Foster,D.A., 1988, The role of tonalites and mafic dikes in the generation of the Idaho Batholith:
J.Geol., v.96, pp.31-46.

Jakes,P.,& White,A.J.R., 1972, Hornblendes from calc-alkaline volcanic rocks of island arcs and continental margins:
Am.Min., v.57, pp.887-902.

Johnson,M.R.W.,& Dalziel,I.W.D., 1966, Metamorphosed Lamprophyres and the Late Thermal History of the Moines:
Geol.Mag., v.103(3), pp.240-249.

Johnstone,G.S., Smith,D.I.,& Harris, 1969, The Moinian assemblage of Scotland:
in:North Atlantic:geology and cont. drift
Am.Ass.Pet.Geol.Mem.12. pp.159-180.

Joplin,G.A., 1935, A note on the origin of Basic xenoliths in plutonic rocks, with special reference to their grain size:
Geol.Mag., v.72, pp.227-234.

Joplin,G.A., 1959, On the origin and occurrence of basic bodies associated with discordant bathyliths:
Geol.Mag., v.xcvi(5), pp.351-373.

Karner,F.R., 1968, Two generations of sphene in Trunk Lake Granite, Southeastern Maine:
Proc.N.Dak.Acad.Sci., v.22, pp.96-103.

Kolbe,P.& Taylor,S.R., 1966, Major and trace element relationships in granodiorites and granites from Australia and South Africa:
Contr.Min.Pet., v.12, pp.202-222.

Koljonen,T.,& Rosenberg,R.J., 1974, REE in granitic rocks:
Lithos, v.7, pp.249-261.

Kostyuk,A.E.,& Sobolev,V.S., 1969, Paragenetic types of calciferous amphiboles of metamorphic rocks:
Lithos, v.2, pp.67-81.

Lacroix,A., 1893, Les enclaves des roches volcaniques:
Protat, Macon, pp.770.

Leake,B.E., 1965, The relationship between composition of calciferous amphiboles and grade of metamorphism:
From: Controls of metamophism.
Ed. W.S.Pitcher and G.W.Flinn, pp.299-318

Leake,B.E., 1971, On aluminous and edenitic hornblendes:
Min.Mag., v.38, pp.289-407.

Leake,B.E., 1978, Nomenclature of amphiboles:
Min.Mag., v.42, pp.533-563.

Lee,D.E.,& Dodge,F.C.W., 1964, Accessory minerals in some granitic rocks in California and Nevada as a function of calcium content:
Am.Min., v.49, pp.1660-1669.

Leedal,G.P.,1951, The Cluanie Igneous Intrusion, Inverness-shire and Ross-shire: Q.J.G.S., v.cviii(1), pp.35-64.

Loewinson-Lessing,F.J., 1940, Petrography: Gosgeolizdat, Leningrad-Moscow.

Marston,R.J., 1971, The Foyers Granitic Complex, Inverness-shire, Scotland: Q.J.G.S.Lond., v.126, pp.331-368.

Mason,B, 1966, Principles of Geochemistry. Wiley & Sons.

Mason,D.R., 1986, Magmatic ferromagnesian inclusions in granitoid plagioclase cores, Barrington Tops granodiorite, New South Wales, Australia: Am.Min., v.71, pp.1314-1321.

Maury,R.C., Didier,J.,& Lameyre,J., 1978, Comparative magma/xenolith relationships in some volcanic and plutonic rocks from the French Massif Central: Contrib.Min.Pet., v.66, pp.401-408.

MacDonald,G.A.,& Katsura,T., 1965, Eruption of Lassen Peak, Cascade Range, California in 1915: Evidence of mixed magmas: Geol.Soc.Am.Bull., v.76, pp.475-482.

MacDonald,R., Rock,N.M.S., Rundle,C.C.,& Russell,O.J., 1986, Relationships between late Caledonian lamprophyric, syenitic and granitic magmas in a differentiated dyke, Southern Scotland: Min.Mag., v.50, pp.547-557.

MacGregor,A.G.,& Kennedy,W.Q.,1932, The Morvern-Strontian Granite: Sum.Prog.Geol.Surv. (for 1931)pt.2 pp.105-119.

McBirney,A.R., 1980, Mixing and unmixing of magmas: J.Vol.Geoth.Res., v.7, pp.357-371.

McCarthy,T.S.,& Hasty,R.A., 1976, Trace element distribution patterns and their relationship to the crystallization of granitic melts: Geochim.Cosmochim.Acta., v.40, pp.1351-1358.

McCarthy,T.S.,& Kable,E.J.D., 1978, On the behaviour of rare earth elements during partial melting of granitic rock: Chem.Geol., v.22, pp.21-29.

McCarthy,T.S.,& Robb,L.J., 1978, On the relationship between cumulus mineralogy and trace and alkali element chemistry in an Archaen granite from the Baberton region, South Africa:
Geochim.Cosmochim.Acta., v.42, pp.21-26.

McCarthy,T.S.,& Groves,D.I., 1979, The Blue Tier Batholith, Northeastern Tasmania:
Contrib.Min.Pet., v.71, pp.193-209

Mercy,E.L.P.,1965, Caledonian Igneous Activity:
Geology of Scotland ed.G.Y.Craig
Chapter 7, pp.229-267.

Miller,C.F.,& Mittlefehldt,D.W., 1982, Depletion of LREE in felsic magmas:
Geol., v.10, pp.129-133.

Miller,J.A.,& Brown,P.E., 1965, Potassium-Argon ages studies in Scotland:
Geol.Mag., v.102(2),pp.106-134.

Munro,M., 1965, Some structural features of the Caledonian granitic complex of Strontian Argyllshire:
Scott.J.of Geol., v.1(2), pp.152-175.

Munro,M., 1973, Structures in the south-eastern portion of the Strontian granitic complex, Argyllshire:
Scott.J.of Geol., v.9(2), pp.99-108.

Nakamura,N., 1974, Distribution of REE, Ba, Fe, Mg, Na and K in carbonaceous and ordinary chondrites:
Geochim. Cosmochim. Acta., v.38, pp.757-775.

Nash,W.P.,& Crecraft,H.R., 1985, Partition coefficients for trace elements in silicic magmas.
Geochim.Cosmochim.Acta., v.49, pp.2309-2322.

Nicholls,G.D., 1950, The Glenelg-Ratagain Igneous Complex:
Q.J.G.S., v.cvi, pp.309-344.

Nockolds,S.R., 1933, Some theoretical aspects of contamination in acid magmas:
J.Geol., v.41, pp.561-590.

Nockolds,S.R., 1933, The contaminated tonalites of Loch Awe, Argyllshire:
Q.J.G.S., v.XC(3), pp.302-321.

Nockolds,S.R., 1940, The Garabal Hill-Glen Fyne Igneous Complex:
Q.J.G.S., v.xcvi, pp.451-511.

Nockolds,S.R., 1954, Average chemical compositions of some igneous rocks:
Bull.Geol.Soc.Am., v.65, pp.1007-1032.

Nockolds,S.R., 1966, The behaviour of some elements during fractional crystallization of magma:
Geochim.Cosmochim.Acta., v.30, pp.267-278

Nockolds,S.R.,& Allen,R., 1953, The geochemistry of some igneous rock series:
Geochim.Cosmochim.Acta., v.4, pp.105-142.

Nockolds,S.R.,& Mitchell,R.L., 1946, The geochemistry of some Caledonian Plutonic rocks: A study in the relationship between the major and trace elements of igneous rocks and their minerals:
Trans.Roy.Soc.Edin., v.lxi, pp.533-575.

Noyes,H.J., Wones,D.R.,& Frey,F.A., 1983, A tale of two plutons: Petrographic and mineralogic constraints on the petrogenesis of the Red Lake and Eagle Peak Plutons, Central Sierra Nevada, California:
J.Geol., v.91(4), pp.353-379.

Noyes,H.J., Frey,F.A.,& Wones,D.R., 1983, A tale of two plutons: Geochemical evidence bearing on the origin and differentiation of the Red Lake and Eagle Peak Plutons, Central Sierra Nevada, California:
J.Geol., v.91(5), pp.487-509.

O'Hara,M.J., 1977, Geochemical evolution during fractional crystallization of a periodically refilled magma chamber:
Nature. v.266, pp.503-507.

Pabst,A., 1928, Observations on inclusions in the granitic rocks of the Sierra Nevada:
Univ.Calif.Publ.Bull., Dept.Geol.Sci. v.17, pp.325-387.

Pabst,A., 1936, Orientation of minerals in "autoliths":
Am.Min., v.21, pp.68.

Pankhurst,R.J., 1974, Rb-Sr whole rock chronology of Caledonian events in northeast Scotland:
Bull.Geol.Soc.Am., v.85, pp.345-350.

Pankhurst,R.J., 1979, Isotope and trace element evidence for the origin and evolution of Caledonian granites in the Scottish Highlands:
From: Origin of Granite Batholiths:
ed. M.P.Atherton & J.Tarney, pp.18-33.

Pankhurst,R.J.,& Sutherland,D.S., 1982, Caledonian granites and diorites of Scotland and Ireland: Igneous Rocks of the British Isles. Ed. by D.S.Sutherland, pp.149-190.

Pearce,J.A.,& Norry,M.J., 1979, Petrogenetic implications of Ti, Zr, Y and Nb variations in volcanic rocks: Contrib.Min.Pet., v.69, pp.33-47.

Phillips,J.A., 1880, On concretionary patches and fragments of other rocks contained in granite: Q.J.G.S.Lond., v.xxxvi, pp.1-22.

Phillips,W.J., 1956, The Criffell-Dalbeattie Granodiorite Complex: Q.J.G.S., v.cxii(2), no.446, pp.221-239.

Phillips,W.J., Fuge,R.,& Phillips,N., 1981, Convection and crystallization in the Criffell-Dalbeattie pluton: J.G.S.Lond., v.138, pp.351-366.

Pidgeon,R.T.,& Aftalion,M., 1978, Cogenetic and inherited zircon U-Pb systems in granites: Palaeozoic granites of Scotland and England: From: Crustal evolution in northwestern Britain and adjacent regions; Geol.J.Spec.Issue No.10, pp.183-248.

Piwinskii,A.J., 1968, Studies of batholithic feldspars: Sierra Nevada, California: Contrib.Min.Pet., v.17, pp.204-223.

Piwinskii,A.J.,& Wyllie,P.J., 1968, Experimental studies of igneous rock series: A zoned pluton in the Wallowa Batholith, Oregon: J.Geol., v.76, pp.205-234.

Potts,P.J., 1987, A handbook of silicate rock analysis: Blackie, Glasgow.

Powell,D., 1974, Stratigraphy and structure of the western Moine and the problem of Moine orogenesis: Jl.Geol.Soc.Lond., v.130, pp.575-593.

Read,H.H., 1931, The hybrids of Ach'uaine type: The Geology of Central Sutherland: Geol.Surv.Mem.Scot., H.M.S.O., chap.IX.

Read,H.H., 1961, Aspects of Caledonian Magmatism in Britain: Liver.& Manch.Geol.J., v.2, pp.653-683.

Reid.Jr,J.B., Evans,O.C.,& Fates,D.G., 1983, Magma mixing in granitic rocks of the central Sierra Nevada, California:

Ear.Pl.Sci.Lett., v.66, pp.243-261.

Ringwood,A.E., 1974, The petrological evolution of island arc systems:
J.Geol.Soc.Lond., v.130, pp.183-204.

Ringwood,A.E., 1975, Composition and petrology of the Earth's mantle.
publ. McGraw-Hill.

Rock,N.M.S.,& Leake,B.E., 1984, The International Mineralogical Association amphibole nomenclature scheme: computerization and its consequences:
Min.Mag., v.48, pp.211-227.

Rock.N.M.S., Hunter,R.H., 1987, Late Caledonian dyke swarms of northern Britain: spatial and temporal intimacy between lamprophyric and granitic magmatism around the Ross of Mull pluton, Inner Hebrides:
Geol.Rund., v.76, pp.805-826.

Rogers,G.,& Dunning,G.R., 1989, Geochronology of Appinitic and related granitic magmatism in Western Highlands of Scotland: Constraints on timing of transcurrent fault movement:
Terra Abstracts, v.1, pp.11-12 (abstract).
J.Geol.Soc.Lond., in press.

Sabine,P.A., 1963, The Strontian Granite Complex, Argyllshire:
Geol.Surv.Gt.Br.Bull., v.20, pp.6-42.

Sawka,W.N., 1988, REE and trace element variations in minerals and hornblende from strongly zoned McMurry Meadows Pluton, California:
Trans.R.Soc.Edin., v.79, pp.157-168.

Scott,J.F., 1928, General Geology and Physiography of Morvern, Argyll:
Trans.G.Soc.Glasg., v.xviii, pp.149-189.

Shannon,R.D., 1976, Revised effective ionic radii and systematic studies of interatomic distances in halides and chalcogenides:
Acta.Crystallogr., v.A32, pp.751-767.

Shaw,D.M., 1968, A review of K-Rb fractionation trends by covariance analysis:
Geochim.Cosmochim.Acta., v.32, pp.573.

Shaw,D.M., 1977, Trace element behaviour during anatexis:
Magma genesis Bull., v.96, pp.189-213.

Shaw,S.E.,& Flood,R.H., 1981, The New England Batholith, E. Australia: Geochemical variation in time and space:
J.Geophy.Res., v.86(B11), pp.10530-10544.

Smith,D.I., 1979, Caledonian minor intrusions of the N. Highlands of Scotland: The Caledonides of the British Isles-rd. Geological Society of London, pp.683-697.

Snoke,A.W., Quick,J.E.,& Bowman,H.R., 1981, Bear Mountain Igneous Complex, Klamath Mountains, California: an ultrabasic to silicic calc-alkaline suite: J.Pet., v.22(4), pp.501-552.

Soper,N.J., 1964, Conditions in the metamorphic Caledonides during the period of late orogenic cooling: Geol.Mag., v.101, pp.567-568.

Sparks,R.S.J., Pinkerton,H.,& MacDonald,R., 1977, The transport of xenoliths in magmas: Ear.Pl.Sci.Lett., v.35, pp.234-238.

Streckeisen,A., 1975, To each plutonic rock its proper name: Ear.Sci.Rev., v.12, pp.1-33.

Strong,D.F., 1979, The Mount Peyton Batholith, Central Newfoundland: A bimodal Calc-alkaline suite: J.Pet., v.20(1), pp.119-138.

Sweatman,T.R.,& Long,J.V.P., 1969, Quantitative electron - probe microanalysis of rock forming minerals: J.Pet., v.10, pp.332-379.

Taylor,S.R., 1965, The application of trace element data to problems in petrology: Phys.Chem.Earth., v.6, pp.133-213.

Taylor,S.R., 1969, Trace element chemistry of Andesites and associated calc-alkaline rocks: Ore.Dept.G.Min.Ind.Bull., v.65, pp.43-63.

Taylor,T.R., Vogel,T.A.,& Wilbrand,J.T., 1980, The composite dikes at Mount Desert Island, Maine: An example of coexisting acidic and basic magmas: J.Geol., v.88, pp.433-444.

Thirlwall,M.F., 1979, The petrochemistry of the British Old Red Sandstone volcanic province: Ph.D. Thesis, Edinburgh University.

Thirlwall,M.F., 1981, Implications for Caledonian plate tectonic models of chemical data from volcanic rocks of the British Old Red Sandstone: J.Geol.Soc.Lond., v.138, pp.123-138.

Thirlwall,M.F., 1982, Systematic variation in chemistry and Nd-Sr isotopes across a Caledonian calc-alkaline volcanic arc: implications for source materials:
Ear.Pl.Sci.Lett., v.58, pp.27-50.

Thompson,M.,& Walsh,J.N.,1983, A handbook of inductively coupled plasma spectrometry:
Blackie, Glasgow, pp.273.

Tindle,A.G.,& Pearce,J.A., 1981, Petrogenetic modelling of in situ fractional crystallization in the zoned Loch Doon Pluton, Scotland:
Contrib.Min.Pet., v.78, pp.196-207.

Tindle,A.G.,& Pearce,J.A., 1983, Assimilation and partial melting of continental crust: evidence from the mineralogy and geochemistry of autoliths and xenoliths:
Lithos. v.16, pp.185-202.

Tindle,A.G., McGarvie,D.W.,& Webb,P.C., 1988, The role of hybridization and crystal fractionation in the evolution of the Cairnsmore of Carsphairn Intrusion, Southern Uplands of Scotland:
J.Geol.Soc.Lond., v.145, pp.11-21.

Togashi,S., 1984, Sr variation by fractional crystallizatio for volcanic rocks from island arcs and continental margins:
Chem.Geol., v.51(1-2), pp.41-53.

Turekian,K.K.,& Wedepohl,W.H., 1961, Distribution of the elements in some major units of the earth's crust:
Bull.Geol.Soc.Am., v.72, pp.175-192.

Tyler,I.M.,& Ashworth,J.R., 1981, Garnet zoning and re-equilibration in the Strontian area, Scotland:
Min.Mag., v.44, pp.293-300.

Tyler,I.M.,& Ashworth,J.R.,1982, Sillimanite - Potash assemblages in graphitic pelites, Strontian area, Scotland:
Contrib.Mineral.Petrol., v.81, pp.18-29.

Veblen,D.R.,& Ribbe,P.H., 1982, Reviews in Mineralogy v.9B:
Amphiboles: Petrology and Experimental Phase relations:
Amphiboles in the Igneous Environment
Chapter 3, pp.355-390

Verhoogen,J., 1962, Distribution of titanium between silicates and oxides in igneous rocks:
Am.J.Sci., v.260, pp.211-220.

Vernon,R.H.,& Flood,R.H., 1982, Some problems in the interpretation of microstructures in granitoid rocks: New England Geology. pp.201-210.

Vernon,R.H., 1983, Restite,xenoliths and microgranitoid enclaves in granites: J.& Proc.Roy.Soc.of N.S.W.. v.116, pp.77-103.

Vernon,R.H., Etheridge,M.A.,& Wall,V.J.,1983, Magma mixing in the development of metaluminous Granitoid Suites of the Moruya Batholith around Tuross Head, NSW: Abst.Geol.Soc.Aust.. v.9, pp.185.

Vernon,R.H., 1984, Microgranitoid enclaves in granites - globules of hybrid magma quenched in a plutonic environment: Nature. v.309, pp.438-439.

Wager,L.R.,& Bailey,E.B., 1953, Basic magma chilled against acid magma: Nature. v.172, pp.68-70.

Wager,L.R.,& Brown,G.M., 1968, Layered Igneous Rocks: publ. Oliver & Boyd.

Walker,G.P.L.,& Skelhorn,R.R.,1966, Some associations of acid and basic igneous rocks: Earth Sci.Rev.. v.2, pp.93-109.

Walsh,J.N.,& Howie,W., 1980, An evaluation of the performance of an inductively coupled plasma source spectrometer for the determination of major and trace constituents of silicate rocks and minerals: Min.Mag.. v.43, pp.967-974.

Walsh,J.N.,Buckley,F.,& Barker,J., 1981, The simultaneous determination of the rare earth elements in rocks using inductively coupled plasma source spectrometry: Chem.Geol.. v.33, pp.141-153.

Watson,J., 1964, Conditions in the Metamorphic Caledonides during the period of Late-Orogenic cooling: Geol.Mag.. v.101, pp.457-465.

White,A.J.R.,& Chappell,B.W., 1977, Ultrametamorphism and Granitoid Genesis: Tectonophysics: v.43, pp.7-22.

Whitten,D.G.A.,& Brooks,J.R.V., 1979, The Penguin Dictionary of Geology.

Wiebe,R.A., 1973, Relations between co-existing basaltic and granitic magmas in a composite dyke: Am.J.Sci., v.273, pp.130-151.

Wiebe,R.A., 1980, Commingling of contrasted magmas in the plutonic environment: Examples from the Nain Anorthositic Complex: J.Geol., v.80, pp.197-209.

Wiebe,R.A.,& Wild,T., 1983, Fractional crystallization and magma mixing in the Tigalak Layered Intrusion, the Nain Anorthositic Complex, Labrador: Contrib.Min.Pet., v.84, pp.327-344.

Wilkinson,J.F.G., Vernon,R.H.,& Shaw,S.E., 1964, The petrology of an adamellite-porphyrite from the New England batholith (NSW): J.Pet., v.5, pp.461-488.

Wilshire,H.G., 1969, Mineral layering in the Twin Lakes granodiorite, Colorado: Geol.Soc.Am.Mem. 115. pp.235-261. Ed. L.H.Larsen.

Winchester,J.A., 1974, The zonal pattern of regional metamorphism in the Scottish Caledonides: Jl.Geol.Soc.Lond., v.130, pp.509-524.

Wones & Gilbert 1982, see D.R.Veblen & P.H.Ribbe.

Wright,A.E.,& Bowes,D.R., 1979, Geochemistry of the appinite suite: The Caledonides of the British Isles-rd. Geol.Soc.Lond., pp.699-704.

Wyborn,D.,& Chappell,B.W., 1986, The petrogenetic significance of chemically related plutonic and volcanic rock units: Geol.Mag., v.123(6), pp.619-628.

Wyllie,P.J., Cox,K.G.,& Biggar,G.M., 1962, The habit of apatite in synthetic systems and igneous rocks: J.Pet., v.3(2), pp.238-243.

Znamenskii,E.B., Konysova,V.V., Krinberg,I.A., Popolitov,E.I. Flerova,K.V.,& Tsykhanskii,V.D., 1962, Distribution of titanium, niobium and tantalum in granitic rocks containing sphene: Geochem., v.9, pp.919-925.

ERRATA - ADDITION TO REFERENCES

Bussell,M.A., 1988, Structure and petrogenesis of a mixed-magma ring dyke in the Peruvian Coastal Batholith: eruptions from a zoned magma chamber: Trans.R.Soc.Edin:Ear.Sci.. v.79, pp.87-104.

Carmichael,I.S.E., Turner,F.J., & Verhoogen,J., 1974, Igneous Petrology: New York: McGraw-Hill.

Dorais,M.J., Whitney,J.A., & Roden,M.F., 1990, Origin of Mafic enclaves in the Dinkey Creek Pluton Central Sierra Nevada, California: J.Pet.. v.31(4), pp.853-881.

Ehlers,E.G., 1972, The interpretation of Geological Phase Diagrams. publ. Freeman & Co.

Ewart,A., 1982, The mineralogy and petrology of Tertiary-Recent orogenic volcanic rocks: with special reference to the andesitic-basaltic compositional range. In: Andesites: orogenic andesites and related rocks, pp.26-87. ed.Thorpe; publ. Chichester - Wiley.

Holden,P., Halliday,A.N., & Stephens,W.E., 1987, Neodymium and strontium isotope content of microdiorite enclaves points to mantle input to granitoid production: Nature. v.330, pp.53-56.

Huang,W.L., & Wyllie,P.J., 1975, Melting reactions in the system NaAlSi3O8 - KAlSi2O8 - SiO2 to 35 kilobars, dry and with excess water: J.Geol.. v.83, pp.737-748.

Johannes,W., 1983a, Metastable melting in the granite and related systems: In Migmatites, Melting & Metamorphism. eds.Atherton,M.P., & Gribble,C.D. publ. Shiva, Nantwich., pp.27-36.

Johannes,W., 1984, Beginning of melting in the granite system Qz - Or - Ab - An - H2O: Contrib.Min.Pet.. v.86, pp.264-273.

Lange,R.A., & Carmichael,I.S.E., 1990, Hydrous basaltic andesites associated with minette and related lavas in western Mexico: J.Pet.. v.31, pp.1225-1259.

Peccerillo,A., & Taylor,S.R., 1975, Geochemistry of Upper Cretaceous volcanic rocks from the Pontic Chain northern Turkey: Bull.Volcan.. v.39(4), pp.557-569.

Steiner,J.C., Jahns,R.H., & Luth,W.C., 1975, Crystallization of alkali feldspars and quartz in the haplogranite system NaAlSi2O8 - SiO2 - H2O at 4kb: Geol.Soc.Am.Bull., v.86, pp.83-98.

Stephens, & Halliday, 1984, Geochemical contrasts between late Caledonian granitoid plutons of northern, central and southern Scotland: Trans.R.Soc.Edin:Ear.Sci., V.75, pp.259-273.

Thorpe,R.S., 1982, Andesites: orogenic andesites and related rocks: ed.R.S.Thorpe; publ. Chichester-Wiley.

Von Platen,H., 1965, Experimental anatexis and genesis of migmatites: In: Controls of Metamorphism: pp.202-218. eds.Pitcher,W.S., & Flinn,G.W. publ.Oliver & Boyd, Edinburgh, Scotland.

Winkler,H.G.F., 1974, Petrogenesis of Metamorphic Rocks. publ.Springer-Verlag, New York; 3rd.Ed.

APPENDIX A SAMPLE LOCALITITES AND ROCK TYPES

THE STRONTIAN COMPLEX

N.B The change in the prefixes for xenoliths (X to XG) or granites (SGXXVI to SG7) has no significance, but is simply the change in collecting seasons.

SAMPLE	GRID REF	ROCK TYPE
X38	7681-5325	Type 2
X39	7686-5322	Type 1B
X40	7703-5323	Type 1A
X43	7957-5310	Type 1B
X44	7945-5316	Type 1B
X69	7780-6075	Type 1B
X75	7820-6091	Type 1B
X81	7845-6105	Type 1B
X100	7906-6107	Type 1B
X113	7911-6104	Type 1B
X116	7930-6108	Type 4
X119	7997-6123	Type 4
X140	8064-6101	Type 2
X142	8091-6118	Type 1B
X143	8091-6118	Type 2
X144	8091-6118	Type 2
X146	8191-6090	Type 4
X150	8252-6081	Type 2
X160	8271-6086	Type 1B
X166	8045-5912	Type 1B
X170A	8244-6560	Type 1A
X171A	8236-6552	Type 1A
X172	8236-6545	Type 2
X173	8236-6542	Type 1A
X176	7777-5008	Type 2
X177	7915-5058	Type 3
X178	8007-5375	Type 1B
X179	8007-5375	Type 1B
X180	7607-4811	Type 3
X181	7620-5460	Type 2
X182	7620-5460	Type 1B
XG01	7562-5338	Type 5
XG0	8136-5510	Type 1A
XG1	7625-5493	Type 1
XG2	7624-5493	Type 2
XG3	7625-5491	Type 1B
XG3A	7625-5491	Type 1A
XG4	7886-6114	Type 5
XG5	7886-6114	Type 5
XG6	7884-6115	Type 1B
XG7	7881-6115	Type 1B
XG8	7875-6114	Type 3
XG9	7875-6114	Type 5
XG11	7721-5690	Type 2
XG12	7721-5690	Type 5
XG13	7721-5690	Type 5

XG14	7721-5688	Type 1B
XG15	7756-5655	Type 5
XG18	7756-5655	Type 3
XG19	7773-5626	Type 1B
XG20	7797-5605	Type 4
XG20A	7797-5605	Type 1B
XG21	7797-5606	Type 2
XG21A	7797-5605	Type 5
XG22	7797-5606	Type 1B
XG22A	7797-5606	Type 2
XG22B	7797-5606	Type 1B
XG23	7798-5604	Type 1A
XG24	7448-5080	Type 1B
XG24A	7796-5606	Type 1B
XG25	7456-5084	Type 2
XG26	7458-5089	Type 2
XG27	7459-5090	Type 4
XG28	7474-5126	Type 2
XG29	7474-5126	Type 1B
XG30	7482-5150	Type 5
XG31	7524-5279	Type 1A
XG32	7524-5279	Type 1A
XG33	7599-5389	Type 2
XG34	7680-5534	Type 2
XG35	7680-5534	Type 2
XG36	7680-5534	Type 2
XG37	7680-5534	Type 5
XG39	7745-5548	Type 5
XG40	7748-5547	Type 5
XG41	7749-5547	Type 5
XG43	7755-5646	Type 5
XG44	7784-5547	Type 2
XG45	7789-5532	Type 1B
XG46	7797-5606	Type 4
XG47	7796-5604	Type 4
XG48	7796-5604	Type 2
XG48A	7796-5604	Type 1A
XG50	7717-5706	Type 1A
XG51	7622-5464	Type 1A
XG52	7622-5465	Type 1B
XG53	7622-5466	Type 1B
XG54	7622-5466	Type 1B
XG55	7622-5466	Type 4
XG56	7622-5466	Type 4
XG57	7622-5467	Type 1B
XG58	7622-5467	Type 1B
XG59	7620-5465	Type 1A
XG60	7620-5466	Type 5
XG61A	7621-5471	Type 2
XG61B	7621-5471	Type 2
XG61C	7621-5471	Type 2
XG62	7621-5471	Type 2
XG63	7621-5471	Type 4
XG64A	7620-5467	Type 1B
XG64B	7620-5467	Type 1B
XG65	7620-5467	Type 1A

XG66	7622-5463	Type 5
XG67	7718-5710	Type 2
XG68	7725-5732	Type 2
XG69	7711-5788	Type 1A
XG70	7711-5788	Type 5
XG71	7711-5788	Type 5
XG74	7722-5824	Type 1B
XG75	7730-5839	Type 1B
XG77	7803-5935	Type 2
XG78	8599-6069	Type 4
XG80	8598-6069	Type 2
XG81	8597-6069	Type 2
XG82	8521-6091	Type 1B
XG84	8490-6093	Type 1B
XG85	8488-6097	Type 2
XG87	8423-6102	Type 2
XG88	8421-6102	Type 4
XG89	8418-6101	Type 2
XG90	8417-6101	Type 1B
XG91	8421-6102	Type 2
XG92	8394-6097	Type 1A
XG93	7931-6009	Type 5
XG94	7933-6011	Type 5
XD1	7933-6011	Type 2
XD1A	7933-6011	Type 1A
XD2	7933-6011	Type 5
MX	7618-5462	Moine
MX1	7792-5314	Moine
MX2	7773-5320	Moine
MX2A	7773-5320	Moine
MX3	6040-6103	Moine
SGI	7541-5312	Tonalitic Gdi
SGII	7557-5330	Tonalitic Gdi
SGIII	7430-5034	Tonalitic Gdi
SGIV	7475-5130	Biotite Granite
SGV	7475-5130	Tonalitic Gdi
SGVI	7475-5130	Biotite Granite
SGVIA	7475-5130	Biotite Granite
SGVII	7620-5463	Granitic Sheet ctG
SGVIII	7620-5467	Granitic Sheet ctG
SGIX	7720-5742	Tonalitic Gdi
SGX	7621-5463	Granitic Sheet ctG
SGXI	7722-5741	Tonalitic Gdi
SGXII	7709-5770	Tonalitic Gdi
SGXV	7404-5036	Granitic Sheet fG
SGXVI	7402-5036	Granitic Sheet fG
SGXVII	7402-5036	Granitic Sheet fG
SGXVIII	7405-5037	Granitic Sheet fG
SGXIX	7405-5036	Granitic Sheet fG
SGXX	8122-5501	Biotite Granite
SGXXI	8272-5418	Tonalitic Gdi
SGXXII	8502-5299	Porphyritic Gdi
SGXXIII	8599-6059	Tonalitic Gdi
SGXXV	8521-6091	Tonalitic Gdi
SGXXVI	8418-6101	Tonalitic Gdi
SGXXVII	7933-6011	Porphyritic Gdi

SG7	8096-6017	Porphyritic Gdi
SG11	7409-4955	Tonalitic Gdi
SG14	7681-5323	Porphyritic Gdi
SG17	7433-4899	Tonalitic Gdi
SG18	7990-5301	Biotite Granite
SG19	7956-5310	Biotite Granite
SG20	7867-5321	Biotite Granite
SG21	7794-5314	Porphyritic Gdi
SG25	7948-4866	Biotite Granite
SG27	8116-4798	Biotite Granite
SG29	7576-4766	Porphyritic Gdi
SG41	8091-6117	Porphyritic Gdi
SG42	8252-6080	Porphyritic Gdi
SG43	8114-5667	Biotite Granite
SG44	8073-5863	Porphyritic Gdi
SG45	8178-4768	Biotite Granite
SG46	8043-5282	Biotite Granite
SG47	8054-5276	Biotite Granite
SG48	8133-5277	Biotite Granite
SG49	8199-5261	Porphyritic Gdi
SG51	8363-5247	Porphyritic Gdi
SG53A	8235-6545	Tonalitic Gdi
SG55	7832-4848	Biotite Granite
SG56	7787-4844	Biotite Granite
SG57	8045-6205	Porphyritic Gdi
SG58	7983-5282	Biotite Granite
SG59	7964-5246	Biotite Granite
SG61	7907-5157	Biotite Granite
SG62	7914-5105	Biotite Granite
SG63	7876-4783	Biotite Granite
SG64	7838-4736	Biotite Granite
SG65	7879-4665	Biotite Granite
SG66	7848-4640	Biotite Granite
SG67	7768-4554	Biotite Granite
SG68	7939-4405	Biotite Granite
SG69	7879-4417	Biotite Granite
SG71	7760-4465	Biotite Granite
SG72	7748-4485	Biotite Granite
SG73	7410-4084	Biotite Granite
SG78	7494-4387	Biotite Granite
SG80	7458-4473	Tonalitic Gdi
SG82	7449-4513	Tonalitic Gdi
SG85	7436-4650	Tonalitic Gdi
SG86	7993-5339	Biotite Granite
SG87	8003-5376	Biotite Granite
SG88	8037-5437	Biotite Granite
SG89	8033-5467	Biotite Granite
SG90	7861-4945	Biotite Granite
SG91	7833-4881	Biotite Granite
SG92	7608-4810	Porphyritic Gdi
SG93	7745-5985	Tonalitic Gdi
G140	8064-6002	Porphyritic Gdi
G24	7447-5080	Tonalitic Gdi
GX42	7755-5545	Tonalitic Gdi
GX7	7881-6115	Tonalitic Gdi
SGC1	7417-5049	Tonalitic Gdi

fG1	8093-6017	Granitic Sheet fG
fG2	8155-6018	Granitic Sheet fG
GR1	7678-5323	Granitic Sheet fG
GS3	7939-6018	Granitic Sheet
GS3A	7939-6018	Granitic Sheet
AP1	7756-5657	Aplitic Vein
AP2	7794-5542	Aplitic Vein
AP3	7621-5464	Aplitic Vein
AP4	7845-6105	Aplitic Vein
P1	7746-5547	Pegmatite
V1	7621-5466	Dioritic Xenolith
E1	7729-5316	Caledonian Dyke
E2	7729-5317	Caledonian Dyke
E3	7729-5317	Caledonian Dyke
L1	7703-5323	Caledonian Dyke
D1	7935-6012	Poikilitic Biotite Diorite
D1i	7935-6013	Poikilitic Biotite Diorite
D2	7935-6014	Poikilitic Biotite Diorite
D3	7935-6015	Hbl-Biot Diorite
D3A	7935-6015	Hbl-Biot Diorite
D4	7939-6018	Poikilitic Biotite Diorite
D5	7940-6020	Poikilitic Biotite Diorite
D5A	7940-6020	Poikilitic Biotite Diorite
D6	7945-6018	Poikilitic Biotite Diorite
D7	7951-6021	Poikilitic Biotite Diorite
D7A	7951-6021	Poikilitic Biotite Diorite
D8	7955-6022	Poikilitic Biotite Diorite
D9	7958-6023	Poikilitic Biotite Diorite
D10	7714-5801	Poikilitic Biotite Diorite
D11	7718-5811	Hbl-Biot Diorite
D12	7721-5817	Hbl-Biot Diorite
D13	7723-5823	Hbl-Biot Diorite
D14	7724-5827	Hbl-Biot Diorite
D17	7523-5334	Hbl-Biot Diorite
D19	7536-5349	Hornblende Diorite
D20	7533-5353	Hornblende Diorite
D24	7611-5494	Hbl-Biot Diorite
D25	7605-5512	"Spotted" Diorite
D27	7620-5556	Hbl-Biot Diorite
D28	7654-5630	"Spotted" Diorite
D29	7791-5310	Biotite Diorite
D32	7555-5380	Biotite Diorite
D33	7846-6106	Hbl-Biot Diorite
D35	7847-6108	Hornblende Diorite
D37	7854-6110	Hbl-Biot Diorite
D38	7858-6112	Hbl-Biot Diorite
D40	7860-6113	"Spotted" Diorite
D41	7863-6115	Hornblende Diorite
D43	7867-6116	"Spotted" Diorite
D44	7509-5241	Hornblende Diorite
D45	7507-5243	"Spotted" Diorite
D47	7856-6118	Hbl-Biot Diorite
D48	7759-5982	"Spotted" Diorite
D50	7754-5988	Biotite Diorite
D51	7751-5991	Hbl-Biot Diorite
D53	7749-5993	Hornblende Diorite

D54	7749-5993	Hornblende Diorite
D55	7897-5059	Poikilitic Biotite Diorite
D57	7903-5060	Poikilitic Biotite Diorite
D58	7745-5995	Hbl-Biot Diorite
D58A	7885-5053	"Spotted" Diorite
D59A	7874-5044	Biotite Diorite
D60	7743-5997	Hornblende Diorite
D60A	7866-5033	Hbl-Biot Diorite
D61	7741-5998	Hornblende Diorite
D63	7877-5039	Net-Veined Diorite
D64	7871-5040	Net-Veined Diorite
D65	7858-5046	Net-Veined Biotite Diorite
D67	7560-4698	Hbl-Biot Diorite
D68	7563-4701	Hornblende Diorite
D69	7855-5084	Poikilitic Biotite Diorite
D70	7850-5081	Net-Veined Diorite
D71	7859-5070	Biotite Diorite
D72	7851-6109	Hbl-Biot Diorite
D73	7853-5086	Net-Veined Diorite
D74	7855-5097	"Spotted" Diorite
D76	7867-5087	Net-Veined Diorite
D77	7850-5084	Poikilitic Biotite Diorite
D80	7550-4659	Hbl-Biot Diorite

APPENDIX B WHOLE ROCK GEOCHEMICAL ANALYSES

Table B.1: STRONTIAN HOST ROCKS

Table B.2: XENOLITHS

Table B.3: MAFIC DIORITES

Table B.4: MISCELLANEOUS

Table B.5: RARE EARTH ELEMENTS

All Grid References for these analyzed samples are given in Appendix A.

KEY TO TABLES

TGD - refers to the tonalitic granodiorite

PGD - refers to the porphyritic granodiorite

BGT - refers to the biotite granite

Late - refers to the late granitic sheets

N.B Types 1A, 1B, 2, 3, 4 and 5 refer to the classification of xenoliths given in Chapter 5.

Rubh. - refers to the Rubha-na-Sroine diorite

Lidd. - refers to the Liddesdale diorite

Shet. - refers to the long Sheet diorite

Ranac. - refers to the Ranachan diorite

Uile. - refers to the Uileann diorite

L.Tea.- refers to the Loch Tearnait diorite

Dyke - refers to the Caledonian dykes

Aplite - refers to Aplite vein

Pegmt. - refers to pegmatite vein

APPENDIX B

Table B.1: WHOLE ROCK ANALYSIS OF THE STRONTIAN HOST ROCKS

	SGI TGD	SGII TGD	SGIII TGD	SGIV BGT	SGV TGD	SGVI BGT
MAJOR ELEMENTS						
SiO_2	65.00	63.75	64.50	69.00	62.50	72.50
TiO_2	0.63	0.55	0.50	0.35	0.83	0.25
Al_2O_3	14.20	15.10	15.20	15.70	13.90	13.70
FeO*	3.70	3.05	3.45	0.75	4.40	1.45
MnO	0.04	0.03	0.04	0.01	0.04	0.01
MgO	2.55	2.25	2.60	0.50	3.35	0.80
CaO	3.90	3.80	4.50	2.30	4.00	1.60
Na_2O	4.47	4.68	4.50	5.45	4.39	4.99
K_2O	3.28	3.20	2.74	3.35	2.88	3.07
P_2O_5	0.28	1.09	0.16	0.01	0.02	0.02
H_2O	1.04	1.34	0.80	1.18	2.32	1.24
CO_2	0.05	0.00	0.03	0.48	1.73	0.74
Total	99.14	98.84	99.01	99.07	100.35	100.37
NORMS						
Q	15.43	14.82	15.04	20.01	15.37	28.59
C	-	-	-	0.07	0.35	1.03
Or	19.38	18.91	16.19	19.79	17.02	18.14
Ab	37.81	39.58	38.06	46.09	37.13	42.20
An	9.00	10.75	13.19	8.31	8.77	3.13
Lc	-	-	-	-	-	-
Ne	-	-	-	-	-	-
Di	6.65	0.80	6.40	-	-	-
Wo	-	-	-	-	-	-
Hy	6.59	8.02	6.76	1.59	12.33	3.34
Ol	-	-	-	-	-	-
Mt	1.38	1.13	1.28	0.28	1.64	0.54
Il	1.20	1.04	0.95	0.66	1.58	0.47
Ap	0.66	2.58	0.38	0.02	0.05	0.05
Cc	0.11	-	0.07	1.09	3.93	1.68
TRACE ELEMENTS						
Ba	910	1120	1055	735	890	455
Cr	85	132	85	60	90	8
Cu	16	18	17	11	19	26
Li	18	20	20	2	16	2
Ni	47	37	37	1	56	9
Rb	68	58	65	83	65	70
Sc	7	5	5	-	9	2
Sr	870	1075	890	660	780	470
V	98	61	67	13	88	24
Y	15	13	13	4	17	7
Zn	63	44	51	17	67	26

APPENDIX B

Table B.1: WHOLE ROCK ANALYSIS OF THE STRONTIAN HOST ROCKS

	SGVIa BGT	SGVII Late	SGVIII Late	SGIX TGD	SGX Late	SGXI TGD
MAJOR ELEMENTS						
SiO_2	69.75	68.50	68.00	66.50	66.00	59.00
TiO_2	0.50	0.49	0.55	0.55	0.65	0.90
Al_2O_3	12.90	14.50	14.60	14.40	14.50	14.80
FeO*	3.01	2.20	3.10	3.55	3.05	5.60
MnO	0.02	0.03	0.04	0.04	0.03	0.07
MgO	2.20	1.80	1.85	2.60	2.15	4.30
CaO	1.40	3.10	2.30	4.15	3.50	5.30
Na_2O	4.45	4.33	4.40	4.60	4.54	4.39
K_2O	2.73	3.13	3.05	3.03	3.03	2.93
P_2O_5	0.17	0.14	0.17	0.24	0.70	0.35
H_2O	2.52	1.56	1.34	1.10	0.84	1.18
CO_2	0.95	0.05	0.05	0.05	0.14	0.11
Total	100.60	99.83	99.45	100.81	99.13	98.93
NORMS						
Q	26.35	22.41	-	16.60	18.83	5.79
C	0.49	-	-	-	-	-
Or	16.13	18.49	-	17.90	17.90	17.31
Ab	37.64	36.62	-	38.91	38.40	37.13
An	5.83	10.89	-	9.70	10.24	12.03
Lc	-	-	-	-	-	-
Ne	-	-	-	-	-	-
Di	-	2.62	-	7.30	1.35	9.13
Wo	-	-	-	-	-	-
Hy	8.30	5.10	-	6.36	7.34	11.65
Ol	-	-	-	-	-	-
Mt	1.12	0.82	-	1.32	1.13	2.08
Il	0.95	0.93	-	1.04	1.23	1.71
Ap	0.40	0.33	-	0.57	1.66	0.83
Cc	0.00	0.11	-	0.11	0.32	0.25
TRACE ELEMENTS						
Ba	420	995	992	920	985	930
Cr	30	35	55	72	102	175
Cu	19	15	20	17	21	34
Li	8	24	26	30	26	41
Ni	30	24	74	44	31	68
Rb	68	78	75	70	85	88
Sc	7	5	8	7	6	13
Sr	410	730	874	975	815	915
V	60	54	67	69	60	107
Y	14	13	15	14	14	19
Zn	61	41	52	48	46	80

APPENDIX B

Table B.1: WHOLE ROCK ANALYSIS OF THE STRONTIAN HOST ROCKS

	SGXII TGD	SGXV Late	SGXVI Late	XVII Late	XVIII Late	XIX Late
MAJOR ELEMENTS						
SiO_2	63.50	73.00	72.50	72.50	73.50	71.00
TiO_2	0.73	0.30	0.18	0.39	0.29	0.29
Al_2O_3	14.50	13.80	13.20	13.50	13.20	13.50
FeO*	3.80	1.55	1.10	0.85	1.60	1.45
MnO	0.04	0.02	0.01	0.02	0.02	0.02
MgO	2.55	0.70	0.45	1.00	0.80	0.80
CaO	5.00	2.00	1.60	2.20	2.00	1.90
Na_2O	4.64	4.04	4.05	4.03	3.79	4.10
K_2O	2.58	3.35	3.83	2.98	3.00	3.30
P_2O_5	0.24	0.00	0.01	0.02	0.03	-
H_2O	0.88	1.48	1.10	1.92	1.62	1.78
CO_2	0.72	0.25	0.55	0.65	0.16	0.72
Total	99.18	100.49	98.58	100.06	100.01	98.86
NORMS						
Q	14.86	31.42	31.26	33.11	34.36	30.65
C	-	0.47	0.78	1.20	0.53	1.40
Or	15.24	19.79	22.63	17.61	17.72	19.50
Ab	39.24	34.17	34.25	34.08	32.05	34.68
An	11.13	8.34	4.39	6.67	8.71	4.87
Lc	-	-	-	-	-	-
Ne	-	-	-	-	-	-
Di	6.13	-	-	-	-	-
Wo	-	-	-	-	-	-
Hy	6.80	3.15	2.16	2.90	3.47	3.29
Ol	-	-	-	-	-	-
Mt	1.41	0.58	0.41	0.32	0.59	0.54
Il	1.39	0.57	0.34	0.74	0.55	0.55
Ap	0.57	0.00	0.02	0.05	0.07	0.00
Cc	1.64	0.57	1.25	1.48	0.36	1.64
TRACE ELEMENTS						
Ba	1025	795	665	715	645	695
Cr	100	95	150	150	70	125
Cu	13	6	5	7	9	6
Li	27	20	11	17	27	25
Ni	43	3	2	13	5	7
Rb	70	98	93	85	88	103
Sc	7	2	1	2	3	2
Sr	1035	480	380	455	470	365
V	74	25	15	33	25	24
Y	15	7	9	10	9	8
Zn	50	30	22	34	37	31

APPENDIX B

Table B.1: WHOLE ROCK ANALYSIS OF THE STRONTIAN HOST ROCKS

	XX BGT	XXI TGD	XXII PGD	XXIII TGD	XXV TGD	XXVI TGD
MAJOR ELEMENTS						
SiO_2	72.00	63.90	66.50	63.00	62.50	69.00
TiO_2	0.28	0.73	0.55	0.68	0.63	0.48
Al_2O_3	14.30	15.60	15.10	16.60	15.50	14.60
FeO*	1.45	3.85	2.60	3.60	4.15	2.00
MnO	0.01	0.04	0.03	0.05	0.05	0.02
MgO	0.55	2.46	1.65	2.55	3.30	1.40
CaO	1.75	3.08	3.15	4.75	5.00	2.45
Na_2O	4.36	4.73	4.68	5.45	4.91	4.41
K_2O	3.48	3.10	3.42	1.93	2.08	3.40
P_2O_5	0.02	0.22	0.14	0.23	0.30	0.09
H_2O	1.08	2.20	1.56	1.22	0.94	1.20
CO_2	0.08	0.45	0.08	0.14	0.09	0.08
Total	99.36	100.36	99.46	100.20	99.45	99.13
NORMS						
Q	28.46	14.54	17.47	10.80	11.39	22.97
C	0.42	0.44	-	-	-	-
Or	20.56	18.32	20.21	11.40	12.29	20.09
Ab	36.88	40.00	39.58	46.09	41.53	37.30
An	8.04	11.00	10.10	15.14	14.12	10.01
Lc	-	-	-	-	-	-
Ne	-	-	-	-	-	-
Di	-	-	3.33	4.89	6.60	0.85
Wo	-	-	-	-	-	-
Hy	2.67	9.61	4.76	7.27	9.06	4.72
Ol	-	-	-	-	-	-
Mt	0.54	1.43	0.97	1.34	1.54	0.74
Il	0.53	1.39	1.04	1.29	1.20	0.91
Ap	0.05	0.52	0.33	0.55	0.71	0.21
Cc	0.18	1.02	0.18	0.32	0.20	0.18
TRACE ELEMENTS						
Ba	895	1005	1125	605	1055	855
Cr	22	37	37	30	105	60
Cu	7	14	11	27	9	16
Li	35	40	25	35	13	23
Ni	3	36	25	36	12	50
Rb	107	80	93	70	40	83
Sc	1	7	4	8	3	8
Sr	545	905	885	1120	745	1125
V	22	77	51	69	39	82
Y	7	18	13	15	11	14
Zn	30	66	47	70	86	69

APPENDIX B

Table B.1: WHOLE ROCK ANALYSIS OF THE STRONTIAN HOST ROCKS

	XXVII PGD	SG7 PGD	SG11 TGD	SG14 PGD	SG17 TGD	SG18 BGT
MAJOR ELEMENTS						
SiO_2	70.00	64.00	61.50	64.00	65.00	74.00
TiO_2	0.48	0.73	1.03	1.55	0.75	0.45
Al_2O_3	14.50	16.00	15.80	15.60	15.90	14.20
FeO*	2.20	5.30	5.60	4.05	4.10	1.20
MnO	0.02	0.06	0.08	0.06	0.05	0.02
MgO	1.39	2.85	3.90	2.65	2.60	0.65
CaO	2.80	3.20	3.60	3.00	2.70	1.10
Na_2O	4.55	4.90	4.30	4.89	4.75	4.40
K_2O	3.60	2.90	2.63	2.97	2.10	3.45
P_2O_5	0.09	0.35	0.33	0.32	0.26	0.05
H_2O	1.32	0.48	0.24	1.08	0.64	0.94
CO_2	-	0.08	0.05	-	0.08	0.08
Total	100.95	100.85	99.06	100.17	98.93	100.54
NORMS						
Q	22.14	12.13	11.63	13.84	18.93	31.92
C	-	0.01	0.24	-	1.72	1.54
Or	21.27	17.13	15.54	17.55	12.41	20.38
Ab	38.48	41.44	36.37	41.36	40.17	37.21
An	8.52	13.08	15.39	11.85	11.19	4.62
Lc	-	-	-	-	-	-
Ne	-	-	-	-	-	-
Di	3.88	-	-	0.75	-	-
Wo	-	-	-	-	-	-
Hy	3.46	12.36	14.88	8.65	10.25	2.35
Ol	-	-	-	-	-	-
Mt	0.82	1.97	2.08	1.51	1.52	0.45
Il	0.91	1.39	1.96	2.94	1.42	0.85
Ap	0.21	0.83	0.78	0.76	0.62	0.12
Cc	0.00	0.18	0.11	0.00	0.18	0.18
TRACE ELEMENTS						
Ba	925	988	879	1067	561	878
Cr	145	75	100	60	60	10
Cu	9	24	40	24	27	11
Li	11	20	28	24	24	35
Ni	17	95	101	92	79	38
Rb	77	57	77	57	62	112
Sc	3	10	13	10	9	4
Sr	700	1248	978	1226	1054	556
Y	42	89	123	85	87	27
Y	11	20	24	19	20	18
Zn	86	63	83	63	66	40

APPENDIX B

Table B.1: WHOLE ROCK ANALYSIS OF THE STRONTIAN HOST ROCKS

	SG19 BGT	SG20 BGT	SG21 PGD	SG25 BGT	SG27 BGT	SG29 PGD
MAJOR ELEMENTS						
SiO_2	73.00	74.00	63.50	72.00	72.50	63.50
TiO_2	0.25	0.06	0.84	0.20	0.70	0.98
Al_2O_3	14.00	14.20	16.00	15.00	15.00	15.00
FeO*	1.30	0.75	4.20	1.00	1.20	4.45
MnO	0.02	0.01	0.07	0.01	0.02	0.06
MgO	0.85	0.50	2.45	0.60	0.65	2.80
CaO	1.20	0.80	2.90	0.85	1.10	2.60
Na_2O	4.05	4.50	4.70	4.70	4.50	4.45
K_2O	3.70	3.47	2.93	3.73	3.67	3.03
P_2O_5	0.07	0.03	0.32	0.06	0.07	0.35
H_2O	0.74	0.74	1.24	0.76	0.66	1.34
CO_2	0.05	0.03	0.13	0.08	0.05	-
Total	99.23	99.09	99.28	98.99	100.12	98.56
NORMS						
Q	31.26	31.90	14.64	27.68	29.16	15.54
C	1.44	1.73	0.89	2.02	1.91	0.51
Or	21.86	20.50	17.31	22.04	21.68	17.90
Ab	34.25	38.06	39.75	39.75	38.06	37.64
An	5.18	3.58	11.47	3.32	4.68	10.61
Lc	-	-	-	-	-	-
Ne	-	-	-	-	-	-
Di	-	-	-	-	-	-
Wo	-	-	-	-	-	-
Hy	3.30	2.06	9.88	2.38	1.94	10.81
Ol	-	-	-	-	-	-
Mt	0.48	0.28	1.56	0.37	0.45	1.65
Il	0.47	0.11	1.60	0.38	1.33	1.86
Ap	0.17	0.07	0.76	0.14	0.17	0.83
Cc	0.11	0.07	0.30	0.18	0.11	0.00
TRACE ELEMENTS						
Ba	928	391	940	894	837	1175
Cr	20	10	65	12	10	75
Cu	10	10	20	10	10	17
Li	29	42	30	56	43	17
Ni	51	40	88	39	40	87
Rb	82	130	65	130	107	66
Sc	4	3	10	3	3	10
Sr	716	352	1055	503	563	1117
V	33	17	91	21	24	95
Y	9	7	21	10	8	19
Zn	33	34	70	39	39	72

APPENDIX B

Table B.1: WHOLE ROCK ANALYSIS OF THE STRONTIAN HOST ROCKS

	SG41 PGD	SG42 PGD	SG43 BGT	SG44 PGD	SG45 BGT	SG46 BGT
MAJOR ELEMENTS						
SiO_2	62.00	61.00	72.50	64.00	75.00	73.00
TiO_2	0.98	1.30	0.17	1.04	0.20	0.22
Al_2O_3	15.90	13.80	15.00	15.60	14.20	14.60
FeO*	4.40	6.70	1.10	4.60	1.00	1.05
MnO	0.06	0.11	0.02	0.06	0.02	0.01
MgO	3.00	4.70	0.70	2.90	0.60	0.60
CaO	3.85	4.25	1.05	3.00	0.80	1.00
Na_2O	5.00	4.30	4.50	4.90	4.40	4.30
K_2O	2.93	2.77	3.43	2.67	3.55	3.80
P_2O_5	0.37	0.46	0.09	0.37	0.03	0.05
H_2O	0.54	1.10	1.28	1.12	1.02	1.22
CO_2	0.08	0.08	0.03	0.10	0.05	0.08
Total	99.11	100.57	99.87	100.36	100.87	99.93
NORMS						
Q	9.39	9.63	29.77	14.09	33.04	30.37
C	-	-	2.26	0.32	1.86	1.90
Or	17.31	16.37	20.27	15.77	20.97	22.45
Ab	42.29	36.37	38.06	41.44	37.21	36.37
An	12.30	10.18	4.43	11.83	3.46	4.13
Lc	-	-	-	-	-	-
Ne	-	-	-	-	-	-
Di	3.14	5.99	-	-	-	-
Wo	-	-	-	-	-	-
Hy	9.72	14.90	2.82	11.14	2.40	2.41
Ol	-	-	-	-	-	-
Mt	1.64	2.49	0.41	1.71	0.37	0.39
Il	1.86	2.47	0.32	1.98	0.38	0.42
Ap	0.88	1.09	0.21	0.88	0.07	0.12
Cc	0.18	0.18	0.07	0.23	0.11	0.18
TRACE ELEMENTS						
Ba	967	820	979	942	807	793
Cr	70	135	15	80	10	12
Cu	22	25	13	20	10	11
Li	18	33	35	18	40	42
Ni	87	124	48	87	39	42
Rb	57	60	115	55	140	135
Sc	10	18	4	10	3	3
Sr	1243	984	608	1097	470	459
V	93	131	27	91	22	23
Y	20	31	11	20	8	9
Zn	66	101	42	69	38	41

APPENDIX B

Table B.1: WHOLE ROCK ANALYSIS OF THE STRONTIAN HOST ROCKS

	SG47 BGT	SG48 BGT	SG49 PGD	SG51 PGD	SG53A TGD	SG55 BGT
MAJOR ELEMENTS						
SiO_2	73.00	71.00	66.50	66.50	66.00	73.50
TiO_2	0.21	0.32	0.55	0.48	0.62	0.30
Al_2O_3	14.80	15.10	15.80	16.20	15.80	14.20
FeO*	0.90	1.75	3.10	3.00	3.20	1.00
MnO	0.02	0.03	0.04	0.04	0.04	0.02
MgO	0.69	0.90	2.00	1.80	2.00	0.65
CaO	0.85	0.90	2.20	2.00	2.60	0.90
Na_2O	4.50	4.70	4.63	5.05	4.70	4.40
K_2O	3.43	3.43	2.90	2.93	2.70	3.55
P_2O_5	0.05	0.09	0.23	0.21	0.21	0.05
H_2O	0.80	1.06	1.36	1.44	1.38	0.90
CO_2	0.05	0.08	0.25	0.13	0.05	0.05
Total	99.30	99.35	99.56	99.77	99.30	99.52
NORMS						
Q	30.80	27.02	20.81	18.60	19.21	31.38
C	2.38	2.42	2.18	1.89	1.04	1.72
Or	20.27	20.27	17.13	17.31	15.95	20.97
Ab	38.06	39.75	39.16	41.71	39.75	37.21
An	3.57	3.37	7.83	7.73	11.21	3.82
Lc	-	-	-	-	-	-
Ne	-	-	-	-	-	-
Di	-	-	-	-	-	-
Wo	-	-	-	-	-	-
Hy	2.49	3.87	7.87	7.36	7.87	2.36
Ol	-	-	-	-	-	-
Mt	0.33	0.65	1.15	1.12	1.19	0.37
Il	0.40	0.61	1.04	0.91	1.18	0.57
Ap	0.12	0.21	0.55	0.50	0.50	0.12
Cc	0.11	0.18	0.57	0.30	0.11	0.11
TRACE ELEMENTS						
Ba	849	1024	740	813	835	791
Cr	30	20	55	35	40	10
Cu	10	11	15	13	13	10
Li	49	49	45	41	31	56
Ni	36	50	66	58	71	41
Rb	110	127	75	90	67	127
Sc	4	4	7	6	8	4
Sr	542	648	846	863	1037	530
V	25	33	66	63	70	25
Y	12	11	17	16	20	6
Zn	40	53	58	59	56	37

APPENDIX B

Table B.1: WHOLE ROCK ANALYSIS OF THE STRONTIAN HOST ROCKS

	SG56 BGT	SG57 PGD	SG58 BGT	SG59 BGT	SG61 BGT	SG62 BGT
MAJOR FLEMENTS						
SiO_2	72.50	64.00	72.00	71.50	72.50	73.00
TiO_2	0.21	1.00	0.25	0.28	0.18	0.32
Al_2O_3	14.60	15.50	15.30	15.30	15.30	14.60
FeO*	1.10	4.30	1.20	1.25	1.35	1.10
MnO	0.02	0.06	0.02	0.02	0.02	0.02
MgO	0.60	2.85	0.70	0.80	0.70	0.50
CaO	0.90	2.85	1.10	1.30	1.25	0.80
Na_2O	4.40	4.68	4.60	4.45	4.72	4.70
K_2O	3.70	3.07	3.50	3.23	3.10	3.85
P_2O_5	0.03	0.35	0.06	0.09	0.08	0.07
H_2O	1.16	1.04	0.94	0.99	0.66	0.40
CO_2	0.05	0.05	0.05	0.08	0.05	0.05
Total	99.27	99.75	99.72	99.28	99.91	99.41
NORMS						
Q	29.71	14.17	28.29	29.28	29.22	28.45
C	1.91	0.25	2.21	2.52	2.22	1.53
Or	21.86	18.14	20.68	19.08	18.32	22.75
Ab	37.21	39.58	38.91	37.64	39.92	39.75
An	3.95	11.54	4.75	5.35	5.36	3.20
Lc	-	-	-	-	-	-
Ne	-	-	-	-	-	-
Di	-	-	-	-	-	-
Wo	-	-	-	-	-	-
Hy	2.50	10.72	2.81	3.07	3.10	2.07
Ol	-	-	-	-	-	-
Mt	0.41	1.60	0.45	0.46	0.50	0.41
Il	0.40	1.90	0.47	0.53	0.34	0.61
Ap	0.07	0.83	0.14	0.21	0.19	0.17
Cc	0.11	0.11	0.11	0.18	0.11	0.11
TRACE ELEMENTS						
Ba	697	871	790	900	863	762
Cr	12	65	20	10	15	12
Cu	11	20	10	11	11	10
Li	44	18	47	44	52	37
Ni	44	88	38	44	46	44
Rb	110	62	117	110	100	145
Sc	3	9	4	4	4	4
Sr	505	1009	524	544	584	453
V	24	86	27	30	29	26
Y	8	20	10	15	14	15
Zn	41	65	42	49	70	44

APPENDIX B

Table B.1: WHOLE ROCK ANALYSIS OF THE STRONTIAN HOST ROCKS

	SG63 BGT	SG64 BGT	SG65 BGT	SG66 BGT	SG67 BGT	SG68 BGT
MAJOR ELEMENTS						
SiO_2	73.00	73.00	73.00	73.00	73.50	74.00
TiO_2	0.29	0.20	0.17	0.20	0.20	0.17
Al_2O_3	14.60	14.60	14.60	14.80	15.00	14.20
FeO*	0.95	1.10	0.90	0.95	0.95	1.10
MnO	0.01	0.02	0.01	0.01	0.01	0.02
MgO	0.65	0.65	0.40	0.50	0.50	0.60
CaO	0.50	0.90	0.62	0.80	0.90	0.65
Na_2O	4.85	4.45	4.45	4.40	4.45	4.35
K_2O	3.80	3.75	3.80	3.60	3.75	3.85
P_2O_5	0.07	0.06	0.03	0.06	0.06	0.08
H_2O	1.36	0.54	1.18	1.12	0.58	1.02
CO_2	0.03	0.08	0.10	0.05	0.08	0.05
Total	100.11	99.34	99.26	99.49	99.98	100.09
NORMS						
Q	28.20	29.81	30.65	31.12	30.62	31.57
C	1.84	1.92	2.35	2.27	2.12	2.01
Or	22.45	22.16	22.45	21.27	22.16	22.75
Ab	41.02	37.64	37.64	37.21	37.64	36.79
An	1.83	3.57	2.25	3.26	3.57	2.39
Lc	-	-	-	-	-	-
Ne	-	-	-	-	-	-
Di	-	-	-	-	-	-
Wo	-	-	-	-	-	-
Hy	2.30	2.65	1.81	2.07	2.07	2.57
Ol	-	-	-	-	-	-
Mt	0.35	0.41	0.33	0.35	0.35	0.41
Il	0.55	0.38	0.32	0.38	0.38	0.32
Ap	0.17	0.14	0.07	0.14	0.14	0.19
Cc	0.07	0.18	0.23	0.11	0.18	0.11
TRACE ELEMENTS						
Ba	816	725	680	729	758	607
Cr	5	10	10	10	10	10
Cu	10	10	10	10	10	10
Li	42	54	37	45	57	47
Ni	37	44	31	40	40	45
Rb	125	150	135	132	135	150
Sc	3	3	3	3	3	4
Sr	619	460	403	454	445	442
V	23	23	19	22	21	23
Y	10	13	10	10	10	11
Zn	40	44	39	41	44	41

APPENDIX B

Table B.1: WHOLE ROCK ANALYSIS OF THE STRONTIAN HOST ROCKS

	SG69 BGT	SG71 BGT	SG72 BGT	SG73 BGT	SG78 BGT	SG80 TGD
MAJOR ELEMENTS						
SiO_2	73.50	72.50	72.50	70.00	70.00	68.00
TiO_2	0.18	0.30	0.20	0.26	0.48	0.65
Al_2O_3	14.60	14.20	14.60	15.50	15.90	16.60
FeO*	0.75	1.00	1.00	1.75	1.70	2.60
MnO	0.01	0.01	0.01	0.25	0.02	0.03
MgO	0.40	0.60	0.65	1.00	0.85	1.30
CaO	0.60	0.85	0.75	1.30	1.60	2.20
Na_2O	4.43	4.50	4.55	4.53	4.63	5.20
K_2O	3.96	3.75	3.84	3.13	3.20	1.83
P_2O_5	0.06	0.05	0.07	0.07	0.14	0.17
H_2O	1.08	0.90	0.99	1.20	1.00	1.74
CO_2	0.03	0.05	0.05	0.10	0.08	0.05
Total	99.59	98.71	99.21	99.09	99.59	100.37
NORMS						
Q	30.68	29.23	28.71	26.91	26.18	23.78
C	2.15	1.43	1.88	2.70	2.43	2.59
Or	23.40	22.16	22.69	18.49	18.91	10.81
Ab	37.47	38.06	38.48	38.31	39.16	43.98
An	2.39	3.57	2.95	5.36	6.52	9.49
Lc	-	-	-	-	-	-
Ne	-	-	-	-	-	-
Di	-	-	-	-	-	-
Wo	-	-	-	-	-	-
Hy	1.62	2.22	2.51	4.63	3.40	5.34
Ol	-	-	-	-	-	-
Mt	0.28	0.37	0.37	0.65	0.63	0.97
Il	0.34	0.57	0.38	0.49	0.91	1.23
Ap	0.14	0.12	0.17	0.17	0.33	0.40
Cc	0.07	0.11	0.11	0.23	0.18	0.11
TRACE ELEMENTS						
Ba	537	767	826	962	1084	305
Cr	10	12	9	30	22	45
Cu	8	10	11	18	13	17
Li	30	54	49	36	40	23
Ni	40	36	43	55	47	73
Rb	162	132	150	97	92	82
Sc	3	3	3	5	5	2
Sr	359	431	436	622	759	975
V	17	22	24	38	39	60
Y	10	9	10	11	16	8
Zn	33	38	44	57	47	51

APPENDIX B

Table B.1: WHOLE ROCK ANALYSIS OF THE STRONTIAN HOST ROCKS

	SG82 TGD	SG85 TGD	SG86 BGT	SG87 BGT	SG88 BGT	SG89 BGT
MAJOR ELEMENTS						
SiO_2	64.00	65.50	74.00	72.50	71.00	72.00
TiO_2	0.90	0.75	0.21	0.32	0.17	0.39
Al_2O_3	15.30	16.40	14.20	15.10	16.40	15.00
FeO*	4.40	3.40	1.25	1.20	1.00	1.40
MnO	0.06	0.05	0.02	0.02	0.01	0.02
MgO	3.00	1.95	0.65	0.65	0.60	0.80
CaO	3.10	3.10	0.95	1.10	0.75	1.60
Na_2O	4.53	4.75	4.45	4.45	4.35	4.70
K_2O	2.70	2.66	3.60	3.55	3.63	3.43
P_2O_5	0.26	0.24	0.03	0.08	0.03	0.07
H_2O	0.84	1.24	1.14	0.60	1.06	0.28
CO_2	0.05	0.08	0.08	0.05	0.08	0.05
Total	99.14	100.12	100.57	99.62	99.08	99.74
NORMS						
Q	15.32	17.72	31.12	29.65	29.20	26.78
C	0.03	0.83	1.52	2.25	4.21	0.93
Or	15.95	15.72	21.27	20.97	21.45	20.27
Ab	38.31	40.17	37.64	37.64	36.79	39.75
An	13.36	13.30	4.01	4.62	3.02	7.16
Lc	-	-	-	-	-	-
Ne	-	-	-	-	-	-
Di	-	-	-	-	-	-
Wo	-	-	-	-	-	-
Hy	11.38	7.79	2.81	2.57	2.43	3.07
Ol	-	-	-	-	-	-
Mt	1.64	1.26	0.46	0.45	0.37	0.52
Il	1.71	1.42	0.40	0.61	0.32	0.74
Ap	0.62	0.57	0.07	0.19	0.07	0.17
Cc	0.11	0.18	0.18	0.11	0.18	0.11
TRACE ELEMENTS						
Ba	908	946	1014	847	740	792
Cr	90	60	20	12	12	12
Cu	22	18	11	11	10	11
Li	25	20	47	43	42	47
Ni	88	72	51	45	44	50
Rb	72	67	120	127	115	105
Sc	10	9	4	4	3	4
Sr	1037	1045	670	581	472	501
V	91	79	32	28	23	25
Y	19	23	13	15	10	13
Zn	63	56	41	38	33	47

APPENDIX B

Table B.1: WHOLE ROCK ANALYSIS OF THE STRONTIAN HOST ROCKS

	SG90 BGT	SG91 BGT	SG92 PGD	SG93 TGD	G140 PGD	G24 TGD
MAJOR ELEMENTS						
SiO_2	70.50	71.50	59.00	64.00	63.00	65.00
TiO_2	0.25	0.18	1.26	1.00	1.00	0.66
Al_2O_3	15.30	15.00	16.50	14.80	15.50	16.10
FeO*	1.40	1.20	5.45	6.65	4.45	4.10
MnO	0.02	0.02	0.07	0.10	0.06	0.07
MgO	0.85	0.80	3.95	3.80	3.00	2.90
CaO	1.10	1.10	3.90	0.48	3.00	3.00
Na_2O	4.66	4.53	4.60	4.45	4.80	4.95
K_2O	3.58	3.55	2.47	1.96	3.07	1.80
P_2O_5	0.09	0.06	0.41	0.52	0.37	0.28
H_2O	1.40	1.04	1.30	1.40	1.32	1.38
CO_2	0.03	0.08	0.13	0.05	0.05	0.08
Total	99.18	99.05	99.04	99.21	99.62	100.31
NORMS						
Q	25.83	27.89	7.99	22.58	12.00	17.80
C	2.05	2.04	0.45	5.85	-	1.41
Or	21.15	20.97	14.59	11.58	18.14	10.63
Ab	39.41	38.31	38.91	37.64	40.60	41.87
An	4.68	4.56	15.85	1.33	11.69	12.55
Lc	-	-	-	-	-	-
Ne	-	-	-	-	-	-
Di	-	-	-	-	0.37	-
Wo	-	-	-	-	-	-
Hy	3.42	3.17	14.43	15.98	11.09	11.18
Ol	-	-	-	-	-	-
Mt	0.52	0.45	2.03	2.47	1.65	1.52
Il	0.47	0.34	2.39	1.90	1.90	1.25
Ap	0.21	0.14	0.97	1.23	0.88	0.66
Cc	0.07	0.18	0.30	0.11	0.11	0.18
TRACE ELEMENTS						
Ba	1004	883	990	704	1077	426
Cr	13	15	110	195	70	60
Cu	13	11	57	38	24	18
Li	54	51	30	21	17	32
Ni	46	43	103	146	92	85
Rb	120	125	72	47	57	52
Sc	4	4	13	15	10	9
Sr	633	584	1243	1408	1173	1031
V	32	28	118	122	93	81
Y	13	11	20	25	19	20
Zn	51	43	73	88	67	60

APPENDIX B

Table B.1: WHOLE ROCK ANALYSIS OF THE STRONTIAN HOST ROCKS

	GX42 TGD	GX7 TGD	SGC1 TGD	fG1 Late	fG2 Late	GR1 Late
MAJOR ELEMENTS						
SiO_2	55.00	61.00	62.00	72.00	71.00	70.00
TiO_2	1.25	0.75	0.80	0.36	0.46	0.35
Al_2O_3	15.60	15.20	14.50	14.40	14.60	15.20
FeO*	7.65	4.05	4.05	1.40	1.85	1.70
MnO	0.12	0.04	0.01	0.02	0.03	0.03
MgO	5.50	3.20	3.30	0.65	0.80	1.20
CaO	4.82	4.95	5.45	1.30	1.60	1.40
Na_2O	4.90	4.99	4.20	4.50	4.45	4.50
K_2O	2.55	2.90	2.95	3.75	3.53	3.75
P_2O	0.74	0.32	0.24	0.09	0.14	0.12
H_2O	1.20	1.42	1.30	0.72	0.78	1.30
CO_2	0.03	0.11	0.11	0.10	0.10	0.08
Total	99.36	98.93	98.91	99.29	99.34	99.62
NORMS						
Q	0.00	7.47	11.79	27.76	26.98	24.57
C	-	-	-	1.03	0.12	0.67
Or	15.07	17.13	17.43	22.16	20.86	22.16
Ab	41.44	42.20	35.52	38.06	37.64	38.06
An	13.05	10.52	12.01	5.23	6.39	5.66
Lc	-	-	-	-	-	-
Ne	-	-	-	-	-	-
Di	4.74	9.09	10.30	-	-	-
Wo	-	-	-	-	-	-
Hy	12.64	7.27	6.88	2.74	3.51	4.51
Ol	-	-	-	-	-	-
Mt	2.84	1.51	1.51	0.52	0.69	0.63
Il	2.37	1.42	0.15	0.68	0.87	0.66
Ap	1.75	0.76	0.57	0.21	0.33	0.28
Cc	0.07	0.25	0.25	0.23	0.23	0.18
TRACE ELEMENTS						
Ba	377	915	780	804	912	1033
Cr	225	67	60	20	25	30
Cu	33	15	19	15	18	17
Li	70	13	23	14	25	22
Ni	160	53	50	51	59	56
Rb	87	55	78	105	105	97
Sc	16	7	8	4	5	5
Sr	980	1000	870	583	636	627
V	151	78	86	35	44	42
Y	21	14	18	10	13	13
Zn	121	57	54	36	45	44

APPENDIX B

Table B.2 WHOLE ROCK ANALYSES OF XENOLITHS

SAMPLE	X38	X39	X40	X43	X44	X69
TYPE	Type 2	Type 1B	Type 1A	Type 1B	Type 1B	Type 1B
MAJOR ELEMENTS						
SiO_2	55.00	52.00	60.00	55.50	54.50	60.00
TiO_2	1.20	1.43	0.98	1.03	1.75	0.90
Al_2O_3	16.50	17.60	15.10	16.00	17.00	15.60
FeO*	7.80	8.40	6.40	7.30	7.45	6.00
MnO	0.10	0.08	0.07	0.14	0.12	0.09
MgO	5.65	4.90	4.00	5.50	5.00	4.40
CaO	3.90	4.00	3.70	4.20	3.95	3.50
Na_2O	5.00	4.40	3.37	5.00	5.05	4.90
K_2O	2.45	2.02	3.43	2.05	2.55	2.08
P_2O_5	0.43	0.38	0.39	0.43	0.56	0.23
H_2O	1.54	3.12	2.84	1.52	0.92	1.32
CO_2	0.03	1.00	0.03	0.03	0.05	0.08
Total	99.60	99.33	100.30	98.69	98.90	99.09
NORM						
Q	-	3.04	11.76	-	-	7.89
C	-	4.13	0.12	-	0.21	-
Or	14.48	11.93	20.27	12.11	15.07	12.29
Ab	42.29	37.21	28.50	42.29	42.71	41.44
An	15.35	11.04	15.62	15.17	15.62	14.44
Lc	-	-	-	-	-	-
Ne	-	-	-	-	-	-
Di	0.81	-	-	2.16	-	0.74
Wo	-	-	-	-	-	-
Hy	13.41	20.07	16.15	19.74	12.00	16.48
Ol	5.68	-	-	0.16	4.38	-
Mt	2.90	3.12	2.38	2.71	2.77	2.23
Il	2.28	2.72	1.86	1.96	3.32	1.71
Ap	1.02	0.90	0.92	1.02	1.33	0.55
Cc	0.07	2.27	0.07	0.07	0.11	0.18
TRACE ELEMENTS						
Ba	330	342	1125	200	282	222
Cr	140	175	140	150	155	110
Cu	66	151	102	54	38	87
Li	47	56	38	77	93	44
Ni	136	131	159	150	125	127
Rb	85	85	97	110	167	80
Sc	18	21	15	18	17	15
Sr	999	1109	926	657	784	714
V	156	170	131	130	148	129
Y	16	23	23	24	24	18
Zn	115	118	94	117	123	98

APPENDIX B

Table B.2 WHOLE ROCK ANALYSES OF XENOLITHS

SAMPLE	X75	X81	X100	X113	X116	X119
TYPE	Type 1B	Type 1B	Type 1B	Type 1B	Type 4	Type 4
MAJOR ELEMENTS						
SiO_2	57.00	54.00	55.50	55.00	56.00	54.00
TiO_2	1.83	1.35	1.28	1.35	1.70	1.75
Al_2O_3	17.20	16.40	16.00	15.60	17.00	16.20
FeO*	7.40	7.75	7.70	8.10	7.10	8.65
MnO	0.09	0.13	0.12	0.13	0.09	0.12
MgO	3.90	6.30	6.10	6.10	4.30	5.85
CaO	3.60	5.30	4.20	4.60	4.10	3.70
Na_2O	5.35	4.50	4.75	4.67	5.20	4.75
K_2O	2.36	2.30	2.82	2.45	2.30	3.07
P_2O	0.48	1.01	0.76	0.61	0.66	0.66
H_2O	1.22	0.84	0.82	1.40	1.16	0.44
CO_2	0.08	0.05	0.08	0.05	0.05	0.03
Total	100.50	99.93	100.13	100.06	99.66	99.21
NORM						
Q	2.18	-	-	-	1.10	0.00
C	0.64	-	-	-	0.20	-
Or	13.94	13.59	16.66	14.48	13.59	18.14
Ab	42.25	38.06	40.17	39.50	43.98	40.17
An	14.22	17.76	14.02	14.38	15.71	13.82
Lc	-	-	-	-	-	-
Ne	-	-	-	-	-	-
Di	-	1.31	1.09	3.36	-	0.03
Wo	-	-	-	-	-	-
Hy	15.74	16.24	15.92	16.81	16.59	9.29
Ol	-	4.44	4.41	3.25	-	9.42
Mt	2.75	2.88	2.86	3.01	2.64	3.22
Il	3.48	2.56	2.43	2.56	3.23	3.32
Ap	1.14	2.39	1.80	1.45	1.56	1.56
Cc	0.18	0.11	0.18	0.11	0.11	0.07
TRACE ELEMENTS						
Ba	465	901	295	245	356	311
Cr	65	150	165	230	80	160
Cu	107	25	20	66	105	79
Li	38	31	62	34	36	53
Ni	86	144	186	161	94	131
Rb	80	82	125	87	80	128
Sc	13	16	18	20	14	18
Sr	1166	1009	786	798	1111	793
V	176	156	155	163	162	178
Y	20	29	24	23	20	17
Zn	106	112	131	125	107	129

APPENDIX B

Table B.2 WHOLE ROCK ANALYSES OF XENOLITHS

SAMPLE	X140	X142	X143	X144	X146	X150
TYPE	Type 2	Type 1B	Type 2	Type 2	Type 4	Type 2
MAJOR ELEMENTS						
SiO_2	53.50	56.00	57.00	55.50	54.00	54.50
TiO_2	1.37	1.41	1.30	1.55	1.24	1.35
Al_2O_3	14.80	18.05	16.00	15.90	17.00	16.80
FeO*	8.80	7.00	7.00	7.90	8.10	7.80
MnO	0.14	0.09	0.10	0.12	0.11	0.12
MgO	6.60	3.95	5.00	5.25	5.60	5.55
CaO	4.70	4.30	3.90	4.10	3.80	5.30
Na_2O	4.40	5.57	4.40	5.20	5.10	5.05
K_2O	2.70	2.03	2.85	2.10	2.93	2.02
P_2O_5	0.55	0.57	0.63	0.51	0.57	0.55
H_2O	1.54	1.66	1.54	0.90	1.30	1.16
CO_2	0.05	0.05	0.05	0.03	0.05	0.03
Total	99.15	100.68	99.77	99.05	99.80	100.22
NORM						
Q	-	-	3.70	-	-	3.73
C	-	0.36	0.21	-	0.01	0.22
Or	15.95	11.99	16.84	12.41	17.31	0.12
Ab	37.21	47.11	37.21	43.98	43.13	42.71
An	12.67	17.29	14.92	13.85	14.81	22.51
Lc	-	-	-	-	-	-
Ne	-	-	-	-	-	-
Di	5.46	-	-	2.41	-	-
Wo	-	-	-	-	-	-
Hy	11.19	14.82	18.89	17.37	2.86	21.17
Ol	8.09	0.91	-	1.22	13.78	-
Mt	3.27	2.60	2.60	2.94	3.01	2.90
Il	2.60	2.68	2.47	2.94	2.35	2.56
Ap	1.30	1.35	1.49	1.21	1.35	1.30
Cc	0.11	0.11	0.11	0.07	0.11	0.07
TRACE ELEMENTS						
Ba	366	386	343	347	417	316
Cr	3	65	120	150	115	105
Cu	126	102	61	47	82	187
Li	47	25	41	31	58	46
Ni	215	89	126	115	127	102
Rb	97	55	102	70	105	65
Sc	20	14	16	21	18	19
Sr	881	1288	926	1108	1001	1097
V	168	150	147	172	167	180
Y	17	21	18	21	14	24
Zn	129	92	108	111	119	104

APPENDIX B

Table B.2 WHOLE ROCK ANALYSES OF XENOLITHS

SAMPLE	X160	X166	X170A	X171A	X172	X173
TYPE	Type 1B	Type 1B	Type 1A	Type 1A	Type 2	Type 1A
MAJOR ELEMENTS						
SiO_2	53.50	58.00	71.00	65.50	60.50	54.75
TiO_2	2.10	1.20	0.14	0.73	0.98	1.90
Al_2O_3	16.90	16.20	16.80	17.80	15.30	15.40
FeO*	8.70	5.85	0.90	3.50	5.40	7.30
MnO	0.13	0.09	0.02	0.05	0.08	0.13
MgO	4.40	3.50	0.60	1.25	4.05	5.30
CaO	4.40	4.22	1.70	2.00	4.10	5.45
Na_2O	5.40	6.50	5.45	5.00	4.53	4.80
K_2O	2.15	2.00	2.44	2.50	2.75	1.73
P_2O_5	0.80	0.44	0.06	0.28	0.32	0.66
H_2O	0.80	0.76	0.54	0.94	0.48	1.56
CO_2	0.10	0.05	0.03	0.05	0.03	0.05
Total	99.38	98.81	99.67	99.60	98.52	99.03
NORM						
Q	-	-	25.30	20.24	8.56	1.50
C	-	-	2.32	4.02	-	-
Or	12.70	11.82	14.42	14.77	16.25	10.22
Ab	45.67	54.97	46.09	42.29	38.31	40.60
An	15.53	9.13	7.85	7.78	13.30	15.37
Lc	-	-	-	-	-	-
Ne	-	-	-	-	-	-
Di	0.36	7.01	-	-	3.85	5.68
Wo	-	-	-	-	-	-
Hy	7.80	7.48	2.38	6.20	13.23	16.32
Ol	7.43	2.20	-	-	-	-
Mt	3.23	2.17	0.33	1.30	2.01	2.71
Il	3.99	2.28	0.27	1.39	1.86	3.61
Ap	1.90	1.04	0.14	0.66	0.76	1.56
Cc	0.23	0.11	0.07	0.11	0.07	0.11
TRACE ELEMENTS						
Ba	359	1317	588	1236	471	413
Cr	70	85	0	20	105	120
Cu	34	54	10	20	79	57
Li	31	15	19	46	25	29
Ni	96	95	51	52	102	73
Rb	72	40	57	100	77	70
Sc	13	15	3	8	14	25
Sr	1148	2248	1140	1509	818	872
V	169	134	21	70	114	166
Y	21	14	8	13	18	39
Zn	104	67	32	90	76	99

APPENDIX B

Table B.2 WHOLE ROCK ANALYSES OF XENOLITHS

SAMPLE	X176	X177	X178	X179	X180	X181
TYPE	Type 2	Type 3	Type 1B	Type 1B	Type 3	Type 2
MAJOR ELEMENTS						
SiO_2	69.50	54.50	67.00	69.50	54.00	65.50
TiO_2	0.55	1.40	0.56	0.46	1.35	0.75
Al_2O_3	15.30	11.60	15.60	15.20	16.40	14.20
FeO*	2.70	9.25	3.25	3.00	7.45	3.85
MnO	0.04	0.20	0.06	0.06	0.11	0.06
MgO	1.85	10.45	2.00	1.85	5.55	2.75
CaO	1.80	5.50	1.90	1.65	5.30	3.25
Na_2O	5.05	2.70	5.35	5.05	4.95	4.10
K_2O	1.80	2.75	1.87	1.90	1.93	3.43
P_2O_5	0.21	0.80	0.25	0.18	0.48	0.25
H_2O	1.32	1.20	1.28	0.88	1.99	1.50
CO_2	0.05	0.08	0.08	0.05	0.03	0.05
Total	100.17	100.42	99.20	99.78	99.54	99.69
NORM						
Q	26.28	0.83	21.21	25.88	-	17.59
C	2.39	-	2.11	2.39	-	-
Or	10.63	16.25	11.05	11.23	11.40	20.27
Ab	42.71	22.84	45.25	42.71	41.87	34.68
An	7.24	11.42	7.29	6.69	16.84	10.22
Lc	-	-	-	-	-	-
Ne	-	-	-	-	-	-
Di	-	8.13	-	-	4.96	3.20
Wo	-	-	-	-	-	-
Hy	7.01	32.28	8.07	7.56	10.45	8.79
Ol	-	-	-	-	5.72	-
Mt	1.00	3.44	1.21	1.12	2.77	1.43
Il	1.04	2.66	1.06	0.87	2.56	1.42
Ap	0.50	1.90	0.59	0.43	1.14	0.59
Cc	0.11	0.18	0.18	0.11	0.07	0.11
TRACE ELEMENTS						
Ba	251	717	275	287	442	982
Cr	50	500	40	50	200	105
Cu	15	36	27	48	22	50
Li	65	92	112	112	32	22
Ni	79	294	64	74	140	91
Rb	122	220	137	130	55	82
Sc	8	23	8	8	18	11
Sr	591	639	545	538	1129	783
V	64	172	67	64	148	81
Y	12	32	18	14	27	16
Zn	86	166	87	89	96	57

APPENDIX B

Table B.2 WHOLE ROCK ANALYSES OF XENOLITHS

SAMPLE	X182	XG01	XG0	XG1	XG2	XG3
TYPE	Type 1B	Type 5	Type 1A	Type 1A	Type 2	Type 1B
MAJOR ELEMENTS						
SiO_2	59.00	54.50	62.50	53.50	52.50	54.00
TiO_2	1.40	1.55	0.94	1.77	1.63	1.29
Al_2O_3	14.50	16.60	15.60	16.00	15.80	15.60
FeO*	6.75	7.90	4.15	7.30	7.15	7.10
MnO	0.11	0.11	0.05	0.09	0.09	0.10
MgO	4.50	5.30	2.10	5.70	5.20	5.70
CaO	4.60	3.40	3.35	6.85	7.90	6.25
Na_2O	4.45	5.05	4.73	5.05	5.35	5.02
K_2O	2.24	2.70	3.48	2.68	2.13	2.75
P_2O_5	0.44	0.60	0.56	0.44	0.44	0.41
H_2O	1.20	1.72	0.98	1.56	1.64	1.42
CO_2	0.03	0.10	0.09	0.23	0.11	0.16
Total	99.21	99.53	98.52	101.16	99.94	99.79
NORM						
Q	8.06	-	11.89	-	-	-
C	-	0.86	-	-	-	-
Or	13.23	15.95	20.56	15.83	12.58	16.25
Ab	37.64	42.71	40.00	36.73	34.51	39.01
An	12.98	12.32	11.06	13.08	12.82	11.92
Lc	-	-	-	-	-	-
Ne	-	-	-	3.24	5.82	1.87
Di	5.49	-	1.08	13.35	18.43	12.44
Wo	-	-	-	-	-	-
Hy	14.53	14.32	8.22	-	-	-
Ol	-	4.36	-	9.94	7.31	10.68
Mt	2.51	2.94	1.54	2.71	2.66	2.64
Il	2.66	2.94	1.79	3.36	3.10	2.45
Ap	1.04	1.42	1.33	1.04	1.04	0.97
Cc	0.07	0.23	0.20	0.52	0.25	0.36
TRACE ELEMENTS						
Ba	468	297	889	266	244	328
Cr	180	150	70	135	250	187
Cu	48	54	23	97	110	68
Li	34	48	91	39	42	57
Ni	142	128	24	92	78	117
Rb	77	110	120	100	80	105
Sc	18	16	8	17	19	18
Sr	728	795	630	897	1046	1018
V	140	154	71	160	157	142
Y	26	13	40	26	26	27
Zn	100	118	108	126	114	120

APPENDIX B

Table B.2 WHOLE ROCK ANALYSES OF XENOLITHS

SAMPLE	XG3A	XG4	XG5	XG6	XG7	XG8
TYPE	Type 1A	Type 5	Type 5	Type 1B	Type 1B	Type 3
MAJOR ELEMENTS						
SiO_2	56.00	60.00	54.50	50.25	54.50	54.00
TiO_2	1.41	1.41	1.27	1.33	1.13	1.28
Al_2O_3	14.90	15.50	15.50	12.30	15.60	16.20
FeO*	6.85	4.60	7.85	7.50	6.25	6.80
MnO	0.09	0.10	0.10	0.14	0.09	0.07
MgO	5.30	5.50	6.70	8.90	5.50	4.55
CaO	7.00	5.00	5.64	9.90	7.25	5.90
Na_2O	4.90	5.28	4.80	3.43	4.99	5.05
K_2O	2.30	2.18	3.20	2.50	2.10	2.83
P_2O_5	0.51	0.59	0.71	0.81	0.50	0.44
H_2O	1.52	1.22	1.14	1.84	1.20	1.68
CO_2	0.11	0.09	0.08	0.28	0.00	0.11
Total	100.90	101.47	101.49	99.17	99.11	98.91
NORM						
Q	-	4.21	-	-	-	-
C	-	-	-	-	-	-
Or	13.59	12.88	18.91	14.77	12.41	16.72
Ab	41.44	44.66	38.46	24.04	42.08	41.13
An	11.88	12.16	11.30	10.79	13.97	13.19
Lc	-	-	-	-	-	-
Ne	-	-	1.16	2.69	0.07	0.86
Di	15.20	6.54	9.35	25.03	15.09	10.15
Wo	-	-	-	-	-	-
Hy	7.82	13.96	-	-	-	-
Ol	2.96	-	14.23	12.39	8.83	9.13
Mt	2.55	1.71	2.92	2.79	2.32	2.53
Il	2.68	2.68	2.41	2.53	2.15	2.43
Ap	1.21	1.40	1.68	1.92	1.19	1.04
Cc	0.25	0.20	0.18	0.64	0.00	0.25
TRACE ELEMENTS						
Ba	296	274	338	780	871	641
Cr	100	90	120	270	87	60
Cu	104	45	59	38	33	130
Li	43	49	66	32	26	24
Ni	99	106	109	154	112	56
Rb	88	93	130	53	60	90
Sc	18	17	17	25	15	14
Sr	1027	944	766	1263	1107	1132
V	136	137	150	175	120	124
Y	24	24	18	29	20	16
Zn	123	114	126	111	96	83

APPENDIX B

Table B.2 WHOLE ROCK ANALYSES OF XENOLITHS

SAMPLE	XG9	XG11	XG12	XG13	XG14	XG15
TYPE	Type 5	Type 2	Type 5	Type 5	Type 1B	Type 5
MAJOR ELEMENTS						
SiO_2	53.50	57.00	53.50	53.50	57.00	52.00
TiO_2	1.73	1.13	1.43	1.24	1.15	1.51
Al_2O_3	16.40	15.10	17.60	16.20	14.80	16.70
FeO*	7.35	7.00	6.75	6.55	6.00	7.70
MnO	0.08	0.07	0.07	0.09	0.09	0.08
MgO	4.85	4.55	5.40	5.50	4.60	5.20
CaO	6.60	5.85	4.40	6.85	6.05	5.85
Na_2O	5.40	5.01	5.45	5.20	4.75	5.20
K_2O	2.35	2.18	3.25	2.35	2.33	3.03
P_2O_5	1.01	0.58	0.51	0.57	0.36	0.98
H_2O	1.18	1.70	1.92	1.78	1.44	1.46
CO_2	0.11	0.03	0.09	0.11	0.07	0.11
Total	100.56	100.19	100.36	99.94	98.64	99.82
NORM						
Q	-	1.66	-	-	2.62	-
C	-	-	-	-	-	-
Or	13.88	12.88	19.20	13.88	13.77	17.90
Ab	42.19	42.37	38.92	39.06	40.17	35.69
An	13.58	12.28	13.97	13.93	12.19	13.29
Lc	-	-	-	-	-	-
Ne	1.89	-	3.89	2.67	-	4.49
Di	9.62	10.38	3.19	12.61	12.15	7.01
Wo	-	-	-	-	-	-
Hy	-	12.94	-	-	11.05	-
Ol	9.81	-	12.84	9.82	-	11.93
Mt	2.73	2.60	2.51	2.43	2.23	2.86
Il	3.29	2.15	2.72	2.35	2.18	2.87
Ap	2.39	1.38	1.21	1.35	0.85	2.32
Cc	0.25	0.07	0.20	0.25	0.16	0.25
TRACE ELEMENTS						
Ba	483	388	408	307	372	420
Cr	185	70	60	115	65	75
Cu	41	149	44	66	86	37
Li	34	44	79	48	41	68
Ni	68	54	104	95	88	92
Rb	75	88	128	78	85	135
Sc	12	14	7	15	15	9
Sr	1100	961	955	862	940	993
V	131	131	122	121	120	153
Y	21	17	9	24	17	30
Zn	92	92	105	111	93	117

APPENDIX B

Table B.2 WHOLE ROCK ANALYSES OF XENOLITHS

SAMPLE	XG18	XG19	XG20	XG20A	XG21	XG21A
TYPE	Type 3	Type 1B	Type 4	Type 1B	Type 2	Type 5
MAJOR ELEMENTS						
SiO_2	49.50	56.00	59.50	59.00	52.50	53.50
TiO_2	1.23	1.08	0.98	0.95	1.28	1.35
Al_2O_3	8.60	15.80	15.10	15.00	14.90	15.80
FeO*	12.60	7.00	5.20	5.20	8.00	6.80
MnO	0.26	0.10	0.06	0.07	0.12	0.09
MgO	10.85	5.65	4.10	4.30	6.80	5.40
CaO	8.85	4.63	6.10	6.55	7.20	7.15
Na_2O	1.10	5.02	4.50	4.20	4.43	5.10
K_2O	3.80	2.44	2.25	2.08	2.49	2.53
P_2O_5	0.96	0.47	0.40	0.32	0.44	0.64
H_2O	1.90	1.50	1.50	1.70	1.44	1.00
CO_2	0.11	0.09	0.03	0.08	0.08	0.14
Total	99.75	99.78	99.71	99.44	99.67	99.50
NORM						
Q	-	-	7.44	8.14	-	-
C	-	-	-	-	-	-
Or	22.45	14.42	13.29	12.29	14.71	14.95
Ab	9.30	42.46	38.06	35.52	34.15	37.76
An	7.31	13.38	14.36	15.94	13.42	12.76
Lc	-	-	-	-	-	-
Ne	-	-	-	-	1.80	2.91
Di	23.99	4.81	10.58	11.26	15.27	14.25
Wo	-	-	-	-	-	-
Hy	16.87	14.57	9.83	10.07	-	-
Ol	8.77	2.87	-	-	12.49	9.16
Mt	4.68	2.60	1.93	1.93	2.97	2.53
Il	2.34	2.05	1.86	1.80	2.43	2.56
Ap	2.28	1.11	0.95	0.76	1.04	1.52
Cc	0.25	0.20	0.07	0.18	0.18	0.32
TRACE ELEMENTS						
Ba	718	314	792	778	321	396
Cr	290	130	80	47	245	80
Cu	45	126	54	50	96	44
Li	55	42	25	21	35	35
Ni	175	103	69	75	133	92
Rb	130	83	58	53	80	63
Sc	31	17	12	14	19	16
Sr	201	947	1007	915	941	1179
V	238	142	101	101	136	147
Y	73	19	18	19	20	16
Zn	190	111	77	77	117	102

APPENDIX B

Table B.2 WHOLE ROCK ANALYSES OF XENOLITHS

SAMPLE	XG22	XG22A	XG22B	XG23	XG24	XG24A
TYPE	Type 1B	Type 2	Type 1B	Type 1A	Type 1B	Type 1B
MAJOR ELEMENTS						
SiO_2	52.00	52.50	53.50	54.50	55.00	58.00
TiO_2	1.15	1.03	1.16	1.38	1.55	1.08
Al_2O_3	15.90	15.80	15.50	16.20	17.40	16.20
FeO*	6.90	7.40	6.75	6.45	7.15	5.70
MnO	0.09	0.10	0.11	0.08	0.18	0.07
MgO	5.20	6.20	6.00	4.70	3.70	4.25
CaO	8.10	5.85	7.40	6.40	4.50	4.70
Na_2O	5.01	4.60	5.05	5.10	5.00	4.90
K_2O	1.93	2.93	1.93	2.43	2.15	2.35
P_2O_5	0.48	0.52	0.35	0.45	0.37	0.41
H_2O	1.72	1.60	2.18	2.16	2.12	1.42
CO_2	0.08	0.00	0.11	0.08	0.08	0.14
Total	98.56	98.52	100.04	99.92	99.19	99.22
NORM						
Q	-	-	-	-	1.08	4.27
C	-	-	-	-	-	-
Or	11.40	17.31	11.40	14.36	12.70	13.88
Ab	35.07	35.55	39.24	43.13	42.29	41.44
An	15.20	13.82	13.93	14.14	18.69	15.28
Lc	-	-	-	-	-	-
Ne	3.96	1.82	1.88	-	-	-
Di	17.28	9.54	15.96	11.45	0.58	3.62
Wo	-	-	-	-	-	-
Hy	-	-	-	0.30	15.29	14.02
Ol	8.06	13.17	9.85	8.30	-	-
Mt	2.56	2.75	2.51	2.40	2.66	2.12
Il	2.18	1.96	2.20	2.62	2.94	2.05
Ap	1.14	1.23	0.83	1.07	0.88	0.97
Cc	0.18	0.00	0.25	0.18	0.18	0.32
TRACE ELEMENTS						
Ba	380	412	293	794	321	926
Cr	70	260	110	115	85	150
Cu	195	113	107	34	63	75
Li	28	41	28	25	37	26
Ni	74	128	122	77	98	74
Rb	63	103	63	73	90	60
Sc	19	15	19	14	20	14
Sr	1179	1014	1013	1107	1016	1199
V	147	133	134	113	163	116
Y	16	16	21	26	39	27
Zn	102	123	102	93	101	86

APPENDIX B

Table B.2 WHOLE ROCK ANALYSES OF XENOLITHS

SAMPLE	XG25	XG26	XG27	XG28	XG29	XG30
TYPE	Type 2	Type 2	Type 4	Type 2	Type 1B	Type 5
MAJOR ELEMENTS						
SiO_2	53.00	55.00	56.00	51.75	58.75	57.00
TiO_2	1.08	1.35	1.33	0.95	0.90	1.09
Al_2O_3	14.20	15.80	16.20	14.30	14.10	14.50
FeO*	7.80	6.25	6.25	8.00	6.50	5.80
MnO	0.12	0.08	0.08	0.14	0.07	0.08
MgO	6.75	4.85	3.35	7.25	5.40	5.30
CaO	6.85	5.65	7.00	7.40	4.10	5.85
Na_2O	4.34	5.01	5.10	4.65	4.50	4.99
K_2O	1.70	1.98	2.03	2.05	2.68	2.19
P_2O	0.25	0.41	0.30	0.44	0.41	0.44
H_2O	2.82	3.04	1.92	1.52	2.06	1.46
CO_2	0.11	0.14	0.11	0.11	0.14	0.09
Total	99.02	99.56	99.67	98.56	99.61	98.78
NORM						
Q	-	0.13	0.88	-	5.50	1.50
C	-	-	-	-	-	-
Or	10.04	11.70	11.99	12.11	15.83	12.88
Ab	36.71	42.37	43.13	33.98	38.06	42.20
An	14.25	14.78	15.32	12.10	10.37	10.74
Lc	-	-	-	-	-	-
Ne	-	-	-	2.90	-	-
Di	14.06	7.81	13.66	16.99	5.18	11.95
Wo	-	-	-	-	-	-
Hy	9.67	13.72	7.12	-	17.38	12.76
Ol	5.89	-	-	13.12	-	-
Mt	2.90	2.32	2.32	2.97	2.42	2.16
Il	2.05	2.56	2.53	1.80	1.71	2.07
Ap	0.59	0.97	0.71	1.04	0.97	1.04
Cc	0.25	0.32	0.25	0.25	0.32	0.20
TRACE ELEMENTS						
Ba	317	368	429	293	291	239
Cr	175	100	55	155	115	272
Cu	64	91	203	97	30	34
Li	38	25	27	33	48	51
Ni	135	66	47	142	126	120
Rb	60	68	65	78	103	88
Sc	22	16	15	23	9	14
Sr	870	1089	1077	829	730	799
V	129	110	130	129	102	104
Y	16	25	26	19	10	12
Zn	123	89	89	117	102	105

APPENDIX B

Table B.2 WHOLE ROCK ANALYSES OF XENOLITHS

SAMPLE	XG31	XG32	XG33	XG34	XG35	XG36
TYPE	Type 1A	Type 1A	Type 2	Type 2	Type 2	Type 2
MAJOR ELEMENTS						
SiO_2	53.25	67.90	51.50	50.00	53.75	53.00
TiO_2	1.15	0.48	2.13	1.14	1.18	1.48
Al_2O_3	16.60	16.30	15.20	16.50	14.90	14.80
FeO*	7.75	2.55	9.20	9.20	7.10	8.70
MnO	0.08	0.02	0.10	0.11	0.10	0.13
MgO	4.18	1.43	6.35	7.45	5.70	6.00
CaO	6.45	4.15	5.40	3.90	6.80	4.30
Na_2O	5.10	5.03	4.55	4.60	4.90	4.25
K_2O	2.78	1.88	3.38	2.35	2.35	3.15
P_2O_5	0.89	0.13	1.05	0.49	0.59	0.71
H_2O	1.46	0.84	1.86	3.70	1.90	1.92
CO_2	0.03	0.08	0.08	0.74	0.90	0.63
Total	99.71	100.77	100.79	100.17	100.17	99.07
NORM						
Q	-	20.60	-	-	-	-
C	-	-	-	2.19	-	-
Or	16.42	11.11	19.97	13.88	13.88	18.61
Ab	39.17	42.54	34.43	38.91	41.44	35.95
An	14.20	16.35	11.08	11.47	11.73	12.01
Lc	-	-	-	-	-	-
Ne	2.15	-	2.19	-	-	-
Di	9.66	2.35	6.76	-	10.07	0.57
Wo	-	-	-	-	-	-
Hy	-	4.72	-	5.94	5.03	6.38
Ol	9.67	-	14.67	15.93	8.00	4.74
Mt	2.88	0.95	3.42	3.42	2.64	3.23
Il	2.18	0.91	4.05	2.17	2.24	2.81
Ap	2.11	0.31	2.49	1.16	1.40	1.68
Cc	0.07	0.18	0.18	1.68	2.05	1.43
TRACE ELEMENTS						
Ba	540	768	333	349	283	370
Cr	135	77	147	257	90	175
Cu	184	28	61	58	51	64
Li	45	22	72	60	40	58
Ni	49	17	102	146	75	157
Rb	100	53	163	95	83	125
Sc	11	4	11	16	17	18
Sr	1037	1094	778	713	838	773
V	159	42	169	46	132	174
Y	29	11	21	12	24	17
Zn	102	53	150	144	111	132

APPENDIX B

Table B.2 WHOLE ROCK ANALYSES OF XENOLITHS

SAMPLE	XG37	XG39	XG40	XG41	XG43	XG44
TYPE	Type 5	Type 5	Type 5	Type 5	Type 5	Type 2
MAJOR ELEMENTS						
SiO_2	52.75	53.50	52.50	53.50	50.00	53.50
TiO_2	1.58	1.45	1.59	1.20	1.30	1.25
Al_2O_3	14.60	15.80	15.50	18.30	15.60	15.70
FeO*	6.90	9.20	8.65	6.70	8.15	7.40
MnO	0.11	0.12	0.10	0.06	0.11	0.09
MgO	6.25	5.90	6.58	4.40	6.80	5.15
CaO	7.20	3.70	3.40	3.85	6.30	6.55
Na_2O	4.70	4.50	4.39	5.68	4.23	4.90
K_2O	2.55	2.94	3.55	2.88	3.05	2.38
P_2O	0.69	0.86	0.65	0.81	0.45	0.64
H_2O	1.66	1.86	2.32	1.42	2.14	1.24
CO_2	0.74	0.03	0.11	0.09	0.37	0.09
Total	99.73	99.85	99.34	98.89	98.49	98.89
NORM						
Q	-	-	-	-	-	-
C	-	0.62		0.99	-	-
Or	15.07	17.37	20.97	17.02	18.02	14.06
Ab	39.48	38.06	37.13	45.99	29.02	41.44
An	11.22	12.55	11.93	13.24	14.58	13.82
Lc	-	-	-	-	-	-
Ne	0.15	-	-	1.11	3.66	-
Di	12.31	-	-	-	9.21	11.30
Wo	-	-	-	-	-	-
Hy	-	5.64	5.58	-	-	0.02
Ol	11.18	5.76	13.58	12.44	14.70	10.38
Mt	2.56	3.42	3.22	2.49	3.03	2.75
Il	3.00	2.75	3.02	2.28	2.47	2.37
Ap	1.64	2.04	1.54	1.92	1.07	1.52
Cc	1.68	0.07	0.25	0.20	0.84	0.20
TRACE ELEMENTS						
Ba	325	312	373	372	452	451
Cr	120	195	90	120	140	205
Cu	68	29	94	69	43	140
Li	44	57	72	58	53	43
Ni	117	123	122	80	137	80
Rb	90	117	143	100	100	80
Sc	18	16	17	11	19	17
Sr	835	790	787	1273	963	1167
V	135	172	164	144	149	144
Y	23	16	11	12	11	18
Zn	123	130	144	114	135	114

APPENDIX B

Table B.2 WHOLE ROCK ANALYSES OF XENOLITHS

SAMPLE	XG45	XG46	XG47	XG48	XG48A	XG50
TYPE	Type 1B	Type 4	Type 4	Type 2	Type 1A	Type 1A
MAJOR ELEMENTS						
SiO_2	55.50	54.25	56.00	51.50	55.00	53.75
TiO_2	1.20	1.32	1.30	1.44	1.35	1.30
Al_2O_3	15.00	15.60	15.00	15.60	16.20	15.90
FeO*	6.50	6.75	6.40	7.15	7.40	7.65
MnO	0.09	0.09	0.09	0.10	0.09	0.10
MgO	5.90	5.40	5.20	5.55	5.30	6.20
CaO	6.50	6.90	6.60	7.45	6.30	6.10
Na_2O	5.20	5.05	4.73	5.02	5.15	5.20
K_2O	2.10	2.40	2.25	2.15	2.50	2.70
P_2O_5	0.44	0.18	0.50	0.49	0.50	0.52
H_2O	1.22	2.06	1.32	2.04	0.78	1.50
CO_2	0.14	0.09	0.11	0.11	0.08	0.08
Total	99.79	100.09	99.49	98.60	100.64	100.99
NORM						
Q	-	-	0.52	-	-	-
C	-	-	-	-	-	-
Or	12.41	14.18	13.29	12.70	14.77	15.95
Ab	43.98	39.22	40.00	34.42	42.72	37.63
An	11.39	12.82	13.06	13.69	13.71	12.08
Lc	-	-	-	-	-	-
Ne	-	1.89	-	4.35	0.45	3.44
Di	13.76	15.88	12.68	15.65	11.16	11.54
Wo	-	-	-	-	-	-
Hy	3.68	-	12.53	-	-	-
Ol	7.49	8.58	-	9.15	10.59	12.36
Mt	2.42	2.51	2.38	2.66	2.75	2.84
Il	2.28	2.51	2.47	2.73	2.56	2.47
Ap	1.04	0.43	1.19	1.16	1.19	1.23
Cc	0.32	0.20	0.25	0.25	0.18	0.18
TRACE ELEMENTS						
Ba	420	513	552	349	420	256
Cr	145	80	132	125	100	230
Cu	67	67	96	169	130	38
Li	50	31	33	27	37	66
Ni	132	108	104	92	84	120
Rb	80	75	65	55	80	120
Sc	16	15	16	17	17	16
Sr	1210	1169	1169	1022	1126	777
V	127	132	130	136	144	134
Y	23	26	23	19	13	16
Zn	108	102	96	105	102	111

APPENDIX B

Table B.2 WHOLE ROCK ANALYSES OF XENOLITHS

SAMPLE	XG51	XG52	XG53	XG54	XG55	XG56
TYPE	Type 1A	Type 1B	Type 1B	Type 1B	Type 4	Type 4
MAJOR ELEMENTS						
SiO_2	64.75	67.50	66.00	65.50	61.75	63.50
TiO_2	0.65	0.75	0.65	0.68	0.58	0.73
Al_2O_3	14.30	10.60	13.90	13.90	14.20	13.60
FeO*	3.95	4.05	4.35	3.90	4.40	4.05
MnO	0.05	0.05	0.06	0.05	0.05	0.05
MgO	2.90	3.20	3.40	3.30	3.60	3.30
CaO	3.25	4.75	3.60	5.25	5.50	4.80
Na_2O	4.43	4.33	4.33	4.23	4.30	4.23
K_2O	3.28	2.83	2.98	2.70	2.43	2.95
P_2O_5	0.24	0.26	0.25	0.26	0.22	0.22
H_2O	1.44	0.76	1.34	1.08	1.56	1.30
CO_2	0.11	0.08	0.08	0.05	0.11	0.14
Total	99.34	99.15	100.93	100.89	98.70	98.86
NORM						
Q	15.38	20.19	16.94	16.44	12.00	14.33
C	-	-	-	-	-	-
Or	19.38	16.72	17.61	15.95	14.36	17.43
Ab	37.47	36.62	36.62	35.78	36.37	35.78
An	9.45	1.14	9.70	10.97	12.28	9.42
Lc	-	-	-	-	-	-
Ne	-	-	-	-	-	-
Di	3.57	16.34	4.88	10.53	10.42	9.75
Wo	-	-	-	-	-	-
Hy	9.25	3.78	10.36	6.78	8.34	7.26
Ol	-	-	-	-	-	-
Mt	1.47	1.51	1.62	1.45	1.64	1.51
Il	1.23	1.42	1.23	1.29	1.10	1.39
Ap	0.57	0.62	0.59	0.62	0.52	0.52
Cc	0.25	0.18	0.18	0.11	0.25	0.32
TRACE ELEMENTS						
Ba	795	730	824	1156	923	1083
Cr	52	60	105	187	130	130
Cu	44	27	38	65	64	75
Li	37	29	33	45	42	39
Ni	50	82	79	83	83	83
Rb	100	88	88	78	80	85
Sc	10	11	14	14	17	15
Sr	862	712	846	990	1090	994
V	77	81	102	91	111	104
Y	19	19	23	18	21	20
Zn	65	65	90	77	83	86

APPENDIX B

Table B.2 WHOLE ROCK ANALYSES OF XENOLITHS

SAMPLE	XG57	XG58	XG59	XG60	XG61A	XG61B
TYPE	Type 1B	Type 1B	Type 1A	Type 5	Type 2	Type 2
MAJOR ELEMENTS						
SiO_2	64.50	62.00	63.25	64.00	63.50	62.00
TiO_2	0.62	0.73	0.72	0.78	0.70	0.75
Al_2O_3	15.40	14.60	14.10	14.50	13.40	13.70
FeO*	4.20	4.00	4.00	4.15	4.65	4.30
MnO	0.06	0.05	0.05	0.04	0.06	0.05
MgO	2.70	3.30	2.90	3.00	4.10	3.85
CaO	2.80	5.30	5.20	4.10	6.00	5.80
Na_2O	4.40	4.39	4.35	4.30	4.10	4.25
K_2O	2.95	3.00	3.10	2.73	2.20	2.63
P_2O_5	0.30	0.19	0.22	0.24	0.09	0.18
H_2O	1.06	1.18	1.20	1.44	0.98	1.10
CO_2	0.13	0.05	0.05	0.14	0.09	0.09
Total	99.12	98.78	99.14	99.42	99.87	98.70
NORM						
Q	15.33	10.63	12.79	15.88	14.38	11.56
C	-	-	-	-	-	-
Or	17.43	17.72	18.32	16.13	13.00	15.54
Ab	37.21	37.13	36.79	36.37	34.68	35.95
An	13.56	11.28	9.80	12.21	11.67	10.54
Lc	-	-	-	-	-	-
Ne	-	-	-	-	-	-
Di	2.04	10.86	11.54	4.60	13.67	13.28
Wo	-	-	-	-	-	-
Hy	9.86	6.66	5.33	9.01	8.15	7.20
Ol	-	-	-	-	-	-
Mt	1.56	1.49	1.49	1.54	1.73	1.60
Il	1.18	1.39	1.37	1.48	1.33	1.42
Ap	0.71	0.45	0.52	0.57	0.21	0.43
Cc	0.30	0.11	0.11	0.32	0.20	0.20
TRACE ELEMENTS						
Ba	801	882	913	819	828	892
Cr	65	95	45	52	105	172
Cu	34	44	49	33	40	50
Li	35	36	38	45	30	37
Ni	82	82	69	68	71	74
Rb	90	80	95	93	65	73
Sc	10	12	12	9	16	14
Sr	812	930	846	861	793	843
V	88	95	89	83	101	91
Y	17	22	21	21	19	18
Zn	64	77	74	77	71	65

APPENDIX B

Table B.2 WHOLE ROCK ANALYSES OF XENOLITHS

SAMPLE	XG61C	XG62	XG63	XG64A	XG64B	XG65
TYPE	Type 2	Type 2	Type 4	Type 1B	Type 1B	Type 1A
MAJOR ELEMENTS						
SiO_2	64.00	64.25	64.50	64.50	65.50	60.00
TiO_2	0.62	0.73	0.75	0.73	0.73	1.05
Al_2O_3	14.00	13.50	13.70	14.40	14.80	15.20
FeO*	4.05	4.45	3.95	3.75	3.70	5.55
MnO	0.05	0.05	0.04	0.04	0.04	0.07
MgO	3.90	3.90	3.60	2.80	2.80	3.95
CaO	5.70	5.55	5.10	5.20	4.60	6.15
Na_2O	4.03	4.15	4.15	4.31	4.35	4.95
K_2O	2.48	2.40	2.75	2.93	2.66	2.23
P_2O_5	0.07	0.21	0.17	0.22	0.19	0.36
H_2O	1.22	1.60	1.54	1.12	1.28	1.40
CO_2	0.05	0.08	0.05	0.09	0.09	0.09
Total	100.17	100.87	100.30	100.09	100.74	101.00
NORM						
Q	14.79	15.27	15.41	14.95	17.01	5.81
C	-	-	-	-	-	-
Or	14.65	14.18	16.25	17.31	15.72	13.18
Ab	34.08	35.10	35.10	36.45	36.79	41.87
An	12.79	11.13	10.64	11.30	13.01	12.68
Lc	-	-	-	-	-	-
Ne	-	-	-	-	-	-
Di	11.84	11.72	10.65	10.10	6.47	12.08
Wo	-	-	-	-	-	-
Hy	7.94	8.29	7.42	5.45	7.15	9.04
Ol	-	-	-	-	-	-
Mt	1.51	1.65	1.47	1.39	1.38	2.06
Il	1.18	1.39	1.42	1.39	1.39	1.99
Ap	0.17	0.50	0.40	0.52	0.45	0.85
Cc	0.11	0.18	0.11	0.20	0.20	0.20
TRACE ELEMENTS						
Ba	948	906	911	832	892	443
Cr	70	170	155	57	50	105
Cu	44	82	46	35	34	51
Li	36	39	30	36	39	43
Ni	69	69	69	55	57	73
Rb	70	80	73	83	83	93
Sc	15	15	13	10	10	13
Sr	830	880	804	797	838	761
V	90	92	83	74	76	104
Y	17	17	15	17	18	23
Zn	68	74	65	56	62	83

APPENDIX B

Table B.2 WHOLE ROCK ANALYSES OF XENOLITHS

SAMPLE	XG66	XG67	XG68	XG69	XG70	XG71
TYPE	Type 5	Type 2	Type 2	Type 1A	Type 5	Type 5
MAJOR ELEMENTS						
SiO_2	63.50	62.00	53.00	52.00	53.00	48.00
TiO_2	0.78	0.75	1.47	1.64	1.08	1.29
Al_2O_3	14.00	14.20	16.30	16.70	15.00	9.80
FeO*	4.10	4.65	6.50	8.95	7.45	9.05
MnO	0.05	0.07	0.10	0.11	0.12	0.14
MgO	3.20	4.60	4.80	5.70	6.90	12.05
CaO	4.75	3.85	6.90	3.60	6.70	8.10
Na_2O	4.55	4.99	5.80	4.53	4.65	1.45
K_2O	2.63	2.12	2.14	3.20	2.55	4.40
P_2O_5	0.25	0.37	0.84	0.80	0.35	1.52
H_2O	1.84	1.38	1.84	1.82	2.02	2.64
CO_2	0.48	0.09		0.45	0.25	1.10
Total	100.13	99.06	99.69	99.50	100.07	99.54
NORM						
Q	14.28	10.33	-	-	-	-
C	-	-	-	2.20	-	-
Or	15.54	12.53	12.64	18.91	15.07	26.00
Ab	38.48	42.20	39.53	38.31	36.12	12.26
An	10.02	10.09	12.13	9.97	12.53	7.24
Lc	-	-	-	-	-	-
Ne	-	-	5.16	-	1.74	-
Di	7.17	4.84	13.42	-	13.57	12.84
Wo	-	-	-	-	-	-
Hy	8.23	13.60	-	11.26	-	11.97
Ol	-	-	7.98	8.12	13.01	14.98
Mt	1.52	1.73	2.42	3.33	2.77	3.36
Il	1.48	1.42	2.79	3.11	2.05	2.45
Ap	0.59	0.88	1.99	1.90	0.83	3.60
Cc	1.09	0.20	0.00	1.02	0.57	2.50
TRACE ELEMENTS						
Ba	729	269	221	444	473	1525
Cr	195	100	110	105	115	457
Cu	38	47	86	41	75	88
Li	32	53	53	58	52	45
Ni	75	107	62	134	139	403
Rb	83	85	90	112	85	128
Sc	11	15	17	15	20	18
Sr	853	896	901	764	840	606
V	85	105	165	196	131	130
Y	19	14	31	13	13	23
Zn	77	90	111	135	117	129

APPENDIX B

Table B.2 WHOLE ROCK ANALYSES OF XENOLITHS

SAMPLE	XG74	XG75	XG77	XG78	XG80	XG81
TYPE	Type 1B	Type 1B	Type 2	Type 4	Type 2	Type 2
MAJOR ELEMENTS						
SiO_2	53.50	52.50	55.00	57.00	63.50	51.75
TiO_2	1.20	1.54	1.30	1.48	0.92	1.50
Al_2O_3	16.60	16.80	16.00	16.00	14.00	16.50
FeO*	7.90	7.50	7.75	6.60	5.00	7.10
MnO	0.11	0.07	0.09	0.07	0.05	0.09
MgO	5.50	3.90	5.20	4.20	3.60	4.85
CaO	5.28	6.30	5.80	6.57	4.15	7.10
Na_2O	4.28	5.64	5.26	4.83	4.30	4.41
K_2O	2.57	2.44	2.62	2.29	2.13	2.20
P_2O_5	0.76	0.91	0.26	0.37	0.16	0.39
H_2O	1.62	0.86	1.24	1.46	1.60	2.72
CO_2	0.05	0.03	0.09	0.05	0.11	1.25
Total	99.36	98.48	100.61	100.91	99.52	99.86
NORM						
Q	-	-	-	1.62	16.12	-
C	-	-	-	-	-	-
Or	15.18	14.42	15.48	13.53	12.58	13.00
Ab	36.20	39.84	42.18	40.85	36.37	37.30
An	18.50	13.33	12.32	15.22	12.62	18.74
Lc	-	-	-	-	-	-
Ne	-	4.26	1.25	-	-	-
Di	1.96	9.63	11.52	11.87	5.05	4.89
Wo	-	-	-	-	-	-
Hy	15.23	-	-	10.30	11.09	9.55
Ol	3.79	8.46	10.66	-	-	4.62
Mt	2.94	2.79	2.88	2.45	1.86	2.64
Il	2.28	2.92	2.47	2.81	1.75	2.85
Ap	1.80	2.16	0.62	0.88	0.38	0.92
Cc	0.11	0.07	0.20	0.11	0.25	2.84
TRACE ELEMENTS						
Ba	1137	717	263	652	589	919
Cr	187	95	90	102	155	130
Cu	42	59	94	70	25	131
Li	26	31	36	22	33	49
Ni	56	44	69	42	59	57
Rb	68	63	108	68	85	93
Sc	18	12	15	13	10	21
Sr	1488	1357	753	1041	1030	1127
V	172	134	124	115	86	133
Y	39	15	12	13	7	20
Zn	102	93	90	77	74	90

APPENDIX B

Table B.2 WHOLE ROCK ANALYSES OF XENOLITHS

SAMPLE	XG82	XG84	XG85	XG87	XG88	XG89
TYPE	Type 1B	Type 1B	Type 2	Type 2	Type 4	Type 2
MAJOR ELEMENTS						
SiO_2	54.00	50.75	53.00	50.50	54.50	52.50
TiO_2	1.03	1.73	1.43	1.83	1.45	1.16
Al_2O_3	15.40	16.40	16.60	16.20	16.70	14.00
FeO*	7.05	8.20	6.70	7.95	7.20	8.60
MnO	0.09	0.10	0.12	0.10	0.09	0.16
MgO	6.00	4.90	5.15	5.20	4.50	7.80
CaO	4.60	7.35	7.70	8.55	7.20	7.30
Na_2O	5.55	4.60	4.90	4.60	5.30	3.65
K_2O	1.78	1.60	1.73	2.00	1.85	2.55
P_2O_5	0.48	0.71	0.43	0.43	0.56	0.30
H_2O	2.46	2.92	1.86	2.14	1.00	1.72
CO_2	0.09	0.09	0.08	0.08	0.09	0.11
Total	98.53	99.35	99.69	99.57	100.44	99.85
NORM						
Q	-	-	-	-	-	-
C	-	-	-	-	-	-
Or	10.52	9.45	10.22	11.82	10.93	15.07
Ab	46.94	38.91	40.25	30.48	44.47	30.87
An	11.86	19.93	18.20	17.66	16.32	14.29
Lc	-	-	-	-	-	-
Ne	-	-	0.64	4.57	0.19	-
Di	5.86	9.21	13.48	17.38	12.33	15.55
Wo	-	-	-	-	-	-
Hy	5.10	1.21	-	-	-	4.78
Ol	10.08	9.94	8.84	8.14	8.45	11.45
Mt	2.62	3.05	2.49	2.95	2.68	3.20
Il	1.96	3.29	2.72	3.48	2.75	2.20
Ap	1.14	1.68	1.02	1.02	1.33	0.71
Cc	0.20	0.20	0.18	0.18	0.20	0.25
TRACE ELEMENTS						
Ba	596	697	1083	801	586	692
Cr	145	60	50	45	52	385
Cu	19	54	115	60	123	73
Li	37	36	35	32	35	42
Ni	117	55	71	80	57	168
Rb	70	58	53	48	50	85
Sc	16	16	17	17	15	21
Sr	702	1342	1486	1457	1355	925
V	122	161	132	164	134	132
Y	11	19	18	29	24	19
Zn	108	96	96	99	93	123

APPENDIX B

Table B.2 WHOLE ROCK ANALYSES OF XENOLITHS

SAMPLE	XG90	XG91	XG92	XG93	XG94	XD1
TYPE	Type 1B	Type 2	Type 1A	Type 5	Type 5	Type 2
MAJOR ELEMENTS						
SiO_2	53.00	52.00	43.00	51.75	51.50	50.25
TiO_2	1.20	1.48	3.58	1.40	1.08	1.18
Al_2O_3	16.30	16.20	12.90	16.00	16.00	13.00
FeO*	6.50	7.40	13.50	7.80	8.50	8.05
MnO	0.09	0.12	0.30	0.09	0.12	0.14
MgO	5.15	5.75	7.59	6.40	6.15	8.85
CaO	6.55	7.10	11.00	5.20	4.50	8.50
Na_2O	5.00	4.64	2.30	5.05	4.45	3.80
K_2O	2.09	2.10	2.00	2.93	3.58	2.03
P_2O_5	0.44	0.50	0.32	0.49	0.52	0.69
H_2O	2.28	1.54	2.36	1.52	1.98	2.10
CO_2	0.11	0.09	0.14	0.08	0.11	0.13
Total	98.71	98.91	98.99	98.71	98.49	98.71
NORM						
Q	-	-	-	-	-	-
C	-	-	-	-	-	-
Or	12.35	12.41	11.82	17.31	21.15	11.99
Ab	41.54	37.44	8.75	34.61	33.41	29.33
An	15.87	17.18	18.97	12.34	13.12	12.43
Lc	-	-	-	-	-	-
Ne	0.40	0.98	5.80	4.39	2.29	1.52
Di	10.55	11.48	26.51	7.87	4.15	19.60
Wo	-	-	-	-	-	-
Hy	-	-	-	-	-	-
Ol	9.92	11.16	12.25	13.99	15.94	14.83
Mt	2.42	2.75	5.02	2.90	3.16	2.99
Il	2.28	2.81	6.80	2.66	2.05	2.24
Ap	1.04	1.19	0.76	1.16	1.23	1.64
Cc	0.25	0.20	0.32	0.18	0.25	0.30
TRACE ELEMENTS						
Ba	550	588	474	578	855	430
Cr	145	162	163	170	80	255
Cu	117	55	30	52	16	104
Li	32	35	41	115	129	28
Ni	92	112	111	158	161	153
Rb	63	60	78	118	173	80
Sc	16	16	48	13	14	22
Sr	1221	1179	324	948	597	800
V	114	132	371	138	127	176
Y	24	27	75	18	25	36
Zn	96	111	160	150	208	102

APPENDIX B

Table B.2 WHOLE ROCK ANALYSES OF XENOLITHS

SAMPLE	XD1A	XD2	MOINE	MX	MX1	MX2
TYPE	Type 1A	Type 5		Moine	Moine	Moine
MAJOR ELEMENTS						
SiO_2	52.75	55.00	79.50	77.80	57.00	66.00
TiO_2	1.70	1.08	0.13	0.12	1.10	0.39
Al_2O_3	15.70	16.80	10.70	11.30	19.40	17.90
FeO*	7.40	6.88	0.80	0.80	5.90	2.25
MnO	0.08	0.09	0.01	0.01	0.06	0.02
MgO	5.35	5.50	0.40	0.02	2.90	1.35
CaO	6.30	4.45	0.55	0.90	3.80	2.50
Na_2O	5.33	5.10	2.40	2.95	5.30	5.80
K_2O	2.25	2.65	3.73	5.45	2.33	2.13
P_2O_5	0.98	0.49		0.01	0.40	0.15
H_2O	2.10	1.18	0.84	1.02	1.20	1.54
CO_2	0.13	0.07	0.05	0.03	0.10	0.15
Total	100.06	99.28	99.11	100.41	99.49	100.18
NORM						
Q	-	-	-	38.18	3.77	16.65
C	-	-	-	-	2.44	2.22
Or	13.29	15.66	-	32.20	13.77	12.58
Ab	42.13	43.13	-	24.95	44.83	49.05
An	12.28	15.13	-	1.50	15.61	10.47
Lc	-	-	-	-	-	-
Ne	1.60	-	-	-	-	-
Di	9.50	2.67	-	1.58	-	-
Wo	-	-	-	0.39	-	-
Hy	-	7.26	-	-	12.60	5.45
Ol	10.82	8.53	-	-	-	-
Mt	2.75	2.56	-	0.30	2.19	0.84
Il	3.23	2.05	-	0.23	2.09	0.74
Ap	2.32	1.16	-	0.02	0.95	0.36
Cc	0.30	0.16	-	0.07	0.23	0.34
TRACE ELEMENTS						
Ba	1168	400	1160	850	996	398
Cr	160	130	5	60	70	30
Cu	112	96	18	6	64	20
Li	131	33	10	6	55	25
Ni	150	65	51	3	66	54
Rb	85	90	90	120	75	57
Sc	13	16	3	0	12	3
Sr	1116	930	367	425	1531	1155
V	174	155	25	17	121	54
Y	78	13	3	3	20	8
Zn	150	94	20	16	88	42

APPENDIX B

Table B.2 WHOLE ROCK ANALYSES OF XENOLITHS

SAMPLE	MX2A	MX3
TYPE	Moine	Moine
MAJOR ELEMENTS		
SiO_2	69.50	59.00
TiO_2	0.32	1.00
Al_2O_3	16.50	17.00
FeO*	1.60	6.65
MnO	0.02	0.07
MgO	1.20	4.22
CaO	1.80	3.20
Na_2O	5.35	4.00
K_2O	2.77	2.85
P_2O_5	0.15	0.28
H_2O	0.78	0.90
CO_2	0.18	0.05
Total	100.16	99.22
NORM		
Q	22.42	9.69
C	2.21	2.31
Or	16.37	16.84
Ab	45.25	33.83
An	6.81	13.73
Lc	-	-
Ne	-	-
Di	-	-
Wo	-	-
Hy	4.42	16.97
Ol	-	-
Mt	0.59	2.47
Il	0.61	1.90
Ap	0.36	0.66
Cc	0.41	0.11
TRACE ELEMENTS		
Ba	885	565
Cr	30	200
Cu	13	273
Li	22	27
Ni	48	104
Rb	80	105
Sc	4	19
Sr	1075	733
V	47	148
Y	8	42
Zn	44	84

APPENDIX B

Table B.3: WHOLE ROCK ANALYSES OF THE MAFIC DIORITES

	D1 Rubh.	D1i Rubh.	D2 Rubh.	D3 Rubh.	D3A Rubh.	D4 Rubh.
MAJOR ELEMENTS						
SiO_2	52.00	50.00	51.00	54.00	54.25	57.50
TiO_2	0.95	0.83	0.98	0.96	0.62	0.43
Al_2O_3	10.80	10.80	11.30	11.00	9.70	9.20
FeO*	7.85	7.40	7.80	7.40	6.90	5.60
MnO	0.13	0.13	0.14	0.11	0.10	0.09
MgO	11.03	12.50	12.10	10.85	12.45	11.10
CaO	8.90	9.00	8.40	7.90	8.00	7.35
Na_2O	2.38	2.48	2.65	2.83	2.50	1.95
K_2O	2.45	2.43	2.90	2.73	3.10	3.88
P_2O_5	0.59	0.52	0.62	0.43	0.24	0.03
H_2O	2.16	2.00	2.30	1.66	1.44	1.54
CO_2	0.11	0.70	0.13	0.23	0.09	0.05
Total	99.35	98.78	100.31	100.10	99.39	98.71
NORM						
Q	-	-	-	-	-	3.15
	-	-	-	-	-	-
Or	14.48	14.36	17.13	16.13	18.32	22.92
Ab	20.13	20.97	22.41	23.94	21.14	16.49
An	11.55	11.16	10.38	9.25	6.09	4.90
Lc	-	-	-	-	-	-
Ne	-	-	-	-	-	-
Di	22.41	20.44	21.07	20.49	25.03	24.68
Wo	-	-	-	-	-	-
Hy	16.47	7.30	2.21	17.64	14.27	22.10
Ol	6.01	15.63	18.53	5.08	8.77	-
Mt	2.92	2.75	2.90	2.75	2.56	2.08
Il	1.80	1.58	1.86	1.82	1.18	0.82
Ap	1.40	1.23	1.47	1.02	0.57	0.07
Cc	0.25	1.59	0.30	0.52	0.20	0.11
TRACE ELEMENTS						
Ba	780	705	830	815	805	675
Cr	430	417	375	415	430	278
Cu	33	33	30	39	26	46
Li	25	25	24	18	18	13
Ni	287	292	262	280	258	278
Rb	80	83	95	88	78	75
Sc	23	22	21	20	20	17
Sr	790	640	830	555	615	525
V	149	132	139	98	128	77
Y	30	24	28	17	20	15
Zn	92	83	87	80	76	66

APPENDIX B

Table B.3: WHOLE ROCK ANALYSES OF THE MAFIC DIORITES

	D5 Rubh.	D5A Rubh.	D6 Rubh.	D7 Rubh.	D7A Rubh.	D8 Rubh.
MAJOR ELEMENTS						
SiO_2	55.75	51.50	52.75	49.75	53.00	49.00
TiO_2	1.23	1.05	0.96	0.98	0.83	0.90
Al_2O_3	9.50	12.20	12.40	10.70	10.70	10.00
FeO*	6.80	7.40	7.00	8.10	7.73	8.70
MnO	0.09	0.13	0.11	0.13	0.12	0.14
MgO	10.90	11.10	9.80	12.25	11.60	13.51
CaO	8.80	8.20	8.30	8.70	9.35	9.65
Na_2O	2.28	2.85	3.18	2.50	2.87	2.19
K_2O	2.50	2.23	3.25	2.74	2.80	2.43
P_2O_5	0.50	0.63	0.65	0.15	0.50	0.53
H_2O	1.52	1.62	1.30	2.76	1.34	1.92
CO_2	0.11	-	0.09	0.28	0.11	0.09
Total	99.97	98.91	99.79	99.03	100.95	99.06
NORM						
Q	3.46	-	-	-	-	-
	-	-	-	-	-	-
Or	14.77	13.18	19.20	16.19	16.54	14.36
Ab	19.28	24.10	26.90	20.18	24.27	17.44
An	8.31	13.91	9.97	9.89	8.05	10.28
Lc	-	-	-	-	-	-
Ne	-	-	-	0.52	-	0.59
Di	24.96	18.06	21.08	24.35	27.44	26.77
Wo	-	-	-	-	-	-
Hy	21.58	10.94	0.28	-	1.78	-
Ol	-	11.08	15.11	19.51	15.86	21.55
Mt	2.53	2.75	2.60	3.01	2.87	3.23
Il	2.34	1.99	1.82	1.86	1.58	1.71
Ap	1.19	1.49	1.54	0.36	1.19	1.26
Cc	0.25	-	0.20	0.64	0.25	0.20
TRACE ELEMENTS						
Ba	655	910	1030	855	830	695
Cr	300	430	272	520	340	337
Cu	65	32	35	36	38	41
Li	23	24	18	25	20	23
Ni	254	238	173	170	155	338
Rb	73	93	90	93	80	75
Sc	22	20	21	23	24	23
Sr	490	915	1020	725	725	772
V	145	140	145	148	132	132
Y	21	28	26	29	25	26
Zn	74	83	81	86	82	88

APPENDIX B

Table B.3: WHOLE ROCK ANALYSES OF THE MAFIC DIORITES

	D9 Rubh.	D10 Lidd.	D11 Lidd.	D12 Lidd.	D13 Lidd.	D14 Lidd.
MAJOR ELEMENTS						
SiO_2	50.00	49.00	48.00	48.00	50.50	57.00
TiO_2	0.80	1.00	1.28	1.15	1.25	1.43
Al_2O_3	10.20	10.10	9.10	11.00	12.90	16.20
FeO*	8.35	10.30	9.30	9.35	8.75	7.00
MnO	0.14	0.22	0.15	0.16	0.14	0.05
MgO	13.60	13.90	13.40	11.95	9.95	3.75
CaO	9.85	10.30	11.25	11.05	9.15	5.70
Na_2O	2.23	1.98	1.92	2.08	3.04	4.47
K_2O	2.48	1.92	1.32	1.73	2.32	2.23
P_2O_5	0.54	0.34	0.09	0.34	0.48	0.81
H_2O	1.48	1.78	2.22	1.94	2.12	2.08
CO_2	0.40	0.15	0.50	0.20	0.11	0.06
Total	100.08	100.98	98.52	98.95	100.71	100.78
NORM						
Q	-	-	-	-	-	5.43
	-	-	-	-	-	-
Or	14.65	11.34	7.80	10.22	13.71	13.18
Ab	18.86	16.75	16.24	17.36	24.65	37.81
An	10.50	13.00	12.32	15.57	14.71	17.56
Lc	-	-	-	-	-	-
Ne	-	-	-	0.12	0.58	-
Di	25.76	27.96	31.72	28.63	21.54	4.12
Wo	-	-	-	-	-	-
Hy	1.34	1.19	5.28	-	-	13.46
Ol	20.91	22.38	15.97	18.44	16.65	-
Mt	3.10	3.83	3.46	3.48	3.25	2.60
Il	1.52	1.90	2.43	2.18	2.37	2.72
Ap	1.28	0.81	0.21	0.81	1.14	1.92
Cc	0.91	0.34	1.14	0.45	0.25	0.14
TRACE ELEMENTS						
Ba	765	670	450	595	763	1280
Cr	435	472	485	455	200	27
Cu	40	31	37	44	36	228
Li	22	25	23	28	23	35
Ni	315	145	175	118	80	13
Rb	75	55	38	50	70	65
Sc	24	31	33	33	24	12
Sr	730	625	475	730	930	1255
V	142	172	183	197	180	224
Y	28	30	27	33	32	28
Zn	96	94	82	99	88	83

APPENDIX B

Table B.3: WHOLE ROCK ANALYSES OF THE MAFIC DIORITES

	D17 Sheet	D19 Sheet	D20 Sheet	D24 Sheet	D25 Sheet	D27 Sheet
MAJOR ELEMENTS						
SiO_2	57.00	55.00	54.00	55.00	55.50	54.50
TiO_2	1.05	1.35	0.91	1.06	1.05	1.17
Al_2O_3	14.00	14.20	12.00	15.00	14.10	15.00
FeO*	8.20	8.40	9.30	8.50	8.60	8.60
MnO	0.13	0.13	0.15	0.13	0.13	0.13
MgO	7.05	6.80	9.90	7.05	7.40	7.25
CaO	5.50	5.10	6.70	5.30	5.30	5.40
Na_2O	3.30	3.45	2.70	3.30	2.95	3.35
K_2O	2.36	2.40	1.96	2.25	2.30	2.36
P_2O_5	0.37	0.39	0.35	0.35	0.36	0.39
H_2O	1.42	1.34	1.44	1.58	1.64	1.74
CO_2	0.10	0.08	0.08	0.08	0.08	0.08
Total	100.48	98.64	99.49	99.60	99.41	99.97
NORM						
Q	5.70	3.55	1.76	3.47	5.47	2.05
	-	-	-	-	-	-
Or	13.94	14.18	11.58	13.29	13.59	13.94
Ab	27.91	29.18	22.84	27.91	24.95	28.33
An	16.42	16.18	14.84	19.48	18.44	18.93
Lc	-	-	-	-	-	-
Ne	-	-	-	-	-	-
Di	6.31	5.26	12.56	3.25	4.03	2.89
Wo	-	-	-	-	-	-
Hy	22.85	22.48	28.54	24.67	25.30	24.80
Ol	-	-	-	-	-	-
Mt	3.05	3.12	3.46	3.16	3.20	3.20
Il	1.99	2.56	1.73	2.01	1.99	2.22
Ap	0.88	0.92	0.83	0.83	0.85	0.92
Cc	0.23	0.02	0.18	0.18	0.18	0.18
TRACE ELEMENTS						
Ba	672	745	609	660	702	813
Cr	290	250	480	270	295	235
Cu	27	31	34	27	29	29
Li	20	23	23	20	22	23
Ni	123	127	181	123	122	116
Rb	62	67	55	57	60	62
Sc	22	22	27	22	22	23
Sr	806	810	745	839	782	1021
V	172	179	166	173	184	194
Y	27	30	29	27	28	30
Zn	84	93	106	89	95	87

APPENDIX B

Table B.3: WHOLE ROCK ANALYSES OF THE MAFIC DIORITES

	D28 Sheet	D29 Beach	D32 Sheet	D33 Ranac.	D35 Ranac.	D37 Ranac.
MAJOR ELEMENTS						
SiO_2	56.50	55.50	56.00	52.50	55.00	53.50
TiO_2	1.18	1.35	1.25	1.85	1.10	1.45
Al_2O_3	13.60	18.40	14.30	9.70	12.40	13.20
FeO*	8.55	6.80	7.80	10.80	8.80	8.85
MnO	0.13	0.09	0.12	0.15	0.13	0.13
MgO	7.25	3.80	5.50	9.90	9.80	8.65
CaO	5.40	4.22	5.70	7.70	5.90	6.00
Na_2O	3.20	5.20	3.45	2.10	2.80	3.00
K_2O	2.05	2.66	2.63	1.88	2.13	2.60
P_2O_5	0.33	0.48	0.41	1.05	0.32	0.76
H_2O	1.82	1.80	1.99	2.30	1.58	1.18
CO_2	0.05	0.03	0.05	0.15	0.05	0.05
Total	100.05	100.32	99.20	100.08	100.01	99.37
NORM						
Q	6.50	-	5.40	4.67	2.85	0.87
	-	0.52	-	-	-	-
Or	12.11	15.72	15.54	11.11	12.58	15.36
Ab	27.06	43.98	29.18	17.76	23.68	25.37
An	16.70	17.61	15.77	22.49	14.98	14.88
Lc	-	-	-	-	-	-
Ne	-	-	-	-	-	-
Di	6.16	-	7.72	15.22	9.54	7.73
Wo	-	-	-	-	-	-
Hy	23.63	12.06	17.47	27.50	28.80	26.29
Ol	-	2.55	-	-	-	-
Mt	3.18	2.53	2.90	4.01	3.27	3.29
Il	2.24	2.56	2.37	3.51	2.09	2.75
Ap	0.78	1.14	0.97	2.49	0.76	1.80
Cc	0.11	0.07	0.11	0.34	0.11	0.11
TRACE ELEMENTS						
Ba	739	795	761	547	668	1143
Cr	290	140	230	450	410	310
Cu	27	114	40	103	43	36
Li	20	42	20	22	21	22
Ni	130	98	114	208	216	179
Rb	55	85	85	50	50	60
Sc	22	16	20	48	30	26
Sr	806	1420	851	518	905	1253
V	166	137	166	290	184	195
Y	27	25	28	69	31	37
Zn	91	100	104	122	94	98

APPENDIX B

Table B.3: WHOLE ROCK ANALYSES OF THE MAFIC DIORITES

	D38 Ranac.	D40 Ranac.	D41 Ranac.	D43 Ranac.	D44 Sheet	D45 Sheet
MAJOR ELEMENTS						
SiO_2	54.00	54.00	55.00	60.00	69.50	54.50
TiO_2	1.40	1.40	1.43	0.75	0.33	1.45
Al_2O_3	12.60	14.00	13.10	9.20	16.80	14.80
FeO*	8.50	7.80	8.60	8.00	2.00	9.00
MnO	0.13	0.12	0.12	0.15	0.02	0.14
MgO	8.65	7.60	7.95	9.00	1.10	6.55
CaO	6.00	5.30	6.00	5.60	2.10	5.50
Na_2O	3.05	3.20	3.15	2.13	4.70	3.50
K_2O	2.33	2.45	2.33	2.30	2.36	2.17
P_2O_5	0.72	0.48	0.45	0.48	0.12	0.37
H_2O	1.74	1.78	1.12	0.86	0.90	1.56
CO_2	0.08	0.53	0.05	0.05	0.08	0.08
Total	99.19	98.65	99.30	98.52	100.01	99.61
NORM						
Q	2.48	3.53	3.30	14.33	26.71	2.94
	-	-	-	-	3.17	-
Or	13.77	14.48	13.77	13.59	13.94	12.82
Ab	25.80	27.06	26.64	18.01	39.75	29.60
An	13.81	16.61	14.73	8.75	9.13	18.27
Lc	-	-	-	-	-	-
Ne	-	-	-	-	-	-
Di	8.63	2.57	9.49	12.52	-	4.94
Wo	-	-	-	-	-	-
Hy	25.52	24.96	23.41	25.03	4.63	22.58
Ol	-	-	-	-	-	-
Mt	3.16	2.90	3.20	2.97	0.74	3.35
Il	2.66	2.66	2.72	1.42	0.63	2.75
Ap	1.71	1.14	1.07	1.14	0.28	0.88
Cc	0.18	1.21	0.11	0.11	0.18	0.18
TRACE ELEMENTS						
Ba	775	751	683	867	1062	623
Cr	310	330	350	350	20	245
Cu	38	36	34	187	17	38
Li	22	24	20	16	24	19
Ni	183	176	198	236	46	101
Rb	60	67	57	50	62	65
Sc	26	24	27	25	5	22
Sr	1203	1145	1030	553	970	747
V	192	174	192	123	44	188
Y	38	30	32	23	12	30
Zn	93	88	89	112	37	94

APPENDIX B

Table B.3: WHOLE ROCK ANALYSES OF THE MAFIC DIORITES

	D47 Ranac.	D48 Lidd.	D50 Lidd.	D51 Lidd.	D53 Lidd.	D54 Lidd.
MAJOR ELEMENTS						
SiO_2	53.00	55.00	53.00	55.50	51.00	49.50
TiO_2	1.53	1.35	1.10	0.93	1.03	1.78
Al_2O_3	13.10	13.20	11.20	7.60	9.70	11.30
FeO*	9.15	8.95	9.10	8.95	9.65	9.50
MnO	0.13	0.13	0.15	0.14	0.15	0.13
MgO	8.00	7.65	11.40	13.85	12.20	10.50
CaO	6.20	5.30	6.00	7.10	9.24	9.10
Na_2O	3.02	3.25	2.63	1.90	2.17	2.62
K_2O	1.80	2.55	2.40	1.30	1.75	1.75
P_2O_5	0.86	0.70	0.51	0.30	0.64	0.89
H_2O	2.16	1.16	1.40	2.12	1.32	1.40
CO_2	0.30	0.08	0.10	0.03	0.25	0.63
Total	99.25	99.32	98.99	99.72	99.10	99.09
NORM						
Q	3.27	3.39	-	5.59	-	-
	-	-	-	-	-	-
Or	10.63	15.07	14.18	7.68	10.34	10.34
Ab	25.54	27.49	22.24	16.07	18.35	22.16
An	16.88	13.90	11.67	8.37	11.56	13.91
Lc	-	-	-	-	-	-
Ne	-	-	-	-	-	-
Di	5.16	5.91	11.32	19.71	22.85	17.18
Wo	-	-	-	-	-	-
Hy	27.76	24.95	29.44	34.55	21.56	17.14
Ol	-	-	2.09	-	5.77	6.81
Mt	3.40	3.33	3.38	3.33	3.59	3.53
Il	1.01	2.56	2.09	1.77	1.96	3.38
Ap	2.04	1.66	1.21	0.71	1.52	2.11
Cc	0.68	0.18	0.23	0.07	0.57	1.43
TRACE ELEMENTS						
Ba	819	752	704	499	693	804
Cr	330	315	410	705	440	390
Cu	43	38	48	29	47	40
Li	22	20	26	15	25	22
Ni	186	186	261	351	256	229
Rb	40	70	72	35	47	40
Sc	28	20	23	25	30	32
Sr	1091	1106	976	553	1048	1655
V	211	178	155	113	166	235
Y	40	32	26	20	29	37
Zn	99	108	97	95	97	90

APPENDIX B

Table B.3: WHOLE ROCK ANALYSES OF THE MAFIC DIORITES

	D55 Uile.	D57 Uile.	D58 Lidd.	D58A Uile.	D59A Uile.	D60 Lidd.
MAJOR ELEMENTS						
SiO_2	53.00	51.00	55.00	55.00	53.00	57.00
TiO_2	1.65	1.65	1.20	1.10	1.45	0.87
Al_2O_3	13.00	11.80	15.40	14.40	12.00	14.00
FeO*	8.40	9.40	9.10	4.45	9.00	7.30
MnO	0.13	0.14	0.08	0.06	0.13	0.11
MgO	8.20	11.20	4.60	3.15	10.10	7.30
CaO	5.95	6.20	5.00	2.70	6.00	4.60
Na_2O	3.51	2.42	4.05	4.05	2.70	3.70
K_2O	3.40	3.20	2.54	3.75	3.20	2.83
P_2O_5	0.76	0.73	1.26	0.47	0.73	0.60
H_2O	1.62	1.82	1.24	0.84	1.20	1.20
CO_2	0.13	0.30	0.15	0.15	0.33	0.08
Total	99.74	99.86	99.62	90.12	99.83	99.58
NORM						
Q	-	-	4.00	15.71	-	3.53
	-	-	0.26	0.24	-	-
Or	20.09	18.91	15.01	22.16	18.91	16.72
Ab	29.69	20.47	34.25	34.25	22.84	31.29
An	9.68	11.89	15.63	9.38	11.18	13.24
Lc	-	-	-	-	-	-
Ne	-	-	-	-	-	-
Di	11.29	9.77	-	-	9.41	4.15
Wo	-	-	-	-	-	-
Hy	10.79	18.63	20.54	11.48	24.72	23.70
Ol	8.50	9.62	-	-	3.28	-
Mt	3.12	3.49	3.38	1.65	3.35	2.71
Il	3.13	3.13	2.28	2.09	2.75	1.65
Ap	1.80	1.73	2.99	1.11	1.73	1.42
Cc	0.30	0.68	0.34	0.34	0.75	0.18
TRACE ELEMENTS						
Ba	1633	1577	751	1205	1243	742
Cr	400	545	60	100	460	265
Cu	31	34	52	20	34	34
Li	37	51	27	33	32	22
Ni	212	267	74	91	247	188
Rb	107	91	72	115	92	80
Sc	22	24	14	11	24	17
Sr	1138	881	2367	988	1044	1301
V	171	176	223	104	173	136
Y	28	27	35	21	29	27
Zn	98	106	102	69	97	90

APPENDIX B

Table B.3: WHOLE ROCK ANALYSES OF THE MAFIC DIORITES

	D60A Uile.	D61 Lidd.	D63 Uile.	D64 Uile.	D65 Uile.	D67 L.Tea.
MAJOR ELEMENTS						
SiO_2	55.00	54.00	61.50	60.00	52.00	60.50
TiO_2	1.10	1.69	1.00	1.35	2.05	0.97
Al_2O_3	12.40	13.30	10.40	14.60	12.30	15.50
FeO*	8.50	8.80	6.65	5.60	9.25	5.55
MnO	0.14	0.12	0.10	0.08	0.13	0.08
MgO	8.85	7.40	6.40	4.20	9.20	4.20
CaO	5.05	4.90	5.30	4.22	5.10	4.00
Na_2O	3.54	3.50	3.05	4.05	3.05	4.50
K_2O	2.93	3.10	2.50	3.70	3.30	2.75
P_2O_5	0.62	1.19	0.64	0.62	0.92	0.44
H_2O	1.42	1.44	1.50	1.88	1.40	1.72
CO_2	0.13	0.08	0.10	0.20	0.05	0.03
Total	99.67	99.51	99.14	100.50	98.75	100.24
NORM						
Q	-	1.20	15.49	8.24	-	8.55
C	-	-	-	-	-	-
Or	17.31	18.32	14.77	21.86	19.50	16.25
Ab	29.94	29.60	25.80	34.25	25.80	38.06
An	9.30	11.43	7.31	10.74	10.13	13.98
Lc	-	-	-	-	-	-
Ne	-	-	-	-	-	-
Di	8.76	3.71	11.41	3.94	7.10	2.27
Wo	-	-	-	-	-	-
Hy	25.49	24.63	16.96	13.20	20.45	14.57
Ol	0.71	-	-	-	5.05	-
Mt	3.16	3.27	2.47	2.08	3.44	2.06
Il	2.09	3.21	1.90	2.56	3.89	1.84
Ap	1.47	2.82	1.52	1.47	2.18	1.04
Cc	0.30	0.18	0.23	0.45	0.11	0.07
TRACE ELEMENTS						
Ba	1005	1623	772	1278	1783	1060
Cr	375	295	270	135	435	95
Cu	43	61	45	25	29	38
Li	30	26	12	33	40	29
Ni	270	175	167	109	246	107
Rb	72	70	47	105	105	60
Sc	17	19	19	14	21	13
Sr	1224	1287	706	1134	6745	1337
V	136	177	133	130	177	120
Y	32	25	23	24	32	21
Zn	97	113	81	80	109	68

APPENDIX B

Table B.3: WHOLE ROCK ANALYSES OF THE MAFIC DIORITES

	D68 L.Tea.	D69 Uile.	D70 Uile.	D71 Uile.	D72 Rana.	D73 Uile.
MAJOR ELEMENTS						
SiO_2	56.00	49.50	56.00	56.00	52.75	48.50
TiO_2	1.45	1.71	1.60	1.85	1.60	2.00
Al_2O_3	17.70	11.20	13.60	15.50	13.60	11.00
FeO*	6.80	9.75	7.20	7.55	8.40	10.05
MnO	0.09	0.14	0.11	0.09	0.12	0.14
MgO	4.10	13.20	6.00	3.80	8.15	13.10
CaO	4.60	6.10	5.05	4.30	6.20	6.05
Na_2O	5.25	2.20	3.80	3.92	3.45	1.80
K_2O	2.30	2.67	3.55	3.45	2.20	3.47
P_2O_5	0.43	0.75	0.76	1.03	0.83	0.80
H_2O	1.36	1.60	1.68	1.30	1.54	1.80
CO_2	0.03	0.03	-	0.43	0.05	0.10
Total	100.11	98.85	99.35	99.22	98.89	98.81
NORM						
Q	-	-	2.16	6.41	-	-
	-	-	-	0.96	-	-
Or	13.59	15.77	20.97	20.38	13.00	20.50
Ab	44.40	18.61	32.14	33.15	29.18	15.22
An	17.95	12.80	9.57	11.89	15.13	11.69
Lc	-	-	-	-	-	-
Ne	-	-	-	-	-	-
Di	1.52	9.87	8.47	-	7.95	9.95
Wo	-	-	-	-	-	-
Hy	14.36	17.80	17.06	15.64	24.06	13.62
Ol	0.76	13.96	-	-	0.06	16.67
Mt	2.53	3.62	2.68	2.81	3.12	3.74
Il	2.75	3.25	3.04	3.51	3.04	3.80
Ap	1.02	1.78	1.80	2.44	1.97	1.90
Cc	0.07	0.07	-	0.98	0.11	0.23
TRACE ELEMENTS						
Ba	555	1212	1237	1480	941	1381
Cr	105	550	210	60	315	725
Cu	52	45	31	89	31	24
Li	35	61	54	54	22	59
Ni	95	344	137	70	150	331
Rb	87	75	96	91	60	145
Sc	15	23	18	15	26	25
Sr	1197	900	1162	1455	1423	648
V	144	174	159	178	182	193
Y	30	29	28	27	34	28
Zn	98	117	87	81	92	119

APPENDIX B

Table B.3: WHOLE ROCK ANALYSES OF THE MAFIC DIORITES

	D74 Uile.	D76 Uile.	D77 Uile.	D80 L.Tea.
MAJOR ELEMENTS				
SiO_2	50.50	61.00	51.75	62.00
TiO_2	1.55	1.10	1.55	0.93
Al_2O_3	14.20	14.90	10.20	15.30
FeO*	8.60	5.70	9.50	5.20
MnO	0.14	0.08	0.14	0.08
MgO	7.60	4.20	11.70	4.10
CaO	6.40	3.40	7.10	3.70
Na_2O	3.25	3.95	2.15	4.35
K_2O	3.01	3.52	2.33	2.60
P_2O_5	0.93	0.59	0.60	0.40
H_2O	1.80	1.18	1.60	1.52
CO_2	1.45	0.08	0.30	0.05
Total	99.43	99.70	98.92	100.22
NORM				
Q	-	10.56	-	11.97
	-	0.01	-	-
Or	17.78	20.80	13.77	15.36
Ab	27.49	33.41	18.18	36.79
An	15.27	12.51	11.30	14.55
Lc	-	-	-	-
Ne	-	-	-	-
Di	1.00	-	14.48	0.71
Wo	-	-	-	-
Hy	20.18	15.63	31.21	14.72
Ol	4.54	-	0.07	-
Mt	3.20	2.12	3.53	1.93
Il	2.94	2.09	2.94	1.77
Ap	2.21	1.40	1.42	0.95
Cc	3.30	0.18	0.68	0.11
TRACE ELEMENTS				
Ba	1478	1239	1058	1011
Cr	270	150	585	105
Cu	64	24	47	27
Li	48	38	63	27
Ni	173	107	304	113
Rb	108	100	75	65
Sc	20	12	28	13
Sr	1479	1132	790	1266
V	176	120	162	121
Y	31	23	26	24
Zn	97	84	107	80

APPENDIX B

Table B.4: WHOLE ROCK ANALYSES OF MISCELLANEOUS SAMPLES

	AP1 Aplite	AP2 Aplite	AP3 Aplite	AP4 Aplite	P1 Pegmt	V1
MAJOR ELEMENTS						
SiO_2	78.00	77.00	76.00	76.50	77.50	65.00
TiO_2	-	0.12	0.08	-	0.05	0.54
Ai_2O_3	11.80	12.90	13.20	12.90	14.10	14.20
FeO	0.55	0.65	0.65	0.40	0.15	4.55
MnO	0.01	0.01	0.01	0.00	0.00	0.07
MgO	0.07	0.20	0.09	0.10	-	3.70
CaO	0.75	1.00	1.40	0.55	0.30	3.50
Na_2O	3.73	4.15	4.35	3.75	3.03	4.20
K_2O	4.03	3.98	4.03	4.65	5.00	2.65
P_2O_5	0.00	0.00	0.00	-	-	0.18
H_2O	1.14	0.52	0.54	0.52	0.66	0.56
CO_2	-	-	0.07	0.08	0.05	0.05
Total	100.08	100.53	100.41	99.45	100.84	99.20
NORM						
Q	38.91	34.98	32.46	35.58	40.21	16.76
C	-	-	-	0.89	3.28	-
Or	23.81	23.51	23.81	27.47	29.54	15.66
Ab	31.55	35.10	36.79	31.72	25.63	35.52
An	3.56	4.82	4.60	2.22	1.17	12.07
Lc	-	-	-	-	-	-
Ne	-	-	-	-	-	-
Di	0.14	0.06	1.63	-	-	3.07
Wo	-	-	-	-	-	-
Hy	0.78	1.07	0.05	0.73	0.10	12.42
Ol	-	-	-	-	-	-
Mt	0.20	0.24	0.24	0.15	0.06	1.69
Il	-	0.23	0.15		0.09	1.03
Ap	-	0.02	-	-	-	0.43
Cc	-	-	0.16	0.18	0.11	0.11
TRACE ELEMENTS						
Ba	600	370	900	446	455	843
Cr	15	25	16	-	7	105
Cu	3	9	5	36	3	70
Li	1	3	6	3	-	29
Ni	-	1	-	44	-	98
Rb	78	105	73	82	148	72
Sc	-	-	-	1	-	13
Sr	365	320	585	360	295	742
V	5	9	11	10	1	92
Y	1	4	5	2	-	15
Zn	6	14	10	15	4	69

APPENDIX B

Table B.4: WHOLE ROCK ANALYSES OF MISCELLANEOUS SAMPLES

	GS3	GS3A	C1 Moine
MAJOR ELEMENTS			
SiO_2	58.50	62.50	77.80
TiO_2	1.01	0.80	0.12
Al_2O_3	13.80	14.90	11.30
FeO	6.50	4.10	0.80
MnO	0.09	0.00	0.01
MgO	5.40	3.00	0.02
CaO	5.18	4.55	0.40
Na_2O	3.78	4.95	1.65
K_2O	2.95	2.99	1.35
P_2O_5	0.41	0.34	0.02
H_2O	2.04	1.36	0.82
CO_2	0.25	0.15	0.03
Total	99.90	99.64	94.31
NORM			
Q	7.11	9.88	72.52
C	-	-	0.12
Or	17.43	17.67	7.98
Ab	31.97	41.87	13.96
An	11.98	9.61	1.66
Lc	-	-	-
Ne	-	-	-
Di	7.64	7.92	-
Wo	-	-	-
Hy	16.05	7.31	1.98
Ol	-	-	-
Mt	2.42	1.52	0.43
Il	1.92	1.52	0.19
Ap	0.97	0.81	0.05
Cc	0.57	0.34	0.07
TRACE ELE			
Ba	820	1125	150
Cr	185	80	25
Cu	26	21	4
Li	21	16	8
Ni	87	48	8
Rb	80	65	38
Sc	12	8	1
Sr	790	1140	150
V	140	82	23
Y	20	18	5
Zn	106	62	18

APPENDIX B

Table B.5: WHOLE ROCK ANALYSES OF RARE EARTH ELEMENTS

	SGVIA BGT	SGVII Late	SGIX TGD	SGXVII Late	SGXVIII Late	SGXXII PGD
La	152	118	145	94	73	112
Ce	103	85	100	61	47	86
Pr	75	67	75	33	33	67
Nd	43	40	29	16	21	40
Sm	25	25	25	15	10	25
Eu	14	14	29	13	10	14
Gd	14	11	14	7	7	11
Dy	6	6	6	3	3	6
Ho	7	7	7	2	4	6
Er	6	4	6	3	4	5
Yb	4	4	2	3	3	4
Lu	5	5	5	3	3	4

	SG29 PGD	SG46 BGT	SG61 BGT	SG82 TGD	SG85 TGD	GX7 TGD
La	197	73	91	124	85	152
Ce	145	48	61	93	82	109
Pr	108	33	50	67	67	75
Nd	73	19	21	41	38	56
Sm	35	15	20	25	25	25
Eu	29	10	14	14	14	29
Gd	18	7	11	14	14	9
Dy	9	3	6	9	9	9
Ho	10	4	6	6	10	6
Er	7	4	5	5	10	6
Yb	5	2	4	5	10	4
Lu	6	3	4	5	9	4

	SGC1 TGD	fG1 Late	fG2 Late	XG3A 1A	XG6 1B	XG18 3
La	109	64	88	194	303	464
Ce	82	44	77	153	243	431
Pr	67	33	58	108	200	367
Nd	32	19	35	70	140	262
Sm	25	15	20	40	75	130
Eu	29	9	14	29	57	71
Gd	14	7	11	21	36	64
Dy	9	4	6	12	15	38
Ho	10	5	6	11	15	43
Er	8	4	5	9	11	30
Yb	6	4	5	6	7	23
Lu	6	4	5	7	7	21

APPENDIX B

Table B.5: WHOLE ROCK ANALYSES OF RARE EARTH ELEMENTS

	XG20 4	XG22B 1B	XG29 1B	XG34 2	XG44 2	XG52 1B
La	133	136	103	79	212	142
Ce	107	102	56	60	132	106
Pr	92	75	42	42	92	75
Nd	44	38	29	27	52	44
Sm	35	30	15	15	30	30
Eu	29	14	12	13	14	29
Gd	18	18	7	11	18	14
Dy	9	9	4	6	9	9
Ho	8	9	4	5	7	7
Er	7	7	3	4	7	6
Yb	5	5	3	4	4	5
Lu	5	6	3	4	6	5

	XG53 1B	XG56 4	XG66 5	XG71 5	X40 1A	X69 1B
La	106	97	97	306	179	103
Ce	95	74	75	234	152	71
Pr	75	58	50	183	125	58
Nd	54	32	24	127	83	41
Sm	30	25	20	60	45	25
Eu	29	14	14	43	29	14
Gd	18	11	11	25	21	14
Dy	9	6	6	12	12	9
Ho	8	6	6	12	12	7
Er	7	6	7	10	9	7
Yb	5	4	4	6	6	5
Lu	6	5	5	6	6	5

	X116 4	X150 2	X177 3	AP1 Aplite	AP4 Aplite	E1 Dyke
La	224	145	209	12	45	130
Ce	148	114	194	9	17	100
Pr	108	92	175	4	8	83
Nd	70	67	135	1	3	54
Sm	35	40	70	2	2	30
Eu	29	29	57	3	3	29
Gd	18	21	32	1	1	18
Dy	10	12	18	1	1	9
Ho	10	10	16	1	1	9
Er	9	8	12	1	1	9
Yb	5	7	9	1	1	4
Lu	6	6	9	2	2	5

APPENDIX B

Table B.5: WHOLE ROCK ANALYSES OF RARE EARTH ELEMENTS

	E3 Dyke	D1 Rubh.	D3A Rubh.	D5 Rubh.	D6 Rubh.	D8 Rubh.
La	130	258	139	133	242	215
Ce	103	210	110	114	184	176
Pr	83	175	92	100	142	150
Nd	48	127	65	65	98	98
Sm	35	65	35	45	55	60
Eu	29	43	29	29	43	43
Gd	18	32	18	21	25	29
Dy	9	15	9	12	12	15
Ho	9	16	9	11	10	14
Er	7	12	7	8	9	12
Yb	5	9	5	6	7	7
Lu	6	9	5	6	6	9

	D9 Rubh.	D11 Lidd.	D12 Lidd.	D13 Lidd.	D25 Shet.	D28 Shet.
La	200	70	161	167	127	118
Ce	178	87	133	156	99	100
Pr	150	83	108	133	83	83
Nd	98	71	78	89	57	62
Sm	60	45	55	55	35	35
Eu	43	43	43	43	29	29
Gd	29	25	29	29	18	18
Dy	15	15	18	15	12	13
Ho	14	14	14	15	14	13
Er	11	10	12	13	9	10
Yb	7	8	9	10	9	8
Lu	8	8	9	9	9	9

	D41 Rana.	D47 Rana.	D58A Uile.	D60 Lidd.	D73 Uile.	D80 L.Tea.
La	100	248	148	248	221	197
Ce	91	202	120	187	177	153
Pr	83	175	100	142	158	125
Nd	60	137	59	100	114	81
Sm	35	75	35	50	60	50
Eu	29	57	29	43	43	43
Gd	21	39	18	25	29	25
Dy	9	21	10	12	15	12
Ho	10	19	11	13	15	11
Er	9	14	10	11	11	9
Yb	6	12	5	8	7	6
Lu	6	9	7	8	7	6

APPENDIX C MICROPROBE ANALYSES

KEY TO TABLES C.1 to C.9 INCLUSIVE

The atomic formulae were calculated on the basis of x oxygens as follows:

MINERAL	NUMBER OF OXYGENS
Amphiboles	23
Biotites	23
Pyroxenes	6

FeO* - Total iron calculated as FeO
\- - element not determined

Sample Numbering

The sample numbering is composed of four parts:

eg. SGIII/TGD/E-hbl/1 or XG64A/1B/Eden/10

Represented as A/B/C/D

Where A is the rock number (refer to Appendix A).

Where B is the type of rock sample.

Where C is the mineral phase:

Acti	-	actinolite			
A-hbl	-	actinolitic-hornblende			
E-hbl	-	edenitic-hornblende			
Eden	-	edenite			
F/P-hbl	-	ferroan/pargasitic hornblende			
Mg-hbl	-	magnesio-hornblende			
Ande.	-	andesine	Olig.	-	oligoclase
Labr.	-	labradorite	Or	-	alkali feldspar
Haem.	-	haematite	Il.	-	ilmenite
Ti-mag.	-	titaniferous-magnetite			
Aug.	-	augite	Opx	-	orthopyroxene
Biot	-	biotite			
Sph	-	sphene	Cp	-	chalcopyrite
Mi	-	millerite	Pe	-	pentlandite
Pt	-	pyrite	Ap	-	apatite

Where D is the analysis number:

C - Core R - Rim M - Middle (between C and R).

APPENDIX C

Table C.1: AMPHIBOLE MICROPROBE ANALYSES

	SGIII TGD E-hbl 1	SGIII TGD Mg-hbl 2	SGIII TGD Eden 3	SGIII TGD Mg-hbl 4	SGIII TGD Eden 5	SGIII TGD Eden 6
SiO2	45.01	47.52	45.57	46.12	45.89	45.49
TiO2	1.05	0.65	0.85	0.88	0.96	0.99
Al2O3	8.29	7.32	8.17	7.97	7.90	8.07
FeO*	15.55	14.83	15.32	15.29	15.19	15.41
MgO	12.33	13.24	12.26	12.55	12.42	12.32
MnO	0.37	0.36	0.35	0.33	0.38	0.35
CaO	12.02	11.83	11.77	11.98	11.89	11.71
Na2O	1.38	0.93	1.01	0.90	1.31	1.44
K2O	0.86	0.64	0.82	0.77	0.80	0.84
Total	96.86	97.32	96.12	96.79	96.74	96.62
Si	6.723	7.074	6.922	6.943	6.613	6.572
Al(iv)	1.277	0.926	1.077	1.057	1.342	1.374
Al(vi)	0.177	0.359	0.385	0.358	-	-
Ti	0.117	0.073	0.097	0.099	0.105	0.108
Fe2+	2.154	1.846	1.947	1.924	1.828	1.859
Mn	0.045	0.045	0.045	0.042	0.046	0.043
Mg	2.738	2.937	2.777	2.816	2.668	2.652
Ca	1.921	1.887	1.916	1.933	1.836	1.812
Na	0.394	0.362	0.403	0.355	0.365	0.405
K	0.162	0.121	0.159	0.148	0.148	0.155

	SGIII TGD Mg-hbl 7	SGIII TGD Eden 8	SGIII TGD Eden. 9	SGIII TGD Eden. 10	SGIII TGD Eden 11	SGIII TGD Eden 12
SiO2	45.46	46.52	46.77	46.79	45.23	45.79
TiO2	1.00	0.77	0.96	1.18	1.14	0.75
Al2O3	8.27	7.58	7.00	7.23	8.01	7.64
FeO*	15.47	14.94	14.67	14.60	15.37	14.93
MgO	12.31	13.02	12.92	13.08	12.25	12.84
MnO	0.39	0.37	0.35	0.34	0.38	0.36
CaO	11.77	11.81	11.70	11.73	11.49	11.91
Na2O	1.52	1.36	1.33	1.44	1.57	1.37
K2O	0.84	0.74	0.67	0.72	0.87	0.72
Total	97.03	97.11	96.37	97.11	96.31	96.31
Si	6.545	6.667	7.019	6.965	6.559	6.591
Al(iv)	1.455	1.281	0.981	1.035	1.369	1.297
Al(vi)	0.405	-	0.262	0.232	-	-
Ti	0.108	0.083	0.118	0.135	0.125	0.081
Fe2+	1.860	1.788	1.838	1.814	1.862	1.798
Mn	0.048	0.045	0.045	0.044	0.046	0.044
Mg	2.642	2.782	2.883	2.896	2.649	2.755
Ca	1.816	1.813	1.883	1.868	1.786	1.836
Na	0.426	0.378	0.378	0.411	0.441	0.384
K	0.154	0.136	0.126	0.143	0.161	0.132

APPENDIX C

Table C.1: AMPHIBOLE MICROPROBE ANALYSES

	SGIII TGD Eden 13	SGVII Late Mg-hbl 1	SGVII Late Mg-hbl 2	SGVII Late Eden 3	SGVII Late Eden 5	SGVII Late Eden 6
SiO2	45.58	48.36	48.49	46.07	44.61	47.07
TiO2	1.09	0.81	0.75	0.99	1.13	1.02
Al2O3	7.98	6.14	5.66	7.15	8.74	7.03
FeO*	15.20	14.58	14.17	15.40	16.60	15.34
MgO	12.40	12.84	13.68	12.28	11.09	12.62
MnO	0.37	0.42	0.38	0.39	0.39	0.39
CaO	11.81	11.74	11.95	11.77	11.70	11.62
Na2O	1.45	1.25	1.11	1.36	1.39	1.46
K2O	0.86	0.59	0.50	0.71	0.91	0.69
Total	96.74	96.73	96.69	96.12	96.56	97.24
Si	6.544	7.198	7.198	6.985	6.771	7.007
Al(iv)	1.351	0.802	0.802	1.015	1.229	0.993
Al(vi)	-	0.264	0.197	0.255	0.341	0.242
Ti	0.118	0.087	0.089	0.108	0.124	0.115
Fe2+	1.825	1.742	1.757	1.963	2.012	1.915
Mn	0.045	0.050	0.044	0.049	0.048	0.047
Mg	2.654	2.838	3.023	2.769	2.399	2.801
Ca	1.816	1.870	1.899	1.910	1.911	1.852
Na	0.404	0.348	0.321	0.383	0.391	0.429
K	0.157	0.108	0.089	0.141	0.181	0.125

	SGVII Late Eden. 8	SGVII Late A-hbl 9	SGVIII Late Mg-hbl 1	SGVIII Late Mg-hbl ?	SGVIII Late A-hbl 3	SGVIII Late Mg-hbl 4
SiO2	45.96	50.01	48.56	47.72	50.59	47.75
TiO2	1.11	0.21	0.71	0.77	0.49	0.75
Al2O3	7.54	4.61	5.89	6.33	4.20	6.49
FeO*	15.74	13.80	14.34	14.65	13.01	14.75
MgO	12.01	14.34	13.41	13.11	14.65	12.97
MnO	0.37	0.39	0.36	0.32	0.35	0.33
CaO	11.85	12.19	11.99	12.08	12.13	11.97
Na2O	1.38	0.84	1.21	1.10	0.83	1.22
K2O	0.79	0.29	0.54	0.61	0.34	0.63
Total	96.75	96.68	97.01	96.69	96.59	96.86
Si	6.915	7.379	7.185	6.661	7.445	7.109
Al(iv)	1.085	0.621	0.815	1.040	0.555	0.889
Al(vi)	0.255	0.177	0.215	0.000	0.175	0.260
Ti	0.125	0.025	0.080	0.815	0.055	0.078
Fe2+	1.978	1.703	1.778	1.711	1.600	1.827
Mn	0.044	0.044	0.039	0.042	0.044	0.040
Mg	2.689	3.157	2.958	2.726	3.208	2.878
Ca	1.911	1.924	1.901	1.803	1.909	1.911
Na	0.429	0.248	0.358	0.302	0.229	0.361
K	0.125	0.053	0.101	0.117	0.070	0.119

APPENDIX C

Table C.1: AMPHIBOLE MICROPROBE ANALYSES

	SGVIII Late Mg-hbl 5	SGVIII Late Eden 6	SGVIII Late Mg-hbl 7	SGVIII Late A-hbl 8	SGVIII Late Mg-hbl 9	SGVIII Late Eden 10
SiO2	48.09	44.73	47.60	50.21	48.75	45.92
TiO2	0.66	1.62	0.85	0.45	0.58	1.29
Al2O3	6.47	8.79	6.49	5.02	5.56	7.79
FeO*	14.66	15.89	14.90	13.57	13.91	15.76
MgO	13.11	11.16	12.85	14.29	13.72	11.79
MnO	0.35	0.34	0.34	0.39	0.38	0.35
CaO	12.02	11.69	11.79	12.09	12.04	11.86
Na2O	1.15	1.56	1.24	0.92	1.01	1.45
K2O	0.59	0.88	0.61	0.42	0.47	0.78
Total	97.10	96.66	96.67	97.36	96.42	96.99
Si	7.135	6.755	7.105	7.348	7.239	6.898
Al(iv)	0.865	1.245	0.895	0.652	0.761	1.100
Al(vi)	0.265	0.315	0.255	0.227	0.219	0.269
Ti	0.070	0.181	0.099	0.055	0.065	0.145
Fe2+	1.819	2.006	1.862	1.661	1.727	1.987
Mn	0.041	0.045	0.039	0.052	0.039	0.042
Mg	2.901	2.515	2.855	3.102	3.038	2.644
Ca	1.909	1.897	1.878	1.898	1.921	1.921
Na	0.340	0.454	0.391	0.263	0.279	0.411
K	0.090	0.163	0.111	0.087	0.080	0.139

	SGVIII Late Mg-hbl 11	SGVIII Late Eden 12	SGVIII Late Mg-hbl 13	SGVIII Late Mg-hbl 14	SGVIII Late Mg-hbl 15	SGIX TGD Eden 1C
SiO2	47.83	46.88	46.44	47.63	47.84	46.63
TiO2	0.64	0.89	0.58	0.84	0.66	1.25
Al2O3	6.67	6.96	6.66	6.62	6.46	6.52
FeO*	14.67	15.00	13.91	14.68	15.14	14.49
MgO	12.85	12.53	12.79	12.85	12.91	13.21
MnO	0.34	0.34	0.31	0.38	0.32	0.39
CaO	12.03	11.93	11.66	11.81	11.95	11.29
Na2O	0.99	1.28	0.91	1.28	1.18	1.60
K2O	0.57	0.68	0.52	0.62	0.59	0.71
Total	96.59	96.49	93.78	96.71	97.05	96.09
Si	7.129	7.029	7.111	7.075	7.125	7.014
Al(iv)	0.870	0.970	0.889	0.925	0.875	0.986
Al(vi)	0.301	0.259	0.307	0.245	0.255	0.169
Ti	0.069	0.101	0.065	0.095	0.067	0.141
Fe2+	1.831	1.879	1.784	1.826	1.889	1.824
Mn	0.039	0.050	0.036	0.038	0.041	0.051
Mg	2.862	2.798	2.916	2.855	2.856	2.963
Ca	1.920	1.918	1.914	1.889	1.911	1.821
Na	0.279	0.381	0.276	0.378	0.342	0.468
K	0.101	0.119	0.110	0.121	0.101	0.138

APPENDIX C

Table C.1: AMPHIBOLE MICROPROBE ANALYSES

	SGIX TGD Eden 2R	SGIX TGD Eden 3C	SGIX TGD Eden 4C	SGIX TGD Eden 5R	SGIX TGD Eden 6C	SGIX TGD Eden 7R
SiO2	47.47	46.91	46.79	47.33	47.82	47.19
TiO2	1.36	1.08	1.05	1.19	1.13	1.23
Al2O3	6.24	6.43	6.66	6.25	6.22	6.51
FeO*	13.81	14.48	14.59	14.27	13.92	14.44
MgO	13.35	13.04	13.06	13.05	13.40	12.77
MnO	0.38	0.38	0.41	0.40	0.37	0.40
CaO	11.38	11.51	11.31	11.36	11.61	11.38
Na2O	1.61	1.36	1.60	1.51	1.34	1.51
K2O	0.72	0.62	0.73	0.64	0.62	0.75
Total	96.32	95.81	96.20	96.00	96.43	96.18
Si	7.094	7.065	7.030	7.101	7.123	7.079
Al(iv)	0.906	0.935	0.970	0.899	0.877	0.921
Al(vi)	0.194	0.208	0.210	0.208	0.216	0.230
Ti	0.154	0.123	0.119	0.136	0.127	0.139
Fe2+	1.726	1.824	1.834	1.792	1.735	1.812
Mn	0.049	0.049	0.053	0.051	0.048	0.052
Mg	2.975	2.927	2.924	2.919	2.975	2.855
Ca	1.822	1.857	1.821	1.828	1.853	1.830
Na	0.440	0.400	0.468	0.441	0.388	0.441
K	0.138	0.119	0.141	0.122	0.119	0.144

	SGX Late Mg-hbl 1	SGX Late Mg-hbl 2	SGX Late Eden 3	SGX Late F/P-hbl 4	SGX Late Mg-hbl 5	SGX Late Mg-hbl 6
SiO2	47.31	46.71	47.05	45.88	48.13	48.22
TiO2	1.11	1.15	1.11	1.11	0.78	0.77
Al2O3	6.30	6.97	6.78	7.67	5.89	5.87
FeO*	15.10	15.12	15.24	15.51	14.80	14.31
MgO	12.99	12.91	12.86	12.40	13.37	13.72
MnO	0.40	0.38	0.39	0.36	0.40	0.41
CaO	11.69	11.92	11.73	11.99	11.95	11.81
Na2O	1.28	1.26	1.37	1.35	1.02	1.13
K2O	0.60	0.62	0.62	0.74	0.53	0.54
Total	96.78	97.04	97.15	97.01	96.87	96.78
Si	7.069	6.964	7.000	6.396	7.145	7.162
Al(iv)	0.929	1.036	1.000	1.255	0.845	0.837
Al(vi)	0.181	0.185	0.119	0.000	0.178	0.189
Ti	0.125	0.125	0.125	0.115	0.091	0.091
Fe2+	1.889	1.886	1.899	1.808	1.835	1.767
Mn	0.051	0.044	0.053	0.041	0.045	0.047
Mg	2.889	2.873	2.855	2.578	2.956	3.033
Ca	1.865	1.912	1.878	1.791	1.901	1.880
Na	0.381	0.359	0.401	0.368	0.301	0.321
K	0.090	0.125	0.119	0.133	0.090	0.102

APPENDIX C

Table C.1: AMPHIBOLE MICROPROBE ANALYSES

	SGX Late Eden 7	SGX Late Eden 8	SGX Late A-hbl 9	SGXIII TGD Eden 1R	SGXIII TGD Eden 2C	SGXIII TGD Eden 3C
SiO2	47.43	46.95	48.90	47.95	47.19	47.56
TiO2	1.16	0.84	0.94	0.71	1.15	0.77
Al2O3	6.42	6.80	5.31	6.38	6.96	6.72
FeO*	14.71	15.50	14.46	14.48	14.73	14.56
MgO	13.17	12.43	13.52	13.03	12.87	13.43
MnO	0.44	0.39	0.42	0.39	0.38	0.37
CaO	11.71	11.71	11.74	11.53	11.66	10.90
Na2O	1.31	1.28	1.19	1.29	1.43	9.30
K2O	0.62	0.67	0.45	0.66	0.73	1.23
Total	96.97	96.57	96.93	96.42	97.10	104.84
Si	7.055	7.037	7.247	7.155	7.020	7.101
Al(iv)	0.945	0.961	0.752	0.845	0.980	0.899
Al(vi)	0.182	0.247	0.175	0.278	0.243	0.284
Ti	0.135	0.101	0.105	0.080	0.129	0.087
Fe2+	1.833	1.951	1.789	1.807	1.833	1.818
Mn	0.053	0.045	0.053	0.050	0.049	0.048
Mg	2.924	2.778	2.982	2.900	2.855	2.989
Ca	1.868	1.879	1.861	1.844	1.859	1.745
Na	0.375	0.387	0.338	0.373	0.413	0.269
K	0.125	0.119	0.089	0.127	0.139	0.236

	SGXIII TGD Eden 4C	SGXIII TGD Mg-hbl 5C	SGXIII TGD Eden 1	SGXIII TGD Eden 2	SGXIII TGD Eden 3	SGXIII TGD Eden 4
SiO2	46.88	48.19	46.58	46.40	47.28	47.36
TiO2	1.09	1.21	0.99	0.91	1.19	1.22
Al2O3	6.98	6.34	7.39	7.64	6.51	6.85
FeO*	14.88	14.22	14.50	14.82	13.96	14.29
MgO	12.71	13.43	12.94	12.74	13.61	13.27
MnO	0.41	0.36	0.36	0.35	0.42	0.37
CaO	11.51	11.76	11.79	11.81	11.69	11.53
Na2O	1.40	1.23	1.43	1.42	1.42	1.54
K2O	0.75	0.64	0.76	0.76	0.65	0.66
Total	96.61	97.38	96.74	96.85	96.73	97.09
Si	7.017	7.113	6.965	6.935	7.035	7.029
Al(iv)	0.983	0.887	1.035	1.065	0.965	0.971
Al(vi)	0.250	0.217	0.235	0.285	0.185	0.229
Ti	0.124	0.135	0.109	0.098	0.135	0.135
Fe2+	1.863	1.756	1.817	1.851	1.726	1.775
Mn	0.052	0.046	0.050	0.044	0.051	0.039
Mg	2.837	2.954	2.889	2.838	3.019	2.937
Ca	1.846	1.860	1.889	1.895	1.868	1.839
Na	0.407	0.352	0.417	0.413	0.421	0.441
K	0.144	0.122	0.141	0.143	0.119	0.121

APPENDIX C

Table C.1: AMPHIBOLE MICROPROBE ANALYSES

	SGXIII TGD Eden 5	SGXIII TGD Mg-hbl 6	SGXIII TGD Eden 7	SGXIII TGD Eden 8	SGXIII TGD Eden 9	SGXIII TGD Eden 10
SiO2	46.82	48.59	46.81	46.22	47.07	46.81
TiO2	1.09	0.87	1.03	1.01	0.99	1.17
Al2O3	6.99	5.76	7.27	7.64	7.10	7.11
FeO*	14.28	13.70	14.54	15.02	14.51	14.44
MgO	13.37	14.26	13.05	12.65	13.19	13.20
MnO	0.37	0.36	0.35	0.41	0.38	0.38
CaO	11.72	11.87	11.77	11.67	11.74	11.79
Na2O	1.47	1.19	1.46	1.52	1.44	1.43
K2O	0.69	0.51	0.72	0.78	0.65	0.72
Total	96.80	97.11	97.00	96.92	97.07	97.05
Si	6.971	7.159	6.965	6.909	7.000	6.965
Al(iv)	1.029	0.836	1.035	1.089	1.000	1.035
Al(vi)	0.201	0.169	0.255	0.258	0.245	0.215
Ti	0.125	0.095	0.115	0.115	0.111	0.135
Fe2+	1.781	1.689	1.806	1.889	1.809	1.796
Mn	0.044	0.041	0.041	0.051	0.039	0.044
Mg	2.971	3.129	2.899	2.819	2.919	2.931
Ca	1.979	1.878	1.878	1.869	1.869	1.877
Na	0.429	0.341	0.442	0.455	0.418	0.411
K	0.125	0.101	0.140	0.141	0.121	0.143

	SGXIII TGD Eden 11	SGXXVI TGD A-hbl 2R	SGXXVI TGD A-hbl 3R	SGXXVI TGD Mg-hbl 4C	SGXXVI TGD Mg-hbl 5R	SGXXVI TGD Eden 6R
SiO2	46.39	49.52	49.89	47.72	48.61	48.26
TiO2	1.08	0.81	0.95	0.97	0.88	1.31
Al2O3	7.41	5.19	5.25	6.65	6.17	6.44
FeO*	14.73	14.46	14.21	16.24	15.34	14.41
MgO	12.99	13.37	13.26	11.94	12.65	12.96
MnO	0.38	0.52	0.51	0.59	0.51	0.49
CaO	11.62	11.78	11.66	11.57	11.71	11.83
Na2O	1.48	1.07	1.11	1.21	1.07	1.33
K2O	0.78	0.49	0.47	0.68	0.61	0.63
Total	96.86	97.21	97.31	97.57	97.55	97.66
Si	6.929	7.306	7.334	7.102	7.187	7.114
Al(iv)	1.069	0.694	0.665	0.898	0.813	0.886
Al(vi)	0.237	0.211	0.245	0.269	0.264	0.233
Ti	0.125	0.090	0.105	0.109	0.099	0.146
Fe2+	1.835	1.785	1.747	2.022	1.898	1.777
Mn	0.042	0.066	0.065	0.076	0.064	0.063
Mg	2.889	2.940	2.907	2.649	2.789	2.848
Ca	1.861	1.864	1.838	1.846	1.856	1.869
Na	0.441	0.307	0.318	0.350	0.310	0.381
K	0.139	0.094	0.089	0.129	0.115	0.120

APPENDIX C

Table C.1: AMPHIBOLE MICROPROBE ANALYSES

	SGXXVI TGD A-hbl 7C	G24 TGD Mg-hbl 1R	G24 TGD Eden 2C	G24 TGD Eden 3M	G24 TGD Mg-hbl 4C	G24 TGD Mg-hbl 5R
SiO2	49.40	46.27	45.80	45.76	46.83	46.10
TiO2	0.95	0.71	1.00	0.97	0.84	0.93
Al2O3	5.46	7.57	7.79	8.07	6.74	7.42
FeO*	14.34	15.25	15.19	15.57	14.53	14.81
MgO	13.45	12.17	12.22	12.23	12.95	12.47
MnO	0.53	0.41	0.41	0.43	0.41	0.40
CaO	11.68	11.73	11.47	11.55	11.86	11.69
Na2O	1.14	1.18	1.38	1.44	1.08	1.17
K2O	0.49	0.77	0.83	0.86	0.67	0.78
Total	97.44	96.06	96.09	96.88	95.91	95.37
Si	7.269	6.980	6.916	6.870	7.048	6.966
Al(iv)	0.731	1.020	1.084	1.130	0.952	1.034
Al(vi)	0.218	0.327	0.304	0.300	0.245	0.288
Ti	0.106	0.081	0.114	0.111	0.095	0.106
Fe2+	1.765	1.925	1.920	1.956	1.829	1.872
Mn	0.067	0.053	0.054	0.055	0.052	0.052
Mg	2.950	2.739	2.751	2.736	2.906	2.809
Ca	1.842	1.896	1.856	1.859	1.913	1.894
Na	0.325	0.345	0.403	0.421	0.317	0.345
K	0.094	0.150	0.162	0.165	0.130	0.152

	G24 TGD Mg-hbl 6C	G24 TGD Mg-hbl 7R	G24 TGD Mg-hbl 8M	G24 TGD Eden 9M	SG49 PGD Mg-hbl 1	SG49 PGD Mg-hbl 2
SiO2	46.98	46.35	47.11	45.45	48.21	48.56
TiO2	1.15	0.89	0.73	0.96	1.02	0.84
Al2O3	6.76	7.60	7.15	7.65	5.99	5.83
FeO*	14.23	15.14	14.79	15.06	14.05	13.91
MgO	13.05	12.63	12.80	12.24	13.45	13.59
MnO	0.41	0.40	0.36	0.42	0.48	0.43
CaO	11.75	11.77	11.91	11.46	11.86	11.91
Na2O	1.12	1.12	0.99	1.42	1.22	1.19
K2O	0.68	0.77	0.64	0.83	0.59	0.56
Total	96.13	96.67	96.48	95.49	96.87	96.82
Si	7.041	6.946	7.043	6.911	7.145	7.235
Al(iv)	1.548	1.054	0.957	1.633	0.855	0.763
Al(vi)	0.237	0.290	0.303	0.282	0.198	0.262
Ti	0.130	0.101	0.082	0.111	0.115	0.099
Fe2+	1.785	1.898	1.849	1.915	1.745	1.739
Mn	0.052	0.051	0.047	0.055	0.062	0.054
Mg	2.915	2.820	2.853	2.775	1.975	3.019
Ca	1.888	1.890	1.909	1.868	1.888	1.901
Na	0.327	0.325	0.289	0.421	0.356	0.359
K	0.132	0.147	0.123	0.163	0.106	0.108

APPENDIX C

Table C.1: AMPHIBOLE MICROPROBE ANALYSES

	SG49 PGD Mg-hbl 3	SG49 PGD Mg-hbl 4	SG49 PGD Mg-hbl 5	SG49 PGD Mg-hbl 6	SG93 TGD Acti 1	SG93 TGD Acti 2
SiO2	48.21	47.71	47.54	48.38	52.90	53.23
TiO2	0.68	0.92	0.99	0.83	0.29	0.19
Al2O3	6.03	6.48	6.16	5.91	3.06	1.97
FeO*	14.03	14.18	13.87	13.82	9.87	11.29
MgO	13.42	13.42	13.45	13.73	17.29	18.00
MnO	0.41	0.48	0.44	0.46	0.27	0.29
CaO	11.95	11.92	11.92	11.93	12.57	12.22
Na2O	1.13	1.31	1.21	1.12	0.44	0.37
K2O	0.56	0.61	0.64	0.58	0.19	0.12
Total	96.42	97.03	96.22	96.76	96.88	97.68
Si	7.195	7.129	7.168	7.175	7.605	7.645
Al(iv)	0.805	0.868	0.831	0.825	0.395	0.327
Al(vi)	0.265	0.279	0.278	0.205	0.125	-
Ti	0.081	0.111	0.108	0.089	0.035	0.015
Fe2+	1.743	1.769	1.748	1.709	1.184	1.354
Mn	0.053	0.058	0.054	0.045	0.034	0.034
Mg	2.976	2.991	3.026	3.035	3.707	3.848
Ca	1.904	1.911	1.930	1.901	1.936	1.881
Na	0.321	0.359	0.362	0.316	0.121	0.103
K	0.107	0.101	0.126	0.101	0.034	0.017

	SG93 TGD Acti 3	SG93 TGD Mg-hbl 4	SG93 TGD Mg-hbl 5	SG93 TGD Mg-hbl 6	SG93 TGD Mg-hbl 7	SG93 TGD Mg-hbl 8
SiO2	52.14	49.46	46.35	45.97	48.14	47.73
TiO2	0.36	0.84	1.39	1.94	0.97	1.01
Al2O3	3.41	5.53	7.68	7.97	6.21	6.37
FeO*	10.34	11.91	13.19	11.59	12.65	12.55
MgO	16.87	15.30	13.53	13.32	14.34	14.19
MnO	0.31	0.31	0.27	0.28	0.31	0.26
CaO	12.41	12.00	11.97	11.97	11.97	12.00
Na2O	0.65	1.11	1.29	1.24	1.14	1.19
K2O	0.26	0.49	0.77	0.79	0.58	0.59
Total	96.75	96.95	96.44	95.07	96.31	95.89
Si	7.548	7.235	6.915	6.905	7.135	7.099
Al(iv)	0.451	0.765	1.085	1.095	0.865	0.900
Al(vi)	0.118	0.182	0.255	0.315	0.225	0.229
Ti	0.045	0.095	0.145	0.217	0.107	0.115
Fe2+	1.252	1.455	1.655	1.445	1.567	1.555
Mn	0.034	0.041	0.035	0.041	0.042	0.036
Mg	3.634	3.331	3.011	2.978	3.165	3.145
Ca	1.921	1.879	1.920	1.929	1.889	1.909
Na	0.173	0.321	0.355	0.355	0.321	0.341
K	0.052	0.076	0.141	0.139	0.101	0.101

APPENDIX C

Table C.1: AMPHIBOLE MICROPROBE ANALYSES

	SG93 TGD Mg-hbl 9	SG93 TGD Mg-hbl 10	SG93 TGD Mg-hbl 11	SG93 TGD Mg-hbl 12	SG93 TGD Mg-hbl 13	SG93 TGD Mg-hbl 14
SiO2	47.47	47.50	48.05	48.17	48.33	48.41
TiO2	1.26	1.19	1.03	1.04	0.96	1.04
Al2O3	6.77	6.63	6.07	6.67	6.02	6.30
FeO*	12.81	13.11	12.97	12.54	1251.00	12.54
MgO	14.01	13.95	14.04	14.18	14.47	14.15
MnO	0.31	0.29	0.26	0.28	0.31	0.28
CaO	11.99	11.89	12.12	12.29	12.09	12.15
Na2O	1.19	1.33	1.05	0.99	1.09	1.09
K2O	0.62	0.65	0.57	0.58	0.55	0.56
Total	96.43	96.54	96.16	96.74	1334.82	96.52
Si	7.045	7.055	7.135	7.105	7.135	7.145
Al(iv)	0.955	0.945	0.862	0.895	0.865	0.855
Al(vi)	0.225	0.215	0.211	0.225	0.185	0.245
Ti	0.145	0.135	0.115	0.115	0.105	0.115
Fe2+	1.589	1.615	1.621	1.549	1.545	1.545
Mn	0.042	0.041	0.039	0.035	0.041	0.038
Mg	3.089	3.089	3.099	3.117	3.188	3.109
Ca	1.909	1.891	1.929	1.939	1.917	1.919
Na	0.337	0.375	0.299	0.283	0.321	0.319
K	0.121	0.121	0.099	0.106	0.101	0.099

	SG93 TGD A-hbl 15	SG93 TGD A/Mg-hbl 16	SG93 TGD Mg-hbl 17	D1 Rubh. A-hbl 1R	D1 Rubh. A-hbl 2C	D1 Rubh. A-hbl 6M
SiO2	49.83	49.11	47.32	51.54	50.55	50.79
TiO2	0.64	0.86	1.15	0.71	0.91	0.74
Al2O3	4.84	5.47	6.92	4.69	5.30	5.46
FeO*	11.63	11.76	13.00	10.13	10.88	10.06
MgO	15.21	14.85	13.98	15.55	15.14	15.55
MnO	0.32	0.26	0.29	0.22	0.27	0.23
CaO	12.04	12.18	12.04	11.89	11.76	11.92
Na2O	0.97	1.01	1.26	1.03	1.17	1.03
K2O	0.39	0.49	0.64	0.40	0.52	0.52
Total	95.87	95.99	96.60	96.16	96.50	96.30
Si	7.345	7.249	7.019	7.490	7.367	7.381
Al(iv)	0.656	0.751	0.982	0.510	0.633	0.619
Al(vi)	0.189	0.209	0.231	0.294	0.278	0.318
Ti	0.071	0.097	0.125	0.079	0.100	0.082
Fe2+	1.424	1.455	1.611	1.232	1.327	1.223
Mn	0.039	0.035	0.039	0.028	0.034	0.029
Mg	3.345	3.265	3.089	3.367	3.290	3.370
Ca	1.901	1.925	1.922	1.852	1.837	1.858
Na	0.278	0.283	0.356	0.291	0.331	0.292
K	0.079	0.088	0.121	0.075	0.099	0.097

APPENDIX C

Table C.1: AMPHIBOLE MICROPROBE ANALYSES

	D1 Rubh. A-hbl 9	D2 Rubh. Acti 1R	D2 Rubh. A-hbl 2C	D2 Rubh. Acti 4R	D2 Rubh. A-hbl 5R	D2 Rubh. A-hbl 6R
SiO2	51.44	52.26	50.05	53.52	50.64	51.58
TiO2	0.48	0.66	0.89	0.41	0.79	0.65
Al2O3	4.61	4.14	5.06	3.17	5.17	4.62
FeO*	10.04	9.54	10.50	9.15	10.36	9.60
MgO	15.91	16.56	15.71	17.30	15.79	16.20
MnO	0.25	0.21	0.26	0.22	0.25	0.23
CaO	11.99	12.27	11.93	12.29	12.05	12.24
Na2O	0.94	0.82	1.06	0.66	1.06	0.83
K2O	0.43	0.35	0.48	0.23	0.47	0.37
Total	96.09	96.81	95.94	96.95	96.58	96.32
Si	7.482	7.519	7.336	7.652	7.359	7.469
Al(iv)	0.518	0.481	0.664	0.348	0.641	0.531
Al(vi)	0.274	0.222	0.211	0.188	0.246	0.258
Ti	0.054	0.072	0.100	0.045	0.088	0.071
Fe2+	1.222	1.149	1.287	1.095	1.259	1.164
Mn	0.031	0.027	0.033	0.027	0.032	0.029
Mg	3.449	3.552	3.431	3.688	3.420	3.497
Ca	1.870	1.893	1.875	1.884	1.877	1.899
Na	0.267	0.229	0.301	0.185	0.300	0.235
K	0.081	0.065	0.090	0.043	0.088	0.069

	D2 Rubh. Acti 7R	D2 Rubh. A-hbl 8C	D8 Rubh. A-hbl 1	D8 Rubh. A-hbl 2	D8 Rubh. A-hbl 3	D8 Rubh. Acti 4
SiO2	52.77	51.58	50.84	50.69	52.49	52.88
TiO2	0.40	0.55	0.64	0.27	0.40	0.30
Al2O3	3.62	4.52	5.85	4.84	4.18	3.67
FeO*	9.11	9.71	8.57	8.27	8.14	8.05
MgO	16.83	16.12	17.68	18.37	18.51	18.69
MnO	0.24	0.24	0.20	0.22	0.19	0.21
CaO	12.01	12.10	12.12	12.10	12.12	12.23
Na2O	0.80	0.96	1.29	1.15	1.03	0.92
K2O	0.29	0.40	0.34	0.37	0.26	0.18
Total	96.07	96.18	97.53	96.28	97.32	97.13
Si	7.619	7.485	7.255	7.331	7.465	7.525
Al(iv)	0.381	0.515	0.735	0.669	0.535	0.475
Al(vi)	0.236	0.260	0.235	0.147	0.165	0.138
Ti	0.045	0.061	0.065	0.025	0.045	0.035
Fe2+	1.100	1.179	1.019	0.998	0.965	0.956
Mn	0.030	0.030	0.031	0.026	0.025	0.031
Mg	3.622	3.487	3.756	3.961	3.921	3.969
Ca	1.859	1.882	1.846	1.876	1.845	1.855
Na	0.226	0.272	0.359	0.330	0.291	0.258
K	0.055	0.075	0.055	0.069	0.051	0.041

APPENDIX C

Table C.1: AMPHIBOLE MICROPROBE ANALYSES

	D8 Rubh. A-hbl 5	D8 Rubh. A-hbl 6	D8 Rubh. A-hbl 7	D8 Rubh. A-hbl 8	D8 Rubh. A-hbl 9	D8 Rubh. A-hbl 10
SiO2	52.04	50.90	50.54	51.84	51.58	51.57
TiO2	0.69	0.53	0.43	0.54	0.63	0.60
Al2O3	4.09	4.88	5.13	4.41	4.41	4.44
FeO*	8.73	8.92	8.95	8.07	9.27	8.28
MgO	18.01	17.82	17.91	18.19	17.66	17.99
MnO	0.19	0.23	0.19	0.21	0.23	0.21
CaO	11.89	11.87	12.06	12.19	11.77	12.13
Na2O	1.07	1.22	1.20	1.04	1.18	1.09
K2O	0.32	0.41	0.49	0.29	0.37	0.27
Total	97.03	96.78	96.90	96.78	97.10	96.58
Si	7.445	7.375	7.286	7.433	7.411	7.405
Al(iv)	0.545	0.621	0.711	0.575	0.589	0.595
Al(vi)	0.138	0.211	0.161	0.167	0.149	0.165
Ti	0.075	0.055	0.045	0.061	0.067	0.063
Fe2+	1.045	1.079	1.079	0.955	1.111	0.991
Mn	0.033	0.029	0.032	0.033	0.029	0.031
Mg	3.835	3.855	3.851	3.879	3.785	3.847
Ca	1.819	1.848	1.857	1.865	1.805	1.866
Na	0.301	0.401	0.321	0.301	0.321	0.322
K	0.055	0.055	0.080	0.055	0.058	0.059

	D8 Rubh. Acti 12	D8 Rubh. A-hbl 13	D11 Lidd. Mg-hbl 1	D11 Lidd. A-hbl 2	D11 Lidd. Mg-hbl 3	D11 Lidd. Eden 4
SiO2	52.95	50.94	50.02	50.56	49.39	48.03
TiO2	0.36	0.91	1.06	0.98	0.87	1.07
Al2O3	3.78	4.39	5.33	5.14	5.97	7.01
FeO*	7.65	8.71	9.72	9.56	9.71	9.33
MgO	18.49	17.81	17.29	16.95	16.50	16.90
MnO	0.20	0.21	0.18	0.15	0.17	0.19
CaO	12.19	11.98	11.67	12.17	11.75	11.73
Na2O	0.86	1.16	1.03	1.02	1.29	1.47
K2O	0.14	0.38	0.33	0.38	0.48	0.51
Total	96.62	96.49	96.63	96.91	96.13	96.24
Si	7.549	7.357	7.245	7.302	7.202	7.011
Al(iv)	0.451	0.641	0.755	0.697	0.797	0.989
Al(vi)	0.183	0.110	0.155	0.172	0.232	0.221
Ti	0.045	0.095	0.115	0.105	0.095	0.115
Fe2+	0.908	1.045	1.174	1.154	1.179	1.141
Mn	0.025	0.033	0.026	0.017	0.022	0.026
Mg	3.933	3.845	3.731	3.646	3.582	3.676
Ca	1.859	1.855	1.809	1.884	1.842	1.833
Na	0.239	0.324	0.295	0.295	0.357	0.421
K	0.034	0.059	0.069	0.069	0.081	0.087

APPENDIX C

Table C.1: AMPHIBOLE MICROPROBE ANALYSES

	D11 Lidd. Mg-hbl 5	D11 Lidd. A-hbl 6	D11 Lidd. A-hbl 7	D12 Lidd. Mg-hbl 1M	D12 Lidd. A-hbl 2C	D12 Lidd. A-hbl 3M
SiO2	49.37	51.34	49.89	48.46	49.90	50.44
TiO2	1.23	0.96	1.04	0.80	0.82	0.42
Al2O3	5.63	4.39	5.28	6.27	4.94	4.81
FeO*	9.19	9.18	9.84	10.85	11.57	10.51
MgO	17.10	17.64	16.86	15.23	15.34	15.76
MnO	0.16	0.17	0.18	0.24	0.30	0.24
CaO	11.99	11.72	11.63	12.09	11.73	12.30
Na2O	1.12	1.04	1.22	1.13	1.11	0.76
K2O	0.43	0.31	0.45	0.49	0.43	0.27
Total	96.22	96.75	96.39	95.56	96.14	95.51
Si	7.188	7.389	7.255	7.164	7.334	7.409
Al(iv)	0.812	0.610	0.745	0.836	0.665	0.591
Al(vi)	0.149	0.139	0.162	0.258	0.191	0.242
Ti	0.131	0.105	0.115	0.090	0.092	0.047
Fe2+	1.119	1.107	1.199	1.343	1.423	1.291
Mn	0.017	0.017	0.031	0.031	0.038	0.031
Mg	3.707	3.790	3.645	3.357	3.361	3.450
Ca	1.871	1.808	1.809	1.916	1.848	1.936
Na	0.314	0.294	0.339	0.327	0.317	0.218
K	0.087	0.052	0.082	0.093	0.081	0.051

	D12 Lidd. A-hbl 4M	D12 Lidd. A-hbl 5R	D12 Lidd. A-hbl 6C	D12 Lidd. Acti 7M	D12 Lidd. A-hbl 8R	D12 Lidd Mg-hbl 9M
SiO2	49.38	49.91	49.89	51.73	50.23	47.96
TiO2	0.53	0.79	0.79	0.47	0.71	0.91
Al2O3	5.52	5.33	5.14	3.91	5.04	6.79
FeO*	10.71	11.22	10.74	10.44	11.08	11.29
MgO	15.91	15.16	15.57	15.98	15.66	14.79
MnO	0.29	0.25	0.27	0.25	0.25	0.26
CaO	11.64	12.21	12.05	12.23	11.97	11.78
Na2O	1.23	0.90	1.01	0.64	0.98	1.34
K2O	0.51	0.39	0.42	0.19	0.39	0.56
Total	95.72	96.16	95.88	95.84	96.31	95.68
Si	7.269	7.319	7.325	7.544	7.344	7.104
Al(iv)	0.731	0.681	0.675	0.456	0.656	0.896
Al(vi)	0.228	0.241	0.215	0.217	0.215	0.290
Ti	0.059	0.088	0.088	0.052	0.079	0.102
Fe2+	1.319	1.376	1.320	1.275	1.355	1.399
Mn	0.037	0.032	0.034	0.032	0.032	0.033
Mg	3.491	3.313	3.408	3.473	3.412	3.264
Ca	1.837	1.920	1.896	1.913	1.876	1.870
Na	0.353	0.258	0.289	0.182	0.279	0.386
K	0.096	0.075	0.080	0.036	0.073	0.107

APPENDIX C

Table C.1: AMPHIBOLE MICROPROBE ANALYSES

	D12 Lidd. F-Parg 10M	D19 Lidd. A-hbl 1	D19 Lidd. A-hbl 2	D19 Lidd. A-hbl 3	D19 Shet. Mg-hbl 4	D19 Lidd. A-hbl 5
SiO2	40.63	49.69	51.01	50.28	48.29	49.23
TiO2	2.82	0.51	0.43	0.52	0.99	0.69
Al2O3	12.15	5.62	4.79	5.37	6.82	5.72
FeO*	15.11	12.02	11.39	12.15	12.72	11.90
MgO	10.75	15.06	15.71	15.12	14.17	14.98
MnO	0.26	0.31	0.28	0.32	0.26	0.33
CaO	11.75	12.22	12.19	12.23	12.13	11.92
Na2O	1.84	0.83	0.83	0.83	0.95	0.98
K2O	1.44	0.37	0.33	0.35	0.58	0.44
Total	96.75	96.63	96.96	97.17	96.91	96.19
Si	6.183	7.285	7.409	7.325	7.105	7.256
Al(iv)	1.817	0.715	0.591	0.675	0.895	0.735
Al(vi)	0.363	0.258	0.229	0.252	0.292	0.252
Ti	0.323	0.055	0.035	0.055	0.106	0.088
Fe2+	1.924	1.471	12.389	1.478	1.564	1.467
Mn	0.034	0.035	0.035	0.029	0.035	0.042
Mg	2.438	3.284	3.339	3.278	3.102	3.288
Ca	1.916	1.919	1.901	1.909	1.909	1.889
Na	0.543	0.246	0.221	0.279	0.265	0.278
K	0.280	0.070	0.057	0.065	0.106	0.083

	D19 Lidd. Mg-hbl 6	D19 Lidd. Mg-hbl 7	D19 Lidd. Mg-hbl 8	D19 Lidd. Mg-hbl 9	D19 Lidd Mg-hbl 10	D19 Shet. Eden 11
SiO2	47.50	48.19	49.43	48.97	47.86	46.12
TiO2	0.82	0.81	0.59	0.74	0.89	1.20
Al2O3	7.30	6.80	5.98	6.21	7.25	8.27
FeO*	13.03	12.86	12.14	11.98	12.93	13.61
MgO	13.77	14.20	14.76	14.47	13.83	13.09
MnO	0.28	0.29	0.27	0.29	0.32	0.30
CaO	12.20	12.08	12.28	12.14	12.17	12.08
Na2O	1.12	1.08	0.80	0.94	1.07	1.24
K2O	0.65	0.56	0.42	0.48	0.59	0.77
Total	96.67	96.87	96.67	96.22	96.91	96.68
Si	7.029	7.099	7.245	7.215	7.057	6.871
Al(iv)	0.967	0.900	0.755	0.785	0.944	1.129
Al(vi)	0.311	0.289	0.285	0.295	0.321	0.320
Ti	0.089	0.089	0.055	0.076	0.095	0.135
Fe2+	1.606	1.577	1.488	1.478	1.599	1.699
Mn	0.042	0.041	0.038	0.035	0.043	0.035
Mg	3.036	3.121	3.219	3.178	3.039	2.907
Ca	1.937	1.909	1.928	1.917	1.917	1.923
Na	0.322	0.302	0.237	0.255	0.298	0.357
K	0.121	0.090	0.081	0.079	0.099	0.143

APPENDIX C

Table C.1: AMPHIBOLE MICROPROBE ANALYSES

	D19 Lidd. Mg-hbl 12	D19 Lidd. Mg-hbl 13	D19 Lidd. A-hbl 14	D19 Shet. Eden 15	D19 Lidd. Mg-hbl 16	D19 Lidd. Mg-hbl 17
SiO2	47.07	48.44	50.44	46.81	47.65	48.52
TiO2	1.28	0.97	0.49	1.27	1.11	0.76
Al2O3	7.65	7.17	5.37	7.54	7.09	6.67
FeO*	13.40	12.95	11.74	13.39	13.16	12.86
MgO	13.72	14.16	15.47	13.52	13.96	14.09
MnO	0.32	0.32	0.29	0.33	0.32	0.30
CaO	11.87	12.00	12.18	11.87	11.83	12.03
Na2O	1.38	1.16	0.89	1.41	1.21	1.06
K2O	0.74	0.63	0.41	0.73	0.65	0.54
Total	97.43	97.80	97.28	96.87	96.98	96.83
Si	6.942	7.075	7.325	6.925	7.025	7.135
Al(iv)	1.055	0.925	0.675	1.075	0.975	0.856
Al(vi)	0.274	0.295	0.252	0.235	0.265	0.288
Ti	0.137	0.105	0.055	0.142	0.125	0.089
Fe2+	1.651	1.578	1.418	1.653	1.615	1.577
Mn	0.038	0.037	0.029	0.044	0.037	0.038
Mg	3.009	3.078	3.345	2.987	3.055	3.099
Ca	1.868	1.878	1.889	1.884	1.867	1.899
Na	0.378	0.344	0.245	0.497	0.355	0.301
K	0.139	0.121	0.057	0.142	0.119	0.099

	D19 Lidd. Eden 18	D41 Rana. A-hbl 1	D41 Rana. A-hbl 2	D41 Rana. A-hbl 3	D41 Rana. Mg-hbl 4	D41 Rana. A-hbl 5
SiO2	46.52	50.09	50.05	48.71	49.55	50.60
TiO2	1.20	0.66	0.72	0.97	0.92	0.63
Al2O3	8.12	5.22	5.19	6.43	5.37	4.69
FeO*	13.79	10.90	10.72	11.06	10.90	10.47
MgO	13.03	16.18	16.18	15.56	16.11	16.70
MnO	0.29	0.22	0.22	0.23	0.20	0.22
CaO	11.98	12.29	12.13	12.11	12.19	12.24
Na2O	1.29	0.97	1.01	1.28	1.10	0.93
K2O	0.79	0.44	0.43	0.42	0.47	0.41
Total	97.01	96.97	96.65	96.77	96.81	96.89
Si	6.901	7.285	7.295	7.295	7.225	7.335
Al(iv)	1.109	0.715	0.705	0.705	0.775	0.656
Al(vi)	0.327	0.175	0.185	0.402	0.152	0.138
Ti	0.135	0.069	0.075	0.105	0.105	0.067
Fe2+	1.708	1.327	1.307	1.352	1.328	1.275
Mn	0.037	0.026	0.028	0.026	0.028	0.031
Mg	2.878	3.502	3.509	3.389	3.489	3.612
Ca	1.909	1.912	1.889	1.896	1.899	1.898
Na	0.378	0.279	0.278	0.368	0.321	0.257
K	0.136	0.087	0.076	0.087	0.078	0.067

APPENDIX C

Table C.1: AMPHIBOLE MICROPROBE ANALYSES

	D41 Rana. A-hbl 6	D41 Rana. Mg-hbl 7	D41 Rana. Mg-hbl 8	D41 Rana. Mg-hbl 9	D41 Rana. A-hbl 10	D41 Rana. Mg-hbl 11
SiO2	49.93	47.61	47.27	49.43	50.05	48.89
TiO2	0.77	1.32	1.16	1.09	0.67	1.10
Al2O3	5.39	7.21	7.34	5.48	5.08	5.53
FeO*	10.84	11.72	12.43	10.66	10.92	10.93
MgO	15.93	14.75	14.35	16.00	15.93	15.82
MnO	0.23	0.22	0.26	0.22	0.23	0.24
CaO	12.36	11.99	12.22	12.16	12.38	12.27
Na2O	0.86	1.33	1.25	1.05	0.96	0.99
K2O	0.44	0.66	0.69	0.52	0.40	0.49
Total	96.75	96.81	96.97	96.61	96.62	96.26
Si	7.265	6.995	6.966	7.215	7.305	7.185
Al(iv)	0.735	1.005	1.034	0.785	0.695	0.815
Al(vi)	0.195	0.245	0.236	0.165	0.185	0.135
Ti	0.088	0.150	0.132	0.125	0.065	0.125
Fe2+	1.320	1.439	1.531	1.299	1.328	1.336
Mn	0.026	0.026	0.035	0.028	0.031	0.031
Mg	3.454	3.231	3.151	3.478	3.455	3.456
Ca	1.932	1.889	1.929	1.899	1.939	1.929
Na	0.244	0.371	0.354	0.301	0.278	0.277
K	0.087	0.123	0.123	0.078	0.081	0.077

	D41 Rana. A-hbl 12	D41 Rana. A-hbl 13	D41 Rana. Mg-hbl 14	D41 Rana. A-hbl 15	D63 Uile. A-hbl 1	D63 Uile. Eden 2
SiO2	49.57	50.37	49.34	51.11	50.20	48.21
TiO2	0.81	0.64	0.96	0.60	0.70	1.07
Al2O3	5.25	5.07	5.61	4.76	4.47	5.95
FeO*	9.96	10.58	11.17	10.81	12.36	13.12
MgO	16.18	16.22	15.82	16.42	15.34	14.47
MnO	0.21	0.22	0.21	0.24	0.28	0.25
CaO	12.07	12.35	12.18	12.48	12.03	11.89
Na2O	1.05	0.82	1.04	0.75	1.16	1.46
K2O	0.45	0.41	0.48	0.37	0.40	0.61
Total	95.55	96.68	96.81	97.34	96.94	97.03
Si	7.278	7.325	7.211	7.347	7.344	7.115
Al(iv)	0.721	0.675	0.791	0.655	0.651	0.885
Al(vi)	0.201	0.195	0.178	0.160	0.119	0.145
Ti	0.089	0.073	0.105	0.067	0.079	0.115
Fe2+	1.292	1.288	1.355	1.278	1.512	1.623
Mn	0.033	0.027	0.028	0.027	0.036	0.035
Mg	3.544	3.511	3.435	3.521	3.345	3.184
Ca	1.898	1.921	1.911	1.929	1.878	1.880
Na	0.303	0.227	0.298	0.199	0.341	0.425
K	0.082	0.061	0.078	0.178	0.081	0.121

APPENDIX C

Table C.1: AMPHIBOLE MICROPROBE ANALYSES

	D63 Uile. Acti 3	D63 Uile. A-hbl 4	D63 Uile. Mg-hbl 5	D63 Uile. A-hbl 6	D63 Uile. Acti 7	D63 Uile. A-hbl 8
SiO2	52.16	50.17	48.55	50.45	52.62	48.92
TiO2	0.31	0.54	0.71	0.49	0.14	0.47
Al2O3	3.26	4.49	5.21	4.22	2.55	5.01
FeO*	11.24	12.82	12.37	12.27	11.15	13.00
MgO	16.28	15.22	15.06	15.49	16.61	14.72
MnO	0.23	0.24	0.23	0.24	0.26	0.26
CaO	12.45	12.09	12.09	12.08	12.09	12.19
Na2O	0.79	1.02	1.25	1.08	0.53	1.13
K2O	0.24	0.43	0.49	0.37	0.22	0.45
Total	96.96	97.02	95.96	96.69	96.17	96.15
Si	7.560	7.348	7.205	7.419	7.665	7.269
Al(iv)	0.440	0.652	0.795	0.583	0.331	0.731
Al(vi)	0.117	0.122	0.115	0.144	0.111	0.144
Ti	0.035	0.061	0.078	0.055	0.019	0.055
Fe2+	1.358	1.566	1.544	1.509	1.356	1.616
Mn	0.026	0.026	0.028	0.028	0.037	0.035
Mg	3.518	3.352	3.341	3.388	3.606	3.259
Ca	1.933	1.901	1.929	1.899	1.889	1.937
Na	0.226	0.299	0.367	0.301	0.161	0.321
K	0.052	0.088	0.081	0.082	0.035	0.089

	D63 Uile. A-hbl 9	D63 Uile. Acti 10	D63 Uile. A-hbl 11	D63 Uile. A-hbl 12	D63 Uile. A-hbl 13	D63 Uile. Eden 14
SiO2	50.04	53.73	50.36	49.24	50.76	47.97
TiO2	0.43	0.37	0.43	0.68	0.47	0.76
Al2O3	4.07	4.29	4.22	5.09	4.21	6.23
FeO*	11.92	11.73	12.10	12.47	12.00	13.42
MgO	15.86	13.82	15.56	14.66	15.53	13.94
MnO	0.24	0.20	0.27	0.27	0.22	0.27
CaO	12.24	11.31	12.09	12.09	12.23	12.14
Na2O	0.99	0.82	1.03	1.26	1.03	1.37
K2O	0.34	0.39	0.35	0.43	0.36	0.56
Total	96.13	96.66	96.41	96.19	96.81	96.66
Si	7.378	7.755	7.399	7.275	7.421	7.110
Al(iv)	0.621	0.250	0.601	0.725	0.582	0.890
Al(vi)	0.099	0.481	0.132	0.165	0.141	0.197
Ti	0.045	0.045	0.045	0.078	0.055	0.089
Fe2+	1.467	1.411	1.478	1.555	1.467	1.665
Mn	0.029	0.028	0.043	0.035	0.028	0.035
Mg	3.489	2.978	4.311	3.229	3.378	3.082
Ca	1.933	1.755	1.909	1.917	1.909	1.933
Na	0.278	0.221	0.299	0.365	0.299	0.392
K	0.077	0.056	0.082	0.088	0.078	0.106

APPENDIX C

Table C.1: AMPHIBOLE MICROPROBE ANALYSES

	D63 Uile. Acti 15	D63 Uile. A-hbl 16	E1 Dyke A-hbl 1	E1 Dyke Mg-hbl 2	E1 Dyke Mg-hbl 4	E1 Dyke Mg-hbl 5
SiO2	54.03	50.31	50.34	44.17	49.07	49.31
TiO2	0.12	0.45	0.68	0.41	0.90	0.66
Al2O3	1.45	4.11	5.25	8.18	5.86	5.97
FeO*	9.76	12.10	12.15	13.70	12.70	12.74
MgO	18.00	15.64	15.15	16.78	14.84	14.75
MnO	0.23	0.26	0.28	0.22	0.30	0.29
CaO	12.72	12.29	12.28	7.85	11.79	12.17
Na2O	0.41	0.99	0.96	0.68	1.08	0.93
K2O	0.10	0.36	0.42	0.56	0.48	0.50
Total	96.82	96.51	97.51	92.55	97.02	97.32
Si	7.763	7.389	7.307	6.789	7.205	7.212
Al(iv)	0.240	0.611	0.693	1.201	0.705	0.790
Al(vi)	-	0.121	0.213	0.281	0.305	0.241
Ti	0.015	0.055	0.078	0.045	0.095	0.067
Fe2+	1.165	1.478	1.473	1.767	1.555	1.553
Mn	0.029	0.039	0.034	0.031	0.038	0.044
Mg	3.851	3.432	3.278	3.855	3.251	3.211
Ca	1.955	1.928	1.909	1.302	1.852	1.911
Na	0.121	0.281	0.261	0.199	0.299	0.255
K	0.021	0.079	0.069	0.121	0.078	0.076

	E1 Dyke A-hbl 6	E1 Dyke Mg-hbl 7	E1 Dyke A-hbl 8	E1 Dyke Mg-hbl 9	E1 Dyke Mg-hbl 10	E1 Dyke Mg-hbl 11
SiO2	49.76	48.84	49.70	48.36	48.74	49.25
TiO2	0.78	0.84	0.70	0.91	0.79	0.69
Al2O3	5.46	6.11	5.46	6.19	5.98	5.68
FeO*	12.35	12.90	12.35	13.05	12.60	12.51
MgO	15.01	14.43	14.98	14.15	14.53	14.72
MnO	0.30	0.26	0.30	0.29	0.25	0.28
CaO	12.15	12.13	12.23	11.99	12.14	12.24
Na2O	1.01	1.06	1.02	1.09	1.05	0.89
K2O	0.46	0.51	0.46	0.56	0.52	0.45
Total	97.28	97.08	97.20	96.59	96.60	96.71
Si	7.255	7.177	7.255	7.145	7.175	7.241
Al(iv)	0.745	0.821	0.744	0.853	0.825	0.759
Al(vi)	0.205	0.238	0.212	0.244	0.225	0.229
Ti	0.087	0.090	0.078	0.099	0.088	0.079
Fe2+	1.506	1.588	1.506	1.619	1.548	1.536
Mn	0.035	0.035	0.042	0.035	0.035	0.035
Mg	3.258	3.156	3.267	3.121	3.194	3.222
Ca	1.901	1.909	1.909	1.899	1.920	1.924
Na	0.280	0.299	0.278	0.321	0.301	0.247
K	0.087	0.078	0.082	0.099	0.106	0.088

APPENDIX C

Table C.1: AMPHIBOLE MICROPROBE ANALYSES

	E1 Dyke Mg-hbl 12	E1 Dyke E-hbl 13	E1 Dyke Mg-hbl 14	E1 Dyke Mg-hbl 15	E1 Dyke A-hbl 16	E3 Dyke A-hbl 1R
SiO2	48.09	43.03	48.86	47.77	49.92	49.69
TiO2	0.72	1.20	0.62	0.86	0.70	0.52
Al2O3	6.63	10.08	5.98	6.83	5.27	0.51
FeO*	13.05	15.72	12.84	13.41	12.18	12.60
MgO	14.13	11.32	14.84	13.88	15.06	15.02
MnO	0.28	0.30	0.30	0.30	0.26	0.32
CaO	12.15	11.91	11.88	12.03	12.01	12.13
Na2O	1.07	1.57	0.91	1.18	1.09	0.98
K2O	0.54	0.98	0.50	0.60	0.44	0.42
Total	96.66	96.11	96.73	96.86	96.93	92.19
Si	7.105	6.558	7.199	7.067	7.298	7.294
Al(iv)	0.895	1.442	0.801	0.931	0.702	0.706
Al(vi)	0.255	0.371	0.238	0.255	0.211	0.176
Ti	0.081	0.135	0.072	0.101	0.083	0.061
Fe2+	1.619	2.006	1.577	1.656	1.497	1.543
Mn	0.044	0.036	0.038	0.037	0.035	0.044
Mg	3.111	2.573	3.255	3.065	3.277	3.289
Ca	1.931	1.951	1.867	1.090	1.888	1.905
Na	0.298	0.458	0.255	0.341	0.321	0.282
K	0.097	0.183	0.078	0.099	0.078	0.071

	E3 Dyke A-hbl 2C	E3 Dyke Eden 3	E3 Dyke Mg-hbl 4	E3 Dyke Mg-hbl 5	E3 Dyke Mg-hbl 7M	E3 Dyke Mg-hbl 8R
SiO2	49.55	46.40	48.41	47.58	48.47	48.39
TiO2	0.69	0.98	0.96	0.95	0.88	0.85
Al2O3	5.29	7.69	5.97	6.51	6.09	6.16
FeO*	12.80	14.62	13.40	13.65	13.20	13.40
MgO	14.68	13.27	14.00	13.89	14.21	14.02
MnO	0.33	0.31	0.33	0.32	0.29	0.29
CaO	12.12	11.86	12.06	12.03	12.15	12.06
Na2O	1.02	1.27	1.17	1.25	1.14	1.12
K2O	0.47	0.73	0.57	0.59	0.51	0.61
Total	84.15	97.13	96.87	96.77	96.94	96.90
Si	7.276	6.905	7.155	7.065	7.146	7.140
Al(iv)	0.724	1.090	0.841	0.935	0.855	0.860
Al(vi)	0.193	0.255	0.211	0.205	0.221	0.222
Ti	0.079	0.105	0.105	0.105	0.095	0.097
Fe2+	1.569	1.819	1.655	1.698	1.625	1.649
Mn	0.044	0.035	0.035	0.042	0.042	0.035
Mg	3.210	2.944	3.076	3.065	3.121	3.089
Ca	1.905	1.899	1.909	1.909	1.919	1.907
Na	0.299	0.365	0.342	0.365	0.355	0.319
K	0.088	0.142	0.101	0.109	0.078	0.124

APPENDIX C

Table C.1: AMPHIBOLE MICROPROBE ANALYSES

	E3 Dyke A-hbl 9M	E3 Dyke Mg-hbl 10M	E3 Dyke A-hbl 11M	E3 Dyke Mg-hbl 12	E3 Dyke Mg-hbl 13	E3 Dyke Mg-hbl 14
SiO2	49.63	48.08	49.55	48.94	47.53	48.15
TiO2	0.80	0.68	0.67	0.61	1.03	0.94
Al2O3	5.22	6.16	5.12	5.77	6.56	6.19
FeO*	12.86	13.50	12.69	13.05	13.71	13.53
MgO	14.71	14.05	14.77	14.34	13.68	13.65
MnO	0.35	0.29	0.31	0.33	0.31	0.33
CaO	12.08	12.11	12.05	12.06	12.06	12.05
Na2O	1.06	1.16	1.01	1.07	1.24	1.21
K2O	0.46	0.55	0.47	0.50	0.62	0.60
Total	97.17	96.58	96.64	96.67	96.74	96.65
Si	7.275	7.135	7.295	7.211	7.065	7.135
Al(iv)	0.725	0.865	0.701	0.790	0.935	0.865
Al(vi)	0.175	0.205	0.195	0.223	0.205	0.225
Ti	0.091	0.080	0.075	0.072	0.115	0.105
Fe2+	1.578	1.676	1.567	1.605	1.706	1.678
Mn	0.042	0.035	0.039	0.042	0.042	0.044
Mg	3.221	3.104	3.243	3.145	3.039	3.019
Ca	1.899	1.926	1.899	1.899	1.919	1.918
Na	0.301	0.338	0.277	0.298	0.355	0.362
K	0.076	0.107	0.081	0.082	0.121	0.101

	E5A Dyke A-hbl 1	E5A Dyke A-hbl 2	E5A Dyke A-hbl 3	E5A Dyke A-hbl 4	E5A Dyke A-hbl 5	E5A Dyke A-hbl 6
SiO2	49.53	50.42	49.52	49.87	49.51	49.44
TiO2	0.63	0.63	0.77	0.50	0.52	0.55
Al2O3	5.40	4.79	5.38	5.33	5.20	5.42
FeO*	12.91	12.53	12.76	12.71	12.73	13.02
MgO	14.69	15.15	14.78	14.83	14.79	14.50
MnO	0.31	0.31	0.33	0.26	0.32	0.32
CaO	12.07	11.89	11.85	12.18	12.12	12.15
Na2O	0.97	0.95	1.08	0.96	1.01	0.99
K2O	0.44	0.41	0.44	0.41	0.42	0.44
Total	96.95	97.08	96.91	97.05	96.62	96.83
Si	7.275	7.378	7.267	7.305	7.285	7.272
Al(iv)	0.725	0.621	0.731	0.695	0.706	0.727
Al(vi)	0.195	0.210	0.199	0.218	0.189	0.208
Ti	0.071	0.067	0.099	0.055	0.066	0.061
Fe2+	1.587	1.528	1.566	1.557	1.567	1.599
Mn	0.037	0.036	0.038	0.035	0.038	0.044
Mg	3.221	3.309	3.244	3.239	3.255	3.181
Ca	1.899	1.865	1.855	1.910	1.909	1.917
Na	0.282	0.255	0.301	0.264	0.278	0.282
K	0.079	0.078	0.078	0.071	0.078	0.088

APPENDIX C

Table C.1: AMPHIBOLE MICROPROBE ANALYSES

	E5A Dyke A-hbl 7	E5A Dyke A-hbl 8	E5A Dyke A-hbl 9	E5A Dyke A-hbl 10	E5A Dyke A-hbl 11	E5A Dyke A-hbl 12
SiO2	50.06	50.18	51.68	49.89	49.97	51.69
TiO2	0.51	0.35	0.36	0.61	0.45	0.36
Al2O3	4.87	4.71	3.83	5.09	5.08	3.89
FeO*	12.45	12.24	11.72	12.63	12.56	11.50
MgO	14.84	15.20	16.02	15.11	15.02	15.99
MnO	0.29	0.33	0.29	0.28	0.32	0.29
CaO	12.05	12.28	12.48	12.02	12.19	12.28
Na2O	0.99	0.81	0.70	0.91	0.89	0.73
K2O	0.40	0.33	0.28	0.42	0.39	0.30
Total	96.46	96.43	97.36	96.96	96.87	97.03
Si	7.365	7.375	7.478	7.305	7.321	7.495
Al(iv)	0.635	0.621	0.522	0.695	0.688	0.505
Al(vi)	0.215	0.190	0.139	0.185	0.202	0.155
Ti	0.055	0.035	0.045	0.071	0.055	0.045
Fe2+	1.525	1.502	1.417	1.545	1.535	1.389
Mn	0.039	0.035	0.034	0.039	0.038	0.028
Mg	3.251	3.328	3.452	3.298	3.278	3.455
Ca	1.899	1.944	1.939	1.788	1.909	1.909
Na	0.278	0.221	0.191	0.256	0.241	0.218
K	0.079	0.055	0.052	0.076	0.081	0.065

	E5A Dyke Mg-hbl 13
SiO2	47.46
TiO2	0.65
Al2O3	5.59
FeO*	12.51
MgO	14.32
MnO	0.28
CaO	13.48
Na2O	0.99
K2O	0.49
Total	95.77
Si	7.111
Al(iv)	0.890
Al(vi)	0.100
Ti	0.072
Fe2+	1.566
Mn	0.036
Mg	3.195
Ca	2.160
Na	0.288
K	0.090

APPENDIX C

Table C.1: AMPHIBOLE MICROPROBE ANALYSES

	E5A Dyke Mg-hbl 14	E5A Dyke Mg-hbl 15	E5A Dyke Mg-hbl 16	E5A Dyke Mg-hbl 17	XG65 Type 1A Mg-hbl 1	XG65 1A Eden 3
SiO2	48.59	48.71	50.21	48.72	46.94	46.32
TiO2	0.85	0.57	0.37	0.55	0.71	0.74
Al2O3	5.96	5.88	4.67	5.29	6.40	7.45
FeO*	13.16	12.98	12.24	12.77	14.83	15.60
MgO	14.36	14.32	15.25	14.63	12.98	12.53
MnO	0.32	0.30	0.33	0.32	0.38	0.38
CaO	12.03	12.14	12.26	12.07	11.87	10.97
Na2O	1.12	0.99	0.83	1.12	1.21	1.13
K2O	0.55	0.50	0.35	0.43	0.61	1.06
Total	96.94	96.39	96.51	95.90	95.93	96.18
Si	7.167	7.205	7.367	7.243	7.069	6.989
Al(iv)	0.829	0.795	0.632	0.756	0.930	1.010
Al(vi)	0.201	0.235	0.178	0.172	0.209	0.309
Ti	0.095	0.062	0.045	0.065	0.081	0.081
Fe2+	1.616	1.608	1.498	1.588	1.864	1.967
Mn	0.035	0.035	0.044	0.044	0.045	0.045
Mg	3.155	3.154	3.326	3.236	2.914	2.819
Ca	1.899	1.928	1.929	1.919	1.919	1.776
Na	0.321	0.284	0.244	0.321	0.362	0.326
K	0.101	0.088	0.082	0.087	0.126	0.199

	XG65 1A Mg-hbl 7	XG65 1A Mg-hbl 9	XG65 1A Mg-hbl 10	XG7 1B Mg-hbl 1C	XG7 1B Mg-hbl 2M	XG7 1B Mg-hbl 4R
SiO2	47.52	46.42	47.11	48.10	48.27	48.71
TiO2	0.70	0.95	0.83	0.85	1.05	0.95
Al2O3	6.53	7.04	6.31	6.28	6.36	6.29
FeO*	14.96	15.40	14.79	14.21	13.99	14.16
MgO	12.82	12.32	12.73	13.01	13.14	13.23
MnO	0.35	0.39	0.33	0.34	0.35	0.38
CaO	12.05	11.90	11.84	11.89	11.64	11.87
Na2O	1.06	1.26	1.17	1.04	1.17	1.20
K2O	0.57	0.70	0.62	0.64	0.66	0.62
Total	96.56	96.38	95.73	96.36	96.63	97.41
Si	7.105	6.985	7.105	7.170	7.163	7.175
Al(iv)	0.895	1.015	0.895	0.830	0.837	0.825
Al(vi)	0.255	0.255	0.235	0.273	0.277	0.269
Ti	0.081	0.109	0.091	0.096	0.118	0.106
Fe2+	1.868	1.925	1.867	1.772	1.737	1.745
Mn	0.044	0.045	0.025	0.044	0.045	0.048
Mg	2.855	2.765	2.855	2.890	2.906	2.905
Ca	1.931	1.919	1.909	1.900	1.852	1.873
Na	0.305	0.347	0.341	0.302	0.338	0.345
K	0.107	0.116	0.121	0.122	0.127	0.118

APPENDIX C

Table C.1: AMPHIBOLE MICROPROBE ANALYSES

	XG7 1B Mg-hbl 5R	XG7 1B Mg-hbl 6M	XG7 1B Mg-hbl 7M	XG7 1B Mg-hbl 8R	XG7 1B Mg-hbl 9M	XG24 1B Eden 1
SiO2	48.16	48.26	47.42	48.27	47.98	44.92
TiO2	1.27	1.37	1.03	1.02	2.98	1.09
Al2O3	6.03	6.12	6.76	6.22	5.57	8.45
FeO*	13.62	13.39	14.43	13.87	13.28	15.67
MgO	13.46	13.54	12.76	13.23	13.54	12.03
MnO	0.37	0.37	0.37	0.37	0.29	0.36
CaO	11.54	11.56	11.78	11.67	11.62	11.71
Na2O	1.25	1.32	1.23	1.28	0.79	1.57
K2O	0.60	0.60	0.69	0.63	0.67	0.91
Total	96.30	96.53	96.47	96.56	96.72	96.71
Si	7.164	7.154	7.082	7.169	7.097	6.775
Al(iv)	0.836	0.846	0.918	0.831	0.903	1.225
Al(vi)	0.222	0.224	0.273	0.259	0.069	0.285
Ti	0.143	0.153	0.117	0.115	0.333	0.125
Fe2+	1.695	1.661	1.803	1.723	1.643	1.975
Mn	0.047	0.047	0.048	0.047	0.037	0.045
Mg	2.984	2.991	2.840	2.929	2.986	2.708
Ca	1.839	1.837	1.885	1.858	1.843	1.902
Na	0.362	0.381	0.358	0.370	0.229	0.453
K	0.116	0.114	0.133	0.120	0.127	0.181

	XG24 1B Eden 2	XG24 1B Eden 3	XG24 1B Eden 4	XG24 1B Eden 5	XG24 1B Eden 6	XG24 1B Eden 7
SiO2	44.86	45.09	45.36	45.19	45.40	44.55
TiO2	1.10	1.05	0.90	1.01	1.04	1.01
Al2O3	8.38	8.46	8.09	8.42	8.27	8.42
FeO*	15.42	15.55	15.27	15.50	15.46	15.62
MgO	12.14	12.01	12.46	12.17	12.23	12.00
MnO	0.37	0.37	0.37	0.37	0.37	0.38
CaO	11.80	11.80	11.78	11.79	11.88	11.79
Na2O	1.54	1.54	1.44	0.13	1.36	1.50
K2O	0.89	0.94	0.82	0.88	0.84	0.91
Total	96.50	96.81	96.49	95.46	96.85	96.18
Si	6.785	6.800	6.835	6.798	6.825	6.756
Al(iv)	1.215	1.200	1.165	1.202	1.175	1.241
Al(vi)	0.275	0.309	0.285	0.298	0.325	0.270
Ti	0.125	0.119	0.099	0.117	0.115	0.121
Fe2+	1.953	1.955	1.927	1.952	1.935	1.978
Mn	0.045	0.051	0.045	0.045	0.045	0.045
Mg	2.727	2.701	2.796	2.730	2.743	2.719
Ca	1.909	1.899	1.900	1.898	1.909	1.918
Na	0.445	0.455	0.416	0.397	0.401	0.435
K	0.159	0.179	0.162	0.162	0.158	0.178

APPENDIX C

Table C.1: AMPHIBOLE MICROPROBE ANALYSES

	XG24 1B Eden 8	XG24 1B Eden 9	XG24 1B Eden 10	XG24 1B Eden 11	XG24 1B Eden 12	XG24 1B Eden 13
SiO2	45.79	45.10	45.53	45.16	44.89	45.28
TiO2	0.76	1.04	0.80	1.05	1.11	1.07
Al2O3	8.33	8.54	8.02	8.48	8.36	8.45
FeO*	15.50	15.70	15.27	15.76	15.42	15.57
MgO	12.12	11.82	12.52	11.96	12.44	12.05
MnO	0.36	0.38	0.37	0.36	0.36	0.37
CaO	12.07	11.77	11.88	11.85	11.77	11.97
Na2O	1.19	1.49	1.41	1.45	1.53	1.46
K2O	0.80	0.93	0.82	0.89	0.87	0.91
Total	96.92	96.77	96.62	96.96	96.75	97.13
Si	6.858	6.799	6.845	6.798	6.765	6.795
Al(iv)	1.142	1.202	1.155	1.204	1.243	1.205
Al(vi)	0.334	0.321	0.275	0.303	0.255	0.295
Ti	0.090	0.120	0.089	0.121	0.125	0.115
Fe2+	1.944	1.978	1.918	1.991	1.945	1.955
Mn	0.045	0.048	0.048	0.047	0.046	0.045
Mg	2.709	2.655	2.809	2.678	2.798	2.699
Ca	1.935	1.899	1.909	1.909	1.909	1.918
Na	0.342	0.435	0.421	0.422	0.455	0.435
K	0.162	0.179	0.161	0.158	0.158	0.181

	XG24 1B Eden 14	XG24 1B Eden 15	XG64A 1B Mg-hbl 1	XG64A 1B Mg-hbl 2	XG64A 1B Eden 3	XG64A 1B Eden 5
SiO2	45.14	44.79	47.14	47.56	46.67	46.19
TiO2	1.07	1.02	0.76	0.88	1.04	1.13
Al2O3	8.42	8.33	6.70	6.43	6.85	7.32
FeO*	15.77	15.50	15.17	14.89	15.33	15.60
MgO	11.96	12.28	12.86	12.87	12.46	12.21
MnO	0.37	0.38	0.39	0.37	0.41	0.39
CaO	11.86	11.84	12.06	11.79	11.91	11.73
Na2O	1.51	1.49	1.06	1.30	1.29	1.38
K2O	0.91	0.90	0.60	0.63	0.66	0.71
Total	97.01	96.53	96.74	96.72	96.62	96.66
Si	6.789	6.767	7.049	7.105	7.009	6.945
Al(iv)	1.211	1.231	0.951	0.895	0.991	1.055
Al(vi)	0.292	0.273	0.234	0.235	0.224	0.245
Ti	0.118	0.118	0.089	0.098	0.115	0.125
Fe2+	1.978	1.958	1.894	1.858	1.918	1.959
Mn	0.053	0.045	0.053	0.044	0.043	0.054
Mg	2.687	2.747	2.864	2.864	2.791	2.736
Ca	1.921	1.918	1.931	1.885	1.909	1.887
Na	0.435	0.442	0.305	0.377	0.378	0.397
K	0.182	0.178	0.107	0.125	0.117	0.144

APPENDIX C

Table C.1: AMPHIBOLE MICROPROBE ANALYSES

	XG64A 1B Mg-hbl 6	XG64A 1B Mg-hbl 7	XG64A 1B E-hbl 8	XG64A 1B Eden 10	XG64A 1B Mg-hbl 11	X181 2 Eden 1
SiO2	47.52	46.71	44.19	46.23	47.27	46.44
TiO2	0.98	1.03	1.19	0.96	0.96	1.19
Al2O3	6.18	6.75	8.74	6.62	6.51	7.33
FeO*	14.78	15.20	16.79	15.35	14.93	15.05
MgO	13.02	12.49	11.22	12.48	12.72	12.48
MnO	0.39	0.38	0.38	0.37	0.41	0.37
CaO	11.80	11.81	11.89	11.59	11.66	11.82
Na2O	1.27	1.26	1.43	1.33	1.32	1.41
K2O	0.59	0.66	0.92	0.63	0.65	0.63
Total	96.53	96.29	96.75	95.56	96.43	96.72
Si	7.115	7.025	6.709	7.015	7.085	6.949
Al(iv)	0.895	0.975	1.292	0.985	0.915	1.051
Al(vi)	0.195	0.215	0.283	0.205	0.235	0.242
Ti	0.111	0.121	0.135	0.109	0.114	0.135
Fe2+	1.847	1.917	2.131	1.951	1.867	1.878
Mn	0.047	0.035	0.047	0.045	0.047	0.044
Mg	2.898	2.798	2.544	2.827	2.843	2.786
Ca	1.899	1.909	1.932	1.887	1.873	1.896
Na	0.378	0.362	0.421	0.383	0.376	0.413
K	0.101	0.122	0.179	0.127	0.121	0.125

	X181 2 Eden 2	X181 2 Mg-hbl 3	X181 2 Mg-hbl 4	X181 2 Mg-hbl 5	X181 2 Eden 6	X181 2 A-hbl 7
SiO2	44.83	47.25	47.41	47.93	45.34	50.69
TiO2	1.47	0.89	0.80	0.80	0.99	0.35
Al2O3	8.16	6.60	6.53	6.16	8.31	4.56
FeO*	15.84	14.74	14.68	14.37	15.96	12.96
MgO	11.66	12.95	12.89	13.24	11.75	14.78
MnO	0.35	0.32	0.32	0.37	0.34	0.33
CaO	11.65	11.94	12.01	11.89	11.86	12.28
Na2O	1.53	1.12	1.13	1.16	1.40	0.72
K2O	0.81	0.61	0.62	0.58	0.81	0.35
Total	96.30	96.42	96.39	96.50	96.76	97.02
Si	6.795	7.067	7.095	7.125	6.835	7.412
Al(iv)	1.205	0.931	0.905	0.875	1.165	0.587
Al(vi)	0.255	0.269	0.245	0.215	0.325	0.205
Ti	0.165	0.101	0.089	0.099	0.111	0.035
Fe2+	2.011	1.842	1.834	1.809	2.099	1.581
Mn	0.049	0.037	0.044	0.046	0.049	0.043
Mg	2.626	2.889	2.877	2.957	2.632	3.222
Ca	1.889	1.918	1.924	1.908	1.917	1.932
Na	0.456	0.321	0.323	0.342	0.424	0.211
K	0.161	0.109	0.125	0.101	0.165	0.070

APPENDIX C

Table C.1: AMPHIBOLE MICROPROBE ANALYSES

	X181 2 Eden 8	X181 2 Mg-hbl 9	X181 2 A-hbl 10	X181 2 Eden 11	X181 2 Mg-hbl 12	X181 2 A-hbl 13
SiO2	45.05	47.47	48.85	47.13	48.40	49.21
TiO2	0.89	0.75	0.49	1.05	0.67	0.36
Al2O3	8.70	6.67	5.49	6.74	5.87	5.44
FeO*	16.34	14.85	13.90	14.81	14.08	14.21
MgO	11.40	12.94	13.89	12.91	13.51	13.70
MnO	0.37	0.39	0.33	0.37	0.33	0.32
CaO	11.75	11.88	12.09	11.83	11.97	12.14
Na2O	1.34	1.20	0.87	1.36	1.12	0.84
K2O	0.87	0.64	0.47	0.71	0.56	0.43
Total	96.71	96.79	96.38	96.91	96.51	96.65
Si	6.809	7.085	7.255	7.025	7.211	7.285
Al(iv)	1.191	0.915	0.745	0.971	0.789	0.715
Al(vi)	0.360	0.252	0.222	0.216	0.255	0.225
Ti	0.099	0.079	0.055	0.115	0.072	0.045
Fe2+	2.055	1.855	1.720	1.845	1.756	1.765
Mn	0.055	0.052	0.040	0.044	0.044	0.043
Mg	2.567	2.878	3.080	2.877	3.001	3.022
Ca	1.909	1.899	1.931	1.889	1.909	1.932
Na	0.399	0.342	0.255	0.401	0.321	0.235
K	0.161	0.121	0.082	0.137	0.102	0.078

	X181 2 Mg-hbl 14	X181 2 A-hbl 15	X181 2 A-hbl 16	XG25 2 Eden 1R	XG25 2 Eden 2C	XG25 2 Eden 3R
SiO2	48.36	49.87	49.15	46.61	47.05	46.71
TiO2	0.77	0.45	0.67	0.89	0.98	0.98
Al2O3	5.84	4.68	5.63	7.39	7.31	7.53
FeO*	14.05	13.18	14.03	15.42	15.21	15.34
MgO	13.82	14.53	13.75	12.17	12.25	12.19
MnO	0.40	0.34	0.31	0.38	0.40	0.39
CaO	11.90	12.11	12.16	11.54	11.51	11.51
Na2O	1.16	0.92	0.94	1.37	1.39	1.41
K2O	0.55	0.37	0.48	0.77	0.77	0.77
Total	96.85	96.45	97.12	96.54	96.87	96.83
Si	7.175	7.356	7.255	6.999	7.026	6.987
Al(iv)	0.825	0.641	0.745	1.001	0.974	1.013
Al(vi)	0.185	0.173	0.225	0.308	0.314	0.316
Ti	0.078	0.055	0.073	0.102	0.111	0.110
Fe2+	1.755	1.621	1.731	1.937	1.900	1.919
Mn	0.035	0.042	0.038	0.049	0.052	0.051
Mg	3.063	3.190	3.022	2.724	2.727	2.720
Ca	1.889	1.919	1.926	1.857	1.843	1.845
Na	0.343	0.282	0.256	0.400	0.403	0.410
K	0.101	0.078	0.078	0.148	0.147	0.148

APPENDIX C

Table C.1: AMPHIBOLE MICROPROBE ANALYSES

	XG25 2 Eden 4R	XG25 2 Eden 5M	XG25 2 Eden 6M	XG25 2 Mg-hbl 7M	XG25 2 Eden 8C	XG44 2 Eden 1
SiO2	46.19	46.69	47.16	48.16	47.02	46.96
TiO2	0.91	0.98	0.85	0.68	1.02	1.02
Al2O3	7.63	7.46	7.27	6.48	7.27	7.02
FeO*	15.41	15.24	14.94	14.23	15.19	14.53
MgO	12.11	12.17	12.51	13.08	12.52	13.21
MnO	0.39	0.36	0.37	0.39	0.37	0.34
CaO	11.59	11.68	11.52	11.59	11.47	11.68
Na2O	1.34	1.32	1.32	1.18	1.42	1.43
K2O	0.82	0.80	0.74	0.61	0.75	0.73
Total	96.39	96.70	96.68	96.40	97.03	96.92
Si	6.955	6.993	7.043	7.170	7.011	6.995
Al(iv)	1.045	1.007	0.957	0.830	0.989	1.005
Al(vi)	0.310	0.312	0.323	0.308	0.291	0.225
Ti	0.104	0.111	0.097	0.077	0.115	0.115
Fe2+	1.941	1.910	1.867	1.773	1.895	1.809
Mn	0.050	0.046	0.048	0.050	0.047	0.035
Mg	2.719	2.718	2.784	2.903	2.782	2.933
Ca	1.870	1.875	1.844	1.849	1.833	1.855
Na	0.392	0.385	0.384	0.341	0.411	0.421
K	0.158	0.154	0.141	0.117	0.143	0.141

	XG44 2 Mg-hbl 2	XG44 2 Mg-hbl 3	XG44 2 Eden 4	XG44 2 Eden 5	XG44 2 Mg-hbl 6	XG44 2 Mg-hbl 7
SiO2	47.55	47.48	46.07	47.53	47.40	47.03
TiO2	0.85	0.87	1.05	0.88	0.91	0.94
Al2O3	6.84	6.67	7.21	6.70	6.71	6.91
FeO*	14.16	14.03	14.52	14.15	14.11	14.23
MgO	13.45	13.46	12.82	13.50	13.55	13.26
MnO	0.29	0.33	0.32	0.32	0.34	0.31
CaO	12.00	12.02	11.71	11.87	11.88	12.37
Na2O	1.25	1.18	1.47	1.32	1.27	1.28
K2O	0.65	0.66	0.78	0.65	0.69	0.69
Total	97.04	96.70	95.95	96.92	96.86	97.02
Si	7.047	7.065	6.955	7.055	7.055	6.995
Al(iv)	0.953	0.935	1.045	0.954	0.945	1.005
Al(vi)	0.240	0.235	0.245	0.221	0.235	0.205
Ti	0.098	0.098	0.121	0.099	0.099	0.105
Fe2+	1.755	1.744	1.832	1.778	1.755	1.774
Mn	0.035	0.044	0.042	0.043	0.044	0.044
Mg	2.975	2.987	2.878	2.988	3.009	2.943
Ca	1.906	1.914	1.899	1.890	1.899	1.967
Na	0.356	0.339	0.441	0.377	0.365	0.388
K	0.124	0.125	0.142	0.119	0.122	0.121

APPENDIX C

Table C.1: AMPHIBOLE MICROPROBE ANALYSES

	XG44 2 Eden 8	XG44 2 Mg-hbl 9	XG44 2 A-hbl 10	XG44 2 Eden 11	XG44 2 Eden 12	XG44 2 Eden 13
SiO2	47.68	47.51	49.57	47.02	46.74	47.39
TiO2	1.06	0.91	0.70	1.08	0.98	0.93
Al2O3	6.62	6.81	5.09	6.95	7.03	6.78
FeO*	14.06	14.55	12.92	14.44	14.51	14.40
MgO	13.52	13.27	14.57	13.25	13.09	13.29
MnO	0.34	0.34	0.35	0.35	0.33	0.37
CaO	11.87	12.00	11.92	11.84	11.75	11.81
Na2O	1.32	1.27	1.13	1.39	1.42	1.46
K2O	0.69	0.70	0.48	0.71	0.73	0.67
Total	97.16	97.36	96.73	97.03	96.58	97.10
Si	7.065	7.045	7.297	7.015	6.985	7.045
Al(iv)	0.935	0.963	0.700	0.985	1.015	0.955
Al(vi)	0.215	0.231	0.199	0.235	0.225	0.223
Ti	0.115	0.099	0.079	0.125	0.107	0.105
Fe2+	1.745	1.809	1.598	1.802	1.813	1.786
Mn	0.045	0.044	0.043	0.045	0.044	0.044
Mg	2.989	2.932	3.188	2.899	2.918	2.946
Ca	1.889	1.898	1.887	1.889	1.885	1.884
Na	0.377	0.388	0.318	0.388	0.413	0.428
K	0.125	0.121	0.088	0.142	0.143	0.125

	XG44 2 Eden 14	XG44 2 Mg-hbl 15	XG61B 2 Mg-hbl 1R	XG61B 2 Mg-hbl 2R	XG61B 2 Mg-hbl 3C	XG61B 2 A-hbl 5M
SiO2	46.87	47.43	48.62	48.72	48.04	50.15
TiO2	1.31	0.89	0.70	0.69	0.86	0.46
Al2O3	7.17	6.69	5.69	5.96	5.88	4.82
FeO*	14.67	14.03	13.79	14.18	14.07	13.17
MgO	12.97	13.48	13.70	13.37	13.31	14.29
MnO	0.34	0.33	0.33	0.31	0.32	0.33
CaO	11.64	11.95	11.84	11.81	11.85	11.87
Na2O	1.53	1.22	0.96	1.05	0.98	0.81
K2O	0.74	0.64	0.51	0.52	0.52	0.40
Total	97.24	96.66	96.14	96.61	95.83	96.30
Si	6.975	7.055	7.236	7.224	7.192	7.399
Al(iv)	1.025	0.945	0.764	0.776	0.808	0.601
Al(vi)	0.225	0.235	0.235	0.268	0.230	0.239
Ti	0.145	0.099	0.079	0.078	0.098	0.052
Fe2+	1.821	1.744	1.717	1.759	1.762	1.626
Mn	0.048	0.037	0.042	0.040	0.041	0.042
Mg	2.877	2.999	3.039	2.956	2.971	3.143
Ca	1.856	1.887	1.888	1.877	1.901	1.878
Na	0.441	0.356	0.279	0.304	0.286	0.232
K	0.144	0.119	0.098	0.099	0.101	0.077

APPENDIX C

Table C.1: AMPHIBOLE MICROPROBE ANALYSES

	XG61B 2 A-hbl 6C	XG61B 2 Mg-hbl 7M	XG61B 2 Mg-hbl 8C	XG61C 2 Mg-hbl 1	XG61C 2 Mg-hbl 2	XG61C 2 Mg-hbl 3
SiO2	49.68	47.60	48.43	48.08	47.59	48.96
TiO2	0.40	1.04	0.88	0.96	0.83	0.62
Al2O3	4.93	6.68	6.11	6.34	6.04	5.60
FeO*	13.22	14.31	13.90	13.63	13.51	13.18
MgO	14.22	12.83	13.44	13.75	13.57	14.26
MnO	0.33	0.31	0.31	0.31	0.33	0.29
CaO	11.89	11.87	11.87	11.98	12.69	12.15
Na2O	0.91	1.10	1.07	1.18	1.12	1.01
K2O	0.39	0.61	0.59	0.54	0.53	0.47
Total	95.97	96.35	96.60	96.77	96.21	96.54
Si	7.367	7.104	7.185	7.121	7.107	7.235
Al(iv)	0.633	0.896	0.815	0.886	0.893	0.765
Al(vi)	0.230	0.281	0.254	0.234	0.165	0.205
Ti	0.045	0.117	0.099	0.109	0.098	0.077
Fe2+	1.640	1.786	1.726	1.698	1.687	1.633
Mn	0.042	0.040	0.040	0.044	0.044	0.043
Mg	3.144	2.854	2.972	3.029	3.024	3.135
Ca	1.891	1.898	1.887	1.901	2.028	1.922
Na	0.263	0.320	0.307	0.343	0.323	0.289
K	0.074	0.118	0.113	0.102	0.107	0.088

	XG61C 2 A-hbl 4	XG61C 2 A-hbl 5	XG61C 2 A-hbl 6	XG61C 2 Acti 7	XG61C 2 Mg-hbl 8	XG61C 2 Mg-hbl 9
SiO2	49.45	49.71	49.78	52.15	48.27	49.05
TiO2	0.71	0.54	0.54	0.07	0.84	0.68
Al2O3	5.39	5.24	5.00	2.91	6.28	5.63
FeO*	12.87	13.04	13.17	12.32	13.89	13.10
MgO	14.69	14.63	14.65	15.68	13.63	14.27
MnO	0.30	0.31	0.32	0.27	0.30	0.33
CaO	12.12	12.10	12.17	12.70	12.07	12.16
Na2O	0.95	0.85	0.93	0.32	1.13	0.94
K2O	0.43	0.42	0.41	0.11	0.56	0.47
Total	96.91	96.84	96.97	96.53	96.97	96.63
Si	7.265	7.305	7.315	7.611	7.135	7.195
Al(iv)	0.735	0.695	0.685	0.389	0.865	0.805
Al(vi)	0.195	0.205	0.185	0.119	0.235	0.255
Ti	0.080	0.061	0.061	0.008	0.099	0.079
Fe2+	1.579	1.598	1.615	1.508	1.721	1.605
Mn	0.035	0.035	0.044	0.035	0.037	0.044
Mg	3.212	3.206	3.203	3.411	3.003	3.121
Ca	1.906	1.907	1.915	1.991	1.909	1.913
Na	0.264	0.247	0.264	0.087	0.321	0.264
K	0.088	0.088	0.071	0.017	0.099	0.088

APPENDIX C

Table C.1: AMPHIBOLE MICROPROBE ANALYSES

	XG61C 2 Mg-hbl 10	XG61C 2 A-hbl 11	XG61C 2 A-hbl 12	XG61C 2 Mg-hbl 13	XG61C 2 A-hbl 14	XG61C 2 A-hbl 15
SiO2	47.20	50.02	49.64	48.90	48.92	50.92
TiO2	1.03	0.64	0.55	0.78	0.67	0.40
Al2O3	6.93	4.93	5.23	5.61	5.34	4.26
FeO*	14.53	12.38	13.28	13.33	13.00	13.02
MgO	13.02	14.89	14.57	14.06	14.50	14.88
MnO	0.31	0.29	0.29	0.29	0.31	0.26
CaO	11.84	12.14	12.10	11.95	12.09	12.18
Na2O	1.26	0.86	0.95	1.11	0.98	0.60
K2O	0.62	0.35	0.41	0.48	0.45	0.44
Total	96.74	96.50	97.02	96.51	96.26	96.96
Si	7.044	7.355	7.295	7.235	7.255	7.126
Al(iv)	0.962	0.653	0.705	0.765	0.745	0.703
Al(vi)	0.262	0.202	0.195	0.215	0.165	-
Ti	0.115	0.067	0.055	0.086	0.077	0.042
Fe2+	1.809	1.522	1.632	1.655	1.609	1.524
Mn	0.036	0.038	0.044	0.036	0.037	0.031
Mg	2.898	3.263	3.191	3.101	3.212	3.104
Ca	1.889	1.909	1.909	1.887	1.928	1.826
Na	0.366	0.244	0.255	0.323	0.287	0.164
K	0.121	0.079	0.078	0.077	0.079	0.079

	XG89 2 Mg-hbl 1M	XG89 2 Mg-hbl 2M	XG89 2 Mg-hbl 3C	XG89 2 Eden 4R	XG39 2 Mg-hbl 5R	XG89 2 Eden 6M
SiO2	48.13	47.66	48.73	47.47	46.80	47.19
TiO2	1.13	0.84	1.00	1.22	1.04	1.31
Al2O3	6.00	6.71	5.63	6.74	6.53	6.41
FeO*	13.51	14.35	12.92	14.27	13.96	13.88
MgO	13.92	13.45	14.75	13.36	13.49	13.37
MnO	0.38	0.38	0.36	0.37	0.37	0.39
CaO	11.82	11.79	11.38	11.74	11.81	11.65
Na2O	1.20	1.16	1.15	1.30	1.06	1.30
K2O	0.60	0.66	0.54	0.71	0.66	0.69
Total	96.69	97.00	96.46	97.18	95.72	96.19
Si	7.134	7.072	7.199	7.037	7.039	7.060
Al(iv)	0.866	0.928	0.801	0.963	0.961	0.940
Al(vi)	0.184	0.247	0.181	0.216	0.198	0.192
Ti	0.127	0.094	0.113	0.137	0.119	0.148
Fe2+	1.676	1.782	1.597	1.770	1.756	1.737
Mn	0.049	0.048	0.046	0.048	0.048	0.050
Mg	3.076	2.974	3.248	2.951	3.025	2.982
Ca	1.877	1.875	1.802	1.865	1.904	1.868
Na	0.346	0.334	0.332	0.376	0.311	0.378
K	0.115	0.127	0.102	0.136	0.127	0.133

APPENDIX C

Table C.1: AMPHIBOLE MICROPROBE ANALYSES

	XG89 2 Mg-hbl 7M	XG89 2 Eden 8C	XG89 2 Eden 9C	XG4 5 Mg-hbl 1M	XG4 5 Eden 2R	XG4 5 Eden 3M
SiO2	47.82	47.26	45.95	48.65	47.45	47.11
TiO2	1.14	1.31	1.57	0.73	0.86	1.05
Al2O3	6.42	6.83	7.73	5.89	6.37	6.41
FeO*	13.86	14.38	14.75	14.08	14.41	14.16
MgO	13.48	13.10	12.90	13.87	13.62	13.66
MnO	0.38	0.40	0.38	0.37	0.37	0.39
CaO	11.89	11.63	10.11	11.71	11.61	11.63
Na2O	1.11	1.33	0.95	1.27	1.46	1.37
K2O	0.66	0.74	2.12	0.58	0.68	0.70
Total	96.76	96.98	96.46	97.15	96.83	96.48
Si	7.098	7.026	6.911	7.185	7.067	7.039
Al(iv)	0.902	0.974	1.089	0.815	0.933	0.961
Al(vi)	0.222	0.225	0.282	0.213	0.186	0.170
Ti	0.128	0.147	0.178	0.081	0.097	0.118
Fe2+	1.722	1.789	1.855	1.740	1.795	1.770
Mn	0.049	0.052	0.049	0.047	0.047	0.051
Mg	2.981	2.903	2.893	3.053	3.025	3.043
Ca	1.891	1.853	1.630	1.854	1.853	1.863
Na	0.321	0.386	0.278	0.364	0.424	0.399
K	0.125	0.142	0.408	0.110	0.130	0.134

	XG4 5 A-hbl 4M	XG4 5 Mg-hbl 5R	XG4 5 Mg-hbl 6R	XG4 5 Eden 7C	XG4 5 Mg-hbl 8C	XG4 5 Eden 9C
SiO2	49.38	48.76	48.19	47.45	48.44	47.81
TiO2	0.70	0.91	0.71	1.27	0.84	1.07
Al2O3	5.18	5.45	6.12	6.43	5.59	5.94
FeO*	13.40	13.33	14.41	13.89	13.68	14.01
MgO	14.42	14.18	13.54	13.53	14.19	13.67
MnO	0.39	0.38	0.38	0.40	0.36	0.38
CaO	11.77	11.66	11.81	11.59	11.77	11.70
Na2O	1.23	1.28	1.31	1.48	1.19	1.35
K2O	0.49	0.59	0.63	0.72	0.55	0.65
Total	96.96	96.54	97.10	96.76	96.61	96.58
Si	7.274	7.223	7.142	7.057	7.185	7.121
Al(iv)	0.726	0.777	0.858	0.943	0.815	0.879
Al(vi)	0.175	0.176	0.213	0.186	0.164	0.165
Ti	0.078	0.103	0.081	0.143	0.094	0.120
Fe2+	1.652	1.652	1.787	1.728	1.698	1.746
Mn	0.049	0.048	0.049	0.052	0.047	0.049
Mg	3.166	3.132	2.992	3.000	3.137	3.036
Ca	1.859	1.852	1.877	1.848	1.871	1.868
Na	0.353	0.369	0.378	0.428	0.343	0.390
K	0.094	0.112	0.120	0.138	0.106	0.124

APPENDIX C

Table C.2: PLAGIOCLASE MICROPROBE ANALYSES

	SGIII TGD Ande. 1	SGIII TGD Ande. 2	SGIII TGD Ande. 3	SGIII TGD Ande. 4	SGIII TGD Ande. 5	SGIII TGD Ande. 6
SiO2	61.66	60.77	61.95	61.79	61.71	61.21
Al2O3	23.54	24.02	23.44	23.30	23.44	23.61
Fe2O3	0.11	0.15	0.13	0.14	0.17	0.16
MgO	-	-	-	-	-	-
CaO	4.75	5.33	4.66	4.67	4.75	4.96
BaO	-	0.09	-	0.04	0.03	0.02
Na2O	8.93	8.53	8.92	8.84	8.74	8.73
K2O	0.28	0.35	0.28	0.41	0.43	0.42
Total	99.27	99.24	99.38	99.19	99.27	99.11
Ab	64.0	60.1	64.4	63.5	62.8	61.9
Or	2.0	2.5	2.0	3.0	3.1	2.9
An	34.0	37.5	33.6	33.5	34.1	35.2

	SGIII TGD Ande. 7	SGIII TGD Ande. 8	SGIII TGD Ande. 9	SGIII TGD Ande. 10	SGIII TGD Ande. 11	SGVII Late Olig. 2R
SiO2	61.49	61.86	61.76	62.06	61.99	64.39
Al2O3	23.47	23.15	23.43	23.31	23.16	21.93
Fe2O3	0.12	0.12	0.12	0.17	0.15	0.15
MgO	-	-	-	-	-	-
CaO	4.64	4.64	4.84	4.56	4.37	2.72
BaO	0.03	-	0.07	0.04	0.03	0.06
Na2O	9.09	8.98	8.78	8.91	9.01	9.59
K2O	0.21	0.23	0.36	0.43	0.33	0.25
Total	99.05	98.98	99.36	99.48	99.04	99.09
Ab	65.2	64.8	62.7	64.1	65.7	76.4
Or	1.5	1.7	2.6	3.1	2.4	2.0
An	33.3	33.5	34.7	32.8	31.9	21.6

APPENDIX C

Table C.2: PLAGIOCLASE MICROPROBE ANALYSES

	SGVII Late Olig. 3M	SGVII Late Ande. 4M	SGVII Late Ande. 5C	SGVII Late Ande. 6C	SGVII Late Ande. 7	SGVII Late Ande. 8
SiO2	62.82	62.82	61.90	62.63	62.34	62.78
Al2O3	22.92	23.12	23.63	23.21	22.95	22.82
Fe2O3	0.12	0.09	0.09	0.09	0.17	0.16
MgO	-	-	-	-	-	-
CaO	3.93	4.11	4.75	4.38	4.08	3.97
BaO	0.07	0.03	0.02	-	0.03	0.03
Na2O	9.47	9.33	9.05	9.02	9.11	9.16
K2O	0.25	0.22	0.19	0.27	0.44	0.36
Total	99.58	99.72	99.63	99.60	99.12	99.28
Ab	69.4	68.3	64.7	66.0	66.8	67.9
Or	1.8	1.6	1.3	2.0	3.2	2.7
An	28.8	30.1	34.0	32.0	30.0	29.4

	SGVII Late Olig. 9R	SGVII Late Ande. 10R	SGVII Late Ande. 11R	SGVII Late Ande. 12C	SGVII Late Olig. 13R	SGVII Late Ande. 14M
SiO2	62.66	62.63	61.87	62.41	63.09	61.55
Al2O3	22.97	23.00	23.35	23.16	22.85	23.79
Fe2O3	0.09	0.07	0.14	0.13	0.14	0.11
MgO	-	-	-	-	-	-
CaO	4.07	4.18	4.51	4.28	4.00	5.04
BaO	0.01	0.01	-	-	0.04	-
Na2O	9.46	9.40	9.16	9.37	9.51	8.87
K2O	0.13	0.17	0.32	0.23	0.31	0.18
Total	99.39	99.46	99.35	99.58	99.94	99.54
Ab	69.3	68.4	65.5	67.5	68.8	63.0
Or	0.9	1.2	2.3	1.6	2.2	1.3
An	29.8	30.4	32.2	30.9	29.0	35.7

APPENDIX C

Table C.2: PLAGIOCLASE MICROPROBE ANALYSES

	SGVII Late Ande. 15C	SGVII Late Ande. 16	SGVIII Late Olig. 1R	SGVIII Late Olig. 2M	SGVIII Late Olig. 3M	SGVIII Late Olig. 4C
SiO2	61.23	61.15	63.78	62.72	62.89	62.96
Al2O3	24.06	23.97	22.38	22.92	22.71	22.64
Fe2O3	0.12	0.08	0.11	0.12	0.16	0.09
MgO	-	-	-	-	-	-
CaO	5.35	5.22	3.32	3.88	3.74	3.86
BaO	0.08	0.03	0.01	-	0.01	-
Na2O	8.81	8.76	9.81	9.38	9.63	9.58
K2O	0.15	0.16	0.24	0.29	0.35	0.19
Total	99.80	99.37	99.65	99.31	99.49	99.32
Ab	61.5	61.9	73.3	69.2	70.2	70.3
Or	1.1	1.2	1.8	2.2	2.6	1.4
An	37.4	36.9	24.9	28.6	27.2	28.3

	SGVIII Late Olig. 5R	SGVIII Late Olig. 7R	SGVIII Late Ande. 8R	SGVIII Late Ande 9C	SGVIII Late Ande. 10C	SGVIII Late Ande. 11R
SiO2	62.61	62.91	62.51	62.75	62.22	62.49
Al2O3	22.88	23.04	22.97	22.84	23.21	23.48
Fe2O3	0.07	0.05	0.10	0.14	0.17	0.05
MgO	-	-	-	-	-	-
CaO	3.99	4.06	4.23	4.16	4.41	4.57
BaO	0.03	-	0.03	0.01	0.03	0.01
Na2O	9.59	9.62	9.41	9.21	9.03	9.15
K2O	0.21	0.08	0.19	0.44	0.47	0.13
Total	99.38	99.76	99.44	99.55	99.54	99.88
Ab	69.5	69.9	68.0	66.7	64.9	66.1
Or	1.5	0.6	1.4	3.2	3.4	0.9
An	29.0	29.5	30.6	30.1	31.7	33.0

APPENDIX C

Table C.2: PLAGIOCLASE MICROPROBE ANALYSES

	SGVIII Late Olig. 12R	SGVIII Late Ande. 13C	SGVIII Late Olig. 14R	SGVIII Late Ande. 15C	SGVIII Late Ande. 16R	SGVIII Late Ande. 17M
SiO2	62.72	61.92	63.24	62.72	61.11	62.28
Al2O3	22.92	23.36	22.35	23.02	24.08	23.10
Fe2O3	0.12	0.14	0.11	0.18	0.10	0.21
MgO	-	-	-	-	-	-
CaO	3.99	4.62	3.53	4.12	5.28	4.45
BaO	-	0.01	-	0.08	0.11	0.08
Na2O	9.39	8.74	9.60	9.27	8.63	9.05
K2O	0.24	0.29	0.22	0.36	0.27	0.39
Total	99.38	99.08	99.05	99.75	99.58	99.56
Ab	69.0	64.0	71.9	67.4	60.8	65.1
Or	1.7	2.2	1.7	2.5	1.9	2.8
An	29.3	33.8	26.4	30.1	37.3	32.1

	SGVIII Late Ande. 18C	SGIX TGD Ande. 1R	SGIX TGD Olig. 2R	SGIX TGD Ande. 3C	SGIX TGD Olig. 4R	SGIX TGD Ande. 5R
SiO2	62.11	61.64	62.33	62.87	64.47	59.95
Al2O3	23.36	22.78	22.07	22.64	21.92	22.09
Fe2O3	0.10	0.14	0.13	0.18	0.14	0.14
MgO	-	0.02	0.02	0.01	0.01	-
CaO	4.49	4.47	3.64	4.09	3.43	4.39
BaO	0.03	0.10	0.08	0.17	0.06	0.12
Na2O	9.04	9.01	9.73	9.11	9.51	8.36
K2O	0.33	0.32	0.20	0.51	0.37	0.49
Total	99.46	98.48	98.20	99.58	99.91	95.54
Ab	65.2	65.0	71.7	66.4	71.4	63.1
Or	2.4	2.3	1.5	3.8	2.7	3.7
An	32.4	32.4	26.8	29.8	25.8	33.1

APPENDIX C

Table C.2: PLAGIOCLASE MICROPROBE ANALYSES

	SGIX TGD Ande. 6	SGIX TGD Olig. 7R	SGIX TGD Ande. 8M	SGIX TGD Ande. 9C	SGX Late Olig. 13	SGX Late Ande. 14
SiO2	63.24	65.87	63.05	62.47	62.79	62.13
Al2O3	23.32	22.09	22.92	23.19	22.68	22.83
Fe2O3	0.17	0.17	0.15	0.11	0.11	0.12
MgO	0.02	0.01	0.01	0.01	-	-
CaO	4.49	3.45	4.46	4.82	3.75	4.15
BaO	0.17	0.06	0.07	0.08	0.06	-
Na2O	8.85	9.62	8.79	8.79	9.59	9.30
K2O	0.50	0.34	0.41	0.42	0.21	0.23
Total	100.76	101.61	99.86	99.89	99.19	98.76
Ab	63.9	71.7	64.3	62.7	70.8	68.0
Or	3.7	2.6	3.1	2.9	1.5	1.7
An	32.4	25.7	32.6	34.4	27.7	30.3

	SGX Late Ande. 15	SGX Late Ande. 16	SGX Late Ande. 17	SGX Late Ande. 18	SGX Late Ande. 19	SGXIII TGD Ande. 1R
SiO2	62.30	61.49	61.03	60.99	61.35	63.84
Al2O3	22.94	23.69	23.59	23.32	22.72	22.52
Fe2O3	0.17	0.15	0.12	0.14	0.17	0.11
MgO	-	-	-	-	-	0.01
CaO	4.22	4.86	4.99	4.57	4.53	4.19
BaO	0.05	0.05	0.11	0.01	0.13	-
Na2O	9.26	8.79	8.73	8.84	8.77	9.27
K2O	0.32	0.30	0.27	0.47	0.44	0.28
Total	99.26	99.33	98.84	98.34	98.11	100.22
Ab	67.1	63.0	62.4	63.7	63.8	67.4
Or	2.3	2.2	1.9	3.4	3.2	2.1
An	30.6	34.8	35.7	32.9	33.0	30.5

APPENDIX C

Table C.2: PLAGIOCLASE MICROPROBE ANALYSES

	SGXIII TGD Ande. 2M	SGXIII TGD Ande. 4R	SGXIII TGD Ande. 5M	SGXIII TGD Ande. 7C	SGXIII TGD Ande. 8R	SGXIII TGD Ande. 9C
SiO2	63.05	63.52	62.93	63.25	63.64	63.03
Al2O3	23.02	22.52	22.56	22.56	22.54	22.79
Fe2O3	0.11	0.15	0.08	0.19	0.19	0.11
MgO	0.01	0.01	0.01	0.01	0.01	0.01
CaO	4.75	4.04	4.14	4.22	4.00	4.33
BaO	-	-	-	-	-	-
Na2O	8.84	9.18	9.19	8.96	9.28	9.11
K2O	0.41	0.37	0.19	0.57	0.17	0.21
Total	100.19	99.79	99.10	99.76	99.83	99.59
Ab	63.2	67.6	68.0	65.2	69.0	66.7
Or	2.9	2.7	1.4	4.1	1.3	1.6
An	33.9	29.7	30.6	30.7	29.7	31.7

	SGXIII TGD Ande. 10R	SGXIII TGD Ande. 11M	SGXIII TGD Ande. 12C	SGXIII TGD Olig. 1	SGXIII TGD Ande. 2	SGXIII TGD Ande. 3
SiO2	63.22	61.66	62.07	62.44	61.96	61.98
Al2O3	22.37	23.51	23.09	23.02	23.02	23.21
Fe2O3	0.21	0.09	0.11	0.14	0.19	0.21
MgO	0.02	0.02	0.01	-	-	-
CaO	3.94	5.41	4.72	4.06	4.52	4.53
BaO	-	-	-	-	0.09	0.05
Na2O	9.32	8.36	8.76	9.53	8.99	8.82
K2O	0.41	0.36	0.35	0.27	0.49	0.56
Total	99.49	99.41	99.11	99.46	99.26	99.36
Ab	68.2	59.2	63.3	68.7	64.2	63.4
Or	3.0	2.6	2.6	1.9	3.5	4.0
An	28.8	28.2	34.1	29.4	32.3	32.6

APPENDIX C

Table C.2: PLAGIOCLASE MICROPROBE ANALYSES

	SGXIII TGD Ande. 4	SGXIII TGD Ande. 5	SGXIII TGD Ande. 6R	SGXIII TGD Ande. 7M	SGXIII TGD Ande. 8C	SGXIII TGD Olig. 9R
SiO2	61.86	62.08	62.78	61.98	61.13	62.83
Al2O3	23.33	23.37	23.13	23.39	23.76	22.57
Fe2O3	0.19	0.17	0.16	0.13	0.14	0.12
MgO	-	-	-	-	-	-
CaO	4.43	4.46	4.12	4.39	5.12	3.52
BaO	0.12	0.11	0.04	0.05	0.08	0.02
Na2O	8.96	9.12	9.29	9.15	8.63	8.93
K2O	0.55	0.37	0.33	0.32	0.43	1.04
Total	99.44	99.68	99.85	99.41	99.29	99.03
Ab	64.3	65.3	67.6	66.0	60.8	66.2
Or	3.9	2.7	2.4	2.3	3.1	7.7
An	31.8	32.0	30.0	31.7	36.1	26.1

	SGXIII TGD Ande. 10M	SGXIII TGD Ande. 11C	SGXIII TGD Olig. 12R	SGXIII TGD Ande. 13M	SGXIII TGD Ande. 14R	SGXIII TGD Ande. 15M
SiO2	61.87	61.59	63.06	62.48	62.07	61.94
Al2O3	23.53	23.66	22.76	23.04	23.39	23.37
Fe2O3	0.08	0.14	0.09	0.11	0.17	0.15
MgO	-	-	-	-	-	-
CaO	4.77	4.87	3.99	4.31	4.45	4.39
BaO	0.06	0.07	0.07	0.01	-	0.12
Na2O	9.18	8.95	9.51	9.24	8.85	8.67
K2O	0.24	0.27	0.24	0.17	0.28	0.45
Total	99.73	99.55	99.72	99.36	99.21	99.09
Ab	64.7	63.5	69.2	67.3	64.9	64.1
Or	1.7	1.9	1.7	1.2	2.1	3.4
An	33.6	34.6	29.1	31.4	33.0	32.5

APPENDIX C

Table C.2: PLAGIOCLASE MICROPROBE ANALYSES

	SGXIII TGD Ande. 16C	SGXIII TGD Ande. 17	SGXIII TGD Ande. 18	SGXXVI TGD Olig. 1R	SGXXVI TGD Ande. 3M	SGXXVI TGD Ande. 4M
SiO2	61.65	62.36	62.12	64.08	63.34	63.49
Al2O3	23.14	23.09	23.33	22.49	23.35	22.96
Fe2O3	0.16	0.14	0.15	0.05	0.13	0.07
MgO	-	-	-	0.02	0.02	0.01
CaO	4.58	4.09	4.25	3.51	4.55	4.45
BaO	0.02	0.02	0.11	-	-	-
Na2O	8.55	9.33	9.15	9.54	8.67	8.86
K2O	0.54	0.25	0.33	0.15	0.33	0.15
Total	98.64	99.28	99.44	99.84	100.39	99.99
Ab	62.6	68.2	66.5	72.3	64.0	
Or	3.9	1.8	2.4	1.1	2.4	
An	33.5	30.0	31.1	26.6	33.6	

	SGXXVI TGD Ande. 7M	G24 TGD Ande. 1R	G24 TGD Ande. 2M	G24 TGD Ande. 3R	G24 TGD Ande. 4M	G24 TGD Ande. 5C
SiO2	64.29	62.11	61.74	60.54	61.37	62.22
Al2O3	22.78	23.45	23.37	23.26	23.58	23.59
Fe2O3	0.13	0.14	0.09	0.15	0.09	0.09
MgO	0.01	0.02	0.02	0.02	0.02	0.02
CaO	3.93	4.79	4.76	6.13	4.83	4.75
BaO	-	-	-	-	-	-
Na2O	9.17	8.63	8.77	8.63	8.71	8.72
K2O	0.25	0.42	0.27	0.28	0.26	0.24
Total	100.56	99.56	99.02	99.01	98.86	99.63
Ab	68.7	62.3	63.5	57.3	63.0	63.6
Or	1.9	3.0	2.0	1.9	1.0	1.7
An	29.4	34.7	34.5	40.8	35.1	34.7

APPENDIX C

Table C.2: PLAGIOCLASE MICROPROBE ANALYSES

	G24 TGD Ande. 6C	G24 TGD Ande. 7M	G24 TGD Ande. 8M	G24 TGD Ande. 9R	G24 TGD Ande. 10M	SG49 PGD Ande. 1R
SiO2	61.18	61.19	62.09	61.94	62.22	62.69
Al2O3	23.51	24.05	23.37	23.54	23.45	23.05
Fe2O3	0.13	0.09	0.07	0.06	0.13	0.11
MgO	0.02	0.02	0.02	0.02	0.02	-
CaO	4.88	5.49	4.73	4.67	4.77	4.12
BaO	-	-	-	-	-	0.07
Na2O	8.73	8.21	8.71	8.87	8.63	9.45
K2O	0.32	0.21	0.27	0.14	0.45	0.23
Total	98.77	99.26	99.26	99.24	99.67	99.72
Ab	62.7	59.0	63.5	64.8	62.3	68.5
Or	2.3	1.5	2.0	1.0	3.3	1.6
An	35.0	39.5	34.5	34.2	34.4	29.9

	SG49 PGD Ande. 2M	SG49 PGD Ande. 3C	SG49 PGD Ande. 4	SG49 PGD Ande. 5R	SG49 PGd Ande. 6R	SG49 PGD Ande. 7
SiO2	62.37	62.72	62.09	62.93	62.74	62.89
Al2O3	23.06	22.86	23.29	22.68	22.88	22.78
Fe2O3	0.16	0.20	0.17	0.17	0.16	0.18
MgO	-	-	-	-	-	-
CaO	4.21	4.17	4.48	4.01	4.04	4.15
BaO	0.06	-	-	-	0.08	0.07
Na2O	9.15	9.15	9.02	9.31	9.32	9.28
K2O	0.43	0.44	0.37	0.44	0.45	0.47
Total	99.44	99.54	99.42	99.54	99.67	99.82
Ab	66.3	66.5	65.0	67.6	67.5	66.8
Or	3.1	3.2	2.7	3.2	3.3	3.4
An	30.6	30.3	32.3	29.2	29.2	29.9

APPENDIX C

Table C.2: PLAGIOCLASE MICROPROBE ANALYSES

	SG49 PGD Ande. 8	SG49 PGD Ande. 9	SG49 PGD Ande. 10	SG49 PGD Ande. 11R	SG49 PGD Olig. 12C	SG49 PGD Olig. 13
SiO2	61.64	61.72	62.03	62.35	62.79	63.16
Al2O3	23.49	23.45	23.41	22.83	22.95	22.58
Fe2O3	0.16	0.14	0.16	0.16	0.12	0.19
MgO	-	-	-	-	-	-
CaO	4.50	4.58	4.46	4.00	3.88	3.85
BaO	0.02	0.02	-	0.01	0.06	0.03
Na2O	8.93	8.97	9.08	9.15	9.38	9.13
K2O	0.33	0.44	0.25	0.15	0.16	0.51
Total	99.07	99.32	99.39	98.65	99.34	99.45
Ab	64.9	64.1	65.9	68.8	69.9	67.7
Or	2.4	3.2	1.8	1.1	1.2	3.8
An	32.7	32.7	32.3	30.1	28.9	28.5

	SG49 PGD Ande. 14	SG49 PGD Ande. 15	SG49 PGD Ande. 16	SG49 PGD Ande. 17	SG49 PGD Ande. 18	SG49 PGD Olig. 19
SiO2	62.69	62.16	62.25	61.76	61.58	62.91
Al2O3	22.82	23.36	23.12	23.61	23.63	22.87
Fe2O3	0.18	0.16	0.16	0.15	0.19	0.18
MgO	-	-	-	-	-	-
CaO	3.96	4.61	4.29	4.92	4.98	3.96
BaO	0.04	0.02	-	-	-	-
Na2O	8.85	8.91	8.98	8.68	8.62	9.24
K2O	0.37	0.39	0.49	0.37	0.47	0.32
Total	98.91	99.61	99.29	99.49	99.47	99.48
Ab	67.2	63.9	65.3	62.1	61.2	68.3
Or	2.7	2.8	3.6	2.7	3.3	2.4
An	30.1	33.2	31.1	35.2	35.4	29.3

APPENDIX C

Table C.2: PLAGIOCLASE MICROPROBE ANALYSES

	SG78 BGT Ande. 1R	SG78 BGT Ande. 2C	SG78 BGT Ande. 4R	SG78 BGT Olig. 5C	SG78 BGT Ande. 6C	SG78 BGT Ande. 7R
SiO2	62.39	61.68	62.28	62.65	60.29	62.46
Al2O3	22.86	23.74	23.11	22.72	24.48	23.02
Fe2O3	0.13	0.08	0.10	0.09	0.11	0.07
MgO	-	-	-	-	-	-
CaO	4.22	4.97	4.41	3.80	5.84	4.19
BaO	-	0.09	-	0.04	-	0.02
Na2O	9.28	8.98	9.10	9.55	8.49	9.33
K2O	0.22	0.13	0.31	0.24	0.23	0.23
Total	99.10	99.67	99.31	99.09	99.44	99.32
Ab	67.6	63.8	65.9	70.3	58.3	67.8
Or	1.6	0.9	2.2	1.7	1.6	1.7
An	30.8	35.3	31.9	28.0	40.1	30.5

	SG78 BGT Labr. 8C	SG78 BGT Olig. 9R	SG78 BGT Olig. 10M	SG78 BGT Olig. 11C	SG78 BGT Ande. 14R	SG93 TGD Ande. 1
SiO2	56.74	63.12	62.37	63.21	62.38	61.62
Al2O3	22.95	22.67	22.91	22.39	22.85	23.62
Fe2O3	0.11	0.09	0.12	0.06	0.09	0.14
MgO	-	-	-	-	-	-
CaO	11.85	3.73	3.94	3.53	4.15	4.54
BaO	0.06	-	0.02	-	0.02	0.02
Na2O	7.04	9.66	9.55	9.77	9.28	9.16
K2O	0.06	0.21	0.25	0.20	0.22	0.22
Total	98.81	99.48	99.16	99.16	98.99	99.32
Ab	37.1	71.0	69.5	72.4	68.0	65.8
Or	0.3	1.5	1.8	0.5	4.6	1.6
An	62.5	27.5	28.7	26.1	30.4	32.6

APPENDIX C

Table C.2: PLAGIOCLASE MICROPROBE ANALYSES

	SG93 TGD Ande. 2R	SG93 TGD Ande. 3C	SG93 TGD Ande. 4R	SG93 TGD Ande. 5M	SG93 TGD Ande. 6C	SG93 TGD Ande. 7R
SiO2	61.24	61.86	62.07	60.77	62.02	61.55
Al2O3	23.85	23.28	23.16	23.94	22.95	23.08
Fe2O3	0.17	0.16	0.12	0.13	0.16	0.11
MgO	-	-	-	-	-	-
CaO	5.21	4.57	4.34	5.29	4.45	4.27
BaO	0.08	0.05	0.05	0.05	0.01	-
Na2O	8.59	9.09	9.19	8.69	9.10	9.33
K2O	0.42	0.30	0.32	0.22	0.35	0.21
Total	99.56	99.31	99.25	99.09	99.04	98.55
Ab	60.4	65.1	66.4	61.2	65.4	67.6
Or	3.1	2.2	2.3	1.6	2.5	1.5
An	36.5	32.7	31.3	37.2	32.1	30.9

	SG93 TGD Ande. 8M	SG93 TGD Ande. 9C	SG93 TGD Ande. 10R	SG93 TGD Ande. 11M	SG93 TGD Ande. 12C	SG93 TGD Ande. 13
SiO2	61.44	61.99	61.86	61.32	61.43	62.39
Al2O3	23.34	23.09	23.07	23.33	23.37	23.01
Fe2O3	0.16	0.16	0.14	0.14	0.13	0.16
MgO	-	-	-	-	-	-
CaO	4.71	4.29	4.19	4.77	4.82	4.32
BaO	-	0.03	0.01	0.05	0.09	0.04
Na2O	9.06	9.13	9.04	8.87	8.95	9.32
K2O	0.23	0.43	0.45	0.35	0.32	0.27
Total	98.94	99.12	98.76	98.83	99.11	99.51
Ab	64.7	65.9	66.1	63.4	63.5	67.1
Or	1.6	3.1	3.3	2.5	2.3	1.8
An	33.7	31.0	30.6	34.1	34.2	31.1

APPENDIX C

Table C.2: PLAGIOCLASE MICROPROBE ANALYSES

	SG93 TGD Ande. 14	SG93 TGD Olig. 15	SG93 TGD Ande. 16	XG32 1A Ande. 1	XG32 1A Ande. 2	XG32 1A Ande. 3
SiO2	61.91	61.64	61.68	61.28	61.72	59.42
Al2O3	23.09	22.94	23.05	23.72	23.43	24.92
Fe2O3	0.16	0.78	0.15	0.09	0.11	0.13
MgO	-	0.24	-	-	-	-
CaO	4.29	3.25	4.28	5.09	4.64	6.48
BaO	0.08	0.12	0.02	-	0.06	0.04
Na2O	9.25	8.27	9.14	8.75	8.91	7.88
K2O	0.26	0.65	0.37	0.21	0.29	0.28
Total	99.04	97.89	98.69	99.14	99.16	99.15
Ab	67.0	67.9	66.3	62.3	64.4	53.8
Or	1.9	5.4	2.7	1.5	2.1	1.9
An	31.1	26.7	31.0	36.3	33.5	44.3

	XG32 1A Ande. 4M	XG32 1A Ande. 5	XG32 1A Labr. 6C	XG32 1A Ande. 7	XG32 1A Ande. 8	XG32 1A Ande. 9
SiO2	62.21	59.61	57.19	59.99	58.99	61.32
Al2O3	23.17	24.96	26.33	24.56	25.33	23.44
Fe2O3	0.21	0.09	0.13	0.10	0.09	0.19
MgO	-	-	-	-	-	-
CaO	4.33	6.33	8.23	5.91	6.78	4.76
BaO	0.07	0.05	0.03	0.09	0.06	0.06
Na2O	9.03	7.82	6.89	8.24	7.84	8.94
K2O	0.27	0.28	0.21	0.19	0.17	0.21
Total	99.29	99.14	99.01	99.08	99.26	98.92
Ab	66.3	54.1	45.1	57.5	53.0	64.3
Or	1.9	2.0	1.3	1.3	1.2	1.5
An	31.8	43.9	53.6	41.2	45.8	34.2

APPENDIX C

Table C.2: PLAGIOCLASE MICROPROBE ANALYSES

	XG32 1A Ande. 10	XG32 1A Ande. 11	XG32 1A Ande. 12	XG32 1A Ande. 13	XG32 1A Ande. 15	XG32 1A Ande. 16
SiO2	61.14	61.73	60.81	61.34	62.12	61.79
Al2O3	22.95	23.42	24.17	23.35	23.21	23.16
Fe2O3	0.13	0.12	0.11	0.08	0.11	0.17
MgO	-	-	-	-	-	-
CaO	4.37	4.64	5.43	4.48	4.45	4.45
BaO	-	0.08	0.06	0.08	-	-
Na2O	8.91	9.03	8.55	8.86	9.18	9.09
K2O	0.27	0.25	0.26	0.27	0.22	0.22
Total	97.77	99.27	99.39	98.46	99.29	98.88
Ab	65.7	64.9	60.0	65.1	66.3	66.1
Or	2.0	1.8	1.9	2.0	1.6	1.6
An	32.3	33.3	38.1	32.9	32.1	32.3

	XG32 1A Ande. 17	XG32 1A Labr. 18M	XG32 1A Ande. 19M	XG65 1A Olig. 1R	XG65 1A Olig. 2C	XG65 1A Olig. 3
SiO2	61.25	58.26	60.35	62.67	62.69	62.62
Al2O3	23.55	25.71	24.28	22.55	22.70	22.82
Fe2O3	0.33	0.15	0.21	0.12	0.08	0.15
MgO	-	-	-	-	-	-
CaO	4.78	7.31	5.43	3.85	3.90	3.91
BaO	-	-	-	0.03	0.09	-
Na2O	9.04	7.35	8.46	9.51	9.59	9.43
K2O	0.21	0.24	0.22	0.24	0.18	0.20
Total	99.16	99.02	98.95	98.97	99.23	99.13
Ab	64.4	49.4	60.1	69.9	70.1	69.6
Or	1.5	1.5	1.5	1.7	1.3	1.5
An	34.1	49.1	38.4	28.3	28.6	28.9

APPENDIX C

Table C.2: PLAGIOCLASE MICROPROBE ANALYSES

	XG65 1A Olig. 4	XG65 1A Olig. 5C	XG65 1A Ande. 6R	XG65 1A Ande. 7C	XG65 1A Olig. 8R	XG65 1A Olig. 9C
SiO2	62.85	61.99	61.97	62.43	62.18	62.32
Al2O3	22.73	23.59	23.02	22.99	22.76	22.81
Fe2O3	0.19	0.09	0.09	0.08	0.10	0.08
MgO	0.05	-	-	-	-	-
CaO	3.92	2.99	4.41	4.17	3.95	4.03
BaO	-	0.06	-	-	0.01	-
Na2O	9.59	8.77	8.54	9.39	9.53	9.47
K2O	0.18	0.91	0.11	0.18	0.18	0.19
Total	99.51	98.40	98.14	99.24	98.71	98.90
Ab	70.1	69.2	65.4	68.3	69.8	69.1
Or	1.3	7.2	0.9	1.3	1.3	1.5
An	28.6	23.6	33.7	30.4	28.9	29.4

	XG65 1A Ande. 10	XG65 1A Olig. 11	XG65 1A Olig. 12	XG65 1A Olig. 13	XG65 1A Ande. 14	XG65 1A Ande. 15
SiO2	60.47	61.55	62.73	62.48	62.47	59.91
Al2O3	24.23	22.13	22.59	22.62	23.05	25.03
Fe2O3	0.10	0.12	0.27	0.28	0.24	0.20
MgO	-	-	-	-	-	-
CaO	5.61	3.66	3.89	3.79	4.21	6.06
BaO	-	-	-	-	-	-
Na2O	8.58	9.64	9.66	9.61	9.44	7.57
K2O	0.15	0.17	0.21	0.19	0.14	0.23
Total	99.14	97.27	99.35	98.97	99.55	99.00
Ab	59.9	71.6	70.2	70.7	68.5	54.6
Or	1.0	1.3	1.5	1.4	1.0	1.6
An	39.1	27.1	28.3	27.9	30.5	43.8

APPENDIX C

Table C.2: PLAGIOCLASE MICROPROBE ANALYSES

	XG65 1A Ande. 16	XG65 1A Olig. 18	XG7 1B Ande. 1R	XG7 1B Ande. 2R	XG7 1B Ande. 3M	XG7 1B Ande. 4C
SiO2	61.89	62.17	63.39	62.53	62.79	63.33
Al2O3	23.62	22.82	22.71	22.99	22.87	22.70
Fe2O3	0.25	0.67	0.21	0.19	0.18	0.17
MgO	-	0.03	0.01	-	-	-
CaO	4.66	3.87	4.48	4.71	4.61	4.44
BaO	-	-	-	-	-	-
Na2O	8.79	9.47	8.61	8.45	8.68	8.61
K2O	0.17	0.32	0.58	0.64	0.54	0.64
Total	99.38	99.35	99.99	99.51	99.67	99.89
Ab	64.5	69.3	62.9	61.3	62.7	63.0
Or	1.7	2.3	4.3	4.6	3.9	4.6
An	34.8	28.4	32.8	34.1	33.4	32.4

	XG7 1B Ande. 5M	XG7 1B Ande. 6R	XG7 1B Ande. 7M	XG7 1B Ande. 8C	XG7 1B Ande. 9M	XG7 1B Ande. 10C
SiO2	62.31	63.91	63.03	62.53	63.31	61.88
Al2O3	23.42	22.69	22.68	23.23	22.74	23.32
Fe2O3	0.09	0.19	0.19	0.16	0.19	0.14
MgO	-	-	-	0.01	0.01	-
CaO	5.09	4.41	4.58	4.95	4.11	4.92
BaO	-	-	-	-	-	-
Na2O	8.49	8.70	8.66	8.61	9.03	8.47
K2O	0.27	0.55	0.57	0.35	0.62	0.43
Total	99.67	100.45	99.71	99.84	100.01	99.16
Ab	61.3	63.7	62.7	61.9	65.6	61.3
Or	2.1	4.0	4.0	2.6	4.5	3.1
An	36.6	32.3	33.2	35.5	29.9	35.6

APPENDIX C

Table C.2: PLAGIOCLASE MICROPROBE ANALYSES

	XG24 1B Ande. 1R	XG24 1B Ande. 2M	XG24 1B Ande. 3	XG24 1B Ande. 4R	XG24 1B Ande. 5R	XG24 1B Ande. 6M
SiO2	62.34	61.53	61.66	60.96	61.69	61.30
Al2O3	23.49	23.71	23.57	23.53	23.48	23.59
Fe2O3	0.16	0.14	0.13	0.34	0.19	0.15
MgO	-	-	-	-	-	-
CaO	4.53	4.85	4.81	4.81	4.89	4.78
BaO	0.01	-	0.03	-	0.15	-
Na2O	9.22	8.90	8.91	8.83	8.87	9.03
K2O	0.21	0.33	0.29	0.33	0.32	0.24
Total	99.96	99.46	99.40	98.80	99.59	99.09
Ab	66.1	63.3	63.6	63.2	63.0	64.3
Or	1.5	2.3	2.1	2.4	2.3	1.7
An	32.5	34.4	34.3	34.4	34.7	34.0

	XG24 1B Ande. 7M	XG24 1B Ande. 8C	XG24 1B Ande. 9	XG24 1B Ande. 10R	XG24 1B Ande. 11R	XG24 1B Ande. 12R
SiO2	60.88	61.43	61.18	60.36	59.43	61.29
Al2O3	23.77	23.41	23.82	23.89	24.79	23.54
Fe2O3	0.12	0.17	0.13	0.14	0.09	0.25
MgO	-	-	-	-	-	-
CaO	5.09	4.88	5.07	4.97	6.12	4.67
BaO	0.04	-	0.02	0.04	-	-
Na2O	8.82	8.80	8.79	8.70	8.07	9.04
K2O	0.29	0.36	0.23	0.27	0.26	0.19
Total	99.01	99.05	99.24	98.37	98.76	98.98
Ab	62.1	62.7	62.4	62.4	55.9	65.0
Or	2.0	2.6	1.6	2.0	1.8	1.4
An	35.9	34.7	36.0	35.6	42.3	33.6

APPENDIX C

Table C.2: PLAGIOCLASE MICROPROBE ANALYSES

	XG24 1B Ande. 13M	XG24 1B Ande. 14C	XG24 1B Ande. 15R	XG24 1B Ande. 16M	XG24 1B Ande. 17C	XG64A 1B Ande. 1
SiO2	61.26	59.22	61.36	59.14	59.56	62.53
Al2O3	23.56	24.52	23.57	24.99	24.94	22.95
Fe2O3	0.16	0.11	0.13	0.09	0.15	0.13
MgO	-	-	-	-	-	-
CaO	4.85	5.73	5.02	6.44	6.48	4.14
BaO	0.07	0.04	-	0.01	0.05	-
Na2O	8.98	8.52	8.91	7.92	7.88	9.53
K2O	0.27	0.19	0.21	0.30	0.28	0.15
Total	99.15	98.33	99.20	98.89	99.34	99.43
Ab	63.7	59.0	63.1	54.0	53.8	69.0
Or	1.9	1.3	1.4	2.0	1.9	1.0
An	34.4	39.7	35.5	44.0	44.2	30.0

	XG64A 1B Ande. 2	XG64A 1B Ande. 3	XG64A 1B Ande. 3A	XG64A 1B Olig. 6R	XG64A 1B Olig. 7	XG64A 1B Ande. 8
SiO2	60.69	61.26	62.29	62.26	62.15	62.87
Al2O3	24.04	22.85	22.78	22.49	22.33	22.52
Fe2O3	0.21	0.09	0.21	0.08	0.23	0.17
MgO	-	-	-	-	-	-
CaO	5.36	4.57	4.07	3.93	3.84	3.52
BaO	0.16	-	0.18	-	-	0.04
Na2O	8.70	9.06	9.26	9.56	9.47	7.84
K2O	0.28	0.14	0.20	0.15	0.18	0.29
Total	99.44	97.97	98.99	98.47	98.20	97.25
Ab	60.6	65.8	68.4	70.1	70.2	67.3
Or	2.0	1.0	1.5	1.1	1.3	2.5
An	37.4	33.2	30.1	28.8	28.5	30.2

APPENDIX C

Table C.2: PLAGIOCLASE MICROPROBE ANALYSES

	XG64A 1B Ande. 9M	XG64A 1B Ande. 10	XG64A 1B Ande. 11M	XG64A 1B Ande. 12	X181 2 Olig. 1R	X181 2 Olig. 2R
SiO2	61.65	62.18	62.08	61.92	62.83	62.97
Al2O3	23.35	23.14	23.41	23.20	23.25	22.54
Fe2O3	0.12	0.13	0.26	0.13	0.13	0.13
MgO	-	-	-	-	-	-
CaO	4.38	4.09	4.53	4.39	4.05	3.56
BaO	-	0.04	-	-	-	0
Na2O	8.07	8.38	7.33	7.99	9.64	9.47
K2O	0.18	0.18	0.23	0.24	0.25	0.23
Total	97.75	98.14	97.84	97.87	100.15	98.90
Ab	63.8	66.2	60.6	63.3	69.1	71.4
Or	1.5	1.5	1.9	1.9	1.8	1.8
An	34.7	32.3	37.5	34.8	29.1	26.8

	X181 2 Olig. 3M	X181 2 Ande. 4C	X181 2 Olig. 5R	X181 2 Olig. 7R	X181 2 Ande. 8C	X181 2 Olig. 9R
SiO2	63.11	62.17	62.98	62.88	63.36	63.29
Al2O3	22.86	22.91	22.68	22.71	23.89	22.56
Fe2O3	0.14	0.14	0.14	0.12	0.11	0.15
MgO	-	-	-	-	-	-
CaO	3.84	4.24	3.64	3.96	4.51	3.47
BaO	0.03	0.10	0.03	0.01	0.02	0.07
Na2O	9.64	8.61	9.73	9.42	9.10	9.94
K2O	0.23	0.42	0.20	0.17	0.20	0.19
Total	99.85	98.59	99.40	99.27	101.19	99.67
Ab	70.2	64.9	71.7	69.5	65.9	73.1
Or	1.7	3.2	1.5	1.3	1.5	1.4
An	28.1	31.9	26.8	29.2	32.6	25.5

APPENDIX C

Table C.2: PLAGIOCLASE MICROPROBE ANALYSES

	X181 2 Olig. 10M	X181 2 Olig. 11R	X181 2 Ande. 12C	X181 2 Olig. 13R	X181 2 Olig. 14M	X181 2 Olig. 15R
SiO2	63.31	63.07	59.88	63.13	63.24	62.89
Al2O3	22.29	22.60	24.67	22.35	22.29	22.62
Fe2O3	0.17	0.15	0.17	0.11	0.12	0.12
MgO	-	-	-	-	-	-
CaO	2.54	3.71	6.04	3.46	3.48	3.49
BaO	0.06	0.03	0.01	-	-	0.03
Na2O	10.07	9.79	8.38	9.62	9.67	9.48
K2O	0.65	0.16	0.16	0.19	0.22	0.23
Total	99.09	99.51	99.31	98.86	99.02	98.86
Ab	76.1	71.7	57.5	72.4	72.3	71.8
Or	4.9	1.2	1.1	1.5	1.6	1.7
An	19.0	27.1	41.4	26.1	26.1	26.5

	X181 2 Labr. 16C
SiO2	57.68
Al2O3	26.34
Fe2O3	0.09
MgO	-
CaO	7.87
BaO	0.01
Na2O	7.29
K2O	0.14
Total	99.42
Ab	47.6
Or	0.9
An	51.5

APPENDIX C

Table C.2: PLAGIOCLASE MICROPROBE ANALYSES

	XG25 2 Ande. 1R	XG25 2 Ande. 2M	XG25 2 Ande. 3C	XG25 2 Ande. 4C	XG25 2 Ande. 5M	XG25 2 Ande. 6M
SiO2	63.03	62.88	61.89	62.55	62.54	63.04
Al2O3	22.97	23.13	23.47	23.26	22.98	22.94
Fe2O3	0.08	0.14	0.08	0.14	0.10	0.12
MgO	-	0.01	0.01	-	0.01	-
CaO	4.20	4.39	4.92	4.67	4.17	4.22
BaO	-	-	-	-	-	-
Na2O	8.89	8.78	8.32	8.62	8.85	8.72
K2O	0.23	0.27	0.26	0.37	0.25	0.35
Total	99.4	99.6	98.95	99.61	98.9	99.39
Ab	66.7	65.3	61.6	63.1	66.7	65.6
Or	1.7	2.0	1.9	2.7	1.9	2.7
An	31.6	32.7	36.5	34.2	31.4	31.7

	XG25 2 Ande. 7R	XG25 2 Ande. 8M	XG25 2 Ande. 9R	XG25 2 Ande. 10R	XG44 2 Olig. 1R	XG44 2 Olig. 2C
SiO2	63.38	64.15	63.78	63.21	62.38	63.38
Al2O3	22.83	23.00	22.77	22.94	22.76	22.57
Fe2O3	0.15	0.11	0.15	0.22	0.22	0.08
MgO	0.01	-	0.01	0.01	-	-
CaO	3.99	4.26	4.17	4.13	3.80	3.49
BaO	-	-	-	-	0.01	0.01
Na2O	9.03	8.93	8.74	9.01	9.72	9.91
K2O	0.26	0.23	0.36	0.23	0.19	0.05
Total	99.65	100.68	99.98	99.75	99.08	99.49
Ab	68.0	66.5	65.9	67.4	70.9	73.7
Or	2.0	1.8	2.7	1.7	1.4	0.2
An	30.0	31.7	31.4	30.9	27.7	26.1

APPENDIX C

Table C.2: PLAGIOCLASE MICROPROBE ANALYSES

	XG44 2 Olig. 3R	XG44 2 Ande. 5R	XG44 2 Ande. 6M	XG44 2 Olig. 7R	XG44 2 Ande. 8C	XG44 2 Olig. 9
SiO2	62.57	62.17	61.63	63.64	62.22	62.52
Al2O3	22.82	22.83	23.52	22.12	23.28	22.72
Fe2O3	0.21	0.23	0.12	0.07	0.09	0.13
MgO	-	-	-	-	-	-
CaO	3.99	4.04	4.80	3.02	4.19	3.89
BaO	0.01	0.05	0.05	0.04	-	0.03
Na2O	9.44	9.31	9.06	9.85	9.15	9.59
K2O	0.30	0.21	0.24	0.38	0.21	0.24
Total	99.34	98.84	99.42	99.12	99.14	99.12
Ab	68.8	68.7	64.3	74.3	67.5	69.9
Or	2.2	1.5	1.6	2.9	1.5	1.8
An	29.0	29.8	34.1	22.8	31.0	28.3

	XG44 2 Ande. 10	XG44 2 Ande. 11	XG44 2 Ande. 12R	XG44 2 Olig. 13C	XG44 2 Ande. 14R	XG44 2 Ande. 15M
SiO2	61.55	62.21	62.82	62.02	62.47	62.19
Al2O3	23.57	23.08	23.05	23.14	23.29	23.27
Fe2O3	0.12	0.09	0.17	0.11	0.10	0.16
MgO	-	-	-	-	-	-
CaO	4.83	4.34	4.22	3.78	4.35	4.41
BaO	0.01	0.07	-	0.08	0.03	-
Na2O	9.05	9.34	9.55	8.99	9.31	9.19
K2O	0.23	0.22	0.21	Q.44	0.24	0.28
Total	99.36	99.35	100.02	98.56	99.79	99.5
Ab	64.1	67.2	68.3	68.1	66.9	66.2
Or	1.6	1.6	1.5	3.4	1.8	2.0
An	34.3	31.2	30.2	28.5	31.3	31.8

APPENDIX C

Table C.2: PLAGIOCLASE MICROPROBE ANALYSES

	XG44 2 Ande. 16C	XG61B 2 Olig. 1R	XG61B 2 Ande. 2M	XG61B 2 Olig. 3R	XG61B 2 Olig. 4R	XG61B 2 Ande. 5R
SiO2	61.77	64.06	60.58	64.63	63.77	62.05
Al2O3	23.33	22.53	24.31	22.53	22.53	23.64
Fe2O3	0.17	0.11	0.07	0.11	0.09	0.05
MgO	-	0.02	0.01	0.03	0.02	0.01
CaO	4.72	3.75	6.06	3.65	3.56	4.97
BaO	0.09	-	-	-	-	-
Na2O	8.97	9.41	8.06	9.42	9.44	8.73
K2O	0.42	0.21	0.26	0.22	0.21	0.14
Total	99.47	100.09	99.35	100.59	99.62	99.59
Ab	63.6	70.3	56.1	70.9	71.4	63.0
Or	3.1	1.6	1.8	1.7	1.6	1.0
An	33.3	28.1	42.1	27.4	27.0	36.0

	XG61B 2 Ande. 6C	XG61B 2 Olig. 8R	XG61B 2 Olig. 9R	XG61B 2 Ande. 10C	XG61C 2 Olig. 1	XG61C 2 Olig. 2
SiO2	63.57	63.25	63.42	60.58	62.61	62.35
Al2O3	22.91	21.98	22.68	24.16	22.82	2.59
Fe2O3	0.11	0.09	0.11	0.08	0.12	0.08
MgO	0.01	0.01	0.01	0.03	-	-
CaO	4.16	3.75	3.91	5.88	3.84	3.67
BaO	-	-	-	-	0.03	0.02
Na2O	9.07	9.44	9.33	8.05	9.40	9.64
K2O	0.28	0.26	0.21	0.21	0.26	0.18
Total	100.11	98.78	99.67	98.99	99.08	78.53
Ab	67.1	70.2	69.4	56.9	69.6	71.4
Or	2.1	1.9	1.5	1.5	1.9	1.3
An	30.8	27.9	29.1	41.6	28.5	27.3

APPENDIX C

Table C.2: PLAGIOCLASE MICROPROBE ANALYSES

	XG61C 2 Ande. 3M	XG61C 2 Olig. 4	XG61C 2 Olig. 5	XG61C 2 Olig. 6	XG61C 2 Ande. 7	XG61C 2 Olig. 8
SiO2	61.77	61.41	62.96	62.58	60.76	62.97
Al2O3	23.36	22.91	22.56	22.72	23.17	21.28
Fe2O3	0.07	0.12	0.09	0.09	0.07	0.09
MgO	-	-	-	-	-	-
CaO	4.73	3.86	3.82	3.65	4.68	2.53
BaO	-	-	0.02	0.06	0.01	0.09
Na2O	9.04	9.64	9.53	9.59	8.91	7.34
K2O	0.19	0.14	0.14	0.14	0.16	3.87
Total	99.16	98.08	99.12	98.83	97.76	98.17
Ab	64.7	70.7	70.6	71.7	64.8	53.4
Or	1.3	1.0	1.1	1.0	1.2	28.2
An	33.9	28.3	28.3	27.3	34.0	18.4

	XG61C 2 Olig. 9	XG61C 21 Olig. 10R	XG61C 2 Ande. 11C	XG61C 2 Olig. 12R	XG61C 2 Olig. 13R	XG61C 2 Olig. 14M
SiO2	62.68	62.73	59.98	63.72	62.84	62.84
Al2O3	22.75	22.81	24.43	22.07	22.49	22.48
Fe2O3	0.11	0.08	0.10	0.08	0.09	0.11
MgO	-	-	-	-	-	-
CaO	3.83	3.83	5.81	3.04	3.93	3.84
BaO	0.06	-	0.03	0.03	0.07	-
Na2O	9.48	9.56	8.37	9.92	9.44	9.33
K2O	0.29	0.19	0.22	0.19	0.29	0.36
Total	99.2	99.2	98.94	99.05	99.15	98.96
Ab	69.7	70.4	58.1	75.4	69.1	68.9
Or	2.2	1.4	1.6	1.5	2.1	2.7
An	28.1	28.2	40.3	23.1	28.8	28.4

APPENDIX C

Table C.2: PLAGIOCLASE MICROPROBE ANALYSES

	XG61C 2 Olig. 15M	XG61C 2 Ande. 16C	XG61C 2 Ande. 17C	XG61C 2 Olig. 18M	XG61C 2 Olig. 19R	XG61C 2 Olig. 20R
SiO2	63.27	61.28	59.20	63.28	62.69	62.94
Al2O3	22.22	23.27	25.30	22.28	22.81	22.51
Fe2O3	0.10	0.13	0.09	0.13	0.09	0.13
MgO	-	-	-	-	-	-
CaO	3.44	4.81	6.69	3.64	3.65	3.79
BaO	-	0.01	-	0.03	0.03	0.05
Na2O	9.66	8.87	7.87	9.51	9.55	9.49
K2O	0.32	0.26	0.19	0.34	0.28	0.26
Total	99.01	98.63	99.34	99.21	99.1	99.17
Ab	72.1	63.6	53.3	70.5	70.9	70.0
Or	2.3	1.9	1.3	2.5	2.1	2.0
An	25.6	34.5	45.4	27.0	27.0	28.0

	XG89 2 Ande. 1R	XG89 2 Ande. 2R	XG89 2 Ande. 3R	XG89 2 Ande. 4R	XG89 2 Ande. 5R	XG89 2 Ande. 6C
SiO2	62.69	61.95	62.15	61.79	62.02	61.07
Al2O3	22.74	22.91	23.42	23.49	22.74	23.16
Fe2O3	0.21	0.09	0.09	0.09	0.12	0.11
MgO	0.01	-	0.01	-	-	-
CaO	4.17	4.62	4.79	5.03	4.47	5.15
BaO	-	-	-	-	-	-
Na2O	9.12	8.89	8.92	8.68	9.18	8.66
K2O	0.35	0.28	0.29	0.22	0.23	0.28
Total	99.29	98.74	99.67	99.3	98.76	98.43
Ab	66.8	64.5	63.7	62.3	66.1	61.5
Or	2.6	2.0	2.1	1.6	1.7	2.1
An	30.6	33.5	34.2	36.1	32.2	36.4

APPENDIX C

Table C.2: PLAGIOCLASE MICROPROBE ANALYSES

	XG89 2 Ande. 7R	XG89 2 Ande. 8C	XG89 2 Ande. 9C	XG89 2 Ande. 10R	XG4 5 Olig. 1R	XG4 5 Ande. 2R
SiO2	59.81	61.98	60.76	62.05	62.89	62.61
Al2O3	23.86	22.85	23.38	22.91	22.91	22.85
Fe2O3	0.11	0.13	0.11	0.10	0.16	0.12
MgO	0.01	-	-	-	-	-
CaO	5.86	4.57	5.05	4.34	3.76	4.19
BaO	-	-	-	-	-	-
Na2O	7.31	8.95	8.78	9.20	9.13	8.99
K2O	1.34	0.31	0.29	0.27	0.43	0.24
Total	98.3	98.79	98.37	98.87	99.28	99
Ab	50.4	64.7	62.1	66.6	68.5	67.2
Or	9.2	2.2	2.1	1.9	3.3	1.6
An	40.4	33.1	35.7	31.5	28.2	31.2

	XG4 5 Olig. 3C	XG4 5 Ande. 4C	XG4 5 Ande. 5R	XG4 5 Olig. 6R	XG4 5 Olig. 7R	XG4 5 Olig. 8M
SiO2	62.59	62.42	62.62	63.09	62.85	61.89
Al2O3	22.53	22.96	22.78	22.26	22.22	23.56
Fe2O3	0.12	0.15	0.09	0.15	0.11	0.09
MgO	-	0.02	0.01	0.02	0.01	-
CaO	3.76	4.12	3.96	3.56	3.38	4.81
BaO	-	-	-	-	-	-
Na2O	9.20	9.06	9.09	9.17	9.47	8.68
K2O	0.32	0.26	0.16	0.34	0.25	0.26
Total	98.52	98.99	98.71	98.59	98.29	99.29
Ab	69.3	67.4	68.8	70.1	72.2	63.2
Or	2.4	1.9	1.2	2.6	1.9	1.7
An	28.3	30.6	30.0	27.3	25.9	35.1

APPENDIX C

Table C.2: PLAGIOCLASE MICROPROBE ANALYSES

	XG4 5 Olig. 9R	XG4 5 Ande. 10R	XG4 5 Ande. 11C	XG4 5 Olig. 12
SiO2	64.01	62.09	62.07	63.53
Al2O3	22.21	22.85	23.15	22.37
Fe2O3	0.15	0.18	0.17	0.15
MgO	0.02	0.01	0.02	0.01
CaO	3.33	4.26	4.55	3.74
BaO	-	-	-	-
Na2O	9.39	8.59	8.50	9.11
K2O	0.15	0.52	0.31	0.32
Total	99.26	98.5	98.77	99.23
Ab	72.5	64.1	63.6	
Or	1.1	3.9	2.3	
An	25.4	32.0	34.1	

MAFIC DIORITES

	D1 Rubh. Olig. 1M	D2 Rubh. Olig. 1R	D2 Rubh. Ande. 2C	D2 Rubh. Olig. 3R	D2 Rubh. Olig. 4M	D2 Rubh. Olig. 5R
SiO2	63.21	66.33	64.82	64.94	64.77	65.99
Al2O3	21.18	21.58	22.38	22.28	22.15	21.68
Fe2O3	0.04	0.12	0.11	0.10	0.11	0.13
MgO	-	0.02	0.01	0.01	-	0.01
CaO	2.99	2.37	3.42	3.41	3.40	2.48
BaO	-	-	-	-	-	-
Na2O	9.79	9.89	9.18	9.30	9.22	9.88
K2O	0.22	0.24	0.36	Q.33	0.35	0.15
Total	97.43	100.55	100.28	100.37	100	100.32
Ab	75.3	79.1	71.1	71.0	71.0	78.7
Or	1.6	1.9	2.5	2.5	2.7	1.1
An	23.1	20.0	26.4	26.5	26.3	20.2

APPENDIX C

Table C.2: PLAGIOCLASE MICROPROBE ANALYSES

	D2 Rubh. Ande. 6R	D2 Rubh. Olig. 7R	D2 Rubh. Olig. 8M	D2 Rubh. Olig. 9C	D8 Rubh. Olig. 1M	D8 Rubh. Olig. 2
SiO2	62.03	65.67	66.07	64.04	62.02	63.15
Al2O3	23.94	21.61	22.12	22.52	23.24	22.36
Fe2O3	0.11	0.10	0.11	0.08	0.11	0.15
MgO	0.02	-	0.01	0.02	-	-
CaO	5.21	2.69	3.12	3.54	3.91	3.56
BaO	-	-	-	-	0.05	-
Na2O	8.23	9.73	9.22	9.19	9.54	9.67
K2O	0.34	0.23	0.34	0.36	0.09	0.14
Total	99.88	100.03	100.99	99.75	98.96	99.03
Ab	60.4	77.0	73.0	70.2	70.5	72.3
Or	2.1	2.0	3.0	2.7	0.1	1.1
An	37.5	21.0	24.0	27.1	28.8	26.6

	D8 Rubh. Olig. 3	D8 Rubh. Olig. 4	D8 Rubh. Olig. 5	D8 Rubh. Olig. 6	D8 Rubh. Olig. 7R	D8 Rubh. Olig. 8
SiO2	62.99	62.59	63.33	63.11	64.05	63.71
Al2O3	22.62	22.69	22.36	22.59	21.94	22.21
Fe2O3	0.14	0.19	0.23	0.09	0.05	0.07
MgO	-	-	-	-	-	-
CaO	3.75	3.54	3.26	3.47	2.57	2.84
BaO	-	0.02	0.07	0.04	-	-
Na2O	9.63	9.56	9.89	9.76	10.32	10.13
K2O	0.12	0.15	0.19	0.14	0.05	0.06
Total	99.25	98.74	99.33	99.2	98.98	99.02
Ab	71.3	72.1	74.1	73.0	79.7	77.8
Or	0.9	1.2	1.4	1.0	0.4	0.4
An	27.8	26.7	24.5	26.0	19.9	21.8

APPENDIX C

Table C.2: PLAGIOCLASE MICROPROBE ANALYSES

	D8 Rubh. Olig. 9	D8 Rubh. Olig. 10	D8 Rubh. Ande. 11C	D8 Rubh. Olig. 12	D11 Lidd. Ande. 1	D11 Lidd. Olig. 2
SiO2	63.01	62.98	61.23	62.96	60.87	62.25
Al2O3	22.48	22.52	24.05	22.79	23.65	22.68
Fe2O3	0.15	0.12	0.11	0.16	0.13	0.14
MgO	-	-	-	-	-	-
CaO	3.58	3.71	4.88	3.69	4.85	3.82
BaO	0.01	0.06	0.05	0.04	0.04	0.05
Na2O	9.57	9.64	8.81	9.55	8.99	9.62
K2O	0.13	0.08	0.06	0.09	0.15	0.07
Total	98.93	99.11	99.19	99.28	98.68	98.63
Ab	72.0	71.8	64.1	71.6	64.3	71.2
Or	1.0	0.6	0.5	0.7	1.1	0.5
An	27.0	27.6	35.4	27.7	34.6	28.3

	D11 Lidd. Ande. 3	D11 Lidd. Olig. 4	D11 Lidd. Ande. 5	D11 Lidd. Olig. 6M	D11 Lidd. Ande. 7M	D11 Lidd. Olig. 8R
SiO2	61.36	62.10	61.29	62.39	59.97	63.37
Al2O3	23.66	23.18	23.36	22.79	24.35	22.11
Fe2O3	0.21	0.14	0.13	0.12	0.09	0.13
MgO	-	0.02	-	-	-	-
CaO	4.89	3.18	4.63	4.03	5.83	3.05
BaO	0.08	0.05	0.01	0.04	0.02	-
Na2O	8.98	9.56	9.01	9.49	8.38	10.15
K2O	0.14	0.30	0.13	0.09	0.04	0.09
Total	99.32	98.53	98.56	98.95	98.68	98.9
Ab	64.1	73.3	65.4	69.7	58.9	76.4
Or	1.0	2.3	1.0	0.7	0.3	0.7
An	34.9	24.4	33.6	29.6	40.8	22.9

APPENDIX C

Table C.2: PLAGIOCLASE MICROPROBE ANALYSES

	D11 Lidd. Olig. 9	D11 Lidd. Olig. 10	D11 Lidd. Olig. 11	D12 Lidd. Ande. 1R	D12 Lidd. Ande. 2M	D12 Lidd. Labr. 3C
SiO2	63.37	62.27	62.63	59.28	59.76	58.17
Al2O3	21.84	22.59	22.71	24.92	24.87	25.57
Fe2O3	0.15	0.12	0.11	0.07	0.08	0.08
MgO	-	-	-	0.02	0.02	0.02
CaO	2.99	3.67	3.85	6.61	6.47	7.28
BaO	0.02	0.11	0.04	-	-	-
Na2O	10.09	9.63	9.62	7.91	8.03	7.39
K2O	0.11	0.12	0.09	0.15	0.19	0.17
Total	98.57	98.51	99.05	98.96	99.42	98.68
Ab	76.5	71.8	71.0	54.0	55.0	50.2
Or	0.8	0.9	0.7	1.0	1.0	1.3
An	22.7	27.3	28.3	45.0	44.0	48.5

	D12 Lidd. Labr. 4R	D12 Lidd. Ande. 5C	D12 Lidd. Ande. 6M	D12 Lidd. Ande. 7M	D12 Lidd. Ande. 8C	D12 Lidd. Ande. 9M
SiO2	57.78	57.10	61.25	60.59	62.35	62.04
Al2O3	26.15	26.53	23.67	24.04	22.79	23.32
Fe2O3	0.05	0.26	0.09	0.09	0.12	0.08
MgO	0.02	0.35	0.01	0.02	0.02	0.01
CaO	8.11	3.27	4.87	5.62	4.18	4.57
BaO	-	-	-	-	-	-
Na2O	6.86	6.44	8.72	8.25	9.16	8.99
K2O	0.15	3.36	0.14	0.23	0.22	0.14
Total	99.12	97.31	98.75	98.84	98.84	99.15
Ab	45.2	39.3	63.5	58.0	68.0	65.1
Or	1.1	25.7	1.0	2.0	2.0	1.8
An	53.7	25.0	35.5	40.0	30.0	33.1

APPENDIX C

Table C.2: PLAGIOCLASE MICROPROBE ANALYSES

	D12 Lidd. Olig. 10R	D12 Lidd. Olig. 11R	D12 Lidd. Ande. 12R	D19 Shet. Ande. 1R	D19 Shet. Labr. 2C	D19 Shet. Labr. 3
SiO2	64.09	62.73	60.61	61.05	58.99	57.78
Al2O3	22.54	22.44	23.86	24.34	25.84	26.62
Fe2O3	0.08	0.09	0.09	0.19	0.12	0.09
MgO	0.02	-	-	-	-	-
CaO	3.53	3.43	5.39	5.24	7.51	8.24
BaO	-	-	-	0.05	0.05	0.03
Na2O	9.41	9.61	8.54	8.60	7.57	7.14
K2O	0.24	0.12	0.09	0.15	0.23	0.18
Total	99.91	98.42	98.58	99.62	100.31	100.08
Ab	71.0	72.8	61.0	60.7	49.4	45.9
Or	2.0	0.9	0.7	1.1	1.5	0.2
An	27.0	26.3	38.3	38.2	49.1	52.9

	D19 Shet. Ande. 4	D19 Shet Ande. 5R	D19 Shet Ande. 6M	D19 Shet. Ande. 7R	D19 Shet. Labr. 8C	D19 Shet. Ande. 9R
SiO2	59.04	59.26	60.41	61.78	61.71	61.70
Al2O3	25.63	25.49	24.65	23.89	23.85	23.86
Fe2O3	0.09	0.09	0.04	0.18	0.17	0.17
MgO	-	-	-	-	-	-
CaO	6.98	6.93	5.81	5.07	5.02	5.02
BaO	0.02	0.07	0.06	-	0.09	0.09
Na2O	7.77	7.81	8.52	8.97	8.88	8.88
K2O	0.17	0.22	0.12	0.21	0.15	0.15
Total	99.7	99.87	99.61	100.1	99.87	99.87
Ab	52.1	52.2	58.9	63.1	63.2	63.2
Or	1.2	1.5	0.9	1.4	1.1	1.1
An	46.7	46.3	40.2	35.5	35.7	35.7

APPENDIX C

Table C.2: PLAGIOCLASE MICROPROBE ANALYSES

	D19 Shet. Ande. 10C	D19 Shet. Labr. 11R	D19 Shet Ande. 12M	D19 Shet. Ande. 13C	D19 Shet Ande. 14R	D19 Shet. Ande. 15C
SiO2	60.88	58.19	59.15	61.24	60.65	59.99
Al2O3	24.37	26.17	25.62	24.23	24.32	24.81
Fe2O3	0.15	0.11	0.10	0.12	0.15	0.10
MgO	-	-	-	-	-	-
CaO	5.63	7.80	7.13	5.38	5.71	6.22
BaO	-	-	0.02	-	0.07	-
Na2O	8.50	7.25	7.66	8.43	8.49	8.07
K2O	0.26	0.21	0.24	0.38	0.29	0.28
Total	99.79	99.73	99.92	99.78	99.68	99.47
Ab	59.1	47.5	50.9	59.4	58.6	55.4
Or	1.8	1.4	1.6	2.7	2.0	1.9
An	39.1	51.1	47.5	37.9	39.4	42.7

	D41 Rana. Ande. 1	D41 Rana. Ande. 2R	D41 Rana. Perth. 3R	D41 Rana. Ande. 4R	D41 Rana. Ande. 5	D41 Rana. Ande. 6M
SiO2	60.83	61.88	63.07	60.33	61.65	61.09
Al2O3	23.33	23.17	21.09	24.41	23.12	23.64
Fe2O3	0.13	0.17	0.12	0.08	0.07	0.08
MgO	-	-	-	-	-	-
CaO	4.25	4.23	2.10	5.63	4.64	4.74
BaO	0.15	0.17	0.06	0.03	-	-
Na2O	9.01	9.03	5.67	8.53	9.17	8.95
K2O	0.40	0.46	6.59	0.14	0.16	0.26
Total	98.1	99.11	98.7	99.15	98.81	98.76
Ab	65.9	65.8	39.5	59.7	65.5	64.1
Or	3.0	3.4	45.9	0.9	1.1	1.9
An	31.1	30.8	14.6	39.4	33.3	34.0

APPENDIX C

Table C.2: PLAGIOCLASE MICROPROBE ANALYSES

	D41 Rana. Ande. 7M	D41 Rana. Ande. 8R	D41 Rana. Ande. 9M	D41 Rana. Ande. 10C	D41 Rana. Ande. 11R	D41 Rana. Ande. 12M
SiO2	60.41	61.09	61.69	61.22	61.94	61.74
Al2O3	24.18	23.59	23.37	23.34	23.37	23.40
Fe2O3	0.18	0.15	0.11	0.12	0.11	0.09
MgO	-	-	-	-	-	-
CaO	5.35	4.76	4.67	4.41	4.55	4.62
BaO	0.11	0.06	0.02	0.04	0.09	0.08
Na2O	8.44	8.84	8.97	9.04	9.08	8.96
K2O	0.38	0.39	0.32	0.29	0.28	0.35
Total	99.05	98.88	99.15	98.46	99.42	99.24
Ab	59.5	63.1	64.2	65.7	65.2	64.3
Or	2.7	2.8	2.3	2.1	2.1	2.5
An	37.8	34.1	33.5	32.2	32.7	33.2

	D41 Rana. Ande. 13C	D41 Rana. Ande. 14C	D41 Rana. Ande. 15M	D41 Rana. Ande. 16C	D63 Uile. Olig. 1M	D63 Uile. Olig. 2R
SiO2	61.68	61.61	60.98	61.56	62.14	63.27
Al2O3	23.29	23.60	23.89	23.53	22.79	22.12
Fe2O3	0.16	0.12	0.12	0.12	0.12	0.07
MgO	-	-	-	-	-	-
CaO	4.51	4.68	4.89	4.54	3.52	2.74
BaO	-	0.11	-	0.05	0.02	0.08
Na2O	8.91	9.09	8.82	9.09	9.56	9.88
K2O	0.43	0.20	0.25	0.25	0.27	0.41
Total	98.98	99.41	98.95	99.14	98.42	98.57
Ab	64.3	65.1	63.1	65.5	71.6	75.8
Or	3.1	1.5	1.8	1.8	2.1	3.1
An	32.6	33.5	35.1	32.7	26.3	21.1

APPENDIX C

Table C.2: PLAGIOCLASE MICROPROBE ANALYSES

	D63 Uile. Olig. 3R	D63 Uile. Olig. 16	D63 Uile. Olig. 17	E1 Dyke Ande. 2	E1 Dyke Ande. 3M	E1 Dyke Ande. 4
SiO2	63.15	63.05	63.14	62.22	61.96	61.39
Al2O3	22.49	22.26	22.13	22.65	23.24	23.62
Fe2O3	0.14	0.11	0.14	0.16	0.13	0.11
MgO	-	-	-	-	-	-
CaO	3.22	2.99	2.94	4.15	4.24	4.95
BaO	0.03	0.03	0.06	0.07	0.03	0.06
Na2O	9.86	9.84	9.96	9.26	9.15	8.81
K2O	0.17	0.28	0.25	0.27	0.27	0.23
Total	99.06	98.56	98.62	98.78	99.02	99.17
Ab	74.4	75.0	75.7	67.6	67.1	63.0
Or	1.3	2.2	1.9	2.0	1.8	1.6
An	24.3	22.8	22.4	30.4	31.1	35.4

	E1 Dyke Ande. 5	E1 Dyke Ande. 6	E1 Dyke Ande. 7	E1 Dyke Ande. 8C	E1 Dyke Ande. 9	E1 Dyke Ande. 10
SiO2	62.36	62.29	62.44	61.16	62.23	60.55
Al2O3	23.19	23.11	22.99	23.85	23.32	24.21
Fe2O3	0.13	0.11	0.22	0.14	0.19	0.19
MgO	-	-	-	-	-	-
CaO	4.23	4.22	4.24	5.11	4.22	5.56
BaO	0.04	-	-	0.09	0.05	0.02
Na2O	9.24	9.26	9.28	8.89	9.13	8.52
K2O	0.25	0.22	0.24	0.13	0.25	0.20
Total	99.44	99.21	99.41	99.37	99.39	99.25
Ab	67.3	67.6	67.4	62.9	67.1	60.0
Or	1.8	1.6	1.7	0.9	1..9	1.0
An	30.9	30.8	30.9	36.2	31.0	39.0

APPENDIX C

Table C.2: PLAGIOCLASE MICROPROBE ANALYSES

	E1 Dyke Olig. 11R	E1 Dyke Ande. 12	E1 Dyke Ande. 13	E1 Dyke Olig. 14M	E1 Dyke Ande. 15	E1 Dyke Olig. 16
SiO2	63.21	62.05	61.08	63.28	61.59	62.92
Al2O3	22.78	23.16	23.91	22.59	23.63	22.76
Fe2O3	0.11	0.16	0.09	0.14	0.15	0.15
MgO	-	-	-	-	-	-
CaO	3.75	4.09	5.01	3.36	4.77	3.69
BaO	0.08	-	0.02	0.09	0.05	-
Na20	9.68	9.26	8.75	9.72	8.84	9.53
K20	0.19	0.22	0.18	0.19	0.27	0.29
Total	99.8	98.94	99.04	99.37	99.3	99.34
Ab	71.1	68.2	62.8	73.2	63.7	70.5
Or	1.4	1.6	1.2	1.5	1.9	2.2
An	27.5	30.2	36.0	25.3	34.4	27.3

	E1 Dyke Olig. 17	E3 Dyke Olig. 1	E3 Dyke Ande. 2	E3 Dyke Olig. 3	E3 Dyke Olig. 4R	E3 Dyke Olig. 5R
SiO2	62.87	62.71	62.71	62.65	62.99	62.23
Al2O3	22.92	22.97	23.01	22.93	22.68	22.97
Fe2O3	0.13	0.12	0.13	0.09	0.23	0.19
MgO	-	-	-	-	-	-
CaO	3.83	3.99	4.12	3.76	3.93	4.04
BaO	0.09	-	0.03	0.02	0.08	0.07
Na20	9.34	9.41	9.28	9.42	9.45	9.29
K20	0.31	0.17	0.20	0.26	0.26	0.31
Total	99.49	99.37	99.48	99.13	99.62	99.1
Ab	69.3	69.3	68.2	70.1	69.3	68.1
Or	2.3	1.3	1.5	1.9	1.9	2.3
An	28.4	29.4	30.3	28.0	28.8	29.6

APPENDIX C

Table C.2: PLAGIOCLASE MICROPROBE ANALYSES

	E3 Dyke Olig. 6M	E3 Dyke Ande. 7C	E3 Dyke Ande. 8R	E3 Dyke Ande. 9R	E3 Dyke Olig. 10C	E3 Dyke Or. 11M
SiO2	63.99	61.04	62.51	61.54	62.29	63.58
Al2O3	22.24	23.92	22.70	23.32	22.93	18.96
Fe2O3	0.14	0.12	0.32	0.17	0.14	0.08
MgO	-	-	-	-	-	0.02
CaO	3.25	4.88	4.11	4.22	3.92	-
BaO	-	0.03	-	-	0.05	1.32
Na2O	9.85	8.66	9.33	9.16	9.33	0.85
K2O	0.24	0.42	0.27	0.33	0.30	14.96
Total	99.71	99.07	99.24	98.74	98.96	99.77
Ab	73.8	62.1	68.0	66.8	68.8	5.4
Or	1.8	3.2	2.0	2.4	2.2	94.6
An	24.3	34.7	30.0	30.8	29.0	-

	E3 Dyke Ande. 12M	E3 Dyke Olig. 13	E3 Dyke Olig. 14M	E3 Dyke Olig. 15	E3 Dyke Ande. 16	E5A Dyke Olig. 1
SiO2	62.13	62.36	61.76	62.83	61.59	64.06
Al2O3	23.26	23.00	23.15	22.76	23.24	22.26
Fe2O3	0.10	0.13	0.11	0.14	0.14	0.11
MgO	-	-	-	-	-	-
CaO	4.28	4.03	3.98	3.83	4.27	3.12
BaO	-	0.06	0.04	-	0.12	0.04
Na2O	9.24	9.42	9.34	9.53	9.25	9.81
K2O	0.23	0.25	0.19	0.23	0.24	0.23
Total	99.24	99.25	98.57	99.32	98.85	99.63
Ab	67.2	68.8	69.1	70.1	67.2	74.6
Or	1.7	1.8	1.5	1.7	1.8	1.8
An	31.1	29.4	29.4	28.2	31.0	23.6

APPENDIX C

Table C.2: PLAGIOCLASE MICROPROBE ANALYSES

	E5A Dyke Olig. 2	E5A Dyke Olig. 3	E5A Dyke Olig. 4	E5A Dyke Olig. 5M	E5A Dyke Olig. 6	E5A Dyke Ande. 7
SiO2	63.93	62.84	63.58	64.09	62.73	61.91
Al2O3	22.16	22.48	22.17	22.01	22.95	23.28
Fe2O3	0.10	0.09	0.14	0.15	0.10	0.18
MgO	-	-	-	-	-	-
CaO	3.23	3.31	3.31	2.83	3.86	4.28
BaO	0.06	0.07	-	-	-	0.04
Na2O	9.64	9.80	9.71	9.82	9.41	8.95
K2O	0.24	0.12	0.30	0.29	0.21	0.41
Total	99.36	98.71	99.21	99.19	99.26	99.05
Ab	73.5	74.1	72.9	75.8	69.8	65.6
Or	1.9	0.9	2.3	2.3	1.6	3.0
An	24.6	25.0	24.8	21.9	28.6	31.6

	E5A Dyke Ande. 8	E5A Dyke Ande. 9R	E5A Dyke Ande. 10	E5A Dyke Ande. 11	E5A Dyke Ande. 12	E5A Dyke Olig. 13
SiO2	62.75	61.16	61.98	62.46	61.62	62.64
Al2O3	22.81	23.02	23.35	22.94	22.85	22.71
Fe2O3	0.17	0.19	0.14	0.16	1.05	0.13
MgO	-	-	-	-	-	-
CaO	4.10	4.43	4.53	4.13	4.00	3.68
BaO	-	0.08	0.08	0.02	0.04	-
Na2O	9.09	8.91	8.80	9.06	9.33	9.47
K2O	0.40	0.37	0.44	0.43	0.39	0.13
Total	99.32	98.16	99.32	99.2	99.28	98.76
Ab	66.9	64.9	63.9	66.5	68.0	71.3
Or	2.9	2.7	3.2	3.2	2.8	1.0
An	30.2	32.4	32.9	30.3	29.2	27.7

APPENDIX C

Table C.2: PLAGIOCLASE MICROPROBE ANALYSES

	E5A Dyke Ande. 15M	L1 Dyke Olig. 1M	L1 Dyke Olig. 2	L1 Dyke Ande. 5M	L1 Dyke Olig. 6R	L1 Dyke Ande 7C
SiO2	62.16	63.03	62.08	61.74	63.42	61.87
Al2O3	23.16	23.05	23.14	23.63	22.31	23.48
Fe2O3	0.18	0.37	0.10	0.13	0.10	0.17
MgO	-	-	-	-	-	-
CaO	4.13	3.77	4.00	4.59	1.95	4.25
BaO	0.04	-	0.03	-	-	0.07
Na2O	9.36	9.64	9.52	8.81	8.49	8.98
K2O	0.19	0.26	0.15	0.21	1.06	0.42
Total	99.22	100.12	99.02	99.11	97.33	99.24
Ab	68.5	70.8	69.6	64.7	73.7	65.8
Or	1.4	1.9	1.1	1.8	9.2	3.1
An	30.1	27.7	29.3	33.7	17.1	31.1

APPENDIX C

Table C.3: BIOTITE MICROPROBE ANALYSES

	SGIII TGD Biot 1	SGIII TGD Biot 2	SGIII TGD Biot 3	SGIII TGD Biot 4	SGIII TGD Biot 5	SGIII TGD Biot 6
SiO2	37.29	37.23	37.14	37.38	37.44	36.67
TiO2	2.77	2.85	3.01	3.17	2.85	2.95
Al2O3	14.75	14.69	14.56	14.82	14.63	14.85
FeO*	16.95	16.73	17.30	17.05	17.15	17.09
MgO	13.52	13.38	13.41	13.06	13.39	13.23
MnO	0.22	0.22	0.25	0.22	0.23	0.23
CaO	-	-	-	-	-	-
Na2O	0.11	0.10	0.10	0.11	0.12	0.14
K2O	9.49	9.52	9.48	9.42	9.55	9.56
F	0.28	0.41	0.39	0.33	0.38	0.23
Total	95.38	95.13	95.64	95.56	95.74	94.95
Structural Formulae						
Si	5.619	5.622	5.596	5.621	5.627	5.568
Al(iv)	2.380	2.378	2.404	2.379	2.373	2.431
Al(vi)	0.239	0.237	0.182	0.247	0.218	0.227
Ti	0.314	0.324	0.341	0.359	0.322	0.337
Fe2+	2.137	2.113	2.181	2.144	2.156	2.171
Mn	0.028	0.028	0.032	0.028	0.029	0.029
Mg	3.038	3.013	3.011	2.927	3.002	2.994
Ca	-	-	-	-	-	-
Na	0.033	0.029	0.030	0.033	0.036	0.041
K	1.826	1.834	1.822	1.806	1.831	1.853

	SGIII TGD Biot 7	SGIII TGD Biot 8	SGVII Late Biot 1	SGVII Late Biot 2	SGVII Late Biot 3	SGVII Late Biot 4
SiO2	37.11	37.34	37.44	37.01	37.28	37.29
TiO2	2.31	3.05	2.53	2.53	2.47	2.72
Al2O3	14.98	14.79	14.67	14.65	14.83	14.67
FeO*	17.31	16.76	17.43	17.57	17.73	17.67
MgO	13.62	13.49	13.43	13.05	13.27	13.25
MnO	0.26	0.24	0.26	0.26	0.26	0.28
CaO	-	-	-	-	-	-
Na2O	0.12	0.16	0.09	0.06	0.08	0.11
K2O	9.46	9.37	9.46	9.40	9.28	9.39
F	0.33	0.26	0.33	0.33	0.28	0.40
Total	95.50	95.46	95.64	94.86	95.48	95.78
Structura						
Si	5.597	5.614	5.637	5.627	5.625	5.613
Al(iv)	2.403	2.286	2.362	2.373	2.375	2.387
Al(vi)	0.261	0.235	0.241	0.252	0.262	0.217
Ti	0.262	0.345	0.287	0.289	0.281	0.308
Fe2+	2.183	2.108	2.194	2.234	2.373	2.225
Mn	0.033	0.031	0.033	0.033	0.034	0.035
Mg	3.061	3.024	3.014	2.958	2.985	2.974
Ca	-	-	-	-	-	-
Na	0.360	0.046	0.026	0.019	0.023	0.033
K	1.821	1.797	1.816	1.823	1.786	1.804

APPENDIX C

Table C.3: BIOTITE MICROPROBE ANALYSES

	SGVII Late Biot 6	SGVII Late Biot 7	SGVII Late Biot 8	SGVII Late Biot 9	SGVIII Late Biot 1	SGVIII Late Biot 2
SiO2	37.24	37.02	37.14	36.94	36.40	36.92
TiO2	2.50	2.18	2.92	2.75	2.95	3.14
Al2O3	14.42	14.89	14.42	14.41	14.52	14.51
FeO*	17.39	17.66	17.96	17.85	18.63	17.62
MgO	13.31	13.87	13.17	13.15	13.04	12.79
MnO	0.27	0.25	0.26	0.27	0.25	0.25
CaO	-	-	-	-	-	-
Na2O	0.09	0.11	0.11	0.10	0.11	0.07
K2O	9.39	8.40	9.19	9.24	8.42	9.04
F	0.51	0.31	0.38	0.24	0.43	0.35
Total	95.12	94.69	95.55	94.95	94.75	94.69
Structura						
Si	5.640	5.606	5.611	5.619	5.548	5.615
Al(iv)	2.359	2.394	2.389	2.381	2.452	2.385
Al(vi)	0.215	0.264	0.178	0.201	0.156	0.215
Ti	0.285	0.248	0.331	0.314	0.338	0.359
Fe2+	2.203	2.237	2.269	2.270	2.375	2.242
Mn	0.034	0.032	0.034	0.035	0.032	0.033
Mg	3.005	3.131	2.965	2.982	2.963	2.899
Ca	-	-	-	-	-	-
Na	0.028	0.032	0.031	0.029	0.031	0.022
K	1.814	1.623	1.772	1.794	1.638	1.754

	SGVIII Late Biot 3	SGVIII Late Biot 4	SGVIII Late Biot 5	SGVIII Late Biot 6	SGVIII Late Biot 8	SGIX TGD Biot 1R
SiO2	37.00	37.13	35.88	37.43	36.52	37.31
TiO2	3.20	3.19	2.63	2.79	3.43	2.98
Al2O3	14.34	14.47	14.69	14.64	14.45	13.58
FeO*	17.78	18.01	18.58	17.61	17.83	16.99
MgO	12.68	12.72	13.37	13.01	12.09	13.29
MnO	0.25	0.21	0.22	0.21	0.24	0.24
CaO	-	-	-	-	-	-
Na2O	0.10	0.07	0.08	0.08	0.01	0.13
K2O	9.42	9.44	8.12	9.57	9.23	9.84
F	0.39	0.34	0.16	0.32	0.37	-
Total	95.16	95.58	93.73	95.66	94.17	94.36
Structura						
Si	5.618	5.614	5.524	5.643	5.599	5.970
Al(iv)	2.382	2.385	2.475	2.358	2.401	2.030
Al(vi)	0.184	0.194	0.191	0.244	0.210	0.532
Ti	0.366	0.363	0.304	0.316	0.396	0.359
Fe2+	2.258	2.277	2.392	2.221	2.287	2.275
Mn	0.031	0.027	0.028	0.026	0.031	0.033
Mg	2.869	2.867	3.069	2.923	2.764	3.169
Ca	-	-	-	-	-	-
Na	0.030	0.020	0.023	0.023	0.029	0.042
K	1.824	1.822	1.595	1.840	1.806	2.009

APPENDIX C

Table C.3: BIOTITE MICROPROBE ANALYSES

	SGIX TGD Biot 2C	SGIX TGD Biot 3	SGX Late Biot 1	SGX Late Biot 2	SGX Late Biot 3	SGX Late Biot 4
SiO2	37.14	37.37	36.49	37.23	37.35	36.95
TiO2	3.45	3.49	2.44	2.67	2.55	2.65
Al2O3	13.38	13.58	14.36	14.59	14.41	14.46
FeO*	17.47	17.12	18.04	17.31	17.55	18.09
MgO	13.11	13.20	13.34	13.41	13.45	13.30
MnO	0.24	0.24	0.25	0.28	0.29	0.29
CaO	-	-	-	-	-	-
Na2O	0.10	0.07	0.07	0.09	0.09	0.08
K2O	9.86	9.97	9.11	9.35	9.18	9.15
F	-	-	0.43	0.51	0.44	0.37
Total	94.75	95.04	94.53	95.44	95.31	95.34
Structura						
Si	5.938	5.943	5.582	5.615	5.642	5.599
Al(iv)	2.062	2.057	2.418	2.285	2.358	2.401
Al(vi)	0.460	0.489	0.171	0.208	0.207	0.181
Ti	0.415	0.418	0.281	0.303	0.290	0.302
Fe2+	2.336	2.277	2.307	2.182	2.217	2.292
Mn	0.033	0.033	0.033	0.037	0.037	0.037
Mg	3.124	3.129	3.042	3.015	3.028	3.004
Ca	-	-	-	-	-	-
Na	0.033	0.024	0.022	0.027	0.026	0.025
K	2.012	2.024	1.777	1.800	1.770	1.769

	SGX Late Biot 5	SGX Late Biot 6	SGX Late Biot 7	SGX Late Biot 8	SGX Late Biot 9	SGX Late Biot 10
SiO2	37.05	36.85	37.02	36.28	36.99	36.97
TiO2	2.62	2.73	2.85	2.62	2.52	2.86
Al2O3	14.35	14.48	14.28	14.34	14.49	14.50
FeO*	18.27	18.13	18.45	18.99	18.31	17.82
MgO	13.38	13.28	13.08	13.49	13.32	13.15
MnO	0.26	0.26	0.26	0.28	0.28	0.34
CaO	-	-	-	-	-	-
Na2O	0.06	0.09	0.10	0.06	0.09	0.09
K2O	8.78	9.04	9.06	9.15	8.77	9.32
F	0.34	0.42	0.25	0.31	0.31	0.35
Total	95.11	95.28	95.35	95.52	95.08	95.40
Structura						
Si	5.618	5.587	5.616	5.548	5.613	5.599
Al(iv)	2.381	2.413	2.383	2.452	2.387	2.401
Al(vi)	0.184	0.174	0.170	0.132	0.206	0.187
Ti	0.298	0.311	0.323	0.302	0.287	0.325
Fe2+	2.317	2.298	2.341	2.429	2.323	2.257
Mn	0.034	0.033	0.033	0.036	0.036	0.044
Mg	3.024	2.999	2.958	3.076	3.012	2.968
Ca	-	-	-	-	-	-
Na	0.017	0.028	0.029	0.018	0.028	0.026
K	1.699	1.749	1.755	1.591	1.697	1.801

APPENDIX C

Table C.3: BIOTITE MICROPROBE ANALYSES

	SGX Late Biot 11	SGXIII TGD Biot	SGXIII TGD Biot 1C	SGXIII TGD Biot 2M	SGXIII TGD Biot 3C	SGXIII TGD Biot 4C
SiO2	37.08	37.75	37.57	37.36	37.36	37.56
TiO2	3.94	2.42	2.64	2.73	3.07	2.81
Al2O3	13.83	14.19	14.08	14.06	13.85	14.21
FeO*	18.20	17.02	17.53	17.03	17.44	17.01
MgO	12.69	13.27	12.97	13.36	12.95	13.08
MnO	0.27	0.27	0.25	0.22	0.24	0.27
CaO	-	-	-	0.01	-	-
Na2O	0.14	0.14	0.09	0.11	0.12	0.09
K2O	9.18	9.70	9.79	9.80	9.71	9.78
F	-	-	-	-	-	-
Total	95.33	94.76	94.92	94.68	94.74	94.81
Structura						
Si	5.592	5.996	5.978	5.951	5.957	5.968
Al(iv)	2.408	2.004	2.022	2.049	2.043	2.032
Al(vi)	0.050	0.654	0.620	0.592	0.561	0.630
Ti	0.446	0.290	0.317	0.328	0.369	0.337
Fe2+	2.295	2.262	2.332	2.269	2.326	2.260
Mn	0.034	0.036	0.034	0.031	0.033	0.037
Mg	2.852	3.142	3.076	3.171	3.077	3.098
Ca	-	-	-	0.001	-	-
Na	0.042	0.045	0.029	0.036	0.037	0.029
K	1.767	1.966	1.988	1.992	1.977	1.984

	SGXIII TGD Biot 1	SGXIII TGD Biot 2	SGXIII TGD Biot 3	SGXIII TGD Biot 4	SGXIII TGD Biot 5	SGXIII TGD Biot 6
SiO2	37.26	37.56	37.34	37.54	37.08	37.32
TiO2	2.79	2.65	2.87	2.84	2.85	2.61
Al2O3	14.56	14.57	14.52	14.74	14.39	14.51
FeO*	16.70	16.91	16.95	16.82	17.01	16.99
MgO	13.85	13.90	13.74	13.58	13.52	13.71
MnO	0.24	0.25	0.21	0.23	0.21	0.24
CaO	-	-	-	-	-	-
Na2O	0.07	0.08	0.10	0.11	0.08	0.11
K2O	9.47	9.42	9.53	9.51	9.31	9.36
F	0.37	0.35	0.26	0.25	0.18	0.32
Total	95.31	95.69	95.52	95.62	94.63	95.17
Structura						
Si	5.616	5.635	5.622	5.638	5.633	5.636
Al(iv)	2.384	2.364	2.378	2.362	2.367	2.364
Al(vi)	0.201	0.214	0.199	0.246	0.211	0.218
Ti	0.317	0.299	0.325	0.321	0.326	0.297
Fe2+	2.105	2.122	2.135	2.112	2.162	2.147
Mn	0.030	0.032	0.027	0.029	0.027	0.031
Mg	3.111	3.108	3.083	3.041	3.062	3.087
Ca	-	-	-	-	-	-
Na	0.019	0.025	0.030	0.033	0.025	0.031
K	1.821	1.804	1.830	1.823	1.804	1.805

APPENDIX C

Table C.3: BIOTITE MICROPROBE ANALYSES

	SGXIII TGD Biot 7	SGXIII TGD Biot 8	SGXIII TGD Biot 9	SGXIII TGD Biot 10	SGXXVI TGD Biot 1R	SGXXVI TGD Biot 2
SiO2	37.44	37.27	37.29	37.53	36.84	35.53
TiO2	2.89	2.63	2.59	2.69	2.81	1.78
Al2O3	14.67	14.87	14.56	14.90	13.85	14.28
FeO*	16.65	16.69	15.91	16.56	18.89	19.43
MgO	13.66	13.64	14.13	13.80	12.72	14.27
MnO	0.23	0.23	0.24	0.28	0.35	0.36
CaO	-	-	-	-	0.01	0.01
Na2O	0.08	0.11	0.10	0.09	0.13	0.06
K2O	9.41	9.44	9.05	9.43	9.23	7.66
F	0.39	0.29	0.31	0.31	-	-
Total	95.42	95.17	94.18	95.59	94.83	93.38
Structura						
Si	5.627	5.620	5.652	5.627	5.906	5.763
Al(iv)	2.373	2.380	2.348	2.373	2.094	2.237
Al(vi)	0.225	0.264	0.253	0.260	0.524	0.495
Ti	0.327	0.298	0.295	0.303	0.340	0.219
Fe2+	2.093	2.105	2.016	2.077	2.533	2.636
Mn	0.029	0.029	0.032	0.036	0.049	0.050
Mg	3.061	3.066	3.192	3.085	3.038	3.450
Ca	-	-	-	-	0.002	0.003
Na	0.025	0.031	0.030	0.029	0.042	0.019
K	1.805	1.816	1.750	1.803	1.889	1.587

	SGXXVI TGD Biot 3C	SGXXVI TGD Biot 4	G24 TGD Biot 1C	G24 TGD Biot 2C	G24 TGD Biot 3M	G24 TGD Biot 4C
SiO2	36.83	36.42	37.00	37.39	33.07	37.20
TiO2	2.14	2.45	3.19	3.03	1.57	3.00
Al2O3	14.26	13.97	14.43	14.42	15.14	14.61
FeO*	18.72	18.78	17.07	17.28	19.03	17.31
MgO	12.98	13.07	12.66	12.78	16.17	12.64
MnO	0.36	0.38	0.26	0.26	0.31	0.27
CaO	0.02	0.02	-	0.01	0.09	0.01
Na2O	0.07	0.18	0.09	0.09	0.08	0.15
K2O	9.15	8.58	9.94	9.95	4.31	9.92
F	-	-	-	-	-	-
Total	94.53	93.85	94.64	95.21	89.77	95.11
Structura						
Si	5.909	5.882	5.906	5.931	5.493	5.910
Al(iv)	2.091	2.118	2.094	2.069	2.507	2.090
Al(vi)	0.608	0.543	0.621	0.626	0.458	0.646
Ti	0.260	0.298	0.383	0.362	0.197	0.359
Fe2+	2.512	2.537	2.279	2.293	2.644	2.300
Mn	0.050	0.052	0.035	0.036	0.044	0.037
Mg	3.105	3.147	3.012	3.021	4.002	2.994
Ca	0.004	0.004	-	0.003	0.018	0.002
Na	0.023	0.056	0.031	0.029	0.027	0.048
K	1.875	1.770	2.025	2.014	0.915	2.011

APPENDIX C

Table C.3: BIOTITE MICROPROBE ANALYSES

	G24 TGD Biot 5C	G24 TGD Biot 6C	G24 TGD Biot 7M	G24 TGD Biot 8M	SG49 PGD Biot 1	SG49 PGD Biot 2
SiO2	37.38	36.83	37.23	36.76	36.59	37.28
TiO2	3.02	3.18	2.97	2.97	2.59	2.70
Al2O3	14.44	14.25	14.43	14.56	14.63	14.60
FeO*	17.25	17.38	17.28	17.57	16.94	16.10
MgO	12.89	12.62	12.84	12.73	14.22	13.84
MnO	0.25	0.29	0.24	0.27	0.34	0.27
CaO	-	0.01	-	-	-	-
Na2O	0.10	0.18	0.11	0.09	0.11	0.12
K2O	9.94	9.70	9.72	9.89	8.59	9.36
F	-	-	-	-	0.35	0.44
Total	95.27	94.44	94.82	94.84	94.36	94.71
Structura						
Si	5.923	5.899	5.924	5.870	5.562	5.633
Al(iv)	2.077	2.101	2.076	2.310	2.438	2.366
Al(vi)	0.622	0.590	0.631	0.612	0.182	0.234
Ti	0.361	0.383	0.356	0.358	0.296	0.307
Fe2+	2.287	2.329	2.299	2.347	2.153	2.034
Mn	0.035	0.040	0.033	0.037	0.044	0.035
Mg	3.045	3.014	3.047	3.029	3.221	3.118
Ca	-	0.002	-	-	-	-
Na	0.032	0.057	0.033	0.031	0.031	0.034
K	2.009	1.983	1.974	2.015	1.667	1.806

	SG49 PGD Biot 3	SG49 PGD Biot 4	SG49 PGD Biot 5	SG49 PGD Biot 6	SG49 PGD Biot 7	SG49 PGD Biot 8
SiO2	37.40	36.74	37.74	37.48	37.36	37.24
TiO2	2.78	2.64	2.55	2.62	2.25	2.93
Al2O3	14.92	15.03	14.78	14.71	14.87	14.79
FeO*	16.43	15.97	16.41	17.35	16.61	17.06
MgO	13.29	13.77	13.78	13.37	13.77	13.16
MnO	0.31	0.38	0.32	0.33	0.30	0.32
CaO	-	-	-	-	-	-
Na2O	0.09	0.09	0.11	0.09	0.11	0.10
K2O	9.45	9.02	9.65	9.40	9.35	9.47
F	0.34	0.49	0.57	0.42	0.36	0.54
Total	95.01	94.13	95.91	95.77	94.98	95.61
Structura						
Si	5.641	5.579	5.642	5.632	5.639	5.604
Al(iv)	2.359	2.421	2.358	2.368	2.361	2.396
Al(vi)	0.293	0.269	0.246	0.237	0.285	0.226
Ti	0.316	0.302	0.287	0.296	0.256	0.332
Fe2+	2.073	2.028	2.051	2.181	2.097	2.146
Mn	0.039	0.049	0.040	0.041	0.039	0.041
Mg	2.987	3.117	3.071	2.995	3.099	2.953
Ca	-	-	-	-	-	-
Na	0.028	0.027	0.031	0.280	0.034	0.029
K	1.818	1.747	1.841	1.802	1.800	1.819

APPENDIX C

Table C.3: BIOTITE MICROPROBE ANALYSES

	SG49 PGD Biot 9	SG49 PGD Biot 10	SG78 BGT Biot 1	SG78 BGT Biot 2	SG78 BGT Biot 3	SG78 BGT Biot 4
SiO2	37.29	37.39	36.86	36.97	36.57	36.89
TiO2	2.41	2.62	3.12	3.04	2.87	2.66
Al2O3	14.81	14.66	14.95	14.54	14.68	14.81
FeO*	16.96	16.72	17.54	17.98	17.99	18.45
MgO	13.36	13.49	12.01	12.41	12.12	12.01
MnO	0.29	0.26	0.31	0.36	0.38	0.39
CaO	-	-	-	-	-	-
Na2O	0.09	0.08	0.09	0.11	0.10	0.10
K2O	9.59	9.46	9.71	9.23	9.63	9.75
F	0.42	0.38	0.87	1.06	1.17	1.30
Total	95.22	95.06	95.46	95.70	95.51	96.36
Structura						
Si	5.634	5.646	5.579	5.580	5.549	5.580
Al(iv)	2.366	2.354	2.421	2.419	2.450	2.419
Al(vi)	0.270	0.254	0.245	0.167	0.176	0.222
Ti	0.273	0.298	0.355	0.345	0.327	0.303
Fe2+	2.142	2.112	2.220	2.270	2.284	2.335
Mn	0.038	0.034	0.040	0.046	0.049	0.051
Mg	3.008	3.037	2.709	2.793	2.742	2.709
Ca	-	-	-	-	-	-
Na	0.028	0.025	0.029	0.032	0.031	0.030
K	1.848	1.822	1.875	1.778	1.864	1.881

	SG78 BGT Biot 5	SG78 BGT Biot 6	SG78 BGT Biot 7	SG78 BGT Biot 8	SG78 BGT Biot 9	SG93 TGD Biot 1
SiO2	36.86	37.05	37.29	37.30	37.14	37.26
TiO2	3.01	3.18	2.86	2.52	2.93	4.13
Al2O3	14.67	14.64	14.95	14.78	14.67	14.24
FeO*	18.11	18.23	17.45	17.45	17.73	15.96
MgO	12.27	12.08	12.48	12.68	12.67	13.80
MnO	0.35	0.36	0.39	0.31	0.37	0.15
CaO	-	-	-	-	-	-
Na2O	0.11	0.10	0.13	0.12	0.12	0.13
K2O	9.62	9.67	9.62	9.43	9.61	9.50
F	0.70	0.51	0.76	0.87	0.93	0.06
Total	95.70	95.82	95.93	95.46	96.17	95.23
Structura						
Si	5.582	5.604	5.606	5.628	5.582	5.605
Al(iv)	2.418	2.395	2.394	2.371	2.418	2.395
Al(vi)	0.200	0.214	0.255	0.257	0.181	0.129
Ti	0.343	0.362	0.323	0.286	0.331	0.467
Fe2+	2.293	2.306	2.195	2.202	2.228	2.007
Mn	0.045	0.046	0.049	0.039	0.047	0.019
Mg	2.769	2.725	2.797	2.852	2.838	3.095
Ca	-	-	-	-	-	-
Na	0.032	0.031	0.038	0.035	0.036	0.037
K	1.858	1.867	1.846	1.815	1.841	1.824

APPENDIX C

Table C.3: BIOTITE MICROPROBE ANALYSES

	SG93 TGD Biot 2	SG93 TGD Biot 3	SG93 TGD Biot 4	SG93 TGD Biot 5	SG93 TGD Biot 6	SG93 TGD Biot 7
SiO2	37.17	37.28	37.32	37.06	36.89	37.24
TiO2	4.24	3.80	3.59	3.78	3.85	3.55
Al2O3	14.23	14.56	14.39	14.40	14.40	14.24
FeO*	15.91	15.37	15.42	15.37	15.40	15.59
MgO	13.63	14.18	14.21	14.21	13.80	14.29
MnO	0.15	0.19	0.17	0.16	0.18	0.16
CaO	-	-	-	-	-	-
Na2O	0.12	0.12	0.12	0.13	0.11	0.12
K2O	9.56	9.54	9.49	9.34	9.58	9.39
F	0.17	0.19	0.24	0.28	0.25	0.32
Total	95.18	95.23	94.95	94.73	94.46	94.90
Structura						
Si	5.596	5.590	5.613	5.584	5.586	5.607
Al(iv)	2.404	2.409	2.387	2.415	2.413	2.392
Al(vi)	0.121	0.165	0.164	0.143	0.157	0.135
Ti	0.480	0.429	0.407	0.428	0.439	0.402
Fe2+	2.003	1.927	1.939	1.937	1.950	1.963
Mn	0.019	0.025	0.022	0.021	0.023	0.021
Mg	3.059	3.170	3.186	3.192	3.116	3.206
Ca	-	-	-	-	-	-
Na	0.035	0.036	0.034	0.039	0.033	0.035
K	1.836	1.825	1.820	1.796	1.849	1.805

	SG93 TGD Biot 8	SG93 TGD Biot 9	SG93 TGD Biot 10	SG93 TGD Biot 11	SG93 TGD Biot 12	D1 Rubh. Biot 1M
SiO2	37.02	37.05	37.42	37.20	37.38	38.40
TiO2	3.53	3.52	3.37	3.24	3.42	2.91
Al2O3	14.32	14.44	14.52	14.26	14.68	13.84
FeO*	15.62	15.90	15.94	16.00	15.94	14.24
MgO	14.13	13.79	13.90	14.25	13.88	14.94
MnO	0.16	0.18	0.18	0.17	0.20	0.14
CaO	-	-	-	-	-	-
Na2O	0.12	0.12	0.13	0.11	0.12	0.16
K2O	9.49	9.44	9.49	9.34	9.53	9.62
F	0.27	0.28	0.18	0.33	0.17	-
Total	94.66	94.72	95.13	94.90	95.32	94.25
Structura						
Si	5.595	5.601	5.627	5.611	5.612	6.039
Al(iv)	2.405	2.398	2.372	2.388	2.387	1.961
Al(vi)	0.146	0.174	0.201	0.146	0.209	0.606
Ti	0.401	0.400	0.381	0.367	0.386	0.345
Fe2+	1.975	2.011	2.005	2.018	2.001	1.873
Mn	0.021	0.023	0.023	0.021	0.026	0.020
Mg	3.184	3.106	3.117	3.204	3.107	3.502
Ca	-	-	-	-	-	-
Na	0.036	0.036	0.037	0.033	0.035	0.050
K	1.829	1.821	1.821	1.798	1.825	1.930

APPENDIX C

Table C.3: BIOTITE MICROPROBE ANALYSES

	D1 Rubh. Biot 2M	D1 Rubh. Biot 3M	D1 Rubh. Biot 4M	D1 Rubh. Biot 5M	D1 Rubh. Biot 6C	D1 Rubh. Biot 7M
SiO2	38.47	38.47	38.53	38.47	38.98	38.85
TiO2	3.33	2.94	3.04	3.05	3.17	3.14
Al2O3	13.88	13.89	13.75	13.76	13.84	14.00
FeO*	14.54	14.30	14.82	14.39	14.54	14.33
MgO	14.84	14.94	14.97	14.89	14.44	14.91
MnO	0.15	0.14	0.16	0.14	0.13	0.14
CaO	-	-	0.05	-	0.01	-
Na2O	0.18	0.23	0.13	0.12	0.20	0.24
K2O	9.44	9.41	9.28	9.77	9.61	9.42
F	-	-	-	-	-	-
Total	94.83	94.32	94.73	94.59	94.92	95.03
Structura						
Si	6.015	6.040	6.033	6.037	6.085	6.047
Al(iv)	1.985	1.960	1.967	1.963	1.915	1.953
Al(vi)	0.573	0.612	0.571	0.583	0.632	0.617
Ti	0.393	0.348	0.358	0.360	0.373	0.368
Fe2+	1.901	1.878	1.941	1.889	1.899	1.866
Mn	0.021	0.019	0.021	0.019	0.018	0.020
Mg	3.459	3.496	3.494	3.484	3.361	3.460
Ca	-	-	0.010	-	0.002	-
Na	0.057	0.071	0.040	0.038	0.062	0.073
K	1.884	1.885	1.855	1.957	1.915	1.872

	D1 Rubh. Biot 8R	D1 Rubh. Biot 9M	D1 Rubh. Biot 10M	D2 Rubh. Biot 1R	D2 Rubh. Biot 2C	D2 Rubh. Biot 3C
SiO2	38.74	38.19	38.28	37.52	38.39	36.71
TiO2	3.18	2.77	3.22	3.32	3.33	2.93
Al2O3	13.87	14.03	13.89	13.56	13.97	14.50
FeO*	13.99	14.08	13.99	13.46	13.62	14.18
MgO	15.08	15.16	15.03	15.09	15.69	16.36
MnO	0.15	0.15	0.14	0.15	0.15	0.14
CaO	-	-	-	-	-	0.13
Na2O	0.14	0.13	0.25	0.17	0.14	0.09
K2O	9.64	9.50	9.44	9.49	9.74	7.97
F	-	-	-	-	-	-
Total	94.79	94.01	94.24	92.76	95.03	93.01
Structura						
Si	6.046	6.015	6.011	5.988	5.976	5.818
Al(iv)	1.954	1.985	1.989	2.012	2.024	2.182
Al(vi)	0.598	0.620	0.584	0.540	0.541	0.527
Ti	0.374	0.329	0.381	0.400	0.390	0.350
Fe2+	1.827	1.855	1.839	1.797	1.773	1.880
Mn	0.020	0.020	0.019	0.021	0.021	0.019
Mg	3.508	3.557	3.518	3.589	3.642	3.864
Ca	-	-	-	-	-	0.023
Na	0.042	0.041	0.077	0.053	0.042	0.029
K	1.920	1.910	1.891	1.934	1.935	1.612

APPENDIX C

Table C.3: BIOTITE MICROPROBE ANALYSES

	D2 Rubh. Biot 4C	D2 Rubh. Biot. 5M	D2 Rubh. Biot 6C	D2 Rubh. Biot 7M	D8 Rubh. Biot 1	D8 Rubh. Biot 2
SiO2	38.42	38.35	38.32	38.33	37.29	38.35
TiO2	3.13	3.36	3.02	2.59	3.13	2.86
Al2O3	14.05	14.09	13.78	14.17	14.76	14.42
FeO*	13.65	14.11	14.02	13.27	12.13	11.83
MgO	15.71	15.15	15.01	16.22	17.59	17.86
MnO	0.13	0.15	0.13	0.12	0.12	0.09
CaO	-	-	-	-	-	-
Na2O	0.11	0.09	0.17	0.10	0.04	0.41
K2O	9.48	9.81	9.77	9.57	8.21	8.60
F	-	-	-	-	0.14	0.13
Total	94.68	95.11	94.22	94.37	93.41	94.55
Structura						
Si	5.990	5.979	6.030	5.989	5.553	5.654
Al(iv)	2.010	2.021	1.970	2.011	2.447	2.345
Al(vi)	0.573	0.568	0.587	0.600	0.144	0.161
Ti	0.368	0.395	0.358	0.306	0.351	0.317
Fe2+	1.781	1.840	1.845	1.735	1.510	1.458
Mn	0.018	0.020	0.019	0.017	0.014	0.012
Mg	3.651	3.521	3.521	3.777	3.904	3.924
Ca	-	-	-	-	-	-
Na	0.036	0.030	0.053	0.030	0.116	0.117
K	1.888	1.953	1.962	1.908	1.560	1.618

	D8 Rubh. Biot 3	D8 Rubh. Biot 4	D8 Rubh. Biot 5	D8 Rubh. Biot 6	D8 Rubh. Biot 7	D8 Rubh. Biot 8
SiO2	38.24	38.38	38.14	38.39	38.34	38.38
TiO2	2.93	2.67	2.51	2.89	2.40	2.78
Al2O3	14.88	14.88	14.65	14.45	14.88	14.55
FeO*	11.93	11.89	11.62	11.56	11.50	11.69
MgO	17.84	17.94	18.29	17.95	18.31	18.01
MnO	0.10	0.10	0.09	0.10	0.12	0.12
CaO	-	-	-	-	-	-
Na2O	0.43	0.42	0.31	0.42	0.43	0.42
K2O	8.80	8.82	8.93	8.73	8.80	8.70
F	0.18	0.18	0.25	0.14	0.16	0.17
Total	95.33	95.28	94.79	94.63	94.94	94.82
Structura						
Si	5.602	5.621	5.615	5.653	5.627	5.643
Al(iv)	2.398	2.378	2.385	2.346	2.373	2.356
Al(vi)	0.171	0.191	0.158	0.161	0.200	0.164
Ti	0.323	0.294	0.278	0.319	0.265	0.308
Fe2+	1.461	1.457	1.431	1.424	1.411	1.437
Mn	0.013	0.012	0.012	0.013	0.015	0.014
Mg	3.896	3.917	4.013	3.939	4.005	3.946
Ca	-	-	-	-	-	-
Na	0.121	0.121	0.090	0.119	0.123	0.120
K	1.644	1.647	1.677	1.640	1.648	1.632

APPENDIX C

Table C.3: BIOTITE MICROPROBE ANALYSES

	D8 Rubh. Biot 9	D8 Rubh. Biot 10	D8 Rubh. Biot 11	D8 Rubh. Biot 12	D8 Rubh. Biot 13	D8 Rubh. Biot 14
SiO2	38.62	37.63	37.34	38.33	37.34	37.44
TiO2	1.54	3.05	2.94	2.10	3.30	3.28
Al2O3	14.98	14.52	14.60	14.99	14.98	14.99
FeO*	11.08	12.09	12.07	11.28	11.99	12.05
MgO	18.94	17.98	17.58	18.17	17.36	17.19
MnO	0.09	0.11	0.11	0.09	0.08	0.12
CaO	-	-	-	-	-	-
Na2O	0.38	0.44	0.25	0.33	0.49	0.45
K2O	8.82	8.08	9.33	8.86	8.80	8.71
F	0.25	0.29	0.20	0.19	0.17	0.18
Total	94.70	94.19	94.42	94.34	94.51	94.41
Structura						
Si	5.663	5.572	5.556	5.651	5.533	5.550
Al(iv)	2.337	2.427	2.443	2.349	2.467	2.449
Al(vi)	0.253	0.106	0.117	0.256	0.149	0.169
Ti	0.169	0.339	0.329	0.233	0.368	0.365
Fe2+	1.359	1.497	1.502	1.391	1.486	1.494
Mn	0.012	0.130	0.014	0.011	0.010	0.015
Mg	4.140	3.967	3.900	3.993	3.834	3.798
Ca	-	-	-	-	-	-
Na	0.107	0.127	0.073	0.095	0.140	0.130
K	1.650	1.526	1.770	1.666	1.663	1.647

	D11 Lidd. Biot 1	D11 Lidd. Biot 2	D11 Lidd. Biot 3	D11 Lidd. Biot 4	D11 Lidd. Biot 5	D11 Lidd. Biot 8
SiO2	37.93	38.12	37.44	37.73	37.87	38.34
TiO2	2.80	3.32	2.84	4.38	2.09	3.29
Al2O3	14.93	14.82	15.14	14.29	14.70	14.57
FeO*	12.99	11.91	12.94	12.79	13.92	12.35
MgO	16.58	17.39	16.73	16.12	16.31	17.02
MnO	0.07	0.07	0.09	0.05	0.08	0.08
CaO	-	-	-	-	-	-
Na2O	0.22	0.43	0.22	0.43	0.13	0.38
K2O	9.12	8.51	9.10	8.51	8.97	8.62
F	0.25	0.29	0.34	0.27	0.28	0.19
Total	94.89	94.86	94.84	94.57	94.35	94.84
Structura						
Si	5.617	5.601	5.553	5.596	5.659	5.647
Al(iv)	2.383	2.398	2.447	2.403	2.340	2.352
Al(vi)	0.223	0.169	0.199	0.096	0.248	0.177
Ti	0.312	0.366	0.317	0.489	0.235	0.365
Fe2+	1.609	1.463	1.605	1.586	1.739	1.522
Mn	0.008	0.009	0.012	0.006	0.009	0.010
Mg	3.660	3.809	3.698	3.563	3.633	3.737
Ca	-	-	-	-	-	-
Na	0.063	0.124	0.062	0.124	0.037	0.108
K	1.724	1.596	1.722	1.609	1.711	1.619

APPENDIX C

Table C.3: BIOTITE MICROPROBE ANALYSES

	D11 Lidd. Biot 9	D11 Lidd. Biot 10	D11 Lidd. Biot 12	D12 Lidd. Biot 1M	D12 Lidd. Biot 2R	D12 Lidd. Biot 3R
SiO2	37.85	37.49	36.92	37.64	37.38	37.56
TiO2	3.69	3.48	3.39	2.58	2.58	2.95
Al2O3	14.43	14.84	15.01	14.53	14.79	14.41
FeO*	12.48	10.32	13.03	14.07	14.55	14.36
MgO	16.69	18.58	16.14	15.78	15.13	15.42
MnO	0.07	0.07	0.08	0.13	0.15	0.15
CaO	-	-	-	-	-	-
Na2O	0.39	0.37	0.39	0.21	0.18	0.17
K2O	8.77	8.92	8.45	9.71	9.64	9.68
F	0.29	0.22	0.16	-	-	-
Total	94.66	94.29	93.57	94.65	94.40	94.70
Structura						
Si	5.604	5.525	5.542	5.903	5.891	5.897
Al(iv)	2.396	2.474	2.458	2.097	2.109	2.103
Al(vi)	0.122	0.104	0.198	0.590	0.640	0.565
Ti	0.411	0.386	0.384	0.305	0.306	0.349
Fe2+	1.545	1.272	1.636	1.847	1.918	1.886
Mn	0.008	0.009	0.009	0.018	0.021	0.021
Mg	3.683	4.082	3.612	3.688	3.553	3.608
Ca	-	-	-	-	-	-
Na	0.111	0.106	0.114	0.064	0.055	0.052
K	1.657	1.677	1.619	1.944	1.938	1.939

	D12 Lidd. Biot 6R	D12 Lidd. Biot 7C	D12 Lidd. Biot 8M	D19 Shet. Biot 1	D19 Shet. Biot 2	D19 Shet. Biot 3
SiO2	37.68	37.53	36.97	37.25	37.31	37.20
TiO2	3.20	2.66	3.11	3.55	3.74	3.31
Al2O3	14.41	14.56	14.50	14.91	14.86	14.99
FeO*	14.75	14.24	14.56	16.03	16.20	16.23
MgO	14.92	15.51	14.73	13.65	13.47	13.57
MnO	0.17	0.15	0.14	0.18	0.20	0.18
CaO	-	-	0.02	-	-	-
Na2O	0.17	0.19	0.19	0.13	0.13	0.10
K2O	9.65	9.63	9.58	9.34	9.40	9.39
F	-	-	-	0.16	0.25	0.13
Total	94.95	94.47	93.80	95.20	95.56	95.10
Structura						
Si	5.907	5.901	5.871	5.595	5.588	5.599
Al(iv)	2.093	2.099	2.129	2.405	2.412	2.400
Al(vi)	0.571	0.600	0.586	0.234	0.212	0.259
Ti	0.378	0.315	0.372	0.401	0.421	0.375
Fe2+	1.934	1.873	1.935	2.014	2.030	2.043
Mn	0.023	0.022	0.020	0.023	0.025	0.023
Mg	3.487	3.634	3.486	3.057	3.009	3.044
Ca	-	-	0.005	-	-	-
Na	0.053	0.061	0.061	0.038	0.038	0.030
K	1.932	1.934	1.941	1.790	1.797	1.803

APPENDIX C

Table C.3: BIOTITE MICROPROBE ANALYSES

	D19 Shet. Biot 4	D19 Shet. Biot 5	D19 Shet. Biot 6	D19 Shet. Biot 8	D19 Shet. Biot 9	D19 Shet. Biot 10
SiO2	37.27	37.39	37.43	37.32	37.18	36.68
TiO2	3.36	3.09	3.26	3.51	3.09	3.56
Al2O3	14.95	15.01	14.89	15.04	15.07	14.91
FeO*	16.79	16.25	15.86	15.80	15.93	15.61
MgO	13.22	14.21	13.96	13.83	14.17	13.58
MnO	0.16	0.17	0.19	0.17	0.17	0.17
CaO	-	-	-	-	-	-
Na2O	0.13	0.13	0.15	0.11	0.09	0.14
K2O	9.43	8.89	9.25	9.44	9.34	9.45
F	0.09	0.13	0.09	0.26	0.14	0.15
Total	95.40	95.27	95.08	95.48	95.18	94.25
Structura						
Si	5.608	5.600	5.619	5.583	5.583	5.568
Al(iv)	2.392	2.400	2.380	2.416	2.417	2.432
Al(vi)	0.259	0.249	0.254	0.235	0.249	0.235
Ti	0.379	0.348	0.368	0.395	0.349	0.406
Fe2+	2.113	2.035	1.991	1.977	2.001	1.981
Mn	0.021	0.021	0.024	0.022	0.022	0.022
Mg	2.965	3.173	3.125	3.083	3.170	3.074
Ca	-	-	-	-	-	-
Na	0.039	0.037	0.044	0.032	0.027	0.042
K	1.809	1.699	1.771	1.801	1.789	1.831

	D19 Shet. Biot 11	D19 Shet. Biot 12	D19 Shet. Biot 13	D41 Rana. Biot 1	D41 Rana. Biot 2	D41 Rana. Biot 3
SiO2	37.71	37.26	37.36	37.01	36.73	37.62
TiO2	3.85	3.66	3.73	3.10	3.05	3.57
Al2O3	14.94	15.06	14.93	14.81	14.68	14.31
FeO*	15.64	15.57	16.08	14.85	15.85	14.84
MgO	14.07	13.66	13.44	15.61	15.32	15.17
MnO	0.21	0.19	0.19	0.19	0.15	0.16
CaO	-	-	-	-	-	-
Na2O	0.12	0.13	0.12	0.11	0.11	0.11
K2O	9.39	9.34	9.42	8.96	8.73	9.36
F	0.19	0.26	0.12	0.29	0.35	0.28
Total	96.12	95.13	95.39	94.93	94.97	95.42
Structura						
Si	5.594	5.588	5.603	5.538	5.516	5.607
Al(iv)	2.406	2.412	2.397	2.461	2.484	2.392
Al(vi)	0.207	0.249	0.242	0.150	0.115	0.121
Ti	0.430	0.412	0.421	0.349	0.345	0.400
Fe2+	1.941	1.953	2.016	1.858	1.990	1.850
Mn	0.027	0.025	0.024	0.025	0.019	0.020
Mg	3.111	3.054	3.004	3.482	3.430	3.370
Ca	-	-	-	-	-	-
Na	0.034	0.039	0.035	0.033	0.034	0.032
K	1.778	1.787	1.802	1.710	1.672	1.781

APPENDIX C

Table C.3: BIOTITE MICROPROBE ANALYSES

	D41 Rana. Biot 4	D41 Rana. Biot 5	D41 Rana. Biot 6	D41 Rana. Biot 7	D41 Rana. Biot 8	D41 Rana. Biot 9
SiO2	37.53	37.07	36.90	37.25	37.31	36.79
TiO2	3.56	3.46	3.35	3.26	3.17	3.21
Al2O3	14.12	14.48	14.49	14.39	14.68	14.54
FeO*	14.79	14.45	14.79	14.79	14.47	14.68
MgO	15.44	15.29	15.29	15.46	15.53	15.79
MnO	0.16	0.14	0.16	0.14	0.13	0.17
CaO	-	-	-	-	-	-
Na2O	0.10	0.10	0.14	0.16	0.14	0.11
K2O	9.21	9.53	9.13	9.31	9.23	9.01
F	0.35	0.35	0.27	0.29	0.22	0.48
Total	95.26	94.87	94.52	95.05	94.88	94.78
Structura						
Si	5.599	5.559	5.554	5.576	5.580	5.517
Al(iv)	2.400	2.441	2.445	2.423	2.419	2.483
Al(vi)	0.083	0.119	0.125	0.116	0.168	0.086
Ti	0.400	0.391	0.379	0.367	0.357	0.362
Fe2+	1.845	1.812	1.861	1.853	1.810	1.841
Mn	0.021	0.018	0.020	0.170	0.017	0.022
Mg	3.434	3.418	3.431	3.450	3.461	3.529
Ca	-	-	-	-	-	-
Na	0.029	0.031	0.040	0.046	0.041	0.033
K	1.753	1.823	1.753	1.778	1.761	1.724

	D41 Rana. Biot 10	D41 Rana. Biot 11	D41 Rana. Biot 12	D41 Rana. Biot 13	D63 Uile. Biot 1	D63 Uile. Biot 2
SiO2	37.11	37.14	37.57	37.06	36.72	35.46
TiO2	2.95	3.31	2.47	3.66	2.38	2.03
Al2O3	14.78	14.57	14.85	14.01	14.33	15.21
FeO*	14.77	14.67	14.29	14.77	16.52	16.74
MgO	15.81	15.45	15.84	14.88	14.46	15.71
MnO	0.16	0.14	0.14	0.12	0.18	0.19
CaO	-	-	-	-	-	-
Na2O	0.11	0.10	0.14	0.12	0.09	0.07
K2O	8.94	9.55	9.04	9.24	9.68	7.35
F	0.26	0.29	0.41	0.23	0.22	0.25
Total	94.89	95.22	94.75	94.09	94.58	93.01
Structura						
Si	5.551	5.555	5.509	5.607	5.589	5.431
Al(iv)	2.449	2.445	2.391	2.392	2.410	2.568
Al(vi)	0.157	0.123	0.222	0.105	0.161	0.178
Ti	0.332	0.372	0.277	0.416	0.272	0.234
Fe2+	1.848	1.834	1.784	1.869	2.103	2.144
Mn	0.021	0.018	0.018	0.015	0.024	0.025
Mg	3.525	3.445	3.526	3.355	3.282	3.587
Ca	-	-	-	-	-	-
Na	0.032	0.029	0.041	0.034	0.029	0.022
K	1.705	1.822	1.723	1.783	1.881	1.436

APPENDIX C

Table C.3: BIOTITE MICROPROBE ANALYSES

	D63 Uile. Biot 3	D63 Uile. Biot 4	D63 Uile. Biot 5	D63 Uile. Biot 6	D63 Uile. Biot 7	D63 Uile. Biot 8
SiO2	37.35	36.79	37.10	36.12	37.19	36.76
TiO2	2.68	3.58	2.33	2.60	2.06	2.19
Al2O3	14.36	14.66	14.45	14.54	14.77	14.41
FeO*	17.23	17.35	16.65	16.90	17.05	16.77
MgO	14.09	13.82	14.39	14.05	14.32	14.33
MnO	0.17	0.18	0.15	0.16	0.18	0.18
CaO	-	-	-	-	-	-
Na2O	0.08	0.09	0.09	0.12	0.08	0.08
K2O	9.36	9.59	9.19	9.42	8.73	9.49
F	0.21	0.31	0.15	0.21	0.22	0.31
Total	95.53	96.37	94.50	94.12	94.60	94.52
Structura						
Si	5.625	5.569	5.630	5.535	5.628	5.597
Al(iv)	2.375	2.431	2.369	2.465	2.372	2.403
Al(vi)	0.174	0.184	0.215	0.162	0.262	0.183
Ti	0.304	0.293	0.266	0.299	0.234	0.251
Fe2+	2.170	2.196	2.113	2.166	2.158	2.135
Mn	0.021	0.023	0.019	0.021	0.023	0.023
Mg	3.162	3.118	3.255	3.209	3.231	3.253
Ca	-	-	-	-	-	-
Na	0.025	0.027	0.026	0.037	0.025	0.025
K	1.798	1.852	1.779	1.842	1.686	1.844

	D63 Uile. Biot 10	E1 Dyke Biot 1	E1 Dyke Biot 2	E1 Dyke Biot 3	E1 Dyke Biot 4	E1 Dyke Biot 5
SiO2	36.45	37.32	37.50	37.08	36.82	37.37
TiO2	1.51	3.08	3.05	3.14	3.25	3.34
Al2O3	15.14	14.68	14.74	14.56	14.77	14.40
FeO*	17.95	16.17	16.21	16.36	16.36	16.19
MgO	14.19	14.12	14.02	13.96	13.72	13.98
MnO	0.18	0.16	0.19	0.18	0.20	0.19
CaO	-	-	-	-	-	-
Na2O	0.06	0.09	0.11	0.08	0.10	0.11
K2O	8.28	9.44	9.48	9.37	9.30	9.39
F	0.20	0.24	0.21	0.24	0.08	0.31
Total	93.96	95.30	95.51	94.97	94.60	95.28
Structura						
Si	5.571	5.607	5.621	5.597	5.581	5.617
Al(iv)	2.429	2.392	2.379	2.402	2.418	2.383
Al(vi)	0.299	0.206	0.226	0.188	0.220	0.169
Ti	0.174	0.348	0.344	0.357	0.370	0.378
Fe2+	2.294	2.031	2.032	2.066	2.074	2.035
Mn	0.023	0.021	0.024	0.024	0.026	0.024
Mg	3.234	3.162	3.132	3.142	3.100	3.131
Ca	-	-	-	-	-	-
Na	0.017	0.025	0.032	0.025	0.031	0.033
K	1.614	1.809	1.812	1.804	1.798	1.801

APPENDIX C

Table C.3: BIOTITE MICROPROBE ANALYSES

	E1 Dyke Biot 6	E1 Dyke Biot 7	E1 Dyke Biot 8	E1 Dyke Biot 9	E1 Dyke Biot 10	E1 Dyke Biot 11
SiO2	37.44	37.26	37.62	36.82	36.99	37.41
TiO2	3.22	3.38	3.49	2.60	3.22	3.39
Al2O3	14.49	14.36	14.57	14.21	14.37	14.66
FeO*	16.32	16.16	15.98	15.97	16.26	16.42
MgO	14.09	14.06	13.89	14.12	14.01	13.90
MnO	0.20	0.18	0.17	0.21	0.19	0.20
CaO	-	-	-	-	-	-
Na2O	0.08	0.11	0.10	0.08	0.09	0.11
K2O	9.11	9.29	9.27	8.86	9.46	9.33
F	0.17	0.31	0.16	0.24	0.25	0.28
Total	95.12	95.11	95.25	93.11	94.84	95.70
Structura						
Si	5.628	5.609	5.640	5.649	5.596	5.599
Al(iv)	2.372	2.391	2.359	2.351	2.403	2.400
Al(vi)	0.196	0.156	0.215	0.219	0.159	0.186
Ti	0.364	0.382	0.393	0.300	0.367	0.381
Fe2+	2.051	2.034	2.003	2.049	2.058	2.055
Mn	0.025	0.023	0.022	0.027	0.024	0.025
Mg	3.158	3.154	3.105	3.230	3.160	3.103
Ca	-	-	-	-	-	-
Na	0.023	0.032	0.029	0.024	0.026	0.031
K	1.746	1.783	1.774	1.734	1.825	1.781

	E1 Dyke Biot 12	E1 Dyke Biot 13	E1 Dyke Biot 14	E3 Dyke Biot 1	E3 Dyke Biot 2	E3 Dyke Biot 3
SiO2	36.79	36.93	37.18	37.20	37.07	37.07
TiO2	3.06	2.78	2.87	3.13	3.04	3.10
Al2O3	14.48	13.93	14.82	14.44	14.47	14.40
FeO*	15.84	16.24	17.61	16.68	16.57	16.77
MgO	13.96	13.94	14.08	13.60	13.79	13.85
MnO	0.17	0.17	0.19	0.22	0.22	0.18
CaO	-	-	-	-	-	-
Na2O	0.10	0.08	0.09	0.08	0.05	0.09
K2O	8.85	9.02	8.58	9.70	9.62	9.56
F	0.26	0.26	-	0.32	0.48	0.34
Total	93.51	93.35	95.42	95.37	95.31	95.36
Structura						
Si	5.615	5.664	5.644	5.612	5.592	5.592
Al(iv)	2.385	2.335	2.355	2.387	2.408	2.408
Al(vi)	0.219	0.182	0.297	0.179	0.165	0.153
Ti	0.351	0.321	0.327	0.355	0.344	0.351
Fe2+	2.022	2.083	2.012	2.105	2.090	2.116
Mn	0.022	0.022	0.024	0.028	0.028	0.023
Mg	3.175	3.187	3.186	3.058	3.100	3.115
Ca	-	-	-	-	-	-
Na	0.031	0.023	0.028	0.023	0.016	0.026
K	1.723	1.765	1.663	1.867	1.850	1.841

APPENDIX C

Table C.3: BIOTITE MICROPROBE ANALYSES

	E3 Dyke Biot 4	E3 Dyke Biot 5	E3 Dyke Biot 6	E3 Dyke Biot 7	E3 Dyke Biot 8	E3 Dyke Biot 10
SiO2	37.03	37.28	36.92	37.09	36.57	36.80
TiO2	2.94	3.00	3.23	3.02	3.21	3.20
Al2O3	14.47	14.55	14.47	14.22	14.27	14.23
FeO*	16.63	16.58	16.67	16.75	16.68	16.63
MgO	13.94	13.89	13.60	13.49	13.57	13.62
MnO	0.22	0.20	0.21	0.22	0.19	0.19
CaO	-	-	-	-	-	-
Na2O	0.10	0.09	0.07	0.08	0.11	0.09
K2O	9.49	9.61	9.73	9.59	9.57	9.64
F	0.40	0.38	0.41	0.44	0.24	0.46
Total	95.22	95.58	95.31	94.90	94.41	94.86
Structura						
Si	5.589	5.603	5.579	5.624	5.582	5.587
Al(iv)	2.140	2.397	2.421	2.376	2.418	2.413
Al(vi)	0.164	0.179	0.155	0.165	0.149	0.133
Ti	0.334	0.339	0.367	0.345	0.368	0.365
Fe2+	2.099	2.084	2.107	2.124	2.129	2.112
Mn	0.028	0.025	0.027	0.028	0.025	0.024
Mg	3.137	3.113	3.063	3.050	3.088	3.082
Ca	-	-	-	-	-	-
Na	0.030	0.027	0.020	0.023	0.033	0.026
K	1.827	1.844	1.875	1.855	1.863	1.868

	E5A Dyke Biot 1	E5A Dyke Biot 2	E5A Dyke Biot 3	E5A Dyke Biot 4	E5A Dyke Biot 5	E5A Dyke Biot 6
SiO2	37.25	37.06	37.17	37.55	37.20	37.29
TiO2	2.47	2.89	2.92	2.62	2.13	2.70
Al2O3	14.70	14.66	14.54	14.72	14.85	14.63
FeO*	16.56	16.75	16.58	16.45	16.34	16.06
MgO	13.96	13.94	13.78	13.99	14.23	14.07
MnO	0.19	0.22	0.19	0.19	0.18	0.20
CaO	-	-	-	-	-	-
Na2O	0.09	0.06	0.06	0.07	0.09	0.09
K2O	9.55	9.54	9.37	9.29	9.30	9.39
F	0.36	0.27	0.29	0.47	0.21	0.27
Total	95.13	95.39	94.90	95.35	94.53	94.70
Structura						
Si	5.621	5.585	5.619	5.636	5.633	5.635
Al(iv)	2.378	2.414	2.380	2.364	2.366	2.365
Al(vi)	0.236	0.191	0.210	0.239	0.284	0.239
Ti	0.279	0.328	0.332	0.296	0.243	0.307
Fe2+	2.089	2.112	2.096	2.064	2.070	2.029
Mn	0.025	0.028	0.024	0.025	0.024	0.026
Mg	3.139	3.133	3.106	1.131	3.212	3.169
Ca	-	-	-	-	-	-
Na	0.026	0.017	0.017	0.021	0.270	0.027
K	1.838	1.834	1.807	1.778	1.796	1.809

APPENDIX C

Table C.3: BIOTITE MICROPROBE ANALYSES

	E5A Dyke Biot 7	E5A Dyke Biot 9	E5A Dyke Biot 10	E5A Dyke Biot 11	E5A Dyke Biot 12	L1 Dyke Biot 2
SiO2	37.44	37.54	37.30	37.35	37.42	36.45
TiO2	2.64	2.37	2.64	2.58	2.84	2.90
Al2O3	14.67	14.63	14.57	14.49	14.48	14.97
FeO*	15.91	16.34	16.10	15.69	16.42	16.15
MgO	14.02	14.62	14.25	14.53	13.89	14.43
MnO	0.20	0.20	0.18	0.21	0.22	0.17
CaO	-	-	-	-	-	-
Na2O	0.09	0.07	0.07	0.10	0.11	0.09
K2O	9.26	9.04	9.45	9.15	9.38	8.48
F	0.26	0.30	0.32	0.38	0.31	0.33
Total	94.49	95.11	94.88	94.48	95.07	93.97
Structura						
Si	5.658	5.638	5.628	5.639	5.641	5.533
Al(iv)	2.341	2.361	2.372	2.361	2.359	2.466
Al(vi)	0.271	0.229	0.219	0.218	0.214	0.211
Ti	0.300	0.267	0.299	0.293	0.322	0.331
Fe2+	2.010	2.053	2.031	1.982	2.071	2.051
Mn	0.026	0.025	0.024	0.026	0.028	0.220
Mg	3.157	3.272	3.204	3.269	3.121	3.264
Ca	-	-	-	-	-	-
Na	0.028	0.021	0.021	0.029	0.032	0.027
K	1.784	1.732	1.819	1.763	1.803	1.643

	L1 Dyke Biot 3	L1 Dyke Biot 4	L1 Dyke Biot 5	L1 Dyke Biot 6
SiO2	36.30	37.42	36.90	37.39
TiO2	2.89	2.74	2.95	3.00
Al2O3	14.98	14.98	14.65	14.65
FeO*	15.80	16.00	15.97	15.71
MgO	14.51	14.42	14.07	14.18
MnO	0.16	0.17	0.18	0.19
CaO	-	-	-	-
Na2O	0.05	0.08	0.06	0.08
K2O	8.69	9.13	9.21	9.49
F	0.26	0.32	0.27	0.19
Total	93.64	95.26	94.26	94.88
Structura				
Si	5.529	5.605	5.599	5.632
Al(iv)	2.470	2.395	2.400	2.368
Al(vi)	0.218	0.249	0.219	0.233
Ti	0.331	0.308	0.336	0.339
Fe2+	2.013	2.004	2.027	1.978
Mn	0.020	0.220	0.024	0.024
Mg	3.295	3.218	3.181	3.183
Ca	-	-	-	-
Na	0.014	0.025	0.017	0.024
K	1.688	1.745	1.782	1.822

APPENDIX C

Table C.3: BIOTITE MICROPROBE ANALYSES

	XG32 1A Biot 1	XG32 1A Biot 2	XG32 1A Biot 3	XG32 1A Biot 4	XG32 1A Biot 5	XG32 1A Biot 6
SiO2	36.05	36.75	36.69	36.77	36.69	37.02
TiO2	2.49	3.14	3.32	3.39	2.92	2.73
Al2O3	15.06	15.24	15.01	14.96	15.02	15.13
FeO*	17.87	17.88	17.75	18.39	18.47	18.21
MgO	12.45	12.22	12.16	12.18	12.04	12.49
MnO	0.21	0.27	0.26	0.24	0.23	0.26
CaO	-	-	-	-	-	-
Na2O	0.09	0.08	0.08	0.07	0.10	0.09
K2O	9.10	9.47	9.28	9.16	9.38	9.53
F	0.28	0.17	0.26	0.22	0.21	0.15
Total	93.6	95.22	94.81	95.38	95.06	95.61
Structural Formulae						
Si	5.565	5.576	5.584	5.575	5.592	5.602
Al(iv)	2.434	2.423	2.415	2.425	2.408	2.398
Al(vi)	0.307	0.303	0.277	0.248	0.290	0.301
Ti	0.289	0.359	0.380	0.386	0.335	0.311
Fe2+	2.308	2.269	2.259	2.331	2.353	2.304
Mn	0.028	0.034	0.034	0.031	0.030	0.033
Mg	2.864	2.764	2.759	2.753	2.736	2.818
Ca	-	-	-	-	-	-
Na	0.027	0.025	0.023	0.022	0.030	0.025
K	1.792	1.833	1.803	1.773	1.824	1.839

	XG32 1A Biot 7	XG32 1A Biot 8	XG32 1A Biot 9	XG32 1A Biot 10	XG32 1A Biot 11	XG65 1A Biot 1
SiO2	36.79	36.62	36.32	36.46	36.41	36.81
TiO2	2.51	2.49	2.86	3.52	3.26	2.75
Al2O3	15.26	15.52	15.14	14.97	14.79	14.62
FeO*	18.33	18.23	18.23	17.97	18.33	17.84
MgO	12.39	11.75	12.50	12.01	11.76	12.72
MnO	0.25	0.28	0.25	0.23	0.25	0.25
CaO	-	-	-	-	-	-
Na2O	0.05	0.09	0.07	0.07	0.07	0.08
K2O	9.21	9.30	9.27	9.36	9.17	9.39
F	0.32	0.17	0.30	0.25	0.21	0.22
Total	95.11	94.45	94.94	94.84	94.25	94.68
Structura						
Si	5.589	5.605	5.538	5.560	5.592	5.618
Al(iv)	2.410	2.395	2.462	2.439	2.407	2.381
Al(vi)	0.322	0.404	0.259	0.251	0.271	0.249
Ti	0.287	0.287	0.328	0.404	0.377	0.316
Fe2+	2.330	2.334	2.325	2.292	2.354	2.277
Mn	0.032	0.036	0.032	0.030	0.033	0.033
Mg	2.806	2.682	2.841	2.730	2.692	2.894
Ca	-	-	-	-	-	-
Na	0.015	0.026	0.021	0.022	0.022	0.024
K	1.785	1.817	1.804	1.822	1.797	1.829

APPENDIX C

Table C.3: BIOTITE MICROPROBE ANALYSES

	XG65 1A Biot 2	XG65 1A Biot 3	XG65 1A Biot 4	XG65 1A Biot 5	XG65 1A Biot 6	XG65 1A Biot 7
SiO2	36.35	36.50	36.22	36.25	36.64	36.58
TiO2	3.34	3.25	3.40	3.35	3.29	3.24
Al2O3	14.40	14.29	14.47	14.28	14.21	14.35
FeO*	18.07	17.87	17.95	17.78	18.03	18.29
MgO	12.21	12.41	12.31	12.25	12.16	12.43
MnO	0.28	0.27	0.24	0.27	0.27	0.27
CaO	-	-	-	-	-	-
Na2O	0.07	0.05	0.07	0.07	0.11	0.09
K2O	9.57	9.63	9.66	9.47	9.55	9.65
F	0.29	0.32	0.39	0.22	0.42	0.37
Total	94.58	94.59	94.71	93.94	94.68	95.27
Structura						
Si	5.577	5.594	5.550	5.593	5.610	5.576
Al(iv)	2.423	2.406	2.450	2.407	2.389	2.424
Al(vi)	0.182	0.176	0.163	0.189	0.176	0.154
Ti	0.385	0.374	0.392	0.388	0.379	0.371
Fe2+	2.319	2.290	2.300	2.294	2.308	2.332
Mn	0.036	0.035	0.032	0.035	0.035	0.035
Mg	2.792	2.836	2.813	2.817	2.776	2.825
Ca	-	-	-	-	-	-
Na	0.021	0.017	0.021	0.021	0.032	0.028
K	1.873	1.883	1.889	1.864	1.866	1.878

	XG65 1A Biot 8	XG65 1A Biot 9	XG65 1A Biot 10	XG7 1B Biot 1M	XG7 1B Biot 2C	XG7 1B Biot 3M
SiO2	36.81	36.90	36.43	37.18	37.81	37.44
TiO2	3.38	3.11	2.78	3.82	3.73	2.62
Al2O3	14.24	14.49	14.38	13.80	13.79	14.08
FeO*	17.77	17.91	17.79	17.19	17.10	16.63
MgO	12.54	12.56	12.68	12.35	12.58	13.25
MnO	0.27	0.25	0.25	0.22	0.25	0.22
CaO	-	-	-	-	-	-
Na2O	0.05	0.09	0.10	0.11	0.18	0.14
K2O	9.66	9.55	9.58	9.76	9.38	9.63
F	0.33	0.36	0.39	-	-	-
Total	95.05	95.22	94.38	94.43	94.82	94.01
Structura						
Si	5.607	5.607	5.592	5.947	5.995	5.986
Al(iv)	2.303	2.392	2.407	2.053	2.005	2.014
Al(vi)	0.164	0.203	0.195	0.549	0.574	0.641
Ti	0.387	0.355	0.321	0.460	0.445	0.315
Fe2+	2.263	2.276	2.285	2.300	2.269	2.225
Mn	0.035	0.032	0.032	0.030	0.035	0.031
Mg	2.848	2.845	2.901	2.944	2.974	3.158
Ca	-	-	-	-	-	-
Na	0.016	0.028	0.030	0.035	0.056	0.044
K	1.878	1.851	1.876	1.992	1.897	1.965

APPENDIX C

Table C.3: BIOTITE MICROPROBE ANALYSES

	XG7 1B Biot 4M	XG7 1B Biot 5R	XG7 1B Biot 6M	XG7 1B Biot 7M	XG24 1B Biot 1	XG24 1B Biot 2
SiO2	37.67	37.23	37.54	37.33	36.55	36.80
TiO2	3.52	3.07	3.21	3.73	2.97	3.02
Al2O3	13.77	13.84	13.61	13.70	14.62	14.83
FeO*	17.05	17.01	17.14	17.41	17.03	16.97
MgO	13.10	13.03	13.00	12.66	13.74	13.36
MnO	0.22	0.23	0.25	0.23	0.20	0.23
CaO	-	-	-	-	-	-
Na2O	0.11	0.14	0.15	0.10	0.11	0.12
K2O	9.51	9.56	9.62	9.56	8.83	9.71
F	-	-	-	-	0.36	0.48
Total	94.95	94.11	94.52	94.72	94.41	95.52
Structura						
Si	5.969	5.962	5.989	5.949	5.560	5.554
Al(iv)	2.031	2.038	2.011	2.051	2.439	2.446
Al(vi)	0.542	0.575	0.549	0.523	0.181	0.193
Ti	0.420	0.371	0.386	0.448	0.339	0.342
Fe2+	2.259	2.613	2.287	2.320	2.166	2.142
Mn	0.031	0.032	0.034	0.032	0.026	0.029
Mg	3.095	3.111	3.091	3.008	3.115	3.007
Ca	-	-	-	-	-	-
Na	0.036	0.043	0.047	0.033	0.033	0.036
K	1.923	1.953	1.958	1.945	1.714	1.869

	XG24 1B Biot 3	XG24 1B Biot 4	XG24 1B Biot 5	XG24 1B Biot 6	XG24 1B Biot 7	XG24 1B Biot 8
SiO2	37.06	36.51	36.89	36.87	36.97	36.65
TiO2	2.37	2.82	3.07	3.16	3.14	3.27
Al2O3	15.27	14.84	14.45	14.54	14.70	14.77
FeO*	16.34	17.11	17.12	16.99	17.16	17.25
MgO	14.02	13.23	13.32	13.25	13.25	13.17
MnO	0.27	0.27	0.22	0.24	0.21	0.25
CaO	-	-	-	-	-	-
Na2O	0.10	0.11	0.12	0.07	0.10	0.09
K2O	9.54	9.53	9.59	9.58	9.49	9.65
F	0.34	0.51	0.26	0.29	0.34	0.30
Total	95.31	94.93	95.04	94.99	95.36	95.4
Structura						
Si	5.576	5.548	5.599	5.593	5.584	5.548
Al(iv)	2.423	2.452	2.400	2.406	2.416	2.452
Al(vi)	0.284	0.206	0.184	0.193	0.202	0.183
Ti	0.268	0.322	0.350	0.360	0.357	0.372
Fe2+	2.056	2.175	2.173	2.155	2.167	2.184
Mn	0.035	0.035	0.029	0.031	0.027	0.032
Mg	3.144	2.998	3.012	2.996	2.984	2.971
Ca	-	-	-	-	-	-
Na	0.029	0.031	0.035	0.021	0.031	0.029
K	1.832	1.847	1.856	1.855	1.829	1.864

APPENDIX C

Table C.3: BIOTITE MICROPROBE ANALYSES

	XG24 1B Biot 9	XG24 1B Biot 10	XG24 1B Biot 11	XG24 1B Biot 12	XG24 1B Biot 13	XG64A 1B Biot 1
SiO2	37.14	37.20	37.17	36.69	37.27	36.74
TiO2	3.21	2.68	2.89	3.06	2.99	3.43
Al2O3	14.86	15.14	15.12	14.79	14.57	14.27
FeO*	16.78	16.62	16.68	16.99	17.15	18.00
MgO	13.47	14.10	13.44	13.29	13.23	12.69
MnO	0.24	0.22	0.21	0.23	0.23	0.26
CaO	-	-	-	-	-	-
Na2O	0.08	0.10	0.09	0.08	0.09	0.07
K2O	9.48	8.76	9.63	9.63	9.58	9.20
F	0.32	0.31	0.21	0.23	0.38	0.35
Total	95.58	95.13	95.44	94.99	95.49	95.01
Structura						
Si	5.583	5.587	5.595	5.568	5.620	5.591
Al(iv)	2.417	2.422	2.404	2.432	2.379	2.409
Al(vi)	0.216	0.257	0.277	0.214	0.209	0.150
Ti	0.363	0.302	0.327	0.349	0.340	0.392
Fe2+	2.109	2.088	2.099	2.157	2.163	2.291
Mn	0.030	0.028	0.027	0.029	0.029	0.034
Mg	3.019	3.156	3.016	3.007	2.974	2.878
Ca	-	-	-	-	-	-
Na	0.025	0.031	0.027	0.026	0.029	0.022
K	1.818	1.677	1.849	1.864	1.842	1.786

	XG64A 1B Biot 2	XG64A 1B Biot 3	XG64A 1B Biot 4	XG64A 1B Biot 5	XG64A 1B Biot 6	XG64A 1B Biot 7
SiO2	37.09	36.44	36.55	36.31	36.99	37.01
TiO2	3.22	3.39	3.28	3.12	3.16	3.06
Al2O3	14.42	14.48	14.41	14.59	14.63	14.24
FeO*	18.01	18.06	17.74	17.27	17.95	18.05
MgO	12.72	12.25	12.58	12.57	12.69	12.58
MnO	0.23	0.25	0.23	0.26	0.27	0.24
CaO	-	-	-	-	-	-
Na2O	0.08	0.08	0.08	0.04	0.08	0.07
K2O	9.38	9.35	9.46	8.86	9.21	9.27
F	0.35	0.39	0.30	0.33	0.29	0.32
Total	95.5	94.69	94.63	93.35	95.27	94.84
Structura						
Si	5.613	5.573	5.588	5.596	5.605	5.640
Al(iv)	2.386	2.426	2.411	2.404	2.395	2.359
Al(vi)	0.186	0.185	0.186	0.247	0.217	0.198
Ti	0.366	0.389	0.377	0.362	0.259	0.351
Fe2+	2.280	2.310	2.268	2.226	2.275	2.300
Mn	0.029	0.032	0.030	0.034	0.034	0.031
Mg	2.869	2.794	2.866	2.887	2.868	2.858
Ca	-	-	-	-	-	-
Na	0.023	0.024	0.025	0.013	0.023	0.023
K	1.811	1.825	1.845	1.743	1.779	1.802

APPENDIX C

Table C.3: BIOTITE MICROPROBE ANALYSES

	XG64A 1B Biot 8	XG64A 1B Biot 9	XG64A 1B Biot 10	XG64A 1B Biot 11	X181 2 Biot 1	X181 2 Biot 2
SiO2	37.22	37.10	36.94	36.78	36.71	36.96
TiO2	3.14	3.21	3.34	3.36	2.66	2.24
Al2O3	14.23	14.24	14.06	14.49	14.40	14.74
FeO*	17.99	17.95	17.86	17.71	17.88	17.62
MgO	12.88	12.82	13.11	12.76	12.91	13.26
MnO	0.25	0.28	0.25	0.28	0.24	0.24
CaO	-	-	-	-	-	-
Na2O	0.09	0.06	0.09	0.08	0.07	0.12
K2O	9.12	9.28	9.23	9.33	9.29	9.22
F	0.38	0.44	0.39	0.35	0.42	0.51
Total	95.3	95.38	95.27	95.137	94.58	94.91
Structura						
Si	5.636	5.619	5.602	5.584	5.609	5.612
Al(iv)	2.364	2.381	2.398	2.416	2.390	2.387
Al(vi)	0.175	0.160	0.116	0.177	0.204	0.249
Ti	0.357	0.365	0.381	0.384	0.305	0.256
Fe2+	2.278	2.274	2.265	2.249	2.286	2.237
Mn	0.032	0.036	0.032	0.036	0.020	0.032
Mg	2.906	2.894	1.963	2.889	2.941	3.002
Ca	-	-	-	-	-	-
Na	0.025	0.019	0.026	0.023	0.022	0.036
K	1.761	1.793	1.786	1.808	1.811	1.786

	X181 2 Biot 3	X181 2 Biot 5	X181 2 Biot 6	X181 2 Biot 7	X181 2 Biot 8	X181 2 Biot 9
SiO2	37.09	36.77	36.97	36.58	36.64	36.64
TiO2	2.52	2.67	2.93	2.89	3.19	2.63
Al2O3	14.48	14.37	14.46	14.39	13.86	14.49
FeO*	17.49	17.92	17.57	17.75	17.34	17.64
MgO	13.24	13.20	13.18	13.33	12.92	13.61
MnO	0.24	0.26	0.23	0.20	0.20	0.25
CaO	-	-	-	-	-	-
Na2O	0.11	0.11	0.10	0.08	0.08	0.10
K2O	9.55	9.18	9.18	8.67	9.45	9.05
F	0.39	0.34	0.39	0.43	0.34	0.37
Total	95.11	94.82	95.01	94.32	94.02	94.78
Structura						
Si	5.629	5.603	5.608	5.583	5.630	5.575
Al(iv)	2.370	2.396	2.391	2.416	2.369	2.425
Al(vi)	0.219	0.185	0.193	0.171	0.140	0.173
Ti	0.287	0.306	0.334	0.332	0.368	0.302
Fe2+	2.218	2.283	2.228	2.266	2.228	2.245
Mn	0.031	0.034	0.029	0.026	0.027	0.032
Mg	2.995	2.999	2.981	3.032	2.959	3.087
Ca	-	-	-	-	-	-
Na	0.034	0.032	0.029	0.025	0.024	0.031
K	1.849	1.784	1.777	1.689	1.854	1.756

APPENDIX C

Table C.3: BIOTITE MICROPROBE ANALYSES

	X181 2 Biot 10	XG25 2 Biot 1M	XG25 2 Biot 2R	XG25 2 Biot 3M	XG25 2 Biot 4C	XG25 2 Biot 5R
SiO2	36.83	36.65	36.77	36.58	37.03	34.67
TiO2	3.35	3.33	3.11	2.74	3.18	2.87
Al2O3	14.76	14.20	14.13	14.19	14.19	14.03
FeO*	17.42	17.29	17.54	17.31	16.89	17.24
MgO	12.36	12.82	12.86	13.54	12.59	13.51
MnO	0.22	0.23	0.23	0.24	0.23	0.23
CaO	-	-	0.01	0.03	-	0.06
Na2O	0.09	0.13	0.24	0.10	0.12	0.11
K2O	9.46	9.77	9.27	8.68	9.69	7.92
F	0.39	-	-	-	-	-
Total	94.88	94.42	94.16	93.41	93.92	90.64
Structura						
Si	5.598	5.873	5.898	5.887	5.942	5.760
Al(iv)	2.402	2.127	2.102	2.113	2.058	2.240
Al(vi)	0.243	0.556	0.569	0.580	0.627	0.508
Ti	0.382	0.402	0.376	0.333	0.385	0.359
Fe2+	2.215	2.317	2.353	2.331	2.268	2.395
Mn	0.029	0.032	0.032	0.034	0.032	0.034
Mg	2.801	3.061	3.075	3.249	3.013	3.345
Ca	-	-	0.003	0.006	-	0.013
Na	0.026	0.042	0.075	0.032	0.037	0.035
K	1.835	1.998	1.897	1.783	1.985	1.679

	XG44 2 Biot 1	XG44 2 Biot 2	XG44 2 Biot 3	XG44 2 Biot 4	XG44 2 Biot 5	XG44 2 Biot 6
SiO2	36.77	36.89	36.97	37.11	35.49	37.23
TiO2	2.18	3.22	3.16	2.92	3.43	3.17
Al2O3	14.53	14.27	14.31	14.15	14.06	14.20
FeO*	16.91	16.58	16.97	16.50	17.85	16.92
MgO	14.39	13.35	13.86	13.74	13.17	13.70
MnO	0.24	0.21	0.24	0.24	0.24	0.22
CaO	-	-	-	-	-	-
Na2O	0.08	0.12	0.11	0.12	0.07	0.09
K2O	8.68	9.69	9.29	9.49	8.46	9.60
F	0.51	0.34	0.39	0.32	0.23	0.49
Total	94.29	94.67	95.3	94.59	93	95.62
Structura						
Si	5.589	5.611	5.581	5.638	5.514	5.606
Al(iv)	2.410	2.389	2.418	2.362	2.486	2.394
Al(vi)	0.192	0.169	0.128	0.171	0.088	0.126
Ti	0.250	0.368	0.359	0.333	0.401	0.359
Fe2+	2.149	2.109	2.143	2.097	2.319	2.130
Mn	0.031	0.027	0.030	0.031	0.032	0.028
Mg	3.259	3.026	3.119	3.113	3.051	3.076
Ca	-	-	-	-	-	-
Na	0.023	0.036	0.033	0.035	0.023	0.027
K	1.684	1.881	1.789	1.839	1.676	1.844

APPENDIX C

Table C.3: BIOTITE MICROPROBE ANALYSES

	XG442 Biot 7	XG442 Biot 8	XG442 Biot 9	XG442 Biot 10	XG442 Biot 11	XG442 Biot 12
SiO2	37.17	37.00	37.35	37.47	36.82	37.27
TiO2	2.68	3.54	3.24	3.48	3.47	3.04
Al2O3	14.49	14.34	14.37	14.13	14.19	14.33
FeO*	16.93	17.01	17.00	16.99	16.94	16.62
MgO	13.86	13.34	13.40	13.29	13.45	13.77
MnO	0.23	0.22	0.20	0.26	0.22	0.23
CaO	-	-	-	-	-	-
Na2O	0.07	0.11	0.08	0.07	0.11	0.07
K2O	9.48	9.67	9.69	9.66	9.63	9.58
F	0.37	0.43	0.33	0.36	0.48	0.35
Total	95.28	95.66	95.66	95.71	95.31	95.26
Structura						
Si	5.611	5.577	5.623	5.637	5.572	5.622
Al(iv)	2.389	2.423	2.377	2.362	2.428	2.378
Al(vi)	0.190	0.125	0.172	0.144	0.102	0.171
Ti	0.304	0.402	0.367	0.394	0.395	0.345
Fe2+	2.138	2.144	2.140	2.137	2.144	2.097
Mn	0.030	0.029	0.026	0.033	0.029	0.029
Mg	3.118	2.996	3.006	2.981	3.034	3.097
Ca	-	-	-	-	-	-
Na	0.022	0.032	0.024	0.021	0.032	0.022
K	1.826	1.859	1.862	1.854	1.859	1.845

	XG61B2 Biot 1M	XG61B2 Biot 2M	XG61B2 Biot 3M	XG61B2 Biot 4M	XG61B2 Biot 5C	XG61B2 Biot 6M
SiO2	37.55	36.82	37.29	37.49	37.04	37.32
TiO2	2.39	3.38	3.04	3.07	3.06	3.13
Al2O3	14.32	14.05	14.02	14.00	14.26	14.19
FeO*	17.59	17.32	17.25	17.33	17.59	17.10
MgO	13.19	12.78	12.88	12.98	12.86	12.84
MnO	0.22	0.21	0.20	0.22	0.21	0.20
CaO	-	-	-	0.21	-	0.02
Na2O	0.08	0.10	0.11	0.10	0.12	0.10
K2O	9.75	9.81	9.90	9.58	9.83	9.83
F	-	-	-	-	-	-
Total	95.09	94.47	94.69	94.98	94.97	94.73
Structura						
Si	5.962	5.896	5.949	5.954	5.902	5.943
Al(iv)	2.038	2.104	2.060	2.046	2.098	2.057
Al(vi)	0.642	0.549	0.577	0.576	0.582	0.608
Ti	0.286	0.407	0.365	0.368	0.367	0.375
Fe2+	2.336	2.320	2.302	2.302	2.344	2.277
Mn	0.030	0.029	0.028	0.031	0.029	0.028
Mg	3.121	3.050	3.064	3.073	3.055	3.048
Ca	-	-	-	0.036	-	0.004
Na	0.026	0.032	0.035	0.033	0.037	0.032
K	1.977	2.005	2.017	1.942	1.999	1.998

APPENDIX C

Table C.3: BIOTITE MICROPROBE ANALYSES

	XG61B 2 Biot 7	XG61B 2 Biot 8M	XG61B 2 Biot 9M	XG61C 2 Biot 2	XG61C 2 Biot 3	XG61C 2 Biot 4
SiO2	37.34	36.98	37.35	37.10	36.14	37.23
TiO2	3.33	2.80	3.02	3.11	3.13	2.97
Al2O3	14.09	14.35	14.05	14.54	14.67	14.45
FeO*	17.36	17.43	17.26	16.94	17.46	17.02
MgO	12.84	13.04	12.96	13.54	13.41	13.78
MnO	0.21	0.20	0.21	0.18	0.18	0.19
CaO	-	-	-	-	-	-
Na2O	0.09	0.08	0.09	0.08	0.11	0.08
K2O	9.82	9.52	9.83	9.38	8.92	9.00
F	-	-	-	0.21	0.28	0.29
Total	95.08	94.4	94.77	95.08	94.3	95.01
Structura						
Si	5.931	5.911	5.949	5.609	5.524	5.620
Al(iv)	2.069	2.089	2.051	2.390	2.476	2.379
Al(vi)	0.570	0.616	0.588	0.201	0.168	0.192
Ti	0.398	0.337	0.363	0.354	0.361	0.337
Fe2+	2.306	2.331	2.300	2.142	2.232	2.149
Mn	0.029	0.028	0.029	0.023	0.024	0.025
Mg	3.041	3.107	3.078	3.051	3.055	3.101
Ca	-	-	-	-	-	-
Na	0.030	0.027	0.029	0.024	0.032	0.024
K	1.991	1.941	2.000	1.810	1.739	1.734

	XG61C 2 Biot 5	XG61C 2 Biot 6	XG61C 2 Biot 7	XG61C 2 Biot 8	XG61C 2 Biot 9	XG61C 2 Biot 11
SiO2	37.17	37.32	37.44	36.10	36.52	37.26
TiO2	3.09	3.25	3.44	2.78	3.11	3.04
Al2O3	14.50	14.51	14.42	14.41	14.21	14.22
FeO*	16.81	17.03	16.83	17.12	17.03	16.89
MgO	13.48	13.39	13.65	13.97	13.69	13.56
MnO	0.20	0.19	0.17	0.18	0.16	0.18
CaO	-	-	-	-	-	-
Na2O	0.10	0.09	0.09	0.15	0.13	0.08
K2O	8.89	9.36	9.38	8.85	9.12	9.26
F	0.18	0.35	0.33	0.31	0.33	0.29
Total	94.42	95.49	95.75	93.87	94.3	94.78
Structura						
Si	5.638	5.617	5.614	5.535	5.575	5.647
Al(iv)	2.362	2.383	2.386	2.464	2.425	2.353
Al(vi)	0.231	0.191	0.162	0.140	0.133	0.186
Ti	0.353	0.368	0.388	0.321	0.357	0.346
Fe2+	2.132	2.143	2.110	2.196	2.174	2.140
Mn	0.026	0.025	0.022	0.023	0.021	0.024
Mg	3.048	3.003	3.050	3.194	3.115	3.063
Ca	-	-	-	-	-	-
Na	0.031	0.027	0.027	0.046	0.039	0.024
K	1.720	1.797	1.793	1.731	1.777	1.789

APPENDIX C

Table C.3: BIOTITE MICROPROBE ANALYSES

	XG61C 2 Biot 12	XG89 2 Biot 1C	XG89 2 Biot 2R	XG89 2 Biot 3C	XG89 2 Biot 4M	XG89 2 Biot 5M
SiO2	37.34	37.52	37.48	37.66	36.84	37.50
TiO2	2.94	2.70	4.06	3.45	2.65	3.12
Al2O3	14.49	13.95	13.47	13.90	14.12	14.01
FeO*	17.23	17.06	17.00	17.37	17.38	17.26
MgO	13.62	13.67	12.79	12.86	14.05	13.26
MnO	0.19	0.24	0.26	0.27	0.27	0.25
CaO	-	-	0.01	-	0.03	-
Na2O	0.12	0.09	0.20	0.09	0.09	0.09
K2O	9.35	9.73	9.72	9.80	8.88	9.58
F	0.44	-	-	-	-	-
Total	95.72	94.96	94.99	95.4	94.31	95.07
Structura						
Si	5.611	5.955	5.954	5.959	5.878	5.946
Al(iv)	2.388	2.045	2.046	2.041	2.122	2.054
Al(vi)	0.178	0.566	0.476	0.553	0.535	0.565
Ti	0.333	0.323	0.486	0.411	0.319	0.372
Fe2+	2.165	2.264	2.259	2.300	2.320	2.288
Mn	0.025	0.032	0.036	0.037	0.038	0.034
Mg	3.052	3.235	3.029	3.034	3.342	3.133
Ca	-	-	0.002	-	0.006	-
Na	0.034	0.030	0.063	0.028	0.028	0.031
K	1.792	1.971	1.970	1.980	1.808	1.938

	XG89 2 Biot 6C	XG89 2 Biot 7M	XG89 2 Biot 8M	XG89 2 Biot 9M	XG89 2 Biot 10M	XG4 5 Biot 1R
SiO2	37.29	37.26	38.25	37.58	37.65	36.96
TiO2	3.36	3.15	3.19	3.39	3.67	2.81
Al2O3	13.73	13.91	13.99	13.67	13.83	13.68
FeO*	17.38	17.46	16.98	17.00	16.85	16.93
MgO	13.15	12.99	13.15	13.01	12.90	13.82
MnO	0.27	0.28	0.25	0.26	0.24	0.23
CaO	-	0.01	-	-	-	-
Na2O	0.09	0.11	0.10	0.14	0.10	0.22
K2O	9.49	9.25	9.62	9.61	9.71	9.92
F	-	-	-	-	-	-
Total	94.76	94.42	95.53	94.66	94.95	94.57
Structura						
Si	5.938	5.948	6.014	5.981	5.968	5.910
Al(iv)	2.070	2.052	1.986	2.019	2.032	2.090
Al(vi)	0.509	0.566	0.607	0.546	0.552	0.490
Ti	0.403	0.379	0.378	0.406	0.439	0.339
Fe2+	2.315	2.331	2.233	2.263	2.234	2.264
Mn	0.038	0.038	0.034	0.036	0.033	0.031
Mg	3.121	3.092	3.081	3.086	3.049	3.295
Ca	-	0.002	-	-	-	-
Na	0.029	0.036	0.033	0.043	0.032	0.070
K	1.929	1.885	1.930	1.953	1.964	2.024

APPENDIX C

Table C.3: BIOTITE MICROPROBE ANALYSES

	XG45 Biot 2C	XG45 Biot 3M	XG45 Biot 4M	XG45 Biot 5M	XG45 Biot 6C	XG45 Biot 7C
SiO2	36.93	37.39	37.32	37.35	37.62	37.32
TiO2	3.45	3.39	3.43	3.15	2.87	3.41
Al2O3	13.48	14.05	13.84	13.83	14.01	13.78
FeO*	17.39	17.46	17.24	17.37	17.17	17.32
MgO	13.47	13.46	13.59	13.36	13.71	13.36
MnO	0.23	0.23	0.23	0.24	0.25	0.25
CaO	-	-	-	-	0.03	-
Na2O	0.16	0.18	0.05	0.18	0.18	0.11
K2O	9.95	10.00	10.04	9.81	10.03	10.08
F	-	-	-	-	-	-
Total	95.06	96.16	95.74	95.29	95.87	95.63
Structura						
Si	5.891	5.884	5.896	5.926	5.928	5.908
Al(iv)	2.109	2.116	2.104	2.074	2.080	2.092
Al(vi)	0.427	0.492	0.474	0.513	0.523	0.480
Ti	0.415	0.403	0.408	0.377	0.341	0.407
Fe2+	2.320	2.299	2.278	2.305	2.263	2.293
Mn	0.031	0.032	0.031	0.033	0.034	0.034
Mg	3.201	3.157	3.200	3.159	3.220	3.154
Ca	-	-	-	-	0.007	-
Na	0.050	0.056	0.017	0.056	0.056	0.033
K	2.025	2.008	2.024	1.987	2.018	2.037

	XG45 Biot 8C
SiO2	37.41
TiO2	3.37
Al2O3	13.79
FeO*	17.52
MgO	13.22
MnO	0.24
CaO	-
Na2O	0.10
K2O	10.10
F	-
Total	95.75
Structura	
Si	5.918
Al(iv)	2.082
Al(vi)	0.492
Ti	0.401
Fe2+	2.318
Mn	0.033
Mg	3.117
Ca	-
Na	0.033
K	2.039

APPENDIX C

Table C4: OXIDE MICROPROBE ANALYSIS

	SGIII TGD Haem. 2	SGIII TGD Haem. 5	SGVIII Late Ti-Mg 1	SGVIII Late Haem. 2	SGIX TGD Ti-Mg 1	G24 TGD Ti-Mg 2
SiO2	0.28	0.05	0.04	0.06	0.01	0.05
TiO2	0.03	0.07	20.41	0.03	16.80	21.73
Al2O3	0.10	0.18	0.09	0.06	0.07	0.08
Cr2O3	0.01	0.75	0.15	0.06	0.17	0.04
FeO*	89.73	90.01	69.49	89.71	73.20	69.68
MgO	0.03	0.06	0.07	-	0.09	0.12
MnO	0.02	0.12	0.35	0.02	0.35	0.30
Total	90.20		90.60		90.69	92.00

	SG49 PGD Haem. 1	SG49 PGD Haem. 2	SG49 PGD Haem. 3	SG49 PGD Haem. 4	SG78 BGT Haem. 1	XG7 1B Ilm. 1
SiO2	0.37	-	0.08	0.05	0.03	0.06
TiO2	0.07	0.05	0.06	0.04	0.08	46.72
Al2O3	0.19	0.02	0.01	0.02	0.04	0.03
Cr2O3	0.37	0.40	0.40	0.19	0.13	-
FeO*	88.54	90.03	90.03	90.14	90.27	46.96
MgO	0.10	0.06	-	-	-	0.54
MnO	0.09	-	0.06	0.02	0.05	2.64
Total	89.73		90.64			96.95

	XG7 1B Ilm. 2	XG7 1B Ilm. 3	XG44 2 Haem 1	XG44 2 Haem. 2	XG44 2 Haem. 3	XG89 2 Ti-Mg 1
SiO2	0.05	0.03	0.03	0.03	0.04	0.07
TiO2	42.17	42.68	0.06	0.11	0.07	10.66
Al2O3	0.04	0.02	0.05	0.12	0.08	0.04
Cr2O3	-	0.04	0.70	0.69	0.87	0.14
FeO*	52.26	49.04	90.29	90.02	89.84	78.36
MgO	0.46	0.01	0.04	0.01	-	0.06
MnO	0.87	2.56	0.07	0.09	0.07	0.06
Total	95.85	94.38	91.24		90.97	89.39

APPENDIX C

Table C4: OXIDE MICROPROBE ANALYSIS

	XG89 2 Ilm. 2	XG4 5 Ti-Mg 1	XG4 5 Ti-Mg 2
SiO2	0.08	-	0.01
TiO2	49.07	17.09	20.12
Al2O3	0.03	0.05	0.02
Cr2O3	-	0.21	0.21
FeO*	43.77	75.12	70.10
MgO	0.43	0.11	0.12
MnO	2.74	0.21	0.46
Total	96.12	92.79	91.04

APPENDIX C

Table C.5: PYROXENE MICROPROBE ANALYSES

	D11 Lidd Aug. 1	D11 Lidd Aug. 2	D11 Lidd Aug. 3	D11 Lidd Aug. 4	D11 Lidd Aug. 5	D11 Lidd Opx. 6
SiO2	52.78	53.84	51.01	52.31	52.91	52.75
TiO2	0.45	0.43	0.54	0.56	0.40	0.09
Al2O3	2.86	2.75	4.78	3.94	3.41	1.36
Cr2O3	0.07	0.02	0.07	0.13	0.01	0.03
FeO*	7.46	7.27	7.92	7.47	7.38	14.60
MgO	19.26	19.52	18.19	0.15	0.17	0.46
MnO	0.14	0.17	0.15	18.81	19.07	23.29
CaO	11.90	12.04	12.12	12.11	12.17	1.27
Na2O	0.69	0.64	0.89	0.83	0.75	0.26
TOTAL	95.61	96.68	95.67	96.31	96.27	94.11
Structural Formulae						
Si	1.980	1.99	1.92	1.95	1.97	2.02
Al(iv)	0.02	0.01	0.08	0.05	0.03	-
Al(vi)	0.11	0.11	0.14	0.13	0.12	0.06
Ti	0.01	0.01	0.02	0.02	0.01	0.00
Cr	0.00	0.00	0.00	0.00	-	0.00
Fe2+	0.23	0.23	0.25	0.23	0.23	0.47
Mn	0.00	0.01	0.01	0.01	0.01	0.02
Mg	1.08	1.08	1.02	1.05	1.06	1.33
Ca	0.48	0.48	0.49	0.48	0.49	0.05
Na	0.050	0.05	0.07	0.06	0.05	0.02
Wo	27.0	26.90	28	27.40	27.40	2.60
En	60.0	60.50	58	59.30	59.70	72.10
Fs	13.0	12.60	14	13.20	12.90	25.30

APPENDIX C

Table C.5: PYROXENE MICROPROBE ANALYSES

	D11 Lidd Aug. 7	D11 Lidd Opx 8	D11 Lidd Opx 9	D11 Lidd Opx. 10	D11 Lidd Aug. 11	D11 Lidd Opx. 12
SiO2	55.40	55.34	55.34	56.05	54.42	54.92
TiO2	0.08	0.03	0.04	0.03	0.27	0.13
Al2O3	1.54	0.24	0.41	0.27	2.78	1.79
Cr2O3	0.03	0.03	0.01	0.02	0.08	0.03
FeO*	5.73	13.70	14.25	13.66	9.89	13.79
MgO	21.00	24.79	24.75	0.44	21.90	0.53
MnO	0.19	0.49	0.53	24.99	0.36	23.54
CaO	12.44	1.54	0.76	0.78	6.83	1.51
Na2O	0.32	0.07	0.06	0.05	0.59	0.33
TOTAL	96.73	96.23	96.15	96.29	97.12	96.57
Structura						
Si	2.03	2.05	2.05	2.07	2.00	2.03
Al(iv)	-	-	-	-	0.00	-
Al(vi)	0.07	0.01	0.02	0.01	0.12	0.08
Ti	0.00	0.00	0.00	0.00	0.01	0.00
Cr	0.00	0.00	-	-	0.00	0.00
Fe2+	0.18	0.43	0.44	0.42	3.03	0.43
Mn	0.01	0.02	0.02	0.01	0.01	0.02
Mg	1.15	1.37	1.37	1.38	1.20	1.30
Ca	0.49	0.06	0.030	0.03	0.27	0.06
Na	0.02	0.01	0.00	0.00	0.04	0.02
Wo	27.0	3.3	1.7	1.70	15.2	3.50
En	63.3	73.8	74.3	75.20	67.7	72.60
Fs	9.7	22.9	24.0	23.10	17.2	23.90

APPENDIX C

Table C.5: PYROXENE MICROPROBE ANALYSES

	D11 Lidd Opx 13
SiO2	51.39
TiO2	0.35
Al2O3	3.39
Cr2O3	0.06
FeO*	14.41
MgO	21.62
MnO	0.61
CaO	0.77
Na2O	0.06
TOTAL	92.66
Structura	
Si	1.99
Al(iv)	0.01
Al(vi)	0.14
Ti	0.010
Cr	0.00
Fe2+	0.47
Mn	0.020
Mg	1.25
Ca	0.03
Na	0.01
Wo	1.9
En	71.4
Fs	26.7

APPENDIX C

Table C.6: SPHENE MICROPROBE ANALYSES

	SGIII TGD Sph 1	SGIII TGD Sph 2	SGIII TGD Sph 3	SGIII TGD Sph 4	SGIII TGD Sph 5	SGIII TGD Sph 6
SiO2	29.78	29.58	28.44	29.53	29.02	28.74
TiO2	37.28	37.04	36.47	37.44	36.49	36.06
Al2O3	1.12	1.04	1.13	0.93	1.01	1.08
FeO*	1.29	1.44	1.77	1.27	1.53	1.55
MnO	0.11	0.10	0.11	0.10	0.08	0.09
CaO	27.51	27.46	27.02	27.91	26.70	26.72
Na2O	0.03	0.02	0.03	0.05	0.08	0.05
Total	97.12	96.68	94.97	97.23	94.91	94.29

	SGVII Late Sph 1	SGVII Late Sph 2	SGVII Late Sph 3	SGVII Late Sph 5	SGVIII Late Sph 1	SGVIII Late Sph 2
SiO2	29.79	28.67	29.66	29.59	29.86	29.54
TiO2	36.86	36.46	37.24	37.63	37.79	35.44
Al2O3	1.09	0.97	1.04	1	0.93	1.45
FeO*	1.50	1.55	1.33	1.16	1.04	2.04
MnO	0.08	0.04	0.08	0.06	0.07	0.08
CaO	27.74	26.24	27.61	27.82	27.54	27.26
Na2O	0.04	0.05	0.04	0.03	0.03	0.04
Total	97.10	93.98	97.00	97.29	97.26	95.85

	SGVIII Late Sph 3	SGVIII Late Sph 4	SGVIII Late Sph 5	SGVIII Late Sph 6	SGVIII Late Sph 7	SGVIII Late Sph 8
SiO2	29.87	29.86	29.92	29.79	29.63	30.07
TiO2	37.59	37.81	37.76	37.83	36.25	37.26
Al2O3	1.08	0.87	1.08	0.96	1.30	1.21
FeO*	1.14	1.11	1.26	1.21	1.93	1.58
MnO	0.09	0.07	0.08	0.12	0.11	0.09
CaO	27.64	27.81	28.32	27.73	27.55	28.31
Na2O	0.05	0.03	0.01	0.02	0.03	0.02
Total	97.46	97.56	98.43	97.66	96.80	98.54

APPENDIX C

Table C.6: SPHENE MICROPROBE ANALYSES

	SGIX TGD Sph 1C	SGIX TGD Sph 2C	SGX Late Sph 1	SGX Late Sph 2	SGX Late Sph 3	SGX Late Sph 4
SiO2	29.94	28.52	29.39	29.69	28.92	29
TiO2	37.83	34.89	37.12	37.76	36.17	36.29
Al2O3	0.76	1.11	1.09	1.06	1.07	1.06
FeO*	0.95	1.73	1.38	1.36	1.70	1.59
MnO	-	-	0.05	0.11	0.09	0.07
CaO	27.62	26.84	27.59	28.35	26.54	26.72
Na2O	-	-	0.02	0.02	0.03	0.05
Total	97.10	93.09	96.64	98.35	94.52	94.78

	SGX Late Sph 4	SGX Late Sph 5	SGX Late Sph 6	SGX Late Sph 7	SGXIII TGD Sph 1	SGXIII TGD Sph 2
SiO2	29	28.97	29.03	28.94	29.55	29.34
TiO2	36.29	37.33	36.23	36.33	36.88	36.61
Al2O3	1.06	0.96	1.19	1.09	1.14	1.20
FeO*	1.59	1.27	1.63	1.62	1.61	1.54
MnO	0.07	0.08	0.08	0.10	0.09	0.10
CaO	26.72	27.48	26.88	26.99	27.48	27.61
Na2O	0.05	0.03	0.03	0.04	0.03	0.01
Total	94.78	96.12	95.07	95.11	96.78	96.41

	SGXIII TGD Sph 3	SGXIII TGD Sph 4	SGXIII TGD Sph 5	SGXIII TGD Sph 6	SGXIII TGD Sph 7	SGXIII TGD Sph 8
SiO2	29.65	29.33	29.59	30.09	29.96	29.67
TiO2	36.81	37.33	37.96	37.60	37.49	37.14
Al2O3	1.15	0.89	0.87	1.04	1.06	1.12
FeO*	1.52	1.31	1.02	1.36	1.44	1.55
MnO	0.11	0.12	0.06	0.08	0.11	0.10
CaO	27.62	27.22	27.59	28.22	28.07	27.81
Na2O	0.03	0.03	0.04	0.02	0.04	0.01
Total	96.89	96.23	97.13	98.41	98.17	97.40

APPENDIX C

Table C.6: SPHENE MICROPROBE ANALYSES

	SGXIII TGD Sph 1R	SGXIII TGD Sph 2C	SGXXVI TGD Sph 1C	SGXXVI TGD Sph 2C	G24 TGD Sph 1C	G24 TGD Sph 2R
SiO2	29.96	28.95	29.49	29.47	29.71	29.85
TiO2	37.09	35.68	37.20	36.97	36.83	36.18
Al2O3	0.98	1.07	0.87	0.98	1.09	1.32
FeO*	1.22	1.74	1.18	1.45	1.05	1.35
MnO	-	-	-	-	-	-
CaO	27.56	25.98	26.94	27.27	26.85	27.20
Na2O	-	-	-	-	-	-
Total	96.81	93.42	95.68	96.14	95.53	95.90

	G24 TGD Sph 3C	SG49 PGD Sph 1	SG49 PGD Sph 2	SG49 PGD Sph 3	SG49 PGD Sph 4	SG49 PGD Sph 5
SiO2	29.46	30.15	29.60	30.48	30.20	29.54
TiO2	36.80	37.85	37.05	37.95	38.33	37.11
Al2O3	1.05	0.99	0.95	1.01	0.96	1.08
FeO*	1.07	1.14	1.37	1.20	1.19	1.50
MnO	-	0.12	0.08	0.08	0.08	0.10
CaO	26.95	28.41	27.36	28.47	28.53	27.74
Na2O	-	-	0.02	0.04	0.02	0.03
Total	95.33	98.66	96.43	99.23	99.31	97.10

	SG49 PGD Sph 6	SG49 PGD Sph 7	SG49 PGD Sph 8	SG78 BGT Sph 1	SG78 BGT Sph 2	SG78 BGT Sph 3
SiO2	29.56	29.51	29.65	29.92	29.41	29.38
TiO2	36.51	36.43	37.48	36.79	36.15	36.15
Al2O3	1.09	1.13	1.02	1.32	1.41	1.39
FeO*	1.84	1.87	1.67	1.42	1.75	1.71
MnO	0.08	0.13	0.12	0.13	0.11	0.08
CaO	27.16	27.26	27.69	28.09	27.94	27.11
Na2O	0.02	0.02	0.01	0.01	0.05	0.02
Total	96.26	96.35	97.64	97.68	96.82	95.84

APPENDIX C

Table C.6: SPHENE MICROPROBE ANALYSES

	SG78 BGT Sph 4	SG78 BGT Sph 5	SG78 BGT Sph 6	D1 Rubh Sph 1	D11 Lidd Sph 1	D11 Lidd Sph 2
SiO2	29.06	29.89	29.04	30.07	29.54	29.57
TiO2	36.05	37.21	35.77	35.75	37.46	36.38
Al2O3	1.06	1.20	1.27	1.29	1.19	1.37
FeO*	1.70	1.32	1.73	1.44	1.46	1.61
MnO	0.06	0.09	0.13	-	0.04	0.02
CaO	26.73	27.99	26.52	26.51	28.03	27.62
Na2O	0.02	0.04	0.04	-	0.02	-
Total	94.68	97.74	94.50	95.06	97.74	96.57

	D19 Shet Sph 1	D19 Shet Sph 2	D19 Shet Sph 3	D19 Shet Sph 4	D19 Shet Sph 5	D41 Rana Sph 1
SiO2	29.91	29.70	29.74	29.92	29.78	29.60
TiO2	38.33	37.72	37.65	37.12	36.94	37.25
Al2O3	0.88	1.07	0.99	1.16	1.27	1.14
FeO*	0.72	0.91	0.98	1.16	1.25	1
MnO	0.06	0.08	0.08	0.06	0.06	0.04
CaO	28.20	27.59	27.54	27.51	27.53	27.83
Na2O	-	0.03	0.04	0.01	0.03	0.02
Total	98.10	97.10	97.02	96.94	96.86	96.88

	D41 Rana Sph 2	D41 Rana Sph 3	D41 Rana Sph 4	D41 Rana Sph 5	D41 Rana Sph 6	D63 Uil Sph 1
SiO2	29.82	29.33	28.74	29.58	29.37	28.95
TiO2	36.98	37.81	36.17	37.73	37.27	37.27
Al2O3	1.43	0.89	1.13	0.93	1.07	0.98
FeO*	1.15	0.83	1.10	0.81	0.96	1.22
MnO	0.05	0.06	0.06	0.06	27.19	0.04
CaO	28.15	27.61	26.84	27.81	-	27.48
Na2O	0.03	0.03	0.02	0.03		0.03
Total	97.61	96.56	94.06	96.95	95.86	95.97

APPENDIX C

Table C.6: SPHENE MICROPROBE ANALYSES

	D63 Uil Sph 2	D63 Uil Sph 3	D63 Uil Sph 4	D63 Uil Sph 5	D63 Uil Sph 6	D63 Uil Sph 7
SiO2	29.13	29.63	29.08	29.97	29.53	30.01
TiO2	36.89	36.87	36.91	37.44	37.83	37.49
Al2O3	1.07	1.15	1.11	1.12	1.08	1.04
FeO*	1.45	1.53	1.47	1.43	1.27	1.23
MnO	0.10	0.04	0.02	0.08	0.07	0.07
CaO	27.56	28.39	27.56	28.51	28.32	28.51
Na2O	0.05	0.03	0.03	0.02	0.03	0.03
Total	96.25	97.64	96.18	98.57	98.13	98.38

	D63 Uil Sph 3	D63 Uil Sph 4	D63 Uil Sph 5	D63 Uil Sph 6	D63 Uil Sph 7	XG32 1A Sph 1
SiO2	29.63	29.08	29.97	29.53	30.01	29.76
TiO2	36.87	36.91	37.44	37.83	37.49	37.12
Al2O3	1.15	1.11	1.12	1.08	1.04	1.32
FeO*	1.53	1.47	1.43	1.27	1.23	1.46
MnO	0.04	0.02	0.08	0.07	0.07	0.12
CaO	28.39	27.56	28.51	28.32	28.51	28.28
Na2O	0.03	0.03	0.02	0.03	0.03	-
Total	97.64	96.18	98.57	98.13	98.38	98.06

	XG32 1A Sph 2	XG32 1A Sph 3	XG32 1A Sph 4	XG32 1A Sph 5	XG32 1A Sph 6	XG32 1A Sph 7
SiO2	29.31	29.46	29.60	29.21	29.57	29.59
TiO2	37.31	37.14	37.19	36.19	36.78	36.88
Al2O3	1.09	1.21	1.17	1.28	1.29	1.21
FeO*	1.19	1.44	1.26	1.41	1.43	1.34
MnO	0.09	0.08	0.10	0.12	0.08	0.12
CaO	27.82	28.57	28.07	27.23	27.56	27.85
Na2O	0.02	0.03	0.01	0.06	0.03	0.01
Total	96.83	97.93	97.40	95.50	96.74	97.00

APPENDIX C

Table C.6: SPHENE MICROPROBE ANALYSES

	XG65 1A Sph 1	XG65 1A Sph 2	XG65 1A Sph 4	XG65 1A Sph 5	XG65 1A Sph 6	XG65 1A Sph 7
SiO2	29.43	29.13	29.49	29.42	29.97	30.06
TiO2	37.31	36.75	36.60	37.78	36.27	37.24
Al2O3	0.87	0.99	1.12	0.93	1.06	1.23
FeO*	1.19	1.33	1.69	1.21	1.46	1.46
MnO	0.09	0.11	0.09	0.09	0.05	0.13
CaO	27.61	27.17	27.66	27.48	26.83	28.16
Na2O	0.01	0.03	0.03	0.03	0.05	0.02
Total	96.51	95.51	96.68	96.94	95.69	98.30

	XG24 1B Sph 1	XG24 1B Sph 2R	XG24 1B Sph 3C	XG24 1B Sph 4R	XG24 1B Sph 5M	XG24 1B Sph 6
SiO2	29.39	29.24	29.84	29.74	29.58	29.91
TiO2	37.95	37.67	37.39	37.95	38.23	36.95
Al2O3	0.89	0.79	1.01	0.87	0.85	1.37
FeO*	0.99	0.93	1.09	0.96	0.86	1.29
MnO	0.09	0.09	0.09	0.08	0.10	0.08
CaO	28.27	28.35	28.15	28.32	28.32	28.26
Na2O	0.02	0.01	0.03	0.03	0.06	0.03
Total	97.60	97.08	97.60	97.95	98.00	97.89

	XG24 1B Sph 7	XG24 1B Sph 8	XG24 1B Sph 9	XG24 1B Sph 10	XG64A 1B Sph 1	XG64A 1B Sph 2
SiO2	29.54	29.58	28.87	29.37	29.79	30.03
TiO2	37.86	37.71	37.92	37.53	37.23	37.33
Al2O3	0.82	0.90	0.89	0.93	1.12	1.08
FeO*	0.98	0.97	0.87	1.04	1.44	1.57
MnO	0.09	0.11	0.08	0.08	0.09	0.05
CaO	28.14	28.06	28.06	27.87	28.21	28.35
Na2O	0.04	0.03	0.04	0.01	0.02	0.03
Total	97.47	97.36	96.73	96.83	97.90	98.44

APPENDIX C

Table C.6: SPHENE MICROBROBE ANALYSES

	XG64A 1B Sph 3	XG64A 1B Sph 4	XG64A 1B Sph 5R	XG64A 1B Sph 6C	XG64A 1B Sph 7	XG64A 1B Sph 8
SiO2	29.45	29.64	29.81	29.76	29.76	29.82
TiO2	37.43	37.62	37.56	36.95	37.36	37.98
Al2O3	0.88	0.92	1.06	1.11	1.04	0.92
FeO*	1.18	0.88	1.43	1.45	1.17	1.08
MnO	0.07	0.08	0.09	0.06	0.06	0.07
CaO	27.69	28.01	28.36	28.22	27.70	28.28
Na2O	0.03	0.03	0.03	0.03	0.03	0.04
Total	96.73	97.18	98.34	97.58	97.12	98.19

	XG64A 1B Sph 9	X181 2 Sph 1	X181 2 Sph 2	X181 2 Sph 3	X181 2 Sph 4	X181 2 Sph 5
SiO2	29.83	29.85	29.90	29.57	29.93	29.93
TiO2	37.14	37.10	36.97	37.41	37.53	37.58
Al2O3	1.06	1.21	1.26	1.01	1.07	1.04
FeO*	1.38	1.46	1.51	1.08	1.24	1.28
MnO	0.09	0.08	0.06	0.08	0.05	0.07
CaO	28.14	28.15	28.12	27.88	28.07	27.97
Na2O	0.03	0.02	0.04	0.03	0.02	0.03
Total	97.67	97.87	97.86	97.06	97.91	97.90

	X181 2 Sph 6	X181 2 Sph 7	X181 2 Sph 8	X181 2 Sph 9	XG44 2 Sph 1	XG44 2 Sph 2
SiO2	29.84	29.96	29.57	29.53	29.41	30.28
TiO2	36.59	36.84	38.13	37.56	37.75	36.97
Al2O3	1.26	1.28	0.87	0.98	0.99	1.25
FeO*	1.65	1.66	1.03	1.12	1.15	1.75
MnO	0.05	0.06	0.06	0.06	0.09	0.08
CaO	27.70	28.17	27.96	27.81	28.29	28.25
Na2O	0.05	0.04	0.03	0.02	0.01	0.02
Total	97.14	98.01	97.65	97.08	97.69	98.60

APPENDIX C

Table C.6: SPHENE MICROBROBE ANALYSES

	XG44 2 Sph 3	XG44 2 Sph 4	XG44 2 Sph 5	XG61B 2 Sph 1C	XG61B 2 Sph 2C	XG61B 2 Sph 3R
SiO2	29.73	29.96	29.59	29.38	29.88	29.94
TiO2	37.98	37.09	36.88	36.72	36.96	36.56
Al2O3	0.79	1.11	1.06	1.05	1.19	1.15
FeO*	1.04	1.48	1.43	1.37	1.34	1.24
MnO	0.07	0.08	0.09	-	-	-
CaO	28.02	27.96	28.12	26.93	27.82	27.50
Na2O	0.03	0.03	0.03	-	-	-
Total	97.66	97.71	97.20	95.45	97.19	96.39

	XG61B 2 Sph 4C	XG61C 2 Sph 1	XG61C 2 Sph 2	XG61C 2 Sph 3	XG61C 2 Sph 4	XG61C 2 Sph 5
SiO2	29.59	29.79	30.06	29.67	29.49	29.35
TiO2	36.39	37.48	37.69	38.49	37.42	37.52
Al2O3	1.03	1.15	1.18	0.80	1.09	0.89
FeO*	1.31	1.31	1.24	0.83	1.17	1.18
MnO	-	0.07	0.04	0.07	0.06	0.07
CaO	26.96	28.33	28.64	28.26	27.86	27.60
Na2O	-	0.03	-	0.03	0.03	0.03
Total	95.28	98.16	98.85	98.15	97.12	96.64

	XG61C 2 Sph 6	XG61C 2 Sph 7	XG61C 2 Sph 8	XG4 5 Sph 1R	XG4 5 Sph 2C	XG4 5 Sph 3M
SiO2	29.83	29.64	29.57	30.57	28.94	29.57
TiO2	37.57	36.35	38.61	37.13	36.71	38.04
Al2O3	1.13	1.28	0.81	1.37	0.94	0.82
FeO*	1.26	1.59	0.86	0.95	1.49	1.12
MnO	0.06	0.08	0.07	-	-	-
CaO	28.43	28.11	28.45	26.85	26.79	27.65
Na2O	0.03	0.02	0.05	-	-	-
Total	98.31	97.07	98.42	96.87	94.87	97.20

APPENDIX C

Table C.6: SPHENE MICROBROBE ANALYSES

	E1 Dyke Sph 1	E1 Dyke Sph 2	E1 Dyke Sph 3	E3 Dyke Sph 1	E3 Dyke Sph 2	E3 Dyke Sph 3
SiO2	29.78	29.04	29.48	29.42	29.22	29.71
TiO2	37.40	36.51	36.92	37.87	37.37	38.04
Al2O3	1.06	1.07	1.21	0.87	0.97	0.83
FeO*	1.13	1.16	1.23	0.94	0.97	0.84
MnO	0.07	0.02	0.04	0.04	0.07	0.07
CaO	27.89	27.15	27.94	27.87	27.72	27.81
Na2O	0.02	-	0.03	0.03	0.02	0.02
Total	97.35	94.95	96.85	97.04	96.34	97.32

	E3 Dyke Sph 4	E3 Dyke Sph 5	E3 Dyke Sph 6	E3 Dyke Sph 7	E5A Dyke Sph 1	E5A Dyke Sph 2
SiO2	29.63	29.56	29.61	29.41	29.97	29.77
TiO2	38.08	37.56	37.92	37.49	37.64	37.68
Al2O3	0.99	1.08	1.02	1.05	1.06	1.07
FeO*	1.03	1.10	0.93	1.09	1.44	1.31
MnO	0.05	0.06	0.06	0.04	0.07	0.08
CaO	28.23	28.14	27.72	27.91	28.65	28.12
Na2O	0.03	0.01	0.01	0.02	0.01	0.01
Total	98.04	97.51	97.27	97.01	98.84	98.04

	E5A Dyke Sph 3	E5A Dyke Sph 4	E5A Dyke Sph 5	E5A Dyke Sph 6
SiO2	29.15	29.40	28.97	29.38
TiO2	35.79	36.31	35.26	37.08
Al2O3	0.99	1.19	1.49	1.05
FeO*	1.52	1.60	2.09	1.48
MnO	0.05	0.05	0.06	0.06
CaO	27.41	27.92	27.64	27.89
Na2O	-	0.01	0.02	0.02
Total	94.91	96.48	95.53	96.96

APPENDIX C

Table C.7: SULPHIDE MICROPROBE ANALYSES

	D8 Rubh Pt1	D8 Rubh Pt2	D8 Rubh Pt3	D8 Rubh Pt4	D8 Rubh Pt5	D8 Rubh Pt6
Fe	45.83	45.09	45.87	46.19	45.73	45.80
Co	0.13	1.35	0.19	0.08	0.21	0.19
Ni	0.49	0.18	0.37	0.51	0.16	0.02
Cu	-	-	0.04	0.03	-	-
S	53.42	53.51	53.70	53.51	53.53	53.55
Total	99.87	100.13	100.17	100.32	99.63	99.56

	D8 Rubh Pt7	D8 Rubh Pt8	D8 Rubh Mi 1	D8 Rubh Mi 2	D8 Rubh Mi 3	D8 Rubh Cp 1
Fe	44.95	46.39	2.27	1.51	1.19	30.70
Co	0.97	0.06	0.01	0.05	-	0.06
Ni	0.07	0.08	60.57	60.83	61.38	0.01
Cu	-	0.02	0.08	0.07	0.06	32.66
S	53.57	53.54	35.57	35.55	35.58	35.07
Total	99.56	100.09	98.50	98.01	98.21	98.50

	D8 Rubh Cp 1	D8 Rubh Cp 2	D8 Rubh Cp 3	D11 Lidd Cp 1	D11 Lidd Cp 2	D11 Lidd Cp 3
Fe	30.70	30.77	30.66	30.17	30.69	30.74
Co	0.06	0.06	0.05	0.04	0.03	0.05
Ni	0.01	0.13	0.16	0.11	2.18	0.04
Cu	32.66	31.95	32.12	32.97	30.59	32.34
S	35.07	35.11	35.23	35.08	34.94	34.99
Total	98.50	98.02	98.22	98.37	98.43	98.16

APPENDIX C

Table C.7: SULPHIDE MICROPROBE ANALYSES

	D11 Lidd Cp 4	D11 Lidd Cp 5	D11 Lidd Cp 6	D11 Lidd Pt1	D11 Lidd Pt2	D11 Lidd Pt3
Fe	30.41	30.59	30.41	46.16	46.61	46.57
Co	0.06	0.03	0.05	0.15	0.08	0.03
Ni	-	0.03	0.06	0.24	0.05	0.21
Cu	32.61	32.18	32.44	0.03	-	0.03
S	35.16	34.94	35.16	53.68	53.79	53.60
Total	98.24	97.77	98.12	100.26	100.53	100.44

	D11 Lidd Pt4	D11 Lidd Pt5	D11 Lidd Pt6	D11 Lidd Pt7	D11 Lidd Pt8	D11 Lidd Pt9
Fe	46.04	45.14	46.24	45.72	45.77	45.55
Co	0.06	1.28	0.29	0.32	0.81	0.51
Ni	0.30	0.03	0.05	0.55	0.05	0.06
Cu	0.03	0.01	0.01	-	0.04	0.03
S	53.48	53.51	53.52	53.37	53.55	53.38
Total	99.91	99.97	100.11	99.96	100.22	99.53

	D11 Lidd Pt10	D11 Lidd Pt11	D11 Lidd Pt12	D11 Lidd Pe 1	D11 Lidd Pe 2	D11 Lidd Mi 1
Fe	46.29	45.82	45.49	31.59	31.71	0.45
Co	0.07	0.09	0.39	0.04	0.05	0.26
Ni	0.14	0.21	0.07	33.72	33.52	61.99
Cu	0.04	0.03	0.05	0.04	0.06	0.08
S	53.43	53.44	53.52	33.43	33.47	35.68
Total	99.97	99.59	99.52	98.82	98.81	98.46

APPENDIX C

Table C.7: SULPHIDE MICROPROBE ANALYSES

	D11 Lidd Mi 2	D11 Lidd Mi 3	D11 Lidd Mi 4	D19 Shet Pt1	D19 Shet Pt2	D19 Shet Pt3
Fe	0.46	2.37	1.33	45.85	45.76	46.07
Co	0.26	0.81	0.29	0.16	0.10	0.08
Ni	62.23	60.18	61.59	0.18	0.12	0.28
Cu	0.04	0.36	0.08	0.04	0.03	0.01
S	35.58	35.57	35.58	53.42	53.62	53.47
Total	98.57	99.29	98.87	99.65	99.63	99.91

	D19 Shet Pt4	D19 Shet Pt5	D19 Shet Pt6	D19 Shet Pt7	D19 Shet Pt8	D19 Shet Cp 1
Fe	45.71	46.16	46.34	46.15	45.86	30.24
Co	0.07	0.07	0.06	0.07	0.14	0.06
Ni	0.25	0.07	0.09	0.05	0.06	0.03
Cu	0.05	-	0.03	0.01	0.07	32.11
S	53.49	53.56	53.29	53.48	53.58	35.19
Total	99.57	99.86	99.81	99.76	99.71	97.63

	D19 Shet Cp 2	D19 Shet Cp 3	D19 Shet Cp 4	D19 Shet Cp 5	D19 Shet Cp 6	D41 Rana Pt1
Fe	30.07	30.21	29.97	30.46	30.37	45.91
Co	0.04	0.04	0.03	0.04	0.03	0.13
Ni	0.07	0.02	-	0.04	0.01	0.08
Cu	32.64	32.52	32.57	32.44	32.66	-
S	34.97	34.97	34.94	35.06	35.10	53.70
Total	97.79	97.76	97.51	98.04	98.17	99.82

APPENDIX C

Table C.7: SULPHIDE MICROPROBE ANALYSES

	D41 Rana Pt2	D41 Rana Pt3	D41 Rana Pt4	D41 Rana Pt5	D63 Uil Pt1	D63 Uil Pt2
Fe	45.91	45.36	45.68	46.07	46.09	45.94
Co	0.18	0.62	0.17	0.05	0.05	0.06
Ni	0.07	0.11	0.05	0.05	0.14	0.05
Cu	0.06	0.01	0.01	0.04	0.01	0.04
S	53.57	53.58	53.62	53.29	53.41	53.44
Total	99.79	99.68	99.53	99.50	99.70	99.53

	D63 Uil Pt3	D63 Uil Pt4	D63 Uil Pt5	D63 Uil Pt6	D63 Uil Pt7	D63 Uil Pt8
Fe	45.07	46.26	45.35	46.16	46.03	45.87
Co	1.24	0.06	1.01	0.05	0.05	0.42
Ni	0.05	0.09	0.04	0.03	0.17	0.14
Cu	0.03	-	0.04	0.03	0.04	0.03
S	53.33	53.34	53.62	53.38	53.27	53.33
Total	99.72	99.75	100.06	99.65	99.56	99.79

	D63 Uil Pt9	D63 Uil Pt10	D63 Uil Pt11	D63 Uil Cp 1	D63 Uil Cp 2	D63 Uil Cp 3
Fe	45.68	46.43	45.87	31.01	33.03	30.60
Co	0.06	0.06	0.17	0.03	0.05	0.01
Ni	0.33	0.05	0.18	0.02	0.64	0.02
Cu	0.03	-	0.02	31.32	29.13	31.81
S	53.48	53.49	53.43	35.43	35.16	34.92
Total	99.58	100.03	99.67	97.81	98.01	97.36

APPENDIX C

Table C.7: SULPHIDE MICROPROBE ANALYSES

	D63 Uil Cp 4	D63 Uil Cp 5	D63 Uil Cp 6	D63 Uil Cp 7
Fe	30.37	31.19	30.42	31.18
Co	0.01	0.03	0.04	0.03
Ni	0.02	0.02	1.25	0.02
Cu	31.57	32.29	31.15	26.28
S	34.98	34.91	35.06	35.06
Total	96.95	98.44	97.92	92.57

APPENDIX C

Table C.8: ALKALI FELDSPAR MICROPROBE ANALYSES

1	SGIII TGD Or 1	SGVII Late Or 1M	SGVIII Late Or 6M	SGIX TGD Or 2R	SGX Late Or 1	SGX Late Or 2
SiO2	63.43	64.63	63.57	64.84	64.90	64.38
TiO2	-	-	-	-	-	-
Al2O3	18.83	18.76	18.44	18.46	19.16	18.82
FeO*	0.07	0.09	0.10	0.14	0.05	0.05
MgO	-	-	-	0.01	-	-
CaO	-	-	-	0.06	-	-
BaO	0.58	0.46	0.49	0.59	0.65	0.46
Na2O	1.34	1.07	0.64	1.67	0.98	1.06
K2O	14.40	15.00	15.49	14.74	15.11	14.71
Total	98.65	100.01	98.73	100.51	100.85	99.48
K	91.44	93.3	96.10	89.4	93.9	93.30
Na	8.56	6.7	3.90	10.1	6.1	6.70
Ca	-	-	-	0.4	-	-

1	SGX Late Or 3	SGX Late Or 4	SGX Late Or 5	SGX Late Or 6	SGX Late Or 7	SGX Late Or 8
SiO2	64.09	64.77	64.05	64.06	64.15	63.18
TiO2	-	-	-	-	-	-
Al2O3	18.76	19.17	18.81	18.53	18.67	18.97
FeO*	0.07	0.06	0.11	0.11	0.12	0.11
MgO	0.01	0.01	0.01	-	-	0.01
CaO	-	-	-	-	-	-
BaO	0.49	0.46	0.30	0.51	0.64	0.68
Na2O	0.94	4.49	1.81	1.98	2.09	1.57
K2O	14.94	9.86	13.64	13.37	13.03	14.02
Total	99.30	98.82	98.73	98.56	98.70	98.54
K	94.10	68.70	88.30	87.10	86.20	89.9
Na	5.90	31.30	11.70	12.90	13.80	10.1
Ca	-	-	-	-	-	-

APPENDIX C

Table C.8: ALKALI FELDSPAR MICROPROBE ANALYSES

1	SGX Late Or 9	SGX Late Or 10	SGX Late Or 11	SGX Late Or 12	SGX Late Or 13	SGX Late Or 14
SiO2	63.21	63.59	63.86	64.23	63.74	63.79
TiO2	-	-	-	-	-	-
Al2O3	18.24	18.68	18.79	18.59	18.96	18.67
FeO*	0.12	0.12	0.09	0.11	0.09	0.08
MgO	0.02	0.01	-	0.01	0.01	0.01
CaO	-	-	-	-	-	-
BaO	1.11	0.57	0.55	0.44	0.53	0.43
Na2O	1.71	1.43	1.54	1.62	2.75	1.12
K2O	13.16	14.33	13.86	13.94	12.52	14.66
Total	97.57	98.73	98.69	98.94	98.60	98.76
K	88.50	90.90	90	89.60	82	92.90
Na	11.50	9.10	10	10.40	18	7.10
Ca	-	-	-	-	-	-

1	SGX Late Or 15	SGXIII TGD Or 1R	SGXIII TGD Or 2C	SGXIII TGD Or 3C	SGXIII TGD Or 4M	SGXXVI TGD Or 1R
SiO2	63.56	64.62	64.54	63.86	64.39	64.11
TiO2	-	-	-	-	-	-
Al2O3	18.83	18.71	18.47	18.15	18.24	18.54
FeO*	0.05	0.08	0.07	0.06	0.05	0.11
MgO	0.01	0.01	0.01	0.02	0.02	0.01
CaO	-	0.03	-	0.01	0.01	0.03
BaO	0.63	1.02	1.27	-	-	0.64
Na2O	1.34	1.59	0.97	0.69	0.94	1.34
K2O	14.25	14.43	15.23	15.88	15.05	15.06
Total	98.67	100.49	100.56	98.67	98.70	99.84
K	91.40	89.8	93.90	95.70	93.80	91.6
Na	8.60	9.9	6	4.20	5.80	8.1
Ca	-	0.3	0.10	0.10	0.40	0.2

APPENDIX C

Table C.8: ALKALI FELDSPAR MICROPROBE ANALYSES

	SGXXVI TGD Or	SGXXVI TGD Or	SGXXVI TGD Or	SGXXVI TGD Or	SGXXVI TGD Or	SG78 BGT Or
1	2C	3R	4R	5M	6C	12
SiO2	64.24	64.83	64.49	64.27	65.81	64.21
TiO2	-	-	-	-	-	-
Al2O3	18.58	18.65	18.37	18.51	18.46	18.72
FeO*	0.08	0.08	0.11	0.11	0.11	0.04
MgO	0.01	0.02	0.02	0.02	0.02	0.01
CaO	0.03	0.02	0.04	0.01	0.02	-
BaO	1.05	0.59	0.98	0.61	0.41	0.60
Na2O	1.44	1.59	1.23	1.28	1.36	0.74
K2O	14.61	14.82	15.01	14.95	15.05	15.29
Total	100.04	100.60	100.25	99.76	101.24	99.01
K	90.8	90.20	92.10	92	91.60	95.4
Na	8.9	9.70	7.60	7.90	8.30	4.6
Ca	0.2	0.10	0.30	0.10	0.10	-

	SG78 BGT Or	D63 Uile. Or	D63 Uile. Or	D63 Uile. Or	D63 Uile. Or	D63 Uile. Or
1	13	4	5	6	7	8
SiO2	63.82	63.49	62.98	62.64	62.91	63.40
TiO2	-	-	-	-	-	-
Al2O3	18.76	18.81	18.88	18.87	18.93	18.80
FeO*	0.03	0.09	0.06	0.07	0.09	0.04
MgO	0.02	-	-	-	-	-
CaO	-	-	-	-	-	-
BaO	0.59	0.67	0.78	0.78	0.72	0.65
Na2O	0.60	0.71	0.68	0.74	0.96	0.98
K2O	15.49	15.44	15.43	15.36	14.99	14.93
Total	99.31	99.21	98.81	98.46	98.60	98.80
K	96.3	95.60	95.8	95.4	94	93.90
Na	3.7	4.40	4.2	4.6	6	6.10
Ca	-	-	-	-	-	-

APPENDIX C

Table C.8: ALKALI FELDSPAR MICROPROBE ANALYSES

	D63 Uile. Or 9	D63 Uile. Or 10	D63 Uile. Or 11	D63 Uile. Or 12	D63 Uile. Or 13	D63 Uile. Or 14
1						
SiO2	63.15	62.22	63.96	62.44	62.92	64.02
TiO2	-	-	-	-	-	-
Al2O3	18.62	18.76	18.68	18.91	19.02	18.49
FeO*	0.11	0.05	0.09	0.07	0.10	0.11
MgO	-	0.01	-	-	-	0.02
CaO	-	-	-	-	-	-
BaO	0.59	0.63	0.42	0.61	0.89	0.46
Na2O	1.27	1.25	1.07	1.38	1.60	1.14
K2O	14.43	14.64	15.08	14.54	14	14.41
Total	98.17	97.56	99.30	97.95	98.53	98.65
K	91.90	92.10	93.40	91.30	89.70	92.60
Na	8.10	7.90	6.60	8.70	10.30	7.40
Ca	-	-	-	-	-	-

	D63 Uile. Or 15	XG32 1A Or 14	XG64A 1B Or 4	XG64A 1B Or 5	XG65 1A Or 13	XG61C 2 Or 13
1						
SiO2	63.02	63.26	63.73	63.59	63.81	63.55
TiO2	-	-	-	-	0.01	-
Al2O3	18.72	18.89	18.49	18.63	18.36	18.51
FeO*	0.11	0.07	0.04	0.08	0.09	0.18
MgO	0.01	0.02	0.01	-	0.01	-
CaO	-	-	-	-	-	-
BaO	0.53	1.73	0.13	0.67	-	-
Na2O	0.46	0.86	1.29	1.17	1.00	1.22
K2O	15.77	14.65	14.43	14.27	14.21	14.26
Total	98.62	99.48	98.12	98.41	97.49	97.72
K	97.20	94.4	91.80	92.4	93.40	92.1
Na	2.80	5.6	8.20	7.6	6.60	7.9
Ca	-	-	-	-	-	-

APPENDIX C

Table C.8: ALKALI FELDSPAR MICROPROBE ANALYSES

	E1 Dyke Or	E5A Dyke Or	L1 Dyke Or	L1 Dyke Or
1	1	14	1	2
SiO2	63.36	64.05	63.63	62.59
TiO2	-	-	-	-
Al2O3	19.10	18.63	19.06	18.69
FeO*	0.06	0.14	0.13	0.15
MgO	-	-	0.01	-
CaO	-	-	-	-
BaO	1.95	0.62	1.70	-
Na2O	1.34	1.03	1.09	1.13
K2O	13.52	14.69	14.49	14.52
Total	99.33	99.16	100.11	97.08
K	91.0	93.4	93	92.8
Na	9.0	6.6	7	7.2
Ca	-	-	-	-

APPENDIX C

Table C.9: APATITE MICROPROBE ANALYSES

	SGIII TGD Ap 1	SGIII TGD Ap 2	SGVII Late Ap 1	SGVII Late Ap 3	SGVII Late Ap 3	SGIX TGD Ap 1C
SiO2	1.22	0.41	0.23	0.24	0.22	-
Al2O3	-	0.01	0.01	0.03	0.02	-
CaO	55.52	55.51	55.43	55.42	55.43	54.29
FeO*	0.06	0.07	0.40	0.38	0.26	0.07
MnO	0.04	0.03	0.04	0.04	0.07	0.03
MgO	-	-	-	-	-	0.01
P2O5	41.90	41.36	41.34	41.79	41.61	40.31
F	4.32	4.93	4.55	3.60	4.40	3.98
Total	103.06	102.32	101.60	101.50	102.01	98.69

	SGIX TGD Ap 2C	SGXXVI TGD Ap 1	G24 TGD Ap 1	SG49 PGD Ap 1	SG49 PGD Ap 2	SG49 PGD Ap 3
SiO2	-	-	-	0.03	0.19	0.23
Al2O3	-	-	-	-	0.02	0.01
CaO	54.23	55.13	54.76	55.45	55.66	55.58
FeO*	0.03	0.05	0.02	0.38	0.07	0.07
MnO	0.03	0.06	0.01	0.07	0.05	0.05
MgO	0.01	-	0.01	-	-	-
P2O5	40.17	41.41	40.28	40.53	41.59	41.49
F	3.56	4.11	3.87	4.24	4.65	4.28
Total	98.03	100.76	98.95	100.70	102.23	101.71

	SG93 TGD Ap 1	D1 Rubh Ap 1C	D1 Rubh Ap 2	D1 Rubh Ap 3	D2 Rubh Ap 1	D2 Rubh Ap 2C
SiO2	0.31	-	-	-	-	-
Al2O3	-	-	-	-	-	-
CaO	54.71	53.58	53.80	53.28	54.12	54.05
FeO*	0.31	0.23	0.01	0.07	0.05	0.06
MnO	0.03	0.03	0.01	0.01	0.02	-
MgO	-	0.03	0.01	-	-	0.01
P2O5	40.92	39.63	39.54	39.08	40.54	40.39
F	3.91	3.26	3.33	3.63	3.18	3.24
Total	100.19	96.76	96.70	96.07	97.91	97.75

APPENDIX C

Table C.9: APATITE MICROPROBE ANALYSES

	D2 Rubh Ap 3M	D8 Rubh Ap 1	D8 Rubh Ap 2	D8 Rubh Ap 3	D8 Rubh Ap 4	D8 Rubh Ap 5
SiO2	-	0.29	0.34	0.19	0.36	0.44
Al2O3	-	-	-	-	-	-
CaO	53.96	54.47	54.45	54.86	54.57	54.57
FeO*	0.02	0.06	0.11	0.09	0.11	0.10
MnO	0.01	0.04	0.04	0.08	0.06	0.05
MgO	0.02	-	-	-	-	-
P2O5	40.07	41.12	41.07	41.51	40.88	40.54
F	3.04	3.49	3.19	4.15	3.30	3.62
Total	97.12	99.47	99.20	100.88	99.28	99.32

	D8 Rubh Ap 6	D11 Lidd Ap 1	D11 Lidd Ap 2	D11 Lidd Ap 3	D11 Lidd Ap 4	D11 Lidd Ap 5
SiO2	0.19	0.29	0.23	0.33	0.24	0.30
Al2O3	-	0.01	0.02	0.03	0.03	-
CaO	54.89	54.27	54.98	54.49	55.01	54.84
FeO*	0.05	0.65	0.03	0.09	0.03	0.03
MnO	0.05	0.05	0.02	0.05	0.03	0.06
MgO	-	-	-	-	-	-
P2O5	41.51	40.58	41.51	40.95	41.55	41.44
F	3.27	3.72	3.62	4.17	3.86	3.32
Total	99.96	99.57	100.41	100.11	100.75	99.99

	D11 Lidd Ap 6	D19 Shet Ap 1	D19 Shet Ap 2	D19 Shet Ap 3	D41 Rana Ap 1	D41 Rana Ap 2
SiO2	0.33	0.20	0.31	0.29	0.15	0.16
Al2O3	0.01	0.03	0.04	-	-	-
CaO	54.50	55.27	54.88	54.84	55.50	55.48
FeO*	0.02	0.19	0.07	0.04	0.03	-
MnO	0.01	0.07	0.06	0.04	-	0.05
MgO	-	-	-	-	-	-
P2O5	40.79	41.66	40.92	41.21	41.77	41.63
F	3.87	3.81	3.98	3.62	4.12	4.16
Total	99.53	101.03	100.26	100.04	101.57	101.48

APPENDIX C

Table C.9: APATITE MICROPROBE ANALYSES

	D41 Rana Ap 3	D41 Rana Ap 4	D41 Rana Ap 5	D63 Uil Ap 1	D63 Uil Ap 2	D63 Uil Ap 3
SiO2	0.21	0.22	0.24	0.32	0.34	0.32
Al2O3	0.01	0.01	-	0.07	-	0.07
CaO	55.51	55.45	55.69	55.62	55.12	55.72
FeO*	0.05	0.12	0.03	0.23	0.46	0.11
MnO	0.04	0.03	0.05	0.06	0.01	0.04
MgO	-	-	-	-	-	-
P2O5	41.74	41.86	41.78	42.02	40.68	41.83
F	4.70	4.59	4.38	3.66	3.71	4.02
Total	102.26	102.28	102.17	101.98	100.32	102.11

	D63 Uil Ap 4	D63 Uil Ap 5	D63 Uil Ap 6	XG7 1B Ap 1	XG25 2 Ap 1	XG25 2 Ap 2
SiO2	0.30	1.61	0.27	-	-	-
Al2O3	0.01	0.49	0.01	-	-	-
CaO	55.38	54.42	55.53	54.01	54.36	54.73
FeO*	0.02	0.07	0.14	0.03	0.02	-
MnO	0.04	0.06	0.03	0.02	-	0.01
MgO	-	-	-	-	0.02	-
P2O5	41.03	41.36	41.41	39.69	42.38	42.40
F	3.41	4.51	4.32	3.94	3.66	4.03
Total	100.19	102.52	101.71	97.69	100.44	101.17

	XG25 2 Ap 3	XG44 2 Ap 1	XG44 2 Ap 2	XG44 2 Ap 3	XG44 2 Ap 4	XG89 2 Ap 1C
SiO2	-	0.27	0.33	1.86	3.41	-
Al2O3	-	0.04	0.03	0.52	1.08	-
CaO	54.61	55.04	55.06	51.71	49.16	54.57
FeO*	0.33	0.05	0.27	1.06	1.63	0.01
MnO	0.01	0.04	-	0.05	0.05	-
MgO	0.01	-	-	-	-	0.02
P2O5	42.16	41.30	41.34	39.17	37.17	40.36
F	3.71	3.78	4.28	4.83	3.85	3.91
Total	100.83	100.52	101.31	99.20	96.35	98.87

APPENDIX C

Table C.9: APATITE MICROPROBE ANALYSES

	XG89 2 Ap 2C	XG4 5 Ap 1	E1 Dyke Ap 1	E3 Dyke Ap 1	E3 Dyke Ap 2	E3 Dyke Ap 3
SiO2	-	-	0.48	0.15	0.26	0.12
Al2O3	-	-	0.01	-	-	-
CaO	54.61	54.31	55.40	55.62	55.30	55.73
FeO*	0.21	0.05	0.04	0.23	0.12	0.29
MnO	0.01	-	0.05	0.04	0.06	0.07
MgO	0.01	0.05	-	-	-	-
P2O5	40.58	38.81	41.49	41.63	41.07	41.52
F	3.74	4.19	4.05	4.34	4.22	4.50
Total	99.16	97.41	101.52	102.01	101.03	102.23

	E3 Dyke Ap 4	E3 Dyke Ap 5
SiO2	0.12	0.22
Al2O3	0.01	0.03
CaO	55.66	55.49
FeO*	0.10	0.09
MnO	0.05	0.05
MgO	-	-
P2O5	41.69	41.59
F	4.75	3.72
Total	102.28	101.19

APPENDIX D ANALYTICAL TECHNIQUES

D.1 BULK ROCK MAJOR AND TRACE ELEMENT ANALYSIS

Samples of approximately 1kg were collected for the host Strontian rocks and the mafic diorites, while the xenoliths' sample depended on its size. Samples were split using a geological hammer or a conventional rock spliter composed of two steel plates forced together by a hydraulic mechanism. A sample of each rock type was kept back for hand specimen identification as well as for cutting of 30$\frac{1}{2}$ thin sections. The rest of the sample was cleaned of all the organic material on its surface and washed in in distilled water. These samples were then broken into small (<5mm) pieces using a Sturtevant hardened-steel jaw crusher. A split of each sample at this stage was retained. The rest was ground to a very fine powder (<30$\frac{1}{2}$) using a tungsten carbide "Tema" disc mill. The resultant powder was stored in glass jars.

These initial stages of preparation lead to contamination of the samples with tungsten and cobalt (an impurity in the tungsten carbide), therefore these elements have not been analyzed.

The sample powders were then dried in an oven at 105 ºC for 24 hours prior to use. Two methods of sample preparation were used to allow a wide range of of major and trace elements to be determined. The two techniques are detailed below and are evaluated in Thompson & Walsh (1983) and Potts (1987).

D.1.1 Preparation of solution for major element analysis using a Lithium Metaborate fusion

1. Dry powders at 105 ºC for 24 hours.
2. Accurately weigh 0.25g of sample powder. Make up to 1.5g with lithium Metaborate (Spectroflux*) and mix carefully. Transfer to clean graphite crucible. Twelve samples are fused in each batch.
3. Fuse at 1050 ºC for twenty minutes.
4. Whilst the samples are fusing, measure 150ml of approximately 3.5% HNO_3** into some wide neck plastic bottles and place a clean magnetic stirring bar in each.
5. Transfer the sample directly from the crucible to the bottles immediately after removing each one from the furnace.
6. Stir until all dissolved.
7. Add 5ml of 10% Caesium chloride*** (Spec Pure*) solution.
8. Filter the solutions into 250ml plastic volumetric flasks using Whatman No. 54 papers. Make upto volume with deionized water.
9. Transfer to labelled 250ml polythene bottles and store in fridge.

All chemicals are analytical reagent grade.

* Trade mark of Johnson Matthey Chemicals Ltd.

** 1 litre of 3.5% HNO_3 is made by adding 50ml of concentrated acid to a few hondred mls of deionized water. Make upto 1000ml in a volumetric flask.

*** 1 litre of 10% Caesium chloride is made by adding 126.70g of CsCl (Spec Pure*) to a few hundred mls of deionized water. Make upto 1000ml in a volumetric flask.

The lithium metaborate fusion solution was used for the analysis of SiO_2, Al_2O_3, TiO_2, FeO*, MgO, MnO, Na_2O, K_2O and Rb by atomic absorption spectrometry (AAS). A 1000 times dilution factor (0.25g of sample in 250ml) allows direct measurement of the major elements without further dilution. Rb, an alkali metal, is very sensitive by AAS, but is easily ionized, therefore CsCl was added to all solutions as an ionization suppressant. Details of the operating conditions are given in Table 1.1. Calibrations were made using a number of standard reference materials (SRM) containing a similar matrix to the samples. SRM's were also included in each run to assess the analytical accuracy of the method. Silica was also determined by colorimetry as a result of it being so abundant in acid rocks and with the possibility of it percipitating from the solutions. In addition to the major elements listed above, P_2O_5 was also determined using a fusion solution. Phosphorus is relatively insensitive by AAS therefore the concentration was determined by colorimetry. Both methods are described below.

D.1.2 Determination of silica by colorimetry

Reagents to be prepared on the day of use.

i. Ammonium molybdate solution (Analar):
Dissolve 6.0g of $(NH_4)6MO_7O_{24}.4H_2O$ in 1lt of water.

ii. Tartaric acid solution (Analar):
Dissolve 16.0g of $H_2C_2H_4O_6$ in 1litre of water.

iii. Reducing solution:
Dissolve in 1 litre of water:
0.28g of Na sulphite (Analar);
3.6g of Na Metabisulphite; and
0.06g of 1-amino-2 napthol-4 sulphonic acid (GPR)

Method: Transfer 200µl aliquots of the unknown samples into a series of 60ml plastic bottles. Add 10ml of molybdate solution to each and leave for 10 minutes. Add 10ml of tartaric acid solution to each bottle. Then add 10ml of reducing solution to each and leave for at least 45 minutes. Fill a 1cm light path cuvettes to 5mm from the top. The absorbance of each solution was measured at 640nm using the Pye Unicam SP6-550 UV/VIS Spectrophotometer.

D.1.3 **Determination of phosphorus by colorimetry**

Preparation of the 1000ppm solution

Dissolve 0.4264g of Di-Ammonium Hydrogen Orthophosphate [$(NH_4)2HPO_4$] in 100ml of deionized water. Store in a plastic bottle.

Preparation of the standards

A standard was chosen which has virtually no phosphorus eg. NIM-G (0.02% P_2O_5). Transfer 10ml aliquots of NIM-G to a series of plastic bottles. Then transfer 25, 50 and 100 l of the 1000ppm standard solution to each bottle to give a set of standards containing 0.569%, 1.139% and 2.267% P_2O_5 respectively.

Preparation of reagents for the determination of phosphorus by colorimetry

Prepare just before use. Dissolve 1.25g of Ammonium Molybdate (AR) in 56ml of 25% vol/vol Sulphuric acid (H_2SO_4) in a 250ml beaker. Partially dissolve 20g of Ascorbic acid (AR) in 40ml of deionized water and add to the acidified molybdate solution. Then dissolve 0.10g of Antimony Potassium Tartrate in 10ml of deionized water and add this to the mixture and stir well. Dissolve 25.0g of Hydroxylammonium Chloride 120ml of deionized water. Mix thoroughly and add this to the 250ml beaker. When the solution is clear, transfer to a 250ml volumetric flask and make upto volume with deionized water. Transfer solutions in the order proportions shown directly into 1cm light path cuvettes:

200 microlitres sample

2500 microlitres deionized water

500 microlitres reagent

Allow the cuvettes to stand for 1 hour undisturbed. Measure absorbance of each solution at 880nm using the Pye Unicam SP6-550 UV/VIS Spectrphotometer.

D.1.4 **Determination of Water - using the Modified Penfold Tube method**

1. Preparation of reagent

Dry anhydrous Sodium tungstate (Na_2WO_4) at 125 °C overnight.

Weigh approximately 0.5g of the unknown sample and note exact weight. Add 2.0g of the Na_2WO_4 and mix well. Transfer into a pyrex test-tube. Next weigh in a boat a piece of filter paper/blotting paper (6 x 6cm). Note the weight of boat + paper. Roll the paper into a coil and place in the end of the test-tube. Place a stopper, with a hole drilled in it, in the end of the test-tube. Set up the test-tube in a cooling jacket. Place the cooling jacket with the tube at a height where it will receive maximum heat from a Meeker burner. Heat the closed end of the tube till the sample has melted

completely. Remove from heat, remove the bung and then with the aid of a glass rod and policeman draw out the paper, rotating it to capture all the trapped moisture. Place the paper in the weighing boat and reweigh the two.

Subtract the original weight of boat + paper from the second weight of boat + paper. This value is the weight in grams of water contained in the sample:

$$\frac{\text{Weight of water in grams}}{\text{Weight of sample in grams}} \times 100 = \% \text{ water in sample}$$

D.1.5 Determination of Carbon Dioxide

i. Reagents - 50% vol/vol HCL (AR)

ii. Prepare two standards of 0% and 4% CO_2 for calibration. The blank is 10ml of deionized water. For the 4% CO_2 weigh 0.495g of NBSIB (an argillaceous limestone standard) in a disposable weighing boat and transfer into a 100ml quickfit conical flask using 10ml deionized water (dispensed from an automatic pipette). The unknown samples weigh 0.5g into a conical flask (as before) and wash in with 10ml of deionized water. Place a magnetic stirring bar into the flask.

iii. Set up the equipment and ensure that both taps are open. inject 5ml of 50% HCL using an automatic pipette. As soon as acid injection is completed close both taps and remove the auto pipette from site. Evolution of CO_2 will cause a displacement of the liquid in the U-tube and the amount of displacement is proportional to the amount of CO_2 in the sample.

D.1.6 Preparation of solution for trace element analysis using an open acid digestion

1. Dry powder at 105 °C for 24 hours.
2. Place 0.5g of accurately weighed powder into a PTFE beaker and moisten with 2ml of cold deionized water.
3. Add 10ml of 48% Hydrofluoric acid followed by 8ml of 60% Perchloric acid ($HClO_4$).
4. Slowly decompose on a hot plate at 230 °C. Take to near dryness but do not dry. *
5. Allow to cool. Add 5ml Perchloric acid.
6. Evaporate slowly on a hot plate to near dryness but do not dry.
7. Add 10ml of 50% v/v HCL and digest slowly for about 10 mins on a hot plate.
8. Allow to cool. Transfer to a 50ml volumetric flask and make upto volume with deionized water. Store in a labelled plastic bottle.

* Stages 3 and 4 were repeated if an incomplete digestion occurred.

This open acid digestion was used for the analysis of Ba, Cr, Cu, Li, Ni, Sc, Sr, V.Y and Zn by ICPAES. facilities were made available at the Department of Geology , Kings College London using a Philips Pv8120 1.5m path length simultaneous ICPAES. Details of the Philips system are given elsewhere (Walsh et al 1981). A summary of the operating parameters, spectral wavelengths and detection limits are given in Table 1.1. Calibrations were made using (SRM) prepared at the same time as the samples. SRM's were also used to assess the analytical accuracy and precision. The limits of detection, based on real rock samples are given in Table 1.1.

D.1.7 Determination of Rare Earth Elements

After the major and trace elements were determined, a number of the samples were chosen for REE analysis. A wide choice of rock types were used to give as wide a range as possible. The solutions for REE analysis are prepared in the same way as for trace elements (D.1.6).

i. Preparation of the ion exchange columns:

   a. Load the glass columns with a 10cm height resin bed (Dowex AG50W-x12, 200-400 mesh).

   b. Wash the columns first with 50ml deionized water.

   c. To prepare the resin for the sample pass through 200ml of 1.0N HCL and discard this.

   d. Load the sample onto the columns with 50ml of deionized water.

   e. Once the sample has passed through, wash through with 450ml of 1.7N HCL and discard.

   f. Then pass through 500ml of 4.0N HCL and filter with Whatman No.50 filter paper and collect these washings.

   g. Boil off to complete dryness, having transferred to a smaller beaker in the process.

   h. The samples are then ready for analysis, when 5ml Nitric acid are added just before.

At the end of each day the resin should be collected into one large beaker and mixed together, so as to homogenize it, in case any contamination has occurred. A blank is passed through with every batch of samples to assist with recalculation and also to help in case of any change in the resin or acid.

D.1.8 Electron Microprobe Analysis

Thirty six representative samples were chosen for microprobe analysis. facilities were made available at the Department of Geology, Experimental Petrology Unit, Edinburgh University, using two wavelength dispersive electron microprobes. The first is a Cambridge Instruments Microscan V and the second a Cameca Camebax Microbeam (France). Correction techniques (after Sweatman & Long 1969) were applied to both machines.

Polished sections were prepared from thin sections initially cut to 3.0mm and subsequently ground down to approximately 80μ using a Logitech rotary grinder. the sections were than polished on a rotary polisher using 14μ, 6μ, 1μ and 0.25μ diamond paste to attain a relief free surface. Prior to microprobe analysis, samples are coated with a carbon film to increase the conductitvity of the surface.

Table 1.1

Machine: Pye Unicam SP1900 Atomic Absorption Spectrometer
Elements analyzed: Si, Ti, Al, Fe, Mg, Mn, Ca, Na, K, Rb.

Element	Wavelength	Current ma	Bandpass	Fuel
Al	309.27	10	200	N_2O 5.0 C_2H_2 4.5
Ca	422.7	10	100	N_2O 5.0 C_2H_2 4.0
Fe	248.8	15	100	N_2O 5.0 C_2H_2 3.1
Mg	285.2	4	200	N_2O 5.0 C_2H_2 3.5
Mn	279.5	12	100	Air 5.0 C_2H_2 1.1
K	766.5	8	200	Air 5.0 C_2H_2 1.0
Rb	780.6	emission	300	Air 5.0 C_2H_2 1.2
Si	251.6	15	100	N_2O 5.0 C_2H_2 4.6
Na	589.0	8	200	Air 5.0 C_2H_2 1.0
Ti	365.4	15	100	N_2O 5.0 C_2H_2 4.5

N.B Precision is better than 1% for all elements.

Machine: Philips PV 8210 1.5m ICP Atomic Emission Spectrometer
Elements analyzed: Ba, Cr, Cu, Li, Ni, Sc, Sr, V, Y, Zn and the REE.

Element	Wavelength nm	Practical detection limit* μg g -1
Ba	455.40	1
Cr	267.72	5
Cu	324.75	2
Li	670.78	2
Ni	231.60	5
Sc	361.38	1
Sr	407.77	1
V	290.88	2
Y	371.03	1
Zn	213.86	5

Rare Earth Elements			Chondrite**
La	398.85	0.75	0.329
Ce	418.66	0.86	0.865
Pr	422.29	0.16	0.122
Nd	430.36	0.67	0.630
Sm	359.26	0.11	0.203
Eu	389.17	0.02	0.077
Gd	335.05	0.14	0.276
Dy	353.17	0.05	0.343
Ho	345.60	0.02	0.076
Er	390.63	0.08	0.226
Yb	328.94	0.04	0.220
Lu	261.54	0.01	0.034

Precision is better than 0.5% and accuracy is between 0.7 tp 1.0%

* Walsh & Howe 1980 & Thompson and Walsh 1983
** Nakamura 1974

Operating parameters for REE and trace element determination by ICPAES:

Coolant gas flow	15.01min-1
Auxiliary gas flow	01min-1
Injector gas flow	1.21min-1
Sample uptake rate	2.0mlmin-1
Observation zone above coil	15-19mm
Power input	1.0Kw (50MHz)

Machine: Microscan V, Cambridge Instruments

Gun potential	20 kilovolts
Probe current	30 nanoamps

Elements analyzed:

- Rubidium Acid Phthalate (RAP) crystal on Ka line - F, Na, Mg, Al & Si.
- Quartz crystal on Ka line - K, Ca, Ti, Cr, Mn & Fe.
- Quartz crystal on La line - Ba.

Machine: Camebax, Cameca France

Gun potential	20 kilovolts
Probe current	20 nanoamps

Elements analyzed:

- Thallium Acid Phthalate (TAP) crystal on Ka line - F, Na, Mg, Al & Si.

- Pentaerythritol (PET) crystal on Ka line - K, Ca, Ti & Ba.
- Lithium Fluoride (LiF) crystal on Ka line - Cr, Mn, Fe & Ni.

All the above data holds for the major silicate phases of pyroxenes, amphiboles, micas, opaques and feldspars.

Standards

F - Magnesium Fluoride
K - Orthoclase
Mg - Periclase
Ba - Barytes
Si & Ca - Wollastonite
Al - Corundum
Na - Jadeite
Ti - Rutile
Cr, Mn, Fe & Ni - Individual "Specpure" metals

TITLE THE XENOLITHIC SUITE OF THE STRONTIAN GRANITE

AUTHOR Barbara M. Kruszewska

UNIVERSITY London Polytechnic, C.N.A.A. 1990